

DISSERTATION ZUR ERLANGUNG DES DOKTORGRADES
DER FAKULTÄT FÜR CHEMIE UND PHARMAZIE
DER LUDWIG-MAXIMILIANS-UNIVERSITÄT MÜNCHEN

**Organic Nitrates in Energetic Materials Research:
From PETN Sensitivity to TNT Replacements**



Tobias Lenz

aus

München, Deutschland

2023

Erklärung

Diese Dissertation wurde im Sinne von § 7 der Promotionsordnung vom 28. November 2011 von Herrn Prof. Dr. Thomas M. Klapötke betreut.

Eidesstattliche Versicherung

Diese Dissertation wurde eigenständig und ohne unerlaubte Hilfe erarbeitet.

München, 19.12.2023

(Tobias Lenz)

Dissertation eingereicht am 27.10.2023

1. Gutachter: Prof. Dr. Thomas M. Klapötke

2. Gutachter: Prof. Dr. Konstantin L. Karaghiosoff

Mündliche Prüfung am 07.12.2023

DANKSAGUNG

Ich möchte diese Gelegenheit nutzen, um den folgenden Personen und Organisationen, ohne die die Fertigstellung dieser Dissertation nicht möglich gewesen wäre, meinen herzlichen Dank auszusprechen:

Ich bin meinem Doktorvater, Herrn Prof. Thomas Klapötke (tmk), dankbar für die große Unterstützung während dieser Forschungsreise. Sie haben mich immer mit spannenden Projekten aus der Industrie herausgefordert und mich sehr offen und vertrauensvoll betreut.

Herrn Prof. Karaghiosoff (Conny) danke ich für seine nahbare Art und gute Laune. Bei Fragen zu NMR-Spektroskopie oder Röntgenstrukturen stehst du stets mit enthusiastischen Antworten zur Seite. Danke, dass du es mir ermöglicht hast am Röntgendiffraktometer zu lernen und auch mal dran rumzuschrauben :).

Bei Herrn Dr. Jörg Stierstorfer (Jörg) möchte ich mich für die persönliche Betreuung und direkte Art bedanken. Von Beginn an hast du mir den Rücken gestärkt und mich zusammen mit tmk in der EMTO GmbH aufgenommen.

An dieser Stelle möchte ich mich auch bei allen Industriepartnern für die lehrreichen Einblicke, vielen Gespräche und die erfolgreichen Kooperationen bedanken. Darunter sind Dr. Moritz Mühlemann (BIAZZI SA), Ralf Weber (Austin Powder) and Dr. Jens Wutke (SSE Group).

Frau Irene Scheckenbach danke ich für ihre freundliche Art und ihren positiven Einfluss auf die gesamte Gruppe. Bei organisatorischem Wirrwarr behalten sie stets einen klaren Kopf.

Herrn Dr. Burkhardt Krumm und Frau Brigitte Breitenstein sowie der Zentralen Analytik sei für die zuverlässigen und schnellen Messungen gedankt.

Für das Gelingen meiner Arbeit spielten meine Laborkollegen im Arbeitskreis Klapötke eine unersetzliche Rolle. Im Laufe der Zeit sind aus diesen kollegialen Beziehungen echte Freundschaften entstanden, und ich möchte mich besonders bei Maxi Benz, Willi Cremers, Marcus Lommel, Michi Gruhne, Alex Harter, Lukas Bauer, Jasmin Lechner und Elena Reinhardt bedanken. Ihre Unterstützung und Zusammenarbeit haben nicht nur meine Forschung, sondern auch meine Zeit im Labor zu einer wertvollen und bereichernden Erfahrung gemacht. Die Geschichten und Erinnerungen mit euch sind so zahlreich und lebendig, dass sie allein ein ganzes Buch füllen könnten. Daher habe ich sie hier nur in Stichpunkten festgehalten, damit wir sie bei Gelegenheit wieder aufleben lassen können. Ulux und Tubu, Radltouren, Maxis Praktikanten (speziell Absturz A.), Andechs Ausflug, Marcus und Michi das Dream Team, die Feststofftonne und das Telefon, Weihnachtsschießen, Corona Bierpong.

Besonderer Dank gilt an dieser Stelle den Laborpartnern in meinem Rücken. Maxi mit dir habe ich mich immer gemessen und wir haben uns gegenseitig motiviert aber vor allem freundschaftlich unterstützt. Ich habe die Diskussionen und Feiern sehr genossen, auch wenn

sich beides gelegentlich vermischt hat. Deine Entschlossenheit in vielen Angelegenheiten hat mich beeindruckt, und ich bin sicher, dass du deinen Weg erfolgreich fortsetzen wirst. Marcus, ich danke dir von Herzen für deine enorme Inspiration. Du setzt den Standard immer noch ein Stück höher, selbst wenn er bereits für mich hoch war, und achtest auf jedes Detail. Dein aufrichtiges Interesse daran, anderen zu helfen, und deine bemerkenswerte Zuhörbereitschaft sind Eigenschaften, die ich bewundere.

Jetzt möchte ich meinen Praktikanten, Ersel Parigi, Niklas Kölbl, Jürgen Kuch, Lukas Eberhardt, Sabrina Dörrich, Mohamed Mouzayek, Sandra Klotz und Michael Thoma, von Herzen danken. Durch euren engagierten Einsatz habt ihr meine Arbeit erheblich erleichtert und einen bedeutenden Beitrag zur Fertigstellung dieser Doktorarbeit geleistet.

Mein aufrichtiger Dank gilt allen anderen, die in irgendeiner Weise an dieser Arbeit beteiligt waren. Ihre Beiträge und Unterstützung haben maßgeblich zum Erfolg dieser Forschung beigetragen.

Mein herzlicher Dank gilt meiner Familie, meinen Eltern Martina und Andreas, für ihre unerschütterliche Unterstützung, ihre Ermutigung und ihr Verständnis während dieser schwierigen und lohnenden Reise. Bei meiner Schwester, Isabella, möchte ich mich ganz besonders für die erholsamen Semesterferien in Budapest bedanken aber natürlich auch dafür, dass du immer Zeit für mich hast.

Meiner Freundin Inessa möchte ich von Herzen für ihre liebevolle Geduld mit mir und meiner Forschung danken. Du warst immer an meiner Seite und hast mich nicht nur in meiner akademischen, sondern auch in meiner persönlichen Entwicklung bedingungslos unterstützt. Dafür danke ich dir von Herzen. ❤️

Table of Content

1	Introduction	10
1.1	From Deflagration to Detonation	10
1.2	Classification	12
1.2.1	Propellants	13
1.2.2	Pyrotechnics	14
1.2.3	High Explosives	15
1.3	Characterization	20
1.3.1	Sensitivity	20
1.3.2	Toxicity	22
1.3.3	Thermal Sensitivity and Stability	22
1.3.4	Performance	23
1.4	Next-generation Energetic Materials	23
1.4.1	Requirements	23
1.4.2	Toxicity Requirements	25
1.4.3	Synthesis	26
1.5	The Special Role of PETN	28
1.5.1	Manufacturing	29
1.5.2	Mechanical Sensitivity	30
2	Motivation and Objectives	32
3	Summary and Conclusion	33
3.1	Sensitivity of PETN	33
3.1.1	Laboratory Grade	33
3.1.2	During Manufacturing	34
3.2	Nitrato- and Azidoalkyl Containing Energetic Materials	37
3.2.1	PETN Derivatives	38
3.2.2	Tetrazole Derivatives	40

3.2.3	1,2,3-Triazole Derivatives.....	45
3.2.4	Nitropyrazole Derivatives	46
3.2.5	Polycyclic Derivatives.....	47
3.3	Most Promising Energetic Materials.....	48
3.4	Trends	49
4	Literature	50
5	Appendix	55
5.1	Publications	56
5.1.1	Impact and Friction Sensitivities of PETN: I. Sensitivities of the Pure and Wetted Material	56
5.1.2	Impact and Friction Sensitivities of PETN: II. Sensitivities of the Acidic Material During Manufacturing.....	76
5.1.3	About the Azido Derivatives of Pentaerythritol Tetranitrate.....	116
5.1.4	Melt Castable Derivatives of Pentaerythritol Tetranitrate	136
5.1.5	Nitratoethyl-5H-tetrazoles: Improving the Oxygen Balance through the Application of Organic Nitrates in Energetic Coordination Compounds.....	195
5.1.6	Tuning the Properties of 5-Azido and 5-Nitramino-tetrazoles by Diverse Functionalization - General Concepts for Future Energetic Materials.....	275
5.1.7	Evolving the Scope of 5,5'-Azobistetrazoles in the Search for High-Performing Green Energetic Materials.....	326
5.1.8	Isomerism of Nitratoalkylazoles.....	368
5.1.9	4,5-Bisnitratomethyl and Similar Representatives of the Rare Class of 2-Nitro-1,2,3-triazoles	401
5.1.10	Synthesis and Characterization of Azido- and Nitratoalkyl Nitropyrazoles as Potential Melt-Cast Explosives	431
5.1.11	Polyazido-methyl Derivatives of Prominent Oxadiazole and Isoxazole Scaffolds: Synthesis, Explosive Properties, and Evaluation.....	489

1 Introduction

This chapter will give an overview of the development and characterization of energetic materials. As the field and the applications are constantly evolving and can be very diverse, an important selection will be covered. The focus is placed on the synthesis and properties of explosive materials. The explosive pentaerythritol tetranitrate (PETN) is discussed in detail since the main part of the work deals with the sensitivity of PETN, its derivatives, or organic nitrates in general.

1.1 From Deflagration to Detonation

Combustion, deflagration, and detonation are exothermic oxidation reactions with different velocities. Combustion is dominated by the oxidation of fuel, heat, and chain reactions and no pressure is built up. [1] Subsonic combustion, where the noise of the flame can be heard and pressure is building up, is called deflagration. This deflagration can be self-accelerating until it reaches the local speed of sound in the material. Then a transition to a detonation is observed with the release of a shock wave. The shockwave can propagate into unreacted material, causing compression and a self-sustaining reaction. The transition from deflagration to detonation is called DDT. Compounds like diazo dinitrophenol (DDNP), mercury fulminate, and tetrazene undergo DDT. [2] The linear burning rate of a material r (m s^{-1}) depends on β ($\beta = f(T)$) and increases proportionally to the pressure p on the material. The index α describes the pressure dependence of the burning rate of the material, for $\alpha < 1$ a deflagration, and $\alpha > 1$ a detonation is observed. [1]

$$r = \beta p^\alpha$$

In a confined space, pressure reaches higher values and a detonation is more likely to be triggered. Compounds like lead azide, silver azide, and silver fulminate are so reactive that immediate detonation after ignition is observed. [2] Furthermore, less sensitive explosives like PETN or Hexanitrostilbene (HNS) can be initiated by a shock from hot metallic plasma (in an exploding foil initiator (EFI)). [3] Adiabatic compression (from force applied) of small gas bubbles (from inclusions or glass beads) can also lead to heat and shock release that can initiate explosives. [4-6]

In the detonation, a chemical reaction zone moves at a constant velocity, pressure, and temperature, while heat is released (Figure 1). The reaction zone is accompanied by a shockwave that compresses unreacted material in front. The specific volume ($V_0 = 1/\rho_0$) is decreased and the pressure p is increased (V_0 to V_1 and p_0 to p_1) along the shock adiabat

(Hugoniot adiabat). The compression leads to temperature increase and initiation of the reaction. Pressure and volume at the end of the reaction zone are defined as V_2 and p_2 . [1, 7] The reaction products are in chemical dynamic equilibrium, $\Delta G = 0$ (Chapman-Jouguet condition). [8] A line can be drawn from the pressure-volume correlation at each stage called the Rayleigh line. The slope of this line corresponds to the detonation velocity. Chapman and Jouguet stated that the Rayleigh line is tangential to the shock adiabat at the equilibrium point (p_2, V_2). This is called the Chapman-Jouguet point or C-J point. [9] This model is simplified for ideal detonations and can be applied well for calculations. Real detonations are three-dimensional and show uneven, wave-like reaction zones.

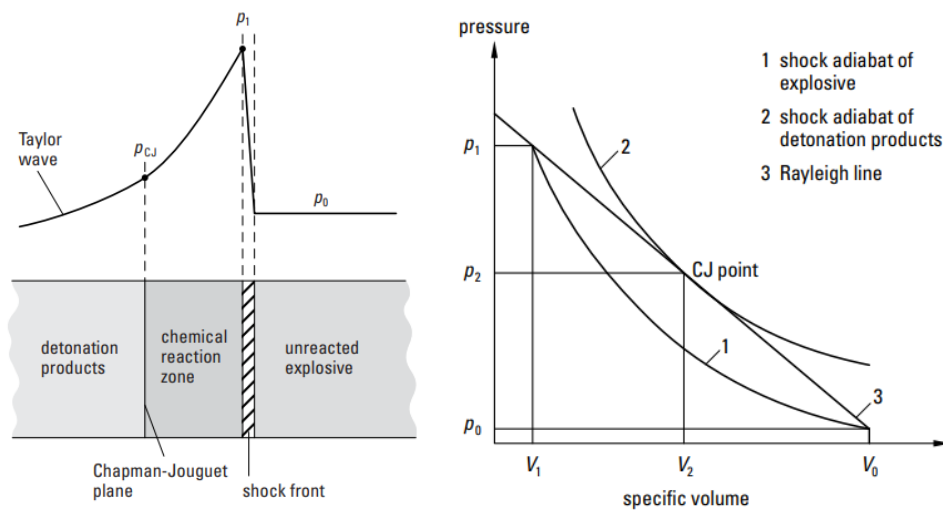


Figure 1 Detonation process and structure of the wave (left) and shock adiabats of explosives and detonation products with Rayleigh line (right). (reproduced from [1])

1.2 Classification

Energetic materials can be divided into propellants, pyrotechnics, and explosives (Figure 2). Whereas explosives are typically subdivided into primary and secondary explosives. Materials used to transition the detonation between these explosives can be counted to the class of booster explosives. Individual compounds are mixed with binders, plasticizers or other substances to be used for the respective application. Individual compounds can also be applied in different categories. [1-2, 10-11] Nitroglycerin (NG) is used in Dynamite as a secondary explosive and also in double or triple-based formulations as part of the propellant charge. [10]

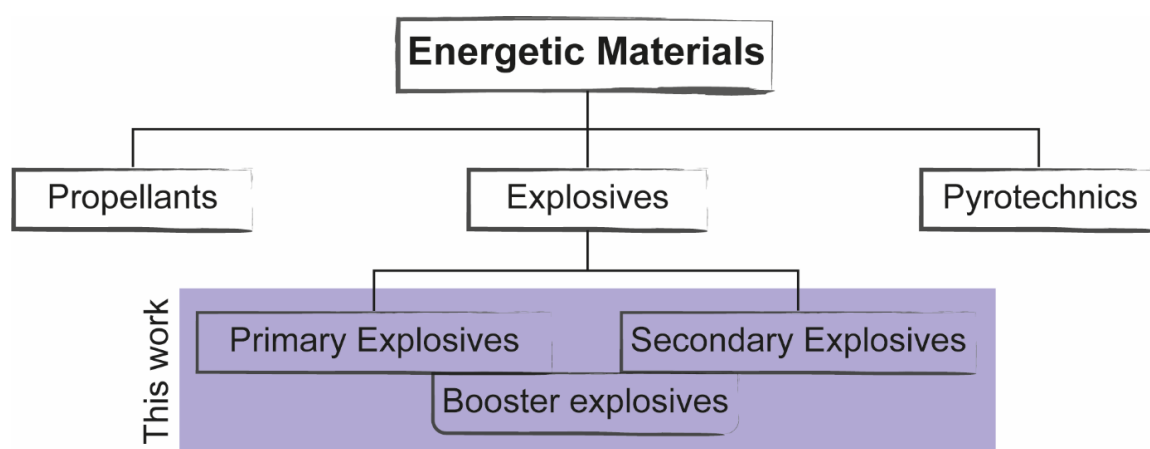


Figure 2 Classification of energetic materials.

Another classification based on the area of application into civil and military is also possible. Civil explosives are used in the demolition, quarrying, mining, construction, tunneling, and seismic industries. The main requirements for civil explosives are very safe handling, low price, regional availability, and environmental neutrality. [12] For military explosives, the price is of less concern if a high performance can be achieved. Military materials must be very stable under storage conditions, highly reliable, and safe enough to withstand rough handling. Of course, the military uses civil explosives and vice versa, but this classification shows the main interests of the two fields. When developing new materials this is of special interest. For mining, mainly mass-producible, safe, and cheap materials (ammonium nitrate) are of interest, complex synthesis procedures and expensive starting materials must be avoided. When developing a military explosive, expensive materials, and multi-step synthesis might be acceptable if the performance is worth it (e.g. CL-20 [13]).

The accidental discovery of black powder (BP) was the beginning of the development of energetic materials (~ 220 BC). BP is a physical mixture of potassium nitrate, carbon, and sulfur. Energy is released through their solid-state reaction. Long after BP was discovered

and used as an explosive, at the end of the 19th century, the principle of combination of oxidizer and fuel in one molecule was a milestone on the way to more powerful materials. [1] To get an overview of the materials and their development, they are categorized in the following.

1.2.1 Propellants

Propellants are mainly used to accelerate projectiles or rockets, by the generation of large amounts of hot gas (Figure 3). BP was the first discovered and still used propellant. With a burn rate of 600-800 m s⁻¹ it does not generate a shock wave under standard conditions. [1] As a result, the effect is not crushing, but pushing. With the discovery of nitrocellulose (NC) (Schönbein 1846 [14]), obtained by nitration of cellulose, a single-base gun propellant was developed in the middle of the 19th century. It burns smokeless without leaving any residue. Another organic nitrate, nitroglycerin (NG) (Sobrero 1847 [14]), was discovered one year later and forms, in combination with NC, double-base propellants. This mixture shows enhanced power at the cost of higher combustion temperatures, causing erosion and muzzle flash. To counter those drawbacks nitroguanidine NQ is added to NG and NC as the main component. NG can be replaced by other nitrates (e.g. ethylene glycol dinitrate) to finetune the properties of the propellant to their respective use. While triple-base propellants maintain good performance, the combustion temperature is lower than that of the single-base mixtures. [15] Due to the high temperatures reached, CO reacts with iron in the barrel to form iron carbide, leading to corrosion. Furthermore, the importance of the heat of combustion (Q in J g⁻¹) can be seen in the equation for the estimation of the projectile velocity (u): [1]

$$u = \left(\frac{2m Q \eta}{M} \right)^{0.5}$$

m : mass of charge in g; M : mass of projectile, η : constant.

Replacing carbon-based propellants with nitrogen-rich materials increases the N₂/CO ratio. This leads to the formation of iron nitride and longer lifetimes of the barrel. [16] Here triaminoguanidinium azotetrazolate (TAGzT) has proven to be effective. [17] The propulsion of rockets requires lower pressures than gun propellants (70 bar vs 4000 bar), while a high specific impulse I_{sp} is also of main importance. The I_{sp} describes the change of impulse (Newton-second) per mass propellant and therefore the efficiency of the propellant. Modern-day solid rocket motors use composite materials made of ammonium perchlorate (AP) or nitrate (AN) as oxidizers, metals (e.g. Al), and binders. Double-base propellants are still used for lower-performance applications. [1] In 2018 AP was classified as an endocrine disruptor by the European Chemicals Agency, due to its influence on

thyroid hormone production. [18] Ammonium dinitramide (ADN) is a potential candidate to replace AP. ADN shows a high heat of formation and a high oxidizing potential but a low thermal stability (T_d : 135 °C). [19] New research materials often derive from trinitroethanol. [20] Liquid rocket fuels can be monopropellants (hydrazine or hydrogen peroxide) and bipropellants (H_2/O_2 , monomethylhydrazine (MMH) / HNO_3). Hypergolic mixtures are igniting after less than 20 ms and are very reliable. Used are carcinogenic hydrazine derivatives (like MMH) with oxidizing HNO_3 or N_2O_4 . [21]

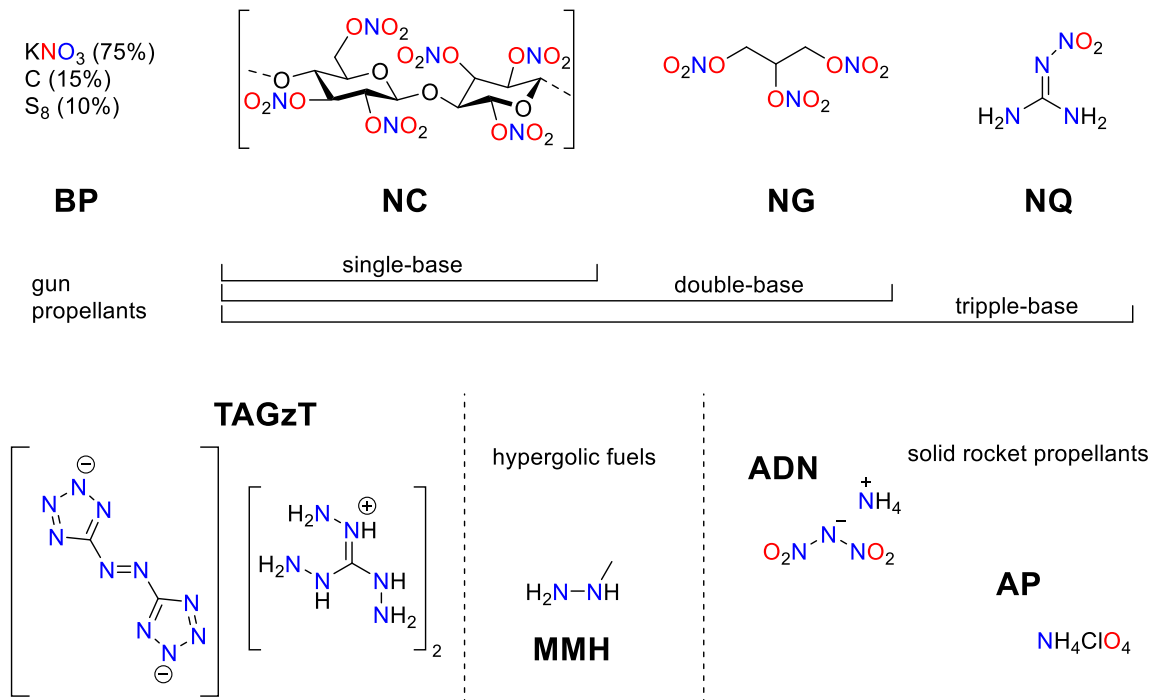


Figure 3 Energetic materials used as propellants.

1.2.2 Pyrotechnics

The art of pyrotechnics focuses on visual, sound, or heat effects through exothermic reactions of physical mixtures. Important parameters are, for example, burning rate, smoke density, or color intensity. The reaction is typically a solid-state reaction of a physical mixture of oxidizers, reducing agents, and additives. The applications and formulations are very diverse, therefore only a selection will be discussed. [1] Flame-generating pyrotechnics are used for electric matches or in percussion caps. Primer compositions in percussion caps contain initiating substances that are discussed in more detail below (see 1.2.3.1 Primary explosives). Examples are SINOXID consisting of lead styphnate LS (primary explosive), tetrazene (sensitizer), barium nitrate/ antimony sulfide/ calcium silicide (pyrotechnic system), or lead-free (SINTOX) consisting of diazodinitrophenol (DDNP, primary explosive), tetrazene (sensitizer), zinc peroxide/ titanium. [22] Delay charges can

be gasless or gassy and are further distinguished by their burn time. BP or mixtures of oxidizing metal salts and elemental fuels are commonly used. Probably the best-known pyrotechnic class is the light generated from the field of fireworks for civil applications. In the military, chemically generated light is used as a signal, for illumination, or as a marker. Typical mixtures contain perchlorates, nitrates, and NC. Metals like Mg can be added to increase the flame temperature. The color is achieved by the addition of Sr (red), Ba (green), or Na (yellow) salts. Research focuses on the replacement of heavy metals (Ba->B₄C or Sr->Li) to reduce toxicity. [23]

1.2.3 High Explosives

High explosives can be divided into either primary explosives or secondary explosives. Primary explosives will trigger the reaction whereas secondary explosives represent the main charge and decide on the effect of the charge. This concept is called the explosive train and is explained exemplarily on a detonator (Figure 4). [2] The explosion is triggered by a simple initiating impulse SII, like a flame, heat, impact, friction, or electrostatic discharge event. Here an electric igniter sets off the primary explosive by a flame and hot particles. [2] The primary explosive undergoes deflagration to detonation and emits a shockwave. Then a larger amount of secondary explosive is initiated and transmits the shockwave to the main charge. The main charge (large amount) consists of less sensitive material and is not part of the standard detonator. Between the detonator and the main charge, booster charges of higher sensitivities might be used for very insensitive main charges or to avoid problems in detonation propagation of the main charge.

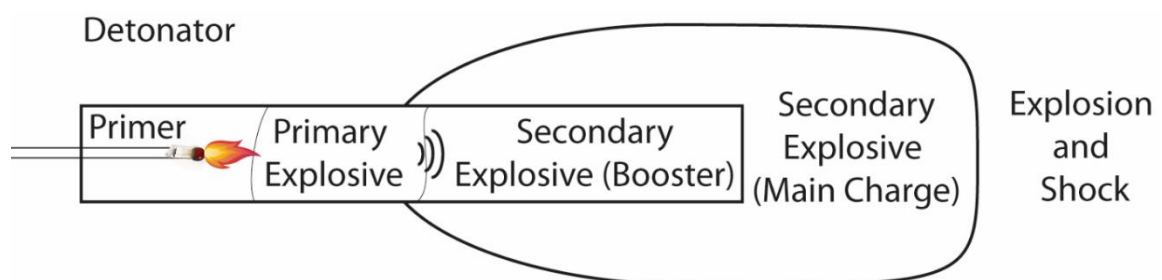


Figure 4 Explosive train as described by Matyáš and Pachman. [2]

1.2.3.1 Primary explosives

Primary explosives (also called initiating substances or primers) are used to start the explosive train through mechanical, electrical, or thermal stimulus (Figure 5). Depending on the output, detonating or burning results are sought. Compositions of mainly or neat detonating substances trigger detonation. Ignition mixtures (also called primers) contain smaller amounts of primary explosives for sensitization but do not undergo DDT. Generally high sensitivity towards impact, friction, and electrostatic combined with a fast transition to detonation is necessary whereas the detonation velocity is of less concern. [1-2] The first compound used in blasting caps and for ignition was mercury fulminate (MF). Due to the high price and toxicity of mercury, it was replaced in a lengthy process by lead azide (LA) and lead styphnate (LS) after the end of the 19th century. [1] LA is typically used if detonations are wanted whereas LS is used in primer caps. [2] Those lead salts are still the commonly most used primary explosives today and replacement is a long-lasting process. Lead exposure causes harm to humans and the environment, everyday exposure is a main issue, and training grounds show high lead levels that need to be decontaminated. [24] Possible next-generation materials for LA are silver azide (AgN₃), copper(I) 5-nitrotetrazolate (DBX-1) [25], and nickel hydrazine nitrate (NHN) [26]. DDNP [27] (in SINTOX) or KDNP [28] are replacements for LS, although heavy metal free they are nitrophenols. Most of the potential or used replacements either contain heavy metals

Summarized development of primary explosives

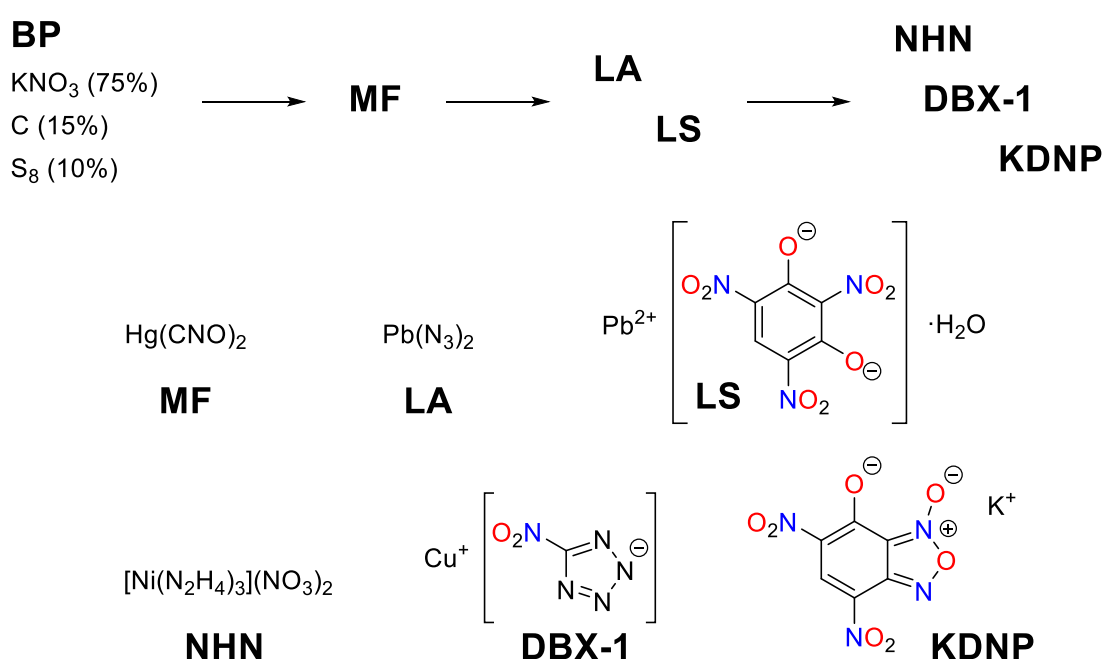


Figure 5 Overview of the simplified development of primary explosives.

or are constructed of nitrophenols. The heavy metal compounds themselves and their combustion products are toxic. There are discussions about nitroaromatic compounds showing a general mutagenic effect. [29] Nevertheless, the toxicity of the reaction products can be reduced by using DBX-1 or DDNP. The concept of energetic coordination compounds, ECCs, leads to a high variety of compounds with tunable properties. Here anions, mostly azide and perchlorate, are combined with a metal center, mostly copper, and nitrogen-rich ligands like tetrazole derivatives. Recently the refinement of copper azide with 1-methyltetrazole showed promising results for lead azide and styphnate replacements. [30]

1.2.3.2 Secondary high explosives

Secondary explosives are characterized by a less sensitive character towards mechanical stimuli or sparks. This is necessary for safe handling because secondary explosives represent the main charge of most explosive devices. Pentaerythritol tetranitrate (PETN) is often referred to be the border between primary and secondary explosives and discussed in a special chapter (1.5 The Special Role of PETN). As it does not undergo DDT in smaller amounts without confinement it is counted as the secondary explosives or might be referred to as booster explosive material. The developed materials often derive from picric acid (PA) in the military sector or Dynamite form NG in the civil sector (Figure 6). Both (PA and NG) are now outdated materials that were developed at the end of the 19th century. PA was found to form primary explosive salts by the reaction with metal shells. NG production still causes devastating accidents, and the produced Dynamite can freeze or leak out sensitive NG. [15, 31]

PA is mainly replaced by 2,4-Dinitroanisole (DNAN) or more powerful 2-Methyl-1,3,5-trinitrobenzene (TNT) mixed with more powerful explosives. The materials are highly compatible, moderately or insensitive, and can be melted in a reasonable temperature range (80-100 °C). [10] The two materials belong to the class of melt-castable explosives a field that needs replacements. Toxicity and production of TNT cause problems for humans and the environment (see 1.3.2 Toxicity). Materials mixed with melt-cast explosives are the nitramine explosives Hexogen (RDX) and Octogen (HMX) or 5-nitrotriazolone (NTO). Mixtures used for military purposes are e.g. Comp. B (RDX, TNT, wax), IMX 101 (DNAN, NTO, NQ) or Comp. C4 (RDX, plasticizer, binder). [1, 15, 32] The more powerful melt-cast bis(1,2,4-oxadiazole)bis(methylene) dinitrate BOM recently developed by the LANL, and the Army research laboratory could replace and outperform TNT. The sensitivity and complex synthesis of BOM are still problems to overcome. [33] Toxic nitramines and nitroaromatic compounds could further be replaced by advanced materials like bis(hydroxylammonium) 5,5'-bitetrazole-1,1'-dioxide (TKX-50), hexanitrohexaazaisowurtzitane (CL-20) or octanitrocubane (ONC). [1]

Summarized development of secondary explosives

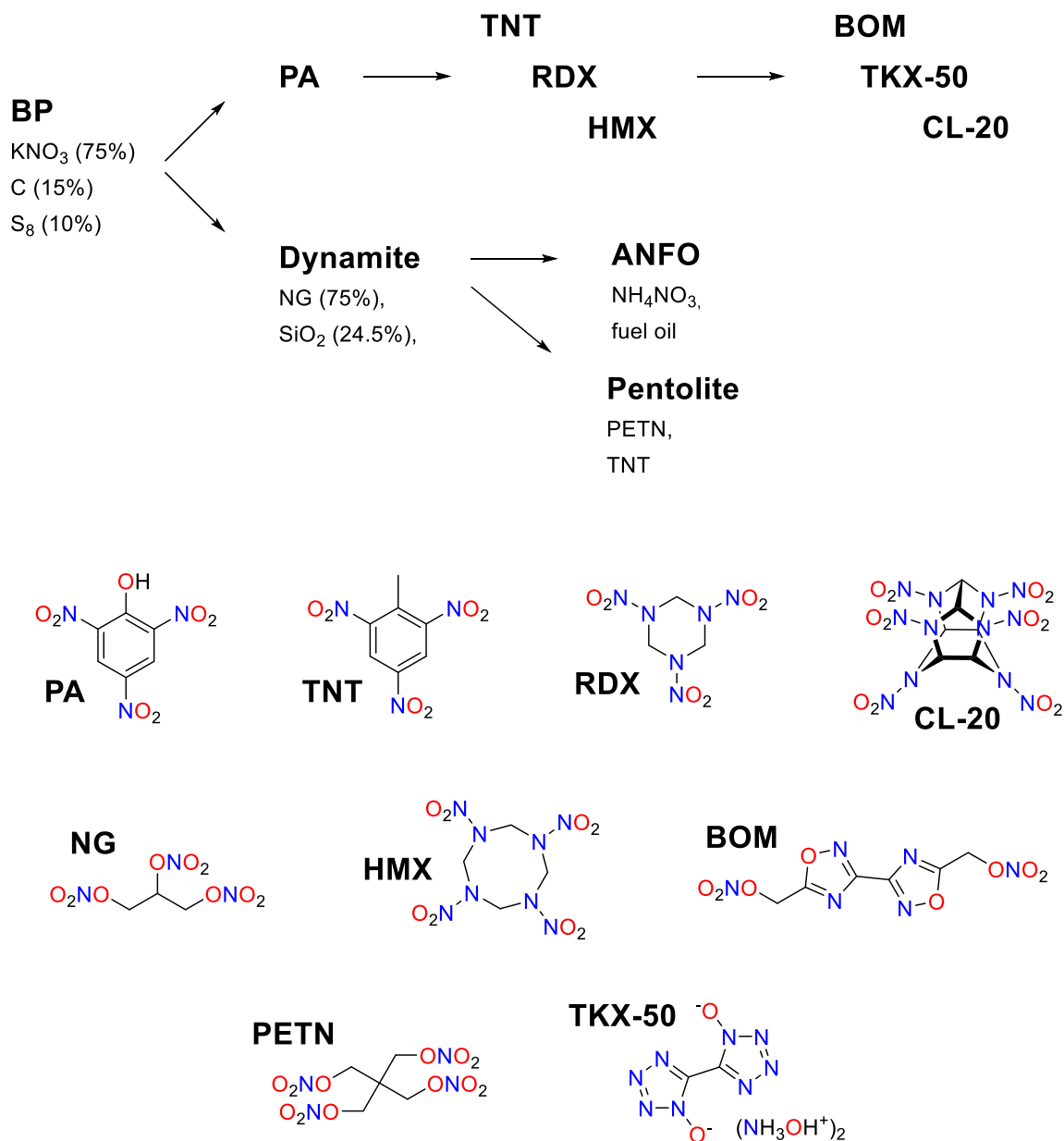


Figure 6 Overview of the simplified development of secondary explosives.

In the civil sector, ammonium nitrate (AN) based explosives displaced the NG-ones due to lower sensitivity, cheaper synthesis, and more practical handling. [1] Due to their cap insensitivity, they are sometimes referred to as tertiary explosives. AN is mixed with fuel oil, resulting in ammonium nitrate fuel oil (ANFO) explosives, that are typically applied as emulsions. Emulsions are sensitized by glass or plastic beads as well as generated gas bubbles. After compression of the material, the gas bubbles collapse releasing a shockwave. This results in a complete and more uniform detonation. ANFOs can be applied in powder form, patronized, or by direct pumping into the boreholes. [1] Ammonium

nitrate is known to cause devastating explosions. Oppau or Beirut is just the tip of the iceberg. Recently, it was shown that ANFO trucks that transport only a few tons of explosives can undergo detonation after catching on fire. [34]

To reliably initiate ANFO mixtures, a larger mass of booster explosive is necessary. Typically, Pentolite, a mixture of PETN and TNT is used. Production of Pentolite through demilitarized TNT caused serious accidents in the past. [35]

Another subclass of secondary explosives are the thermally stable explosives. Hexanitrostilbene (HNS), which is derived from TNT, withstands 320 °C and can be used for fuel fire-resistant devices or hot oil deep drilling applications. Triaminotrinitrobenzene (TATB) is also used as a thermally stable explosive. The stability in HNS derives from the large conjugated π -system whereas TATB shows alternating amino and nitro groups, both typical concepts to achieve very stable explosives. [1]

1.3 Characterization

The characterization of energetic materials covers the sensitivity, toxicity, thermal behavior, and performance parameters of energetic materials. The comparison with existing materials is useful to evaluate the relative performance.

1.3.1 Sensitivity

Before handling larger amounts of unknown explosives impact (IS), friction (FS) and electrostatic discharge (ESD) sensitivity should be analyzed (Figure 7). Impact and friction sensitivity measurements are highly standardized, while there is no general procedure for ESD measurements.



Figure 7 Mechanical sensitivity measurement with BAM friction tester (left) and impact tester (right).

The IS is the oldest known sensitivity test and can be applied by a simple hammer strike for rough estimation (roughly 4 J, enough for PETN). More advanced setups are the BAM Fallhammer, used in our group, or the American ESL type 12 drophammer. Procedures are available in the “UN Recommendations on the Transport of Dangerous Goods” or STANAG 4489. [36-37] Generally, values from different procedures and institutes are not comparable and care has to be taken when comparing measurements on similar machines from different institutions as the evaluation is very operator-dependent. Furthermore, compounds like PETN are easy to evaluate whereas TNT evaluation is more complex. [38] Our group uses the BAM apparatus and the “UN Recommendations on the Transport of Dangerous Goods” procedure. Mechanical energy is applied to the sample by employing weights with options of 1 kg, 5 kg, or 10 kg, dropped from a specific height within the range of 10 to 40 cm. The energy transferred to the sample through this method varies between 1 and 40 J. In terms of test outcomes, the results can be categorized as “no reaction”, “decomposition”, or “explosion”. These outcomes are further categorized into “positive” for an explosion or “negative” for other events. (STANTAG 4489 would count a decomposition as a positive result!). The “one out of six” method used, is a testing procedure wherein six trials are conducted at a specific energy level. The objective is to observe at least one

positive result during these six trials, while trials conducted at lower energy levels must yield negative results. Consequently, this approach is employed to identify the lower detonation limit, a parameter that differs from and is not directly comparable to the E_{50} , 50% probability value (for PETN, 1/6: 3 J, H_{50} : 5 J). For transportation, the material is considered to be an unstable explosive with $IS \leq 2$ J. A more general distinction can be made between insensitive (> 40 J), moderately sensitive (35-40 J), sensitive (4-35 J), and very sensitive (< 4 J) materials. [37]

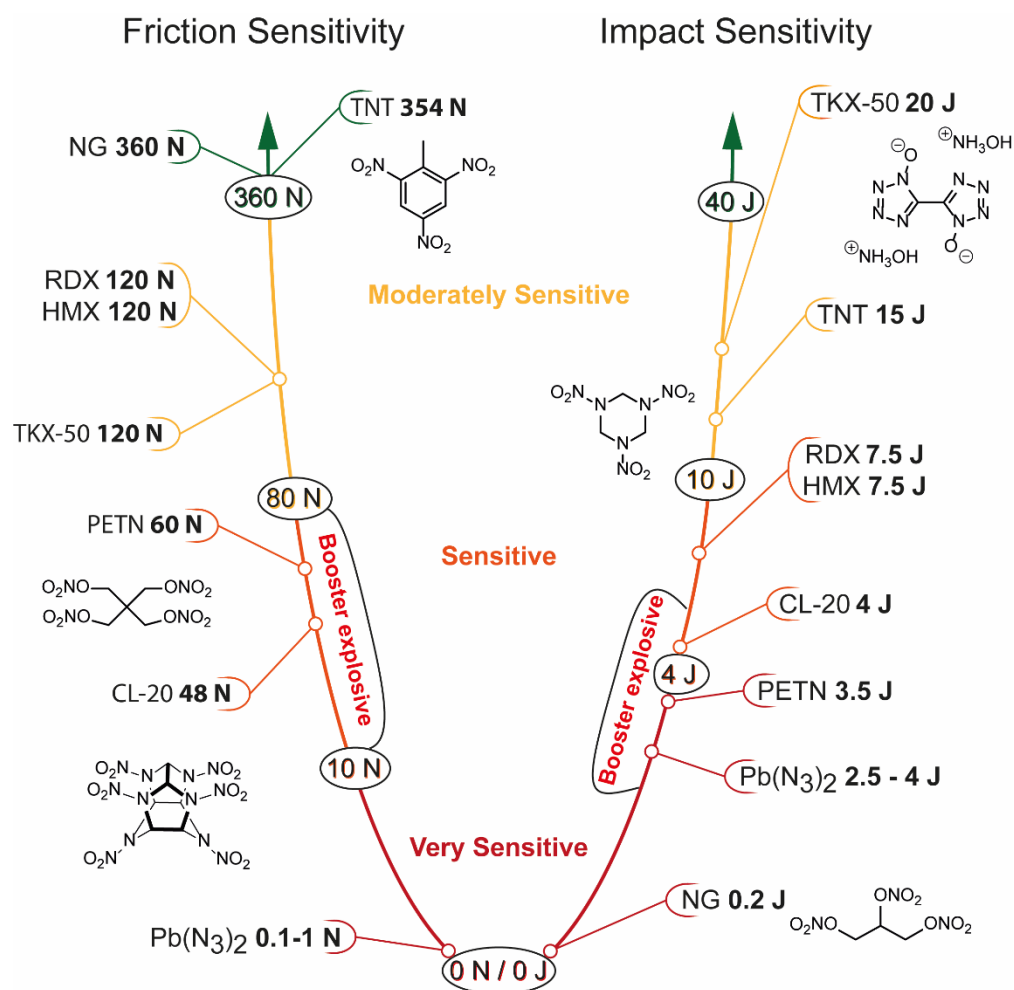


Figure 8 Impact and friction sensitivities of explosives trinitrotoluene flakes (TNT), nitroglycerin (NG), hexogen (RDX), octogen (HMX), bishydroxylammonium 5,5'-bistetrazole-1,1'-dioxide (TKX-50), pentaerythritol tetranitrate (PETN), hexanitroisowurtzitane technical (CL-20), lead azide ($Pb(N_3)_2$). [10, 31]

Manipulation of explosives often results in friction events. Many accidents are derived from scratching surfaces or loosening bolts. Throughout history, various friction sensitivity (FS) devices have been employed, with the BAM friction tester emerging as the most widely utilized. The combination of FS and IS covers the mechanical sensitivity of an energetic material. Procedures for FS are again given by the "Recommendations on the Transport of Dangerous Goods" and STANAG 4487. [37, 39] Force is applied on a porcelain peg

implemented in a lever arm that is loaded with weight. A porcelain plate is fixed within a screw clamp fastened to a steel table below the peg. When activated, the plate moves back and forth by one centimeter. During this motion, friction is generated between the porcelain peg positioned above the porcelain plate. Forces between 0.1 and 360 N can be applied to the material placed between the surfaces. Results are evaluated in the same way as for the IS. The porcelain surface, the placement of the material, and the operator are the main uncertainty factors. With a FS of < 80 N the material is categorized as an unstable explosive and is considered unsafe for transportation. FS can be distinguished more precisely in insensitive (> 360 N), moderately sensitive (80-360 N), sensitive (10-80 N), and very sensitive (< 10 N) materials. [37] The sensitivities of common explosives are visualized in Figure 8. Liquid compounds, such as NG, typically exhibit low levels of friction sensitivity. An examination of NC also reveals that the IS and FS of solid substances can significantly differ, but in the case of most materials like PETN, RDX, or TKX-50, their sensitivity to impact tends to be similar compared to their respective sensitivity to friction.

1.3.2 Toxicity

Toxicity and mutagenicity are an increasingly important factor in the evaluation of new substances. Computational methods are increasingly getting better in this area, but *in vitro* and *in vivo* tests are required. *In vitro*, mutagenicity against the bacteria *Salmonella typhimurium* can be measured by the bacterial reverse mutation test (Ames test). [40] Aquatic toxicity can be estimated by the influence of a compound on the bacteria *Aliivibrio fischeri*. [41] Water-insoluble compounds like most organic nitrates cannot be measured. *In vivo* measurements are costly and ethically unacceptable at an early stage.

1.3.3 Thermal Sensitivity and Stability

Thermal sensitivity can be understood as the temperature necessary for decomposition, ignition, or detonation whereas thermal stability represents the stability at elevated temperatures over time. Differential thermal analysis (DTA) is applied to roughly analyze for endothermic and exothermic signals. The onset temperature, extrapolated reaction beginning, is typically determined. It must be mentioned here that for sharp signals, the onset is close to the actual beginning of the thermal event, whereas for broad signals the onset can be significantly later than the actual beginning of the temperature difference. This concludes that the process of the thermal behavior is of more interest than the neat value. Endothermic signals refer to melting, phase transition, or evaporation. Exothermic peaks are attributed to decomposition events. Melting can be proven by analysis through

a standard melting point analysis. More complex behavior can be further investigated through thermogravimetric analysis (TGA) or differential scanning calorimetry (DSC). Both devices are usually not part of the standard analytics as the sensitive measurement crucibles can be destroyed by heavy decomposition or detonation.

1.3.4 Performance

The performance is typically calculated with the EXPLO [42] code in the first step. The heat of explosion (Q_{C-J}), the detonation pressure (p_{C-J}), and the detonation velocity (D_{C-J}) are considered the main performance parameters. Most important for the determination of those are the density and heat of formation (HOF). [1] The density can be determined by single crystal structure measurement or pycnometric analysis. The heat of combustion can be experimentally determined by bomb calorimetry. Then, using Hess's law, the HOF can be calculated thereof. For initial screening, it is convenient to calculate the heat of formation using the quantum chemistry method CBS-4M and the method of atomization energies. To calculate energies of sublimation or vaporization Trouton's rule is applied. [43] Calculation of lattice energies and lattice enthalpies is performed by Jenkin's method. [44] The HOF of TKX-50 was calculated with this method to be $\Delta_f H^\circ$ (TKX-50, theoretically): 447 kJ mol^{-1} [45], later determination by measurement showed a 50% decreased value $\Delta_f H^\circ$ (TKX-50, measured): $213.4 \pm 1.2 \text{ kJ mol}^{-1}$ [46]. Although the detonation velocity remains in the same area (9698 [45] vs. 9642 m s^{-1} [46]) parameters like the detonation pressure are differing by a large amount (42.4 [45] vs. 37.0 GPa [46]). This shows that the calculation of the heat of formation only gives a rough estimation that should be proven by calorimetry.

1.4 Next-generation Energetic Materials

In the individual classes of energetic materials, we have seen that development to date has mainly been through optimization of performance, safety, or application changes. Modern materials can be manufactured and used safely to the greatest possible extent. The industry is familiar with their hazards and has learned to control them better over the decades. Today, environmental factors and performance are the main driving forces for the development of new materials. In the following, important characterization methods are critically discussed and benchmark values for different classes of explosives are given.

1.4.1 Requirements

The development of new explosive products has always been linked to the discovery of new explosives and the invention of special devices or mixtures (Mercury fulminate in the first detonator caps; NG with binder). Those devices were then optimized, and explosives

were exchanged for less toxic or more powerful materials: LA replacing MF; and ANFO replacing Dynamite. New inventions, like shock tubes [47], open new application areas with different requirements. Energetic material research either focuses on drop-in replacements for existing devices or materials for new applications.

To create a new type of explosive that can be easily integrated, we need to understand the necessary requirements. Therefore, the properties of used explosives are shown in Table 1. Demands for new materials are derived from the properties of existing materials

Table 1 Requirements for next-generation energetic materials.

Replacement	Used in	Issue	Candidates	Requirements	Source
LA (primary)	Detonator	toxic (lead)	NHN or DBX-1	<ul style="list-style-type: none"> - balanced sensitivity - fast DDT - initiation of secondary - T_m: >90 °C - T_d: ≥ 150 °C 	[1-2]
LS (primary)	Primer cap	toxic (lead)	DDNP	<ul style="list-style-type: none"> neat: <ul style="list-style-type: none"> - T_m: >90 °C - T_d: ≥ 150 °C in mixtures: <ul style="list-style-type: none"> - no DDT - low erosion - high flame temperature 	[1-2]
TNT or DNAN (melt-cast secondary)	Comp. B., IMX-101 or Pentolite	toxic, wastewater, and low performance	BOM	<ul style="list-style-type: none"> - T_m: 75-115 °C - T_d: ≥ 180 °C - ΔT_{m-d}: ≥ 100 °C - D: ≥ 7600 m s⁻¹ - ρ: ≥ 1.76 g cm⁻³ - IS: ≥ 8 J - FS: ≥ 120 N 	[48]
RDX or HMX (secondary)	IMX-101 or PBX	toxic	CL-20, TKX-50	<ul style="list-style-type: none"> - T_d: ≥ 180 °C - IS: ≥ 7 J - FS: ≥ 120 N - D: ≥ 8500 m s⁻¹ - P_{C-J}: ≥ 340 kbar 	[1]

and the opinions of experts in the field of explosives. Desirable properties that count for all materials are heavy metal free, non-toxic, mass-producible (primaries less than secondaries), affordable, long-term chemically stable, compatible with shell, and compatible in used mixtures.

1.4.2 Toxicity Requirements

The impact on humans and nature can be divided into three parts: production, handling, and residues. LA massively contaminates training grounds and expensive soil recovery is necessary while everyday shooting leads to higher lead blood levels for soldiers. Heavy and toxic metals persist after their use and therefore need to be replaced urgently where humans are affected. Other materials like TNT, DDNP, or other nitrobenzenes are toxic themselves and cause problems to the environment due to their production. The blood system and liver of humans are damaged through exposure to TNT. [49] There is evidence that all nitroaromatic substances could interact with DNA. [29] Red and pink wastewater is produced in large amounts and without proper treatment causes damage to the environment. [50] RDX is one of the most used explosives and pollution in air water and soil is detected especially around training grounds. The nitramine is toxic because it harms the nervous system, urinary system, and prostate of animals, and evidence for carcinogenic potential is shown. [51-52] Whereas automation and safety precaution are permanently getting better it might be acceptable to continue using toxic substances under controlled conditions if their residue and use does not impact humans or nature.

Tetrazoles and organic nitrates are often discussed as replacements for traditional explosives or are already used. Both are proven to be biologically active and are used in drugs. However, biological activity and use as a drug are not necessarily associated with a positive effect on humans and the environment. Tetrazole exhibits a variety of effects, including antifungal, antihypertensive, and antihistaminic properties. [53-55] 5-Aminotetrazole (5-AT) showed no mutagenic effects and no toxicity up to 623 mg 5-AT/kg (over 14 days) in rats. [56] The use of tetrazoles in future energetic materials is likely and could be environmentally friendly without negative effects on humans. Organic nitrates are used in drugs to release nitric oxide (NO) in vivo. In 1998 the discovery of NO as a signaling molecule in the cardiovascular system was awarded with the Nobel prize. [57] The nitrates PETN or NG are used as vasodilators, which widen the blood vessels, causing a decrease in blood pressure. They are commonly used to treat angina pectoris (chest tightness). [58] The exposure of organic nitrates is limited due to their water insolubility. PETN has been used for decades without observations of significant mutagenic or toxic potential, only headaches are observed as side effects in a few cases. [59-61]

1.4.3 Synthesis

The following synthetic strategies are often applied to achieve explosive materials: [1]

- high nitrogen content
- close to zero oxygen balance (OB)
 - high density
 - ionic character
- conjugated π -system

Nitrogen-rich compounds show an increased density due to the higher weight of nitrogen compared to carbon. The explosion leads to mainly inert nitrogen as a reaction product and a large energy release due to exothermic nitrogen triple bond formation ($BDE(N\equiv N) = 954 \text{ kJ mol}^{-1}$). [1] The nitrogen bond energy per two-electron bond is increasing with the order of the bond. In comparison, the carbon triple bond is less stable than three times the carbon single bond. The well-known azido functionality is typically part of the synthesis or final structure of nitrogen bonds (Figure 9). Azides can be applied in ionic (lead azide), aliphatic, or aromatic positions. The azo bridge can be synthesized through simple oxidation of amines and is often applied in combination with azoles (five-membered aromatic rings containing nitrogen). Pentazole is the most favorable, but hardly accessible, all-nitrogen azole. Current research is focused on the isolation of ionic derivatives. [62] Tetrazole, an explosive itself, is obtained by a reaction of triethyl orthoformate with azide and ammonium chloride with a 60% yield. [63] The acidic azole crystallizes with a density of 1.529 g cm^{-3} and shows a positive heat of formation ($\Delta_f H_m = 237 \text{ kJ mol}^{-1}$). [64-65] The decomposition of neutral tetrazole is observed at $188 \text{ }^\circ\text{C}$ whereas, salt formation stabilizes the compound. Tetrazole can be functionalized at the *N1* or *N2* position to remove the acidity. Through differing synthetic strategies, nitrogen-rich 5-substituted amino [66] or azido tetrazole [67] can be synthesized. To access more functional sites at the azole, triazoles or pyrazoles can be used.



Figure 9 High nitrogen motifs commonly used in energetic materials to increase the performance.

A good oxygen balance is of high priority as the reaction proceeds much faster when oxidizer and fuel are combined in one molecule. Suitable energetic oxygen-rich groups are the nitrato, nitramino, and nitro functionality. Those groups can be applied in aliphatic

positions as shown for nitrate and nitramino in this work. While nitramino, aromatic nitrimino, and nitro groups are commonly found in aromatic positions of energetic materials, the presence of the nitrate group in such positions is hardly known [68]. Heterocyclic motifs can also improve the oxygen balance. Here oxadiazoles and furoxanes are often used as energetic motives (Figure 10).



Figure 10 Motifs commonly used in energetic materials with high combined nitrogen and oxygen content used to tune the oxygen balance.

A high density can be achieved mainly by a high nitrogen and oxygen content, as both atoms show a greater atomic mass. Ionic interactions can also have a positive effect on the density (furoxanes or TKX-50). [1] Also, very tensioned rings show elevated densities (ONC, CL-20). In the cubane motif, the carbon single bond is deformed to a 90° angle. This stored strain energy contributes to increased energetic performance. [1] Acidic protons can be removed by ionic derivatization. This can increase thermal stability and density depending on the ions used. Sensitive acids can be transferred to silver or potassium salts to synthesize primary explosives. Nitrogen-rich ionic derivatives, if insensitive enough, can be used as secondary explosives. [1]

1.5 The Special Role of PETN

The tetranitrate of pentaerythritol is a highly symmetric nitrate ester melting at 141 °C and decomposing at about 180 °C. In its synthesis, the corresponding alcohol pentaerythritol (PE) undergoes a chemical reaction with white-fuming nitric acid, resulting in the formation of the ester. The so-obtained aliphatic energetic compound is characterized by a carbon framework that functions as a fuel source for the highly oxidizing nitrate esters. With a high density of 1.77 g cm⁻³ and a detonation velocity of 8400 m s⁻¹, its performance is closer to RDX than to TNT. [10, 69] PETN is often used to distinguish between primary and secondary explosives. It can be easily initiated by an initial shock wave of a primary explosive. Gram scales of PETN can be burned in an open environment showing deflagration whereas confined material can undergo a DDT. Pressed to a total maximum density TMD of 70-75%, a 5 mm thick and confined rod of PETN detonates 15 mm after the ignition point. [70] Samples with higher or lower TMD lead to longer transition distances. At 93% TMD, no detonation occurs after 150 mm, concluding that a dead-pressing effect occurs similar to that of MF and DDNP. [2, 71] PETN is used in detonators to accelerate a shockwave. [72] It can be initiated by a primary explosive (Figure 4) or an exploding foil. The exploding foil initiator EFI is interesting as no sensitive primary explosive is necessary to initiate detonation. [3] PETN is also used to accelerate a shockwave from the detonator to a tertiary or insensitive secondary explosive. So-called cap-sensitive booster charges typically consist of mixtures of PETN and TNT, called Pentolite. Dynamite, containing nitroglycerin, was employed in the past; however, like numerous other liquid aliphatic nitrate esters, it has been associated with the occurrence of headaches. The next-generation materials, now avoiding toxic TNT, could consist of PETN (sensitizer), AN, and binder/emulsifier. [73] Mixtures with superfine PETN (ca. 5 µm) were shown to be more shock-sensitive and propagate better than coarse material. [74-75] PETN is further used as a secondary explosive in shock tubes, detonating cords, sheet explosives, or mixtures such as SEMTEX®. Shock tubes are non-explosive fuses, consisting of a thin plastic tube coated with explosive material on the inside. [47] Shock tubes and EFI open new requirements for initiating materials. These concepts generate slower shockwaves that could initiate less sensitive material and enhance overall safety. For detonating cord, PETN with good quality is enclosed in a tube and fixed in it by fibers. The cord is flexible and can be wrapped around trees, put in boreholes, or used as a detonating fuse. It is mainly used for mining and demolition with charges of 5 to 100 g (PETN)/meter. [76] In the case of sheet explosives, PETN is encased within a rubber-like, elastic matrix. These pliable sheets have found utility in applications such as metal

the acid, the NO₂ content and concentration must be controlled. The NO₂ concentration should be below 0.4% and the acid concentration around 85%. Higher NO₂ concentrations catalyze decomposition with much faster rates at concentrations between 65-75%. [80] The reaction mixture is cured at lower temperatures to finalize precipitation. The obtained crude material contains occluded acid in the crystal and is not long-term stable. Stabilization with carbonate in mixtures is possible resulting in stabilized PETN with reduced shelf life and stability. [81] To obtain better shelf life and stability crude PETN is dissolved in hot acetone and neutralized with ammonia. [82] Crystallization is achieved through the addition of water and cooling. The resulting recrystallized PETN is stable. [83] Neutralization with carbonate is reported but more complex due to the low solubility of carbonate salts in acetone. In the laboratory, PETN can be obtained by a similar reaction from pure PE in nitric acid. [84] Through the dissolution of crude PETN in organic solvents, followed by the extraction of the acid using aqueous carbonate solutions, laboratory-grade pure PETN can be yielded.

1.5.2 Mechanical Sensitivity

The mechanical sensitivity of PETN is investigated in the first part of this work. Particle size effects and crystallization techniques are a recent topic in PETN investigations. Research on safety during the manufacturing process was rare and therefore investigated (3.1.1 Laboratory Grade). Here, a short introduction to the sensitivity of PETN and the relevance of measurement procedures is given.

Mechanical sensitivity is understood as the impact and friction sensitivity of a material. It depends on various influencing factors. In an overview study, Marrs *et al.* have shown that detonation of dry PETN, in contrast to TNT, can be reliably evaluated by acoustic measurement. Furthermore, they have proven that one laboratory can measure reliably over years and variations with other laboratories can be large. [38] The variation of measurements performed by different institutes is a commonly observed phenomenon. [85-87] This concludes that sensitivities can only be compared if they are measured by one institute under highly standardized conditions. At best, the values are compared within one study or series. General comparison of sensitivities, especially of hardly exploding materials or measurement of different probabilities (1/6 vs E₅₀), must be done with great care.

The mechanical sensitivities are reported to decrease by the addition of water, wax, and TNT, or by the synthesis of ultrafine PETN. The effects of heating are inconsistently reported to increase or decrease sensitivity. The exact effects are shown in Table 2.

Table 2 Impact and friction sensitivities of PETN as measured neat (standard) and in modified mixtures (influenced). For the μm -sized sample, the percent of positive results at a certain energy is given. When centimeters are given for IS or FS, the exact load or detailed apparatus is not clearly described in the source.

influence	standard PETN		influenced Sample		Source
	IS	FS	IS	FS	
water 9%	4 J	54 N	25 J	60 N	[88]
water 15%	4 J	54 N	25 J	72 N	[88]
water 9%	4 J	54 N	25 J	80 N	[89]
water 20%	2-3 J	25-40 cm	4-5 J	> 150 cm	[84]
vacuum dry	3 ± 0.5 J	-	2 J	-	[90]
TNT 10%	4.1 J	64 N	6.3 J	96 N	[91]
wax 10%	4.1 J	64 N	10 J	174 N	[91]
μm -sized	100% (~ 5.5 J)	-	14-80% (~ 5.5 J)	-	[92]
0.27 μm	5.1 J, 6.1 J	-	7.8 J, 8.8 J	-	[93]
100 μm	3 J	60 N	2.8 J	135 N	[94]
0.5 μm (spray-dried)	3 J	60 N	5.5 J	202 N	[94]
heating 55 °C	20.8 cm	-	24.8 cm	-	[95]
heating 65 °C	20.8 cm	-	27.3 cm	-	[95]
heating 65 °C	~ 40 cm	-	~ 20 cm	-	[96]
heating 148 °C	> 43 cm	-	3-4 cm	-	[84]

2 Motivation and Objectives

Part 1: Sensitivity of PETN

Large-scale manufacturing of PETN has a long history dating back to the 1930s. Despite this extensive tradition and knowledge, the occurrence of accidents within plants remains a persistent concern. Most of those accidents happen through mechanical force leading to an explosion. Literature addressing the safety aspects of explosive production is rare and to achieve optimization or implement process changes, a more comprehensive understanding of the mechanical sensitivity is required. Furthermore, it is a fact that sensitivity data cannot reliably be compared between different institutes (see chapter 1.5.2 Mechanical Sensitivity). We decided to start a large examination of the sensitivity of PETN when mixed with water and under various manufacturing scenarios. This research received support from BIAZZI, the industrial plant designer, as well as the manufacturers Austin Powder and the SSE group. With the data obtained, it is anticipated that a more comprehensive assessment of the hazards associated with the production and handling of PETN can be achieved. This information has the potential to improve existing designs and safety regulations .

Part 2: Nitrato- and Azidoalkyl Containing Energetic Materials

Although TNT is extensively used as a melt castable explosive, its widespread use has raised concerns regarding toxicity and the generation of problematic wastewater (see chapter 1.3.2 Toxicity). The current shortages, coupled with increased demand, are worsening the situation. The alternative replacement, DNAN, is an insensitive, nitroaromatic material, but considerably less powerful. From research, only a few compounds have demonstrated the potential to replace TNT, and many of them suffer from drawbacks like expensive synthesis, relatively high sensitivity or toxicity. This results in a justified motivation to synthesize new materials that are melt castable and can potentially replace TNT or DNAN. The objective is to create stable and cost-effective melt castable materials by utilizing less-toxic building blocks. Our focus is on combining azido- and nitratoalkyl groups with specific backbones such as pentaerythritol, tetrazole, or triazoles to achieve the desired properties. We defined them for a TNT replacement as follows (see chapter 1.4.1 Requirements):

$$\begin{aligned} T_m(\text{melting point}): & 75\text{-}115 \text{ }^\circ\text{C}, T_d(\text{decomposition point}): \geq 180 \text{ }^\circ\text{C}, \\ \Delta T_{m-d}(\text{temperature difference between melting and decomposition point}): & \geq 100 \text{ }^\circ\text{C}, \\ D(\text{detonation velocity}): & > 7600 \text{ m s}^{-1}, \rho(\text{density}): 1.76 \text{ g cm}^{-3}, \\ \text{IS}(\text{impact sensitivity}): & \geq 8 \text{ J, FS}(\text{friction sensitivity}): \geq 120 \text{ N}. \end{aligned}$$

3 Summary and Conclusion

This work is divided into two main topics: the sensitivity of pentaerythritol tetranitrate and the evaluation of nitrate- and azidoalkylazoles as potential TNT replacements. Both topics are related to the use of organic nitrates as oxidizing elements. The sensitivity investigation, which involves close collaboration with the industry, covers synthesis and material science. In contrast, the second topic is fundamental research, focusing on the synthesis and characterization of new energetic materials. At the end of this work, you will find a discussion of observed trends in structure-property relationships and an overview of the most promising energetic materials.

3.1 Sensitivity of PETN

The industrial production and use of organic nitrates have always been a dangerous business. To better understand the risks during the manufacturing of PETN, we started this investigation. The project was a cooperation of the industrial plant designer BIAZZI and the manufacturer Austin Powder, combined with the LMU as a scientific research lab. Later, the SSE group joined the investigation and provided material directly from the production plant in Brigg, Swiss.

It is a fact that sensitivity data cannot reliably be compared between different institutes (see chapter 1.5.2 Mechanical Sensitivity). As a result, we laid the groundwork for our experiments using laboratory grade PETN and observed that gradually increasing the water content desensitizes PETN. This is covered in the first chapter 3.1.1 Laboratory Grade. Having the pure and wet PETN data to compare we investigated the sensitivity of dry and wet PETN in three industrial cases covered in chapter 3.1.2 During Manufacturing.

3.1.1 Laboratory Grade

A literature review revealed that high-accuracy mechanical sensitivity data is hard to obtain, and good standardization must be done before. Furthermore, data on wet PETN by the UN and the ICI is controversial. (1.5.2 Mechanical Sensitivity) Initial trials led to improved sample preparations and the observation of water loss during measurements. We measured the water content before and after each test using Karl-Fischer titration and found that water loss was minimal, in the lower percentage range.

Pure PETN with a mean particle size of 300 μm consisting of partly intergrown blocks was used as sample. We investigated the sensitivity of the PETN dried and after wetting with up to 35% water (Figure 11). In the dry state, a sensitivity of 3.5 ± 0.5 J and 50 ± 4 N was observed. The addition of water showed a general decrease in sensitivity correlating with the amount of water. The impact sensitivity decreases exponentially up to 10% water and

16.7 ±2.4 J. The friction sensitivity shows a linear decrease to 15% and 87 ±8 N. Water contents of up to 25% show stagnating mechanical sensitivity values. Increasing the water content further results in decreased sensitivities of 25 ±0 J and 105 ±8 N. Observations indicate the inhibition of propagation rather than the inhibition of detonation.

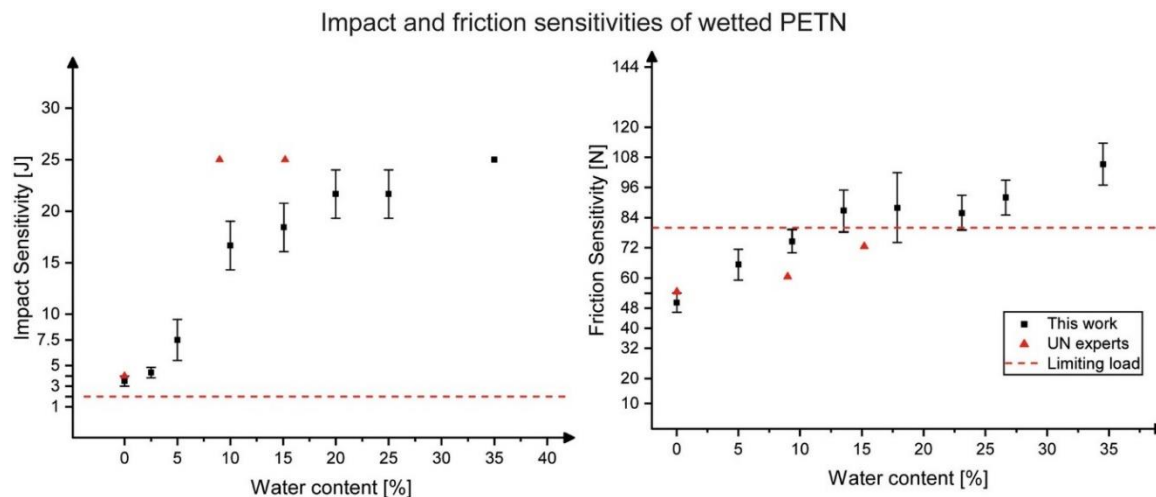
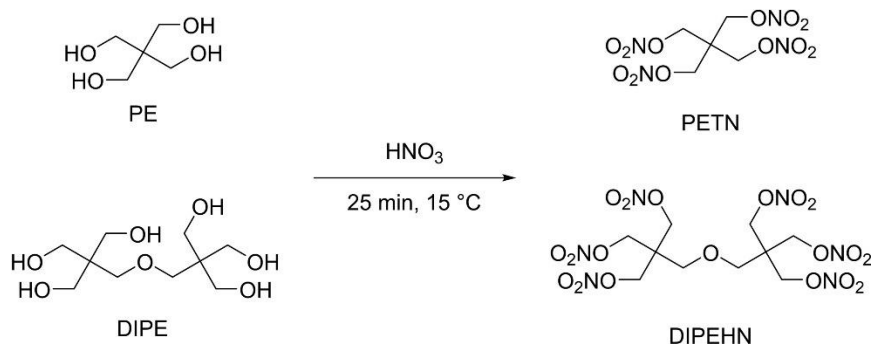


Figure 11 The mechanical sensitivities of wetted PETN ranging from 0 to 35% water with impact sensitivity (left) and friction sensitivity (right) are shown.

When PETN contains less than 10% water, it is a sensitive material and should be handled like dry material. With 15% water, the friction forces are a major concern whereas impact is less relevant. Rough surfaces and shear stress should be avoided. Further addition of water is desensitizing, but the material stays sensitive. The loss or settling of water presents a significant risk.

3.1.2 During Manufacturing

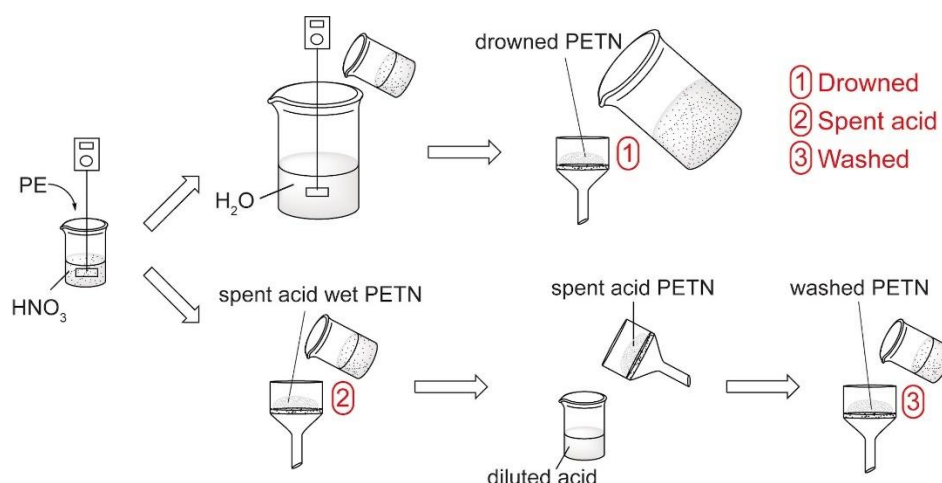
To increase the safety of manufacturing of PETN, the mechanical sensitivities during the process were investigated. We started to develop a small-scale industrial reactor in close cooperation with the industry.



Scheme 2 Synthesis of industrial crude PETN.

The goal was to simulate emergency procedures and standard process conditions of a real plant. The batch-flow process of BIAZZI was used as orientation. A mixture of pentaerythritol containing 0.1, 0.8, and 1.3% dipentaerythritol (DIPE) was nitrated on a 30 g scale (Scheme 2).

The first case investigated is called emergency drowning and applied in a malfunction situation (Scheme 3). Here the reactor content is poured in a large amount of water to dilute the nitric acid and stop the reaction. The second and third investigated case is part of the regular nitration. In the second case, acidic PETN is taken from the finished reaction mixture of 85% nitric acid, called spent acid. This spent acid wet sample was investigated. The third measurement series was done after washing the spent acid wet PETN resulting in washed PETN. Impact and friction sensitivity measurements were conducted on dry and wet material, with liquid contents of up to 35%. The DIPE content was varied in three steps to investigate its influence.



Scheme 3 Synthesis of the three different grades of PETN.

We found that DIPE does not influence the mechanical sensitivity to a measurable degree. No dried sample showed to be more sensitive than PETN. Drowning and washing results in a very similar product concerning its sensitivity. Both are desensitized by wetting whereas the friction sensitivity is less affected and stays around 84 N between 10 to 35% liquid content. The impact sensitivity is decreased to around 20 J at 10% and higher liquid contents. A high friction sensitivity was observed for spent acid-wet PETN during nitration with mostly 48-72 N. The spent acid can sensitize the material to 36 N at 16% acid content. The impact sensitivity decreases with higher acid content. This decrease is marginally less than for the washed and drowned samples (Figure 12).

Therefore, drowning and washing yields a product that can be handled like the final recrystallized product. Only the nitration step shows a high-risk potential due to friction-

sensitive material, that is sensitized by spent acid. The impact sensitivity is generally decreased, the wetter the sample is.

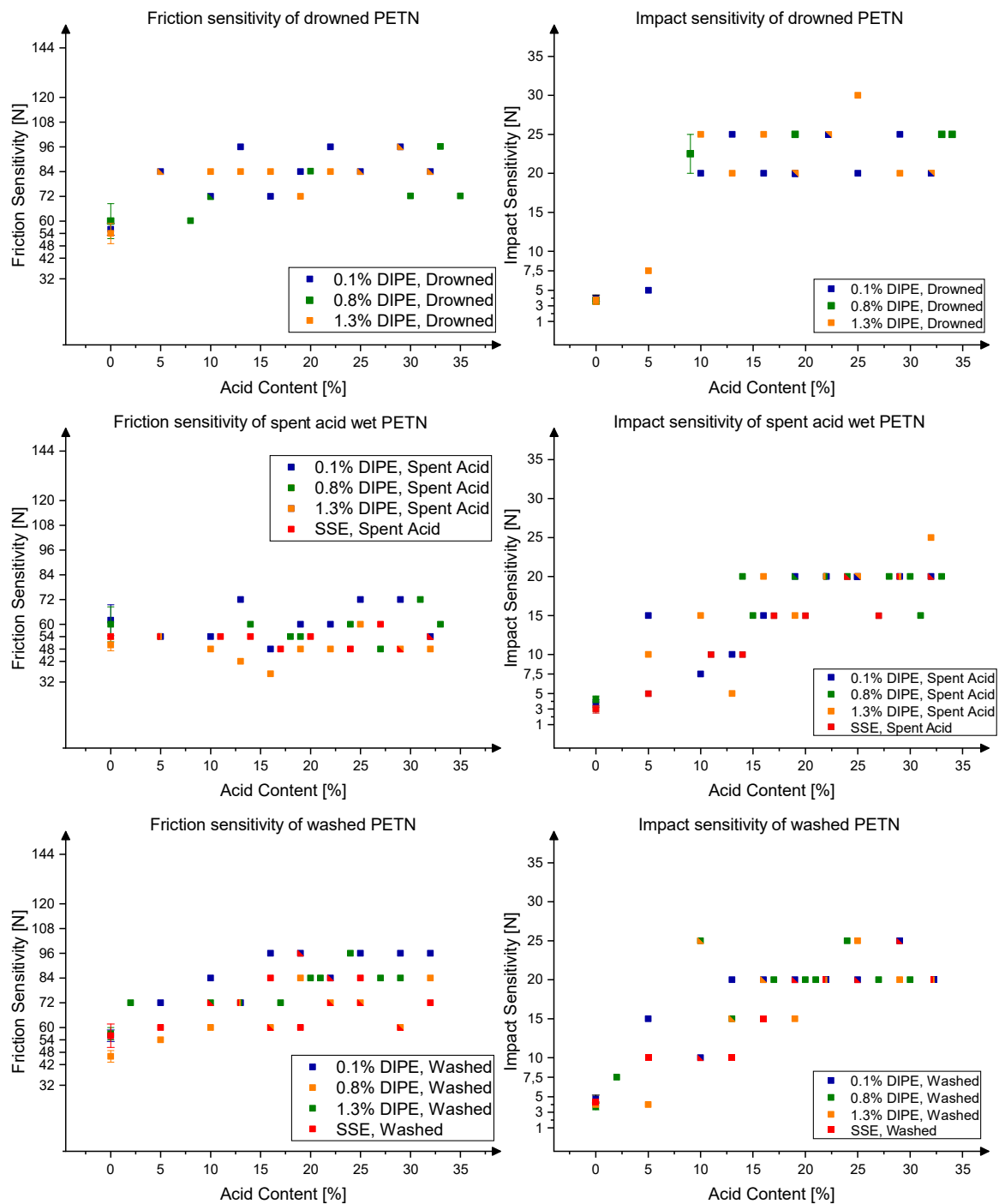
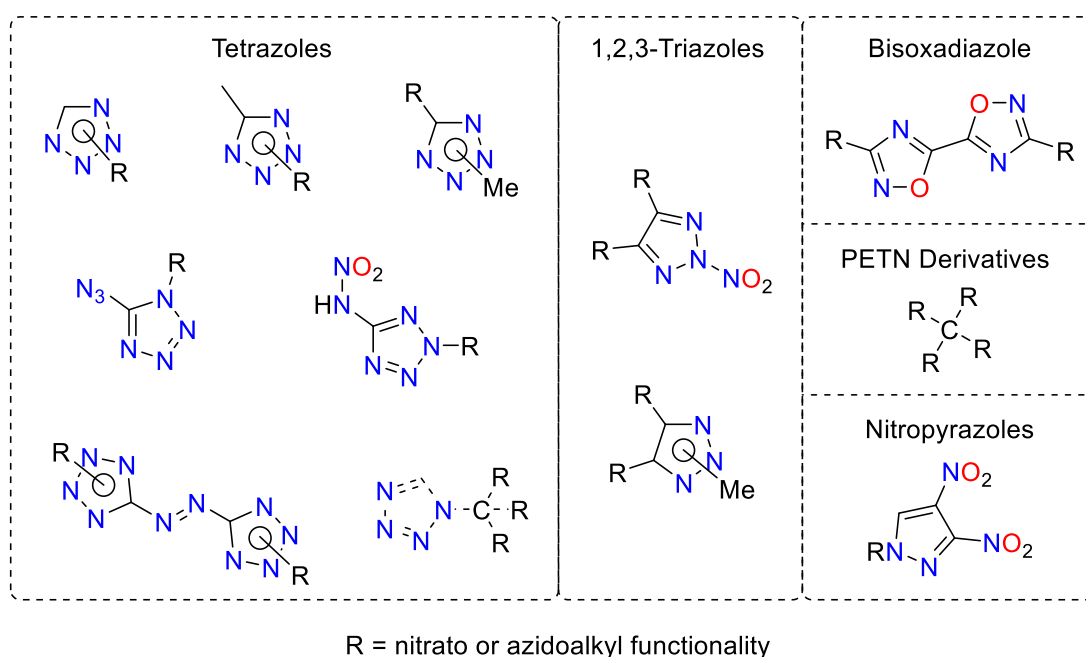


Figure 12 Friction and impact sensitivities of drowned, spent acid wet, and washed samples containing respective liquids in amounts of 0-35 %.

3.2 Nitrate- and Azidoalkyl Containing Energetic Materials

Following the first part of the work, PETN derivatives containing azides, 1*H*-tetrazoles, amines, nitramines, and their salts were prepared. The pentaerythritol building block consists only of hydro-carbon, nevertheless the high content of functional groups can lead to powerful materials. Furthermore, the energetic building blocks of 5*H*-tetrazole, 5-methyltetrazole, 1- or 2-methyltetrazole, 5-azidotetrazole, 5-nitraminetetrazole, 5,5'-azobistetrazole, 2-nitro-1,2,3-triazole, 1 or 2-methyl-1,2,3-triazole, 3-nitropyrazole, 4-nitropyrazole, 3,4-dinitropyrazole, 3,3'-bis-1,2,4-oxadiazole, 3,3'-bis-1,2-oxazole and furazan as well as furoxan based 1,2,4-oxadiazole-polycyclic structures were functionalized with nitrate- or azidoalkyl chains (Scheme 4). Azoles and oxadiazoles show preferable enthalpy of formations (e.g. tetrazole: 200 kJ mol⁻¹). Tetrazoles show mainly inert nitrogen as a reaction product and can be combined with oxidizing nitrate groups for a more even oxygen balance. Triazoles and pyrazoles are best combined with nitro groups, which lowers the enthalpy of formation, but increases the density and oxygen balance. Oxazoles provide oxygen in the ring and combination with oxidizing moieties can further improve the performance.



Scheme 4 Structural motives that are combined with nitrate- and azidoalkyl functionalities.

3.2.1 PETN Derivatives

We initiated the investigation by examining the nitrate- and azidoalkyl functionalities in almost pure form to gain a comprehensive understanding of their impact on the physicochemical properties. We synthesized azide and nitrate derivatives of pentaerythritol with high yields by first performing azide exchange on the corresponding bromo derivatives, followed by nitration using in-situ generated acetyl nitrate. The physicochemical properties were evaluated and compared (Figure 13). Mechanical sensitivities exhibit an increasing trend from PETN to TAPE, with only liquid TAPEMN demonstrating decreased friction sensitivity compared to PETN. The observed sensitivities could be explained through Hirshfeld analysis of the crystal structures. A progressive decrease in the melting point is observed from PETN to TAPEMN, with each azide exchanged causing a decrease of 50-60°C. The thermal stability of the organic nitrates is restricted to 180°C, while the tetraazide exhibits a stability of 218 °C. Possessing a melting point of 82 °C and a detonation velocity of 8092 m s⁻¹, MAPETN stands out as a high-performance melt-cast explosive. However, its high sensitivity relative to TNT makes it unsuitable as a replacement. While the tetraazide exhibits the capability to initiate PETN, its liquid state above 44 °C introduces practical handling challenges. The calculated performance of the azido derivatives falls below that of PETN, primarily attributed to lower densities and oxygen balances. Nevertheless, the investigation highlights the potential of carbon-bonded azides as prospective candidates for new initiating or melt-cast explosives. It is noteworthy, however, that in this scenario, either the thermal or mechanical properties do not meet the required standards for primary or secondary explosives. We have made the hypothesis that the modification of functional side groups, leading to increased hydrogen bonding, would result in an elevation of the melting point and a decrease in sensitivity - therefore solving the issues of the azido compounds above.

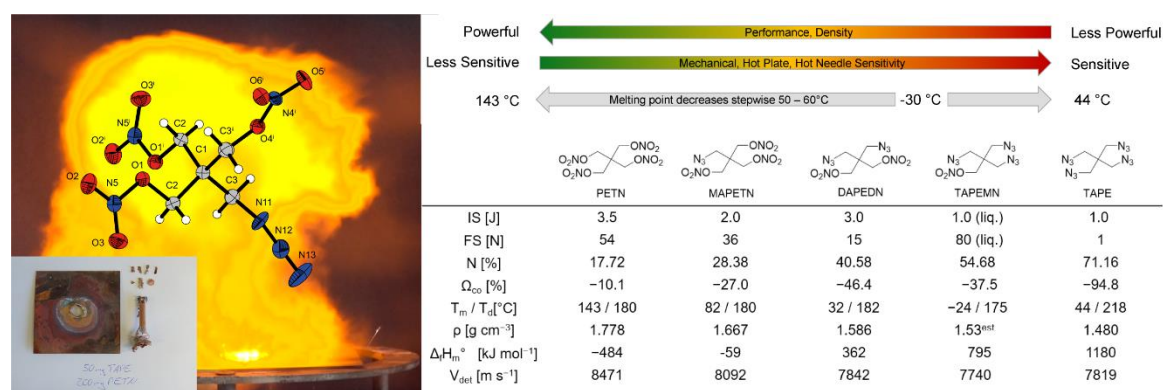
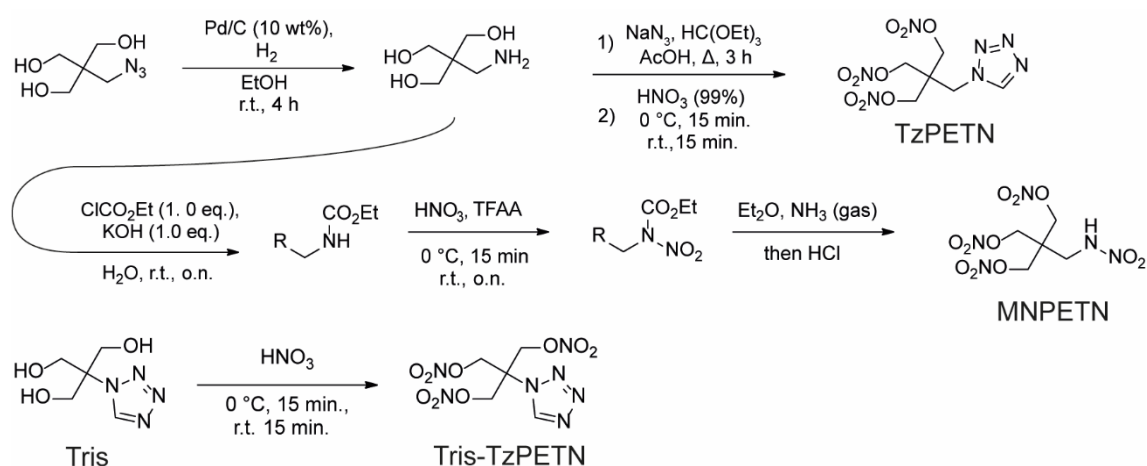


Figure 13 Results of the study about azido derivatives of PETN.

To access amino, 1*H*-tetrazole, and nitramino derivatives a synthesis strategy starting from the azidoalcohol was elaborated. Reduction to the amine made a following tetrazole formation to tetrazolo PETN (TzPETN) possible. To yield mono (MNPETN) and dinitramino PETN (DNPEDN), several steps were necessary including protection of the amine. In advance, the widely used and easily available buffer substance Tris was reacted to the tetrazole and nitrated to Tris-TzPETN in only two steps (Scheme 5).



Scheme 5 Synthesis of TzPETN (top), MNPETN (middle), and Tris-TzPETN (bottom).

The targeted increase of melting points and decrease of sensitivities showed success, yielding melting points ranging from 64 to 126 °C and sensitivities ranging from 2 to 10 J for impact and 80 to 360 N for friction sensitivity (Figure 14). While achieving high performance and oxygen balances close to zero, there is a trade-off in the form of less efficient synthesis procedures and, in some cases, partially reduced decomposition temperatures. Water-insoluble MNPETN exhibits significantly decreased sensitivity while maintaining good thermal stability (ΔT_{m-d} : 116 °C) and performance. Salt formation of the nitramines yielded a strong decrease in thermal stability, whereas sometimes the energetic performance was improved. The tetrazoles exhibit undesirable sensitivity to impact, with Tris-TzPETN being more powerful and less stable than TzPETN, which is, on the other hand, a balanced and otherwise applicable melt-cast material. The findings suggest methyl-bridged nitramine and tetrazoles should be considered for the development of new melt-cast energetic materials. Concluding the investigations on PETN derivatives as melt-cast explosives, we demonstrated the potential of nitrate- and azidoalkyl functionalities to surpass many properties of TNT. The central problem is the mostly high sensitivity, whereby the cause probably lies with the high amount of sensitive functional groups. By only reducing the number of functional groups, less sensitive but uncompetitive

compounds would be obtained. Therefore, we investigated further backbones in the next chapters.

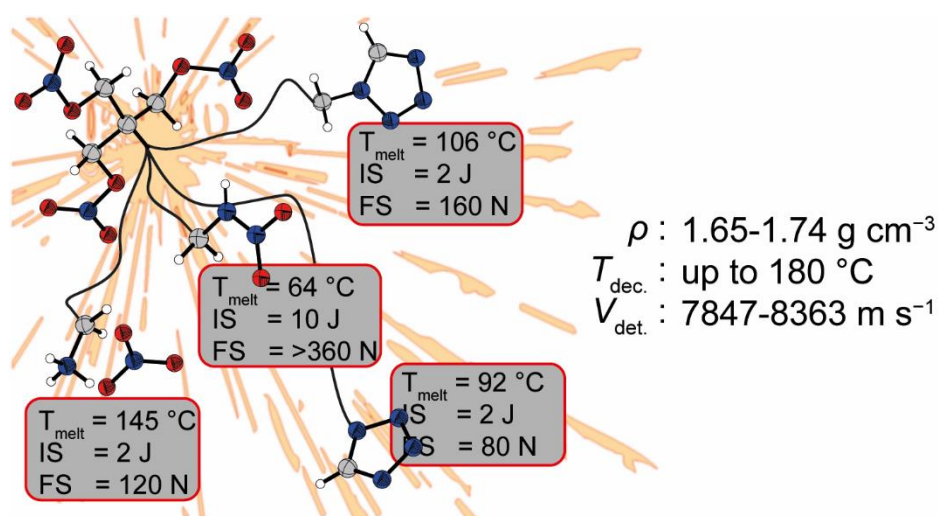


Figure 14 Overview of mono-substituted PETN derivatives and their properties.

3.2.2 Tetrazole Derivatives

The use of tetrazoles already showed promising results when using pentaerythritol as the backbone. In the following studies, we focused on nitrate- and azidoalkylazoles to obtain less sensitive but powerful explosives. Azoles possess a positive enthalpy of formation (e.g. tetrazole: 200 kJ mol⁻¹) and are densely packed.

We started with the combination of the nitrateethyl group and 1*H*-tetrazole (Figure 15). The neat azole was reacted with chloroethanol and nitrated in a second step, yielding the 1-nitrateethyltetrazole (1-NET) and the corresponding *N*2-isomer (2-NET). The 1-isomer was also obtained by cyclization of acetyl-protected aminoethanol followed by nitration. Both isomers were found to be melting at 24-25 °C and are sensitive towards impact but not friction force. Positive heat of formations and densities around 1.55 g cm⁻¹ result in detonation velocities and pressures higher than TNT. Due to the low melting point, the compounds cannot be used in their pure form. However, due to the low steric hindrance on the tetrazole, energetic coordination compounds ECCs could be obtained. The copper, silver, manganese, and zinc metal ions were combined with either oxidizing anions such as dinitramide or sensitizing anions like azide and fulminate.

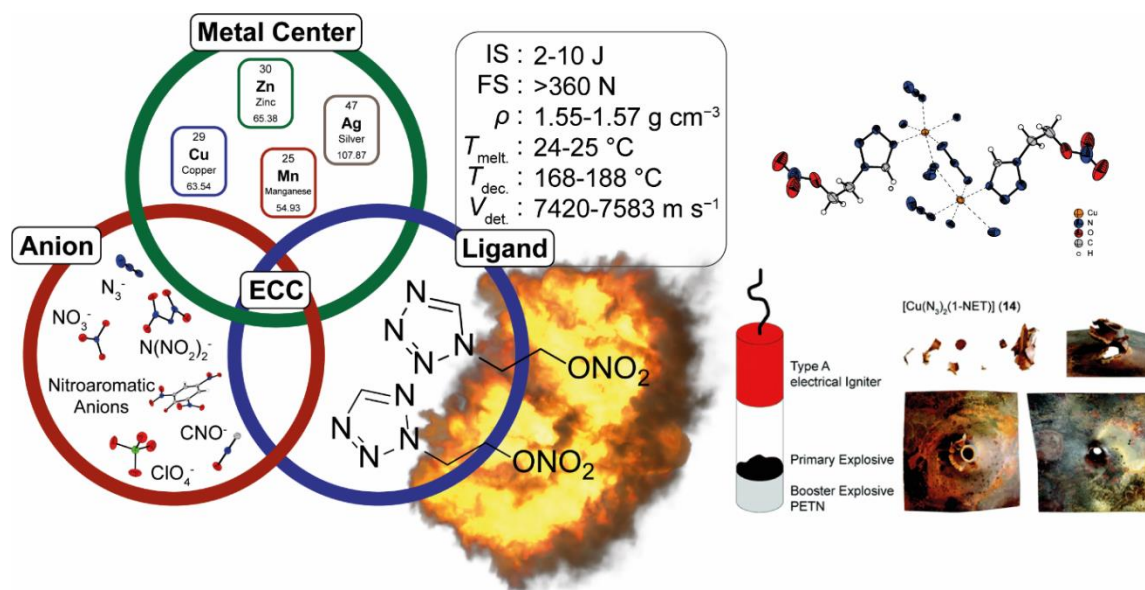
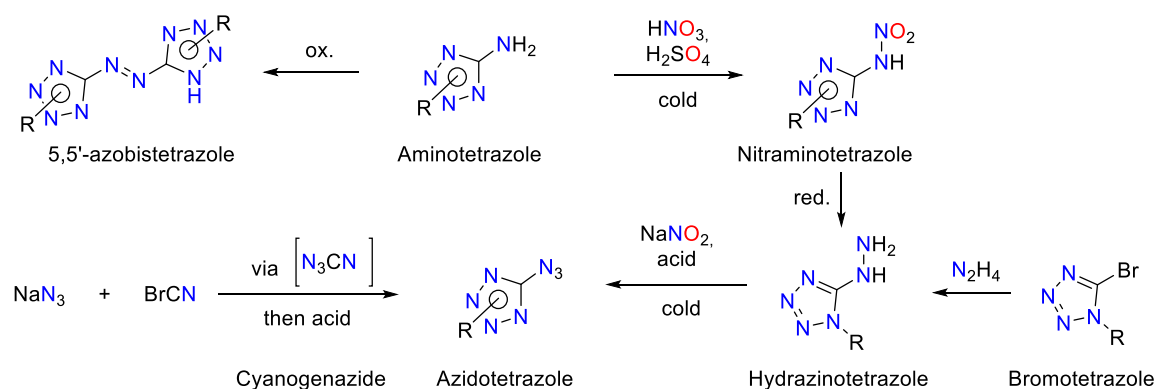


Figure 15 Overview of nitroethyltetrazoles and their corresponding ECCs.

Some decomposition temperatures are higher than that of the neutral compounds, but mostly moderately stable complexes are obtained. The copper azide complex of 1-NET is a primary explosive that can initiate PETN in a detonator setup. If the complex is irradiated by a laser, detonation occurs. Having a nonenergetic proton at the 5-position of tetrazole left space for improvement. Functionalization with further energetic groups was conducted to increase the performance and the melting point. Therefore, the nitrogen-rich azidotetrazole was combined with nitrato- and azidoethyl functionalities. Azidotetrazoles are among the most sensitive structure motifs known and we were curious to know if the sensitivity can be influenced by the alkyl chain. A manageable synthesis route for azidotetrazoles starts from the functionalized 5-hydrazinotetrazoles. Diazotization with the *in situ* generated nitrosyl cation in water leads to the 5-azidotetrazoles within minutes (Scheme 6).



Scheme 6 Synthesis strategies aimed at achieving nitrogen-rich and highly energetic azole backbones.

In this way, 5-azido-1-azidoethyltetrazole (5-A-1-AET) and 5-azido-1-nitratoethyltetrazole (5-A-1-NET) could be synthesized and characterized (Figure 16). 5-A-1-AET was found to be the most sensitive compound of this work although it is a liquid. With a melting point of about $-20\text{ }^{\circ}\text{C}$, the diazide is liquid and was crystallized at low temperatures. The corresponding nitrate solidifies at $45\text{ }^{\circ}\text{C}$ and shows a high but manageable sensitivity. The introduction of the azide at the 5-position of 1-NET resulted in a complete sensitivity shift while the melting point, density, and detonation velocity were remarkably increased. Furthermore, the 1 and 2-methylated azidotetrazoles were synthesized and found to show very high sensitivities and melting points of 20 to $62\text{ }^{\circ}\text{C}$. Alkylation was not able to adjust the sensitivity to a reasonable level and the melting point of the 5-azides was still too low for applicational use, but surprisingly later than for the *1H*-tetrazole. With the oxygen-balanced nitraminotetrazole as the backbone, we expected more hydrogen bonding, resulting in less sensitive, powerful, and low-melting ionic derivatives. As the organic nitrate is thermally not stable enough, we decided to synthesize the well accessible 5-nitramino-2-azidoethyltetrazole through functionalized aminotetrazole and nitration with mixed acid.

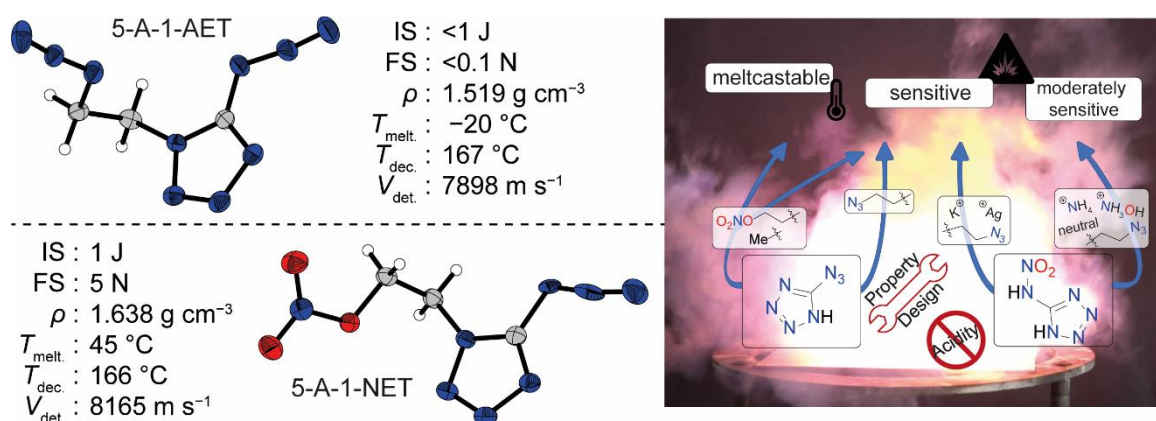


Figure 16 Physicochemical properties of 5-A-1-AET and 5-A-1-NET (left) and scope of the work on azido and nitraminotetrazoles(right).

The neutral compound is not stable, but ionic derivatives show melting points above $100\text{ }^{\circ}\text{C}$. The ammonium salt is moderately sensitive with a performance level of PETN. The thermal stabilities are the weakness of the 5-azido and 5-nitraminotetrazoles of this study. Conjugated π -systems are known to show increased thermal stabilities, and because of the good accessibility of aminotetrazole, we focused on the 5,5'-azobistetrazole backbone in combination with the nitrato and azidoalkyl group (Scheme 6). The alkylated aminotetrazoles were oxidized using *tert*-butyl hypochlorite yielding the azo derivatives. The synthesis is beneficial because of short reaction times and yields of 80% and higher. Both 1-isomers exhibit higher melting points and thermal stabilities. The nitrates are denser and have higher melting but are less stable compared to the azides.

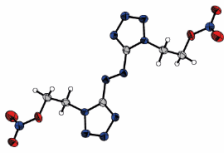
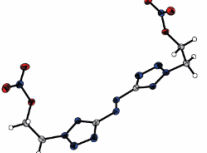
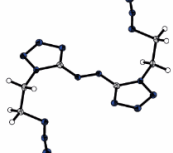
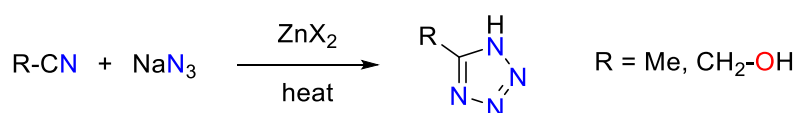
	Azo-1-NET	Azo-2-NET	Azo-1-AET	Azo-2-AET
				
IS [J]	2	< 1	4	< 1
FS [N]	60	20	6	0.2
ESD [J]	0.1	1.5	0.25	0.75
ρ [g cm ⁻³]	1.702	1.676	1.605	1.539
T_{melt}/T_{dec} [°C]	167/179	-/97	147/188	72/140
V_{det} [m s ⁻¹]	8179	8060	8148	7801

Figure 17 Physicochemical properties of nitrate- and azidoalkyl-5,5'-azobistetrazoles.

The sensitivity of all compounds was unexpectedly high with the 2-isomer being more sensitive. With the high nitrogen and energy content of azido, nitramino, or azotetrazoles we were looking into the direction of more and more sensitive and unstable explosives. Therefore, we decided to increase the carbon content to achieve balanced stability at the cost of oxygen balance and detonation performance. As the increasing alkyl character was believed to decrease the melting point, we decided to concentrate on the higher melting and well-accessible organic nitrate compounds.



Scheme 7 Huisgen 1,3-dipolar cycloaddition towards tetrazoles with X representing an halide.

With 5-methyltetrazole we selected a backbone accessible through [2+3] cycloaddition in one step from acetonitrile and azide (Scheme 7). Functionalization with chloroethanol and nitration yielded completely insensitive 5-methyl-1-nitrateethyltetrazole (5-M-1-NET) and the *N*2-isomer 5-M-2-NET. Both are withstanding 190 °C but differ strongly in their melting points with a difference of 130 °C. An unexpected observation was the melting of 5-M-1-NET at 110 °C which is 85 °C higher than the 5*H*-derivative 1-NET at a comparable density. The high carbon contents are leading to weaker oxygen balances and detonation performances, still enough to outperform TNT and insensitive DNAN. To counter the performance issue, we decided to shorten the alkyl chain to obtain 5-methyl-1-nitratomethyltetrazole (5-M-1-NMT) (Figure 18). A higher density, better oxygen balance, and improved detonation performance were achieved at the cost of moderate to high sensitivities and decreased thermal stability. The 2-isomer decomposed upon nitration and was not accessible. This already indicated the lower stability of the *N*-methyl group, which

we expected, as both energetic functionalities are bound to the same methyl-carbon. Furthermore, the tetrazolate or nitrate ions are stable by themselves and could act as leaving groups. To stabilize the nitromethyl functionality, we switched the connection to the heterocycle from *N1* to *C5*. Therefore, we investigated the chemistry of 5-hydroxymethyltetrazole toward nitration. The acidic azole was nitrated yielding the corresponding nitratomethyl carboxylic acid, glycolic acid nitrate, in a controlled decomposition reaction. To stabilize the azole, methylation was performed before the nitration step, leading to 1-methyl-5-nitratomethyltetrazole (1-M-5-NMT) and the corresponding *N2*-isomer (2-M-5-NMT) (Figure 18).

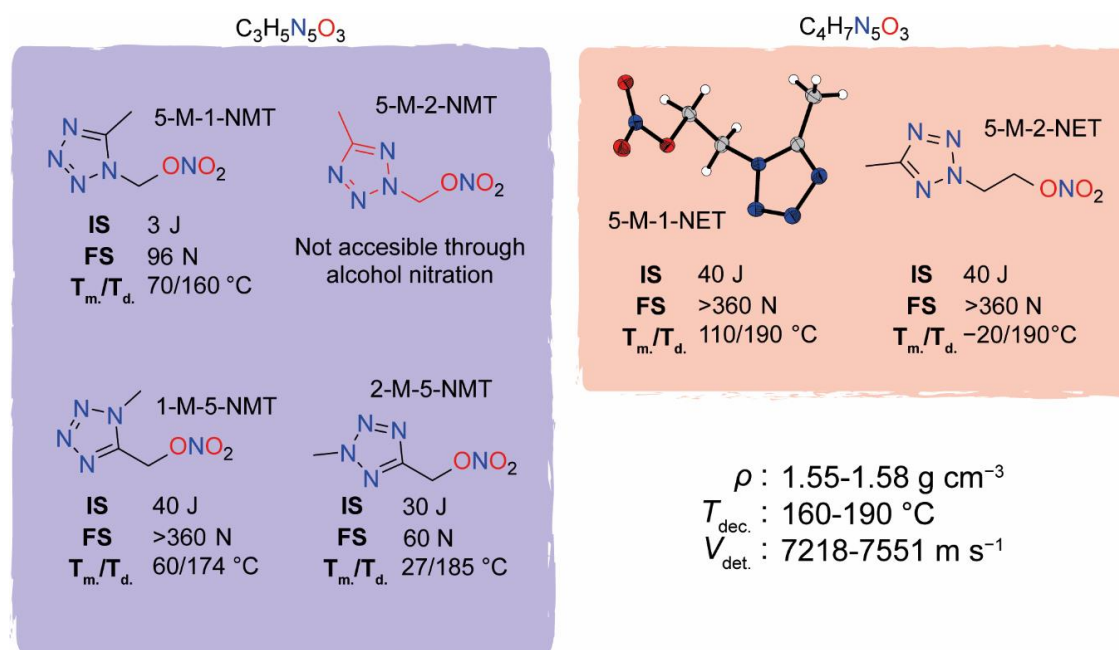


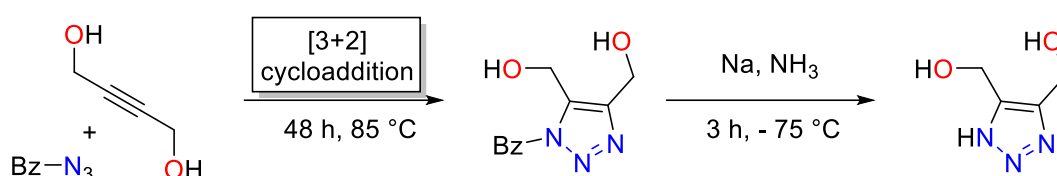
Figure 18 Physicochemical properties of C₃H₅N₅O₃ (left) and C₄H₇N₅O₃ (right) nitratoalkyltetrazole isomers.

Both are thermally more stable than the structural isomer 5-M-1-NMT. 1-M-5-NMT melts at 60 °C and decomposes at 174 °C while being insensitive and more powerful than TNT with 11% higher detonation velocity. The corresponding 2-isomer is moderately impact sensitive but as friction sensitive as PETN, furthermore having a little lower density and a low melting point of 27 °C.

Concluding the results of tetrazole chemistry, the combining of nitrate- or azidoalkyl functionalities with the 5*H*-tetrazole moiety yielded low melting explosives. The introduction of azido, nitramino, or azo functionalities at the 5-position increased the melting points and performance but resulted in unpractical, sensitive materials. The introduction of carbon at the 5-position of tetrazole results in manageable melt-cast explosives, outperforming TNT in terms of sensitivity and performance.

3.2.3 1,2,3-Triazole Derivatives

For the study of 1,2,3-triazoles, the building block 4,5-bishydroxymethyltriazole was synthesized for the first time. Here, the preferable C-linkage of the nitratomethyl group was targeted. A click reaction of protected azide with the alkyne yielded the acidic triazole after reductive deprotection with sodium (Scheme 8).



Scheme 8 Click reaction towards benzyl-protected intermediate followed by reductive deprotection towards 4,5-bishydroxymethyltriazole.

Nitration of this compound yielded the remarkably energetic bisnitratomethyl-2-nitrotriazole (BNMNT), a representative of the rare class of 2-nitro-1,2,3-triazoles. The presence of the N-NO₂ group at the N2 position was confirmed through X-ray diffraction and ¹⁵N NMR. Four additional N2 nitrated triazoles were synthesized for general verification, with two demonstrating high energetic characteristics. BNMNT exhibits a high density (1.764 g cm⁻³), high detonation velocity (8590 m s⁻¹), sensitivities of a primary explosive, and a positive oxygen balance towards CO. The azidomethyl derivatives are also sensitive and show lower densities while maintaining similar stability (Figure 19).

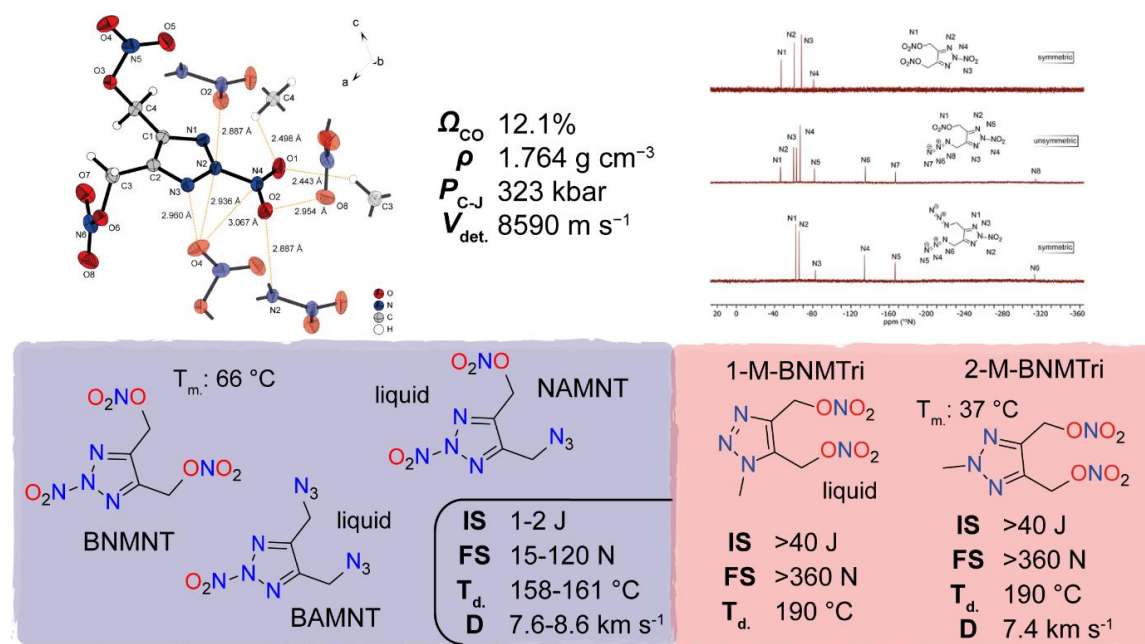


Figure 19 Physicochemical properties of energetic materials derived from 4,5-bishydroxymethyl-1,2,3-triazole.

The combination of alkylated azoles with nitrates and azides showed success for moderate sensitivity and performance, a little higher than TNT. To obtain higher detonation velocities and pressures the density needed to be increased. In the context of practical applications, the short shelf life (months) and high sensitivities are problematic for N-nitro azoles. Therefore, we decided to deactivate the acidic triazole before nitration through methylation. This yielded 1-methyl-4,5-bisnitratomethyl-1,2,3-triazole (1-M-BNMTri) and the corresponding *N*2-isomer (2-methyl-4,5-bisnitratomethyl-1,2,3-triazole (1-M-BNMTri)). Both are thermally stable up to 190 °C and insensitive. The melting point of the symmetric 2-isomer is higher but, with 37 °C, not ideal for applicational purposes. The oxygen balance and detonation parameters are better than that of TNT.

3.2.4 Nitropyrazole Derivatives

We decided to start with well-accessible moderately sensitive nitropyrazoles as the backbone. 3-Nitropyrazole, 4-nitropyrazole, and 3,4-dinitropyrazole were combined with nitrate- or azidomethyl and ethyl functionalities. Azide exchange yielded unexpected and seldomly observed ortho-azido functionalized nitropyrazoles that are very sensitive but scientifically interesting. The investigation concludes that azido compounds possess higher thermal stability and heat of formation in comparison to their nitrate ester counterparts. However, this advantageous feature is accompanied by a trade-off in the form of decreased melting points, resulting in some compounds being liquid at room temperature. The nitrate ester compounds exhibit higher densities, thereby positively impacting their detonation parameters. Noteworthy are the properties of 1-nitratomethyl-3,4-dinitropyrazole (NM-3,4-DNP) and the ethyl derivative (NE-3,4-DNP), among others.

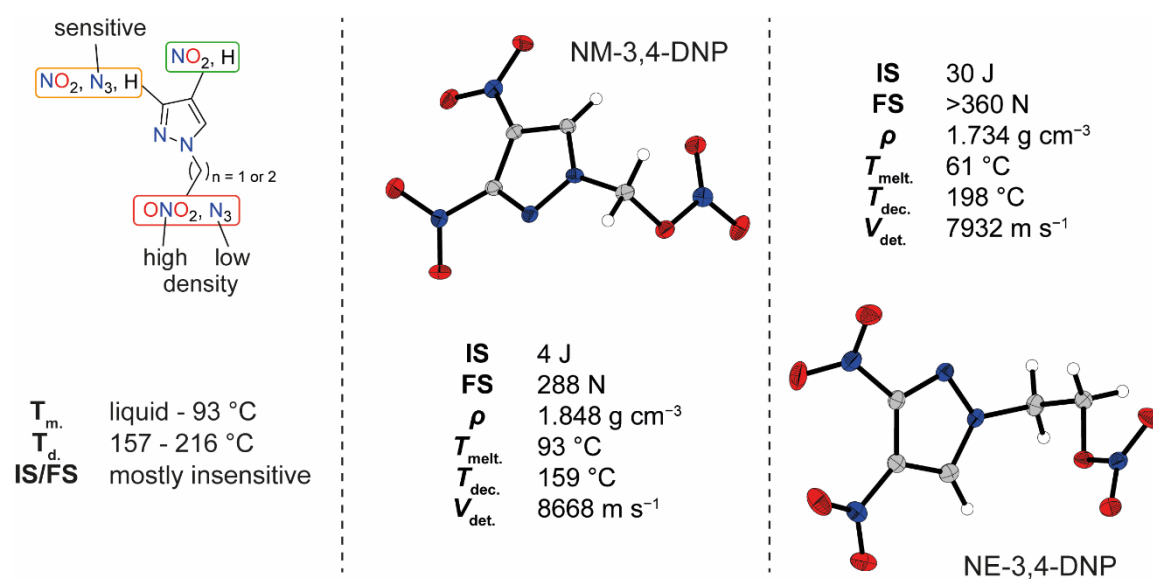


Figure 20 Physicochemical properties of energetic materials derived from nitropyrazoles.

NM-3,4-DNP demonstrates a notable detonation velocity of 8668 m s^{-1} , while NE-3,4-DNP shows preferable thermal characteristics with a melting point of $61 \text{ }^\circ\text{C}$ and a decomposition temperature of $198 \text{ }^\circ\text{C}$ (Figure 20). Furthermore, both compounds exhibit favorable compatibility with HMX and RDX. NM-3,4-DNP surpasses the performance of widely utilized PETN and HMX in the SSRT, suggesting its potential as a highly energetic material.

3.2.5 Polycyclic Derivatives

An alternative approach for achieving high densities, circumventing the utilization of potentially carcinogenic nitroaromatic compounds, involves employing bi- or tricyclic backbones. Oxazole, oxadiazole, furazane, and furoxane-containing backbones were evaluated with C-connected azidomethyl functionalities. The compound 3,3'-bis-azidomethyl-5,5'-bis-1,2,4-oxadiazole, abbreviated as DAMBO, has precisely achieved the ideal melting range for emerging melt-cast explosives (Figure 21).

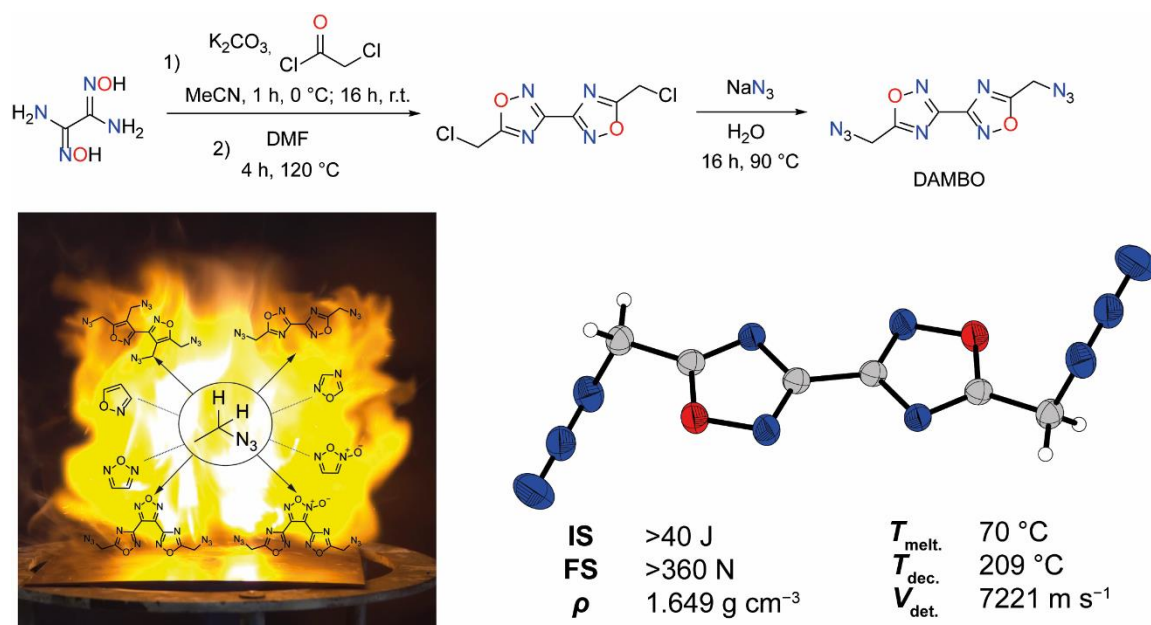


Figure 21 Synthesis and physicochemical properties of 3,3'-bis-azidomethyl-5,5'-bis-1,2,4-oxadiazole (DAMBO).

DAMBO exhibits a melting point of $70 \text{ }^\circ\text{C}$ and undergoes decomposition at $209 \text{ }^\circ\text{C}$, a remarkable $139 \text{ }^\circ\text{C}$ later. Synthesis of DAMBO is conveniently accomplished through a two-step process with excellent yield, starting from diaminoglyoxime, chloroacetyl chloride, and sodium azide. In terms of performance, DAMBO surpasses TNT while maintaining nearly identical crystallographic density. Particularly noteworthy is DAMBO's exceptional insensitivity to both impact and friction, with impact sensitivity exceeding 40 J and friction sensitivity surpassing 360 N .

3.3 Most Promising Energetic Materials

In terms of practical applicability, the most promising compounds from this thesis are as follows:

TNT or DNAN replacements:

1. **5-M-1-NET** (5-methyl-1-nitratoethyltetrazole) is an insensitive material, showing a 6% increased detonation velocity compared to TNT and 16% to DNAN. The synthesis is affordable and leaves space for improvement. With a melting point of 110 °C and a decomposition temperature of 190 °C, melt casting is possible. (work in progress)
2. **NE-3-NP** (nitratoethyl-3-nitropyrazole) is insensitive, performs similarly to TNT and surpasses DNAN by 15% in terms of detonation velocity. Its melting (78 °C) and decomposition (198 °C) points fall within the desired range with a 120 °C difference. The synthesis is straightforward and affordable, but there may be concerns regarding the toxicity of pyrazole. (work in progress)
3. **DAMBO** (3,3'-bis-azidomethyl-5,5'-bis-1,2,4-oxadiazole) is insensitive, shows a 5% increase in detonation velocity compared to TNT and a 16% increase to DNAN. With a 140°C difference between its melting (70 °C) and decomposition (209 °C) points, which is the largest among all the candidates, it can be melted with a higher degree of safety. The synthesis is scalable and straightforward.
4. **MNPETN** (mononitramino pentaerythritol trinitrate) exhibits moderate sensitivity to impact (10 J) and is insensitive to friction (>360 N). It reveals outstanding performance, with a 22% increase in detonation velocity and a 67% increase in detonation pressure when compared to TNT. Its melting point is at 64 °C, and decomposition occurs at 170 °C. The synthesis is more complex and costlier.

Primary explosives:

1. **[Cu(N₃)₂(1-NET)]** (Copper (II) azido 1-nitratoethyl-5*H*-tetrazole) is a possible lead azide replacement. The complex is capable to initiate PETN while maintaining manageable sensitivities (3 J, 1 N, 14 mJ). It can be synthesized affordably, with the only limitation being its early decomposition at 122 °C.
2. **TAPE** (Tetraazido pentaerythritol) is also capable to initiate PETN. A one-step synthesis using commercially available starting materials and a high decomposition temperature of 218°C are significant advantages. However, its applicability is limited due to a low melting point of 44°C.

3.4 Trends

The research covers a total of 58 new energetic materials, categorized into three groups: 30 compounds containing nitratealkyl functionalities, 22 compounds azidoalkyl functionalities, and 4 compounds that possess both functionalities.

12 Pairs of analogous compounds, containing either a nitratealkyl group or an azidoalkyl group were evaluated. As expected, the heat of formation of the azides was notably higher in comparison to the nitrates, although at the cost of a reduced oxygen balance. The density and melting points of the nitrates were detected to be generally higher in all cases. For the density, a mean increase of $0.21 \pm 0.09 \text{ g cm}^{-3}$ was calculated, which does not consistently correlate with the number of functionalities exchanged. Higher oxygen balances, coupled with the density trend, result in significantly elevated detonation pressures ($+6.7 \pm 2.6 \text{ GPa}$) and velocities ($+607 \pm 329 \text{ m s}^{-1}$) for the organic nitrates compared to the azide analogues. When comparing the melting temperatures, a difference of $47 \pm 30 \text{ }^\circ\text{C}$ was observed, with all organic nitrates exhibiting higher melting than the azides. Thermal stability is not consistently predefined by these functionalities, especially in the case of unstable compounds like the 2-nitro-1,2,3-triazoles. Nevertheless the decomposition temperature of all azides was higher than that of the nitrates, with an increase of $18 \pm 14 \text{ }^\circ\text{C}$. A very descriptive and clear example is provided by the complete series of all azidonitrate derivatives of pentaerythritol tetranitrate in chapter 3.2.1 PETN Derivatives.

For the mechanical sensitivities, no clear general trend could be observed. Sensitive nitrates tend to have extremely sensitive azide derivatives (Tetraazido PETN or 1-azidoethyl-5-azidotetrazole) whereas moderately sensitive nitrates can show completely insensitive azido derivatives (3,3'-bis-azidomethyl-5,5'-bis-1,2,4-oxadiazole).

At this point, another crucial observation comes into play. When working with tetrazoles, isomers were often obtained. It was observed that when the structures were more elongated and less bulky, the melting points tended to be lower. For instance, the *N2* isomers of tetrazole mostly melt at lower temperatures than the corresponding *N1* isomers (for 5*H*-tetrazoles, 5,5'-azobistetrazoles, 5-methyltetrazole, 5-nitratomethyltetrazoles). Surprisingly, an elongation of the alkyl chain, from methyl to ethyl, and subsequent increase in degrees of freedom did not always result in a decrease in the melting point, emphasizing the difficulty of melting point predictions based on empirical observations.

4 Literature

- [1] T. M. Klapötke, *Chemistry of High-Energy Materials* 6th edn. De Gruyter, Berlin/Boston **2022**.
- [2] R. Matyáš; J. Pachman, *Primary Explosives*. Springer Berlin, Heidelberg **2013**.
- [3] J. R. Stroud; D. L. Ornellas, *Flying-plate detonator using a high-density high explosive*, US4788913A, US Energy, **1988**.
- [4] Y. Cai; F. P. Zhao; Q. An; H. A. Wu; W. A. Goddard III; S. N. Luo, Shock response of single crystal and nanocrystalline pentaerythritol tetranitrate: Implications to hotspot formation in energetic materials. *J. Chem. Phys.* **2013**, *139*, 164704.
- [5] F. P. Bowden; K. Singh, Size Effects in the Initiation and Growth of Explosion. *Nature* **1953**, *172*, 378.
- [6] P. J. Rae; P. M. Dickson, Some Observations About the Drop-weight Explosive Sensitivity Test. *J. dynamic behavior mater.* **2021**, *7*, 414.
- [7] S. N. Bulusu, *Chemistry and Physics of Energetic Materials*. Kluwer Academic Publishers, Dordrecht **1990**.
- [8] P. W. Cooper, *Explosives Engineering*. Wiley-VCH, Weinheim **1996**.
- [9] D. L. Chapman, VI. On the rate of explosion in gases. The London, Edinburgh, and Dublin Philosophical Magazine and Journal of Science **1899**, *47*, 90.
- [10] R. M. J. Köhler, A. Homburg, *Explosivstoffe*. Wiley-VCH, Weinheim **2008**; Vol. 10.
- [11] J. P. Agrawal; R. D. Hodgson, *Organic Chemistry of Explosives*. John Wiley & Sons Ltd., West Sussex **2007**.
- [12] M. A. Cook, *The Science of Industrial Explosives*. IRECO Chemicals, **1974**.
- [13] U. R. Nair; R. Sivabalan; G. M. Gore; M. Geetha; S. N. Asthana; H. Singh, Hexanitrohexaazaisowurtzitane (CL-20) and CL-20-based formulations (review). *Combust., Explos. Shock Waves* **2005**, *41*, 121.
- [14] J. Gartz, *Vom griechischen Feuer zum Dynamit: eine Kulturgeschichte der Explosivstoffe* 1st edn. E. S. Mittler & Sohn, Hamburg-Berlin-Bonn **2007**.
- [15] T. Urbanski, *Chemistry and Technology of Explosives*. Pergamon Press Ltd., Oxford **1984**; Vol. 4.
- [16] P. J. Conroy; C. S. Leveritt; J. K. Hirvonen; J. D. Demaree, *The Role of Nitrogen In Gun Tube Wear And Erosion; US Army Research Laboratory Weapons and Materials Research*. Directorate Aberdeen Proving Ground, MD 21005, **2004**.
- [17] R. M. Doherty, Novel Energetic Materials for Emerging Needs, 9th-IWCP on Novel Energetic Materials and Applications, Lericci (Pisa), Italy, **2003**.
- [18] ECHA, BAuA, Chemicals Substance evaluation of ammonium perchlorate, **2016**, EC No 232-235-1, <https://echa.europa.eu/information-on-chemicals/evaluation/community-rolling-action-plan/corap-table/-/dislist/details/0b0236e1807e9ab1> (05.09.2023).
- [19] I. B. Mishra; T. P. Russell, Thermal stability of ammonium dinitramide. *Thermochim. Acta* **2002**, *384*, 47.
- [20] C. C. Unger; M. Holler; B. Krumm; T. M. Klapötke, Oxygen-Rich Bis(trinitroethyl esters): Suitable Oxidizers as Potential Ammonium Perchlorate Replacements. *Energy Fuels* **2020**, *34*, 16469.
- [21] F. Barato, Review of Alternative Sustainable Fuels for Hybrid Rocket Propulsion. *Aerospace* **2023**, *10*, 643.
- [22] R. Hagel; K. Redecker, Sintox - A New, Non-Toxic Primer Composition by Dynamit Nobel AG. *Propellants, Explos., Pyrotech.* **1986**, *11*, 184.

- [23] S. Kanitkar; D. Haynes; E. M. Sabolsky; B. Chorpeneing, A review of colored light production by pyrotechnic materials. *Propellants, Explos., Pyrotech.* **2023**, n/a, e202300012.
- [24] M. A. S. Laidlaw; G. Filippelli; H. Mielke; B. Gulson; A. S. Ball, Lead exposure at firing ranges—a review. *Environ Health* **2017**, *16*, 34.
- [25] J. W. Fronabarger; M. D. Williams; W. B. Sanborn; J. G. Bragg; D. A. Parrish; M. Bichay, DBX-1 – A Lead Free Replacement for Lead Azide. *Propellants, Explos., Pyrotech.* **2011**, *36*, 541.
- [26] Z. Shunguan; W. Youchen; Z. Wenyi; M. Jingyan, Evaluation of a New Primary Explosive: Nickel Hydrazine Nitrate (NHN) complex. *Propellants, Explos., Pyrotech.* **1997**, *22*, 317.
- [27] L. V. Clark, Diazodinitrophenol, a Detonating Explosive. *Ind. Eng. Chem.* **1933**, *25*, 663.
- [28] J. W. Fronabarger; M. D. Williams; W. B. Sanborn; D. A. Parrish; M. Bichay, KDNP – A Lead Free Replacement for Lead Styphnate. *Propellants, Explos., Pyrotech.* **2011**, *36*, 459.
- [29] V. Purohit; A. K. Basu, Mutagenicity of Nitroaromatic Compounds. *Chem. Res. Toxicol.* **2000**, *13*, 673.
- [30] M. H. H. Wurzenberger; M. Lommel; M. S. Gruhne; N. Szimhardt; J. Stierstorfer, Refinement of Copper(II) Azide with 1-Alkyl-5H-tetrazoles: Adaptable Energetic Complexes. *Angew. Chem. Int. Ed.* **2020**, *59*, 12367.
- [31] T. M. Klapötke, *Energetic Materials Encyclopedia* 2nd edn. De Gruyter, Berlin/Boston **2021**.
- [32] J. P. Agrawal, *High Energy Materials*. Wiley-VCH Verlag GmbH & Co., Weinheim **2010**.
- [33] E. C. Johnson; J. J. Sabatini; D. E. Chavez; R. C. Sausa; E. F. C. Byrd; L. A. Wingard; P. E. Guzmán, Bis(1,2,4-oxadiazole)bis(methylene) Dinitrate: A High-Energy Melt-Castable Explosive and Energetic Propellant Plasticizing Ingredient. *Org. Process Res. Dev.* **2018**, *22*, 736.
- [34] Gov. of Western Australia, Incident Alert, *Ammonium nitrate emulsion tanker trailer explosion*; East Perth WA, 2022.
- [35] U.S. Chemical Safety Board, *Sierra Chemical Co. High Explosives Accident*; 1998.
- [36] NATO, *STANAG 4489*, **1999**.
- [37] U. N. Recommendations on the Transport of Dangerous Goods – Manual of Tests and Criteria; New York and Geneva, **2019**.
- [38] F. W. Marrs; V. W. Manner; A. C. Burch; J. D. Yeager; G. W. Brown; L. M. Kay; R. T. Buckley; C. M. Anderson-Cook; M. J. Cawkwell, Sources of Variation in Drop-Weight Impact Sensitivity Testing of the Explosive Pentaerythritol Tetranitrate. *Ind. Eng. Chem. Res.* **2021**, *60*, 5024.
- [39] NATO, *STANAG 4487*, **2009**.
- [40] "Oecd" Test No. 471: *Bacterial Reverse Mutation Test*, **2020**.
- [41] T. M. Klapötke; R. Scharf; J. Stierstorfer; C. C. Unger, Toxicity Assessment of Energetic Materials by Using the Luminescent Bacteria Inhibition Test. *Propellants, Explos., Pyrotech.* **2021**, *46*, 114.
- [42] M. Suceška; M. Dobrićević; V. Bohanek; B. Stimac, Estimation of Explosive Energy Output by EXPLO5 Thermochemical Code. *Z. Anorg. Allg. Chem.* **2021**, *647*, 231.
- [43] D. Mc Lachlan; R. J. Marcus, The statistical-mechanical basis of Trouton's rule. *J. Chem. Educ.* **1957**, *34*, 460.
- [44] H. D. B. Jenkins, *Chemical Thermodynamics at a Glance*. Wiley-VCH, **2008**.
- [45] N. Fischer; D. Fischer; T. M. Klapötke; D. G. Piercey; J. Stierstorfer, Pushing the limits of energetic materials – the synthesis and characterization of dihydroxylammonium 5,5'-bistetrazole-1,1'-diolate. *J. Mater. Chem.* **2012**, *22*, 20418.
- [46] T. M. Klapötke; S. Cudziło; W. A. Trzciński, An Answer to the Question about the Energetic Performance of TKX-50. *Propellants, Explos., Pyrotech.* **2022**, *47*, e202100358.
- [47] P. A. Persson, Fuse, US3590739A, **1971**.

- [48] M. Benz; A. Delage; T. M. Klapötke; M. Kofen; J. Stierstorfer, A rocky road toward a suitable TNT replacement – A closer look at three promising azoles. *Propellants, Explos., Pyrotech.* **2023**, *48*, e202300042.
- [49] B. S. Levine; E. M. Furedi; D. E. Gordon; J. J. Barkley; P. M. Lish, Toxic Interactions of the Munitions Compounds TNT and RDX in F344 Rats¹². *Toxicol. Sci.* **1990**, *15*, 373.
- [50] S. W. Maloney; V. M. Boddu; K. K. Phull; O. J. Hao, *TNT Redwater Treatment by Wet Air Oxidation*; Army Corps of Engineering: Champaign, IL, USA, **1994**.
- [51] L. C. B. Crouse; M. W. Michie; M. J. Major; R. B. M.S.; Lee; H. I. Paulus, *Subchronic Oral Toxicity of RDX in Rats*; U.S. Army Center for Health Promotion and Preventive Medicine; Aberdeen Proving Ground: Aberdeen, MD, USA, **2006**.
- [52] T. Blessinger; L. D'amico; R. Subramaniam; C. Brinkerhoff, *Toxicological Review of RDX*; U.S. Environmental Protection Agency: Washington, DC, USA, 2018.
- [53] V. A. Ostrovskii; R. E. Trifonov; E. A. Popova, Medicinal chemistry of tetrazoles. *Russ Chem Bull* **2012**, *61*, 768.
- [54] P. B. Mohite; V. H. Bhaskar, In vitro evaluation of tetrazoles as a novel class of Antimycobacterium tuberculosis agents. *Adv Pharm Bull* **2012**, *2*, 31.
- [55] E. A. Popova; R. E. Trifonov; V. A. Ostrovskii, Tetrazoles for biomedicine. *Russ. Chem. Rev.* **2019**, *88*, 644.
- [56] V. H. Adams; M. A. Bazar; E. N. Reinke; A. R. Buckalew; W. S. Eck, In vitro and in vivo effects of 5-aminotetrazole (5-AT), an energetic compound. *Regul Toxicol Pharmacol* **2020**, *111*, 104573.
- [57] <https://www.nobelprize.org/prizes/medicine/1998/press-release> (13.09.2023)
- [58] L. Morbidelli; B. Bonavida, *Therapeutic Application of Nitric Oxide in Cancer and Inflammatory Disorders*. Academic Press, **2019**.
- [59] J. R. Bucher; J. Huff; J. K. Haseman; S. L. Eustis; H. S. Lilja; A. S. Murthy, No evidence of toxicity or carcinogenicity of pentaerythritol tetranitrate given in the diet to F344 rats and B6C3F1 mice for up to two years. *J Appl Toxicol* **1990**, *10*, 353.
- [60] U.S. Department of Health and Human Services, *Toxicology and carcinogenesis studies of pentaerythritol tetranitrate with 80% D-lactose monohydrate (PETN, NF) in F344/N rats and B6C3F1 mice (feed studies)*. (NTP TR 365). Research Triangle Park; Public Health Service; National Institutes of Health, **1989**.
- [61] D. D. Petersen; J. Swartout, *Provisional Peer-Reviewed Toxicity Values for Pentaerythritol Tetranitrate (PETN)*. U.S. Environmental Protection Agency; **2021**.
- [62] C. Zhang; C. Sun; B. Hu; C. Yu; M. Lu, Synthesis and characterization of the pentazolate anion *cyclo-N₅⁻* in (N₅)₆(H₃O)₃(NH₄)₄Cl. *Science* **2017**, *355*, 374.
- [63] T. M. Klapötke; M. Stein; J. Stierstorfer, Salts of 1H-Tetrazole – Synthesis, Characterization and Properties. *Z. Anorg. Allg. Chem.* **2008**, *634*, 1711.
- [64] R. Goddard; O. Heinemann; C. Kruger, [alpha]-1H-1,2,3,4-Tetrazole. *Acta Cryst.* **1997**, *C53*, 590.
- [65] W. S. Mcewan; M. W. Rigg, The Heats of Combustion of Compounds Containing the Tetrazole Ring. *J. Am. Chem. Soc.* **1951**, *73*, 4725.
- [66] J. S. Mihina; R. M. Herbst, The Reactio of Nitriles with Hydrazoic Acid: Synthesis of Monosubstituted Tetrazoles. *J. Org. Chem.* **1950**, *15*, 1082.
- [67] F. D. Marsh, Cyanogen azide. *J. Org. Chem.* **1972**, *37*, 2966.
- [68] G. H. Hakimalahi; H. Sharghi; H. Zarrinmayeh; A. Khalafi-Nezhad, The Synthesis and Application of Novel Nitrating and Nitrosating Agents. *HCA* **1984**, *67*, 906.

- [69] E. Berlow; R. H. Barth; J. E. Snow, *The Pentaerythritols*. Reinhold Publishing Corporation, New York **1958**.
- [70] P. E. Luebcke; P. M. Dickson; J. E. Field, Deflagration-to-detonation transition in granular pentaerythritol tetranitrate. *J. Appl. Phys.* **1996**, *79*, 3499.
- [71] P. Schulze; I. Lopez-Pulliam; E. Heatwole; T. Feagin; G. Parker, The deflagration-to-detonation transition (DDT) in high density pentaerythritol tetranitrate (PETN). *AIP Conf. Proc.* **2020**, 2272.
- [72] D. C. Claessen, *Verfahren zur Herstellung von Zündsätzen für Sprengkapseln*, DE370574C, **1913**.
- [73] H. U. Rehman, *Water-in-oil explosive emulsion composition*, NOF Corp., US4664729, **1987**.
- [74] H. H. Fassnacht; E. Wuesthoff, *Ammoniumnitratsprengstoff*, EIDP Inc., DE1130342, **1962**.
- [75] C. D. Forrest, *Superfine PETN thin layer slurry explosive*, Teledyne Mccormick Selph, US4012246A, **1979**.
- [76] As sold by Austin Powder company.
- [77] B. T. Fedoroff; O. E. Sheffield, *Encyclopedia of explosives and related items* Vol. 4. US Dept of the Army Picatinny Arsenal United States of America, Springfield **1969**.
- [78] Explosia Special application explosives - Semtex; **2020**.
- [79] R. S. Gow, The Manufacture and Properties of Pentaerythritol Tetranitrate (PETN); ICI Research Brochure No.46: Research Department, Nobel Division, Stevenson, **1955**.
- [80] I. Rodger; J. D. Mcirvine, The decomposition of spent PETN nitration acids. *Can. J. Chem. Eng.* **1963**, *41*, 87.
- [81] M. Van der Merwe, F. C. Fouche, M. von Abo, PETN Stability Study The 17th International Annual Conference of Analysis of Propellants and Explosives **1986**.
- [82] M. F. Foltz Aging of Pentaerythritol tetranitrate (PETN); Lawrence Livermore National Laboratory: **2009**.
- [83] D. M. Chambers Perspectives on PETN Decomposition; Lawrence Livermore National Laboratory: Livermore, **2002**.
- [84] R. S. Gow, The Manufacture and Properties of Pentaerythritol Tetranitrate (PETN); ICI Research Brochure No.46: Research Department, Nobel Division, Stevenson, **1955**.
- [85] G. W. Brown; M. M. Sandstrom; D. N. Preston; C. J. Pollard; K. F. Warner; D. N. Sorensen; D. L. Remmers; J. J. Phillips; T. J. Shelley; J. A. Reyes; P. C. Hsu; J. G. Reynolds, Statistical Analysis of an Inter-Laboratory Comparison of Small-Scale Safety and Thermal Testing of RDX. *Propellants, Explos., Pyrotech.* **2015**, *40*, 221.
- [86] R. M. Doherty; D. S. Watt, Relationship Between RDX Properties and Sensitivity. *Propellants, Explos., Pyrotech.* **2008**, *33*, 4.
- [87] L. K. Peter Lüth Ringversuch mit dem Fallhammer gemäß Abs. 1.6.2 Mechanische Empfindlichkeit (Schlag) der Methode A.14 Explosionsgefahr 2011; BAM Bundesanstalt für Materialforschung und -prüfung: Berlin, **2013**.
- [88] Un/SCETDG/49/Inf.9, **2016**.
- [89] Un/ SCETDG /47/Inf.8, **2015**.
- [90] C. S. Coffey; V. F. De Vost, Impact Testing of Explosives and Propellants. *Propellants Explos. Pyrotech.* **1995**, *20*, 105.
- [91] Jakub Selesovsky; Jiri Pachman; M. Hanus Changes in Sensitiveness of Phlegmatized High Explosives after Artificial Aging, Proceedings of the 21st Seminar on New Trends in Research of Energetic Materials (NTREM), University of Pardubice, Pardubice, Czech **2003**.

- [92] J. E. Balzer; J. E. Field; M. J. Gifford; W. G. Proud; S. M. Walley, High-speed photographic study of the drop-weight impact response of ultrafine and conventional PETN and RDX. *Combust. Flame* **2002**, *130*, 298.
- [93] X. Song; Y. Wang; C. An, Thermochemical properties of nanometer CL-20 and PETN fabricated using a mechanical milling method. *AIP Advances* **2018**, *8*, 065009.
- [94] J. T. Tisdale; L. G. Hill; A. L. Duque, Production of desensitized, ultrafine PETN powder. *Powder Technol.* **2022**, *396*, 152.
- [95] N. Lease; L. Kay; D. E. Chavez; D. Robbins; V. W. Manner, Increased handling sensitivity of molten erythritol tetranitrate (ETN). *J. Hazard. Mater.* **2019**, *367*, 546.
- [96] G. Zhang; B. L. Weeks, A Device for Testing Thermal Impact Sensitivity of High Explosives. *Propellants Explos. Pyrotech.* **2010**, *35*, 440.

5 Appendix

The appendix section presents the most important publications, complete with the corresponding supporting information. The arrangement corresponds to the sequence in which they are discussed in the summary and conclusion. Additionally, a Curriculum Vitae, and a comprehensive bibliography have been appended.

Impact and Friction Sensitivities of PETN: I. Sensitivities of the Pure and Wetted Material

Thomas M. Klapötke,^{*,[a]} Guillaume Lemarchand,^[b] Tobias Lenz,^{*,[a]} Moritz Mühlemann,^[b] Jörg Stierstorfer,^[a] and Ralf Weber^[c]

Dedicated in Memoriam to Prof. Dr. Peter Elsner

Abstract: Pentaerythritol tetranitrate (PETN) is a sensitive and brisant explosive. PETN is transported wetted (25%) with water to limit its impact and friction sensitivities. Literature on its sensitivities in function of its water content is controversial as the measurements were performed by several operators and laboratories rendering difficult to compare the values. Literature studies of mechanical sensitivity methods show the weaknesses and problems of mechanical measurements. Indeed, it is important to analyze a

sample with standardized machines and by a single operator. During this work, pure PETN samples with water contents of 0 to 35% were prepared and the water content was measured by Karl-Fischer titration. The sensitivities were analyzed by the "BAM Fallhammer" and the "BAM Friction Apparatus". The resulting trends were analyzed and discussed with regard to their meaning for handling safety. The study should help to better assess dangers when working with wet PETN (10–25%) in order to avoid accidents.

Keywords: PETN · Explosives · Impact Sensitivity · Friction Sensitivity · Testing and Assessment

1 Introduction

1.1 About Pentaerythritol Tetranitrate

The Tetranitrate of pentaerythritol, PETN, is a versatile explosive used in boosters, detonating cords, detonators etc. [1–3] Industrial PETN large-scale manufacturing has a long tradition reaching back to the 1930's, but accidents still occur on plants. After nitration, the nitrate is filtered, washed, neutralized, and mostly recrystallized. [4] In a dry state, an impact sensitivity of 3–4 J and a friction sensitivity of about 60 N renders the material sensitive to very sensitive. [5–6] To ensure safe packing and transportation, traditionally water is added. The sensitivity of dry pentaerythritol tetranitrate is extensively studied, but surprisingly very few data is known on the impact and friction sensitivities of the wetted material. In the ICI research brochure no. 46 by Gow, it is stated that the mechanical sensitivity is gradually decreasing, from 2–3 J to 5–6 J with rising water content, from 0% to 35%. [7] Coffey et al. measured impact sensitivities of PETN with a particle size of 5 µm. At a vacuum dry state (<0.1% water), PETN shows an increased sensitivity of 2 J compared to air dry with 3 ± 0.5 J. [8] More recent data is measured by the UN in the report UN/SCETDG/47/INF.8. The Spanish experts show that a water content of 9% decreases the sensitivities to 25 J and 80 N. [9] In the following report UN/SCETDG/49/INF.9 the German experts discovered an inhomogeneous distribution of water in the delivered samples. Homogenized samples were measured dry, 4 J and 54 N, with 9% water, 25 J and 60 N, and 15.2%

water, 25 J and 72 N. [10] A large decrease in impact sensitivity besides a rather small decrease in friction sensitivity is observed. From a purely economic point of view, the lowest possible water content is beneficial, whereas insensitive material is preferable for safe handling and transportation. A complete set of data is necessary so that the appropriate water content can be selected for each application and the danger can be better assessed (Figure 1).

In this study, the influence of water on the mechanical sensitivity of pure PETN is investigated. The difference between pure and industrial PETN is the presence of small

[a] T. M. Klapötke, T. Lenz, J. Stierstorfer
Energetic Materials Research, Department of Chemistry, University of Munich (LMU), Butenandtstr. 5–13, München, D-81377, Germany

*e-mail: tmk@cup.uni-muenchen.de
tolech@cup.uni-muenchen.de

[b] G. Lemarchand, M. Mühlemann
BIAZZI SA, Chemin de la Tavallaz 25, 1816 Chailly/Montreux, Switzerland

[c] R. Weber
Austin Powder Technology GmbH
Zum Elberskamp 24, 57413 Finnentrop, Germany

Supporting information for this article is available on the WWW under <https://doi.org/10.1002/prop.202200150>

© 2022 The Authors. Propellants, Explosives, Pyrotechnics published by Wiley-VCH GmbH. This is an open access article under the terms of the Creative Commons Attribution License, which permits use, distribution and reproduction in any medium, provided the original work is properly cited.



Figure 1. The importance of mechanical sensitivity.

amounts of Dipentaerythritol hexanitrate (DPEHN) in the industrial PETN. A study on the properties of industrial PETN is ongoing.

1.2 Assessment of Impact Sensitivities

The traditional method to detect a reaction towards a mechanical stimulus is the determination of the impact sensitivity (Figure 2). When enough impact energy or more accurate plastic deformation is applied on a sample, ignition can occur [11]. The ignition sites are called hotspots and are caused through adiabatic shear bands and gas compression [12–14]. For PETN the initiation through hotspots is believed to happen at 400 to 500 °C [15].

The “ERL Type 12 Drop Weight Impact Sensitivity Apparatus” [16] and the “BAM Fallhammer” [17] are two widely used and established instruments. The ERL machine has a plane anvil on which the sample is hit by a striker sitting above it. The energy on the striker is generated by a 2.5 kg weight. In contrast, the BAM apparatus uses a sample holder that confines the sample and is exchanged every measurement. A 1 kg, 5 kg, or 10 kg weight from a certain height (1–40 cm) delivers an energy of 1–40 J on the sample.



Figure 2. Friction and impact test apparatus used in this work.

Single test results are “no reaction”, “decomposition” or “explosion” and those are assigned to the result “positive” or “negative” depending on the procedure.

At the end of a test series an energy is determined at which a certain probability of a positive result is given. Typically, an E50, 50% probability, value is determined on the ERL device, usually with the Bruerton or Neyer D method [18–19]. The detection is often performed with the help of measuring instruments (microphone etc.). In every case strict criteria should be defined before the experiment and one should be aware of possible pitfalls when using technical help [20]. The BAM device can be used for E50 values but more common are “one out of six” measurements. The one out of six method means that at least one positive result occurs in six trials at certain energy, but six negative results are obtained with lower energy. Therefore, the lower detonation limit is detected, which is different and not directly comparable to the 50% probability value. The detonation is usually detected by the operator which is possible because the sample is confined and the positive result is usually audible [17].

The Fallhammer method comes with some general drawbacks. Depending on the apparatus and its wear, different energies than the theoretically calculated are delivered into the sample. Energy is lost due to elastic deformation or friction of the apparatus [8]. Several studies were performed to compare sensitivity results of different institutions. With uniform test regulations and identical samples, large deviations between different laboratories are observed. This is the case for both BAM and ERL instruments [21–23]. An intense study by Marrs et al. shows that Fallhammer experiments with PETN are reproducible over decades at the same institute, with some deviation. Furthermore, it becomes clear that PETN is excellently suited to evaluate experiments acoustically [24]. There are some materials (e.g. thallium azide) where it is difficult to detect the actual sensitive character via this method [25]. All studies attribute deviations to the operator, protocol, or environment. It can be concluded that the comparison of data between laboratories should be done with care.

1.3 Assessment of Friction Sensitivities

The friction sensitivity testing is the second most used mechanical sensitivity test (Figure 2). Over time the “BAM friction apparatus” [17] has become established, but friction tests with an impact component such as the Ball Drop Impact Test [26] are also known. The friction measurement in combination with the impact test gives a good overview of the mechanical sensitivity of a material. The BAM apparatus consists of a fixed porcelain peg and a moving porcelain plate. The plate is moved one centimeter forth and then returns to the starting position. The peg is part of a one-sided lever and the force is generated by nine different weights that can be fixed in six notches on the lever. Thus 0.5 to

360 N force can act on the specimen. Evaluation is similar to the impact test, E50 is determined with STANAG [27], one out of ten with LLNL [28–29] and one out of six with the UN procedure [17]. Drawbacks are comparable to those of the impact method. The porcelain surfaces and the operation of the apparatus are major uncertainty factors.

2 Experimental Section

2.1 Sample Specification

A sample of pure PETN delivered from the “Fraunhofer ICT” was used for this study. The purity was determined by elemental analysis, IR spectroscopy and ^1H , ^{13}C and ^{14}N NMR. Thermal properties were determined by differential thermal analysis (DTA) and differential scanning calorimetry (DSC) (Supporting Information). The DSC measurements show that no change in the melting or decomposition point is observed due to wetting.

The morphology of the dry sample was analyzed by scanning electron microscopy (SEM) and optical microscopy. The particle size distribution was analyzed using sieves with a mesh size of 100, 300, 500, 600, and 1000 micrometers.

Analysis of pentaerythritol tetranitrate: DTA (5°C min^{-1} , onset): 143°C (melt.); Sensitivities: BAM Fallhammer: 3.5 J, friction tester: 54 N; IR (ATR) $\tilde{\nu}$ (cm^{-1}) = 2986 (w), 2904 (w), 1638 (s), 1630 (s), 1473 (m), 1396 (w), 1305 (m), 1283 (s), 1266 (s), 1036 (m), 998 (s), 939 (m), 833 (s), 752 (s), 701 (s), 619 (s), 458 (m); Elem. Anal. ($\text{C}_5\text{H}_8\text{N}_4\text{O}_{12}$, $316.15 \text{ g mol}^{-1}$)

calcd.: C 19.00, H 2.55, N 17.72%. Found: C 19.01, H 2.28, N 17.47%; ^1H NMR (DMSO- D_6 , 400 MHz, ppm) $\delta = 4.70$ (s, 8H); ^{13}C NMR (DMSO- D_6 , 101 MHz, ppm) $\delta = 70.3, 40.8$; ^{14}N NMR (DMSO- D_6 , 29 MHz, ppm) $\delta = -45$.

The morphology and particle size distribution are shown in Figure 3. The nitrate ester crystallizes in elongated blocks that are partly grown together. The crystal surface is smooth and the edges are sharp and not crushed. The mean particle size is at 200 to 400 μm . Particles below 100 and above 600 μm are rare.

2.2 Sample Preparation

About one and a half gram of dry PETN was weight in and wetted to the desired water content. The sample was shaken for two hours with an overhead shaker and additionally mixed with a spatula directly before each measurement. As water is only attached loosely to the crystalline material it evaporates, settles, or attaches to the walls of the vessel. Therefore, the water content was determined by coulometric Karl-Fischer titration with a 899 coulometer and 860 KF Thermoprep oven from Metrohm. [30] Before and after each friction sensitivity measurement a representative sample (ca. 20 mg) was taken. This sample was analysed by the Karl-Fischer device using the oven method. Therefore, water was extracted from the sample oven (80°C) into the cell (nitrogen flow). A sample was considered dry at water content below 0.1%. Table 1 shows the measured water contents after preparation and after a friction sensitivity measurement was performed. The average of three meas-

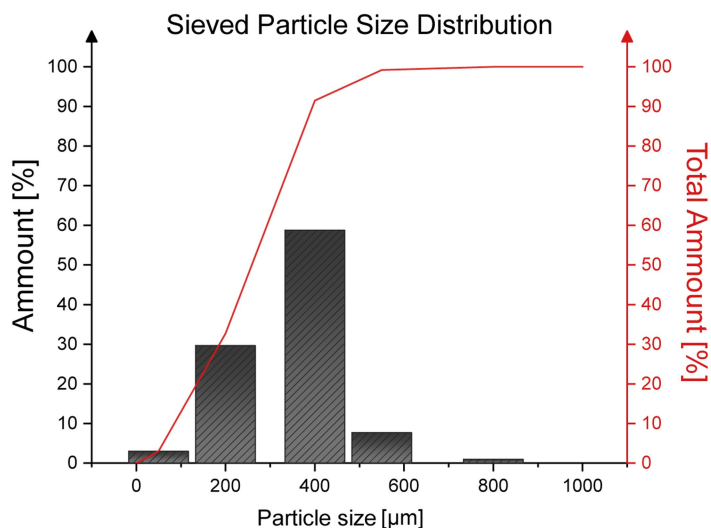
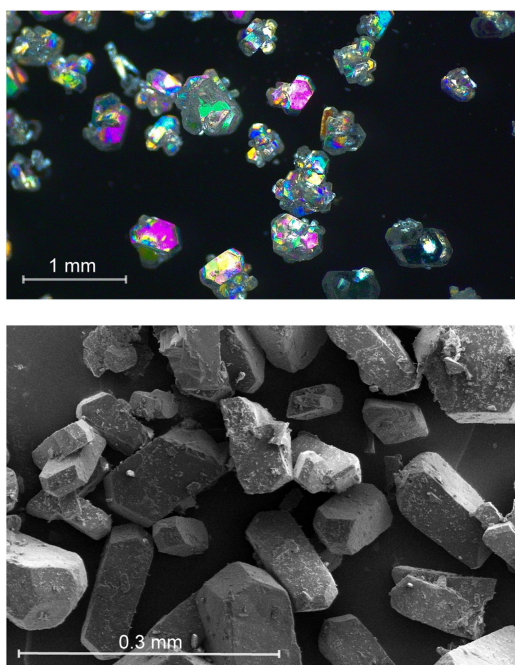


Figure 3. Optical microscop image (top left), SEM image at 350x magnification (bottom left) and particle size distribution (right).

Table 1. Water content as determined by coulometric Karl-Fischer titration. A triple determination with standard deviation is shown.

Water content	Initial [%]	After friction sensitivity determination [%][31]
dry	< 0.1	< 0.1
5 %	4.6 ± 0.1	4.3 ± 0.3
10 %	9.5 ± 0.2	9.4 ± 0.1
15 %	14.7 ± 0.7	13.5 ± 0.7
20 %	19.0 ± 0.7	17.9 ± 0.7
25 %	25.3 ± 0.9	23.1 ± 1.6
30 %	30.3 ± 2.3	26.6 ± 1.9
35 %	36.4 ± 2.3	34.5 ± 0.25

urements was calculated and given with its standard deviation. At 5–20% water the samples taken shows to be drier than initially prepared. This is believed to happen due to evaporation and the separation of water. In contrast at 25% and higher the samples show higher water contents.

At this point, water begins to separate from the PETN and when a sample is taken water attaches to the spatula due to surface tension. The water content generally drops a few percent during sensitivity measurement with a larger deviation at higher contents. (The raw data can be found in the Supporting Information).

2.3 Sensitivity Measurement

The impact sensitivities were determined on a “BAM Fallhammer” by Reichel & Partner. Steel rings and collars are purchased from OZM Research (2020). For 1–5 J the 1 kg weight and for energies above that the 5 kg weight were used. The contact surfaces of the guiding rail and the weight was greased with powdered graphite [32]. The result “explosion” was assigned to a positive test and “decomposition” or “no reaction” was assigned to a negative test. The samples were taken with a cylindrical 40 mm³ measure and tapped directly into the sample holder. The friction sensitivities were measured on a “BAM Friction Apparatus” by Reichel & Partner. Porcelain plates and pegs are purchased from OZM Research (2020). The surface of new (2020) and old plates, which appear much rougher, was compared with the Keyence 3D profilometer VR-5200 [33]. The two plates were scanned and analyzed for their surface heights and profiles (Figure 4). The older plate shows significantly fewer and wider grooves with greater differences in height. Whereas the newer plates consist of many small furrows with less depth. It is believed that this contributes to the sensitivity especially for different particle sizes. Therefore, only the newer 2020 plates were used.

A small amount of sample about 20 to 30 mm³ was taken and put on the porcelain plate underneath the porcelain peg. Due to the adherent nature of the sample, accurate dosing and placement was difficult. This was also due to the fact that fast handling was necessary to prevent the

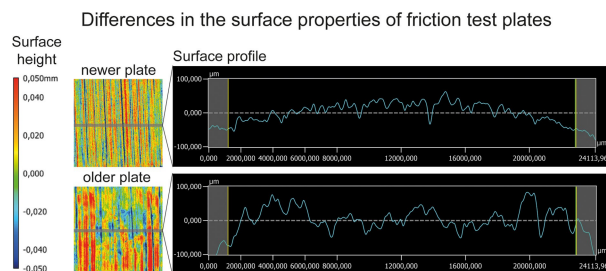


Figure 4. Surface height and profile of BAM friction test plates.

sample from drying out. Three different phenomena were observed which are shown in Figure 5. The sample can be offset from the center of the plate. When the peg is moved down on the sample it distributes differently. (1.) If the sample is in front of the peg, the PETN-water mass forms a slippery film where the peg might slide on. (2.) The sample is placed in the center and a mix of sliding and scratching of the porcelain surfaces is observed. (3.) The sample is placed behind the moving direction of the peg and mostly scratching is observed. It is believed that case (3.) shows the highest and case (1.) the lowest sensitivity. In this work mostly, methods (1.) and (2.) were used. For the determination specifically, the one out of six methods (1 of 6) was selected, as the lower detonation limit is determined. When it comes to safety assessment this value is more reasonable than an E50.

As the accuracy of those measurements is limited, each measurement was done triple and the standard deviations were calculated. The machines (Figure 2) and procedures are described in ST/SG/AC.10/11/Rev.6 (s. 13.4.2.3.3).[17]

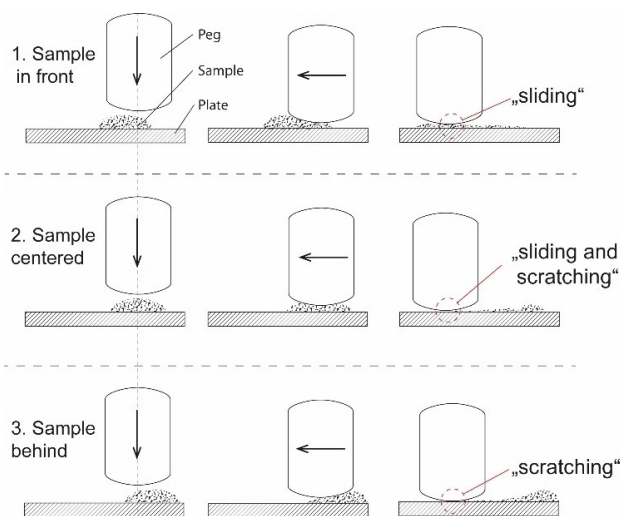


Figure 5. Differences in the way the sample is placed between the porcelain parts within the BAM friction tester.

3 Results and Discussion

The mechanical sensitivities of pure PETN were determined ranging from a dry sample to water contents up to 35%. The measurements were repeated three times and the mean value with standard deviation is given. The red colored triangles indicate literature known measurements on BAM devices. The red line indicates the limiting load for safe transportation according to the United Nations handbook "Transport of Dangerous Goods".

3.1 Impact Sensitivity

The impact sensitivity of the dry sample is at 3.5 ± 0.5 J and therefore similar to the UN measurements (red). The explosion of the dry sample is sharp and clearly audible. Adding water of an amount of 2.5 % is not decreasing the sensitivity remarkably. An energy necessary for explosion of



Figure 6. Fallhammer specimen holder after various tests. Negative tests remain closed (bottom left) positive tests are usually opened through the detonation (bottom right).

4.3 ± 0.5 J is observed. At 5% water, the sensitivity decreases slightly while the deviation increases to 7.5 ± 2.0 J. Wetting to 10% causes a strong decrease in sensitivity with 16.7 ± 2.4 J. For 20% and 25% water content, no explosion is observed below 20 J with a mean sensitivity of 21.7 ± 2.4 J. With a water content of 35%, a sensitivity of 25 J was measured in a single determination. In the regions of lower water contents, an exponential decrease of the sensitivity is observed. From 10% and higher the sensitivity decreases only slightly with the addition of more water. The measurement results of the UN experts show slightly lower sensitivities.

Dry samples or samples wetted up to 5% mainly show complete conversion of the sample when a positive result is detected (Figure 6). The higher the water content, the lower the conversion. With the lower conversion, the noise of the positive result is generally less loud. It is believed, that the desensitizer, in this case water, inhibits propagation. Whereas it is not given that initiation is diminished by the addition of water. It cannot be excluded, that small initiation sites that are not propagating are formed. Furthermore, great care should be taken against drying out or settling of the water when working with wet PETN. In contrast to wax or plastic, water is only loosely attached to PETN and separates over time.

3.2 Friction Sensitivity

The dry sample shows a friction sensitivity of 50 ± 4 N with loud and partly propagating explosions [34]. This is comparable to the results by the UN experts. The water contents in Figure 7 are corrected to the actual water contents after measurement from Table 1. Wetting causes the sensi-

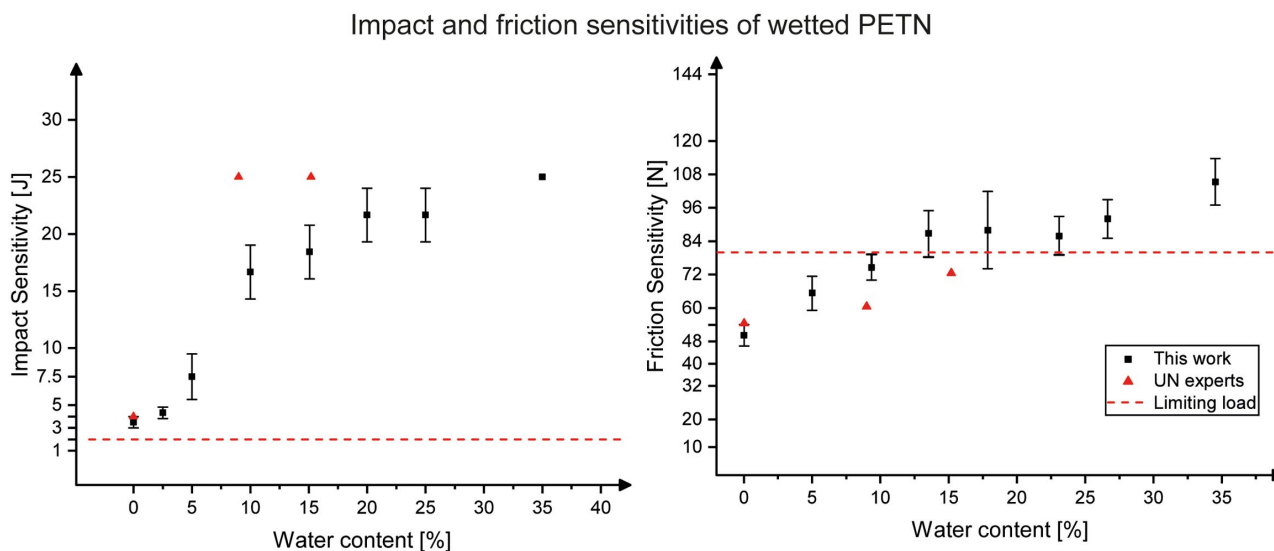


Figure 7. Mechanical sensitivities of wetted PETN ranging from 0 to 35% water. Left: Impact sensitivity, Right: Friction sensitivity.

tivity to drop linear to 87 ± 8 N at 15% water. The sensitivity keeps in this range until 25% water. Up to 35%, a decrease is observed with a sensitivity of 105 ± 8 N. The measurements by the UN experts are slightly more sensitive which can be attributed to different samples (Figure 7 red triangles).

The noise and propagation of the explosion decreases when water is added. This reduction in the intensity of a positive result is not captured by the measurement or evaluation. Often, very quiet crackling can be heard that is barely audible with hearing protection, which makes evaluation difficult. We also believe that mainly propagation is inhibited and initiation is less detected due to the decreasing noise of very small explosions.

4 Conclusion

Impact and friction sensitivity measurements are two well established methods for the determination of mechanical sensitivity. The literature was reviewed carefully showing that good accuracy can only be achieved through high standardization.

PETN with a mean particle size of 200 to 400 μm , crystallized in partly intergrown blocks, was used. The water loss during sensitivity determination was detected by Karl-Fischer titration and found to be in the lower percent area.

The dry sample shows a sensitivity of 3.5 ± 0.5 J and 50 ± 4 N. When wetted the mechanical sensitivity is generally decreased. The impact sensitivity shows an exponential decrease up to 10% water to 7.5 ± 2.0 J. The friction sensitivity is decreasing linear up to 15% and 87 ± 8 N. Between 15 and 25% water content, the mechanical sensitivities stagnate. Up to 35% water, a decrease is observed to 25 J and 105 ± 8 N. The authors believe, like stated before, that desensitization is caused by inhibition of propagation. The initiation can still occur in wet samples.

For the handling, it can be concluded that PETN below 10% water is still sensitive and should be handled as the dry material. Above 15% water, impact forces are of less concern but sensitivity towards friction and shear is still given. Smooth or soft surfaces (Teflon, plastic) and low shear stress are beneficial. Rough surfaces (metal, porcelain) and mixtures with hard particles (sand) should be avoided. Higher water contents (35%) are reducing the sensitivity further but in every case, the material stays sensitive to moderately sensitive.

Wet samples always tend to separate and release water and get therefore dry and sensitive again. Wet PETN delivered in larger containers or bags shows a separation of water due to condensation or settling. The water content represents an average value and lower water contents can be expected at the top layer.

Acknowledgements

For financial support of this work by Ludwig-Maximilian University (LMU), the Office of Naval Research (ONR) under grant no. ONR N00014-19-1-2078 and the Strategic Environmental Research and Development Program (SERDP) under contract no. W912HQ19C0033 are gratefully acknowledged. Open Access funding enabled and organized by Projekt DEAL.

References

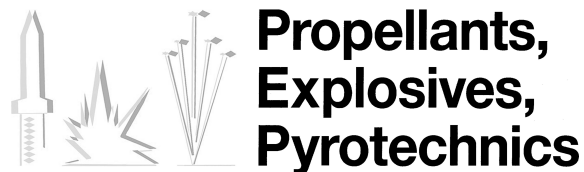
- [1] J. P. Agrawal, *High Energy Materials*. WILEY-VCH Verlag GmbH & Co., Weinheim 2010.
- [2] R. M. J. Köhler, A. Homburg, *Explosivstoffe*. WILEY-VCH Verlag GmbH, Weinheim 2008, Vol. 10.
- [3] T. M. Klapötke, *Chemistry of High-Energy Materials*. Walter de Gruyter GmbH, Berlin/Boston 2019, Vol. 5.
- [4] E. Berlow, R. H. Barth, J. E. Snow, *The Pentaerythritols*. Reinhold Publishing Corporation, New York 1958.
- [5] R. Matyáš, J. Šelešovský, T. Musil, Sensitivity to friction for primary explosives. *J. Hazard. Mater.* 2012, 213–214, 236.
- [6] T. M. Klapötke, *Energetic Materials Encyclopedia*. De Gruyter, 2018, doi:10.1515/9783110442922.
- [7] R. S. Gow *The Manufacture and Properties of Pentaerythritol Tetranitrate (PETN)*; ICI Research Brochure No.46: Research Department, Nobel Division, Stevenson, 1955.
- [8] C. S. Coffey, V. F. De Vost, Impact Testing of Explosives and Propellants. *Propellants Explos. Pyrotech.* 1995, 20, 105.
- [9] United Nations, *Transport of Pentaerythrite Tetranitrate (PETN) with less than 25% of water but more than 9% of water*; UN/SCETDG/47/INF.8, Geneva, 2015.
- [10] United Nations, *Transport of Pentaerythrite Tetranitrate (PETN) with less than 25% of water but more than 9% of water*; UN/SCETDG/49/INF.9, Geneva, 2016.
- [11] S. N. Heavens, J. E. Field., D. Tabor, The ignition of a thin layer of explosive by impact. *Proceedings of the Royal Society of London. A. Mathematical and Physical Sciences* 1974, 338, 77.
- [12] Y. Cai, F. P. Zhao, Q. An, H. A. Wu, W. A. Goddard III, S. N. Luo, Shock response of single crystal and nanocrystalline pentaerythritol tetranitrate: Implications to hotspot formation in energetic materials, *J. Chem. Phys.* 2013, 139, 164704.
- [13] J. E. Balzer, J. E. Field, M. J. Gifford, W. G. Proud, S. M. Walley, High-speed photographic study of the drop-weight impact response of ultrafine and conventional PETN and RDX. *Combust. Flame* 2002, 130, 298.
- [14] C. A. Handley, B. D. Lambourn, N. J. Whitworth, H. R. James, W. J. Belfield, Understanding the shock and detonation response of high explosives at the continuum and meso scales. *Appl. Phys. Rev.* 2018, 5, 011303.
- [15] F. P. Bowden, O. A. Gurton, Initiation of solid explosives by impact and friction: the influence of grit. *Proceedings of the Royal Society of London. Series A. Mathematical and Physical Sciences* 1949, 198, 337.
- [16] L. R. Simpson, M. F. Foltz, *LLNL small-scale drop-hammer impact sensitivity test*; United States, 1995.
- [17] United Nations, *Recommendations on the Transport of Dangerous Goods: Manual of Tests and Criteria*; New York and Geneva, 2015.
- [18] NATO STANAG 4489; 1999.
- [19] D. Preston, G. Brown, C. B. Skidmore, B. L. Reardon, D. A. Parkinson, Small-scale explosives sensitivity safety testing: A departure from Bruceton. *AIP Conf. Proc.* 2012, 1426, 713.

- [20] D. N. Preston, G. W. Brown, B. C. Tappan, D. M. Oshwald, J. R. Koby, M. L. Schoonover, Drop weight impact measurements of HE sensitivity: modified detection methods. *J. Phys. Conf. Ser.* **2014**, *500*, 182033.
- [21] G. W. Brown, M. M. Sandstrom, D. N. Preston, C. J. Pollard, K. F. Warner, D. N. Sorensen, D. L. Remmers, J. J. Phillips, T. J. Shelley, J. A. Reyes, P. C. Hsu, J. G. Reynolds, Statistical Analysis of an Inter-Laboratory Comparison of Small-Scale Safety and Thermal Testing of RDX. *Propellants Explos. Pyrotech.* **2015**, *40*, 221.
- [22] R. M. Doherty, D. S. Watt, Relationship Between RDX Properties and Sensitivity. *Propellants Explos. Pyrotech.* **2008**, *33*, 4.
- [23] L. Kurth, P. Lüth, *Ringversuch mit dem Fallhammer gemäß Abs. 1.6.2 Mechanische Empfindlichkeit (Schlag) der Methode A.14 Explosionsgefahr 2011*; BAM Bundesanstalt für Materialforschung und -prüfung: Berlin, **2013**.
- [24] F. W. Marrs, V. W. Manner, A. C. Burch, J. D. Yeager, G. W. Brown, L. M. Kay, R. T. Buckley, C. M. Anderson-Cook, M. J. Cawkwell, Sources of Variation in Drop-Weight Impact Sensitivity Testing of the Explosive Pentaerythritol Tetranitrate. *Ind. Eng. Chem. Res.* **2021**, *60*, 5024.
- [25] P. J. Rae, P. M. Dickson, Some Observations About the Drop-weight Explosive Sensitivity Test. *J. dynamic behavior mater.* **2021**, *7*, 414.
- [26] M. S. Gruhne, M. Lommel, M. H. H. Wurzenberger, N. Szimhardt, T. M. Klapötke, J. Stierstorfer, OZM Ball Drop Impact Tester (BIT-132) vs. BAM Standard Method – a Comparative Investigation. *Propellants Explos. Pyrotech.* **2020**, *45*, 147.
- [27] NATO STANAG 4487; **2009**.
- [28] P. C. Hsu, *A Brief Description of the Small-scale Safety Testing Systems at Lawrence Livermore National Laboratory*; United States, **2008**.
- [29] L. R. Simpson, M. F. Foltz, *LLNL Small-Scale Friction sensitivity (BAM) Test*; United States, **1996**.
- [30] One measurement takes approx. 20 min at room temperature.
- [31] https://www.metrohm.com/en_us/products/2/8600010.html (accessed 04/2022).
- [32] The decomposition products cause coating and corrosion on the device. Regular cleaning with a brush and cloth, as well as lubrication with graphite are necessary. Our experience shows that a dirty instrument determines a lower sensitivity (e.g. PETN 5 J).
- [33] <https://www.keyence.de/landing/lpc/vr6000.jsp> (accessed 04/2022).
- [34] T. M. Klapötke, G. Lemarchand, T. Lenz, M. Mühlemann, J. Stierstorfer, R. Weber, PETN - A Sensitivity Study, *Proceedings of the 23rd Seminar on New Trends in Research of Energetic Materials*, Pardubice, **2020**, pp 496.

Manuscript received: May 26, 2022

Revised manuscript received: June 20, 2022

Version of record online: August 2, 2022



Supporting Information

Impact and Friction Sensitivities of PETN: I. Sensitivities of the Pure and Wetted Material

Thomas M. Klapötke,* Guillaume Lemarchand, Tobias Lenz,* Moritz Mühlemann, Jörg Stierstorfer, and Ralf Weber© 2022 The Authors. Propellants, Explosives, Pyrotechnics published by Wiley-VCH GmbH. This is an open access article under the terms of the Creative Commons Attribution License, which permits use, distribution and reproduction in any medium, provided the original work is properly cited.

Impact and Friction Sensitivities of PETN: I. Sensitivities of the Pure and Wetted Material

Thomas M. Klapötke^{*[a]}, Guillaume Lemarchand^[b], Tobias Lenz^{*[a]}, Moritz Mühleman^[b],
Jörg Stierstorfer^[a], and Ralf Weber^[c]

[a] T. M. Klapötke, T. Lenz, J. Stierstorfer; Energetic Materials Research, Department of Chemistry, University of Munich (LMU), Butenandtstr. 5–13, D-81377, Germany, E-mail: tolech@cup.uni-muenchen

[b] G. Lemarchand, M. Mühleman; BIAZZI SA, Chemin de la Tavallaz 25, 1816 Chailly/Montreux, Switzerland

[c] R. Weber; Austin Powder Technology GmbH, Zum Elberskamp 24, 57413 Finnentrop, Germany

Supporting Information

Contents

1. General Analytics	2
2. Water content	4
3. Impact Sensitivities	7
4. Friction Sensitivity	9

1. General Analytics

General: ^1H , ^{13}C and ^{14}N spectra were recorded on BRUKER AMX 400 instruments. The samples were measured at room temperature in standard NMR tubes (\varnothing 5 mm). Chemical shifts are reported as δ values in ppm relative to the residual solvent peaks of $[\text{D}_6]\text{DMSO}$ (δ_{H} : 2.50, δ_{C} : 39.5). Solvent residual signals and chemical shifts for NMR solvents were referenced against tetramethylsilane (TMS, $\delta = 0$ ppm) and nitromethane. Unless stated otherwise, coupling constants were reported in Hertz (Hz) and for the characterization of the observed signal multiplicities the following abbreviations were used: s (singlet), m (multiplet) and br (broad). Infrared spectra (IR) were recorded from 4000 cm^{-1} to 400 cm^{-1} on a PERKIN ELMER Spectrum BX- 59343 instrument with a SMITHS DETECTION DuraSamplIR II Diamond ATR sensor. The absorption bands are reported in wave-numbers (cm^{-1}). Decomposition temperatures were measured via differential thermal analysis (DTA) with an OZM Research DTA 552-Ex instrument at a heating rate of $5\text{ K}\cdot\text{min}^{-1}$ and in a range of room temperature to $400\text{ }^\circ\text{C}$. The particle size distribution was analyzed using sieves with a mesh size of 100, 300, 500, 600 and 1000 micrometer.

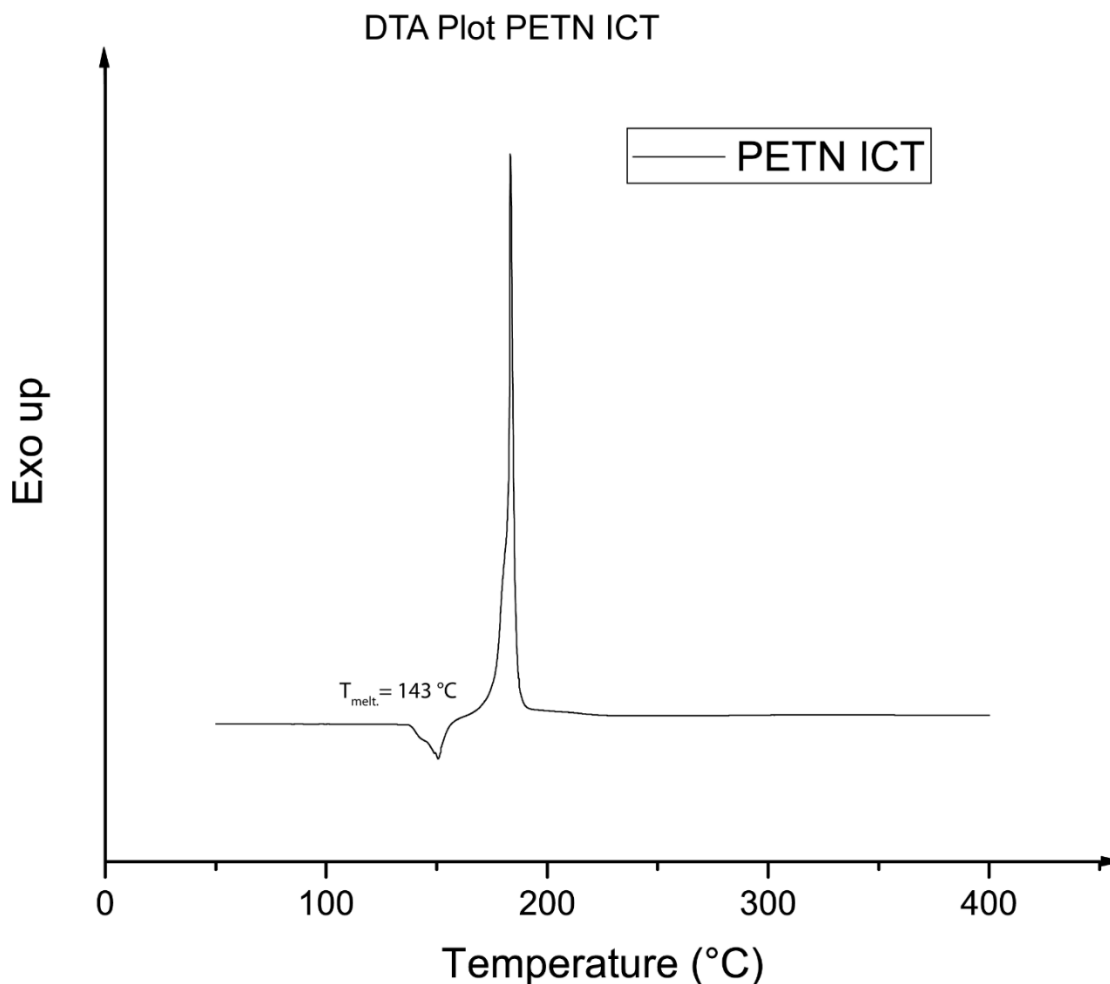
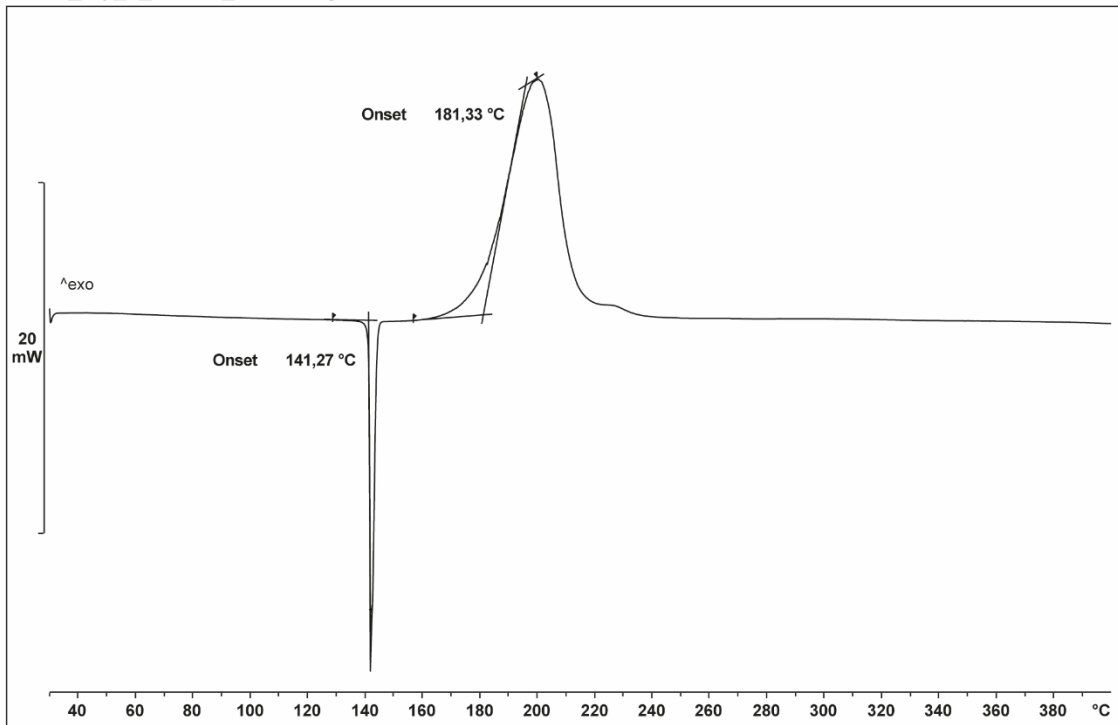


Figure 1 DTA plot of the dry PETN sample used for this study. (20 mg at $5\text{ K}\cdot\text{min}^{-1}$)

PETN_dry_5_°C/min_3,0100 mg



PETN_15%wet_5_°C/min_3,4800 mg

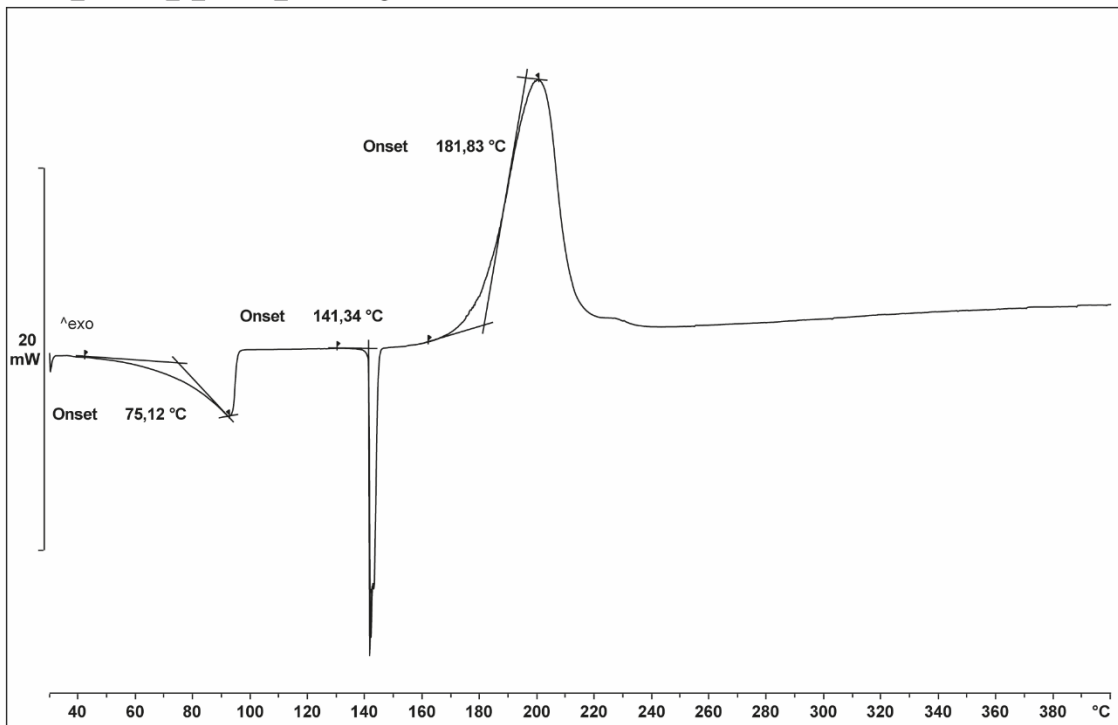


Figure 2 DSC plot of dry (top) and wetted (bottom) PETN. (5 K·min⁻¹)

2. Water content

Defined water 5%

	measured water before [%]	measured water after [%]	FS [N]	average water loss [%]
Probe 1	4,61	4,25	64	
Probe 2	4,78	4,53	72	
Probe 3	4,53	4,02	60	
Average	4,64	4,27	65,3	0,37
Standard deviation	0,13	0,26	6,1	

Defined water 10%

	measured water before [%]	measured water after [%]	FS [N]	average water loss [%]
Probe 1	9,56	9,22	80	
Probe 2	9,6	9,42	72	
Probe 3	9,24	9,43	72	
Average	9,47	9,36	74,7	0,11
Standard deviation	0,20	0,12	4,6	

Defined water 15%

	measured water before [%]	measured water after [%]	FS [N]	average water loss [%]
Probe 1	14,14	12,84	96	
Probe 2	14,48	14,25	84	
Probe 3	15,56	13,5	80	
Average	14,73	13,53	86,7	1,20
Standard deviation	0,74	0,71	8,3	

Defined water 20%

	measured water before [%]	measured water after [%]	FS [N]	average water loss [%]
Probe 1	18,23	17,53	72	
Probe 2	19,59	18,68	96	
Probe 3	19,14	17,41	96	
Average	18,99	17,87	88,0	1,11
Standard deviation	0,70	0,70	13,9	

Defined water 25%

	measured water before [%]	measured water after [%]	FS [N]	average water loss [%]
Probe 1	24,63	23,88	84	
Probe 2	24,48	20,7	96	
Probe 3	26,12	22,88	84	
Probe 4	25,80	24,90	80	
Average	25,26	23,09	86,0	2,17
Standard deviation	0,91	1,63	6,9	

Defined water 30%

	measured water before [%]	measured water after [%]	FS [N]	average water loss [%]
Probe 1	29,15	27,87	96	
Probe 2	32,9	27,61	96	
Probe 3	28,7	24,41	84	
Average	30,25	26,63	92,0	3,62
Standard deviation	2,31	1,93	6,9	

Defined water 35%

	measured water before [%]	measured water after [%]	FS [N]	average water loss [%]
Probe 1	33,76	34,58	112	
Probe 2	37,37	34,25	108	
Probe 3	38,12	34,75	96	
Average	36,42	34,53	105,3	1,89
Standard deviation	2,33	0,25	8,3	

3. Impact Sensitivities

Water [%]	E [J]		E [J]
35	30	N N E	25
	25	E	
	20	N N N N N N	
25	20	E	20
	15	N N N N N N	
25	25	N E	25
	20	N N N N N N	
25	25	N N N N N E	20
	20	N N N N N E	
	15	N N N N N N	
20	20	E	20
	15	N N N N N N	
20	30	E	25
	25	N N E	
	20	N N N N N N	
20	20	N E	20
	15	N N N N N N	
15	35	E	20
	30	N E	
	25	N N E	
	20	N N N N N E	
15	20	N N N N E	15
	15	N N N N E	
	10	N N N N N N	
15	20	N E E	20
	15	N N N N N N	
10	25	N E	15
	20	N N N E	
	15	E	
	10	N N N N N N	
10	20	N N E	20
	15	N N N N N N	
10	20	N E	15
	15	N N E	
	10	N N N N N N	

4. Friction Sensitivity

Water [%]	E [J]		E [J]
34.25	112	E	108
	108	N N E	
	96	N N N N N N	
34.75	120	E	96
	112	E	
	108	E	
	96	E	
	84	N N N N N N	
34.58	128	E	112
	120	N N E	
	112	N N E	
		N N N N N N	
27.61	120	E	96
	112	E	
	108	E	
	96	N N E	
	84	N N N N N N	
27.87	128	N N N E	96
	120	E	
	112	E	
	108	E	
	96	N N N E	
	84	N N N N N N	
24.41	120	E	84
	108	N N N E	
	96	E	
	84	N E	
	80	N N N N N N	

24.90 108 E
 96 N N E
 84 N N N E
 80 N N N E **80**
 72 N N N N N N

22.88 112 E
 108 N N E
 96 E
 84 N N E **84**
 80 N N N N N N

23.88 120 E
 112 E
 108 E
 96 E N E **96**
 84 N N N N N N

20.70 120 E
 112 E
 108 N E
 96 N N E
 84 N N N N E **84**
 80 N N N N N N

17.53 108 E
 96 N E
 84 E
 80 E
 72 N N N E **72**
 64 N N N N N N

18.68 120 E
 108 E
 96 N N E **96**
 84 N N N N N N

Impact and Friction Sensitivities of PETN: II. Sensitivities of the Acidic Material During Manufacturing

Thomas M. Klapötke,^{*,[a]} Guillaume Lemarchand,^[b] Tobias Lenz,^{*,[a]} Moritz Mühlemann,^[b] Jörg Stierstorfer,^[a] Fabian Venetz,^[c] Ralf Weber,^[d] and Jens Wutke^[c]

Dedicated to Professor Wolfgang Weigand on the occasion of his 65th birthday

Abstract: In this second part of our work on the sensitivity of pentaerythritol tetranitrate (PETN) the investigations focus on the manufacturing process. Literature about the explosive during production is very rare and optimization or changes in the process demand more in-depth knowledge of the safety parameters. Therefore, the industrial process is imitated in a small-scale laboratory reactor. Then impact

and friction sensitivities of emergency drowned, spent acid wet and acid washed PETN are investigated. In advance, PETN samples were taken from the filter of the SSE production and measured in the same manner. It becomes clear at which point a sensitive material is expected in the process. The data will improve handling safety and plant design.

Keywords: PETN · Explosives · Impact Sensitivity · Friction Sensitivity · Testing and Assessment

1 Introduction

The highly energetic nitrate ester of pentaerythritol (PETN) has been successful in various fields for decades. Easy to initiate and moderately sensitive, the compound is suitable in boosters (Pentolite), detonating cords (neat PETN in plastic tubes), detonators (combined with $\text{Pb}(\text{N}_3)_2$ [1]) or in other formulations (Semtex) [2–3]. Furthermore, PETN is used as a vasodilator to treat angina pectoris [4]. The white crystalline material melts at 141 °C and the decomposition starts at about 20 °C above that [5]. Due to the insolubility in water, it already precipitates during nitration and can be crystallized from many organic solvents [6]. Industrial manufacturing of pentaerythritol tetranitrate goes back to the 1930s [7]. The established methods are often used for good reason. Optimizing or changing the process poses risks and unintentional conversion of material would have disastrous consequences. However, optimization can be useful for economic, safety and environmental aspects. Changes in the supply industry or new legislation can also force changes in the process [9].

Pure common explosives are extensively characterized. In Figure 1 mechanical sensitivities of nine energetic materials are compared. PETN shows to be in the area of a sensitive to very sensitive booster explosive. It is more sensitive than TNT, RDX or TKX-50 but less sensitive than lead azide. In contrast to the pure compounds, much less is known about the properties during manufacturing. To be prepared for future changes or to optimize the existing process, it is necessary to examine the individual manufacturing processes more closely. Here the mechanical sensitivities during the manufacturing of pentaerythritol tetranitrate are inves-

tigated further. The production of PETN has developed since the first synthesis in 1894 [10]. Nitration with pure nitric acid followed by filtration, neutralization and recrystallization is now the state-of-the-art process. Pentaerythritol usually contains about 0.8% dipentaerythritol. Some stability and sensitivity data of crude material is available but a comparison to today's processes is hardly possible. The ICI Explosives Canada investigated two charges of crude PETN to use the acidic product in booster production [11]. The crude PETN (filtrated after nitration) is slightly less thermally stable. The dry materials show similar impact sensitivities to recrystallized PETN. Desensitization through wetting is less

[a] T. M. Klapötke, T. Lenz, J. Stierstorfer
Energetic Materials Research, Department of Chemistry,
University of Munich (LMU),
Butenandtstr. 5–13, 81377 München, Germany
*e-mail: tmk@cup.uni-muenchen.de
tolech@cup.uni-muenchen.de

[b] G. Lemarchand, M. Mühlemann
BIAZZI SA, Chemin de la Tavallaz 25,
1816 Chailly/Montreux, Switzerland

[c] F. Venetz, J. Wutke
Société Suisse des Explosifs,
Fabrikstrasse 48, 3900 Brig, Switzerland

[d] R. Weber
Austin Powder Technology GmbH,
Zum Elberskamp 24, 57413 Finnentrop, Germany

© 2023 The Authors. Propellants, Explosives, Pyrotechnics published by Wiley-VCH GmbH. This is an open access article under the terms of the Creative Commons Attribution License, which permits use, distribution and reproduction in any medium, provided the original work is properly cited.

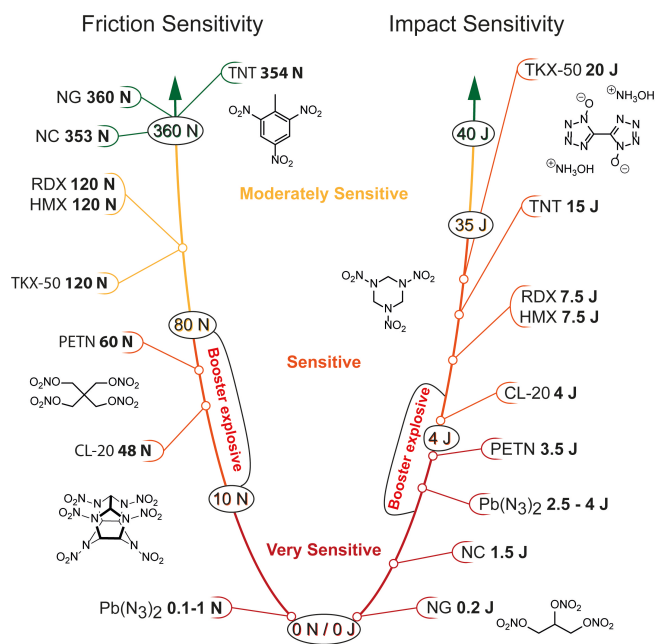


Figure 1. Impact and friction sensitivities of common explosives Trinitrotoluene flakes (TNT), Nitroglycerin (NG), Hexogen (RDX), Octogen (HMX), Dihydroxylammonium-5,5'-bistetrazole-1,1'-dioxide (TKX-50), Pentaerythritol tetranitrate (PETN), Hexanitroisowurtzitan technical (CL-20I), Lead azide ($\text{Pb}(\text{N}_3)_2$) [5, 8].

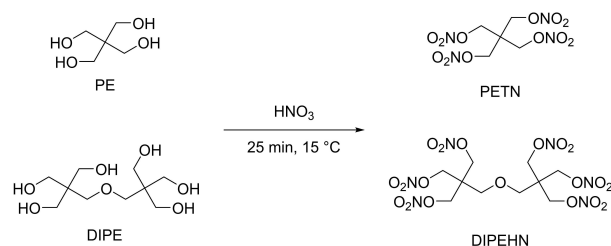
effective for crude material. This indicates differences in the behavior towards mechanical influences.

To better understand the hazards during production the impact and friction sensitivities of emergency drowned, crude acidic and washed PETN are investigated in this work. This should make the existing production safer and prepare for future changes. The sensitivity of water-wet pure PETN is discussed in part one of this series [12]. Some parts of this work are already published at the NTREM [13] and IEC conferences [14] and are shown here for comparison.

2 Experimental Section

Caution: PETN is a highly explosive material, especially sensitive to impact, friction, electrostatic discharge and temperature. When handling, protective measures must be taken depending on the quantity. The reactor setup and procedures were developed as safely as possible, in coordination with BIAZZI and Austin Powder. A solidly grounded reactor with a PTFE stirrer is recommended. Screw fittings and other sources of friction should be avoided or adequately lubricated with silicone grease. Manipulation of the PETN should be done only with soft materials, preferably wet. Wearing Kevlar gloves, wrist and hearing protection behind a blast shield during critical manipulation is recommended.

To synthesize pentaerythritol tetranitrate the corresponding alcohol pentaerythritol is nitrated (Scheme 1). In



Scheme 1. The reaction toward industrial PETN.

industrial production nitric acid with a concentration of > 99% is used nowadays. The NO_2 content should be low and checked, as it hurts spent acid stability [15]. The pentaerythritol usually has a content of about 0.8% of its mono ether dipentaerythritol. The nitration in this work is carried out based on the BIAZZI continuous process.

In Figure 2 three simulated industrial scenarios are shown. To not risk an uncontrolled reaction in the event of a malfunction in the plant, the reactor content can be drowned (1) in an excess of water. The controlled process begins with the nitration and filtration of the precipitated material. In the case of spent acid wet PETN (2), the properties of the nitrated material in its residual acid, the spent acid, are examined. Filtration of the spent acid PETN is followed by washing with diluted acid. The sensitivities of this washed product (3) are investigated as well.

2.1 Laboratory and Industrial Samples

Pentaerythritol with contents of 0.1, 0.8 and 1.3% DIPE are used for nitration. The nitric acid shows a concentration of > 99% and a low NO_2 content (< 0.3%). The nitration was performed in a double-jacketed glass reactor with external cooling and mechanical stirring. Further information about the used materials and the setup can be found in the supporting information. Three different types of PETN were produced: drowned PETN, spent acid wet PETN and washed PETN. The goal was to show the consecutive sensitivities

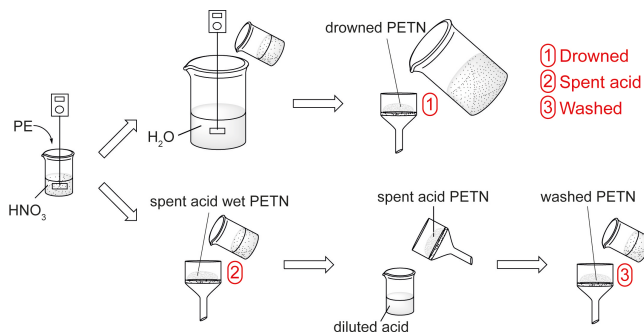


Figure 2. Synthesis of the three different qualities.

from the dry to 35% wet samples. Therefore, samples were taken from the filter and analyzed for their acid content by either titration or gravimetrically. If necessary the filtrated acid was added to adjust the acid content of the sample. As shown in part I, mixtures of PETN with water tend to be inhomogeneous and lose water during the measurements [12]. It is estimated that the given acid contents vary in the lower percent area.

Synthesis of PETN suspension: A grounded double-jacketed reactor (100 mL) with external cooling and mechanical stirring (500 rpm) was loaded with fuming nitric acid (99.1%, 50 mL, 75 g, 5 Parts). Pentaerythritol (15.0 g, 110 mmol, 1 Part) containing dipentaerythritol (0.1 or 0.8 or 1.3%) was added in small portions over 25 min at $15 \pm 3^\circ\text{C}$. A suspension (a) of PETN in 86% aqueous nitric acid is obtained.

(1) **Drowning:** The suspension (a) was poured onto water (8-fold amount, 400 mL) which was mechanically stirred (800 rpm). The resulting drowning acid (11.5%, aqueous nitric acid) was separated from the acidic PETN by suction filtration using a plastic funnel.

(2) **Spent Acid:** The suspension (a) was cooled to 5°C and stirred for 30 min. The spent acid was removed by suction filtration over an Omnipore™ 10 μm filter and plastic funnel. On the filter spent acid-wet PETN is obtained.

(3) **Washed:** The spent acid-wet PETN was dried for 15 min on the filter. Then the crude PETN was transferred into washing acid (150 mL, 11%, aqueous nitric acid) and mechanically stirred (500 rpm) for 5 min. Suction filtration with a plastic funnel was done to separate the washing acid.

Furthermore, the “*Société Suisse des Explosifs*” was kind enough to provide industrially manufactured PETN samples from their plant. Spent acid wet material was taken directly from the filter after nitration. Then after water-washing and filtration, a second wet sample was taken. This is especially useful to compare laboratory results with industrial production.

In addition, “*Austin Powder Technology*” has provided detonating cord. A cord with 40 g PETN per meter was opened, freed from plastic threads and used for this study.

2.2 Morphology and Particle Size

The dry samples were analyzed by sieving and scanning electron microscopy. The complete data can be found in the supporting information. The data relevant for differentiation are presented in Figure 3.

The samples prepared in the LMU laboratory (0.1–1.3% DIPE) are comparable in terms of crystal shape and size. Neither the dipentaerythritol content nor the process step has a measurable effect. The PETN is crystalizing in regular blocks that are partly intergrown. The predominant particle size is 100–300 μm with 74% or more by weight.

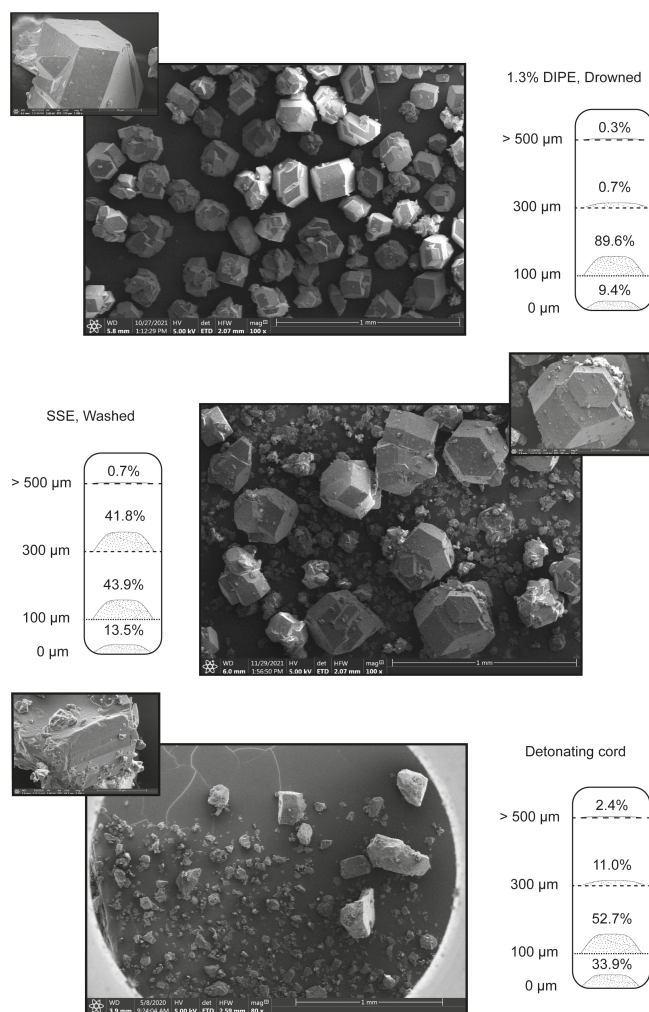


Figure 3. Particle size distribution and scanning electron microscopy pictures of drowned, washed and detonating cord PETN from different sources.

The spent acid wet sample obtained by SSE crystallized as intergrown blocks and agglomerates of smaller crystals. The particles are between 100 and 500 μm with 85%, thus coarser than the laboratory material. The washed sample shows comparable but smaller crystals in the SEM image. The main particles of detonating cord are 0–300 μm , thus finer than the LMU and SSE samples. On the SEM image, some large fragments are visible that are accompanied by smaller irregular crystals.

Because of manual sieving and electrostatic effects, sieving for smaller particle sizes is less accurate. Furthermore, loosely bound agglomerates and strongly intergrown crystals are hard to distinguish. For future work particle size determination through laser diffraction is recommended. Agglomerates can be broken up by ultrasound and intergrown crystals will stay connected.

3 Mechanical Sensitivities

To better assess the hazards of handling and the safety of the plant, knowledge of the sensitivity of PETN is essential. Mechanical sensitivity measurements are long-established methods to classify the hazards of energetic materials.

Over the years, several methods have been developed, but only a few have gained acceptance. Highly standardized and commonly used are the BAM devices described in the report "Transport of Dangerous Goods. Manual of Tests and Criteria" of the UN [16]. The drop hammer simulates a uniaxial impact on the specimen. This generates heat, shear force and adiabatic compression [17–24]. On the other hand, the friction tester simulates shear forces between roughened porcelain surfaces.

In this way, both devices can simulate a large part of the forces occurring in production. The lower detonation limit is determined with the "one out of six" method. In the following, the results of various samples from the industry and laboratory are compared and conclusions are drawn about the handling of the samples.

3.1 Reference Samples

No comparable or standardized values are available for impact and friction sensitivities during production. Recrystallized PETN from detonating cord and water-wet industrial PETN [25–26] are presented as a reference to better understand the sensitivities obtained. Furthermore, in part I. of our work the sensitivities of wet pure PETN are determined and discussed [12].

In Table 1 the sensitivities of detonating cord and industrial PETN are given. The dry samples show 3–4 J impact and 53–59 N friction sensitivity. The wet samples are desensitized in impact sensitivity to 25 J (9–15% water). The friction sensitivities for the wet samples vary from 60–80 N (9–15% water) depending on the institute measuring. The limiting sensitivities for transportation by the United Nations are 2 J and 80 N [16]. The friction sensitivity of PETN is therefore the larger concern.

Table 1. Impact and friction sensitivities of reference samples [25–26] compared with the UN limits for transportation [16].

PETN	Water [%]	IS [J]	FS [N]
Detonating cord ^[a]	dry	3	56 ± 3
Dried [26]	dry	4	54
Wetted [26]	9	25	60
Wet [25]	9	> 25	80
As delivered [26]	15	25	72
UN Transportation limit [16]	–	2	80

[a] Measured at LMU.

3.2 After Drowning

In the case of an emergency on a plant, the reactor is usually poured, drowned, into an excess of water. Then cleaning and disposal are necessary. To ensure safe and efficient working, the mechanical sensitivities of the dry and wet material must be known. In Figure 4 the measured friction and impact sensitivities of drowned PETN are shown. The colors indicate the different DIPE contents in the starting material.

For the friction sensitivities, a slightly decreasing trend is observed. The wetter the material the lower the sensitivities. The dry material shows to react at around 60 N, which is comparable to pure PETN. The sensitivities then decrease to around 84 N (15% wet). Until 35% drowning acid content the sensitivities stay unchanged. The DIPE content does not have a significant influence that can be detected.

The impact energy necessary for detonation is also increasing with higher drowning acid contents. The dry material shows to be around 4 J, like pure PETN. When wetted, an increase above 20 J (10% wet) is observed. Above 10% drowning acid, the sensitivities stagnate around 20–25 J.

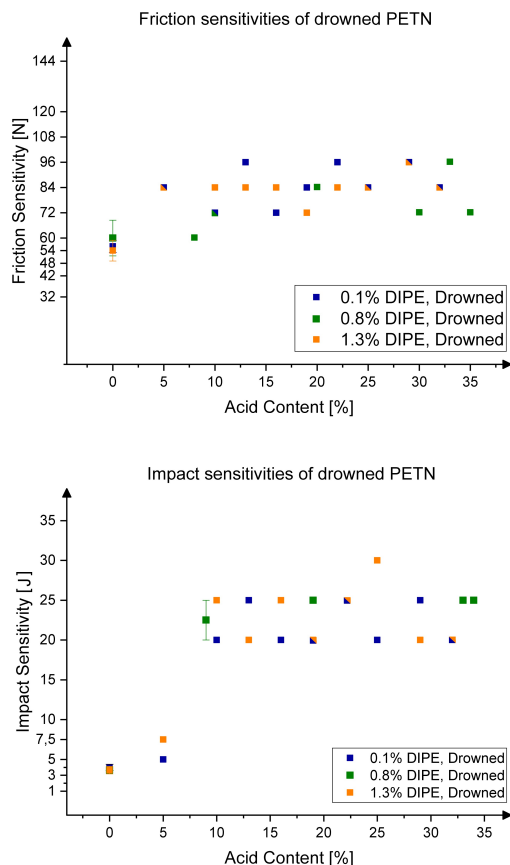


Figure 4. Friction and impact sensitivities of drowned samples containing drowning acid in amounts of 0–35%.

3.3 After Nitration

In today's PETN nitration process, the product is precipitated directly from the nitric acid. Through the reaction the acid is diluted to around 85% concentration, then called spent acid. The crystallization causes acid to be occluded within the crystal. These suspensions are mechanically stressed by pumping and filtration. In Figure 5 the friction and impact sensitivities of the spent acid wet and dry material are given. Furthermore, the LMU samples are compared with the industrial SSE PETN after nitration. The LMU samples and SSE samples are in line with the trend and are comparable.

Unexpectedly, increased friction sensitivities are observed for many spent acid-wet samples. The dry materials show sensitivities around 60 N. When wetted, the sensitivities mostly stagnate between 48 and 72 N. The 1.3% DIPE sample was measured with only 36 N at 16% acid content. This increase in sensitivity was not observed in any other form or mixture of PETN.

The impact sensitivities, in contrast, show a decreasing trend. With around 4 J the dry material is comparable to pure PETN. The decrease slowly takes place when wetting up to 15% acid. In this area of decrease, the deviations are

rather high and no concrete statement can be made. Between 15–35% acid the impact sensitivities are around 15–20 J.

3.4 After Nitration and Washing

After the nitration and filtration, the crude PETN is washed with diluted nitric acid (11%). This suspension is then stressed through vigorous stirring, filtration and pumping. The mechanical sensitivities of the washed samples are represented in Figure 6 and compared with the washed sample taken from the SSE production.

The friction sensitivities are slightly decreasing when more washing acid is present. This trend can also be observed for the SSE sample. The dry samples show sensitivities around 54 N, similar to pure PETN. The addition of acid causes the sensitivities to slightly decrease up to around 84 N (20% wet). The SSE samples show to be slightly more sensitive than the LMU samples but the deviations, in general, are rather high. For the SSE and the 1.3% DIPE sample a sensitivity of 60 N is observed at 29% wet. A general decrease is detected but some exceptions are present and caution is advised.

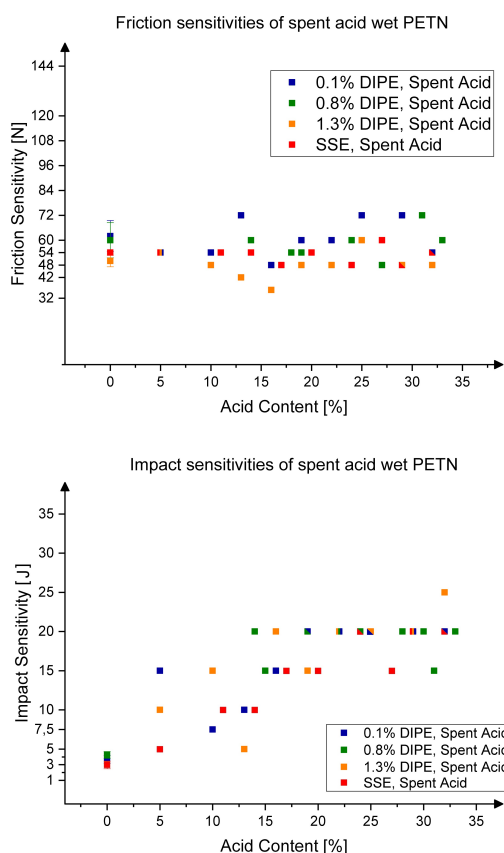


Figure 5. Friction and impact sensitivities of PETN after nitration containing spent acid in amounts of 0–35%.

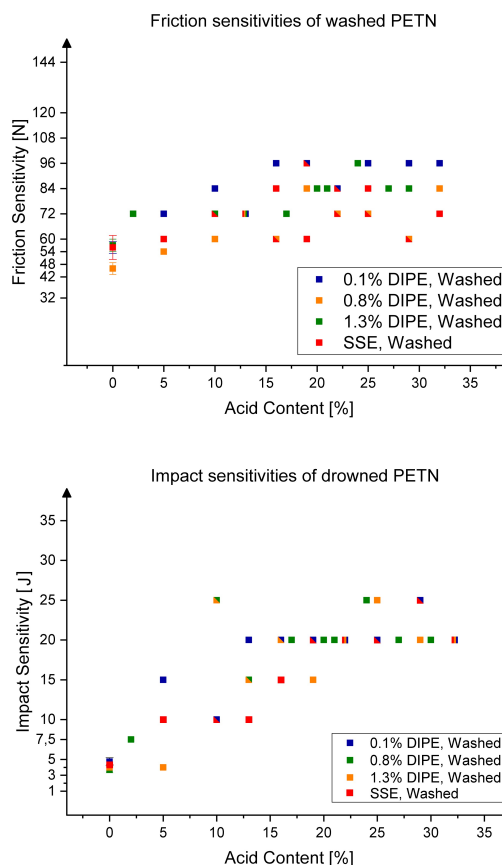


Figure 6. Friction and impact sensitivities of washed PETN containing washing acid in amounts of 0–35%.

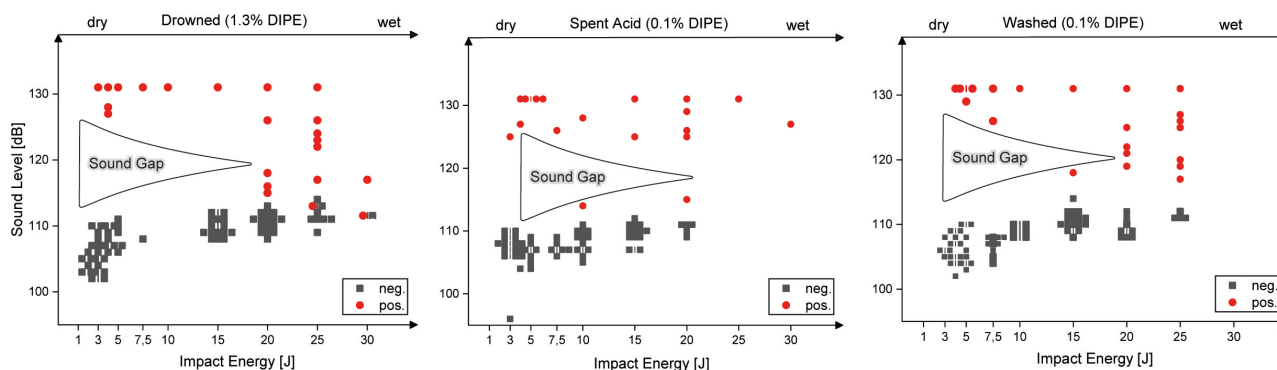


Figure 7. Sound level of impact sensitivity tests at different DIPE contents and drop energies. Red dots are evaluated by the operator as positive results, grey squares are negative results.

The impact sensitivities again show a different trend. A strong decrease with rising acid content is observed. The dry material is tested to be around 4 J. When washing acid is added desensitization takes place. Above 16% acid content the sensitivities stagnate at 15–20 J. The area of decrease again shows large deviations and is of high uncertainty. Above 15% acid the sensitivities are 20–25 J. The SSE samples show a comparable trend with the LMU samples.

3.5 Sound Level of Impact Sensitivities

After the first few impact measurements, it was audible that the detonations of the wet samples are less violent. Often residues of unreacted material were found in those test sleeves. To record this information, the noise level was detected in dB using a microphone about 30 cm away. Any kind of detonation was counted as a positive result regardless of how loud it was. In Figure 7 the sound levels of the drop experiments are shown. Positive results, detonations, are marked in red and negative results in grey. The negative results tend to stay between 100–115 dB. This noise is generated by the impact of the weight and increases with the mass of the weight. The explosions of the dry materials are in the area of 130 dB (maximum measurable value). The operator can evaluate the result using the microphone alone. When the samples are wet and incomplete conversion happens the noise of the detonation is decreasing. This can happen up to a point where the detonation is quieter than the basic noise of the machine. The operator can clearly distinguish the detonation and background but the microphone does not. For the acoustic evaluation of TNT impact tests, similar problems are observed by Marrs et al. [27].

The drowned and washed samples both show a strong decrease in noise when the conversion of the material is incomplete. Nevertheless, there are wet samples that show full conversion accompanied by a violent sound. The spent acid wet samples are generally more violent and show less

incomplete conversion. The incomplete conversion means that the sample initiates but the detonation does not propagate. The diluted acid does inhibit detonation propagation. However, initiation of PETN in spent acid, showed to propagate more easily.

4 Conclusion

The goal of this work was to outline the differences between PETN during manufacturing and the known final product. Therefore, PETN was synthesized from PE with 0.1 to 1.3% DIPE. The mechanical sensitivities were investigated after emergency drowning, during nitration, and after washing the crude product. No dry sample was found more sensitive than industrial PETN. Altering the DIPE content did not change the sensitivities significantly. The drowned and the washed samples are acting very similarly towards wetting. Both are desensitized by higher liquid contents whereas the effect is much more dominant for the impact sensitivities. The effect appears to be linear at least up to 25% liquid content. For the PETN during nitration, a drastic difference is observed. The wet material showed to be more friction sensitive than industrial PETN. The impact sensitivities are decreased when the material is wet.

It can be concluded that spent acid wet PETN represents the greatest hazard in the process. Drowning or washing leads to a product that is comparable sensitive to the final product. In general, friction sensitivities show to be the greater concern. Soft materials and careful manipulation are recommended.

Acknowledgments

For financial support of this work by Ludwig-Maximilian University (LMU), the Office of Naval Research (ONR) under Grant No. ONR N00014-19-1-2078 and the Strategic Environmental Research and Development Program (SERDP) under Contract No. W912HQ19C0033 are gratefully acknowledged. The authors thank Stefan Huber, Maxi Benz and Lukas Eberhardt for their help and sci-

entific exchange. Open Access funding enabled and organized by Projekt DEAL.

Data Availability Statement

Data may be requested via the authors.

References

- [1] D. C. Claessen, Verfahren zur Herstellung von Züandsätzen für Sprengkapseln, Zündhütchen und Großzündungen, 265025, Kaiserliches Patentamt, 1913.
- [2] T. M. Klapötke, *Chemistry of High-Energy Materials*, Walter de Gruyter GmbH, Berlin/Boston 2022, 6th edn.
- [3] R. M. J. Köhler, A. Homburg, *Explosivstoffe*, WILEY-VCH Verlag GmbH, Weinheim 2008; Vol. 10.
- [4] New Drugs, *Can. Med. Assoc. J.* 1959, 80, 997.
- [5] T. M. Klapötke, *Energetic Materials Encyclopedia*, Walter de Gruyter GmbH, Berlin/Boston 2021, 2nd edn.
- [6] R. N. Roberts, R. H. Dinegar, Solubility of Pentaerythritol Tetranitrate, *J. Phys. Chem.* 1958, 62, 1009.
- [7] E. Berlow, R. H. Barth, J. E. Snow, *The Pentaerythritols*; Reinhold Publishing Corporation, New York 1958.
- [8] R. Matyáš, J. Pachman, *Primary Explosives*, Springer Berlin, Heidelberg, 2013.
- [9] REACH: <https://echa.europa.eu/de/regulations/reach/understanding-reach> (accessed 24.08.2022).
- [10] T. Urbanski, *Chemistry and Technology of Explosives*, Pergamon Press Ltd., Oxford 1984; Vol. 4.
- [11] S. Boisvert, R. Deshais, *Characterization of Crude PETN*; ICI Explosives Canada: Quebec, 1992.
- [12] T. M. Klapötke, G. Lemarchand, T. Lenz, M. Mühlemann, J. Stierstorfer, R. Weber, Impact and Friction Sensitivities of PETN: I. Sensitivities of the Pure and Wetted Material, *Propellants Explos. Pyrotech.* 2022, 47, e202200150.
- [13] T. Lenz, T. M. Klapötke, J. Stierstorfer, M. Mühlemann, G. Lemarchand, R. Weber, Impact and friction sensitivity of acidic PETN; In: J. Pachmán & J. Selesovsky (Eds), Proc. 24th Seminar of the New Trends in Research of Energetic Materials. University of Pardubice, Pardubice, Czech Republic, pp. 142–149.
- [14] T. Lenz, T. M. Klapötke, J. Stierstorfer, M. Mühlemann, G. Lemarchand, R. Weber, Impact and friction sensitivities of PETN during manufacture, *International Explosives Conference, London 2022*, n/a.
- [15] I. Rodger, J. D. McIrvine, The decomposition of spent PETN nitration acids, *The Canadian Journal of Chemical Engineering* 1963, 41, 87.
- [16] United Nations, *Recommendations on the Transport of Dangerous Goods – Manual of Tests and Criteria*, New York and Geneva, 2015.
- [17] S. M. Walley, J. E. Field, M. W. Greenaway, Crystal sensitivities of energetic materials, *Mater. Sci. Technol.* 2006, 22, 402.
- [18] J. E. Balzer, J. E. Field, M. J. Gifford, W. G. Proud, S. M. Walley, High-speed photographic study of the drop-weight impact response of ultrafine and conventional PETN and RDX, *Combust. Flame* 2002, 130, 298.
- [19] S. N. Heavens, J. E. Field, D. Tabor, The ignition of a thin layer of explosive by impact, *Proceedings of the Royal Society of London, A. Mathematical and Physical Sciences* 1974, 338, 77.
- [20] P. Politzer, J. S. Murray, Impact sensitivity and crystal lattice compressibility/free space, *J. Mol. Model.* 2014, 20, 2223.
- [21] C. S. Coffey, V. F. De Vost, Impact Testing of Explosives and Propellants, *Propellants Explos. Pyrotech.* 1995, 20, 105.
- [22] F. P. Bowden, O. A. Gurton, Initiation of solid explosives by impact and friction: the influence of grit, *Proceedings of the Royal Society of London. Series A. Mathematical and Physical Sciences* 1949, 198, 337.
- [23] Y. Cai, F. P. Zhao, Q. An, H. A. Wu, W. A. Goddard III, S. N. Luo, Shock response of single crystal and nanocrystalline pentaerythritol tetranitrate: Implications to hotspot formation in energetic materials, *J. Chem. Phys.* 2013, 139, 164704.
- [24] P. J. Rae, P. M. Dickson, Some Observations About the Drop-weight Explosive Sensitivity Test, *Journal of Dynamic Behavior of Materials* 2021, 7, 414.
- [25] United Nations, *Transport of pentaerythrite tetranitrate (PETN) with less than 25 % of water but more than 9 % of water*, UN/SCETDG/47/INF.8, Geneva, 2015.
- [26] United Nations, *Transport of pentaerythrite tetranitrate (PETN) with less than 25 % of water but more than 9 % of water*, UN/SCETDG/49/INF.9, Geneva, 2016.
- [27] F. W. Marrs, V. W. Manner, A. C. Burch, J. D. Yeager, G. W. Brown, L. M. Kay, R. T. Buckley, C. M. Anderson-Cook, M. J. Cawkwell, Sources of Variation in Drop-Weight Impact Sensitivity Testing of the Explosive Pentaerythritol Tetranitrate, *Ind. Eng. Chem. Res.* 2021, 60, 5024–5033.

Manuscript received: October 23, 2022

Revised manuscript received: December 5, 2022

Version of record online: January 31, 2023

Impact and Friction Sensitivities of PETN:

II. Sensitivities of the Acidic Material During Manufacturing

Thomas M. Klapötke^[a], Guillaume Lemarchand^[b], Tobias Lenz^[a], Moritz Mühlemann^[b], Jörg Stierstorfer^[a], Fabian Venetz^[c], Ralf Weber^[d], and Jens Wutke^[c]

[a] T. M. Klapötke, T. Lenz, J. Stierstorfer; Energetic Materials Research, Department of Chemistry, University of Munich (LMU), Butenandtstr. 5-13, D-81377, Germany, E-mail: tolech@cup.uni-muenchen

[b] G. Lemarchand, M. Mühlemann; BIAZZI SA, Chemin de la Tavallaz 25, 1816 Chailly/Montreux, Switzerland

[c] F. Venetz, J. Wutke; Société Suisse des Explosifs, Fabrikstrasse 48, 3900 Brig, Switzerland

[d] R. Weber; Austin Powder Technology GmbH, Zum Elberskamp 24, 57413 Finnentrop, Germany

Supporting Information

Contents

1 Specification of Starting Materials.....	1
2 Reactor and Materials	3
3 Sensitivity Data.....	4
4 Morphology and Particle Size	31

1 Specification of Starting Materials

1.1 Specification of Nitric Acid

The nitric acid for nitration was analyzed and total acidity, as well as nitrous acid content, was determined by titration. For the total acidity, titration with sodium hydroxide, and for nitrous acid content, titration with permanganate solution, was applied. The specification, as well as the analysis, are shown in Table 1, detailed titration methods are described in the experimental part. The nitric acid used was delivered by Honeywell with a nominal purity >99%. Titration analysis concludes a nitric acid content of 99.00% and a nitrous acid content of 0.07%.

Table 1. Analysis result for nitric acid.

	Honeywell HNO ₃	Method
Total acidity (A')	99.10%	Titration NaOH
HNO ₃ (A)	99.00%	Calculated
HNO ₂ (B)	0.07%	Titration KMnO ₄
Water	<0.93%	Calculated

In Figure 1 the different acids and their nitrous acid contents are given. It is visible that in this case, the color correlates with the HNO₂ content. A clear to slightly yellow nitric acid is more likely to show low nitrous acid contents, but the analysis is always mandatory. High nitrous acid contents are known to cause fume off during nitration.

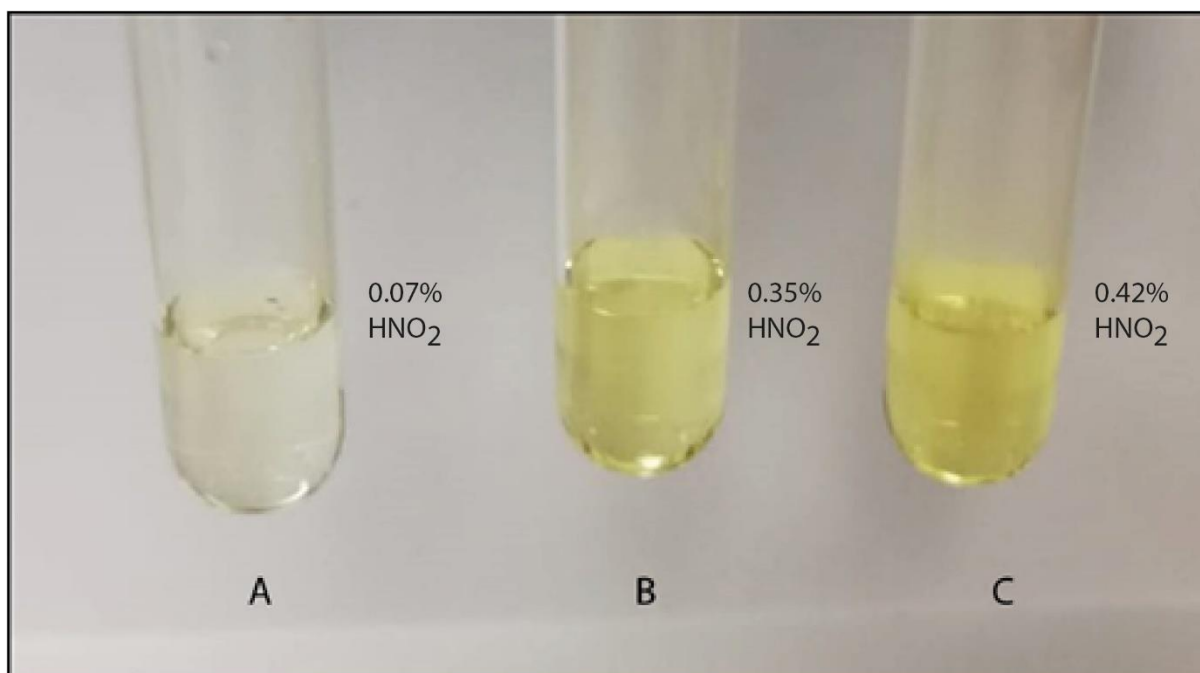


Figure 1. HNO₂ content of different suppliers and grades of nitric acid. Left: fresh nitric acid used for this study, middle and right: older stored nitric acid.

1.2 Specification of Pentaerythritol

The PE and DIPE samples were provided by Austin powder. The received materials were produced and analyzed by Perstorp. The specification and analysis data are collected in Table 2. The PE sample containing content of 1.3% DIPE was produced from PE containing 0.1% DIPE and pure DIPE. A mixture of 100.00 g PE (0.1) and 1.34 g DIPE was shaken in a 3D globular mixer for 24 h to achieve mixed PE (1.3).

Table 2. Specification (by BIAZZI) and analysis results for PE from Perstorp (McArthur).

	Specification	PE (0.1) Perstorp	PE (0.8) Perstorp	DIPE Perstorp	Mixed PE (1.3)
MonoPE [%]	96.5 ... 98.	99.5	99%	-	98.2
DiPE content [%]	0.7 ... 1.5	0.1	0.8%	91	1.3
Melting point [°C]	263 ± 1	263	-	-	-
Hydroxyl content [%]	49 min.	-	49.8%	-	-
Hydroxyl number [mg/g]	1'616 min.	1646	-	1324	-
Ash [%]	0.01 Max.	0.001	0.000%	-	-

2 Reactor and Materials

For nitration, a reactor similar to the industrial process was developed in collaboration with BIAZZI (Figure 2). Thus, a scale of up to 30 g PETN is possible. A double-jacketed glass reactor is cooled with an electric cooling unit using an aqueous magnesium nitrate solution (28%). Standard polyol cooling liquids should be avoided because of their exothermic reaction with nitric acid. Stirring was performed with a mechanical stirrer and a PTFE screw propeller. Heavy agitation is known to cause static electricity. Therefore, the reaction vessel is additionally equipped with a stainless-steel-grounding. Furthermore, all screw connections are lubricated with vaseline to reduce friction forces in case of PETN contamination. A safety shield can be placed in front of the reactor during the addition of PETN and the completion of the reaction. Underneath the vessel, a plastic basin is placed for spill containment.

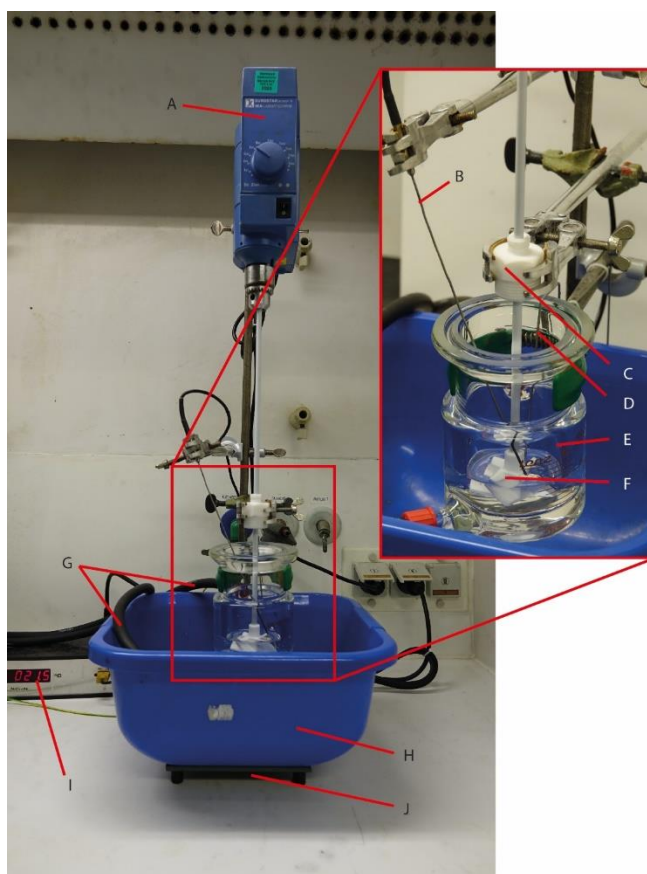


Figure 2. Reactor setup showing: A – mechanical stirrer, B,I – thermometer with digital display, C – Teflon stabilization, D – grounding, E – 100 mL double jacket reactor vessel, F – PTFE screw propeller, G – connection to cryostat, H – collecting basin, J – stand.

3 Sensitivity Data

The raw data of the mechanical sensitivity tests are presented in the chapters 3.1 - 3.23. Each test is performed according to the BAM procedure described in "Transport of Dangerous Goods. Manual of Tests and Criteria" of the UN. It is distinguished between an "Explosion" (E, positive result) and "No explosion" (N, negative result). The positive result gained with the lowest energy is stated as "impact sensitivity" or "friction sensitivity" of the respective material.

3.1 Friction Sensitivities – Drowned (0.1% DIPE)

Acid content [%]	E [N]		E [N]
0	72	E	
	60	E	60
	54	N N N N N N N	
0	60	N N N N N E	60
	54	N N N N N N N	
0	60	N E	
	54	N N E	54
	48	N N N N N N N	
5	120	E	
	108	E	
	96	N E	
	84	N N N E	84
	72	N N N N N N N	
10	120	E	
	96	E	
	84	E	84
	72	N N N N N N N	
13	120	N E	
	96	E	96
	84	N N N N N N N	
16	108	E	
	96	E	
	84	N N N E	84
	72	N N N N N N N	
19	120	N E	
	108	N E	
	96	E	
	84	N N N	84
	72	N N N N N N N	
22	108	E	
	96	E	96
	84	N N N N N N N	

Acid content [%]	E [N]	E [N]
25	120	E
	108	E
	96	N N E
	84	E
	72	N N N N N N
		84
29	120	E
	108	E
	96	N E
	84	N N N N N N
		96
32	120	E
	108	E
	96	N N E
	84	N N N N N N ? E
		84
		N N N N N N

3.2 Impact Sensitivities – Drowned (0.1% DIPE)

Acid content [%]	E [J]	E [J]
0	5	E
	4	N N E
	3	N N N N N N
		4
0	4	E
	3	N N N N N N
		4
0	4	N N E
	3	N N N N N N
		4
5	15	E
	10	N E
	7.5	N N N E
	5	N N N E
	4	N N N N N N
		5
10	25	N N E
	20	N N N N E
	15	N N N N N N
		20
13	25	N N N N N E
	20	N N N N N N
		25
16	25	N E
	20	N E
	15	N N N N N N
		20
19	25	E
	20	E
	15	N N N N N N
		20
		5
		88

Acid content [%]	E [J]		E [J]
22	25	N E	25
	20	N N N N N N N	
25	25	N N E	20
	20	N N E	
	15	N N N N N N N	
29	25	E	25
	20	N N N N N N N	
32	25	N E	20
	20	N E	
	15	N N N N N N N	

3.3 Friction Sensitivities – Spent acid wet (0.1% DIPE)

Acid content [%]	E [N]		E [N]
0	120	E	72
	96	E	
	84	N N E	
	72	E	
	60	N N N N N N N	
0	72	E	60
	60	E	
	54	N N N N N N N	
0	72	E	54
	60	N N E	
	54	E	
	48	N N N N N N N	
5	96	N N E	54
	84	E	
	72	N N N N E	
	60	E	
	54	N N N E	
	48	N N N N N N N	
10	96	E	54
	84	E	
	72	N E	
	60	E	
	54	N N N E	
	48	N N N N N N N	
13	96	E	72
	84	N E	
	72	N E	
	60	N N N N N N N	

Acid content [%]	E [N]		E [N]
16	72	E	
	60	? N E	
	54		N N E
	48		E
	42		N N N N N N
			48
19	96	N E	
	84		E
	72		N N N N E
	60		E
	54		N N N N N N
			60
22	72	E	
	60	N E	
	54		N N N N N N
			60
25	96	E	
	84	E	
	72	E	
	60		N N N N N N
			72
29	96	E	
	84	E	
	72	N E	
	60		N N N N N N
			72
32	96	E	
	84	E	
	72	E	
	60	? N N E	
	54		N N N N N E
	48		N N N N N N
			54

3.4 Impact Sensitivities – Spent acid wet (0.1% DIPE)

Acid content [%]	E [J]		E [J]
0	5	E	
	4	E	
	3		N N N N N E
	2		N N N N N N
			3
0	5	N E	
	4		N N N E
	3		N N N N N N
			4
0	5	N E	
	4		N E
	3		N N N N N N
			4

Acid content [%]	E [J]		E [J]
5	15	E	15
	10	N N N N N N N	
10	20	E	7.5
	15	E	
	10	N N N E	
	7.5	N E	
	5	N N N N N N N	
13	20	N N N E	10
	15	N N E	
	10	N E	
	7.5	N N N N N N N	
16	20	N E	15
	15	N N N E	
	10	N N N N N N N	
19	20	N E	20
	15	N N N N N N N	
22	25	E	20
	20	E	
	15	N N N N N N N	
25	25	E	20
	20	N E	
	15	N N N N N N N	
29	30	E	20
	25	E	
	20	N E	
	15	N N N N N N N	
32	30	E	20
	25	E	
	20	N N E	
	15	N N N N N N N	

3.5 Friction Sensitivities – Washed (0.1% DIPE)

Acid content [%]	E [N]		E [N]
0	84	E	54
	72	E	
	60	E	
	54	N N E	
	48	N N N N N N N	
0	60	E	54
	54	N N N E	
	48	N N N N N N N	

Acid content [%]	E [N]		E [N]
0	60	E	60
	54	N N N N N N N	
5	84	N N N N E	72
	72	N N N N E	
	60	N N N N N N N	
10	96	E	84
	84	N E	
	72	N N N N N N N	
13	96	N N E	72
	84	E	
	72	N N N N E	
	60	N N N N N N N	
16	120	N E	96
	96	N N N E	
	84	N N N N N N N	
19	120	N E	96
	96	E	
	84	N N N N N N N	
22	120	N E	84
	96	E	
	84	N N N N E	
	72	N N N N N N N	
25	120	E	96
	96	E E	
	84	N N N N N	
29	120	N E	96
	96	N N N N E	
	84	N N N N N N N	
32	120	E	96
	96	N N E	
	84	N N N N N N N	

3.6 Impact Sensitivities – Washed (0.1% DIPE)

Acid content [%]	E [J]		E [J]
0	7.5	N N N N N E	5
	5	E	
	4	N N N N N N N	
0	7.5	E	5
	5	N N N N N ? E	
	4	N N N N N N N	

Acid content [%]	E [J]		E [J]
0	5	N N E	4
	4	N E	
	3	N N N N N N	
5	25	E	15
	20	N E	
	15	N E	
	10	N N N N N N	
10	25	N E	10
	20	E	
	15	N E	
	10	E	
	7.5	N N N N N N	
13	25	E	20
	20	E	
	15	N N N N N N	
16	25	E	20
	20	N E	
	15	N N N N N N	
19	25	N N E	20
	20	N E	
	15	N N N N N N	
22	25	N N E	20
	20	N N N E	
	15	N N N N N N	
25	25	E	20
	20	N E	
	15	N N N N N N	
29	25	E	25
	20	N N N N N N	
32	25	E	20
	20	E	
	15	N N N N N N	

3.7 Friction Sensitivities – Drowned (0.8% DIPE)

Acid content [%]	E [N]		E [N]
0	72	E	54
	60	E	
	54	E	
	48	N N N N N N	

Acid content [%]	E [N]		E [N]
0	84	E	60
	72	N E	
	60	N N N N N N	
0	96	E	54
	84	E	
	72	E	
	60	E	
	54	N N N E	
0	48	N N N N N N	60
	84	N E	
0	72	E	60
	60	N E	
	54	N N N N N N	
	84	N E	
8	96	N E	60
	84	E	
	72	N N N E	
	60	N N ? E	
	54	N N N N N N	
10	96	E	72
	84	N N N E	
	72	N N N N E	
	60	N N N N N N	
15	120	E	96
	108	E	
	96	N N N N N ? E	
	84	N N N N N N	
20	96	E	84
	84	N E	
	72	N N N N N N	
30	96	? E	72
	84	E	
	72	N N N N N E	
	60	N N N N N N	
31	120	N N E	96
	96	N N N E	
	84	N N N N N N	
33	96	N N N E	96
	84	N N N N N N	

Acid content [%]	E [N]	E [N]
35	120 E	
	96 N N E	
	84 N E	
	72 ? E	72
	60 N N N N N N	

3.8 Impact Sensitivities – Drowned (0.8% DIPE)

Acid content [%]	E [J]	E [J]
0	10 E	
	7.5 E	
	5 E	
	4 E	
	3 N E	3
	2 N N N N N N	
0	5 E	
	4 E	4
	3 N N N N N N	
0	5 N E	
	4 E	4
	3 N N N N N N	
0	5 E	
	4 E	4
	3 N N N N N N	
9	35 E	
	30 N N E	
	25 N N E	25
	20 N N N N N N	
	15 N	
	10 N	
9	25 E	
	20 N N N N N E	20
	15 N N N N N N	
	10 N	
17	25 E	25
	20 N N N N N N	
	15 N	
	10 N	
19	25 E	
	20 N N N N N N	20
	15 N	
	10 N	

Acid content [%]	E [J]		E [J]
32	25	E	25
	20	N N N N N N N	
	15	N	
33	30	E	25
	25	N E	
	20	N N N N N N N	
	15	N	
	10	N	
34	30	E	25
	25	N E	
	20	N N N N N N N	
	15	N	
38	35	E	25
	30	N N E	
	25	N N E	
	20	N N N N N N N	
	15	N	
	10	N	

3.9 Friction Sensitivities – Spent acid wet (0.8% DIPE)

Acid content [%]	E [N]		E [N]
0	120	E	60
	96	N E	
	84	E	
	72	N E	
	60	N N N N N E	
	54	N N N N N N N	
0	84	E	72
	72	N E	
	60	N N N N N N N	
0	120	E	60
	84	E	
	72	N E	
	60	N N E	
	54	N N N N N N N	

Acid content [%]	E [N]	E [N]
0	96	E
	80	E
	72	N N E
	60	N E
	54	N N E
	48	N N N N N E
	40	N N N 3xN
48		
14	120	E
	96	E
	84	N E
	72	E
	60	N N E
60		
54	N N N N N N	
18	96	E
	84	E
	72	E
	60	E
	54	N N N N E
	48	N N N N N N
54		
19	96	E
	84	E
	72	N N E
	60	N E
	54	N N E
	48	N N N N N N
54		
23	84	E
	72	N E
	60	N N E
	54	N N N N E
	48	N N N N N N
54		
24	96	E
	84	E
	72	E
	60	N N N N N E
	54	N N N N N N
60		
22	72	E
	60	N E
	54	N N N N N N
60		

Acid content [%]	E [N]	E [N]
27	120	N E
	96	E
	84	N N N N N E
	72	E
	60	N N N E
	54	N E
	48	N N E
	42	6xN
31	84	N N E
	72	N E
	60	N N N N N N
33	360	E
	240	N E
	192	E
	160	N E
	144	N E
	120	N E
	96	N N N E
	84	E
	72	N N E
	60	E
54	6xN	

3.10 Impact Sensitivities – Spent acid wet (0.8% DIPE)

Acid content [%]	E [J]	E [J]
0	5	N E
	4	N E
	3	N N N N N N
0	7.5	E
	5	N N E
	4	N N N N N N
0	7.5	E
	5	N N N N E
	4	E
	3	N N N N N N
0	5	E
	4	N E
	3	N N N N N N
14	25	E
	20	N E
	15	N N N N N N

Acid content [%]	E [J]		E [J]
19	25	E	20
	20	N E	
	15	N N N N N N	
13	20	N N N E	10
	15	N N E	
	10	N E	
	7.5	N N N N N N	
15	25	E	15
	20	N E	
	15	N N N ? N N E	
	10	N N N N N N	
22	25	N	20
	20	N N N N N E	
	15	N N N N N N	
24	25	E	20
	20	N N N E	
	15	N N N N N N	
28	25	E	20
	20	N N E	
	15	N N N N N N	
30	25	E	20
	20	N E	
	15	N N N N N N	
31	30	E	20
	25	E	
	20	N E	
	15	N N N N N E	
	10	N N N N N N	
33	20	E	20
	15	N N N N N N	
	10	N	
	5	N	

3.11 Friction Sensitivities – Washed (0.8% DIPE)

Acid content [%]	E [N]		E [N]
0	72	N E	54
	60	N E	
	54	E	
	48	N N N N N N	

Acid content [%]	E [N]	E [N]
0	72	E
	60	E
	54	N N N N N N N
60		
0	84	E
	72	N E
	60	N N E
	54	N N N N N N N
60		
2	108	E
	96	N N E
	84	N N N E
	72	N E
	60	N N N N N N N
72		
10	96	E
	84	N ? N E
	72	E
	60	N N N N N N N
72		
13	96	E
	84	E
	72	N N E
	60	N N N N N N N
72		
17	96	N E
	84	N N E
	72	N N E
	60	N N N N N N N
72		
20	96	E
	84	E
	72	N N N N N N N
84		
21	120	E
	108	N N E
	96	E
	84	N E
	72	N N N N N N N
84		
24	96	N E
	84	N N N N N N N
96		
27	120	N E
	96	N E
	84	N N N N N E
	72	N N N N N N N
84		
30	120	N E
	96	E
	84	E
	72	N N N N N N N
84		

17

100

3.12 Impact Sensitivities – Washed (0.8% DIPE)

Acid content [%]	E [J]		E [J]
0	5	N N N N N E	4
	4	N N N N N N E	
	3	N N N N N N N	
0	4	N N E	4
	3	N N N N N N	
0	4	N E	4
	3	N N N N N N	
0	5	N E	3
	4	N E	
	3	N N N E	
	2	N N N N N N	
2	20	N E	10
	15	N E	
	10	N N E	
	7.5	N N N N N E	
	5	N N N N N N	
10	30	N N E	25
	25	N E	
	20	N N N N N N	
13	30	N E	15
	25	N E	
	20	E	
	15	N N N N N E	
	10	N N N N N N	
17	30	N N E	20
	25	N E	
	20	N N N E	
	15	N N N N N N	
20	30	E	20
	25	N N E	
	20	N N N N E	
	15	N N N N N N	
20	30	E	20
	25	N E	
	20	N N N E	
	15	N N N N N N	
24	25	E	25
	20	N N N N N N	

Acid content [%]	E [J]		E [J]
27	30	E	20
	25	N E	
	20	N E	
	15	N N N N N N	
30	30	E	20
	25	N E	
	20	N N N E	
	15	N N N N N N	

3.13 Friction Sensitivities – Drowned (1.3% DIPE)

Acid content [%]	E [N]		E [N]
0	72	N N N N E	60
	60	N E	
	54	N N N N N N	
0	60	E	54
	54	N E	
	48	N N N N N N	
0	72	E	48
	60	N N E	
	54	N E	
	48	N N N N N E	
	42	N N N N N N	
5	96	E	84
	84	N N E	
	72	N N N N N N	
10	120	N E	84
	96	N E	
	84	E	
	72	N N N N N N	
13	96	E	84
	84	N N N ? E	
	72	N N N N N N	
16	96	N N N N E	84
	84	N N N N N E	
	72	N N N N N N	
19	96	E	72
	84	N E	
	72	N N E	
	60	N N N N N N	

Acid content [%]	E [N]		E [N]
22	96	E	
	84	N N N N N E	84
	72	N N N N N N N	
25	96	N N E	
	84	N N N E	84
	72	N N N N N N N	
29	96	N E	96
	84	N N N N N N N	
32	120	E	
	96	N E	
	84	N N ? N E	84
	72	N N N N N N N	

3.14 Impact Sensitivities – Drowned (1.3% DIPE)

Acid content [%]	E [J]		E [J]
0	4	N N N E	
	3	N N E	3
	2	N N N N N N N	
0	4	N N E	4
	3	N N N N N N N	
0	5	N N N E	
	4	N N N N E	4
	3	N N N N N N N	
5	25	E	
	20	E	
	15	E	
	10	E	
	7.5	N E	7.5
	5	N N N N N N N	
10	25	E	25
	20	N N N N N N N	
13	25	N E	
	20	N N N N E	20
	15	N N N N N N N	
16	25	E	25
	20	N N N N N N N	
19	25	E	
	20	N N E	20
	15	N N N N N N N	
22	25	E	25
	20	N N N N N N N	

Acid content [%]	E [J]									E [J]
25	30	N	E							30
	25			N	N	N	N	N	N	
29	30	E								20
	25		N	E						
	20				E					
	15					N	N	N	N	
32	25	N	E							20
	20			E						
	15				N	N	N	N	N	

3.15 Friction Sensitivities – Spent acid wet (1.3% DIPE)

Acid content [%]	E [N]									E [N]				
0	60	N	N	E						54				
	54				N	E	E							
	48						N	N	N		N	N	N	
0	54	E								48				
	48		N	N	N	E								
	42						N	N	N		N	N	N	
0	54	N	E							48				
	48			N	N	?	E							
	42							N	N		N	N	N	N
5	60	E								54				
	54		N	N	N	N	N	E						
	48								N		N	N	N	N
10	60	E								48				
	54		N	E										
	48				E									
	42						N	N	N		N	N	N	
13	60	N	E							42				
	54			N	N	N	E							
	48							E						
	42								N		N	N	E	
	32										N	N	N	N
16	48	N	N	N	E					36				
	42					E								
	36						N	N	N		E			
	32								N		N	N	N	N
19	60	N	E							48				
	54			N	E									
	48					E								
	42						N	N	N		N	N	N	

Acid content [%]	E [N]		E [N]
22	60	N N N E	
	54		N N N E
	48		E
	42		N N N N N N
25	60	E	60
	54	N N N N N N	
29	60	E	
	54	N E	
	48		N N N N N E
	42		N N N N N N
32	84	E	
	72	E	
	60	N N E	
	54		N E
	48		E
	42		N N N N N N

3.16 Impact Sensitivities – Spent acid wet (1.3% DIPE)

Acid content [%]	E [J]		E [J]
0	4	E	
	3	N N E	3
	2		N N N N N N
0	5	E	
	4	N N E	
	3		N N N N N E
2		N N N N N N	
0	3	N N N N E	3
	2		N N N N N N
5	15	E	
	10	N N E	10
	7.5		N N N N N N
10	20	N N E	
	15		N N E
	10		N N N N N N
13	20	N N E	
	15		N N N N N E
	10		N N N N E
	7.5		N E
	5		N E
	4		6xN

Acid content [%]	E [J]		E [J]
16	20	N N N N N E	20
	15	N N N N N N N	
19	25	N E	15
	20	N E	
	15	N N N N E	
	10	N N N N N N N	
22	25	E	20
	20	N N N N N E	
	15	N N N N N N	
25	25	E	20
	20	E	
	15	N N N N N N	
29	25	N E	20
	20	N E	
	15	N N N N N N	
32	25	N E	25
	20	N N N N N N	

3.18 Friction Sensitivities – Washed (1.3% DIPE)

Acid content [%]	E [N]		E [N]
0	60	E	42
	54	N N E	
	48	E	
	42	E	
	36	N N N N N N	
0	60	N E	48
	54	E	
	48	N N N E	
	42	N N N N N N	
0	60	N E	48
	54	E	
	48	N E	
	42	N N N N N N	
5	84	N N ? E	54
	72	N E	
	60	E	
	54	N N N N E	
	48	N N N N N N	

Acid content [%]	E [N]	E [N]
10	96	E
	84	E
	72	N N N N N E
	60	N N E
	54	N N N N N N
13	84	E
	72	E
	60	N N N N N N
16	96	E
	84	N E
	72	N E
	60	E
	54	N N N N N N
19	96	E
	84	E
	72	N N N N N N
22	96	N E
	84	N E
	72	N N N N N E
	60	N N N N N N
25	108	E
	96	E
	84	N N N E
	72	N N N N E
	60	N N N N N N
29	108	E
	96	N N E
	84	N E
	72	N E
	60	N N E
	54	N N N N N N
32	108	E
	96	E
	84	? E
	72	N N N N N

3.19 Impact Sensitivities – Washed (1.3% DIPE)

Acid content [%]	E [J]	E [J]
0	5	E
	4	N E
	3	N N N N N N

24

107

Acid content [%]	E [J]		E [J]
0	4	E	4
	3	N N N N N N N	
0	5	E	4
	4	N E	
	3	N N N N N N N	
5	20	E	4
	15	N N E	
	10	N N N E	
	7.5	E	
	5	N N E	
	4	E	
	3	N N N N N N N	
10	25	E	
	20	N N N N N N N	
13	25	N E	15
	20	E	
	15	N N E	
	10	N N N N N N N	
16	25	N N E	20
	20	N N E	
	15	N N N N N N N	
19	25	E	15
	20	N N N N E	
	15	N N N N E	
	10	N N N N N N N	
22	25	E	20
	20	N E	
	15	N N N N N N N	
25	25	N N E	25
	20	N N N N N N N	
29	25	N N N E	20
	20	N E	
	15	N N N N N N N	
32	25	N N N E	20
	20	N E	
	15	N N N N N N N	

3.20 Friction Sensitivities – Spent acid wet (SSE)

Acid content [%]	E [N]		E [N]
0	60	N N N N N E	54
	54	E	
	48	N N N N N N N	
0	54	N N N N N E	54
	48	N N N N N N N	
0	54	N N N E	54
	48	N N N N N N N	
5	72	N E	54
	60	E	
	54	N E	
	48	N N N N N N N	
16	120	E	54
	108	E	
	84	E	
	72	E	
	60	E	
	54	N N E	
	48	N N N N N N N	
19	84	E E	54
	72	N N N N N E	
	60	E	
	54	E	
	48	N N N N N N N	
22	84	E	48
	72	E	
	60	N E	
	54	N N E	
	48	N N E	
42	N N N N N N N		
25	84	E	54
	72	N E	
	60	N E	
	54	N N N N E	
	48	N N N N N N N	
29	84	N E	48
	72	E	
	60	E	
	54	N N N N E	
	48	E	
	42	N N N N N N N	

Acid content [%]	E [N]											E [N]
29	72	N	N	E								
	60				E							
	54					E						
	48						E					48
	42							N	N	N	N	N
32	84	E										
	72		E									
	60			N	N	N	N	E				60
	54								N	N	N	N
32	84	E										
	72		E									
	60			E								
	54				E							
	48					N	N	N	N	N	N	

3.21 Impact Sensitivities – Spent acid wet (SSE)

Acid content [%]	E [J]											E [J]
0	5	E										
	4		E									
	3			N	N	N	N	E				3
	2								N	N	N	N
0	3	N	E									3
	2			N	N	N	N	N	N			
0	3	N	N	E								3
	2				N	N	N	N	N	N		
5	10	N	N	E								
	7.5				E							
	5					N	N	N	N	N	E	5
	4									N	N	N
16	30	E										
	25		E									
	20			E								
	15				E							
	10					E						10
	7.5						N	N	N	N	N	N
19	30	E										
	25		E									
	20			E								
	15				E							
	10					N	N	N	E			10

	7.5		N	N	N	N	N	N				
Acid content [%]	E [J]								E [J]			
22	25	E										
	20		E									
	15			N	E				15			
	10					N	N	N	N	N	N	
25	25	E										
	20		E									
	15			N	N	E			15			
	10						N	N	N	N	N	N
29	25	E										
	20		N	E					20			
	15				N	N	N	N	N	N		
29	25	E										
	20		N	E					20			
	15				N	N	N	N	N	N		
32	25	E										
	20		E									
	15			N	E				15			
	10					N	N	N	N	N	N	
32	30	E										
	25		E									
	20			N	N	N	N	N	E	20		
	15							N	N	N	N	N

3.22 Friction Sensitivities – Washed (SSE)

Acid content [%]	E [N]									E [N]			
0	72	E											
	60		N	N	E								
	54				N	N	E						
	48							E		48			
	42								N	N	N	N	N
0	60	E								60			
	54		N	N	N	N	N	N					
0	60	N	N	E						60			
	54				N	N	N	N	N	N			
5	84	E											
	72		N	N	N	E	E						
	60							N	N	N	E	60	
	54								N	N	N	N	N

Acid content [%]	E [N]		E [N]
10	96	E	72
	84	E	
	72	N N N N N E	
	60	N N N N N N	
13	96	N E	72
	84	E	
	72	E	
	60	N N N N N N	
16	96	E	84
	84	N N N E	
	72	N N N N N N	
19	96	N N E	96
	84	N N N N N N	
22	96	N N N N E	84
	84	E	
	72	N N N N N N	
25	108	N N N E	84
	96	E	
	84	N N N E	
	72	N N N N N N	
29	84	N N N E	60
	72	N N N N E	
	60	N N N E	
	54	N N N N N N	
32	84	N E	72
	72	E	
	60	N N N N N N	
32	120	E	72
	96	E E	
	84	N E	
	72	N E	
	60	N N N N N N	
32	72	E	72
	60	N N N N N N	
29	84	N N E	60
	72	E	
	60	E	
	54	N N N N N N	
29	72	E	72
	60	N N N N N	

Acid content [%]	E [N]		E [N]
16	96	E	60
	84	E	
	72	E	
	60	E	
	54	N N N N N N	
22	72	N N N N N E	72
	60	N N N N N N	
19	96	E	60
	84	N N N N E	
	72	N N E	
	60	E	
	54	N N N N N N	
25	96	E	72
	84	N E	
	72	N E	
	60	N N N N N N	

3.23 Impact Sensitivities – Washed (SSE)

Acid content [%]	E [J]		E [J]
0	5	E	4
	4	N E	
	3	N N N N N N	
0	5	E	5
	4	N N N N N N	
0	5	E	4
	4	E	
	3	N N N N N N	
5	20	E	10
	15	E	
	10	E	
	7.5	N N N N N N	
10	20	E	10
	15	N N N E	
	10	N N N N E	
	7.5	N N N N N N	
13	25	E	10
	20	E	
	15	E	
	10	N N N E	

		7.5	N N N N N N									
Acid content [%]	E [J]									E [J]		
16	25	E								15		
	20	E										
	15		N	N	E							
	10					N	N	N	N		N	N
19	25	N	N	E						20		
	20				N	E						
	15					N	N	N	N		N	N
22	25	N	N	E						20		
	20				N	N	E					
	15						N	N	N		N	N
25	25	E								20		
	20		N	E								
	15				N	N	N	N	N		N	
29	25	E								25		
	20		N	N	N	N	N	N				
32	30	E								20		
	25		N	E								
	20				N	N	N	N	E			
	15							N	N		N	N

4 Morphology and Particle Size

After drying, until no more weight was lost, the particle size distribution was determined. Therefore, the sample was sieved and every fraction was weighed. Sieves with a mesh size of 1000, 600, 500, 300 and 100 µm were used and the fractions were described with the mean grain sizes between two sieves. The results are shown in Figure 3.

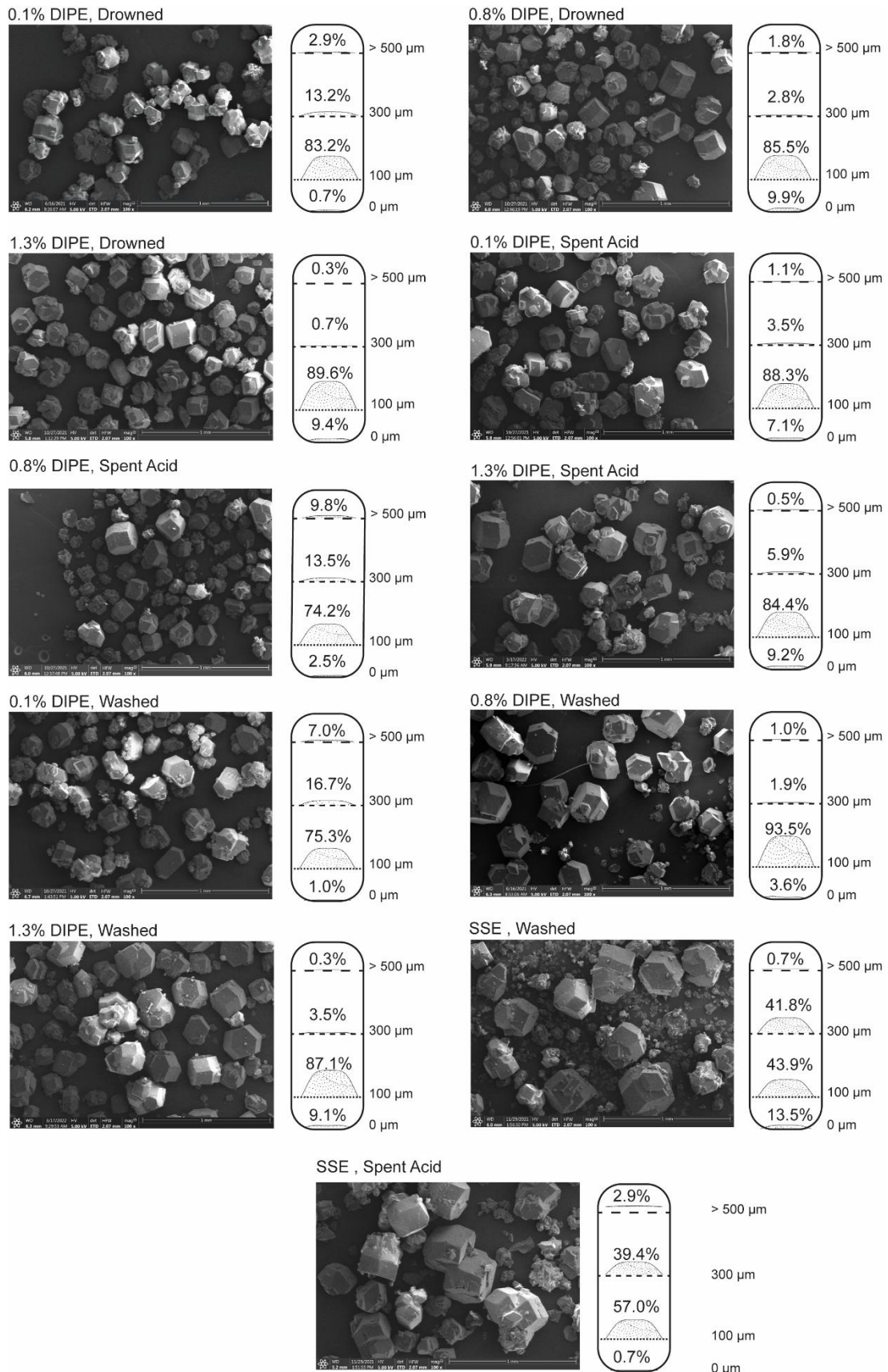


Figure 3. REM images and particle size distribution of the investigated samples.

About the Azido Derivatives of Pentaerythritol Tetranitrate

Tobias Lenz,^[a] Thomas M. Klapötke,^{*[a]} Moritz Mühlemann,^[b] and Jörg Stierstorfer^[a]

Dedicated to Professor Dr. Peter Klüfers on the occasion of his 70th birthday.

Abstract: With the first ever synthesis of monoazidopentaerythritol trinitrate, a comparative study of the properties of all azidonitrate derivatives from pentaerythritol tetranitrate (PETN) to tetraazidopentaerythritol (TAPE) was possible. The azides were prepared by halogen azide exchange and the remaining alcohols were then converted into the organic nitrate esters using acetyl nitrate. The resulting compounds pentaerythritol tetranitrate (PETN), monoazidopentaerythritol mononitrate (MAPETN), diazidopentaerythritol dinitrate (DAPEDN), triazidopentaerythritol mononitrate (TAPEMN), tetraazidopentaerythritol (TAPE) were analyzed for their chemical (XRD, NMR, EA, IR)

and energetic properties (DTA/DSC, impact and friction sensitivity) and presented for comparison. An interesting trend of decreasing melting points from PETN to the triazide was observed, with the monoazide found to meet the thermal requirements for a melt-castable explosive. The mechanical sensitivities were successfully explained by Hirshfeld analysis. The energetic properties were calculated with the EXPLO5 code and show a decreasing performance towards the highly sensitive tetraazido derivative. Furthermore, PETN was successfully initiated with its tetraazido derivative TAPE.

Keywords: energetic materials · nitrate esters · azides · PETN · sensitivities

1 Introduction

Since 1867 when Alfred Nobel invented dynamite, organic nitrates are ubiquitous in the field of energetic materials. While nitroglycerine, contained in dynamite and propellants, has been replaced in many fields, due to its headache causing properties and high sensitivity, the tetranitrate of pentaerythritol finds a wide range of applications. It is characterized by a favorable one-step synthesis, low toxicity, and high performance. The explosive, shortened PETN, is used in both the military and civilian sectors. The nitrate can be found as the main charge in grenades and shaped charges or as a booster charge in detonators. PETN is also available as detonating cord, in which tubes are filled with PETN, which can then be flexibly wrapped around trees or inserted into boreholes. Furthermore PETN is used in Semtex or sheet explosives. In mixtures with TNT, PETN is known as pentolite for mining operations. A pentolite booster is needed to transfer the energy from the detonator to

the more insensitive, often ammonium nitrate-based main charge. This is one of the reasons why PETN is often referred to as the boundary between primary and secondary explosives [1].

Because PETN is such a well-known explosive, several attempts have been made to modify it. Functionalities like polynitramino [2], nitrate salts [3], amine [4] or nitrocarbamate [5] were introduced. Furthermore, sila [6] and oxophosphine [4] derivatives are known. Herein we report the synthesis of all azido derivatives from pentaerythritol tetranitrate to tetraazidopentaerythritol. In Figure 1 the molecular structures of Pentaerythritol tetranitrate (PETN), Monoazidopentaerythritol trinitrate (MAPETN), Dia-

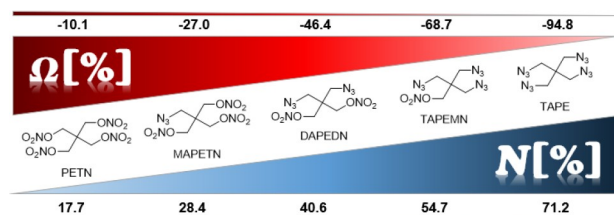


Figure 1. Oxygen balance (Ω_{CO_2}) and nitrogen content of PETN, MAPETN, DAPEDN, TAPEMN, TAPE.

[a] T. Lenz, T. M. Klapötke, J. Stierstorfer
Department of Chemistry
Energetic Materials Research
Ludwig Maximilian University of Munich
Butenandtstr. 5–13
81377 Munich, Germany
*e-mail: tmk@cup.uni-muenchen.de

[b] M. Mühlemann
BIAZZI SA
Chemin de la Tavallaz 25
CH-1816 Chailly/Montreux, Switzerland

Supporting information for this article is available on the WWW under <https://doi.org/10.1002/prop.202000265>

© 2021 The Authors. Propellants, Explosives, Pyrotechnics published by Wiley-VCH GmbH. This is an open access article under the terms of the Creative Commons Attribution License, which permits use, distribution and reproduction in any medium, provided the original work is properly cited.

zidopentaerythritol dinitrate (DAPEDN), Triazidopentaerythritol mononitrate (TAPEMN), and Tetraazidopentaerythritol (TAPE) are given with corresponding oxygen balance and nitrogen content. Whereas the properties of PETN are well characterized, there is only a little literature on the azidonitrate derivatives. DAPEDN and TAPEMN were synthesized for the first time through oxetane ring opening by Frankel and Wilson [7]. The reported liquid DAPEDN was later found to be solid at room temperature [8]. TAPE is well known as an organic building block but the energetic properties are poorly characterized [9]. In this work, all five compounds are synthesized and their properties are compared. The best oxygen balance can be observed for PETN with -10% , where the explosion energy is largely released by the oxidation of the carbon skeleton. By exchanging nitrate with azide, the nitrogen content enriches and the oxygen balance decreases. For TAPE the nitrogen content is at a maximum of 71% . Other than for PETN, the formation of nitrogen is the cause of high energy output.

2 Experimental Section

CAUTION! All investigated azidonitrates are explosive and sensitive materials. Although no incidents were observed during preparation and handling of these compounds, safety precautions (such as wearing a leather coat, face shield, Kevlar sleeves, Kevlar gloves, earthed equipment, and ear-plugs) should be drawn especially when manipulating dry materials.

2.1 Tetraazidopentaerythritol (TAPE)

1,3-Dibromo-2,2-bis(bromomethyl)propane (0.50 g, 1.4 mmol) was dissolved in DMF (10 mL) and sodium azide (1.02 g, 15.7 mmol) was added. The mixture was heated 10 h at 100°C . The completion of the reaction was checked by TLC. Then the solvent was evaporated under reduced pressure. Water was added to the residue and the mixture was extracted with ethyl acetate ($\times 3$). The solvent was dried over MgSO_4 , filtrated and evaporated to dryness, yielding TAPE (0.19 g, 0.8 mmol, 60%) as a colorless crystalline solid. DTA (5 K min^{-1}): 44°C (endo), 218°C (dec.). $^1\text{H NMR}$ ($\text{DMSO-}d_6$, 400 MHz, ppm): $\delta = 3.40$ (s, 8H). $^{13}\text{C NMR}$ ($\text{DMSO-}d_6$, 100 MHz, ppm): $\delta = 51.7, 43.6$. $^{14}\text{N NMR}$ ($\text{DMSO-}d_6$, 29 MHz, ppm): $\delta = -133, -175$. FT-IR (ATR): $\tilde{\nu} = 2956$ (w), 2929 (m), 2868 (w), 2221 (w), 2175 (w), 2087 (vs), 1444 (s), 1352 (m), 1287 (s), 1269 (vs), 1246 (s), 1153 (m), 1123 (w), 945 (m), 908 (m), 895 (s), 653 (m), 634 (m), 599 (m), 556 (m), 463 (s) cm^{-1} . EA calcd. for $\text{C}_5\text{H}_8\text{N}_{10}\text{O}_3$ (236.20 g mol^{-1}): C 25.43, N 71.16, H 3.41%; found: C 25.75, N 70.36, H 3.43%. IS: $< 1\text{ J}$; FS: 1 N.

2.2 General Procedure for Organic Nitrate Formation

To a solution of acetic acid anhydride (5 parts) and glacial acetic acid (1 part), nitric acid (1 part) was added dropwise at $5\text{--}10^\circ\text{C}$ under stirring. After the solution was cooled down to 5°C , the azido compound (0.4 M for MAPE, 0.3 M for DAPE, 0.2 M for TriAPE) was added carefully in portions and the reaction is stirred 20 min at 5°C . After completion, the solution is poured on ice water (20 parts).

2.3 Monoazidopentaerythritol Trinitrate (MAPETN)

Following the general procedure, 2-(azidomethyl)-2-(hydroxymethyl)propane-1,3-diol (0.50 g, 3.6 mmol), acetic acid anhydride (7.5 mL), glacial acetic acid (1.5 mL), nitric acid (1.5 mL) were used. After addition to water the precipitating solid was extracted with ethyl acetate ($\times 3$) and residues of acid were neutralized with sodium bicarbonate. The solvent was dried over MgSO_4 , filtrated and evaporated to dryness, yielding MAPETN (0.79 g, 2.7 mmol, 86%) as a colorless crystalline solid. DTA (5 K min^{-1}): 82°C (endo), 180°C (dec.). $^1\text{H NMR}$ ($\text{DMSO-}d_6$, 400 MHz, ppm): $\delta = 4.63$ (s, 6H), 3.69 (s, 2H). $^{13}\text{C NMR}$ ($\text{DMSO-}d_6$, 100 MHz, ppm): $\delta = 71.1, 50.1, 41.5$. $^{14}\text{N NMR}$ ($\text{DMSO-}d_6$, 29 MHz, ppm): $\delta = -46, -137$. $^{15}\text{N NMR}$ ($\text{DMSO-}d_6$, 41 MHz, ppm): $\delta = -43.8, -134.5, -172.0, -317.1$. FT-IR (ATR): $\tilde{\nu} = 2111$ (m), 1635 (vs), 1467 (w), 1304 (m), 1273 (vs), 1026 (m), 999 (m), 846 (vs), 754 (s), 737 (m), 707 (m), 690 (m), 643 (w), 621 (m) cm^{-1} . EA calcd. for $\text{C}_5\text{H}_8\text{N}_6\text{O}_9$ (296.15 g mol^{-1}): C 20.28, N 28.38, H 2.72%; found: C 20.33, N 28.14, H 2.72%; IS: 2 J; FS: 36 N.

2.4 Diazidopentaerythritol Dinitrate (DAPEDN)

Following the general procedure, 2,2-bis(azidomethyl)propane-1,3-diol (0.50 g, 2.7 mmol), acetic acid anhydride (7.5 mL), glacial acetic acid (1.5 mL) and nitric acid (1.5 mL) were used. After addition to water the precipitating solid was extracted with ethyl acetate ($\times 3$) and residues of acid were neutralized with sodium bicarbonate. The solvent was dried over MgSO_4 , filtrated and evaporated to dryness, yielding DAPETN (0.66 g, 2.4 mmol, 88%) as a colorless crystalline solid. DTA (5 K min^{-1}): 32°C (endo), 182°C (dec.). $^1\text{H NMR}$ ($\text{DMSO-}d_6$, 400 MHz, ppm): $\delta = 4.56$ (s, 4H), 3.60 (s, 4H). $^{13}\text{C NMR}$ ($\text{DMSO-}d_6$, 100 MHz, ppm): $\delta = 71.7, 50.7, 42.2$. $^{14}\text{N NMR}$ ($\text{DMSO-}d_6$, 29 MHz, ppm): $\delta = -42, -134$. FT-IR (ATR): $\tilde{\nu} = 2104$ (vs), 1661 (m), 1633 (vs), 1465 (m), 1451 (m), 1363 (m), 1278 (vs), 1271 (vs), 1256 (vs), 1028 (m), 1001 (s), 923 (m), 853 (vs), 755 (s), 725 (s), 708 (s), 655 (m), 625 (m), 554 (m) cm^{-1} . EA calcd. for $\text{C}_5\text{H}_8\text{N}_8\text{O}_6$ (276.17 g mol^{-1}): C 21.75, N 40.58, H 2.92%; found: C 21.79, N 40.77, H 2.85%; IS: 3 J; FS: 15 N.

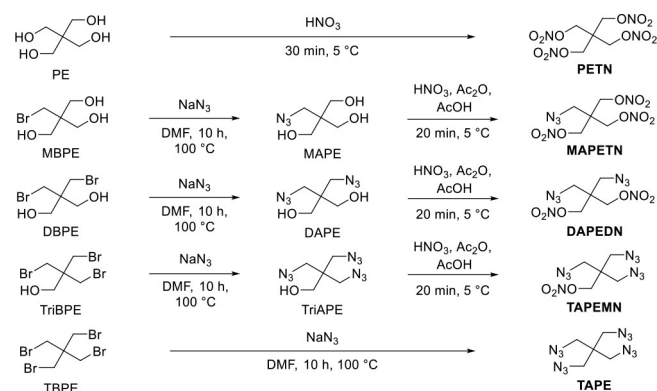
2.5 Triazidopentaerythritol Mononitrate (TAPEMN)

Following the general procedure, 3-azido-2,2-bis (azidomethyl)propan-1-ol (0.50 g, 2.4 mmol), acetic acid anhydride (7.5 mL), glacial acetic acid (1.5 mL), nitric acid (1.5 mL) were used. After addition to water the precipitating solid was extracted with dichloromethane ($\times 3$) and residues of acid were neutralized with sodium bicarbonate. The solvent was dried over MgSO_4 , filtered and evaporated to dryness, yielding TAPETN (0.50 g, 1.9 mmol, 82%) as a yellowish liquid. DTA (5 K min^{-1}): -24°C (endo), 180°C (dec.). $^1\text{H NMR}$ ($\text{DMSO-}d_6$, 400 MHz, ppm): $\delta = 4.49$ (s, 2H), 3.50 (s, 6H). $^{13}\text{C NMR}$ ($\text{DMSO-}d_6$, 100 MHz, ppm): $\delta = 72.2$, 51.3, 42.9. $^{14}\text{N NMR}$ ($\text{DMSO-}d_6$, 29 MHz, ppm): $\delta = -42$, -134 , -173 . FT-IR (ATR): $\tilde{\nu} = 2938$ (w), 2874 (vw), 2094 (vs), 1635 (s), 1451 (m), 1365 (w), 1273 (vs), 1009 (m), 847 (s), 754 (m), 708 (m), 644 (m), 601 (w), 552 (m) cm^{-1} . EA calcd. for $\text{C}_5\text{H}_8\text{N}_{10}\text{O}_3$ (256.19 g mol^{-1}): C 23.44, N 54.68, H 3.15%; found: C 23.90, N 55.51, H 2.92%; IS: < 1 J; FS: 80 N.

3 Results and Discussion

3.1 Synthesis

An overview of the synthesis is given in Scheme 1. On an industrial scale, PETN is synthesized from the corresponding alcohol by nitration with white fuming nitric acid. The pentaerythritol scaffold can be brominated with hydrogen bromide to the solid mono (MBPE) [10], di (DBPE) [11], and tri (TriBPE) [12] or by treatment with phenyl chloride and sodium bromide to the tetrabromide (TBPE) [13]. In this work, the bromide functionality was replaced by an azide functionality through exchange with sodium azide to prepare MAPE, DAPE, TriAPE, TAPE in good yields. The resulting azido alcohols were then converted to the corresponding nitrate esters. It was observed, that for the synthesis of MAPETN with nitric acid, mixtures of PETN and the desired azido nitrate were yielded. A more selective nitrate for-



Scheme 1. Synthesis of azido and nitrate derivatives of pentaerythritol (PE).

mation with acetyl nitrate leads the wanted azido nitrates MAPETN, DAPEDN, and TAPEMN in good yields.

All azido nitrates were analyzed by ^1H , ^{13}C , and ^{14}N NMR in $\text{DMSO-}d_6$. The chemical shift of protons next to the nitrate is decreasing stepwise from PETN with 4.70 ppm to TAPEMN with 4.49 ppm. The shifts of the protons next to azide are decreasing from MAPETN 3.69 to TAPE 3.40 ppm. In the carbon NMR increasing shifts for the centered carbon from PETN 40.8 ppm to TAPE 43.6 ppm are observed. The nitrate bound carbons show the same trend from PETN 70.3 to TAPEMN 72.2 ppm. This is also the case for shifts of azide bound carbons from MAPETN 50.1 to 51.7 ppm for TAPE. The ^{14}N shifts of the nitrates can be observed in the region of -45 ppm. The β nitrogen of the azide was observed at about -135 and in some cases the γ nitrogen shows in the range of -175 ppm. The ^{15}N NMR of MAPETN in $\text{DMSO-}d_6$ (Figure 2) shows four resonances for nitrogen, one of the nitrates and three of the azide. The chemical shift for nitrate is observed at -43.8 ppm, which is typical for primary organic nitrates. The nitrogen of the azide can be found at -134.5 , -172.0 , and -317.1 ppm, typical shifts for azide.

3.2 Crystallographic Data

The crystal structures of PETN and TAPE are known to literature. Crystals of MAPETN and DAPEDN and TAPE were obtained by evaporation of the extraction solvent. On the crystals of MAPETN and DAPEDN and TAPE, low-temperature single-crystal X-ray diffraction experiments were performed. TAPE was measured at low temperature to decrease the rotation of the azide functionality. TAPEMN shows to be solid below -24°C but all efforts to obtain a crystal structure failed. Both highly symmetric molecules, PETN with $P4_2/c$ and TAPE with $I4_1/a$ crystallize in tetragonal space groups. The azido-nitrates MAPETN and DAPEDN crystallize in the orthorhombic space group $Pbcn$. The room

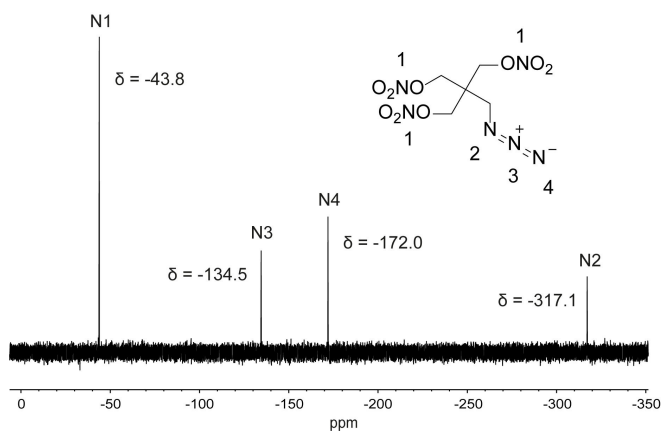


Figure 2. ^{15}N NMR of MAPETN in $\text{DMSO-}d_6$. N3 is identified through ^{14}N NMR in advance.

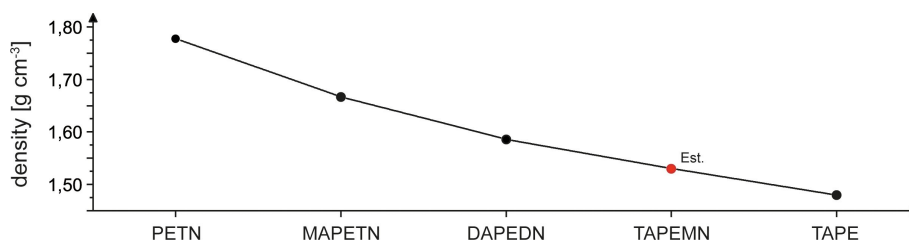


Figure 3. Room temperature densities of the azido-nitrates.

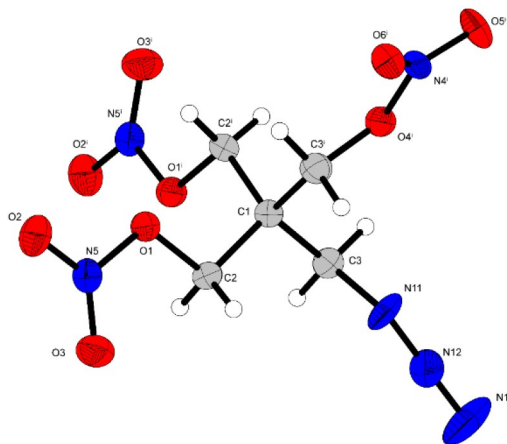


Figure 4. Molecular structure (thermal ellipsoids represent 50% probability) of MAPETN. Selected bond lengths [Å] and angles [°]: C1-C2 1.527(2), O1-C2 1.448(2), O1-N5 1.393(2), O2-N5 1.195(2), O3-N5 1.209(2), C1-C3 1.528(2), C3-N11 1.548(13), N11-N12 1.241(17), N12-N13, 1.090(17), O1-C2-C1 106.74(13), O2-N5-O1, 113.62(13), C1-C3-N11 104.0(5), N12-N11-C3 113.9(11), N13-N12-N11 169.2(14).

temperature densities were calculated from the crystal structure densities and it shows, that a linear decrease in density is taking place. (Figure 3) PETN shows the highest density with 1.778 g cm^{-3} followed by MAPETN with 1.667 g cm^{-3} . DAPEDN shows a slightly lower density of 1.586 g cm^{-3} and the TAPE has the lowest density with 1.480 g cm^{-3} . The density of TAPEMN is estimated to follow the trend and should therefore be in the area of 1.53 g cm^{-3} .

Intramolecular distances and torsion angles are given underneath the Figures 4–6. Bond length and torsion angles of all compounds are similar to the already discussed and reported PETN [14] or TAPE [15]. For MAPETN a disorder in the structure is observed. For every other molecule the azide and nitrate functionality at C3 changes position. Therefore, an azide and nitrate are bound to the C3 and C3' at 50% each. For simplicity, only the nitrate group at C3' and the azide group at C3 is represented in Figure 4.

MAPETN shows stabilizing intermolecular interactions of O2...H 2.51 Å, O6...H 2.45 Å and O5-H 2.48 Å. Furthermore,

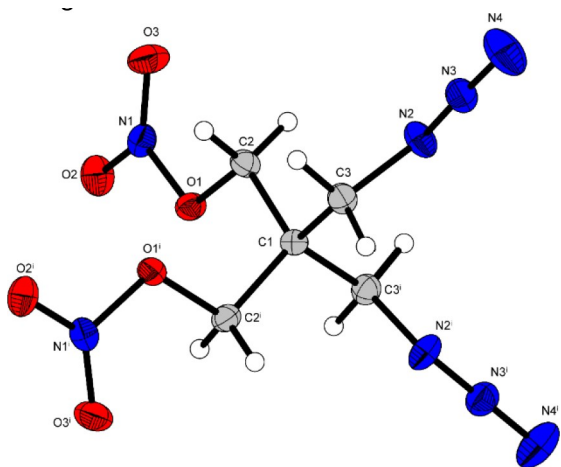


Figure 5. Molecular structure (thermal ellipsoids represent 50% probability) of DAPEDN. Selected bond lengths [Å] and angles [°]: C1-C2 1.524(2), O1-C2 1.449(2), O1-N1 1.399(2), O2-N1 1.201(2), O3-N1 1.205(2), C1-C3 1.532(2), N2-C3 1.480(2), N3-N2 1.236(2), N3-N4 1.126(2), O1-C2-C1 106.93(10), N1-O1-C2 112.52(10), O2-N1-O1 112.97(11), N2-C3-C1 108.05(10), N3-N2-C3 114.07(12), N4-N3-N2 172.75(16).

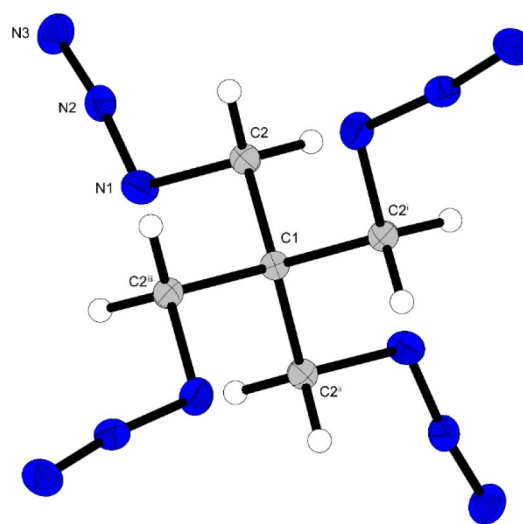


Figure 6. Molecular structure (thermal ellipsoids represent 50% probability) of TAPE. Selected bond lengths [Å] and angles [°]: C1-C2 1.529(1), N1-C2 1.487(1), N2-N1 1.233(1), N2-N3 1.133(1), N1-C2-C1 109.07(7), N2-N1-C2 114.62(8), N3-N2-N1 173.02(10).

the N1...H interaction with 2.46 Å is stabilizing intermolecular.

For DAPEDN the nitrate oxygen O2 shows attractive interactions with distances of O2...H 2.45 Å. The O3...H distance with 2.75 Å is much less attractive. The nitrogen N4 is interacting with hydrogen bound at C2. These N...H interactions with 2.65 Å are in the area of the added van der Waals radii ($VdW_{N+H} = 2.65$ Å).

In the structure of the tetraazide TAPE interactions of the two polarized azide nitrogen atoms, N1 and N3 with hydrogen are observed. The distance N...H 2.86 Å is longer than the sum of the van der Waals radii of N...H and longer than in DAPEDN.

3.3 Hirshfeld Analysis

Hirshfeld surfaces of PETN, DAPEDN, and TAPE were generated and their Fingerprint plots were calculated (Figure 7). The distance of interactions can be calculated by the addition of the distance d_e and d_i . Therefore, points in the lower left region represent close interactions. The percentage of the different interactions is visualized in the bar dia-

gram below [16]. MAPETN shows a disorder of the nitrate and azide positions, so a Hirshfeld analysis could not be performed.

PETN shows the most stabilizing and relatively close attractive O...H interactions. These stabilizing interactions are decreasing in number for the higher nitrogen content derivatives, up to an extreme for TAPE where no O...H interactions are possible. The decrease of O...H interactions goes along with an increase in less attractive N...H interactions. These interactions are stabilizing for DAPEDN because of their relatively short distance. For TAPE the distance of N...H interactions increases and the stabilization is therefore less. The decrease of stabilizing interaction agrees with the increasing sensitivity. Attractive interactions are decreasing from PETN to DAPEDN to TAPE.

Destabilizing effects in the crystal structure are O...O, N...N, O...N, or H...H repulsive interactions. PETN shows a high amount of relatively close O...O repulsion. For DAPEDN relatively close O...O and O...N repulsions are found. TAPE shows weak repulsive N...N interactions but very strong H...H repulsion. The hydrogen repulsion is very close and therefore very destabilizing. The repulsive effects are in-

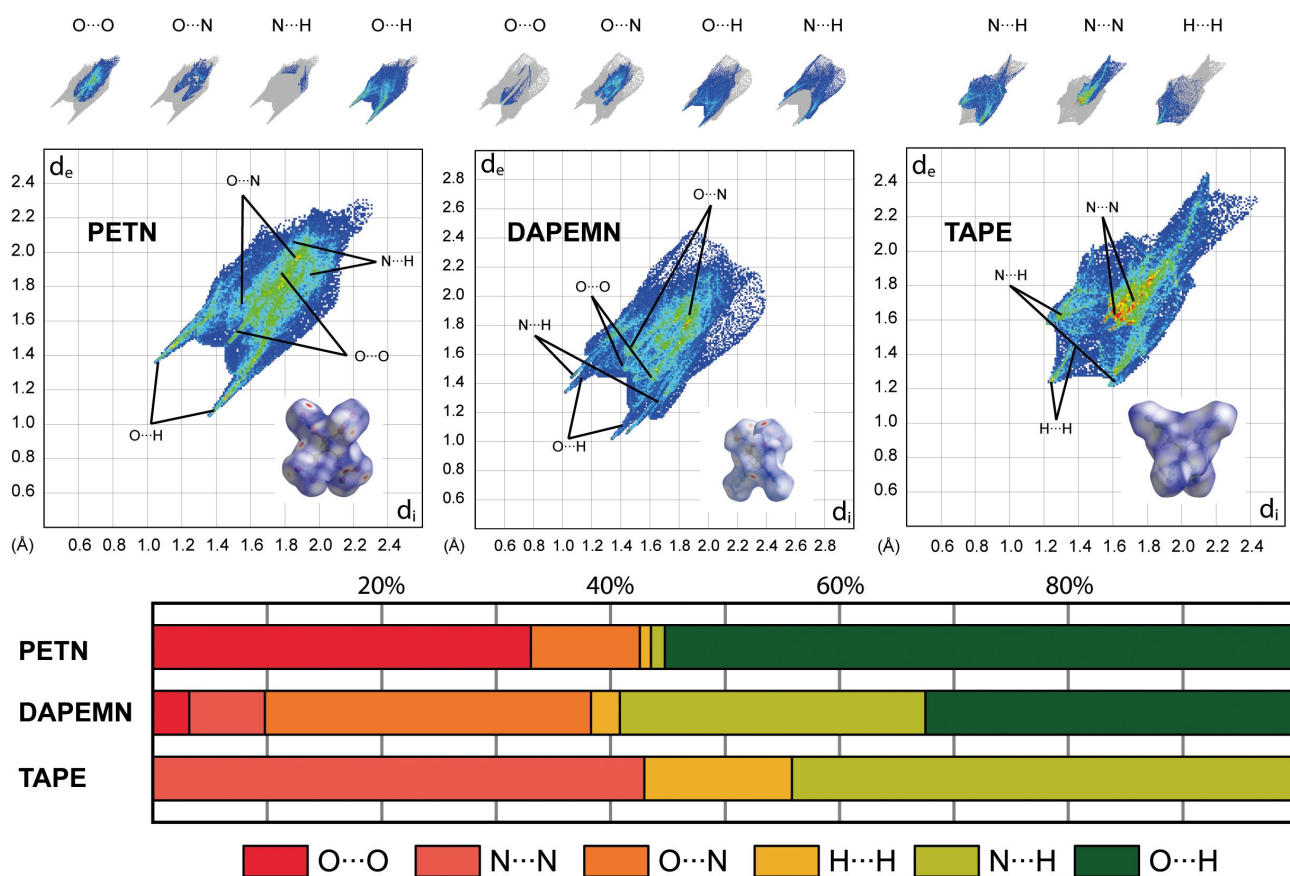


Figure 7. Two-dimensional fingerprint plots of PETN, DAPEDN, and TAPE together with their Hirshfeld surfaces. The atomic contacts percentage contribution to the Hirshfeld surface can be obtained from the bar chart.

creasing from PETN to DAPEDN to TAPE, which is also associated with the increasing sensitivity.

Hirshfeld analysis clearly shows that the derivatives containing nitrates show very stabilizing O...H interactions that compensate for the repulsive O...O, O...N interactions. For the high nitrogen-containing derivatives, O...H is replaced by weaker N...H stabilization, and repulsion is caused by

close H...H contacts. The Hirshfeld analysis agrees with the increasing sensitivity towards TAPE.

3.4 Physicochemical Properties

3.4.1 Thermal Analysis

The thermal behavior was investigated by differential thermal analysis (DTA), hotplate, and hot needle test. TAPEMN was also analyzed by low-temperature DSC as it shows a melting point of -24°C . The DTA curves of the five investigated compounds are shown in Figure 8. The tetraazide is the most thermally stable compound with a decomposition at 218°C . All compounds with a nitrate functionality decompose at about 180°C like PETN. Remarkable is that, from PETN to TAPEMN, the melting point decreases gradually by $50\text{--}60^\circ\text{C}$ with each azide exchanged, starting from PETN with 143°C to TAPEMN with -24°C (Table 1). The asymmetric triazide shows the lowest melting point due to the disturbed crystal packing. The highly symmetric TAPE is melting at 44°C and not following the trend. This stability is a consequence of the high symmetry within the crystal. With a melting point of 82°C and a decomposition point of 180°C , MAPETN is a melt cast explosive, melting in the area of TNT and decomposing about 100°C earlier [1c].

Upon fast heating on a hot plate (HP), the nitrate rich PETN and MAPETN are deflagrating. The more nitrogen-rich compounds DAPEDN, TAPEMN, and TAPE are detonating violently on the hot plate.

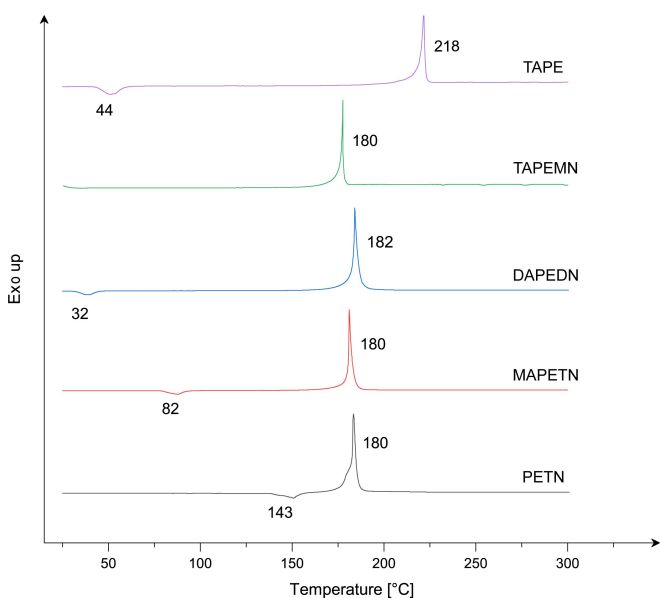


Figure 8. DTA plot of all analyzed pentaerythritol azido-nitrates at a heating rate of 5 Kmin^{-1} .

Table 1. Physicochemical properties of PETN, MAPETN, DAPEDN, TAPEMN, TAPE, $\text{Pb}(\text{N}_3)_2$, RDX.

	PETN	MAPETN	DAPEDN	TAPEMN	TAPE	$\text{Pb}(\text{N}_3)_2$ [1c]	RDX [1c]
Formula	$\text{C}_5\text{H}_8\text{N}_4\text{O}_9$	$\text{C}_5\text{H}_8\text{N}_6\text{O}_9$	$\text{C}_5\text{H}_8\text{N}_8\text{O}_6$	$\text{C}_5\text{H}_8\text{N}_{10}\text{O}_3$	$\text{C}_5\text{H}_8\text{N}_{12}$	PbN_6	$\text{C}_3\text{H}_6\text{N}_6\text{O}_6$
M [g mol^{-1}]	316.14	296.15	276.06	256.19	236.20	291.24	222.12
IS [J] ^[a]	3.5	2.0	3.0	1	< 1	2.5–4	7.5
FS [N] ^[b]	54	36	15	80	1	0.1–1	120
N [%] ^[c]	17.7	28.4	40.6	54.7	71.2	28.86	37.84
Ω [%] ^[d]	−10.1	−27.0	−46.4	−68.7	−94.8	−	−21.61
T_{melt} [$^\circ\text{C}$] ^[e]	143	82	32	−24	44	−	−
T_{dec} [$^\circ\text{C}$] ^[f]	180	180	182	175	218	320–360	210
Density (298 K) [g cm^{-3}] ^[g]	1.778	1.667	1.586	1.53 ^{Est.}	1.480	4.71	1.800
$\Delta_f H_m^\circ$ [kJ mol^{-1}] ^[h]	−484	−59	362	795	1180	−	31
<i>Detonation parameters calculated with EXPLO5V6.05</i>							
$-\Delta_f U^\circ$ [kJ kg^{-1}] ^[i]	6166	5702	5532	5427	5074	1639	5740
T_E [K] ^[j]	4038	3849	3747	3588	3213	−	3745
p_{C-J} [GPa] ^[k]	31.3	27.8	24.2	21.2	20.5	−	33.6
D [m s^{-1}] ^[l]	8471	8092	7842	7740	7819	5180	8801
Gas vol. [L kg^{-1}] ^[m]	744	771	809	820	799	308	711

[a] Impact sensitivity (BAM Drophammer, 1 of 6), [b] Friction sensitivity (BAM friction tester, 1 of 6), [c] Nitrogen content, [d] Oxygen balance towards CO_2 ,

[e] Melting point from DTA (5 Kmin^{-1} , onset), [f] Decomposition temperature from DTA (5 Kmin^{-1} , onset), [g] Calculated density from low temperature X-ray diffraction,

[h] Calculated (CBS-4M) heat of formation, [i] Heat of explosion, [j] Explosion temperature, [k] Detonation pressure, [l] Detonation velocity, [m] Volume of detonation gases (assuming only gaseous products).

As the hotplate test shows the reaction of an unconfined sample against heating, the hot needle (HN) test is performed on substances fixed and confined with adhesive tape. The contact of a red glowing hot needle causes decomposition of PETN and MAPETN, whereas DAPEDN shows fast deflagration. TAPEMN and TAPE are violently detonating.

3.4.2 Sensitivities and Energetic Properties

Impact and friction sensitivities were determined according to the "UN declaration of dangerous goods" on a BAM Drophammer and a BAM Friction Tester (Figure 9). The basis for a positive test is at least one explosion in six tests. This result is additionally supported by six negative tests with lower energy [17].

A strong increase in the impact sensitivity is observed towards TAPE. The tetranitrate PETN shows an explosion when hit with 3.5 J energy. The monoazide MAPETN shows, as expected, an increased sensitivity of 2 J. Whereas DAPEDN, 3 J, shows a slightly lower impact sensitivity than PETN but higher sensitivity than MAPETN. This unexpected jump in sensitivity can be explained by morphology effects or a consequence of the measurement of probabilities. The liquid TAPEMN shows an impact sensitivity of < 1 J just like the solid TAPE. In short, the impact sensitivity increases with slight jumps from PETN to TAPE. As a liquid TAPEMN is like nitroglycerine highly sensitive to impact < 1 J.

The sensitivity to friction shows a continuous progression to TAPE, except for liquid TAPEMN. For PETN cracking can be observed at 54 N. For the solid azides, heavy detonations are observed at the lower detonation limit. The friction sensitivities are decreasing from 36 N for MAPETN to 15 N for DAPEDN to 1 N for TAPE. With 80 N explosion limit, TAPEMN is the least friction sensitive compound of all derivatives. In short, the friction sensitivity increases from PETN to TAPE, except for less sensitive TAPEMN. The melt-castable explosive MAPETN (2 J, 36 N) shows higher sensitivity than TNT (15 J, 360 N) [1c].

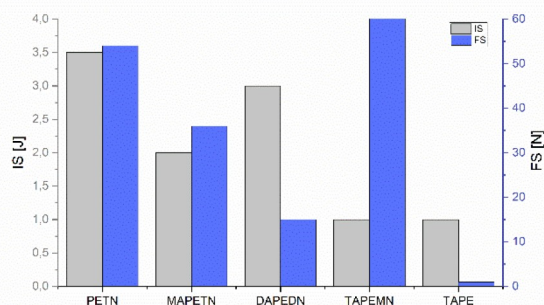


Figure 9. Bar chart of the impact (grey) and friction (blue) sensitivities of the investigated compounds.

The heats of formation were calculated using the atomization method (using Gaussian CBS-4M electronic enthalpies) and the detonation parameters were calculated using the EXPLO5 V6.05 code [18]. (Details of the calculations can be found in the supporting information). For PETN a low heat of formation of -484 kJ mol^{-1} is calculated by this method. Exchange of nitrate with azide causes a stepwise increase in heat of formation (app. 425 kJ per $-\text{ONO}_2 / -\text{N}_3$ exchange) up to TAPE with 1180 kJ mol^{-1} .

PETN shows the best detonation parameters of all investigated compounds, with a detonation velocity of 8.5 km s^{-1} and a pressure of 31.3 GPa. As the density decreases, velocity and pressure also decrease to TAPE with a velocity of 7.8 km s^{-1} and a pressure of 20.5 GPa. The decrease in the performance can be explained due to the decrease in the density of the materials, but as the heat of formation goes up towards TAPE the negative effect of the lower densities is compensated to a certain degree.

As TAPE possesses high thermal stability and a sensitivity typical for primary explosives, classical initiation capability tests were performed. A 200 mg load of PETN was pressed into a copper shell and initiated by 50 mg of its tetraazide derivative TAPE. The result of the experiment is shown in Figure 10 where it is clearly visible that PETN was initiated. As TAPE is melting at 44°C it cannot be easily used as a replacement for the typical initiating primary explosive lead azide. Nevertheless, this experiment shows that organic azides are possible replacements for common initiating explosives. The test failed for the less sensitive DAPEDN therefore the less sensitive compounds were not tested. TAPEMN was not tested as it is a liquid at room temperature.



Figure 10. Positive initiation capability test of TAPE on PETN.

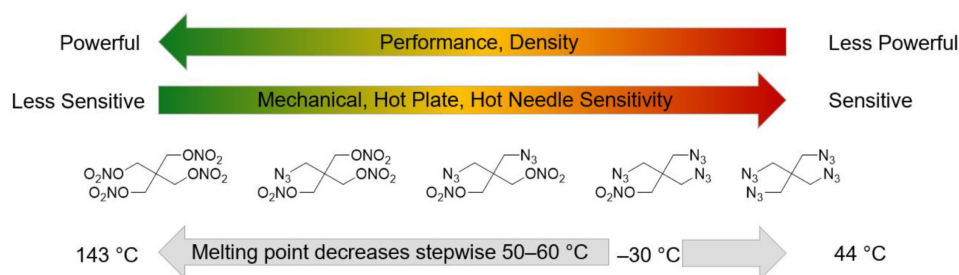


Figure 11. Overview of the properties of the synthesized compounds.

4 Conclusion

Azide and nitrate derivatives of pentaerythritol were synthesized in good yields by azide exchange of the corresponding bromate derivatives, followed by nitration with in-situ generated acetyl nitrate. The properties of the pure compounds were investigated and compared (Figure 11). The mechanical sensitivities are increasing from PETN to TAPE. Only the liquid TAPEMN is less friction sensitive than PETN. The sensitivities are also successfully explained by Hirshfeld analysis. A stepwise decrease of the melting point is observed from PETN to TAPEMN. Every azide exchanged causes a drop of 50–60 °C. The thermal stability of the organic nitrates is limited by 180 °C whereas the tetraazide is stable up to 218 °C.

With a melting point of 82 °C and a detonation velocity of 8.1 km s⁻¹ MAPETN is a high performing melt cast explosive, but the high sensitivity compared to TNT rules it out as a drop-in replacement. The tetraazide is capable to initiate PETN but shows to be liquid above 44 °C which makes it difficult to handle in practice. The calculated performance of the azido derivatives is lower than that of PETN, because of the lower densities and oxygen balance. However, the study shows that carbon bonded azides are possible candidates as new initiating or melt cast explosives, although in this case, the thermal or mechanical properties are not sufficient.

Acknowledgements

For financial support of this work by Ludwig-Maximilian University (LMU), the Office of Naval Research (ONR) under grant no. ONR N00014-19-1-2078 and the Strategic Environmental Research and Development Program (SERDP) under contract no. W912HQ19C0033 are gratefully acknowledged. Further thanks to Prof. Dr. Konstantin Karaghiosoff for the measurement of the ¹⁵N NMR and two dimensional ¹H-¹⁵N HMBC NMR spectra. Open access funding enabled and organized by Projekt DEAL.

Data Availability Statement

No data available.

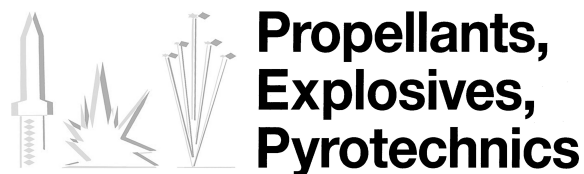
References

- a) J. Köhler, D. R. Meyer, D. I. A. Homburg, *Explosivstoffe*, Tenth Edition, **2008**; b) E. Berlow, R. H. Barth, J. E. Snow, *The Pentaerythritols*, Reinhold Publishing Corporation, New York, **1958**; c) T. M. Klapötke, *Energetic Materials Encyclopedia*, **2018**; d) T. M. Klapötke, *Chemistry of High-Energy Materials*, De Gruyter, Berlin/Boston, **2017**; e) W. P. Walters, J. A. Zukas, *Explosive Effects and Applications*, Springer, New York, **1998**.
- Y.-H. Joo, J. M. Shreeve, Polynitramino compounds outperform PETN, *Chem. Commun.* **2010**, *46*, 142–144.
- M. A. Hiskey, M. J. Hatch, J. C. Oxley, Nitrate Amine Nitrates: Nitrate ester explosives with reduced impact sensitivity, *Propellants Explos. Pyrotech.* **1991**, *16*, 40–42.
- V. W. Manner, M. J. Cawkwell, E. M. Kober, T. W. Myers, G. W. Brown, H. Tian, C. J. Snyder, R. Perriot, D. N. Preston, Examining the chemical and structural properties that influence the sensitivity of energetic nitrate esters, *Chem. Sci.* **2018**, *9*, 3649–3663.
- Q. J. Axthammer, B. Krumm, T. M. Klapötke, Synthesis of Energetic Nitrocarbamates from Polynitro Alcohols and Their Potential as High Energetic Oxidizers, *Eur. J. Org. Chem.* **2015**, *4*, 723–729.
- T. M. Klapötke, B. Krumm, R. Ilg, D. Trögel, R. Tacke, The Sila-Explosives Si(CH₂N₃)₄ and Si(CH₂ONO₂)₄: Silicon Analogues of the Common Explosives Pentaerythrityl Tetraazide, C(CH₂N₃)₄, and Pentaerythritol Tetranitrate, C(CH₂ONO₂)₄, *J. Am. Chem. Soc.* **2007**, *129*, 6908–6915.
- E. R. Wilson, M. B. Frankel, Synthesis of novel energetic compounds. 7. Azido derivatives of pentaerythritol, *J. Org. Chem.* **1985**, *50*, 3211–3212.
- Y. Ou, B. Chen, H. Yan, H. Jia, J. Li, S. Dong, Development of energetic additives for propellants in China, *J. Propul. Power* **1995**, *11*, 838–847.
- W. Hayes, H. M. I. Osborn, S. D. Osborne, R. A. Rastall, B. Romagnoli, One-pot synthesis of multivalent arrays of mannose mono- and disaccharides, *Tetrahedron* **2003**, *59*, 7983–7996.
- S. Wawzonek, A. Matar, C. H. Issidorides, Monobromopentaerythritol, *Org. Synth.* **1958**, *38*, 68–70.
- S. Hussain, *Process for preparing brominated pentaerythritols*, US Patent 4,929,775, Ethyl Corp., USA **1990**.
- Y. Takasu, M. Yoshimitsu, T. Kagawa, H. Shuyama, *Manufacture of tribromoneopentyl alcohol*, JP Patent 07165645, Tosoh Corp, **1995**.
- H. L. Herzog, PENTAERYTHRITYL TETRABROMIDE, *Org. Synth.* **1951**, *31*, 82.
- E. A. Zhurova, A. I. Stash, V. G. Tsirelson, V. V. Zhurov, E. V. Bartashevich, V. A. Potemkin, A. A. Pinkerton, Atoms-in-Molecules Study of Intra- and Intermolecular Bonding in the Pentaery-

About the Azido Derivatives of Pentaerythritol Tetranitrate

- thritol Tetranitrate Crystal, *J. Am. Chem. Soc.* **2006**, *128*, 14728–14734.
- [15] K. A. Lyssenko, Y. V. Nelubina, D. V. Safronov, O. I. Haustova, R. G. Kostyanovsky, D. A. Lenev, M. Y. Antipin, Intermolecular N3...N3 interactions in the crystal of pentaerythrityl tetraazide, *Mendeleev Commun.* **2005**, *15*, 232–234.
- [16] M. A. Spackman, D. Jayatilaka, *Hirshfeld surface analysis, CrystEngComm.* **2009**, *11*, 19–32.
- [17] UN, Recommendations on the Transport of Dangerous Goods – Manual of Tests and Criteria – Fifth revised edition, ST/SG/AC.10/11/Rev.5, **2009**.
- [18] M. Sućeska, EXPLOS Version 6.05.02 **2018**, Zagreb.

Manuscript received: October 6, 2020
Revised manuscript received: January 4, 2021
Version of record online: February 19, 2021



Supporting Information

About the Azido Derivatives of Pentaerythritol Tetranitrate

Tobias Lenz, Thomas M. Klapötke,* Moritz Mühlemann, and Jörg Stierstorfer© 2021 The Authors. Propellants, Explosives, Pyrotechnics published by Wiley-VCH GmbH. This is an open access article under the terms of the Creative Commons Attribution License, which permits use, distribution and reproduction in any medium, provided the original work is properly cited.

About the Azido Derivatives of Pentaerythritol Tetranitrate

Tobias Lenz,^[a] Thomas M. Klapötke,^{*[a]} Moritz Mühlemann,^{**[b]} Jörg Stierstorfer^[a]

[a] T. Lenz, J. Stierstorfer, T. M. Klapötke, Department of Chemistry, Energetic Materials Research, Ludwig Maximilian University of Munich, Butenandtstr. 5-13, 81377 Munich Germany, *e-mail: tmk@cup.uni-muenchen.de

[b] M. Mühlemann, BIAZZI SA, Chemin de la Tavallaz 25, CH-1816 Chailly/Montreux Switzerland

Supporting Information

Contents

Experimental	2
Xray Diffraction.....	4
Theoretical Calculations	7
Hot Plate Test	8
Hot Needle Test	9

1. Experimental

General: ^1H , ^{13}C , ^{14}N and ^{15}N NMR spectra were recorded on JEOL 270 and BRUKER AMX 400 instruments. The samples were measured at room temperature in standard NMR tubes (\varnothing 5 mm). Chemical shifts are reported as δ values in ppm relative to the residual solvent peaks of $[\text{D}_6]\text{DMSO}$ (δ_{H} : 2.50, δ_{C} : 39.5). Solvent residual signals and chemical shifts for NMR solvents were referenced against tetramethylsilane (TMS, $\delta = 0$ ppm) and nitromethane. Unless stated otherwise, coupling constants were reported in Hertz (Hz) and for the characterization of the observed signal multiplicities the following abbreviations were used: s (singlet), m (multiplet) and br (broad). Mass spectra were recorded on a JEOL MStation JMS700 using the EI. Infrared spectra (IR) were recorded from 4000 cm^{-1} to 400 cm^{-1} on a PERKIN ELMER Spectrum BX-59343 instrument with a SMITHS DETECTION DuraSampIR II Diamond ATR sensor. The absorption bands are reported in wave-numbers (cm^{-1}). Decomposition temperatures were measured via differential thermal analysis (DTA) with an OZM Research DTA 552-Ex instrument at a heating rate of $5\text{ K}\cdot\text{min}^{-1}$ and in a range of room temperature to $400\text{ }^\circ\text{C}$. All sensitivities toward impact (IS) and friction (FS) were determined according to BAM (German: Bundesanstalt für Materialforschung und Prüfung) standards using a BAM drop hammer and a BAM friction apparatus by applying the 1 of 6 method. **CAUTION!** All investigated azido and nitrate compounds are potentially explosive materials, although no hazards were observed during preparation and handling these compounds. Nevertheless, safety precautions (such as wearing leather coat, face shield, Kevlar sleeves, Kevlar gloves, earthed equipment and ear plugs) should be drawn especially when manipulating dry material.

Monobromopentaerythritol was synthesized according to literature by bromination of pentaerythritol. Dibromopentaerythritol and tetrabromopentaerythritol were purchased by Merck, tribromopentaerythritol was purchased by TCI.

Typical azide exchange TP1

To a solution of the bromide compound (1 eq.) in DMF, sodium azide (monoazide 2 eq., diazide 3 eq., triazide 4 eq, tetraazide 10 eq.) was added. The mixture was heated 10 h at $100\text{ }^\circ\text{C}$. The completion of the reaction was checked by TLC. Then the solvent was evaporated under reduced pressure.

2-(Azidomethyl)-2-(hydroxymethyl)propane-1,3-diol (MAPE)

Following TP1, 2-(bromomethyl)-2-(hydroxymethyl)propane-1,3-diol (2.00 g, 10 mmol), DMF (40 mL), sodium azide (1.30 g, 20 mmol) was used. Water was added to the residue and then the mixture was extracted with ethyl acetate (15x). The solvent was dried over MgSO_4 and evaporated. After removal of DMF under high vacuum monoazidopentaerythritol (1.37 g, 8.5 mmol, 85%) was yielded. $^1\text{H NMR}$ (DMSO-d_6 , 400 MHz, ppm): $\delta = 4.41$ (t, $J = 5.2$ Hz, 3H), 3.30 (d, $J = 5.2$ Hz, 6H), 3.28 (s, 2H). $^{13}\text{C NMR}$ (DMSO-d_6 , 100 MHz, ppm): $\delta = 60.2$, 51.1, 45.8. $^{14}\text{N NMR}$ (DMSO-d_6 , 29 MHz, ppm): $\delta = -133$, -278; m/z (ESI⁻): (anion). **FT-IR** (ATR): $\tilde{\nu} = 3276$ (m), 2935 (m), 2890 (m), 2098 (vs), 1483 (m), 1463 (m), 1380 (m), 1369 (m), 1272 (m), 1252 (m), 1146 (m), 1024 (vs), 952 (m), 916 (m), 892 (m), 876 (m), 778 (m), 647 (s), 594 (s), 555 (s), 501 (m) cm^{-1} . **EA** calcd. for $\text{C}_5\text{H}_{11}\text{N}_3\text{O}_3$ (161.16 g/mol^{-1}): C 37.26, N 26.07, H 6.88%; found: C 37.28, N 24.69, H 6.57%.

2,2-Bis(azidomethyl)propane-1,3-diol (DAPE)

Following TP1, 2,2-Bis(bromomethyl)-1,3-propanediol (2.50 g, 9.5 mmol), DMF (30 mL), sodium azide (1.85 g, 28.5 mmol) was used. Water was added to the residue and then the mixture was extracted with ethyl acetate (3x). The solvent was dried over MgSO_4 and evaporated to dryness, yielding diazidopentaerythritol (1.72 g, 9.2 mmol, 91%) as a yellowish liquid. $^1\text{H NMR}$ (DMSO-d_6 , 400 MHz, ppm): $\delta = 4.74$ (t, $J = 5.0$ Hz, 2H), 3.29 (s, 4H), 3.27 (d, $J = 5.0$ Hz, 4H). $^{13}\text{C NMR}$ (DMSO-d_6 , 100 MHz, ppm): $\delta = 60.2$, 51.6, 46.0. **FT-IR** (ATR): $\tilde{\nu} = 3353$ (w), 2166 (w), 2093 (vs), 1656 (m), 1448 (m), 1359 (w), 1274 (m), 1125 (w), 1036 (s), 924 (m), 887 (m), 662 (m), 552 (m),

479 (m), 423 (m), 413 (m), 409 (m) cm^{-1} . **EA** calcd. for $\text{C}_5\text{H}_{10}\text{N}_6\text{O}_2$ ($186.18 \text{ g/mol}^{-1}$): C 32.26, N 45.14, H 5.41%; found: C 32.44, N 42.82, H 5.59%; IS: >40 J. FS: 360 N.

3-Azido-2,2-bis(azidomethyl)propan-1-ol (TriAPE)

Following TP1, 3-Bromo-2,2-bis(bromomethyl)-1-propanol (1.25 g, 3.8 mmol), DMF (12 mL), sodium azide (0.97 g, 14.8 mmol) was used. Water was added to the residue and then the mixture was extracted with dichloromethane (3x). The solvent was dried over MgSO_4 , filtrated and evaporated to dryness, yielding triazidopentaerythritol (1.41 g, 6.7 mmol, 87%) as a yellowish liquid. **$^1\text{H NMR}$** (DMSO- d_6 , 400 MHz, ppm): $\delta = 5.05$ (t, $J = 4.9 \text{ Hz}$, 1H), 3.33 (s, 6H), 3.27 (d, $J = 5.0 \text{ Hz}$, 2H). **$^{13}\text{C NMR}$** (DMSO- d_6 , 100 MHz, ppm): $\delta = 59.9, 51.3, 44.7$. **FT-IR** (ATR): $\tilde{\nu} = 3397$ (w), 2937 (w), 2873 (w), 2089 (vs), 1449 (m), 1360 (w), 1284 (s), 1125 (w), 1042 (m), 888 (m), 648 (m), 552 (m), 454 (w), 414 (w) cm^{-1} . **EA** calcd. for $\text{C}_5\text{H}_9\text{N}_9\text{O}$ ($211.19 \text{ g/mol}^{-1}$): C 28.44, N 59.69, H 4.33%; found: C 28.61, N 60.00, H 4.08%; IS: <1 J. FS: 360 N.

Low Temperature DSC of TAPEMN

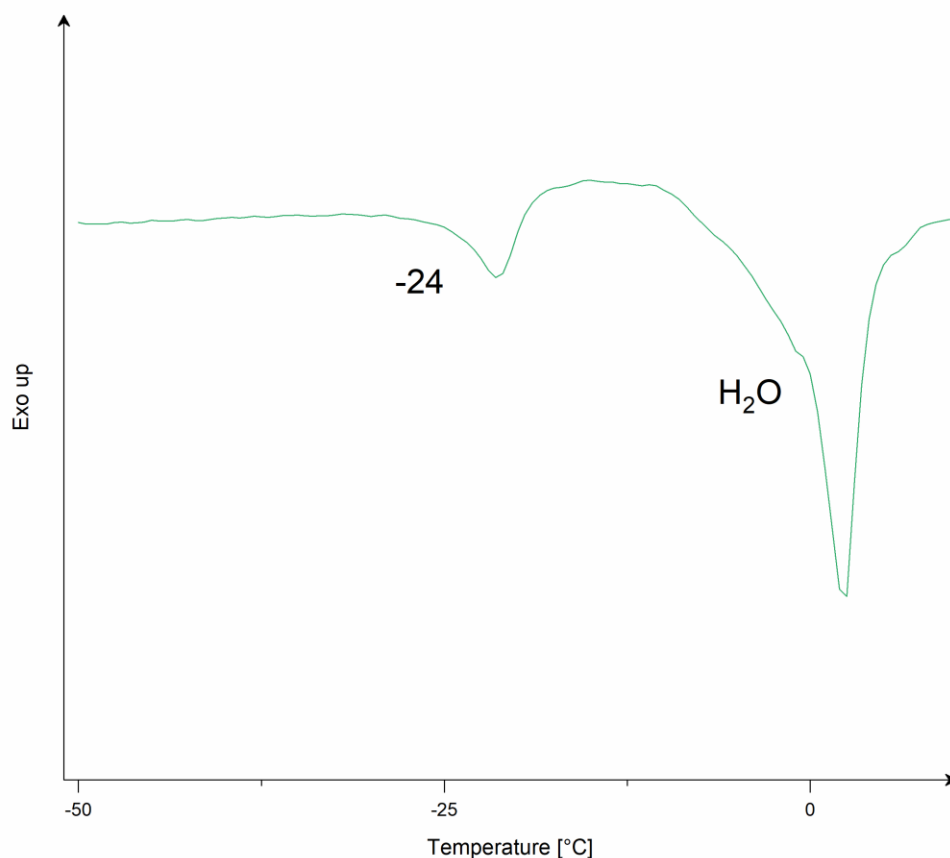


Figure S1 Low temperature DSC of TAPEMN with the melting point at $-24 \text{ }^\circ\text{C}$. (Water is condensed during measurement)

^1H - ^{15}N -HMBC NMR spectra of DAPEDN

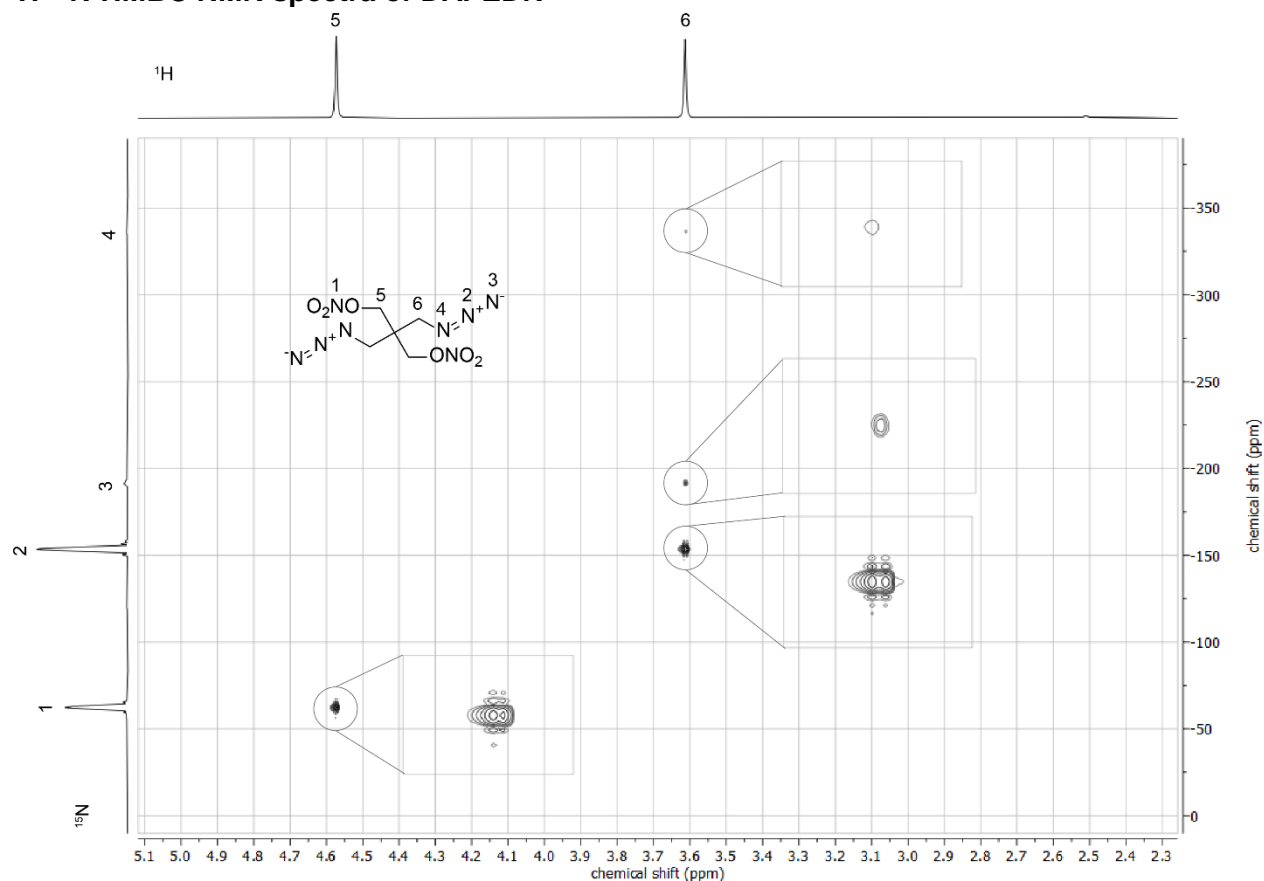


Figure S2 Two-dimensional ^1H - ^{15}N -HMBC NMR spectra of DAPEDN (DMSO- d_6 , 25 °C): $\delta = -62$ (N1), -153 (N2), -192 (N4), -337 ppm (N1).

2. Xray Diffraction

Crystal structure data were obtained by measurements on an Oxford Xcalibur3 diffractometer with a Spellman generator (voltage 50 kV, current 40 mA) and a Kappa CCD area for data collection using Mo-K α radiation ($\lambda = 0.71073 \text{ \AA}$) or a Bruker D8 Venture TXS diffractometer equipped with a multilayer monochromator, a Photon 2 detector and a rotation-anode generator (Mo-K α radiation). The data collection was performed using the CrysAlis RED software.ⁱ The solution of the structure was performed by direct methods and refined by full-matrix least-squares on F2 (SHELXT)ⁱⁱ implemented in the OLEX2ⁱⁱⁱ software suite. The non-hydrogen atoms were refined anisotropically and the hydrogen atoms were located and freely refined. The absorption correction was carried out by a SCALE3 ABSPACK multiscan method.^{iv} The DIAMOND2 plots shown with thermal ellipsoids at the 50% probability level and hydrogen atoms are shown as small spheres of arbitrary radius. The SADABS program embedded in the Bruker APEX3 software was used for multi-scan absorption corrections in all structures.^v

Within the synthesis of the final monoazidopentaerythritoltrinitrate, crystal structures of both intermediates, the monobromide MBPE and the monoazide MAPE were measured.

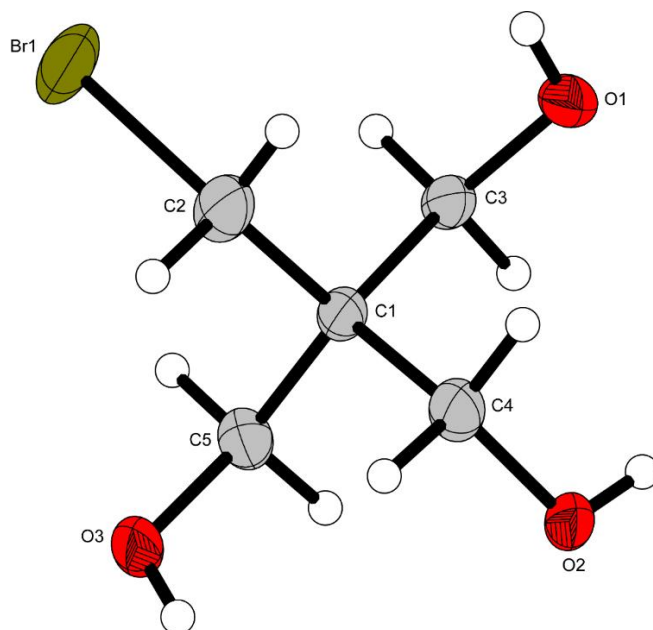


Figure S3 Molecular structure (thermal ellipsoids represent 50% probability) of monobromopentaerythritol MBPE.

MBPE crystallizes in the monoclinic space group with a cell volume of $1622.83(18) \text{ \AA}^3$ and two formula units per cell. The cell constants are $a = 11.7631(7) \text{ \AA}$, $b = 11.5732(8) \text{ \AA}$ and $c = 12.6667(6) \text{ \AA}$, while the density is 1.629 g cm^{-3} at 111 K.

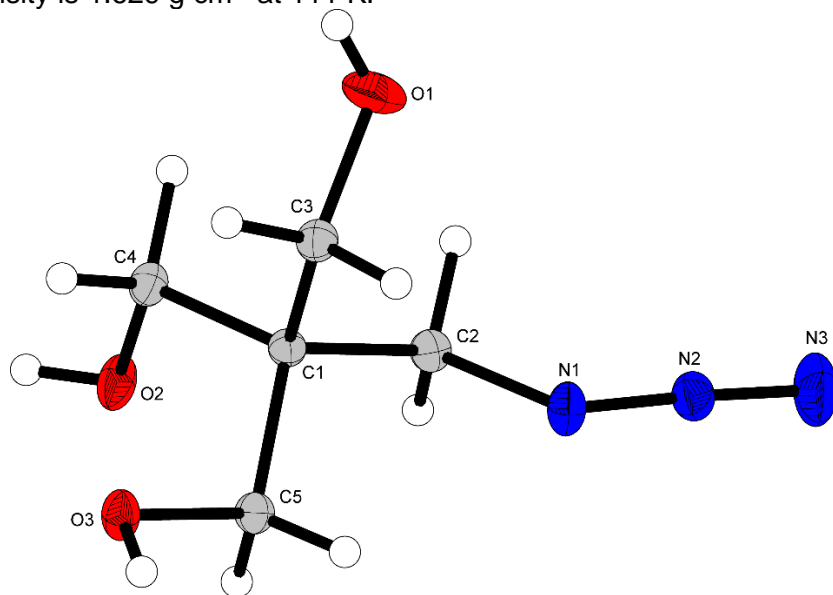


Figure S4 Molecular structure (thermal ellipsoids represent 50% probability) of monoazidopentaerythritol MAPE.

MAPE crystallizes in the monoclinic space group with a cell volume of $1149.55(13) \text{ \AA}^3$ and two formula units per cell. The cell constants are $a = 19.5775(12) \text{ \AA}$, $b = 9.5024(5) \text{ \AA}$ and $c = 8.3850(5) \text{ \AA}$, while the density is 1.410 g cm^{-3} at 124 K.

Table S1 Crystallographic data and structure refinement details for the prepared compounds.

	<i>MBPE</i>	<i>MAPE</i>	<i>MAPETN</i>
Formula	C ₅ H ₁₁ BrO ₃	C ₅ H ₁₁ N ₃ O ₃	C ₅ H ₈ N ₆ O ₉
FW [g mol ⁻¹]	199.05	161.17	296.17
Crystal system	monoclinic	monoclinic	orthorhombic
Space group	C2/c (No. 15)	C2/c (No. 15)	Pbcn (No. 60)
Color / Habit	colorless	colorless	colorless
Size [mm]	0.20 x 0.20 x 0.50	0.05 x 0.15 x 0.48	0.05 x 0.10 x 0.20
a [Å]	11.7631(7)	19.5775(12)	13.1388(9)
b [Å]	11.5732(8)	9.5024(5)	6.6452(4)
c [Å]	12.6667(6)	8.3850(5)	13.1663(9)
α [°]	90	90	90
β [°]	109.763(6)	103.311(6)	90
γ [°]	90	90	90
V [Å ³]	1622.83(18)	1517.98(16)	1149.55(13)
Z	8	8	4
ρ _{calc.} [g cm ⁻³]	1.629	1.410	1.711
μ [mm ⁻¹]	5.009	0.116	0.164
F(000)	800	688	608
λ _{MoKα} [Å]	0.71073	0.71073	0.71073
T [K]	111	124	123
θ Min-Max [°]	2.5, 26.4	2.1, 26.4	3.1, 26.3
Dataset	-14: 14 ; -14: 13 ; -15: 15	-23: 24 ; -11: 7 ; -10: 10	-15: 16 ; -8: 8 ; -16: 16
Reflections collected	4882	6010	8176
Independent refl.	1660	1555	1183
R _{int}	0.024	0.033	0.047
Observed reflections	1409	1258	898
Parameters	126	149	133
R ₁ (obs) ^[a]	0.0269	0.0403	0.0372
wR ₂ (all data) ^[b]	0.0632	0.1057	0.0913
S ^[c]	1.05	1.14	1.07
Resd. dens [e Å ⁻³]	-0.49, 0.47	-0.19, 0.33	-0.15, 0.27
Device type	Oxford Xcalibur3	Oxford Xcalibur3	Oxford Xcalibur3
Solution	SHELXT	SHELXT	SHELXT
Refinement	SHELXL-2018	SHELXL-2018	SHELXL-2018
Absorption correction	multi-scan	multi-scan	multi-scan
CCDC	2035689	2035690	2035691

^[a]R₁ = Σ||F_o|-|F_c||/Σ|F_o|; ^[b]wR₂ = [Σ[w(F_o²-F_c²)²]/Σ[w(F_o²)]^{1/2}; w = [σc²(F_o²)+(xP)²+yP]⁻¹ and P=(F_o²+2F_c²)/3; ^[c]S = {Σ[w(F_o²-F_c²)²]/(n-p)}^{1/2} (n = number of reflections; p = total number of parameters).

3. Theoretical Calculations

All calculations were carried out using the Gaussian G03W (revision B.03) program package.^{vi} The enthalpies (H) and free energies (G) were calculated using the complete basis set (CBS) method of Petersson and coworkers in order to obtain very accurate energies. The CBS models use the known asymptotic convergence of pair natural orbital expressions to extrapolate from calculations using a finite basis set to the estimated complete basis set limit. CBS-4 begins with a HF/3-21G(d) geometry optimization; the zero-point energy is computed at the same level. It then uses a large basis set SCF calculation as a base energy, and a MP2/6-31+G calculation with a CBS extrapolation to correct the energy through second order. A MP4(SDQ)/6-31+(d,p) calculation is used to approximate higher order contributions. In this study we applied the modified CBS-4M method (M referring to the use of minimal population localization) which is a re-parametrized version of the original CBS-4 method and also includes some additional empirical corrections.^{vii} The enthalpies of the gas-phase species M were computed according to the atomization energy method (Eq. 1) (Tables S2–4).^{viii} In the last step the gas-phase heat of formations were converted to the solid/liquid state ones by subtracting the vaporization/sublimation enthalpies (calculated using the Trouton rule).

$$\Delta_f H^p_{(g, M, 298)} = H_{(Molecule, 298)} - \sum H^p_{(Atoms, 298)} + \sum \Delta_f H^p_{(Atoms, 298)} \quad (1)$$

Table S2. CBS-4M results

	$-H^{298} / \text{a.u.}$
PETN	-1314,965678
MAPETN	-1198,954686
DAPEDN	-1082,944608
TAPEMN	-966,93282
TAPE	-850,925082

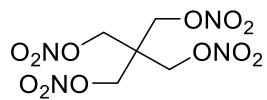
Table S3. Literature values for atomic $\Delta H^p_{f,298} / \text{kcal mol}^{-1}$

	NIST ^{ix}
H	52.1
C	171.3
N	113.0
O	59.6

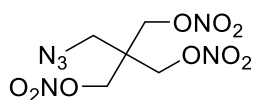
Table S4. Gas phase enthalpies of formation, calculated sublimation/vaporization enthalpies and solid-state heat of formation

M	$\Delta_f H^p(g) / \text{kJ mol}^{-1}$	$\Delta H^p(\text{sub/vap}) / \text{kJ mol}^{-1}$	$\Delta_f H^p(s) / \text{kJ mol}^{-1}$
PETN	-405,8	78,6122	-484,4
MAPETN	8,1	66,7682	-58,7
DAPEDN	419,6	57,3682	362,3
TAPEMN	835,6	40,7835	794,9
TAPE	1241,0	61,5042	1179,5

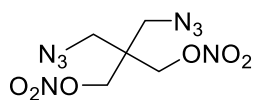
4. Hot Plate Test



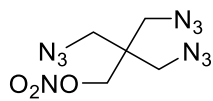
Def.



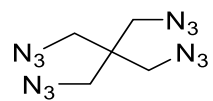
Def.



Det.

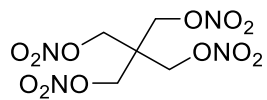


Det.

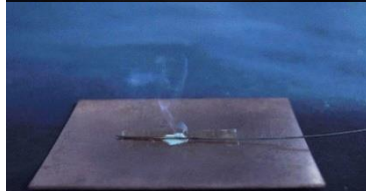
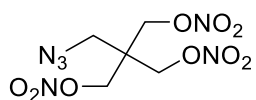


Det.

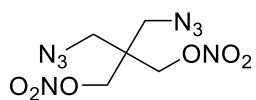
5. Hot Needle Test



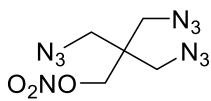
Dec.



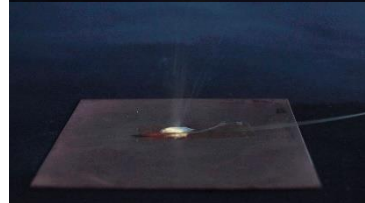
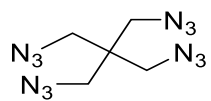
Dec.



Def.



Det.



Det.

References

- ⁱ CrysAlisPro, Oxford Diffraction Ltd. version 171.33.41, **2009**.
- ⁱⁱ G. M. Sheldrick, *Acta Cryst.* **2015**, *A71*, 3–8.
- ⁱⁱⁱ Dolomanov, O. V., Bourhis, L. J., Gildea, R. J., Howard, J. A. K. & Puschmann, *H. J. Appl. Cryst.* **2009**, *42*, 339–341.
- ^{iv} SCALE3 ABSPACK – An Oxford Diffraction program (1.0.4, gui: 1.0.3), Oxford Diffraction Ltd., **2005**.
- ^v APEX3. Bruker AXS Inc., Madison, Wisconsin, USA.
- ^{vi} M. J. Frisch et al., Gaussian 03, Revision B04, Gaussian Inc., Wallingford, CT, **2004**.
- ^{vii} (a) J. W. Ochterski, G. A. Petersson, and J. A. Montgomery Jr., *J. Chem. Phys.* **1996**, *104*, 2598; (b) J. A. Montgomery Jr., M. J. Frisch, J. W. Ochterski G. A. Petersson, *J. Chem. Phys.* **2000**, *112*, 6532.
- ^{viii} (a) L. A. Curtiss, K. Raghavachari, P. C. Redfern, J. A. Pople, *J. Chem. Phys.* **1997**, *106*(3), 1063; (b) E. F. C. Byrd, B. M. Rice, *J. Phys. Chem.* **2006**, *110*(3), 1005–1013; (c) B. M. Rice, S. V. Pai, J. Hare, *Comb. Flame* **1999**, *118*(3), 445–458.
- ^{ix} P. J. Linstrom, W. G. Mallard, Eds., NIST Chemistry WebBook, NIST Standard Reference Database Number 69, June **2005**, National Institute of Standards and Technology, Gaithersburg MD, 20899

Melt Castable Derivatives of Pentaerythritol Tetranitrate

Maximilian Benz,^[a] Thomas M. Klapötke,^{*[a]} Niklas Kölbl,^[a] Jürgen Kuch,^[a] Tobias Lenz,^[a] Ersel Parigi,^[a] and Jörg Stierstorfer^[a]

Abstract: In the search for high-performance and environmentally friendly energetic materials, the derivatization of known materials is an often-applied concept to fulfill modern-day demands. Surprisingly, the long known pentaerythritol tetranitrate (PETN) has only been derivatized to a limited extent. PETN shows a brought application in energetic materials or pharmaceuticals. In this work, the PETN backbone

is modified by introducing nitramine, ionic nitramine, amine, ionic amine and tetrazole functionalities. The obtained and structurally similar compounds allow good comparability and insights into functional group effects on sensitivity, thermal behavior and performance. The functionalizations result in melting points in the range of 64 to 126 °C. Some compounds are therefore potential candidates to replace toxic TNT.

Introduction

Since the discovery of nitroglycerin and PETN, organic nitrates have persisted in energetic materials to this day.^[1] The advantageous single-step synthesis from the associated alcohol leads to compounds with high density, good performance and acceptable thermal stability.^[2] Not only PETN but also the long-known compounds Lead azide, RDX/HMX and TNT have also remained in the industry to this day. Most of those materials used today show unfavorable properties (e.g., toxicity, high sensitivity, harmful to the environment) that one would like to eliminate.^[3] Replacements should fulfill the demand for thermal properties (melt castable or heat-resistant explosives), performance and sensitivity. Furthermore, technological advances and changes in the industry, such as the use of shock tubes, are changing the general demand for new materials.^[4]

With growing commitment, computational chemistry is attempting to enable more targeted synthesis. The prediction of melting points is also continuously improved. For example, it has been shown that the square of molar mass is directly proportional to the melting point of n-alkanes. Non-computational methods for more complex C,H,N,O halogen compounds are also available.^[5] However, due to the complex correlations only some properties can be calculated with meaningful uncertainty, e.g. the initiation by impact can occur by different mechanisms, different measurement standards are applied

worldwide and the deviations and influencing factors are large.^[6] This harms a deeper understanding of the topic. Fundamental understandings, like shock compression experiments on single crystals, that Prof. Gupta is seeking to obtain are associated with immense effort.^[7]

In this interdisciplinary field of understanding the connection between chemical composition and properties, this work contributes to the comparison of some prominent energetic groups: nitramine, ionic nitramine, amine, ionic amine, tetrazole and organic nitrate. Figure 1 shows a selection of research already done in this field. It is shown that the energetic liquid PETN derivatives **A** are less sensitive towards friction than PETN.^[8] The polynitramino PETN **B** synthesized by Shreeve et al. outperforms PETN due to its superior heat of formation and lower sensitivity.^[9] A more comparative study was performed on erythritol tetranitrate derivatives **C** by Lease and Manner et al. They were able to show that the mechanical sensitivity decreases in the order: azido-, nitrate-, nitramino erythritol.^[10] Melting points in a suitable range for melt-castable substances were also achieved. In advance of this study, our group has been working on azidopentaerythritol derivatives **D**.^[11]

This shows that the introduction of azides lowers the melting point and increases the mechanical sensitivity. The group of Chavez et al. synthesized **SMX** with an ideal melting point at 85 °C–86 °C and twice the detonation pressure of TNT.^[12] However, the compound is sensitive and thermally not stable enough to be suitable as a TNT replacement. More energetic nitrates can be found in the review by Sabatini and Johnson.^[13] This includes the most prominent TNT replacement bis(1,2,4-oxadiazole)bis(methylene) dinitrate.^[14] Modification of one nitratomethyl function of the PETN backbone gives great comparability of the functional groups introduced. Furthermore, modification of PETN, with a melting point of 143 °C, will lead to lower melting and melt-castable explosives. The replacement of toxic TNT and the comparison of energetic functional groups is the goal of this work. Therefore azido, amino, ionic derivatives of amino, nitramino, ionic derivatives of nitramino and 1H-tetrazoles were introduced into the pentaerythritol body (Figure 2). Formally, in PETN, the C-bonded nitrate oxygen can be

[a] M. Benz, Prof. Dr. T. M. Klapötke, N. Kölbl, J. Kuch, T. Lenz, E. Parigi, Dr. J. Stierstorfer
 Department of Chemistry
 Ludwig Maximilian University of Munich
 Butenandstr. 5–13, 81337 München (Germany)
 E-mail: tmk@cup.uni-muenchen.de
 Homepage: <http://www.hedm.cup.uni-muenchen.de>

Supporting information for this article is available on the WWW under <https://doi.org/10.1002/chem.202204013>

© 2023 The Authors. Chemistry - A European Journal published by Wiley-VCH GmbH. This is an open access article under the terms of the Creative Commons Attribution License, which permits use, distribution and reproduction in any medium, provided the original work is properly cited.

Known Compounds

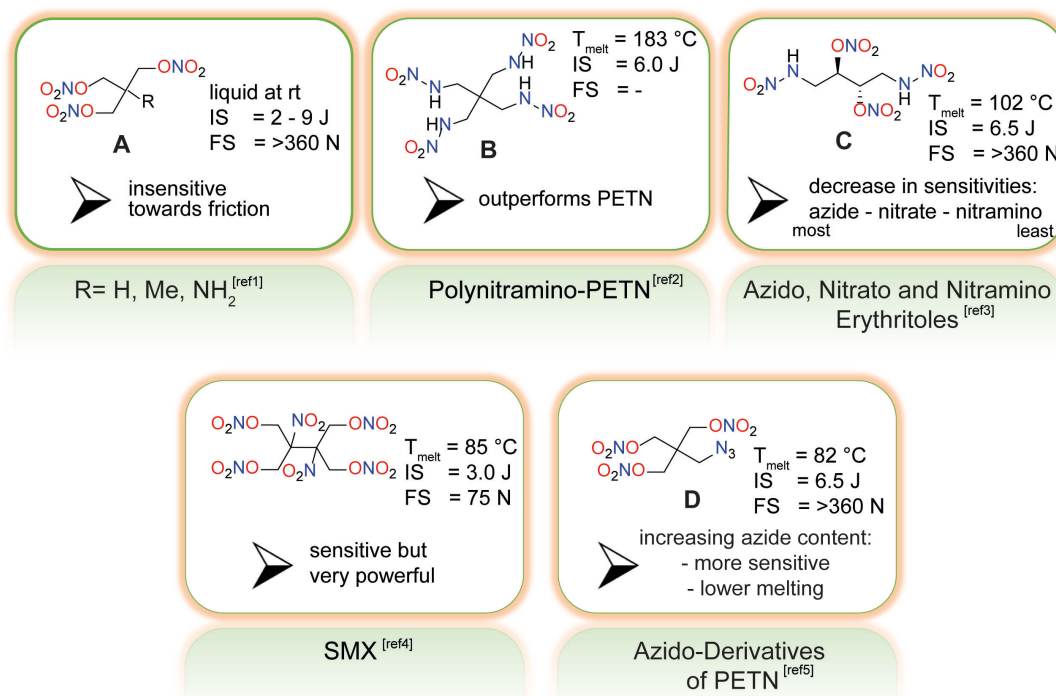


Figure 1. Selection of aliphatic energetic materials with various functionalities. (ref1: [8]; ref2: [9]; ref3: [10]; ref4: [12]; ref5: [11]).

Formal Modifications

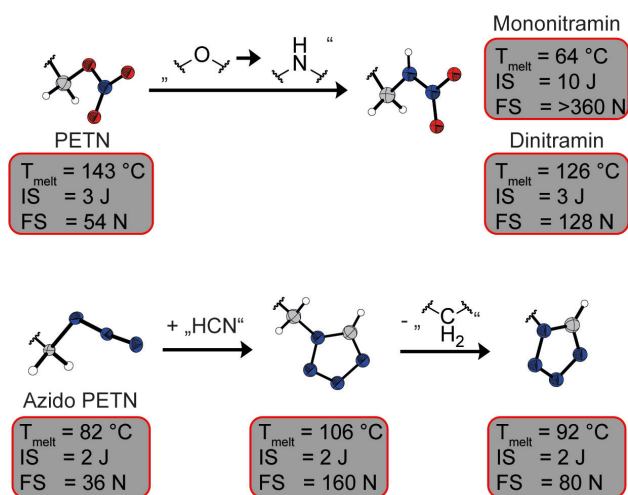


Figure 2. Selection of new compounds synthesized in this paper, together with their interrelationships and properties.

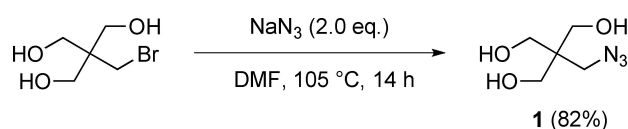
exchanged with an NH group to form the nitramine. Starting from the azido PETN, HCN can formally be added in a [2+3] cycloaddition to form a methyl-bridged tetrazole. The CH_2 group can now be formally removed to obtain a tetrazole bound to the central carbon.

Results and Discussion

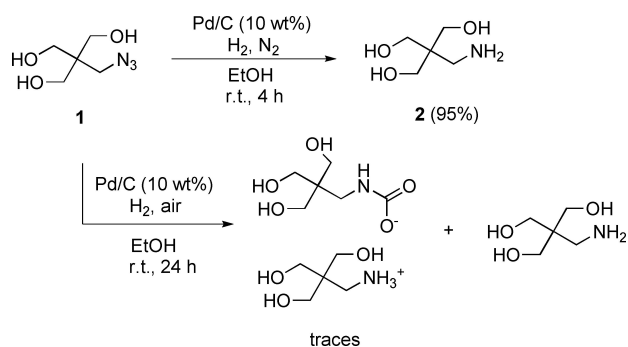
Synthesis

Safety: We have not experienced any incidents or accidental detonations of the compounds. But with the sensitivities present (between primary and secondary explosives), caution is advised. Working with small quantities and protection (kevlar gloves, ear protection, etc.) is strongly recommended.

New high energetic pentaerythritol tetranitrate derivatives were synthesized starting from the commercially available alcohol, pentaerythritol. Bromination yielded monobromopentaerythritol as reported.^[15] By a bromine-azide substitution, the reaction towards monoazidopentaerythritol **1** was performed similarly as previously reported by our group (Scheme 1).^[11] Compound **1** can be recrystallized from a mixture of ethyl acetate and chloroform. It is crucial to have a pure compound that is completely free of dimethylformamide for the following hydrogenation. Purification of the higher azides of pentaery-



Scheme 1. Synthesis of compound **1** starting from monobromopentaerythritol.

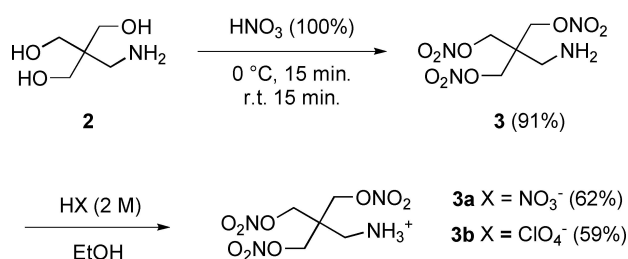


Scheme 2. Synthesis of compound 2 starting from 1.

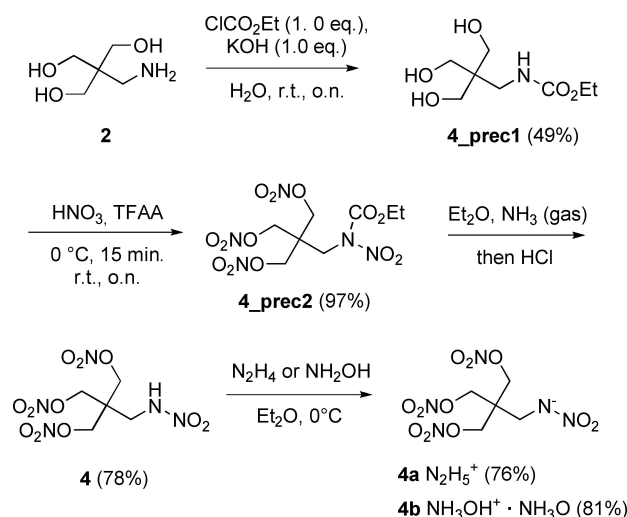
thritol is simpler as they are less water soluble and DMF can be separated much better by washing the organic phase with water.

Reduction of the azide using minimum amounts of palladium on charcoal (10%, 6 mg/mmol) (recovered and refreshed after the reaction) made the monoamine of pentaerythritol 2 accessible in quantitative yields as an off-white solid (Scheme 2). Other than previously reported, purification via the carbamate was not necessary when working under a nitrogen and hydrogen atmosphere.^[16] Nevertheless, the carbamate was discovered as a by-product of early experiments without using an inert gas (X-Ray Structure in the ESI). We achieved the best results by hydrogenation in ethanol with a constant flow of hydrogen over a few hours. The consumption of starting material was checked hourly by TLC.

Monoaminopentaerythritol trinitrate 3 was obtained in excellent yields as a yellowish viscous oil after nitration of 2 (Scheme 3). Purification by column chromatography did not remove the color or changes the physical state. Purification through the salt formation with hydrochloric acid in isopropanol yield the colorless chlorine salt that, when neutralized, gives colorless 2. Further derivatization through a different route was previously done by Hiskey and coworkers, giving the nitrate salt of monoaminopentaerythritol trinitrate 3a.^[16] We obtained compound 3a as a colorless solid through the reaction of 3 with diluted nitric acid. Furthermore, the colorless perchlorate salt 3b was obtained through the reaction of 3 with diluted perchloric acid (Scheme 3). In air, both compounds decompose within days, giving NO_x fumes.



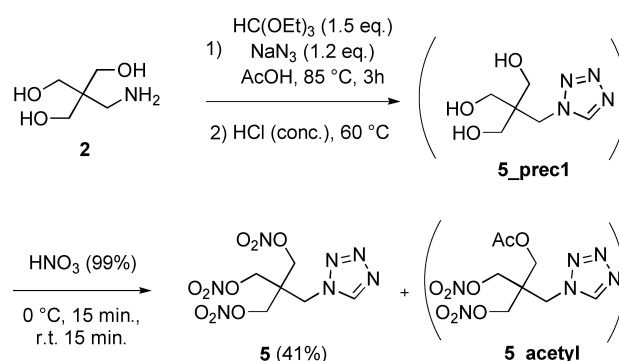
Scheme 3. Synthesis of compound 3 and its ionic derivatives 3a and 3b starting from 2.



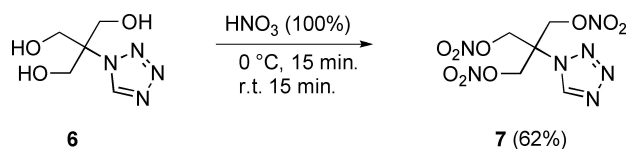
Scheme 4. Synthesis of compound 4 and its ionic derivatives 4a and 4b starting from 2.

The reaction of compound 3 to mononitraminopentaerythritol trinitrate 4 was challenging (Scheme 4). Direct nitration with nitric acid, acetyl nitrate or mixed acid did not yield the required nitramine in one step. The route previously applied by our group, Shreeve or Manner and coworkers was performed successfully to yield 4 in 37% overall yield.^[9,10b,17] First the amine is protected through a reaction with ethyl chloroformate. The protected amine 4_prec1 was then nitrated using a mixture of trifluoroacetic anhydride and nitric acid and the protected nitramine 4_prec2 was obtained as trinitrate. Deprotection with ammonia and precipitation through acidification in water yielded nitramine 4 as a colorless solid. The formation of ionic derivatives of 4 with equimolar amounts of ammonia and potassium hydroxide^[18] did not yield the desired salts in their pure form. The hydrazinium salt 4a and the hydroxylammonium salt with one cocrystalline ammonia oxide 4b could only be obtained by crystallization from ether at 4 °C (Scheme 4). Higher temperatures or protic solvents lead to impure products and decomposition.

Tetrazole ring closure at the amine of 2 was applied with Gaponik conditions (Scheme 5).^[19] The obtained crude 5_prec1



Scheme 5. Synthesis of compound 5 starting from 2.



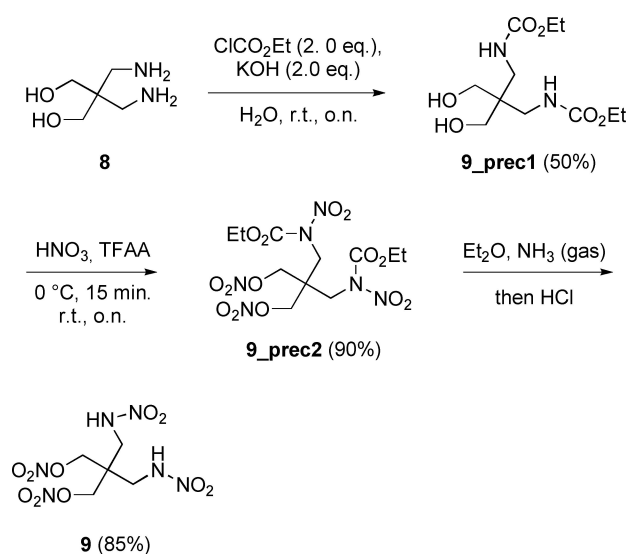
Scheme 6. Synthesis of compound 7 starting from 6.

was directly nitrated in fuming nitric acid. The less polar product was separated by column chromatography. A mono-acetylated side product **5_acetyl** could be identified by NMR and X-ray crystallography in reasonable amounts (ESI). To increase the yield of **5**, the crude intermediate **5_prec1** was heated in concentrated hydrochloric acid to remove the acetyl group before nitration. Thus, the yield was increased to an overall 41% starting from **2**.

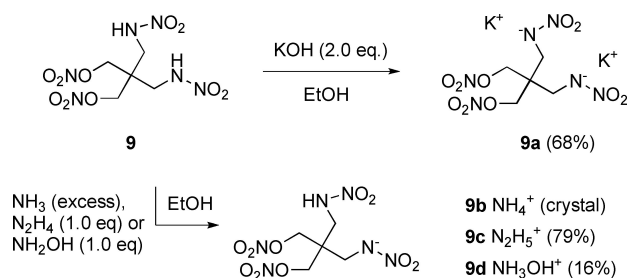
In advance, literature known compound **6** TRIS-alcohol was nitrated to its colorless TRIS-trinitrate **7** in moderate yields (Scheme 6). Isolation of **6** as pure solid showed to be complicated. Nevertheless, the purity of the starting material was not important for nitration to pure **7**.

Several complexation attempts of compounds **5** and **7** failed. No complexation with copper and manganese, nitrates or perchlorates was observed. Instead, the ligands crystallized again.

Attempts to synthesize di- or tri-substituted derivatives were made. During our work on the dinitramine **9**, similar results were published.^[10a] The synthesis is comparable to **4** (Scheme 4). The diamine **8** was further reacted to compound **9_prec1**. After nitration, the protected dinitramine **9_prec2** is yielded. Treatment with gaseous ammonia followed by acidification of the aqueous phase led to the precipitation of dinitraminopentaerythritol dinitrate **9** in very good yields (Scheme 7). Other than for compound **4**, crystal structure measurement with refinement of **9** was possible. Furthermore,



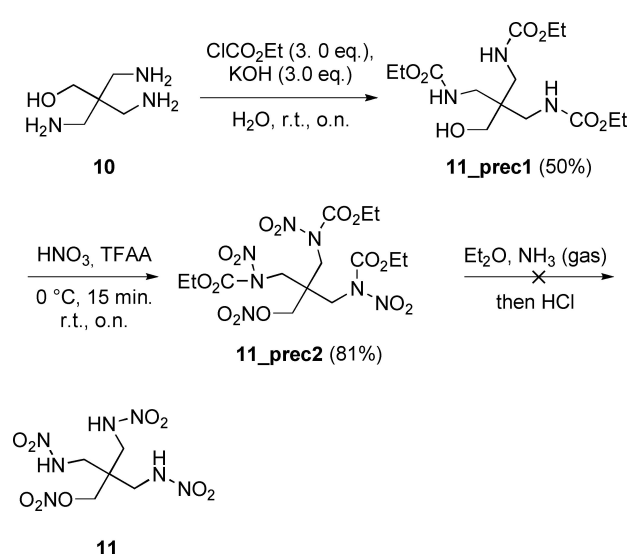
Scheme 7. Synthesis of compound 9 starting from 8.

Scheme 8. Ionic derivatives **9a–d** starting from **9**.

the reaction pathway is proven by crystal structures of the starting material **8** and the two intermediates **9_prec1** and **9_prec2**. Tetrazole ring closure of **8** with a similar procedure to compound **5**, resulted in the recovery of the starting material. Those reactions on diamino alkyl chains are known to show low yields for uneven chain length.

Ionic derivatives of acidic **9** were obtained by reaction with bases (Scheme 8). The potassium salt **9a** precipitates from an ethanolic solution of **9**. With the nitrogen bases ammonia, hydrazine and hydroxylamine only the mono salts could be obtained as they crystalize from ethanol. The ammonia salt **9b** could not be isolated, only a crystal structure was obtained (ESI). The hydrazine **9c** and hydroxylamine **9d** salts were fully characterized.

Furthermore, the tri derivatives were investigated (Scheme 9). Amine **10** was protected with ethyl chloroformate to yield **11_prec1**. The following nitration with trifluoroacetic anhydride yielded **11_prec2** as expected. Several deprotection attempts towards trinitramine **11** failed. Only an impure yellow oil that cannot be purified or reacted selectively is obtained.

Scheme 9. Attempt for the synthesis of **11**.

NMR spectroscopy

Investigation through ^1H and ^{13}C was performed on all compounds (ESI). It can be observed that O-nitration leads to a characteristic change in chemical shift. The shift of the protons of the CH_2 group nearby generally increases from ~ 3.3 to ~ 4.6 ppm and for tetrazole containing compounds from 3.9 to 5.3 ppm. The carbon shifts generally from 62 ppm to 71 ppm. In advance ^{15}N NMR of the compounds **4**, **5** and **7** were measured, revealing the chemical shifts of all nitrogen atoms contained (Figure 3). The nitrogen of all the organic nitrates is at -50 ppm. The nitramino nitrogens of **4** show at -20 ppm for the nitro group and -220 ppm for the amine bearing a proton. The tetrazole nitrogens of **5** and **7** are found between 20 and -170 ppm. The nitrogen bound to two carbons is shifted between -150 and -170 ppm, which matches with the shifts

of similar 1-alkyl-substituted tetrazoles.^[20] The nitrogen bound to only one carbon atom can be observed at -50 to -60 ppm. The more shielded nitrogen atoms are at about -25 ppm for N3 and 10 ppm for N4.

Crystal structures

The mono-substituted PETN derivatives **3a**, **3b**, **4**, **4a**, **4b**, **5** and **7** as well as the side products **2_CO₂** and **5_acetyl** were analyzed by low-temperature single crystal diffraction. For the disubstituted compounds structures of **8**, **9_prec1**, **9_prec2**, **9**, **9a** and **9b** were observed. The structures of **3a**, **4b**, **5**, **7** and **9** are discussed below (Figures 4–9). The structures of **2_CO₂**, **3b**, **4a**, **5_acetyl**, **9_prec1**, **9_prec2**, **9a** and **9b** together with all measurement parameters and refinement data can be found in

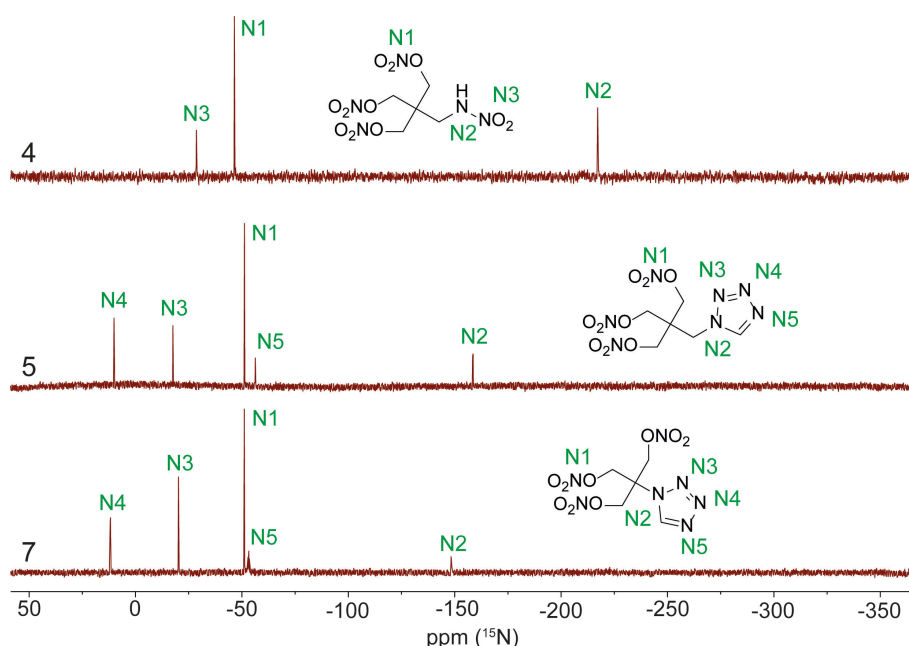


Figure 3. ^{15}N NMR spectra of **4**, **5** and **7** (Acetone- d_6 , 1H coupled).

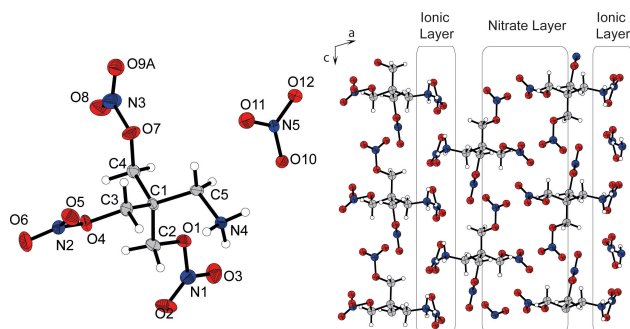


Figure 4. Scheme caption. Formula unit of **3a**. Selected bond length (\AA): C1–C4: 1.537(8), C4–O7: 1.449(8), O7–N3: 1.384(8), N3–O8: 1.195(9), C1–C5: 1.530(8), C5–N4: 1.478(8), N5–O10: 1.252(7). Selected bond angles ($^\circ$): C5–C1–C4: 109.8(5), C1–C4–O7: 106.6(5), O7–N3–O8: 118.2(7), C1–C5–N4: 113.9(5), O10–N5–O11: 122.2(5).

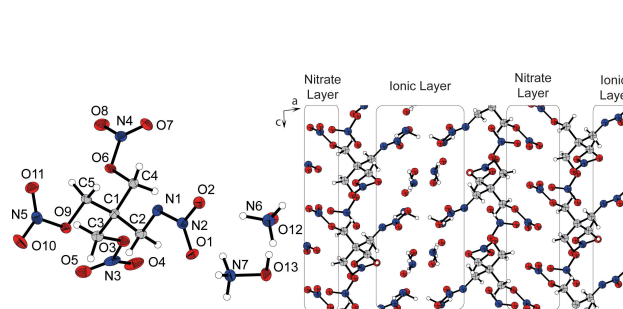


Figure 5. Formula unit of **4b**. Selected bond length (\AA): C1–C4: 1.534(3), C4–O6: 1.451(3), O6–N4: 1.396(2), N4–O7: 1.200(3), C1–C2: 1.535(3), C2–N1: 1.458(3), N1–N2: 1.264(3), N2–O2: 1.312(2), N6–O12: 1.417(3), N7–O13: 1.421(3). Selected bond angles ($^\circ$): C2–C1–C4: 106.9(2), C1–C4–O6: 106.5(2), C4–O6–N4: 113.2(2), O6–N4–O7: 118.5(2), C1–C2–N1: 107.9(2), C2–N1–N2: 114.1(2), N1–N2–O1: 125.6(2).

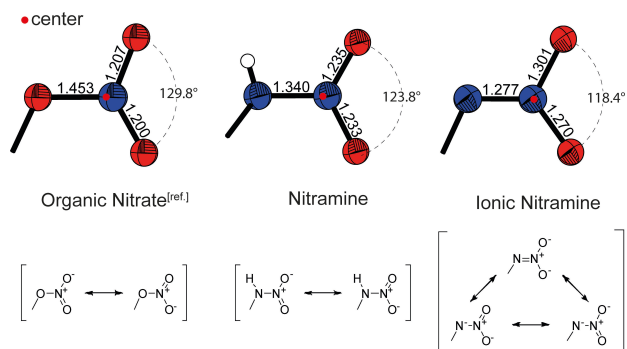


Figure 6. Comparison of bonding and angles of an organic nitrate of PETN, nitramine (**9**) and ionic nitramine (**4b**) with the resulting Lewis structures below.

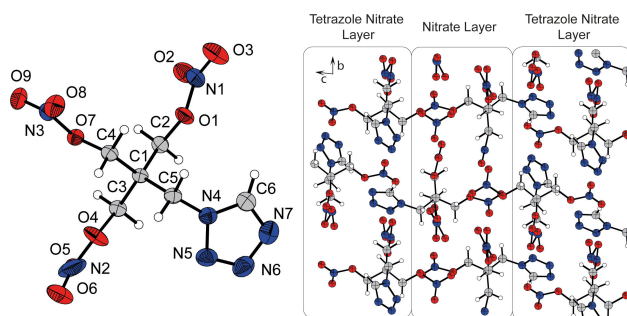


Figure 7. Formula unit of **5**. Selected bond length (Å): C1–C2: 1.5324(1), C2–O1: 1.4374(1), O1–N1: 1.4018(1), N1–O2: 1.2111(1), C1–C5: 1.5446(1), C5–N4: 1.4358(1). Selected bond angles [°]: C5–C1–C2: 112.35(1), C1–C2–O1: 106.06(1), C2–O1–N1: 114.99(1), O1–N1–O3: 111.61(1), C1–C5–N4: 114.84(1).

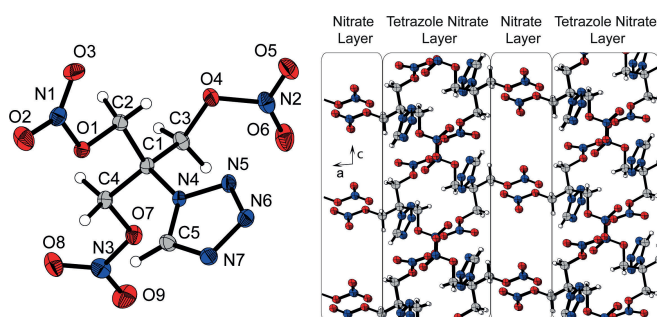


Figure 8. Formula unit of **7**. Selected bond length [Å]: C1–C3: 1.539(2), C3–O4: 1.440(2), O4–N2: 1.413(2), N2–O6: 1.200(2), C1–N4: 1.480(2). Selected bond angles [°]: N4–C1–C3: 110.6(1), C1–C3–O4: 109.9(1), C3–O4–N2: 115.1(1), O4–N2–O6: 119.0(1), N5–N4–C1: 120.7(1).

the Supporting Information. Compound **4** crystallizes in colorless blocks that are suitable for single-crystal diffraction. Due to the structural similarity of the nitrate and nitramino group, the molecules are highly disordered and refinement was impossible. Nevertheless, the structure is proven by the follow-up reactions to the ionic derivatives **4a** and **4b**. The datasets were uploaded to the CSD database and can be accessed free of charge. CSD Deposition numbers: 2232116–2232128.

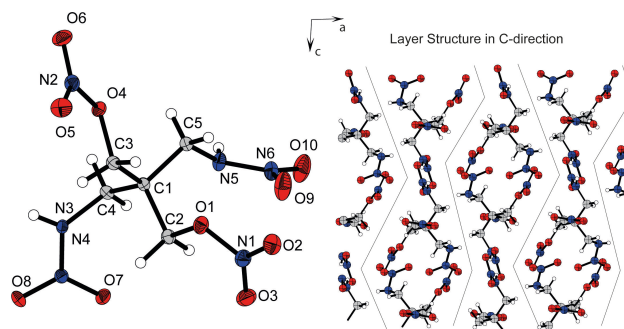


Figure 9. Formula unit of **9**. Selected bond length [Å]: C1–C3: 1.529(3), C3–O4: 1.455(2), O4–N2: 1.394(2), N2–O6: 1.206(2), C1–C5: 1.548(3), C5–N5: 1.455(3), N5–N6: 1.362(2), N6–O9: 1.237(3). Selected bond angles [°]: C1–C3–O4: 106.1(2), C1–C4–N3: 113.8(2), C3–O4–N2: 113.4(1), O5–N2–O6: 129.2(2), C5–N5–N6: 118.4(2), O9–N6–O1.

The nitrate salt **3a** crystallizes in the monoclinic space group $P2_1/c$ with eight molecules in the unit cell. A density of 1.660 g cm^{-3} at 293 K was determined. The four carbon atoms around the central carbon of the pentaerythritol backbone span a tetrahedron with a volume of 1.83 \AA^3 . The C–C distances for the nitrate-bound carbons are 1.50–1.55 Å. The carbon-oxygen bonds are 1.45 Å long. The organic nitrate nitrogen is not in the center of the three oxygens. The N–O bond directed to the carbon-bound oxygen is about 0.20 Å longer than the remaining, 1.20 Å long. The bond between the ammonium functionality and carbon is 1.49 Å, longer than the nitrates are bound to carbon. The planar nitrate shows symmetrically distributed binding with an N–O bond length of 1.25 Å. The O–N–O angles are between 117° and 122° slightly off the ideal 120° because of attractive interactions with the ammonium proton. The three-dimensional structure viewed along the b -axis reveals ionic layers where the ammonium and nitrate are fixed by O–H interactions. Those layers alternate with layers fixed through nitrate-nitrate interactions (Figure 4).

The hydroxylammonium salt of mononitraminopentaerythritol trinitrate **4b** crystallizes with one molecule of ammonia oxide, in the triclinic space group $P-1$. The density is 1.687 g cm^{-3} at 100 K with four molecules in the unit cell. The tetrahedron in the center has a volume of 1.84 \AA^3 . The bond length and angles of the carbon backbone and nitrate functionalities are comparable to compound **3a**. The C–N bond of the nitramine is shorter than that of the ammonium functionality in **3a** with a length of 1.46 Å close to the C–O bonds. In contrast to the nitrate group the nitrogen in the center of the planar nitramino group is well-centered with N–O or N–N bond lengths of 1.26–1.31 Å. The bond distances in the hydroxylammonium cation and the ammonia oxide are comparable with a length of 1.42 Å. In the three-dimensional structure again alternating layers can be observed when viewing along the b -axis. An ionic layer with the deprotonated nitramine and the cationic and neutral hydroxylamine is found. This layer is again alternating with layers of organic nitrates (Figure 5).

Since the electronic situation of several substituents is similar ($-\text{ONO}_2$, $-\text{NH}-\text{NO}_2$, $-\text{N}-\text{NO}_2$), we featured a comparison of those including the crystallographic key properties. In Figure 6 an organic nitrate of PETN, a nitramino group of **9** and an ionic nitramine of **4b** were analyzed and compared. The bond distance shortens from the nitrate (1.45 Å) to the nitramine (1.34 Å) to the anionic nitramine (1.28 Å). The central nitrogen initially shifted to the nitro group and moves further to the center (red dot). Consequently, the outer O–N–O angle changes and becomes smaller from 129.8° to 118.4°. The Lewis structures below clearly show that the N–N bond of the ionic nitramine has a double bond character and therefore must be shorter, which is proven here through the comparison of the bond lengths.

The N-tetrazole derivative of PETN **5** crystallizes in the triclinic space group $P-1$ with two molecules in the unit cell. The density at 123 K is 1.695 g cm⁻³. The tetrahedron volume is 1.84–1.85 Å³. The angles and bond length of the nitrate bearing arms are comparable to the previous structures. The distance of N4 of the tetrazole to the pentaerythritol carbon is 1.44 Å and therefore shorter than the introduced functionality in **3a** and **4b**. The three-dimensional structure reveals a more rigid structure. Alternating layers can be observed along the a -axis. Nitrate-nitrate interactions are part of one layer and tetrazole N–H interactions are part of the other layer (Figure 7).

The trinitrate of the TRIS-tetrazole backbone **7** crystallizes in the monoclinic space group $P2_1/n$ with four molecules in the unit cell. With a density of 1.764 g cm⁻³ at 110 K, **7** shows the highest density of all investigated derivatives. The tetrahedron spanned by the tris-backbone has a volume of 1.80 Å³. Thus, the tetrahedron is smaller than that of all other derivatives. The angles and bond length of the nitratomethyl groups are comparable to the previously discussed. The bond distance of the central carbon to the tetrazole is 1.48 Å and therefore longer than the C–N bond in **5**. The three-dimensional structure, viewed along the b -axis, reveals a similar layer type to **5**. The nitrate layer is dominated by O–H interactions whereas

the tetrazole nitrate layer is dominated by N–H interactions (Figure 8).

Dinitraminopentaerythritol dinitrate **9** crystallizes in the monoclinic space group $P2_1/n$ with four molecules in the unit cell. The density of 1.790 g cm⁻³ at 123 K is higher than the density of the mono derivatives. The inner tetrahedron shows a volume of 1.87 Å³, the largest of all compounds. The carbon nitramin bond is 1.46 Å long and comparable to the C-nitrate or C-tetrazole distances. When a grown supercell is viewed along the b -axis, alternating zic-zac layers can be identified. The whole structure is dominated by CH–O and NH–O hydrogen bonding (Figure 9).

Physico chemical properties

The energetic properties and detonation parameters of compounds **3**, **3a**, **3b**, **4**, **4a**, **4b**, **5**, **7**, **9**, **9a**, **9c** and **9d** are presented in Table 1. All energetic products were analyzed by differential thermal analysis (DTA) with a heating rate of 5 K min⁻¹. The onset temperatures for endothermic and exothermic peaks were determined and are shown in Figure 10. For compounds **4**, **5** and **7** the melting and recrystallization of the melt were proven by optical observation. Pure PETN melts at 143 °C and decomposes shortly thereafter at 180 °C. For a melt cast energetic, it is important to achieve a melting range that can be reached with hot or boiling water possibly under pressure (80–120 °C). Furthermore, the decomposition point should be as far away as possible from the melting point to ensure safe processing. Since organic nitrates usually decompose around 180 °C (onset) and, on closer inspection, often earlier, the distance between melting and decomposition is the critical factor here.

Compounds **4**, **5** and **7** are therefore particularly suitable as melt-castable energetic materials. Compound **4** melts early at 64 °C and decomposes (106 °C higher) at 170 °C. Compound **5** has a significantly higher melting point of 106 °C and decomposition is 74 °C later at 180 °C. Nitratotetrazole **7** shows an

Table 1. Energetic properties and detonation parameters of MAPETN, **3**, **3a**, **3b**, **4**, **4a**, **4b**, **5**, **7**, **9** compared to PETN.

	IS [J] ^[a]	FS [N] ^[b]	ρ [g cm ⁻³] ^[c]	Ω [%] ^[d]	$T_{\text{endo}}/T_{\text{exo}}$ [°C] ^[e]	$\Delta_f H^\circ$ [kJ mol ⁻¹] ^[f]	P_{CJ} [kbar] ^[g]	V_{det} [m s ⁻¹] ^[h]	TNT equiv. ^[i]
TNT	> 15	> 360	1.648	-24.7	81/289	-56	183	6785	1.01
MAPETN	2	36	1.667	0.0	82/180	-59	278	8092	1.57
3	7.5	> 360	-	-5.9	89/153	-	-	-	-
3a	3	120	1.659	7.2	145/145	-423	287	8163	1.68
3b	-	-	1.792	10.8	-/146	-383	317	8484	1.77
4	10	> 360	1.729 ^{pyc}	7.6	64/170	-339	305	8283	1.56
4a	3	120	1.637	-2.3	-/100	-48	293	8363	1.88
4b	4	45	1.709	2.1	73/73	-	-	-	-
5	2	160	1.652	0.0	106/180	-48	252	7847	1.44
7	2	80	1.716	2.6	92/163	-3	292	8258	1.52
9	3	128	1.744	0.0	126/134	-254	302	8352	1.53
9a	3	> 360	1.856	4.1	-/135	-	-	-	-
9c	3	160	-	13.7	-/108	-	-	-	-
9d	15	360	-	-3.2	120/125	-	-	-	-
PETN	3–4	54	1.778	-10.1	143/180	-484	313	8471	1.64

[a] Impact sensitivity (BAM drophammer (1 of 6)). [b] Friction sensitivity (BAM friction tester (1 of 6)). [c] From X-ray diffraction analysis recalculated to 298 K. [d] Oxygen balance with respect to CO. [e] Melting/Decomposition temperature (DTA; $\beta = 5^\circ\text{C min}^{-1}$). [f] Calculated enthalpy of formation (ExpLo5-V6.05.04 code). [g] Detonation pressure at Chapman-Jouguet point (ExpLo5-V6.05.04 code). [h] Detonation velocity. [i] TNT equiv. based on the Power Index.

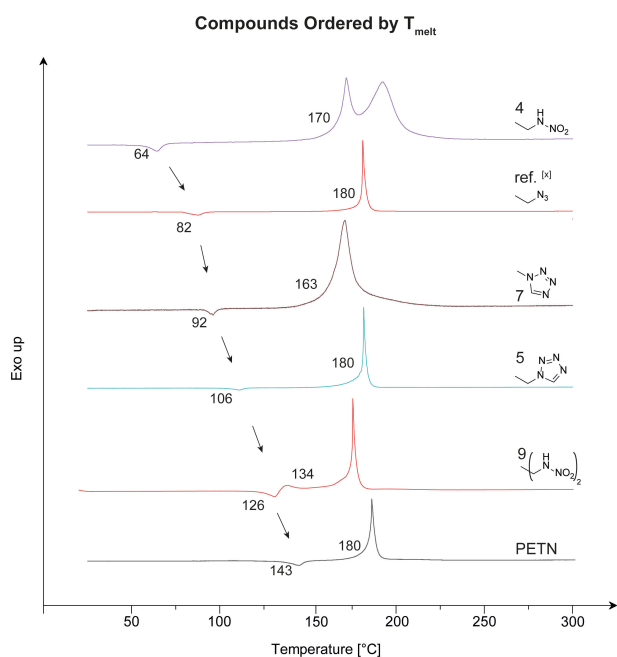


Figure 10. Differential thermal analysis of derivatives compared to PETN and monoazidopentaerythritol trinitrate.^[11]

ideal melting point at 92°C and decomposition at 71°C later. Interestingly compound **9** decomposes right after melting at 126°C–134°C. The formation of ionic derivatives as well as having a nucleophilic amino group lowers the thermal stability and leads to early decompositions below 150°C.

The detonation parameters were calculated using the EXPLO5-V6.05.04 code. The densities were taken from the crystal structures and simply calculated to room temperature densities. The density of compound **7** is measured pycnometrically. The heat of formation is calculated from Gaussian CBS-4 M enthalpies using the atomization method (ESI). The melt cast candidates **4**, **5** and **7** outperform TNT by 1.0–1.5 km s⁻¹. The high densities of **4** and **7** cause them to be more powerful with a detonation velocity of 8.3 km s⁻¹, whereas **5** still shows a good detonation velocity of 7.8 km s⁻¹. The detonation pressures are at 25–31 GPa and correspond to the detonation velocities. The ionic derivatives show properties in the same area, with the perchlorate salt **3b** as the most powerful compound. With a velocity of 8.5 km s⁻¹ and a pressure of 31.7 GPa, it appears more powerful than PETN. TNT equivalents, based on the power index, were calculated from the heat of detonation and the volumes of gas at STP. All calculated compounds outperform TNT by 1.44 to 1.88 times. With the melt cast candidates being close to the power of PETN.

Conclusion

The PETN backbone was modified by several functionalities revealing the influences on thermal, energetic and chemical properties. Mononitramino PETN **4** shows to be remarkably less

sensitive while the thermal stability and performance are largely maintained compared to PETN. Introducing tetrazoles to the PETN backbone, caused the resulting tristetrazole PETN **5** and tetrazole PETN **7** to be less friction sensitive. The formal addition of HCN on the azide of sensitive monoazido PETN causes the resulting tetrazole **5** to be less friction sensitive and shifts the melting point to 26°C higher. Compounds **4**, **5** and **7** are candidates to replace TNT. However, compound **4** shows a low melting point and **5** and **7** are impact sensitive. Due to the low water solubility, the good sensitivity parameters and the high-performance mononitramino PETN **4** is particularly outstanding. Although their synthesis appears to be too complex, this study shows that methyl-bridged nitramine and tetrazoles should be considered for the synthesis of new melt cast energetic material. The introduction of the amine-like **3** or ionic groups like **3a**, **3b**, **4a**, **4b**, **9a**, **9b**, **9c** and **9d** has been shown to decrease the thermal properties but sometimes improve energetic properties.

Experimental Section

Compound 3: Compound **2** (500 mg, 3.70 mmol) was added in portions to HNO₃ (100%, 4 mL) at 0°C–5°C. The resulting mixture was stirred at this temperature for 15 min., then was allowed to warm to r.t. After 15 min the reaction mixture was poured on ice-water and neutralized with NaHCO₃. The solution was extracted with EtOAc (3×100 mL), the combined organic phases were dried over Na₂SO₄ and the solvent was removed under reduced pressure, to provide amine **3** (560 mg, 2.08 mmol, 56%) as a yellowish paste. DTA (5°C min⁻¹): 89°C (melt.), 153°C (dec.), Sensitivities: BAM drop hammer: 7.5 J, BAM friction tester: 360 N, IR (ATR): ν_{\max} [cm⁻¹] = 2935 (w), 1630 (s), 1471 (m), 1374 (m), 1333 (m), 1272 (vs), 1259 (s), 1092 (m), 980 (s), 929 (m), 851 (vs), 826 (s), 753 (s), 725 (s), 715 (s), 613 (s), 591 (s), 557 (m), 418 (s), 411 (s), EA (C₅H₁₀N₄O₉, 270.15 g mol⁻¹): calc.: C 22.23, N 20.74, H 3.73%; found: C 22.63, N 20.18, H 3.75%, ¹H NMR (400 MHz, Methanol-*d*₄): δ (ppm) = 4.67 (s, 6H), 2.91 (s, 2H), ¹³C NMR (101 MHz, Methanol-*d*₄): δ (ppm) = 70.8, 51.1, 43.0.

Compound 4: Amine **3** (5.28 g, 39.1 mmol, 1.0 equiv.) was dissolved in H₂O (100 mL). Then half of the ethyl chloroformate (3.72 mL, 39.1 mmol, 1.0 equiv.) was added dropwise to the solution at 0°C. Afterwards, KOH (2.19 g, 39.1 mmol, 1.0 equiv.) was dissolved in H₂O (120 mL). The potassium hydroxide solution and the remaining ethyl chloroformate were then added dropwise in an alternating manner. The solution was stirred overnight at room temperature. The solvent was removed by a rotation evaporator and a white residue was obtained. This residue was then extracted with EtOH (50 mL) (formed KCl is not soluble). The EtOH then was removed under reduced pressure and compound **4_prec1** was obtained as a white solid (3.98 g, 19.2 mmol, 49%). ¹H NMR (400 MHz, DMSO-*d*₆): δ (ppm) = 6.74 (t, *J* = 6.1 Hz, 1H), 4.27 (t, *J* = 5.4 Hz, 3H), 3.98 (q, *J* = 7.1 Hz, 2H), 3.29 (d, *J* = 4.9 Hz, 6H), 2.99 (d, *J* = 6.2 Hz, 2H), 1.15 (t, *J* = 7.1 Hz, 3H); ¹³C NMR (101 MHz, DMSO-*d*₆): δ (ppm) = 157.2, 61.0, 59.9, 45.1, 40.9, 14.6. Then fuming HNO₃ (99%, 12 mL) was added slowly to TFAA (24 mL) at 5°C. Compound **4_prec1** (0.93 mg, 4.50 mmol) was added in portions at 5–10°C. The yellow solution was then stirred at room temperature overnight. The either orange or clear solution was then added onto ice (50 mL) and extracted with DCM (3×50 mL). The organic phase was then washed with sat. NaHCO₃ solution (3×100 mL) and with brine (1×100 mL). After drying over Na₂SO₄ the solvent was removed under reduced pressure. Yellowish-white solid **4_prec2** was obtained (1.36 g,

3.51 mmol, 78%). ¹H NMR (400 MHz, DMSO-*d*₆): δ (ppm) = 4.67 (s, 6H), 4.41 (s, 2H), 4.31 (q, *J* = 7.1 Hz, 2H), 1.28 (t, *J* = 7.1 Hz, 3H); ¹³C NMR (101 MHz, DMSO-*d*₆): δ (ppm) = 150.7, 71.0, 65.2, 49.0, 42.2, 13.6. Then compound (**4_prec2**) (1.71 g, 3.74 mmol, 1.0 equiv.) was dissolved in Et₂O (50 mL). Afterwards, NH₃-gas was passed into the solution for 20 min. Then the suspension was extracted with water (3 × 25 mL). The aqueous phase was acidified carefully with HCl (2 M). The solution was extracted with EtOAc (3 × 25 mL). The organic phase was dried over Na₂SO₄, filtered and the solvent was removed. Compound **4** was obtained as a white solid (676 mg, 2.14 mmol, 78%). DTA (5 °C min⁻¹): 64 (melt.), 170 °C (dec.); Sensitivities (< 500 μm, crystalline material): BAM drop hammer: 10 J; BAM friction tester: > 360 N; IR (ATR): ν_{max} [cm⁻¹] = 3318 (w), 2903 (w), 1631 (vs), 1590 (s), 1393 (m), 1322 (s), 1265 (vs), 1023 (s), 994 (s), 839 (vs), 752 (s), 702 (s), 622 (s), 526 (s); EA (C₅H₉N₅O₁₁, 315.15 g mol⁻¹): calc.: C 19.06, N 22.22, H 2.88%; found: C 19.31, N 21.95, H 2.73%; ¹H NMR (400 MHz, DMSO-*d*₆): δ (ppm) = 12.32 (s, 1H), 4.61 (s, 6H), 3.78 (s, 2H); ¹³C NMR (101 MHz, DMSO-*d*₆): δ (ppm) = 71.0, 44.1, 41.9; ¹⁵N NMR (41 MHz, Acetone-*d*₆): δ (ppm) = -27.2, -45.0, -215.7.

Compound 5: Amine **3** (1.00 g, 7.39 mmol, 1.0 equiv.), NaN₃ (578 mg, 8.89 mmol, 1.2 equiv.) and triethyl orthoformate (1.84 mL, 11.07 mmol, 1.5 equiv.) were added together and then heated at 40 °C. Dropwise AcOH (4 mL) was added and the solution was heated at 85 °C for 3 h. Afterwards conc. HCl (0.75 mL, 9.00 mmol, 1.2 equiv.) was added slowly. The obtained suspension was filtered off, and conc. HCl (10 mL) was added to the filtrate. After heating at 60 °C for 30 min. the solvent was removed under vacuum to obtain **5_prec1**. ¹H NMR (400 MHz, DMSO-*d*₆): δ (ppm) = 9.21 (s, 1H), 4.41 (s, 2H), 3.26 (s, 6H), ¹³C NMR (101 MHz, DMSO-*d*₆): δ (ppm) = 145.6, 60.4, 46.2, 45.7. This crude material was added in portions to HNO₃ (99%, 8 mL) at 0 °C–5 °C. The resulting mixture was stirred at 0 °C for 15 min., was allowed to warm to r.t. and stirred for another 15 min. Then the reaction mixture was poured on ice-water and neutralized with NaHCO₃. After extraction with EtOAc (3 × 50 mL), the combined organic phases were dried over Na₂SO₄ and the solvent was removed under reduced pressure. The resulting crude was then purified via column chromatography (*i*-Hex/EtOAc, 1:1) to afford colorless solid **5** (974 mg, 3.01 mmol, 41%). DTA (5 °C min⁻¹): 106 °C (melt.), 180 °C (dec.), Sensitivities: BAM drop hammer: 2 J; BAM friction tester: 160 N, IR (ATR): ν_{max} [cm⁻¹] = 3154 (w), 3026 (vw), 2992 (vw), 2904 (w), 1626 (vs), 1467 (m), 1389 (w), 1275 (vs), 1171 (m), 1124 (w), 1096 (m), 1036 (m), 1007 (s), 985 (m), 962 (w), 856 (vs), 773 (m), 753 (s), 729 (m), 709 (s), 696 (m), 661 (m), 631 (m), 623 (m), 454 (m), EA (C₆H₉N₇O₉, 323.18 g mol⁻¹): calc.: C 22.30, N 30.34, H 2.81%; found: C 22.32, N 30.08, H 2.73%, ¹H NMR (400 MHz, DMSO-*d*₆): δ (ppm) = 9.53 (s, 1H), 4.82 (s, 2H), 4.66 (s, 6H); ¹³C NMR (101 MHz, DMSO-*d*₆): δ = 145.5, 70.6, 46.9, 41.3; ¹⁵N NMR (41 MHz, Acetone): δ (ppm) = 11.0 (d, *J* = 3.1 Hz), -16.6 (s), -50.0 (t, *J* = 1.9 Hz), -54.9 (d, *J* = 12.2 Hz), -156.7 (d, *J* = 9.7 Hz).

Compound 7: Compound **6** (1.00 g, 5.74 mmol) was added in portions to HNO₃ (99%, 8 mL) at 0 °C–5 °C. The resulting mixture was stirred at 0 °C for 15 min., was allowed to warm to ambient temperature and stirred for another 15 min. Then the reaction mixture was poured on ice-water and neutralized with NaHCO₃. After extraction with EtOAc (3 × 50 mL), the combined organic phases were dried over Na₂SO₄ and the solvent was removed under reduced pressure leaving colorless crystalline **7** (1.10 g, 3.56 mmol, 62%). DTA (5 °C min⁻¹): 92 °C (melt.), 163 °C (dec.), Sensitivities: BAM drop hammer: 2 J; BAM friction tester: 80 N, IR (ATR): ν_{max} [cm⁻¹] = 3123 (w), 3026 (w), 2922 (w), 1641 (vs), 1380 (m), 1296 (m), 1280 (vs), 1259 (s), 1093 (m), 1035 (s), 1021 (s), 977 (m), 866 (s), 836 (vs), 751 (s), 740 (s), 725 (s), 714 (s), 624 (s), 557 (m); EA (C₅H₇N₇O₉, 309.15 g mol⁻¹): calc.: C 19.43, N 31.72, H 2.28%; found: C 19.79, N 30.40, H 2.45%, ¹H NMR (400 MHz, Acetone-*d*₆): δ (ppm) = 9.68 (s,

1H), 5.47 (s, 6H); ¹³C NMR (101 MHz, Acetone-*d*₆): δ (ppm) = 143.6, 69.9, 62.4; ¹⁵N NMR (41 MHz, Acetone-*d*₆): δ (ppm) = 13.3, -18.4, -49.0, -50.7, -145.1.

CCDC

Deposition Number(s) 2236739 (for **2_CO2**), 2232124 (for **3 a**), 2232126 (for **3 b**), 2232127 (for **4 a**), 2232121 (for **4 b**), 2232120 (for **5**), 2232116 (for **5_acetyl**), 2232122 (for **7**), 2232125 (for **8**), 2232123 (for **9**), 2232117 (for **9_prec1**), 2232118 (for **9_prec2**), 2232128 (for **9 a**), 2232119 (for **9 b**) contain(s) the supplementary crystallographic data for this paper. These data are provided free of charge by the joint Cambridge Crystallographic Data Centre and Fachinformationszentrum Karlsruhe Access Structures service.

Acknowledgements

For financial support of this work by Ludwig-Maximilian University (LMU), the Office of Naval Research (ONR) under grant no. ONR N00014-19-1-2078 and the Strategic Environmental Research and Development Program (SERDP) under contract no. W912HQ19C0033 are gratefully acknowledged. We thank Prof. Dr. Konstantin Karaghiosoff for the measurement of the ¹⁵N NMR spectra and Dr. Peter Mayer for his help with X-ray crystallography measurements. Open Access funding enabled and organized by Projekt DEAL.

Conflict of Interest

The authors declare no conflict of interest.

Data Availability Statement

The data that support the findings of this study are available in the supplementary material of this article.

Keywords: energetic materials · meltcast · nitramine · PETN · tetrazole

- [1] E. Berlow, R. H. Barth, J. E. Snow, *The Pentaerythritols*, Reinhold Publishing Corporation, New York, 1958.
- [2] a) T. M. Klapötke, *Chemistry of High-Energy Materials*, 6th Ed., Walter de Gruyter GmbH, Berlin/Boston, 2022; b) R. M. J. Köhler, A. Homburg, *Explosivstoffe*, Vol. 10, WILEY-VCH Verlag GmbH, Weinheim, 2008; c) J. P. Agrawal, *High Energy Materials*, WILEY-VCH Verlag GmbH & Co., Weinheim, 2010.
- [3] a) T. Blessinger, L. D'Amico, R. Subramaniam, C. Brinkerhoff in *EPA/635/R-18/211Fa*, U. S. Environmental Protection Agency, Washington, 2018; b) Technical Fact Sheet - 2,4,6-Trinitrotoluene (TNT) in *EPA 505-F-21-001*, U. S. Environmental Protection Agency, Washington, 2021.
- [4] P. A. Persson, *US 4220087 A*, 1971.
- [5] a) A. E. Terhemen, *Adv. J. Chem., Sect. A* 2020, 3, 122–130; b) S. V. Bondarchuk, *FirePhysChem* 2022, 2, 160–167; c) S. Song, F. Chen, Y. Wang, K. Wang, M. Yan, Q. Zhang, *J. Mater. Chem.* 2021, 9, 21723–21731.
- [6] a) F. W. Marrs, V. W. Manner, A. C. Burch, J. D. Yeager, G. W. Brown, L. M. Kay, R. T. Buckley, C. M. Anderson-Cook, M. J. Cawkwell, *Ind. Eng. Chem. Res.* 2021, 60, 5024–5033; b) P. J. Rae, P. M. Dickson, *J. Dynamic Behavior Mater.* 2021, 7, 414–424.

- [7] J. M. Winey, K. Zimmerman, Z. A. Dreger, Y. M. Gupta, *J. Phys. Chem. A* **2020**, *124*, 6521–6527.
- [8] a) Virginia, W. Manner, M. J. Cawkwell, E. M. Kober, T. W. Myers, G. W. Brown, H. Tian, C. J. Snyder, R. Perriot, D. N. Preston, *Chem. Sci.* **2018**, *9*, 3649–3663; b) T. W. Myers, C. J. Snyder, V. W. Manner, *Cryst. Growth Des.* **2017**, *17*, 3204–3209.
- [9] a) Y.-H. Joo, J. M. Shreeve, *Chem. Commun.* **2010**, *46*, 142–144; b) R. P. Singh, J. M. Shreeve, *Chem. Eur. J.* **2011**, *17*, 11876–11881.
- [10] a) N. Lease, V. W. Manner, D. E. Chavez, D. Robbins, L. Kay, *AIP Conf. Proc.* **2020**, 2272, 050013; b) N. Lease, L. M. Kay, G. W. Brown, D. E. Chavez, D. Robbins, E. F. C. Byrd, G. H. Imler, D. A. Parrish, V. W. Manner, *J. Org. Chem.* **2020**, *85*, 4619–4626.
- [11] T. Lenz, T. M. Klapötke, M. Mühlemann, J. Stierstorfer, *Propellants Explos. Pyrotech.* **2021**, *46*, 723–731.
- [12] a) D. E. Chavez, M. A. Hiskey, D. L. Naud, D. Parrish, *Angew. Chem. Int. Ed.* **2008**, *47*, 8307–8309; *Angew. Chem.* **2008**, *120*, 8431–8433; b) T. W. Myers, C. J. Snyder, D. E. Chavez, R. J. Scharff, J. M. Veauthier, *Chem. Eur. J.* **2016**, *22*, 10590–10596.
- [13] J. J. Sabatini, E. C. Johnson, *ACS Omega* **2021**, *6*, 11813–11821.
- [14] E. C. Johnson, J. J. Sabatini, D. E. Chavez, R. C. Sausa, E. F. C. Byrd, L. A. Wingard, P. E. Guzmàn, *Org. Process Res. Dev.* **2018**, *22*, 736–740.
- [15] S. Wawzonek, A. Matar, C. H. Issidorides, *Org. Synth.* **2003**, *38*, 68–68.
- [16] M. A. Hiskey, M. J. Hatch, J. C. Oxley, *Propellants Explos. Pyrotech.* **1991**, *16*, 40–42.
- [17] T. Altenburg, T. M. Klapötke, A. Penger, *Cent. Eur. J. Energ. Mater.* **2009**, *6*, 255–275.
- [18] "Formation of the potassium salt in Ethanol yielded crystals of potassium nitrite."
- [19] P. N. Gaponik, V. P. Karavai, Y. V. Grigor'ev, *Chem. Heterocycl. Compd.* **1985**, *21*, 1255–1258.
- [20] a) M. Benz, T. M. Klapötke, T. Lenz, J. Stierstorfer, *Chem. Eur. J.* **2022**, *28*, e202200772; b) M. S. Gruhne, T. Lenz, M. Rösch, M. Lommel, M. H. H. Wurzenberger, T. M. Klapötke, J. Stierstorfer, *Dalton Trans.* **2021**, *50*, 10811–10825.

Manuscript received: December 22, 2022

Accepted manuscript online: January 24, 2023

Version of record online: March 10, 2023

Chemistry–A European Journal

Supporting Information

Melt Castable Derivatives of Pentaerythritol Tetranitrate

Maximilian Benz, Thomas M. Klapötke,* Niklas Kölbl, Jürgen Kuch, Tobias Lenz, Ersel Parigi,
and Jörg Stierstorfer

Table of Contents

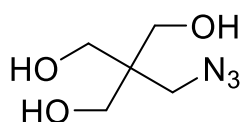
1. Experimental part and general procedures
2. X-ray diffraction
3. Computation
4. NMR Spectroscopy
5. Thermal properties
6. References

1. Experimental part and general procedures

^1H , ^{13}C , ^{14}N and ^{15}N NMR spectra were recorded on *BRUKER AMX 400* instruments. Chemical shifts are referenced with respect to tetramethylsilane ($^1\text{H}/^{13}\text{C}$) and nitromethane ($^{14}\text{N}/^{15}\text{N}$). Infrared spectra (IR) were recorded in the region $4000\text{-}400\text{ cm}^{-1}$ on a *PERKIN ELMER Spectrum BX-59343* instrument with a *SMITHS DETECTION DuraSamplIR II Diamond ATR* sensor. The absorption bands are reported in wavenumbers (cm^{-1}). Decomposition temperatures were measured via differential thermal analysis (DTA) with an *OZM Research DTA 552-Ex* instrument at a heating rate of $5\text{ }^\circ\text{C}/\text{min}$ and in a range of room temperature to $400\text{ }^\circ\text{C}$. All sensitivities toward impact (IS) and friction (FS) were determined according to BAM (Bundesanstalt für Materialforschung und Prüfung) standards using a BAM drop hammer and a BAM friction apparatus by applying the 1 of 6 method.¹ Energetic properties have been calculated with the EXPLO 5 6.04 computer² code using the RT converted X-ray density or the densities measured with a gas pycnometer at 298 K and calculated solid state heats of formation.

Safety: We have not experienced any incidents or accidental detonations of the compounds. But with the sensitivities present (between primary and secondary explosives), caution is advised. Working with small quantities and protection (kevler gloves, ear protection) is recommended.

Compound 1

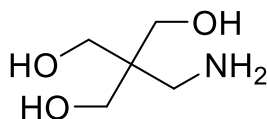


To a solution of monobromopentaerythritol³ (10.0 g, 50.2 mmol, 1.0 eq.) in DMF (150 mL), NaN_3 (6.53 g, 100 mmol, 2.0 eq.) was added and the reaction mixture was stirred overnight at $105\text{ }^\circ\text{C}$. The reaction process was checked by TLC. The solvent was removed under reduced pressure ($80\text{ }^\circ\text{C}$, 10 mbar) and the residue was extracted with EtOAc (10 x 100 mL). The combined organic phases were dried over Na_2SO_4 and the solvent was removed under reduced pressure. The obtained yellow crude solid was recrystallized from chloroform/EtOAc (3:2) to yield colorless azide **1** (6.64 g, 41.2 mmol, 82%).

Full characterization by Klapötke *et al.*⁴

IR (ATR): ν_{\max} [cm^{-1}] = 3258 (m), 2967 (m), 2935 (m), 2889 (m), 2099 (s), 1483 (m), 1463 (m), 1369 (m), 1272 (m), 1252 (m), 1146 (m), 1025 (vs), 951 (m), 915 (m), 893 (m), 876 (m), 647 (s), 596 (s), 555 (s), 501 (m); **^1H NMR (400 MHz, DMSO-*d*₆):** δ (ppm) = 4.41 (t, J = 5.2 Hz, 3H), 3.30 (d, J = 5.2 Hz, 6H), 3.28 (s, 2H).

Compound 2



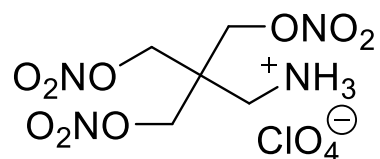
Compound 1 (2.01 g, 12.4 mmol, 1.0 eq.) was dissolved in EtOH (150 mL) and the solution was degassed with N_2 . Pd/C (10 wt.%, 75 mg) was added under N_2 -atmosphere then H_2 was bubbled through the solution. (Caution: fine powdered and dry Pd/C can ignite in air). The reaction mixture was stirred at r.t. for 4 h then filtered over diatomaceous earth and the solvent was removed under reduced pressure to yield colorless amine **2** (1.60 g, 11.8 mmol, 95%).

IR (ATR): ν_{\max} [cm^{-1}] = 3303 (m), 2932 (m), 2875 (m), 1658 (w), 1588 (m), 1469 (m), 1452 (m), 1372 (s), 1274 (m), 1089 (m), 1063 (m), 1021 (vs), 984 (vs), 880 (m), 867 (m), 819 (s), 787 (s), 641 (s), 560 (s), 417 (s); **EA** ($\text{C}_5\text{H}_{13}\text{NO}_3$, 135.16 g mol^{-1}): calc.: C 44.43, N 10.36, H 9.69%; found: (hygroscopic); **^1H NMR (400 MHz, Methanol-*d*₄):** δ (ppm) = 3.55 (s, 6H), 2.73 (s, 2H); **^{13}C NMR (101 MHz, Methanol-*d*₄):** δ (ppm) = 63.8, 45.7, 43.7; **HRMS** (ESI) m/z : [$\text{M} - \text{H}^+$], Calcd. for $\text{C}_5\text{H}_{14}\text{NO}_3$ 136.08954; Found: 136.09680.

type 12, recalculated with $m = 2.5 \text{ kg}$ and $g = 10 \text{ m s}^{-1}$): 7 J for **3a** compared to 3 J for **PETN**.

DTA (5 °C min⁻¹): 145 °C (dec.); **Sensitivities** (< 500 μm , crystalline material): BAM drop hammer: 3 J; BAM friction tester: 120 N; **IR (ATR):** $\nu_{\text{max}} [\text{cm}^{-1}] = 2933 \text{ (w)}, 1633 \text{ (s)}, 1531 \text{ (m)}, 1473 \text{ (m)}, 1465 \text{ (m)}, 1411 \text{ (m)}, 1394 \text{ (m)}, 1375 \text{ (m)}, 1305 \text{ (s)}, 1269 \text{ (vs)}, 1110 \text{ (w)}, 1024 \text{ (s)}, 996 \text{ (s)}, 848 \text{ (vs)}, 824 \text{ (vs)}, 753 \text{ (s)}, 740 \text{ (s)}, 706 \text{ (s)}, 690 \text{ (m)}, 620 \text{ (s)}, 595 \text{ (m)}$; **EA** ($\text{C}_5\text{H}_{11}\text{N}_5\text{O}_{12}$, 333.17 g mol^{-1}): calc.: C 18.03, N 21.02, H 3.33%; found: C 18.32, N 20.78, H 3.23%; **¹H NMR (400 MHz, DMSO-*d*₆):** δ (ppm) = 8.07 (s, 3H), 4.65 (s, 6H), 3.11 (s, 2H); **¹³C NMR (101 MHz, DMSO-*d*₆):** δ (ppm) = 70.2, 39.6, 38.8.

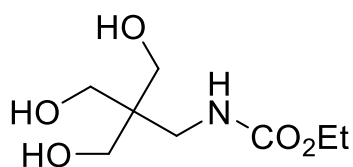
Compound 3b



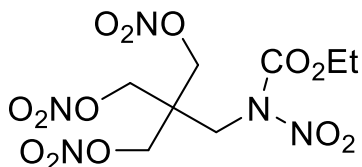
Compound **3** (504 mg, 1.87 mmol, 1.00 eq.) was dissolved in hot HClO₄ (2M, 0.93 ml, 1.87 mmol, 1.00 eq.). The solvent was evaporated until perchlorate salt **3b** (409 mg, 1.15 mmol, 59%) crystallizes as colorless blocks.

DTA (5 °C min⁻¹): 146 °C (dec); **IR (ATR):** $\nu_{\text{max}} [\text{cm}^{-1}] = 3266 \text{ (w)}, 3237 \text{ (w)}, 3094 \text{ (w)}, 1667 \text{ (m)}, 1651 \text{ (s)}, 1632 \text{ (s)}, 1500 \text{ (m)}, 1477 \text{ (m)}, 1279 \text{ (vs)}, 1119 \text{ (m)}, 1103 \text{ (s)}, 1071 \text{ (vs)}, 1029 \text{ (s)}, 1006 \text{ (s)}, 981 \text{ (s)}, 887 \text{ (s)}, 870 \text{ (s)}, 856 \text{ (s)}, 832 \text{ (vs)}, 805 \text{ (s)}, 754 \text{ (s)}, 730 \text{ (m)}, 716 \text{ (s)}, 677 \text{ (m)}, 621 \text{ (s)}, 608 \text{ (s)}$; **EA** ($\text{C}_5\text{H}_{11}\text{ClN}_4\text{O}_{13}$, 370.61 g mol^{-1}): calc.: C 16.20, N 21.12, H 2.99%; found: C 16.23, N 15.12, H 3.06%; **¹H NMR (400 MHz, DMSO-*d*₆):** δ (ppm) = 7.99 (s, 3H), 4.65 (s, 6H), 3.10 (s, 2H); **¹³C NMR (101 MHz, DMSO-*d*₆):** δ (ppm) = 70.2, 39.6, 38.9.

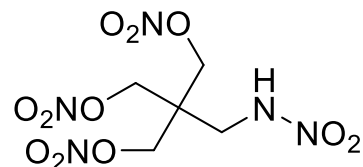
Compound 4 and Intermediates 4_prec1 and 4_prec2



4_prec1



4_prec2



4

Amine **3** (5.28 g, 39.1 mmol, 1.0 eq.) was dissolved in H₂O (100 ml). Then half of ethyl chloroformate (3.72 ml, 39.1 mmol, 1.0 eq) was added dropwise to the solution at 0 °C. Afterwards KOH (2.19 g, 39.1 mmol, 1.0 eq.) was dissolved in H₂O (120 ml). The potassium hydroxide solution and the remaining ethyl chloroformate were then added dropwise in an alternating manner. The solution was stirred over night at room temperature. The solvent was removed under vacuum and a white residue was obtained. This residue was then extracted with EtOH (50 ml) (formed KCl is not soluble). The EtOH then was removed under reduced pressure and compound **4_prec1** was obtained as a white solid (3.98 g, 19.2 mmol, 49%).

¹H NMR (400 MHz, DMSO-*d*₆): δ (ppm) = 6.74 (t, *J* = 6.1 Hz, 1H), 4.27 (t, *J* = 5.4 Hz, 3H), 3.98 (q, *J* = 7.1 Hz, 2H), 3.29 (d, *J* = 4.9 Hz, 6H), 2.99 (d, *J* = 6.2 Hz, 2H), 1.15 (t, *J* = 7.1 Hz, 3H); **¹³C NMR (101 MHz, DMSO-*d*₆):** δ (ppm) = 157.2, 61.0, 59.9, 45.1, 40.9, 14.6.

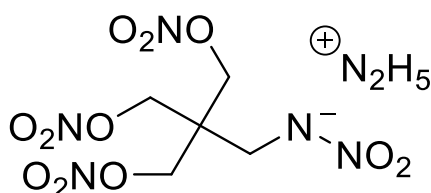
Then fuming HNO₃ (99%, 12 ml) was added slowly to TFAA (24 ml) at 5 °C. Compound **4_prec1** (0.93 mg, 4.50 mmol) was added in portions at 5-10 °C. The yellow solution was then stirred at room temperature overnight. The either orange or clear solution was then added onto ice (50 ml) and extracted with DCM (3 x 50 ml). The organic phase was then washed with sat. NaHCO₃ solution (3 x 100 ml) and with brine (1x 100 ml). After drying over Na₂SO₄ the solvent was removed under reduced pressure. Yellowish solid **4_prec2** was obtained (1.69 g, 4.37 mmol, 97%).

¹H NMR (400 MHz, DMSO-*d*₆): δ (ppm) = 4.67 (s, 6H), 4.41 (s, 2H), 4.31 (q, *J* = 7.1 Hz, 2H), 1.28 (t, *J* = 7.1 Hz, 3H); **¹³C NMR (101 MHz, DMSO-*d*₆):** δ (ppm) = 150.7, 71.0, 65.2, 49.0, 42.2, 13.6.

Then compound **4_prec2** (1.71 g, 3.74 mmol, 1.0 eq.) was dissolved in Et₂O (50 ml). Afterwards NH₃-gas was passed into the solution for 20 min. Then the suspension was extracted with water (3x 25 ml). The aqueous phase was acidified carefully with HCl (2M). The solution was extracted with EtOAc (3x 25 ml). The organic phase was dried with Na₂SO₄, filtered and the solvent was removed. Compound **4** was obtained as a white solid (676 mg, 2.14 mmol, 78%).

DTA (5 °C min⁻¹): 64 °C (melt.), 170 °C (dec.); **Sensitivities** (< 500 μm, crystalline material): BAM drop hammer: 10 J; BAM friction tester: >360 N; **IR (ATR):** v_{\max} [cm⁻¹] = 3318 (w), 2903 (w), 1631 (vs), 1590 (s), 1393 (m), 1322 (s), 1265 (vs), 1023 (s), 994 (s), 839 (vs), 752 (s), 702 (s), 622 (s), 526 (s); **EA** (C₅H₉N₅O₁₁, 315.15 g mol⁻¹): calc.: C 19.06, N 22.22, H 2.88%; found: C 19.31, N 21.952, H 2.73%; **¹H NMR (400 MHz, DMSO):** δ = 12.32 (s, 1H), 4.61 (s, 6H), 3.78 (s, 2H); **¹³C NMR (101 MHz, DMSO):** δ = 71.0, 44.1, 41.9; **¹⁵N NMR (41 MHz, Acetone):** δ = -27.19, -45.02, -215.74.

Compound 4a

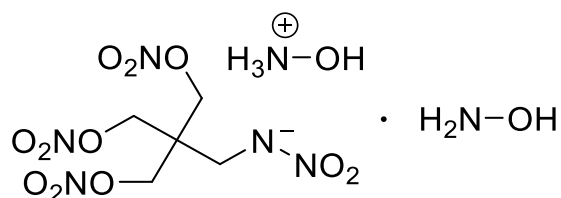


Compound **4** (400 mg, 1.27 mmol, 1.0 eq.) was dissolved in Et₂O (20 mL) and hydrazine monohydrate (62.0 μL, 1.27 mmol, 1.0 eq.) was added. The immediately formed precipitate was filtered off to obtain hydrazinium salt **4a** (337 mg, 0.97 mmol, 76%) as a colorless solid.

DTA (5 °C min⁻¹): 100 °C (dec); **Sensitivities:** BAM drop hammer: 3 J; BAM friction tester: 120 N; **IR (ATR):** v_{\max} [cm⁻¹] = 2911 (w), 2629 (w), 1634 (vs), 1535 (w), 1443 (m), 1424 (m), 1402 (m), 1380 (m), 1270 (vs), 1260 (vs), 1181 (m), 1096 (m), 1026 (m), 995 (s), 935 (m), 852 (vs), 753 (s), 738 (s), 707 (s), 687 (m), 659 (m), 621 (m), 549 (w), 465 (m); **EA** (C₅H₁₃N₇O₁₁, 347.20 g mol⁻¹): calc.: C 17.30, N 28.24, H 3.77%;

found: C 17.62, N 27.55, H 3.65%, $^1\text{H NMR}$ (400 MHz, Methanol- d_4): δ (ppm) = 4.67 (s, 6H), 3.56 (s, 2H), $^{13}\text{C NMR}$ (101 MHz, Methanol- d_4): δ (ppm) = 72.7, 50.9, 43.0.

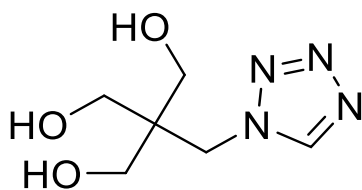
Compound 4b



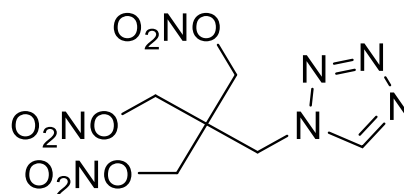
Compound **4** (400 mg, 1.27 mmol, 1.0 eq.) was dissolved in Et₂O (20 mL) and a solution of hydroxylamine (50% aq., 0.16 mL, 2.54 mmol, 2.0 eq.) was added dropwise. The reaction mixture was cooled to 0 °C overnight and the formed precipitate was filtered off to afford hydroxylammonium salt **4b** (391 mg, 1.03 mmol, 81%).

DTA (5 °C min⁻¹): 73 °C (dec.); **Sensitivities**: BAM drop hammer: 4 J; BAM friction tester: 45 N; **IR** (ATR): ν_{max} [cm⁻¹] = 3243 (w), 2924 (w), 2705 (w), 1666 (m), 1628 (vs), 1530 (m), 1467 (m), 1449 (s), 1428 (s), 1383 (m), 1348 (m), 1273 (s), 1243 (s), 1190 (m), 1084 (m), 1032 (s), 994 (s), 929 (m), 861 (vs), 837 (s), 753 (s), 742 (s), 715 (m), 705 (s), 686 (m), 663 (m), 631 (m), 625 (m), 546 (m), 471 (m); **EA** (C₅H₁₅N₇O₁₃, 381.21 g mol⁻¹): calc.: C 15.75, N 25.72, H 3.97%; found: C 16.20, N 25.18, H 3.65%, $^1\text{H NMR}$ (400 MHz, Methanol- d_4): δ (ppm) = 4.66 (s, 6H), 3.66 (s, 2H), $^{13}\text{C NMR}$ (101 MHz, Methanol- d_4): δ (ppm) = 72.4, 49.8-48.2 (between solvent peaks), 43.4; $^{14}\text{N NMR}$ (29 MHz, Methanol- d_4): δ (ppm) = -27, -47.

Compound 5



5_prec1



5

Amine **3** (1.00 g, 7.39 mmol, 1.0 eq.), NaN₃ (578 mg, 8.89 mmol, 1.2 eq.) and triethyl orthoformate (1.84 ml, 11.07 mmol, 1.5 eq.) were added together and then heated at 40 °C. Dropwise AcOH (4 ml) was added and the solution was heated at 85 °C for 3 h. Afterwards conc. HCl (0.75 ml, 9.00 mmol, 1.2 eq.) was added slowly. The obtained suspension was filtered off, and conc. HCl (10 ml) was added to the filtrate. After heating at 60 °C for 30 min. the solvent was removed under vacuum to obtain crude **5_prec1**.

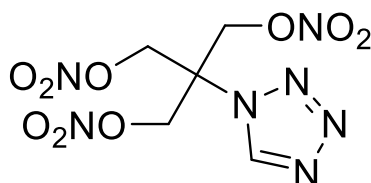
¹H NMR (400 MHz, DMSO-d₆): δ (ppm) = 9.21 (s, 1H), 4.41 (s, 2H), 3.26 (s, 6H), **¹³C NMR (101 MHz, DMSO-d₆):** δ (ppm) = 145.6, 60.4, 46.2, 45.7.

This crude material was added in portions to HNO₃ (99%, 8 mL) at 0 °C-5 °C. The resulting mixture was stirred at 0 °C for 15 min., was allowed to warm to r.t. and stirred for another 15 min. Then the reaction mixture was poured on ice-water and neutralized with NaHCO₃. After extraction with EtOAc (3x 50 mL), the combined organic phases were dried over Na₂SO₄ and the solvent was removed under reduced pressure. The resulting crude was then purified *via* column chromatography (*i*-Hex/EtOAc, 1:1) to afford colorless solid **5** (974 mg, 3.01 mmol, 41%).

DTA (5 °C min⁻¹): 106 °C (melt.), 180 °C (dec.); **Sensitivities:** BAM drop hammer: 2 J; BAM friction tester: 160 N, **IR (ATR):** ν_{max} [cm⁻¹] = 3154 (w), 3026 (vw), 2992 (vw), 2904 (w), 1626 (vs), 1467 (m), 1389 (w), 1275 (vs), 1171 (m), 1124 (w), 1096 (m), 1036 (m), 1007 (s), 985 (m), 962 (w), 856 (vs), 773 (m), 753 (s), 729 (m), 709 (s), 696 (m), 661 (m), 631 (m), 623 (m), 454 (m), **EA** (C₆H₉N₇O₉, 323.18 g mol⁻¹): calc.: C 22.30, N 30.34, H 2.81%; found: C 22.32, N 30.08, H 2.73%, **¹H NMR (400 MHz, DMSO):** δ (ppm) = 9.53 (s, 1H), 4.82 (s, 2H), 4.66 (s, 6H); **¹³C NMR (101 MHz, DMSO):**

$\delta = 145.5, 70.6, 46.9, 41.3$; **^{15}N NMR (41 MHz, Acetone)**: δ (ppm) = 11.0 (d, $J = 3.1$ Hz), -16.6 (s), -50.0 (t, $J = 1.9$ Hz), -54.9 (d, $J = 12.2$ Hz), -156.7 (d, $J = 9.7$ Hz).

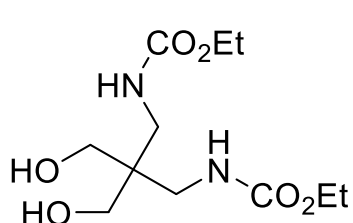
Compound 7



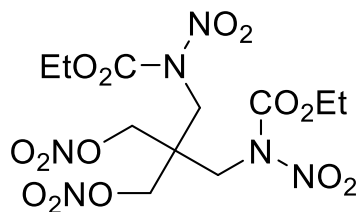
Compound **6**⁶ (1.00 g, 5.74 mmol) was added in portions to HNO_3 (99%, 8 mL) at 0 °C-5 °C. The resulting mixture was stirred at below 5 °C for 15 min., was allowed to warm to r.t. and stirred for another 15 min. Then the reaction mixture was poured on ice-water and neutralized with NaHCO_3 . After extraction with EtOAc (3 x 50 mL), the combined organic phases were dried over Na_2SO_4 and the solvent was removed under reduced pressure leaving colorless crystalline **7** (1.10 g, 3.56 mmol, 62%).

DTA (5 °C min⁻¹): 92 °C (melt.), 163 °C (dec.); **Sensitivities**: BAM drop hammer: 2 J; BAM friction tester: 80 N; **IR (ATR)**: ν_{max} [cm^{-1}] = 3123 (w), 3026 (w), 2922 (w), 1641 (vs), 1380 (m), 1296 (m), 1280 (vs), 1259 (s), 1093 (m), 1035 (s), 1021 (s), 977 (m), 866 (s), 836 (vs), 751 (s), 740 (s), 725 (s), 714 (s), 624 (s), 557 (m); **EA** ($\text{C}_5\text{H}_7\text{N}_7\text{O}_9$, 309.15 g mol⁻¹): calc.: C 19.43, N 31.72, H 2.28%; found: C 19.79, N 30.40, H 2.45%, **^1H NMR (400 MHz, Acetone- d_6)**: δ (ppm) = 9.68 (s, 1H), 5.47 (s, 6H) **^{13}C NMR (101 MHz, DMSO, Acetone- d_6)**: δ (ppm) = 143.6, 69.9, 62.4; **^{15}N NMR (41 MHz, Acetone- d_6)**: δ (ppm) = 13.3, -18.4, -49.0, -50.7, -145.1.

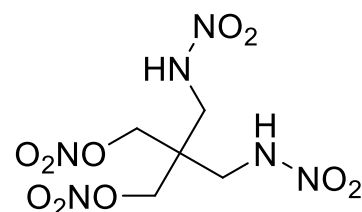
Compound 9 and Intermediates 9_prec1 and 9_prec2



9_prec1



9_prec2



9

Amine **8** (2.45 g, 18.4 mmol, 1.0 eq.) was dissolved in H₂O (50 ml). Then half of ethyl chloroformate (3.47 ml, 36.5 mmol, 2.0 eq) was added dropwise to the solution at 0 °C. Afterwards KOH (2.05 g, 36.5 mmol, 2.0 eq.) was dissolved in H₂O (20 ml). The potassium hydroxide solution and the remaining ethyl chloroformate were then added dropwise in an alternating manner. The solution was stirred over night at room temperature. The solvent was removed by a rotation evaporator and a white residue was obtained. This residue was then extracted with EtOH (50 ml) (formed KCl is not soluble). The EtOH then was removed under reduced pressure and compound **9_prec1** was obtained as a white solid (2.57 g, 9.2 mmol, 50%).

¹H NMR (400 MHz, DMSO-*d*₆): δ (ppm) = 6.79 (t, 6.36 Hz, 2H), 4.35 (s, 2H), 3.98 (q, *J* = 7.08 Hz, 4H), 3.24 (s, 4H), 2.94 (d, *J* = 6.38 Hz, 4H), 1.15 (t, *J* = 7.08 Hz, 6H); **¹³C NMR (101 MHz, DMSO-*d*₆):** δ (ppm) = 157.1, 61.2, 59.9, 45.0, 40.9, 14.6.

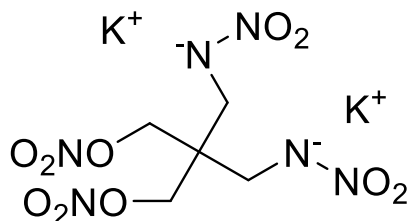
Then fuming HNO₃ (99%, 9 ml) was added slowly to TFAA (18 ml) at 5 °C. Compound **9_prec1** (1.28 g, 4.62 mmol) was added in portions at 5-10 °C. The yellow solution was then stirred at room temperature overnight. The either orange or clear solution was then added onto ice (50 ml) and extracted with DCM (3 x 50 ml). The organic phase was then washed with sat. NaHCO₃ solution (3 x 100 ml) and with brine (1x 100 ml). After drying over Na₂SO₄ the solvent was removed under reduced pressure. Yellowish white solid **9_prec2** was obtained (1.90 g, 4.16 mmol, 90%).

¹H-NMR (400 MHz, DMSO-*d*₆): δ (ppm) = 4.61 (s, 4H), 4.38 (s, 4H), 4.31 (q, *J* = 7.15 Hz, 4H), 1.28 (t, *J* = 7.1 Hz, 6H); **¹³C-NMR (101 MHz, DMSO-*d*₆):** δ (ppm) = 150.8, 71.9, 65.3, 49.7, 43.7, 13.6.

Then compound (**9_prec2**) (1.73 g, 3.78 mmol, 1.0 eq.) was dissolved in Et₂O (50 ml). Afterwards NH₃-gas was passed into the solution for 20 min. Then the suspension was extracted with water (3x 25 ml). The aqueous phase was acidified carefully with HCl (2 M). Compound **9** crystallizes out of solution and was obtained as a colorless solid (1.01 g, 3.21 mmol, 85%).

DTA (5 °C min⁻¹): 64 (melt.), 170 °C (dec.); **Sensitivities** (< 500 μm, crystalline material): BAM drop hammer: 10 J; BAM friction tester: >360 N; **IR (ATR):** v_{\max} [cm⁻¹] = 3318 (w), 2903 (w), 1631 (vs), 1590 (s), 1393 (m), 1322 (s), 1265 (vs), 1023 (s), 994 (s), 839 (vs), 752 (s), 702 (s), 622 (s), 526 (s); **EA** (C₅H₉N₅O₁₁, 315.15 g mol⁻¹): calc.: C 19.06, N 22.22, H 2.88%; found: C 19.31, N 21.952, H 2.73%; **¹H NMR (400 MHz, DMSO):** δ = 12.32 (s, 1H), 4.61 (s, 6H), 3.78 (s, 2H).; **¹³C NMR (101 MHz, DMSO):** δ = 71.0, 44.1, 41.9; **¹⁵N NMR (41 MHz, Acetone):** δ = -27.2, -45.0, -215.7.

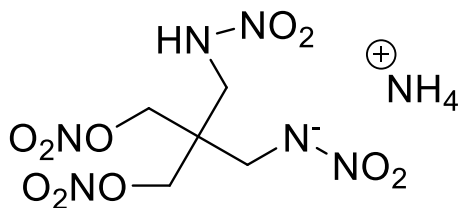
Compound 9a



To a solution of compound **6b** (462 mg, 1.64 mmol, 1.0 eq.) in EtOH (10 ml) was added KOH (184 mg, 3.28 mmol, 2.0 eq.) in EtOH. The white solid potassium salt **9a** (436 mg, 1.12 mmol, 68%) precipitated out of solution. The product was recrystallized from EtOH/H₂O.

DTA (5 °C min⁻¹): 135 °C (dec.); **Sensitivities** (< 500 μm, crystalline material): BAM drop hammer: 3 J; BAM friction tester: >360 N; **IR (ATR):** v_{\max} [cm⁻¹] = 3304 (m), 2930 (m), 2875 (m), 1634 (m), 1590 (m), 1400 (m), 1373 (m), 1268 (s), 1022 (vs), 990 (vs), 864 (s), 823(s), 623 (s), 559 (s); **EA** (C₅H₈K₂N₆O₁₀, 390.35 g/mol): C 15.39, H, 2.07, N 21.53%; found: C 15.71, 2.12, 21.37%, **¹H NMR (400 MHz, D₂O):** δ = 4.71 (s, 4H), 3.54 (s, 4H); **¹³C NMR (101 MHz, D₂O):** δ = 72.9, 51.9, 40.8.

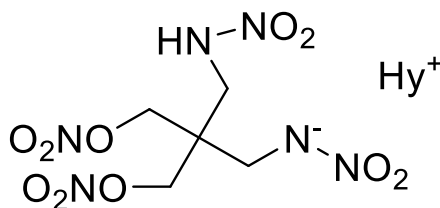
Compound 9b



Compound **9** (250 mg, 0.79 mmol) was dissolved in ammonia (2 M, aq. solution, 5 ml). The solution was left to crystallize and few single crystals suitable for X-ray crystallography were obtained.

EA (C₅H₁₃N₇O₁₀, 331.20 g mol⁻¹): calc.: C 18.13, N 29.60, H 3.96%; found: C 18.73, N 28.86, H 3.67%;

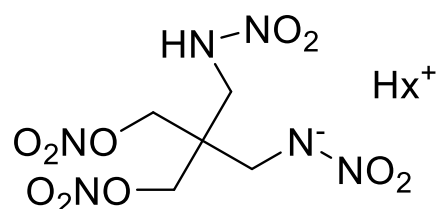
Compound 9c



Compound **9** (403 mg, 1.28 mmol, 1.0 eq.) was dissolved in Et₂O (200 mL) and MeOH (5 mL). Hydrazine monohydrate (62.0 μL, 1.28 mmol, 1.0 eq.) was added and the mixture was cooled to 0 °C overnight. The precipitate was filtered off and washed with Et₂O to afford the colorless hydrazinium salt **9c** (351 mg, 1.01 mmol, 79%).

DTA (5 °C min⁻¹): 108 °C (dec.); **Sensitivities** (< 500 μm, crystalline material): BAM drop hammer: 3 J; BAM friction tester: 160 N; **IR (ATR):** ν_{\max} [cm⁻¹] = 3347 (w), 3211 (w), 2921 (w), 2725 (w), 2606 (w), 1649 (m), 1634 (s), 1624 (s), 1588 (m), 1538 (w), 1447 (s), 1415 (m), 1396 (m), 1378 (m), 1318 (m), 1270 (vs), 1152 (m), 1117(m), 1094 (s), 1031 (m), 1016 (m), 1000 (m), 989 (m), 948 (s), 887 (m), 853 (vs), 823 (s), 753 (s), 726(s), 710 (m), 667 (m), 643 (m), 621 (m), 506 (m), 434 (m); **EA** (C₅H₁₄N₈O₁₀, 346.21 g mol⁻¹): calc.: C 17.35, N 32.37, H 4.08%; found: C 17.58, N 32.53, H 3.80%; **¹H NMR (400 MHz, MeOD):** δ = 4.90 (br s), 4.59 (s, 4H), 3.65 (s, 4H); **¹³C NMR (101 MHz, MeOD):** δ = 73.5, 49.9, 43.6; **¹⁴N NMR (29 MHz, Acetone):** δ = -25, -44.

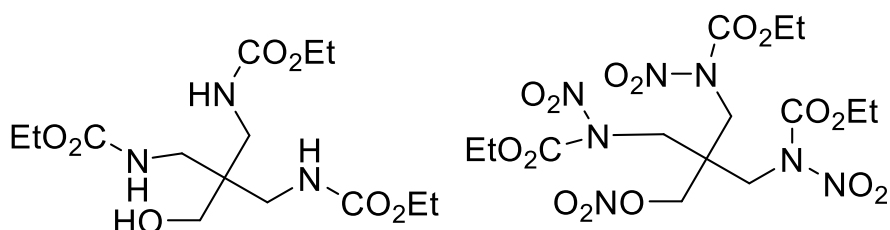
Compound 9d



Compound **9** (596 mg, 1.90 mmol, 1.0 eq.) was dissolved in Et₂O (200 mL) and MeOH (10 mL). Hydroxylamine (0.116 mL, 1.90 mmol, 1.0 eq.) was added and the mixture was stirred at r.t. for 10 minutes before cooled to 0 °C overnight. The precipitate was filtered off to obtain hydroxylamine salt **9d** (104 mg, 0.30 mmol, 16%).

DTA (5 °C min⁻¹): 120 °C (melt.), 125 °C (dec.); **Sensitivities** (< 500 μm, crystalline material): BAM drop hammer: 15 J; BAM friction tester: 360 N; **IR (ATR):** v_{\max} [cm⁻¹] = 3349 (w), 3273 (w), 1630 (s), 1589 (s), 1553 (w), 1465 (w), 1395 (m), 1318 (s), 1268 (s), 1179 (m), 1110 (m), 1091 (m), 1012 (m), 864 (s), 756 (m), 571 (m), 438 (m); **EA** (C₅H₁₃N₇O₁₁, 347.20 g mol⁻¹): calc.: C 17.30, N 28.24, H 3.77%; found: C 17.50, N 27.55, H 3.70%; **¹H NMR (400 MHz, CD₃CN):** δ = 4.52 (s, 4H), 3.72 (s, 4H); **¹³C NMR (101 MHz, CD₃CN):** δ = 72.5, 47.1, 44.0; **¹⁴N NMR (29 MHz, Acetone):** δ = -26, -44, -136.

Intermediates 11_prec1 and 11_prec2



11_prec1

11_prec2

Amine **8** (2.45 g, 18.4 mmol, 1.0 eq.) was dissolved in H₂O (50 ml). Then half of ethyl chloroformate (3.47 ml, 36.5 mmol, 2.0 eq) was added dropwise to the solution at 0 °C. Afterwards KOH (2.05 g, 36.5 mmol, 2.0 eq.) was dissolved in H₂O (20 ml). The

potassium hydroxide solution and the remaining ethyl chloroformate were then added dropwise in an alternating manner. The solution was stirred over night at room temperature. The solvent was removed by a rotation evaporator and a white residue was obtained. This residue was then extracted with EtOH (50 ml) (formed KCl is not soluble). The EtOH then was removed under reduced pressure and compound **9_prec1** was obtained as a white solid (2.57 g, 9.2 mmol, 50%).

¹H NMR (400 MHz, DMSO-*d*₆): δ (ppm) = 6.82 (t, *J* = 6.6 Hz, 3H), 4.32 (q, *J* = 7.1 Hz, 1H), 3.17 (s, *J* = 4.8, 2H), 2.91 (d, *J* = 6.6 Hz, 6H), 1.16 (t, *J* = 7.1 Hz, 9H); **¹³C NMR (101 MHz, DMSO-*d*₆):** δ (ppm) = 157.1, 61.7, 60.0, 45.0, 41.1, 14.6.

Then fuming HNO₃ (99%, 9 ml) was added slowly to TFAA (18 ml) at 5 °C. Compound **9_prec1** (1.28 g, 4.62 mmol) was added in portions at 5-10 °C. The yellow solution was then stirred at room temperature overnight. The either orange or clear solution was then added onto ice (50 ml) and extracted with DCM (3 x 50 ml). The organic phase was then washed with sat. NaHCO₃ solution (3 x 100 ml) and with brine (1x 100 ml). After drying over Na₂SO₄ the solvent was removed under reduced pressure. Yellowish white solid **9_prec2** was obtained (1.90 g, 4.16 mmol, 90%).

¹H-NMR (400 MHz, DMSO-*d*₆): δ (ppm) = 4.50 (s, 2H), 4.36 (s, 6H), 4.31 (q, *J* = 7.2 Hz, 6H), 1.28 (t, *J* = 7.1 Hz, 9H); **¹³C-NMR (101 MHz, DMSO-*d*₆):** δ (ppm) = 151.0, 73.5, 65.3, 51.0, 45.6, 13.6.

2. X-ray diffraction

Crystal structure data were obtained from an Oxford Xcalibur3 diffractometer with a Spellman generator (voltage 50 kV, current 40 mA) and a Kappa CCD area for data collection using Mo- $K\alpha$ radiation ($\lambda = 0.71073 \text{ \AA}$). The data collection was performed using the CRYSTALIS RED software.⁷ Very small crystals were measured on a Bruker D8 Venture TXS system equipped with a multilayer mirror monochromator and a Mo $K\alpha$ rotating anode X-ray tube ($\lambda = 0.71073 \text{ \AA}$). The frames were integrated with the Bruker SAINT software package.⁸ Data were corrected for absorption effects using the Multi-Scan method (SADABS).⁹ The solution of the structure was performed by direct methods and refined by full-matrix least-squares on F² (SHELXT)¹⁰ implemented in the OLEX2¹¹ software suite. The non-hydrogen atoms were refined anisotropically and the hydrogen atoms were located and freely refined. The absorption correction was carried out by a SCALE3 ABSPACK multiscan method.¹² The DIAMOND2 plots shown with thermal ellipsoids at the 50% probability level and hydrogen atoms are shown as small spheres of arbitrary radius. The SADABS program embedded in the Bruker APEX3 software was used for multi-scan absorption corrections in all structures.¹³

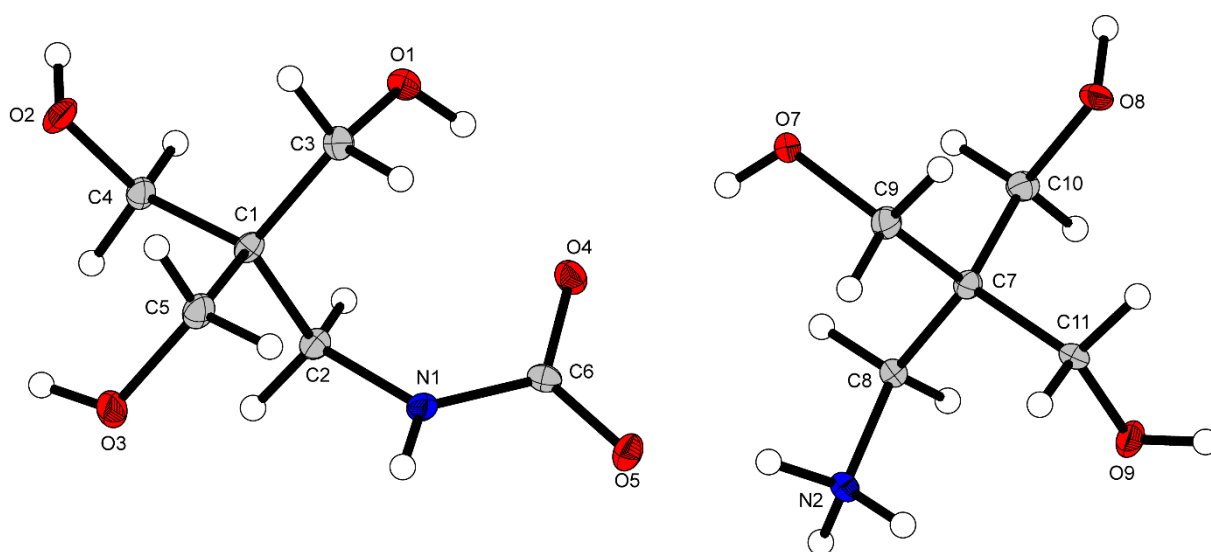


Figure S1. Representation of the molecular unit of **2_CO₂**, showing the atom-labeling scheme. Thermal ellipsoids represent the 50% probability level and hydrogen atoms are shown as small spheres of arbitrary radius.

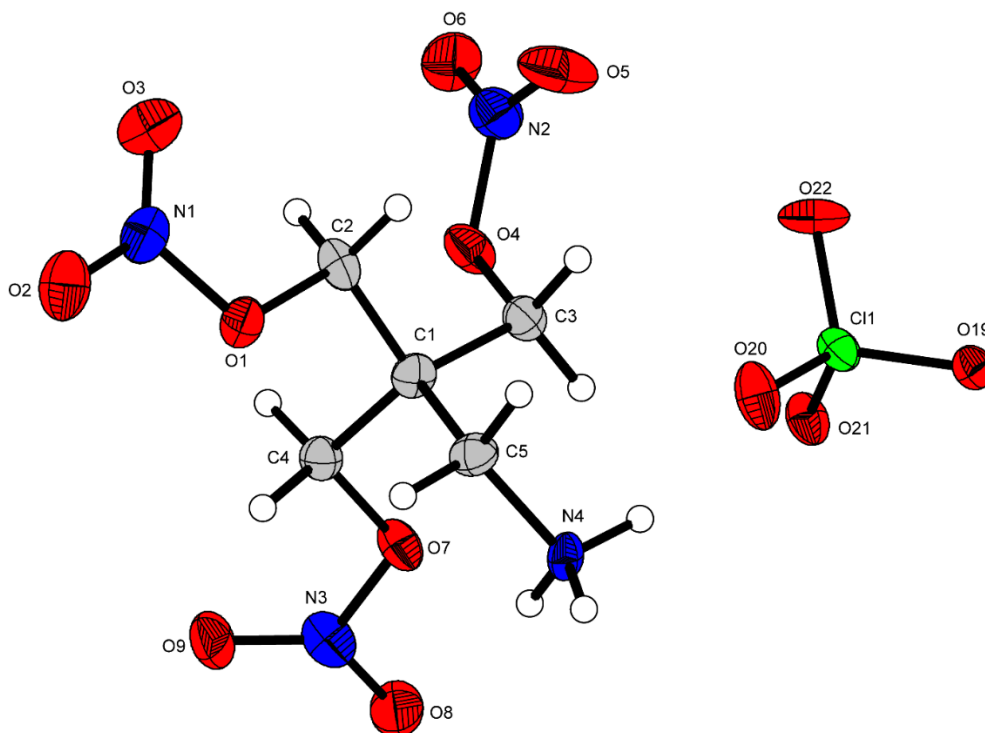


Figure S2. Representation of the molecular unit of **3b**, showing the atom-labeling scheme. Thermal ellipsoids represent the 50% probability level and hydrogen atoms are shown as small spheres of arbitrary radius.

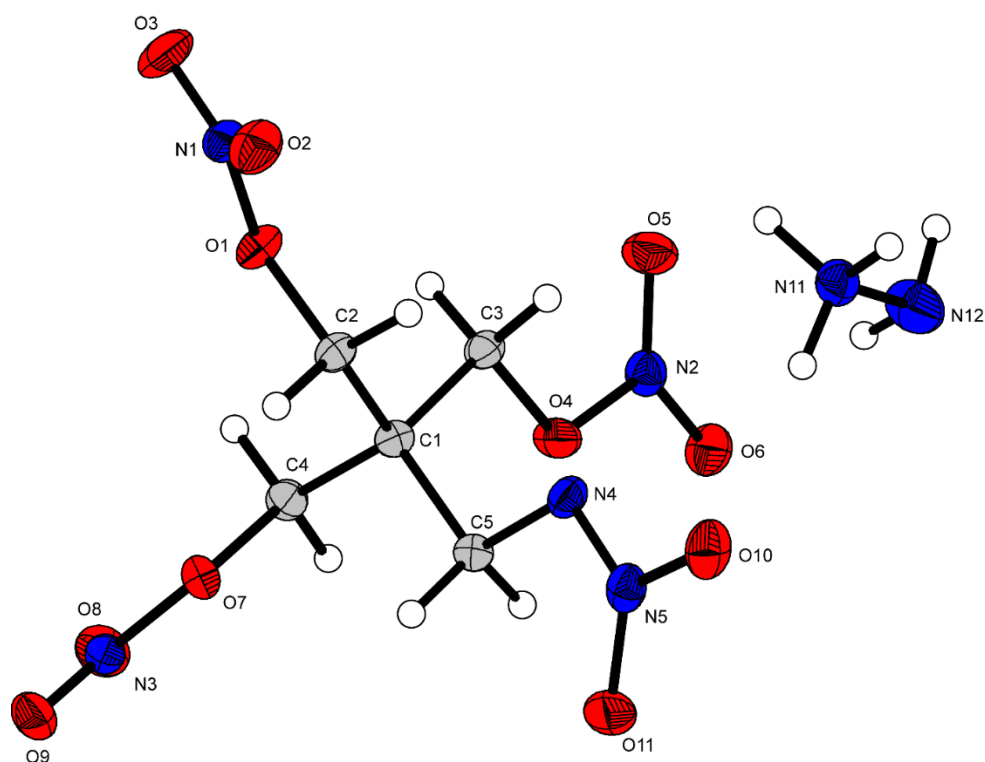


Figure S3. Representation of the molecular unit of **4a**, showing the atom-labeling scheme. Thermal ellipsoids represent the 50% probability level and hydrogen atoms are shown as small spheres of arbitrary radius.

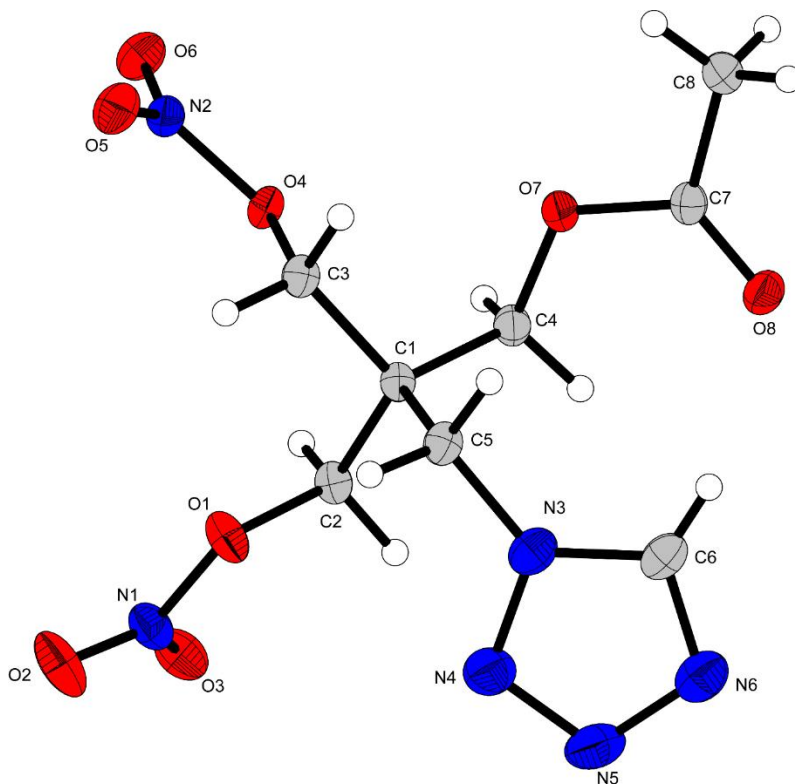


Figure S4. Representation of the molecular unit of **5_acetyl**, showing the atom-labeling scheme. Thermal ellipsoids represent the 50% probability level and hydrogen atoms are shown as small spheres of arbitrary radius.

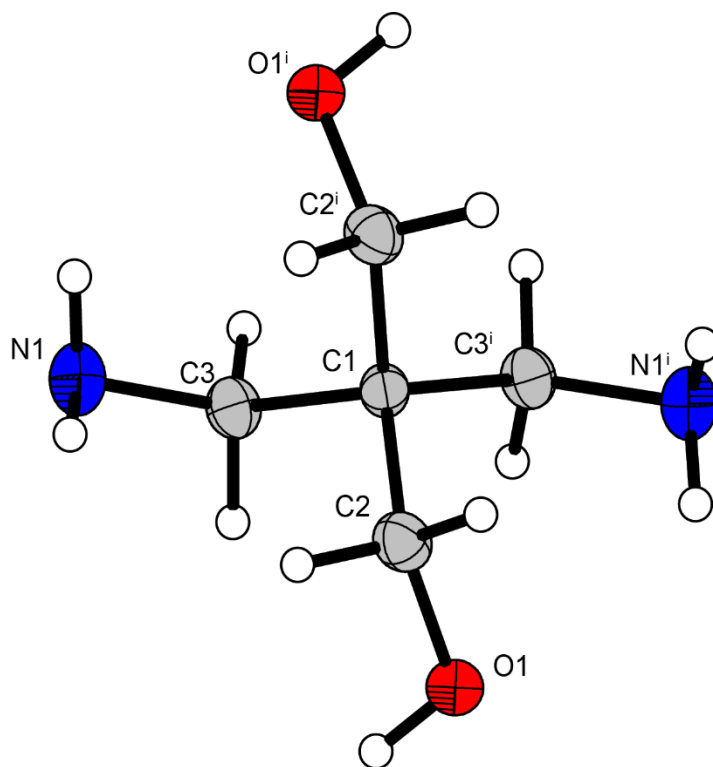


Figure S5 Representation of the molecular unit of **8**, showing the atom-labeling scheme. Thermal ellipsoids represent the 50% probability level and hydrogen atoms are shown as small spheres of arbitrary radius.

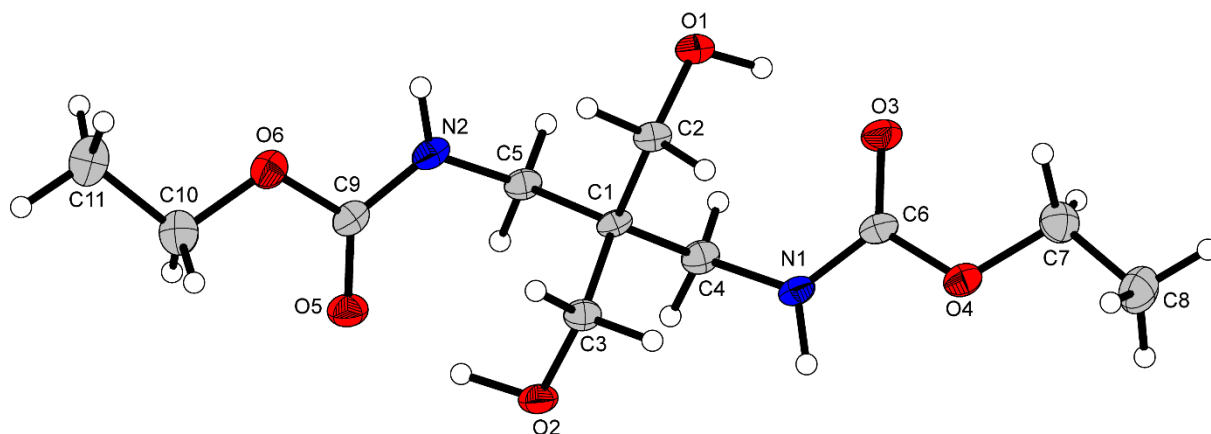


Figure S6 Representation of the molecular unit of **9_prec1**, showing the atom-labeling scheme. Thermal ellipsoids represent the 50% probability level and hydrogen atoms are shown as small spheres of arbitrary radius.

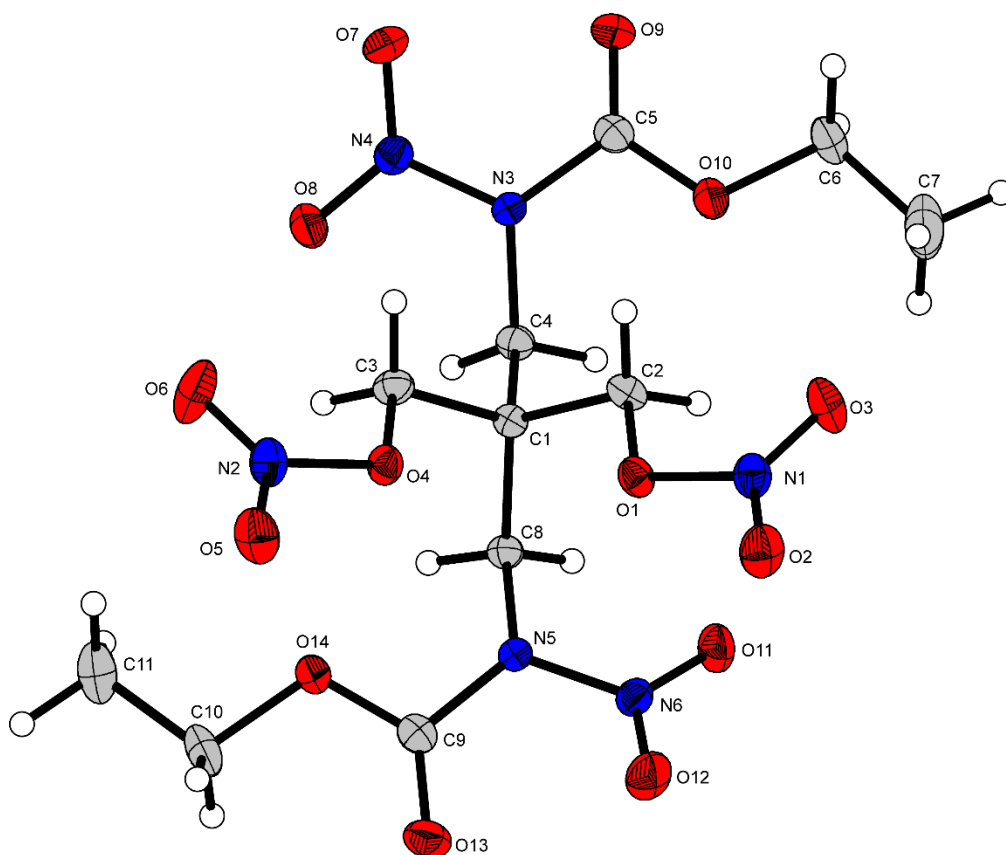


Figure S7 Representation of the molecular unit of **9_prec2**, showing the atom-labeling scheme. Thermal ellipsoids represent the 50% probability level and hydrogen atoms are shown as small spheres of arbitrary radius.

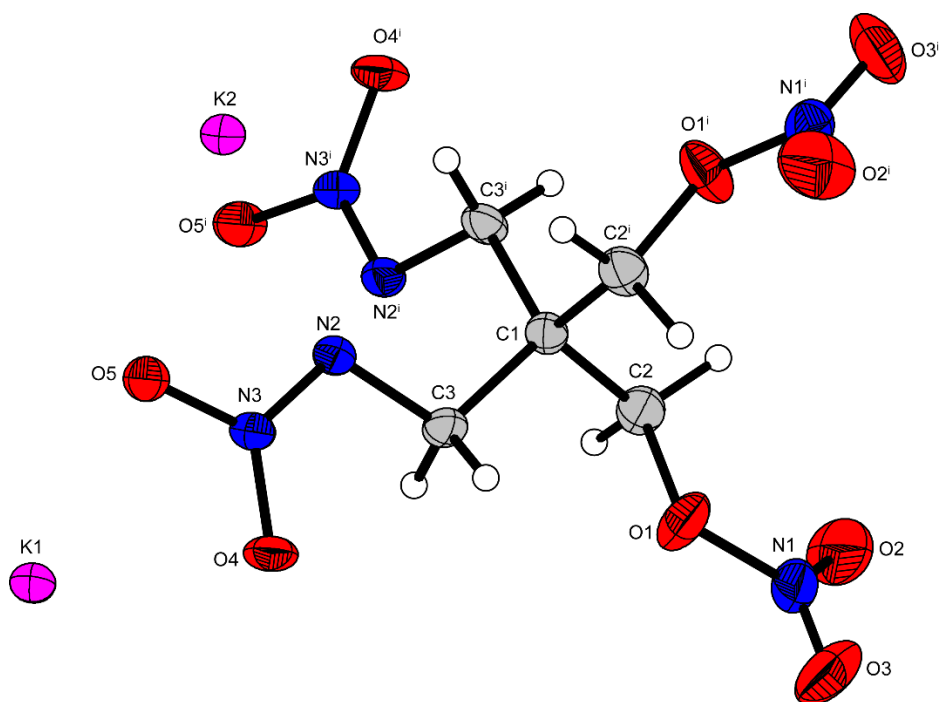


Figure S8 Representation of the molecular unit of **9a**, showing the atom-labeling scheme. Thermal ellipsoids represent the 50% probability level and hydrogen atoms are shown as small spheres of arbitrary radius.

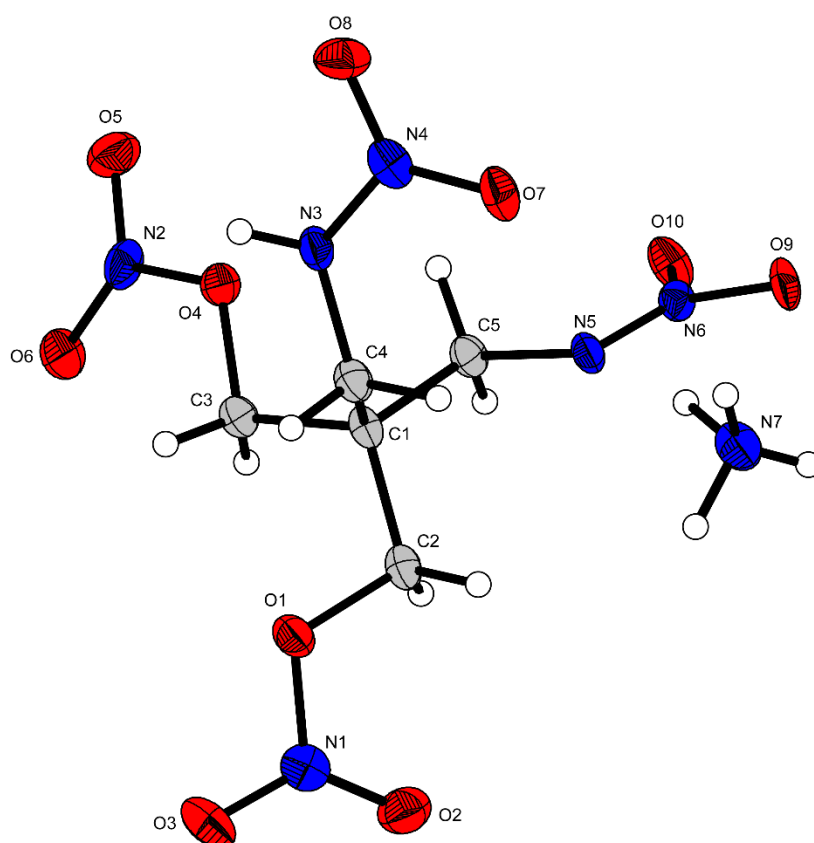


Figure S9 Representation of the molecular unit of **9b**, showing the atom-labeling scheme. Thermal ellipsoids represent the 50% probability level and hydrogen atoms are shown as small spheres of arbitrary radius.

Table S1. Crystallographic data and structure refinement details for the prepared compounds **2_CO2**, **3a** and **3b**.

	2_CO2	3a	3b
Formula	C ₆ H ₁₂ NO ₅ , C ₅ H ₁₄ NO ₃	C ₅ H ₁₁ N ₄ O ₉ , NO ₃	C ₅ H ₁₁ N ₄ O ₉ , ClO ₄
FW [g mol ⁻¹]	314.34	333.19	370.63
Crystal system	monoclinic	monoclinic	orthorhombic
Space group	P21/c (No. 14)	P21/c (No. 14)	Pca21 (No. 29)
Color / Habit	colorless block	colorless block	colorless block
Size [mm]	0.02 x 0.05 x 0.10	0.10 x 0.22 x 0.37	0.10 x 0.36 x 0.44
a [Å]	19.6027(17)	25.773(3)	14.3971(7)
b [Å]	8.7807(7)	7.1108(5)	6.6519(3)
c [Å]	8.5682(7)	15.1047(12)	27.964(2)
α [°]	90	90	
β [°]	96.231(2)	105.551(10)	
γ [°]	90	90	
V [Å ³]	1466.1(2)	2666.9(4)	2678.1(3)
Z	4	8	8
ρ _{calc.} [g cm ⁻³]	1.424	1.660	1.839
μ [mm ⁻¹]	0.121	0.166	0.371
F(000)	680	1376	1520
λ _{MoKα} [Å]	0.71073	0.71073	0.71073
T [K]	102	293	123
θ Min-Max [°]	3.1, 25.3	2.5, 28.7	2.8, 29.2
Dataset	0: 23; -10: 0 ; -10: 10	-26: 33 ; -8: 9 ; -19: 19	-19: 18 ; -8: 8 ; -38: 23
Reflections collected	2888	15306	18542
Independent refl.	2888	6158	5407
R _{int}	0.093	0.073	0.062
Observed reflections	2474	3281	3398
Parameters	228	399	417
R ₁ (obs) ^[a]	0.0802	0.1081	0.0546
wR ₂ (all data) ^[b]	0.1459	0.2916	0.1269
S ^[c]	1.21	1.07	1.03
Resd. dens [e Å ⁻³]	-0.35, 0.38	-0.44, 0.61	-0.51, 0.52
Device type	Bruker D8 Venture TXS	Xcalibur Sapphire3	Xcalibur Sapphire3
Solution	SIR-92	SIR-92	SIR-92
Refinement	SHELXL-2013	SHELXL-2013	SHELXL-2013
Absorption correction	multi-scan	multi-scan	multi-scan
CCDC	2236739	2232124	2232126

^[a]R₁ = $\sum||F_o| - |F_c|| / \sum|F_o|$; ^[b]wR₂ = $[\sum[w(F_o^2 - F_c^2)^2] / \sum[w(F_o^2)]]^{1/2}$; w = $[\sigma c^2(F_o^2) + (xP)^2 + yP]^{-1}$ and P = $(F_o^2 + 2F_c^2) / 3$; ^[c]S = $(\sum[w(F_o^2 - F_c^2)^2] / (n - p))^{1/2}$ (n = number of reflections; p = total number of parameters).

Table S2. Crystallographic data and structure refinement details for the prepared compounds **4a**, **4b**, **5**.

	4a	4b	5
Formula	C ₅ H ₁₃ N ₇ O ₁₁ , N ₂ H ₅	C ₅ H ₈ N ₅ O ₁₁ , H ₃ NO, H ₄ NO	C ₅ H ₇ N ₇ O ₉
FW [g mol ⁻¹]	347.22	381.24	309.18
Crystal system	triclinic	monoclinic	monoclinic
Space group	P-1 (No. 2)	P21/c (No. 14)	P21/n (No. 14)
Color / Habit	colorless block	colourless block	colourless block
Size [mm]	0.10 x 0.10 x 0.50	0.05 x 0.50 x 0.50	0.20 x 0.34 x 0.50
a [Å]	7.8541(6)	16.1267(12)	11.8470(5)
b [Å]	11.7172(8)	7.6433(4)	7.3229(3)
c [Å]	16.0024(7)	11.7734(9)	13.4955(6)
α [°]	96.858(5)	90	90
β [°]	103.993(5)	97.028(7)	96.225(4)
γ [°]	103.161(6)	90	90
V [Å ³]	1367.51(16)	1440.30(17)	1163.89(9)
Z	2	4	4
ρ _{calc.} [g cm ⁻³]	1.686	1.758	1.764
μ [mm ⁻¹]	0.164	0.174	0.169
F(000)	720	792	632
λ _{MoKα} [Å]	0.71073	0.71073	0.71073
T [K]	100	105	110
θ Min-Max [°]	1.8, 26.4	2.5, 26.4	2.2, 26.4
Dataset	-9: 9 ; -14: 14 ; -19: 19	-16: 20 ; -9: 9 ; -14: 8	-14: 14 ; -9: 7 ; -16: 15
Reflections collected	29995	6697	7537
Independent refl.	5596	2947	2377
R _{int}	0.056	0.040	0.025
Observed reflections	4339	1979	2028
Parameters	447	254	190
R ₁ (obs) ^[a]	0.0447	0.0452	0.0316
wR ₂ (all data) ^[b]	0.1124	0.1055	0.0788
S ^[c]	1.07	1.03	1.03
Resd. dens [e Å ⁻³]	-0.27, 0.27	-0.26, 0.30	-0.20, 0.27
Device type	Xcalibur Sapphire3	Xcalibur Sapphire3	Xcalibur Sapphire3
Solution	SIR-92	SIR-92	SIR-92
Refinement	SHELXL-2013	SHELXL-2013	SHELXL-2013
Absorption correction	multi-scan	multi-scan	multi-scan
CCDC	2232127	2232121	2232120

^[a]R₁ = $\sum ||F_o| - |F_c|| / \sum |F_o|$; ^[b]wR₂ = $[\sum [w(F_o^2 - F_c^2)^2] / \sum [w(F_o^2)]]^{1/2}$; $w = [\sigma^2(F_o^2) + (xP)^2 + yP]^{-1}$ and $P = (F_o^2 + 2F_c^2) / 3$; ^[c]S = $(\sum [w(F_o^2 - F_c^2)^2] / (n-p))^{1/2}$ (n = number of reflections; p = total number of parameters).

Table S3 Crystallographic data and structure refinement details for the prepared compounds **5_acetyl**, **7**, **8**.

	5_acetyl	7	8
Formula	C ₈ H ₁₂ N ₆ O ₈	C ₆ H ₉ N ₇ O ₉	C ₅ H ₁₄ N ₂ O ₂
FW [g mol ⁻¹]	320.24	323.20	134.18
Crystal system	triclinic	triclinic	tetragonal
Space group	P-1 (No. 2)	P-1 (No. 2)	P43212 (No. 96)
Color / Habit	colourless block	colourless block	colourless block
Size [mm]	0.35 x 0.50 x 0.50	0.27 x 0.40 x 0.43	0.19 x 0.34 x 0.42
a [Å]	8.0823(8)	7.8591(4)	6.2481(4)
b [Å]	8.2682(8)	11.2910(5)	6.2481(4)
c [Å]	11.0633(12)	14.4491(8)	17.8005(18)
α [°]	78.398(9)	83.473(4)	
β [°]	86.543(8)	86.066(4)	
γ [°]	64.925(10)	84.766(4)	
V [Å ³]	655.70(13)	1266.35(11)	694.91(11)
Z	2	4	4
ρ _{calc.} [g cm ⁻³]	1.622	1.695	1.283
μ [mm ⁻¹]	0.146	0.159	0.098
F(000)	332	664	296
λ _{MoKα} [Å]	0.71073	0.71073	0.71073
T [K]	100	123	129
θ Min-Max [°]	2.8, 26.4	1.8, 29.2	3.5, 26.3
Dataset	-10: 10 ; -7: 10 ; -13: 13	-10: 10 ; -15: 14 ; -19: 19	-7: 7 ; -7: 7 ; -22: 22
Reflections collected	5460	11304	10240
Independent refl.	2685	5820	709
R _{int}	0.025	0.022	0.049
Observed reflections	2003	4099	642
Parameters	247	426	50
R ₁ (obs) ^[a]	0.0472	0.0574	0.0454
wR ₂ (all data) ^[b]	0.1235	0.1452	0.1157
S ^[c]	1.03	1.03	1.09
Resd. dens [e Å ⁻³]	-0.24, 0.80	-0.38, 0.48	-0.16, 0.40
Device type	Xcalibur Sapphire3	Xcalibur Sapphire3	Xcalibur Sapphire3
Solution	SIR-92	SIR-92	SIR-92
Refinement	SHELXL-2013	SHELXL-2013	SHELXL-2013
Absorption correction	multi-scan	multi-scan	multi-scan
CCDC	2232116	2232122	2232125

^[a]R₁ = $\sum ||F_o| - |F_c|| / \sum |F_o|$; ^[b]wR₂ = $[\sum [w(F_o^2 - F_c^2)^2] / \sum [w(F_o^2)]]^{1/2}$; $w = [\sigma^2(F_o^2) + (xP)^2 + yP]^{-1}$ and $P = (F_o^2 + 2F_c^2) / 3$; ^[c]S = $(\sum [w(F_o^2 - F_c^2)^2] / (n-p))^{1/2}$ (n = number of reflections; p = total number of parameters).

Table S4 Crystallographic data and structure refinement details for the prepared compounds **5_acetyl**, **7**, **8**.

	9	9_prec1	9_prec2
Formula	C ₅ H ₁₀ N ₆ O ₁₀	C ₁₁ H ₂₂ N ₂ O ₆	C ₁₁ H ₁₈ N ₆ O ₁₄
FW [g mol ⁻¹]	314.19	278.30	458.31
Crystal system	monoclinic	orthorhombic	monoclinic
Space group	P21/n (No. 14)	P212121 (No. 19)	P21/c (No. 14)
Color / Habit	colorless block	colorless block	colorless block
Size [mm]	0.05 x 0.10 x 0.30	0.02 x 0.20 x 0.50	0.38 x 0.69 x 0.99
a [Å]	10.3324(4)	6.1441(5)	19.9520(14)
b [Å]	8.6759(3)	8.4143(11)	8.1248(7)
c [Å]	13.0669(5)	27.667(3)	11.7677(7)
α [°]	90		90
β [°]	95.474(3)		92.511(6)
γ [°]	90		90
V [Å ³]	1166.01(8)	1430.3(3)	1905.8(2)
Z	4	4	4
ρ _{calc.} [g cm ⁻³]	1.790	1.292	1.597
μ [mm ⁻¹]	0.174	0.105	0.149
F(000)	648	600	952
λ _{MoKα} [Å]	0.71073	0.71073	0.71073
T [K]	123	112	107
θ Min-Max [°]	2.4, 26.4	2.5, 28.3	2.7, 26.4
Dataset	-12: 12 ; -10: 10 ; -16: 16	-8: 8 ; -11: 10 ; -36: 34	-24: 17 ; -5: 10 ; -12: 14
Reflections collected	17019	17999	8011
Independent refl.	2381	3391	3894
R _{int}	0.033	0.097	0.023
Observed reflections	2057	2455	3069
Parameters	230	260	352
R ₁ (obs) ^[a]	0.0424	0.0608	0.0371
wR ₂ (all data) ^[b]	0.1145	0.1328	0.1003
S ^[c]	1.04	1.07	1.05
Resd. dens [e Å ⁻³]	-0.32, 0.74	-0.29, 0.35	-0.21, 0.31
Device type	Xcalibur Sapphire3	Xcalibur Sapphire3	Xcalibur Sapphire3
Solution	SIR-92	SIR-92	SIR-92
Refinement	SHELXL-2013	SHELXL-2013	SHELXL-2013
Absorption correction	multi-scan	multi-scan	multi-scan
CCDC	2232123	2232117	2232118

^[a]R₁ = $\sum ||F_o| - |F_c|| / \sum |F_o|$; ^[b]wR₂ = $[\sum [w(F_o^2 - F_c^2)^2] / \sum [w(F_o^2)]]^{1/2}$; $w = [\sigma^2(F_o^2) + (xP)^2 + yP]^{-1}$ and $P = (F_o^2 + 2F_c^2) / 3$; ^[c]S = $(\sum [w(F_o^2 - F_c^2)^2] / (n-p))^{1/2}$ (n = number of reflections; p = total number of parameters).

Table S5 Crystallographic data and structure refinement details for the prepared compounds **9a** and **9b**.

	9a	9b
Formula	C ₅ H ₈ K ₂ N ₆ O ₁₀	C ₅ H ₉ N ₆ O ₁₀ , H ₄ N
FW [g mol ⁻¹]	390.37	331.22
Crystal system	monoclinic	triclinic
Space group	C2/c (No. 15)	P-1 (No. 2)
Color / Habit	colorless block	colorless block
Size [mm]	0.04 x 0.07 x 0.12	0.06 x 0.07 x 0.32
a [Å]	9.5921(15)	6.3178(10)
b [Å]	19.735(3)	7.9159(10)
c [Å]	7.6025(11)	13.8070(16)
α [°]	90	78.794(10)
β [°]	107.706(5)	81.368(11)
γ [°]	90	71.011(13)
V [Å ³]	1371.0(4)	637.66(16)
Z	4	2
ρ _{calc.} [g cm ⁻³]	1.891	1.725
μ [mm ⁻¹]	0.760	0.166
F(000)	792	344
λ _{MoKα} [Å]	0.71073	0.71073
T [K]	173	100
θ Min-Max [°]	3.2, 26.4	1.5, 26.4
Dataset	-11: 11 ; -24: 24 ; -9: 9	-7: 6 ; -9: 9 ; -17: 14
Reflections collected	13874	5219
Independent refl.	1406	2611
R _{int}	0.043	0.049
Observed reflections	1340	1583
Parameters	123	251
R ₁ (obs) ^[a]	0.0518	0.0606
wR ₂ (all data) ^[b]	0.1165	0.1425
S ^[c]	1.36	1.00
Resd. dens [e Å ⁻³]	-0.66, 0.89	-0.29, 0.32
Device type	Xcalibur Sapphire3	Xcalibur Sapphire3
Solution	SIR-92	SIR-92
Refinement	SHELXL-2013	SHELXL-2013
Absorption correction	multi-scan	multi-scan
CCDC	2232128	2232119

^[a]R₁ = Σ||F_o|-|F_c||/Σ|F_o|; ^[b]wR₂ = [Σ[w(F_o²-F_c²)²]/Σ[w(F_o)²]^{1/2}; w = [σc²(F_o²)+(xP)²+yP]⁻¹ and P=(F_o²+2F_c²)/3; ^[c]S = (Σ[w(F_o²-F_c²)²]/(n-p))^{1/2} (n = number of reflections; p = total number of parameters).

3. Computation

Heat of Formation Computation

All quantum chemical calculations were carried out using the Gaussian G09 program package.¹⁴ The enthalpies (H) and free energies (G) were calculated using the complete basis set (CBS) method of Petersson and co-workers in order to obtain very accurate energies. The CBS models are using the known asymptotic convergence of pair natural orbital expressions to extrapolate from calculations using a finite basis set to the estimated CBS limit. CBS-4 starts with an HF/3-21G(d) geometry optimization; the zero-point energy is computed at the same level. It then uses a large basis set SCF calculation as a base energy, and an MP2/6-31+G calculation with a CBS extrapolation to correct the energy through second order. A MP4(SDQ)/6-31+ (d,p) calculation is used to approximate higher order contributions. In this study, we applied the modified CBS-4M.

Heats of formation of the synthesized ionic compounds were calculated using the atomization method (equation E1) using room temperature CBS-4M enthalpies, which are summarized in Table S5.¹⁵

$$\Delta_f H^{\circ}_{(g, M, 298)} = H_{(Molecule, 298)} - \sum H^{\circ}_{(Atoms, 298)} + \sum \Delta_f H^{\circ}_{(Atoms, 298)} \quad (E1)$$

Table S6. CBS-4M electronic enthalpies for atoms C, H, N and O and their literature values for atomic $\Delta H^{\circ}_{f, 298} / \text{kJ mol}^{-1}$

	$-H^{298}$ [a.u.]	NIST ^[S13]
H	0.500991	218.2
C	37.786156	717.2
N	54.522462	473.1
O	74.991202	249.5

For neutral compounds the sublimation enthalpy, which is needed to convert the gas phase enthalpy of formation to the solid state one, was calculated by the *Trouton* rule.¹⁶ For ionic compounds, the lattice energy (U_L) and lattice enthalpy (ΔH_L) were calculated from the corresponding X-ray molecular volumes according to the equations provided by *Jenkins* and *Glasser*.¹⁷ With the calculated lattice enthalpy the gas-phase enthalpy of formation was converted into the solid state (standard conditions) enthalpy of formation. These molar standard enthalpies of formation (ΔH_m) were used to calculate the molar solid state energies of formation (ΔU_m) according to equation E2.

$$\Delta U_m = \Delta H_m - \Delta n RT \quad (E2)$$

(Δn being the change of moles of gaseous components)

The calculation results are summarized in Table S6.

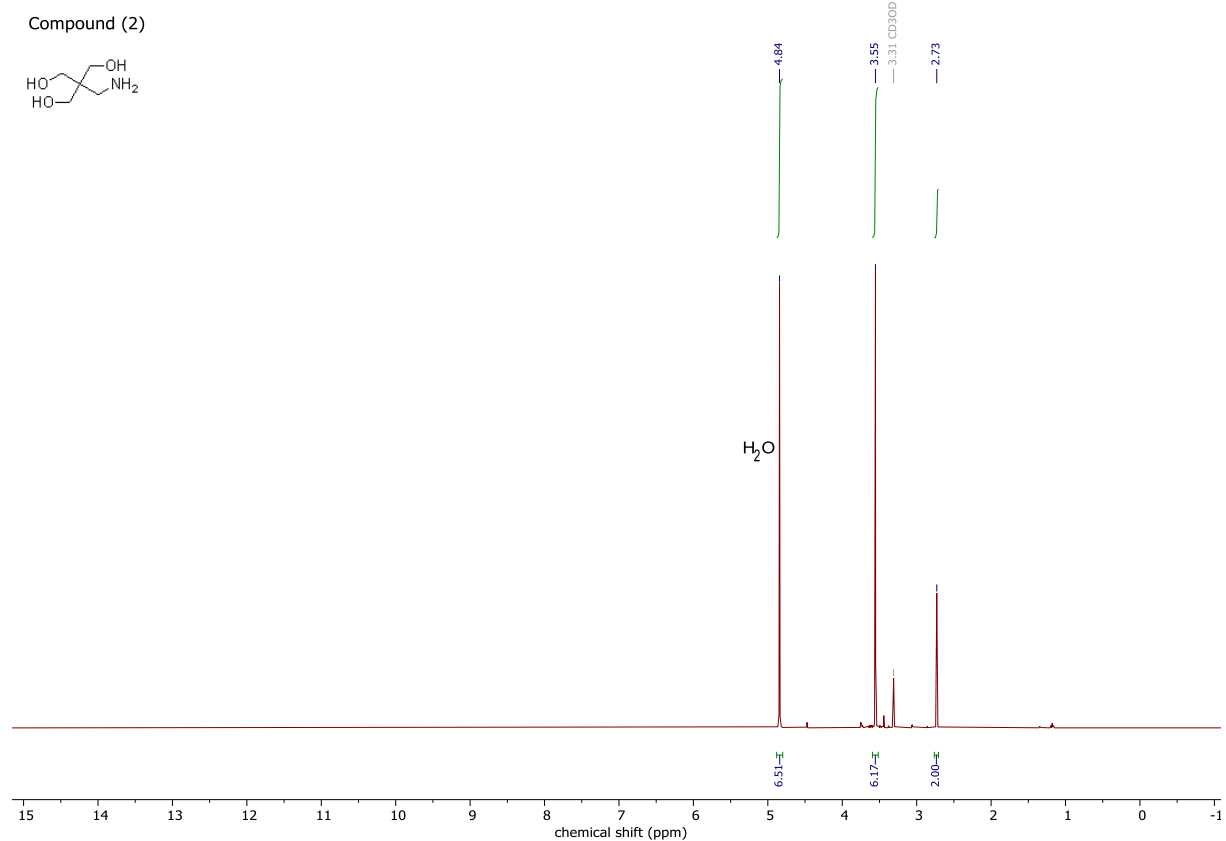
Table S7. Calculation results.

	$-E^{98}$ [a] [a.u.]	$\Delta_f H^\circ(\text{g,M})$ [kJ mol ⁻¹] [b]	V_M [Å ³] [c]	$\Delta U_L; \Delta H_L$ [d] [kJ mol ⁻¹]	$\Delta_f H^\circ(\text{s})$ [e] [kJ mol ⁻¹]	Δn [f]	$\Delta_f U(\text{s})$ [g] [kJ mol ⁻¹]
Cat⁺ (3)	1091,17584	338.7	-	-	-	-	-
NO₃⁻	280.080446	-314.1	-	-	-	-	-
ClO₄⁻	760.171182	-278.2	-	-	-	-	-
3a	-	-	0.333	442.1; 447.1	-422.5	-14.0	-387.8
3b	-	-	0.344	438.8; 443.7	-383.2	-14.5	-347.3
4	1295.116865	-276.6	-	-	-339.2	-12.5	-308.2
Anio.⁻ (4)	1294.599008	-450.3	-	-			
Hy⁺	112.030523	773.4					
4a	-	-	0.704	367.5	-48.1	-15.5	-9.7
5	1292.294989	22.1	-	-	70.2	-12.5	-17.0
7	1253.051998	63.7	-	-	66.39	-11.5	25.8

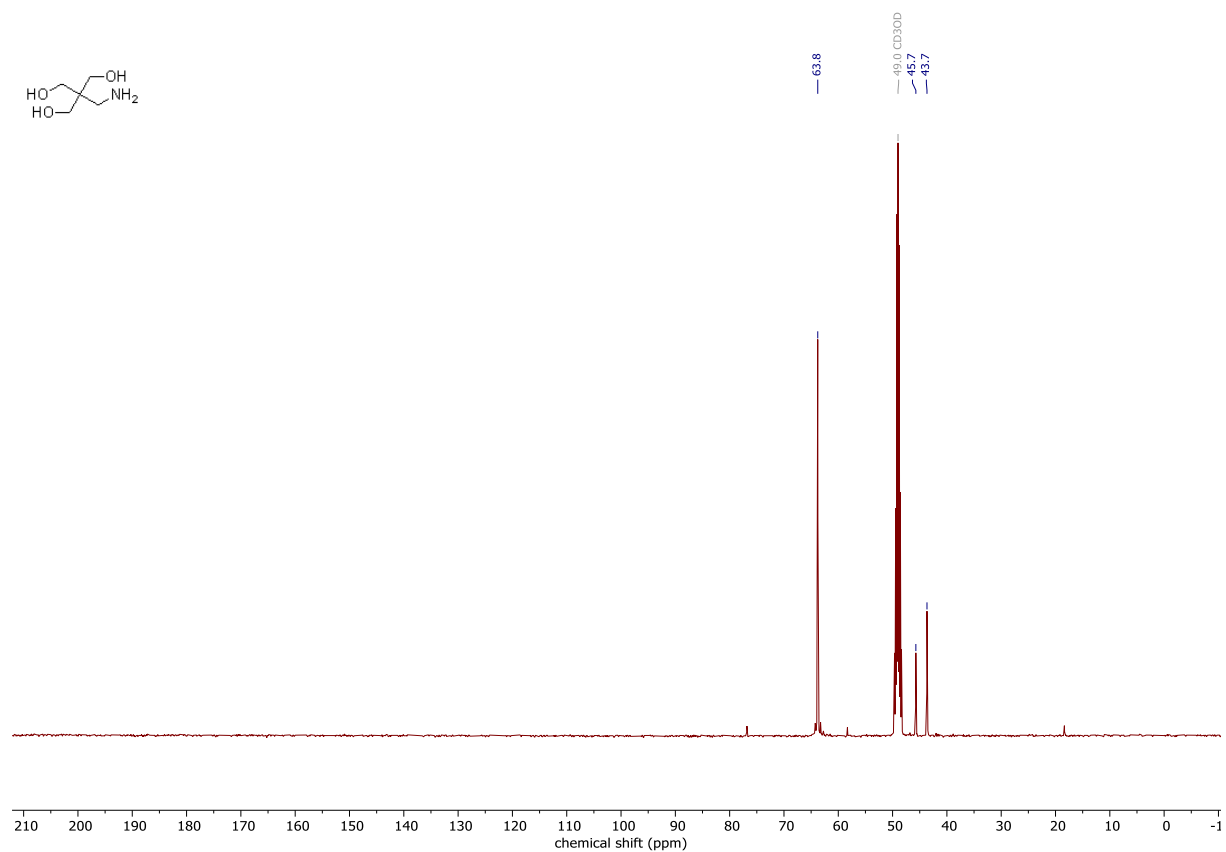
[a] CBS-4M electronic enthalpy; [b] gas phase enthalpy of formation; [c] molecular volumes taken from X-ray structures and corrected to room temperature; [d] lattice energy and enthalpy (calculated using Jenkins and Glasser equations); [e] standard solid state enthalpy of formation; [f] Δn being the change of moles of gaseous components when formed; [g] solid state energy of formation.

4. NMR Spectroscopy

Compound (2), ^1H NMR (400 MHz, MeOH- d_4 , ppm)

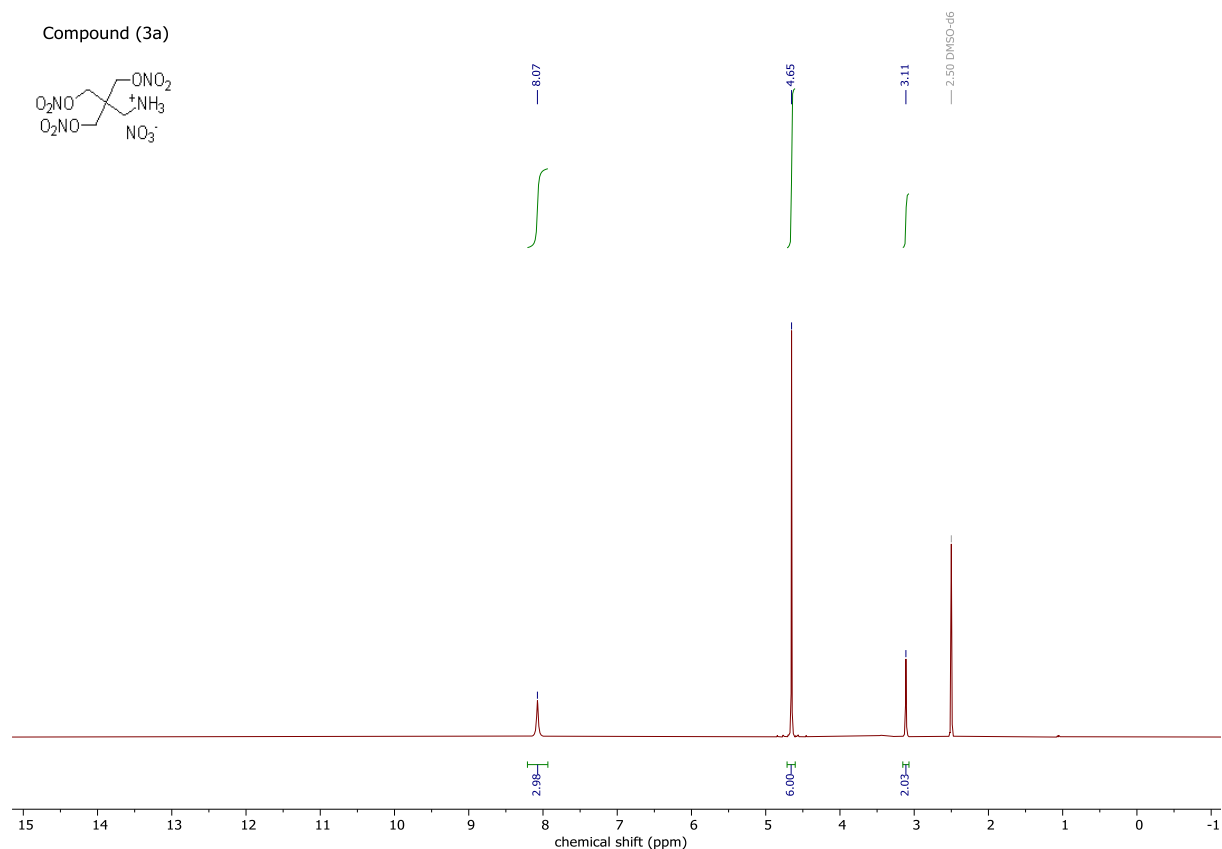


Compound (2), ^{13}C NMR (101 MHz, MeOH- d_4 , ppm)

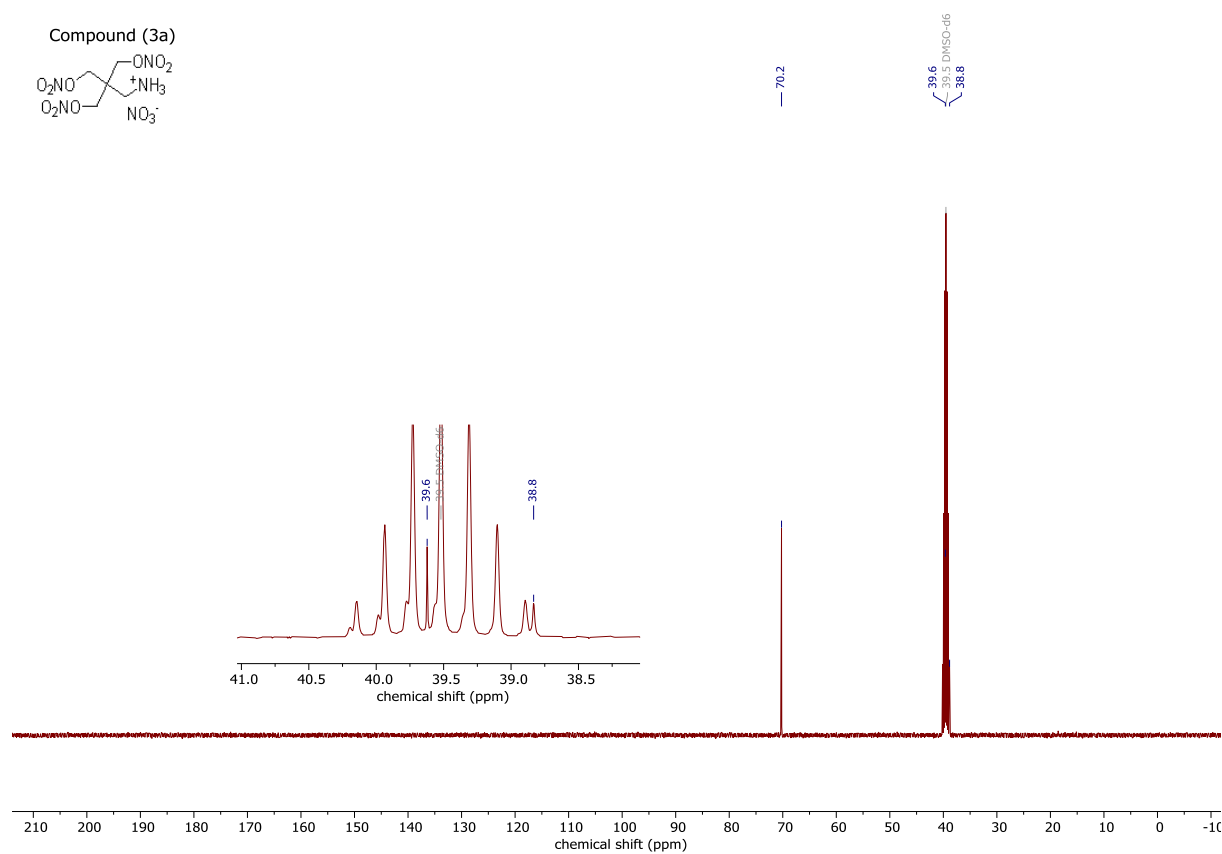


Compound (3), ^1H NMR (400 MHz, MeOH- d_4 , ppm)

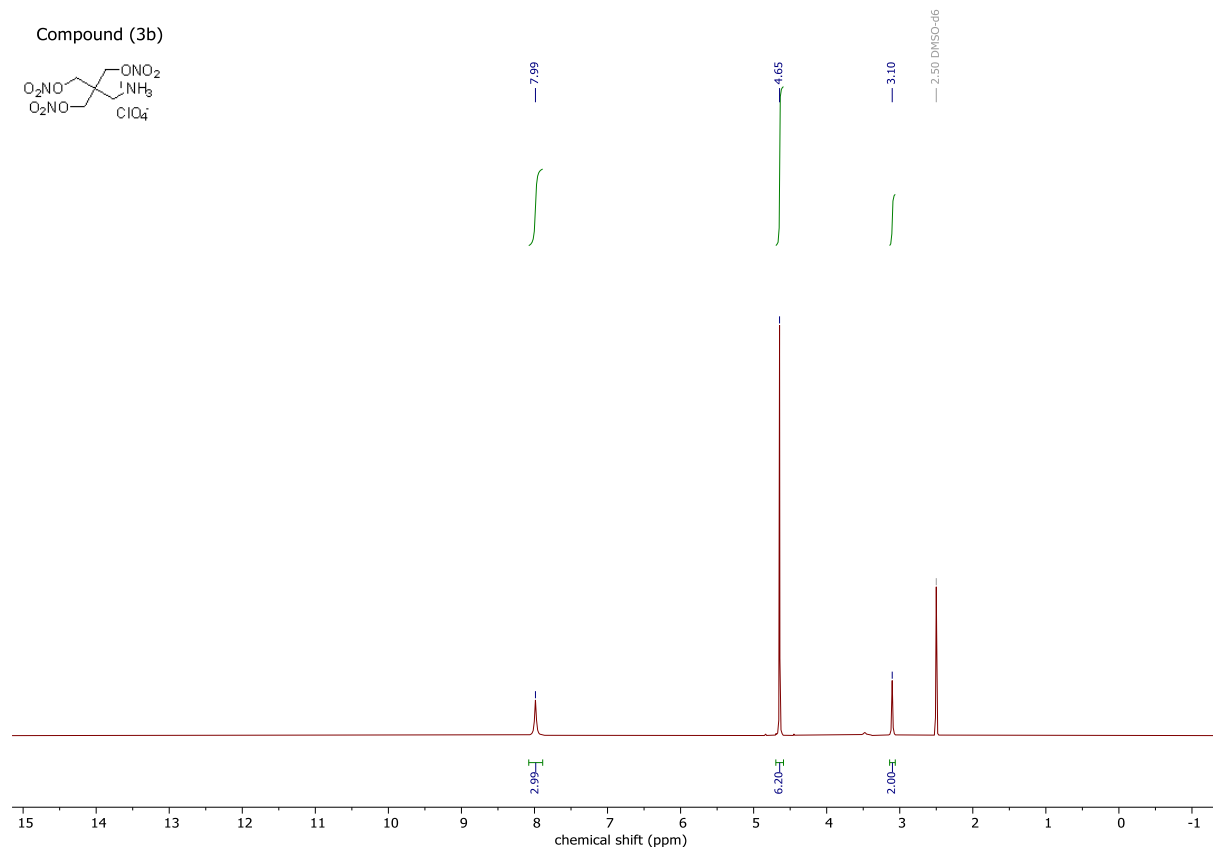
Compound (3a), ¹H NMR (400 MHz, DMSO-d₆, ppm)



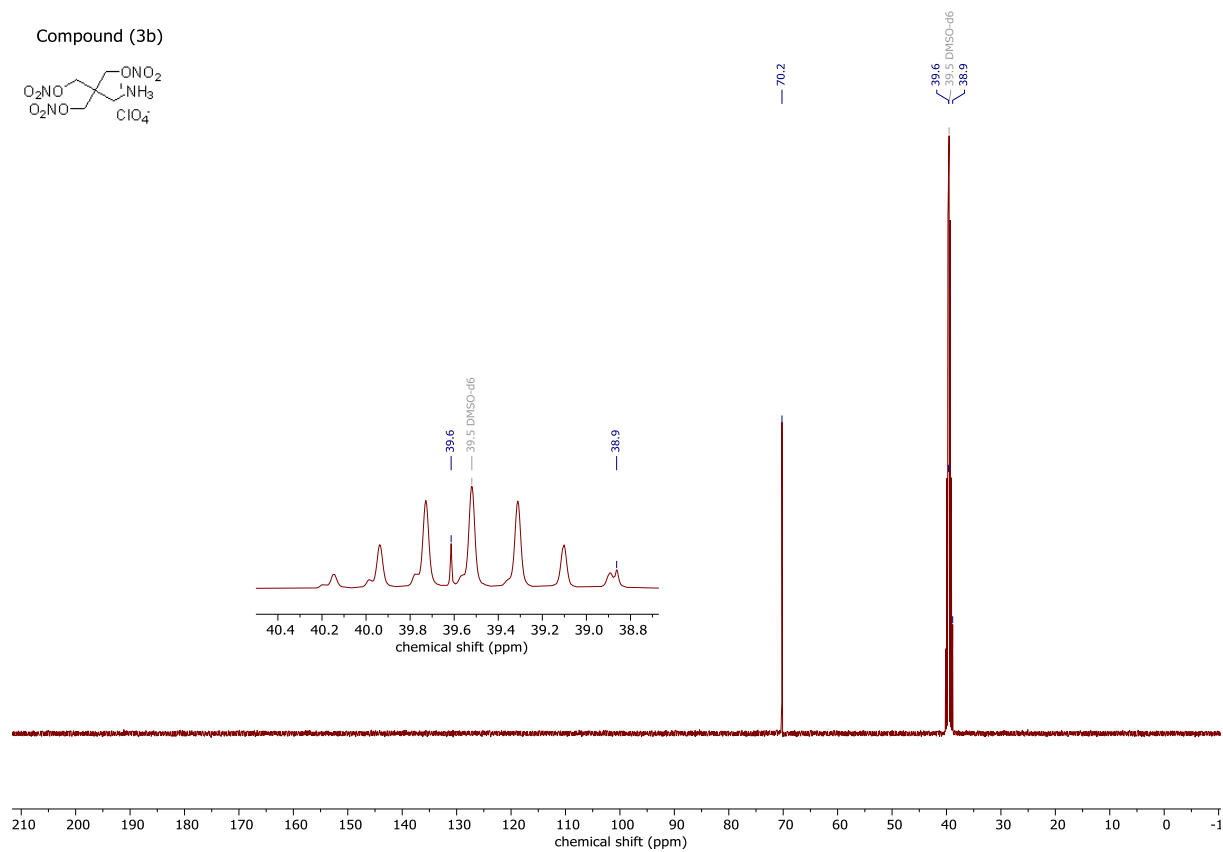
Compound (3a), ¹³C NMR (101 MHz, DMSO-d₆, ppm)



Compound (3b), ¹H NMR (400 MHz, DMSO-d₆, ppm)

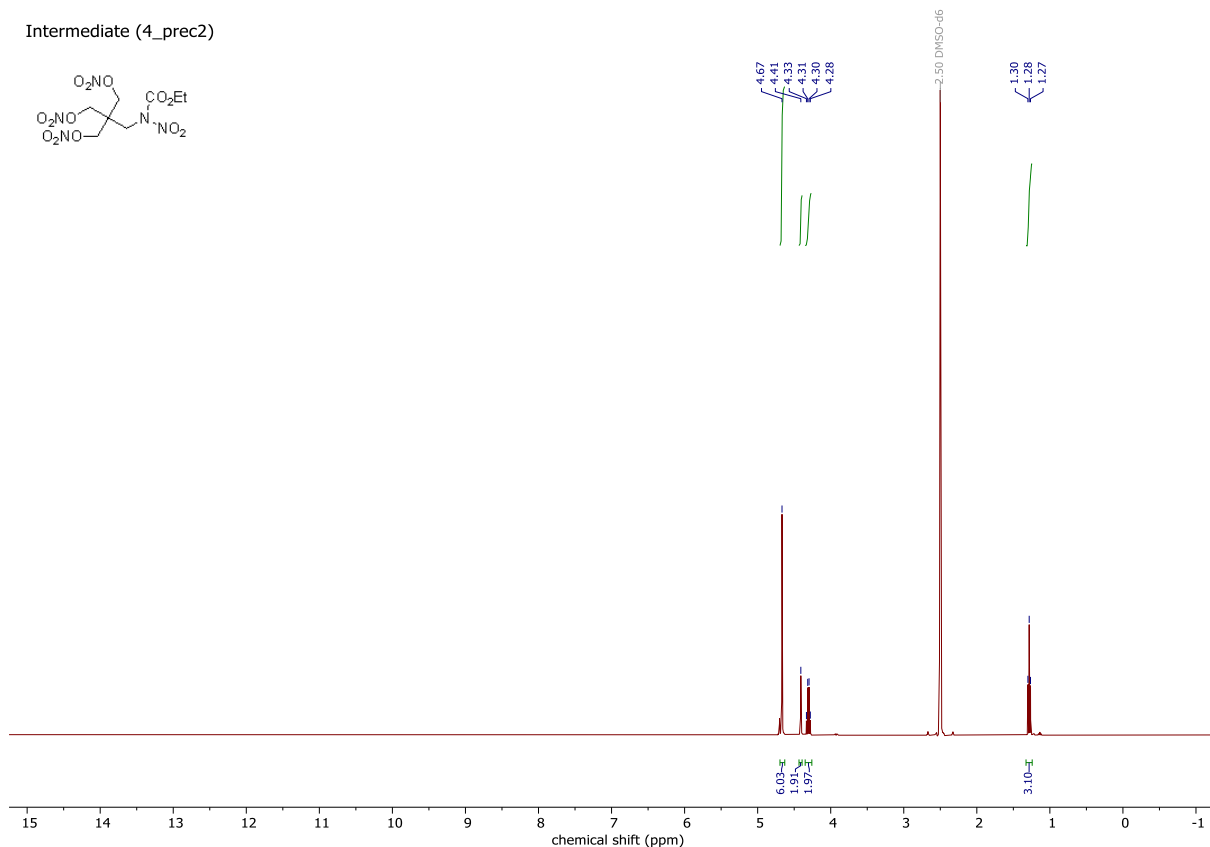
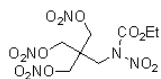


Compound (3b), ¹³C NMR (101 MHz, DMSO-d₆, ppm)



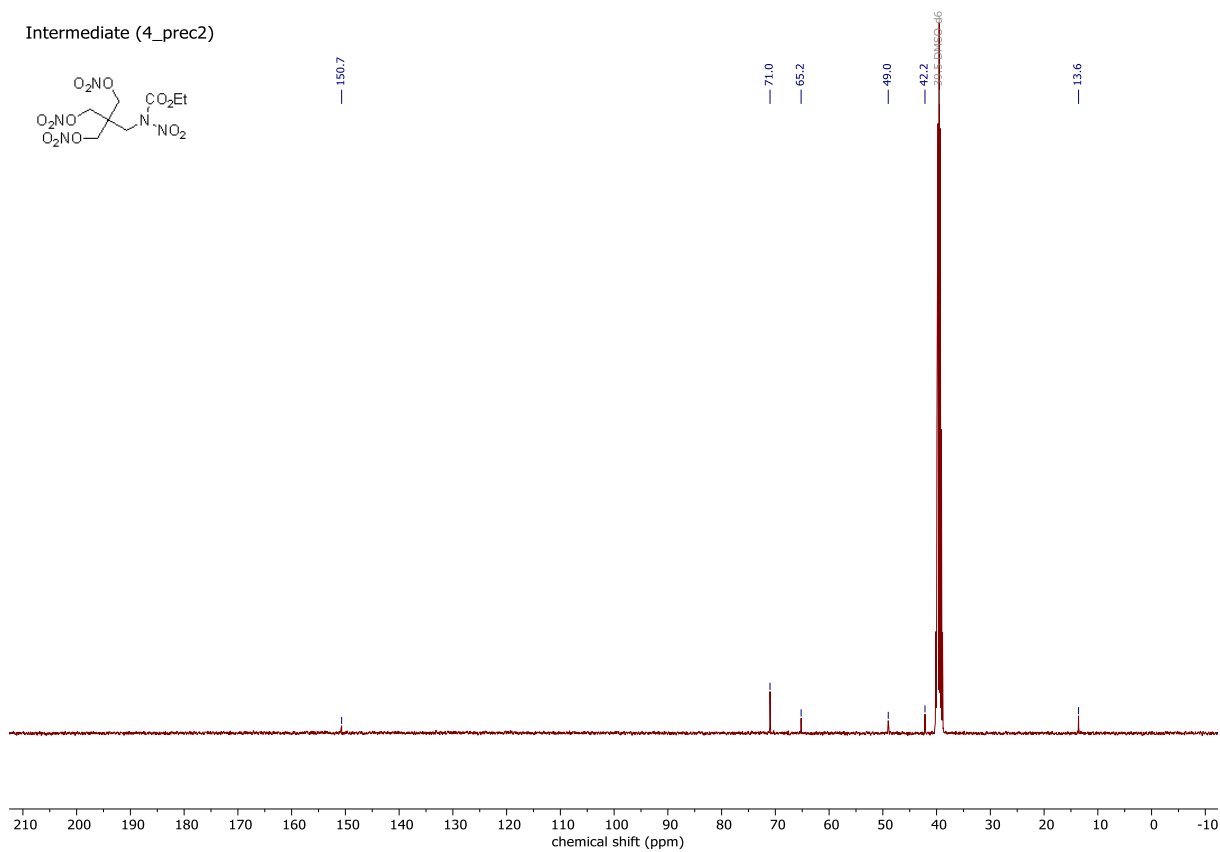
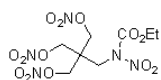
Compound (4_prec2), ¹H NMR (400 MHz, DMSO-d₆, ppm)

Intermediate (4_prec2)

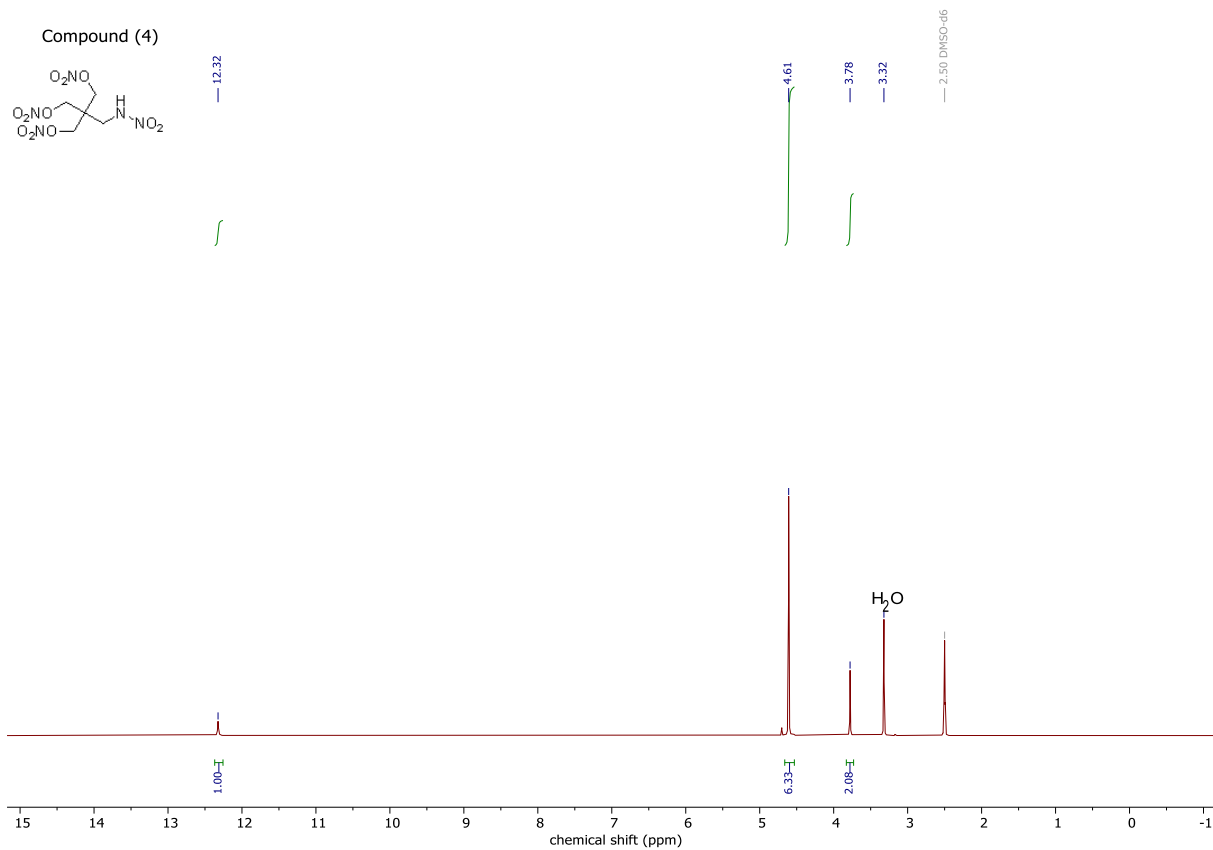


Compound (4_prec2), ¹³C NMR (101 MHz, DMSO-d₆, ppm)

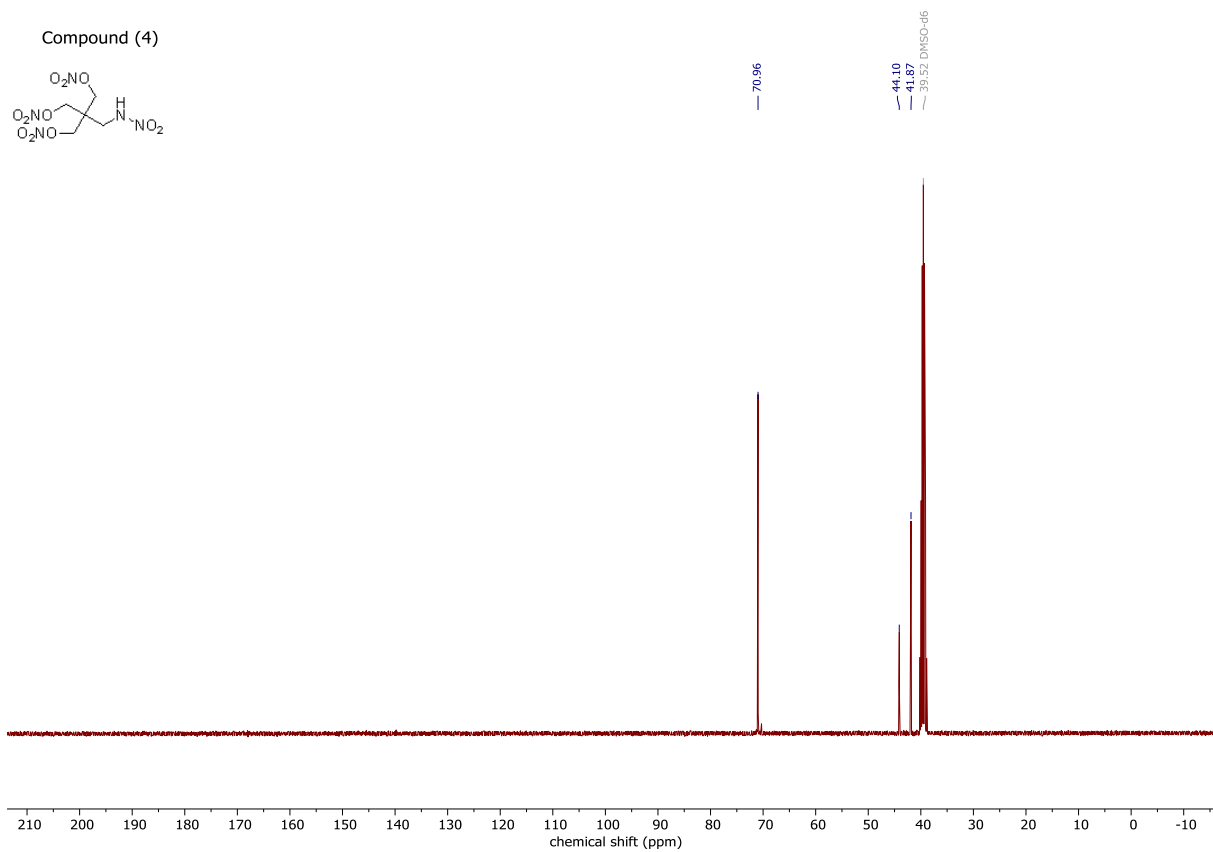
Intermediate (4_prec2)



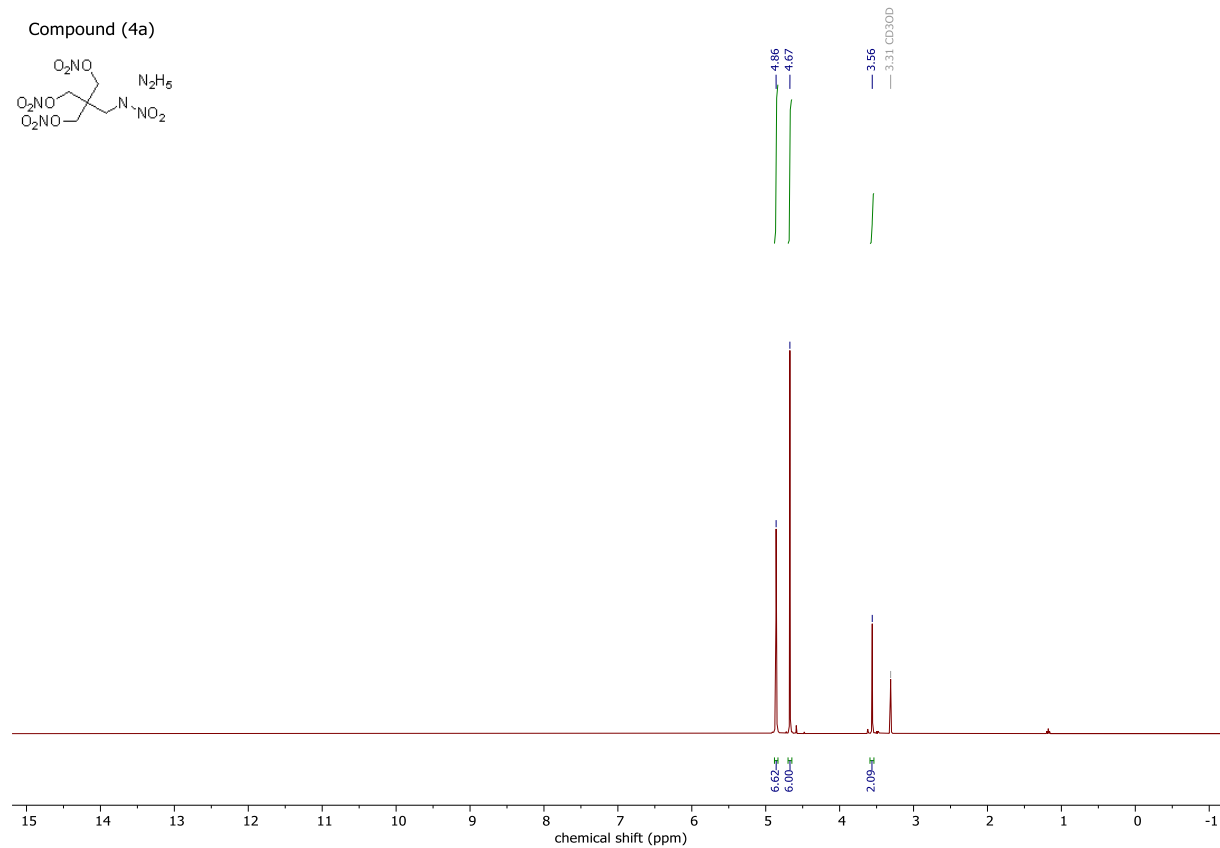
Compound (4), ¹H NMR (400 MHz, DMSO-d₆, ppm)



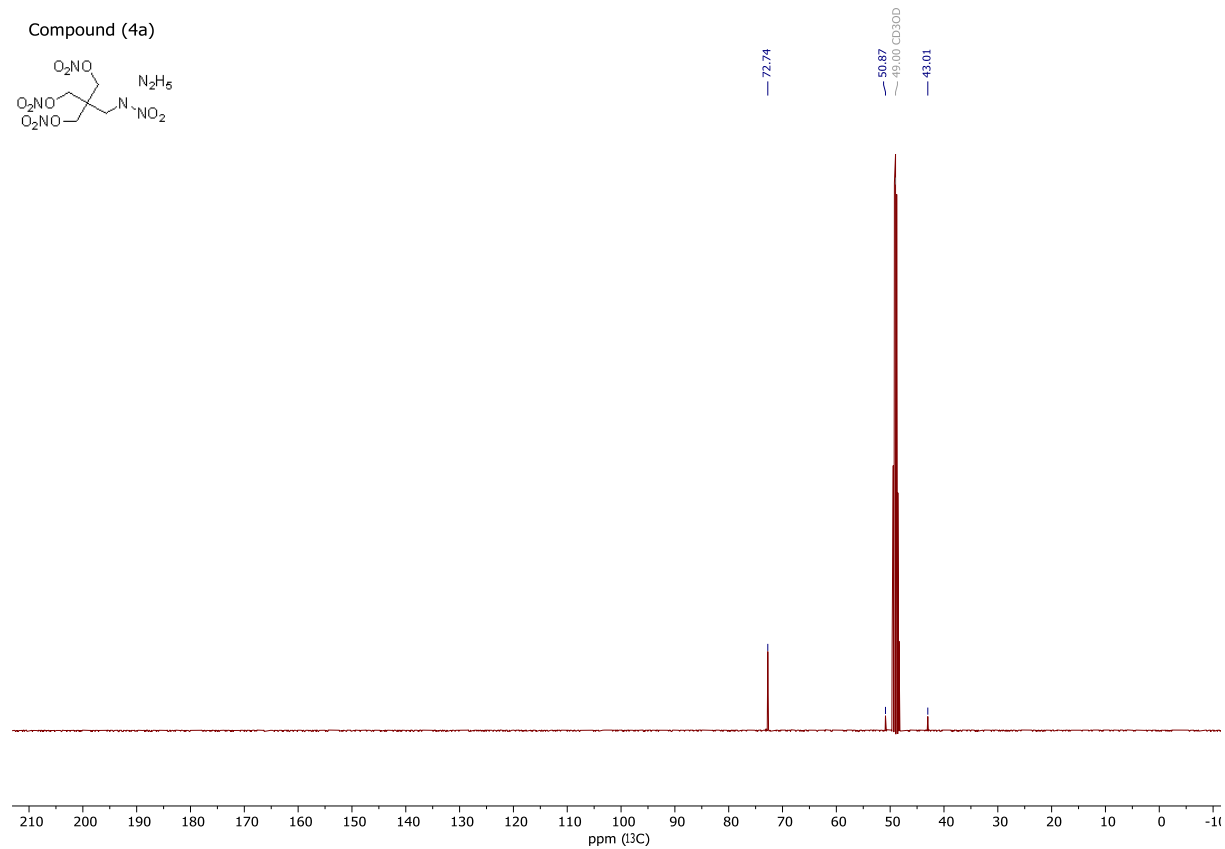
Compound (4), ¹³C NMR (101 MHz, DMSO-d₆, ppm)



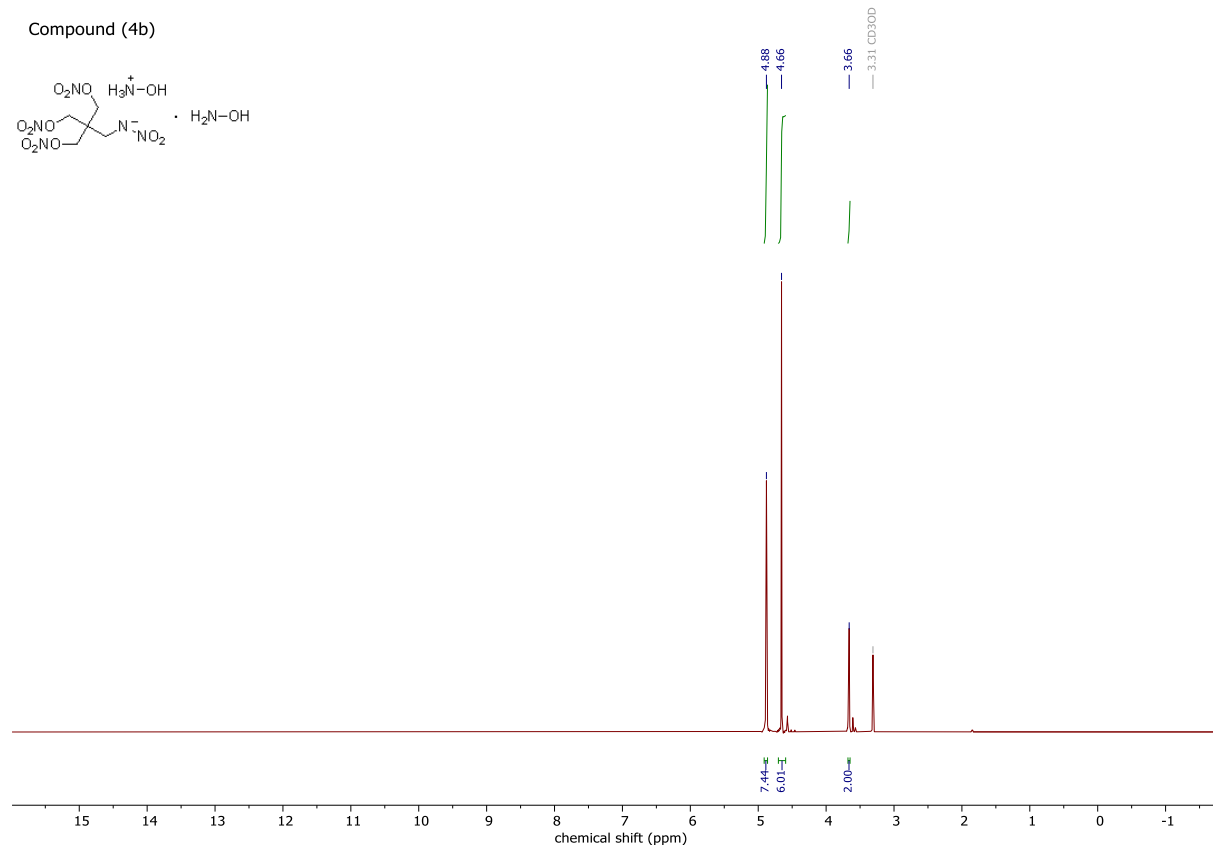
Compound (4a), ¹H NMR (400 MHz, MeOH-d₄, ppm)



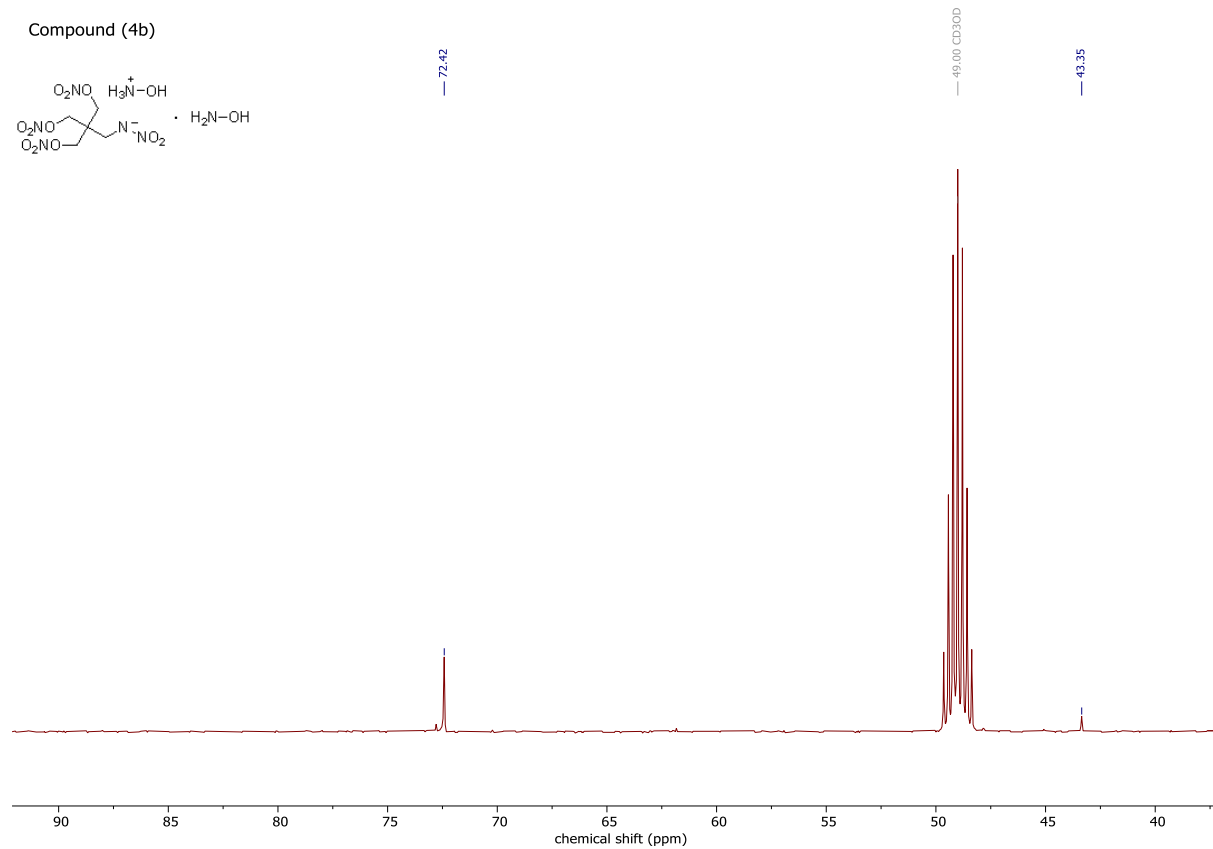
Compound (4a), ¹³C NMR (101 MHz, MeOH-d₄, ppm)



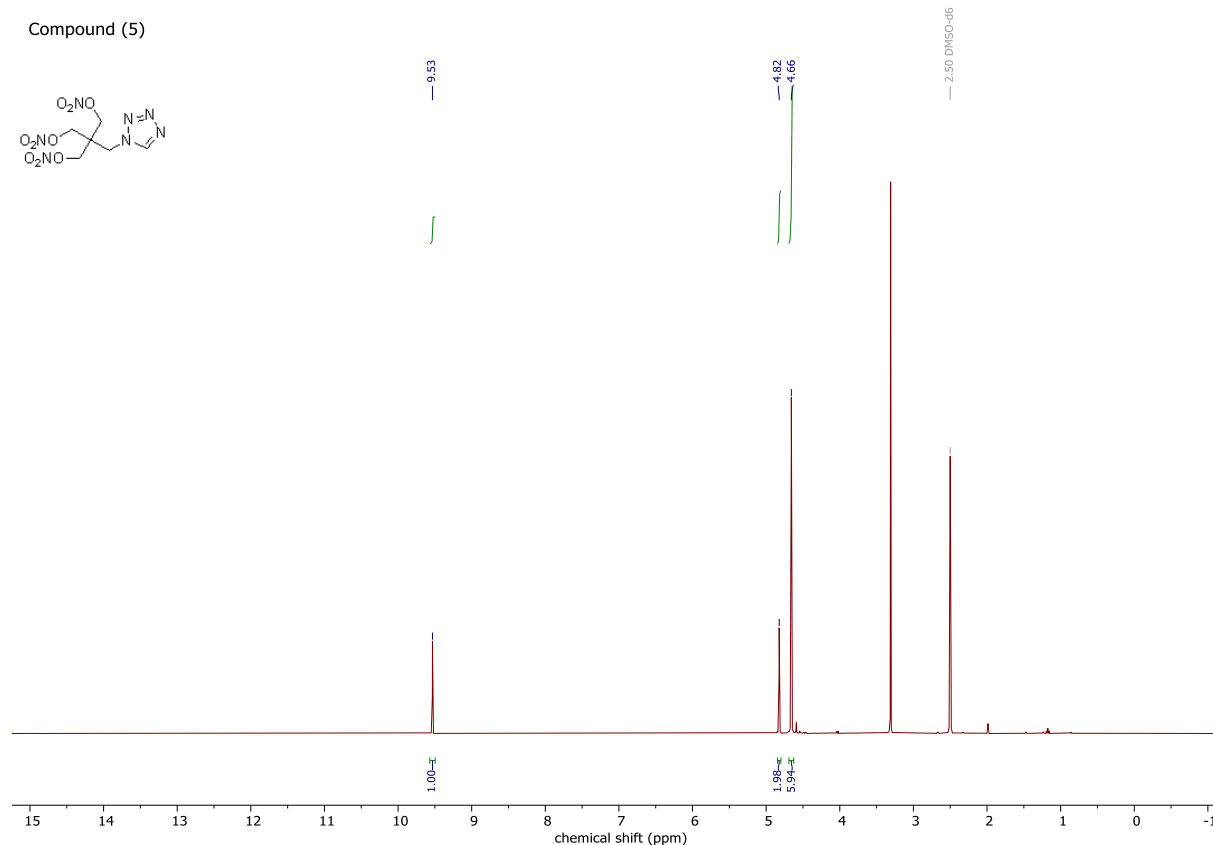
Compound (4b), ¹H NMR (400 MHz, MeOH-d₄, ppm)



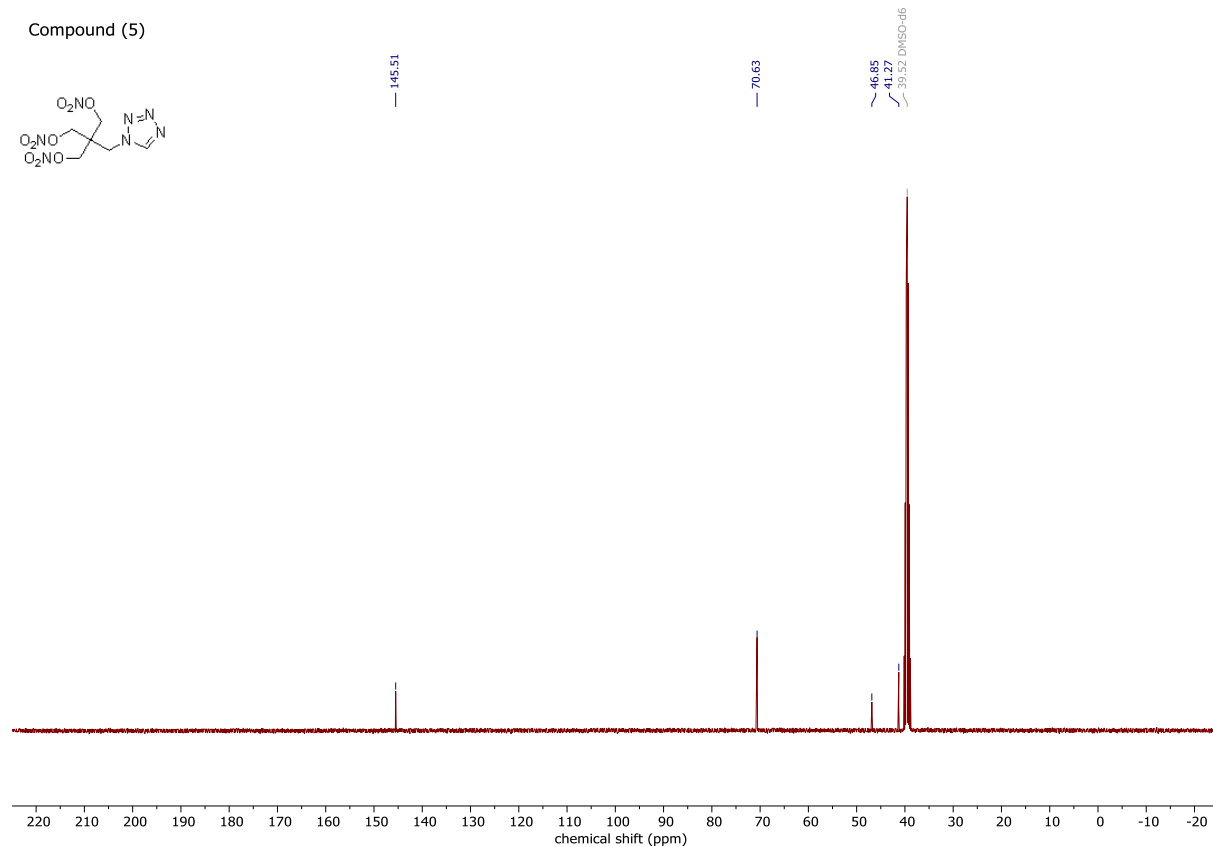
Compound (4b), ¹³C NMR (101 MHz, MeOH-d₄, ppm)



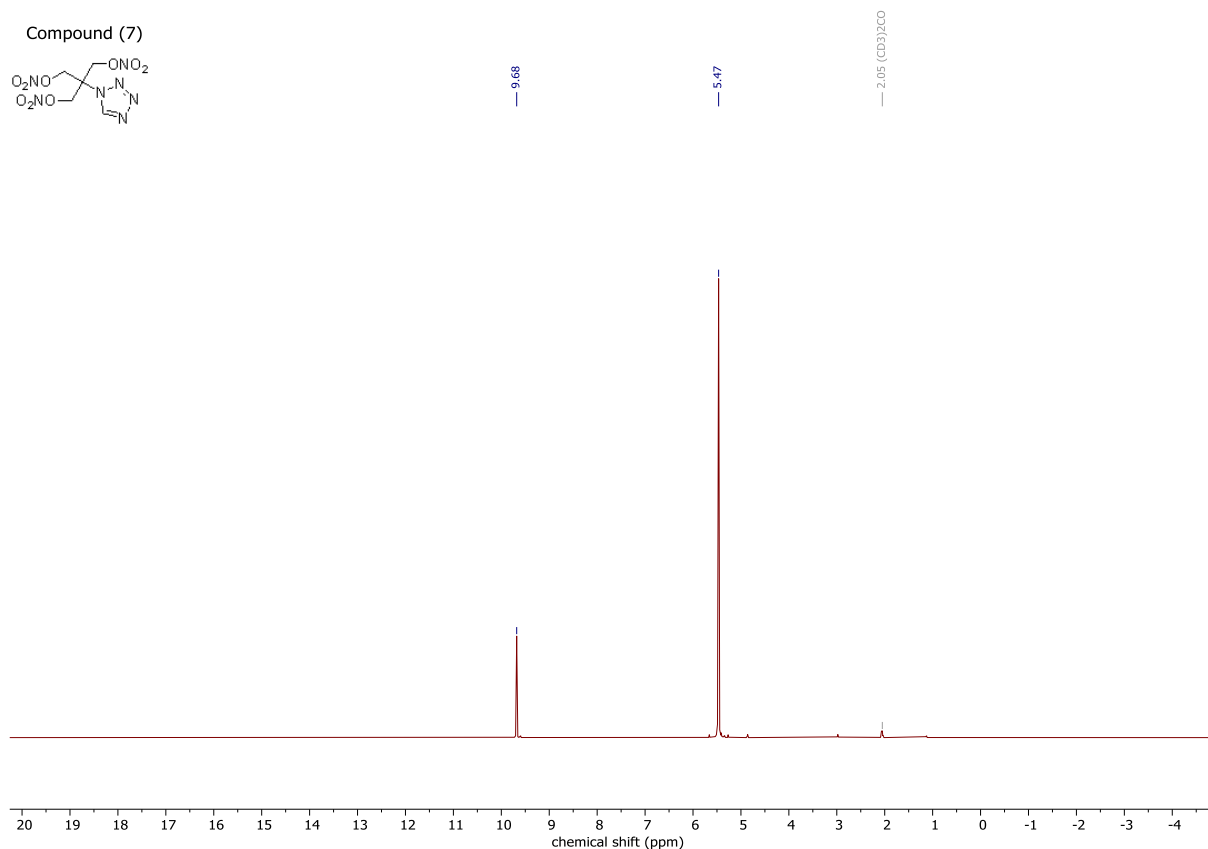
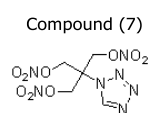
Compound (5), ¹H NMR (400 MHz, DMSO-d₆, ppm)



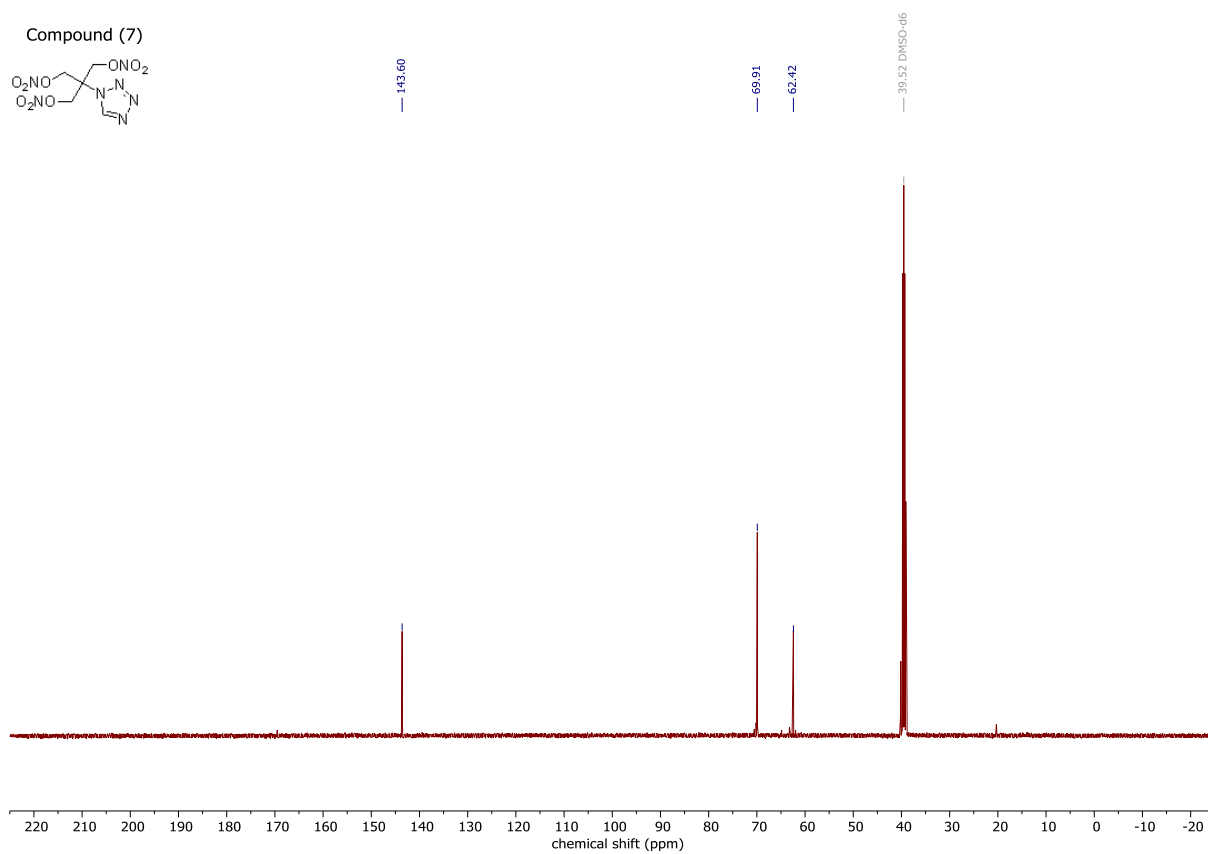
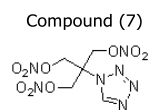
Compound (5), ¹³C NMR (101 MHz, DMSO-d₆, ppm)



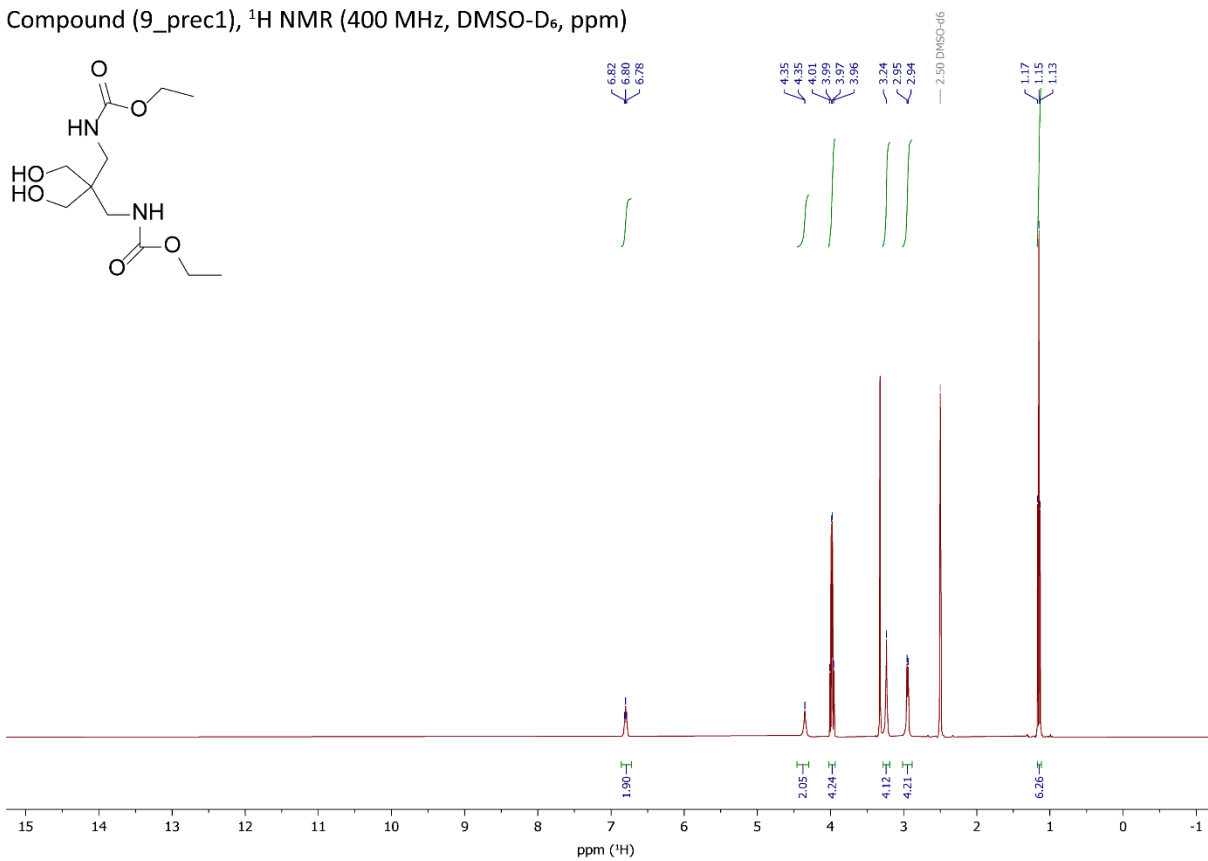
Compound (7), ¹H NMR (400 MHz, Acetone-d₆, ppm)



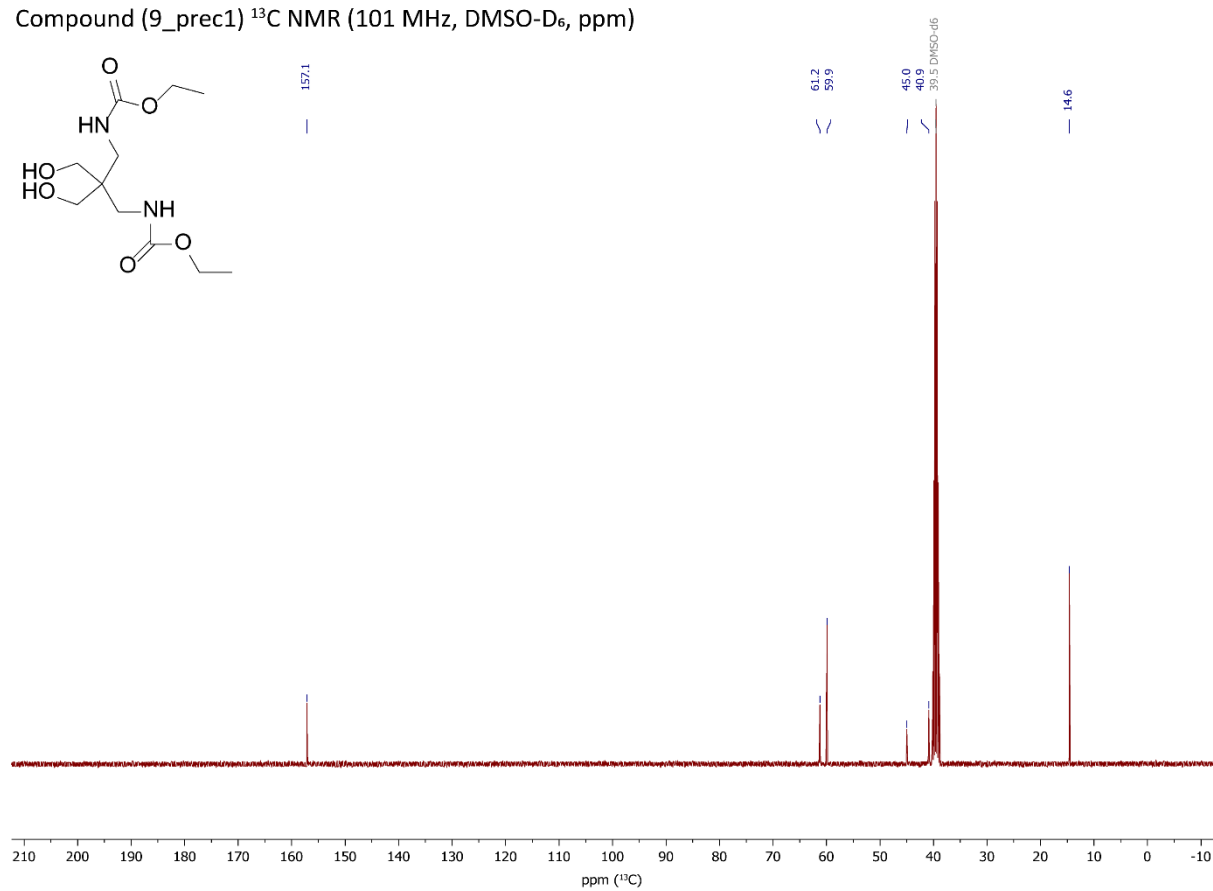
Compound (7), ¹³C NMR (101 MHz, DMSO-d₆, ppm)



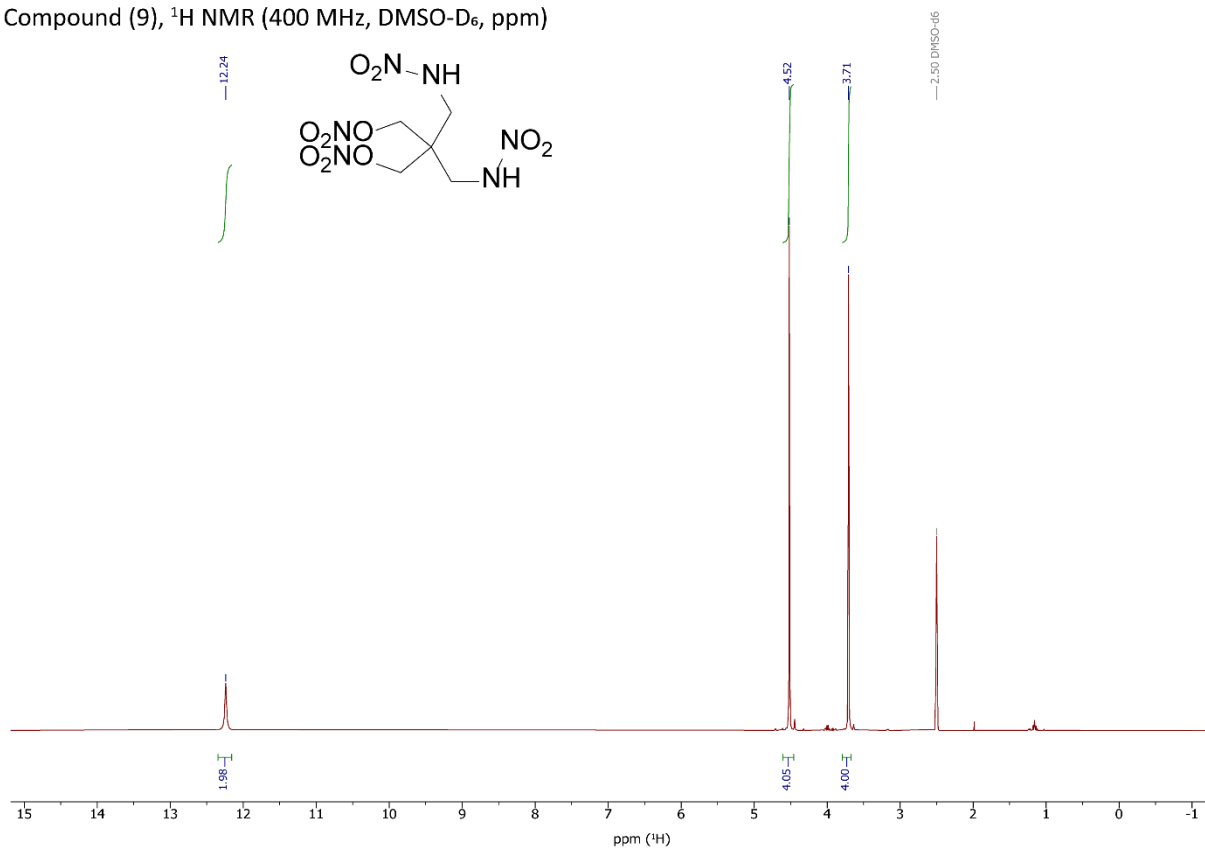
Compound (9_prec1), ^1H NMR (400 MHz, $\text{DMSO-}d_6$, ppm)



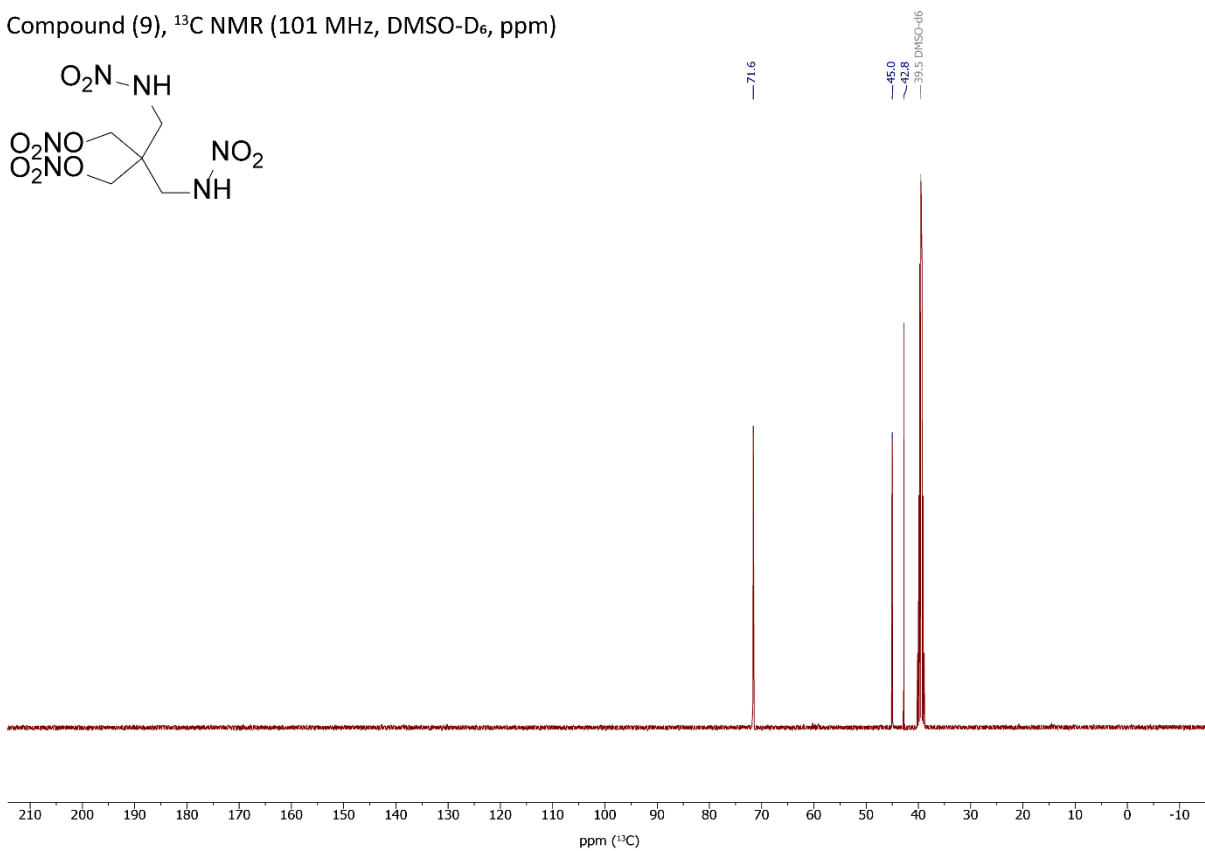
Compound (9_prec1) ^{13}C NMR (101 MHz, $\text{DMSO-}d_6$, ppm)



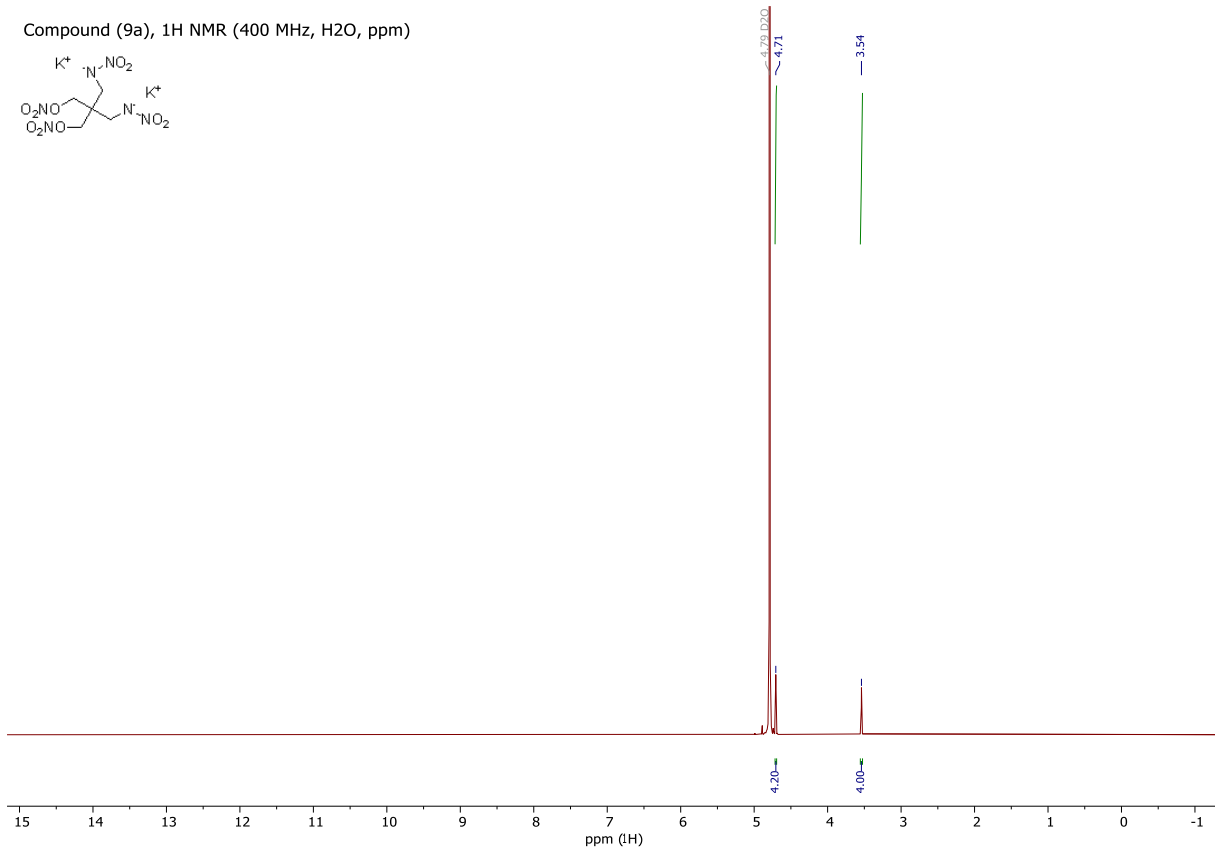
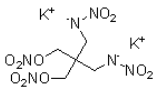
Compound (9), ^1H NMR (400 MHz, DMSO- D_6 , ppm)



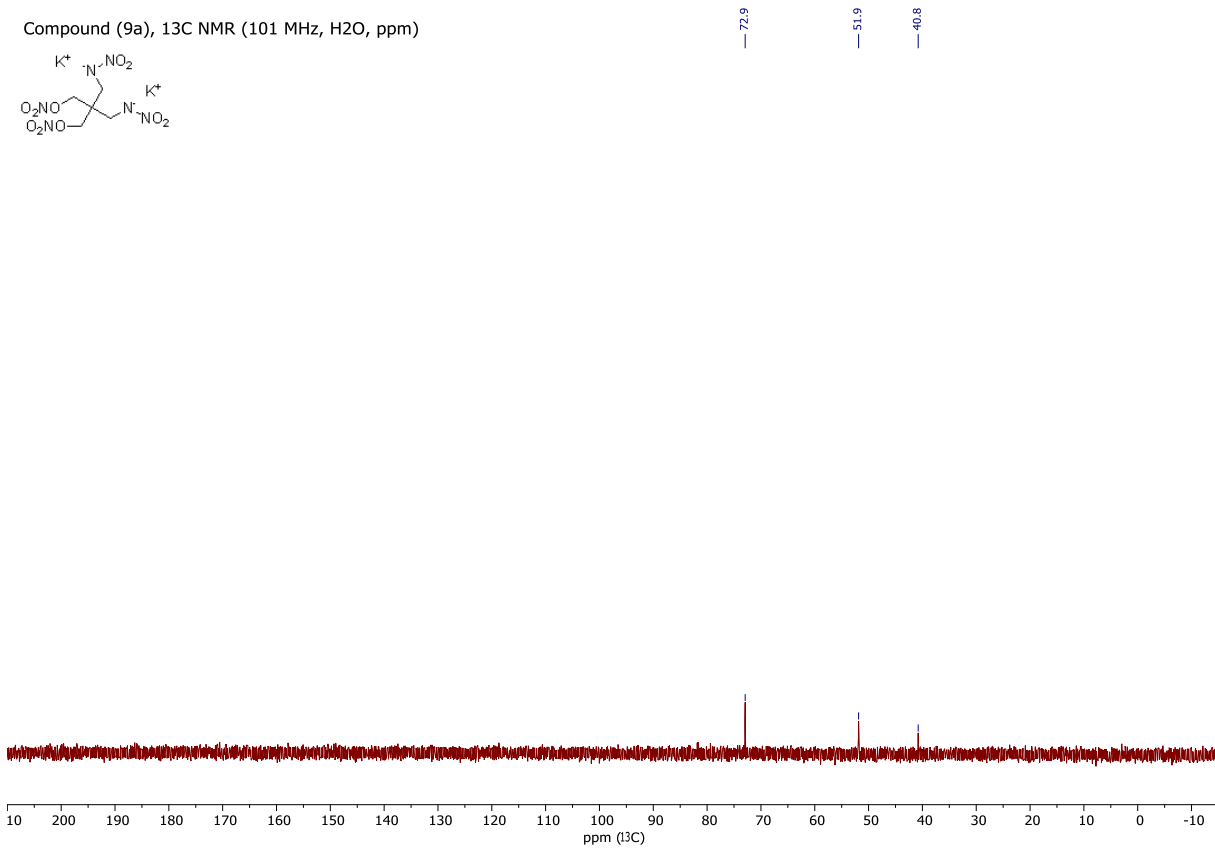
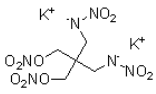
Compound (9), ^{13}C NMR (101 MHz, DMSO- D_6 , ppm)



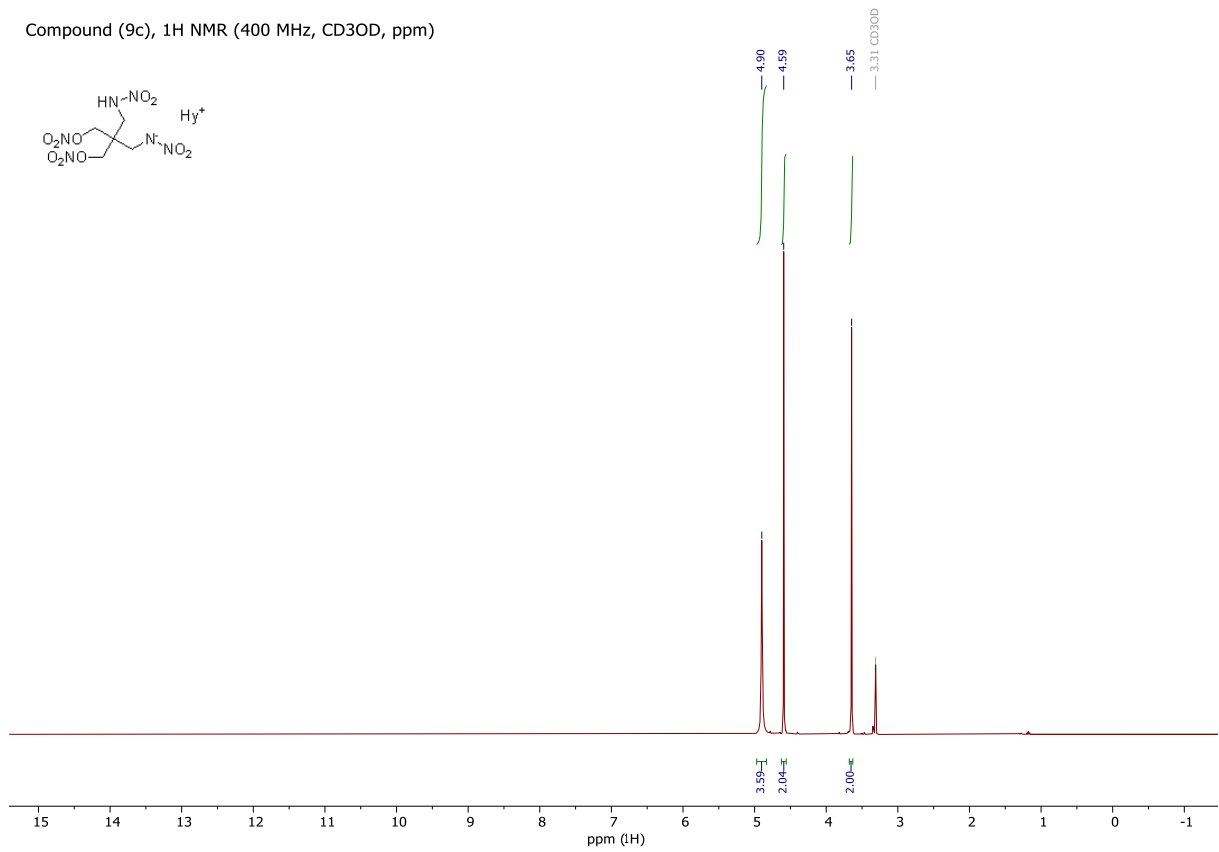
Compound (9a), ¹H NMR (400 MHz, H₂O, ppm)



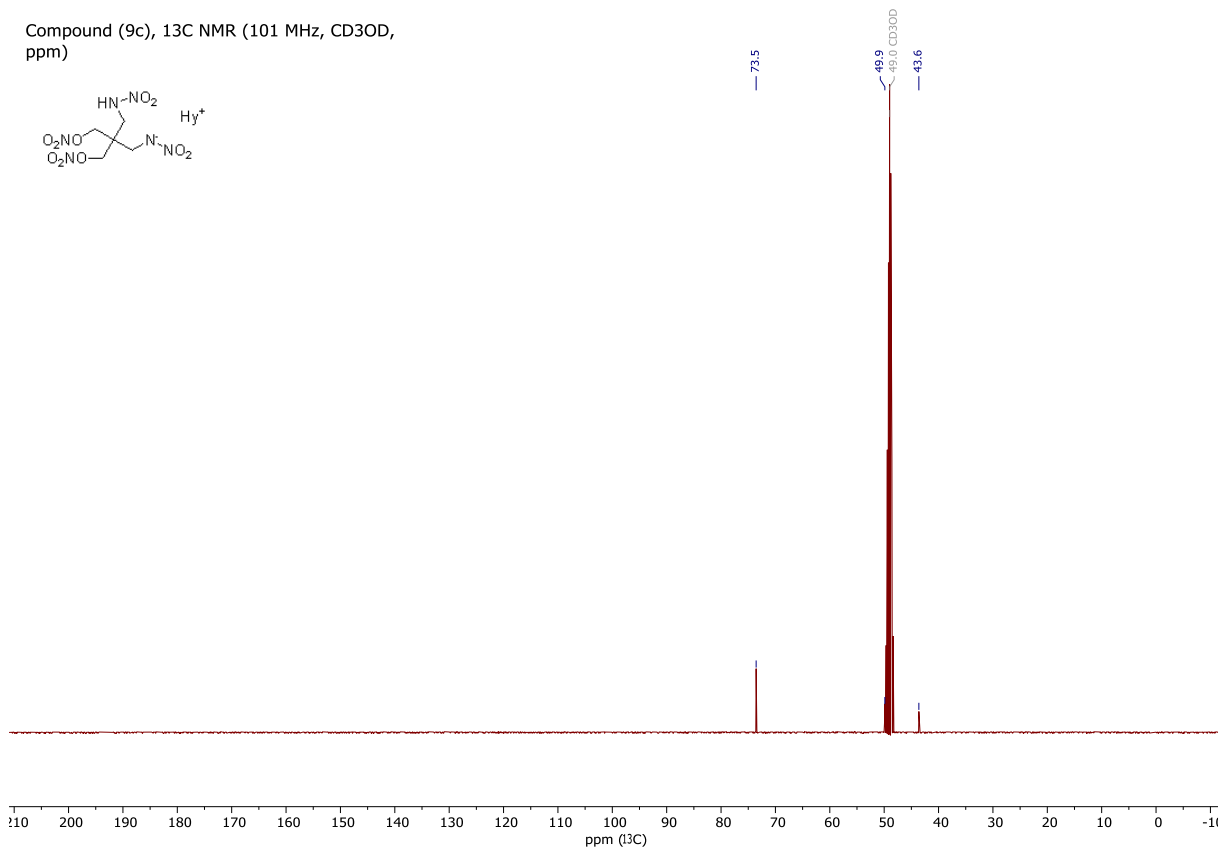
Compound (9a), ¹³C NMR (101 MHz, H₂O, ppm)



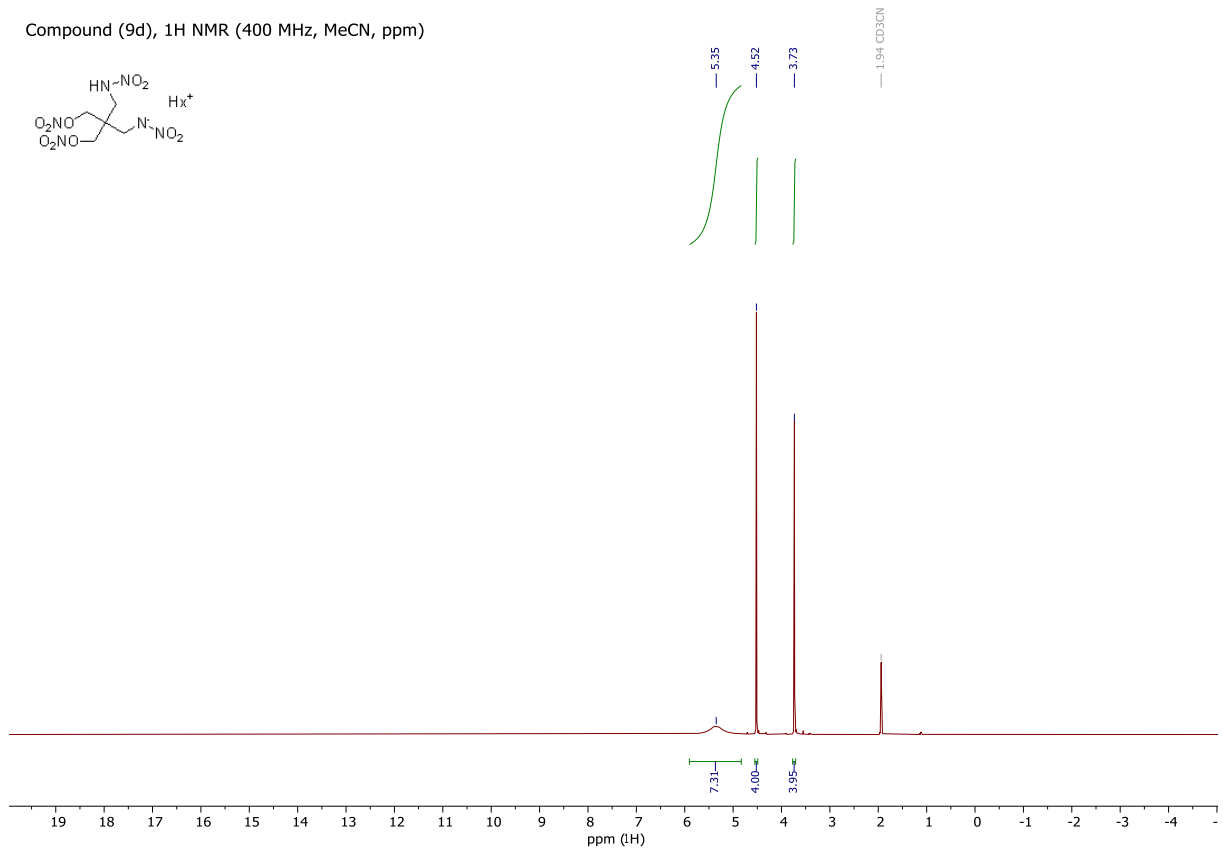
Compound (9c), ¹H NMR (400 MHz, CD₃OD, ppm)



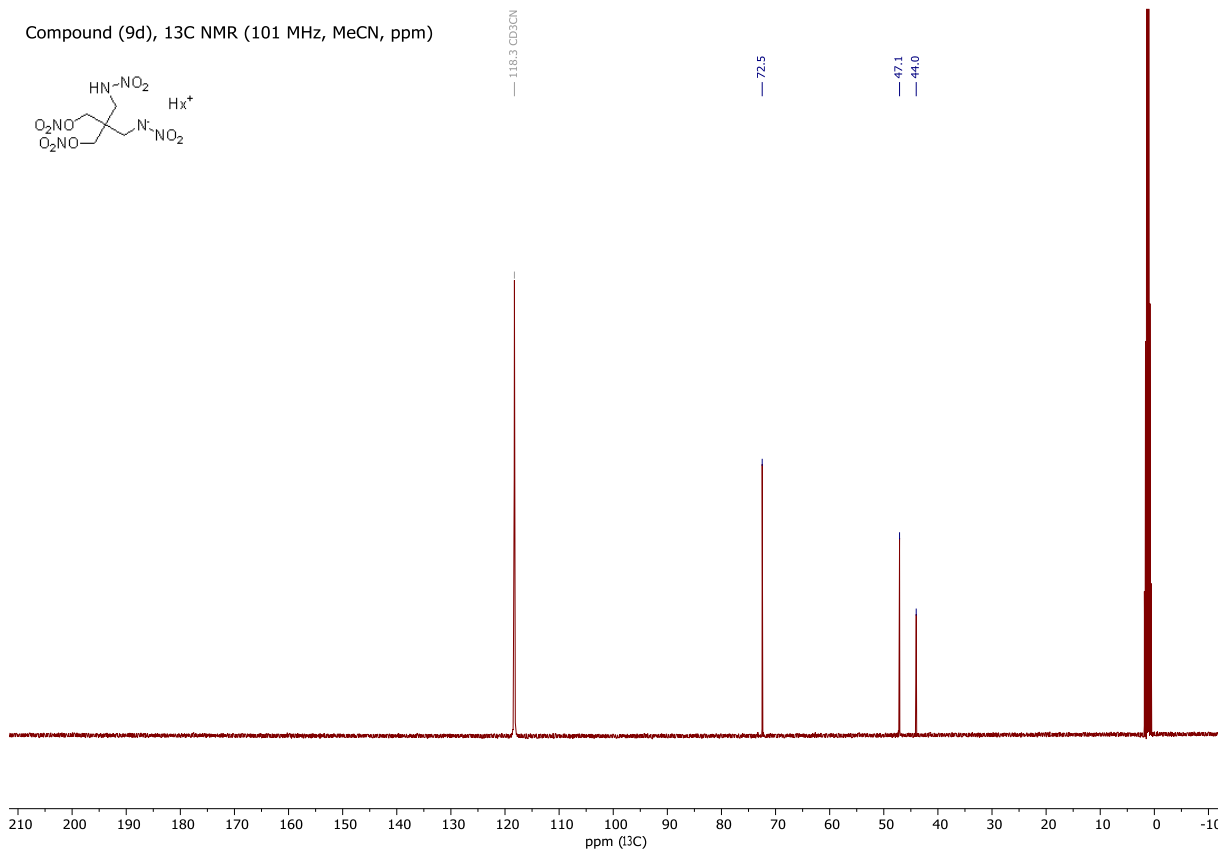
Compound (9c), ¹³C NMR (101 MHz, CD₃OD, ppm)



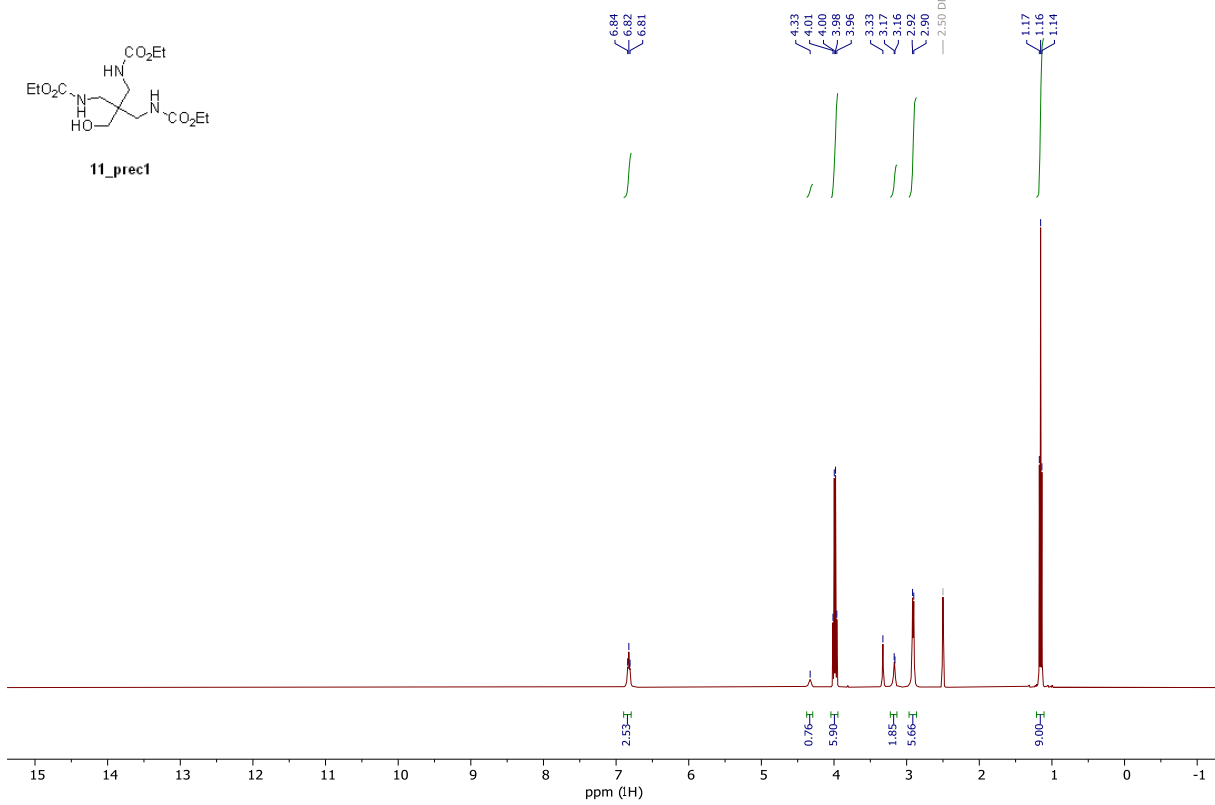
Compound (9d), ¹H NMR (400 MHz, MeCN, ppm)



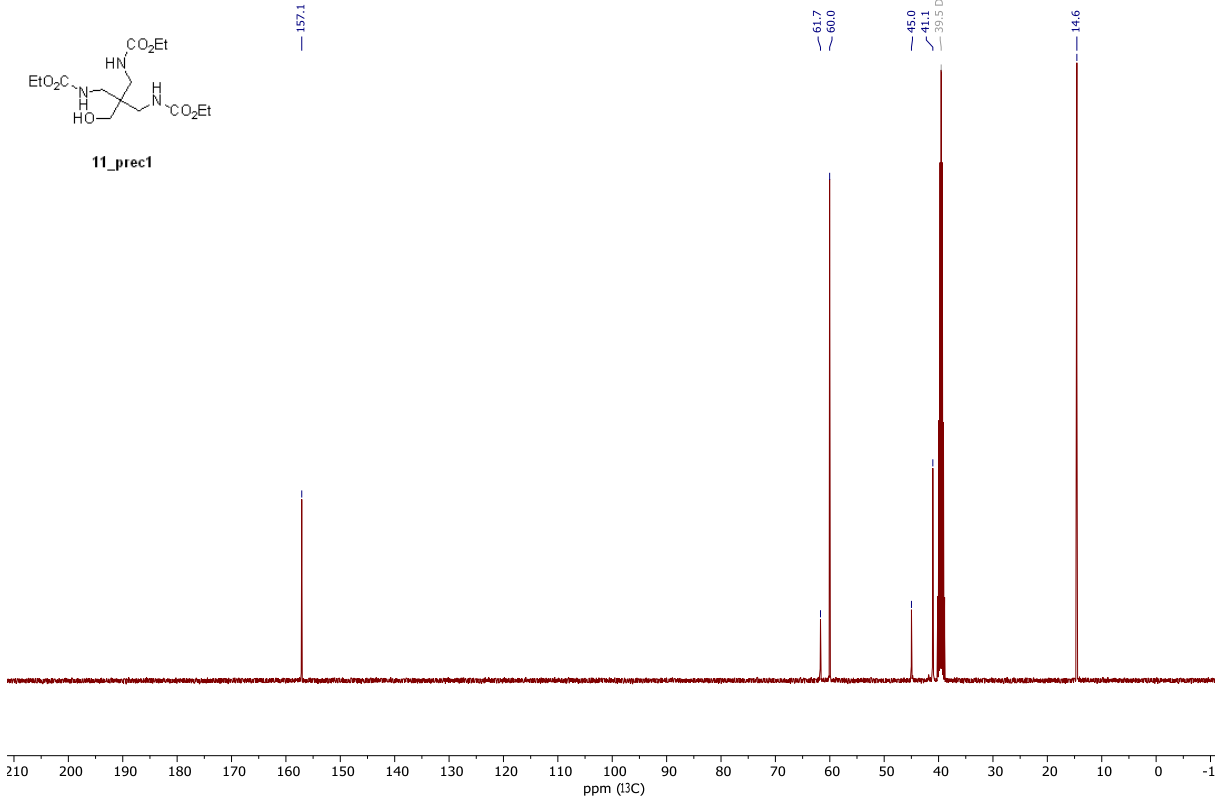
Compound (9d), ¹³C NMR (101 MHz, MeCN, ppm)



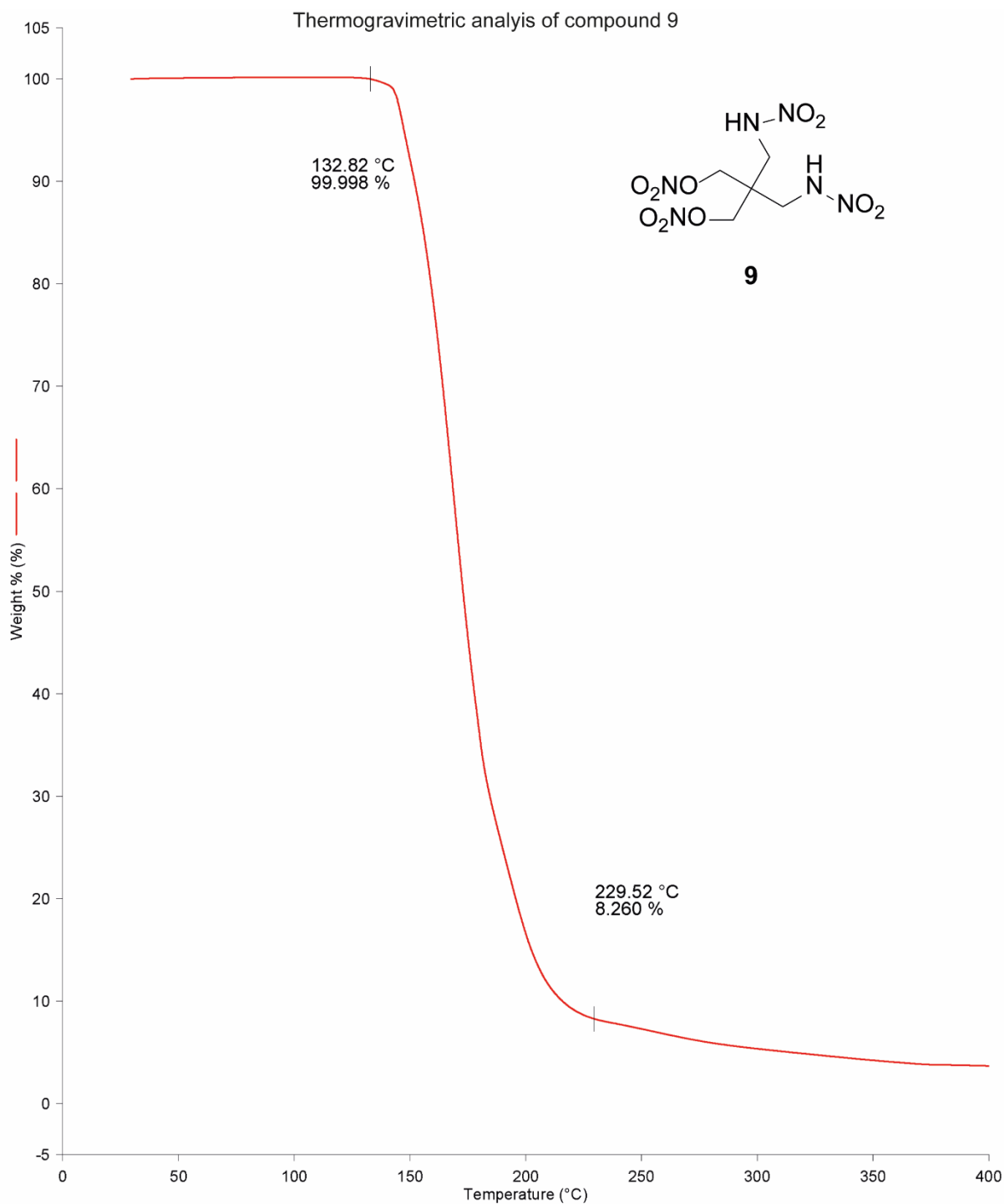
Compound (11_prec1), 1H NMR (400 MHz, DMSO-d6, ppm)



Compound (11_prec1), 13C NMR (101 MHz, DMSO-d6, ppm)



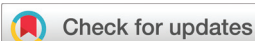
5. Thermal properties



- | | |
|--|--|
| 1) Hold for 1.0 min at 30.00°C | 3) Heat from 400.00°C to 900.00°C at 20.00°C/min |
| 2) Heat from 30.00°C to 400.00°C at 5.00°C/min | 4) Hold for 1.0 min at 900.00°C |

6. References

- ¹ a) Reichel & Partner GmbH, <http://www.reichel-partner.de>; b) Test methods according to the UN Recommendations on the Transport of Dangerous Goods, *Manual of Test and Criteria*, fourth revised edition, United Nations Publication, New York and Geneva, **2003**, ISBN 92–1-139087–7, Sales No. E.03.VIII.2; 13.4.2 Test 3 a (ii) BAM Fallhammer.
- ² M. Sućeska, EXPLO5 V6.02 program, Brodarski Institute, Zagreb, Croatia, **2014**.
- ³ S. Wawzonek, A. Matar, C. H. Issidorides, Monobromopentaerythritol, *Org. Synth.* 1958, **38**, 68.
- ⁴ T. Lenz, T. M. Klapötke, M. Mühlemann, J. Stierstorfer, *Prop., Explos., Pyrotech.* **2021**, **46**, 723.
- ⁵ M. A. Hiskey, M. J. Hatch, J. C. Oxley, Nitrate Amine Nitrates: Nitrate ester explosives with reduced impact sensitivity, *Prop., Explos., Pyrotech.* **1991**, **16**, 40.
- ⁶ P. N. Gaponik, V. P. Karavai, Y. V. Grigorev, Synthesis of 1-substituted tetrazoles by heterocyclization of primary amines, orthoformic ester, and sodium azide, *Chem. heterocycl. Compounds*, 1985, **21**, 1255.
- ⁷ *CrysAlisPro*, Oxford Diffraction Ltd. version 171.33.41, **2009**.
- ⁸ Bruker. SAINT. Bruker AXS Inc., Madison, Wisconsin, USA, **2012**.
- ⁹ Sheldrick, G. M. TWINABS. University of Göttingen, Germany, **1996**.
- ¹⁰ G. M. Sheldrick, *Acta Cryst.* **2015**, **A71**, 3–8.
- ¹¹ O. V. Dolomanov, L. J. Bourhis, R. J. Gildea, J. A. K. Howard, H. Puschmann, *J. Appl. Cryst.* **2009**, **42**, 339–341.
- ¹² *SCALE3 ABSPACK – An Oxford Diffraction program* (1.0.4, gui: 1.0.3), Oxford Diffraction Ltd., **2005**.
- ¹³ *APEX3*. Bruker AXS Inc., Madison, Wisconsin, USA.
- ¹⁴ M. J. Frisch, G. W. Trucks, H. B. Schlegel, G. E. Scuseria, M. A. Robb, J. R. Cheeseman, G. Scalmani, V. Barone, B. Mennucci, G. A. Petersson, H. Nakatsuji, M. Caricato, X. Li, H.P. Hratchian, A. F. Izmaylov, J. Bloino, G. Zheng, J. L. Sonnenberg, M. Hada, M. Ehara, K. Toyota, R. Fukuda, J. Hasegawa, M. Ishida, T. Nakajima, Y. Honda, O. Kitao, H. Nakai, T. Vreven, J. A. Montgomery, Jr., J. E. Peralta, F. Ogliaro, M. Bearpark, J. J. Heyd, E. Brothers, K. N. Kudin, V. N. Staroverov, R. Kobayashi, J. Normand, K. Raghavachari, A. Rendell, J. C. Burant, S. S. Iyengar, J. Tomasi, M. Cossi, N. Rega, J. M. Millam, M. Klene, J. E. Knox, J. B. Cross, V. Bakken, C. Adamo, J. Jaramillo, R. Gomperts, R. E. Stratmann, O. Yazyev, A. J. Austin, R. Cammi, C. Pomelli, J. W. Ochterski, R. L. Martin, K. Morokuma, V. G. Zakrzewski, G. A. Voth, P. Salvador, J. J. Dannenberg, S. Dapprich, A. D. Daniels, O. Farkas, J.B. Foresman, J. V. Ortiz, J. Cioslowski, D. J. Fox, Gaussian 09 A.02, Gaussian, Inc., Wallingford, CT, USA, **2009**.
- ¹⁵ a) J. W. Ochterski, G. A. Petersson, and J. A. Montgomery Jr., *J. Chem. Phys.* **1996**, **104**, 2598–2619; b) J. A. Montgomery Jr., M. J. Frisch, J. W. Ochterski G. A. Petersson, *J. Chem. Phys.* **2000**, **112**, 6532–6542; c) L. A. Curtiss, K. Raghavachari, P. C. Redfern, J. A. Pople, *J. Chem. Phys.* **1997**, **106**, 1063–1079; d) E. F. C. Byrd, B. M. Rice, *J. Phys. Chem. A* **2006**, **110**, 1005–1013; e) B. M. Rice, S. V. Pai, J. Hare, *Comb. Flame* **1999**, **118**, 445–458.
- ¹⁶ M. S. Westwell, M. S. Searle, D. J. Wales, D. H. Williams, *J. Am. Chem. Soc.* **1995**, **117**, 5013–5015; b) F. Trouton, *Philos. Mag.* **1884**, **18**, 54–57.
- ¹⁷ a) H. D. B. Jenkins, H. K. Roobottom, J. Passmore, L. Glasser, *Inorg. Chem.* **1999**, **38**, 3609–3620; b) H. D. B. Jenkins, D. Tudela, L. Glasser, *Inorg. Chem.* **2002**, **41**, 2364–2367.

Cite this: *Dalton Trans.*, 2021, **50**, 10811

Nitratoethyl-5*H*-tetrazoles: improving the oxygen balance through application of organic nitrates in energetic coordination compounds†

Michael S. Gruhne, Tobias Lenz, Markus Rösch, Marcus Lommel, Maximilian H. H. Wurzenberger,  Thomas M. Klapötke  and Jörg Stierstorfer *

1- and 2-Nitratoethyl-5*H*-tetrazole (1-NET and 2-NET) were prepared through nitration of the respective alkyl alcohol using 100% nitric acid. A mixture of 1- and 2-hydroxyethyl-5*H*-tetrazole was obtained after alkylation of 1,5*H*-tetrazole. Also, a one-pot synthesis of 1-hydroxyethyl-5*H*-tetrazole was developed enabling the selective preparation of 1-NET. Both organic nitrates were characterized by ¹H, ¹³C, and ¹H–¹⁵N HMBC NMR spectroscopy. In addition, calculations using the Hirshfeld method and the EXPLO5 code were performed. Principally, 20 energetic coordination compounds involving the d-metals Mn, Cu, Zn, and Ag, each structurally characterized by low temperature single crystal X-ray diffraction, were prepared based on 1-NET and 2-NET. Of these complexes, 18 were obtained as pure bulk materials, and therefore, characterized for impact, friction, and ball drop impact sensitivity, as well as electrostatic discharge and thermal stability using differential thermal analysis. Hot plate and hot needle tests were performed mostly showing strong deflagrations making the complexes candidates for green combustion catalysts. Furthermore, successful PETN initiation experiments were carried out for several complexes and all ECCs were investigated by laser ignition experiments.

Received 9th June 2021,
Accepted 29th June 2021
DOI: 10.1039/d1dt01898a

rsc.li/dalton

Introduction

Ever since the first energetic materials were discovered, research is focused on the improvement of their properties. The explosives widely used today are tailored to specific applications in terms of power, sensitivity, and stability while being cost efficient.¹ In recent years, there has been a worldwide increase in the demand for environmentally friendly and sustainable materials in every area, including the field of energetic materials.² Additionally, regulations such as the REACH directive of the European Union or similar regulations of the US Environmental Protection Agency put pressure on the search for suitable substitutes. In the field of primary explosives commonly used, heavy metal-based lead azide and lead styphnate are harming users and the environment especially when utilized over a long time.³ These two lead salts are therefore classified as substances of very high concern (SVHCs).⁴

In the search for new compounds, great attention is now paid to an environmentally friendly production chain while

still having a cost-efficient synthesis and long-term stability.⁵ The nitrogen-rich tetrazole moiety has proven to be a chameleon for energetic materials.⁶ The simplest representative, 1,5*H*-tetrazole, shows sensitivity toward impact due to its high nitrogen content of 80%, but is also a common reactant due to its straightforward preparation.⁷ Regarding its derivatives, 1-ethyl-5*H*-tetrazole⁸ has proven to be a suitable building block. This structural element has already been successfully used for the introduction of various energetic groups, such as an azido⁹ or trinitromethyl group.¹⁰ The synthesis of haloethyl¹¹ and hydroxyethyl⁹ tetrazole has also been described. An overview on the 1-ethyl-5*H*-tetrazole derivatives, already known in the literature together with unknown representatives of this group, is presented in Chart 1.

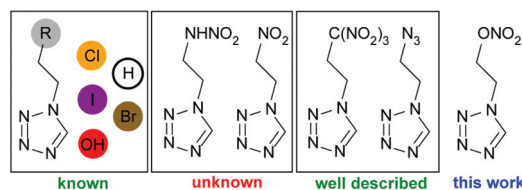


Chart 1 Outline on the tetrazole derivatives based on 1-ethyl-5*H*-tetrazole.^{8–11} Corresponding 2-ethyl-5*H*-tetrazoles and especially 2-nitratoethyl-5*H*-tetrazole, which is also a part of this work, are not shown here.

Department of Chemistry, Ludwig-Maximilians University of Munich, Butenandtstr. 5-13, D-81337 Munich, Germany. E-mail: jstch@cup.uni-muenchen.de;

Fax: +49-89-2180-77007http://www.hedm.cup.uni-muenchen.de

† Electronic supplementary information (ESI) available. CCDC 2080666–2080685. For ESI and crystallographic data in CIF or other electronic format see DOI: 10.1039/d1dt01898a

The ethylene group is favourable because of its easy accessibility from ethylamine hydrochlorides or halides. These starting materials are usually available for purchase at low cost and, with the exception of the trinitromethyl derivative, make the compounds shown in Chart 1 easily accessible.^{8–11}

The reason for the preparation of functionalized tetrazoles is not just to fulfil the need for more nitrogen-rich compounds. They also help to further explore the concept of energetic coordination compounds (ECCs). The aim here is to adjust the properties of the resulting complex as desired by varying the parameters of the central metal, anion, or ligand.¹² A variation of the substitute on the alkyl chain of the 1-ethyl-5*H*-tetrazole building block, for example, affects the solubility, performance, and thermal stability of ECCs. In every case, the anion and central metal (here Mn, Cu, Zn, and Ag) also influence the complex's behaviour. However, in this work, focus is placed on the introduction of an organic nitrate function into the building block to study its effects on the coordination compound.

Organic nitrates are useful for lowering the water solubility of compounds, while increasing the oxygen balance.¹³ As of today, only two tetrazole derivatives with a nitrateoethyl group at the N1 position are known.^{14,15} Both molecules, displayed in Chart 2, are not suitable for use as ligands in promising ECCs. The amino group in the structure on the left, for example, leads to sterically demanding coordination geometries likely leading to the inclusion of aqua ligands and lowering the performance.¹⁶ Nitrimino groups on the other hand are highly acidic, making them more likely to serve as anionic ligands.^{15,17}

Therefore, in this work, focus was placed on the preparation of 1- and 2-nitrateoethyl-5*H*-tetrazole (1-NET and 2-NET). The resulting coordination compounds show an increased oxygen balance, making them interesting for use as energetic combustion catalysts in air bag systems or solid rocket propellants as a potential alternative to basic copper nitrate (BCN).¹⁸

Results and discussion

CAUTION! All investigated compounds are potentially explosive energetic materials (the majority of the compounds lie in the range of primary explosives!), which show increased sensitivities toward various stimuli (*e.g.*, elevated temperatures, impact, friction, or electrostatic discharge). Therefore, proper security precautions (safety glasses, face shield, earthed equipment and shoes, leather jacket, Kevlar gloves, Kevlar sleeves,

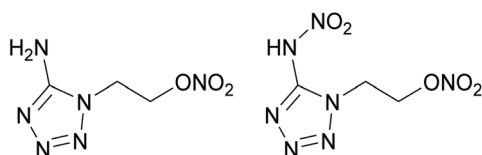


Chart 2 Literature known 1-nitrateoethyltetrazole derivatives.^{14,15}

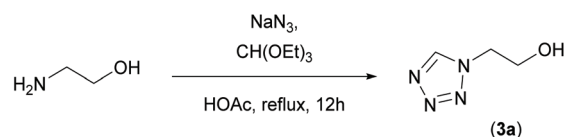
and ear plugs) have to be taken while synthesizing and handling the described compounds.

Synthesis of the ligands

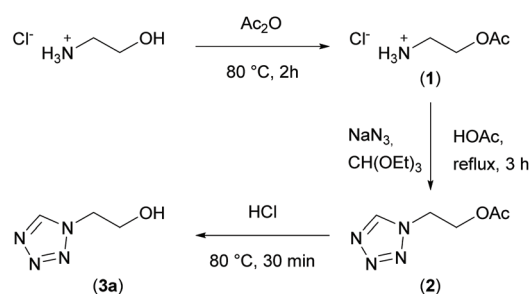
Like most tetrazole derivatives, the ligands can be synthesized in two ways. The first strategy, already described by Gaponik *et al.*, involves the reaction of 2-aminoethanol or the respective hydrochloride together with triethyl orthoformate and sodium azide, yielding only the 1*H*-substituted derivative **3a** (Scheme 1).⁸ However, workup by complexation and subsequent breakdown of the complex with hydrogen sulphide is suggested.

Since the complicated processing of the raw material makes an industrial scale synthesis less promising, the authors have worked out another synthetic pathway toward 1-hydroxyethyl-5*H*-tetrazole (**3a**). As it is assumed that the use of alcohol derivatives together with triethyl orthoformate leads to undesired alkylation products, a modified synthesis of Bays *et al.* was applied.¹⁹ Here, the introduction of a protective group prevents the formation of by-products (Scheme 2). The reaction of 2-aminoethanol hydrochloride with acetic anhydride gave **1** in good yields up to 75%. Subsequently a ring closure reaction was performed resulting in compound **2** in the form of colourless crystals (yield: 61%). This contradicts literature data, describing the substance as a pale-yellow oil.¹⁹ After reacting compound **2** with concentrated hydrochloric acid, 1-hydroxyethyltetrazole (**3**) was obtained in the form of a colourless solid (yield: 93%).

The steps can be carried out sequentially (overall yield: 26%), or by an industrially valuable one-pot synthesis, resulting in an overall yield of 75%. For this purpose, acetic acid formed during the reaction of 2-ethanolamine and acetic anhydride was not removed in the first step. The reaction was cooled down to 40 °C and triethyl orthoformate followed by



Scheme 1 Synthesis of compound **3a** starting from 2-aminoethanol.



Scheme 2 Synthesis of 1-hydroxyethyltetrazole (**3a**) using acetic anhydride.

sodium azide was added. After the addition of further acetic acid, the mixture was refluxed. Subsequently, concentrated hydrochloric acid was added to the hot solution and heating was continued for 30 min. All solvents were removed under reduced pressure and the remaining residue was extracted with hot acetone. The solvent was removed under reduced pressure and the product was dried under high vacuum affording compound **3a** as colourless crystals.

To also obtain 2-hydroxyethyl-5*H*-tetrazole, a classic alkylation, as the second synthetic strategy for the derivatization of tetrazoles, was applied. A reaction of chloroethanol with 1,5*H*-tetrazole involving a base resulted in a mixture of two isomers **3a** and **3b** (Scheme 3) in a 1 : 1 ratio (yield: 88%).²⁰ No separation of the products was carried out.

The nitration of both the isomeric mixture and pure compound **3a** was carried out by adding the alcohol to fuming nitric acid. The reaction of the pure 1-isomer with neutralization and extraction yielded compound **4** (yield: 73%). In the case of the isomeric mixture column chromatography with a solvent gradient was used to separate ligands **4** and **5** (yield **4**: 45%, yield **5**: 43%) (Scheme 4). Compound **5** can be further purified by sublimation, but separation of the isomers is not possible with this method.

Analysis of the ligands

The isomers, thus obtained, were distinguished by infrared spectroscopy (IR) as well as by proton, carbon, and nitrogen NMR spectroscopy. The isomer distribution can easily be followed by integration of the ¹H resonances. Furthermore, ¹H-¹⁵N-HBMC spectra were measured. In the two-dimensional coupled spectra of tetrazole derivatives **4** and **5**, ²*J* and ³*J* couplings between nitrogen and hydrogen were measured. This allows a clear assignment of the isomers (Fig. 1 & 2). In advance, compound **5** was analyzed by one dimensional ¹⁵N NMR to clarify the superimposed shifts at about -62 ppm (Fig. 2, top). The HBMC method used is only showing nitrogen atoms that have a finite ¹H-¹⁵N coupling (>1 Hz) to an immobile hydrogen atom. This is the case here for all nitrogen

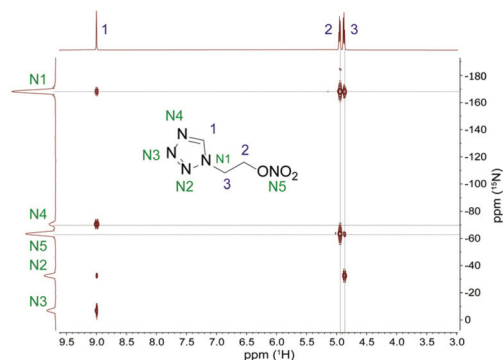


Fig. 1 Two-dimensional ¹H-¹⁵N-HBMC NMR spectra of **4** (MeCN-*d*₃, 25 °C): δ (ppm) = -7.0 (N3), -32.4 (N2), -63.4 (N5), -70.5 (N4), -168.2 (N1).

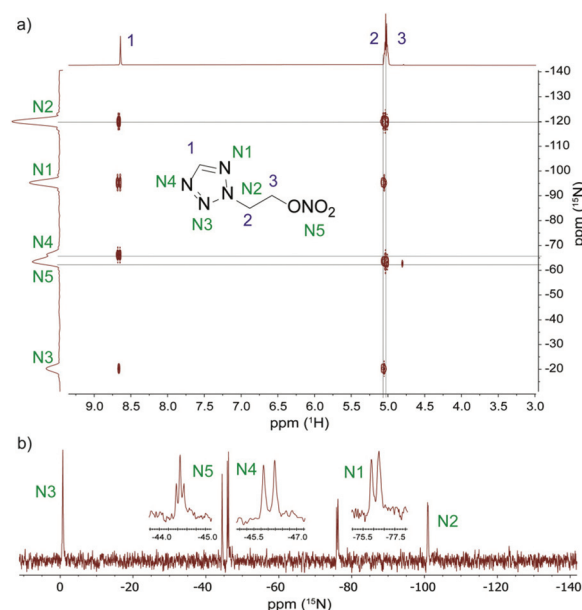
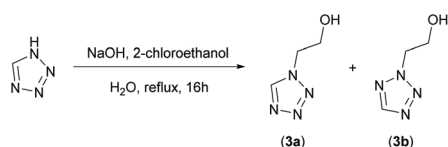
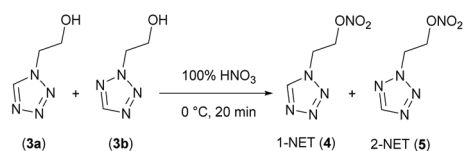


Fig. 2 (a) Two-dimensional ¹H-¹⁵N-HBMC NMR spectra of **5** (acetone-*d*₆, 25 °C): δ (ppm) = -2.0 (N3), -63.5 (N5), -66.4 (N4), -95.3 (N1), -120.1 (N2); (b) ¹⁵N NMR spectra of **5** (acetone-*d*₆, 25 °C).



Scheme 3 Reaction of 1,5*H*-tetrazole with 2-chloroethanol.



Scheme 4 Nitration of 1-hydroxyethyl-5*H*-tetrazole (**3a**) and 2-hydroxyethyl-5*H*-tetrazole (**3b**).

atoms. In addition to the simpler atom assignment due to the coupling, the measurement time is many times shorter than that for traditional ¹⁵N NMR measurements. Additional ¹⁴N NMR shifts can be found in the ESI.†

The crystal structures of precursor **2** (Fig. S1, ESI†) together with the structures of both nitrateoethyl-5*H*-tetrazoles were determined using low temperature single crystal X-ray diffraction (Fig. 3). Compound **4** crystallizes in the monoclinic space group *P2*₁/*n* and possesses an asymmetric unit of two slightly different ordered molecules of 1-NET. Therefore, the unit cell is built up by eight formula units and shows a calculated density of 1.619 g cm⁻³ at 105 K. In contrast, isomeric compound **5** crystallizes in the orthorhombic space group *Pna*2₁. The unit cell contains only four formula units and shows a

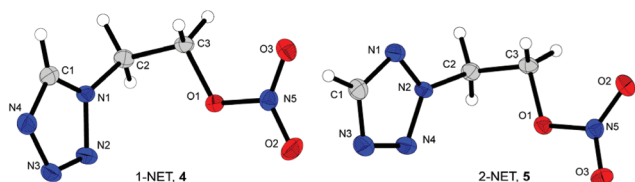


Fig. 3 Formula units of 1-NET (**4**) displayed on the left and 2-NET (**5**) on the right. Selected bond lengths (Å) of **4**: N1–C1 1.334(2), N3–N2 1.2978(19), N4–N3 1.359(2), O1–C3 1.4576(17), O1–N5 1.3927(17), O2–N5 1.2038(18). Selected bond lengths (Å) of **5**: N1–C1 1.327(4), N3–N2 1.326(4), N4–N3 1.318(4), O1–C3 1.456(4), O1–N5 1.394(3), O2–N5 1.216(4). Selected bond angles (°) of **4**: N4–C1–N1 109.32(14), N4–N3–N2 111.18(12), N1–C2–C3 111.19(12), C3–O1–N5 113.22(10), O1–N5–O2 113.09(13), O2–N5–O3 128.78(15). Selected bond angles (°) of **5**: N4–C1–N1 113.2(3), N4–N3–N2 106.1(3), N2–C2–C3 111.5(3), C3–O1–N5 114.1(2), O1–N5–O2 118.0(3), O2–N5–O3 129.2(3).

slightly lower density of 1.584 g cm^{-3} at a temperature of 128 K. The bond distances and angles are similar in both molecules and comparable to those of literature known tetrazole derivatives and organic nitrates.

The crystalline material of the ligands was analysed for their sensitivity toward impact and friction according to the “UN declaration of dangerous goods” with a BAM drop hammer and friction tester.^{21,22} The hard and brittle crystals of **5** ($IS = 2 \text{ J}$) are more sensitive toward impact than the plate like and ductile crystals of **4** ($IS = 10 \text{ J}$). Both ligands are insensitive towards friction ($FS > 360 \text{ N}$).

Hirshfeld surfaces of 1-NET (**4**) and 2-NET (**5**) were generated, and the intermolecular atom interactions were calculated based on the crystallographic data and are visualized in Fig. S8 (ESI†).²³ Attractive and repulsive interactions are comparable for both molecules and therefore the exact location of the interactions in the crystal is of more importance. To investigate the location of the respective interaction, structural elements were investigated (Fig. 4). The strong interactions, visible as red dots on the Hirshfeld surface (Fig. S8, ESI†), were analysed and the interactions are visualized in the structural elements. It becomes clear that compound **4** is arranged in layers. These

layers have an outer part (green, N–H) and a rigid inner part (grey, nitrate–nitrate, O–H). The layers among themselves are only weakly connected (orange, N–N (π), H–H). It is assumed that these properties are responsible for the ductile, layered physical character. In contrast, compound **5** is largely dominated by hydrogen bonding in every direction and cannot be divided into layers.

The crystal is thus fixed in all spatial directions and is clearly more rigid, which is also consistent with the physical properties. With this information, one could explain the lower sensitivity of compound **4**, through its layer like structure.²⁴ Regarding the low sensitivity toward friction we believe that the heat generated through the applied frictional force leads to melting and therefore desensitizing of the samples (the liquid samples are often less sensitive towards friction).⁶ It is questionable if the impact is causing the solid sample to detonate or if a melting process occurs beforehand.²⁵

The heat of formation of **4** and **5** was calculated using the atomization method (Gaussian CBS-4M electronic enthalpies) and the detonation parameters were calculated using the EXPLO5 V6.05 code (Table 1).²⁶ Additional information on the calculations is given in the ESI (Tables S7 & S8†). The heat of formation of 1-NET (**4**) is 27 kJ mol^{-1} which is higher than that of 2-NET (**5**). This leads to a detonation velocity of 7583 m s^{-1} for compound **4**, and a slightly lower value of 7420 m s^{-1} for compound **5**. In Table 1 the most important physico-chemical and calculated properties of **4**, **5**, and TNT are compared. Although the melting points of **4** and **5** are too close to room temperature to classify the energetic materials as suitable melt castable materials, it proves the compatibility of the tetrazole and the nitrate ester moiety.

Synthesis of the ECCs

Many complexes based on monotetrazole ligands are already known in the literature.^{27–29} However, in addition to their

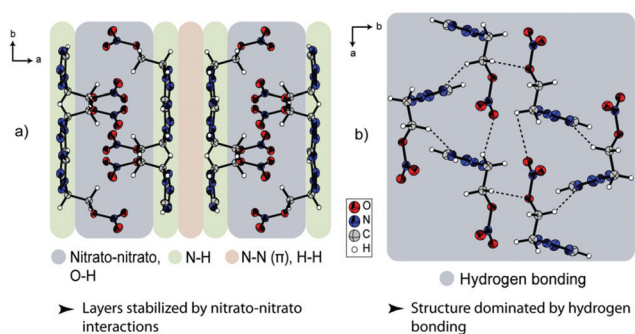


Fig. 4 (a) Structural elements of 1-NET (**4**) along the *c*-axis; (b) structural elements of 2-NET (**5**) along the *c*-axis. The areas showing the same interactions are marked and the type of interaction is noted below the respective structure.

Table 1 Physico chemical and calculated properties of **4**, **5**, and TNT

Compound	4	5	TNT
IS^a [J]	10	2	15
FS^b [N]	>360	>360	>360
$\Omega_{CO_2}^c$ [%]	–55.31	–55.31	–73.96
T_{endo}^d/T_{exo}^e [°C]	25/168	24/188	80/290
ρ^f [g cm^{-3}]	1.55	1.57	1.65
$\Delta_f H_m^g$ [kJ mol^{-1}]	174	147	–59
Detonation parameters calculated with the EXPLO5 V6.05 code			
$-\Delta_f U^{o,h}$ [kJ kg^{-1}]	4861	4689	4406
T_E^i [K]	3336	3268	3176
p_{C-J}^j [GPa]	21.5	20.4	18.3
V_{det}^k [m s^{-1}]	7583	7420	6798
V_0^l [L kg^{-1}]	815	818	640

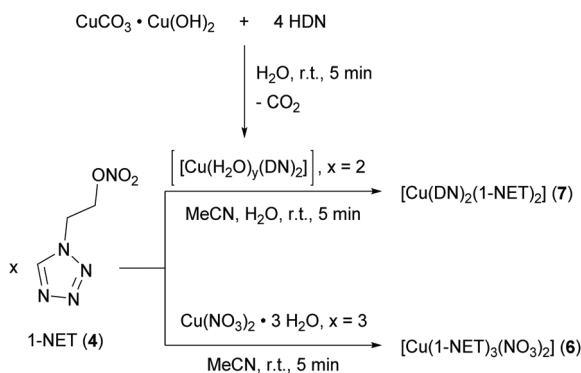
^a Impact sensitivity, (BAM drop hammer, 1 of 6). ^b Friction sensitivity, (BAM friction tester, 1 of 6). ^c Oxygen balance toward CO_2 . ^d Endothermic peak, which indicates melting. ^e Exothermic peak, which indicates decomposition. ^f Calculated density at 298 K. ^g Calculated enthalpy of formation at 298 K. ^h Heat of explosion. ⁱ Detonation temperature. ^j Detonation pressure. ^k Detonation velocity. ^l Volume of detonation gases (assuming only gaseous products).

good performance, these usually exhibit very good water solubility, which is generally not desired in the field of energetic materials. To address this problem, a variety of ECCs containing organic nitrate-based ligands 1-NET (4) and 2-NET (5) were prepared. The resulting complexes should not only exhibit a reduced solubility, but also at the same time maintain their performance.

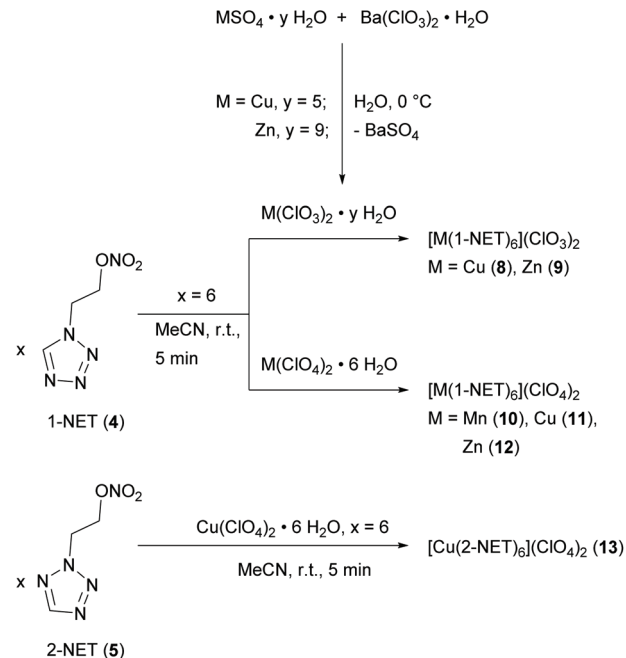
In the first step, several neutral or cationic coordination compounds based on oxidizing anions like nitrate, dinitramide, chlorate, or perchlorate were formed. The role of the ligand is to tune the energy content and sensitivity of the complex. Due to the bad solubility of the ligand, the sole use of water as a green solvent was not possible. Therefore, acetonitrile, or a combination of water and acetonitrile, was applied for the preparation of coordination compounds 6–13. Besides rather easily accessible nitrate anions, the dinitramide anion was made accessible using basic copper carbonate and dinitraminic acid, as published in our previous work (Scheme 5).³⁰ Both metal salts were reacted with stoichiometric amounts of the ligand and crystallized within several days in decent yields up to 96% in the form of single crystals suitable for X-ray diffraction.

Furthermore, the strongly oxidizing chlorate anion was used, as it is also less toxic than the perchlorate anion.³¹ In addition to copper(II) chlorate (8), the less investigated zinc(II) chlorate (9) was also incorporated in an ECC. The respective metal chlorate was made accessible by a reaction of barium chlorate with the respective sulphate salts (Scheme 6).³¹ Both complexes were obtained in the form of single crystals in high yields (80–84%).

Compounds 10–13 were prepared analogous to copper(II) nitrate complex 6 by combining the solutions of the respective metal salt and stoichiometric amounts of the ligand, each dissolved in acetonitrile (Scheme 6). Whereas the use of manganese(II) and zinc(II) perchlorate only led to the isolation of a few single crystals, applying 1-NET (4) to copper(II) perchlorate gave ECC 11 in a satisfying yield (76%). Using 2-NET (5) solely resulted in copper(II) perchlorate complex 13 (yield: 89%). Single crystals suitable for X-ray diffraction were not obtained. Applying 2-NET (5) to copper(II)nitrate, dinitramide or



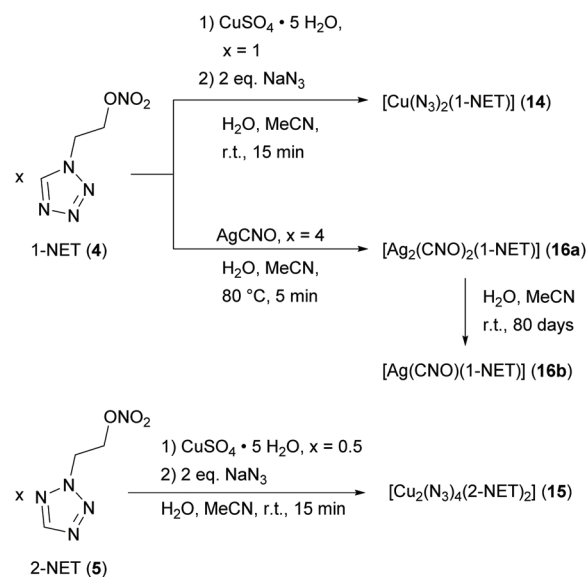
Scheme 5 Preparation of copper(II) complexes 6 and 7.



Scheme 6 Synthesis of coordination compounds 8–13.

different perchlorate salts like manganese(II) or zinc(II), was not successful. The use of iron(II) perchlorate as a building block also did not result in any isolable complexes in either case.

Besides the use of neutral nitrogen-rich ligands as a means of enhancing the performance in nitrate or perchlorate complexes, the concept of ECCs also allows a stabilization of highly sensitive metal salts like copper(II) azide or silver(I) fulminate (Scheme 7). Both synthetic strategies were recently pub-



Scheme 7 Stabilization of copper(II) azide and silver(I) fulminate using 1-NET and 2-NET.

lished by our group.^{32,33} To obtain the copper(II) azide complex **14**, the respective copper(II) sulphate complex is formed *in situ* and further reacted with an aqueous solution of sodium azide. Since the coordination positions remain occupied by the ligands, the formation of pure copper azide is avoided. The complex is formed immediately and precipitates directly and can be filtered off in a very good yield (82%). An elemental analysis pure preparation of compound **15** was not possible using this method, as most likely a side species is formed. Single crystal growth of **14** and **15** was achieved by performing layering experiments. Whereas handling of an extremely sensitive species could be avoided during the preparation of **14** and **15**, pure silver fulminate must be used for obtaining ECC **16a**. The silver salt was dissolved in a warm mixture of water and acetonitrile and an excess of ligand in acetonitrile was added. Single crystals suitable for X-ray diffraction were obtained after two days (yield: 43%). Leaving compound **16a** in its mother liquor for four weeks is resulting in single crystals of the thermodynamic product **16b**.

Another well-studied system is that of trinitrophenolate anions, each of which provides different properties to the respective complex depending on the number of hydroxy groups.²⁹ Compounds **17–22** were prepared in a straight forward manner by the reaction of basic copper carbonate with stoichiometric amounts of the respective acid in boiling water (Schemes 8 & 9). Subsequently, the ligand dissolved in small amounts of acetonitrile was added. Single crystal formation

started within one day, depending on the amount of water used, in sufficient to high yields (68–88%). In the case of compound **18a** no single crystals suitable for X-ray diffraction were obtained but its composition could be verified by elemental analysis. Instead, recrystallization from hot water afforded single crystals of **18b**. Unfortunately, an elemental analysis pure isolation of **18b** was not possible.

By variation of the number of anions added to one equivalent of basic copper carbonate different states of deprotonation of styphnate (HTNR⁻ and TNR²⁻, Scheme 8) or trinitrophenolroglucinate (H₂TNPG⁻ and HTNPG²⁻, Scheme 9) anions could be obtained. In the case of compound **22c**, the addition of 6 equivalents of 2-NET led to the formation of a co-crystal-line species, resulting in a total of three different species based on trinitrophenolroglucinate. Each of these ECCs was obtained pure according to elemental analysis.

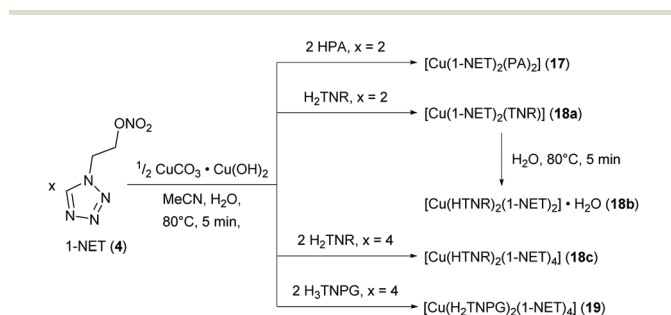
Except side species **18b**, all coordination compounds crystallized without the inclusion of water and were isolated directly from the mother liquor. The crystalline materials were filtered off, washed with small quantities of ice-cold ethanol, and then dried in air overnight.

Crystal structures of the ECCs

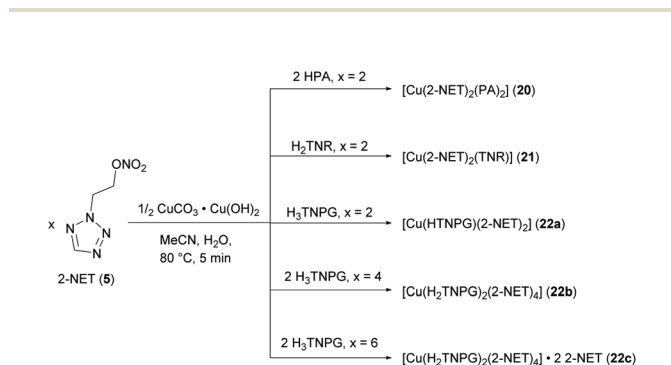
ECCs **6–12** and **14–22** were examined by low-temperature single crystal X-ray diffraction. In the case of compounds **9** and **22b** the measurements allow an indication of the most likely composition, but finalization of the data sets was not possible due to the highly disordered nitrate ethyl moieties. Together with compounds **13** and **18a** in which case no single crystals were obtained, the complexes' composition was finally confirmed by elemental analysis. Details of the structures of compounds **2**, **10**, **12**, **15**, **18b**, **18c**, **19**, **21**, **22a**, and **22c** (Fig. S1–7, ESI†) are given in the ESI† together with the measurement and refinement data of all experiments (Tables S1–S6, ESI†). The crystal datasets were uploaded in the CSD database and can be obtained free of charge.³⁴ All copper(II) complexes, except the nitrate (**6**), and dinitramido (**7**) ECCs, show octahedral coordination spheres around the copper(II) centers. Therefore, typical Jahn–Teller distortions along the respective O–Cu–O or N–Cu–N axes can be observed. Except for ECC **16b**, the ligands are solely coordinating *via* the N₄ nitrogen atom of the tetrazole rings.

The copper(II) nitrate complex **6** crystallizes in the monoclinic space group *P*₂₁/*c* with four formula units per unit cell. The compound possesses a calculated density of 1.888 g cm⁻³ at 99 K. The coordination sphere could either be interpreted as distorted fivefold trigonal bipyramidal (N9–Cu1–O10 147.87 (10)°, O10–Cu1–O13 80.22(8)°), or as distorted seven fold pentagonal bipyramidal (N9–Cu1–O11 96.37(9)°, O11–Cu1–O10 51.93(8)°) depending on whether the longer Cu–O bonds between the central metal and nitrate ligands are included (Cu1–O11 2.695(2) Å, Cu1–O14 2.583(2) Å). In every case, the equatorial positions are occupied by the anionic nitrate ligands, and one ligand moiety (Fig. 5).

The dinitramide complex **7** crystallizes in the monoclinic space group *P*₂₁/*n* with two formula units per unit cell. The



Scheme 8 Preparation of copper(II) picrate (PA), styphnate (HTNR/TNR) and 2,4,6-trinitrophenolroglucinate-based (HTNPG/H₂TNPG) complexes of 1-nitrateethyltetrazole (1-NET, **4**).



Scheme 9 Reaction of basic copper(II) carbonate with several trinitrophenol derivatives and subsequent applications of 2-NET (**5**).

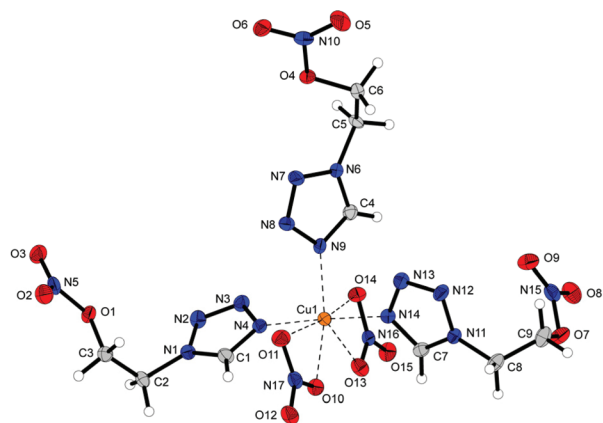


Fig. 5 Formula unit of $[\text{Cu}(\text{1-NET})_3(\text{NO}_3)_2]$ (**6**). Selected bond lengths (Å): Cu1–N9 2.028(3), Cu1–N4 1.973(3), Cu1–N14 1.987(3), Cu1–O10 2.117(2), Cu1–O13 2.268(2). Selected bond angles (°): N9–Cu1–N4 93.87(10), N9–Cu1–N14 89.14(10), N14–Cu1–N4 174.78(11), N4–Cu1–O11 86.03(9).

complex shows a high density of 1.953 g cm^{-3} at 102 K, with only the copper azide and silver fulminate complexes possessing higher densities. The coordination sphere is built up by two ligand moieties and two coordinating dinitramido anions (Fig. 6). This rather uncommon built up was already observed one time by our group employing 1-azidoethyl-5H-tetrazole as the ligand.³⁰ One way of explaining the complexes' coordination geometry is by using two square planar spheres by either the oxygen atoms of the anion or the nitrogen atoms of the anion and ligand. Another possible coordination geometry might be distorted hexagonal bipyramidal. Also, it should be pointed out that in each case the extremely long Cu–O bonds were included. (Cu1–O1 2.8715(17) Å, Cu1–O4 2.8287(17) Å). Therefore, no clear Jahn–Teller distortion can be observed, but a strongly distorted dinitramide anion is evident (O7–N8–N7–O5 25.19(17)°, O6–N8–N6–N7 150.45(16)°).

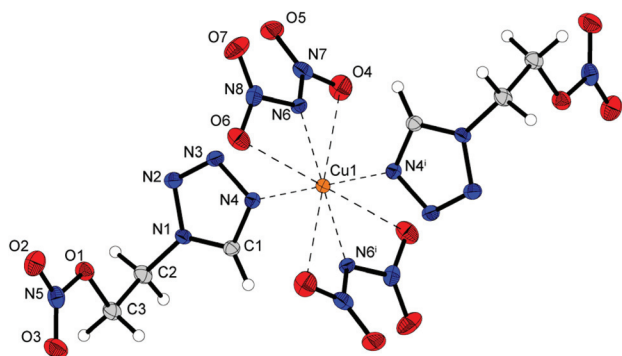


Fig. 6 Coordination environment of $[\text{Cu}(\text{DN})_2(\text{1-NET})_2]$ (**7**). Selected bond lengths (Å): Cu1–N6 1.9978(17), Cu1–N4 1.9735(17). Selected bond angles (°): N4–Cu1–N6 90.02(7), O4–Cu1–N4 90.33(6), O6–Cu1–N4 102.57(6), O6–Cu1–N6 49.13(6), O4–Cu1–N6 49.33(6), N6–N8–O6 111.96(17), N6–N7–O4 110.25(17). Symmetry code: (i) $1 - x, 1 - y, 1 - z$.

The copper(II) chlorate complex **8** crystallizes in the monoclinic space group Cc and the unit cell consists of four formula units. The compound's density of 1.689 g cm^{-3} (at 100 K) is slightly lower than the density observed for the corresponding perchlorate complex **11**. The octahedral coordination sphere is built up by six ligand moieties, whereas some nitrate-groups had to be split due to disorder and are therefore not refined to be anisotropic. The metal perchlorate complexes **10–12** crystallize isotypically in the triclinic space group $P\bar{1}$ with one formula unit per unit cell. The observed densities differ only slightly, with the copper coordination compound showing the highest value (**10** (Mn): 1.681 g cm^{-3} at 123 K; **11** (Cu): 1.727 g cm^{-3} at 114 K; **12** (Zn): 1.719 g cm^{-3}). Each compound shows an octahedral coordination sphere built up by six moieties of 1-NET (**4**), whereas only **11** shows a Jahn–Teller distortion due to its d^9 configuration (Fig. 7).

Copper(II) azide complex **14** crystallizes in the form of brown plates in the triclinic space group $P\bar{1}$. The asymmetric unit consists of two molecular units, whereas the molecular unit is built up by one tetrazole moiety per copper(II) azide. This coordination geometry has already been observed in previous studies.³² The unit cell contains four formula units and shows the highest density of all investigated copper complexes (1.985 g cm^{-3} at 173 K). Each copper centre is surrounded by a strongly distorted octahedral coordination sphere (N11–Cu1–N11ⁱ 77.11(13)) with the 1-NET ligands in the equatorial positions (Fig. 8, part A). The remaining coordination sites are occupied by azido ligands. In addition to that the azide anion shows a bridging behaviour, further linking the copper centres in various ways. Two of the anions show the same binding behaviour and bridge exclusively to the same neighbouring copper centres. This binding behaviour, shown in part C of Fig. 8, leads to the formation of dimers. The remaining equatorial coordinating azide ion, and both moieties in the axial position, exhibit a bridging behaviour as shown in part B of Fig. 8. This further linking of the metal centres leads to the formation of a two-dimensional polymeric network, as displayed in part D (Fig. 8).

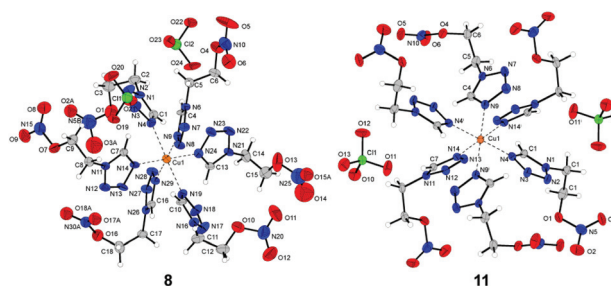


Fig. 7 Formula units of $[\text{Cu}(\text{1-NET})_6](\text{ClO}_3)_2$ (**8**) and $[\text{Cu}(\text{1-NET})_6](\text{ClO}_4)_2$ (**11**). Selected bond lengths (Å) of **8**: Cu1–N4 2.371(8), Cu1–N9 2.048(8), Cu1–N14 2.046(7). Selected bond lengths (Å) of **11**: Cu1–N4 2.022(3), Cu1–N14 2.035(3), Cu1–N9 2.338(3). Selected bond angles (°) of **8**: N4–Cu1–N9 86–1(3), N4–Cu1–N14 92.8(3), N9–Cu1–N14 88.7(3). Selected bond angles (°) of **11**: N9–Cu1–N4 89.48(11), N9–Cu1–N14 88.66(10), N14–Cu1–N4 91.60(11). Symmetry codes of **11**: (i) $1 - x, 1 - y, 1 - z$.

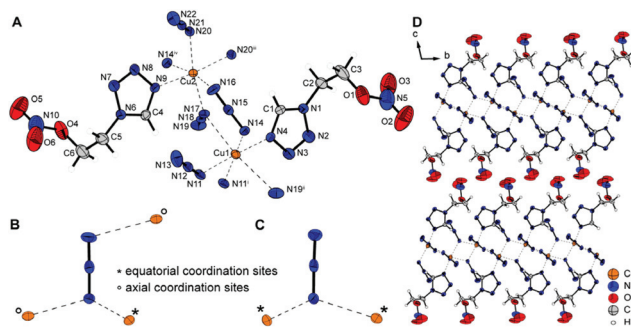


Fig. 8 A: Coordination environment of the copper(II) azide dimer **14**. Selected bond lengths (Å): Cu1–N17 2.497(3), Cu1–N19ⁱⁱ 2.683(3), Cu2–N14^{iv} 2.534(3), Cu2–N16 2.715(3). Selected bond angles (°): N14–Cu1–N19ⁱⁱ 84.62(10), N11ⁱ–Cu1–N4 95.86(11), N11–Cu1–N14 94.55(12), N9–Cu2–N20 95.15(11), N17–Cu2–N16 86.55(10), N16–Cu2–N20 86.85(19), N16–Cu2–N14^{iv} 170.95(10), N20–Cu2–N17 169.31(11). Symmetry codes: (i) $1 - x, 1 - y, 1 - z$; (ii) $-1 + x, y, z$; (iii) $2 - x, 2 - y, 1 - z$; (iv) $1 + x, y, z$. B & C: Coordination modes of the azide anions. D: Polymeric structure of compound **14**.

Silver complex **16a** crystallizes in the form of colourless plates in the monoclinic space group $I2/a$. The unit cell consists of eight formula units and shows the highest density of all investigated compounds with 2.718 g cm^{-3} at 104 K. The molecular unit consists of one 1-NET per two silver fulminate moieties. In addition to the formation of argentophilic Ag–Ag interactions, all centres within the cluster are further linked to each other by the fulminate anions. Two identical cations are bridged by two anions, one *via* the carbon of one fulminate ligand and the other *via* the oxygen atom of the other fulminate ligand, in an alternating order forming twofold coordinated silver chains. This 1D polymeric chain is further coordinated by 1-NET ligands which shifts the linear 2-fold coordination of the silver atoms to a distorted tetrahedral coordination. The resulting fourfold coordination environment around each silver cation has already been observed for silver(I) fulminate complexes based on monotetrazole ligands.³³

Fulminato complex **16b**, based on the same ligand as complex **16a**, on the other hand crystallizes in the monoclinic space group $P2_1/c$ with four formula units. The calculated density of 2.337 g cm^{-3} at 173 K is lower than the one determined for **16a**. The molecular formula in this case consists of only one silver fulminate moiety per 1-NET ligand. Also, the silver atoms are coordinated differently (Fig. 9, bottom). In compound **16b** each silver atom shows only a six-fold coordination sphere, whereas no Ag–O bonds were found. Instead, bridging tetrazole ligands were observed. Every moiety of 1-NET is binding *via* its N4 nitrogen atom together with its N3 position, which is a rather uncommon behaviour of tetrazoles in ECCs. This linking is further connecting the Ag–Ag chains formed by the fulminato ligands, leading to the formation of 2D polymeric sheets.

Overall, both silver fulminate complexes based on 1-NET (**4**) form two dimensional polymeric networks, while the sum formula and the structure of these networks are very different.

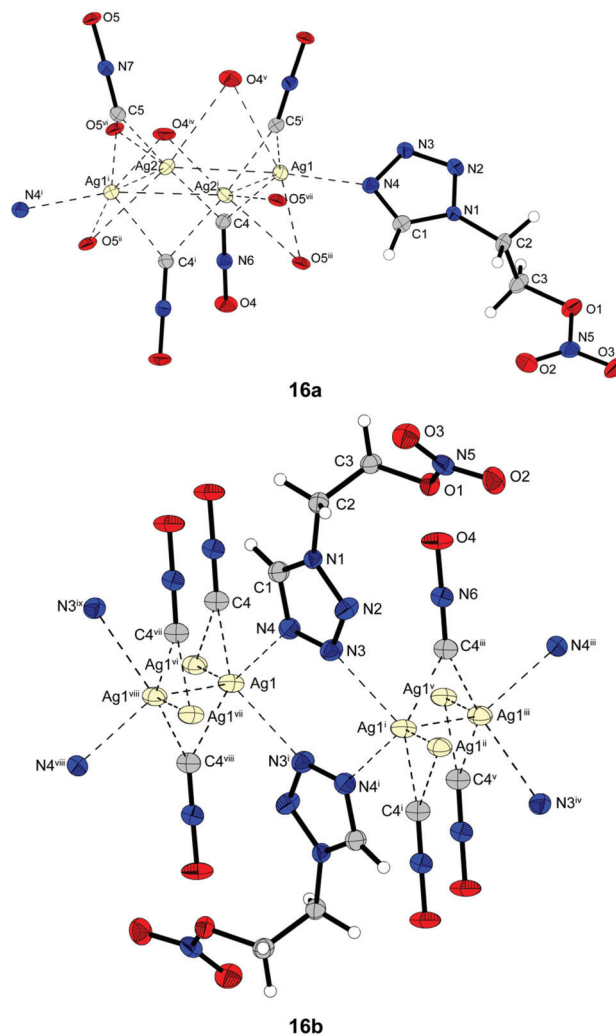


Fig. 9 Extended molecular units of $[\text{Ag}_2(\text{CNO})_2(1\text{-NET})]$ (**16a**) and $[\text{Ag}(\text{CNO})(1\text{-NET})]$ (**16b**). Selected bond lengths (Å) of **16a**: Ag1–N4 2.291(3), Ag2–O5 2.501(3), Ag1–C4 2.236(3), Ag2–C4 2.195(4), Ag1–O4 2.893(3), Ag2–O4 2.846(3), Ag1–C5 2.242(4), Ag2–C5 2.200(4), Ag1–O5 2.698(2), Ag2–O5 2.703(2). Selected bond lengths (Å) of **16b**: Ag1–Ag1^{vi} 3.0106(2), Ag1–C4 2.184(2), Ag1^{vi}–C4 2.247(2), Ag1–N4 2.4260(18), Ag1–N3 2.4692(19). Selected bond angles (°) of **16a**: Ag2–Ag1–N4 161.47(8), Ag1–Ag2–O5 126.02(6), Ag2–Ag1–Ag2 67.284(13), Ag1–Ag2–Ag1 112.694(13), Ag2–C4–Ag1 77.89(11), Ag1–O5–Ag2 64.53(5). Selected bond angles (°) of **16b**: Ag1^{vi}–Ag1–C4 48.10(6), Ag1–C4–Ag1^{vi} 85.59(7), N4–Ag1–N3ⁱ 103.46(6), N4–Ag1–C4^{viii} 106.50(7), N3–Ag1–C4^{viii} 82.16(7). Symmetry codes of **16a**: (i) $1.5 - x, y, 1 - z$; (ii) $x, -1 + y, z$; (iii) $1.5 - x, -1 + y, 1 - z$; (iv) $1.5 - x, 1 + y, 1 - z$; (v) $x, 1 + y, z$; (vi) $2 - x, 2 - y, 1 - z$; (vii) $-0.5, 2 - y, z$. Symmetry codes of **16b**: (i) $1 - x, 1 - y, 1 - z$; (ii) $x, 1.5 - y, -0.5 + z$; (iii) $x, 0.5 - y, -0.5 + z$; (iv) $1x, -0.5 + y, 0.5 - z$; (v) $1 - x, -y, 1z$; (vi) $1 - x, -0.5 + y, 1.5 - z$; (vii) $x, 1 + y, z$; (viii) $1 - x, 0.5 + y, 1.5 - z$; (ix) $x, 1.5 - y, 0.5 + z$.

Both complexes **17** and **20** based on the picrate anion crystallize with the same molecular formula in the form of green plates and blocks, respectively. However, since both complexes crystallize in different space groups (**17**: monoclinic $P2_1/c$; **20**: triclinic $P\bar{1}$), the unit cell of compound **17** consists of four formula units and the one of **20** is made of one unit. Despite

this fact, the densities of both complexes are very similar (**17**: 1.852 g cm⁻³ at 173 K, **20**: 1.890 g cm⁻³ at 132 K). The distorted octahedral coordination sphere is, for picrate-based complexes, structured in the expected manner.^{27,29} Two ligand moieties are arranged in the equatorial positions together with Cu–O bonds formed by the deprotonated hydroxy groups of the anion (Fig. 10). The axial positions are occupied by the

oxygen atoms of picrate's nitro group next to its hydroxy group.

Thermal stability and sensitivity data of the ECCs

Each coordination compound, which could be obtained elemental analysis pure, was investigated by differential thermal analysis (DTA) in the range from 25 to 400 °C at a heating rate of 5 °C min⁻¹. The resulting endothermic processes indicating a melting of the respective compound, a loss of ligand, or a phase transition, together with the exothermic processes, indicating a decomposition, are listed in Table 2. Plots of every DTA spectrum measured can be found in the ESI (Fig. S20–24†). When endothermic processes occurred during DTA measurements, thermogravimetry (TG) analysis was applied at a heating rate of 5 °C min⁻¹ in the range from 30 to 400 °C to ensure that only melting of the respective compound occurred. The TG plots of the chlorate and perchlorate complexes **8**, **9**, **11**, and **13** are illustrated in Fig. 11. Further spectra can be found in the ESI (Fig. S25 & 26†). In the case of **16a**, the second endothermic process indicates a loss of the ligand according to TG measurements. Since no mass loss has been detected for compound **11**, a phase transformation probably takes place here.

Except the nitrate (**6**, $T_{\text{exo}} = 196$ °C) and the trinitrophenolate based complexes **17** ($T_{\text{exo}} = 197$ °C) and **18a** ($T_{\text{exo}} = 195$ °C), none of the compounds' thermal stability exceeds the free ligands' stability. Furthermore, quite low melting points were observed especially for the chlorate and perchlorate complexes **8**, **9**, **11**, and **13**. This is most likely due to the low melting temperatures of the respective ligands (**4**, **5**: $T_{\text{endo}} \leq 25$ °C).

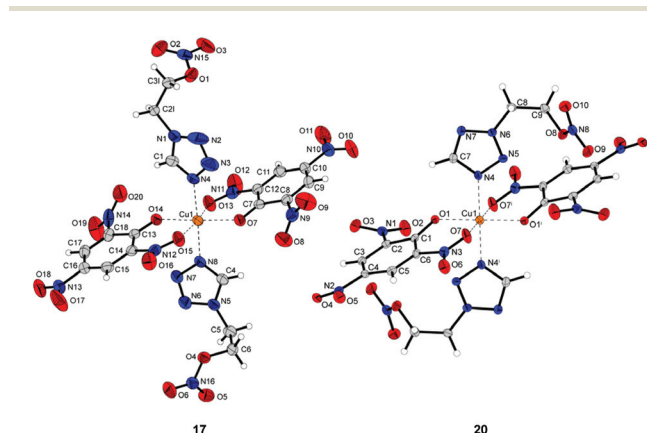


Fig. 10 Molecular units of ECCs **17** and **20**. Selected bond lengths (Å) of **17**: Cu1–N4 1.999(3), Cu1–N8 2.000(3), Cu1–O14 1.919(2), Cu1–O7 1.931(2), Cu1–O13 2.296(2), Cu1–O15 2.412(3). Selected bond lengths (Å) of **20**: Cu1–O1 1.9193(18), Cu1–N4 2.001(2), Cu1–O7 2.430(2). Selected bond angles (°) of **17**: O7–Cu1–O13 81.58(9), O13–Cu1–O14 94.72(9), O14–Cu1–O15 77.39(9), O13–Cu1–N4 88.02(11), N4–Cu1–O15 92.32, N4–Cu1–O14 85.29(10), O14–Cu1–N8 91.67(10). Selected bond angles (°) of **20**: O7–Cu1–O1 76.34(7), O7–Cu1–N4 89.49(8), N4–Cu1–O1 87.10(8). Symmetry code of **20**: (i) 1 – x, 2 – y, 1 – z.

Table 2 Thermal stability measurements^a and sensitivities toward various mechanical stimuli^b

Compound	T_{endo}^c (°C)	T_{exo}^d (°C)	IS ^e (J)	FS ^f (N)	ESD ^g (mJ)	BDIS ^h (mJ)
1-NET	4	25	168	10	>360	n.d.
2-NET	5	24	188	2	>360	n.d.
[Cu(1-NET) ₃ (NO ₃) ₂]	6	121	196	5	48	1080
[Cu(DN) ₂ (1-NET) ₂]	7	—	110	2	7	1080
[Cu(1-NET) ₆](ClO ₃) ₂	8	54	149	2	15	250
[Zn(1-NET) ₆](ClO ₃) ₂	9	71	154	7	14	750
[Cu(1-NET) ₆](ClO ₄) ₂	11	70, 117	165	3	25	480
[Cu(2-NET) ₆](ClO ₄) ₂	13	65	143	2	5	1080
[Cu(N ₃) ₂ (1-NET)]	14	—	122	3	1	14
[Ag ₂ (CNO) ₂ (1-NET)]	16a	96	123	≤1	20	250
[Ag(CNO)(1-NET)]	16b	67, 102 ⁱ	102 ⁱ	9	60	250
[Cu(1-NET) ₂ (PA) ₂]	17	—	197	20	>360	480
[Cu(1-NET) ₂ (TNR)]	18a	—	195	2	96	480
[Cu(HTNR) ₂ (1-NET) ₄]	18c	—	167	5	96	>1500
[Cu(H ₂ TNPG) ₂ (1-NET) ₄]	19	—	108	2	96	1080
[Cu(2-NET) ₂ (PA) ₂]	20	165 ⁱ	165 ⁱ	3	192	1080
[Cu(2-NET) ₂ (TNR)]	21	—	161	≤1	80	750
[Cu(HTNPG)(2-NET) ₂]	22a	—	112	4	324	750
[Cu(H ₂ TNPG) ₂ (2-NET) ₄]	22b	—	105	4	324	750
[Cu(H ₂ TNPG) ₂ (2-NET) ₄] · 2 2-NET	22c	92	105	4	60	750
Pb(TNR)·H ₂ O	—	—	260–310 (ref. 38)	8 (ref. 41)	0.45 (ref. 41)	0.04–1 (ref. 38)
Pb(N ₃) ₂ (RD-1333)	—	—	320–350 (ref. 38)	4 (ref. 41)	≤0.1 (ref. 41)	5–8 (ref. 38)

^a Onset temperatures at a heating rate of 5 °C min⁻¹. ^b Determined by 1 of 6 methods. ^c Endothermic peak, which indicates melting, phase transition, or loss of ligands. ^d Exothermic peak, which indicates decomposition. ^e Impact sensitivity (BAM drophammer test). ^f Friction sensitivity (BAM friction tester). ^g Electrostatic discharge sensitivity (OZM XSpark10). ^h Ball drop impact sensitivity (OZM BIT-132). ⁱ Endothermic signal followed by exothermic signal; n.d.: not determined.

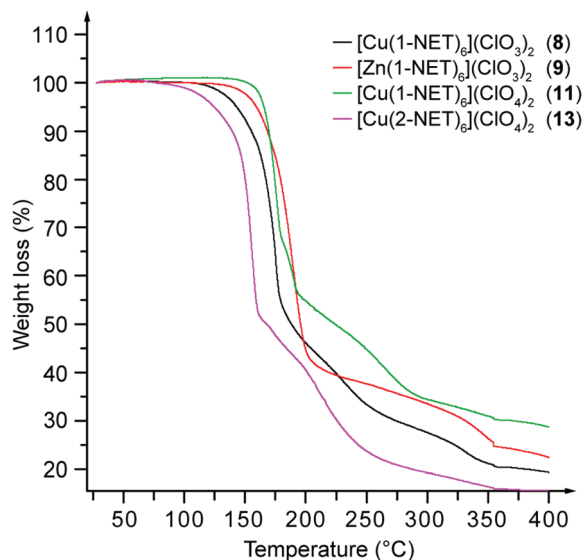


Fig. 11 Thermogravimetric measurements of the copper(II) and zinc(II) chlorate complexes **8** and **9** together with the copper(II) perchlorate complexes **11** and **13** in the range from 30 to 400 °C at a heating rate of 5 °C min⁻¹.

The complexes' low decomposition temperatures are on the one hand again caused by the ligand's properties. Organic nitrates in general are known to possess decomposition temperatures rarely exceeding 180 °C.³⁵ Therefore, it is expected that the compounds' exothermic processes are within this range. On the other hand, catalytic effects might play a crucial role in the decomposition of the ECCs, further limiting the compounds' thermal stability. Thus, similar effects like those observed in the catalytic decomposition of guanidinium nitrate using BCN, probably occur when the complexes are heated.^{18,36}

A detailed look at the compounds' exothermic processes reveals some trends already observed for ECCs in the past. For example, complex **11** ($T_{\text{exo}} = 165$ °C) based on the perchlorate anion is among the most thermally stable compounds, whereas the respective copper(II) chlorate **8** complex ($T_{\text{exo}} = 149$ °C) is less stable.⁹

Also, the decrease in the thermal stability of complexes **20** ($T_{\text{exo}} = 165$ °C) to **22c** ($T_{\text{exo}} = 105$ °C) with an increasing number of hydroxy groups is expected.²⁹ The expected trend of improved thermal stability caused by bridging anions (such as TNR²⁻ and HTNPG²⁻) was only observed for complexes **18a** ($T_{\text{exo}} = 195$ °C), **21** ($T_{\text{exo}} = 161$ °C), and **22a** ($T_{\text{exo}} = 112$ °C).^{9,29} Previous results suggest that the thermal stability of these complexes should be significantly higher than that of the picrate complexes. The drastically lower decomposition temperature of **13** ($T_{\text{exo}} = 143$ °C) was also surprising. Literature data showed rather similar decomposition temperatures for copper(II) perchlorate complexes based on the respective isomers. The reason for this again appears to be the catalytic effects of the central metal on the stability of the organic nitrate of the ligand. Hence, the latest exothermic processes were observed for compounds **6**, **17**, and **18a**. Compounds **16b** ($T_{\text{exo}} = 102$ °C), **22b** ($T_{\text{exo}} = 105$ °C),

and **22c** ($T_{\text{exo}} = 105$ °C) showed the lowest thermal stability of all complexes investigated.

In addition to the compound's thermal stability, great emphasis was placed on the determination of the compounds' sensitivity toward various external stimuli (*e.g.*, impact, friction, ball drop impact sensitivity, and electrostatic discharge). The classification of the compounds regarding the "UN Recommendations on the Transport of Dangerous Goods" should ensure a safe handling of every ECC investigated. Sensitivity measurements were carried out for complexes **6–9**, **11**, **13**, **14**, and **16–22** and ligands **4** and **5**. Further characterization of coordination compounds which could not be isolated elemental analysis pure was waived. Friction sensitivity (FS) measurements showed that, except picrate complex **17**, every ECC is more sensitive than the respective ligand by itself. Copper azide **14** is the most sensitive complex (FS = 1 N), followed by copper(II) perchlorate complex **13** (FS = 5 N), and copper(II) dinitramide complex **7** (FS = 7 N). This is surprising as compound **13** at the same time possesses one of the lowest melting points. In the case of compounds **8** (FS = 15 N), **9** (FS = 14 N), and **11** (FS = 25 N) the low melting point is clearly reducing the compounds' friction sensitivity. Also, it is worth mentioning that the effect of the co-crystallizing 2-NET moieties in compound **22c** on the compound's higher sensitivity toward friction is observed (FS = 60 N). Compared to **22b** (FS = 324 N), lacking the co-crystallizing 2-NET units, the sensitivity is drastically higher. This contradicts the common assumption that energetic materials are less sensitive by introducing co-crystallizing compounds.³⁷

Regarding impact sensitivity (IS) measurements, the effects caused by the low melting points are not as severe as those observed during friction sensitivity measurements. This is reflected by the general impact sensitivity of ≤ 4 J observed for most of the compounds (except **6**, **9**, and **17**). A reason for this might be the ignition of the sample through adiabatic compression or hot spot formation within the setup.²⁵ Also, it is worth mentioning that during impact sensitivity measurements some complexes are tested to be less sensitive than ligand **5** (IS = 2 J). The highest impact sensitivity was observed for styphnate **21** (IS ≤ 1 J), whereas compound **17** (IS = 20 J) showed the lowest sensitivity toward impact.

The low sensitivity of complex **17**, especially compared to ECC **20** based on the same anion, is likely caused by grain size effects. While **17** (FS > 360 N, IS = 20 J) was investigated at a roughly determined grain size <100 μm , the particle size distribution of **20** (FS = 192 N, IS = 3 J) was about 500–1000 μm , possibly making the sample more sensitive. Similar effects are assumed to be responsible for the difference in the sensitivity data for compounds **19** (IS = 2 J, FS = 96 N) and **22b** (IS = 4 J, FS = 324 N). The difference in the sensitivity between the two silver fulminate complexes is due to the content of fulminate in each complex. While in ECC **16a** two fulminate moieties are observed on one ligand, in **16b** only one moiety is found per ligand. Therefore, complex **16a** is clearly more sensitive than **16b**.

Regarding the "UN Recommendations on the Transport of Dangerous Goods", except ECCs **4**, **6**, **9**, and **17**, every com-

pound must at least be classified as sensitive because of impact sensitivity measurements.²¹ Complexes **5**, **7**, **8**, **11**, **13**, **14**, **16a**, and **19–21** even must be considered as very sensitive. The remaining compounds **4**, **9**, and **17** are classified as less sensitive. Taking into account the sensitivity toward friction, the zinc(II) chlorate complex **9** must be rated as very sensitive, with the compounds **7**, **13**, and **14** being extremely sensitive.

The synthesis of several complexes based on 1-NET has again extended the series of ECCs based on alkyl tetrazoles. This suggests a comparison of the complexes with each other, whereby the copper chlorate and perchlorate complexes probably appear to be the most suitable ones, since these, except for the chlorate complex based on 1-methyl-5*H*-tetrazole (MTZ), have the same structure. For this purpose, the data of different complexes known in the literature were compiled and are plotted with the data of ECCs **8** and **13** obtained from this work in the bar charts shown in Fig. 12.^{9,27,31}

The charts generally indicate that a longer carbon chain without an additional energetic group leads to compounds being less sensitive. This is represented through the ECCs based on 1-ethyl-5*H*-tetrazole (ETZ). By adding an energetic group, like an azide (AET) or nitrate (NET), the effect becomes less imminent, and the resulting coordination compounds are even more sensitive than those based on 1-methyl-5*H*-tetrazole, having a shorter carbon chain. Regarding friction sensitivity another general trend can be observed, stating that chlorate complexes are always more sensitive than the ones based on

perchlorate. When it comes to impact sensitivity, this tendency is less clear. It must be noted that the different structure of the methyl tetrazole chlorate complex might influence these findings. Comparing the complexes based on NET and AET shows that with the exception of $[\text{Cu}(\text{AET})_6](\text{ClO}_3)_2$ (IS = 2.5 J), the complexes based on 1-azidoethyl-5*H*-tetrazole are more sensitive.

Because of the already mentioned problems regarding BAM standard impact measurements, in this work, also ball drop impact sensitivity (BDIS) measurements were performed. The device is said to deliver results closer to realistic conditions due to a combination of spin and impact onto the sample.⁴¹ Earlier works of our group showed that there are coherences between the friction and ball drop impact. This work generally supports this thesis, with compounds **7**, **8**, **9**, **14**, **15**, and **21** being tested sensitive during both measurement types. However, the chlorate and perchlorate complexes are less sensitive toward BDIS which is likely due to the compounds' melting point, resulting in crystals absorbing a lot of impact energy. Major exceptions also are compounds **11**, **19b**, and **22c**, which were tested less sensitive than expected. A reason explaining this behaviour might again be the particle size distribution or crystal shape. A high-speed image of the moment of impact of compounds **13** and **14** is displayed in Fig. 13.

Hot plate and hot needle experiments

To get an insight into the compounds' behaviour when exposed to fast heating, hot plate tests were performed for every ECC obtained elemental analysis pure. To run the test, the sample was placed on a copper plate and heated with a Bunsen burner until decomposition. An evaluation of the compounds' reaction when ignited under light confinement was made by performing hot needle tests. For this test the sample was fixed onto a copper plate by using an adhesive tape. Subsequently the compound was penetrated with a red glowing hot needle. Usually, a detonation in at least one of the tests is desired, as this outcome indicates a fast deflagration to detonation transition (DDT), which is an important property of a primary explosive. The DDT is said to allow conclusions to be drawn on how well a primary explosive is capable of igniting pentaerythritol tetranitrate (PETN). Since the substances are intended to rather serve as combustion catalysts than as primary explosives, deflagration or decomposition reactions are desired. The outcome of each test is displayed in Table 3;

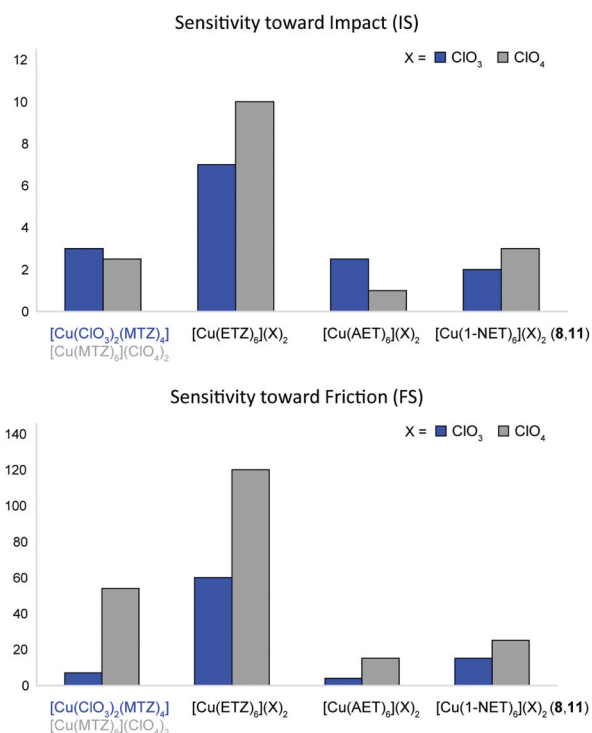


Fig. 12 Bar charts displaying the impact sensitivity (top) and friction sensitivity (bottom) of selected copper(II) chlorate and perchlorate complexes based on various alkyl tetrazoles known in the literature.^{9,27,31}

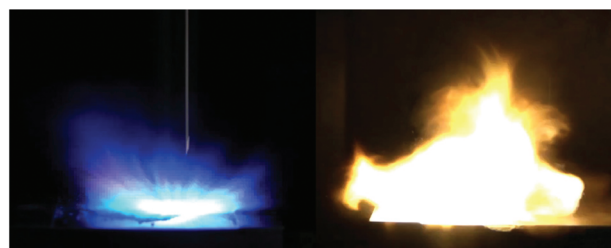


Fig. 13 Moment of detonation during ball drop impact sensitivity measurements of the copper(II) perchlorate (**13**) and copper(II) azide complexes (**14**).

Table 3 Results of hot plate and hot needle experiments^a

Compound	No.	HP	HN	PETN initiation	Laser energy, E^b (mJ)		
					1.7	25.5	51.0
[Cu(1-NET) ₃ (NO ₃) ₂]	6	defl.	defl.	—	dec.	defl.	—
[Cu(DN) ₂ (1-NET) ₂]	7	defl.	defl.	Negative	det.	det.	—
[Cu(1-NET) ₆](ClO ₃) ₂	8	defl.	defl.	—	—	dec.	—
[Zn(1-NET) ₆](ClO ₃) ₂	9	defl.	dec.	—	—	—	—
[Cu(1-NET) ₆](ClO ₄) ₂	11	defl.	defl.	—	—	dec.	—
[Cu(2-NET) ₆](ClO ₄) ₂	13	defl.	defl.	—	—	dec.	—
[Cu(N ₃) ₂ (1-NET)]	14	det.	det.	Positive	—	det.	—
[Ag ₂ (CNO) ₂ (1-NET)]	16a	det.	defl.	Negative	—	—	—
[Ag(CNO)(1-NET)]	16b	det.	dec.	—	—	—	—
[Cu(1-NET) ₂ (PA) ₂]	17	defl.	dec.	—	—	comb.	comb.
[Cu(1-NET) ₂ (TNR)]	18a	defl.	defl.	—	—	comb.	comb.
[Cu(H ₂ TNR) ₂ (1-NET) ₄]	18c	defl.	defl.	—	—	dec.	dec.
[Cu(H ₂ TNPG) ₂ (1-NET) ₄]	19	defl.	dec.	—	—	comb.	comb.
[Cu(2-NET) ₂ (PA) ₂]	20	defl.	defl.	—	—	dec.	dec.
[Cu(2-NET) ₂ (TNR)]	21	defl.	defl.	—	—	comb.	comb.
[Cu(HTNPG)(2-NET) ₂]	22a	defl.	defl.	—	—	comb.	comb.
[Cu(H ₂ TNPG) ₂ (2-NET) ₄]	22b	defl.	dec.	—	dec.	dec.	dec.
[Cu(H ₂ TNPG) ₂ (2-NET) ₄] · 2 2-NET	22c	defl.	defl.	—	det.	comb.	dec.

^a Not tested, comb.: combustion, dec.: decomposition, defl.: deflagration, det.: detonation. ^b Operating parameters: current $I = 7$ A; voltage $U = 4$ V; theoretical maximal output power $P_{\max} = 45$ W; theoretical energy $E_{\max} = 1.7$ –51.0 mJ; wavelength $\lambda = 915$ nm; pulse length $\tau = 1$ –30 ms.

further high-speed images of the tests and details on the setup can be found in the general information in the ESI.†

Deflagration reactions were observed for the majority of the investigated ECCs (Table 3). Only exceptions were copper(II) azide complex **14** (Fig. 14), and silver(I) fulminate **16a**, which detonated during at least one of the experiments, together with compounds **9**, **17**, **19**, and **22b**, only decomposing during at least one of these experiments. Excluding ECCs **14** and **16a** this behaviour indicates their possible use as combustion catalysts. Based on these results, laser ignition experiments, and in the case of **14**, **16a** and because of its strong deflagration, also complex **7**, PETN initiation experiments are of interest. Compound **16b** showed a significant weaker reaction than ECC **16a** due to the lower fulminate content in the complex.

PETN initiation experiments

The compounds which showed the most powerful behaviour during hot plate and hot needle tests have been found to be dinitramide coordination compound **7**, copper(II) azide

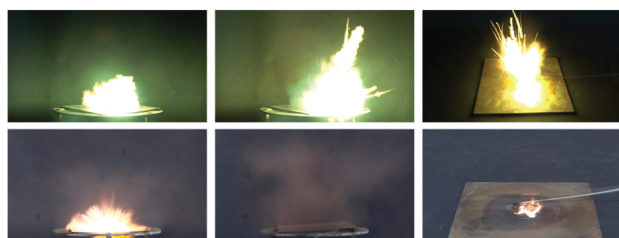


Fig. 14 High-speed images of the results of the hot plate (left and middle) and hot needle tests (the right picture) of the copper(II) dinitramide complex **7** (top) and the copper(II) azide coordination compound **14** (bottom).



Fig. 15 Left: Initiation test setup without a copper witness plate. Right: Result of the initiation experiment of compound **14** toward PETN.

complex **14**, and silver fulminate ECC **16a**. These complexes showed either sharp deflagrations or even detonations during hot plate and hot needle tests. For their potential use as lead-free primary explosives, the compounds were tested for their capability of initiating PETN. Therefore, 200 mg of the booster explosive was loaded into a copper shell and 50 mg of the test substance was filled on top (Fig. 15, left). More details of the test setup can be found in the general methods of the ESI.† A positive DDT from the primary explosive towards PETN is indicated by a hole in the copper witness plate and the fragmentation of the shell. As illustrated in Fig. 15 on the right, compound **14** successfully initiates PETN. In the case of compounds **7**, and **16a** only negative results were obtained.

Laser ignition experiments

Particularly in the field of primary explosives, the safe handling of materials is still severely limited since the mechanical action is in many cases necessary for ignition.¹ For example,

the pyrotechnic charges used in the percussion caps are ignited by the frictional force generated by impact with the anvil. Therefore, the used energetic materials need to possess high sensitivities toward external stimuli like impact and friction. The sensitivity data of the most common primary explosives lead azide and lead styphnate monohydrate are displayed in Table 2. The sensitivity not only affects the safe preparation of the energetic materials, but also makes processing and distribution more difficult.

However, new ways of ignition, which do not require mechanical stimuli, enable the use of less sensitive materials. One method that has received great attention in recent years is ignition through laser irradiation.^{27,42,43} In order to make use of this new technique, every elemental analysis pure ECC prepared in this work was tested for its ignitability by using a laser. Since only coloured compounds are known to react during these experiments, testing of the zinc and silver complexes **9**, and **16** was waived. The outcome of each test and the respective energy used for ignition are displayed in Table 3. Further information on the test setup and the procedure can be found in the general information in the ESI.†

Interestingly not every compounds investigated showed positive results during the laser experiments. A decomposition (Table 3) indicates that no output was observed in the laser setup during laser irradiation. An inspection of the primer cap only showed changes in the colour within the sample. A combustion (Fig. 16, bottom right) was observed for most of the complexes based on trinitrophenolate anions. This is likely caused by the compounds' higher carbon content, resulting in lower energetic compounds. Detonations were observed for compounds **7** and **14**, which was expected with respect to the corresponding hot plate and hot needle tests (Fig. 16, top right

& bottom left). However, the results of complexes **8**, **11**, and **13** were surprising in terms of outcome. In previous experiments, chlorate, and perchlorate complexes proved to exhibit the strongest performance.^{27,28,31} In this case only a slight decomposition within the primer cap was observed after the irradiation. This reinforces the theory that thermal ignition may be the reason for initiation and that the substances' low melting point may be a hindrance to this. Furthermore, pressing the substance into the caps also showed melting because of the force applied during compression. Therefore, these substances are likely to find applications as laser-ignitable energetic components, only as a component of a mixture and not as a neat substance.

Conclusions

A one pot synthesis of 1-hydroxyethyl-5*H*-tetrazole was established in good overall yields by taking advantage of acetyl protection. A mixture of the 1- and 2-hydroxyethyl isomers was prepared by alkylation and after nitration with 100% nitric acid the mixture was separated by chromatographic methods. Both compounds 1-NET (1-nitratoethyl-5*H*-tetrazole) and 2-NET (2-nitratoethyl-5*H*-tetrazole), further used as ligands, were investigated by single crystal XRD and various NMR techniques, including ¹H, ¹³C, ¹⁴N, and ¹H ¹⁵N HMBC. 2-NET was additionally investigated through ¹⁵N NMR to clarify the atom assignment in the HMBC spectrum. BAM sensitivity measurements showed equal values for the friction sensitivity; however much higher impact sensitivities for the 2-isomer were observed. Molecular interactions were investigated to shed light on the sensitivity data. On the basis of Hirshfeld analysis, structural elements were investigated concluding that the rigid structure of 2-NET is likely to cause the increased sensitivity. The tetrazole derivatives were subsequently used for the preparation of 22 different metal (Mn, Cu, Zn, and Ag) complexes. Only acetonitrile and water were used as green solvents, with both the ligands and the resulting ECCs exhibiting a desirable poor solubility in water. Each of these, with the exception of compound **13**, was investigated using low temperature single crystal X-ray diffraction. Thus, 18 of these complexes were obtained elemental analysis pure and subsequently characterized with respect to their sensitivity toward impact, friction, ball drop impact, and electrostatic discharge. In particular, nitrate complex **6** (196 °C) and trinitrophenolate based complexes **17** (197 °C) and **18a** (195 °C) showed very good thermal stabilities, which are outstanding especially for organic nitrates. The improved oxygen balance due to this functional group and the deflagration reactions of the compounds during hot plate and hot needle tests reveal that these compounds can be considered as burn rate catalysts like basic copper nitrate (BCN). However, due to their energetic properties, they simultaneously improve the performance of the mixture. The laser ignition experiments showed that non-classical routes of initiation are also possible for the majority of these additives. Furthermore, these experiments indicate that the dinitramide

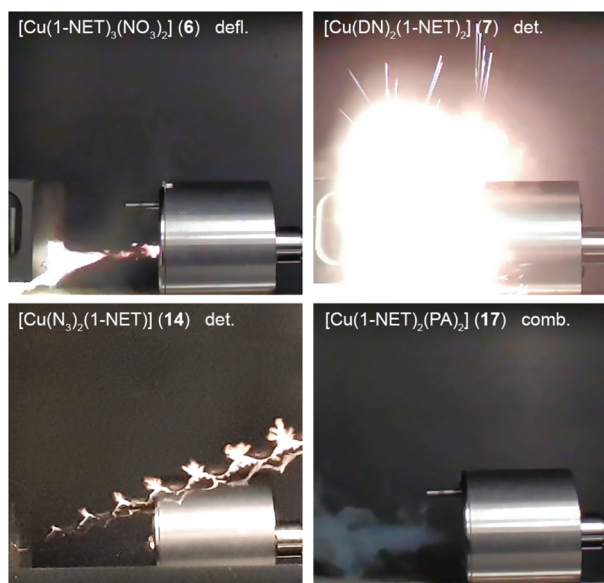


Fig. 16 Single pictures of a high-speed movie of the reaction of ECCs **6**, **7**, **14**, and **17** during laser ignition experiments at an energy of 25.5 mJ.

complex **7** and azide complex **14** in particular are promising candidates as substitutes for BNCP. Because of a positive PETN initiation test, the latter compound is also interesting as a substitute for lead azide or lead styphnate.

Author contributions

The manuscript was written through contributions of all authors. All authors have given approval to the final version of the manuscript.

Conflicts of interest

There are no conflicts to declare.

Acknowledgements

The financial support of this work by the Ludwig-Maximilian University (LMU), the Office of Naval Research (ONR), under grant no. ONR N00014-19-1-2078, and the Strategic Environmental Research and Development Program (SERDP) under contract no. W912HQ19C0033 is gratefully acknowledged. Furthermore, the authors would like to thank Professor Dr Konstantin Karaghiosoff for the measurement of the ^1H - ^{15}N NMR spectra, and Dr Burkhard Krumm for the measurement of the ^{15}N NMR spectrum.

Notes and references

- 1 T. M. Klapötke, *High Energy Materials*, De Gruyter, Berlin, Boston, 5th edn, 2019.
- 2 (a) D. Kumar, G. H. Imler, D. A. Parrish and J. M. Shreeve, *J. Mater. Chem. A*, 2017, **5**, 10437–10441; (b) Y. Tang, K. Li, A. K. Chinnam, R. J. Staples and J. M. Shreeve, *Dalton Trans.*, 2021, **50**, 2143–2148; (c) L. M. Barton, J. T. Edwards, E. C. Johnson, E. J. Bukowski, R. C. Sausa, E. F. C. Byrd, J. A. Orlicki, J. J. Sabatini and P. S. Baran, *J. Am. Chem. Soc.*, 2019, **141**, 12531–12535; (d) J. Ma, H. Yang, J. Tang, G. Zhang, Z. Yi, S. Zhu and G. Cheng, *Dalton Trans.*, 2020, **49**, 4675–4679; (e) N. Lease, L. M. Kay, G. W. Brown, D. E. Chavez, D. Robbins, E. F. C. Byrd, G. H. Imler, D. A. Parrish and V. W. Manner, *J. Org. Chem.*, 2020, **85**, 4619–4626.
- 3 M. A. S. Laidlaw, G. Filippelli, H. Mielke, B. Gulson and A. S. Ball, *Environ. Health*, 2017, **16**, 34.
- 4 (a) Candidate List of substances of very high concern for Authorisation, <https://echa.europa.eu/de>, (accessed May 2021); (b) D. C. Dorman, S. H. Benoff, E. C. Bishop, M. L. Blecker, L. M. Brosseau, R. H. Goldman, J. H. Graziano, S. A. Milz, S. K. Park and M. A. Roberts, *National Research Council Report: Potential Health Risks to DOD Firing-Range Personnel from Recurrent Lead Expo-sure*, National Academies Press, Washington, DC, USA, 2012.
- 5 T. Brinck, *Green Energetic Materials*, John Wiley & Sons Ltd., New York, 1st edn, 2014.
- 6 (a) M. L. Gettings, M. T. Thoenen, E. F. C. Byrd, J. J. Sabatini, M. Zeller and D. G. Piercey, *Chem. – Eur. J.*, 2020, **26**, 14530–14535; (b) N. Fischer, D. Fischer, T. M. Klapötke, D. G. Piercey and J. Stierstorfer, *J. Mater. Chem.*, 2012, **22**, 20418–20422; (c) S. Manzoor, Q. Tariq, X. Yin and J. Zhang, *Def. Technol.*, 2021, DOI: 10.1016/j.dt.2021.02.002; (d) R. Meyer, J. Köhler and A. Homburg, *Explosives*, Wiley-VCH, Weinheim, 7th edn, 2016.
- 7 J. Roh, K. Vávrová and A. Hrabálek, *Eur. J. Org. Chem.*, 2012, 6101–6118.
- 8 P. N. Gaponik and V. P. Karavai, *Chem. Heterocycl. Compd.*, 1985, **21**, 1172–1174.
- 9 (a) P. N. Gaponik, V. P. Karavai and Yu. V. Grigor'ev, *Chem. Heterocycl. Compd.*, 1985, **21**, 1255–1258; (b) M. H. H. Wurzenberger, M. S. Gruhne, M. Lommel, N. Szimhardt, T. M. Klapötke and J. Stierstorfer, *Chem. – Asian J.*, 2019, **14**, 2018–2028.
- 10 T. M. Klapötke, B. Krumm, T. Reith and C. C. Unger, *J. Org. Chem.*, 2018, **83**, 10505–10509.
- 11 (a) M. S. Ghasemzadeh and B. Akhlaghinia, *ChemistrySelect*, 2020, **5**, 6440–6452; (b) A. F. Stassen, M. Grunert, E. Dova, H. Schenk, G. Wiesinger, M. Müller, P. Weinberger, W. Linert, J. G. Haasnoot and J. Reedijk, *Eur. J. Inorg. Chem.*, 2003, **2003**, 2273–2282.
- 12 (a) K. A. McDonald, S. Seth and A. J. Matzger, *Cryst. Growth Des.*, 2015, **15**, 5963–5972; (b) Q. Zhang and J. M. Shreeve, *Angew. Chem., Int. Ed.*, 2014, **53**, 2540–2542; (c) H. Gao, Q. Zhang and J. M. Shreeve, *J. Mater. Chem. A*, 2020, **8**, 4193–4216.
- 13 R. N. Roberts and R. H. Dinegar, *J. Phys. Chem.*, 1958, **62**, 1009–1011.
- 14 N. Fischer, T. M. Klapötke, J. Stierstorfer and C. Wiedemann, *Polyhedron*, 2011, **30**, 2374–2386.
- 15 J. Stierstorfer, K. R. Tarantik and T. M. Klapötke, *Chem. – Eur. J.*, 2009, **15**, 5775–5792.
- 16 L. Zeisel, N. Szimhardt, M. H. H. Wurzenberger, T. M. Klapötke and J. Stierstorfer, *New J. Chem.*, 2019, **43**, 609–616.
- 17 T. M. Klapötke, J. Stierstorfer and B. Weber, *Inorg. Chim. Acta*, 2009, **362**, 2311–2320.
- 18 K. Shiota, H. Matsunaga and A. Miyake, *J. Therm. Anal. Calorim.*, 2015, **121**, 281–286.
- 19 (a) D. E. Bays, *Eu. Pat.*, EP0117368A1, 1982; (b) T. M. Klapötke and S. M. Sproll, *Eur. J. Org. Chem.*, 2010, 1169–1175.
- 20 W. G. Finnegan and R. A. Henry, *J. Org. Chem.*, 1959, **24**, 1565–1567.
- 21 UN Model Regulation: Recommendations on the Transport of Dangerous Goods – Manual of Tests and Criteria, section 13.4.2.3.3, 2015.
- 22 (a) BAM, <http://www.bam.de>, (accessed April May); (b) NATO standardization agreement (STANAG) on explosives, impact sensitivity tests, no. 4489, 1st edn., Sept. 17th, 1999; (c) WI-WEB-Standardarbeitsanweisung 4–5.1.02,

- Ermittlung der Explosionsgefährlichkeit, hier der Schlagempfindlichkeit mit dem Fallhammer, Nov. 8th, 2002; (d) NATO standardization agreement (STANAG) on explosive, friction sensitivity tests, no. 4487, 1st edn., Aug. 22nd, 2002; (e) WIWEB-Standardarbeitsanweisung 4-5.1.03, Ermittlung der Explosionsgefährlichkeit oder der Reibeempfindlichkeit mit dem Reibeapparat, Nov. 8th, 2002.
- 23 (a) M. J. Turner, J. J. McKinnon, S. K. Wolff, D. J. Grimwood, P. R. Spackman, D. Jayatilaka and M. A. Spackman, *CrystalExplorer17*, University of Western Australia, 2017; (b) M. A. Spackman and D. Jayatilaka, *CrystEngComm*, 2009, **11**, 19–32.
- 24 (a) C. Zhang, X. Xue, Y. Cao, Y. Zhou, H. Li, J. Zhou and T. Gao, *CrystEngComm*, 2013, **15**, 6837–6844; (b) Y. Ma, A. Zhang, X. Xue, D. Jiang, Y. Zhu and C. Zhang, *Cryst. Growth Des.*, 2014, **14**, 6101–6114.
- 25 J. G. Reynolds, P. C. Hsu, G. A. Hust, S. A. Strout and H. K. Springer, *Propellants, Explos., Pyrotech.*, 2017, **42**, 1303–1308.
- 26 M. Sućeska, *EXPLO5 Version 6.05 User's Guide*, OZM, Zagreb, Croatia, 2018.
- 27 N. Szimhardt, M. H. H. Wurzenberger, A. Beringer, L. J. Daumann and J. Stierstorfer, *J. Mater. Chem. A*, 2017, **5**, 23753–23765.
- 28 N. Szimhardt, M. H. H. Wurzenberger, L. Zeisel, M. S. Gruhne, M. Lommel and J. Stierstorfer, *J. Mater. Chem. A*, 2018, **6**, 16257–16272.
- 29 M. H. H. Wurzenberger, B. R. G. Bissinger, M. Lommel, M. S. Gruhne, N. Szimhardt and J. Stierstorfer, *New J. Chem.*, 2019, **43**, 18193–18202.
- 30 M. S. Gruhne, M. H. H. Wurzenberger, M. Lommel and J. Stierstorfer, *Chem. Eur. J.*, 2021, **27**, 9112–9123.
- 31 M. H. H. Wurzenberger, N. Szimhardt and J. Stierstorfer, *J. Am. Chem. Soc.*, 2018, **140**, 3206–3209.
- 32 M. H. H. Wurzenberger, M. Lommel, M. S. Gruhne, N. Szimhardt and J. Stierstorfer, *Angew. Chem.*, 2020, **59**, 12367–12370.
- 33 M. H. H. Wurzenberger, M. S. Gruhne, M. Lommel, V. Braun, N. Szimhardt and J. Stierstorfer, *Inorg. Chem.*, 2020, **59**, 17875–17879.
- 34 Crystallographic data for the structures have been deposited with the Cambridge Crystallographic Data Centre.
- 35 T. Lenz, T. M. Klapötke, M. Mühlemann and J. Stierstorfer, *Propellants, Explos., Pyrotech.*, 2021, **46**, 723–731.
- 36 T. Ohtake, S. Date, K. Ikeda and Y. Shiraishi, *Sci. Technol. Energ. Mater.*, 2015, **76**, 39–41.
- 37 (a) L. M. Foroughi, R. A. Wiscons, D. R. Du Bois and A. J. Matzger, *Chem. Commun.*, 2020, **56**, 2111–2114; (b) M. K. Bellas and A. J. Matzger, *Angew. Chem., Int. Ed.*, 2019, **58**, 17185–17188.
- 38 T. M. Klapötke, *Energetic Materials Encyclopedia*, De Gruyter, Berlin, Boston, 2nd edn, 2021.
- 39 OZM Research, <http://www.ozm.cz/en>, (accessed May 2021).
- 40 Military Standard 1751A (MIL-STD-1751A): safety and performance tests for qualification of explosives (high explosives, propellants and pyrotechnics), method 1016, Dec. 11st, 2001.
- 41 M. S. Gruhne, M. Lommel, M. H. H. Wurzenberger, N. Szimhardt, T. M. Klapötke and J. Stierstorfer, *Propellants, Explos., Pyrotech.*, 2020, **45**, 147–153.
- 42 T. W. Myers, J. A. Bjorgaard, K. E. Brown, D. E. Chavez, S. K. Hanson, R. J. Scharff, S. Tretiak and J. M. Veauthier, *J. Am. Chem. Soc.*, 2016, **138**, 4685–4692.
- 43 M. A. Ilyushin, A. A. Kotomin and S. A. Dushenok, *Russ. J. Phys. Chem. B*, 2019, **13**, 119–138.

Supplementary Information

Nitratoethyl-5*H*-tetrazoles: Improving Oxygen Balance through Application of Organic Nitrates in Energetic Coordination Compounds

Michael S. Gruhne, Tobias Lenz, Markus Rösch, Marcus Lommel,
Maximilian H. H. Wurzenberger, Thomas M. Klapötke, and Jörg Stierstorfer*

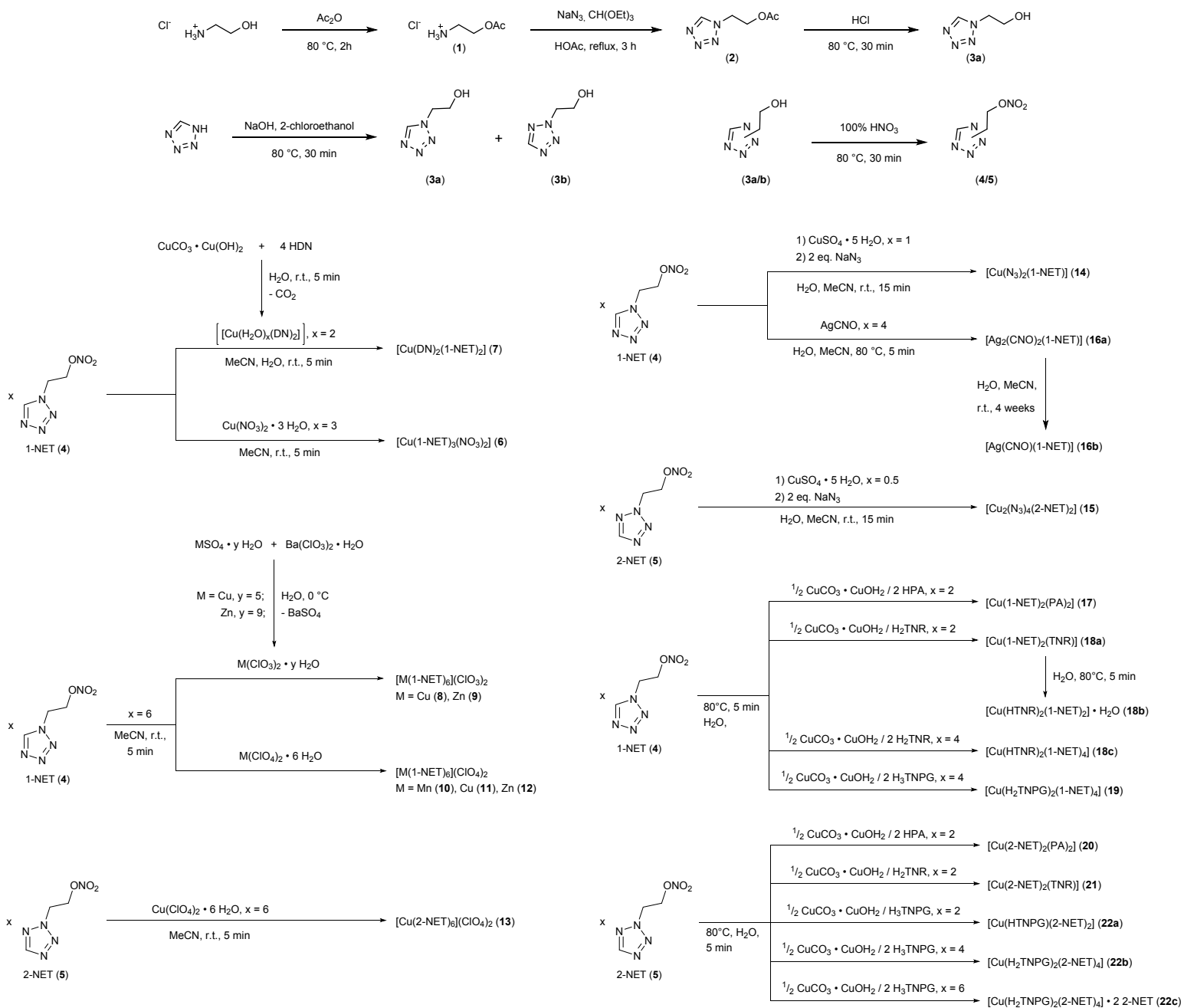
^a Department of Chemistry, Ludwig-Maximilian University of Munich,
Butenandtstr. 5-13, D-81377 Munich, Germany.

Dr. Jörg Stierstorfer, jstch@cup.uni-muenchen.de, FAX +49 89 2180 77007

Table of Contents

1. Compounds Overview
2. Single Crystal X-Ray Diffraction
3. Computations & Hirshfeld Surfaces
5. NMR Spectroscopy of **1, 2, 3, 4** and **5**
4. IR Spectroscopy of **1, 2, 4–9, 11, 13, 14, 16–18b**, and **19–22**
5. DTA Plots of **4–9, 11, 13, 14, 16–18b**, and **19–22**
6. TGA Plots of **4–6, 8, 9, 11, 13, 16, 20**, and **22**
7. Hot Plate & Hot Needle Tests of **6–9, 11, 13, 14, 16–18b**, and **19–22**
8. Experimental Part and General Methods
9. References

1. Compounds Overview



2. Single Crystal X-Ray Diffraction

For all crystalline compounds, an Oxford Xcalibur3 diffractometer with a CCD area detector or Bruker D8 Venture TXS diffractometer equipped with a multilayer monochromator, a Photon 2 detector and a rotating-anode generator were employed for data collection using Mo- K_{α} radiation ($\lambda = 0.7107 \text{ \AA}$). On the Oxford device, data collection and reduction were carried out using the CrysAlisPRO software.^{S1} On the Bruker diffractometer, the data were collected with the Bruker Instrument Service v3.0.21, the data reduction was performed using the SAINT V8.18C software (Bruker AXS Inc., 2011). The structures were solved by direct methods (SIR-92,^{S2} SIR-97,^{S3,S4} SHELXS-97^{S5,S6} or SHELXT^{S7}) and refined by full-matrix least-squares on F^2 (SHELXL^{S5,S6}) and finally checked using the PLATON software^{S8} integrated in the WinGX^{S7} or Olex2^{S8} software suite. The non-hydrogen atoms were refined anisotropically and the hydrogen atoms were located and freely refined. The absorptions were corrected by a SCALE3 ABSPACK or SADABS Bruker APEX3 multi-scan method.^{S11,S12} All DIAMOND2 plots are shown with thermal ellipsoids at the 50% probability level and hydrogen atoms are shown as small spheres of arbitrary radius.

Table S1. Crystallographic data of **2**, **4**, and **5**.

	2	4	5
Formula	C ₅ H ₈ N ₄ O ₂	C ₃ H ₅ N ₅ O ₃	C ₃ H ₅ N ₅ O ₃
FW (g mol ⁻¹)	156.15	159.12	159.12
Crystal system	monoclinic	monoclinic	orthorhombic
Space Group	<i>P2</i> ₁ / <i>c</i>	<i>P2</i> ₁ / <i>c</i>	<i>Pna2</i> ₁
Color / Habit	colorless block	colorless block	colorless needle
Size (mm)	0.31 x 0.50 x 0.50	0.32 x 0.50 x 0.50	0.24 x 0.33 x 0.50
<i>a</i> (Å)	7.6852(9)	20.8315(6)	7.3292(8)
<i>b</i> (Å)	14.3722(13)	6.5682(2)	14.3427(15)
<i>c</i> (Å)	6.6944(6)	9.8140(3)	6.3485(5)
α (°)	90	90	90
β (°)	104.152(10)	103.473(3)	90
γ (°)	90	90	90
<i>V</i> (Å ³)	716.98(13)	1305.85(7)	667.36(11)
<i>Z</i>	4	8	4
ρ _{calc.} (g cm ⁻³)	1.447	1.619	1.584
μ (mm ⁻¹)	0.115	0.143	0.140
<i>F</i> (000)	328	656	328
λ _{MoKα} (Å)	0.71073	0.71073	0.71073
<i>T</i> (K)	106	105	128
θ Min–Max (°)	2.7, 26.4	3.3, 26.4	2.8, 26.4
Dataset	–5:9; –10:17; –8:6	–26:26; –8:8; –12:12	–9:9; –17:17; –7:7
Reflections collected	3119	28160	9133
Independent refl.	1466	2669	1355
<i>R</i> _{int}	0.022	0.030	0.048
Observed reflections	1165	2378	1160
Parameters	132	199	120
<i>R</i> ₁ (obs) ^a	0.0352	0.0339	0.0361
w <i>R</i> ₂ (all data) ^b	0.0830	0.0793	0.0806
Goof ^c	1.07	1.12	1.06
Resd. Dens. (e Å ⁻³)	–0.22, 0.17	–0.17, 0.19	–0.17, 0.19
Absorption correction	multi-scan	multi-scan	multi-scan
Device type	Oxford Xcalibur3	Oxford Xcalibur3	Oxford Xcalibur3
CCDC	2080666	2080674	2080685

^a $R_1 = \sum ||F_o| - |F_c|| / \sum |F_o|$; ^b $wR_2 = [\sum [w(F_o^2 - F_c^2)^2] / \sum [w(F_o^2)]]^{1/2}$; $w = [\sigma^2(F_o^2) + (xP)^2 + yP]^{-1}$ and $P = (F_o^2 + 2F_c^2) / 3$; ^c $Goof = \{\sum [w(F_o^2 - F_c^2)^2] / (n-p)\}^{1/2}$ (n = number of reflections; p = total number of parameters).

Table S2. Crystallographic data of **6–8**.

	6	7	8
Formula	C ₉ H ₁₅ CuN ₁₇ O ₁₅	C ₆ H ₁₀ CuN ₁₆ O ₁₄	C ₁₈ H ₃₀ Cl ₂ CuN ₃₀ O ₂₄
FW (g mol ⁻¹)	664.92	593.84	1185.16
Crystal system	monoclinic	monoclinic	monoclinic
Space Group	<i>P2</i> ₁ / <i>c</i>	<i>P2</i> ₁ / <i>c</i>	<i>Cc</i>
Color / Habit	blue plate	blue plate	blue platelet
Size (mm)	0.08 x 0.38 x 0.50	0.04 x 0.37 x 0.59	0.05 x 0.08 x 0.09
<i>a</i> (Å)	20.6706(13)	13.1234(9)	10.721(3)
<i>b</i> (Å)	7.2984(4)	6.3864(5)	18.897(5)
<i>c</i> (Å)	16.4791(9)	12.8363(8)	23.186(6)
α (°)	90	90	90
β (°)	109.752(7)	110.160(6)	97.284(10)
γ (°)	90	90	90
<i>V</i> (Å ³)	2339.8(3)	1009.92(13)	4660(2)
<i>Z</i>	4	2	4
$\rho_{\text{calc.}}$ (g cm ⁻³)	1.888	1.953	1.689
μ (mm ⁻¹)	1.045	1.193	0.698
<i>F</i> (000)	1348	598	2412
$\lambda_{\text{MoK}\alpha}$ (Å)	0.71073	0.71073	0.71073
<i>T</i> (K)	99	102	100
θ Min–Max (°)	2.5, 26.4	3.2, 26.4	2.2, 26.4
Dataset	–25: 25; –9: 9; –20: 19	–16: 16; –7: 7; –15: 16	–13: 13; –23: 23; –28: 28
Reflections collected	14785	6571	33018
Independent refl.	4786	2048	8963
<i>R</i> _{int}	0.056	0.030	0.058
Observed reflections	3516	1748	7792
Parameters	379	169	659
<i>R</i> ₁ (obs) ^a	0.0442	0.0290	0.0646
<i>wR</i> ₂ (all data) ^b	0.0916	0.0743	0.1824
Goof ^c	1.02	1.08	1.04
Resd. Dens. (e Å ⁻³)	–0.59, 0.57	–0.26, 0.39	–1.04, 0.85
Absorption correction	multi-scan	multi-scan	multi-scan
Device type	Oxford Xcalibur3	Oxford Xcalibur3	Bruker D8 Venture TXS
CCDC	2080679	2080675	2080677

^a $R_1 = \sum ||F_o| - |F_c|| / \sum |F_o|$; ^b $wR_2 = [\sum [w(F_o^2 - F_c^2)^2] / \sum [w(F_o^2)]]^{1/2}$; $w = [\sigma^2(F_o^2) + (xP)^2 + yP]^{-1}$ and $P = (F_o^2 + 2F_c^2) / 3$; ^c $\text{Goof} = \{\sum [w(F_o^2 - F_c^2)^2] / (n-p)\}^{1/2}$ (n = number of reflections; p = total number of parameters).

Table S3. Crystallographic data of **10**, **11**, **12**, and **14**.

	10	11	12	14
Formula	C ₁₈ H ₃₀ Cl ₂ MnN ₃₀ O ₂₆	C ₁₈ H ₃₀ Cl ₂ CuN ₃₀ O ₂₆	C ₁₈ H ₃₀ Cl ₂ N ₃₀ O ₂₆ Zn	C ₆ H ₁₀ Cu ₂ N ₂₂ O ₆
FW (g mol ⁻¹)	1208.56	1217.16	1218.99	613.44
Crystal system	triclinic	triclinic	triclinic	triclinic
Space Group	<i>P</i> -1	<i>P</i> -1	<i>P</i> -1	<i>P</i> -1
Color / Habit	colorless block	blue block	colorless block	brown platelet
Size (mm)	0.11 x 0.18 x 0.47	0.20 x 0.48 x 0.50	0.21 x 0.39 x 0.50	0.01 x 0.03 x 0.03
<i>a</i> (Å)	10.9319(8)	10.8193(9)	10.8769(8)	6.2622(4)
<i>b</i> (Å)	10.9517(6)	10.9055(10)	10.8942(9)	10.5985(8)
<i>c</i> (Å)	12.4811(7)	12.2584(10)	12.4267(12)	15.9381(14)
α (°)	88.318(4)	88.625(7)	68.548(8)	102.119(3)
β (°)	68.294(6)	68.707(8)	88.553(7)	96.226(3)
γ (°)	61.051(7)	61.944(9)	61.016(8)	91.774(3)
<i>V</i> (Å ³)	1194.09(17)	1170.2(2)	1177.8(2)	1026.56(14)
<i>Z</i>	1	1	1	2
$\rho_{\text{calc.}}$ (g cm ⁻³)	1.681	1.727	1.719	1.985
μ (mm ⁻¹)	0.505	0.700	0.754	2.155
<i>F</i> (000)	615	619	620	612
$\lambda_{\text{MoK}\alpha}$ (Å)	0.71073	0.71073	0.71073	0.71073
<i>T</i> (K)	123	114	102	173
θ Min–Max (°)	2.5, 26.4	2.3, 26.4	2.2, 26.4	2.0, 26.4
Dataset	-13: 13; -13: 13; -15: 15	-13:13; -11:13; -15:15	-13:13; -13:12; -15:14	-7: 7; -13: 13; -19: 19
Reflections collected	18055	7824	9471	11434
Independent refl.	4868	4720	4809	4172
<i>R</i> _{int}	0.054	0.037	0.039	0.040
Observed reflections	3535	3314	3302	3184
Parameters	349	349	349	325
<i>R</i> ₁ (obs) ^a	0.0452	0.0538	0.0513	0.0397
<i>wR</i> ₂ (all data) ^b	0.1146	0.1041	0.1045	0.0789
Goof ^c	1.04	1.03	1.04	1.05
Resd. Dens. (e Å ⁻³)	-0.31, 0.58	-0.46, 0.63	-0.45, 0.56	-0.38, 0.39
Absorption correction	multi-scan	multi-scan	multi-scan	multi-scan
Device type	Oxford Xcalibur3	Oxford Xcalibur3	Oxford Xcalibur3	Bruker D8 Venture TXS
CCDC	2080672	2080669	2080683	2080678

^a $R_1 = \sum ||F_0| - |F_c|| / \sum |F_0|$; ^b $wR_2 = [\sum [w(F_0^2 - F_c^2)^2] / \sum [w(F_0^2)^2]]^{1/2}$; $w = [\sigma^2(F_0^2) + (xP)^2 + \gamma P]^{-1}$ and $P = (F_0^2 + 2F_c^2) / 3$; ^c $\text{Goof} = \{ \sum [w(F_0^2 - F_c^2)^2] / (n-p) \}^{1/2}$ (n = number of reflections; p = total number of parameters).

Table S4. Crystallographic data of **15**, **16a**, **16b**, and **17**.

	15	16a	16b	17
Formula	C ₃ H ₅ Cu ₂ N ₁₇ O ₃	C ₅ H ₅ Ag ₂ N ₇ O ₅	C ₄ H ₅ AgN ₆ O ₄	C ₁₈ H ₁₄ CuN ₁₆ O ₂₀
FW (g mol ⁻¹)	454.32	458.90	309.01	837.99
Crystal system	monoclinic	monoclinic	monoclinic	monoclinic
Space Group	<i>P2₁/n</i>	<i>I2/a</i>	<i>P2₁/c</i>	<i>P2₁/c</i>
Color / Habit	brown platelet	colorless platelet	colorless platelet	green platelet
Size (mm)	0.01 x 0.25 x 0.25	0.09 x 0.25 x 0.50	0.02 x 0.07 x 0.10	0.02 x 0.05 x 0.05
<i>a</i> (Å)	15.7453(11)	12.5931(10)	15.0209(6)	8.0432(4)
<i>b</i> (Å)	5.7379(4)	5.6798(3)	5.4770(2)	17.7448(8)
<i>c</i> (Å)	16.3858(14)	31.354(3)	10.6783(5)	21.2063(11)
α (°)	90	90	90	90
β (°)	109.892(9)	90.669(7)	91.237(2)	96.689(2)
γ (°)	90	90	90	90
<i>V</i> (Å ³)	1392.1(2)	2242.5(3)	878.29(6)	3006.1(3)
<i>Z</i>	4	8	4	4
$\rho_{\text{calc.}}$ (g cm ⁻³)	2.168	2.718	2.337	1.852
μ (mm ⁻¹)	3.111	3.525	2.303	0.846
<i>F</i> (000)	896	1744	600	1692
$\lambda_{\text{MoK}\alpha}$ (Å)	0.71073	0.71073	0.71073	0.71073
<i>T</i> (K)	123	104	173	173
θ Min–Max (°)	2.2, 26.4	2.6, 26.4	4.0, 26.4	2.3, 26.4
Dataset	–19: 19; –5: 7; –20: 20	–15: 15; –7: 6; –38: 39	–18: 18; –6: 6; –13: 12	–10: 10; –22: 22; –26: 26
Reflections collected	9140	8676	12974	55744
Independent refl.	2839	2296	1764	6146
<i>R</i> _{int}	0.067	0.030	0.033	0.054
Observed reflections	1971	1864	1672	5073
Parameters	226	172	136	525
<i>R</i> ₁ (obs) ^a	0.0514	0.0251	0.0181	0.0390
<i>wR</i> ₂ (all data) ^b	0.1124	0.0616	0.0423	0.0979
Goof ^c	1.02	1.04	1.06	1.07
Resd. Dens. (e Å ⁻³)	–0.63, 0.75	–0.51, 0.92	–0.65, 0.93	–0.41, 0.56
Absorption correction	multi-scan	multi-scan	multi-scan	multi-scan
Device type	Oxford Xcalibur3	Oxford Xcalibur3	Bruker D8 Venture TXS	Bruker D8 Venture TXS
CCDC	2080684	2080673	2080682	2080680

^a $R_1 = \sum ||F_0| - |F_c|| / \sum |F_0|$; ^b $wR_2 = [\sum [w(F_0^2 - F_c^2)^2] / \sum [w(F_0^2)^2]]^{1/2}$; $w = [\sigma^2(F_0^2) + (xP)^2 + yP]^{-1}$ and $P = (F_0^2 + 2F_c^2) / 3$; ^c $\text{Goof} = \{ \sum [w(F_0^2 - F_c^2)^2] / (n-p) \}^{1/2}$ (n = number of reflections; p = total number of parameters).

Table S5. Crystallographic data of **18b**, **18c**, **19**, and **20**.

	18b	18c	19	20
Formula	C ₁₈ H ₁₆ CuN ₁₆ O ₂₃	C ₂₄ H ₂₄ CuN ₂₆ O ₂₈	C ₂₄ H ₂₄ CuN ₂₆ O ₃₀	C ₁₈ H ₁₄ CuN ₁₆ O ₂₀
FW (g mol ⁻¹)	888.01	1188.23	1220.23	837.99
Crystal system	monoclinic	triclinic	triclinic	triclinic
Space Group	<i>P</i> 2 ₁ / <i>c</i>	<i>P</i> -1	<i>P</i> -1	<i>P</i> -1
Color / Habit	green block	green block	green plate	green block
Size (mm)	0.05 x 0.09 x 0.13	0.08 x 0.19 x 0.47	0.05 x 0.25 x 0.50	0.12 x 0.29 x 0.48
<i>a</i> (Å)	14.2845(14)	8.9977(6)	9.0040(7)	6.5499(4)
<i>b</i> (Å)	22.033(2)	10.9877(7)	10.8642(9)	8.7690(6)
<i>c</i> (Å)	10.1252(9)	12.9353(9)	12.9713(12)	14.0403(11)
α (°)	90	88.113(5)	87.922(7)	71.967(6)
β (°)	99.740(4)	69.868(7)	69.740(8)	89.224(5)
γ (°)	90	66.507(7)	67.742(8)	74.396(5)
<i>V</i> (Å ³)	3140.8(5)	1093.07(15)	1095.07(19)	736.40(10)
<i>Z</i>	4	1	1	1
$\rho_{\text{calc.}}$ (g cm ⁻³)	1.878	1.805	1.850	1.890
μ (mm ⁻¹)	0.822	0.630	0.635	0.864
<i>F</i> (000)	1796	603	619	423
$\lambda_{\text{MoK}\alpha}$ (Å)	0.71073	0.71073	0.71073	0.71073
<i>T</i> (K)	173	101	100	132
θ Min–Max (°)	2.2, 27.5	2.0, 26.4	2.0, 26.4	2.5, 26.4
Dataset	-18: 18; -28: 28; -12: 13	-10: 11; -13: 13; -16: 16	-11: 10; -13: 12; -16: 13	-7: 8; -10: 10; -17: 17
Reflections collected	55212	7022	7691	5569
Independent refl.	7225	4407	4462	3006
<i>R</i> _{int}	0.047	0.025	0.054	0.028
Observed reflections	6349	3673	2743	2432
Parameters	548	435	427	250
<i>R</i> ₁ (obs) ^a	0.0597	0.0429	0.0636	0.0432
<i>wR</i> ₂ (all data) ^b	0.1752	0.1062	0.1326	0.0949
Goof ^c	1.04	1.03	1.03	1.03
Resd. Dens. (e Å ⁻³)	-0.83, 2.36	-0.46, 0.42	-0.57, 0.65	-0.56, 0.48
Absorption correction	multi-scan	multi-scan	multi-scan	multi-scan
Device type	Bruker D8 Venture TXS	Oxford Xcalibur3	Oxford Xcalibur3	Oxford Xcalibur3
CCDC		2080676	2080681	2080671

^a $R_1 = \sum ||F_0| - |F_c|| / \sum |F_0|$; ^b $wR_2 = [\sum [w(F_0^2 - F_c^2)^2] / \sum [w(F_0^2)^2]]^{1/2}$; $w = [oc^2(F_0^2) + (xP)^2 + yP]^{-1}$ and $P = (F_0^2 + 2F_c^2) / 3$; ^c Goof = $\{\sum [w(F_0^2 - F_c^2)^2] / (n-p)\}^{1/2}$ (n = number of reflections; p = total number of parameters).

Table S6. Crystallographic data of **21**, **22a**, and **22c**.

	21	22a	22c
Formula	C ₁₂ H ₁₁ CuN ₁₃ O ₁₄	C ₁₂ H ₁₁ CuN ₁₃ O ₁₅	C ₃₀ H ₃₄ CuN ₃₆ O ₃₆
FW (g mol ⁻¹)	624.88	640.88	1538.48
Crystal system	triclinic	triclinic	triclinic
Space Group	<i>P</i> -1	<i>P</i> -1	<i>P</i> -1
Color / Habit	green plate	dark green block	green platelet
Size (mm)	0.11 x 0.25 x 0.54	0.14 x 0.20 x 0.34	0.06 x 0.30 x 0.38
<i>a</i> (Å)	10.1859(8)	10.3415(6)	8.4568(6)
<i>b</i> (Å)	10.4855(8)	10.4028(6)	11.2204(8)
<i>c</i> (Å)	10.8414(7)	10.8539(6)	16.7588(10)
α (°)	72.332(6)	71.766(5)	101.080(5)
β (°)	77.521(6)	78.429(5)	103.168(5)
γ (°)	81.225(6)	80.742(5)	107.579(6)
<i>V</i> (Å ³)	1072.51(14)	1080.44(11)	1416.56(19)
<i>Z</i>	2	2	1
$\rho_{\text{calc.}}$ (g cm ⁻³)	1.935	1.970	1.804
μ (mm ⁻¹)	1.125	1.123	0.524
<i>F</i> (000)	630	646	783
$\lambda_{\text{MoK}\alpha}$ (Å)	0.71073	0.71073	0.71073
<i>T</i> (K)	102	102	123
θ Min–Max (°)	2.0, 26.4	2.0, 26.4	2.0, 26.4
Dataset	-12:12; -13:13; -13:13	-12: 12; -12: 13; -12: 13	-10:10; -14:14; -20:20
Reflections collected	7539	8987	21342
Independent refl.	4401	4412	5794
<i>R</i> _{int}	0.032	0.028	0.087
Observed reflections	3331	3696	3757
Parameters	364	374	468
<i>R</i> ₁ (obs) ^a	0.0486	0.0348	0.0534
<i>wR</i> ₂ (all data) ^b	0.1363	0.0880	0.1184
Goof ^c	1.06	1.03	1.02
Resd. Dens. (e Å ⁻³)	-0.59, 0.58	-0.37, 0.46	-0.48, 0.72
Absorption correction	multi-scan	multi-scan	multi-scan
Device type	Oxford Xcalibur3	Oxford Xcalibur3	Oxford Xcalibur3
CCDC	2080667	2080670	2080668

^a $R_1 = \sum ||F_0| - |F_c| | / \sum |F_0|$; ^b $wR_2 = [\sum [w(F_0^2 - F_c^2)^2] / \sum [w(F_0^2)]]^{1/2}$; $w = [\sigma^2(F_0^2) + (xP)^2 + yP]^{-1}$ and $P = (F_0^2 + 2F_c^2) / 3$; ^c $\text{Goof} = \{\sum [w(F_0^2 - F_c^2)^2] / (n-p)\}^{1/2}$ (*n* = number of reflections; *p* = total number of parameters).

The tetrazole derivative **2** crystallizes in the form of colorless blocks in the monoclinic space group $P2_1/c$, with four formula units per unit cell. The calculated density of 1.447 g cm^{-3} at 106 K is lower than the densities observed for the tetrazoles **4** and **5**. The methylene groups are, as already observed for the compounds **4** and **5**, arranged in a slightly distorted gauche conformation ($\text{N1-C2-C3-O1} = 69.01(12)^\circ$, Figure S1). The bond lengths and angles in the tetrazole moiety are similar to the ones observed in 1-NET (**4**) and 2-NET (**5**).

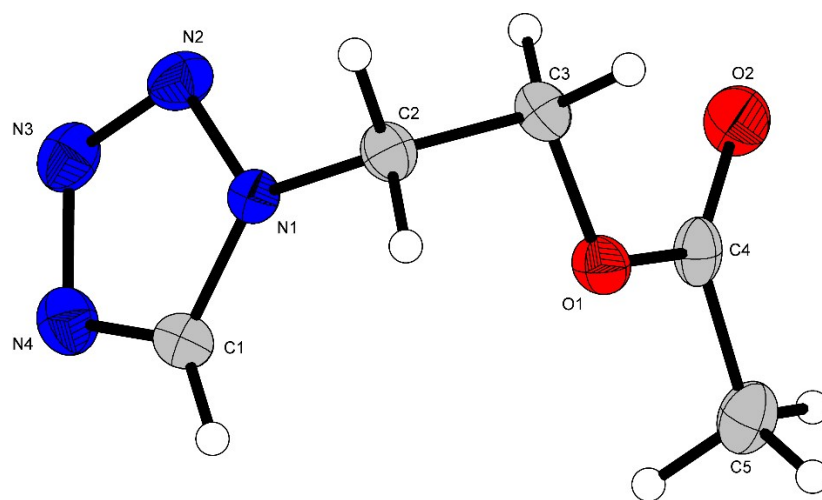


Figure S1. Molecular unit the tetrazole derivative **2**. Selected bond lengths (\AA): N1-C2 1.4620(17), C2-C3 1.5018(19), C3-O1 1.4490(17), O1-C4 1.3448(16), O2-C4 1.2043(17), C4-C5 1.488(2). Selected bond angles ($^\circ$): N1-C2-C3 111.11(11), C2-C3-O1 106.74(11), C3-O1-C4 116.47(10), O1-C4-O2 122.84(13), O1-C4-C5 110.96(13).

The manganese(II) and zinc(II) coordination compounds **10** and **12**, along with the copper(II) perchlorate complex **11**, crystallize isotypically in the triclinic space group $P\bar{1}$ with one formula unit per unit cell. As already stated for the copper complex, the compounds' densities differ only slightly, with compound **11** showing the highest value (**10**: 1.681 g cm^{-3} at 123 K; **11**: 1.727 g cm^{-3} at 114 K; **12**: 1.719 g cm^{-3}). Each perchlorate complex shows an octahedral coordination sphere (Figure S2) built up by six moieties of 1-NET (**4**).

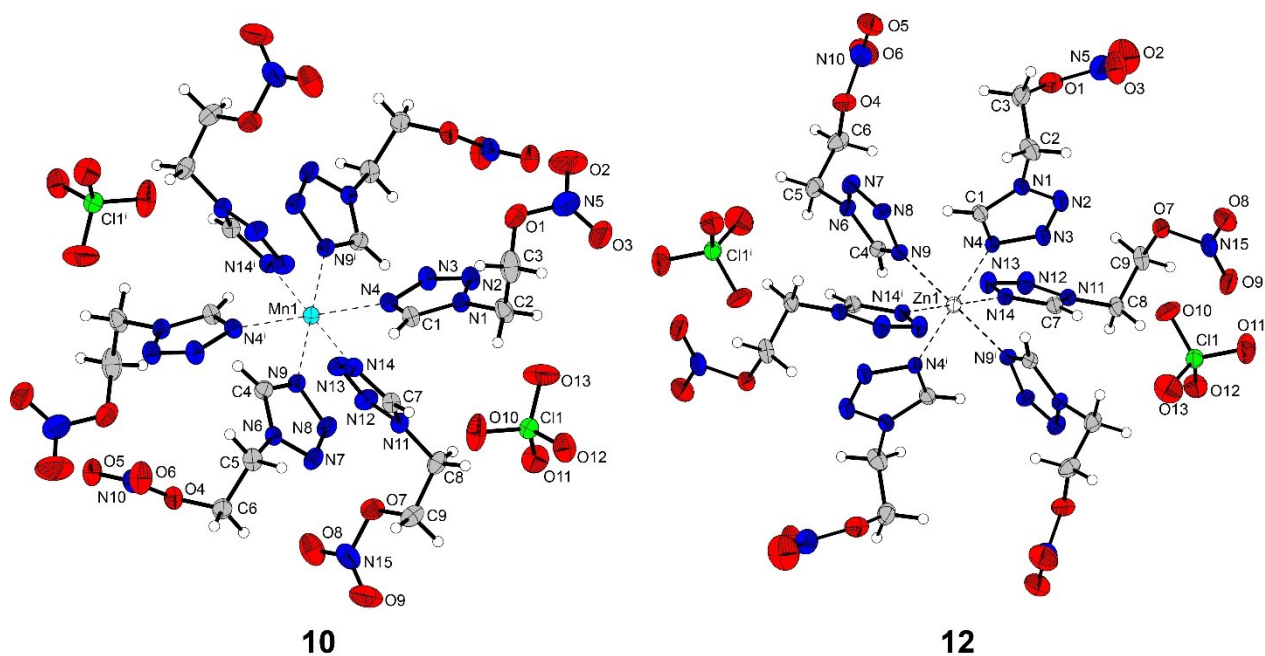


Figure S2. Molecular units of $[\text{Mn}(\text{1-NET})_6](\text{ClO}_4)_2$ (**10**, left) and $[\text{Zn}(\text{1-NET})_6](\text{ClO}_4)_2$ (**12**, right). Selected bond lengths (\AA) of **10**: Mn1–N4 2.23171 (14), Mn–N9 (2.2482(3), Mn1–N14 2.24903(14). Selected bond lengths (\AA) of **12**: Zn1–N4 2.143(3), Zn1–N9 2.154(3), Zn1–N14 2.170(2). Selected bond angles ($^\circ$) of **10**: N9–Mn1–N14 91.803(7), N4–Mn1–N14 86.912(5), N4–Mn1–N9 89.510(7). Selected bond angles ($^\circ$) of **12**: N4–Zn1–N9 92.10(13), N4–Zn1–N14 90.32(11), N9–Zn1–N14 91.67(11). Symmetry code of **10**: (i) $1-x, 1-y, 1-z$. Symmetry code of **12**: (i) $1-x, 2-y, -z$.

In contrast to compound **14**, the copper(II) azide complex **15** crystallizes in the triclinic space group $P\bar{1}$. The asymmetric unit in this case is made up of only one instead of two molecular units and contains two copper azide moieties per tetrazole unit (Figure S3, A). The unit cell is built up by four formula units, resulting in a higher density of 2.168 g cm^{-3} at 123 K. Every copper atom is coordinated octahedrally. While Cu2 is solely coordinated through azide moieties, the other central metal (Cu1) is also complexed by a 2-NET ligand. Every anion is linking between two metal centers, whereas three different types of linking were observed (Figure S3, B). The first mode, represented by the N9–N10–N11 anion, is solely linking Cu1 and Cu2. The N12–N13–N14 and the N15–N16–N17 azide moieties are forming the bonds all originating from the same nitrogen atom. Two of these bonds are within the same asymmetric unit. The third bond is within another asymmetric unit and therefore leading to the formation of 1D polymeric chains. The third coordination mode (N8–N7–N6) is also linking between three copper centers. The first two bonds are again between the same asymmetric unit, the third bond is leading to the formation of 2D polymeric layers (Figure S3, C).

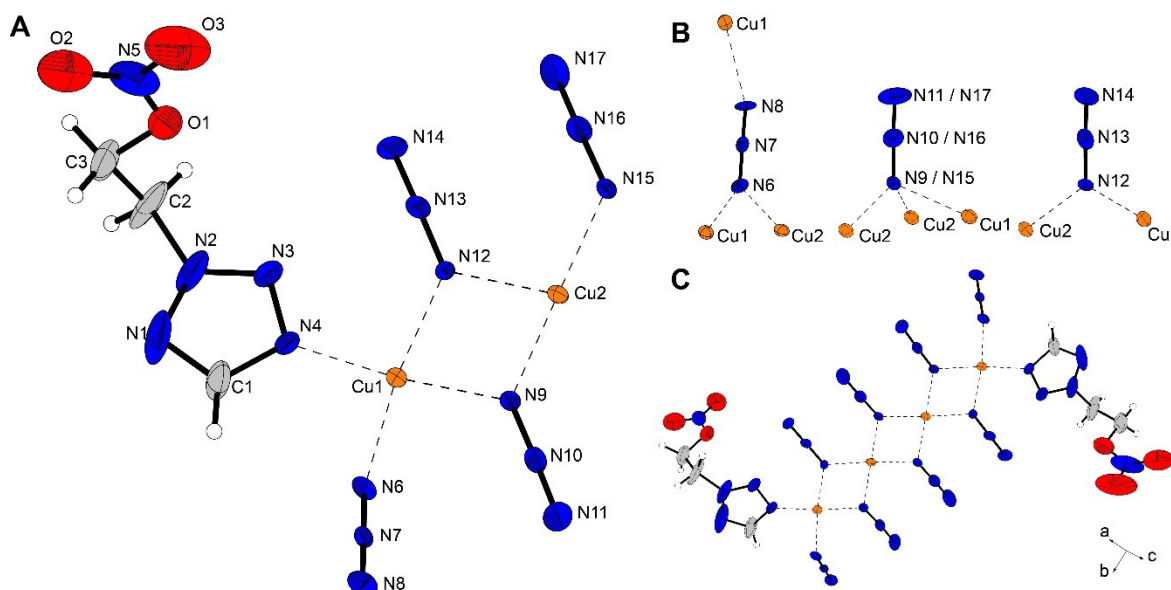


Figure S3. **A:** Molecular unit of complex **15**. Selected bond lengths (Å): Cu1–N4 1.97343(13), Cu1–N6 1.98651(10), Cu1–N9 2.02128(11), Cu1–N12 1.99045(13), Cu2–N9 1.99224(12), Cu2–N12 1.99898(11), Cu2–N15 2.00955(14). Selected bond angles (°): N9–Cu1–N12 77.168(5), N4–Cu1–N6 90.720(5), N9–Cu2–N12 77.643(5). **B:** Coordination modes of the azide anions in **15**. **C:** Section of the polymeric network formed by ECC **15**.

The copper(II) complex **18b**, based on the HTNR⁻ anion crystallizes in the monoclinic space group $P2_1/c$ with four formula units per unit cell. The calculated density of 1.878 g cm⁻³ at 173 K is only slightly higher than the one of **18c** based on the same anion (1.805 g cm⁻³ at 101 K). Like ECC **18c**, an octahedral coordination sphere is formed. However, the coordination sphere found in complex **18b** is built up by two ligand moieties, whereas in coordination compound **18c** four ligand units can be found (Figure S4). Furthermore, the anions and the ligands are arranged in *cis*-conformation and the formed octahedron is strongly distorted ($O14-Cu1-O22 = 162.73(9)^\circ$). The complex is also the only observed coordination compound incorporating an aqua moiety together with NET ligands.

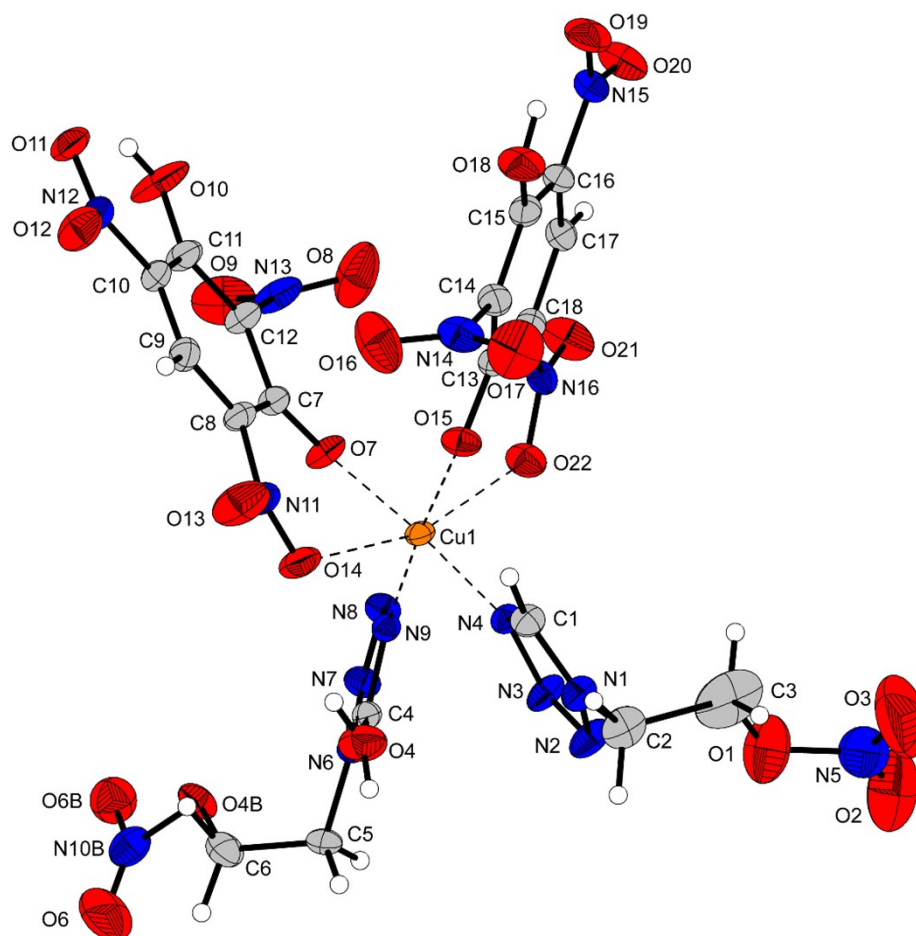


Figure S4. Molecular formula of $[Cu(HTNR)_2(1-NET)_2] \cdot H_2O$ (**18b**). Selected bond lengths (Å): Cu1–N4 2.001(3), Cu1–N9 1.991(3), Cu1–O7 1.950(3), Cu1–O15 1.951(2), Cu1–O14 2.349(3), Cu1–O22 2.306(3). Selected bond angles ($^\circ$): O15–Cu1–N4 86.38(11), O15–Cu1–O7 91.54(10), O15–Cu1–O22 80.83(9).

The copper(II) complexes **18c** and **19**, based on the HTNR or H₂TNPG anions, respectively, crystallize isotypically in the triclinic space group *P*-1 with one formula unit per unit cell. Therefore, the compounds' densities differ only slightly (**18c**: 1.805 g cm⁻³ at 101 K, **19**: 1.850 g cm⁻³ at 100 K). Both ECCs show the same octahedral coordination environment with four tetrazole moieties in the equatorial positions and the two anions in the axial position (Figure 11). In case of ECC **18c** parts of the tetrazole and phenyl moieties were split due to disordering. Therefore, parts of the structure were not refined anisotropically. Furthermore, one of the nitrate groups in compound **19** was split. In both structures **18c** and **19**, one of the ethylene groups had to be split because of a disorder.

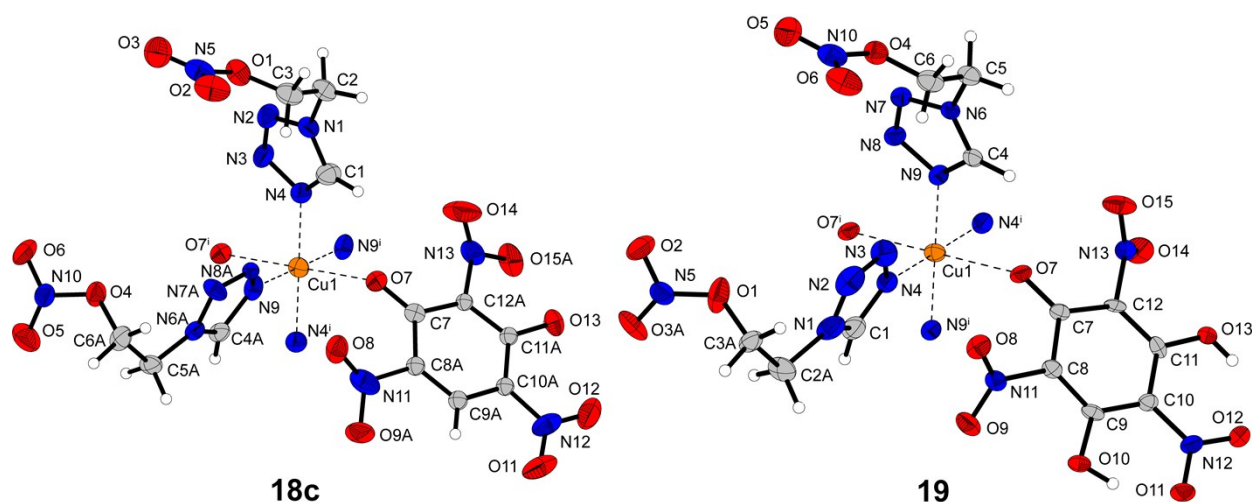


Figure S5. Coordination environment of the complexes [Cu(HTNR)₂(1-NET)₄] (**18c**) and [Cu(H₂TNPG)₂(1-NET)₄] (**19**). Selected bond lengths (Å) of **18c**: Cu1–O7 2.3844(19), Cu1–N9 2.025(3), Cu1–N4 1.985(2). Selected bond lengths (Å) of **19**: Cu1–O7 2.375(3), Cu1–N4 2.011(3), Cu1–N9 1.991(5). Selected bond angles (°) of **18c**: O7–Cu1–N9 88.83(8), O7–Cu1–N4 85.55(8), N4–Cu1–N9 89.29(10). Selected bond angles (°) of **19**: O7–Cu1–N4 89.14(10), O7–Cu1–N9 85.09(12), N4–Cu1–N9 88.81(16) Symmetry code of **18c**: 1–x, 1–y, 1–z. Symmetry code of **19**: –x, 1–y, 1–z.

The coordination compounds **21** and **22a** based on either a styphnate (TNR^{2-}) or 5-hydroxy-2,4,6-trinitroresorcinate (HTNPG^{2-}) anion both crystallize isotypically with similar cell axes and cell volumes in the triclinic space group $P\bar{1}$ with two formula units per unit cell. The additional hydroxy group within the HTNPG^{2-} anions leads to an increased density (**21**: 1.935 g cm^{-3} at 102 K, **22a**: 1.970 g cm^{-3} at 102 K). Every complex shows a distorted octahedral coordination sphere with two ligand moieties in equatorial positions (Figure 12). The remaining equatorial coordination sites are occupied by deprotonated hydroxy groups of the trinitrophenolate ion. The axial positions are taken by nitro groups of the anion, which are closest to the binding hydroxy groups. The binding behaviour of the respective anion leads to the formation of one-dimensional polymeric chains.

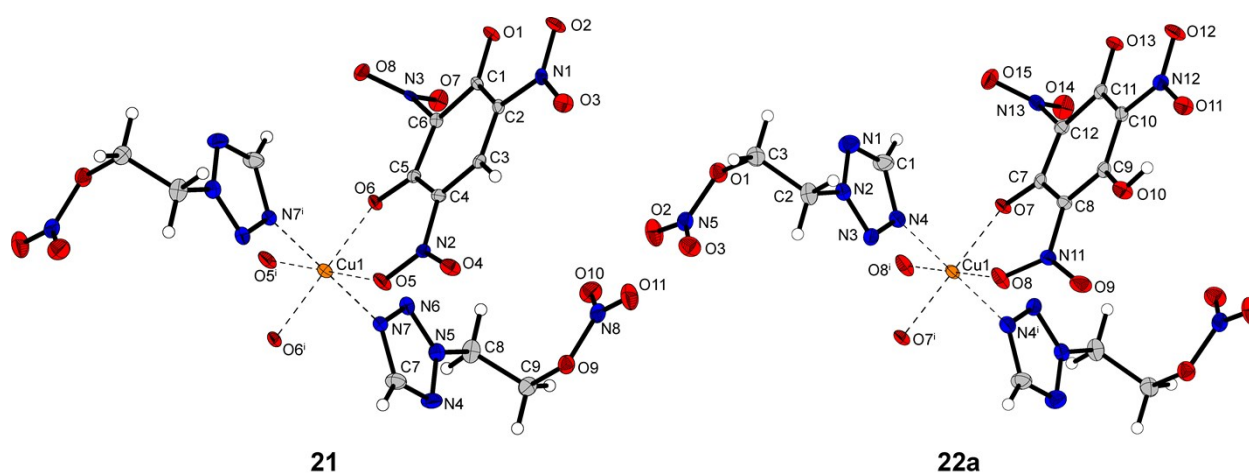


Figure S6. Coordination environments of the complexes $[\text{Cu}(2\text{-NET})_2(\text{TNR})]$ (**21**) and $[\text{Cu}(\text{HTNPG})(2\text{-NET})_2]$ (**22a**). Selected bond lengths (\AA) of **21**: Cu1–O6 1.942(2), Cu1–O5 2.258(3), Cu1–N7 2.022(3). Selected bond lengths (\AA) of **22a**: Cu1–O7 1.9473(16), Cu1–N4 2.027(2), Cu1–O8 2.2396(17). Selected bond angles ($^\circ$) of **21**: O5–Cu1–O6 83.71(9), N7–Cu1–O5 89.93(11), O6–Cu1–N7 88.93(11). Selected bond angles ($^\circ$) of **22a**: O8–Cu1–O7 82.71(7), O8–Cu1–N4 86.46(8), O7–Cu1–N4 88.63(8). Symmetry code of **21**: (i) $1-x, 2-y, -z$. Symmetry code of **22a**: (i) $-x, 1-y, 1-z$.

ECC **22c** crystallizes in the triclinic space group $P\bar{1}$ in the form of green platelets and the unit cell consists of one formula unit. The compound possesses a calculated density of 1.803 g cm^{-3} at 123 K, which is the lowest observed value for all trinitrophenolate complexes based on 2-NET (**5**). The coordination sphere is built up like the 1-NET based complex **19**. Four tetrazole moieties are arranged in the equatorial positions together with anions occupying the axial spots. The major difference to **19**, or **22b**, is that two additional, non-coordinating 2-NET moieties are located within the molecular unit (Figure 13). This behaviour has not been observed among copper complexes based on the H_2TNPG anion. It is likely due to the alkyl chain length of the ligand, allowing the ligand to perfectly fit into the free spots of the structure. This is also favoured by two different conformations of the C–C bond, which were observed within the structure. The co-crystallizing ligand, together with two of the equatorial ligands show a *gauche* conformation ($\text{N10-C11-C12-O1} = 58.4(4)^\circ$, $\text{N15-C14-C15-O16} = 50.1(3)^\circ$), whereas the remaining two ligands are arranged in an *anti*-conformation ($\text{N5-C8-C9-O10} = 172.40(18)^\circ$).

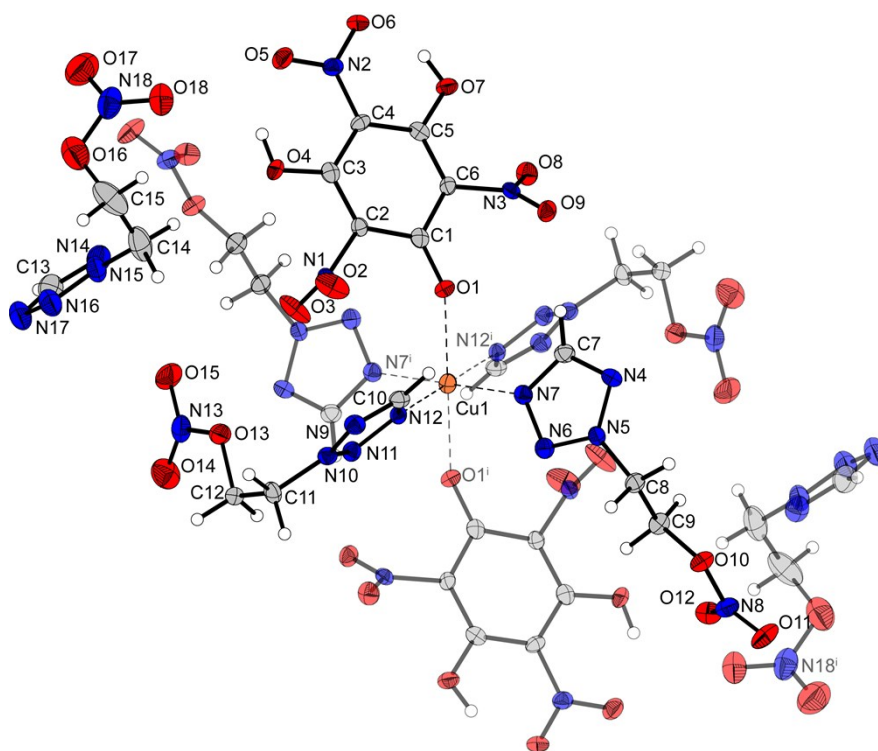


Figure S7. Molecular unit of $[\text{Cu}(\text{H}_2\text{TNPG})_2(2\text{-NET})_4] \cdot 2 \text{ 2-NET}$ (**22c**). Selected bond lengths (\AA): Cu1-O1 2.317(2), Cu1-N7 2.006(2), Cu1-N12 2.043(3). Selected bond angles ($^\circ$): O1-Cu1-N7 84.11(11), O1-Cu1-N12 88.70(11), N7-Cu1-N12 88.71(11). Symmetry code: $1-x, 1-y, 1-z$.

3. Computations & Hishfeld Surfaces

3.1 Computations

All calculations were carried out using the Gaussian G09 program package.^{S13} The enthalpies (H) and free energies (G) were calculated using the complete basis set (CBS) method of Petersson and coworkers in order to obtain very accurate energies. The CBS models use the known asymptotic convergence of pair natural orbital expressions to extrapolate from calculations using a finite basis set to the estimated complete basis set limit. CBS-4 begins with a HF/3-21G(d) geometry optimization; the zero point energy is computed at the same level. It then uses a large basis set SCF calculation as a base energy, and a MP2/6-31+G calculation with a CBS extrapolation to correct the energy through second order. A MP4(SDQ)/6-31+(d,p) calculation is used to approximate higher order contributions. In this study we applied the modified CBS-4M method (M referring to the use of minimal population localization) which is a re-parametrized version of the original CBS-4 method and also includes some additional empirical corrections. The enthalpies of the gas-phase species M were computed according to the atomization energy method (E 1) (Table S7 & 8).^{S13-18}

$$\Delta_f H^\circ_{(g, M, 298)} = H_{(Molecule, 298)} - \sum H^\circ_{(Atoms, 298)} + \sum \Delta_f H^\circ_{(Atoms, 298)} \quad (E1)$$

Table S7. Literature values for atomic ΔH_f° / kcal mol⁻¹

	$-H^{298}$ [a.u.]	NIST ^{S19}
H	0.50091	52.1
C	37.786156	171.3
N	54.522462	113.0
O	74.991202	59.6

In the last step the gas-phase heat of formations were converted to the solid/liquid state ones by subtracting the vaporization/sublimation enthalpies (calculated using the Trouton rule).^{S20,21} The calculation results are summarized in Table S8.

Table S8. CBS-4M results, Gas phase enthalpies of formation, calculated sublimation/vaporization enthalpies and solid-state heat of formation.

Compound	$-H^{298}$ / a.u.	$\Delta_f H^\circ(\text{g})$ / kJ mol^{-1}	$\Delta H^\circ(\text{sub/vap})$ / kJ mol^{-1}	$\Delta_f H^\circ(\text{s})$ / kJ mol^{-1}
4	-615.780788	229.8	56.0522	173.7
5	-615.790916	203.2	56.0522	147.1
TNT	–	–	–	-59.346

3.2 Hirshfeld Surfaces

Hirshfeld surfaces of compound **4** and **5** were generated from the crystal structure data with CrystalExplorer17.⁵²² Fingerprint plots are shown in Figure S5. Interactions are represented by dots in the fingerprint plot and corresponding distances can be calculated by the addition of the distance d_e and d_i . Therefore, the area in the lower left represents close interactions. These close interactions, attractive or repulsive, are represented by red dots on the Hirshfeld surface.

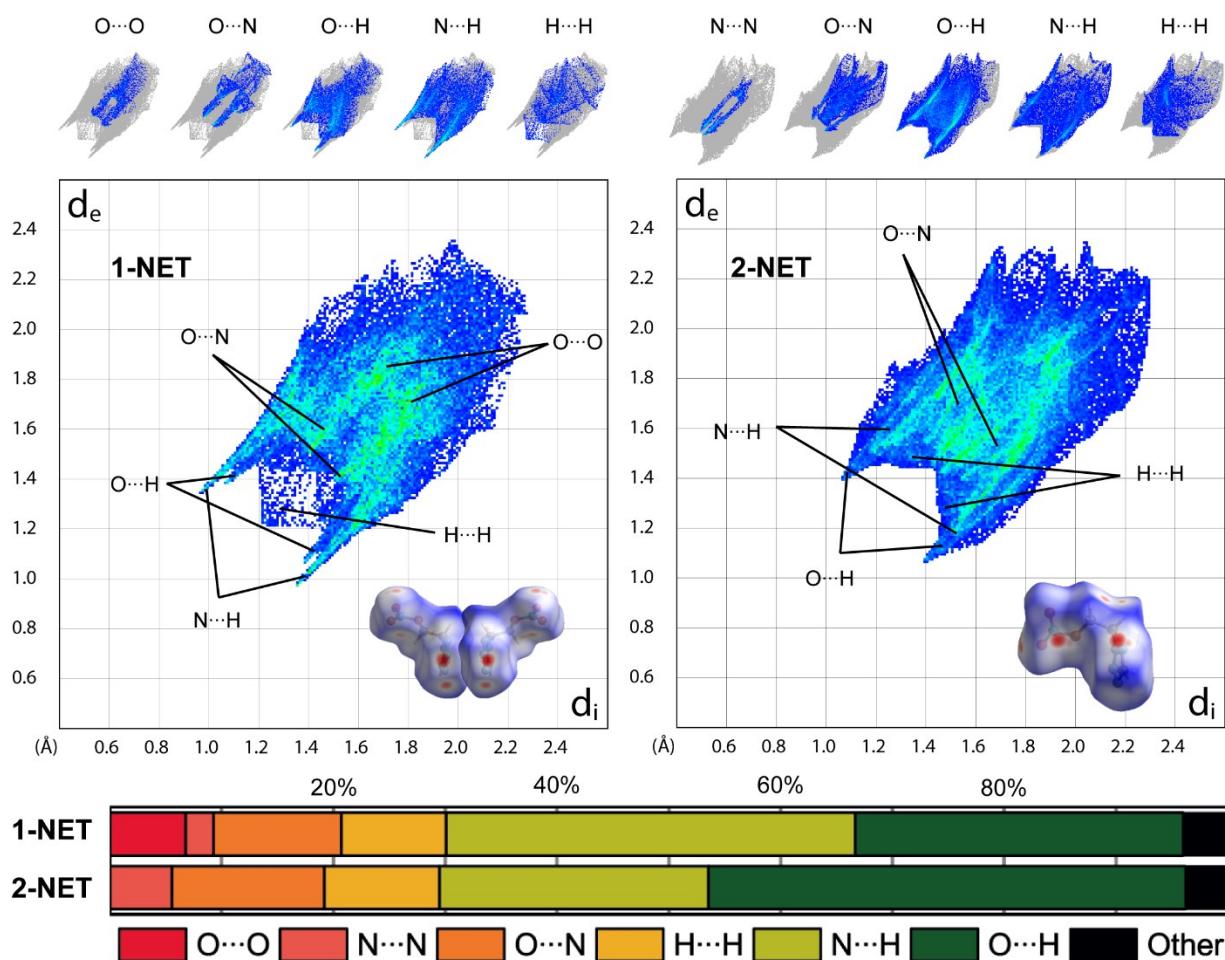


Figure S8. Two-dimensional fingerprint plots of **4** and **5** together with their Hirshfeld surfaces. The areas of the single interactions are represented above the graphs.

4. NMR Spectroscopy of 4 and 5

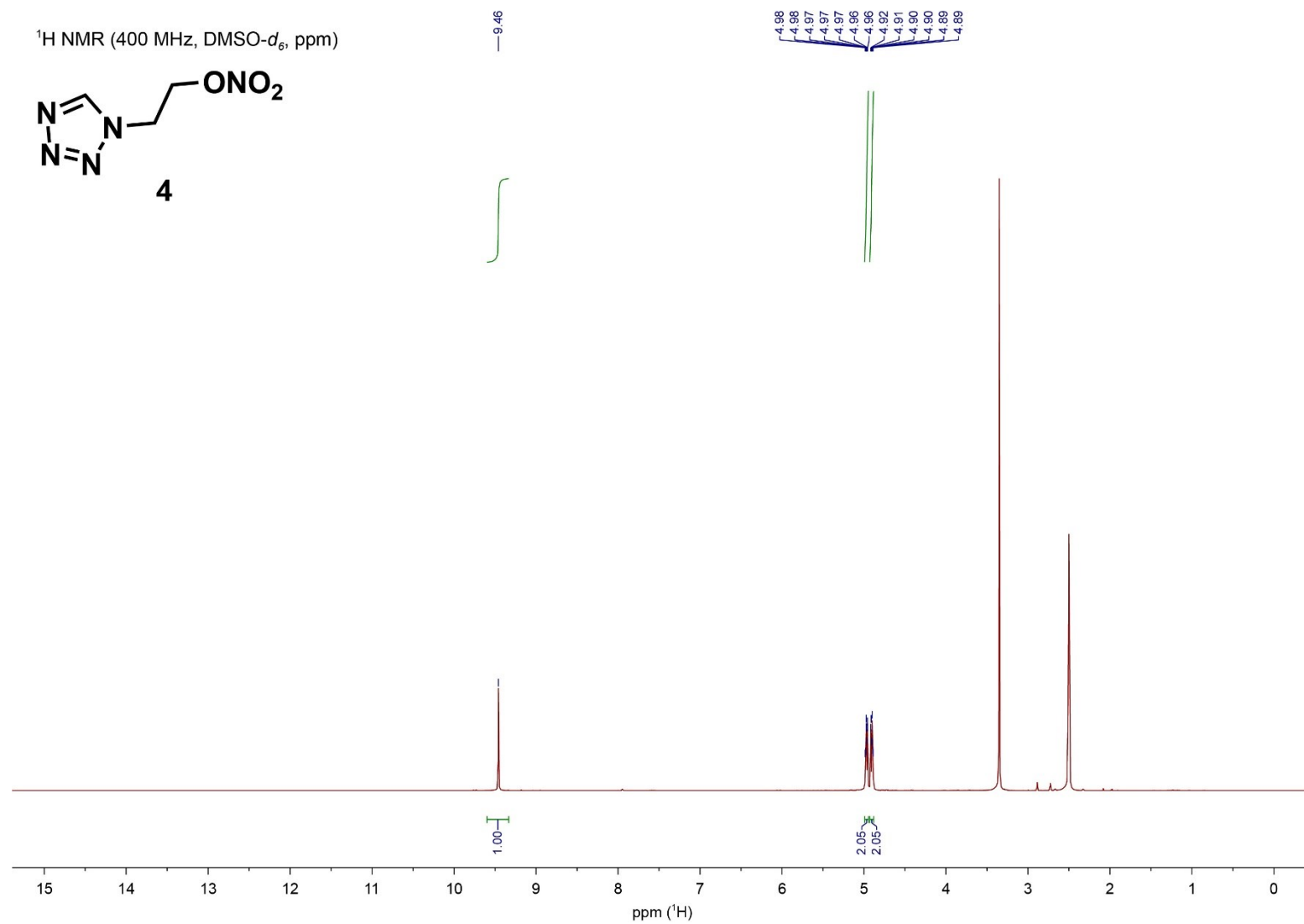


Figure S9. ¹H NMR spectrum of 1-NET (**4**).

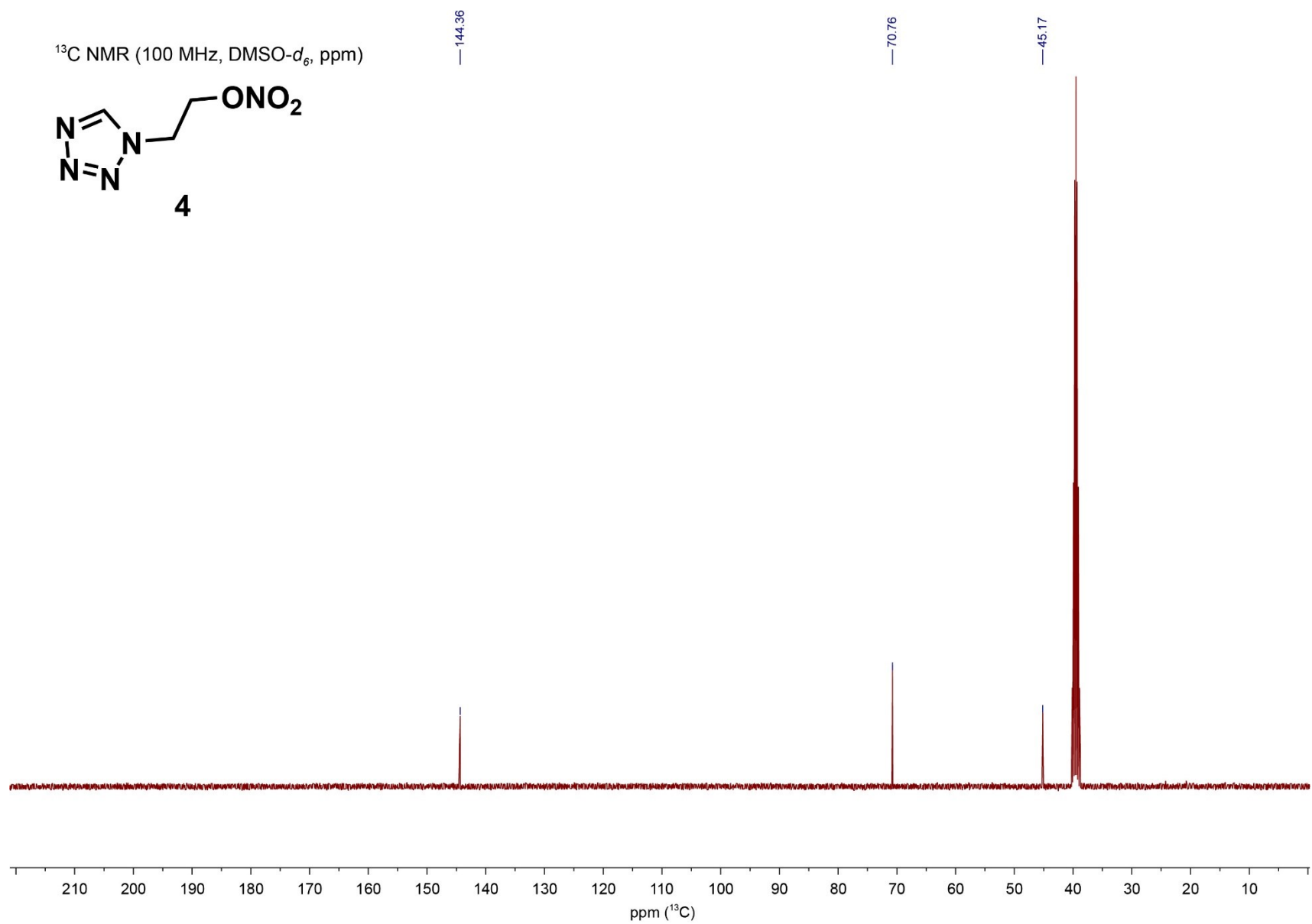


Figure S10. ¹³C NMR spectrum of 1-NET (**4**).

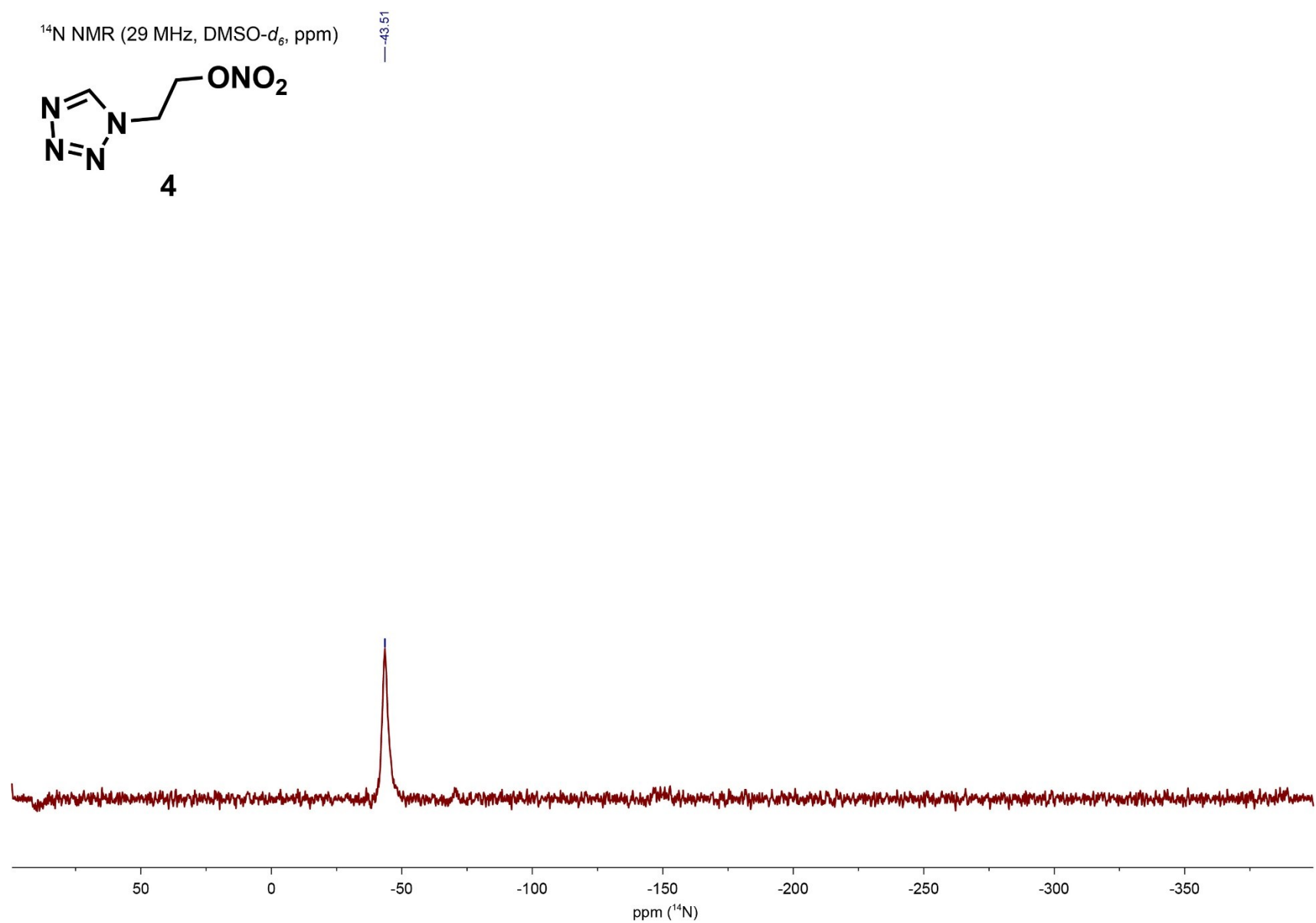


Figure S11. ¹⁴N NMR spectrum of 1-NET (**4**).

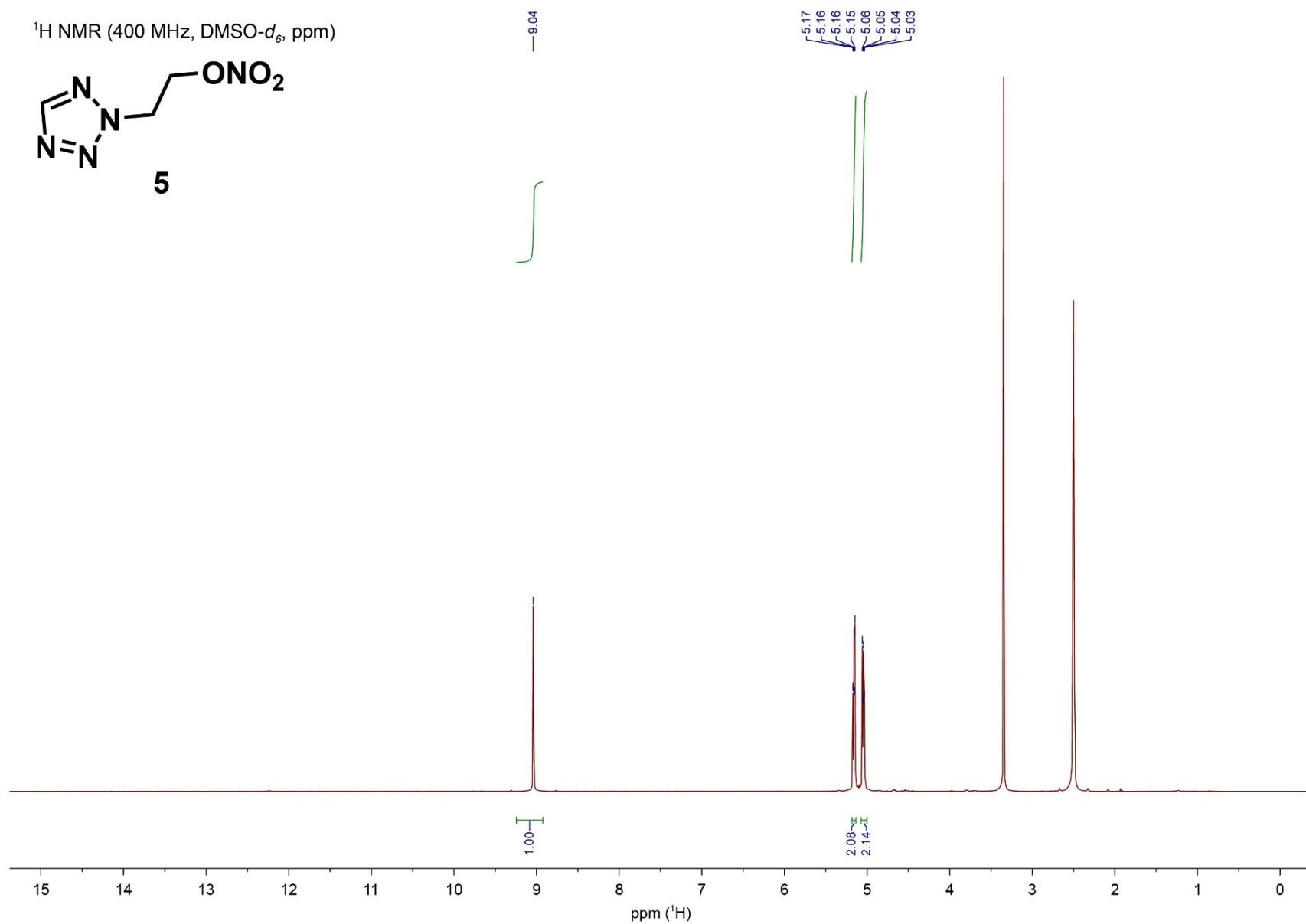


Figure S12. ¹H NMR spectrum of 2-NET (**5**).

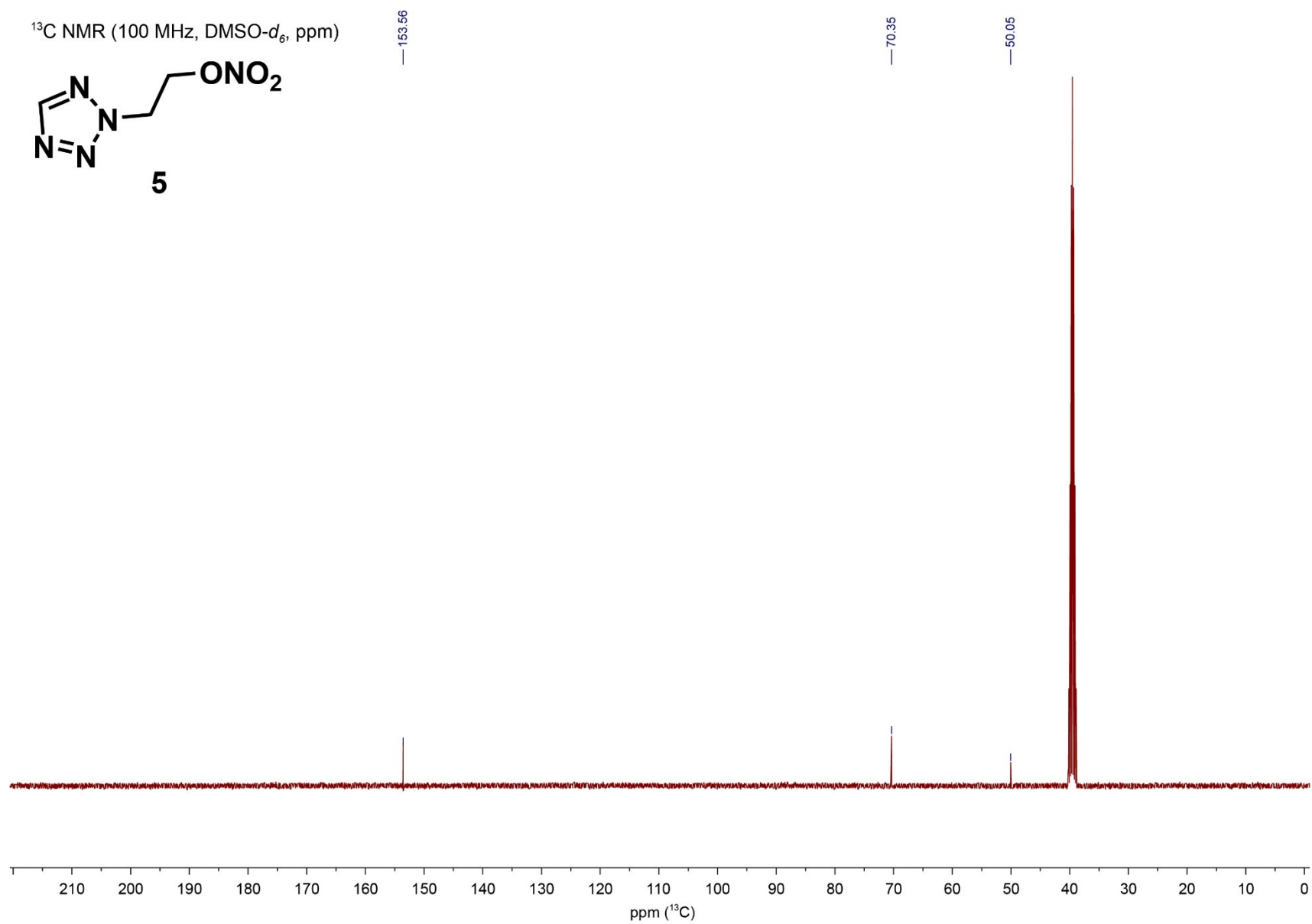


Figure S13. ¹³C NMR spectrum of 2-NET (**5**).

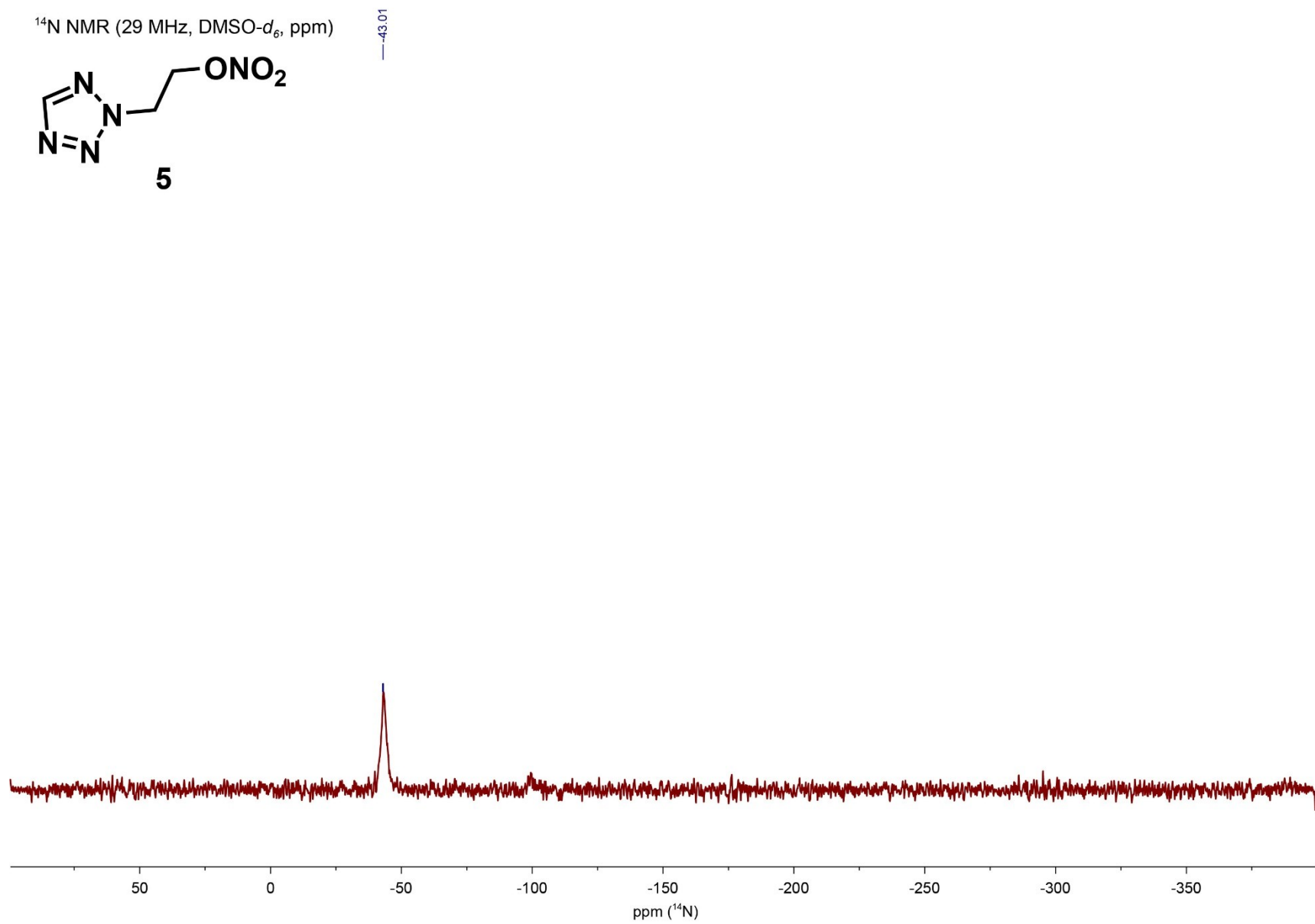


Figure S14. ¹⁴N NMR spectrum of 2-NET (**5**).

4. IR Spectroscopy of 1, 2, 4–9, 11, 13, 14, and 16–22

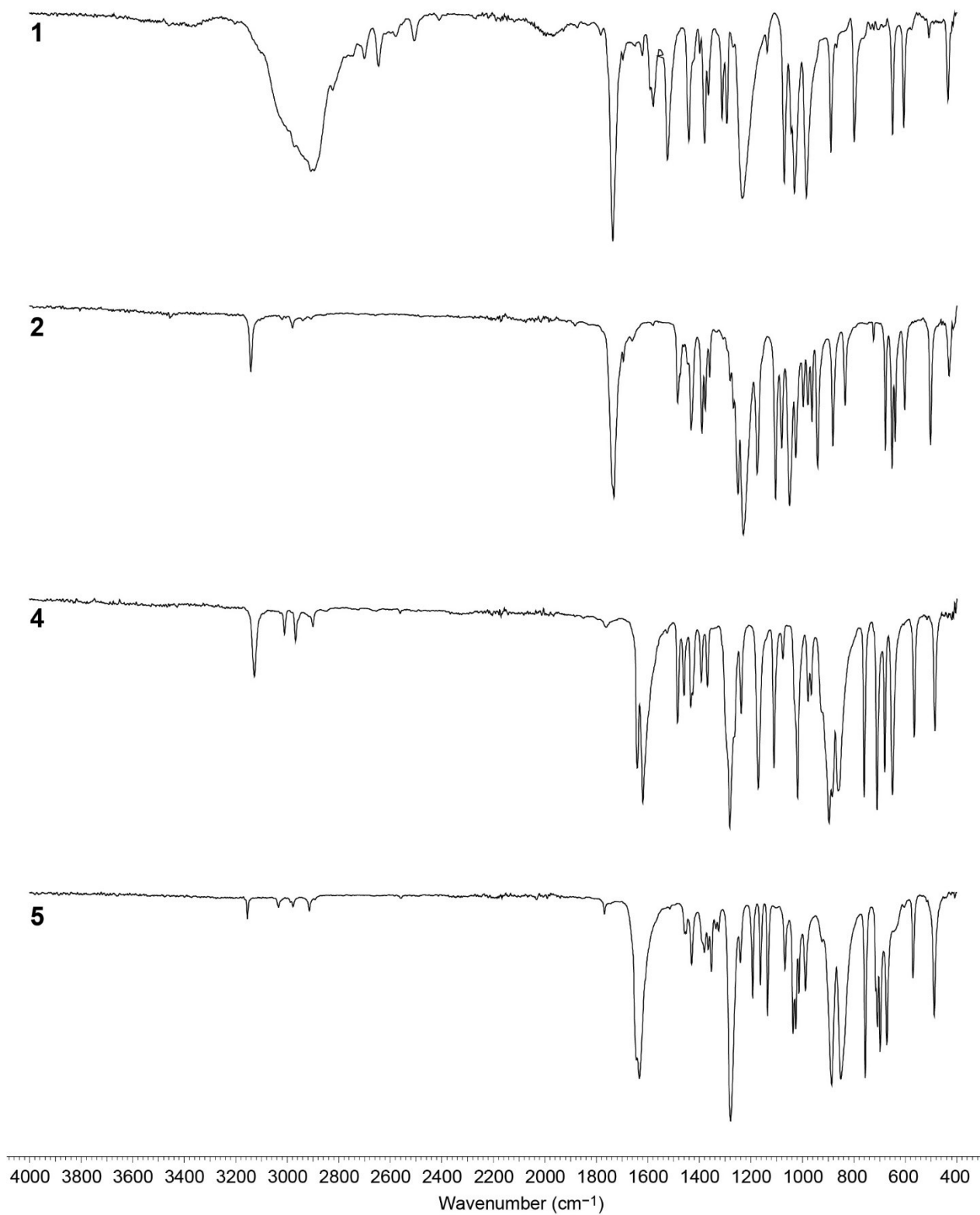


Figure S15. IR spectra of the organic molecules 1, 2, 4, and 5.

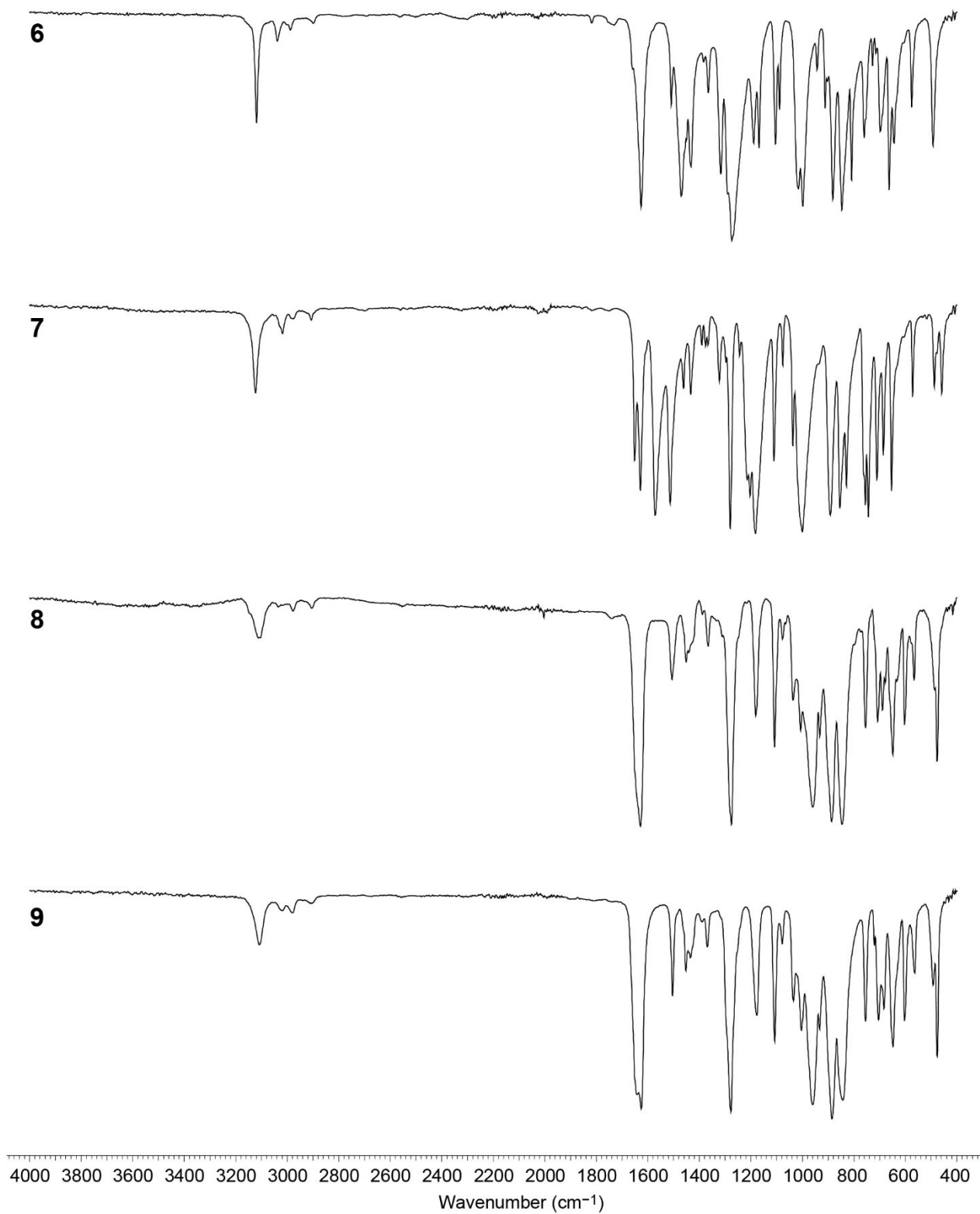


Figure S16. IR spectra of the complexes 6–9.

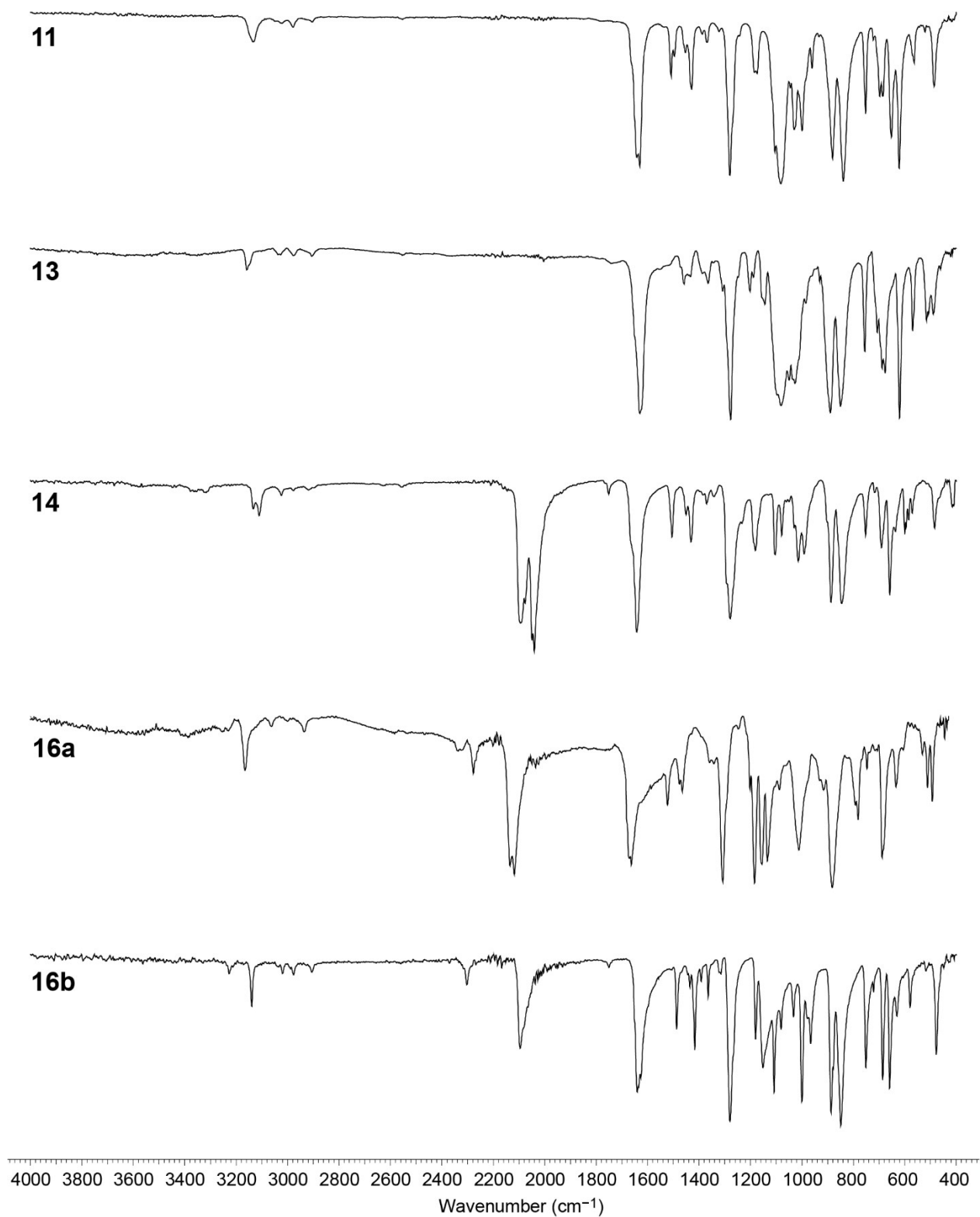


Figure S17. IR spectra of the ECC **11**, **13**, **14**, and **16a–b**.

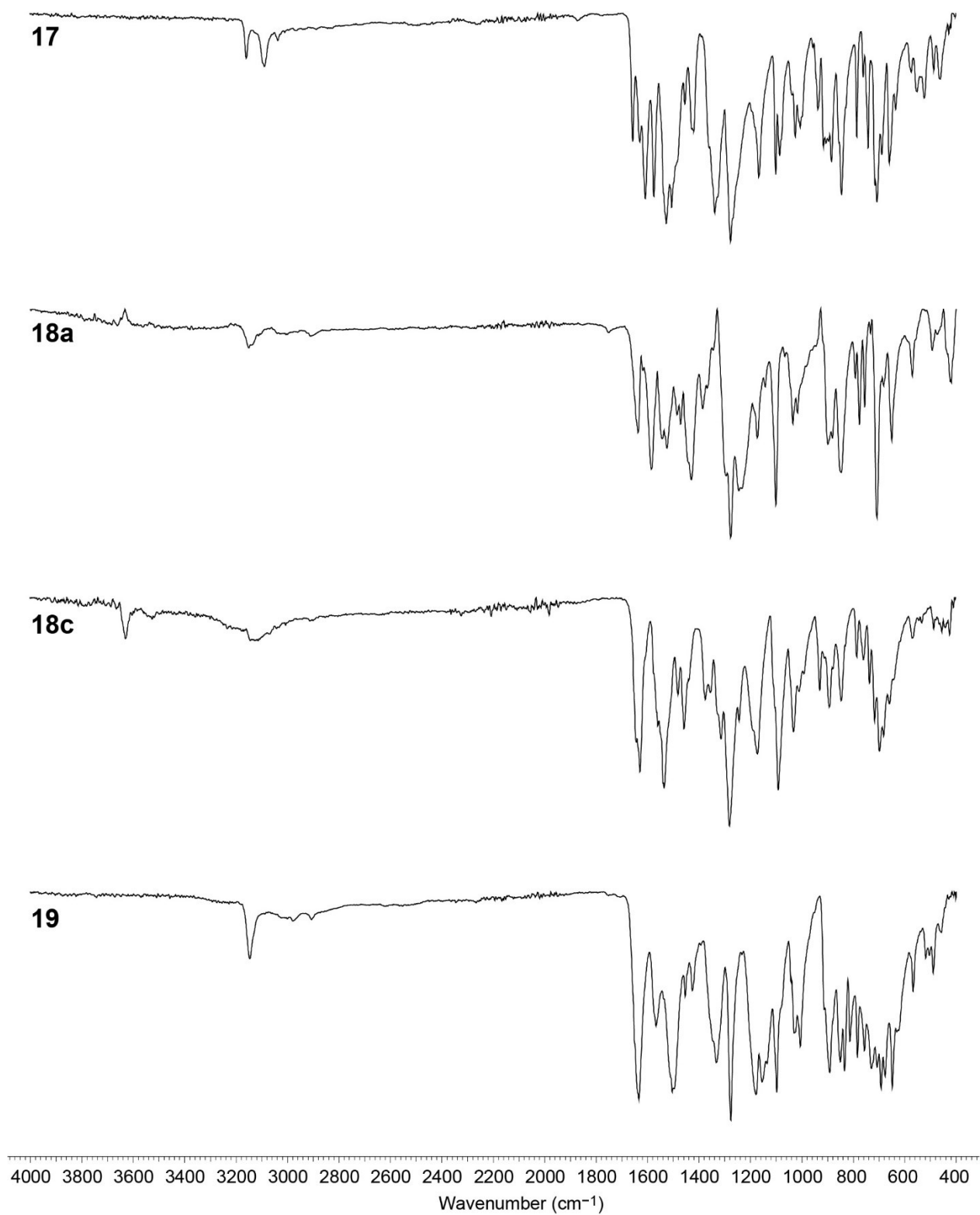


Figure S18. IR spectra of the coordination compounds **17–19** based on various trinitrophenolate anions.

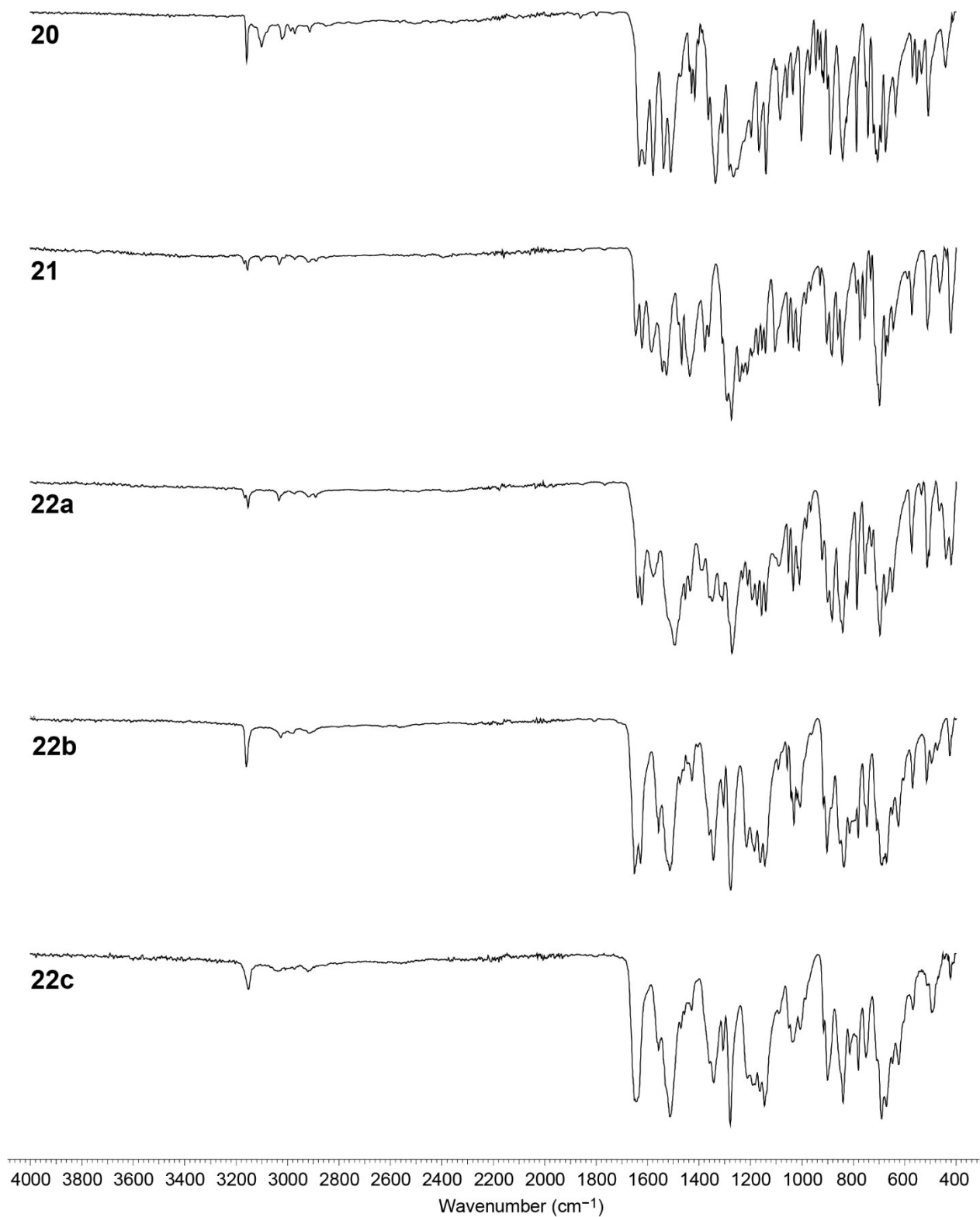


Figure S19. IR spectra of the coordination compounds **20–22**.

5. DTA Plots of 4–9, 11, 13, 14, and 16–22

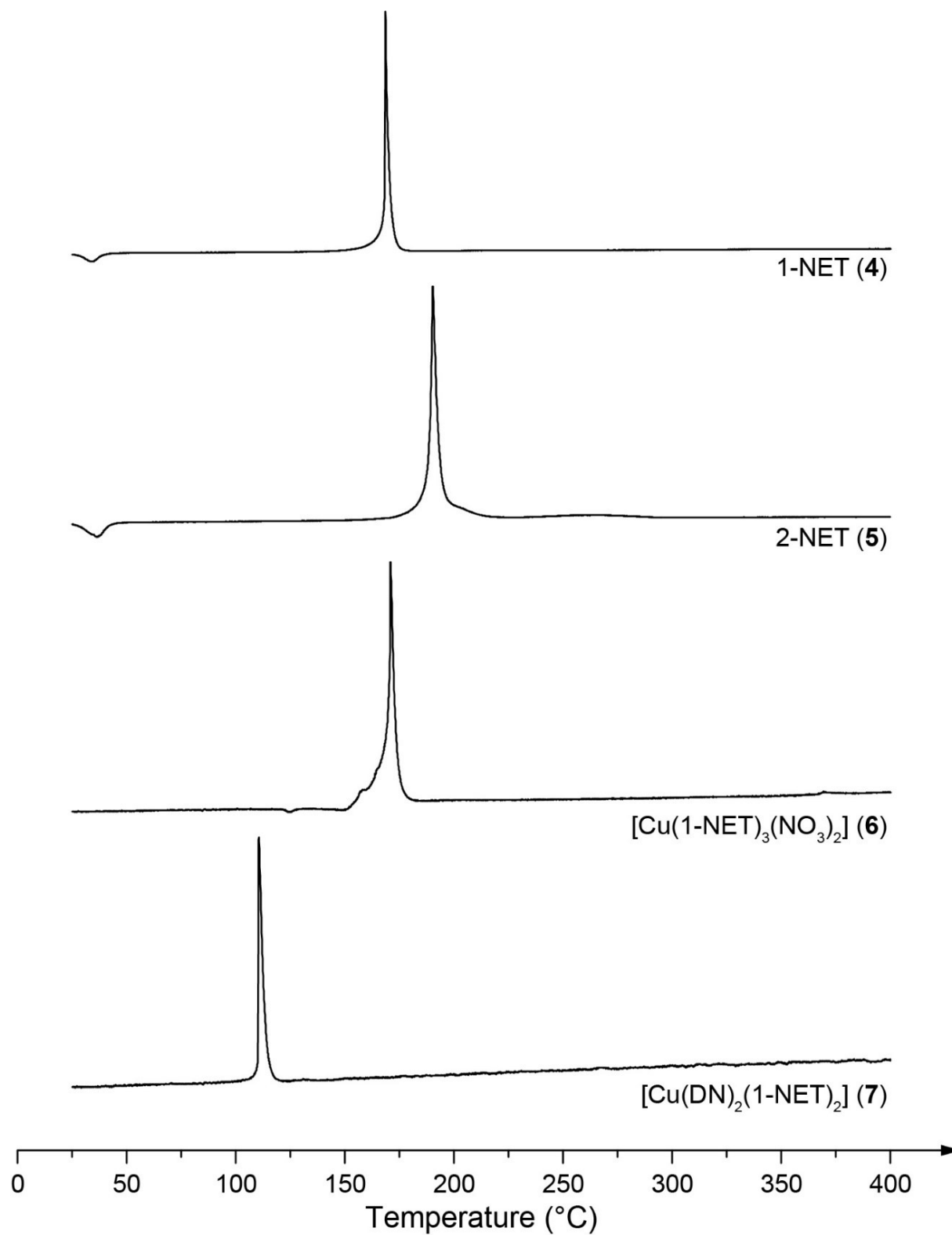


Figure S20. DTA plots of the ligands 4 and 5 together with the complexes 6 and 7.

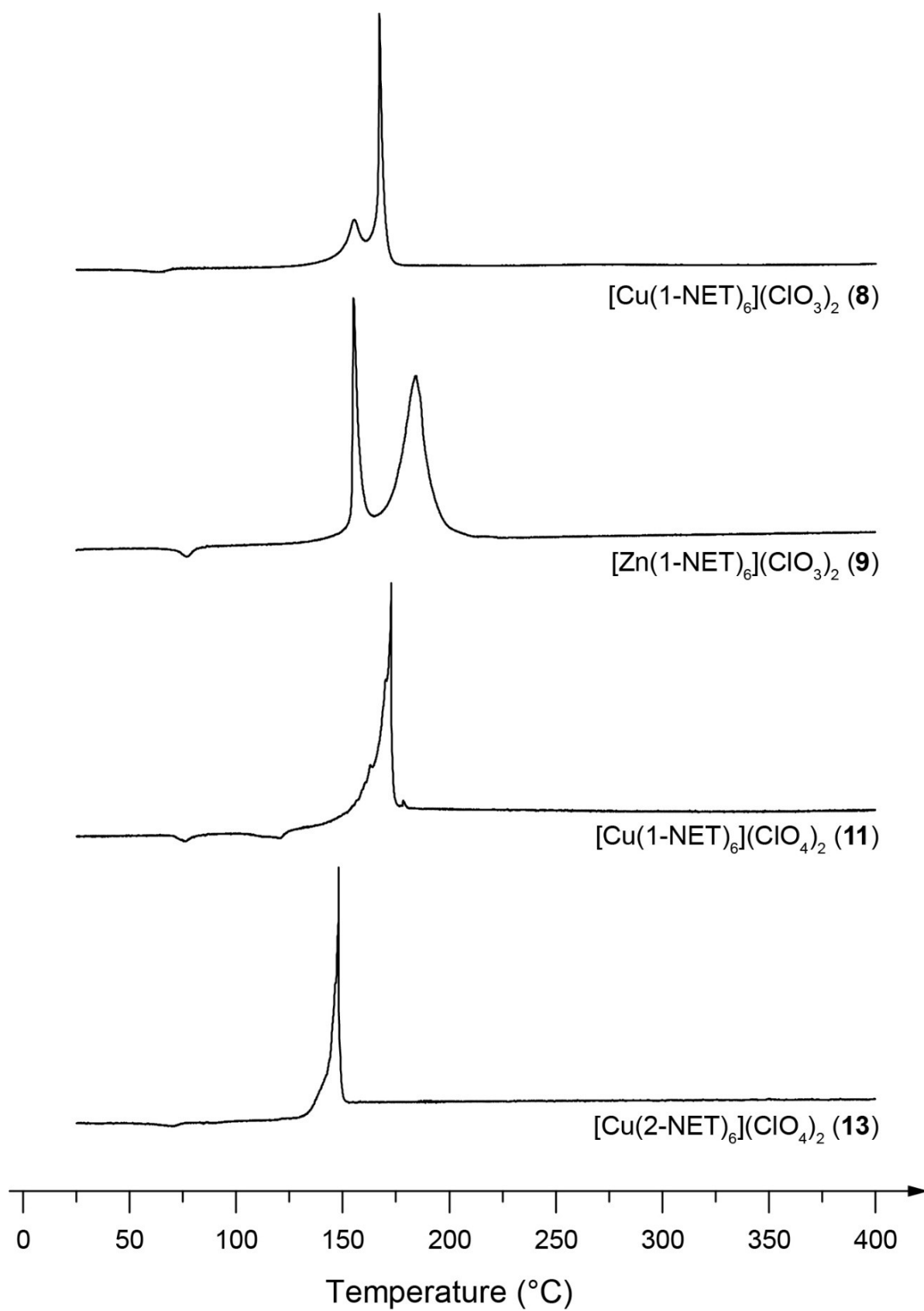


Figure S21. DTA measurements of the compounds **8**, **9**, **11**, and **13**.

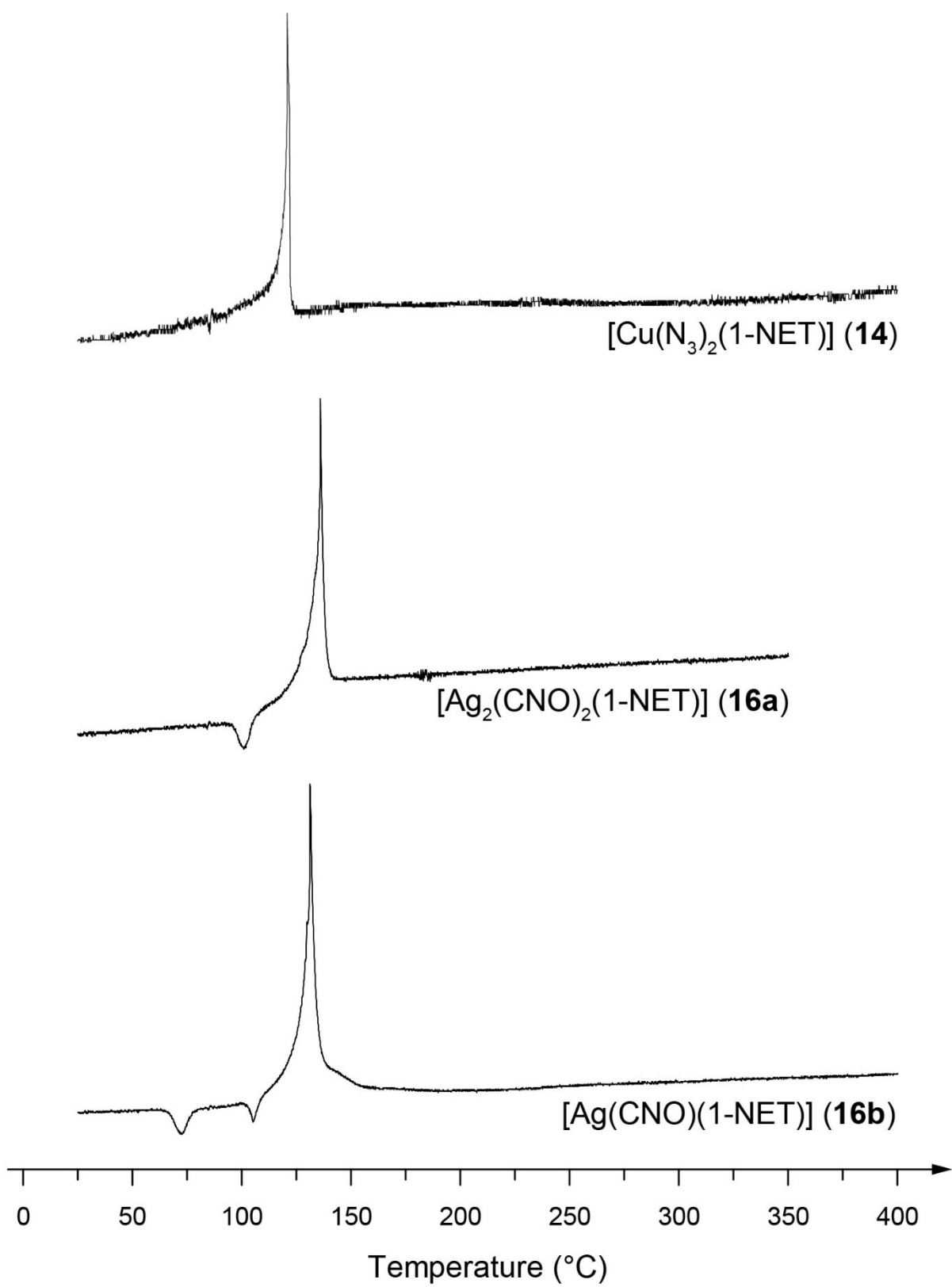


Figure S22. DTA measurements of the complexes **14**, **16a**, and **16b**.

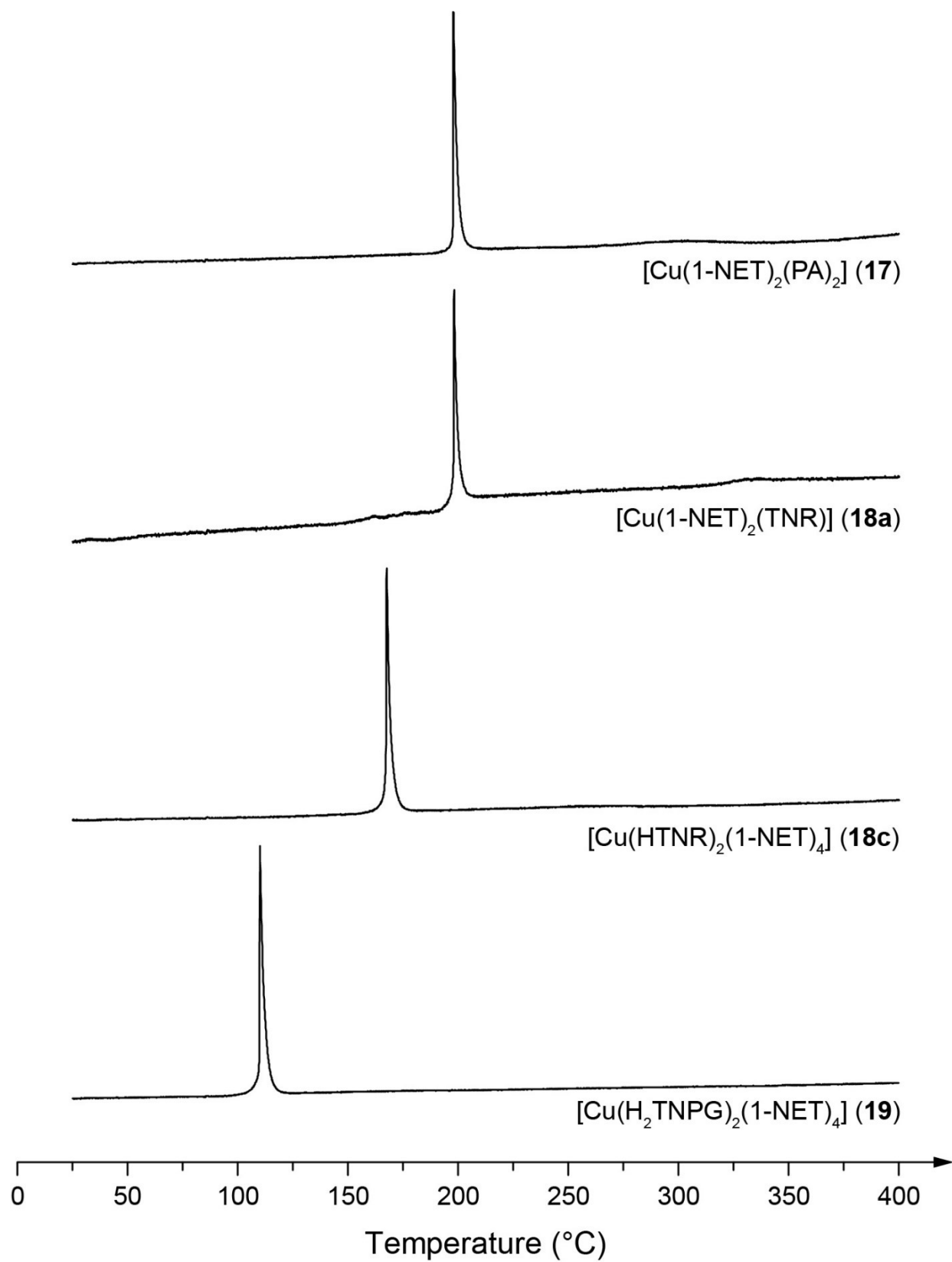


Figure S23. DTA measurements of the trinitrophenolate-based complexes **17–19**.

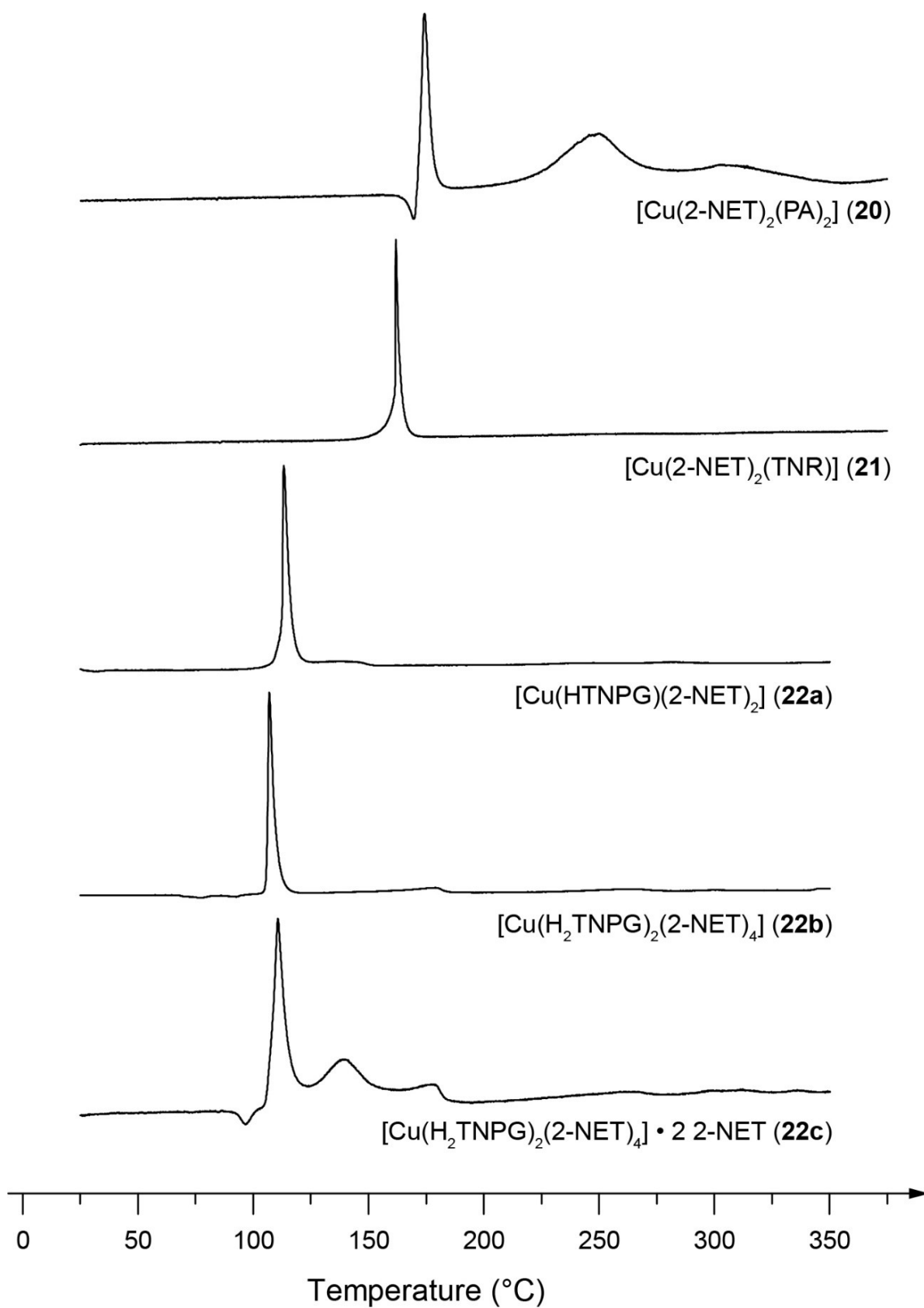


Figure S24. DTA measurements of the trinitrophenolate-based complexes **20–22**.

6. TGA Plots of 4–6, 8, 9, 11, 13, 16, 20, and 22

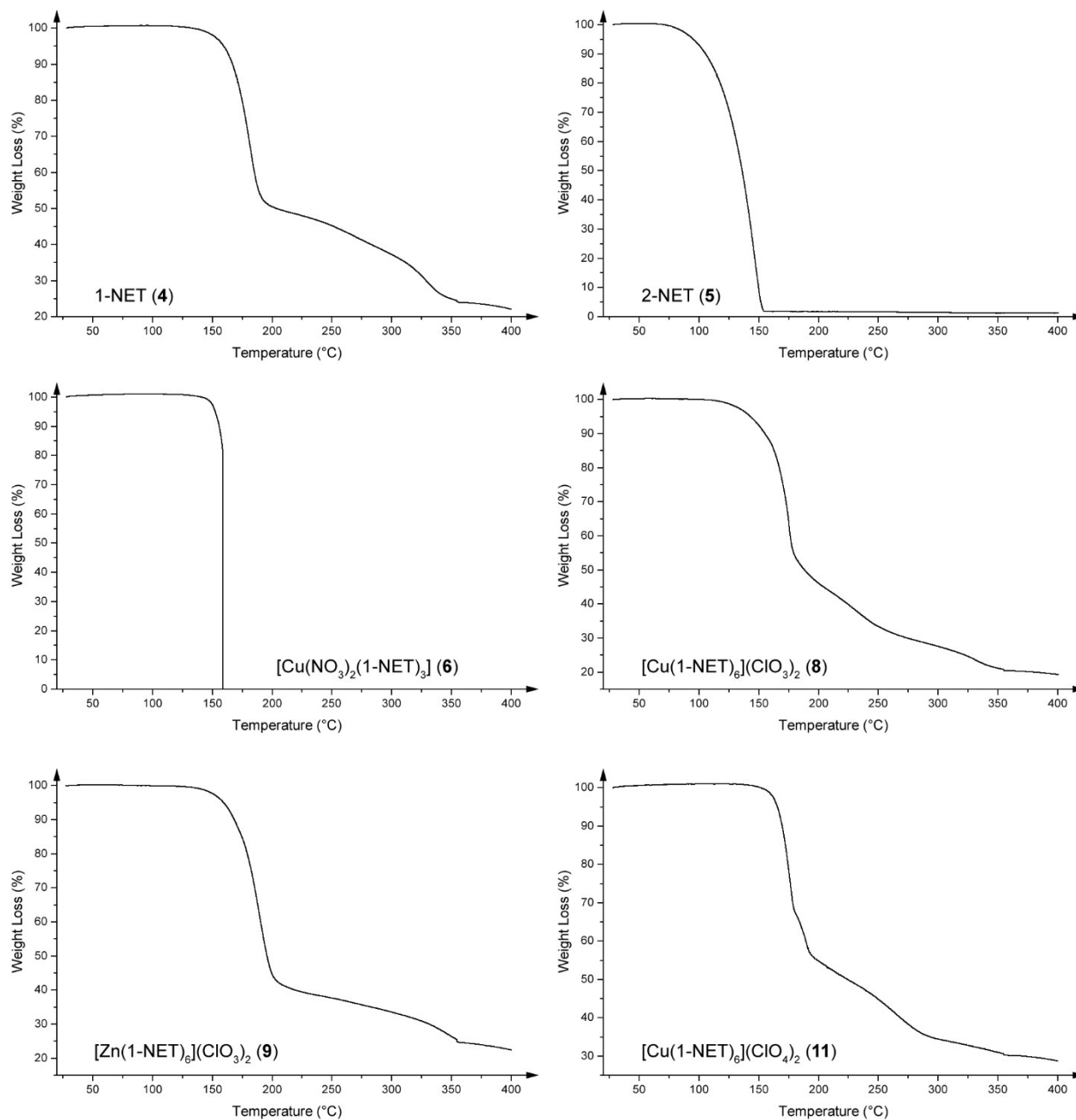


Figure S25. TG measurements of the ligands **4** and **5** together with the complexes **6**, **8**, **9**, and **11**.

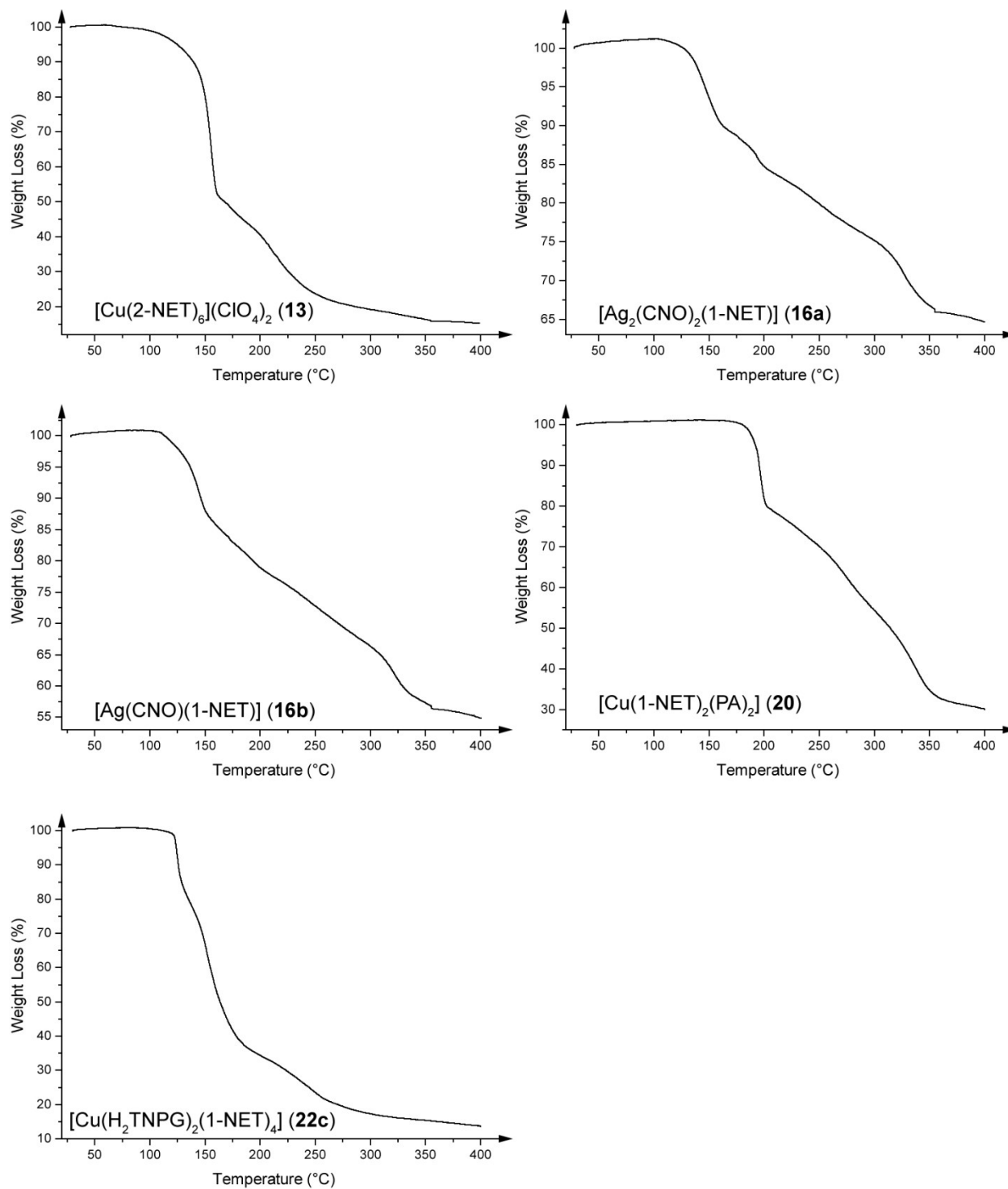


Figure S26. TGA plots of the ECCs **13**, **16a**, **16b**, **20**, and **22c**.

7. Hot Plate & Hot Needle Tests of 6–9, 11, 13, 14, 16–22



Figure S27. Deflagration of the nitrato complex 6 during hot plate (left) and hot needle test (right).



Figure S28. Reaction of the dinitramide complex 7 during hot plate (left) and hot needle test (right).



Figure S29. Deflagration reaction of ECC 8 during hot plate (left) and hot needle test (right).



Figure S30. Deflagration of the zinc chlorate complex 9 during hot plate test.



Figure S31. Reaction of the coordination compound **11** during hot plate (left) and hot needle test (right).

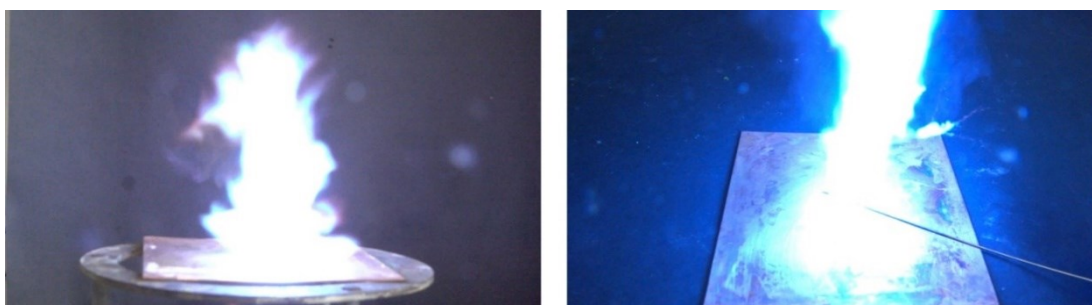


Figure S32. Results of the hot plate (left) and hot needle tests (right) of the ECC **13**.



Figure S33. Detonations of the copper azide complex **14** during hot plate (left) and hot needle test (right).

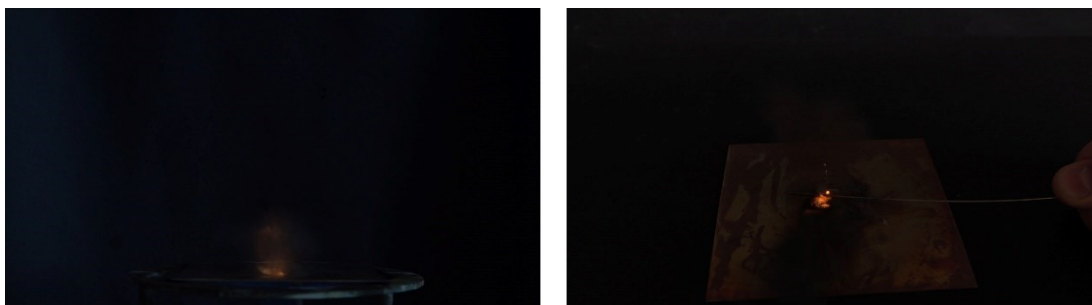


Figure S34. Detonations of the silver fulminate complex **16a** during hot plate (left) and deflagration during hot needle test (right).

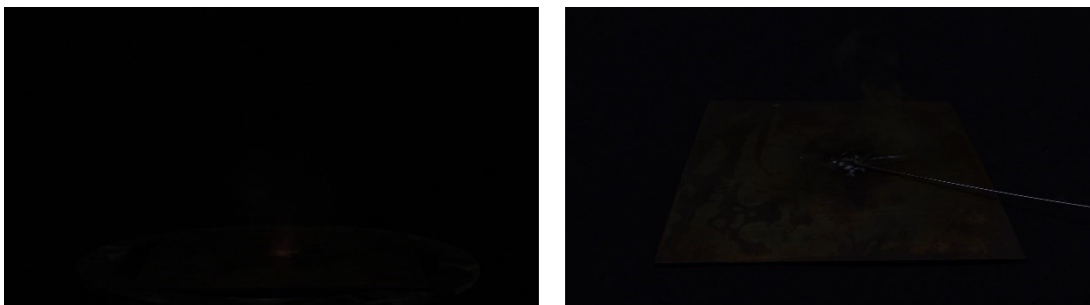


Figure S35. Reactions of the coordination compound **16b** during hot plate (left) and hot needle test (right).



Figure S36. Deflagration of the picrate complex **17** during hot plate test (left) and decomposition during hot needle test (right).

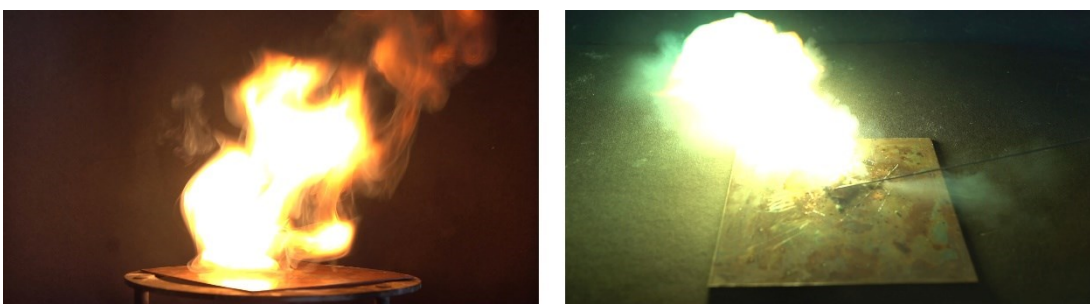


Figure S37. Results of hot plate (left) and hot needle test (right) of compound **18a**.

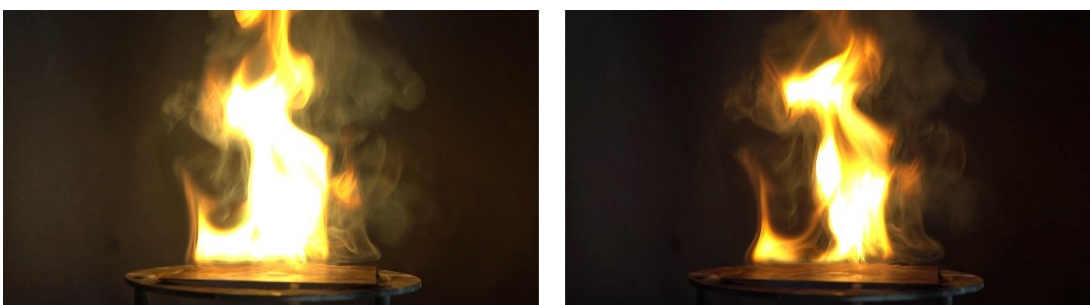


Figure S38. Results of hot plate (left) and hot needle test (right) of compound **18c**.



Figure S39. Coordination compound **19** during hot plate (left) and hot needle (right) testings.



Figure S40. Deflagration of the picrate complex **20** during hot plate test (left) and hot needle tests (right).



Figure S41. Results of hot plate (left) and hot needle test (right) of the styphnate coordination compound **21**.

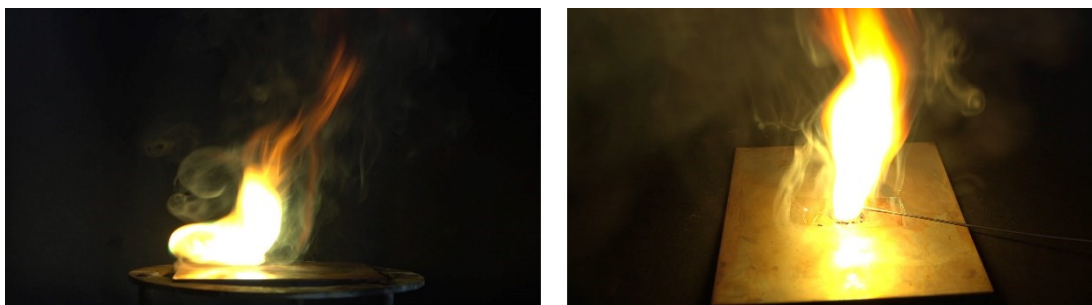


Figure S42. Reactions of ECC **22a** during hot plate (left) and hot needle (right) testings.

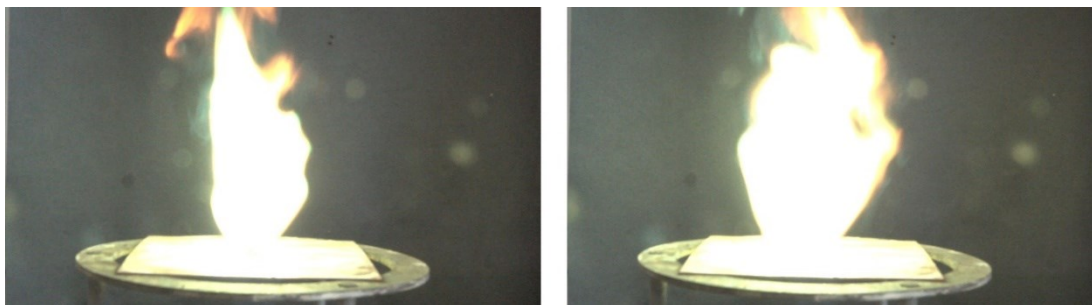


Figure S43. Deflagrations of compound **22b** during hot plate (left) and hot needle tests (right).



Figure S44. Reactions of compound **22c** during hot plate (left) and hot needle tests (right).

8. Experimental Part & General Methods

All chemicals and solvents were employed as received (Sigma-Aldrich, Fluka, Acros, ABCR). ^1H , ^{13}C , ^{14}N , and $^{15}\text{N}\{^1\text{H}\}$, and ^1H - ^{15}N HMBC NMR spectra were recorded at ambient temperature using a JEOL Bruker 27400, Eclipse 270, JEOL EX 400 or a JEOL Eclipse 400 instrument. The chemical shifts quoted in ppm in the text refer to typical standards such as tetramethylsilane (^1H , ^{13}C) nitromethane (^{14}N , ^{15}N) in DMSO- d_6 , acetonitrile- d_3 or acetone- d_6 as the solvent. Endothermic and exothermic events of the described compounds, which indicate melting, loss of crystal water or decomposition, are given as the extrapolated onset temperatures. The samples were measured in a range of 25–400 °C at a heating rate of 5 °C min⁻¹ through differential thermal analysis (DTA) with an OZM Research DTA 552-Ex instrument and in some cases additionally by thermal gravimetric analysis (TGA) with a PerkinElmer TGA4000. Infrared spectra were measured with pure samples on a Perkin-Elmer BXII FT-IR system with a Smith DuraSampler IR II diamond ATR. Determination of the carbon, hydrogen, and nitrogen contents was carried out by combustion analysis using an Elementar Vario El (nitrogen values determined are often lower than the calculated ones' due to their explosive behavior). UV-Vis spectra were recorded in the solid state using a Varian Cary 500 spectrometer in the wavelength range of 350–1000 nm. The step in the absorption intensity at 800 nm is caused by a detector change. Impact sensitivity tests were carried out according to STANAG 4489^{S23} with a modified instruction^{S24} using a BAM (Bundesanstalt für Materialforschung) drophammer.^{S25} Ball drop impact sensitivity tests were determined for selected compounds on an OZM ball drop machine (BIT-132), following MIL-STD-1751A (method 1016) by dropping a free-falling steel ball onto the explosive compound.^{S26,27} Details on the process can be found in the literature.^{S28} Friction sensitivity tests were carried out according to STANAG 4487^{S29} with a modified instruction^{S30} using the BAM friction tester.^{S25,26} The classification of the tested compounds results from the “UN Recommendations on the Transport of Dangerous Goods”.^{S31,32} Additionally, all compounds were tested upon the sensitivity toward electrical discharge using the OZM Electric Spark XSpark10 device.^{S26} Hot plate and hot

needle tests were performed in order to evaluate the potential initiation capability of selected compounds. The samples were fixed on a copper plate underneath adhesive tape and initiated by a red-hot needle. Strong deflagration or detonation of the compound usually indicates a valuable primary explosive. The safe and straightforward hot plate test only shows the behavior of the unconfined sample toward fast heating on a copper plate. It does not necessarily allow any conclusions on a compound's capability as a suitable primary explosive. The laser initiation experiments were performed with a 45 W InGaAs laser diode operating in the single-pulsed mode. The diode is attached to an optical fiber with a core diameter of 400 μm and a cladding diameter of 480 μm . The optical fiber is connected via a SMA type connector directly to the laser and to a collimator. This collimator is coupled to an optical lens, which was positioned in its focal distance ($f = 29.9 \text{ mm}$) to the sample. The lens is shielded from the explosive by a sapphire glass. Approximately 15 mg of the carefully pestled compound to be investigated was filled into a transparent plastic cap (PC), pressed with a pressure force of 1 kN and sealed by a UV-curing adhesive. The confined samples were irradiated at a wavelength of 915 nm, a voltage of 4 V, a current of 7 A and pulse lengths of 1–30 ms. The combined currents and pulse lengths result in an energy output of 1.7–51.0 mJ. Energetic properties have been calculated with the EXPLO5 6.05.04 computer code^{S33} using the, to RT converted, X-ray density and calculated solid state heats of formation. These were computed by the atomization method as described in recently published papers. Electronic enthalpies were calculated with the Gaussian09 software^{S13} suite using the CBS-4M method.

The obtained compounds were washed with acetonitrile when stated, dried overnight in air and used for analytics without further purification.

CAUTION! *All investigated compounds are potentially explosive energetic materials, which show partly increased sensitivities toward various stimuli (e.g. elevated temperatures, impact, friction or electrostatic discharge). Therefore, proper security precautions (safety glass, face shield, earthed equipment and shoes, leather coat, Kevlar gloves, Kevlar sleeves and ear plugs) have to be applied while synthesizing and handling the described compounds.*

2-Aminoethylacetate hydrochloride (1)

2-Aminoethanol hydrochloride (20.0 g, 0.21 mol) was suspended in acetic anhydride (23 g, 0.23 mol).^{S33} The reaction mixture was heated to 80 °C for 2 h. The resulting clear solution was cooled to room temperature. The formed precipitate was filtered off, washed with diethylether (200 mL) and dried in vacuum over night. Compound **1** was obtained as a colorless solid. Yield: 21.4 g (0.153 mol, 75%).

EA (C₄H₁₀ClNO₂, 138.57): calcd: C 34.42, H 7.22, N 10.04%; found: C 34.17, H 7.22, N 10.04%; IR (ATR, cm⁻¹): $\tilde{\nu}$ = 2908 (s), 2895 (s), 2824 (m), 2700 (w), 2646 (w), 2507 (w), 1736 (vs), 1698 (w), 1649 (w), 1622 (w), 1592 (m), 1579 (m), 1524 (s), 1441 (m), 1399 (w), 1380 (m), 1365 (m), 1312 (m), 1293 (m), 1269 (w), 1234 (s), 1137 (w), 1071 (s), 1044 (m), 1031 (s), 985 (s), 890 (s), 868 (w), 799 (m), 651 (m), 607 (m), 436 (m); ¹H NMR (400 MHz, DMSO-*d*₆, 25 °C) δ (ppm) = 8.23 (s, 3H, NH₃), 4.19 (t, ³J_{H-H} = 5.3 Hz, 2H, CH₂), 3.04 (t, ³J_{H-H} = 5.4 Hz, 2H, CH₂), 2.05 (s, 3H, CH₃); ¹³C NMR (101 MHz, DMSO-*d*₆, 25 °C) δ (ppm) = 170.3, 60.4, 37.8, 20.7; HRMS (ESI) for C₄H₁₀ClNO₂ calc. [M-Cl]⁺ 104.0706, found: 104.0707.

2-(1H-tetrazol-1-yl)ethyl acetate (2)

Compound **1** (21.4 g, 0.15 mol) and sodium azide (11.9 g, 0.18 mol) were suspended in triethylorthoformate (91.0 g, 102.1 mL, 0.61 mol).^{S34} Acetic acid (61 mL) was added dropwise

under stirring over a period of 30 min. The suspension was heated to reflux for 3 h. After cooling to RT, the solvent was removed under reduced pressure and the remaining solid was extracted with hot acetone (200 mL). The solvent was evaporated and the remaining colorless oil was dried under high vacuum. The compound solidified yielding 2-(1*H*-tetrazol-1-yl)ethyl acetate (**2**) as colorless block suitable for single crystal X-ray diffraction. Yield: 14.6 g (0.094 mol, 61%).

EA (C₅H₈N₄O₂, 156.15): calcd: C 38.46, H 5.16, N 35.88%; found: C 38.27, H 4.90, N 35.82%; IR (ATR, cm⁻¹): $\tilde{\nu}$ = 2979 (vw), 1731 (s), 1694 (w), 1660 (w), 1483 (m), 1473 (m), 1459 (w), 1444 (w), 1431 (m), 1389 (m), 1376 (m), 1359 (m), 1279 (m), 1267 (m), 1249 (s), 1229 (vs), 1174 (s), 1103 (s), 1080 (s), 1049 (s), 1025 (s), 995 (m), 978 (m), 962 (m), 940 (s), 881 (s), 833 (m), 723 (w), 677 (s), 651 (s), 639 (m), 602 (m), 502 (s), 429 (m); ¹H NMR (400 MHz, DMSO-*d*₆, 25 °C) δ (ppm) = 9.44 (s, 1H, CH), 4.75 (t, ³J_{H-H} = 5.2 Hz, 1H, CH₂), 4.53–4.27 (m, 2H, CH₂), 1.98 (s, 3H, CH₃); ¹³C NMR (101 MHz, DMSO-*d*₆, 25 °C) δ (ppm) = 170.0, 144.3, 61.6, 46.8, 20.4; HRMS (EI) for C₅H₈N₄O₂ calc. [M+H]⁺ 157.0720, found: 157.0714.

1-Hydroxyethyl-5*H*-tetrazole (**3**)

Compound **2** (14.0 g, 0.09 mmol) was dissolved in concentrated hydrochloric acid (10 mL) and stirred at room temperature for 1 h. The solvent was removed under reduced pressure and the resulting colorless oil was dried under high vacuum. The oil solidified yielding compound **3** in the form of colorless blocks. Yield: 8.9 g (0.078 mmol, 87%).

¹H NMR (400 MHz, DMSO-*d*₆, 25 °C) δ (ppm) = 9.33 (s, 1H, CH), 5.11 (s, 2H, OH), 4.50 (t, ³J_{H-H} = 5.3 Hz, 4H, CH₂), 3.78 (t, ³J_{H-H} = 5.3 Hz, 4H, CH₂); ¹³C NMR (101 MHz, DMSO-*d*₆, 25 °C) δ (ppm) = 144.3, 59.1, 50.4; HRMS (EI) for C₃H₆N₄O calc. [M] 114.0542, found: 114.0542.

One-pot synthesis of 1-Hydroxyethyl-5H-tetrazole (**3**)

2-Aminoethanol hydrochloride (19.5 g, 0.20 mol) was suspended in acetic anhydride (22.5 g, 0.22 mol) in a 500 mL three necked roundbottom flask. The reaction mixture was heated to 80 °C for 2 hours. Subsequently the solution was allowed to cool down to 40 °C and triethylorthoformiate (59.3 g, 66.3 mL, 0.40 mol) was added. Sodium azide (15.6 g, 0.24 mol) was added and acetic acid (70 mL) was added dropwise. After the complete addition, the reaction mixture was refluxed for 3 h. Afterwards concentrated hydrochloric acid (40 mL) was added and heating was continued for 30 min. The solution was cooled to RT and the solvent was removed. The remaining suspension was extracted with hot acetone (200 mL) and the solvent was removed *in vacuo*. The remaining colorless oil was dried under high vacuum and solidified. Compound **3** was obtained in the form of colorless blocks. Yield: 17.1 g (0.15 mol, 75%).

Selective preparation of 1-nitratoethyltetrazole (1-NET, **4**)

White fuming nitric acid (12 mL) was cooled to 0 °C and compound **3** (2.0 g, 17.5 mmol) was added dropwise. The temperature was kept below 10 °C during the whole addition. Stirring was continued for 20 min. Subsequently the solution was allowed to warm to room temperature and stirred mechanical for another 20 min. After neutralization using sodium carbonate, the aqueous layer was extracted with dichloromethane (3x, 200 mL). The combined organic layers were dried over magnesium sulfate and the solvent was removed under reduced pressure. The remaining colorless oil was dried under high vacuum and solidified. The tetrazole derivative **4** was obtained in the form of colorless blocks suitable for single crystal X-ray diffraction. Yield: 2.0 g (12.8 mmol, 73%).

Preparation of 1- & 2-nitrateethyltetrazole via alkylation of 1,5*H*-tetrazole (1-NET, **4**; 2-NET, **5**)

1,5*H*-tetrazole (7.0 g, 0.10 mol) was suspended in water (15 mL).^{S35} Sodium hydroxide (4.0 g, 0.10 mol) dissolved in water (15 mL) was added and the solution was heated to reflux. 2-Chloroethanol (10.1 g, 8.3 mL, 0.13 mmol) was added dropwise over the course of 15 min. The reaction mixture was heated to reflux for 12 h. The solvent was removed under reduced pressure and the resulting suspension was extracted with hot acetone (600 mL). Removal of the solvent *in vacuo* afforded a mixture of 1- and 2-hydroxy-5*H*-ethyltetrazole as a yellowish oil in almost quantitative yield (11.2 g, 0.098 mol, 98%). The isomers were not separated.

¹H NMR (400 MHz, DMSO-*d*₆, 25 °C) δ (ppm) = 9.34 (s, 1H, CH), 8.95 (s, 1H, CH), 5.18–4.97 (m, 2H, OH), 4.76–4.66 (m, 2H, CH₂), 4.58–4.43 (m, 2H, CH₂), 3.90 (t, ³*J*_{H-H} = 5.3 Hz, 3H, CH₂), 3.78 (t, ³*J*_{H-H} = 5.2 Hz, 3H, CH₂); ¹³C NMR (101 MHz, DMSO-*d*₆, 25 °C) δ (ppm) = 50.4, 55.4, 59.1, 59.1, 144.3, 153.2.

Subsequently white fuming nitric acid (12 mL) was cooled to 0 °C. The mixture of both tetrazole derivatives (2.1 g, 18.40 mmol) was added dropwise whereas the temperature was kept below 10 °C during the whole addition. After stirring for 20 min the mixture was allowed to warm to RT and stirring was continued for a further 20 min. Sodium carbonate was added until a pH-level of 7. The remaining solution was extracted with dichloromethane (3x, 200 mL). The combined organic layers were dried over magnesium sulfate and the solvent was evaporated under reduced pressure. Purification via flash column chromatography (1:1 ethyl acetate/hexane → pure ethyl acetate) afforded 1-nitrateethyl-5*H*-tetrazole (**4**, 1.31 g, 7.98 mmol, 45%) and 2-nitrateethyltetrazole (**5**, 1.27 g, 8.23 mmol, 43%) as colorless oils. Subjecting the samples to high vacuum led to their solidification, leading to colorless block suitable for X-ray diffraction in case of compound **4**. Single crystals of compound **5** could be achieved through sublimation (40 °C, 0.5 x 10⁻² mbar).

1-NET (4)

EA (C₃H₅N₅O₃, 159.11): calcd: C 22.65, H 3.17, N 44.02%; found: C 22.55, H 3.23, N 43.31%; IR (ATR, cm⁻¹): $\tilde{\nu}$ = 3010 (w), 2967 (w), 2900 (w), 1763 (w), 1641 (s), 1620 (s), 1526 (w), 1485 (m), 1460 (m), 1434 (m), 1427 (m), 1393 (m), 1369 (m), 1282 (vs), 1238 (m), 1172 (s), 1111 (s), 1076 (w), 1019 (s), 978 (m), 966 (m), 897 (vs), 885 (s), 861 (s), 760 (s), 711 (vs), 681 (s), 651 (s), 567 (s), 486 (m); ¹H NMR (400 MHz, DMSO-*d*₆, 25 °C) δ (ppm) = 9.46 (s, 1H, CH), 4.99–4.95 (m, 2H, CH₂), 4.93–4.88 (m, 2H, CH₂); ¹³C NMR (101 MHz, DMSO-*d*₆, 25 °C) δ (ppm) = 144.4, 70.8, 45.2; ¹⁴N NMR (29 MHz, DMSO-*d*₆, 25 °C) δ (ppm) = -43.5; HRMS (ESI) for C₃H₅N₅O₃ calc. [M+H]⁺ 160.0465, found: 160.0467; BAM drophammer: 10 J, BAM friction tester: > 360 N (at grain size \approx 500–1000 μ m).

2-NET (5)

EA (C₃H₅N₅O₃, 159.11): calcd: C 22.65, H 3.17, N 44.02%; found: C 22.94, H 2.87, N 43.83%; IR (ATR, cm⁻¹): $\tilde{\nu}$ = 3033 (vw), 2976 (vw), 2914 (vw), 1768 (vw), 1643 (s), 1632 (s), 1514 (vw), 1456 (w), 1451 (w), 1429 (m), 1380 (w), 1365 (w), 1352 (m), 1335 (w), 1324 (w), 1277 (vs), 1240 (m), 1192 (m), 1162 (m), 1134 (m), 1067 (m), 1035 (s), 1025 (m), 1013 (m), 987 (m), 923 (w), 886 (s), 850 (s), 755 (s), 714 (m), 708 (m), 697 (s), 671 (s), 570 (m), 487 (m); ¹H NMR (400 MHz, DMSO-*d*₆, 25 °C) δ (ppm) = 9.04 (s, 1H, CH), 5.19–5.12 (m, 2H, CH₂), 5.08–5.01 (m, 2H, CH₂); ¹³C NMR (101 MHz, DMSO-*d*₆, 25 °C) δ (ppm) = 153.6, 70.4, 50.1; ¹⁴N NMR (29 MHz, DMSO-*d*₆, 25 °C) δ (ppm) = -43.0; ¹⁵N NMR (41 MHz, Acetone-*d*₆, 25 °C) δ (ppm) = -0.7 (s), -44.5 (t), -46 .1(d), -76.1 (d), 100.9 (m); HRMS (ESI) for C₃H₅N₅O₃ calc. [M+H]⁺ 160.0465, found: 160.0462; BAM drophammer: 2 J, BAM friction tester: > 360 N (at grain size \approx 500–1000 μ m).

[Cu(1-NET)₃(NO₃)₂] (6)

Copper nitrate trihydrate (60.4 mg, 0.25 mmol) was dissolved in acetonitrile (2 mL). Compound **4** was added in stoichiometric amounts in acetonitrile (2 mL). Complex **6** was obtained in the form of blue platelets suitable for X-ray diffraction within a days. Yield: 133.0 mg (0.20 mmol, 81%).

DTA (5 °C min⁻¹) onset: 121 °C (endothermic), 169 °C (exothermic); IR (ATR, cm⁻¹): $\tilde{\nu}$ = 3038 (w), 2987 (vw), 2898 (vw), 1817 (vw), 1731 (vw), 1659 (w), 1625 (s), 1508 (m), 1469 (s), 1449 (m), 1431 (s), 1382 (w), 1364 (m), 1315 (s), 1289 (s), 1273 (vs), 1188 (m), 1167 (m), 1104 (m), 1088 (m), 1015 (s), 997 (s), 942 (w), 911 (m), 902 (m), 881 (s), 846 (s), 808 (s), 759 (m), 726 (w), 714 (w), 697 (m), 662 (s), 643 (m), 575 (m), 492 (m), 449 (vw); EA (C₉H₁₅CuN₇O₁₅, 664.86): calcd: C 16.26, H 2.27, N 35.81%; found: C 16.85, H 2.21, N 35.93%; BAM drophammer: 5 J; BDIS: 14 mJ, BAM friction tester: 48 N; ESD: 1080 mJ (at grain size \approx 500–1000 μ m).

[Cu(DN)₂(1-NET)₂] (7)

Dinitraminic acid was prepared according to our previously published method.^{S36} Basic copper(II) carbonate (55.3 mg, 0.25 mmol) was dissolved in dinitraminic acid (4 mL). Compound **4** was added in stoichiometric amounts. Complex **7** was obtained in the form of blue needle suitable for X-ray diffraction within five days. Yield: 143 mg (0.24 mmol, 96%).

DTA (5 °C min⁻¹) onset: 110 °C (exothermic); IR (ATR, cm⁻¹): $\tilde{\nu}$ = 3018 (w), 2976 (vw), 2906 (vw), 1651 (s), 1628 (s), 1571 (vs), 1513 (s), 1460 (m), 1432 (m), 1389 (w), 1375 (w), 1365 (w), 1322 (m), 1297 (w), 1279 (vs), 1243 (w), 1213 (s), 1202 (s), 1182 (vs), 1109 (s), 1075 (w), 1036 (s), 1000 (vs), 891 (vs), 854 (s), 828 (s), 755 (s), 743 (vs), 710 (s), 685 (s), 653 (s), 571 (m), 487 (m), 477 (w), 458

(m); EA ($C_6H_{10}CuN_{16}O_{14}$, 593.79): calcd: C 12.14, H 1.70, N 37.74%; found: C 12.08, H 1.72, N 37.32%; BAM drophammer: 2 J; BDIS: 14 mJ, BAM friction tester: 7 N; ESD: 1080 mJ (at grain size \approx 500–1000 μ m).

General method for the preparation of ECC 8 & 9

Copper(II) chlorate or Zinc(II) chlorate were prepared according to a literature known method.^{S37} Copper sulfate pentahydrate (62.4 mg, 0.25 mmol) or zinc sulfate heptahydrate (71.9 mg, 0.25 mmol) was dissolved in water (2 mL) and barium chlorate monohydrate (76.1 mg, 0.25 mmol) in water (4 mL) was added. Stirring was continued for 5 min and the solution was filtrated using a syringe filter. The solvent was removed under reduced pressure and acetonitrile was added. Stoichiometric amounts of ligand **4** dissolved in acetonitrile (2 mL) were added and the solution was left for crystalization.

[Cu(1-NET)₆](ClO₃)₂ (**8**)

Blue platelets of complex **8** suitable for single crystal X-ray diffraction were obtained within a week. Yield: 249 mg (0.21 mmol, 84%).

DTA (5 °C min⁻¹) onset: 54 °C (endothermic), 149 °C (exothermic); IR (ATR, cm⁻¹): $\tilde{\nu}$ = 3104 (w), 3035 (vw), 2978 (vw), 2905 (vw), 1743 (vw), 1629 (vs), 1507 (m), 1451 (w), 1443 (w), 1389 (vw), 1367 (w), 1276 (vs), 1181 (m), 1109 (s), 1077 (w), 1065 (w), 1037 (m), 1008 (m), 961 (vs), 933 (s), 887 (vs), 847 (vs), 756 (m), 708 (m), 690 (m), 679 (m), 650 (s), 634 (m), 604 (m), 567 (m), 487 (m), 478 (s); EA ($C_{18}H_{30}CuN_{30}O_{24}$): calcd: C 18.24, H 2.55, N 35.46%; found: C 18.51, H 2.45, N 35.25%;

BAM drophammer: 2 J; BDIS: 55 mJ, BAM friction tester: 15 N; ESD: 250 mJ (at grain size \approx 500–1000 μm).

[Zn(1-NET)₆](ClO₃)₂ (9)

Colorless platelets of complex **9** suitable X-ray diffraction were obtained within a week. Yield: 237 mg (0.20 mmol, 80%).

DTA (5 °C min⁻¹) onset: 71 °C (endothermic), 154 °C (exothermic); IR (ATR, cm⁻¹): $\tilde{\nu}$ = 3020 (vw), 2979 (vw), 2904 (vw), 1643 (s), 1626 (vs), 1505 (m), 1453 (m), 1435 (w), 1390 (w), 1370 (w), 1278 (vs), 1178 (m), 1108 (s), 1079 (w), 1035 (m), 1004 (s), 961 (vs), 934 (s), 886 (vs), 844 (vs), 756 (m), 721 (w), 705 (m), 684 (m), 649 (s), 604 (m), 565 (m), 493 (m), 477 (s); EA (C₁₈H₃₀Cl₂CuN₃₀O₂₄): calcd: C 18.22, H 2.55, N 35.40%; found: C 18.36, H 2.60, N 35.30%; BAM drophammer: 7 J; BDIS: 69 mJ, BAM friction tester: 14 N; ESD: 750 mJ (at grain size \approx 500–1000 μm).

General method for the preparation of ECC 10–13

The respective metal perchlorate (**10**: Mn(ClO₄)₂ • 6 H₂O (90.5 mg, 0.25 mmol); **11**, **13**: Cu(ClO₄)₂ • 6 H₂O (92.6 mg, 0.25 mmol); **12**: Zn(ClO₄)₂ • 6 H₂O (93.1 mg, 0.25 mmol)) was dissolved in acetonitrile (2 mL). For the preparation of the complexes **10–12** stoichiometric amounts of ligand **4** were dissolved in acetonitrile (2 mL) and added. To obtain complex **13**, ligand **5** in acetonitrile (2 mL) was added instead of ligand **4**. The mixture was stirred for 5 min at ambient temperature. Subsequently the solution was left for crystallization.

[Mn(1-NET)₆](ClO₄)₂ (10)

Single crystals in the form of colorless blocks of compound **10** were obtained within two weeks. Due to the low melting point of the complex, it was not possible to isolate the compound on a large scale.

[Cu(1-NET)₆](ClO₄)₂ (11)

Blue blocks of compound **11** suitable for X-ray diffraction were obtained within two days. Yield: 231.2 mg (0.19 mmol, 76%).

DTA (5 °C min⁻¹) onset: 70, 117 °C (endothermic), 165 °C (exothermic); IR (ATR, cm⁻¹): $\tilde{\nu}$ = 3049 (vw), 3021 (vw), 2978 (vw), 2904 (vw), 1642 (s), 1631 (s), 1541 (vw), 1509 (m), 1496 (w), 1453 (w), 1429 (m), 1388 (w), 1369 (w), 1323 (w), 1280 (vs), 1243 (w), 1185 (m), 1175 (m), 1106 (s), 1082 (vs), 1046 (m), 1030 (s), 1000 (s), 961 (m), 934 (w), 882 (s), 839 (vs), 753 (m), 723 (w), 698 (m), 686 (m), 653 (s), 622 (vs), 565 (w), 544 (vw), 522 (w), 486(m); EA (C₁₈H₃₀Cl₂CuN₃₀O₂₆): calcd: C 17.76, H 2.48, N 34.53%; found: C 17.62, H 2.45, N 34.29%; BAM drophammer: 3 J; BDIS: > 200 mJ, BAM friction tester: 25 N; ESD: 480 mJ (at grain size < 100 μm).

[Zn(1-NET)₆](ClO₄)₂ (12)

Colorless blocks of compound **12** suitable for structure determination were obtained within two weeks. Due to the low melting point of the coordination compound, it was not possible to isolate the ECC on a large scale.

[Cu(2-NET)₆](ClO₄)₂ (13)

Blue blocks of compound **13** were obtained within a week. Yield: 270 mg (0.22 mmol, 89%).

DTA (5 °C min⁻¹) onset: 65 °C (endothermic), 143 °C (exothermic); IR (ATR, cm⁻¹): $\tilde{\nu}$ = 3036 (vw), 3027 (vw), 2977 (vw), 2905 (vw), 1742 (vw), 1631 (vs), 1554 (w), 1459 (w), 1434 (w), 1387 (w), 1365 (w), 1345 (vw), 1308 (w), 1278 (vs), 1248 (w), 1203 (w), 1189 (w), 1144 (m), 1096 (s), 1082 (vs), 1050 (s), 1035 (s), 1027 (s), 985 (m), 932 (w), 890 (vs), 850 (vs), 756 (s), 707 (m), 689 (s), 677 (s), 621 (vs), 570 (m), 516 (m), 508 (m), 490 (m), 463 (w); EA (C₁₈H₃₀Cl₂CuN₃₀O₂₆): calcd: C 17.76, H 2.48, N 34.53%; found: C 17.38, H 2.49, N 33.20%; BAM drophammer: 2 J; BDIS: 55 mJ, BAM friction tester: 5 N; ESD: 1080 mJ (at grain size \approx 100–500 μ m).

General method for the preparation of single crystals of ECC 14 & 15

Sodium azide (32.5 mg, 0.50 mmol) and the respective ligand **4** or **5** (238.7 mg, 1.5 mmol) were dissolved in water (6 mL). The solution was carefully layered with a 1:1 mixture of ethanol (4 mL) followed by copper(II) chloride dihydrate (42.6 mg, 0.25 mmol) dissolved in ethanol (6 mL).^{S38}

[Cu(N₃)₂(1-NET)] (14)

Copper(II) sulfate pentahydrate (62.4 mg, 0.25 mmol) was dissolved in water (4 mL) and stoichiometric amounts of ligand **4** were added.^{S38} The solution was heated to 60 °C until the complete dissolution of the ligand. Sodium azide (32.5 mg, 0.50 mmol) dissolved in water (2 mL) was added dropwise over a period of 5 min. Stirring was continued for 15 min. The formed brown precipitate was filtered off and washed with water (20 mL). Coordination compound **14** was obtained as a brown solid. Yield: 64.4 mg (0.21 mmol, 82%).

Single crystals in the form of brown platelets according to the general procedure were obtained within a week.

DTA (5 °C min⁻¹) onset: 122 °C (exothermic); IR (ATR, cm⁻¹): $\tilde{\nu}$ = 3110 (w), 3024 (vw), 2094 (s), 2076 (s), 2050 (vs), 2041 (vs), 1976 (w), 1752 (vw), 1642 (s), 1506 (m), 1450 (w), 1432 (m), 1385 (vw), 1371 (w), 1343 (vw), 1279 (s), 1234 (w), 1181 (m), 1104 (m), 1079 (m), 1061 (w), 1050 (w), 1030 (w), 1015 (m), 992 (m), 903 (w), 887 (s), 846 (s), 753 (m), 718 (vw), 692 (m), 659 (s), 637 (w), 601 (m), 595 (w), 585 (w), 572 (w), 485 (w), 416 (w), 410 (w); EA (C₃H₅CuN₁₁O₃): calcd: C 11.75, H 1.64, N 50.24%; found: C 12.04, H 1.84, N 49.26%; BAM drophammer: 4 J; BDIS: ≤ 4 mJ, BAM friction tester: 1 N; ESD: 14 mJ (at grain size < 100 μm).

[Cu₂(N₃)₄(2-NET)] (15)

Brown platelets of ECC **15** were obtained within two weeks according to the general procedure. An elemental analysis pure isolation of the coordination compound was not possible.

[Ag₂(CNO)₂(1-NET)] (16a)

Complex **16a** was prepared according to a recently published procedure.⁵³⁹ Silver fulminate (37.5 mg, 0.25 mmol) was dissolved in a mixture of water (2 mL) and acetonitrile (2 mL) at 60 °C. Ligand **4** (159.1 mg,) dissolved in acetonitrile (2 mL) were added and stirring was continued for 5 min. Collorless needles of **16a** suitable for X-ray diffraction were isolated within two days. Yield: 49.0 mg (0.11 mmol, 43%).

DTA (5 °C min⁻¹) onset: 96 °C (endothermic), 123 °C (exothermic); IR (ATR, cm⁻¹): $\tilde{\nu}$ = 3032 (vw), 2970 (vw), 2905 (vw), 2311 (w), 2295 (w), 2248 (m), 2106 (s), 2089 (vs), 1641 (s), 1634 (s), 1595 (m), 1558 (m), 1494 (m), 1447 (m), 1436 (m), 1330 (w), 1313 (w), 1279 (vs), 1218 (vw), 1173 (m), 1155 (vs), 1127 (s), 1105 (s), 1058 (m), 983 (s), 901 (m), 887 (m), 853 (vs), 763 (m), 753 (s), 718 (m), 708 (w), 687 (w), 681 (w), 659 (s), 605 (m), 578 (w), 503 (w), 483 (m), 464 (m); EA (C₅H₅Ag₂N₇O₅, 459.88): calcd: C 13.09, H 1.10, N 21.37%; found: C 13.20, H 1.03, N 21.28%; BAM drophammer: ≤ 1 J; BDIS: 8 mJ, BAM friction tester: 20 N; ESD: 250 mJ (at grain size > 1000 μm).

[Ag(CNO)(1-NET)] (16b)

Complex **16b** was formed by leaving the silver fulminate complex 16a for four weeks in a closed vessel in its mother liquor. Yield: 64.8 mg (0.21 mmol, 84%).

DTA (5 °C min⁻¹) onset: 67 °C (endothermic), 102 °C (endothermic followed by exothermic); IR (ATR, cm⁻¹): $\tilde{\nu}$ = 3139 (m), 3019 (w), 2976 (w), 2905 (w), 2303 (w), 2096 (m), 2066 (m), 1640 (s), 1635 (s), 1627 (s), 1487 (m), 1436 (w), 1417 (m), 1365 (w), 1322 (w), 1316 (w), 1280 (vs), 1180 (m), 1152 (s), 1109 (s), 1081 (m), 1034 (m), 1001 (s), 979 (m), 967 (m), 887 (vs), 878 (s), 849 (vs), 752 (s), 722 (w), 687 (s), 660 (s), 631 (m), 580 (m), 478 (m); EA (C₄H₅AgN₆O₄, 308.99): calcd: C 15.55, H 1.63, N 27.20%; found: C 15.57, H 1.62, N 27.31%; BAM drophammer: 9 J; BDIS: 83 mJ, BAM friction tester: 60 N; ESD: 250 mJ (at grain size 100–500 μm).

General procedure for the preparation of the coordination compounds **17–19**

The preparation of the ECC **17–19** was performed according to our previous work.^{S40} Basic copper(II) carbonate (0.25 mmol) was reacted with the corresponding trinitrobenzene derivative based acid (**17**: 115 mg, 0.50 mmol; **18a**: 122.6 mg, 0.50 mmol; **18b**: 61.3 mg, 0.25 mmol; **19**: 131 mg, 0.50 mmol) in water (4 mL) at 80 °C. After the complete dissolution of both compounds, ligand **4** was added in stoichiometric amounts. Mechanical stirring was continued for 5 min. Subsequently the solution was left for crystallization at ambient temperature.

[Cu(1-NET)₂(PA)₂] (**17**)

Single crystals in the form of green platelets of the picrate complex **17** were obtained after two days 360.3 mg (0.43 mmol, 86%).

DTA (5 °C min⁻¹) onset: 197 °C (exothermic); IR (ATR, cm⁻¹): $\tilde{\nu}$ = 3088 (w), 3036 (w), 1656 (m), 1629 (m), 1607 (s), 1574 (s), 1526 (vs), 1506 (s), 1454 (m), 1427 (m), 1419 (m), 1390 (w), 1360 (m), 1338 (s), 1276 (vs), 1166 (s), 1100 (s), 1086 (s), 1037 (m), 1025 (m), 1006 (m), 956 (w), 936 (m), 915 (m), 905 (m), 895 (m), 884 (s), 845 (s), 785 (m), 760 (w), 742 (m), 715 (s), 707 (s), 688 (s), 659 (s), 634 (m), 574 (w), 552 (m), 523 (m), 486 (w), 462 (w), 428 (vw); EA (C₁₈H₁₄CuN₁₆O₂₀, 837.95): calcd: C 25.80, H 1.68, N 26.75%; found: C 25.85, H 1.50, N 26.65%; BAM drophammer: 20 J; BDIS: > 200 mJ, BAM friction tester: > 360 N; ESD: 480 mJ (at grain size < 100 μm).

[Cu(1-NET)₂(TNR)] (**18a**)

Compound **18a** was obtained as dark green blocks suitable for X-ray diffraction within a day. Yield: 250.5 mg (0.40 mmol, 80%).

DTA (5 °C min⁻¹) onset: 195 °C (exothermic); IR (ATR, cm⁻¹): $\tilde{\nu}$ = 2910 (w), 1751 (w), 1636 (m), 1618 (w), 1584 (s), 1543 (m), 1524 (s), 1484 (m), 1471 (m), 1429 (s), 1385 (m), 1367 (m), 1344 (w), 1294 (s), 1276 (vs), 1244 (s), 1232 (s), 1172 (m), 1142 (m), 1100 (s), 1066 (w), 1034 (m), 1016 (m), 959 (w), 944 (w), 898 (m), 880 (m), 847 (s), 791 (m), 775 (m), 755 (m), 708 (vs), 690 (m), 682 (m), 650 (m), 570 (w), 492 (w), 473 (w), 433 (w), 423 (m), 418 (m); EA (C₁₂H₁₁CuN₁₃O₁₄, 624.84): calcd: C 23.07, H 1.77, N 29.14%; found: C 23.30, H 1.658, N 29.90%; BAM drophammer: 2 J; BDIS: 111 mJ, BAM friction tester: 96 N; ESD: 480 mJ (at grain size < 100 μm).

[Cu(HTNR)₂(1-NET)₂] • 2 H₂O (18b)

Single crystals in the form of green blocks of compound **18b** were obtained after one day when recrystallizing complex **18a** in hot water. An elemental analysis pure isolation of the coordination compound was not possible.

[Cu(HTNR)₂(1-NET)₄] (18c)

Compound **18c** was obtained as green blocks suitable for X-ray diffraction within a day. Yield: 332.7 mg (0.28 mmol, 56%).

DTA (5 °C min⁻¹) onset: 167 °C (exothermic); IR (ATR, cm⁻¹): $\tilde{\nu}$ = 3142 (w), 1641 (s), 1627 (s), 1558 (m), 1537 (s), 1533 (s), 1479 (m), 1456 (m), 1436 (m), 1373 (m), 1353 (m), 1312 (s), 1279 (vs), 1242 (m), 1170 (s), 1090 (s), 1030 (m), 1008 (m), 989 (m), 928 (m), 909 (w), 890 (m), 877 (m), 844 (m), 784 (w), 759 (w), 735 (m), 715 (m), 696 (s), 679 (s), 657 (m), 568 (w); EA (C₂₄H₂₄CuN₂₆O₂₈, 1188.16): calcd: C 24.26, H 2.04, N 30.65%; found: C 24.43, H 1.79, N 25.40%; BAM drophammer: 5 J; BDIS: > 200 mJ, BAM friction tester: 96 N; ESD: >1500 mJ (at grain size ≈ 500–1000 μm).

[Cu(H₂TNPG)₂(1-NET)₄] (19)

After two days single crystals in the form of green blocks of ECC **19** were obtained. Yield 414.9 mg (0.34 mmol, 68%).

DTA (5 °C min⁻¹) onset: 169 °C (exothermic); IR (ATR, cm⁻¹): $\tilde{\nu}$ = 3024 (w), 2979 (w), 2907 (w), 1635 (vs), 1568 (m), 1505 (s), 1497 (s), 1454 (m), 1426 (m), 1394 (w), 1333 (s), 1277 (vs), 1233 (w), 1179 (s), 1155 (s), 1136 (s), 1099 (s), 1043 (m), 1030 (s), 1007 (s), 914 (m), 892 (s), 851 (s), 835 (s), 814 (s), 785 (s), 758 (s), 731 (s), 708 (s), 693 (s), 678 (s), 649 (s), 632 (s), 625 (s), 568 (m), 538 (w), 519 (w), 505 (w), 490 (m), 458 (w); EA (C₃H₅CuN₁₁O₃, 1220.15): calcd: C 23.63, H 1.98, N 29.85%; found: C 23.75, H 1.94, N 29.72%; BAM drophammer: 2 J; BDIS: > 200 mJ, BAM friction tester: 96 N; ESD: 1080 mJ (at grain size \approx 500–1000 μ m).

General procedure for the preparation of the coordination compounds 20–22

The coordination compounds **20–22** were prepared according to our previous work.^{S40} Basic copper(II) carbonate (0.25 mmol) was reacted with the corresponding trinitrobenzene derivative based acid (**20**: 115 mg, 0.50 mmol; **21**: 61.3 mg, 0.25 mmol; **22a**: 65.3 mg, 0.25 mmol; **22b–c**: 131 mg, 0.50 mmol) in water (4 mL) at 80 °C. After the complete dissolution of both compounds, ligand **5** was added in stoichiometric amounts. Mechanical stirring was continued for 5 min. Subsequently the solution was left for crystallization at ambient temperature.

[Cu(2-NET)₂(PA)₂] (20)

Single crystals in the form of green platelets of the picrate complex **20** were obtained after two days. Yield: 310.0 mg (0.37 mmol, 74%).

DTA (5 °C min⁻¹) onset: 165 °C (endothermic followed by exothermic); IR (ATR, cm⁻¹): $\tilde{\nu}$ = 3101 (w), 3022 (w), 2987 (w), 2972 (w), 2914 (w), 2850 (vw), 1633 (vs), 1611 (s), 1579 (vs), 1538 (vs), 1510 (vs), 1475 (m), 1471 (m), 1438 (m), 1430 (m), 1417 (m), 1402 (w), 1390 (w), 1364 (s), 1337 (vs), 1309 (s), 1283 (vs), 1267 (vs), 1251 (vs), 1198 (s), 1167 (s), 1141 (vs), 1102 (m), 1085 (s), 1059 (m), 1036 (m), 1003 (s), 970 (m), 947 (m), 933 (w), 922 (m), 916 (m), 901 (m), 890 (s), 843 (s), 827 (s), 788 (s), 752 (m), 744 (s), 723 (s), 714 (s), 706 (s), 693 (s), 676 (s), 637 (m), 571 (m), 554 (m), 536 (m), 510 (s), 442 (m); EA (C₁₈H₁₄CuN₁₆O₂₀, 837.95): calcd: C 25.80, H 1.68, N 26.75%; found: C 25.85, H 1.75, N 26.94%; BAM drophammer: 3 J; BDIS: > 200 mJ, BAM friction tester: 192 N; ESD: 1080 mJ (at grain size \approx 500–1000 μ m).

[Cu(2-NET)₂(TNR)] (21)

The syphnate complex **21** was obtained as green plates suitable for X-ray diffraction in four days. Yield: 249.9 mg (0.40 mmol, 80%).

DTA (5 °C min⁻¹) onset: 161 °C (exothermic); IR (ATR, cm⁻¹): $\tilde{\nu}$ = 3156 (w), 3103 (vw), 3033 (vw), 2971 (vw), 2921 (vw), 2889 (vw), 1647 (m), 1623 (m), 1586 (s), 1543 (s), 1527 (s), 1481 (m), 1468 (s), 1436 (s), 1378 (s), 1363 (m), 1310 (m), 1292 (s), 1274 (vs), 1243 (s), 1228 (s), 1213 (s), 1195 (s), 1171 (s), 1155 (m), 1142 (s), 1105 (s), 1053 (m), 1034 (m), 1018 (m), 1012 (m), 985 (m), 966 (w), 930 (w), 904 (m), 884 (s), 860 (m), 844 (s), 789 (w), 775 (m), 755 (m), 733 (w), 706 (s), 699 (vs), 676 (s), 667 (m), 645 (m), 590 (w), 574 (m), 513 (m), 466 (w), 422 (m); EA (C₁₂H₁₁CuN₁₃O₁₄, 624.84): calcd: C 23.07, H 1.77, N 29.14%; found: C 23.06, H 1.73, N 29.04%; BAM drophammer: \leq 1 J; BDIS: 138 mJ, BAM friction tester: 80 N; ESD: 750 mJ (at grain size < 100 μ m).

[Cu(HTNPG)(2-NET)₂] (22a)

Dark green blocks from compound **22a** suitable for crystal structure determination were obtained within ten days. Yield: 211.5 mg (0.33 mmol, 66%).

DTA (5 °C min⁻¹) onset: 112 °C (exothermic); IR (ATR, cm⁻¹): $\tilde{\nu}$ = 3153 (w), 3033 (w), 2972 (vw), 2919 (vw), 2891 (vw), 1638 (s), 1623 (s), 1578 (m), 1494 (vs), 1454 (s), 1435 (s), 1393 (m), 1386 (m), 1361 (s), 1349 (s), 1317 (s), 1310 (s), 1298 (m), 1272 (vs), 1231 (m), 1212 (s), 1194 (s), 1175 (s), 1157 (s), 1141 (s), 1090 (m), 1053 (m), 1035 (s), 1017 (m), 1010 (m), 983 (w), 966 (w), 922 (m), 901 (s), 883 (s), 849 (s), 842 (s), 824 (s), 786 (s), 754 (m), 730 (m), 711 (s), 697 (s), 675 (s), 649 (s), 574 (m), 537 (vw), 514 (m), 506 (m), 467 (w), 441 (m), 421 (m); EA (C₁₂H₁₁CuN₁₃O₁₅, 640.84): calcd: C 22.49, H 1.73, N 28.41%; found: C 22.31, H 2.02, N 31.87%; BAM drophammer: 4 J; BDIS: > 200 mJ, BAM friction tester: 324 N; ESD: 750 mJ (at grain size \approx 500–1000 μ m).

[Cu(H₂TNPG)₂(2-NET)₄] (22b)

Complex **22b** was isolated after seven days in the form of green plates blocks suitable for single crystal diffraction experiments. Yield: 524.7 mg (0.43 mmol, 86%).

DTA (5 °C min⁻¹) onset: 105 °C (exothermic); IR (ATR, cm⁻¹): $\tilde{\nu}$ = 3026 (w), 2979 (vw), 2913 (vw), 1652 (vs), 1646 (s), 1627 (s), 1558 (s), 1525 (s), 1520 (s), 1515 (s), 1475 (m), 1460 (m), 1446 (w), 1428 (m), 1405 (w), 1361 (s), 1345 (s), 1305 (m), 1278 (vs), 1216 (s), 1185 (s), 1163 (s), 1145 (s), 1092 (w), 1058 (w), 1043 (m), 1031 (s), 1020 (m), 1007 (m), 963 (vw), 917 (m), 903 (s), 886 (m), 853 (s), 837 (s), 815 (s), 794 (m), 782 (s), 747 (s), 710 (s), 693 (s), 688 (s), 681 (s), 671 (s), 649 (m), 626 (s), 605 (m), 570 (m), 515 (m), 497 (w), 475 (w), 425 (w); EA (C₂₄H₂₄CuN₂₆O₃₀, 1220.15): calcd:

C 23.63, H 1.98, N 29.85%; found: C 23.52, H 2.05, N 29.87%; BAM drophammer: 4 J; BDIS: > 200 mJ, BAM friction tester: 324 N; ESD: 750 mJ (at grain size \approx 500–1000 μm).

[Cu(H₂TNPG)₂(2-NET)₄] • 2 2-NET (22c)

The co-crystalizing coordination compound **22c** was isolated after ten days in the form of green platelets suitable for single crystal diffraction experiments. Yield: 523.0 mg (0.34 mmol, 68%).

DTA (5 °C min⁻¹) onset: 92 (endothermic), 105 °C (exothermic); IR (ATR, cm⁻¹): $\tilde{\nu}$ = 1651 (s), 1645 (s), 1558 (m), 1513 (vs), 1471 (m), 1457 (m), 1442 (w), 1429 (m), 1360 (s), 1344 (s), 1307 (m), 1279 (vs), 1213 (s), 1192 (s), 1183 (s), 1164 (s), 1146 (s), 1090 (m), 1051 (m), 1037 (m), 1007 (m), 986 (w), 916 (m), 901 (s), 841 (s), 815 (m), 781 (s), 752 (s), 709 (s), 691 (vs), 672 (s), 648 (s), 624 (s), 569 (m), 514 (w), 509 (w), 497 (m), 491 (m), 469 (w), 424 (w); EA (C₃₀H₃₄CuN₃₆O₃₆, 1538.36): calcd: C 23.42, H 2.23, N 32.78%; found: C 23.37, H 2.16, N 32.82%; BAM drophammer: 4 J; BDIS: > 200 mJ, BAM friction tester: 60 N; ESD: 750 mJ (at grain size \approx 100–500 μm).

9. References

- S1 CrysAlisPRO (Version 171.33.41), Oxford Diffraction Ltd., 2009.
- S2 A. Altomare, G. Cascarano, C. Giacovazzo, and A. Guagliardi, *J. Appl. Crystallogr.*, 1992, **26**, 343.
- S3 A. Altomare, G. Cascarano, C. Giacovazzo, A. Guagliardi, A. G. G. Moliterni, M. C. Burla, G. Polidori, M. Camalli and R. Spagna, SIR97, 2003.
- S4 A. Altomare, M. C. Burla, M. Camalli, G. L. Cascarano, C. Giacovazzo, A. Guagliardi, A. G. G. Moliterni, G. Polidori and R. Spagna, *J. Appl. Crystallogr.*, 1999, **32**, 115.
- S5 G. M. Sheldrick, SHELXL-97, University of Göttingen, Germany, 1997.
- S6 G. M. Sheldrick, *Acta Crystallogr. Sect. A*, 2008, **64**, 112.
- S7 G. M. Sheldrick, *Acta Cryst. A*, 2015, **71**, 3–8.
- S8 A. L. Spek, PLATON, Utrecht University, The Netherlands, 1999.
- S9 L.J. Farrugia, *J. Appl. Cryst.*, 2012, **45**, 849.
- S10 O. V. Dolomanov, L. J. Bourhis, R. J. Gildea, J. A. K. Howard and H. Puschmann, *J. Appl. Cryst.*, 2009, **42**, 339–341.
- S11 Empirical absorption correction using spherical harmonics, implemented in SCALE3 ABSPACK scaling algorithm (CrysAlisPro Oxford Diffraction Ltd., Version 171.33.41, 2009).
- S12 APEX3, Bruker AXS Inc., Madison, Wisconsin, USA.
- S13 M. J. Frisch, G. W. Trucks, H. B. Schlegel, G. E. Scuseria, M. A. Robb, J. R. Cheeseman, G. Scalmani, V. Barone, B. Mennucci, G. A. Petersson, H. Nakatsuji, M. Caricato, X. Li, H.P. Hratchian, A. F. Izmaylov, J. Bloino, G. Zheng, J. L. Sonnenberg, M. Hada, M. Ehara, K. Toyota, R. Fukuda, J. Hasegawa, M. Ishida, T. Nakajima, Y. Honda, O. Kitao, H. Nakai, T. Vreven, J. A. Montgomery, Jr., J. E. Peralta, F. Ogliaro, M. Bearpark, J. J. Heyd, E. Brothers, K. N. Kudin, V. N. Staroverov, R. Kobayashi, J. Normand, K. Raghavachari, A. Rendell, J. C. Burant, S. S. Iyengar, J. Tomasi, M. Cossi, N. Rega, J. M. Millam, M. Klene, J. E. Knox, J. B. Cross, V. Bakken, C. Adamo, J. Jaramillo, R. Gomperts, R. E. Stratmann, O. Yazyev, A. J. Austin, R. Cammi, C. Pomelli, J. W. Ochterski, R. L. Martin, K. Morokuma, V. G. Zakrzewski, G. A. Voth, P. Salvador, J. J. Dannenberg, S. Dapprich, A. D. Daniels, O. Farkas, J.B. Foresman, J. V. Ortiz, J. Cioslowski and D. J. Fox, Gaussian 09 A.02, Gaussian, Inc., Wallingford, CT, USA, 2009.
- S14 J. W. Ochterski, G. A. Petersson and J. A. Montgomery Jr., *J. Chem. Phys.*, 1996, **104**, 2598–2619.

- S15 J. A. Montgomery Jr., M. J. Frisch, J. W. Ochterski and G. A. Petersson, *J. Chem. Phys.*, 2000, **112**, 6532–6542.
- S16 L. A. Curtiss, K. Raghavachari, P. C. Redfern and J. A. Pople, *J. Chem. Phys.*, 1997, **106**, 1063–1079.
- S17 E. F. C. Byrd and B. M. Rice, *J. Phys. Chem. A*, 2006, **110**, 1005–1013.
- S18 B. M. Rice, S. V. Pai and J. Hare, *Comb. Flame*, 1999, **118**, 445–458.
- S19 P. J. Lindstrom and W. G. Mallard, NIST Standard Reference Database Number 69, <http://webbook.nist.gov/chemistry/>, (accessed March 2021).
- S20 M. S. Westwell, M. S. Searle, D. J. Wales and D. H. Williams, *J. Am. Chem. Soc.* 1995, **117**, 5013–5015.
- S21 F. Trouton, *Philos. Mag.* 1884, **18**, 54–57.
- S22 M. J. Turner, J. J. McKinnon, S. K. Wolff, D. J. Grimwood, P. R. Spackman, D. Jayatilaka and M. A. Spackman, *CrystalExplorer17*, University of Western Australia, 2017.
- S23 NATO standardization agreement (STANAG) on explosives, impact sensitivity tests, no. 4489, 1st ed., Sept. 17, 1999.
- S24 WIWEB-Standardarbeitsanweisung 4-5.1.02, Ermittlung der Explosionsgefährlichkeit, hier der Schlagempfindlichkeit mit dem Fallhammer, Nov. 8, 2002.
- S25 BAM, <http://www.bam.de>, (accessed March 2021).
- S26 OZM, <http://www.ozm.cz>, (accessed March 2021).
- S27 Military Standard 1751A (MIL-STD-1751A): safety and performance tests for qualification of explosives (high explosives, propellants and pyrotechnics), method 1016, Dec. 11, 2001.
- S28 M. S. Gruhne, M. Lommel, M. H. H. Wurzenberger, N. Szimhradt, T. M. Klapötke and J. Stierstorfer, *Propellants Explos. Pyrotech.*, 2020, **45**, 147–153.
- S29 NATO standardization agreement (STANAG) on explosive, friction sensitivity tests, no. 4487, 1st ed., Aug. 22, 2002.
- S30 WIWEB-Standardarbeitsanweisung 4-5.1.03, Ermittlung der Explosionsgefährlichkeit oder der Reibeempfindlichkeit mit dem Reibeapparat, Nov. 8, 2002.
- S31 UN Model Regulation: Recommendations on the Transport of Dangerous Goods – Manual of Tests and Criteria, section 13.4.2.3.3, 2015.
- S32 Impact: insensitive > 40 J, less sensitive ≥ 35 J, sensitive ≥ 4 J, very sensitive ≤ 3 J; Friction: insensitive > 360 N, less sensitive = 360 N, sensitive < 360 N and > 80 N, very sensitive ≤ 80 N, extremely sensitive ≤ 10 N. According to the UN Recommendations on the Transport of Dangerous Goods, 5th ed., 2009.

- S33 M. Sućeska, EXPLO5 Version 6.05 User's Guide. Zagreb, Croatia: OZM; 2018.
- S34 R. Seto, K. Matsumoto and T. Endo, *J. Polym. Sci. Pol. Chem.*, 2014, **52**, 1832–1842.
- S35 D. E. Bayes, R. Hayes, P. Blatcher and M. Atkinson, Eu. Pat., 0117368A1, Glaxo Group Ltd., 1982.
- S36 W. Finnegan and R. Henry, *J. Org. Chem.*, 1959, **24**, 1565–1567.
- S37 M. S. Gruhne, M. H. H. Wurzenberger, M. Lommel, J. Stierstorfer, *Chem. Eur. J.* 2021, in press.
- S38 M. H. H. Wurzenberger, N. Szimhardt and J. Stierstorfer, 2018, **140**, 3206–3209.
- S39 M. H. H. Wurzenberger, M. Lommel, M. S. Gruhne, N. Szimhardt and J. Stierstorfer, *Angew. Chem. Int. Ed.*, 2020, **59**, 12367–12370.
- S40 M. H. H. Wurzenberger, M. S. Gruhne, M. Lommel, V. Braun, N. Szimhardt and J. Stierstorfer, *Inorg. Chem.*, 2020, **59**, 17875–17879.
- S41 M. H. H. Wurzenberger, B. R. G. Bissinger, M. Lommel, M. S. Gruhne, N. Szimhardt and J. Stierstorfer, *New J. Chem.*, 2019, **43**, 18193–18202.

Tuning the Properties of 5-Azido and 5-Nitramino-tetrazoles by Diverse Functionalization – General Concepts for Future Energetic Materials

Maximilian Benz⁺,^[a] Thomas M. Klapötke,^{*[a]} Tobias Lenz⁺,^[a] and Jörg Stierstorfer^[a]

Abstract: 5-Azido and 5-nitraminotetrazole backbones are established heterocyclic motifs in the research field of energetic materials synthesis. Despite the high energy content of the compounds, the problem with many derivatives is that their sensitivities are far too high. Functionalization of one of the ring nitrogen atoms is the aim of this study to adjust the sensitivity by inserting nitrateoethyl, azidoethyl and methyl groups. In this context, derivatives of 2-(2-azidoethyl)-5-nitraminotetrazoles (**2**, **2a–2d**), as well as 1-nitrato and 1-azidoethyl substituted 5-azidotetrazole (**7** and **10**) and the methylation products of 5-azidotetrazole (5-azido-1-methyl-tetrazole, **11** and 5-azido-2-methyl-tetrazole,

12) were prepared. The obtained nitrogen-rich compounds were extensively characterized through multinuclear NMR spectroscopy and IR spectroscopy. The structural confinement was checked by X-ray diffraction experiments. The pure samples (verified by elemental analysis) were investigated regarding their behavior toward friction, impact (BAM methods) and electrostatic discharge as well as heating (DTA and DSC). For all metal-free compounds the detonation properties were computed with the EXPLO5 code using their density and heat of formation, calculated based on CBS-4 M level of theory.

Introduction

The application of energetic materials is spread over various fields and thus a material must fulfill suitable criteria.^[1] Explosives are divided into three main categories. A) Sensitive explosives, such as sensitizers, igniters or detonants; B) less sensitive but powerful explosives, secondary explosives; and C) insensitive, tertiary explosives. Many of the materials used were developed before or at the beginning of the 20th century, with only a little focus on sustainability or environmental impact.^[2] The common primary explosives are often heavy metal based, as there are lead azide or styphnate. Their use is found to contaminate training grounds and application sites.^[3] The secondary explosive trinitrotoluene, which is widely used due to its advantageous melt castable properties, shows to have disadvantageous environmental impact and is a possible carcinogenic, as stated by the U.S. Environmental Protection Agency.^[4a] The urgent need for sustainable and environmentally friendly replacements poses major challenges for the energetic

materials community.^[4b] A state-of-the-art synthetic approach consists of derivatization of known oxygen- and nitrogen-rich azoles in combination with short alkyl, azidoalkyl or nitrateoalkyl chains. Sabatini et al. found that bis-5-(nitratomethyl)bis(1,2,4-oxadiazole) (**c**) is suitable to replace trinitrotoluene while showing significantly higher performance data.^[5] Furthermore furazanes^[6], 1,2,3-triazoles^[7], 1,2,4-triazoles^[8], tetrazoles^[9] and pyrazoles^[10] were functionalized by energetic azido or nitrateoalkyl side chains (Figure 1).

In the search for ever higher nitrogen and energy contents, the energetic compounds, 5-nitramino-^[11] and 5-azidotetrazole^[12], arouse attention. Both molecules are intensively studied as free acids^[13] or salinized,^[14] and are promising building blocks due to their straight forward accessibility. Here we report different approaches to reduce the acidity of those high energy and nitrogen-rich tetrazole building blocks. Insights into the changes of the sensitivity are gained. For the 5-nitraminotetrazole replacement of the acidic tetrazole proton by an azidoethyl function led to a monobasic acid (**2**) that was further salinized (**2a–d**) to reduce the acidity, lower the vapor pressure and increase the thermal stability. Also melt-castable primary explosives would be of great interest. Therefore, the acidic proton of 5-azidotetrazole was exchanged by an azidoethyl (**7**), nitrateoethyl (**10**) or methyl (**11**, **12**) functionality. Functionalization reveals compounds that are suitable for various applications (Figure 2).

Synthesis

With the synthetic protocol for 2-(2-azidoethyl)-5-aminotetrazole (**1**) in hand, which was recently published by our group^[9a],

[a] M. Benz,⁺ Prof. Dr. T. M. Klapötke, T. Lenz,⁺ Dr. J. Stierstorfer
Department of Chemistry
Ludwig Maximilian University of Munich
Butenandstr. 5–13, D-81337 Munich (Germany)
E-mail: tmk@cup.uni-muenchen.de
Homepage: <http://www.hedm.cup.uni-muenchen.de>

[†] These authors contribute equality to this work.

Supporting information for this article is available on the WWW under <https://doi.org/10.1002/chem.202200772>

© 2022 The Authors. Chemistry - A European Journal published by Wiley-VCH GmbH. This is an open access article under the terms of the Creative Commons Attribution License, which permits use, distribution and reproduction in any medium, provided the original work is properly cited.

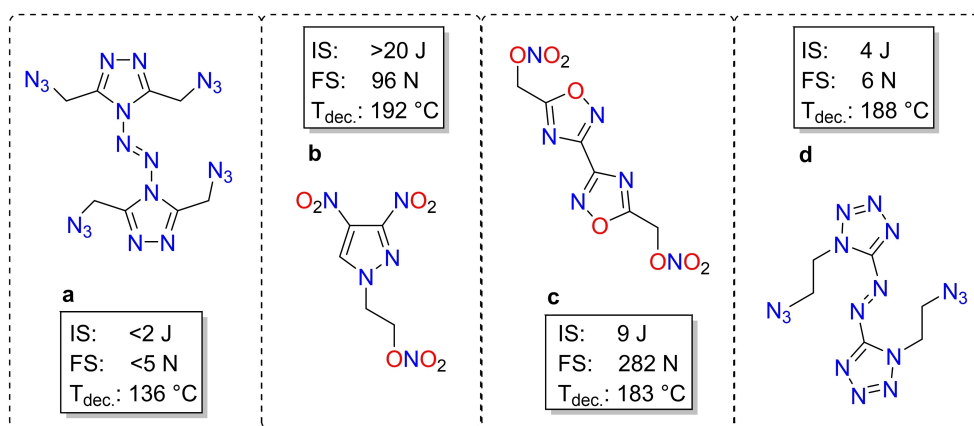


Figure 1. Representatives of energetic N-alkyl substituted azoles. 3,3',5,5'-Tetra(azidomethyl)-4,4'-azo-1,2,4-triazole (a), 1(2-nitrateethyl)-3,4-dinitropyrazole (b), bis(1,2,4-oxadiazole)bis(methylene) dinitrate (c) and 1,1'-bis(2-azidoethyl)-azotetrazole (d).

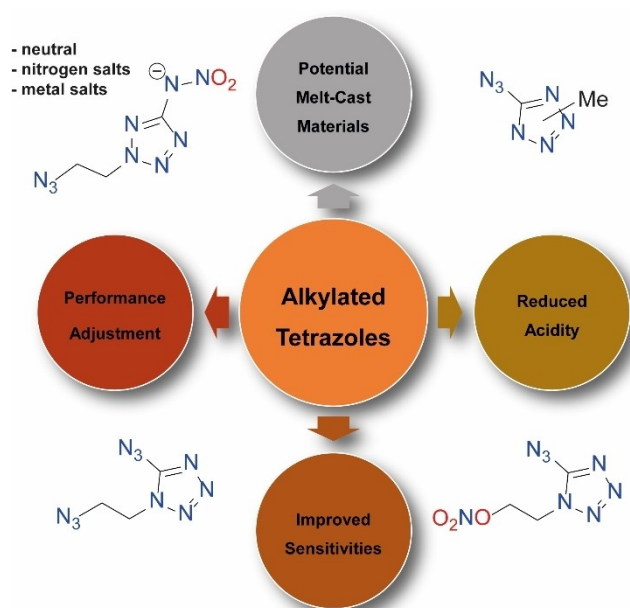
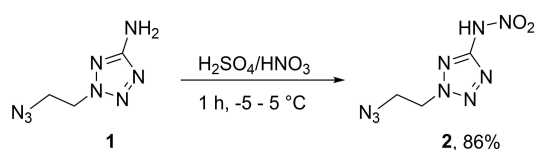


Figure 2. Derivatization of 5-azido- and 5-nitraminotetrazole reveals new applications.

we were investigating suitable conditions to perform the nitration of the amino function to the respective nitraminotetrazole **2**. We found a pre-cooled mixture of sulfuric acid and fuming nitric acid (ratio 8:3) to work best and this yields pure **2** without further purification in 86% yield (Scheme 1).

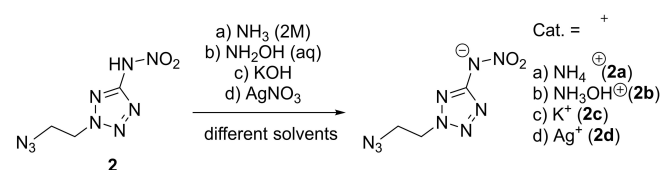


Scheme 1. Nitration of **1** to form the nitramino derivative **2** using mixed acid at low temperatures.

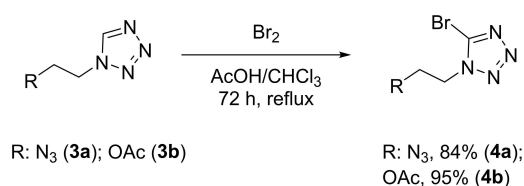
The nitrogen-rich salts **2a** and **2b** as well as the metal salts **2c** and **2d** were obtained by simple acid-base reactions of the free nitramine **2** and the respective base, or in the case of **2d** with AgNO_3 solution (Scheme 2). All compounds were obtained elemental analysis pure and could be analyzed without further purification. In attempting to prepare the hydrazinium salt of **2**, pure **1** was isolated. As has already occurred for other aromatic nitramines^[9b], the reaction with aqueous hydrazine leads to a reduction of the nitramine function to the amine.

To achieve functionalized 5-azidotetrazoles classic bromination of 5*H*-tetrazoles was performed for three days at reflux (Scheme 3). The 1-(2-azidoethyl)-tetrazole (**3a**) was reacted to 1-(2-azidoethyl)-5-bromotetrazole (**4a**) in very good yields. The bromination of 1-(2-acetoxyethyl)-tetrazole (**3b**) was performed similar to the literature,^[15] and 5-bromo-1-(2-acetoxyethyl)-tetrazole (**4b**) was yielded in excellent yields (Scheme 3).

Substitution at the 5-bromo position was then performed by hydrazine. The strong nucleophilicity of hydrazine and the



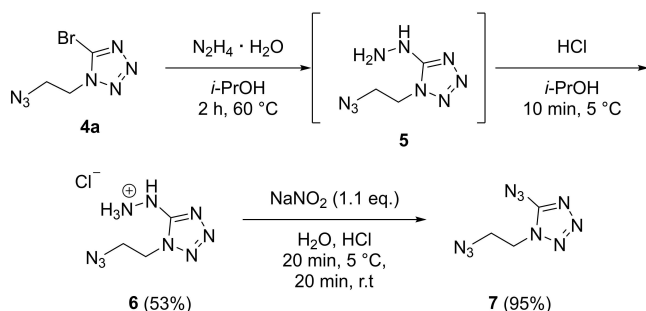
Scheme 2. Preparation of ionic derivatives **2a–2d** starting from the free nitramino derivative **2** through reaction with the respective cation containing reagents.



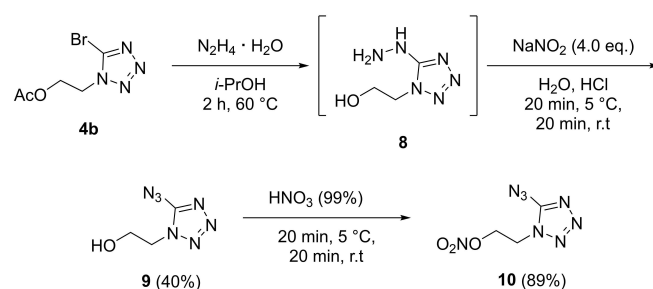
Scheme 3. Bromination of 1-functionalized 5*H*-tetrazoles.

low solubility of the resulting hydrazinium bromide in isopropanol makes bromine-hydrazine exchange possible, even at room temperature. The reaction was performed either at room temperature for three days or at elevated temperature for shorter periods of time. Compound **4a** can be reacted at 60 °C for 2 h to synthesize 1-(2-azidoethyl)-5-hydrazineyltetrazole (**5**). However slow decomposition at room temperature complicated the purification and therefore only a crystal structure and ¹H and ¹³C NMR were measured. To stabilize and purify compound **5** it was precipitated as hydrochloride salt, 1-(2-azidoethyl)-5-hydraziniumtetrazol chloride (**6**), from a concentrated isopropanol solution. The overall reaction from compound **4a** to compound **6** proceeds in acceptable yields. Finally, 1-(2-azidoethyl)-5-azidotetrazole (**7**) was synthesized through reaction of **6** with sodium nitrite under acidic conditions in excellent yields after column chromatography (Scheme 4).

Reaction of compound **4b** with hydrazine over three days at ambient temperature lead to 5-hydrazineyl-1-(2-hydroxyethyl)-tetrazole (**8**). The acetoxy moiety of **4b** reacts with hydrazine to acetohydrazide. Several attempts to purify compound (**8**) failed, only a crystal structure and ¹H and ¹³C NMR were measured. Also, a crystal structure of the hydrochloride was observed by a similar procedure than for **6** (can be found in the Supporting Information). The crude of **5** was reacted with sodium nitrite under acidic conditions to give 5-azido-1-(2-hydroxyethyl)-tetrazole (**9**). After column chromatography the overall yield from **4b** to **9** is 40%. In the last step of the synthesis towards 5-azido-1-(2-nitrateoethyl)-tetrazole (**10**), com-



Scheme 4. Reaction pathway towards 1-(2-azidoethyl)-5-azidotetrazole (**7**) by reacting the 5-position of the tetrazole from bromine to hydrazine to azide.



Scheme 5. Reaction pathway towards 5-Azido-1-(2-nitrateoethyl)-tetrazole (**10**) by bromine-hydrazine exchange followed by reaction with sodium nitrite and the nitration of the hydroxy group to its organic nitrate.

ound **9** was nitrated using white fuming nitric acid in very good yields (Scheme 5).

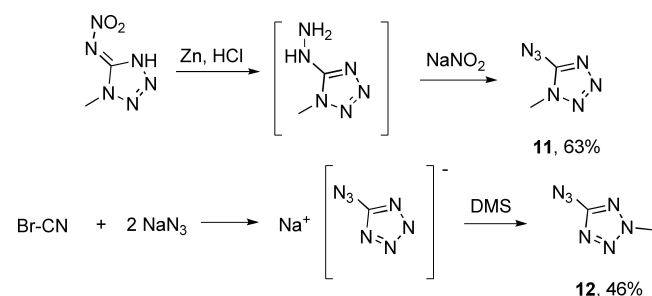
For the synthesis of the two isomers of 5-azido-methyltetrazole, various synthetic pathways had to be pursued as depicted in Scheme 6. Methylation of in situ generated 5-azidotetrazole with dimethyl sulfate produces only the 5-azido-2-methyltetrazole (**12**) isomer due to the two-position directing effect of the azido group. Therefore, an alternative route toward the 5-azido-1-methyltetrazole (**11**) had to be established starting with a 1-methyl substituted tetrazole derivative and subsequent generation of the azide function at position 5.

Thus, we started with 1-methyl-5-nitrimino-4H-tetrazole,^[16] and were able to reduce the nitrimino function with zinc dust under acidic conditions to the respective 5-hydrazino-1-methyltetrazole, which was directly converted to 5-azido-1-methyltetrazole (**11**) through diazotization using one equivalent of sodium nitrite.

Crystal Structures

Crystals suitable for X-ray diffraction experiments could be obtained by recrystallization from different common solvents for **2a**, **2b**, **2d** and **10–12**. Deposition Numbers 2157201 (for **2a**), 2157198 (for **2b**), 2157203 (for **2d**), 2157204 (for **5**), 2157196 (for **6**), 2157199 (for **7**), 2157197 (for **8·HCl**), 2157202 (for **9**), 2157200 (for **10**), 707542 (for **11**) and 707543 (for **12**) contain(s) the supplementary crystallographic data for this paper. These data are provided free of charge by the joint Cambridge Crystallographic Data Centre and Fachinformationszentrum Karlsruhe Access Structures service. Crystalline diazido derivative **7** could be generated and picked by cooling of a saturated solution of **7** in Et₂O at –30 °C since it is a liquid at room temperature. Additional information about the depicted crystal structures and the measuring and computation methods as well as further crystal structures for various precursor compounds (**5**, **6**, **8**, **9**) can be found in the Supporting Information.

Ammonium and hydroxylammonium salts **2a** and **2b** crystallize both in the triclinic space group *P*–1. As expected, the hydroxylammonium derivative has a slightly higher room temperature density (1.624 g cm^{–3} for **2b**) then the respective



Scheme 6. Pathway for selective synthesis of 5-azido-1-methyltetrazole (**11**) through diazotization of 5-hydrazino-1-methyltetrazole and 5-azido-2-methyltetrazole (**12**) through methylation of 5-azidotetrazole.

ammonium salt (1.575 g cm^{-3} for **2a**). The densities are in a range that was expected, when comparing them with related crystal structure densities. As shown in detail in previous studies^[9a,b,d] the densities of *N*-azidoethyl substituted tetrazoles are always well below those of *N*-nitroethyl substituted ones. Compared with the room temperature densities of the hydroxylammonium salts of 1- and 2-nitroethyl-5-nitraminotetrazole (density for both is 1.720 g cm^{-3})^[9e], the density of **2b** is about 0.1 g cm^{-3} lower, which was to be expected due to the substitution at position two.

The three-dimensional configuration of the two salts **2a** and **2b** behave very similarly and can be schematically divided into three different parts depicted in Figure 3 B) Figure 4 B). The interactions in the red areas are exclusively weak van der Waals interactions between the C-H protons of the ethyl groups and

the azide functions. The shortest ones can be found in **2b** (C2-H2 A...N19 2.65 \AA) and are therefore negligible for stability discussion due to their weak character. In the blue region are mainly the tetrazole rings, which also loosely interact with each other through π - π -interactions. But mainly this layer forms both, linking and buffer layer between non-polar, weakly interacting azidoethyl sites and the strongly stabilizing, polar sites consisting of the respective cations and nitramine functions, highlighted in green. In this region of the two crystal structures of **2a** and **2b**, dominated by strong polar interactions, the overall strongest intermolecular, ionic interactions are found. These are formed through all protons of the cations with the respective nitrogen and oxygen atoms of the nitramine function (O1, O2 and N6) as well as with N1 of the tetrazole moiety. The average bond length $d(\text{D-H}\cdots\text{A})$ is 2.06 \AA with O3-

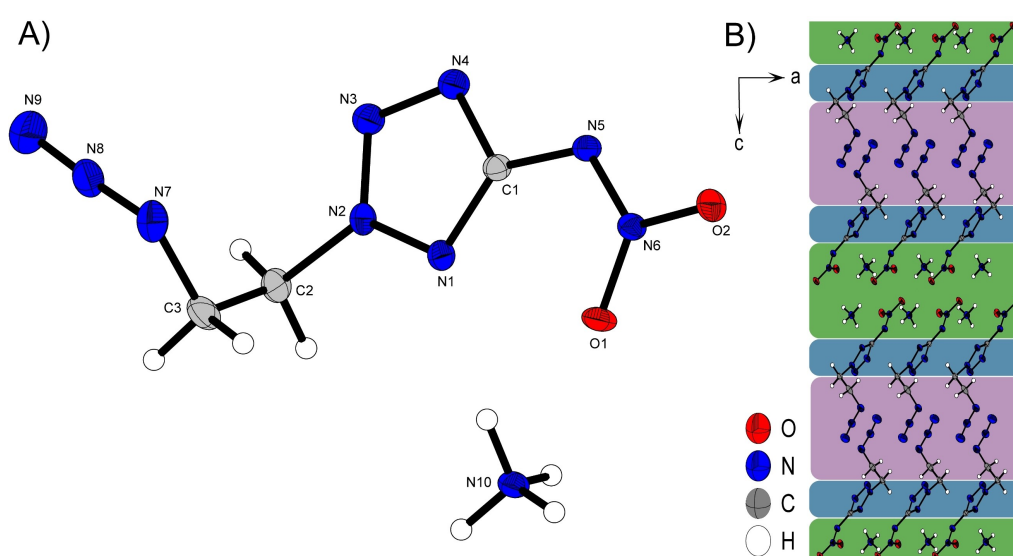


Figure 3. A) Molecular unit of **2a** with thermal ellipsoids drawn at the 50% probability level. Selected bond distances (\AA) and angles [$^\circ$]: C1-N5 1.382(2), C2-N2 1.467(2), N7-N8 1.241(2), N8-N9 1.128(2), N10-H10A...O1 2.10(2), N10-H10B...O2 2.02(2), N10-H10C...N1 2.12(2), N10-H10D...N5 2.05(2), N7-N8-N9 173.6(2), N7-C3-C2-N2 62.08(2), O1-N6-N5-C1 1.7(2); B) Layer structure of **2a** with view along the *b* axis. Green, blue and red regions are labeled based on their different components for intermolecular bond formation.

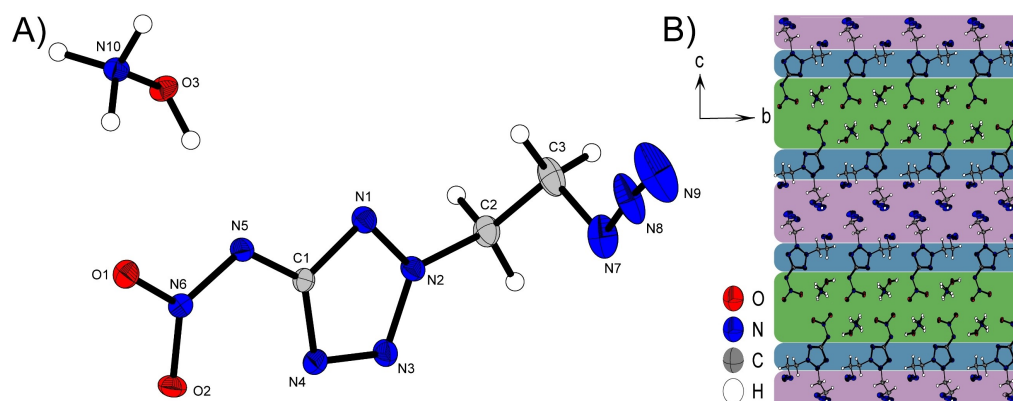


Figure 4. A) Asymmetric unit of **2b** with thermal ellipsoids drawn at the 50% probability level. Selected bond distances (\AA) and angles [$^\circ$]: C1-N5 1.392(3), C2-N2 1.472(3), N7-N8 1.256(3), N8-N9 1.128(4), N10-H10A...O4 2.22(3), N10-H10B...O2 2.08(3), N10-H10C...N11 2.13(3), N10-H10D...O5 2.15(3), O3-H3...N5 1.80(4), N7-N8-N9 173.5(4), N7-C3-C2-N2 69.9(3), O1-N6-N5-C1 0.2(2); B) Layer structure of **2b** with view along the *a* axis. Green, blue and red regions are labeled based on their different components for intermolecular bond formation.

H3...N5 1.80(4) Å being the shortest hydrogen bridge and therefore clearly below the van der Waals radius for a strong interaction.

Compound **2d** crystallizes in the orthorhombic space group *Pbca* with a density of 2.362 g cm⁻³ at 298 K and 16 molecular moieties per unit cell. The structure is mainly characterized by the formation of a close silver-silver contact. The neighboring anions arrange themselves around this structural motif in such manner that the formed argentophilic interaction can be interactively stabilized in the best possible way as depicted in Figure 5 B). Argentophilic interactions are van der Waals contact below a bond distance of 3.44 Å and can be observed in several Ag containing structures.^[17] Compared to the shortest ever measured Ag–Ag contact (2.7599(3) Å)^[18] the silver-silver distance is with a length of 3.0288(11) Å clearly above, but can still be considered as argentophilic interaction.^[19] The Ag–Ag building block is stabilized by four anionic moieties forming several close contacts. These interactions originate from one nitrogen and one oxygen of the nitramine function, the tetrazole nitrogen atoms N1 and N4 as well as from the γ -nitrogen of the azide functionality. These electron donating interactions of the complexing N and O atoms are observed in the range of 2.126(7) Å for Ag1–N14 to 3.154(10) Å for Ag1–N18ⁱⁱ. In order to optimize the assembly around the silver dimer, some unusual arrangements occur within the anion. For example, one nitramine group is clearly twisted out of the plane formed by the tetrazole (N6–N5–C1–N1 29.3(1)^o). However, this rotation improves the complexation of the silver. Nevertheless, this arrangement is unusual for 5-nitraminotetrazoles, which normally bear 5-substituted nitramino groups planar with the tetrazole ring.

Ethyl substituted 5-azidotetrazole derivatives crystallize in the orthorhombic space group *Fdd2* (for **7**) and in the monoclinic space group *P2₁/n* (for **10**). The molecular moieties

are depicted in Figure 6 and Figure 7. The room temperature density of nitraethoxy compound **10** is clearly superior to that of the azidoethyl derivative (1.519 g cm⁻³ for **7**, 1.638 g cm⁻³ for **10**). This trend has also been observed in previous studies^[20], since the nitraethoxy unit offers more possibilities for intermolecular interactions on the one hand and contains more and heavier atoms on the other, which also arrange themselves better in space. Since there are no good opportunities for intermolecular interactions for the present nonpolar residues, the three-dimensional structure of **7** is mainly based on the fact that the azido and azidoethyl substituents avoid each other with a as large spatial distance as possible in order to counteract possible destabilizing interaction (Figure 6 B)).

The three-dimensional pattern of **10** in Figure 7 B) shows the assembly of two molecular units resulting in a linear chain structure of those pairs along *b*. Schematically, a molecular unit of **10** consists of two molecular planes that diverge from each other at an angle of about 112^o. One plane is formed by the azidotetrazole backbone and the second by the ethyl group, in the linear direction of which the nitrate ester is connected (O3–N8–O1–C3 179.5(3)^o; N8–O1–C3–C2 175.1(2)^o). The molecular units within a pair always arrange themselves in an alternating manner, i.e. they are rotated 180^o to each other and thus a nitraethoxy rest is always superimposed with the azido function of its partner molecule.

The 1- and 2-methyl substituted 5-azidotetrazoles both crystallize in monoclinic systems, *P2₁/m* for **11** and *P2₁/c* for **12**. This also results in similar three-dimensional arrangements for both compounds. As shown in Figure 8 B) and Figure 7 B), layers are formed in the illustrated orientations. The alignment to layers is preferred firstly due to the planar character of **11** and **12**, and secondly as a result of the two hydrophobic azido and methyl substituents that do not form a good docking site for pronounced intermolecular interactions. The distances

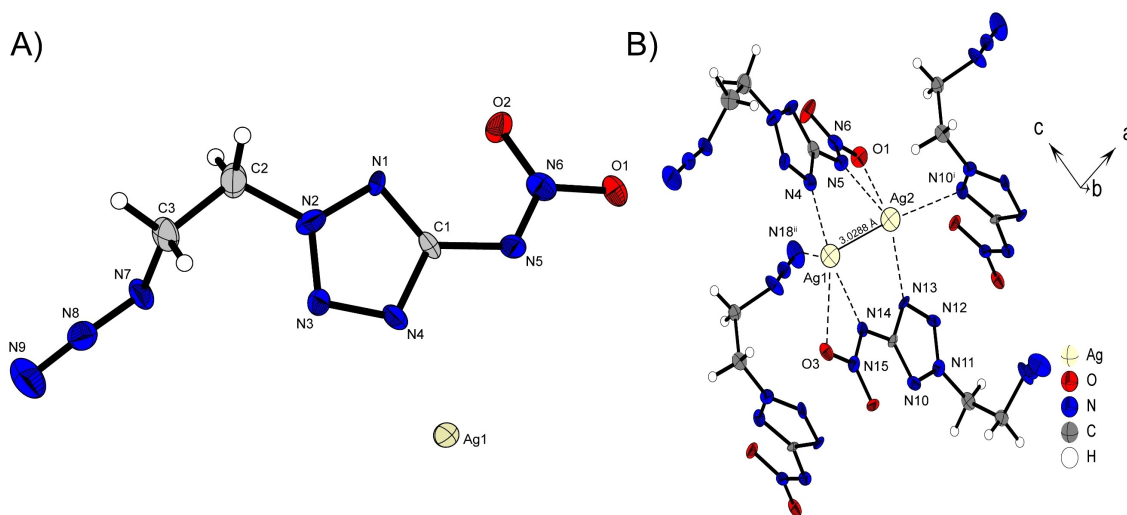


Figure 5. A) Asymmetric unit of **2d** with thermal ellipsoids drawn at the 50% probability level. Selected bond distances (Å) and angles [^o]: Ag1–Ag2 3.0288(11), Ag1–N14 2.126(7), Ag1–O3 2.877(6), Ag1–N4 2.137(7), Ag1–N18ⁱⁱ 3.154(10), Ag2–N13 2.216(7), Ag2–N5 2.201(7), Ag2–O1 2.822(7), Ag2–N10ⁱ 2.489(7), N14–Ag1–N4 167.3(3), N13–Ag2–N5 144.8(3), N15–N14–C4–N10 8.4(1), N6–N5–C1–N1 29.3(1); B) Representation of the argentophilic interaction between Ag1 and Ag2 with anionic moieties involved in the stabilization; Symmetry codes: (i) 0.5 + x, 0.5 – y, 1 – z, (ii) 1 – x, 1 – y, 1 – z.

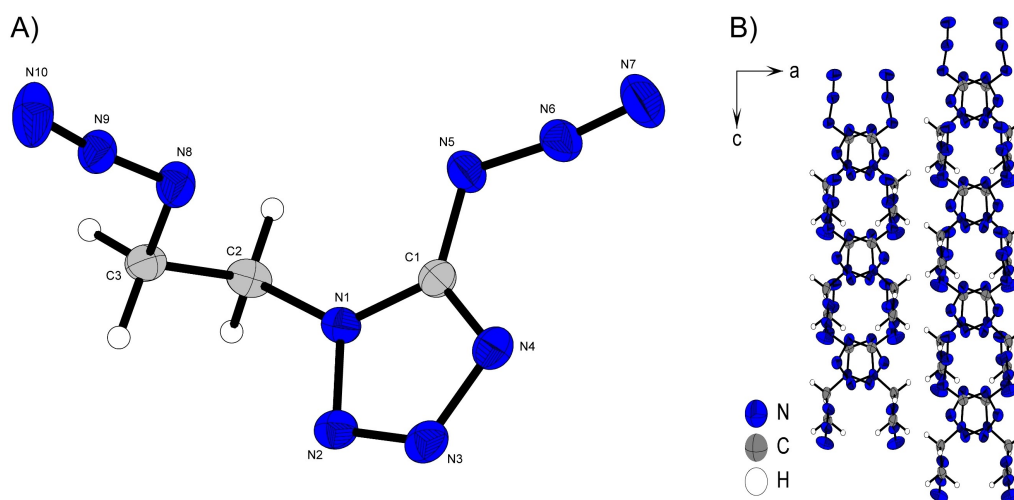


Figure 6. A) Molecular unit of **7** with thermal ellipsoids drawn at the 50% probability level. Selected bond distances (Å) and angles [°]: C1–N5 1.386(4), C2–N1 1.458(4), N5–N6 1.251(4), N6–N7 1.114(4), N8–N9 1.221(4), 1.127(4), N5–N6–N7 171.4(3), N8–N9–N10 172.9(3), N9–N8–C3–C2 171.1(3); B) Layer structure of **9** with view along the *b* axis.

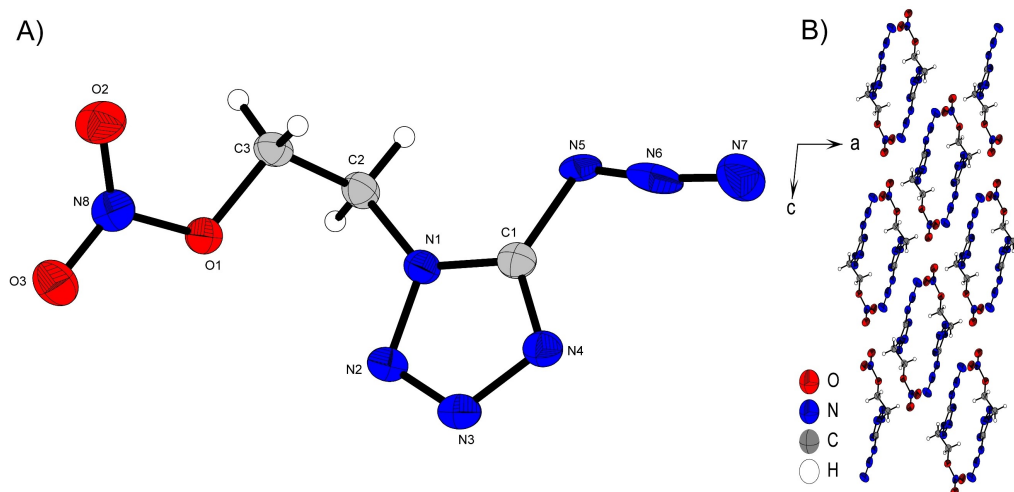


Figure 7. A) Molecular unit of **10** with thermal ellipsoids drawn at the 50% probability level. Selected bond distances (Å) and angles [°]: C1–N5 1.463(4), C2–N1 1.458(4), N5–N6 1.074(4), N6–N7 1.207(4), C3–O1 1.449(4), O1–N8 1.388(3), N5–N6–N7 171.5(3), N1–C2–C3 112.6(2), N6–N5–C1–N1 1.7(3); B) Layer structure of **10** with view along the *b* axis.

between the respective layers of the two 5-azido-methyltetrazoles are in the same range ($d(11)=3.12$ Å, $d(12)=3.31$ Å).

Despite the high structural conformity, the ordering of the molecular moieties within one layer changes as a result of the different substitution positions. **12** forms linear chains along the orientation depicted in Figure 9 B), with the azide group facing the methyl group with its γ -nitrogen (N7), and is therefore tightly embraced by these protons. Since this configuration of molecular units in **12** is more space saving than in the molecular pattern of **11**, significant differences arise in the density of the isomers. **11** comes up with a density of 1.459 g cm⁻³ at 298 K whereas, **12** is about 0.08 g cm⁻³ more dense than its respective one substituted isomer ($\rho(12)=1.542$ g cm⁻³).

NMR Spectroscopy

All compounds were characterized through ¹H and ¹³C{¹H} NMR spectroscopy and the respective resonances are listed in Table 1.

Resonances for the azidoethyl function at position 2 in compounds **2** and **2a–2d** can be found in the range of 4.69–4.94 ppm as multiplets (¹H) and 51.6–53.0 ppm (¹³C) representing the CH₂-group linked to the tetrazole ring and at 3.86–3.97 ppm as multiplets (¹H) and 48.9–49.6 ppm (¹³C) representing the CH₂ protons bonded to N $_{\alpha}$. Additional proton signals for these compounds can be found for **2** (nitramine proton) as broad peak at $\delta=9.69$ ppm and the cationic moieties for **2a** and **2b** at $\delta=7.17$ and 10.03 ppm, respectively. The deprotonation of **2** results in a shift to deeper fields of the tetrazole

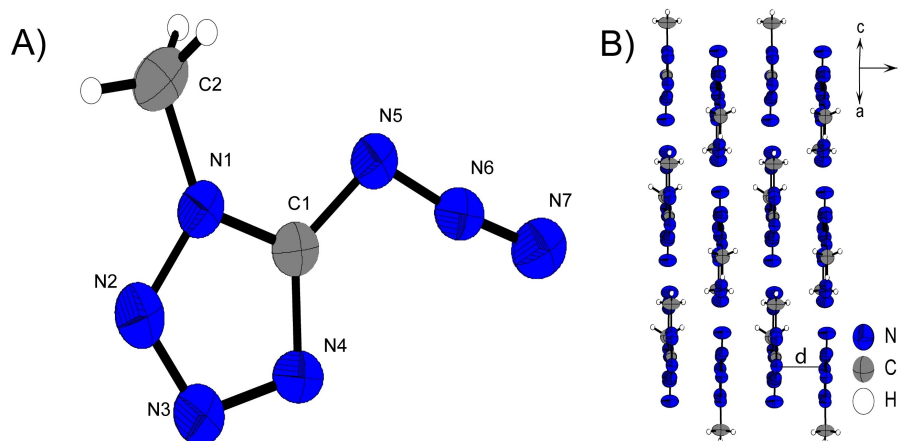


Figure 8. A) Molecular unit of **11** with thermal ellipsoids drawn at the 50% probability level. Selected bond distances (Å) and angles [°]: C1-N5 1.392(3), N5-N6 1.253(2), N6-N7 1.113(3), N1-C2 1.455(3), N2-N1-C2 121.2(2), C1-N1-C2 131.4(2), N5-N6-N7 172.5(2), N6-N5-C1-N4 0.0(2); B) Layer structure of **11**.

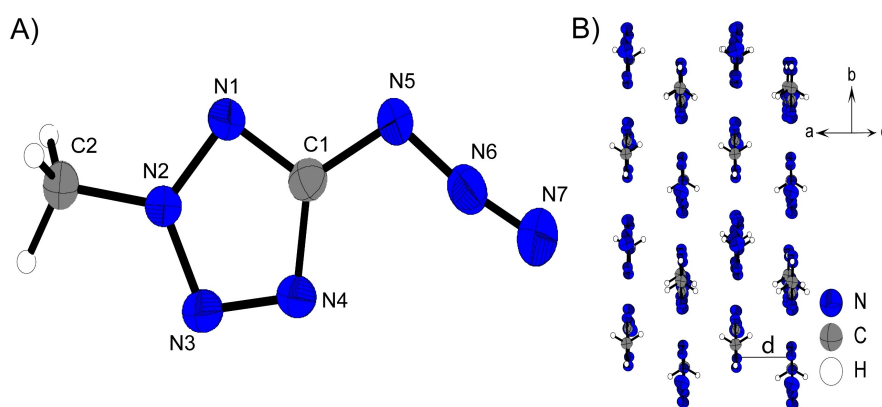


Figure 9. A) Molecular unit of **12** with thermal ellipsoids drawn at the 50% probability level. Selected bond distances (Å) and angles [°]: C1-N5 1.394(2), N5-N6 1.259(2), N6-N7 1.113(2), N2-C2 1.448(2), N1-N2-C2 123.0(1), C2-N2-N3 123.1(1), N5-N6-N7 171.5(2), N6-N5-C1-N4 1.6(2); B) Layer structure of **12**.

Table 1. ^1H and ^{13}C NMR resonances for compounds **2**, **2a–2d**, **7** and **10–12** measured in DMSO- D_6 , chemical shifts are reported in ppm with respect to TMS ($\text{Si}(\text{CH}_3)_4$).

Compound	δ [ppm] ^1H	^{13}C
2	9.69, 4.94, 3.97	157.3, 53.0, 48.9
2a	7.17, 4.69, 3.86	168.3, 51.6, 49.2
2b	10.03, 4.70, 3.87	168.0, 51.7, 49.2
2c	4.69, 3.87	169.0, 51.9, 49.6
2d	4.81, 3.93	166.5, 52.3, 49.0
7	4.20, 3.74	152.8, 49.1, 45.6
10	5.02, 4.68	152.9, 69.8, 43.8
11	3.77	152.9, 33.1
12	4.28	161.9, 40.7

carbon from 157.3 ppm for **2** by about 10 ppm for all ionic derivatives. For compounds **7** and **10** the tetrazole resonance is detected at 153 ppm in the ^{13}C NMR. For the nitrateethyl function of **10** the resonance of the CH_2 lined to the organic nitrate assigns at 5.02 ppm and the CH_2 unit bonded to N1 at 4.68 ppm. The ethylene unit of **7** shows signals at 4.20 and 3.74 ppm.

For the methyl group signals of **11** ($\delta=3.77$ ppm) and **12** ($\delta=4.28$ ppm), the signal for the 2-substitution is shifted to higher fields compared to the 1-substituted one. The ^{13}C shifts for **11** ($\delta(\text{CN}_4)=152.9$ ppm; $\delta(\text{CH}_3)=33.1$ ppm) and **12** ($\delta(\text{CN}_4)=161.9$ ppm; $\delta(\text{CH}_3)=40.7$ ppm) are in good accordance with other alkyl substituted 5-azidotetrazoles.^[21]

Additionally, compounds **2**, **2a** (as representative for the 2-(2-azidoethyl)-5-nitraminotetrazolate anion), **7** and **10–12** were analyzed through proton coupled ^{15}N spectroscopy. The spectra are illustrated in Figure 10. The nitrogen atoms are named as in the corresponding crystal structures. For the tetrazole moieties, signals for all four nitrogen atoms can be found in very similar ranges, depending on the substitution site (1- and 2-substituted). For 1-substituted tetrazoles **7**, **10** and **11** signals appear at around 0 ppm for N3, -13 ppm for N2, -75 ppm for N4 and -170 ppm for N1. For two substituted isomers **2**, **2a** and **12**, the chemical shifts for N3 and N4 do not differ hardly compared with 1-substituted isomers. Values for N1 and N2 can be found around -90 ppm and -102 ppm, respectively.

The same applies to the azide functionalities. Here, however, a distinction must be made between aromatic and alkyl azides.

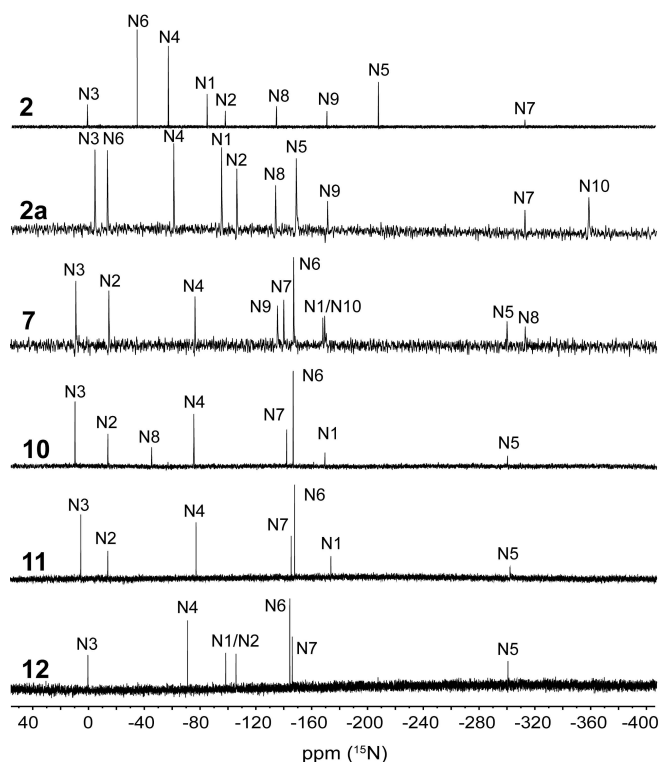


Figure 10. ^{15}N NMR spectra of compounds **2**, **2a**, **7** and **10–12**. Chemical shifts are reported in ppm with respect to MeNO_2 . Measurements of **2**, **2a** and **11–12** were performed in $\text{DMSO-}d_6$, for **7** and **10** in CDCl_3 and in acetone- d_6 , respectively.

Resonances for aromatic azides can be found in the spectra of compounds **7** and **10–12** in typical ranges of around -300 ppm for N_{α} , -145 ppm for N_{β} and -143 ppm for N_{γ} , whereas N_{β} having the highest intensity, followed by N_{γ} and N_{α} being the

less intensive signal. Compared to the aromatic azides, alkyl azide resonances appear high-field shifted at around -315 ppm for N_{α} , -171 ppm for N_{β} and -135 ppm for N_{γ} with equal intensities. These signals are detectable for compounds **2**, **2a** and **7**. In the case of aromatic azides, the signals of N_{β} and N_{γ} appear relatively close together, whereas for alkyl azides, there is a clear gap of around 35 ppm between the two signals. N_{γ} always emerges at higher fields than N_{β} .

Additional signals can be found in the spectra of **2**, **2a** and **10**. These are the nitro group of the protonated nitramine function (N_6) of **2** at -34.7 ppm, the nitro group of the deprotonated nitramine function (N_6) in **2a** at -13.9 ppm and the organic nitrate (N_8) of **10** at -13.3 ppm.

Physico-chemical Properties

Compounds **2**, **2a–2d**, **7** and **10–12** were tested toward the behavior on certain external stimuli as there are impact, friction, electrostatic discharge and temperature (DTA or DSC). The resulting values are listed in Table 2. All investigated compounds can be declined as energetic materials, since they are more or less sensitive facing those external stimuli, according to UN Recommendations on the Transport of Dangerous Goods.^[22] The free acid of 2-azidoethyl-5-nitraminotetrazole **2** is insensitive toward friction and shows an impact sensitivity of 10 J. The two nitrogen-rich salts (**2a** and **2b**) are moderately sensitive, whereas the two metal-containing salts (**2c** and **2d**) are already classified as extremely sensitive with **2d** being the most sensitive compound of the 2-azidoethyl-5-nitramino derivatives ($IS < 1$ J, $FS = 15$ N). All 5-azidotetrazole derivatives (**7**, **10–12**) show impact sensitivities less or equal to 1 J and friction sensitivities of 5 N (for **10**) or below for **7**, **11** and **12** and are therefore classified as sensitive explosives. Metal containing

Table 2. Energetic properties and detonation parameters of **2**, **2a–2d**, **7** and **10–12**.

	2	2a	2b	2c	2d	7*	10	11	12
Formula	$\text{C}_3\text{H}_5\text{N}_9\text{O}_2$	$\text{C}_3\text{H}_8\text{N}_{10}\text{O}_2$	$\text{C}_3\text{H}_8\text{N}_{10}\text{O}_3$	$\text{C}_3\text{H}_4\text{N}_9\text{O}_2\text{K}$	$\text{C}_3\text{H}_4\text{N}_9\text{O}_2\text{Ag}$	$\text{C}_3\text{H}_4\text{N}_{10}$	$\text{C}_3\text{H}_4\text{N}_8\text{O}_3$	$\text{C}_2\text{H}_3\text{N}_7$	$\text{C}_2\text{H}_3\text{N}_7$
M [g mol^{-1}]	199.13	216.17	232.16	237.22	305.99	180.14	200.12	125.11	125.11
IS [J] ^[a]	10	30	9	1	< 1	< 1	1	< 1	< 1
FS [N] ^[b]	360	120	40	30	15	< 0.1	5	< 5	< 5
ESD [mJ] ^[c]	–	100	100	25	13	–	10	50	80
$[g\text{ cm}^{-3}]$ ^[d]	1.60*	1.575	1.624	1.93*	2.362	1.519	1.638	1.459	1.542
N [%] ^[e]	62.4	64.8	60.3	53.1	41.2	77.8	56.0	78.4	78.4
Ω [%] ^[f]	$-28.1/-52.2$	$-37.0/-59.2$	$-27.6/-48.2$	$-20.2/-40.5$	$-15.7/-31.4$	$-44.4/-71.1$	$-16.0/-40.0$	$-44.8/-70.3$	$-44.8/-70.3$
$T_{\text{melt}}/T_{\text{dec}}$ [$^{\circ}\text{C}$] ^[g]	n.d./93	113/172	-171	126/180	-181	-20/167	45/166	20/160	62/162
$\Delta_f H^{\circ}$ [kJ mol^{-1}] ^[h]	647.1	649.1	705.5	–	–	932.7	514.5	594.5	566.9
$\Delta_f U^{\circ}$ [kJ mol^{-1}] ^[i]	666.9	673.9	731.5	–	–	950.1	533.1	606.9	579.3
Explo5 V6.05.02									
$-\Delta_{\text{Ex}} U^{\circ}$ [kJ kg^{-1}] ^[j]	5282	5199	6281	–	–	5123	5409	4769	4563
T_{det} [K] ^[k]	3650	3321	3845	–	–	3535	3872	3383	3199
V_0 [L kg^{-1}] ^[l]	833	889	889	–	–	802	809	817	810
P_{Cl} [kbar] ^[m]	248	256	295	–	–	215	261	202	216
V_{det} [m s^{-1}] ^[n]	8138	8430	8796	–	–	7898	8165	7616	7916

[a] Impact sensitivity (BAM drop hammer (1 of 6)). [b] Friction sensitivity (BAM friction tester (1 of 6)). [c] Electrostatic discharge device (OZM research). [d] From X-Ray diffraction analysis recalculated to 298 K; *pycnometric measurement. [e] Nitrogen content. [f] Oxygen balance with respect to CO/CO_2 [g] Decomposition temperature (DTA/DSC; $\beta = 5$ $^{\circ}\text{C min}^{-1}$). [h] Calculated enthalpy of formation. [i] Energy of formation. [j] Energy of explosion. [k] Detonation temperature. [l] Volume of detonation products (assuming only gaseous products). [m] Detonation pressure at Chapman–Jouguet point. [n] Detonation velocity. *Explo5 V6.05.02 calculation for the theoretical solid state at room temperature.

ionic derivatives **2c** and **2d** are the thermally most stable compounds in this study decomposing at 180 °C and 181 °C, respectively. Nitrogen-rich derivatives **2a** and **2b** decompose around 170 °C, whereby **2a** shows a smooth melting point at 113 °C. The free nitramine **2** is even liquid after long time storage –30 °C and explodes violently at 93 °C. 5-Azidotetrazole derivatives **7** and **10–12** all undergo decomposition between 160 °C and 167 °C and possess a melting point in advance. Compound **7** is liquid at room temperature and melts at about –20 °C, **10**, **11** and **12** are solids at ambient temperatures and melt at 45 °C, 20 °C and 62 °C, respectively. Based on the densities and the calculated enthalpies of formation, the detonation parameters for all metal-free were calculated using the EXPLO5 code. All investigated compounds show highly positive values for their heat of formation, with **9**, containing two azido moieties showing the overall highest heat of formation of $\Delta_f H^0 = 932.7 \text{ kJ mol}^{-1}$. The calculated detonation velocity for **2b** is 8796 ms^{-1} and therefore in the range of RDX ($V_{\text{det}} = 8801 \text{ ms}^{-1}$). The performance parameters of the corresponding ammonium derivative as well as of the neutral compound are significantly lower, since they have both lower density and enthalpy of formation. Ethyl substituted 5-azidotetrazoles **7** and **10** differ about 270 ms^{-1} is their detonation velocity, whereas nitraethyl derivative **10** has the higher value with 8165 ms^{-1} . This trend is in accordance with recently published ethyl substituted 5,5'-azobistetrazoles.^[9a] In terms of detonation parameters, two methyl substituted 5-azidotetrazole (**12**) is clearly superior to its one substituted isomer **11**. The detonation velocities are 7616 ms^{-1} for **11** and 7916 ms^{-1} for **12** and thus exactly 300 ms^{-1} apart, which is mainly attributed to the different densities. Unfortunately, the calculated detonation parameters fell short of expectations due to the low densities of the compounds. Both 5-azidotetrazole backbones and azidoethyl substitutions yield enormous increases in the calculated formation detonation parameters, but the nonpolar properties of the substituents offer only limited opportunities for attractive interactions.

Conclusion

By introducing azidoethyl, nitraethyl and methyl groups to 5-azidotetrazoles, the physico-chemical properties could be specifically modified. Nitraethyl shows a lower sensitivity and a higher melting point (45 °C) with better performance (8165 ms^{-1}) than the respective azidoethyl homologue. Furthermore, the methyl functionalization at N2 not only outperforms its N1-isomer in terms of physico-chemical properties but also shows a much easier synthesis. The melting points of the isomers differ by 40 °C with the 2-isomer melting at 62 °C. The decomposition temperatures of the 5-azides are not altered by functionalization. The sensitivities are all in the area of primary explosives with 1-(2-azidoethyl)-5-azidotetrazole (**7**) being the most sensitive compound which is unusual because this compound is a liquid.

With the synthesis of 2-(2-azidoethyl)-5-nitraminotetrazole (**2**) and its nitrogen rich ionic derivatives (**2a**, **b**) new highly

energetic secondary explosives were discovered. The hydroxylammonium salt **2b** owns the best explosive performance in this study with a detonation velocity of about 8800 ms^{-1} . The metal salts (**2c**, **d**) are more sensitive explosives and as all ionic derivatives in this work stable up to 180 °C.

Acknowledgements

For financial support of this work by Ludwig-Maximilian University (LMU), the Office of Naval Research (ONR) under grant no. ONR N00014-19-1-2078 and the Strategic Environmental Research and Development Program (SERDP) under contract no. W912HQ19C0033 are gratefully acknowledged. We thank Prof. Dr. Konstantin Karaghiosoff for the measurement of the ^{15}N NMR spectra. Open Access funding enabled and organized by Projekt DEAL.

Conflict of Interest

The authors declare no conflict of interest.

Data Availability Statement

The data that support the findings of this study are available from the corresponding author upon reasonable request.

Keywords: azides · energetic materials · NMR spectroscopy · tetrazoles · X-ray diffraction

- [1] a) J. P. Agrawal, R. D. Hodgson, *Organic Chemistry of Explosives*, 1st ed., John Wiley & Sons Inc., Chichester, **2006**; b) J. Köhler, R. Meyer, A. Homburg, *Explosivstoffe*, 10th ed., Wiley-VCH, Weinheim, **2008**.
- [2] T. M. Klapötke, *Chemistry of High-Energy Materials*, 5th ed., De Gruyter, **2019**.
- [3] M. A. S. Laidlaw, G. Filippelli, H. Mielke, B. Gulson, A. S. Ball, *Environ. Health* **2017**, *16*, 34.
- [4] a) U. S. E. P. A., "Technical Fact Sheet – 2,4,6-Trinitrotoluene (TNT)" can be found under <https://www.epa.gov/fedfac/technical-fact-sheet-246-trinitrotoluene-tnt>, **2022**; b) M. L. Gettings, M. T. Thoenen, E. F. C. Byrd, J. J. Sabatini, M. Zeller, D. G. Piercey, *Chem. Eur. J.* **2020**, *26*, 14530.
- [5] E. C. Johnson, J. J. Sabatini, D. E. Chavez, R. C. Sausa, E. F. C. Byrd, L. A. Wingard, P. E. Guzmán, *Org. Process Res. Dev.* **2018**, *22*, 736–740.
- [6] A. B. Sheremetev, S. F. Mel'nikova, E. S. Kokareva, R. E. Nekrutenko, K. V. Strizhenko, K. Y. Suponitsky, T. D. Pham, A. N. Pivkina, V. P. Sinditskii, *Def. Technol.* **2021**.
- [7] P. Gaur, S. Dev, S. Kumar, M. Kumar, A. A. Vargeese, P. Soni, P. F. Siril, S. Ghosh, *ACS Omega* **2017**, *2*, 8227–8233.
- [8] Y. Tang, J. M. Shreeve, *Chem. Eur. J.* **2015**, *21*, 7285–7291.
- [9] a) M. Benz, M. S. Grühne, T. M. Klapötke, N. Krüger, T. Lenz, M. Lommel, J. Stierstorfer, *Eur. J. Org. Chem.* **2021**, 4388–4392; b) N. Fischer, T. M. Klapötke, J. Stierstorfer, C. Wiedemann, *Polyhedron* **2011**, *30*, 2374–2386; c) Y.-H. Joo, J. M. Shreeve, *Angew. Chem. Int. Ed.* **2010**, *49*, 7320–7323; *Angew. Chem.* **2010**, *122*, 7478–7481; d) J. Stierstorfer, K. R. Tarantik, T. M. Klapötke, *Chem. Eur. J.* **2009**, *15*, 5775–5792; e) R. Yang, Z. Dong, Z. Ye, *ChemistrySelect* **2019**, *4*, 14208–14213.
- [10] S. Song, F. Chen, Y. Wang, K. Wang, M. Yan, Q. Zhang, *J. Mater. Chem. A* **2021**, *9*, 21723–21731.
- [11] R. M. Herbst, J. A. Garrison, *J. Org. Chem.* **1953**, *18*, 941–945.
- [12] E. Lieber, D. R. Levering, *J. Am. Chem. Soc.* **1951**, *73*, 1313–1317.

- [13] a) J. Stierstorfer, T. M. Klapötke, A. Hammerl, R. D. Chapman, *Z. Anorg. Allg. Chem.* **2008**, *634*, 1051–1057; b) N. Fischer, T. M. Klapötke, J. Stierstorfer, *Z. Anorg. Allg. Chem.* **2009**, *635*, 271–281.
- [14] a) T. M. Klapötke, J. Stierstorfer, *J. Am. Chem. Soc.* **2009**, *131*, 1122–1134; b) T. Fendt, N. Fischer, T. M. Klapötke, J. Stierstorfer, *Inorg. Chem.* **2011**, *50*, 1447–1458.
- [15] D. E. Bayes (Glaxo Group Limited), EP0117368 A1, **1982**.
- [16] a) J. A. Garrison, R. M. Herbst, *Org. Chem.* **1957**, *22*, 278–283; b) T. M. Klapötke, J. Stierstorfer, *Helv. Chim. Acta* **2007**, *90*, 2132–2150.
- [17] a) M. H. H. Wurzenberger, M. S. Gruhne, M. Lommel, V. Braun, N. Szimhardt, J. Stierstorfer, *Inorg. Chem.* **2020**, *59*, 17875–17879; b) G.-G. Gao, P.-S. Cheng, T. C. W. Mak, *J. Am. Chem. Soc.* **2009**, *131*, 18257–18259; c) Q.-Y. Wang, J. Wang, S. Wang, Z.-Y. Wang, M. Cao, C.-L. He, J.-Q. Yang, S.-Q. Zang, T. C. W. Mak, *J. Am. Chem. Soc.* **2020**, *142*, 12010–12014.
- [18] P. Ai, A. A. Danopoulos, P. Braunstein, K. Y. Monakhov, *Chem. Commun.* **2014**, *50*, 103–105.
- [19] a) H. Schmidbaur, A. Schier, *Angew. Chem. Int. Ed.* **2015**, *54*, 746–784; *Angew. Chem.* **2015**, *127*, 756–797; b) L. Mistry, O. El-Zubir, G. Dura, W. Clegg, P. G. Waddell, T. Pope, W. A. Hofer, N. G. Wright, B. R. Horrocks, A. Houlton, *Chem. Sci.* **2019**, *10*, 3186–3195.
- [20] M. S. Gruhne, T. Lenz, M. Rösch, M. Lommel, M. H. H. Wurzenberger, T. M. Klapötke, J. Stierstorfer, *Dalton Trans.* **2021**, *50*, 10811–10825.
- [21] T. M. Klapötke, S. M. Sproll, *Eur. J. Org. Chem.* **2009**, *2009*, 4284–4289.
- [22] U. Nations, in *Manual of Tests and Criteria*, Vol. ST/SG/AC.10/11/Rev.6 New York and Geneva, **2015**.

Manuscript received: March 10, 2022

Accepted manuscript online: April 13, 2022

Version of record online: May 19, 2022

Chemistry–A European Journal

Supporting Information

Tuning the Properties of 5-Azido and 5-Nitramino-tetrazoles by Diverse Functionalization – General Concepts for Future Energetic Materials

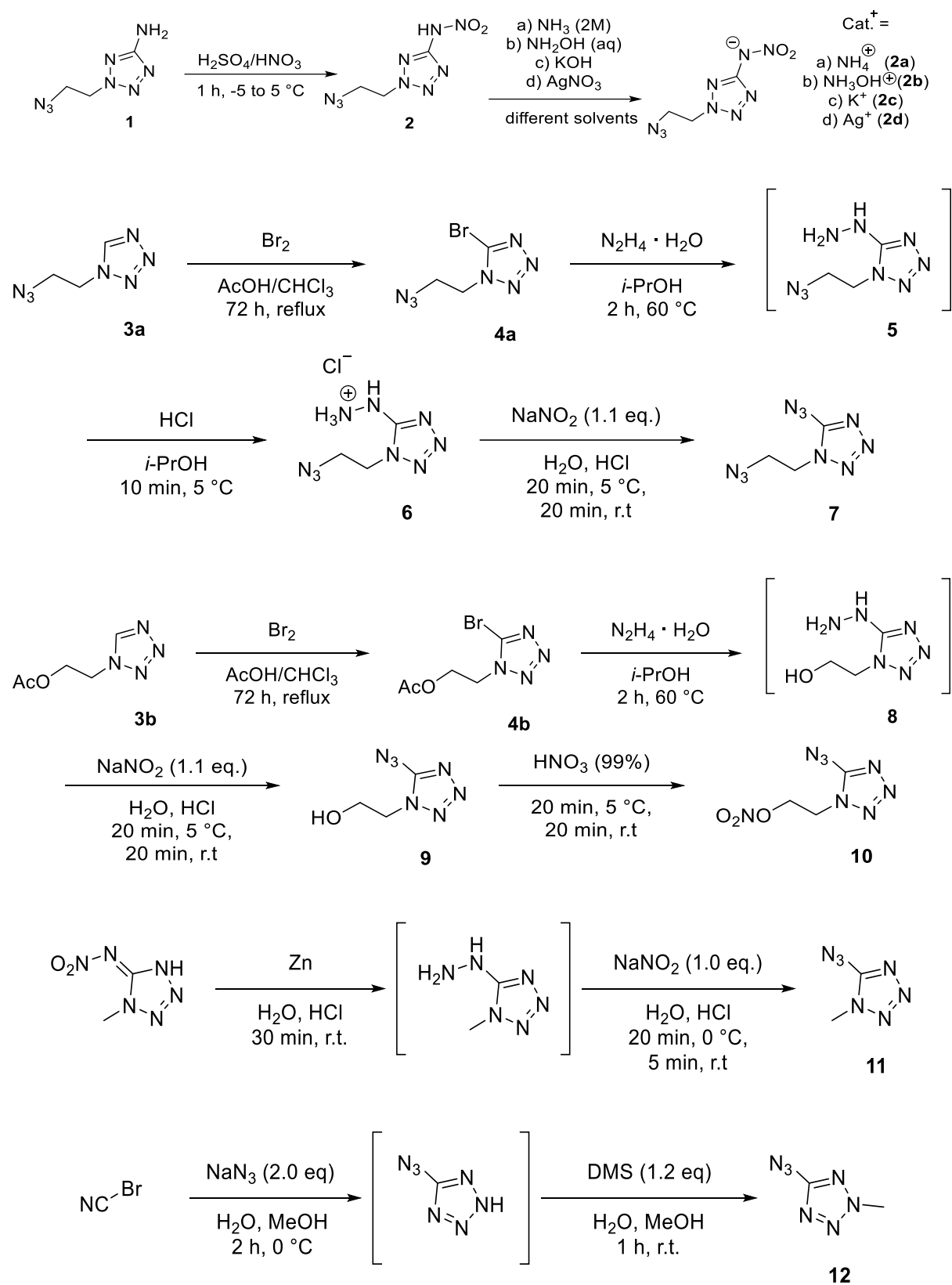
Maximilian Benz, Thomas M. Klapötke,* Tobias Lenz, and Jörg Stierstorfer

Supplementary Information

Table of Contents

1. Experimental part and general procedures
2. Thermal Analysis
3. X-ray diffraction
4. Computation
5. NMR Spectroscopy
6. References

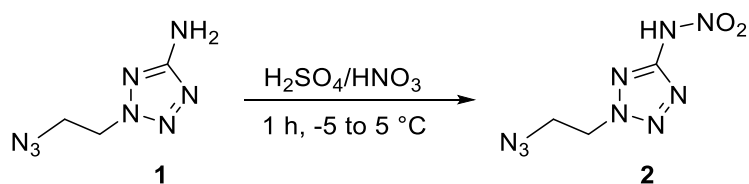
1. Experimental part and general procedures



^1H , ^{13}C , ^{14}N and ^{15}N NMR spectra were recorded on *BRUKER AMX 400* instruments. Chemical shifts are referenced with respect to tetramethylsilane ($^1\text{H}/^{13}\text{C}$) and nitromethane ($^{14}\text{N}/^{15}\text{N}$). Infrared spectra (IR) were recorded in the region $4000\text{-}400\text{ cm}^{-1}$ on a *PERKIN ELMER Spectrum BX-59343* instrument with a *SMITHS DETECTION DuraSamplIR II Diamond ATR* sensor. The absorption bands are reported in wavenumbers (cm^{-1}). Decomposition temperatures were measured via differential thermal analysis (DTA) with an *OZM Research DTA 552-Ex* instrument at a heating rate of $5\text{ }^\circ\text{C}/\text{min}$ and in a range of room temperature to $400\text{ }^\circ\text{C}$. All sensitivities toward impact (IS) and friction (FS) were determined according to BAM (Bundesanstalt für Materialforschung und Prüfung) standards using a BAM drop hammer and a BAM friction apparatus by applying the 1 of 6 method.^[S1] All energetic compounds were tested for sensitivity towards electrical discharge using an *Electric Spark Tester ESD 2010 EN* from OZM. Energetic properties have been calculated with the EXPLO5 6.02 computer ^[S2] code using the RT converted X-ray density or the densities measured with a gas pycnometer at 298 K and calculated solid state heats of formation.

CAUTION! *All investigated compounds are potentially explosive materials. In particular compound 7, 1-(2-azidoethyl)-5-azidotetrazole, is extremely sensitive and tends to explode during solidification. Safety precautions and equipment (such as wearing leather coat, face shield, Kevlar sleeves, Kevlar gloves, earthed equipment and ear plugs) must be used during all manipulations.*

2-(2-Azidoethyl)-5-nitraminetetrazole (2)^[S3]

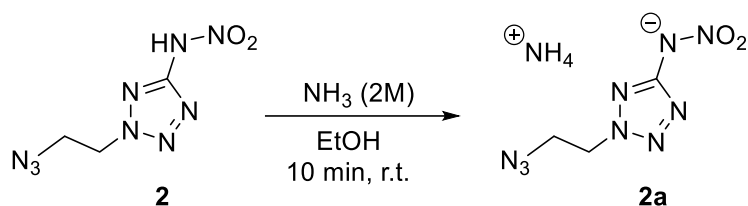


2-(2-Azidoethyl)-5-aminotetrazole (**1**) (1.00 g, 6.50 mmol, 1.0 eq) was dropwise added to a mixture of sulfuric acid (96%, 8.00 mL) and nitric acid (100%, 3.00 mL) keeping the temperature below $5\text{ }^\circ\text{C}$ (**CAUTION!** By rising the temperature above $5\text{ }^\circ\text{C}$, the reaction mixture decomposes exothermically including the formation of large amount of nitrous gases, heat and flames in the reaction flask). The mixture was stirred for 1 h and was allowed to heat to $5\text{ }^\circ\text{C}$. The mixture was poured on ice water (150 mL) and extracted with diethyl ether (3 x 50 mL). After drying over anhydrous sodium sulfate,

the organic solvent was evaporated, the title compound **2** was obtained as slightly brownish liquid (1.16 g, 5.60 mmol, 86%).

DTA (5 °C min⁻¹): 93 °C (dec); Sensitivities: BAM drop hammer: 10 J (liquid), friction tester: 360 N (liquid), ESD: -; IR (ATR) $\tilde{\nu}$ (cm⁻¹) = 3023(w), 2102(s), 1700(w), 1610(s), 1488(m), 1440(m), 1299(vs), 1227(s), 1097(m), 1029(m), 893(m), 827(m), 758(m), 632(m), 554(m), 493(s), 445(m), 435(m), 428(m), 419(m), 412(m); Elem. Anal. (C₃H₅N₉O₂, 199.13 g mol⁻¹) calcd.: C 18.09, H 2.53, N 63.31 %. Found: C 17.94, H 2.82, N 62.37 %; ¹H NMR (DMSO-D₆, 400 MHz, ppm) δ = 9.69 (br s, 1H), 4.94 (m, 2H), 3.97 (m, 2H); ¹³C NMR (DMSO-D₆, 101 MHz, ppm) δ = 157.3, 53.0, 48.9; ¹⁵N NMR (DMSO-D₆, 41 MHz, ppm) δ = 1.0, -34.7, -57.1, -85.0, -98.1, -134.9, -171.2, -208.2, -313.5; HRMS (ESI) *m/z*: [M - H⁺] Calcd for C₃H₄N₉O₂ 198.0493; Found: 198.0492.

Ammonium 2-(2-azidoethyl)-5-nitraminetetrazolate (**2a**)

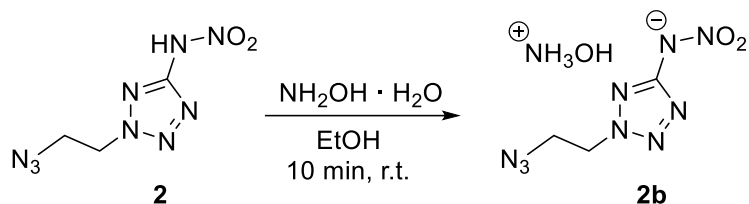


2-(2-Azidoethyl)-5-nitraminetetrazole (**2**) (0.69 g, 3.47 mmol, 1.0 eq) was dissolved in ethanol (25 mL) and ammonia (2M dissolved in ethanol, 1.75 mL, 3.50 mmol, 1.0 eq) was added dropwise. The solvent was reduced and the precipitate was filtered to yield pure ammonium 2-(2-azidoethyl)-5-nitraminetetrazolate (**2a**) (0.66 g, 3.06 mmol, 88%) as brown solid.

DTA (5 °C min⁻¹): 113 °C (melt), 172 °C (dec); Sensitivities: BAM drop hammer: 30 J (\leq 500 μ m), friction tester: 120 N (\leq 500 μ m), ESD: 0.1 J (\leq 500 μ m). IR (ATR) $\tilde{\nu}$ (cm⁻¹) = 3194(s), 2120(s), 1480(s), 1463(s), 1452(s), 1434(s), 1397(s), 1367(s), 1343(s), 1294(vs), 1240(s), 1204(s), 1168(s), 1097(s), 1059(m), 1036(s), 1013(s), 974(s), 953(m), 888(s), 833(s), 771(s), 757(s), 742(m), 699(s), 675(m), 646(m), 560(m), 512(s), 467(s), 448(m); Elem. Anal. (C₃H₈N₁₀O₂, 216.17 g mol⁻¹) calcd.: C 16.67, H 3.73, N 64.80 %. Found: C 16.75, H 3.80, N 63.48 %; ¹H NMR (DMSO-D₆, 400 MHz, ppm) δ = 7.17 (s, 4H), 4.69 (m, 2H), 3.86 (m, 2H); ¹³C NMR (DMSO-D₆,

101 MHz, ppm) δ = 168.3, 51.6, 49.2; ^{15}N NMR (DMSO- D_6 , 41 MHz, ppm) δ = -5.0, -13.9, -61.4, -95.6, -106.5, -134.3, -149.0, -171.4, -312.7, -358.4.

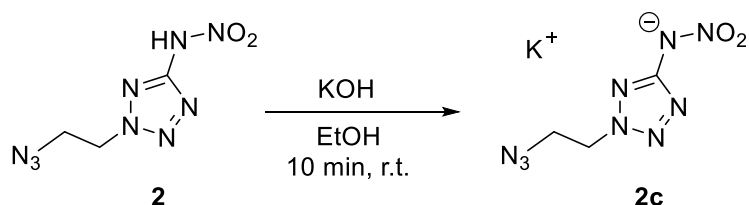
Hydroxylammonium 2-(2-azidoethyl)-5-nitraminotetrazolate (**2b**)



2-(2-Azidoethyl)-5-nitraminotetrazole (**2**) (0.87 g, 4.47 mmol, 1.0 eq) was dissolved in ethanol (18 mL) and aqueous hydroxylamine solution (50% w/w, 0.28 mL, 4.70 mmol, 1.05 eq) was added dropwise. The solvent was reduced and the precipitate was filtered to yield pure hydroxylammonium 2-(2-azidoethyl)-5-nitraminotetrazolate (**2b**) (0.85 g, 3.66 mmol, 82%) as yellow solid.

DTA ($5\text{ }^\circ\text{C min}^{-1}$): $171\text{ }^\circ\text{C}$ (dec); Sensitivities: BAM drop hammer: 9 J ($\leq 500\text{ }\mu\text{m}$), friction tester: 40 N ($\leq 500\text{ }\mu\text{m}$), ESD: 0.1 J ($\leq 500\text{ }\mu\text{m}$). IR (ATR) $\tilde{\nu}$ (cm^{-1}) = 3112(m), 2691(m), 2141(s), 2102(s), 1485(s), 1437(s), 1406(s), 1358(s), 1341(vs), 1290(vs), 1238(s), 1213(s), 1169(vs), 1119(s), 1101(s), 1038(s), 1009(s), 953(m), 897(m), 884(m), 839(m), 775(s), 751(s), 695(m), 688(m), 669(s), 626(s), 555(s), 502(s), 456(s), 441(s); Elem. Anal. ($\text{C}_3\text{H}_8\text{N}_{10}\text{O}_3$, 232.16 g mol^{-1}) calcd.: C 15.52, H 3.47, N 60.33 %. Found: C 14.90, H 3.63, N 59.85 %; ^1H NMR (DMSO- D_6 , 400 MHz, ppm) δ = 10.03 (br s, 4H), 4.70 (m, 2H), 3.87 (m, 2H); ^{13}C NMR (DMSO- D_6 , 101 MHz, ppm) δ = 168.0, 51.7, 49.2; ^{14}N NMR (DMSO- D_6 , 29 MHz, ppm) δ = -3, -13, -134, -173, -359.

Potassium 2-(2-azidoethyl)-5-nitraminotetrazolate (**2c**)

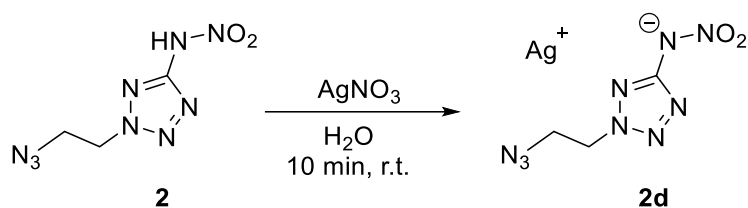


2-(2-Azidoethyl)-5-nitraminotetrazole (**2**) (0.85 g, 4.24 mmol, 1.0 eq) was dissolved in ethanol (18 mL) and potassium hydroxide (0.24 g, 4.24 mmol, 1.0 eq) dissolved in ethanol (8 mL) was added in one portion. The immediately formed solid was filtered

and washed with little amount of cold ethanol to yield potassium 2-(2-azidoethyl)-5-nitraminotetrazolate (**2c**) (0.90 g, 3.80 mmol, 90%) as brownish solid.

DTA (5 °C min⁻¹): 126 °C (melt), 180 °C (dec); Sensitivities: BAM drop hammer: 1 J (≤ 500 μm), friction tester: 30 N (≤ 500 μm), ESD: 25 mJ (≤ 500 μm). IR (ATR) $\tilde{\nu}$ (cm⁻¹) = 2118(s), 2080(m), 1486(s), 1417(s), 1407(s), 1383(s), 1320(vs), 1299(vs), 1261(s), 1208(s), 1099(s), 1041(s), 1006(s), 971(m), 944(m), 883(m), 828(s), 777(s), 760(s), 696(m), 647(m), 557(m), 507(m), 463(m); Elem. Anal. (C₃H₄N₈O₂K, 237.22 g mol⁻¹) calcd.: C 15.19, H 1.70, N 53.14 %. Found: C 15.49, H 1.80, N 52.10 %; ¹H NMR (DMSO-D₆, 400 MHz, ppm) δ = 4.69 (m, 2H), 3.87 (m, 2H); ¹³C NMR (DMSO-D₆, 101 MHz, ppm) δ = 169.0, 51.9, 49.6; ¹⁴N NMR (DMSO-D₆, 29 MHz, ppm) δ = -12, -135, -173.

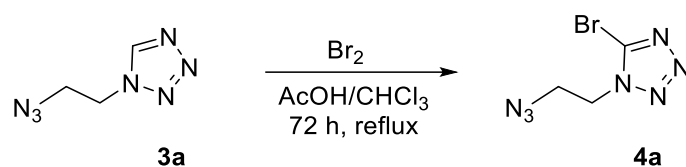
Silver 2-(2-azidoethyl)-5-nitraminotetrazolate (**2d**)



2-(2-Azidoethyl)-5-nitraminotetrazole (**2**) (0.29 g, 1.43 mmol, 1.0 eq) was dissolved in ethanol (5 mL) and silver nitrate (0.25 g, 1.45 mmol, 1.0 eq) dissolved in water (5 mL) was added in one portion. The immediately formed solid was filtered and washed with little amount of cold water to obtain silver 2-(2-azidoethyl)-5-nitraminotetrazolate (**2d**) (0.43 g, 1.40 mmol, 98%) in quantitative yield as beige powder.

DTA (5 °C min⁻¹): 181 °C (dec); Sensitivities: BAM drop hammer: <1 J (≤ 500 μm), friction tester: 15 N (≤ 500 μm), ESD: 13 mJ (≤ 500 μm). IR (ATR) $\tilde{\nu}$ (cm⁻¹) = 2138(s), 2101(s), 1509(s), 1438(s), 1406(s), 1357(s), 1343(s), 1286(vs), 1213(s), 1170(s), 1120(m), 1101(m), 1038(s), 1010(s), 952(m), 884(m), 752(m), 743(m), 694(m), 689(m), 670(s), 626(m), 555(m), 503(m), 456(m), 441(m); Elem. Anal. (C₃H₄N₈O₂Ag, 305.99 g mol⁻¹) calcd.: C 11.78, H 1.32, N 41.20 %. Found: C 11.77, H 1.51, N 40.29 %; ¹H NMR (DMSO-D₆, 400 MHz, ppm) δ = 4.81 (m, 2H), 3.93 (m, 2H); ¹³C NMR (DMSO-D₆, 101 MHz, ppm) δ = 166.5, 52.3, 49.0; ¹⁴N NMR (DMSO-D₆, 29 MHz, ppm) δ = -16, -135.

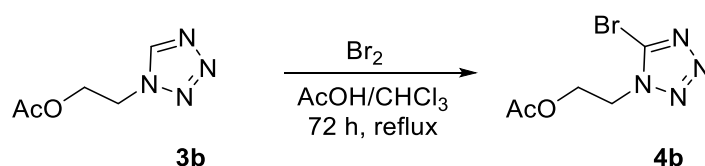
1-(2-Azidoethyl)-5-bromotetrazole (**4a**)



To a solution of 1-(2-azidoethyl)-tetrazole (**3a**) (5.00 g, 35.9 mmol, 1.0 eq) in acetic acid (35 mL) and chloroform (70 mL) was added bromine (11.5 g, 71.8 mmol, 2.0 eq) in chloroform (15 mL). After 72 h at reflux the solvent was evaporated and excess saturated sodium bicarbonate solution was added to the residue. The mixture was extracted with ethyl acetate (3 x 100 mL), the solvent was dried over sodium sulfate and removed to yield 1-(2-azidoethyl)-5-bromotetrazole (**4a**) (6.60 g, 30.3 mmol, 84%) as yellow liquid.

Sensitivities: BAM drop hammer: 40 J (liquid), friction tester: >360 N (liquid); IR (ATR) $\tilde{\nu}$ (cm⁻¹) = 2099(vs), 1455(m), 1429(s), 1414(s), 1398(s), 1352(m), 1286(m), 1248(m), 1228(m), 1180(s), 1123(m), 981(w), 826(w), 663(m), 647(m), 631(m), 494(m); Elem. Anal. (C₃H₄N₇Br, 218.02 g mol⁻¹) calcd.: C 16.53, N 44.97, H 1.85%. Found: C 16.40, N 43.27, H 2.00%; ¹H NMR (DMSO-D₆, 400 MHz, ppm) δ = 4.63 – 4.59 (m, 2H), 3.93 – 3.86 (m, 2H). ¹³C NMR (DMSO-D₆, 101 MHz, ppm) δ = 135.0, 49.1, 42.5; HR-MS (ESI, 70 eV): [C₃H₅N₇Br₂] calcd.: 297.8879 [M – Br], found: 297.8882.

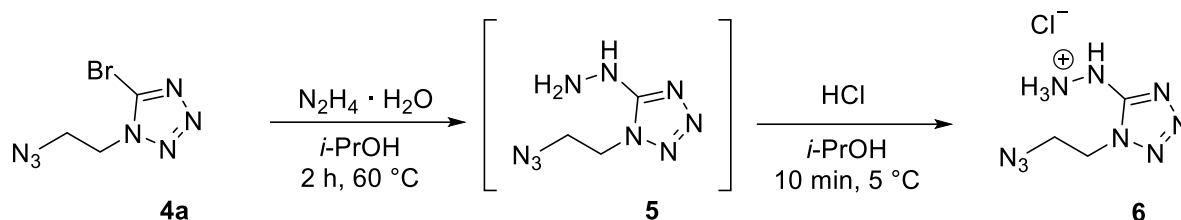
5-Bromo-1-(2-acetoxyethyl)-tetrazole (**4b**)^[S4]



To a solution of 1-(2-acetoxyethyl)-tetrazole (**3b**) (4.1 g, 26 mmol, 1.0 eq) in acetic acid (25 mL) and chloroform (50 mL) was added bromine (2.7 ml, 8.4 g, 52 mmol, 2.0 eq) in chloroform (10 mL). After 72 h at reflux the solvent was evaporated and excess saturated sodium bicarbonate solution was added to the residue. The mixture was extracted with ethyl acetate (3 x 50 mL), the solvent was dried over sodium sulfate and removed to yield 5-bromo-1-(2-chloroethyl)-tetrazole (**4b**) (5.8 g, 25 mmol, 95%) as yellow liquid.

^1H NMR (DMSO- D_6 , 400 MHz, ppm) δ = 4.69 (m, 2H), 4.44 (m, 2H), 1.96 (s, 3H); ^{13}C NMR (DMSO- D_6 , 101 MHz, ppm) δ = 170.0, 135.0, 61.2, 47.4, 20.4;

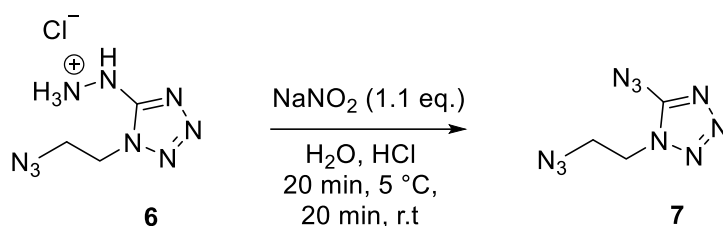
1-(2-Azidoethyl)-5-hydraziniumtetrazole chloride (**6**)



To a solution of 1-(2-azidoethyl)-5-bromotetrazole (**4a**) (1.00 g, 4.57 mmol, 1.0 eq.) in 2-propanol (20 mL) was added hydrazine hydrate (100%, 0.66 mL, 13.70 mmol, 3.0 eq.). After 2 h at 60 °C the solvent was removed and the residue was dissolved in water (50 mL) and extracted with ethyl acetate (3 x 50 mL). The organic phase was dried over sodium sulfate and evaporated to yield a crude oil of 1-(2-azidoethyl)-5-hydrazineyltetrazole (**5**) that forms colorless crystals over time. (^1H NMR (DMSO- D_6 , 400 MHz, ppm) δ = 8.14 (s, 1H), 4.48 (s, 2H), 4.44 – 4.37 (m, 2H), 3.78 – 3.68 (m, 2H). ^{13}C NMR (DMSO- D_6 , 101 MHz, ppm) δ = 158.3, 48.9, 44.9; HR-MS (ESI, 70 eV): $[\text{C}_3\text{H}_8\text{N}_9]$ calcd.: 170.0898 $[\text{M} - \text{H}^+]$, found: 170.0899. The residue was then dissolved in 2-propanol (10 mL) and an excess of a solution of HCl in 2-propanol (4-6 N, 3 mL) was added. After full precipitation and crystallization at 5 °C over night the product was filtered and washed with ether to yield white solid 1-(2-azidoethyl)-5-hydraziniumtetrazole chloride (**6**) (498 mg, 2.42 mmol, 53%).

Sensitivities: BAM drop hammer: >40 J ($\leq 500 \mu\text{m}$), friction tester: >360 N ($\leq 500 \mu\text{m}$); IR (ATR) $\tilde{\nu}$ (cm^{-1}) = 3204(m), 2788(s), 2646(s), 2593(s), 2138(s), 2096(vs), 1599(s), 1570(vs), 1548(s), 1494(s), 1444(s), 1421(s), 1370(m), 1343(s), 1331(m), 1300(s), 1278(s), 1253(m), 1184(m), 1125(m), 1102(s), 1063(m), 1009(s), 971(m), 827(s), 732(s), 667(m), 607(s), 534(s), 486(s); Elem. Anal. ($\text{C}_3\text{H}_8\text{N}_9\text{Cl}$, 205.61 g mol^{-1}) calcd.: C 17.52, H 3.92, N 61.31 %. Found: C 18.01, H 4.09, N 60.24 %; ^1H NMR (D_2O , 400 MHz, ppm) δ = 4.52 – 4.26 (m, 2H), 3.98–3.54 (m, 2H). ^{13}C NMR (DMSO- D_6 , 101 MHz, ppm) δ = 154.6, 48.9, 46.1.; ^{14}N NMR (DMSO- D_6 , 29 MHz, ppm) δ = -135.4, -168.6; HR-MS (ESI, 70 eV): $[\text{C}_3\text{H}_7\text{N}_9\text{Cl}]$ calcd.: 204.0518 $[\text{M} - \text{Cl}^-]$, found: 204.05179.

1-(2-Azidoethyl)-5-azidotetrazole (7)

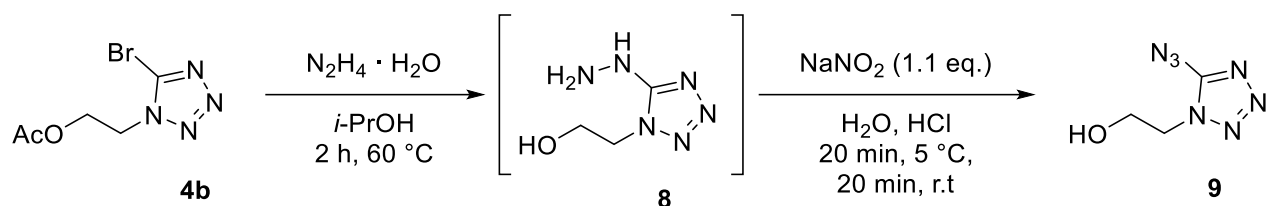


To a solution of 1-(2-azidoethyl)-5-hydraziniumtetrazole chloride (**6**) (200 mg, 0.97 mmol, 1.0 eq) in water (10 mL) and aqueous hydrochloric acid (2N, 2 mL) was added slowly sodium nitrite (74 mg, 1.07 mmol, 1.1 eq.) at 5 °C. After 20 min at 5 °C the solution was stirred at room temperature for further 20 min. Then the reaction was extracted with ether (3 x 20 mL) (using a plastic separation funnel and plastic vessels!). The organic layer was washed with water, dried over sodium sulfate and evaporated under a nitrogen stream to yield a yellowish oil of 5-azido-1-(2-azidoethyl)-tetrazole (**7**). The oil was purified by column chromatography (EtOAc/hex; 8/2; Rf: 0.35) to yield white **7** (265 mg, 1.71 mmol, 40%) (166 mg, 0.92 mmol, 95%) as highly sensitive colorless oil.

(*CAUTION!* The reaction and workup have to be performed very carefully with personal protection and blast shield as the product is highly sensitive. A violent detonation occurred while handling the azido tetrazole with a glass pipette. Therefore, plastic equipment is recommended.)

DTA (5 °C min⁻¹): 167 °C (dec.); Sensitivities: BAM drop hammer: <1 J (liquid), friction tester: <0.1 N (liquid). IR (ATR) $\tilde{\nu}$ (cm⁻¹) = 2156(s), 2101(s), 1531(vs), 1470(m), 1445(m), 1352(w), 1326(m), 1294(m), 1252(m), 1226(m), 1181(m), 1125(w), 1089(m), 827(w), 723(m), 654(m), 636(w), 555(w), 528(m), 502(w), 436(w), 426(w); Elem. Anal. (C₃H₄N₁₀, 180.14 g mol⁻¹) calcd.: C 20.00, H 2.24, N 77.76 %. Found: not determinable; ¹H NMR (DMSO-D₆, 400 MHz, ppm) δ = 4.20 (m, 2H), 3.74 (m, 2H). ¹³C NMR (DMSO D₆, 101 MHz, ppm) δ 152.8, 49.1, 45.6; ¹⁵N NMR (CDCl₃, 41 MHz, ppm) δ = 9.9, -13.9, -76.1, -135.7, -140.2, -147.3, -168.4, -169.7, -301.3, -314.4; HR-MS (ESI, 70 eV): [C₃H₅N₁₀] calcd.: 181.0694 [M - H⁺], found: 181.0695.

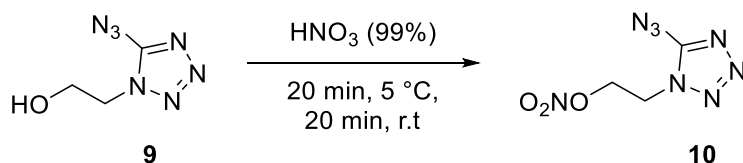
5-Azido-1-(2-hydroxyethyl)-tetrazole (9)



To a solution of 5-bromo-1-(2-acetoxyethyl)-tetrazole (**4b**) (1.00 g, 4.25 mmol, 1.0 eq.) in 2-propanole (25 mL) was added hydrazine hydrate (100%, 0.83 ml, 17.00 mmol, 4.0 eq.). After 72 h at ambient temperature, the precipitated crystals were removed by filtration. The solvent was evaporated to yield a crude mixture of 5-hydrazineyl-1-(2-hydroxyethyl)-tetrazole (**8**) and acetohydrazide. Without further purification the mixture was dissolved in hydrochloric acid (2M, 75 mL) and cooled to 0 – 5 °C. Slowly sodium nitrite (2.65 g, 38.2 mmol, 9.0 eq) in few water was added. After 20 min at 5 °C the solution was allowed to come to room temperature and was then extracted with ethyl acetate (3x50 mL). The organic layer was washed with water, dried over sodium sulfate and evaporated under a nitrogen stream to yield a crude oil of 5-azido-1-(2-hydroxyethyl)-tetrazole (**9**). The oil was purified by column chromatography (EtOAc/hex; 8/2; Rf: 0.35) to yield white crystalline **9** (265 mg, 1.71 mmol, 40%)

DTA (5 °C min⁻¹): 45 °C (melt.), 177 °C (dec.); IR (ATR) $\tilde{\nu}$ (cm⁻¹) = 2944(w), 2156(s), 2134(s), 2101(s), 1531(vs), 1470(m), 1445(m), 1352(w), 1326(m), 1252(m), 1226(m), 1181(m), 1125(w), 1089(m), 827(w), 808(w), 723(m), 654(m), 636(w), 555(w), 528(m); Elem. Anal. ($\text{C}_3\text{H}_5\text{N}_7\text{O}$, 155.12 g mol⁻¹) calcd.: C 23.23, H 3.25, N 63.21 %. Found: C 23.88, H 3.37, N 60.17 %.; ¹H NMR (DMSO-D₆, 400 MHz, ppm) δ = 5.05 (t, *J* = 5.7 Hz, 1H), 4.19 (dd, *J* = 5.7, 4.9 Hz, 2H), 3.74 (q, *J* = 5.5 Hz, 2H). ¹³C NMR (DMSO-D₆, 101 MHz, ppm) δ = 152.6, 58.5, 49.2; ¹⁴N NMR (DMSO-D₆, 29 MHz, ppm) δ = -133.8; HR-MS (EI, 70 eV): [$\text{C}_3\text{H}_5\text{N}_7\text{O}$] calcd.: 155.0556 [M^+], found: 155.0550.

5-Azido-1-(2-nitratoethyl)-tetrazole (10)

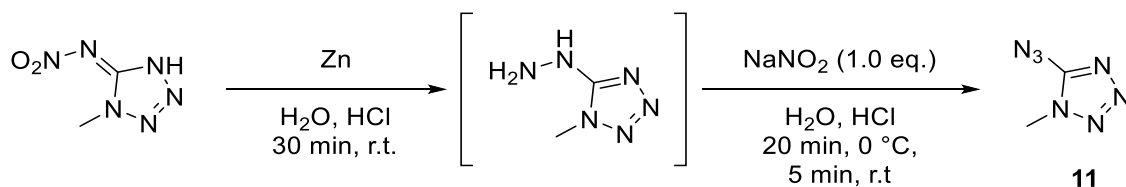


5-Azido-1-(2-nitratoethyl)-tetrazole (**9**) (150 mg, 1.03 mmol) was added to white fuming nitric acid (99%, 2 mL) at 5 °C. After 20 min the reaction was allowed to come to room

temperature and after further 20 min the reaction was quenched on ice. After extraction with ethyl acetate (3x20 mL) and neutralization with saturated sodium bicarbonate solution the organic layer was washed with water, dried over sodium sulfate and evaporated under a nitrogen stream to yield a crude oil of 5-azido-1-(2-nitratoethyl)-tetrazole (**10**). For purification the oil was dissolved in a small amount of methanol (5-10% water) and left for crystallization at 5°C to yield white crystalline **10** (173 mg, 0.87 mmol, 84%)

DTA (5 °C min⁻¹): 45 °C (melt.), 166 °C (dec.); Sensitivities: BAM drop hammer: <1 J, friction tester: 5 N; IR (ATR) $\tilde{\nu}$ (cm⁻¹) = 2967(w), 2923(w), 2158(s), 1745(w), 1635(s), 1534(vs), 1471(m), 1429(m), 1331(m), 1279(vs), 1185(m), 1090(m), 1027(m), 1006(m), 885(s), 840(vs), 754(m), 724(m), 705(m), 659(m), 633(m), 528(m); Elem. Anal. (C₃H₄N₈O₃, 200.12 g mol⁻¹) calcd.: C 18.01, H 2.01, N 55.99 %. Found: C 18.41, H 2.36, N 54.57 %.; ¹H NMR (Acetone-D₆, 400 MHz, ppm) δ = 5.02 (m, 2H), 4.68 (m, 2H); ¹³C NMR (Acetone-D₆, 101 MHz, ppm) δ = 152.9, 69.8, 43.8; ¹⁵N NMR (Acetone-D₆, 41 MHz, ppm) δ = 10.5, -13.3, -44.9, -75.3, -142.3, -147.0, -169.9, -301.7; HR-MS (EI, 70 eV): [C₃H₅N₈O₃] calcd.: 200.0406 [M⁺], found: 200.0404.

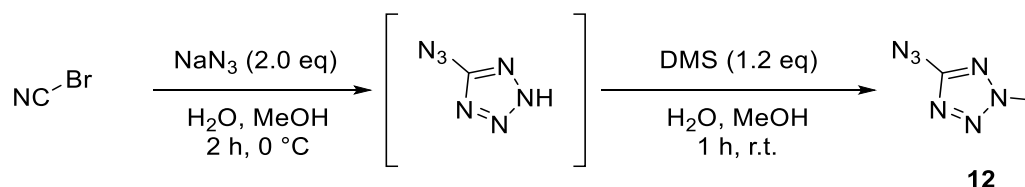
5-Azido-1-methyltetrazole (**11**)



1-Methyl-5-nitriminotetrazole (1.44 g, 10.0 mmol, 1.0 eq) was dissolved in water (10 mL). To this, an excess of zinc powder (2.00 g) was added and the mixture was cooled using an ice bath. Hydrochloric acid (30 mL, 2 M) was added in drops and the mixture was stirred for 30 min at room temperature. After the remained zinc powder was removed by filtration a solution of sodium nitrite (0.65 g, 10.0 mmol, 1.0 eq) in water (10 mL) was added dropwise at temperatures below 0 °C until a clear formation of NO₂ was observed. After stirring the solution for further 5 min, the product was extracted DCM (3 x 20 mL). The organic phases were combined, washed once with hydrochloric acid (2 M) and two times with a concentrated solution of Na₂CO₃. The organic phase was dried using sodium sulfate and evaporated. Liquid **11** (0.78 g, 6.30 mmol, 63%) was remained which could be solidified by cooling in a freezer.

DSC (5 °C min⁻¹): 20 °C (melt.), 160 ° (dec.); Sensitivities: BAM drop hammer: <1 J; friction tester: <5 N; ESD: 50 mJ; EA (C₂H₃N₇, 125.11) calcd.: C 19.20, H 2.42, N 78.38 %; Found: C 19.30, H 2.81, N 78.00; IR (ATR) $\tilde{\nu}$ (cm⁻¹) = 2962 (w), 2160 (vs), 1630 (w), 1547 (s), 1476 (s), 1447 (m), 1413 (m), 1377 (w), 1304 (s), 1259 (s), 1221 (s), 1166 (w), 1092 (m), 1036 (w), 971 (w), 816 (w), 723 (m), 693 (w), 673 (s), 528 (w); ¹H NMR (DMSO-D₆, 400 MHz, ppm) δ = 3.77 (CH₃); ¹³C NMR (DMSO-D₆, 101 MHz, ppm) δ = 152.9, 33.1; ¹⁵N NMR (DMSO-D₆, 41 MHz, ppm) δ = 7.2 (N3), -12.2 (N2, q, ³J_{NH} = 1.6 Hz), -75.6 (N4), -144.0 (N7), -146.5 (N6), -172.6 (N1, q, ²J_{NH} = 2.0 Hz), -301.6 (N5); *m/z* (DEI): 83 (1), 58 (13), 53 (8), 43 (42), 42 (3), 40 (4), 32 (2), 28 (13), 15 (10).

5-Azido-2-methyltetrazole (12)



Cyanogen bromide (0.53 g, 5.00 mmol, 1.0 eq) was dissolved in a mixture of cold water (16 mL) and MeOH (4 mL). To this, a solution of sodium azide (0.65 g, 10.0 mmol, 2.0 eq) was added drop wise while cooling in an ice bath. After 2 h, dimethyl sulfate (0.28 mL, 3.0 mmol, 1.2 eq) was added slowly and the solution was allowed to come to room temperature. After one hour, the precipitate formed was filtered off and washed with a small amount of cold water. The analytically pure **12** (0.29 g, 2.30 mmol, 46%) can be recrystallized from hot water.

DSC (5 °C min⁻¹): 62 °C (melt), 162 °C (dec); Sensitivities: BAM drop hammer: <1 J friction sensitivity: <5 N; ESD: 80 mJ; EA (C₂H₃N₇, 125.11) calcd.: C 19.20, H 2.42, N 78.38 %; Found: C 19.19, H 2.21, N 77.41; IR (ATR) $\tilde{\nu}$ (cm⁻¹) = 3038 (w), 2956 (w), 2417 (w), 2285 (w), 2160 (vs), 1725 (w), 1588 (m), 1550 (s), 1506 (s), 1476 (s), 1421 (m), 1396 (m), 1305 (m), 1259 (w), 1218 (m), 1182 (m), 1091 (w), 1050 (w), 1026 (w), 794 (m), 739 (m), 721 (w), 674 (m), 527 (m); ¹H NMR (DMSO-D₆, 400 MHz, ppm): δ = 4.28 (CH₃); ¹³C NMR (DMSO-D₆, 101 MHz, ppm): δ = 161.9, 40.7; ¹⁵N NMR (DMSO-D₆, 41 MHz, ppm): δ = 0.4 (N1, q, ³J_{NH} = 2.0 Hz), -71.0 (N4), -98.3 (N1, q, ³J_{NH} = 1.9 Hz), -105.7 (N2, q, ²J_{NH} = 2.3 Hz), -144.2 (N6), -146.0 (N7), -300.5 (N5); *m/z* (DEI):

125 (43), 83 (1), 69 (12), 57 (1), 55 (3), 54 (23), 53 (12), 43 (100), 40 (11), 29 (11), 28 (29), 27 (12), 26 (14), 31 (8), 28(29), 18 (14), 15 (48).

2. Thermal Analysis

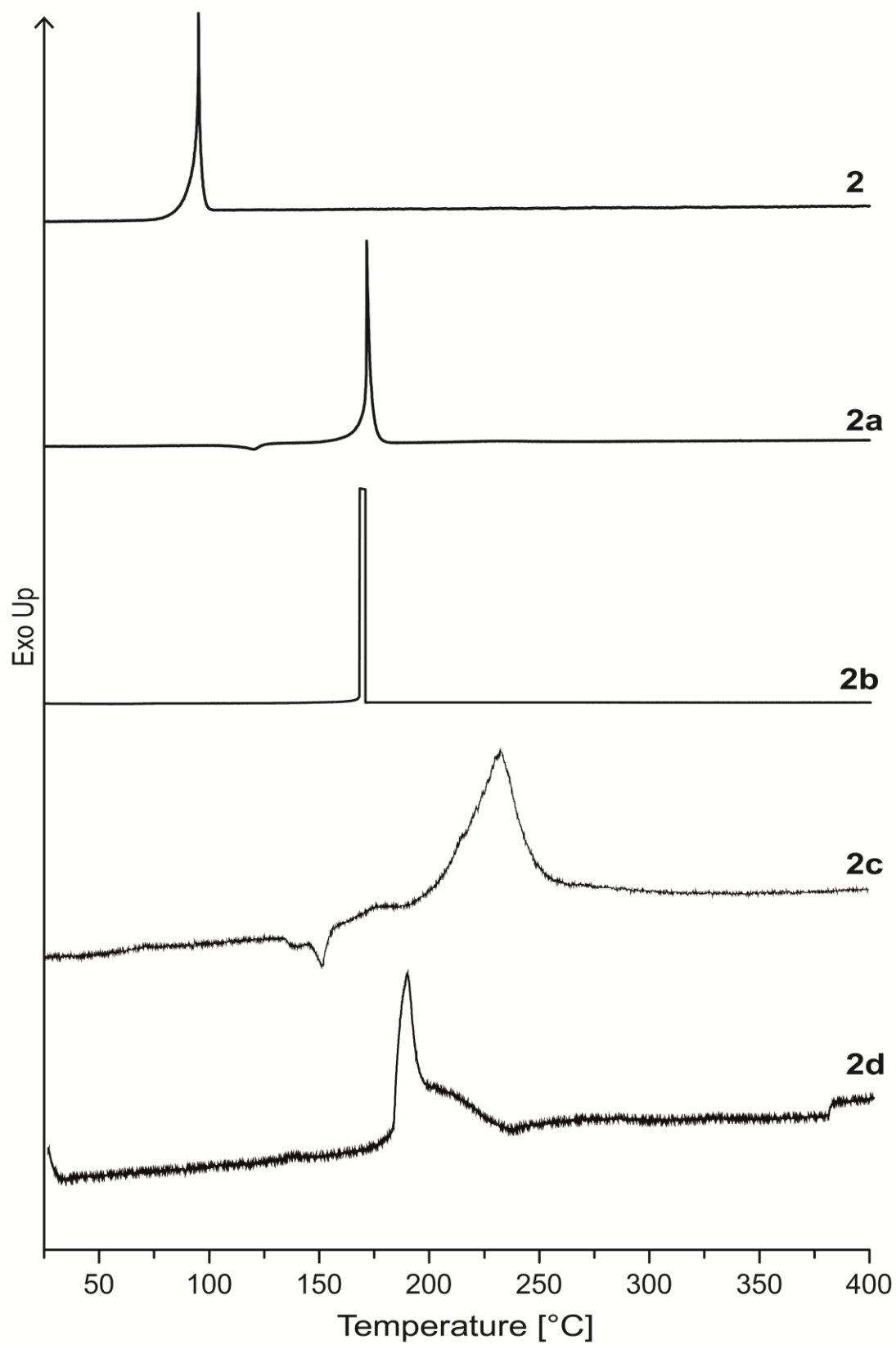


Figure S1. Thermal analysis through DTA of compounds **2** and **2a-2d**.

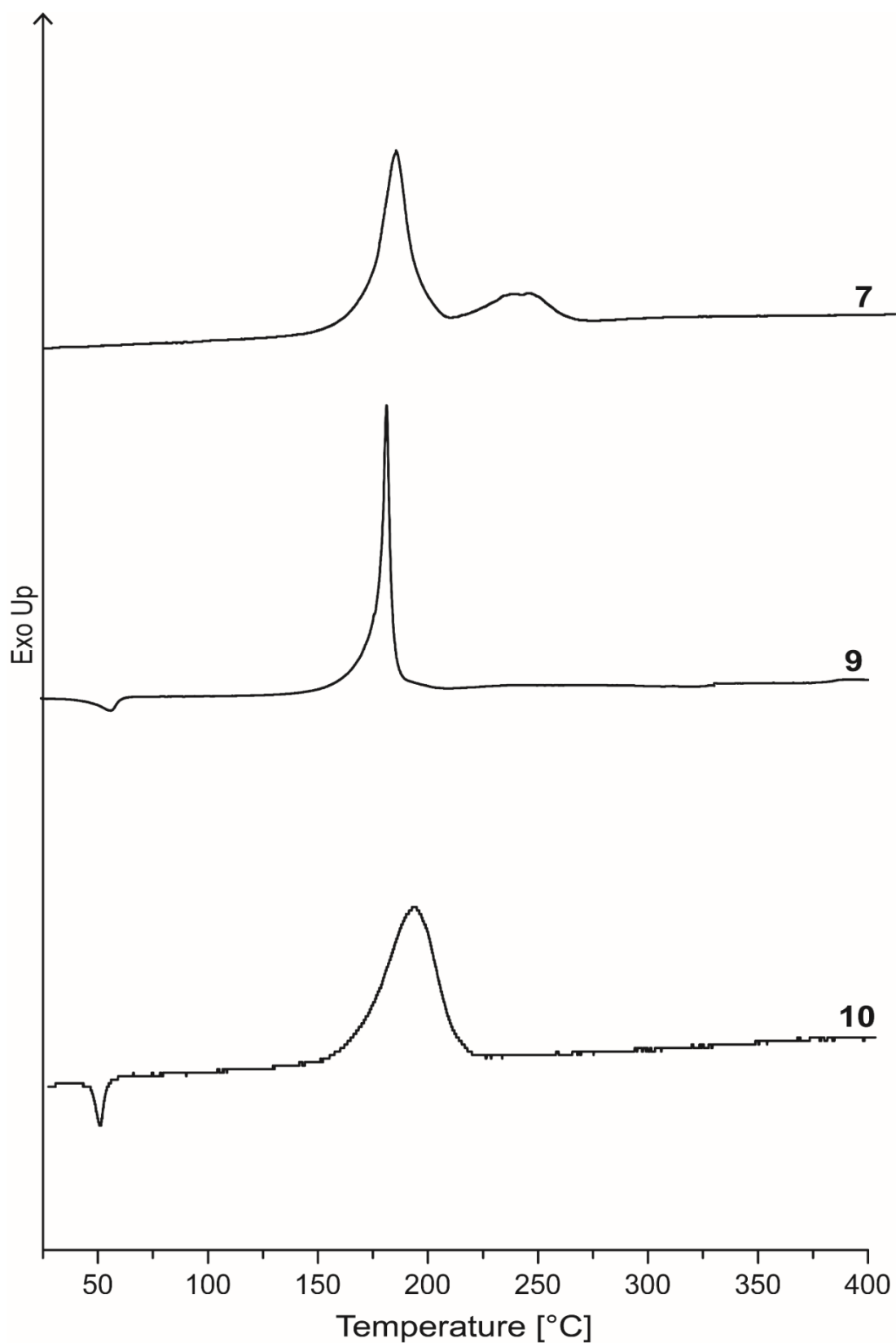


Figure S2. Thermal analysis through DTA of compounds **7** and **9-10**.

3. X-ray diffraction

Crystal structure data were obtained from an Oxford Xcalibur3 diffractometer with a Spellman generator (voltage 50 kV, current 40 mA) and a Kappa CCD area for data collection using Mo- $K\alpha$ radiation ($\lambda = 0.71073 \text{ \AA}$). The data collection was performed using the CRYSTALIS RED software.^[S5] The solution of the structure was performed by direct methods and refined by full-matrix least-squares on F2 (SHELXT)^[S6] implemented in the OLEX2^[S7] software suite. The non-hydrogen atoms were refined anisotropically and the hydrogen atoms were located and freely refined. The absorption correction was carried out by a SCALE3 ABSPACK multiscan method.^[S8] The DIAMOND2 plots shown with thermal ellipsoids at the 50% probability level and hydrogen atoms are shown as small spheres of arbitrary radius. The SADABS program embedded in the Bruker APEX3 software was used for multi-scan absorption corrections in all structures.^[S9]

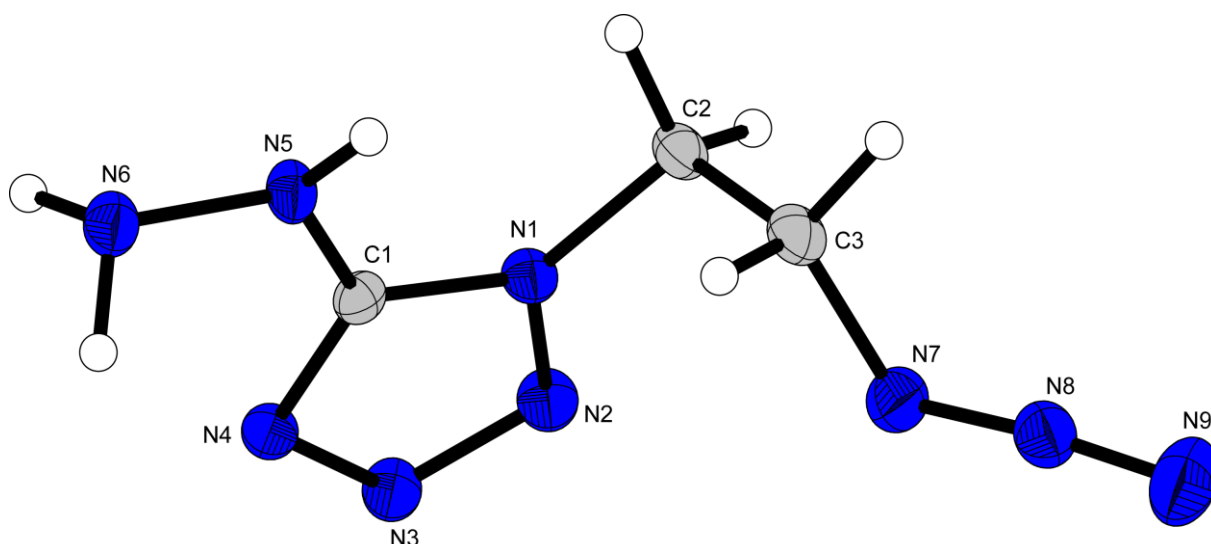


Figure S3. Representation of the molecular unit of **5**, showing the atom-labeling scheme. Thermal ellipsoids represent the 50% probability level and hydrogen atoms are shown as small spheres of arbitrary radius.

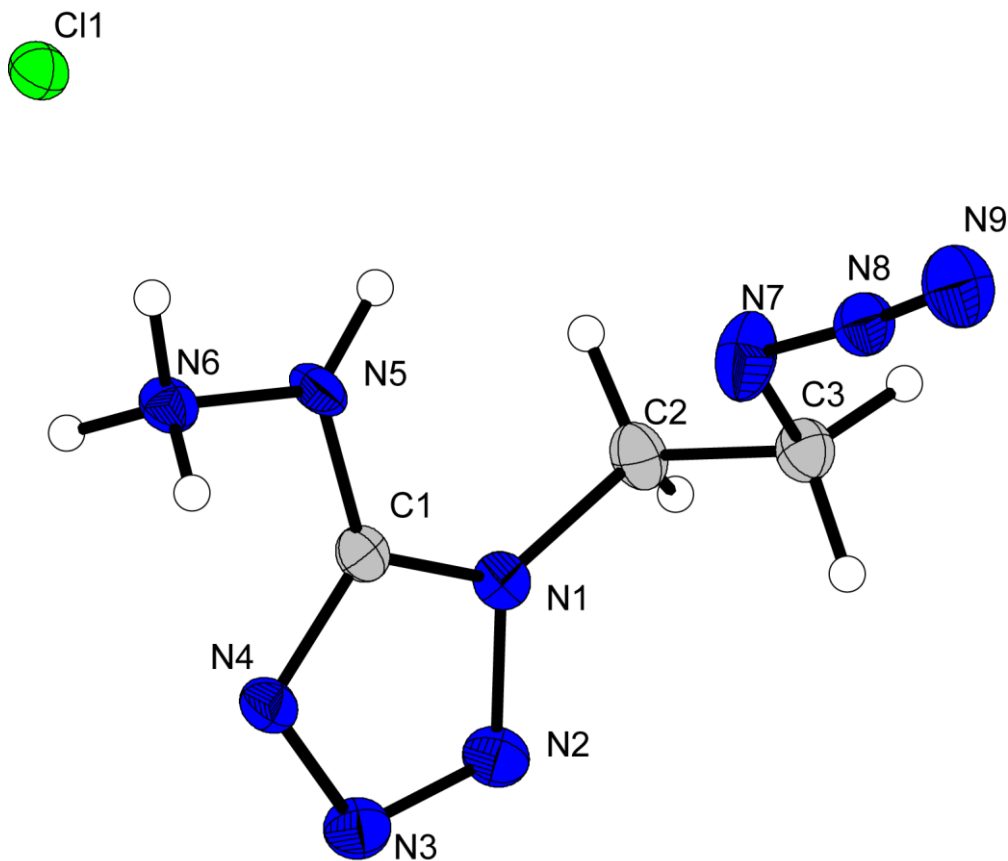


Figure S4. Representation of the molecular unit of **6**, showing the atom-labeling scheme. Thermal ellipsoids represent the 50% probability level and hydrogen atoms are shown as small spheres of arbitrary radius.

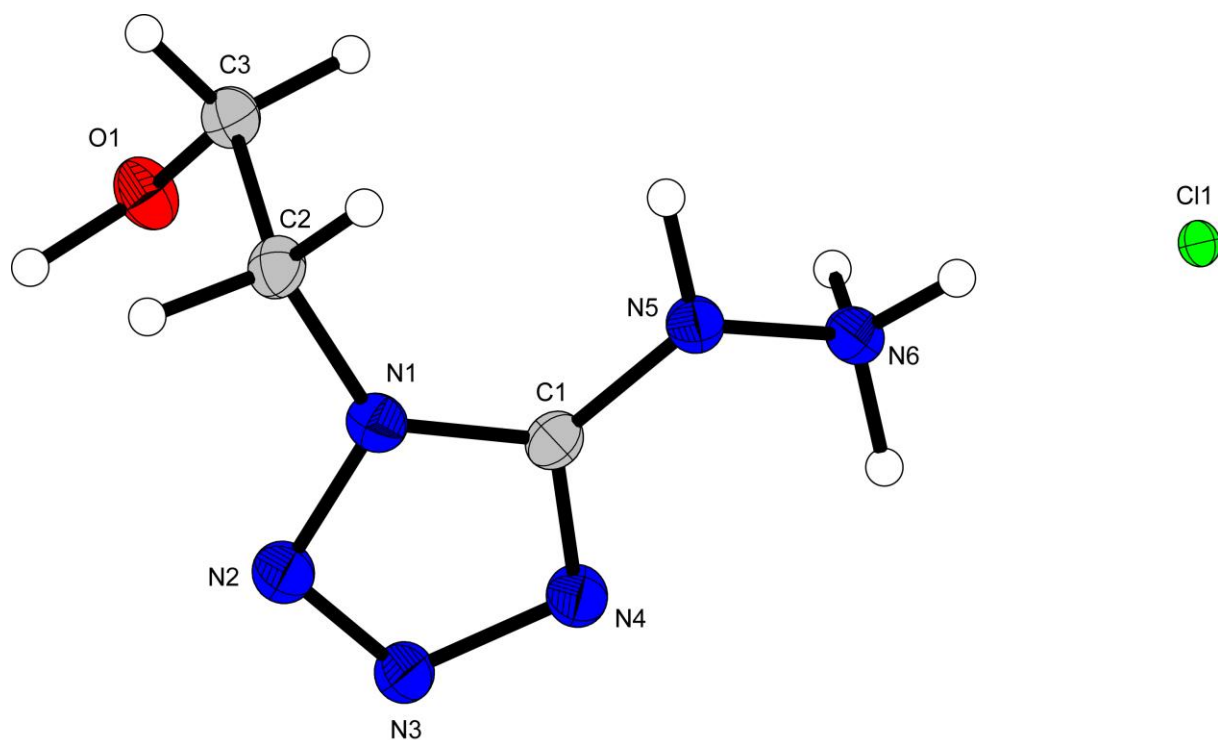


Figure S5. Representation of the molecular unit of **8 · HCl**, showing the atom-labeling scheme. Thermal ellipsoids represent the 50% probability level and hydrogen atoms are shown as small spheres of arbitrary radius.

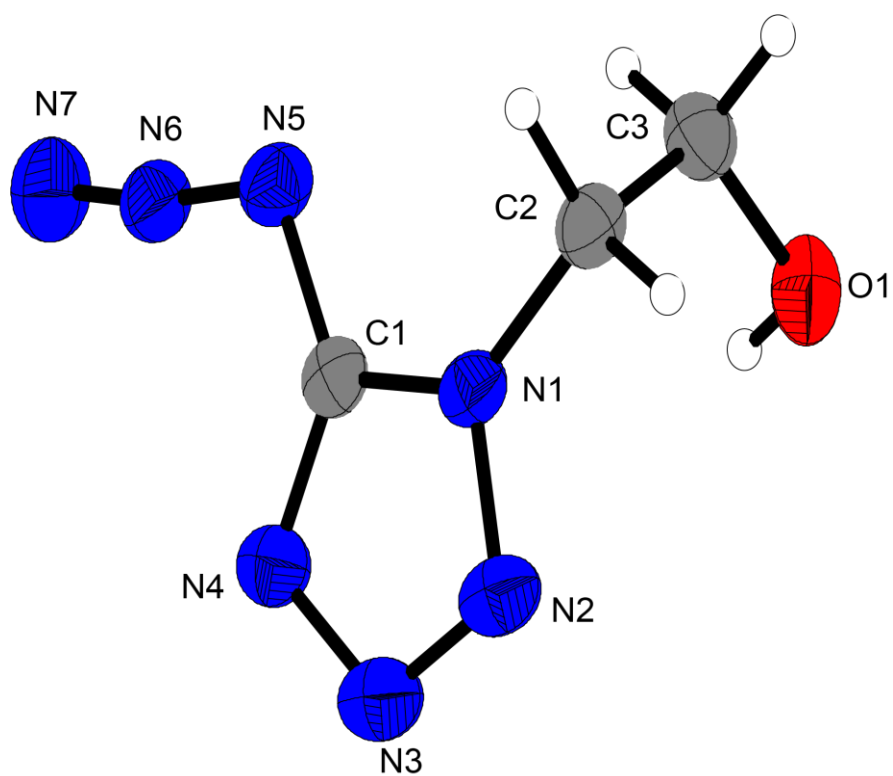


Figure S6. Representation of the molecular unit of **9**, showing the atom-labeling scheme. Thermal ellipsoids represent the 50% probability level and hydrogen atoms are shown as small spheres of arbitrary radius.

Table S1. Crystallographic data and structure refinement details for the prepared compounds **2a**, **2b** and **2d**.

	2a	2b	2d
Formula	C ₃ H ₄ N ₉ O ₂ , NH ₄	C ₃ H ₄ N ₉ O ₂ , NH ₃ OH	Ag ₂ C ₆ H ₈ N ₁₈ O ₄
FW [g mol ⁻¹]	216.19	232.19	612.04
Crystal system	triclinic	triclinic	orthorhombic
Space group	<i>P</i> -1 (No. 2)	<i>P</i> -1 (No. 2)	<i>Pbca</i> (No. 61)
Color / Habit	colorless plate	colorless block	colorless platelet
Size [mm]	0.01 x 0.30 x 0.30	0.30 x 0.30 x 0.50	0.10 x 0.15 x 0.25
a [Å]	4.3043(3)	7.2416(6)	8.9776(6)
b [Å]	6.2716(5)	7.3297(8)	11.1520(12)
c [Å]	16.6686(13)	18.1018(18)	33.395(3)
α [°]	83.082(6)	89.358(9)	
β [°]	88.293(6)	79.717(8)	
γ [°]	84.288(6)	77.681(8)	
V [Å ³]	444.40(6)	923.26(16)	3343.5(5)
Z	2	4	8
ρ _{calc.} [g cm ⁻³]	1.616	1.671	2.432
μ [mm ⁻¹]	0.135	0.144	2.411
F(000)	224	480	2368
λ _{MoKα} [Å]	0.71073	0.71073	0.71073
T [K]	123	105	293
θ Min-Max [°]	2.5, 26.4	2.3, 26.4	2.4, 26.4
Dataset	-5: 5 ; -7: 7 ; -20: 20	-9: 9 ; -9: 7 ; -20: 22	-11: 11 ; -13: 13 ; -41: 41
Reflections collected	6814	7565	28293
Independent refl.	1812	3765	3406
<i>R</i> _{int}	0.035	0.032	0.166
Observed reflections	1427	2433	2254
Parameters	168	353	271
<i>R</i> ₁ (obs) ^[a]	0.0363	0.0485	0.0650
w <i>R</i> ₂ (all data) ^[b]	0.0869	0.1216	0.1368
<i>S</i> ^[c]	1.02	1.03	1.09
Resd. dens [e Å ⁻³]	-0.19, 0.21	-0.24, 0.30	-0.85, 1.58
Device type	Xcalibur Sapphire3	Xcalibur Sapphire3	Xcalibur Sapphire3
Solution	SIR-92	SIR-92	SIR-92
Refinement	SHELXL-2013	SHELXL-2013	SHELXL-2013
Absorption correction	multi-scan	multi-scan	multi-scan
CCDC	2157201	2157198	2157203

^[a] $R_1 = \sum ||F_o| - |F_c|| / \sum |F_o|$; ^[b] $wR_2 = [\sum [w(F_o^2 - F_c^2)^2] / \sum [w(F_o^2)]]^{1/2}$; $w = [\sigma^2(F_o^2) + (xP)^2 + yP]^{-1}$ and $P = (F_o^2 + 2F_c^2) / 3$; ^[c] $S = (\sum [w(F_o^2 - F_c^2)^2] / (n-p))^{1/2}$ (n = number of reflections; p = total number of parameters).

Table S2. Crystallographic data and structure refinement details for the prepared compounds **5-7**.

	5	6	7
Formula	C ₃ H ₇ N ₉	C ₃ H ₈ N ₉ Cl	C ₃ H ₄ N ₁₀
FW [g mol ⁻¹]	169.18	205.63	180.16
Crystal system	monoclinic	monoclinic	orthorhombic
Space group	<i>P2₁/c</i> (No. 14)	<i>P2₁/c</i> (No. 14)	<i>Fdd2</i> (No. 43)
Color / Habit	colorless block	colourless block	colorless block
Size [mm]	0.50 x 0.50 x 0.50	0.10 x 0.50 x 0.50	0.05 x 0.25 x 0.50
a [Å]	6.0070(5)	12.7917(11)	25.526(2)
b [Å]	10.9792(10)	7.7802(6)	12.6485(10)
c [Å]	10.9160(11)	8.8236(6)	9.4801(9)
α [°]	90	90	
β [°]	95.467(7)	101.731(6)	
γ [°]	90	90	
V [Å ³]	716.66(11)	859.80(12)	3060.8(4)
Z	4	4	16
ρ _{calc.} [g cm ⁻³]	1.568	1.589	1.564
μ [mm ⁻¹]	0.120	0.416	0.122
F(000)	352	424	1472
λ _{MoKα} [Å]	0.71073	0.71073	0.71073
T [K]	101	101	102
θ Min-Max [°]	2.6, 29.2	3.1, 26.4	2.8, 26.4
Dataset	-7: 7 ; -13: 5 ; -14: 12	-12: 15 ; -7: 9 ; -10: 11	-31: 31 ; -15: 15 ; -11: 11
Reflections collected	3304	6302	11967
Independent refl.	1627	1755	1568
R _{int}	0.022	0.042	0.062
Observed reflections	1285	1369	1343
Parameters	137	119	135
R ₁ (obs) ^[a]	0.0420	0.0438	0.0366
wR ₂ (all data) ^[b]	0.0985	0.1159	0.0758
S ^[c]	1.04	1.06	1.05
Resd. dens [e Å ⁻³]	-0.19, 0.24	-0.67, 0.62	-0.12, 0.17
Device type	Xcalibur Sapphire3	Xcalibur Sapphire3	Xcalibur Sapphire3
Solution	SIR-92	SIR-92	SIR-92
Refinement	SHELXL-2013	SHELXL-2013	SHELXL-2013
Absorption correction	multi-scan	multi-scan	multi-scan
CCDC	2157204	2157196	2157199

^[a]R₁ = Σ||F_o|-|F_c||/Σ|F_o|; ^[b]wR₂ = [Σ[w(F_o²-F_c²)²]/Σ[w(F_o²)]^{1/2}; w = [σc²(F_o²)+(xP)²+yP]⁻¹ and P=(F_o²+2F_c²)/3; ^[c]S = (Σ[w(F_o²-F_c²)²]/(n-p))^{1/2} (n = number of reflections; p = total number of parameters).

Table S3. Crystallographic data and structure refinement details for the prepared compounds **8** · HCl-**10**.

	8 · HCl	9	10
Formula	C ₃ H ₉ N ₆ OCl	C ₃ H ₅ N ₇ O	C ₃ H ₄ N ₈ O ₃
FW [g mol ⁻¹]	180.61	155.14	200.14
Crystal system	monoclinic	monoclinic	monoclinic
Space group	<i>P2₁/c</i> (No. 14)	<i>P2₁/n</i> (No. 14)	<i>P2₁/n</i> (No. 14)
Color / Habit	colorless block	colorless block	colorless rod
Size [mm]	0.20 x 0.50 x 0.50	0.08 x 0.12 x 0.15	0.10 x 0.20 x 0.50
a [Å]	10.738(3)	8.3335(6)	9.5705(13)
b [Å]	6.5212(11)	8.3390(6)	6.7210(7)
c [Å]	11.244(2)	9.5255(7)	12.3677(16)
α [°]	90	90	90
β [°]	100.26(2)	98.792(7)	97.633(12)
γ [°]	90	90	90
V [Å ³]	774.8(3)	654.18(8)	788.48(17)
Z	4	4	4
ρ _{calc.} [g cm ⁻³]	1.548	1.575	1.686
μ [mm ⁻¹]	0.448	0.127	0.148
F(000)	376	320	408
λ _{MoKα} [Å]	0.71073	0.71073	0.71073
T [K]	104	200	101
θ Min-Max [°]	3.6, 26.4	4.3, 26.0	2.5, 25.7
Dataset	-13: 12 ; -8: 8 ; -14: 14	-10: 10 ; -10: 10 ; -11: 11	-9: 11 ; -8: 8 ; -15: 13
Reflections collected	5599	3070	5590
Independent refl.	1577	1284	1494
R _{int}	0.039	0.022	0.033
Observed reflections	1309	924	1215
Parameters	136	120	143
R ₁ (obs) ^[a]	0.0492	0.0302	0.0595
wR ₂ (all data) ^[b]	0.1418	0.0691	0.1736
S ^[c]	1.09	0.91	1.12
Resd. dens [e Å ⁻³]	-0.42, 0.91	-0.18, 0.15	-0.37, 0.60
Device type	Xcalibur Sapphire3	Xcalibur Sapphire3	Xcalibur Sapphire3
Solution	SIR-92	SIR-92	SIR-92
Refinement	SHELXL-2013	SHELXL-2013	SHELXL-2013
Absorption correction	multi-scan	multi-scan	multi-scan
CCDC	2157197	2157202	2157200

^[a]R₁ = Σ||F_o| - |F_c|| / Σ|F_o|; ^[b]wR₂ = [Σ[w(F_o² - F_c²)²] / Σ[w(F_o)²]^{1/2}; w = [σc²(F_o²) + (xP)² + yP]⁻¹ and P = (F_o² + 2F_c²) / 3; ^[c]S = (Σ[w(F_o² - F_c²)²] / (n - p))^{1/2} (n = number of reflections; p = total number of parameters).

Table S4. Crystallographic data and structure refinement details for the prepared compounds **11** and **12**.

	11	12
Formula	C ₂ H ₃ N ₇	C ₂ H ₃ N ₇
FW [g mol ⁻¹]	125.11	125.11
Crystal system	monoclinic	monoclinic
Space group	<i>P</i> 2 ₁ / <i>m</i> (No. 11)	<i>P</i> 2 ₁ / <i>c</i> (No. 14)
Color / Habit	colorless needle	colorless block
Size [mm]	0.06 x 0.10 x 0.26	0.10 x 0.12 x 0.13
a [Å]	8.7382(4)	6.6219(5)
b [Å]	6.2408(4)	8.7588(7)
c [Å]	10.2986(6)	9.6392(8)
α [°]	90	90
β [°]	90.722(4)	108.858(7)
γ [°]	90	90
V [Å ³]	561.57(6)	529.06(8)
Z	4	4
ρ _{calc.} [g cm ⁻³]	1.480	1.571
μ [mm ⁻¹]	0.115	0.123
F(000)	256	256
λ _{MoKα} [Å]	0.71073	0.71073
T [K]	200	173
θ Min-Max [°]	3.8, 26.0	4.0, 26.0
Dataset	-10: 8 ; -7: 7 ; -12: 8	-5: 8 ; -10: 8 ; -10: 11
Reflections collected	2919	2662
Independent refl.	1206	1037
<i>R</i> _{int}	0.037	0.036
Observed reflections	729	674
Parameters	112	94
<i>R</i> ₁ (obs) ^[a]	0.0320	0.0331
w <i>R</i> ₂ (all data) ^[b]	0.0926	0.0854
<i>S</i> ^[c]	0.97	0.90
Resd. dens [e Å ⁻³]	-0.18, 0.16	-0.16, 0.18
Device type	Xcalibur Sapphire3	Xcalibur Sapphire3
Solution	SIR-92	SIR-92
Refinement	SHELXL-2013	SHELXL-2013
Absorption correction	multi-scan	multi-scan
CCDC	707542	707543

^[a] $R_1 = \sum ||F_o| - |F_c|| / \sum |F_o|$; ^[b] $wR_2 = [\sum [w(F_o^2 - F_c^2)^2] / \sum [w(F_o^2)]]^{1/2}$; $w = [\sigma^2(F_o^2) + (xP)^2 + yP]^{-1}$ and $P = (F_o^2 + 2F_c^2) / 3$; ^[c] $S = (\sum [w(F_o^2 - F_c^2)^2] / (n-p))^{1/2}$ (n = number of reflections; p = total number of parameters).

4. Computation

Heat of Formation Computation

All quantum chemical calculations were carried out using the Gaussian G09 program package.^[S10] The enthalpies (H) and free energies (G) were calculated using the complete basis set (CBS) method of Petersson and co-workers in order to obtain very accurate energies. The CBS models are using the known asymptotic convergence of pair natural orbital expressions to extrapolate from calculations using a finite basis set to the estimated CBS limit. CBS-4 starts with an HF/3-21G(d) geometry optimization; the zero-point energy is computed at the same level. It then uses a large basis set SCF calculation as a base energy, and an MP2/6-31+G calculation with a CBS extrapolation to correct the energy through second order. A MP4(SDQ)/6-31+ (d,p) calculation is used to approximate higher order contributions. In this study, we applied the modified CBS-4M.

Heats of formation of the synthesized ionic compounds were calculated using the atomization method (equation E1) using room temperature CBS-4M enthalpies, which are summarized in Table S5.^[S11, S12]

$$\Delta_f H^{\circ}(\text{g, M, 298}) = H_{(\text{Molecule, 298})} - \sum H^{\circ}_{(\text{Atoms, 298})} + \sum \Delta_f H^{\circ}_{(\text{Atoms, 298})} \quad (\text{E1})$$

Table S5. CBS-4M electronic enthalpies for atoms C, H, N and O and their literature values for atomic $\Delta H^{\circ}_{f,298} / \text{kJ mol}^{-1}$

	$-H^{298}$ [a.u.]	NIST ^[S13]
H	0.500991	218.2
C	37.786156	717.2
N	54.522462	473.1
O	74.991202	249.5

For neutral compounds the sublimation enthalpy, which is needed to convert the gas phase enthalpy of formation to the solid state one, was calculated by the *Trouton* rule.^[S14] For ionic compounds, the lattice energy (U) and lattice enthalpy (ΔH_L) were calculated from the corresponding X-ray molecular volumes according to the equations provided by *Jenkins* and *Glasser*.^[S15] With the calculated lattice enthalpy the gas-phase enthalpy of formation was converted into the solid state (standard conditions)

enthalpy of formation. These molar standard enthalpies of formation (ΔH_m) were used to calculate the molar solid state energies of formation (ΔU_m) according to equation E2.

$$\Delta U_m = \Delta H_m - \Delta n RT \quad (\text{E2})$$

(Δn being the change of moles of gaseous components)

The calculation results are summarized in Table S6.

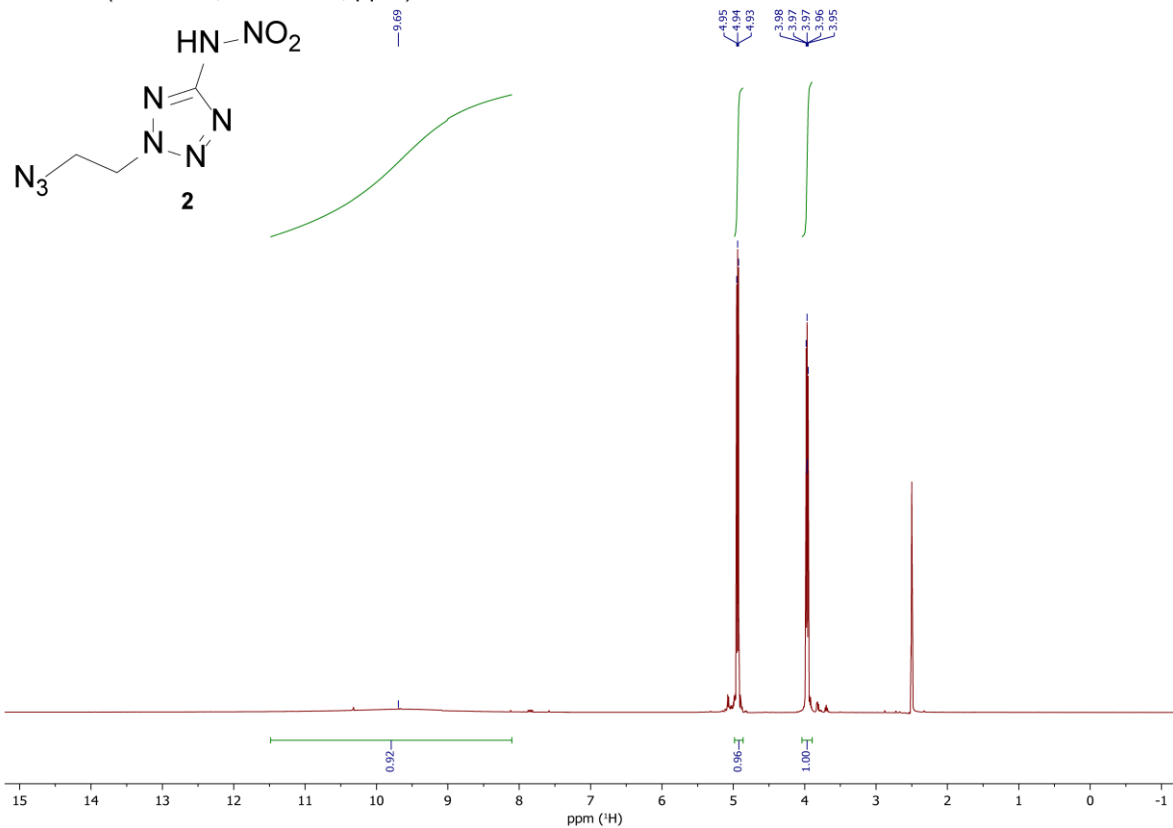
Table S6. Calculation results.

	$-H^{298}$ [a] [a.u.]	$\Delta_f H^\circ(\text{g,M})$ [kJ mol ⁻¹] [b]	V_M [Å ³] [c]	$\Delta U_L; \Delta H_L$ [d] [kJ mol ⁻¹]	$\Delta_f H^\circ(\text{s})$ [e] [kJ mol ⁻¹]	Δn [f]	$\Delta_f U(\text{s})$ [g] [kJ mol ⁻¹]
A⁻ (2)	758.815212	506.6					
NH₄⁺	56.796608	635.3					
NH₃OH⁺	112.630523	773.4					
2	759.333150	680.1	-	-	647.1	-8.0	666.9
2a	-	-	228.0	487.8; 492.8	649.1	-10.0	673.9
2b	-	-	238.0	482.6; 487.6	705.5	-10.5	731.5
7	663.165046	980.3	-	-	932.7	-7.0	950.1
10	779.173027	574.3	-	-	514.5	-7.5	533.1
11	460.540365	649.6	-	-	594.5	-5.0	606.9
12	460.547855	630.0	-	-	566.9	-5.0	579.3

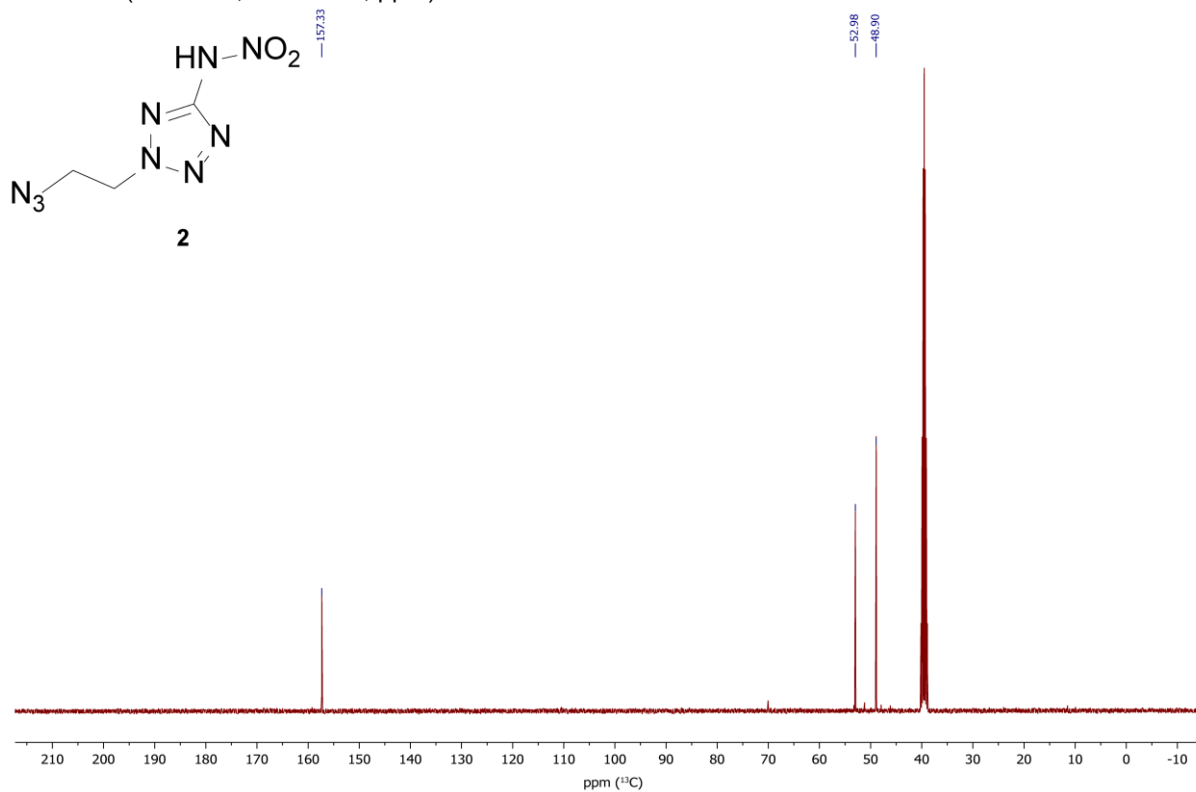
[a] CBS-4M electronic enthalpy; [b] gas phase enthalpy of formation; [c] molecular volumes taken from X-ray structures and corrected to room temperature; [d] lattice energy and enthalpy (calculated using Jenkins and Glasser equations); [e] standard solid state enthalpy of formation; [f] Δn being the change of moles of gaseous components when formed; [g] solid state energy of formation.

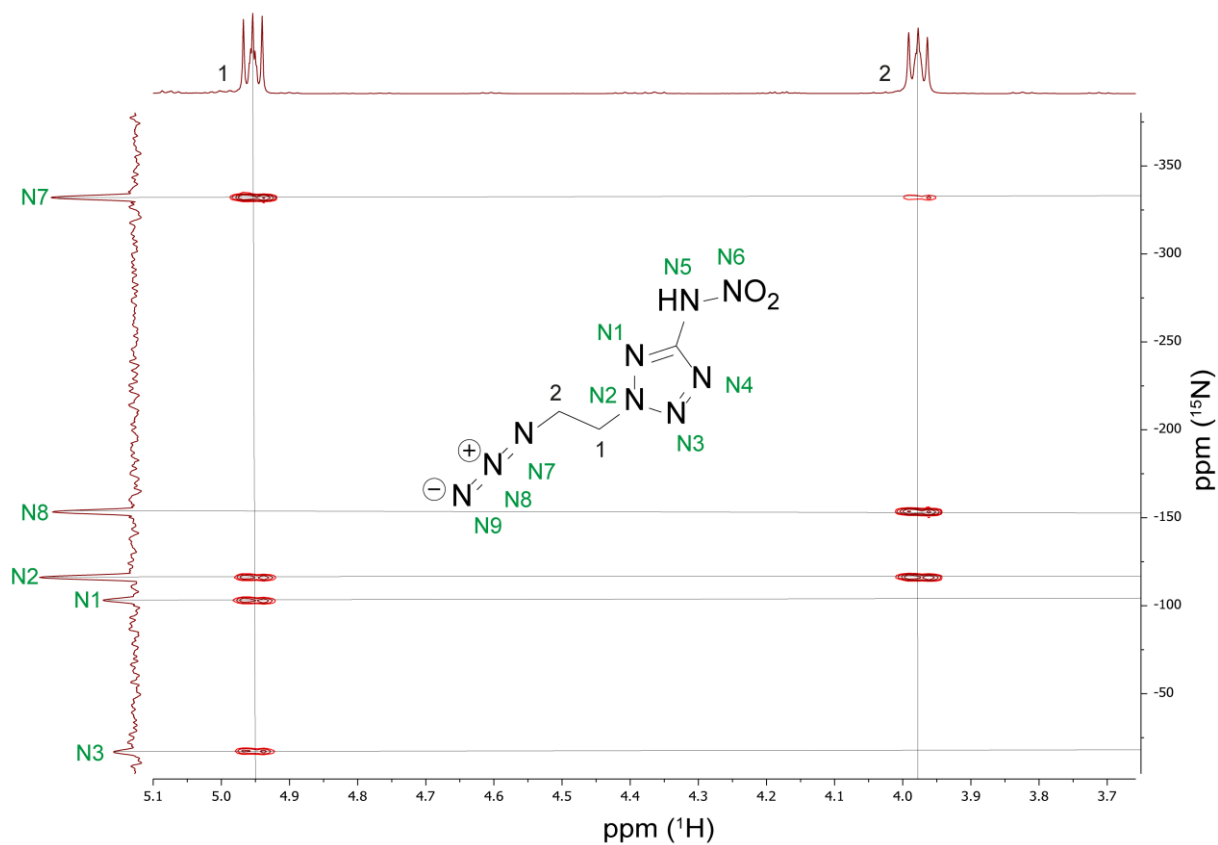
5. NMR Spectroscopy

$^1\text{H-NMR}$ (400 MHz, DMSO-D_6 , ppm)

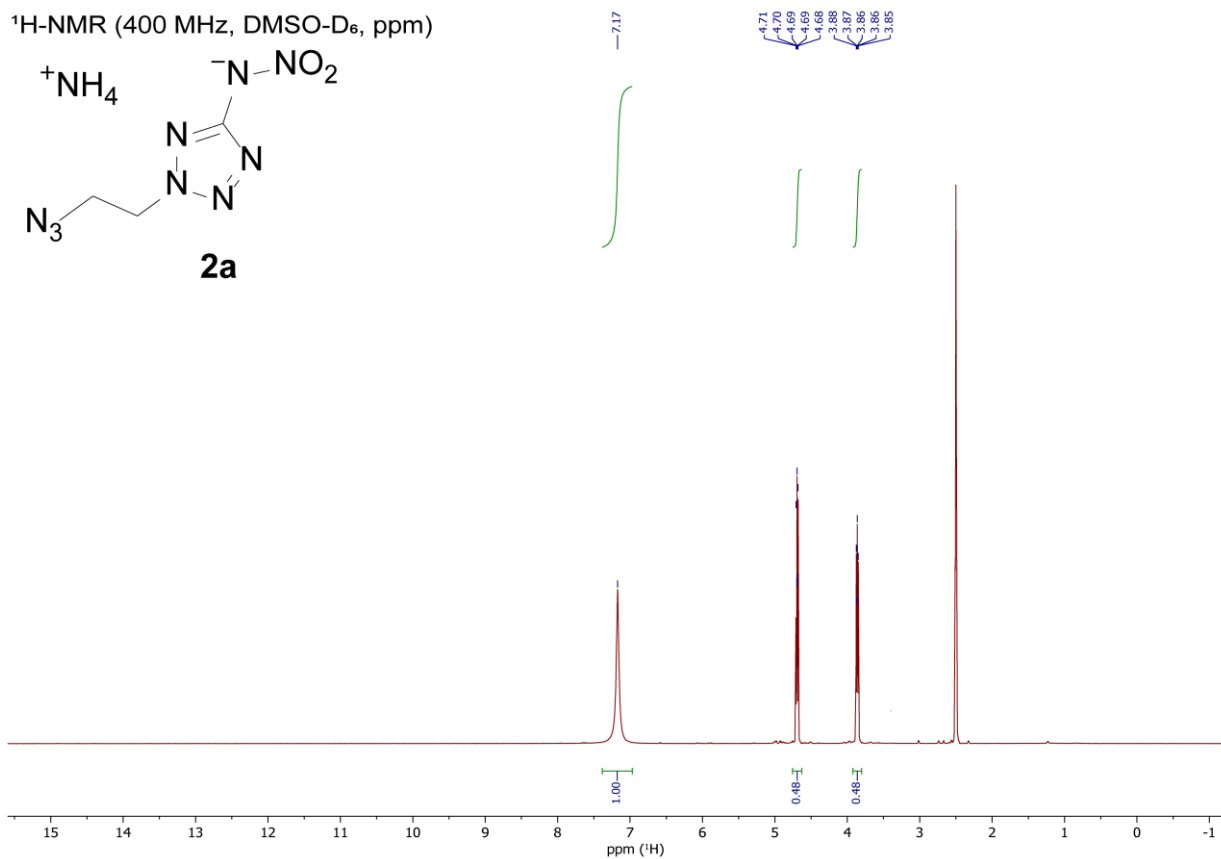
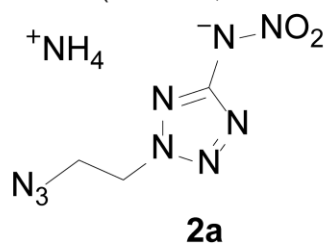


$^{13}\text{C-NMR}$ (101 MHz, DMSO-D_6 , ppm)

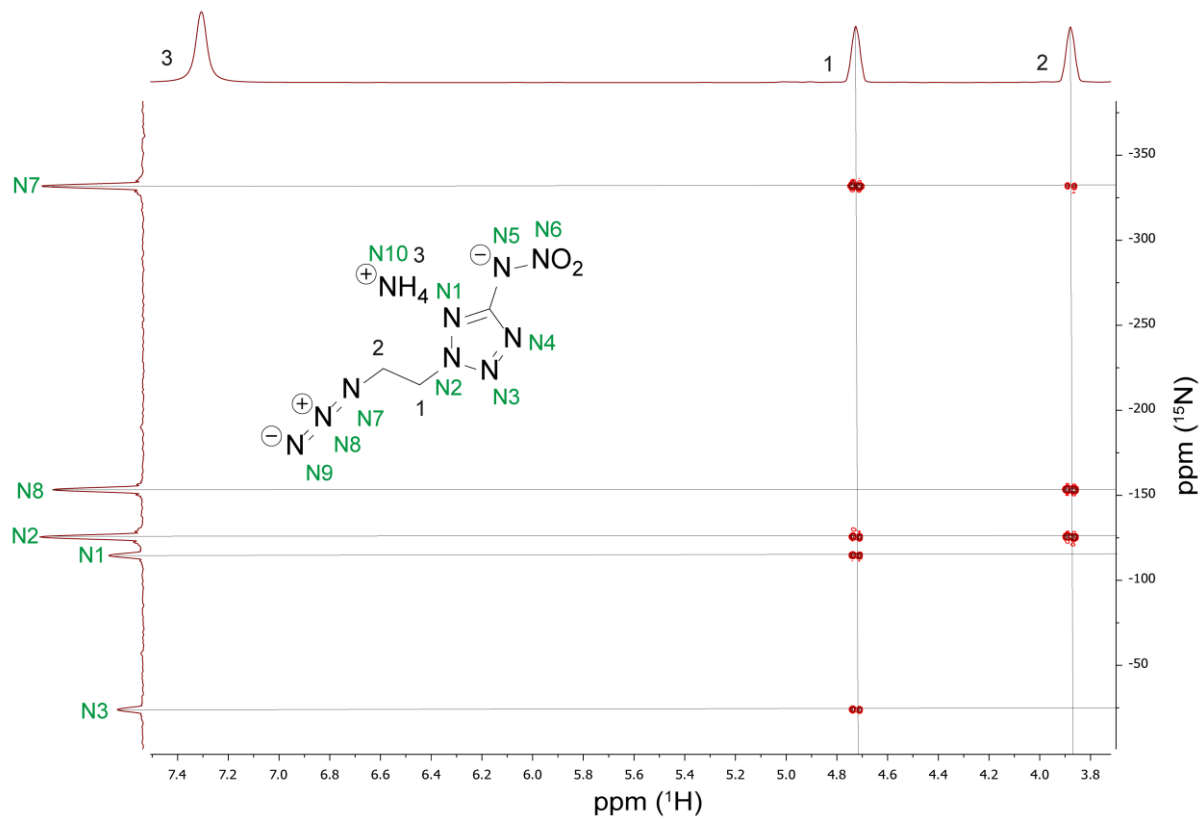
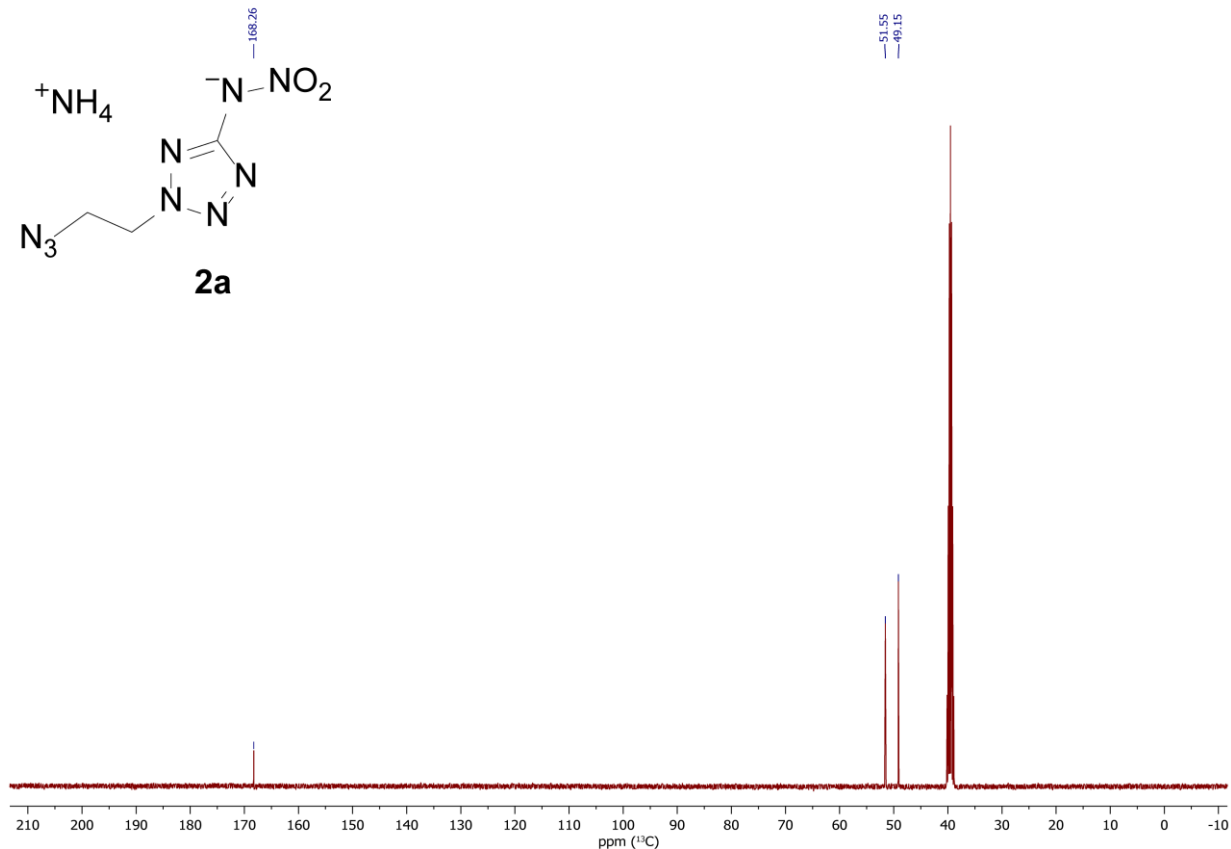
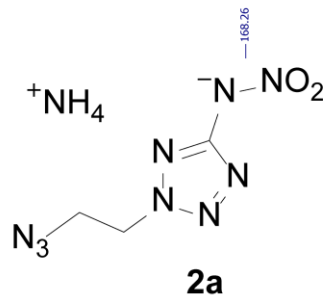




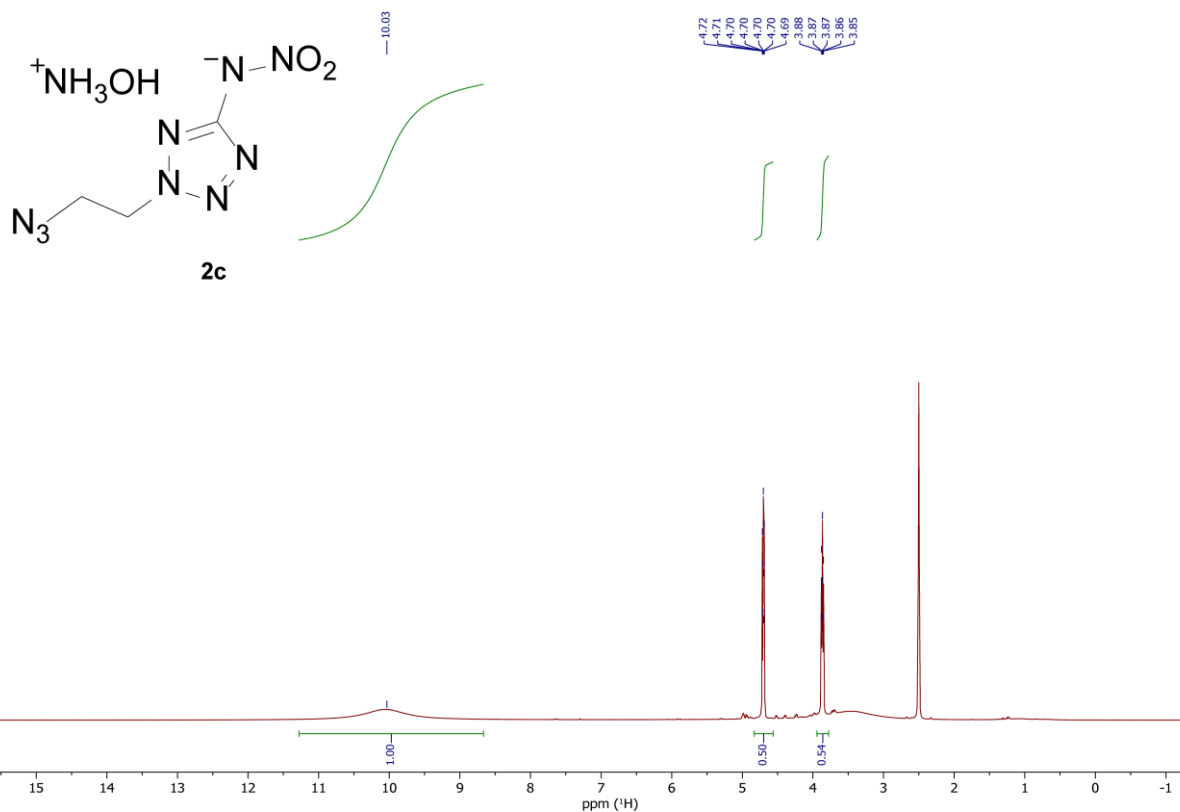
¹H-NMR (400 MHz, DMSO-D₆, ppm)



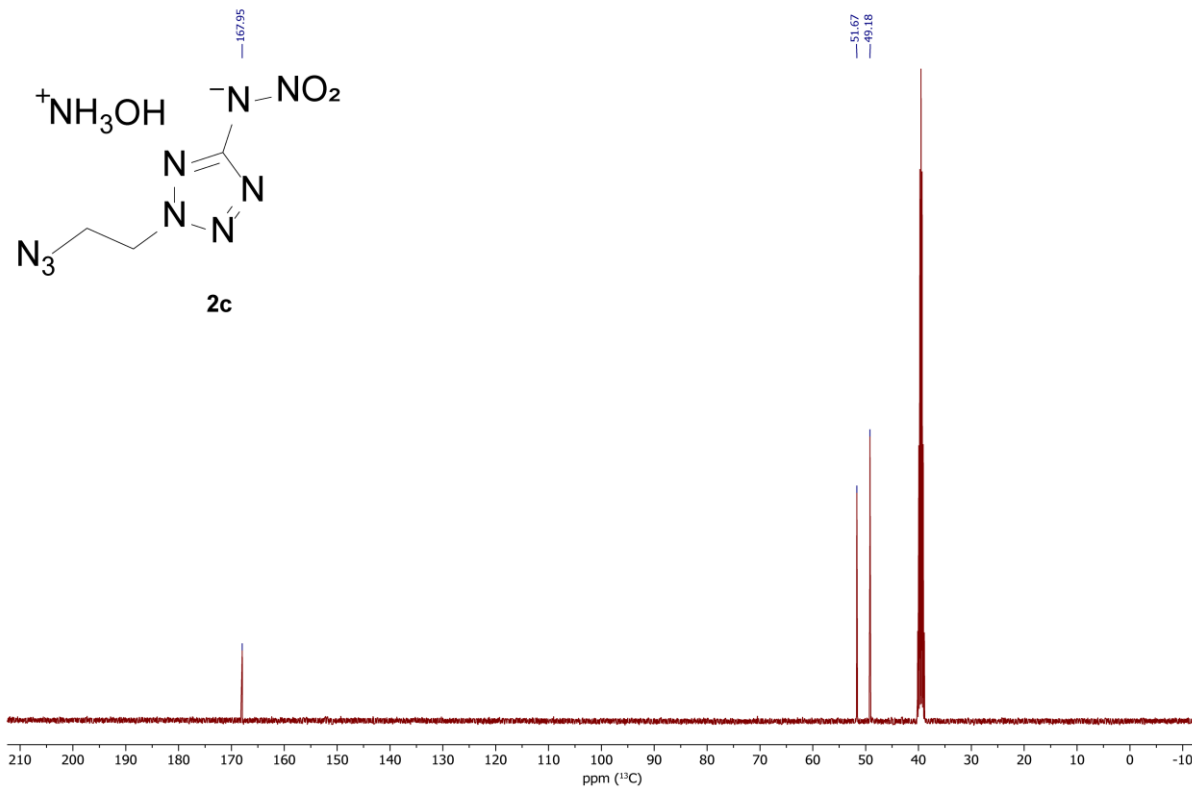
^{13}C -NMR (101 MHz, DMSO- D_6 , ppm)



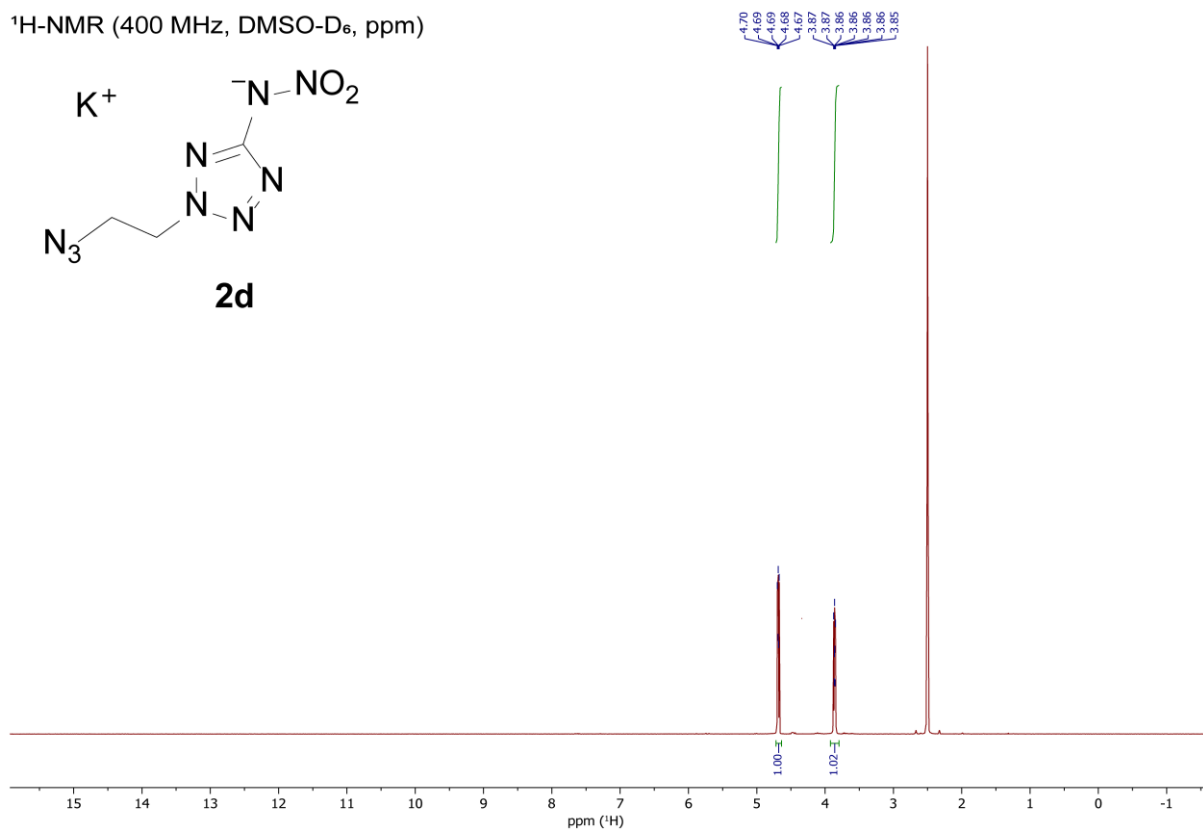
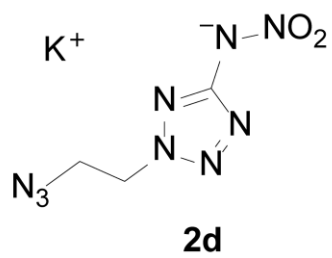
¹H-NMR (400 MHz, DMSO-D₆, ppm)



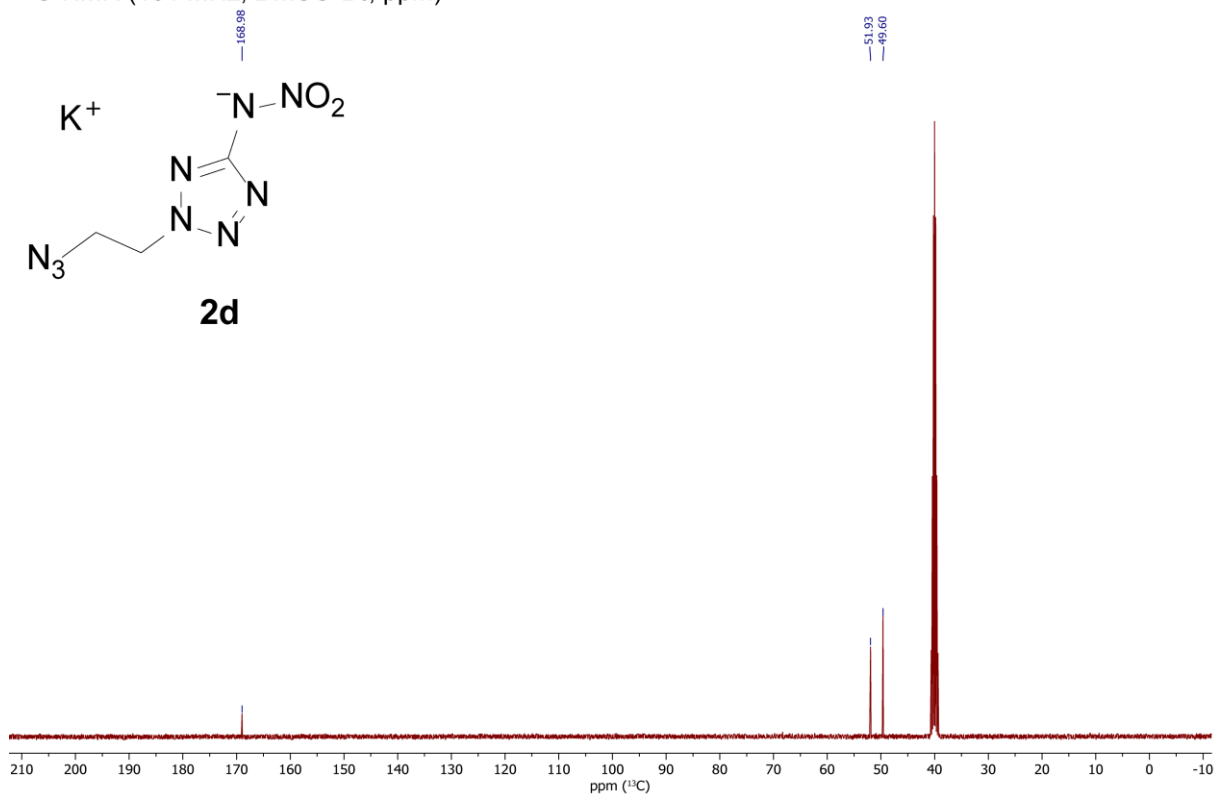
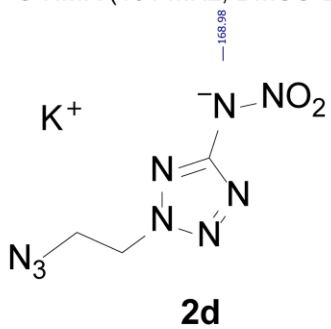
¹³C-NMR (101 MHz, DMSO-D₆, ppm)



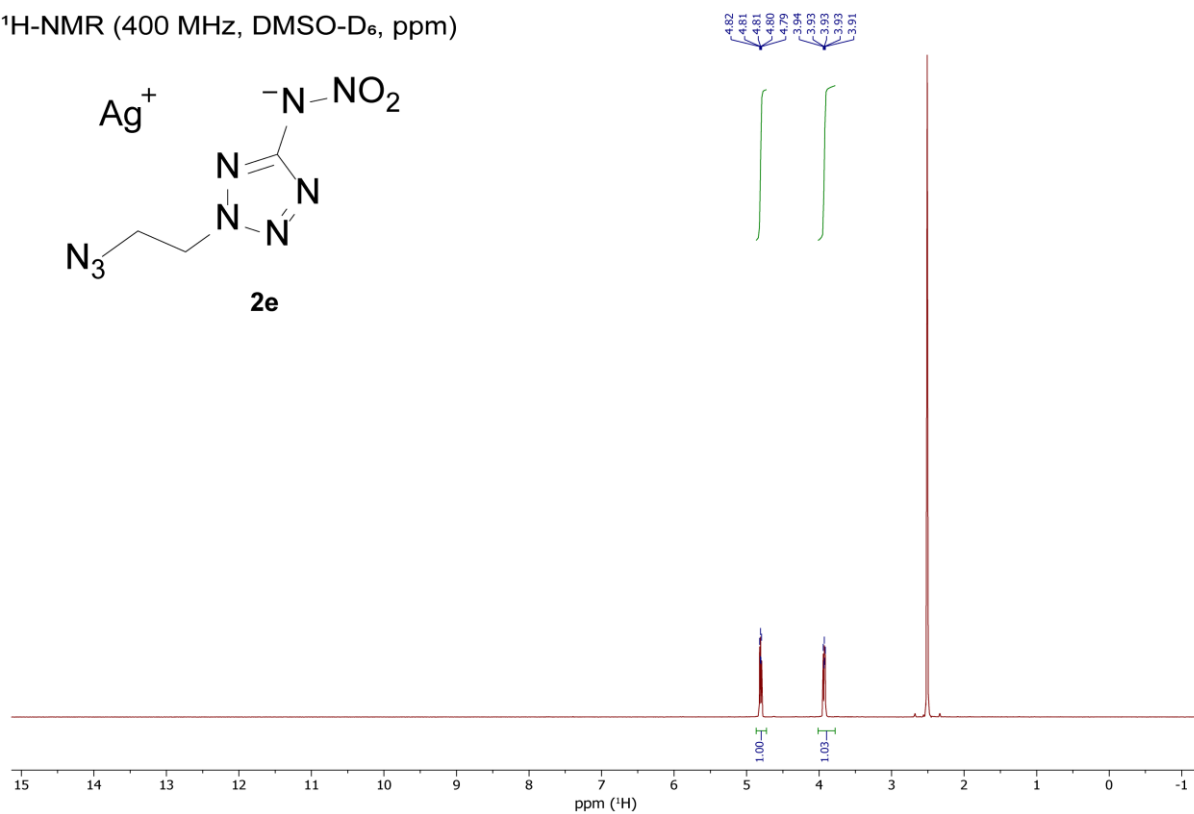
¹H-NMR (400 MHz, DMSO-D₆, ppm)



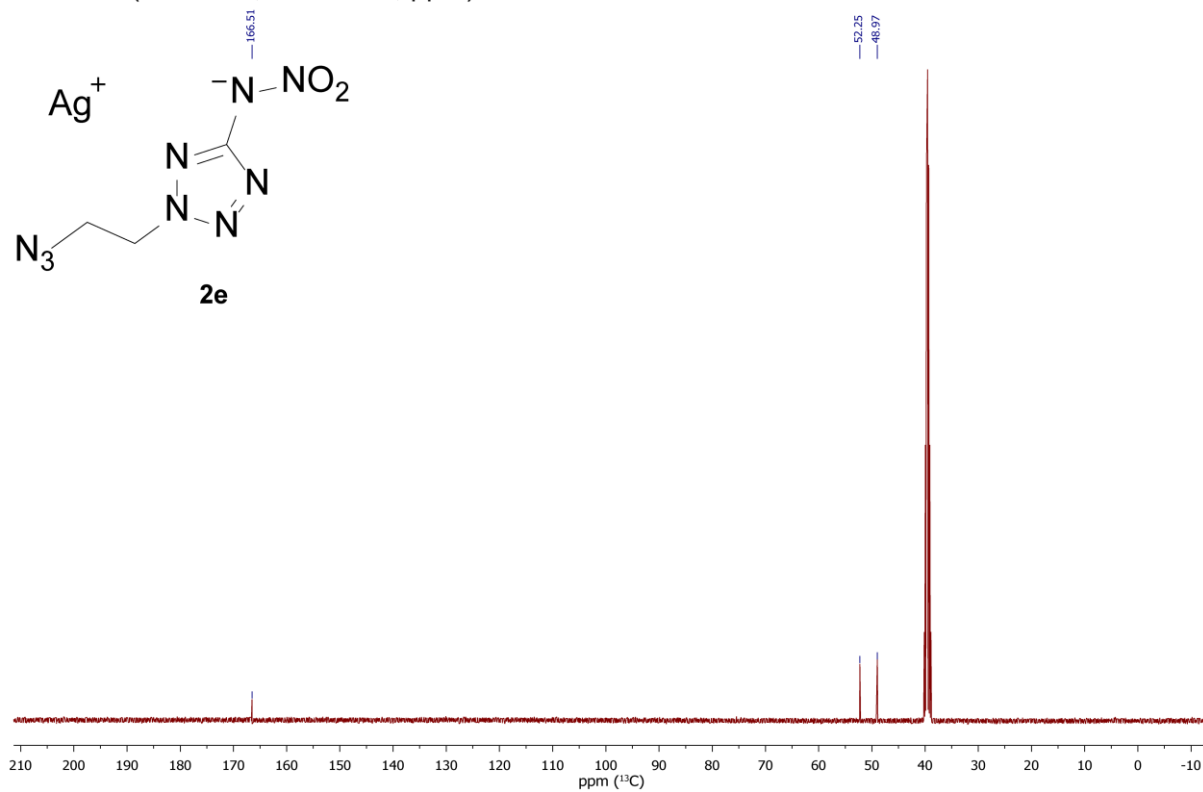
¹³C-NMR (101 MHz, DMSO-D₆, ppm)



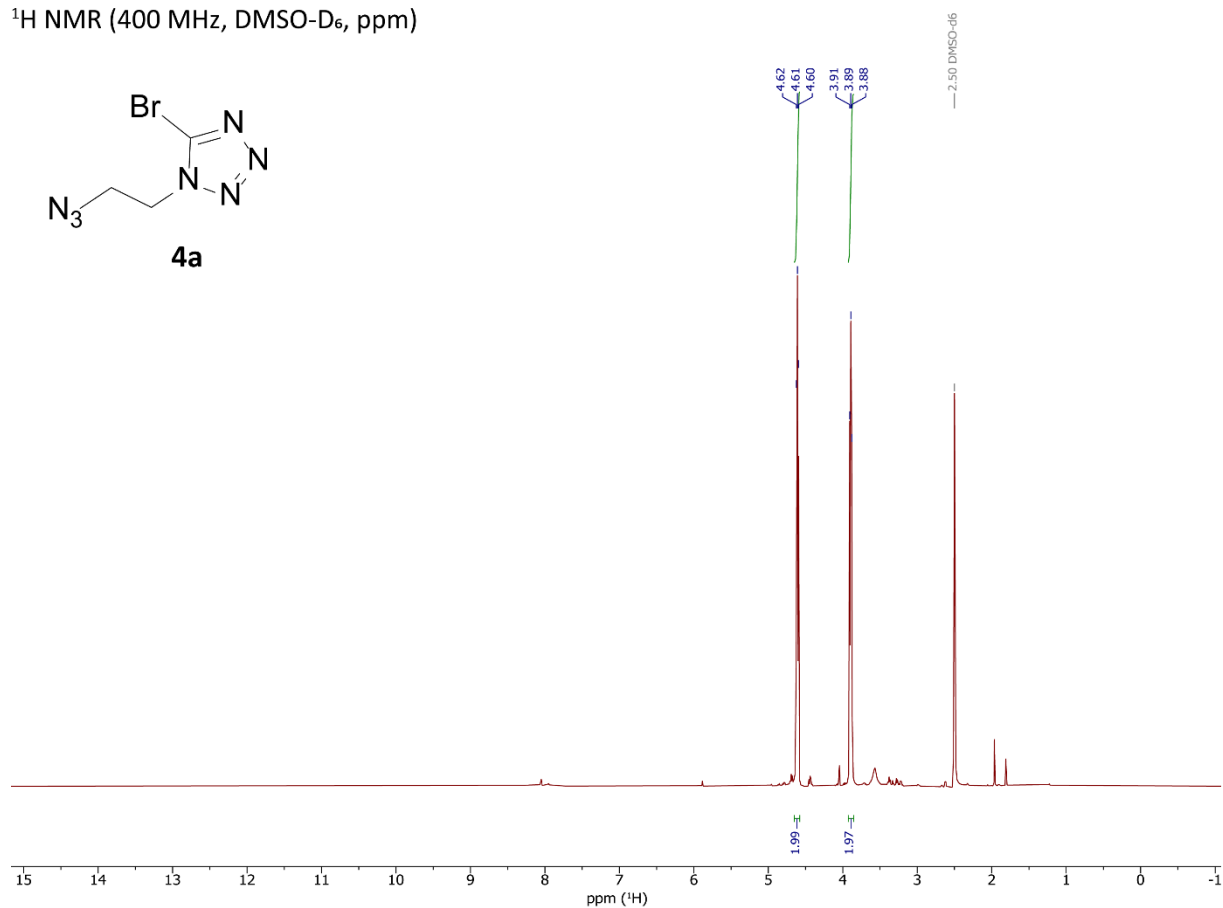
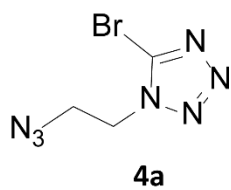
$^1\text{H-NMR}$ (400 MHz, DMSO-D_6 , ppm)



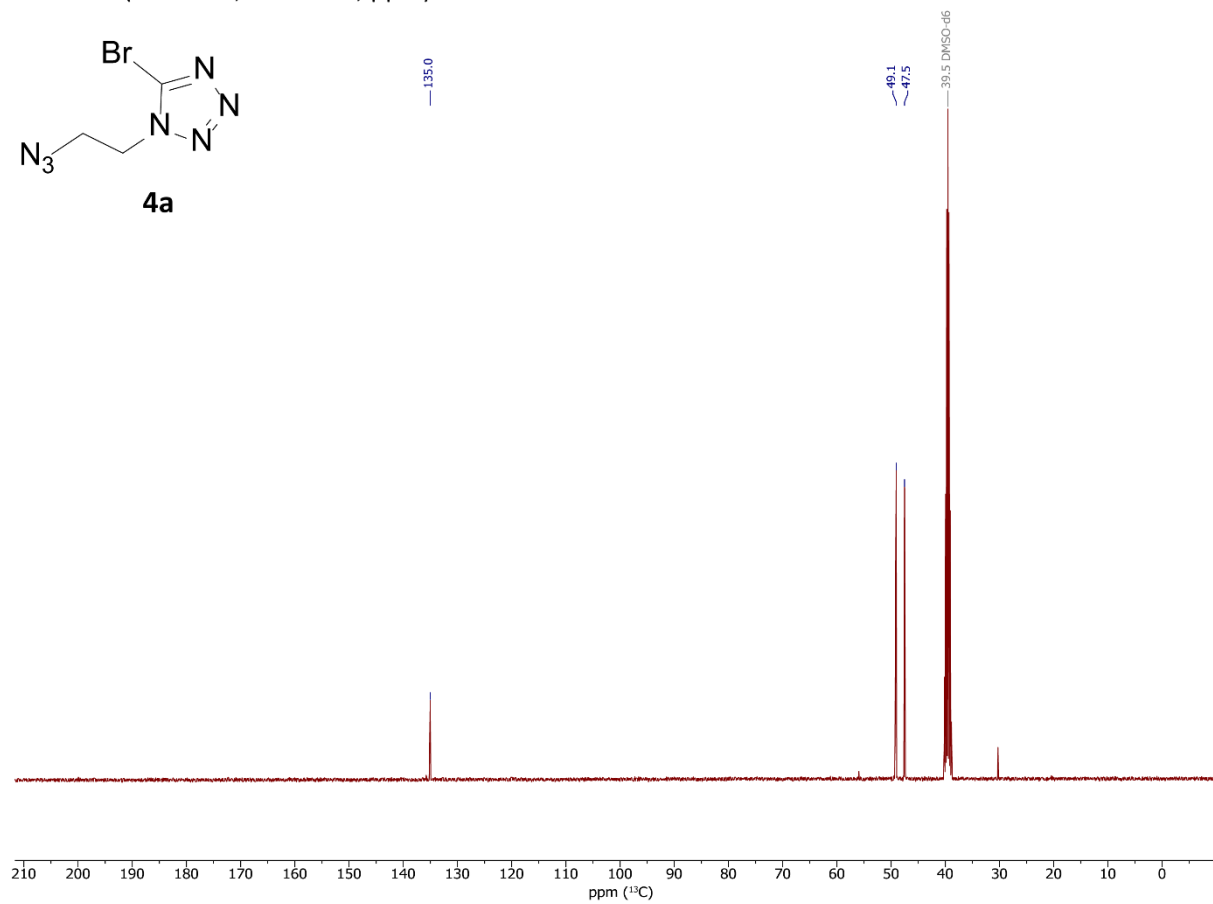
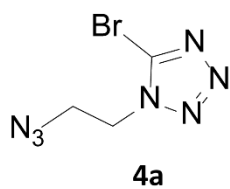
$^{13}\text{C-NMR}$ (101 MHz, DMSO-D_6 , ppm)



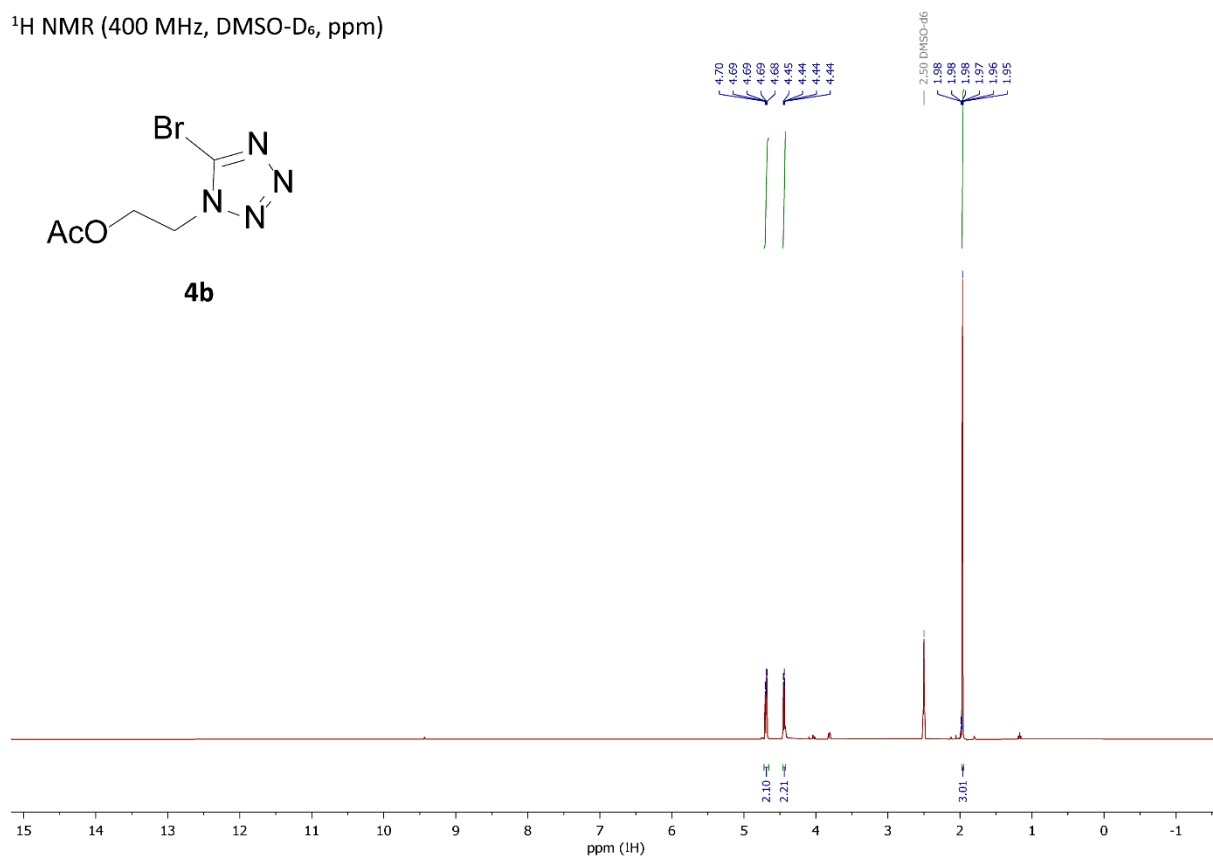
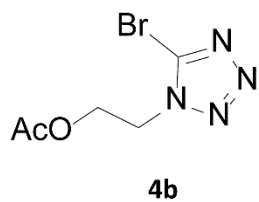
^1H NMR (400 MHz, DMSO- D_6 , ppm)



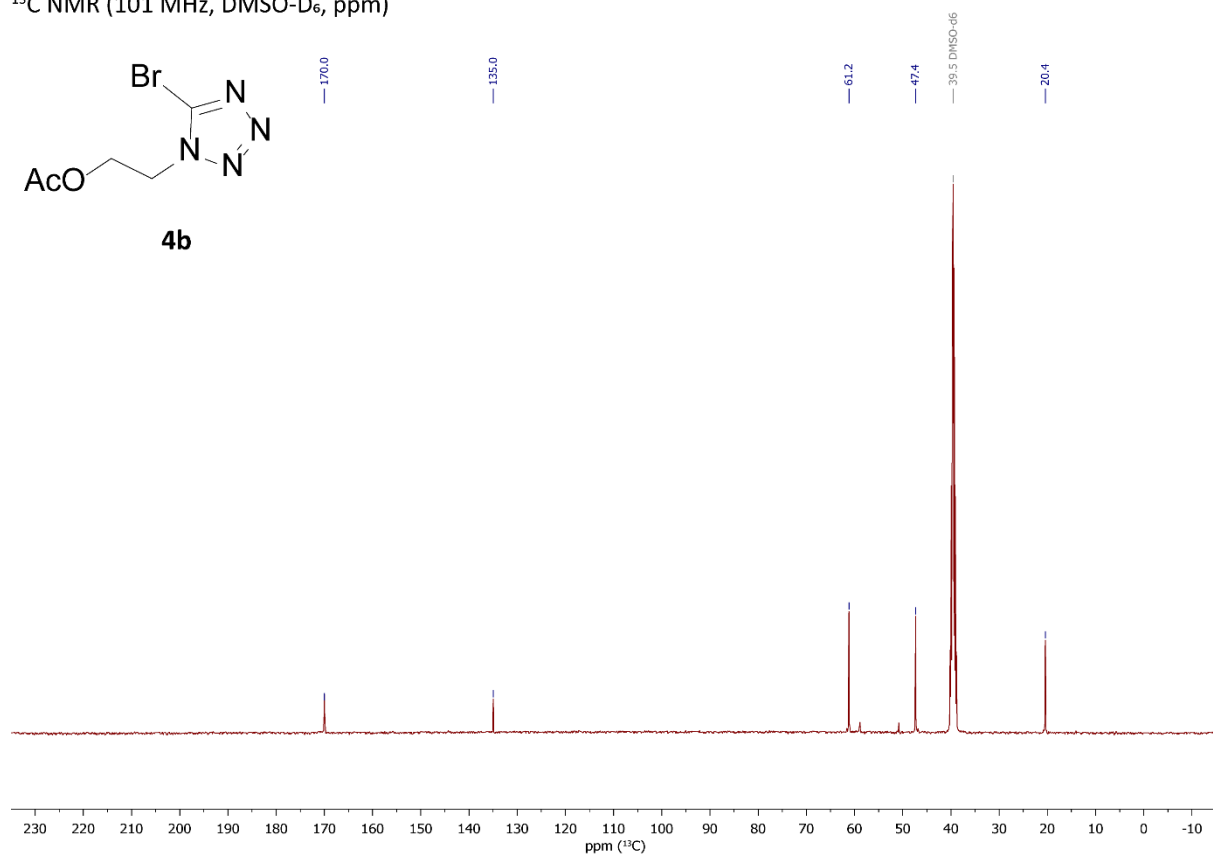
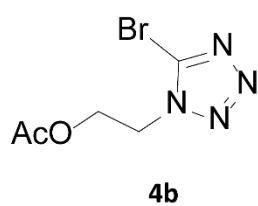
^{13}C NMR (101 MHz, DMSO- D_6 , ppm)



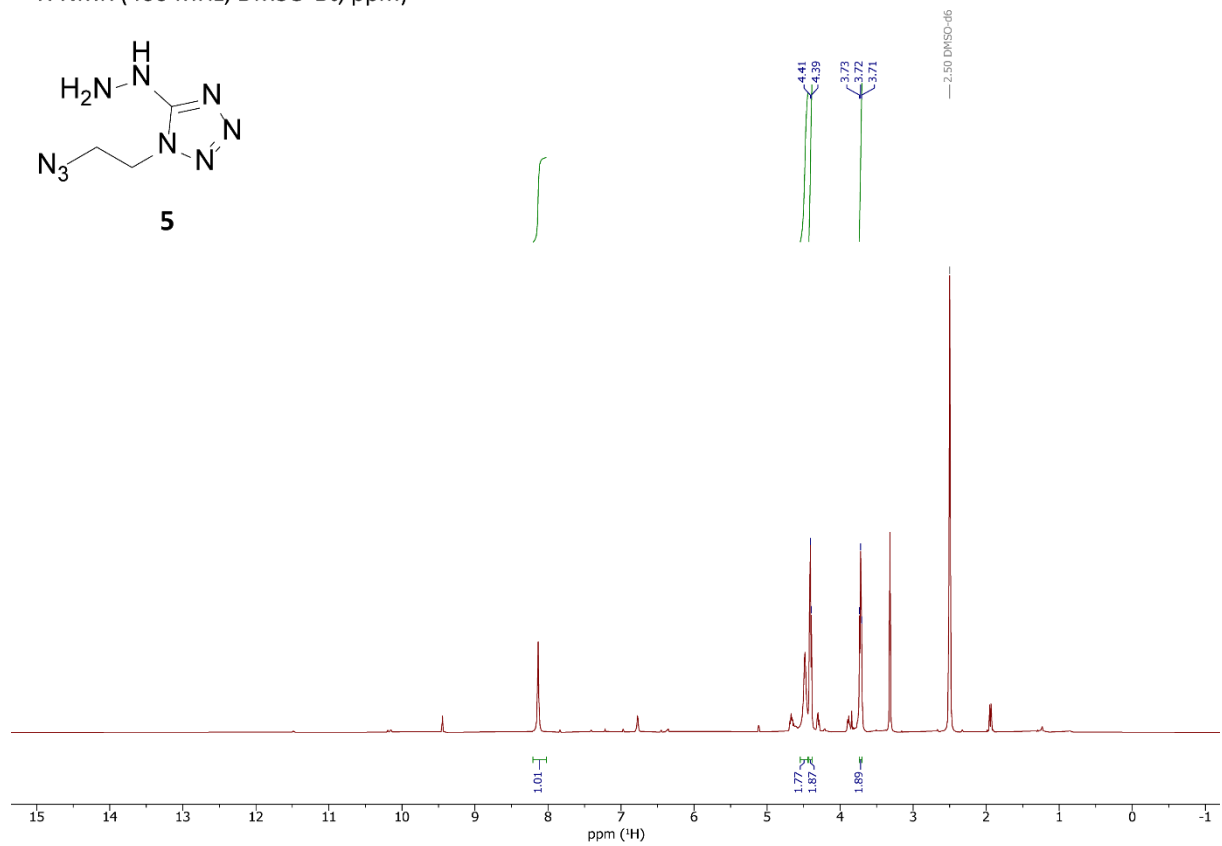
^1H NMR (400 MHz, DMSO- D_6 , ppm)



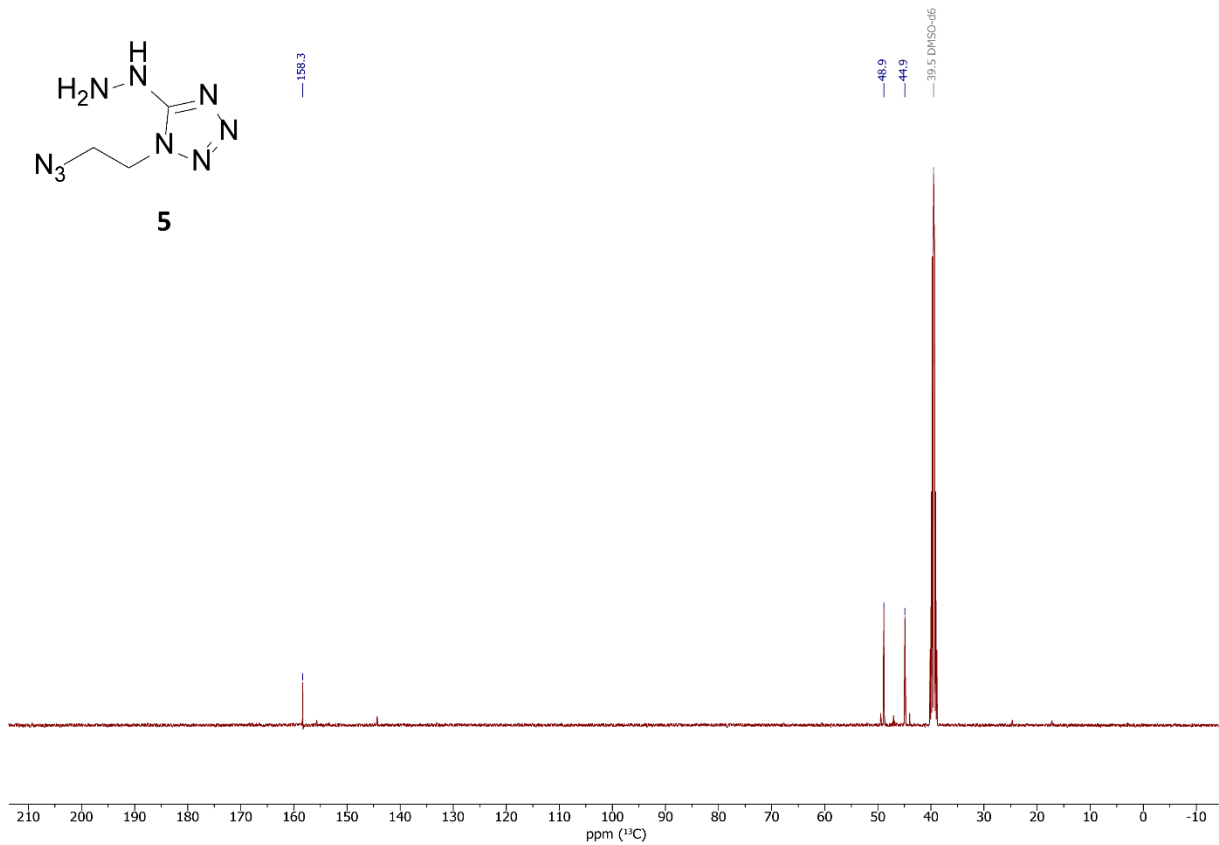
^{13}C NMR (101 MHz, DMSO- D_6 , ppm)



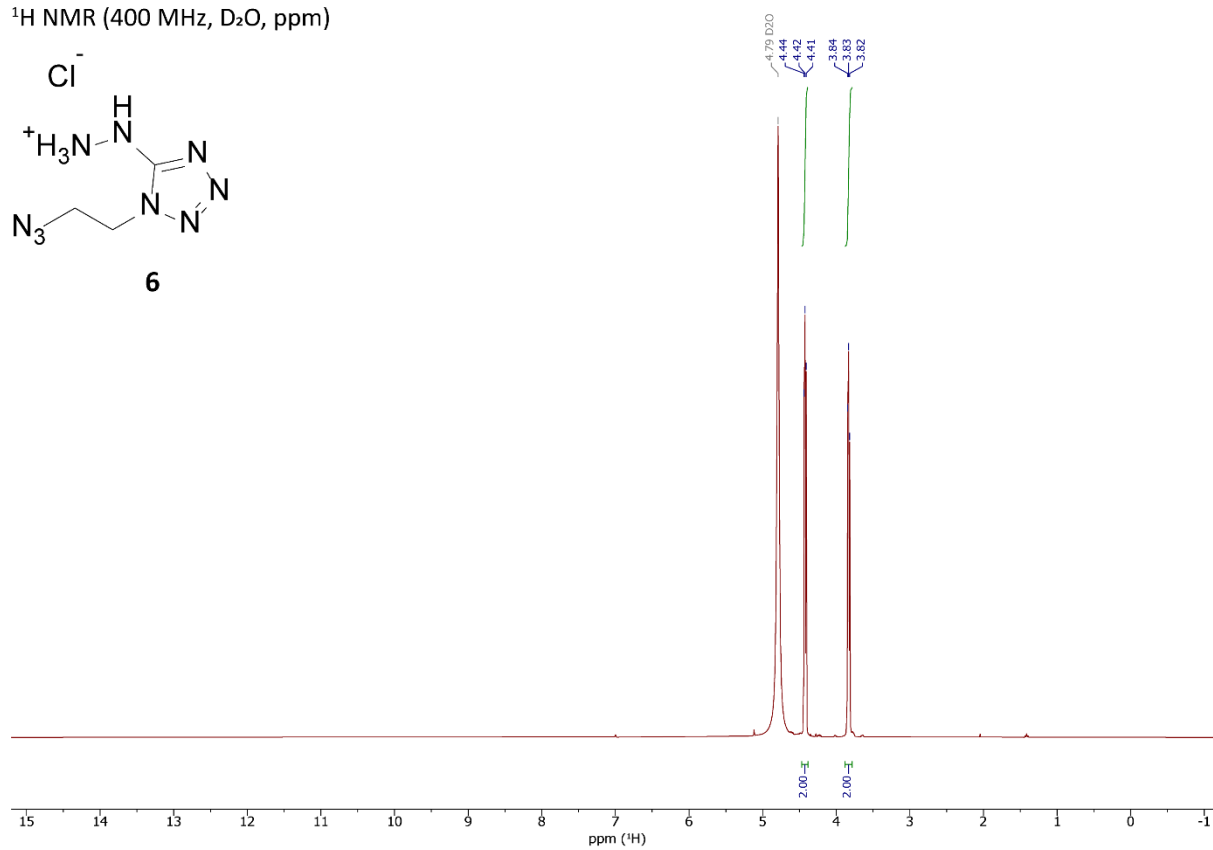
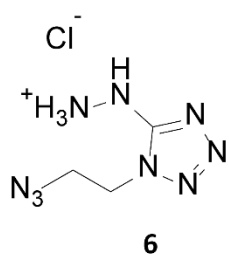
^1H NMR (400 MHz, DMSO- D_6 , ppm)



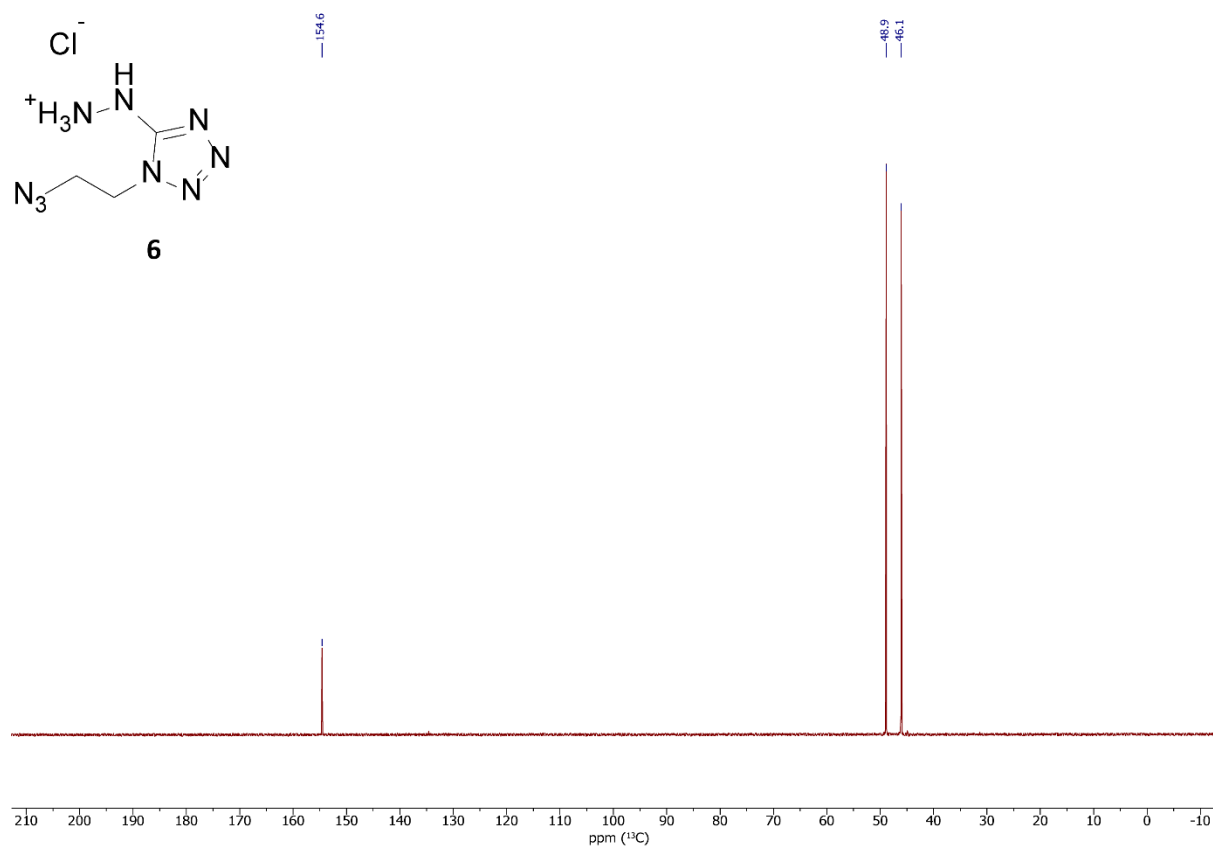
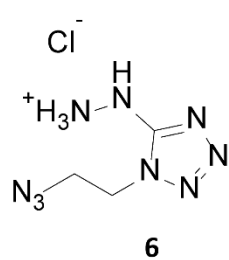
^{13}C NMR (101 MHz, DMSO- D_6 , ppm)



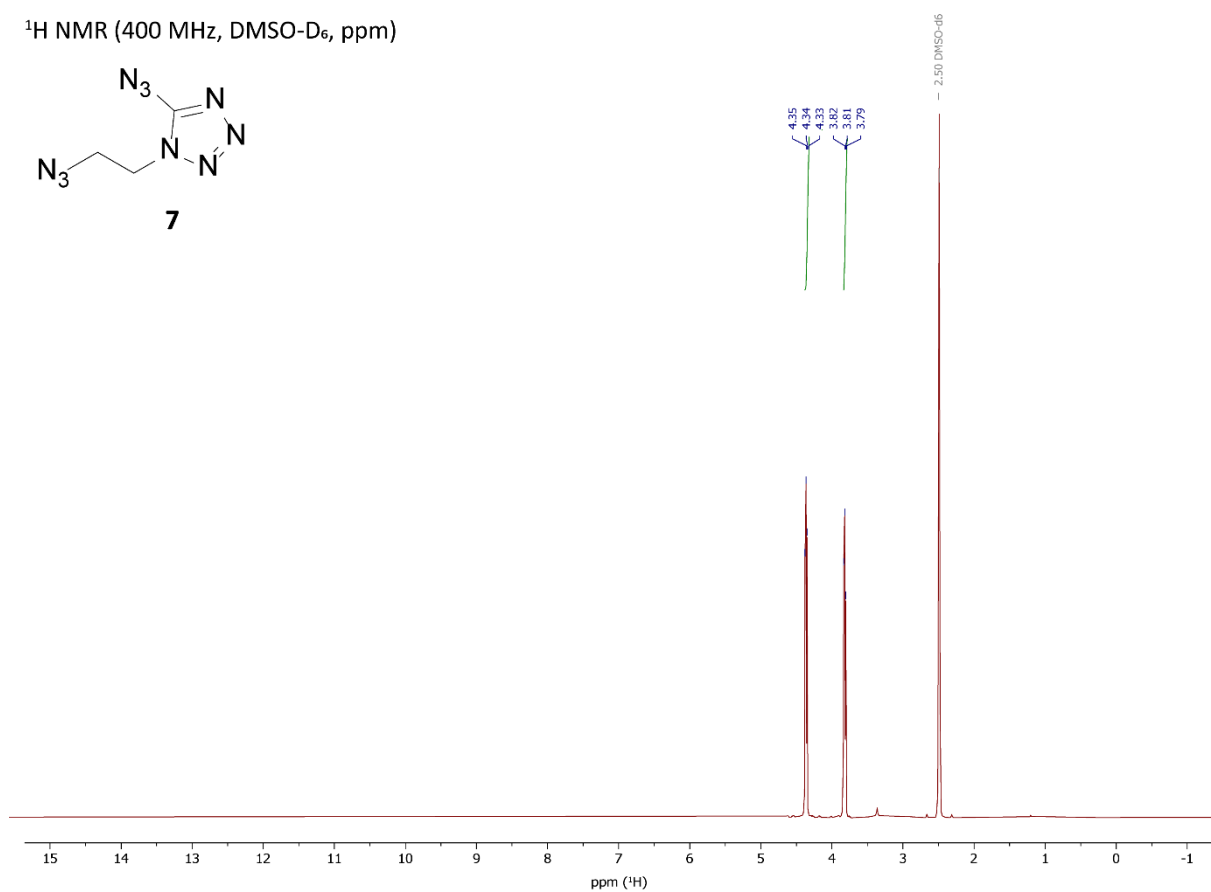
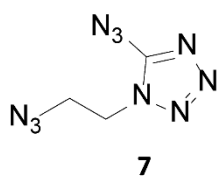
^1H NMR (400 MHz, D_2O , ppm)



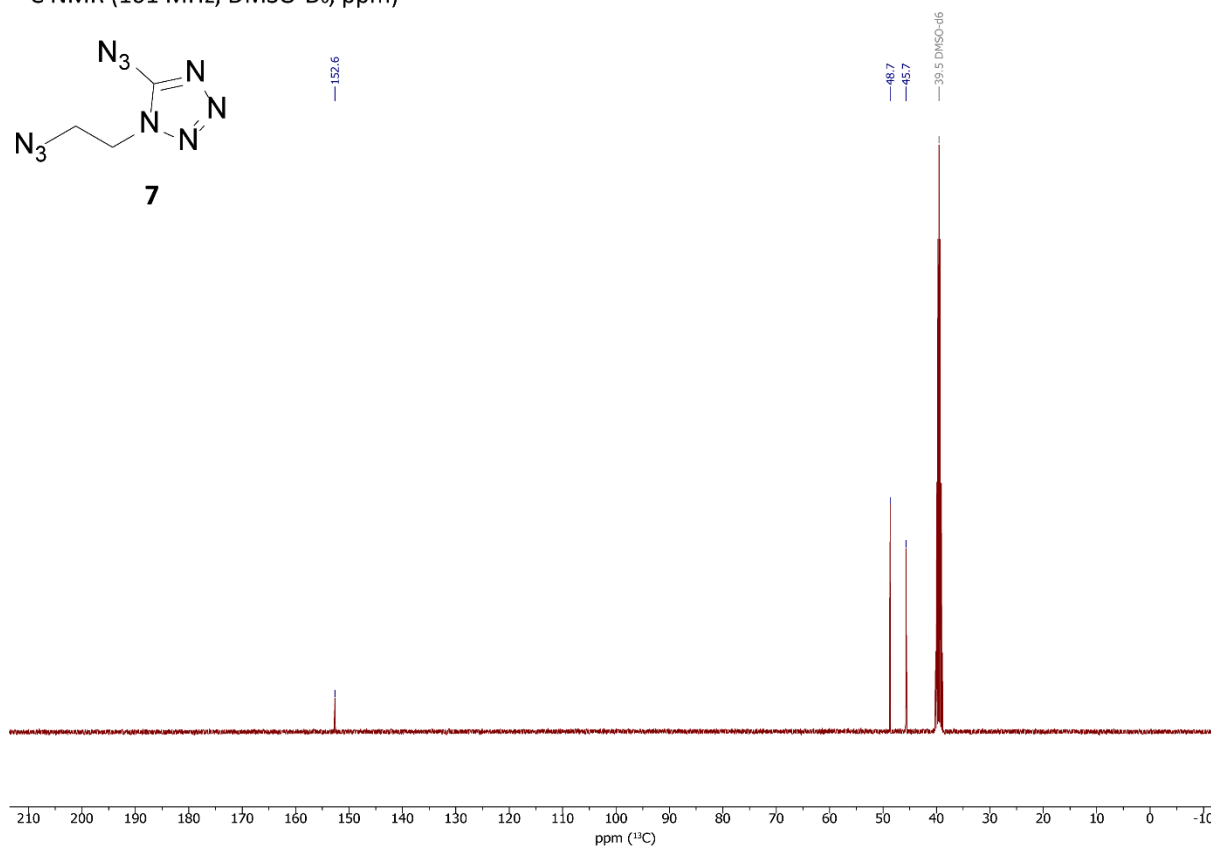
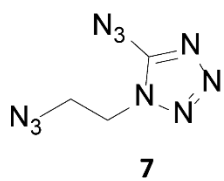
^{13}C NMR (101 MHz, D_2O , ppm)

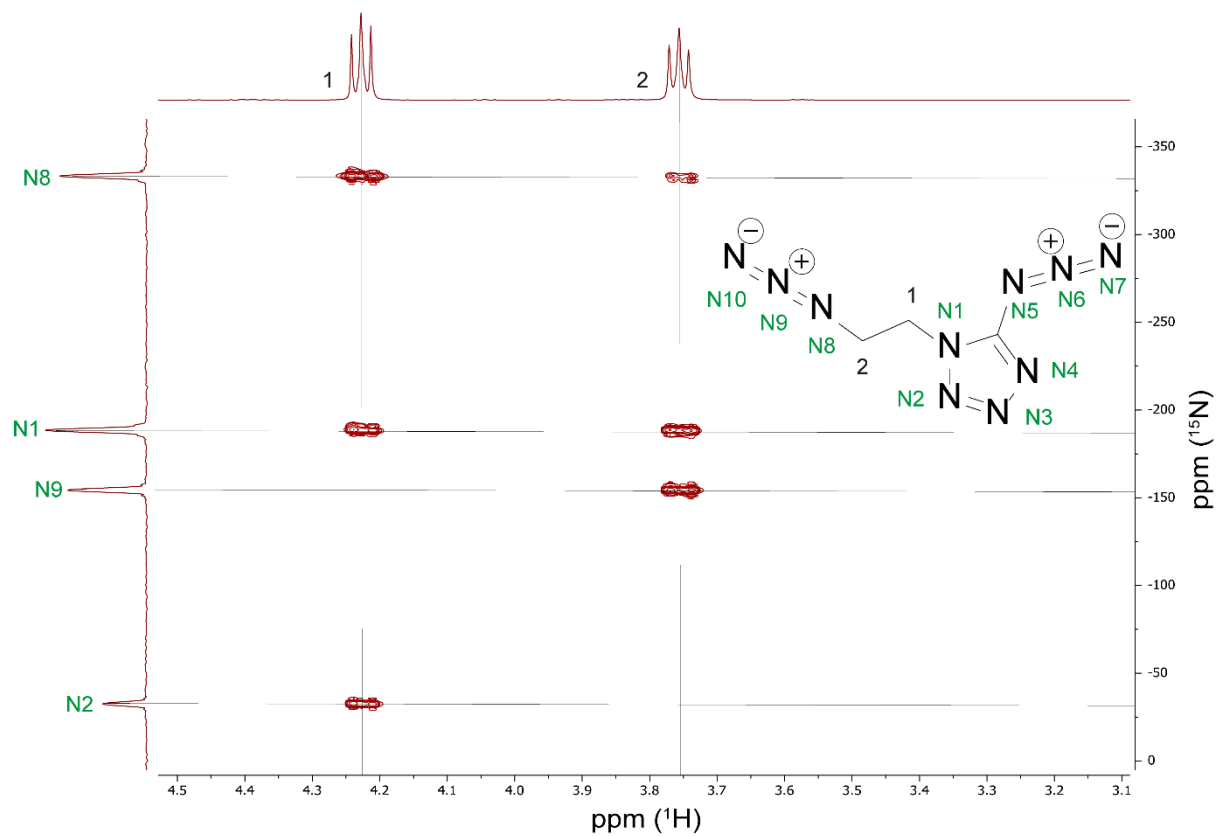


^1H NMR (400 MHz, $\text{DMSO-}d_6$, ppm)

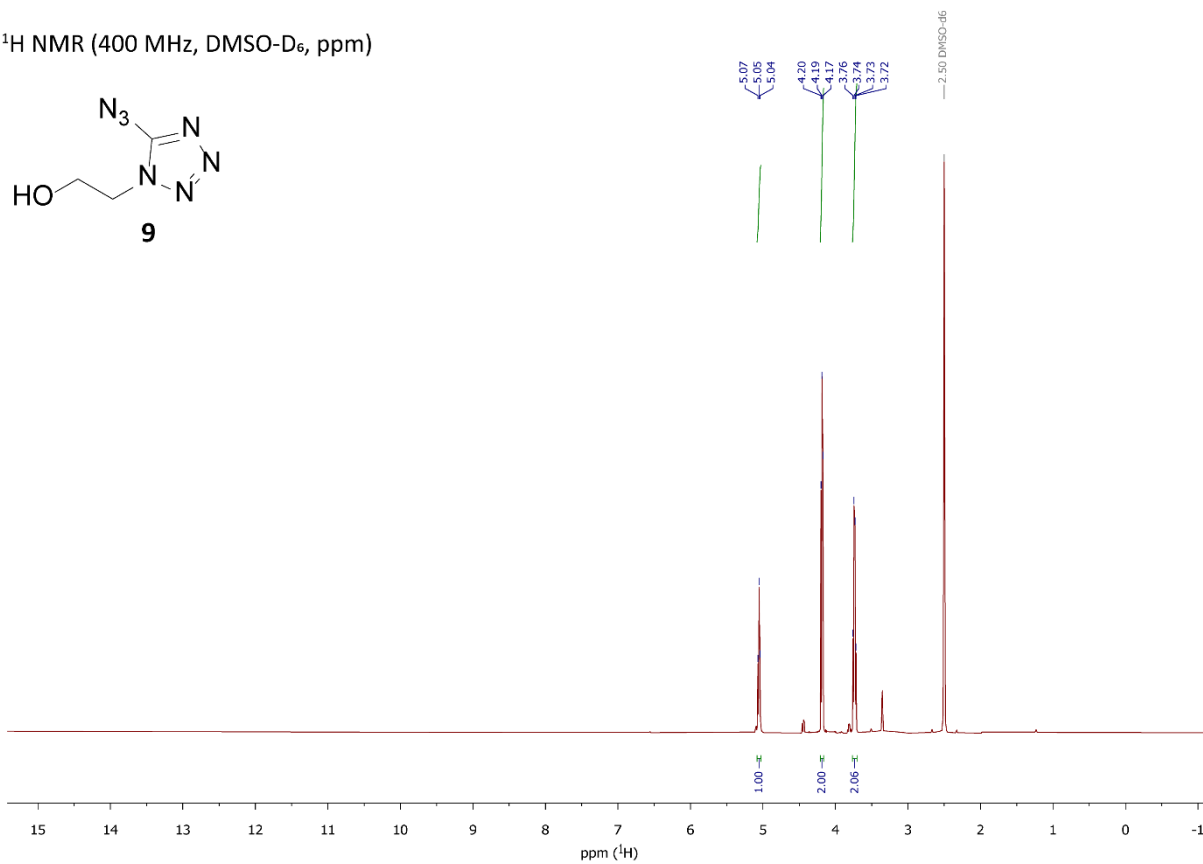


^{13}C NMR (101 MHz, $\text{DMSO-}d_6$, ppm)

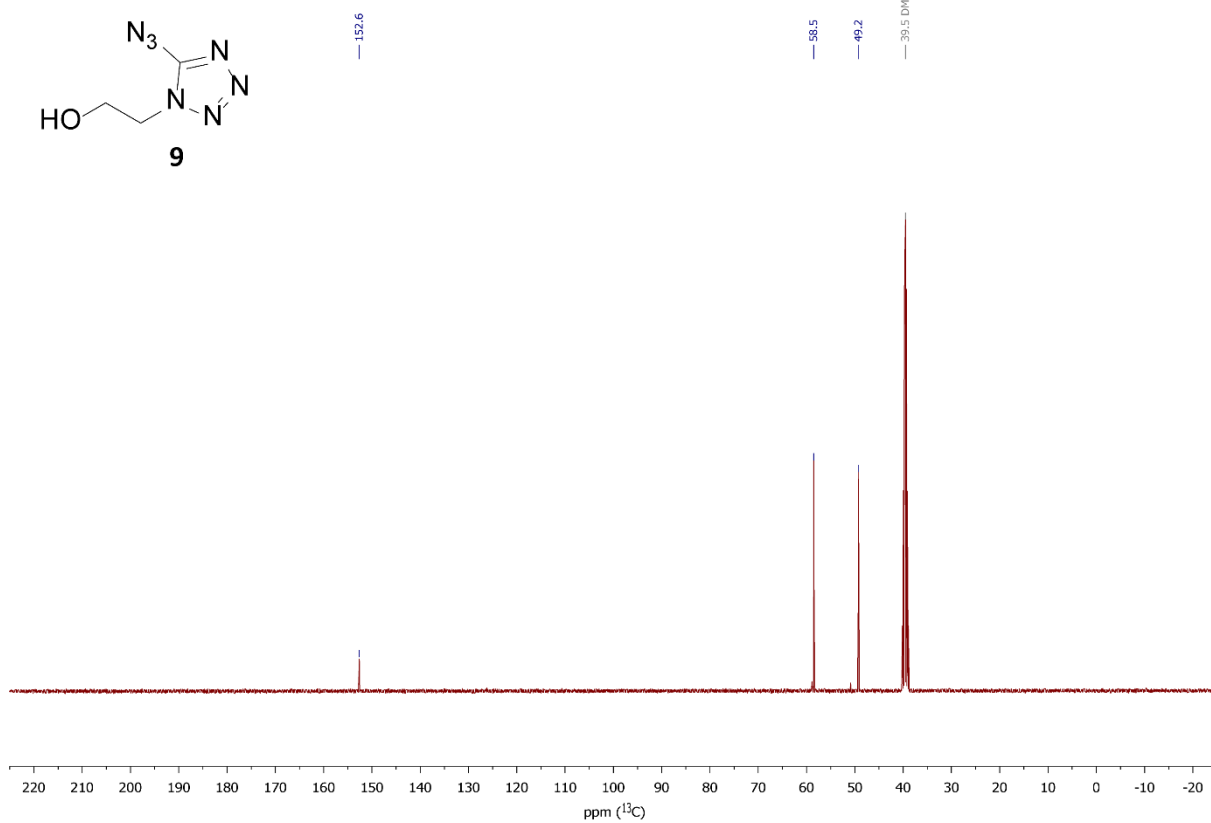
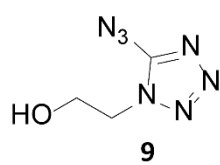




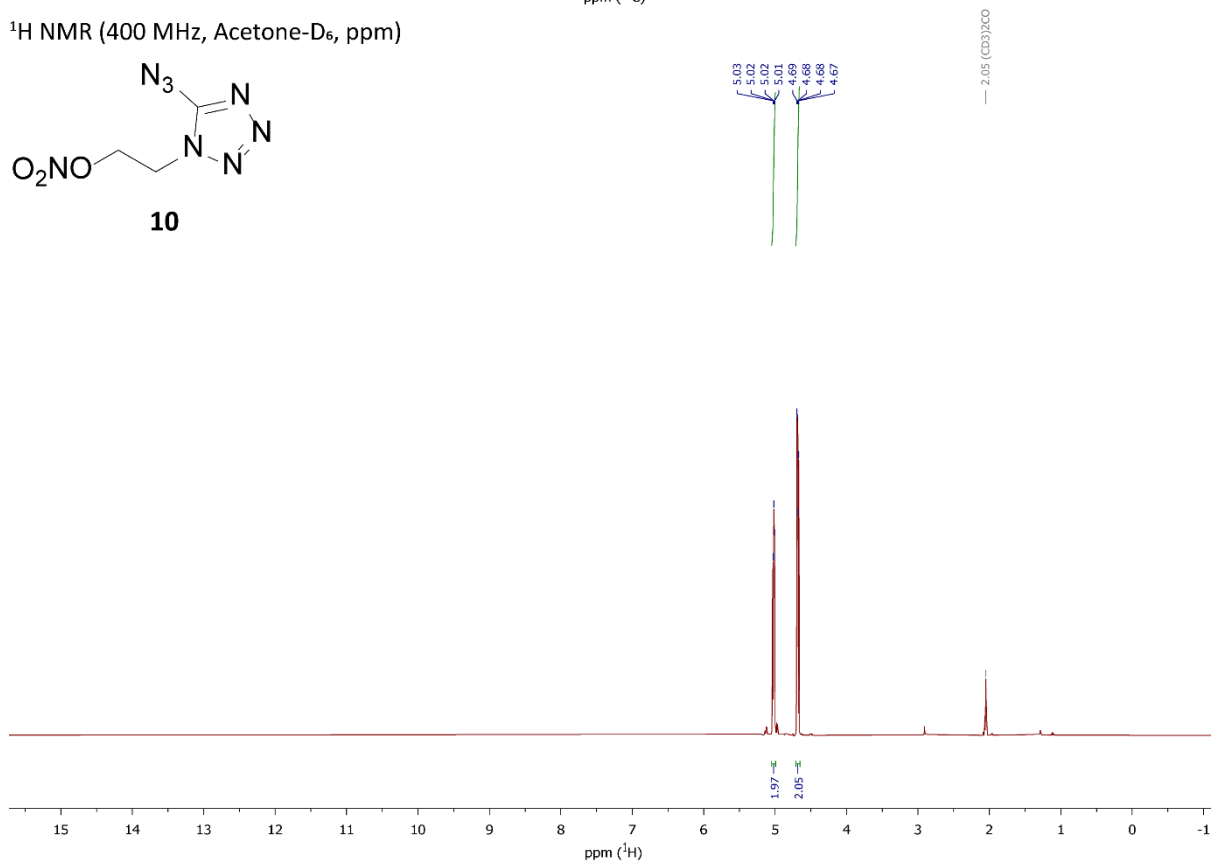
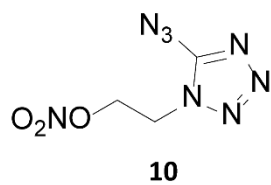
¹H NMR (400 MHz, DMSO-D₆, ppm)



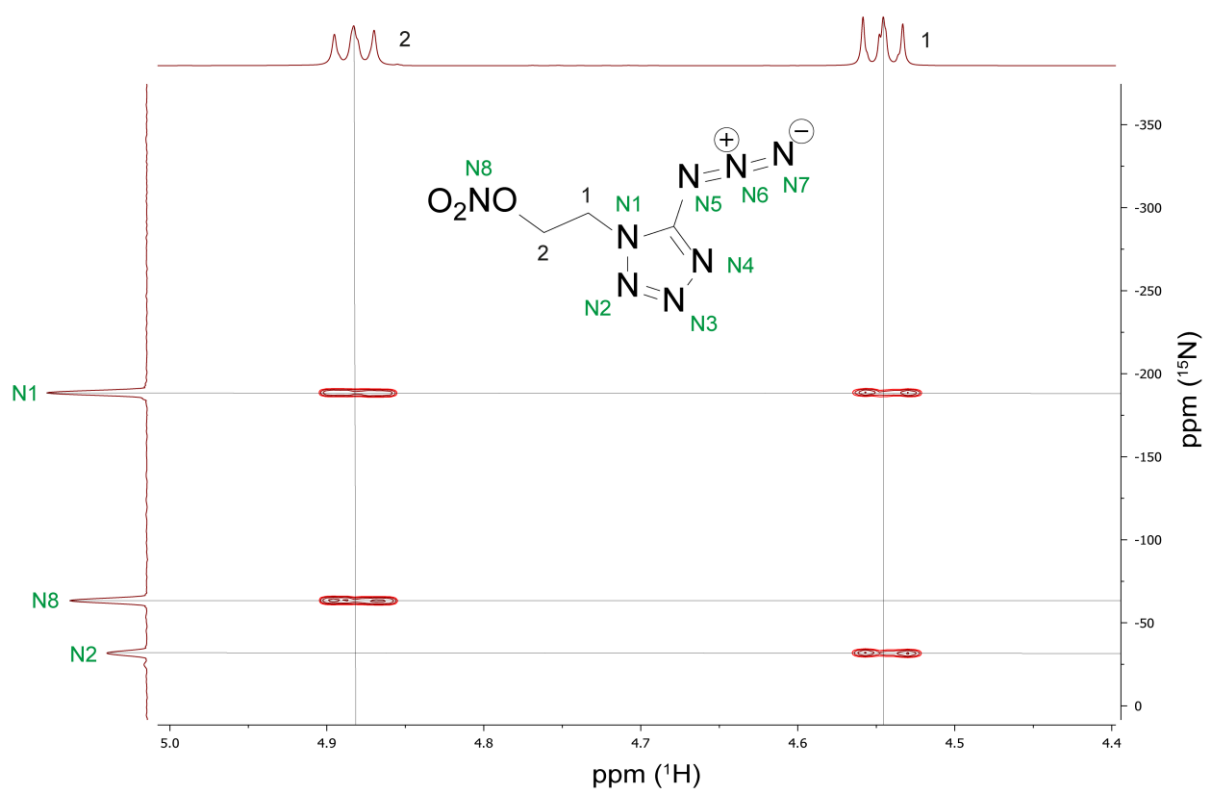
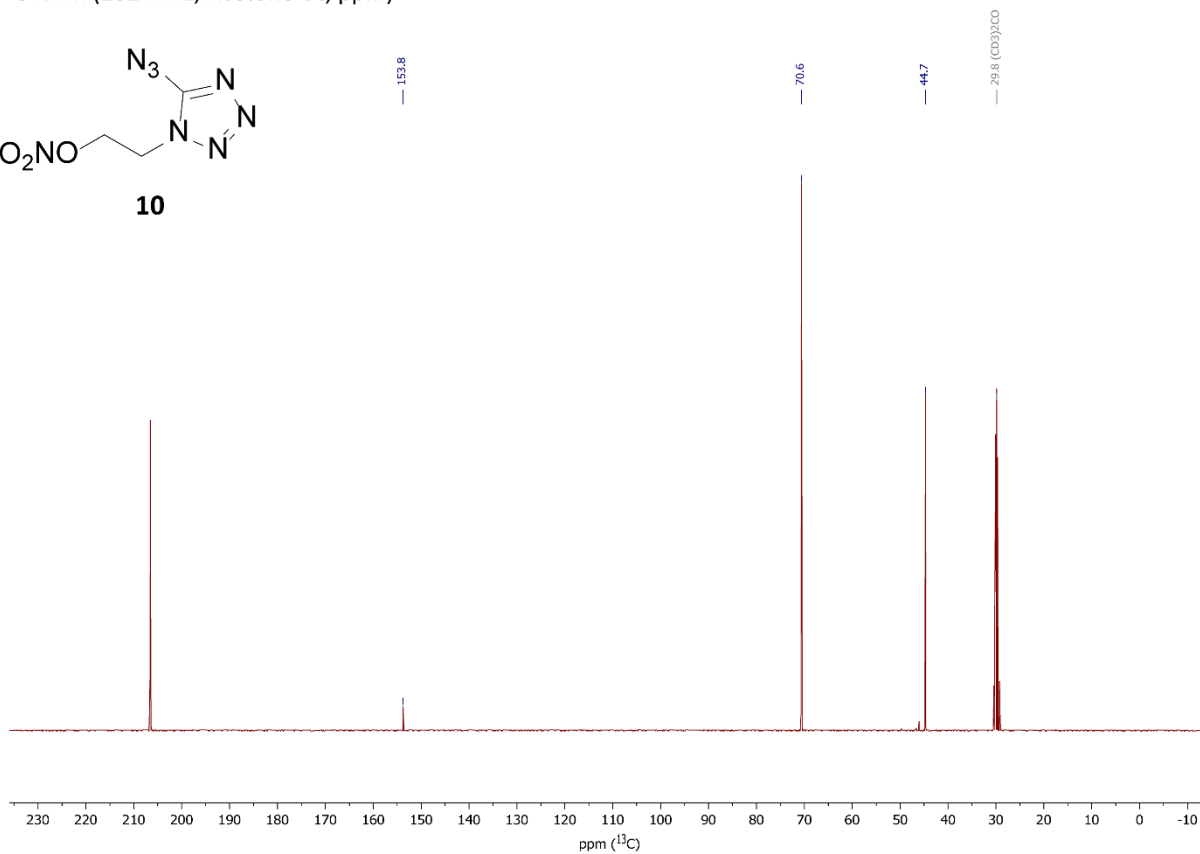
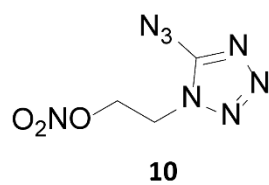
^{13}C NMR (101 MHz, DMSO- D_6 , ppm)



^1H NMR (400 MHz, Acetone- D_6 , ppm)



^{13}C NMR (101 MHz, Acetone- D_6 , ppm)



6. References

- [S1] a) Reichel & Partner GmbH, <http://www.reichelt-partner.de>; b) Test methods according to the UN Recommendations on the Transport of Dangerous Goods, *Manual of Test and Criteria*, fourth revised edition, United Nations Publication, New York and Geneva, **2003**, ISBN 92–1-139087–7, Sales No. E.03.VIII.2; 13.4.2 Test 3 a (ii) BAM Fallhammer.
- [S2] M. Sućeska, EXPLO5 V6.02 program, Brodarski Institute, Zagreb, Croatia, **2014**.
- [S3] R. Yang, Z. Dong, Z. Ye, *ChemistrySelect* **2019**, *4*, 14208-14213.
- [S4] D. E. Bayes (Glaxo Group Limited), EP0117368A1, **1982**.
- [S5] *CrysAlisPro*, Oxford Diffraction Ltd. *version 171.33.41*, **2009**.
- [S6] G. M. Sheldrick, *Acta Cryst.* **2015**, *A71*, 3–8.
- [S7] O. V. Dolomanov, L. J Bourhis, R. J. Gildea, J. A. K. Howard, H. Puschmann, *J. Appl. Cryst.* **2009**, *42*, 339–341.
- [S8] *SCALE3 ABSPACK – An Oxford Diffraction program* (1.0.4, gui: 1.0.3), Oxford Diffraction Ltd., **2005**.
- [S9] *APEX3*. Bruker AXS Inc., Madison, Wisconsin, USA.
- [S10] M. J. Frisch, G. W. Trucks, H. B. Schlegel, G. E. Scuseria, M. A. Robb, J. R. Cheeseman, G. Scalmani, V. Barone, B. Mennucci, G. A. Petersson, H. Nakatsuji, M. Caricato, X. Li, H.P. Hratchian, A. F. Izmaylov, J. Bloino, G. Zheng, J. L. Sonnenberg, M. Hada, M. Ehara, K. Toyota, R. Fukuda, J. Hasegawa, M. Ishida, T. Nakajima, Y. Honda, O. Kitao, H. Nakai, T. Vreven, J. A. Montgomery, Jr., J. E. Peralta, F. Ogliaro, M. Bearpark, J. J. Heyd, E. Brothers, K. N. Kudin, V. N. Staroverov, R. Kobayashi, J. Normand, K. Raghavachari, A. Rendell, J. C. Burant, S. S. Iyengar, J. Tomasi, M. Cossi, N. Rega, J. M. Millam, M. Klene, J. E. Knox, J. B. Cross, V. Bakken, C. Adamo, J. Jaramillo, R. Gomperts, R. E. Stratmann, O. Yazyev, A. J. Austin, R. Cammi, C. Pomelli, J. W. Ochterski, R. L. Martin, K. Morokuma, V. G. Zakrzewski, G. A. Voth, P. Salvador, J. J. Dannenberg, S. Dapprich, A. D. Daniels, O. Farkas, J.B. Foresman, J. V. Ortiz, J. Cioslowski, D. J. Fox, *Gaussian 09 A.02*, Gaussian, Inc., Wallingford, CT, USA, **2009**.

- [S11] a) J. W. Ochterski, G. A. Petersson, and J. A. Montgomery Jr., *J. Chem. Phys.* **1996**, *104*, 2598–2619; b) J. A. Montgomery Jr., M. J. Frisch, J. W. Ochterski G. A. Petersson, *J. Chem. Phys.* **2000**, *112*, 6532–6542.
- [S12] a) L. A. Curtiss, K. Raghavachari, P. C. Redfern, J. A. Pople, *J. Chem. Phys.* **1997**, *106*, 1063–1079; b) E. F. C. Byrd, B. M. Rice, *J. Phys. Chem. A* **2006**, *110*, 1005–1013; c) B. M. Rice, S. V. Pai, J. Hare, *Comb. Flame* **1999**, *118*, 445–458.
- [S13] P. J. Lindstrom, W. G. Mallard (Editors), NIST Standard Reference Database Number 69, <http://webbook.nist.gov/chemistry/> (accessed June **2020**).
- [S14] M. S. Westwell, M. S. Searle, D. J. Wales, D. H. Williams, *J. Am. Chem. Soc.* **1995**, *117*, 5013–5015; b) F. Trouton, *Philos. Mag.* **1884**, *18*, 54–57.
- [S15] a) H. D. B. Jenkins, H. K. Roobottom, J. Passmore, L. Glasser, *Inorg. Chem.* **1999**, *38*, 3609–3620; b) H. D. B. Jenkins, D. Tudela, L. Glasser, *Inorg. Chem.* **2002**, *41*, 2364–2367.

Evolving the Scope of 5,5'-Azobistetrazoles in the Search for High Performing Green Energetic Materials

Maximilian Benz,^[a] Michael S. Gruhne,^[a] Thomas M. Klapötke,^{*[a]} Nina Krüger,^[a] Tobias Lenz,^[a] Marcus Lommel,^[a] and Jörg Stierstorfer^[a]

Dedicated to Professor Konstantin Karaghiosoff on the occasion of his 65th birthday.

The azotetrazole moiety represents a great platform for energetic materials, it offers a planar and nitrogen-rich backbone, combined with a high heat of formation, which easily can be functionalized and tuned. Herein, we start from sodium 5-aminotetrazolate and obtain two isomers by substitution reaction with 2-chloroethanol. Azidoethyl and nitrateethyl substituted azo-tetrazoles were finally synthesized by oxidative azo coupling of the respective *N*-ethyl functionalized 5-aminotetrazole precursors using *tert*-butyl hypochlorite as reagent. All compounds were analyzed through multicore NMR and IR spectroscopy as well as mass spectrometry. All solid compounds were further investigated using low-temperature X-ray crystallography. The purity was verified by CHNO elemental analysis and the decomposition temperature (DTA) and sensitivities toward impact, friction and electrostatic discharged were determined. Based on the CBS-4M calculation results, the energetic properties were calculated using the EXPLO5 code.

In the field of energetic materials, the most common approaches for the synthesis of new molecules are the introduction of cage or ring strain, the oxidation of the carbon backbone, or a raise of the molecule's nitrogen content.^[1] Widely used examples of merging these models are mainly 2,4,6-trinitrotoluene (TNT), cyclotrimethylenetrinitramine (RDX), or hexanitrohexaaza-isowurtzitane (CL-20).^[2–3] However, since TNT in particular, as well as the decomposition products of RDX, turned out to be toxic, an intensive search for a substitute is underway.^[4–5] Suitable substitutes should not only surpass the performance of their predecessors, but also exhibit high thermal stability with low sensitivity.^[6–7] Furthermore, the synthesis should be carried out in a few steps with simple processing while being inexpensive and environmentally friendly. However, the opportunities available here are looking

increasingly exhausted. CL-20 for example is currently part of many studies, trying to compensate the high sensitivity by co-crystallization of insensitive molecules.^[8–9]

In addition to trying to improve known molecules, increasing the nitrogen content also provides a good starting point.^[5] The building blocks represented in this area are primarily azoles. The most nitrogen-rich azole, pentazole, is currently only used as a salt and is extremely difficult to access.^[10–11] The first 5-aminopentazole derivative was only recently detected by NMR spectroscopy by Bannert *et al.*^[12] However, tetrazoles represent a more stable alternative. Currently, these are not considered toxic and are even used in various medicines.^[11,13] Tetrazoles have already found their way into the field of energetic materials, with the best-known representatives in this field probably being TKX-50 or DBX-1.^[14–15] Furthermore, their use as ligands in nitrogen-rich complexes as lead azide or lead styphnate substitutes is being investigated.^[16–17] A particularly interesting moiety because of its detonation parameters improving character, is the azo bridge. In pyrazoles and triazoles, this building block is already widely used.^[18–19] However, since tetrazoles are more limited with respect to their derivatizability, this unit is hardly found so far. Substituents are usually introduced before the azo coupling, and the neutral 5,5'-azobistetrazole (often called simply azotetrazole) is primarily used for the preparation of nitrogen-rich salts. Therefore, only methyl, amino, hydroxy or nitramino derivatives have been prepared by azo coupling of the respective 5-aminotetrazoles (Figure 1) yet.^[20–24]

In this work, we present the synthesis of four new symmetric energetic azotetrazoles, containing azidoethyl or nitrateethyl functionalities. The main access to this substance

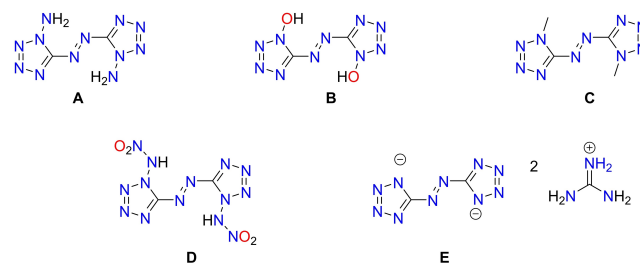


Figure 1. A) 1,1'-Diaminoazotetrazole, B) 1,1'-dihydroxyazotetrazole, C) 1,1'-dimethylazotetrazole, D) 1,1'-dinitraminoazotetrazole, E) bisguanidinium azotetrazolate.

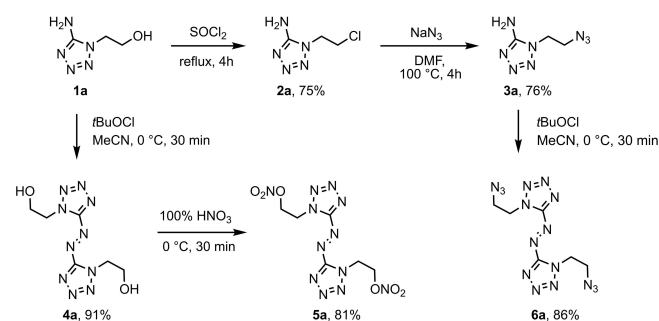
[a] M. Benz, M. S. Gruhne, Prof. Dr. T. M. Klapötke, N. Krüger, T. Lenz, M. Lommel, Dr. J. Stierstorfer
Department of Chemistry, University of Munich (LMU)
Butenandstr. 5–13 (D), 81377 München, Germany
E-mail: tmk@cup.uni-muenchen.de
www.hedm.cup.uni-muenchen.de

Supporting information for this article is available on the WWW under <https://doi.org/10.1002/ejoc.202100747>

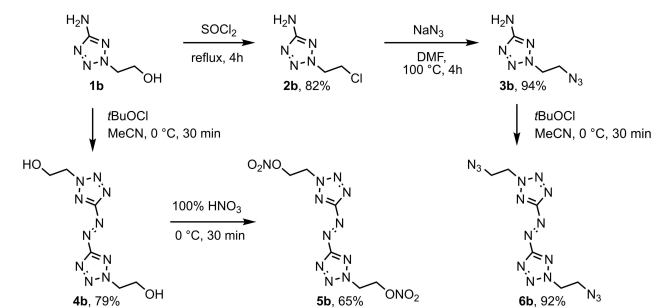
© 2021 The Authors. European Journal of Organic Chemistry published by Wiley-VCH GmbH. This is an open access article under the terms of the Creative Commons Attribution License, which permits use, distribution and reproduction in any medium, provided the original work is properly cited.

class was generated through a well-known reaction of sodium 5-aminotetrazolate with 2-chloroethanol resulting in the formation of the two isomers **1a** and **1b** (Scheme 1 and Scheme 2).^[25] For **1a** and **2a** an additional selective route is the reaction of cyanogen azide with 2-aminoethanol and 2-chloroethylamine hydrochloride, respectively.^[26] Straightforward chlorination of **1a** and subsequent chlorine-azide exchange formed the azidoethyl unit of **3a**.^[27] In order to introduce energetic groups only in the last synthesis step, **2a** was azo-coupled to the corresponding 1,1'-chloroethyl-azotetrazole (**7**, for more information see the SI), but the compound decomposed during the attempt of a chloro-azide exchange. With **1a** and **3a** in hands undergoing oxidative azo coupling with *tert*-butyl hypochlorite (*t*-BuOCl)^[28] in acetonitrile, 1,1'-bis(hydroxyethyl)-azotetrazole (**4a**) and 1,1'-bisazidoethyl-azotetrazole (**6a**) could be synthesized in good yields. Compound **4a** was further nitrated in 100% nitric acid to yield the bis-nitratoethyl compound **5a**. The complete synthetic protocol presented is featuring the use of only industrially accessible chemicals as there are 5-aminotetrazole, chloroethanol, thionyl chloride, sodium azide, *t*-BuOCl and nitric acid, making all products easily available.

Despite the long knowledge of hydroxyethyl-5-aminotetrazoles, hardly any reactions are known about 2-(1-hydroxyethyl)-5-aminotetrazole (**1b**), whereas there are plenty of references about the corresponding 1-isomer **1a** and its derivatives.^[25] Nonetheless, chloromethyl (**2b**) and azidoethyl (**3b**) derivatives could be synthesized in the same manner as for the other isomer (**2a** and **3a**). Oxidation of **1b** followed by nitration



Scheme 1. Synthetic pathway for the synthesis of 1-substituted isomers starting from 1-(2-hydroxyethyl)-5-aminotetrazole (**1a**).



Scheme 2. Synthetic pathway for the synthesis of 2-substituted isomers starting from 2-(2-hydroxyethyl)-5-aminotetrazole (**1b**).

results in the formation of **5b**, which was purified by recrystallization (Scheme 2). To avoid recrystallization, **1b** was protected with a TBS group to prevent the formation of by-products during azo formation or nitration (for more information see the SI compound **8**). However, the above-mentioned reactions led to the cleavage of the protective group. Following the procedure for the preparation of compound **6a**, bis(2,2'-(2,2'-azidoethyl)-azotetrazole (**6b**) was prepared in an identical manner by oxidative dimerization of **3b** using *t*-BuOCl as reagent.

Single crystals suitable for low temperature X-ray diffraction were obtained directly from the reaction mixture (**4a**, **6a**, **6b**) or after recrystallization from dichloromethane (**5a**) or a mixture of acetonitrile and water (**5b**). Details on the structures of the compounds **4a** (CCDC no. 2090053) together with measurement and refinement data of all crystallographically investigated compounds can be found in the Supporting Information (Figures S1–2, Table S1). The datasets were uploaded to the CSD database under the CCDC nos. 2090058 (**5a**), 2090057 (**6a**), 2090056 (**5b**) and 2090054 (**6b**) and can be obtained free of charge. The bond lengths and angles in the 5,5'-azobistetrazole moieties, as well as in the nitratoethyl and azidoethyl groups as substituents on tetrazoles are in accordance with similar structures already described in the literature and are therefore not part of the discussion.^[20–21]

Both nitratoethyl derivatives crystallize in the monoclinic space group *P*2₁/*c* with respectively two (**5a**) or four (**5b**) formula units per unit cell. In both structures, the ethyl groups are rotated out of the plane at approximately the same angle (**5a**: C1–N1–C2–C3 = 92.4(3) °; **5b**: N1–N2–C3–C4 = 83.21(18) °). The inversion symmetry in **5a** results in an opposite position of the two ethyl groups, whereas in **5b**, due to the lack of symmetry, both residues stand away in roughly the same direction (Figure 2).

The azidoethyl derivatives crystallize in a monoclinic space group (**6b**: *P*2₁/*n*) and a triclinic space group (**6a**: *P*-1). As already observed for compounds **5a** and **5b**, the arrangement of the side chains of the molecule is represented by the torsion angle created by the tetrazole and ethyl groups. Since in this case both molecules possess an inversion symmetry, the azidoethyl moieties are located in opposite directions. The torsion angles, however, differ more clearly for **6a** (C1–N1–C2–C3 = 90.4(3) °) and **6b** (N1–N2–C2–C3 = 39.959(7) °) compared to **5a** and **5b** (Figure 3).

All compounds were investigated using ¹H and ¹³C NMR spectroscopy. The CH₂ signals in the proton spectra for the respective ethyl functions, splitting up to doublet of doublet (dd) or multiplet (m) signals, appear, depending on the functional group (–Cl, –OH, –ONO₂, –N₃), in a region of 3.76–5.29 ppm.

Depending on the molecule, additional resonances for the respective OH or NH₂ function are detectable. Successful azo coupling is easily detectable by the disappearance of the NH₂ singlet signal. All investigated compounds show three signals in the ¹³C spectrum. The signals for the tetrazole carbon of the monomers occurs at around 156 ppm for the 1-substituted tetrazoles **1a**–**3a** and 167 ppm for 2-substituted derivatives

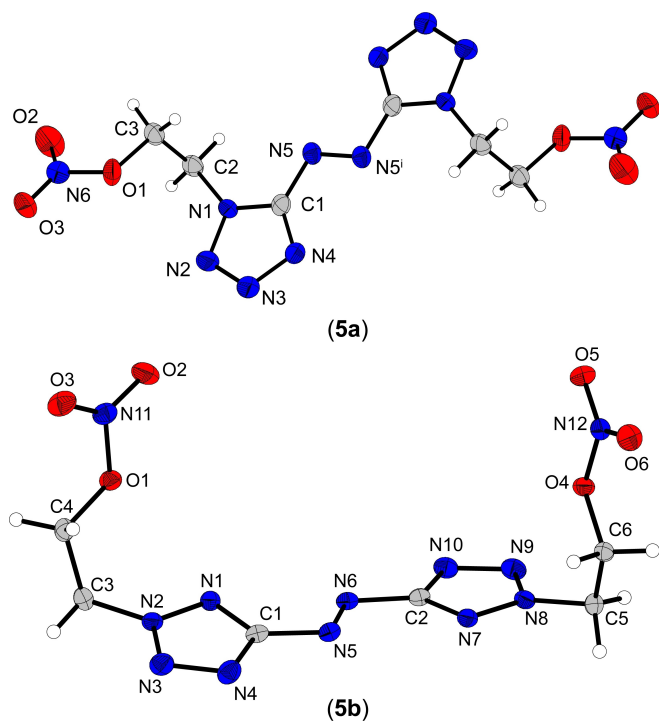


Figure 2. Low temperature crystal structures of the compounds **5a** and **5b**. Selected bond lengths (Å) of **5a**: N5–N5¹ 1.259(3), N1–C2 1.460(3), O1–C3 1.456(3). Selected bond lengths (Å) of **5b**: N5–N6 1.258(2), N2–C3 1.461(2), C4–O1 1.453(2). Selected bond angles (°) of **5a**: N5¹–N5–C1 111.7(2), C1–N1–C2 130.69(18), C3–N6–N7 115.66(19). Selected bond angles (°) of **5b**: N6–N5–C1 112.20(15), N1–N2–C2 123.19(15), C4–O1–N11 113.20(14).

(**1b–3b**) while the respective azo coupled products show a slight downfield shift for this signal. Furthermore, two signals for the ethyl rest are detectable, depending on the particular substitution thereof. As a result of inversion symmetry, for azo coupled compounds **4a,b–6a,b** only the half of the expected number of different resonances is obtained.

Due to poor solubility, ¹⁵N NMR spectra were only measured for **5a** and **6a** (Figure 4). Assignments were only measured for performed on basis of spectra of several azotetrazole^[21] derivatives and 2D ¹H, ¹⁵N HMBSC spectra (for more details see the Supporting Information). Azotetrazole resonances N1–N5 appear homogeneously for both compounds with the nitrogen N5, involved in the azo bridge, as the most downfield shifted signal (117.7 ppm for **6a** and 118.3 ppm for **5a**). Signals N1–N4 arise in the regular range as expected for 1-alkyl-5-amino-tetrazoles. In addition, **5a** shows a signal at –43.6 ppm representing the organic nitrate N6. Nitrogen resonances of the azido function can be detected at –134.8 ppm (N_β), –171.6 ppm (N_γ) and –322.6 ppm (N_α) in the spectrum of **6a**.

Generally, compounds **5a**, **5b**, **6a** and **6b** can be classified^[29] as sensitive to very sensitive energetic materials with high heats of formation (Table 1). The crystallographically determined room temperature densities range from 1.702 g cm^{–3} (**5a**) to 1.539 g cm^{–3} (**6b**), with the 2-substituted isomers each being less dense than the 1-substituted ones. The same applies to the comparison of nitrates and corresponding

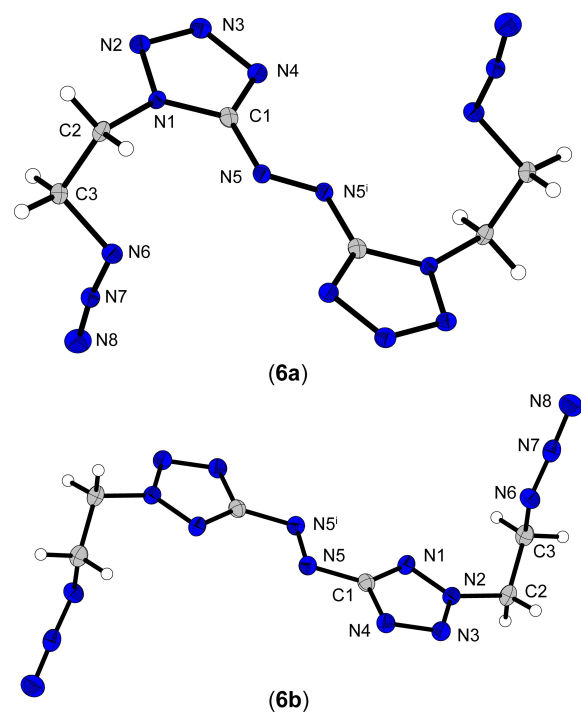


Figure 3. Low temperature crystal structures of the compounds **6a** and **6b**. Selected bond lengths (Å) of **6a**: N5–N5¹ 1.263(4), N1–C2 1.469(3), N6–C3 1.480(3). Selected bond lengths (Å) of **6b**: N5–N5¹ 1.2536(2), N2–C2 1.46606(17), C3–N6 1.4870(2). Selected bond angles (°) of **6a**: N5¹–N5–C1 111.4(3), C1–N1–C2 131.0(2), C3–N6–N7 114.3(2). Selected bond angles (°) of **6b**: N5¹–N5–C1 112.452(8), N1–N2–C2 123.753(10), C3–N6–N7 115.139(11).

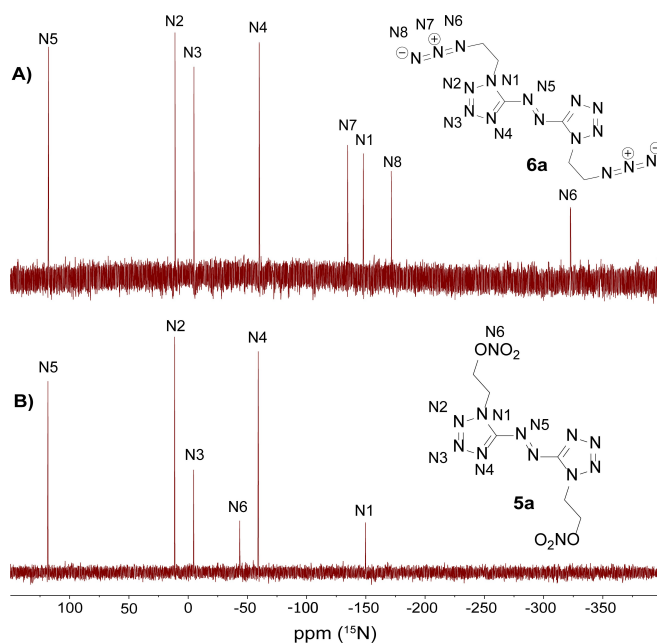


Figure 4. Proton coupled ¹⁵N NMR spectra of **6a** (A) and **5a** (B) measured in DMSO-D₆.

azides within the same substitution position. The calculated detonation parameters, which are closely linked to the

Table 1. Energetic properties and detonation parameters of azo compounds **5a**, **5b**, **6a** and **6b**.

	5a	5b	6a	6b	TNT
Formula	C ₆ H ₈ N ₁₂ O ₆	C ₆ H ₈ N ₁₂ O ₆	C ₆ H ₈ N ₁₆	C ₆ H ₈ N ₁₆	C ₇ H ₅ N ₃ O ₆
<i>M</i> [g mol ⁻¹]	344.21	344.21	304.24	304.24	227.13
IS [J] ^a	2	< 1	4	< 1	15
FS [N] ^b	60	20	6	0.2	353
ESD [J] ^c	0.1	1.5	0.25	0.75	–
ρ [g cm ⁻³] ^d	1.702	1.676	1.605	1.539	1.648
<i>N</i> [%] ^e	48.8	48.8	73.7	73.7	18.5
Ω [%] ^f	–18.6/–46.5	–18.6/–46.5	–52.6/–84.1	–52.6/–84.1	–24.7/–74.0
<i>T</i> _{mel} / <i>T</i> _{dec} [°C] ^g	167/179	–/97	147/188	72/140	80/290
$\Delta_f H^\circ$ [kJ mol ⁻¹] ^h	630.1	613.0	1456.2	1439.2	–55.5
$\Delta_f U^\circ$ [kJ mol ⁻¹] ⁱ	662.3	645.3	1486.0	1468.9	–168.0
EXPLOS V6.05.02					
– $\Delta_{Ex} U$ [kJ kg ⁻¹] ^j	5195	5135	4759	4702	4427
<i>T</i> _{det} [K] ^k	3608	3598	3175	3181	3222
<i>V</i> ₀ [L kg ⁻¹] ^l	782	785	777	782	633
<i>P</i> _{CJ} [kbar] ^m	266	256	233	207	194
<i>V</i> _{det} [m s ⁻¹] ⁿ	8179	8060	8148	7801	6824

[a] Impact sensitivity (BAM drophammer (1 of 6)). [b] Friction sensitivity (BAM friction tester (1 of 6)). [c] Electrostatic discharge sensitivity (OZM XSpark10). [d] From X-ray diffraction analysis recalculated to 298 K. [e] Nitrogen content. [f] Oxygen balance with respect to CO/CO₂. [g] Melting/Decomposition temperature (DTA; $\beta=5^\circ\text{Cmin}^{-1}$). [h] Calculated enthalpy of formation. [i] Calculated energy of formation. [j] Energy of explosion. [k] Detonation temperature. [l] Volume of detonation products (assuming only gaseous products). [m] Detonation pressure at Chapman-Jouguet point. [n] Detonation velocity.

respective density and heat of formation, respond analogously. Organic nitrates **5a** (8179 ms⁻¹) and **5b** (8060 ms⁻¹) both show higher values for detonation velocity than the respective azidoethyl derivatives. Azido compound **6a** (8148 ms⁻¹) is just slightly below the value of **5a**, whereas **6b** (7801 ms⁻¹) differs about 250 ms⁻¹ from the nitrate **5b** due to a higher difference in density. The 1-isomer also achieve higher decomposition temperatures than the 2-isomers. **5a** and **6a** decompose at around 180 °C, whereas **5b** already decomposes shortly below 100 °C. Sensitivity values toward impact and friction for **5a** (IS = 2 J, FS = 60 N) are comparable with those of PETN. As a trend for both, the respective azides and the 2-substituted isomers are more sensitive compared to the 1-substituted homologs. Azide **6b** is the most sensitive compound in this study with IS < 1 J and FS = 0.2 N, which is in the range for primary explosives.

Summarized, we report the synthesis by oxidative azo coupling of several 1- and 2-substituted 5-aminotetrazoles using *tert*-butyl hypochlorite as oxidation agent and characterization (XRD, NMR etc.) of 1- and 2-substituted nitrateoethyl and azidoethyl substituted 5,5'-azotetrazoles and the examination of the utility as energetic materials. The 1-substituted isomers showed more promising results in term of detonation properties and thermal stabilities compared with the respective 2-substituted derivatives. In terms of sensitivity toward external stimuli and the respective calculated energetic parameters azidoethyl derivative **6a** and **6b** could be further investigated for potential application as primary explosives. Organic nitrate **5a** shows the most promising characteristics as it outperforms TNT with a detonation velocity of about 8200 ms⁻¹ and a thermal stability as well as sensitivity values in the same range then PETN. Due to the simple and cheap synthesis, further applications in the field of sensitizers in rocket propellant mixtures are conceivable.

Deposition Numbers 2090058 (for **5a**), 2090057 (for **6a**), 2090056 (for **5b**), and 2090054 (for **6b**) contain the supplementary crystallographic data for this paper. These data are provided free of charge by the joint Cambridge Crystallographic Data Centre and Fachinformationszentrum Karlsruhe Access Structures service www.ccdc.cam.ac.uk/structures.

Acknowledgements

For financial support of this work by Ludwig-Maximilian University (LMU), the Office of Naval Research (ONR) under grant no. ONR N00014-19-1-2078 and the Strategic Environmental Research and Development Program (SERDP) under contract no. W912HQ19C0033 are gratefully acknowledged. We thank Prof. Konstantin Karaghiosoff for NMR measurements. Open access funding enabled and organized by Projekt DEAL.

Conflict of Interest

The authors declare no conflict of interest.

Keywords: Azo compounds · Crystallography · Energetic Material · NMR spectroscopy · Tetrazoles

- [1] H. Gao, J. M. Shreeve, *Chem. Rev.* **2011**, *111*, 7377–7436.
- [2] P. Pagoria, *Propellants Explos. Pyrotech.* **2016**, *41*, 452–469.
- [3] J. Ma, A. K. Chinnam, G. Cheng, H. Yang, J. Zhang, J. M. Shreeve, *Angew. Chem. Int. Ed.* **2021**, *60*, 5497–5504; *Angew. Chem.* **2021**, *133*, 5557–5564.
- [4] T. M. Klapötke, *Chemistry of High-Energy Materials*, De Gruyter, Boston, Berlin, **2017**.
- [5] O. T. O'Sullivan, M. J. Zdilla, *Chem. Rev.* **2020**, *120*, 5682–5744.

- [6] T. M. Klapötke, T. G. Witkowski, *ChemPlusChem* **2016**, *81*, 357–360.
- [7] W.-J. Geng, Q. Ma, Y. Chen, W. Yang, Y.-F. Jia, J.-S. Li, Z.-Q. Zhang, G.-J. Fan, S.-M. Wang, *Cryst. Growth Des.* **2020**, *20*, 2106–2114.
- [8] S.-F. Zhu, Q. Gan, C. Feng, *ACS Omega* **2019**, *4*, 13408–13417.
- [9] Z. Yang, H. Wang, Y. Ma, Q. Huang, J. Zhang, F. Nie, J. Zhang, H. Li, *Cryst. Growth Des.* **2018**, *18*, 6399–6403.
- [10] P. Yin, J. M. Shreeve, *Advances in Heterocyclic Chemistry, Vol. 121*, Academic Press, **2017**, pp. 89–131.
- [11] H. Huang, J. Zhong, L. Ma, L. Lv, J. S. Francisco, X. C. Zeng, *J. Am. Chem. Soc.* **2019**, *141*, 2984–2989.
- [12] K. Banert, T. Pester, *Angew. Chem. Int. Ed.* **2020**, *59*, 12315–12320; *Angew. Chem.* **2020**, *132*, 12413–12418.
- [13] S. Shaaban, A. Negm, A. M. Ashmawy, D. M. Ahmed, L. A. Wessjohann, *Eur. J. Med. Chem.* **2016**, *122*, 55–71.
- [14] N. Fischer, D. Fischer, T. M. Klapötke, D. G. Piercey, J. Stierstorfer, *J. Mater. Chem.* **2012**, *22*, 20418–20422.
- [15] J. W. Fronabarger, M. D. Williams, W. B. Sanborn, J. G. Bragg, D. A. Parrish, M. Bichay, *Propellants Explos. Pyrotech.* **2011**, *36*, 541–550.
- [16] M. H. H. Wurzenberger, M. Lommel, M. S. Gruhne, N. Szimhardt, J. Stierstorfer, *Angew. Chem. Int. Ed.* **2020**, *59*, 12367–12370; *Angew. Chem.* **2020**, *132*, 12466–12469.
- [17] Q. Sun, X. Li, Q. Lin, M. Lu, *J. Mater. Chem. A* **2019**, *7*, 4611–4618.
- [18] M. Zhang, W. Fu, C. Li, H. Gao, L. Tang, Z. Zhou, *Eur. J. Inorg. Chem.* **2017**, *2017*, 2883–2891.
- [19] Y. Tang, J. M. Shreeve, *Chem. Eur. J.* **2015**, *21*, 7285–7291.
- [20] F. Li, X. Cong, Z. Du, C. He, L. Zhao, L. Meng, *New J. Chem.* **2012**, *36*, 1953–1956.
- [21] D. Fischer, T. M. Klapötke, D. G. Piercey, J. Stierstorfer, *Chem. Eur. J.* **2013**, *19*, 4602–4613.
- [22] A. Hammerl, G. Holl, Thomas M. Klapötke, P. Mayer, H. Nöth, H. Piotrowski, M. Warchhold, *Eur. J. Inorg. Chem.* **2002**, *2002*, 834–845.
- [23] D. Fischer, T. M. Klapötke, J. Stierstorfer, N. Szimhardt, *Chem. Eur. J.* **2016**, *22*, 4966–4970.
- [24] T. Küblböck, G. Angé, G. Bikelytė, J. Pokorná, R. Skácel, T. M. Klapötke, *Angew. Chem. Int. Ed.* **2020**, *59*, 12326–12330; *Angew. Chem.* **2020**, *132*, 12425–12429.
- [25] R. A. Henry, W. G. Finnegan, *J. Am. Chem. Soc.* **1954**, *76*, 923–926.
- [26] Y.-H. Joo, J. M. Shreeve, *Org. Lett.* **2008**, *10*, 4665–4667.
- [27] J. Stierstorfer, K. R. Tarantik, T. M. Klapötke, *Chem. Eur. J.* **2009**, *15*, 5775–5792.
- [28] D. E. Chavez, J. C. Bottaro, M. Petrie, D. A. Parrish, *Angew. Chem. Int. Ed.* **2015**, *54*, 12973–12975; *Angew. Chem.* **2015**, *127*, 13165–13167.
- [29] Impact: Insensitive > 40 J, less sensitive ≥ 35 J, sensitive ≥ 4 J, very sensitive ≥ 3 J; friction: Insensitive > 360 N, less sensitive = 360 N, sensitive < 360 N, > 80 N, very sensitive ≥ 80 N, extreme sensitive ≥ 10 N; according to the UN recommendations on the transport of dangerous goods.

Manuscript received: June 25, 2021
Revised manuscript received: July 21, 2021
Accepted manuscript online: July 27, 2021

European Journal of Organic Chemistry

Supporting Information

Evolving the Scope of 5,5'-Azobistetrazoles in the Search for High Performing Green Energetic Materials

Maximilian Benz, Michael S. Gruhne, Thomas M. Klapötke,* Nina Krüger, Tobias Lenz,
Marcus Lommel, and Jörg Stierstorfer

Table of Contents

1. Experimental part
2. NMR spectroscopy
3. X-ray diffraction
4. Thermal Analysis
5. Scanning electron microscopy
6. Computation
7. References

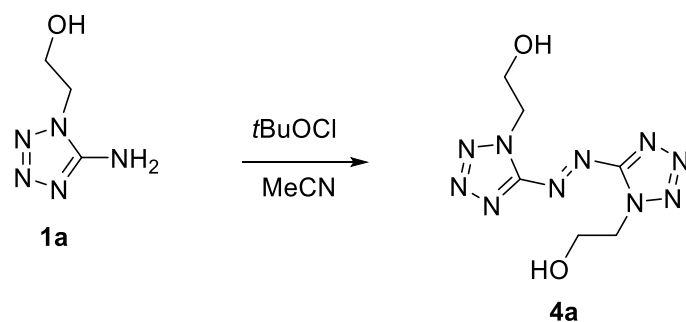
1. Experimental part

^1H , ^{13}C , ^{14}N and ^{15}N NMR spectra were recorded on *BRUKER AMX 400* instruments. Chemical shifts are referenced with respect to tetramethylsilane ($^1\text{H}/^{13}\text{C}$) and nitromethane ($^{14}\text{N}/^{15}\text{N}$). Infrared spectra (IR) were recorded in the region $4000\text{-}400\text{ cm}^{-1}$ on a *PERKIN ELMER Spectrum BX-59343* instrument with a *SMITHS DETECTION DuraSamplIR II Diamond ATR* sensor. Raman spectra were recorded with a Bruker MultiRAM. The absorption bands are reported in wavenumbers (cm^{-1}). Decomposition temperatures were measured via differential thermal analysis (DTA) with an *OZM Research DTA 552-Ex* instrument at a heating rate of $5\text{ }^\circ\text{C}/\text{min}$ and in a range of room temperature to $400\text{ }^\circ\text{C}$. All sensitivities toward impact (IS) and friction (FS) were determined according to BAM (Bundesanstalt für Materialforschung und Prüfung) standards using a BAM drop hammer and a BAM friction apparatus by applying the 1 of 6 method.^[S1] All energetic compounds were tested for sensitivity towards electrical discharge using an *Electric Spark Tester ESD 2010 EN* from OZM. Energetic properties have been calculated with the EXPLO5 6.02 computer^[S2] code using the RT converted X-ray density and calculated solid state heats of formation.

CAUTION! *All investigated compounds are potentially explosive materials. Safety precautions and equipment (such as wearing leather coat, face shield, Kevlar sleeves, Kevlar gloves, earthed equipment and ear plugs) must be used during all manipulations.*

The synthesis of compounds **1a** and **1b** was prepared according to literature known methods by Finnegan et al.^[S3] Compounds **2a** and **3a** were synthesized following the described procedures in the literature.^[S4] These procedures, excluding the work-ups, were used in the same manner for the synthesis of **2b** and **3b**.^[S4]

Bis(1,1'-(2,2'-hydroxyethyl)azotetrazole) (4a)



1-(2-Hydroxyethyl)-5-aminotetrazole (**1a**) (1.00 g, 7.75 mmol, 1.0 eq) was dissolved in MeCN (50 mL) and cooled to 0 °C with an ice bath. *t*BuOCl (2.19 mL, 19.3 mmol, 2.5 eq) was added dropwise and the mixture was stirred for 30 min 0 °C. After further stirring at room temperature for 1 h sodium carbonate (3.00 g) was added to quench the reaction. The solid was filtered off and the filtrate was evaporated to yield bis(1,1'-(2,2'-hydroxyethyl)azotetrazole (**4a**) as orange microcrystalline powder (0.90 g, 3.53 mmol, 91%).

DTA (5 ° min⁻¹): 164 °C (melt), 183 °C (dec).

IR (ATR) $\tilde{\nu}$ (cm⁻¹) = 3467(s), 2955(w), 1615(w), 1517(m), 1483(w), 1457(s), 1428(m), 1378(m), 1352(w), 1326(w), 1255(m), 1146(m), 1058(vs), 1032(s), 1005(m), 947(m), 867(m), 760(s), 745(s), 717(w), 680(s), 549(s), 499(vs), 424(vs).

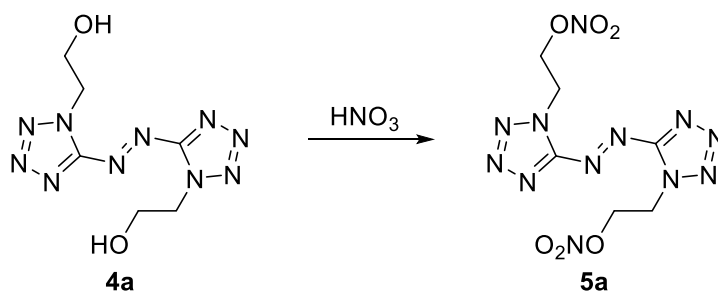
Elem. Anal. (C₆H₁₀N₁₀O₂, 254.21 g mol⁻¹) calcd.: C 28.35, N 55.10, H 3.97%. Found: C 28.22, N 55.22, H 3.89%.

¹H NMR (DMSO-D₆, 400 MHz, ppm) δ = 4.84 (dd, *J* = 5.7, 4.8 Hz, 4H), 3.90 (dd, *J* = 5.7, 4.7 Hz, 4H).

¹³C NMR (DMSO-D₆, 101 MHz, ppm) δ = 159.9, 59.2, 51.3.

HR-MS (ESI, 70 eV): [C₆H₁₀N₁₀O₂] calcd.: 255.1061 (M + H⁺), found: 255.1062.

Bis(1,1'-(2,2'-nitratoethyl))azotetrazole (5a)



Bis(1,1'-(2,2'-hydroxyethyl))azotetrazole (**4a**) (0.70 g, 2.76 mmol, 1.0 eq) was added in portions to HNO₃ (6 mL, 100%) at 0 °C. The mixture was stirred at this temperature for 30 min. The cooling-bath was removed and the mixture was quenched on ice-water (60 mL). The formed precipitate was filtered and washed with little amount of cold water to yield bis(1,1'-(2,2'-nittratoethyl))azotetrazole (**5a**) (0.77 g, 2.23 mmol, 81%) as orange solid.

Sensitivities: BAM drop hammer: 2 J (<100 μm), **friction tester:** 60 N (<100 μm), **ESD:** 100 mJ (<100 μm).

DTA (5 ° min⁻¹): 167 °C (melt), 179 °C (dec).

IR (ATR) $\tilde{\nu}$ (cm⁻¹) = 1630(s), 1452(m), 1427(m), 1280(vs), 1244(w), 1156(m), 1066(m), 1009(w), 987(m), 918(w), 893(vs), 846(s), 751(m), 741(m), 718(w), 710(w), 679(s), 641(m), 572(w), 552(w), 542(w), 496(m), 420(m).

Elem. Anal. (C₆H₈N₁₂O₆, 344.21 g mol⁻¹) calcd.: C 20.94, N 48.83, H 2.34%. Found: C 21.02, N 48.65, H 2.39%.

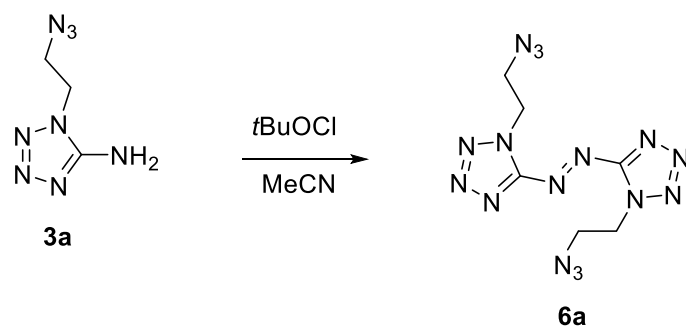
¹H NMR (DMSO-D₆, 400 MHz, ppm) δ = 5.19 (dd, *J* = 5.5, 4.1 Hz, 4H), 5.09 (dd, *J* = 5.5, 4.0 Hz, 4H).

¹³C NMR (DMSO-D₆, 101 MHz, ppm) δ = 159.4, 70.2, 46.3.

¹⁵N NMR (DMSO-D₆, 41 MHz, ppm) δ = 118.3, 11.4, -4.6, -43.6, -59.1, -149.8.

HR-MS (ESI, 70 eV): [C₆H₈N₁₂O₆] calcd.: 343.0617 (M - H⁺), found: 343.0621.

Bis(1,1'-(2,2'-azidoethyl))azotetrazole (**6a**)



1-(2-Azidoethyl)-5-aminotetrazole (**3a**) (1.00 g, 6.49 mmol, 1.0 eq) was dissolved in MeCN (50 mL) and cooled to 0 °C with an ice bath. *t*BuOCl (1.83 mL, 16.2 mmol, 2.5 eq) was added dropwise and the mixture was stirred for 30 min 0 °C. After further stirring at room temperature for 1 h sodium carbonate (3.00 g) was added to quench the reaction. The solid was filtered off and the filtrate was evaporated to yield bis(1,1'-(2,2'-azidoethyl))azotetrazole (**6a**) as pale orange crystals (0.85 g, 2.79 mmol, 86%).

Sensitivities: BAM drop hammer: 4 J (<100 μm), friction tester: 6 N (<100 μm), ESD: 250 mJ (<100 μm).

DTA (5 ° min⁻¹): 147 °C (melt), 188 °C (dec).

IR (ATR) $\tilde{\nu}$ (cm⁻¹) = 2142(vs), 2106(vs), 1500(m), 1444(s), 1425(s), 1372(m), 1342(s), 1291(vs), 1255(m), 1245(s), 1230(s), 1200(m), 1144(s), 1049(m), 1011(m), 949(s), 837(m), 760(s), 738(s), 662(s), 631(vs), 563(vs), 551(s), 489(vs), 422(vs).

Elem. Anal. (C₆H₈N₁₆, 304.24 g mol⁻¹) calcd.: C 23.69, N 73.66, H 2.65%. Found: C 24.27, N 73.10, H 2.74%.

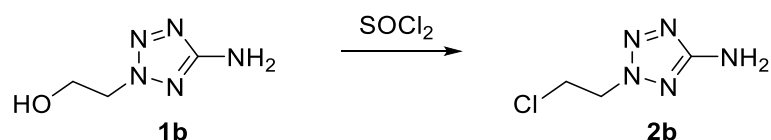
¹H NMR (DMSO-D₆, 400 MHz, ppm) δ = 5.03 – 4.91 (m, 4H), 4.08 – 3.95 (m, 4H).

¹³C NMR (DMSO-D₆, 101 MHz, ppm) δ = 159.5, 49.1, 48.2.

¹⁵N NMR (DMSO-D₆, 41 MHz, ppm) δ = 117.7, 11.0, -5.0, -60.1, -134.8, -148.0, -171.6, -322.6.

HR-MS (ESI, 70 eV): [C₆H₈N₁₆] calcd.: 304.1118 (M), found: 304.1126.

2-(2-Chloroethyl)-5-aminotetrazole (**2b**)^[S4]



2-(2-Hydroxyethyl)-5-aminotetrazole (**1b**) (2.00 g, 15.5 mmol, 1.0 eq) was added to SOCl_2 (6.6 mL) keeping the temperature below 20 °C. After the addition was complete the mixture was refluxed at 80 °C for 4 h. The solvent was removed under reduced pressure and the remaining thionyl chloride was quenched by adding cold ethanol (20 mL) and cold water (20 mL). The solvent was removed under reduced pressure and the crude product was recrystallized from hot benzene to separate 2-(2-chloroethyl)-5-aminotetrazole (**2b**) (1.87 g, 12.7 mmol, 82%) as a slightly brownish oil.

DTA (5 ° min⁻¹) = 201 °C (dec).

IR (ATR) $\tilde{\nu}$ (cm⁻¹) = 3335(m), 3230(w), 1622(s), 1543(vs), 1434(m), 1373(m), 1290(m), 1198(s), 1147(m), 1081(m), 1011(m), 956(m), 908(m), 788(m), 756(s), 668(s), 624(s), 452(s), 436(s), 419(s), 404(s).

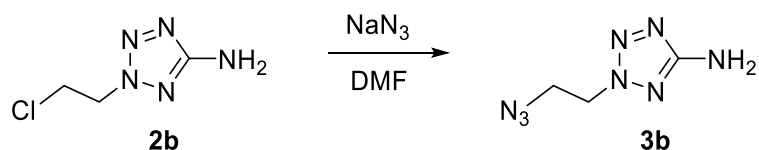
Elem. Anal. ($\text{C}_3\text{H}_6\text{N}_5\text{Cl}$, 147.57 g mol⁻¹) calcd.: C 24.42, N 47.46, H 4.10%. Found: C 24.64, N 47.10, H 4.31%.

¹H NMR (DMSO- D_6 , 400 MHz, ppm) δ = 5.85 (s, 2H), 4.75 (dd, J = 6.0, 5.0 Hz, 2H), 4.07 (dd, J = 6.0, 5.0 Hz, 2H).

¹³C NMR (DMSO- D_6 , 101 MHz, ppm) δ = 167.2, 53.5, 42.1.

HR-MS (ESI, 70 eV): [$\text{C}_3\text{H}_6\text{N}_5\text{Cl}$] calcd.: 148.0384 (M + H⁺), found: 148.0385.

2-(2-Azidoethyl)-5-aminotetrazole (**3b**)^[S4]



2-(2-Chloroethyl)-5-aminotetrazole (**2b**) (1.87 g, 12.7 mmol, 1.0 eq) was solved in DMF (25 mL) and sodium azide (0.91 g, 140.0 mmol, 1.1 eq) was added. The mixture was stirred for 4 h at 100 °C. The solvent was removed under reduced pressure and water (50 mL) was added. The mixture was extracted with EtOAc (3 x 50 mL), the organic phases were dried over anhydrous sodium sulfate and the solvent removed under reduced pressure to yield 2-(2-azidoethyl)-5-aminotetrazole (**3b**) (1.83 g, 11.9 mmol, 94%) as brownish oil.

DTA (5 ° min⁻¹) = 209 °C (dec).

IR (ATR) $\tilde{\nu}$ (cm⁻¹) = 3336(m), 2101(vs), 1622(s), 1542(vs), 1440(m), 1365(m), 1280(m), 1199(s), 1081(m), 1011(m), 790(m), 757(m), 625(s), 553(s), 497(s), 443(s), 416(s), 407(s).

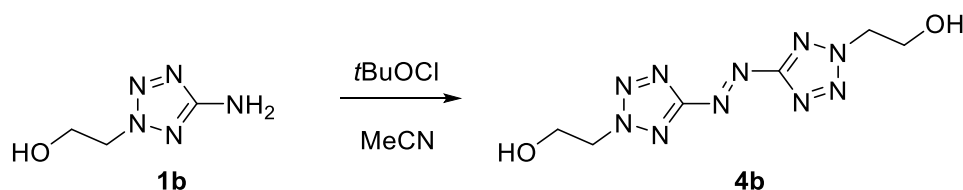
Elem. Anal. (C₃H₆N₅Cl, 154.14 g mol⁻¹) calcd.: C 23.38, N 72.70, H 4.26%. Found: C 23.61, N 72.13, H 4.26%.

¹H NMR (DMSO-D₆, 400 MHz, ppm) δ = 6.07 (s, 2H), 4.66 – 4.54 (m, 2H), 3.86 – 3.76 (m, 2H).

¹³C NMR (DMSO-D₆, 101 MHz, ppm) δ = 167.8, 51.8, 49.5.

HR-MS (ESI, 70 eV): [C₃H₆N₈] calcd.: 155.0788 (M + H⁺), found: 155.0794.

Bis(2,2'-(2,2'-hydroxyethyl)azotetrazole) (4b)



2-(2-Hydroxyethyl)-5-aminotetrazole (**1b**) (1.00 g, 7.75 mmol, 1.0 eq) was dissolved in MeCN (50 mL). *t*BuOCl (2.19 mL, 19.3 mmol, 2.5 eq) was added dropwise and the mixture was stirred for 30 min at ambient temperature. Afterwards, sodium carbonate (3.00 g) was added to quench the reaction. The solid was filtered off and the filtrate was evaporated to yield bis(2,2'-(2,2'-hydroxyethyl)azotetrazole (**4a**) as a yellowish oil (0.78 g, 3.06 mmol, 79%).

DTA (5 ° min⁻¹) = 101 °C (dec).

IR (ATR) $\tilde{\nu}$ (cm⁻¹) = 3361(m), 3224(w), 2950(w), 1739(w), 1633(w), 1524(m), 1469(s), 1397(m), 1363(m), 1195(m), 1066(vs), 1030(s), 956(m), 868(s), 827(m), 764(s), 741(s), 660(s), 601(s), 507(vs), 452(s), 442(s), 415(s), 405(s).

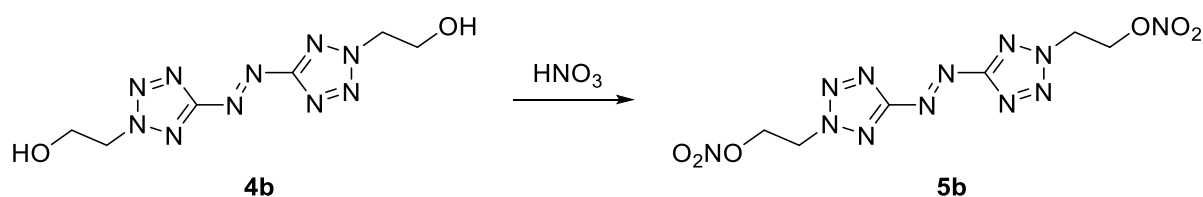
Elem. Anal. (C₆H₁₀N₁₀O₂, 254.21 g mol⁻¹) calcd.: C 28.35, N 55.10, H 3.97%. Found: C 27.91, N 54.02, H 4.61%.

¹H NMR (Acetone-D₆, 400 MHz, ppm) δ = 4.84 – 4.75 (m, 4H), 4.30 (t, *J* = 5.9 Hz, 2H), 4.13 (q, *J* = 5.4 Hz, 4H).

¹³C NMR (Acetone-D₆, 101 MHz, ppm) δ = 167.4, 57.7, 55.9.

HR-MS (ESI, 70 eV): [C₆H₁₀N₁₀O₂] calcd.: 255.1061 (M + H⁺), found: 255.1059.

Bis(2,2'-(2,2'-nitratoethyl))azotetrazole (**5b**)



Bis(2,2'-(2,2'-hydroxyethyl))azotetrazole (**4b**) (0.56 g, 2.20 mmol, 1.0 eq) was added dropwise to HNO₃ (4 mL, 100%) at 0 °C. The mixture was stirred at this temperature for 30 min. The cooling-bath was removed and the mixture was stirred for further 30 min at ambient temperature. Afterwards, the solution was quenched on ice-water (60 mL). The solution was extracted with ethyl acetate (3 x 50 mL). The combined organic phases were dried over anhydrous sodium sulfate and the solvent was reduced to yield bis(2,2'-(2,2'-nitratoethyl))azotetrazole (**5b**) (0.49 g, 1.43 mmol, 65%) as yellowish solid.

Sensitivities: BAM drop hammer: <1 J (<100 μm), **friction tester:** 20 N (<100 μm), **ESD:** 1.5 J (<100 μm).

DTA (5 ° min⁻¹): 97 °C (dec).

IR (ATR) $\tilde{\nu}$ (cm⁻¹) = 1631(s), 1611(s), 1519(w), 1430(m), 1361(m), 1279(vs), 1213(m), 1158(w), 1095(w), 1061(w), 1036(m), 1020(m), 889(vs), 848(s), 772(m), 755(s), 714(s), 706(s), 679(m), 646(m), 637(m), 575(m), 565(m), 508(m), 492(m), 438(m).

Elem. Anal. (C₆H₈N₁₂O₆, 344.21 g mol⁻¹) calcd.: C 20.94, N 48.83, H 2.34%. Found: C 20.19, N 47.99, H 2.27%.

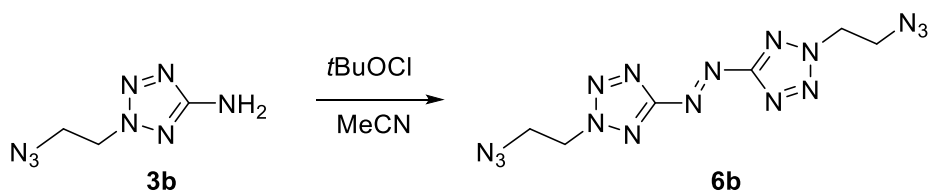
¹H NMR (Acetone-D₆, 400 MHz, ppm) δ = 5.41 – 5.38 (m, 4H), 5.31 – 5.29(m, 4H).

¹³C NMR (Acetone-D₆, 101 MHz, ppm) δ = 172.7, 70.8, 52.5.

¹⁴N NMR (Acetone-D₆, 29 MHz, ppm) δ = -44.

HR-MS (ESI, 70 eV): [C₆H₈N₁₂O₆] calcd.: 379.0384 (M + Cl⁻), found: 379.0389.

Bis(2,2'-(2,2'-azidoethyl))azotetrazole (**6b**)



2-(2-Azidoethyl)-5-aminotetrazole (**3b**) (0.50 g, 3.25 mmol, 1.0 eq) was dissolved in MeCN (50 mL) and cooled to 0 °C with an ice bath. *t*BuOCl (0.92 mL, 8.1 mmol, 2.5 eq) was added dropwise and the mixture was stirred for 30 min at 0 °C. After further stirring at room temperature for 1 h sodium carbonate (1.50 g) was added to quench the reaction. The solid was filtered off and the filtrate was evaporated to yield bis(2,2'-(2,2'-azidoethyl))azotetrazole (**6b**) as low melting orange crystals (0.46 g, 1.50 mmol, 92%).

Sensitivities: BAM drop hammer: <1 J (<100 μm), **friction tester:** 0.2 N (<100 μm), **ESD:** 750 mJ (<100 μm).

DTA (5 ° min⁻¹): 72 °C (melt), 140 °C (dec).

IR (ATR) $\tilde{\nu}$ (cm⁻¹) = 1631(s), 1611(s), 1519(w), 1430(m), 1361(m), 1279(vs), 1213(m), 1158(w), 1095(w), 1061(w), 1036(m), 1020(m), 889(vs), 848(s), 772(m), 755(s), 714(s), 706(s), 679(m), 646(m), 637(m), 575(m), 565(m), 508(m), 492(m), 438(m).

Elem. Anal. (C₆H₈N₁₆, 304.24 g mol⁻¹) calcd.: C 23.69, N 73.66, H 2.65%. Found: C 24.05, N 71.02, H 2.67%.

¹H NMR (Acetone-D₆, 400 MHz, ppm) δ = 5.15 – 5.08 (m, 4H), 4.20 – 4.17 (m, 4H).

¹³C NMR (Acetone-D₆, 101 MHz, ppm) δ = 172.8, 54.3, 50.3.

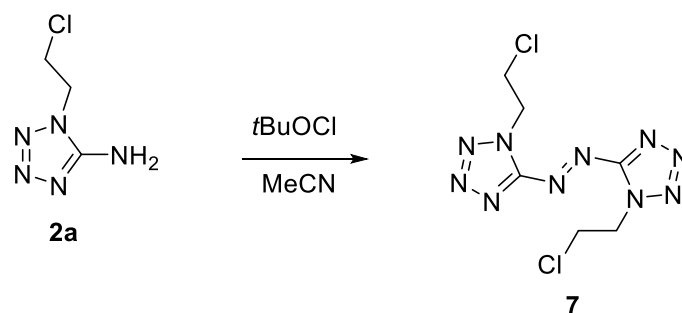
¹⁴N NMR (Acetone-D₆, 29 MHz, ppm) δ = -90, -135, -170, -315.

HR-MS (ESI, 70 eV): [C₆H₈N₁₆] calcd.: 304.1118 (M), found: 304.1124.

Further synthesized substances

Bis(1,1'-(2,2'-chloroethyl)azotetrazole (7)

Bis(1,1'-(2,2'-chloroethyl)azotetrazole (7) was synthesized through oxidative azo coupling starting from 1-(2-chloroethyl)-5-aminotetrazole (2a). The subsequent chlorine-azide exchange failed and ended up with decomposition products.



1-(2-Chloroethyl)-5-aminotetrazole (2a) (1.00 g, 6.80 mmol, 1.0 eq) was dissolved in MeCN (50 mL) and cooled to 0 °C with an ice bath. *t*BuOCl (1.92 mL, 17.0 mmol, 2.5 eq) was added dropwise and the mixture was stirred for 30 min 0 °C. After further stirring at room temperature for 1 h sodium carbonate (3.00 g) was added to quench the reaction. The solid was filtered off and the filtrate was evaporated to yield bis(1,1'-(2,2'-chloroethyl)azotetrazole (7) as orange crystals (0.87 g, 2.99 mmol, 88%).

DTA (5 ° min⁻¹) = 119 °C (melt), 181 °C (dec).

IR (ATR) $\tilde{\nu}$ (cm⁻¹) = 3334(m), 3150(m), 1647(s), 1590(s), 1479(m), 1442(m), 1428(m), 1303(s), 1132(s), 1103(s), 991(m), 944(s), 908(m), 744(m), 681(s), 651(vs), 563(s), 484(s), 451(vs), 436(s), 424(s), 414(s), 406(m).

Elem. Anal. (C₆H₈N₁₀Cl₂, 291.10 g mol⁻¹) calcd.: C 24.76, N 48.12, H 2.77%. Found: C 24.80, N 47.29, H 3.11%.

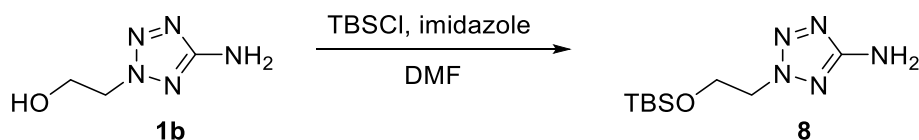
¹H NMR (Acetone-D₆, 400 MHz, ppm) δ = 5.32 (dd, *J* = 6.0, 5.4 Hz, 4H), 4.31 (dd, *J* = 6.0, 5.4 Hz, 4H).

¹³C NMR (Acetone-D₆, 101 MHz, ppm) δ = 161.1, 51.1, 43.0.

HR-MS (ESI, 70 eV): [C₆H₈N₁₀Cl₂] calcd.: 290.0310 (M), found: 290.0317.

1-(2-((*Tert*-butyldimethylsilyl)oxy)ethyl)-5-aminotetrazole (**8**)

1-(2-((*Tert*-butyldimethylsilyl)oxy)ethyl)-5-aminotetrazole (**8**) was prepared using a classic procedure for the TBS protection of alkylic hydroxy groups. **8** should be further reacted to the azo compound but this reaction failed and ended up with decomposition products.



2-(2-Hydroxyethyl)-5-aminotetrazole (**1b**) (1.00 g, 7.75 mmol, 1.0 eq) was dissolved in DMF (10 mL) and imidazole (1.27 g, 18.6 mmol, 2.4 eq) was added. After 10 min, TBSCl (1.52 g, 10.1 mmol, 1.3 eq) was added in one portion and the mixture was stirred overnight. The solvent was evaporated under reduced pressure and water (20 mL) was added. After extraction with EtOAc (3 x 50 mL), the combined organic phases were dried over sodium sulfate and the solvent was evaporated. **8** was obtained after purification using flash column chromatography (*i*Hex/EtOAc: 3:1) as transparent crystals (1.39 g, 5.72 mmol, 74%).

IR (ATR) $\tilde{\nu}$ (cm⁻¹) = 3365(m), 3226(w), 2928(m), 2880(w), 2856(m), 1647(m), 1551(s), 1471(m), 1459(m), 1431(w), 1388(m), 1373(w), 1360(w), 1260(m), 1250(m), 1192(s), 1114(s), 1088(m), 1066(w), 1018(m), 1007(m), 971(w), 935(vs), 840(s), 827(s), 810(s), 797(s), 777(vs), 759(s), 727(s), 682(m), 664(s), 630(s), 574(m), 498(m), 475(m), 442(m), 402(m).

Elem. Anal. (C₉H₂₁N₅OSi, 243.39 g mol⁻¹) calcd.: C 44.41, N 28.78, H 8.70%. Found: C 44.32, N 28.45, H 8.75%.

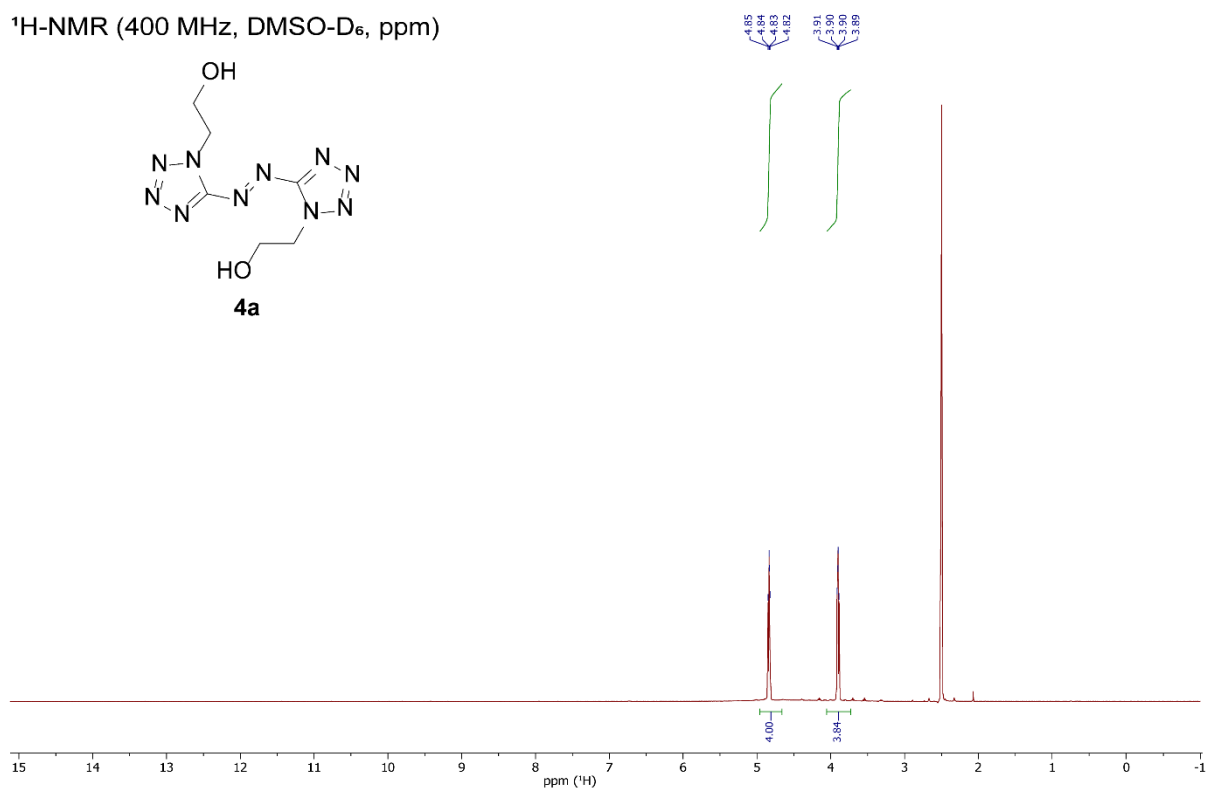
¹H NMR (DMSO-D₆, 400 MHz, ppm) δ = 5.95 (s, 2H), 4.44 (dd, *J* = 5.6, 4.7 Hz, 2H), 3.99 (dd, *J* = 5.6, 4.7 Hz, 2H), 0.77 (s, 9H), -0.07 (s, 6H).

¹³C NMR (DMSO-D₆, 101 MHz, ppm) δ = 167.0, 60.6, 54.5, 25.6, 17.8, -5.6.

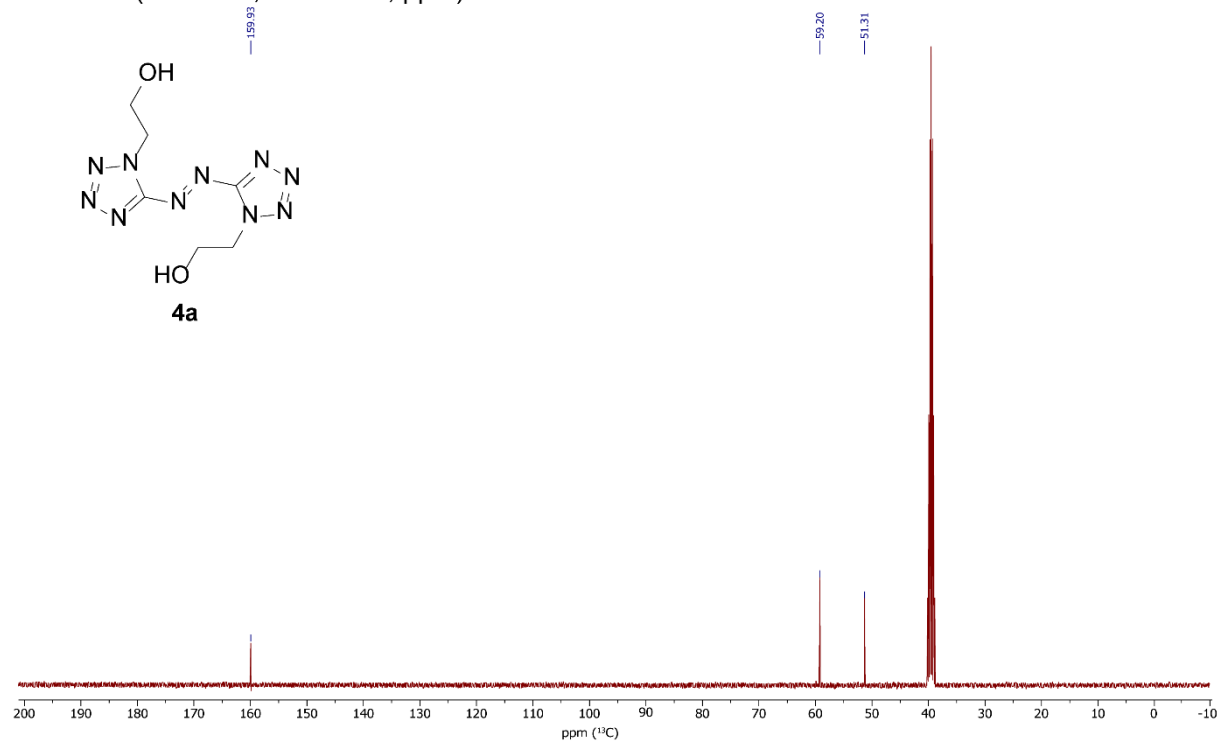
HR-MS (ESI, 70 eV): [C₉H₂₁N₅OSi] calcd.: 244.1588 (M + H⁺), found: 244.1589.

2. NMR spectroscopy

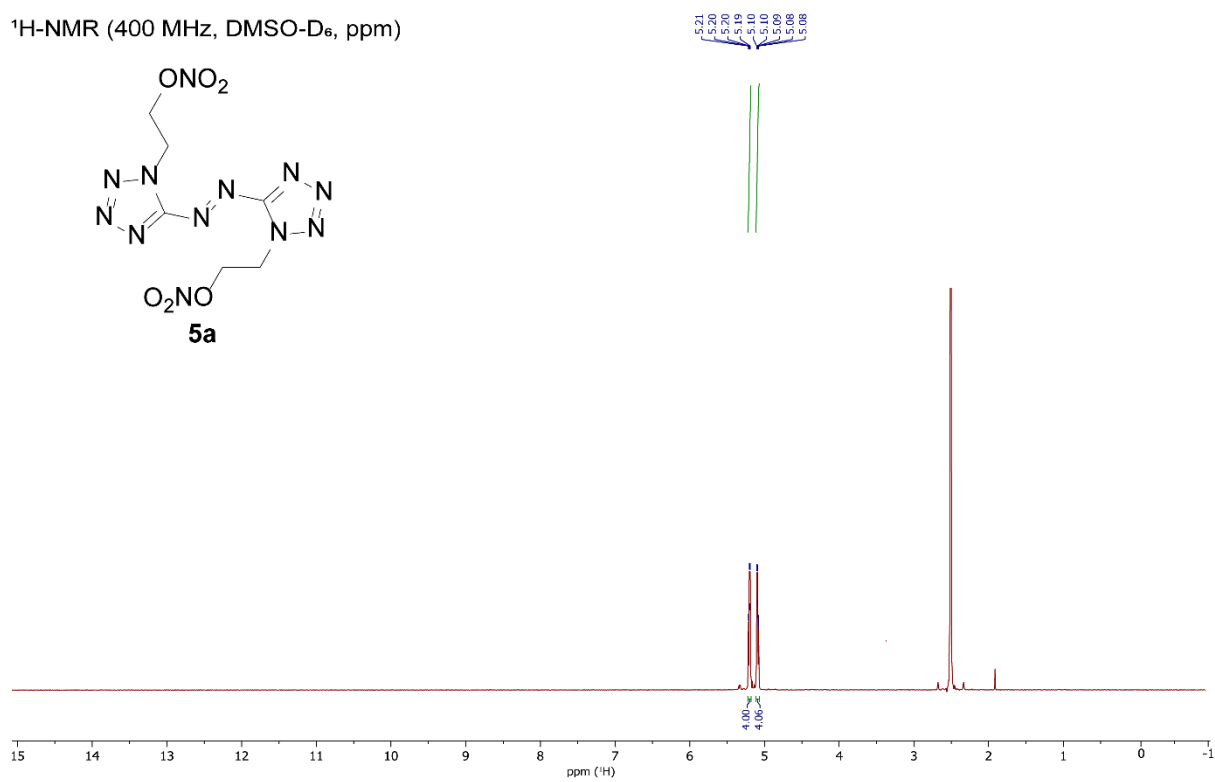
$^1\text{H-NMR}$ (400 MHz, DMSO-D_6 , ppm)



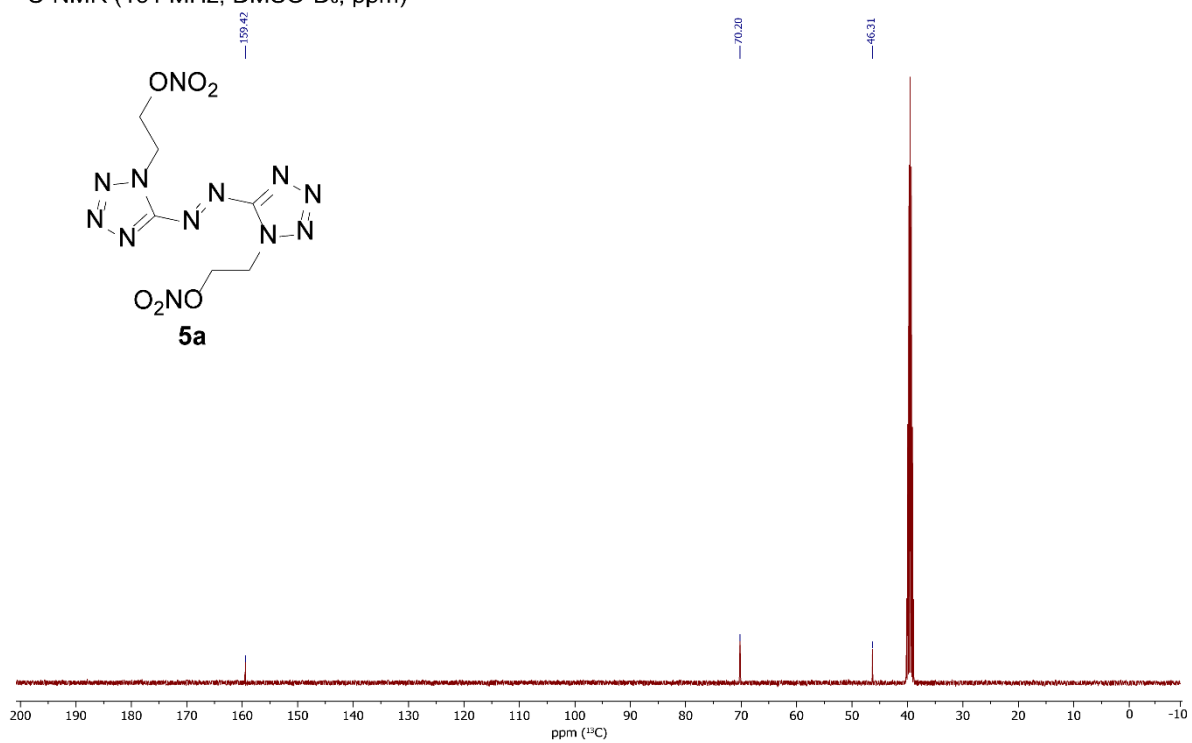
$^{13}\text{C-NMR}$ (101 MHz, DMSO-D_6 , ppm)

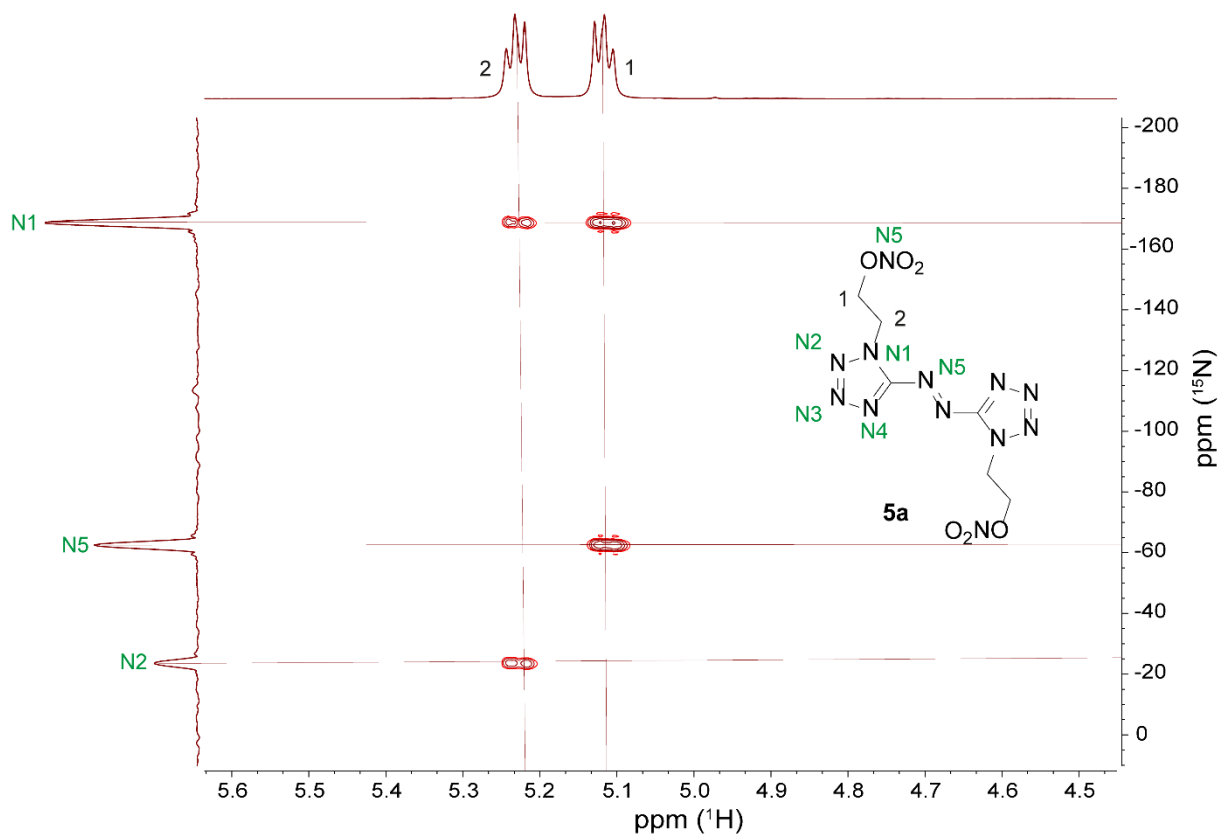


¹H-NMR (400 MHz, DMSO-D₆, ppm)

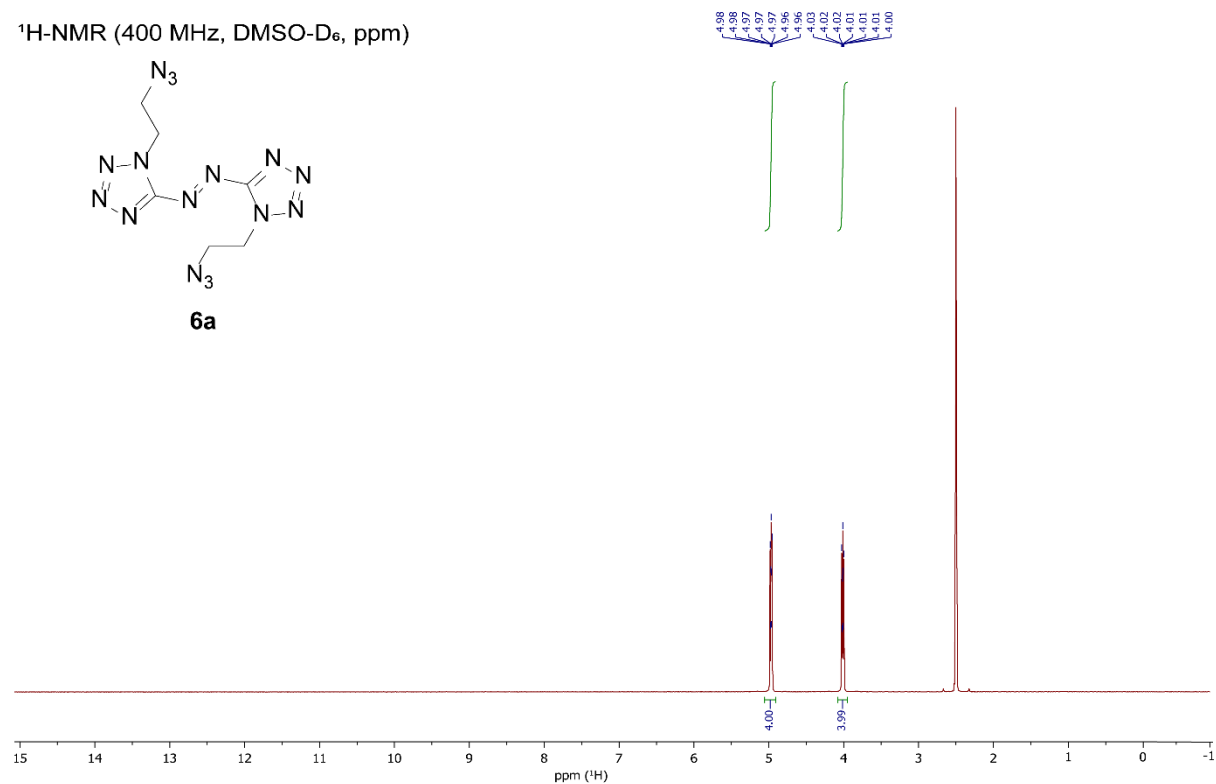


¹³C-NMR (101 MHz, DMSO-D₆, ppm)

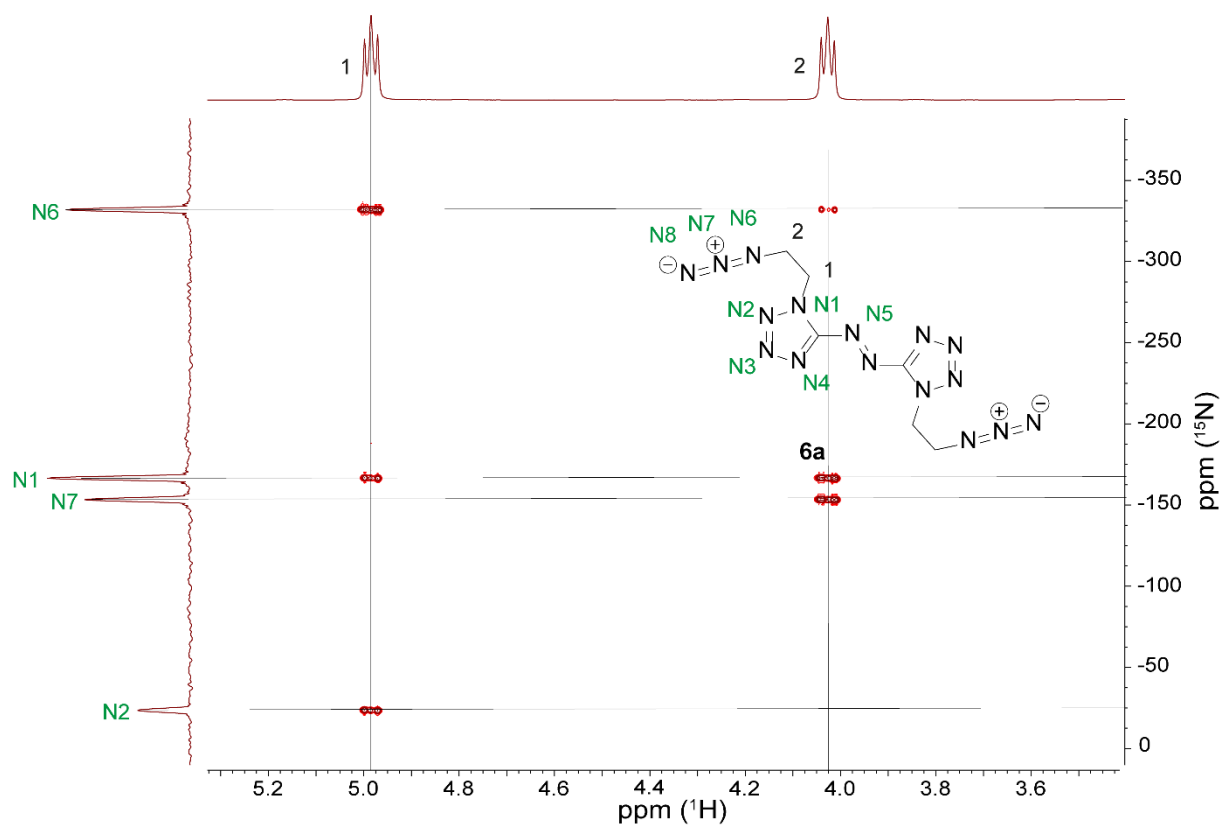
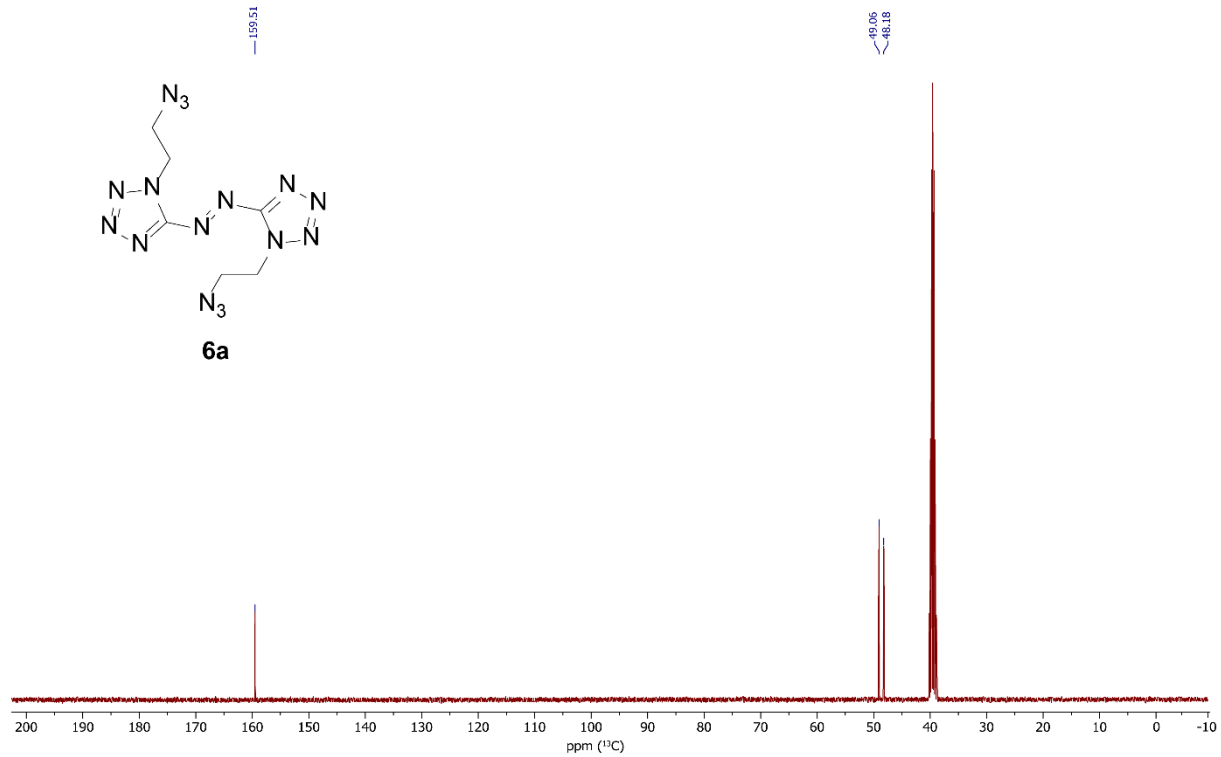




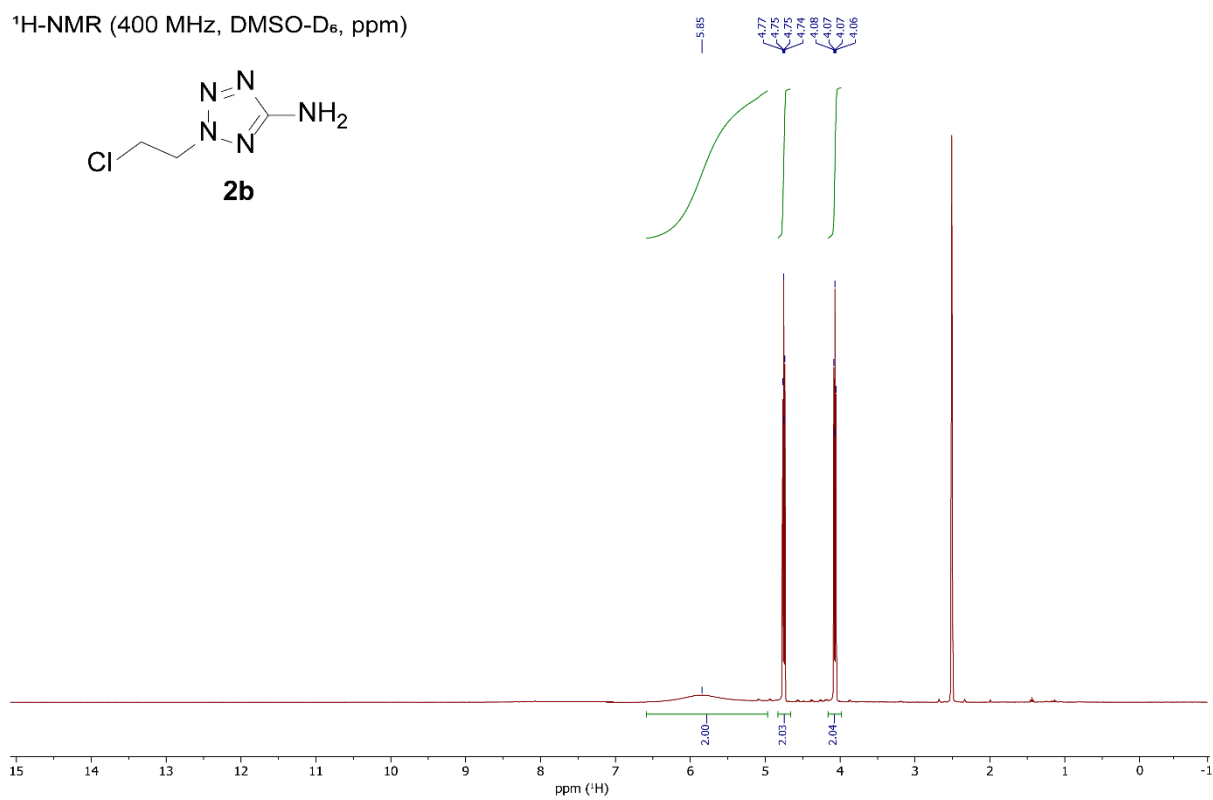
^1H -NMR (400 MHz, DMSO- D_6 , ppm)



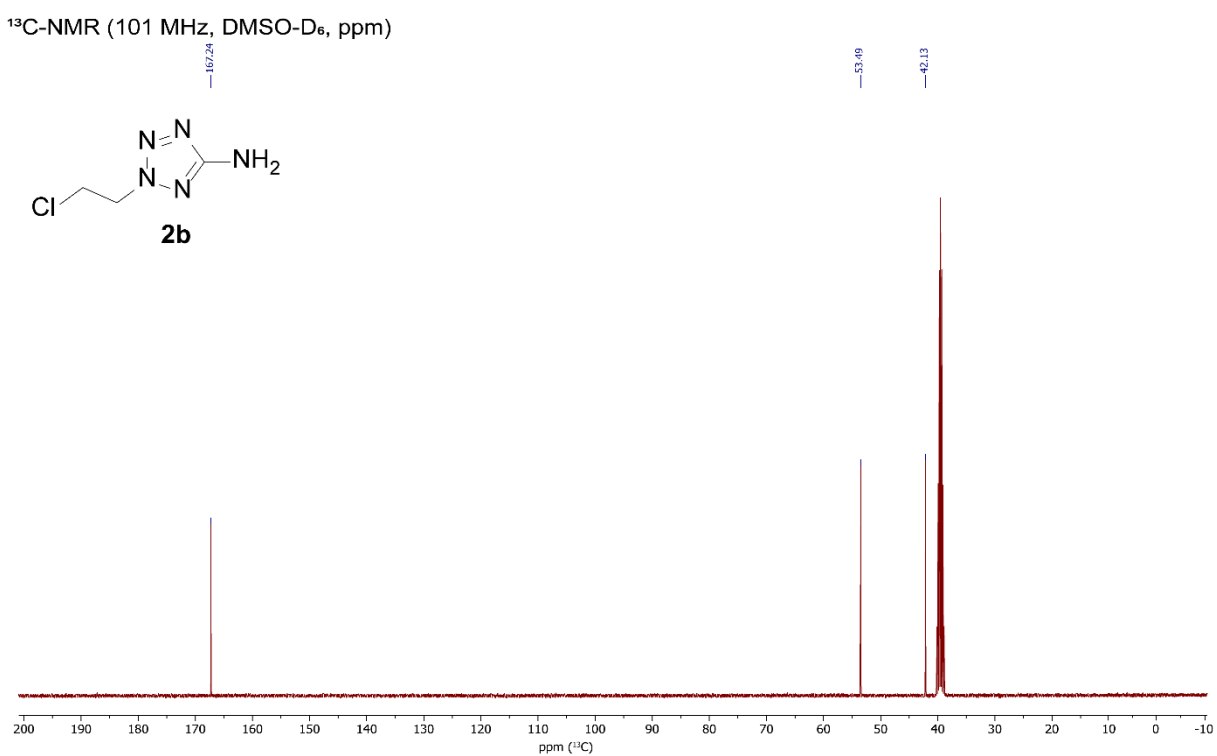
^{13}C -NMR (101 MHz, DMSO- D_6 , ppm)



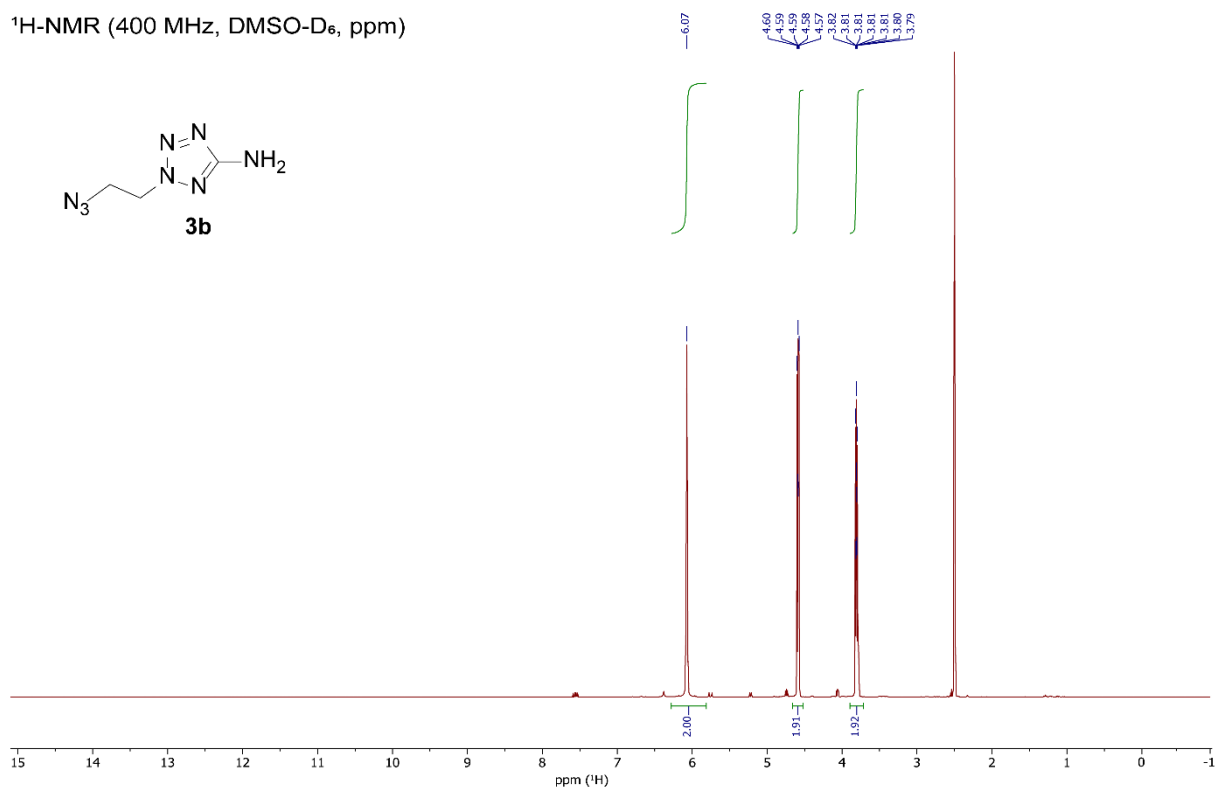
¹H-NMR (400 MHz, DMSO-D₆, ppm)



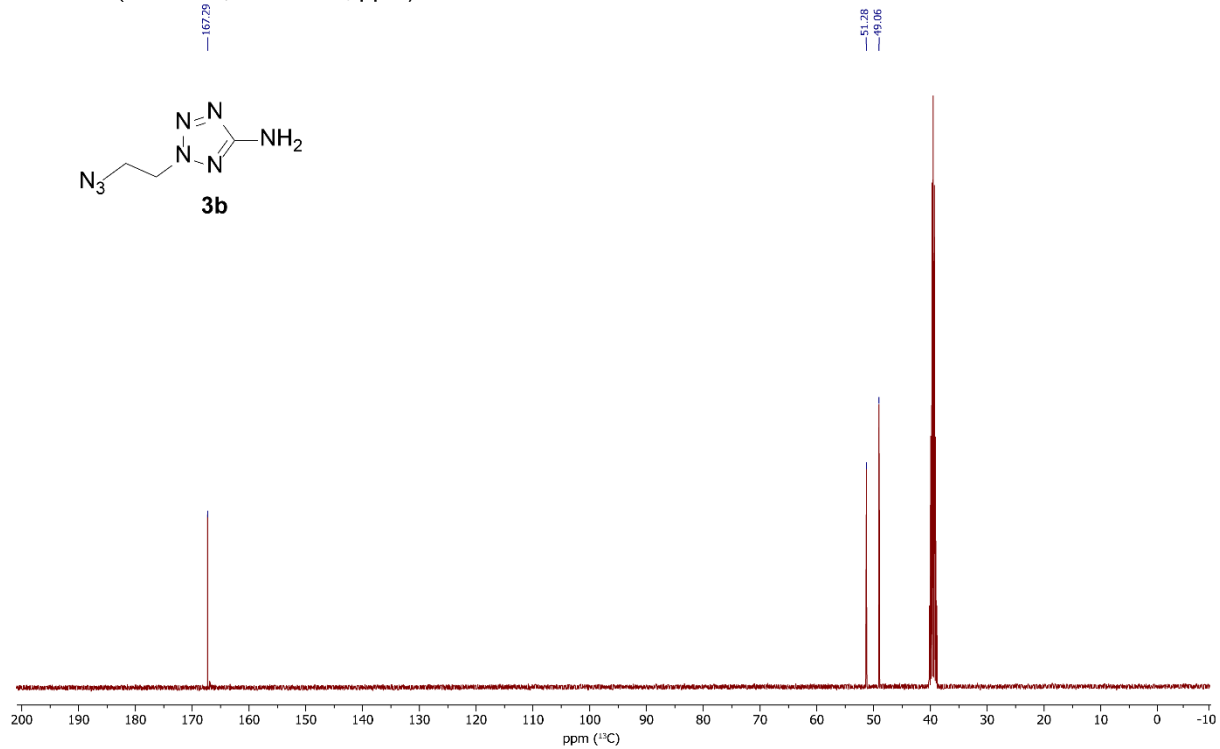
¹³C-NMR (101 MHz, DMSO-D₆, ppm)



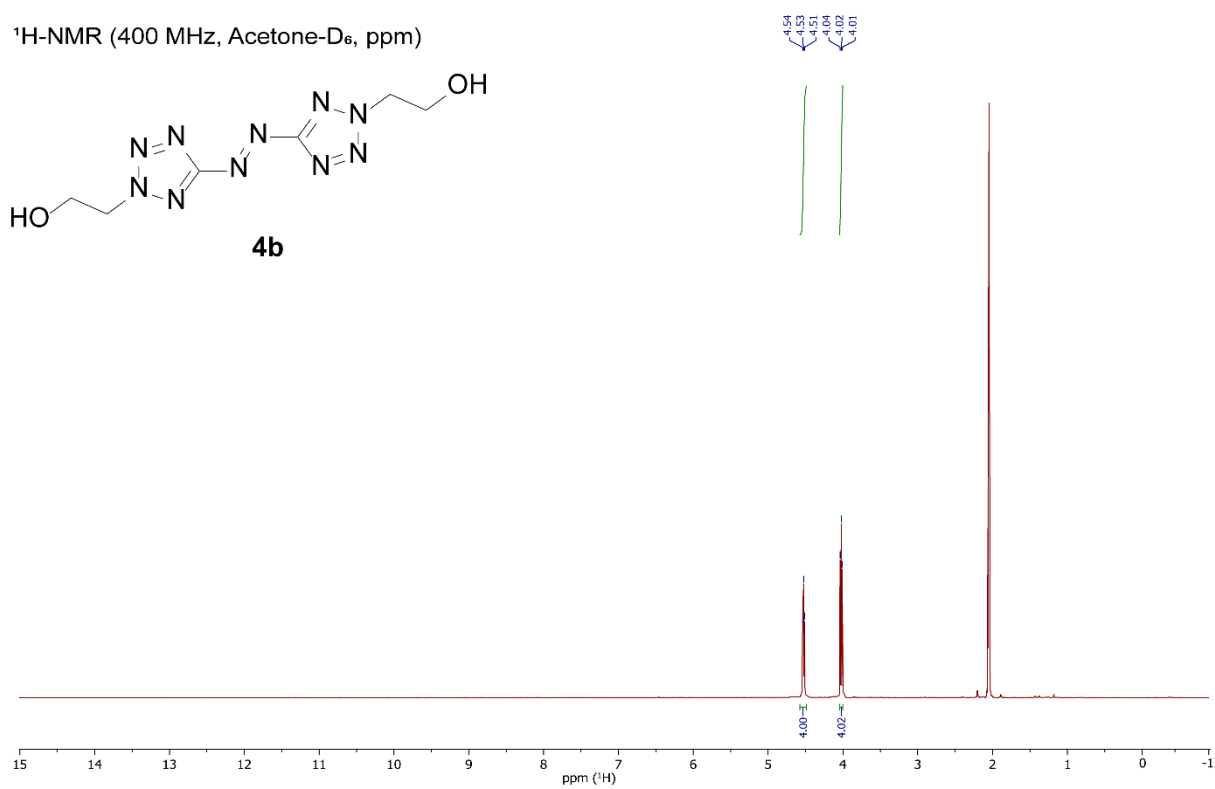
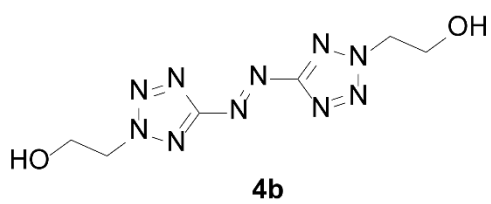
¹H-NMR (400 MHz, DMSO-D₆, ppm)



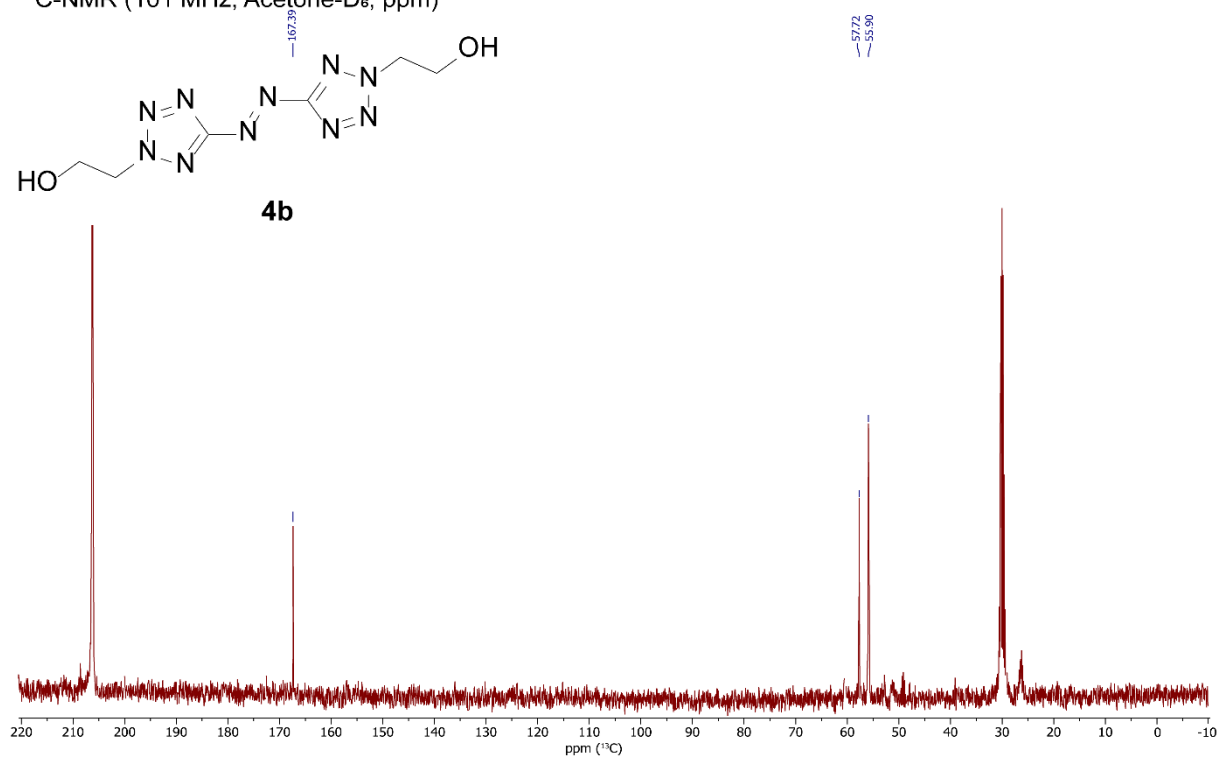
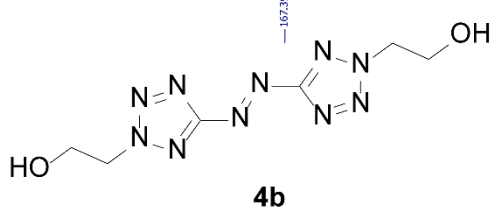
¹³C-NMR (101 MHz, DMSO-D₆, ppm)



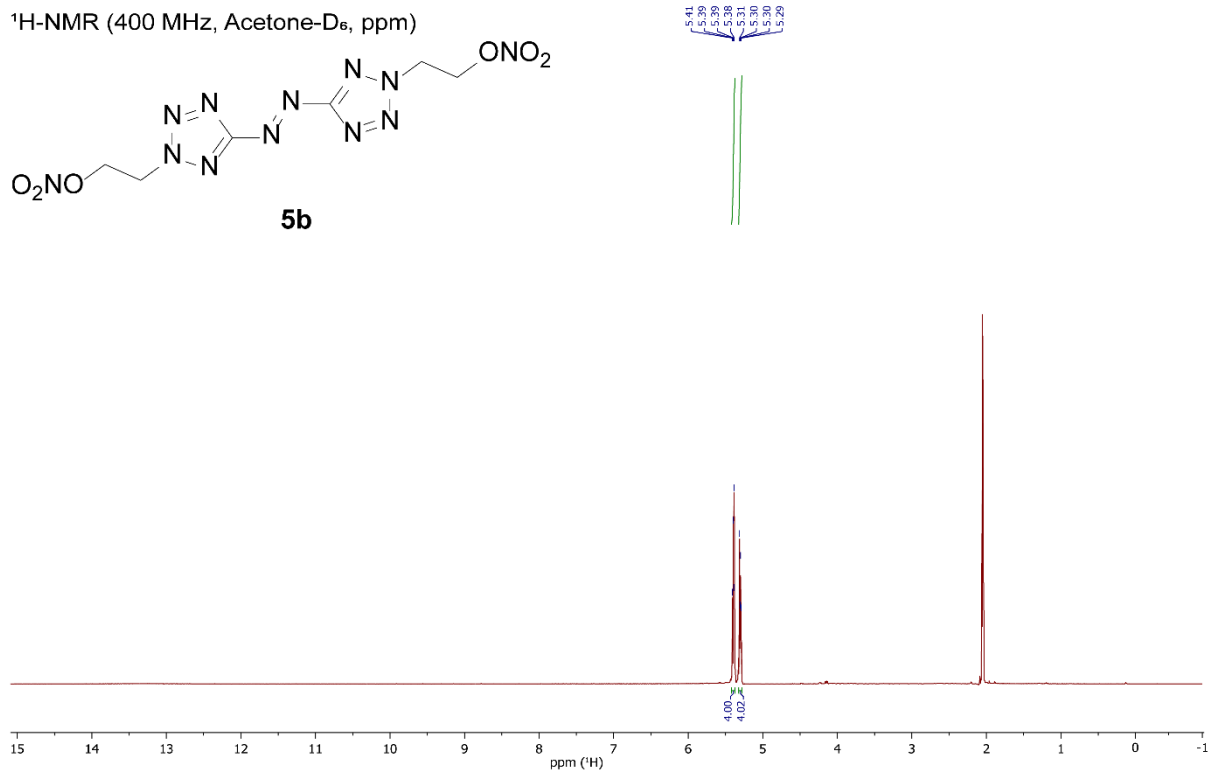
¹H-NMR (400 MHz, Acetone-D₆, ppm)



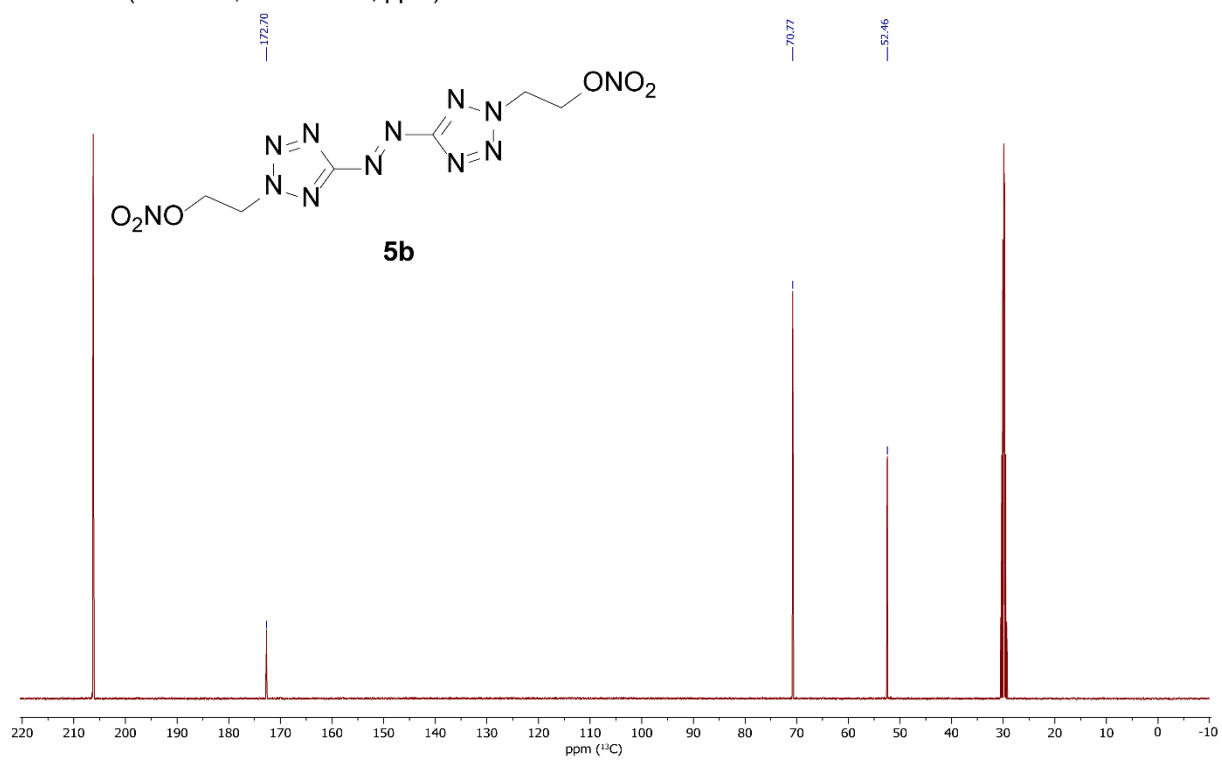
¹³C-NMR (101 MHz, Acetone-D₆, ppm)

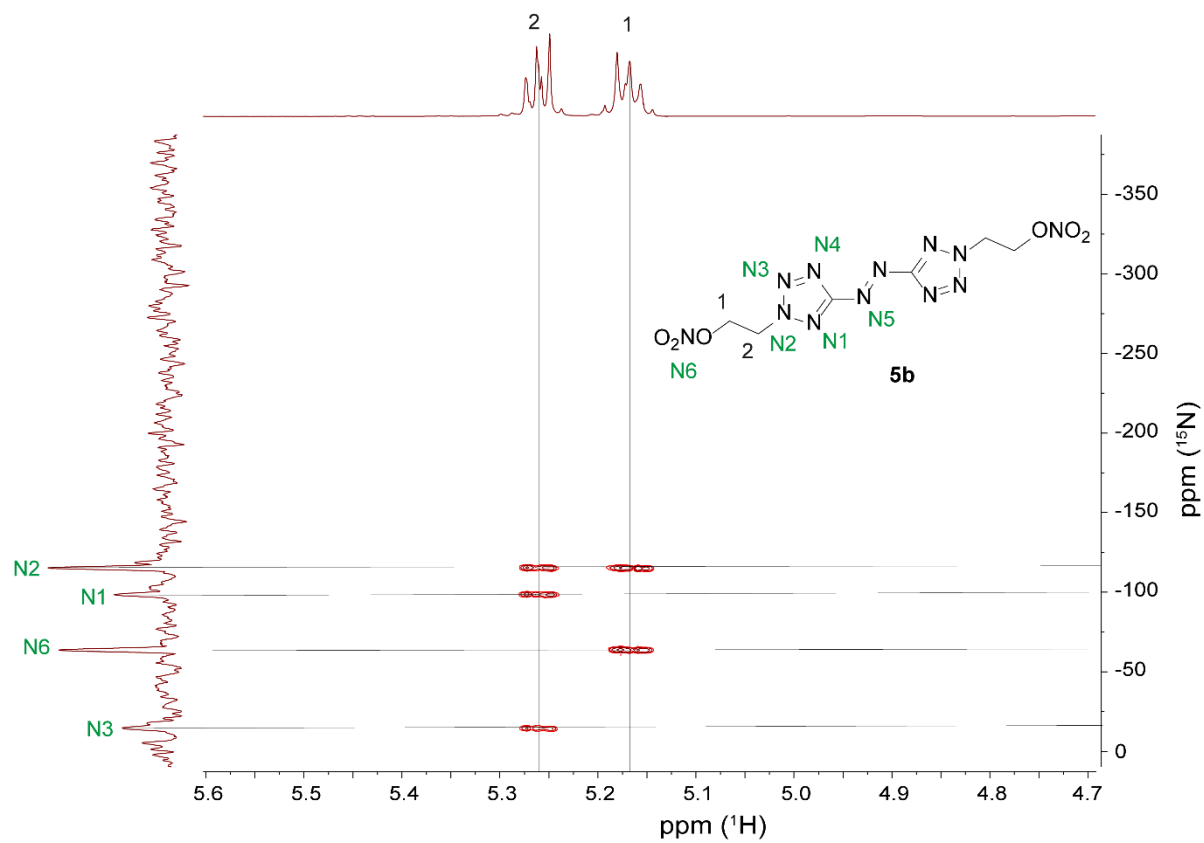


¹H-NMR (400 MHz, Acetone-D₆, ppm)

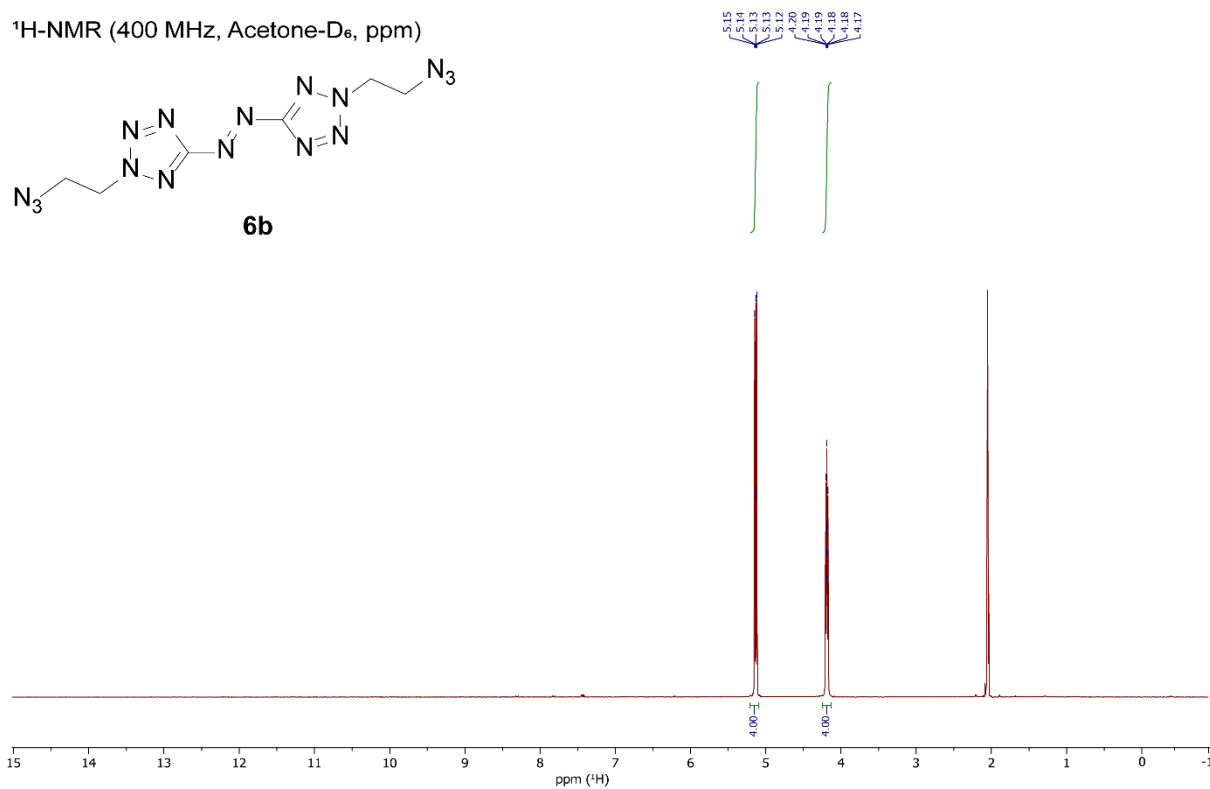


¹³C-NMR (101 MHz, Acetone-D₆, ppm)

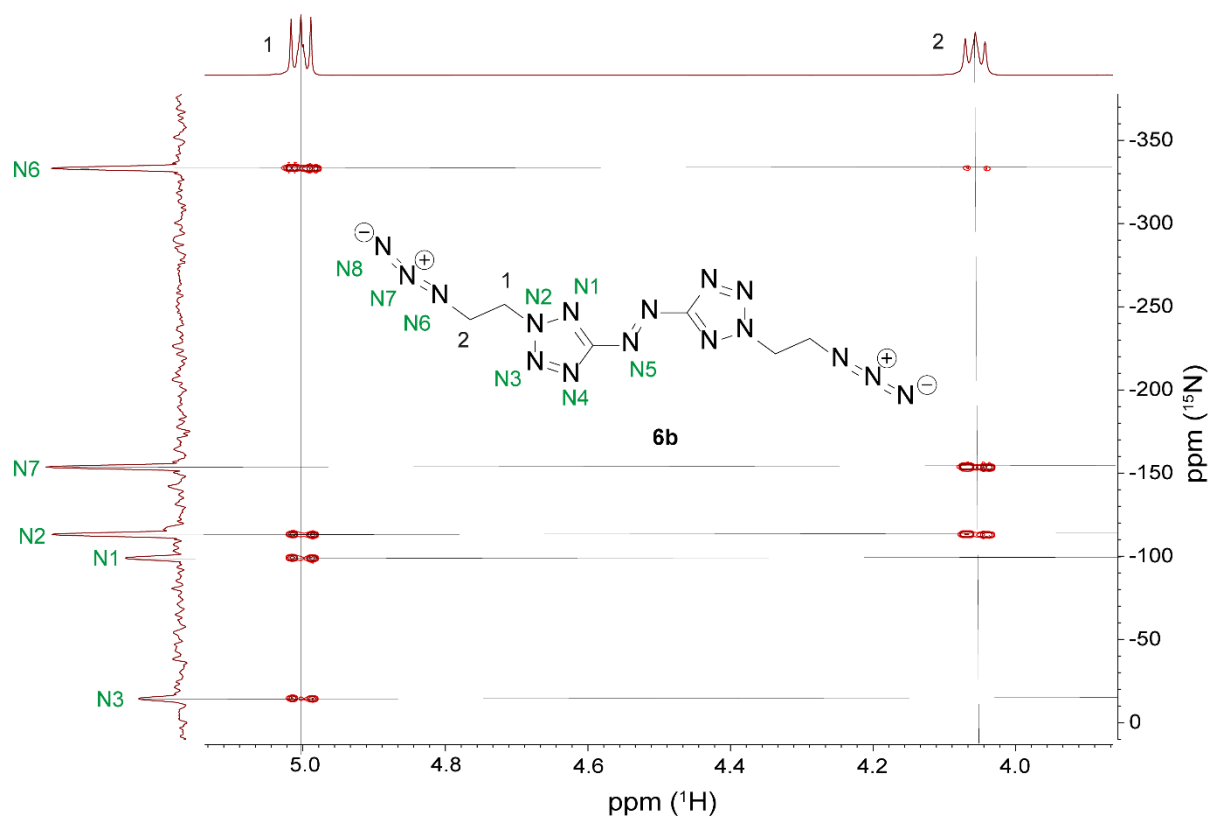
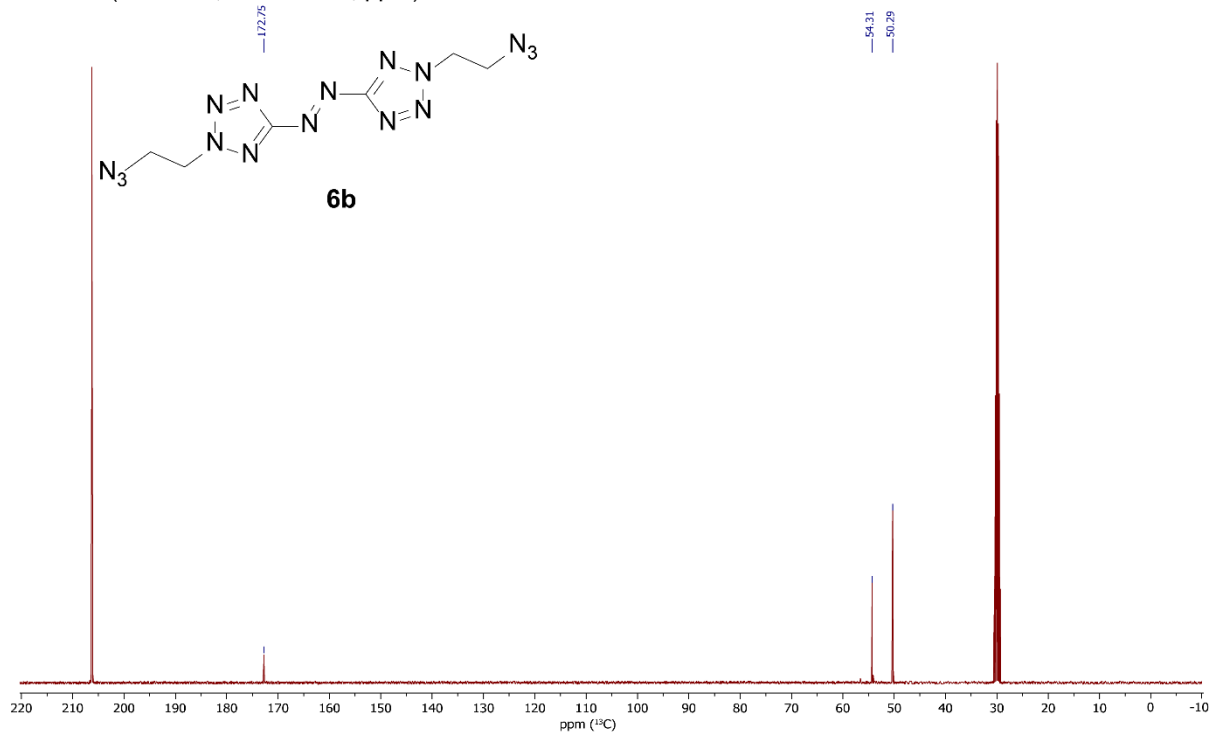




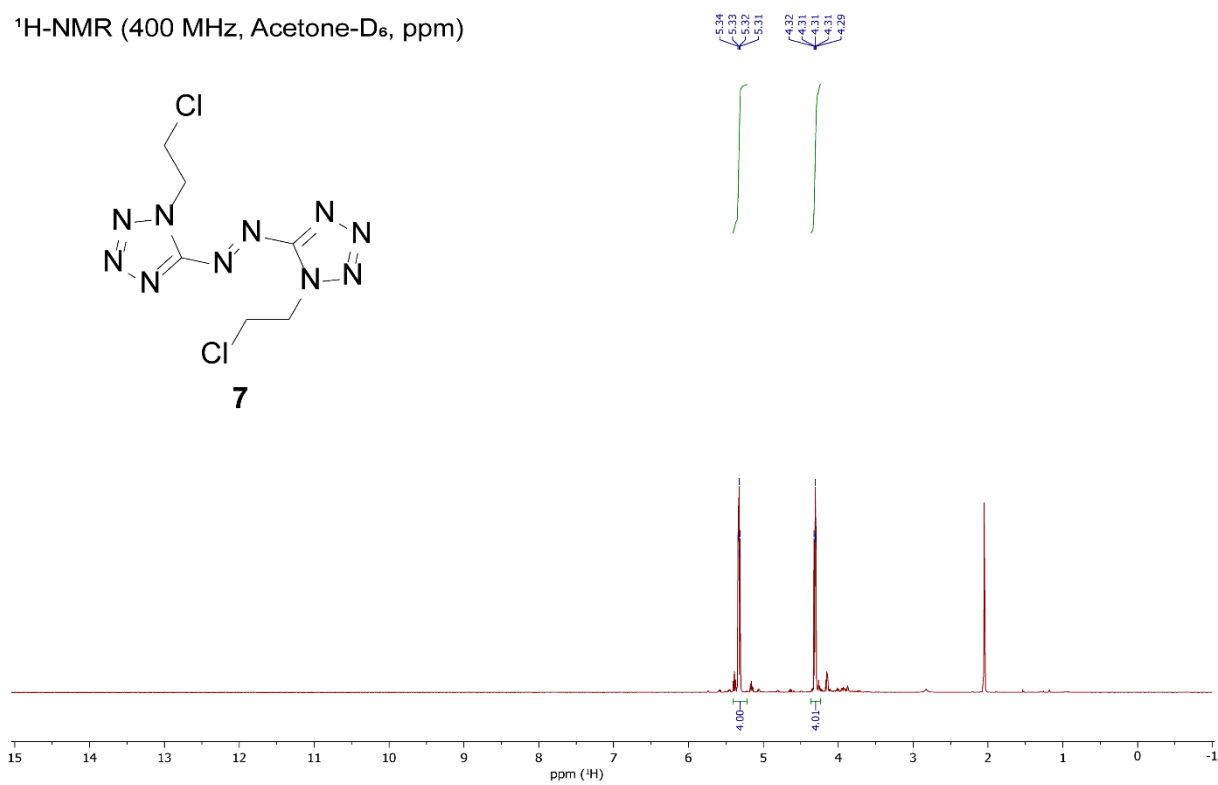
1H-NMR (400 MHz, Acetone-D₆, ppm)



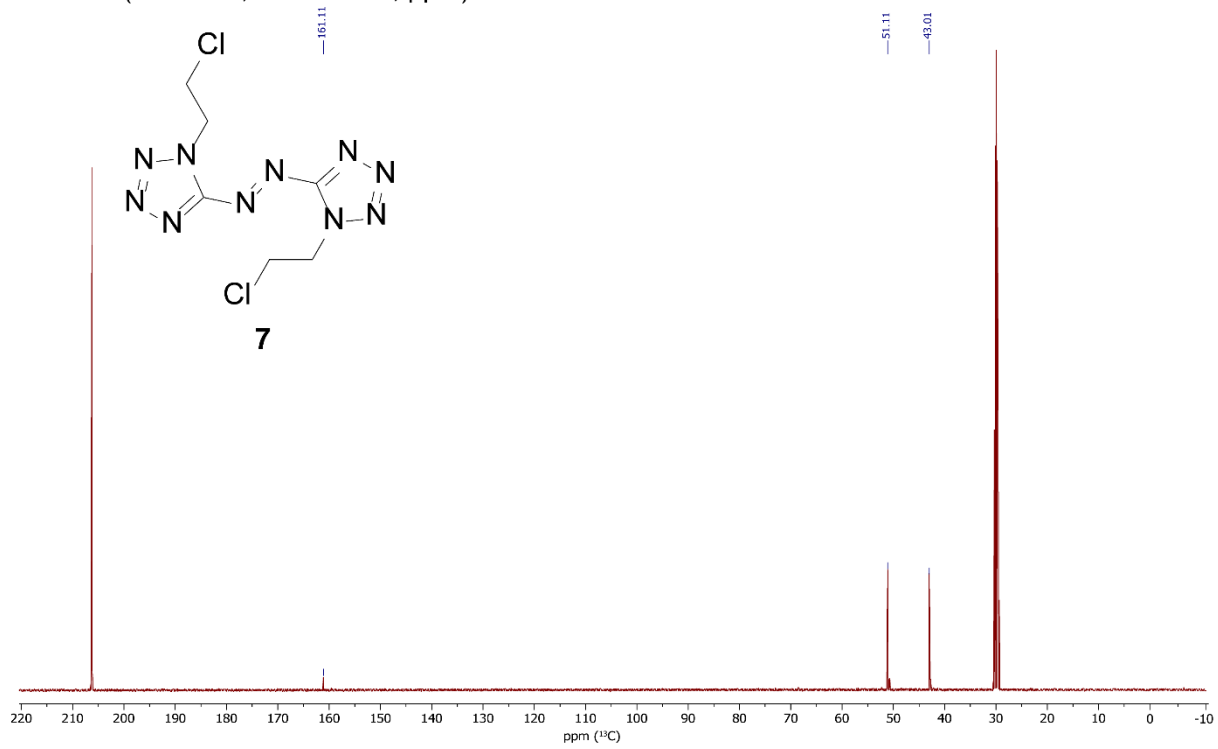
^{13}C -NMR (101 MHz, Acetone- D_6 , ppm)



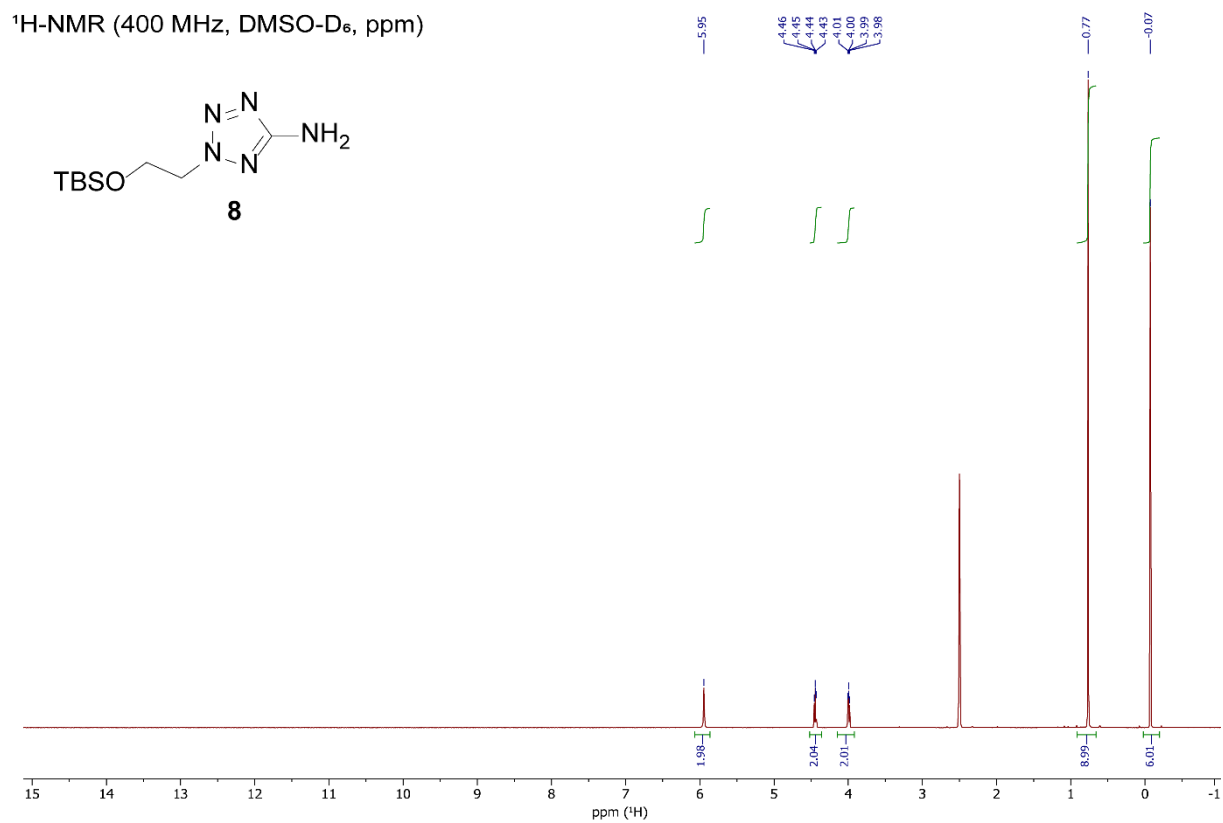
¹H-NMR (400 MHz, Acetone-D₆, ppm)



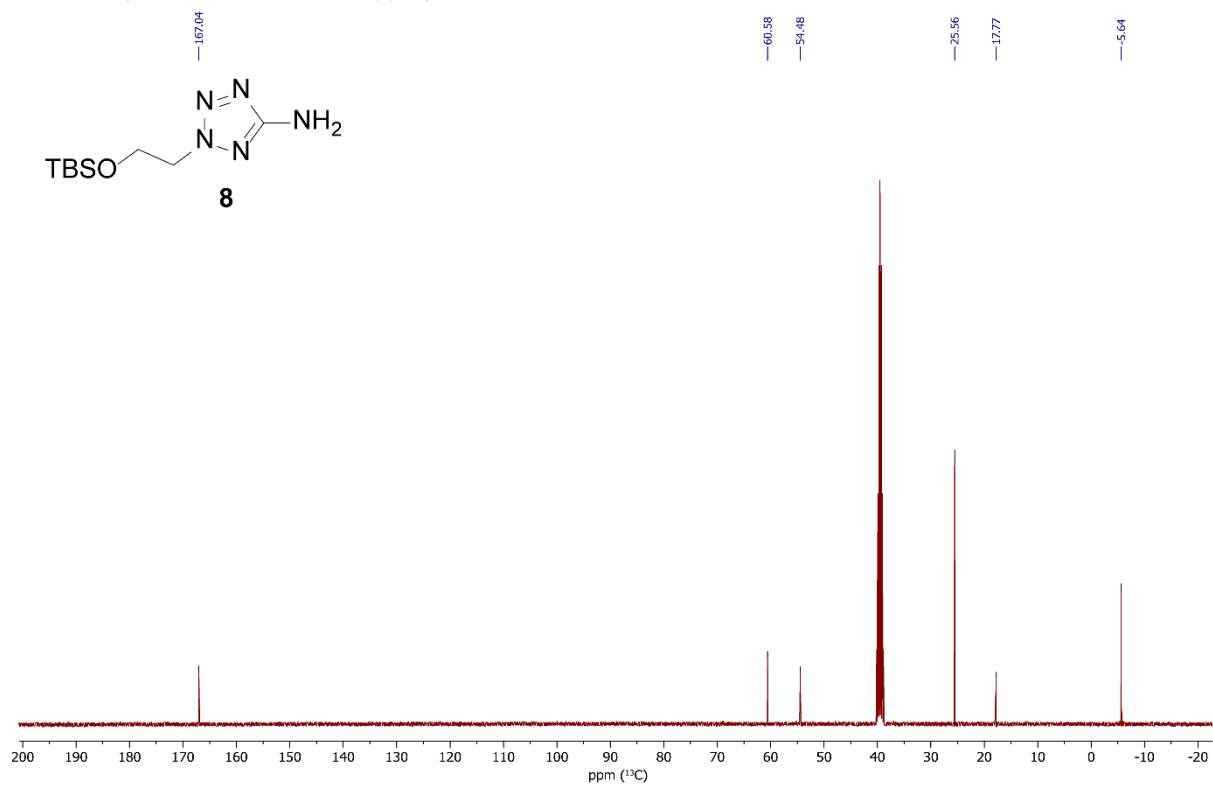
¹³C-NMR (101 MHz, Acetone-D₆, ppm)



¹H-NMR (400 MHz, DMSO-D₆, ppm)



¹³C-NMR (101 MHz, DMSO-D₆, ppm)



3. X-ray Diffraction

Crystal structure data were obtained from an Oxford Xcalibur3 diffractometer with a Spellman generator (voltage 50 kV, current 40 mA) and a Kappa CCD area for data collection using Mo- $K\alpha$ radiation ($\lambda = 0.71073 \text{ \AA}$) or a Bruker D8 Venture TXS diffractometer equipped with a multilayer monochromator, a Photon 2 detector and a rotation-anode generator (Mo- $K\alpha$ radiation). The data collection was performed using the CRYSTALIS RED software.^[S5] The solution of the structure was performed by direct methods and refined by full-matrix least-squares on F² (SHELXT)^[S6] implemented in the OLEX2^[S7] software suite. The non-hydrogen atoms were refined anisotropically and the hydrogen atoms were located and freely refined. The absorption correction was carried out by a SCALE3 ABSPACK multiscan method.^[S8] The DIAMOND2 plots shown with thermal ellipsoids at the 50% probability level and hydrogen atoms are shown as small spheres of arbitrary radius. The SADABS program embedded in the Bruker APEX3 software was used for multi-scan absorption corrections in all structures.^[S9]

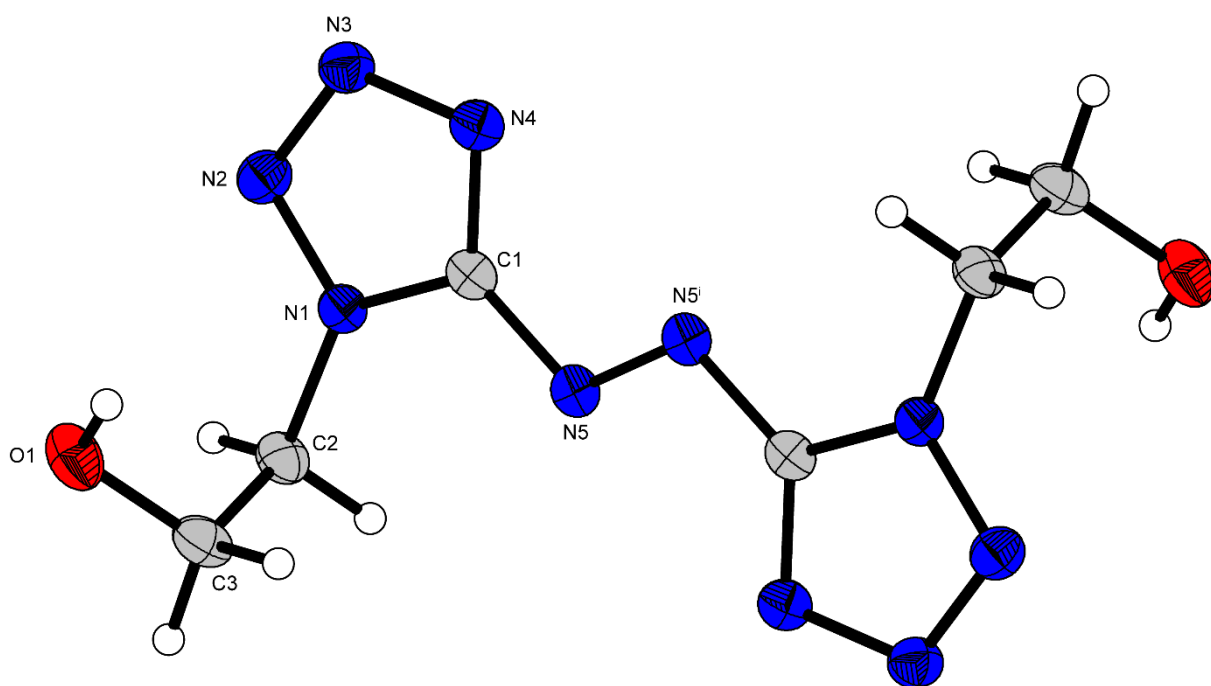


Figure S1. Representation of the molecular unit of bis(1,1'-(2,2'-hydroxyethyl)azotetrazole (**4a**), showing the atom-labeling scheme. Thermal ellipsoids represent the 50% probability level and hydrogen atoms are shown as small spheres of arbitrary radius. Symmetry code: (i) $1-x, -y, 1-z$.

Table S1. Crystallographic data of **4a–6a**.

	4a	5a	6a
Formula	C ₆ H ₁₀ N ₁₀ O ₂	C ₆ H ₈ N ₁₂ O ₆	C ₆ H ₈ N ₁₆
FW [g mol ⁻¹]	254.24	344.24	304.28
Crystal system	monoclinic	monoclinic	triclinic
Space group	<i>P2₁/c</i> (No. 14)	<i>P2₁/c</i> (No. 14)	<i>P</i> -1 (No. 2)
Color / Habit	yellow plate	yellow plate	yellow block
Size [mm]	0.17 x 0.28 x 0.56	0.04 x 0.23 x 0.44	0.08 x 0.15 x 0.25
a [Å]	7.9346(6)	10.6870(19)	5.7863(6)
b [Å]	5.3456(3)	6.3382(7)	6.7887(9)
c [Å]	13.1451(10)	9.7961(11)	8.6292(13)
α [°]	90	90	107.343(13)
β [°]	99.932(7)	99.437(14)	96.706(11)
γ [°]	90	90	104.792(10)
V [Å ³]	549.20(7)	654.57(16)	305.93(8)
Z	2	2	1
ρ _{calc.} [g cm ⁻³]	1.537	1.747	1.652
μ [mm ⁻¹]	0.122	0.154	0.127
F(000)	264	352	156
λ _{MoKα} [Å]	0.71073	0.71073	0.71073
T [K]	101	123	101
θ Min-Max [°]	2.6, 29.1	3.8, 26.4	2.5, 26.4
Dataset	-6: 10 ; -6: 7 ; -17: 16	-11: 13 ; -7: 7 ; -12: 12	-7: 7 ; -8: 8 ; -10: 9
Reflections collected	3398	4795	2265
Independent refl.	1278	1331	2265
<i>R</i> _{int}	0.021	0.056	0.056
Observed reflections	1036	853	1490
Parameters	102	125	117
<i>R</i> ₁ (obs) ^[a]	0.0362	0.0471	0.0390
w <i>R</i> ₂ (all data) ^[b]	0.0863	0.0825	0.1108
<i>S</i> ^[c]	1.07	0.99	0.94
Resd. dens [e Å ⁻³]	-0.23, 0.23	-0.21, 0.20	-0.24, 0.29
Device type	Xcalibur Sapphire3	Xcalibur Sapphire3	Xcalibur Sapphire3
Solution	SIR-92	SIR-92	SIR-92
Refinement	SHELXL-2013	SHELXL-2013	SHELXL-2013
Absorption correction	multi-scan	multi-scan	multi-scan
CCDC	2090053	2090058	2090057

^[a] $R_1 = \frac{\sum ||F_0| - |F_c||}{\sum |F_0|}$; ^[b] $wR_2 = \frac{[\sum [w(F_0^2 - F_c^2)^2]}{\sum [w(F_0^2)]}^{1/2}$; $w = [\sigma^2(F_0^2) + (xP)^2 + yP]^{-1}$ and $P = (F_0^2 + 2F_c^2)/3$; ^[c] $S = (\sum [w(F_0^2 - F_c^2)^2]/(n-p))^{1/2}$ (n = number of reflections; p = total number of parameters).

Table S2. Crystallographic data of **5b** and **6b**.

	5b	6b
Formula	C ₆ H ₈ N ₁₂ O ₆	C ₆ H ₈ N ₁₆
FW [g mol ⁻¹]	344.24	304.28
Crystal system	monoclinic	monoclinic
Space group	<i>P</i> 2 ₁ / <i>c</i> (No. 14)	<i>P</i> 2 ₁ / <i>n</i> (No. 14)
Color / Habit	yellow plate	yellow block
Size [mm]	0.11 x 0.36 x 0.50	0.20 x 0.50 x 0.50
a [Å]	7.4267(7)	5.1580(7)
b [Å]	16.8712(17)	10.7193(15)
c [Å]	11.037(1)	11.548(2)
α [°]	90	90
β [°]	106.561(10)	91.751(12)
γ [°]	90	90
V [Å ³]	1325.5(2)	638.19(17)
Z	4	2
ρ _{calc.} [g cm ⁻³]	1.725	1.584
μ [mm ⁻¹]	0.152	0.121
F(000)	704	312
λ _{MoKα} [Å]	0.71073	0.71073
T [K]	103	101
θ Min-Max [°]	2.3, 29.3	2.6, 29.3
Dataset	-9: 9 ; -21: 21 ; -14: 11	-6: 7 ; -13: 14 ; -14: 15
Reflections collected	9249	5104
Independent refl.	3126	1502
<i>R</i> _{int}	0.032	0.035
Observed reflections	2216	1043
Parameters	249	116
<i>R</i> ₁ (obs) ^[a]	0.0437	0.0444
w <i>R</i> ₂ (all data) ^[b]	0.0949	0.1074
<i>S</i> ^[c]	1.05	1.08
Resd. dens [e Å ⁻³]	-0.31, 0.25	-0.26, 0.20
Device type	Xcalibur Sapphire3	Xcalibur Sapphire3
Solution	SIR-92	SIR-92
Refinement	SHELXL-2013	SHELXL-2013
Absorption correction	multi-scan	multi-scan
CCDC	2090056	2090054

^[a] $R_1 = \sum ||F_0| - |F_c|| / \sum |F_0|$; ^[b] $wR_2 = [\sum [w(F_0^2 - F_c^2)^2] / \sum [w(F_0^2)]]^{1/2}$; $w = [\sigma^2(F_0^2) + (xP)^2 + yP]^{-1}$ and $P = (F_0^2 + 2F_c^2) / 3$; ^[c] $S = (\sum [w(F_0^2 - F_c^2)^2] / (n-p))^{1/2}$ (n = number of reflections; p = total number of parameters).

Table S3. Crystallographic data of **7** and **8**.

	7	8
Formula	C ₆ H ₈ Cl ₂ N ₁₀	C ₉ H ₂₁ N ₅ OSi
FW [g mol ⁻¹]	291.12	243.40
Crystal system	monoclinic	monoclinic
Space group	<i>P</i> 2 ₁ / <i>n</i> (No. 14)	<i>P</i> 2 ₁ / <i>c</i> (No. 14)
Color / Habit	yellow block	colorless platelet
Size [mm]	0.18 x 0.38 x 0.69	0.01 x 0.35 x 0.40
a [Å]	6.9577(5)	16.3221(14)
b [Å]	10.1969(6)	7.0344(7)
c [Å]	8.6636(7)	12.1424(11)
α [°]	90	90
β [°]	109.474(8)	92.685(8)
γ [°]	90	90
V [Å ³]	579.49(8)	1392.6(2)
Z	2	4
ρ _{calc.} [g cm ⁻³]	1.668	1.161
μ [mm ⁻¹]	0.561	0.160
F(000)	296	528
λ _{MoKα} [Å]	0.71073	0.71073
T [K]	135	123
θ Min-Max [°]	3.2, 26.4	2.5, 26.4
Dataset	-8: 8 ; -12: 12 ; -10: 10	-19: 20 ; -8: 8 ; -15: 15
Reflections collected	4250	10764
Independent refl.	1187	2855
<i>R</i> _{int}	0.025	0.057
Observed reflections	1096	1904
Parameters	82	229
<i>R</i> ₁ (obs) ^[a]	0.0340	0.0519
w <i>R</i> ₂ (all data) ^[b]	0.0901	0.1165
<i>S</i> ^[c]	1.14	1.03
Resd. dens [e Å ⁻³]	-0.24, 0.41	-0.24, 0.34
Device type	Xcalibur Sapphire3	Xcalibur Sapphire3
Solution	SIR-92	SIR-92
Refinement	SHELXL-2013	SHELXL-2013
Absorption correction	multi-scan	multi-scan
CCDC	2090055	2091285

^[a] $R_1 = \sum ||F_0| - |F_c|| / \sum |F_0|$; ^[b] $wR_2 = [\sum [w(F_0^2 - F_c^2)^2] / \sum [w(F_0^2)]]^{1/2}$; $w = [\sigma^2(F_0^2) + (xP)^2 + yP]^{-1}$ and $P = (F_0^2 + 2F_c^2) / 3$; ^[c] $S = (\sum [w(F_0^2 - F_c^2)^2] / (n-p))^{1/2}$ (n = number of reflections; p = total number of parameters).

4. Thermal analysis

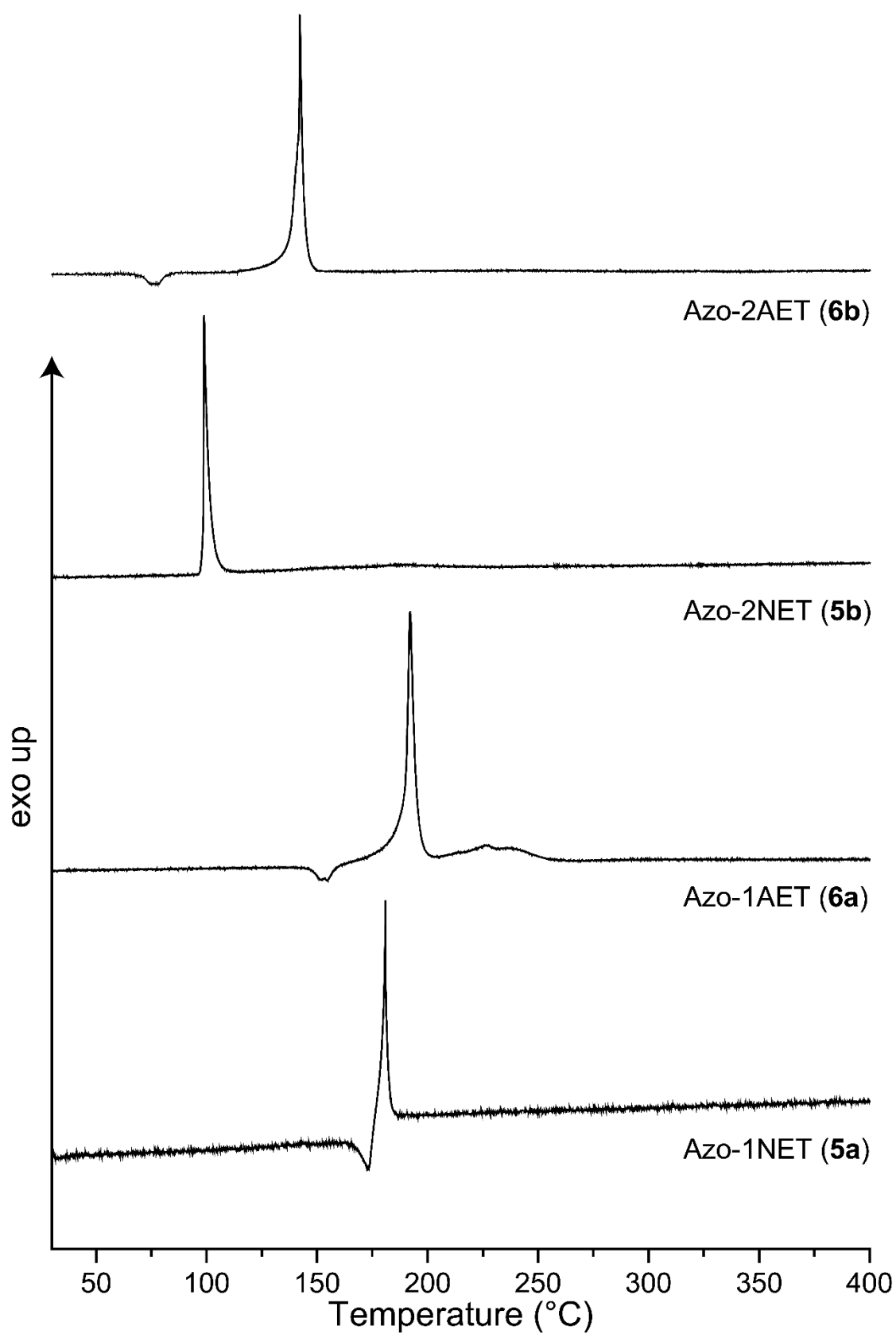


Figure S4. DTA plots of compounds 5a, 5b, 6a and 6b.

5. Scanning electron microscopy

To show the microscopic differences of the gained compounds **5a**, **5b**, **6a** and **6b** scanning electron microscopy (SEM) was performed. In each case, images were taken at low magnification to show the entirety of the crystals and to assess the morphology. Close-up images of the crystals show the surface texture.

Bis(1,1'-(2,2'-nitrateoethyl))azotetrazole (**5a**) crystallizes in very thin plates that tend to form stacks (Figure S5). The crystal surface is very smooth and there is hardly any intergrowth between the crystals

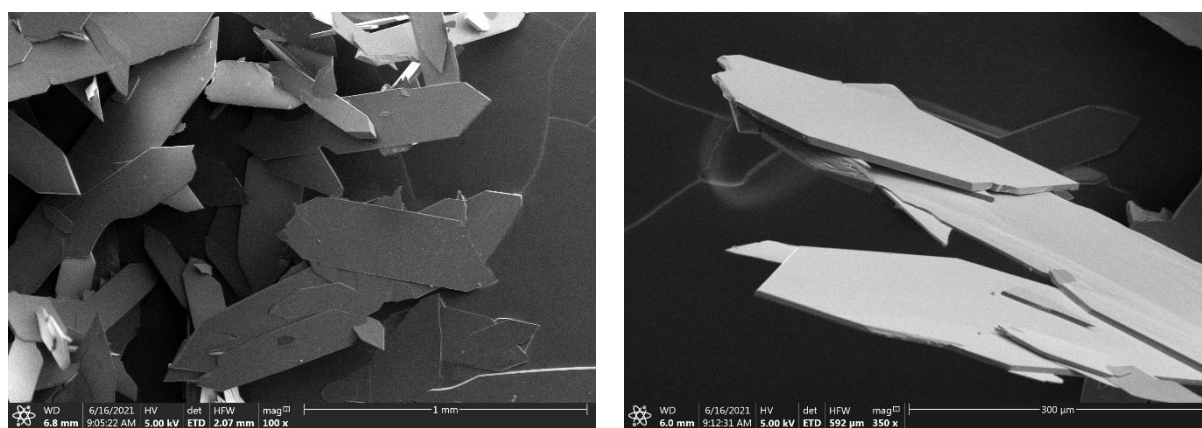


Figure S5. SEM images with 100x magnitude (left) and 350x magnitude (right) of **5a**.

The 2-substituted isomer bis(2,2'-(2,2'-nitrateoethyl))azotetrazole (**5b**) consists of mostly long elongated blocks (Figure S6). The surface of the crystal is rougher than for **5a** and some crystals are intergrown.

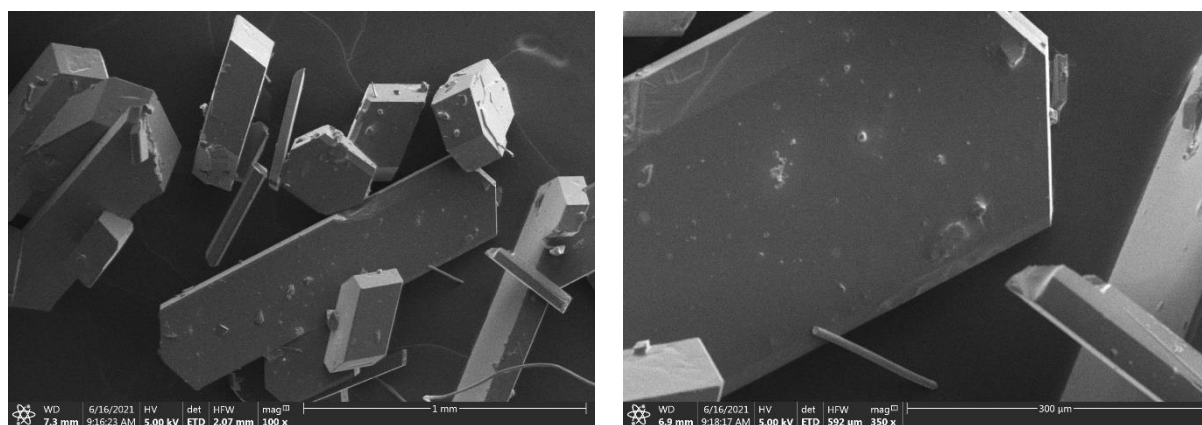


Figure S6. SEM images with 100x magnitude (left) and 350x magnitude (right) of **5b**.

The crystals of bis(1,1'-(2,2'-azidoethyl))azotetrazole (**6a**) form agglomerates of rods and blocks (Figure S7). They are strongly intergrown and exhibit also microcrystalline areas on the surface.

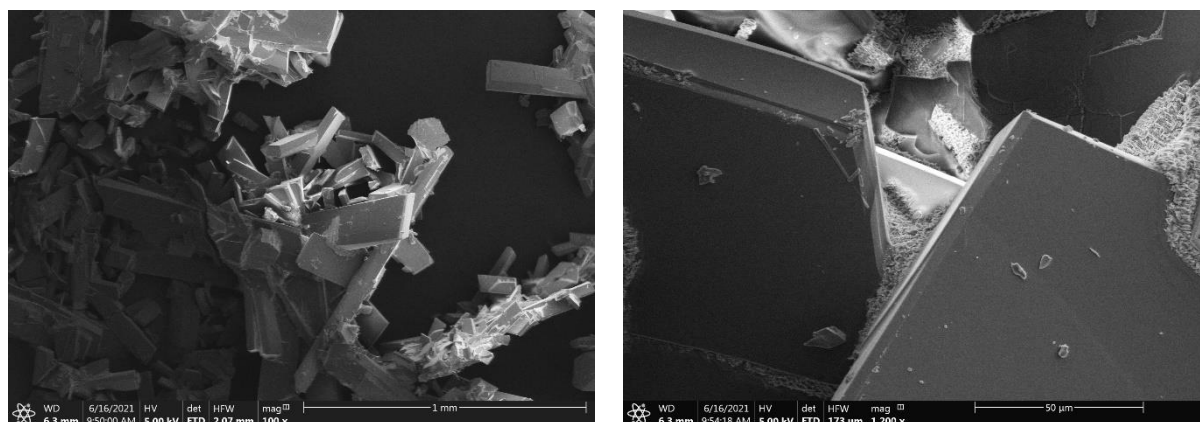


Figure S7. SEM images with 100x magnitude (left) and 1200x magnitude (right) of **6a**.

Bis(1,1'-(2,2'-azidoethyl))azotetrazole (**6b**) shows a different habit than the compounds above (Figure S8). During crystallization large agglomerates are formed with a rigid and porous surface.

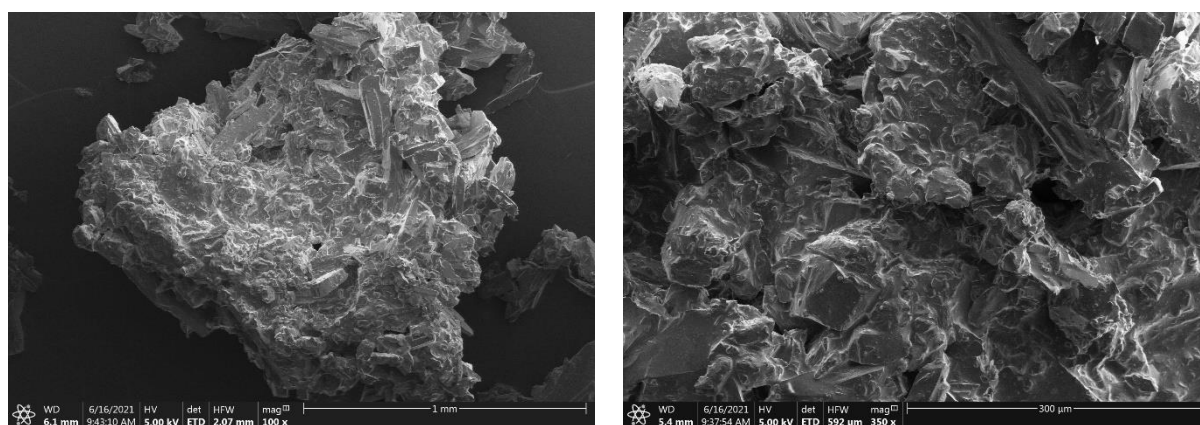


Figure S8. SEM images with 100x magnitude (left) and 350x magnitude (right) of **6b**.

6. Computation

Heat of Formation Computation

All quantum chemical calculations were carried out using the Gaussian G09 program package.^[S10] The enthalpies (H) and free energies (G) were calculated using the complete basis set (CBS) method of Petersson and co-workers in order to obtain very accurate energies. The CBS models are using the known asymptotic convergence of pair natural orbital expressions to extrapolate from calculations using a finite basis set to the estimated CBS limit. CBS-4 starts with an HF/3-21G(d) geometry optimization; the zero-point energy is computed at the same level. It then uses a large basis set SCF calculation as a base energy, and an MP2/6-31+G calculation with a CBS extrapolation to correct the energy through second order. A MP4(SDQ)/6-31+ (d,p) calculation is used to approximate higher order contributions. In this study, we applied the modified CBS-4M.

Heats of formation of the synthesized ionic compounds were calculated using the atomization method (equation E1) using room temperature CBS-4M enthalpies, which are summarized in Table 4.^[S11, S12]

$$\Delta_f H^\circ_{(g, M, 298)} = H_{(Molecule, 298)} - \sum H^\circ_{(Atoms, 298)} + \sum \Delta_f H^\circ_{(Atoms, 298)} \quad (E1)$$

Table S4. CBS-4M electronic enthalpies for atoms C, H, N and O and their literature values for atomic $\Delta_f H^\circ_{298} / \text{kJ mol}^{-1}$

	$-H^{298}$ [a.u.]	NIST ^[S13]
H	0.500991	218.2
C	37.786156	717.2
N	54.522462	473.1
O	74.991202	249.5

For neutral compounds the sublimation enthalpy, which is needed to convert the gas phase enthalpy of formation to the solid state one, was calculated by the *Trouton* rule.^[S14] For ionic compounds, the lattice energy (U_L) and lattice enthalpy (ΔH_L) were calculated from the corresponding X-ray molecular volumes according to the equations provided by *Jenkins* and *Glasser*.^[S15] With the calculated lattice enthalpy the gas-phase enthalpy of formation was converted into the solid state (standard conditions) enthalpy of formation. These molar standard enthalpies of formation (ΔH_m) were used to calculate the molar solid state energies of formation (ΔU_m) according to equation E2.

$$\Delta U_m = \Delta H_m - \Delta n RT \quad (E2)$$

(Δn being the change of moles of gaseous components)

The calculation results are summarized in Table S5.

Table S5. Calculation results.

	$-H^{298}$ [a] [a.u.]	$\Delta_f H^\circ(\text{g,M})$ [kJ mol ⁻¹] [b]	V_M [Å ³] [c]	$\Delta U_L; \Delta H_L$ [d] [kJ mol ⁻¹]	$\Delta_f H^\circ(\text{s})$ [e] [kJ mol ⁻¹]	Δn [f]	$\Delta_f U(\text{s})$ [g] [kJ kg ⁻¹]
5a	1339.702032	712.9	-	-	630.1	13	1924.2
5b	1339.713477	682.8	-	-	613.0	13	1874.6
6a	1107.682135	1535.2	-	-	1456.2	12	4884.3
6b	1107.693998	1504.1	-	-	1439.2	12	4828.3

[a] CBS-4M electronic enthalpy; [b] gas phase enthalpy of formation; [c] molecular volumes taken from X-ray structures and corrected to room temperature; [d] lattice energy and enthalpy (calculated using Jenkins and Glasser equations); [e] standard solid state enthalpy of formation; [f] Δn being the change of moles of gaseous components when formed; [g] solid state energy of formation.

7. References

- [S1] a) Reichel & Partner GmbH, <http://www.reichelt-partner.de>; b) Test methods according to the UN Recommendations on the Transport of Dangerous Goods, *Manual of Test and Criteria*, fourth revised edition, United Nations Publication, New York and Geneva, **2003**, ISBN 92–1-139087–7, Sales No. E.03.VIII.2; 13.4.2 Test 3 a (ii) BAM Fallhammer.
- [S2] Sućeska, M., EXPLO5 V6.02 program, Brodarski Institute, Zagreb, Croatia, **2014**.
- [S3] Finnegan, W. G.; Henry, R. A., Mono-alkylation of Sodium 5-Aminotetrazole in Aqueous Medium, *J. Am. Chem. Soc.* **1954**, *76*, 923–926.
- [S4] a) Finnegan, W. G.; Henry, R. A., N-Vinyl-Tetrazoles, *J. Org. Chem.* **1959**, *24*, 1565–1567; b) Stierstorfer, J., Advanced energetic materials based on 5-aminotetrazole – synthesis, characterization, testing and scale-up, *Dissertation*, **2009**, LMU Munich; c) Fischer, N.; Klapötke, T. M.; Stierstorfer, J.; Wiedemann, C., 1-Nitratoethyl-5-nitriminotetrazole derivatives – Shaping future high explosives, *Polyhedron*, **2011**, *30*, 2374-2386.
- [S5] *CrysAlisPro*, Oxford Diffraction Ltd. *version 171.33.41*, **2009**.
- [S6] Sheldrick, G.M., *Acta Cryst.* **2015**, *A71*, 3–8.
- [S7] Dolomanov, O. V.; Bourhis, L. J.; Gildea, R. J.; Howard, J. A. K.; Puschmann, H., OLEX2: A complete structure solution, refinement and analysis program, *J. Appl. Cryst.* **2009**, *42*, 339–341.
- [S8] *SCALE3 ABSPACK – An Oxford Diffraction program* (1.0.4, gui: 1.0.3), Oxford Diffraction Ltd., **2005**.
- [S9] *APEX3*. Bruker AXS Inc., Madison, Wisconsin, USA.
- [S10] Frisch, M. J.; Trucks, G. W.; Schlegel, H. B.; Scuseria, G. E.; Robb, M. A.; Cheeseman, J. R.; Scalmani, G.; Barone, V.; Petersson, G. A.; Nakatsuji, H.; Li, X.; Caricato, M.; Marenich, A. V.; Bloino, J.; Janesko, B. G.; Gomperts, R.; Mennucci, B.; Hratchian, H. P.; Ortiz, J. V.; Izmaylov, A. F.; Sonnenberg, J. L.; Williams-Young, D.; Ding, F.; Lipparini, F.; Egidi, F.; Goings, J.; Peng, B.; Petrone, A.; Henderson, T.; Ranasinghe, D.; Zakrzewski, V. G.; Gao, J.; Rega, N.; Zheng, G.; Liang, W.; Hada, M.; Ehara, M.; Toyota, K.; Fukuda, R.; Hasegawa, J.; Ishida, M.; Nakajima, T.; Honda, Y.; Kitao, O.; Nakai, H.; Vreven, T.; Throssell, K.; Montgomery, J. A., Jr.; Peralta, J. E.; Ogliaro, F.; Bearpark, M. J.; Heyd, J. J.; Brothers, E. N.; Kudin, K. N.; Staroverov, V. N.; Keith, T. A.; Kobayashi, R.; Normand, J.; Raghavachari, K.;

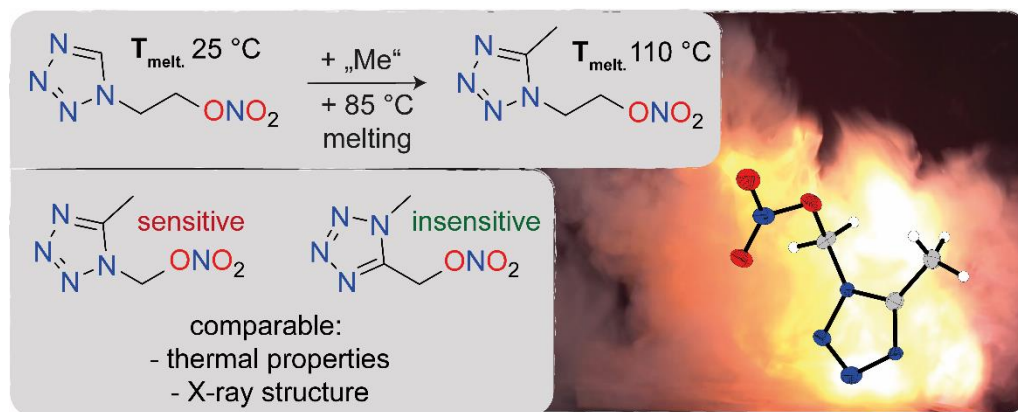
- Rendell, A. P.; Burant, J. C.; Iyengar, S. S.; Tomasi, J.; Cossi, M.; Millam, J. M.; Klene, M.; Adamo, C.; Cammi, R.; Ochterski, J. W.; Martin, R. L.; Morokuma, K.; Farkas, O.; Foresman, J. B.; Fox, D. J., Gaussian 09 A.02, Gaussian, Inc., Wallingford, CT, USA, **2009**.
- [S11] a) Ochterski, J. W.; Petersson, G. A.; Montgomery Jr., J. A., A complete basis set model chemistry. V. Extensions to six or more heavy atoms, *J. Chem. Phys.* **1996**, *104*, 2598–2619; b) Montgomery Jr., J. A.; Frisch, M. J.; Ochterski, J. W.; Petersson, G. A., A complete basis set model chemistry. VII. Use of the minimum population localization method, *J. Chem. Phys.* **2000**, *112*, 6532–6542.
- [S12] a) Curtiss, L. A.; Raghavachari, K.; Redfern, P. C.; Pople, J. A., Assignment of Gaussian-2 and density functional theories for the computation of enthalpies of formation, *J. Chem. Phys.* **1997**, *106*, 1063–1079; b) Byrd, E. F. C.; Rice, B. M., Improved prediction of heats of formation of energetic materials using quantum mechanical calculations, *J. Phys. Chem. A* **2006**, *110*, 1005–1013; c) Rice, B. M.; Pai, S. V.; Hare, J., Predicting heats of formation of energetic materials using quantum mechanical calculations, *Comb. Flame* **1999**, *118*, 445–458.
- [S13] Lindstrom, P. J.; Mallard, W. G., (Editors), NIST Standard Reference Database Number 69, <http://webbook.nist.gov/chemistry/> (accessed June **2020**).
- [S14] Westwell, M. S.; Searle, M. S.; Wales, D. J.; Williams, D. H., Empirical correlations between thermodynamic properties and intermolecular forces, *J. Am. Chem. Soc.* **1995**, *117*, 5013–5015; b) Trouton, F., IV. On molecular latent heat, *Philos. Mag.* **1884**, *18*, 54–57.
- [S15] a) Jenkins, H. D. B.; Roobottom, H. K.; Passmore, J.; Glasser, L., Relationships among ionic lattice energies, molecular (formula unit) volumes and thermochemical radii, *Inorg. Chem.* **1999**, *38*, 3609–3620; b) Jenkins, H. D. B.; Tudela, D.; Glasser, L., Lattice potential energy estimation for complex ionic salts from density measurements, *Inorg. Chem.* **2002**, *41*, 2364–2367.

To be published: Isomerism of Nitratoalkylazoles

Lukas Bauer, Maximilian Benz, Thomas M. Klapötke*, Tobias Lenz, Mohamed Mouzayek, Elena Reinhardt and Jörg Stierstorfer

Department of Chemistry, Ludwig-Maximilians University of Munich, Butenandtstr. 5-13(D), D-81377 Munich, Germany; tmk@cup.uni-muenchen.de

Supporting Information Placeholder



ABSTRACT: In the field of energetic materials, traditional materials with high toxicity or other disadvantages are mostly used. There is an urgent need for trinitrotoluene replacements (TNT), which itself is toxic and its production is problematic due to red wastewater. New materials should be safe to handle, have good performance, and be inexpensive to synthesize. Nitratealkylazoles are known to have low melting points and good energetic properties compared to TNT. In this paper, seven energetic compounds are synthesized starting from 5-methyltetrazole, 5-hydroxymethyltetrazole and 4,5-bishydroxymethyltriazole. The nitrates are characterized in terms of their physical, chemical, and energetic properties. Of those seven compounds, five are solid, melting between 27 to 110 °C, and two are liquid. Methylation and hydroxyalkylation were performed and discussed extensively. The organic nitrate is introduced in the last step so that the synthesis remains safe and scalable. Correlations between the molecular geometry and the melting points are explained. Calculations indicate detonation velocities that are 6-11% higher than those of TNT. A discussion of the effect of isomerism on the properties leads to surprising insights and should help focus and accelerate research on the replacement of TNT.

Introduction

Energetic materials are widely applied as: Primary explosives, secondary explosives and pyrotechnics. The materials applied in these areas were mostly discovered over 100 years ago and many suffer from drawbacks. Explosives are widely used in the military and civil sectors. In the civil sector, cheap and relatively safe ammonium nitrate is mixed with fuel oil, called ANFO, for mining. The large charges are initiated by booster charges consisting of trinitrotoluene (TNT) and pentaerythritol tetranitrate (PETN) mixtures called Pentolite. Still, the booster charges need a blasting cap, containing a primary explosive (e.g. PbN_3), to detonate. In the military sector, more advanced materials like hexogen (RDX), octogen (HMX) or TNT are used as main charges. TNT is melted by hot water ($<100\text{ °C}$), then mixed with other materials or filled directly into shells.[1-4] This melt-cast explosive is moderately sensitive to impact (15 J) but far less powerful than RDX (6798 vs. 8801 m s^{-1}). [5] It damages the liver and blood system if humans are exposed. [6] Furthermore, toxic wastewater is generated during

production which causes environmental damage. [7] This shows the urgent need for TNT replacements.

Energetic material chemists are searching for melt castable replacements with cheap and efficient synthesis, good performance and environmentally friendly character.[8-10] Here organic nitrates combined with nitrogen and oxygen-rich azoles are often used to achieve low melting compounds (Figure 1). [11, 12] In most cases, nitration of the alcohol with highly concentrated HNO_3 is possible and leads to the energetic nitrate. Generally, the decomposition temperatures are around 180 °C or lower. Furthermore, azoles provide a high heat of formation through N_2 formation during decomposition and have a positive effect on the density due to heavier atoms than carbon. Other concepts to achieve low melting explosives include e.g. furoxanes [13] or 1,2,3-triazoles [14].

The Los Alamos National Laboratory and the Army research laboratory are working on the development of a new generation of melt cast explosive, bis(1,2,4-oxadiazole)bis(methylene) dinitrate (BOM). [15] This compound exceeds many of the properties of TNT,

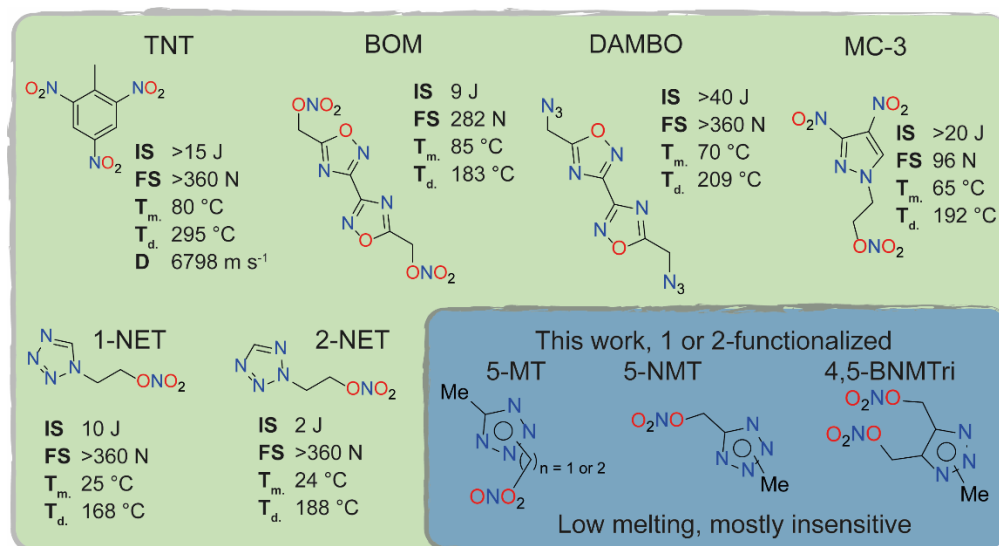


Figure 1 Used and potential next generation melt cast explosives (top row) and low melting nitratoalkylazoles (bottom row).

but the synthesis is complex and the compound is sensitive to mechanical stimuli (BOM-IS: 9 J vs. TNT-IS:15 J). The azide derivative DAMBO shows a lower melting point, and higher decomposition temperature than BOM and is less sensitive. This comes at the cost of a lower density and weaker performance. Especially the lower sensitivity of many azidoalkylazoles is surprising as e.g. many alkylazides are known to be very sensitive. [16]

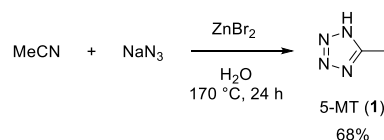
The discovery of nitro pyrazole MC-3 was the result of a machine-learning study. The compound shows high performance and is melting at 65 °C. [17] The nitratoalkyltetrazoles 1-NET and 2-NET give an insight into the influence that isomerism can have. Both compounds are melting at the same temperature, whereas 1-NET is decomposing early and 2-NET is sensitive towards impact. [18] Sabatini and Baran et al. synthesized six stereo- and regioisomers of tetra nitratomethyl cyclobutane nitric esters, concluding that the melting point is the most affected parameter. [19]

In this work we investigated the properties of nitratoalkyl substituted tetrazoles and 1,2,3-triazoles. Starting from 5-methyltetrazole, 5-hydroxymethyltetrazole and 4,5-bishydroxymethyl-1,2,3-triazole, hydroxyalkylation or methylation was performed, followed by nitration yielding seven energetic compounds with different physicochemical properties but comparable energetic performance. Through this it is possible to compare five C₃H₅N₅O₃ nitratoalkyltetrazole isomers.

Synthesis of Starting Materials

5-Methyltetrazole (**1**) is a simple mono-tetrazole derivative. It is mainly characterized by its energetically unfavored C-C unit. Nonetheless, it shows some attractive characteristics, for example, the limiting direction for substitution reaction, which always leads to two different isomers. Although the density of **1** is relatively low ($\rho = 1.349 \text{ g cm}^{-3}$ @ 296 K) [20] it is suited for examining the entire spectrum of energetic derivatization reactions. Particularly for melt-castable explosives, **1** seems to be the ideal platform. The compound itself already contains a decent amount of energy through its tetrazole unit and can easily be equipped with additional energetic groups. Moreover, the hydrophobic methyl function at position 5 indicates a possible melting point in a suitable range, which is essential for the development of melt-castable explosives.

Since the fundamental research on a new compound always requires high quantities of the respective starting material, we first focused on the synthesis and synthetic optimization of **1** (Scheme 1). The main synthesis routes in the literature use acetonitrile as C2 synthon and perform a [2+3] cyclo-addition reaction with sodium azide under different conditions. At regular temperature and pressure transition metal catalysts or complex precursors are required. Another method demands the aid of a pressure tube to increase the reaction temperature and pressure. Therefore, we started with a modified literature procedure by Sharpless et al. [21] The first experiment was examined as stated in the literature. First of all, the conditions are quite confusing, since **1** decomposes at around 155 °C and the reaction temperature is at 170 °C. Therefore, we state that the zinc(II) 5-methyltetrazolate is the present species, which is more temperature stable during the reaction. Nonetheless, we could not obtain the same yield using the exact same protocol (8% vs. 75%). Therefore, we did a reaction optimization and varied several parameters. Our reactions were carried out in a 350 mL pressure tube. As heating source, an oil bath was used. We screened the reaction conditions using a 40 mmol scale with 80 mL of water as solvent. Since **1** is highly water soluble, it is unavoidable to keep the amount of water, especially during the workup process, as low as possible. By reducing the water to a minimum and working with a highly saturated aqueous solution, the yield could be increased to 55%. We expected to further improve the yield by raising the reaction time from 24 h to 48 h. However, the yields decreased to 48%. A similar effect occurs by shortening the reaction time to 16 h (36%). Therefore, the reaction should be performed for about 24 h at 170 °C. We also examined another work-up method. Therefore, we followed the original procedure (precipitation of Zn(OH)₂ with HCl) without saturation of the aqueous solution with MgSO₄. We evaporated our reaction solution under reduced



Scheme 1 Synthesis of 5-methyltetrazole (**5**).

pressure. The formed solid was extracted with 500 mL acetone. After evaporation of the organic phase, **1** was obtained but in low yield (35%) and poor purity (yellowish oil with impurities). After finding the ideal reaction temperature, we varied the equivalents of the reactants, respectively. The different batches with varying amounts of reactants are listed in the following Table 1.

Table 1 Varied reaction conditions and corresponding yields for the synthesis of **1**.

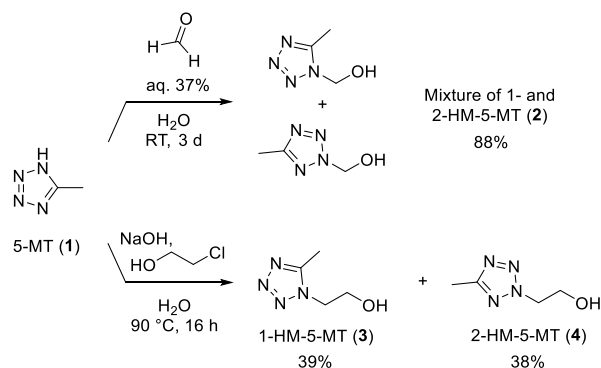
Batch	MeCN (eq.)	NaN ₃ (eq.)	ZnBr ₂ (eq.)	Yield (%)
1	2	1	1	65
2	1	2	1	68
3	1	1	2	51

The best improvement was reached by increasing the equivalents of NaN₃. In this reaction batch, it is noteworthy, that the aqueous solution was heated for 10 min to 90 °C to evaporate the formed HN₃ in order to prevent inhalation. Nonetheless, the published yield of 75% has never been obtained. In the experimental section, the final and optimized reaction protocol is described.

The *N*-alkylation of nitrogen-rich scaffolds proved to be an elegant method to decrease the intrinsic hygroscopicity that many *N*-heterocycles with acidic protons exhibit. Adding to that, the alkyl chain often improves the stability of the explosive and increases the compatibility in formulations of explosive charges.^[22-25] An already established method for *N*-alkylation includes the activation of the heterocycle by deprotonation in water and subsequent alkylation in a polar aprotic solvent.^[26]

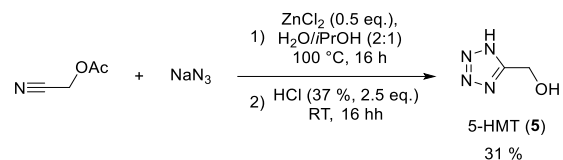
Starting from 5-methyltetrazole (**1**), hydroxymethyl and hydroxyethyl derivatives, were synthesized (unsuccessful recrystallization attempts (chloroform, ether or methanol), the isomeric mixture **2** was used for subsequent reactions.). The hydroxymethyl-5-methyltetrazoles **2** were obtained through the reaction of **1** with a 40% aq. formaldehyde solution, catalyzed by conc. HCl. A solid mixture of isomers **2** comprising 1-hydroxymethyl-5-methyltetrazole and 2-hydroxymethyl-5-methyltetrazole was produced in an 8:1 ratio (¹H NMR) with a yield of 88%. Due to challenges in separating these isomers using column chromatography (*i*Hex:EtOAc or DCM:MeOH), as well as unsuccessful recrystallization attempts (chloroform, ether or methanol), the isomeric mixture **2** was used for subsequent reactions.

The hydroxyethyl-5-methyltetrazoles **3** and **4**, also originating from **1**, were synthesized as an isomeric mixture in a 1:1 ratio through deprotonation and subsequent reaction with 2-chloroethanol under elevated temperatures. The isomers were successfully



Scheme 2 Hydroxyalkylation of 5-methyltetrazole (**1**) with

formaldehyde leading to the isomeric mixture **2** and with chloroethanol to the separated compounds **3** and **4**.

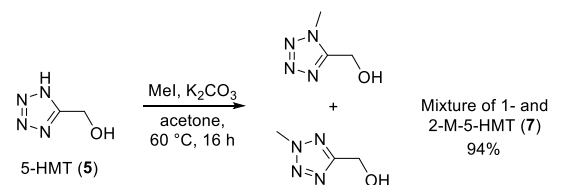


Scheme 3 Synthesis of 5-hydroxymethyltetrazole (**5**) starting from cyanomethyl acetate.

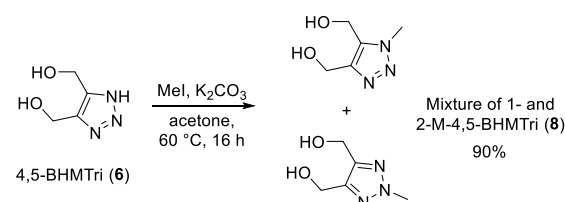
separated using column chromatography, resulting in isolated yields of 39% for 1-hydroxyethyl-5-methyltetrazole (**3**) and 38% for 2-hydroxyethyl-5-methyltetrazole (**4**). Both compounds were obtained as colorless liquids.

5-Hydroxymethyltetrazole (**5**) was prepared from cyanomethyl acetate and sodium azide by utilizing a Lewis acid-promoted tetrazole formation, which was followed by an acidic workup to hydrolyze the ester functionality and yield the corresponding alcohol (Scheme 3).^[27] The alternative synthesis starting from hydroxy acetonitrile showed low and inconsistent yields (0-50%) especially during scale up.^[28] Due to the rapid decomposition of hydroxy acetonitrile, the synthesis via cyanomethyl acetate was preferred and is also described in the experimental section.

Compound **5** and 4,5-bishydroxymethyl-1,2,3-triazole (**6**), the latter was just previously synthesized in our group^[29], were methylated to get rid of the acidic proton and to achieve a low melting end product. The goal was the methylation of tetrazole **5** and triazole **6** in one step without the need for time-consuming purification steps as the obtained crudes will directly be used in the final step of the explosives' preparation regardless. Slightly different methylation methods were tried for compounds **5** and **6** and then evaluated regarding their efficiency and selectivity. All approaches had in common that a regioisomeric mixture of *N*1- and *N*2-methylated heterocycles was obtained. This is due to the isomerism of their anions and adding to that the tautomeric equilibrium neutral triazoles and tetrazoles undergo in solution.^[30, 31] The first preliminary study was conducted by treating both azoles with an equimolar amount of dimethyl sulfate (DMS) as the methylating agent (MA) and sodium bicarbonate as the base. The bicarbonate salt deprotonated **6** as indicated by the gas evolution leading to the corresponding triazolite ion. The respective yields refer to the regioisomeric mixtures of *N*1- and *N*2-methylated tetrazoles **7** and triazoles **8** as they were not separated but isolated. The methylation showed a higher isolated yield for the



Scheme 4 Methylation of **5** with optimized conditions.



Scheme 5 Methylation of **6** with optimized conditions.

methylation of **5**, which might derive from the higher nucleophilicity. Furthermore, methylated triazole mixture **8** is hardly soluble in ethyl acetate while methylated tetrazoles **7** are soluble in ethyl acetate. The presence of two hydroxy moieties in **8** as opposed to only one in **7** most likely results in lower solubility in non-polar solvents. To separate the products from the formed sulfate salt, compounds **7** and **8** are extracted out of the aqueous solution with ethyl acetate which might explain the higher isolated yield of **7** (Table 2). As the yields were not satisfactory and optimization seemed possible, methylation of **6** was repeated with methyl iodide (MI) and different solvent mixtures. When using acetonitrile as the sole solvent, the yield decreased significantly. This might be due to the lower solubility of the bicarbonate salt in an aprotic solvent like acetonitrile. [32] The yield doubled by using acetonitrile/water instead of acetone/water most likely due to the higher solubility of one of the reactants in this mixture. Using MI led to comparable yields compared to DMS and thus, DMS was replaced in the following studies due to its higher toxicity. [33] Although the used methylation reagents are poorly soluble in water at RT, the reactions were carried out at elevated temperatures and therefore it is likely that a significant amount of the MA hydrolysed before reacting with the triazole leading to decreased yields. [34, 35] To avoid decomposition of MI, water was replaced with aprotic polar solvents like acetone and dimethylformamide. Since sodium bicarbonate forms water upon protonation, it was substituted with carbonate salts. At first, caesium carbonate was used as the base due to its higher solubilities in aprotic solvents compared to its analogue alkali metal carbonates. Since the solubility is still not ideal, an excess of the base was used. NMR-analysis showed the presence of a yet not detected side product which probably corresponds to di-methylated triazoles. The reaction was repeated in acetone with an equimolar amount of the base, but the side product was detected again. This observation led to the conclusion that the presence of Cs₂CO₃ results in an additional methylation of the alcohol moiety to form the corresponding methyl ether. There are two aspects that could explain the now occurring change in regioselectivity: Caesium carbonate is the most basic of the alkali carbonates of the group I metals. [36] Additionally, the formed anions are reported to exhibit a special reactivity since they exist in a relatively free state in solution due to the high caesium cation solvation. [37] Therefore, the reaction was repeated with an equimolar amount of potassium carbonate which led to no side-products (Scheme 4 and Scheme 5). The regioisomeric mixture **8** was isolated by simply evaporating the solvent under reduced pressure, taking up the residue in an ethyl acetate-acetone mixture and then filtrating the solution to separate the product from the formed inorganic salt. In both cases any residual methyl iodide was removed by evaporation at reduced pressure and high temperatures. NMR-analysis showed that **7** and **8** were obtained pure already so they could be used in the next step without further purification. The ratio of the isomers was determined via NMR and is approximately 1:1 for both cases. The longer reaction times might have been necessary to ensure a complete conversion of the starting material, especially considering that the water could have decreased the nucleophilicity of the triazolite ion and thus, slowed down the rate of the reaction. [38] The same reaction conditions as above were applied to the methylation of tetrazole **5** to furnish the methylated derivative **7** in quantitative yield. The different reaction conditions and the resulting yields can be seen in Table 2. In conclusion, the conducted studies led to the development of a straightforward procedure with an easy final work-up step that

furnishes both methylated compounds in excellent yields and with good purities.

Table 2 Methylations of **5** and **6** under different reaction conditions with the respective yields of **7** and **8**

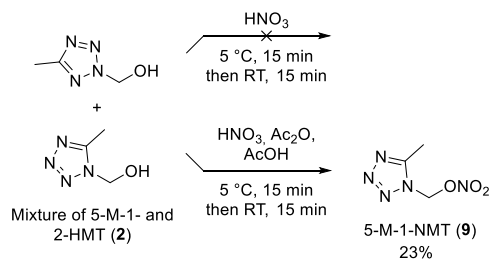
	Solvent	T [°C]	MA	Base	B-Eq.	t [h]	Yield [%]
6	Acetone/H ₂ O (1:1)	100	DMS	NaHCO ₃	1.0	3	19
5	Acetone/H ₂ O (1:1)	100	DMS	NaHCO ₃	1.0	3	39
6	MeCN	80	MI	NaHCO ₃		3	14
6	MeCN/H ₂ O (3:2)	80	MI	NaHCO ₃	1.0	3	36
6	Acetone	60	MI	Cs ₂ CO ₃	6.0	16	x
6	DMF	100	MI	Cs ₂ CO ₃	3.0	16	x
6	Acetone	60	MI	K ₂ CO ₃	1.0	16	90
5	Acetone	60	MI	K ₂ CO ₃	1.0	16	94

MA: Methylation agent, X: side product formation.

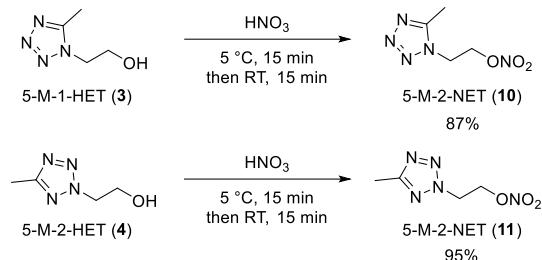
Nitration of the Alcohols

The prepared scaffolds contain hydroxy groups that can be converted into their corresponding nitrate esters. These energetic moieties provide the oxidizing agent in the molecule and lead to oxygen balances closer to zero, therefore resulting in better properties such as a higher detonation velocity and detonation pressure. [3] Additionally, the corresponding organic nitrates of alcohols are less soluble in water, [39] which reduces spreading in the environment. [40] The *O*-nitration of compounds **3**, **4** and **5** as well as of the isomeric mixtures of **2**, **7** and **8** were initially performed with 99% pure white fuming nitric acid under standard conditions for simple organic nitrate formation. The nitration, problems and if necessary modified procedures are discussed in the following. Compound **6** behaves differently when nitrated and is therefore discussed in previous work. [29]

Nitration of the isomeric mixture **2** under standard conditions (99% HNO₃, 5 °C, 15 min) and extraction of the aqueous quenched phase showed no residue (Scheme 6). Strong decomposition was observed when adding **2** to the cold nitric acid. Changing the feeding rate, temperature or reaction time also resulted in strong decomposition indicated by gas release. We believe the decomposition is caused by cleavage of the hydroxy or nitroalkyl group. This would yield **1** which decomposes during nitration as typically observed for acidic 5-substituted tetrazoles (see below "nitration of 5-hydroxymethyltetrazole"). Tetrazole is not able to form stable heterocyclic N-NO₂ nitro groups other than pyrazole [41] or triazole [42]. The nitration was possible by using acetyl nitrate in acetic acid anhydride. This changes not only the nitrating species but furthermore absorbs generated water. With this, 5-methyl-1-nitratomethyltetrazole (**9**) was obtained in a practical yield of 23% (26% yield related to the 1-isomer of the starting material mixture **2**). The nitrate **9** crystallized pure without purification and no 2-nitratomethyl compound was observed. The nitration of **3** and **4** (Scheme 7) was performed under



Scheme 6 Nitration of the regioisomeric mixture **2** yielding nitrate **9**.



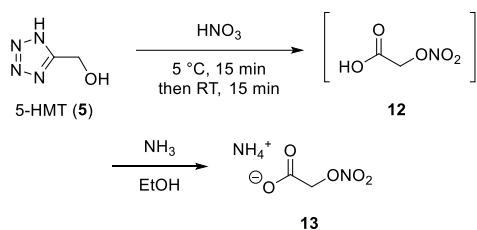
Scheme 7 Nitration of alcohols **3** and **4** to their corresponding nitrates **10** and **11**.

standard nitration conditions and no difficulties were encountered. Compound **10** was obtained in 87% as a crystalline solid and compound **11** in 95% yield as yellowish liquid.

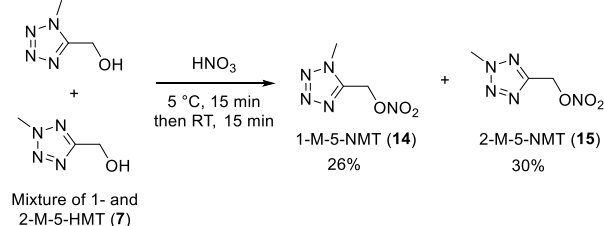
Nitration of 5-hydroxymethyltetrazole (**5**) was attempted under standard conditions (Scheme 8). Gas evolution during addition indicated decomposition and the isolation of the desired tetrazole was not possible. Acidic workup resulted in the formation of liquid glycolic acid nitrate (**12**) which was proven by the formation of the solid ammonia salt (**13**) and X-ray crystallography measurement thereof (ESI). Nitration at cooler temperatures and even reagents like acetyl nitrate or N_2O_5 in acetonitrile showed no success in preventing decomposition.

Nitration of the isomeric mixture of 1- and 2-methylated 5-hydroxymethyltetrazole mixture **7** resulted in the corresponding nitrated compounds 1-methyl-5-nitratomethyltetrazole (**14**) and 2-methyl-5-nitratomethyltetrazole (**15**) that were isolated via flash column chromatography (Scheme 9). The isolated yields of both regioisomers are approximately in a ratio of 1:1 which is in accordance with the NMR ratio of the precursors.

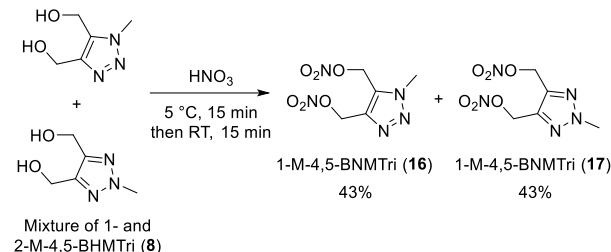
The regioisomeric mixture **8** was treated with nitric acid to furnish the corresponding mixture of nitrate esters. The regioisomers could be separated via flash column chromatography to furnish 1-methyl-4,5-bisnitratomethyltriazazole (**16**) and 2-methyl-4,5-bisnitratomethyltriazazole (**17**) with a combined yield of 86% (Scheme 10). The isolated yields of both regioisomers are in a ratio of 1:1 which is in accordance with the NMR-ratio of the precursors.



Scheme 8 Decomposition of **5** leading to glycolic acid derivatives **12** and **13**.



Scheme 9 Nitration of the isomeric mixture **7** yielding the nitrates **14** and **15**.



Scheme 10 Nitration of the isomeric mixture **8** yielding the nitrates **16** and **17**.

Structures and correlations:

Single crystals of the precursor compounds **2** (N1-isomer), **5** and nitrate compounds **9**, **10**, **13**, **14**, **15** and **17** were obtained directly from the reaction mixture or by crystallization from methanol. X-ray crystallography was performed and the data is depicted in the ESI or can be found in the CSD database under the numbers 2302430-2302436. The refinement of compound **14** does not show a satisfying result. Therefore, the density was calculated from this measurement and a structure is depicted for comparison to compound **9**, but bond distances and angles are not certain enough to be discussed in detail.

No unusual bond lengths and angles were observed. The carbons bound to the heterocycle are at most a few degrees off from the planar aromatic ring. The organic nitrates show comparable angles ($\text{O-NR-O} \pm 2.8^\circ$) and similar bond lengths ($\pm 0.05 \text{ \AA}$). Molecular units and expanded supercells of the nitrates are shown in Figure 2- Figure 6.

The nitrate **9** crystallizes in the orthorhombic space group $P2_12_12_1$ with four formula units per unit cell and a density of 1.616 g cm^{-3} at 123 K (Figure 2). The structure is disordered in such a way that the second tetrazole ring lies twisted in the first ring. Both parts share the nitrate and methyl group. The nitrate-group is twisted out of the planar rest of the molecule by $-66.8(9)^\circ$ (C1-N1A-C2A-O1) or $76.2(18)^\circ$ (C1-N1B-C2B-O2). Viewing along the b -axis of a generated supercell, rods of paired molecules of **9** are observed. The rods are internally attracted by $\text{C-H}\cdots\text{N}$ and externally by $\text{C-H}\cdots\text{O}$ hydrogen bonds.

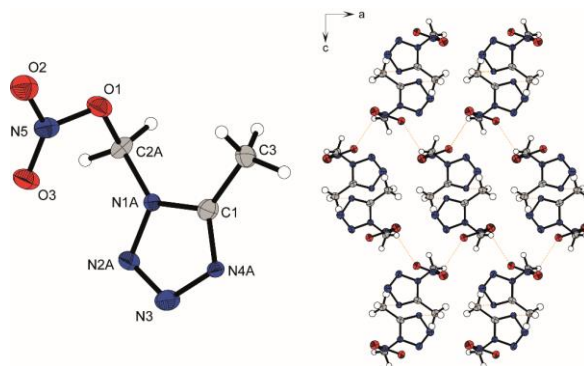


Figure 2 Low temperature crystal structure of **9** with thermal ellipsoids drawn at the 50 % probability level and orange dashed lines indicating hydrogen bonding. Selected bond lengths (\AA): C1-C3 1.475(4), N1A-C2A 1.416(9), O1-C2A 1.480(7), O1-N5 1.371(5), O2 -

N5 1.255(5). Selected bond angles ($^{\circ}$): N5-O1-C2A 114.5(4), O1-C2A-N1A 112.8(5), O2-N5-O3 126.7(4).

Ethyl nitrate **10** crystallizes in the monoclinic space group $P2_1/n$ with four formula units per unit cell and a density of 1.589 g cm^{-3} at 123 K (Figure 3). The ethyl group is at an angle of $-76.8(3)^{\circ}$ to the planar ring (C1-N1-C3-C4). Along the C3-C4 bond, the tetrazole is twisted $-63.6(2)^{\circ}$ against the nitrate (N1-C3-C4-O1). Viewing along the b -axis of the supercell alternating molecules rotated by 180° can be seen in the direction of the a or c -axis. The nitrate ethyl groups of two of those molecules arrange to build four nonclassical hydrogen bonds. The structure is rigidly fixed in other directions by further C-H \cdots O/N hydrogen bonding.

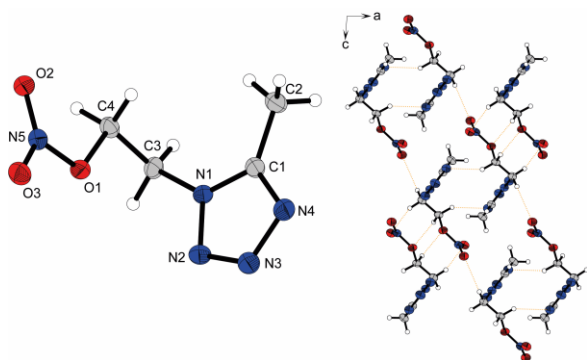


Figure 3 Low temperature crystal structure of **10** with thermal ellipsoids drawn at the 50% probability level and orange dashed lines indicating hydrogen bonding. Selected bond lengths (\AA): C1-C2 1.473(4), N1-C3 1.461(3), O1-C4 1.451(3), O1-N5 1.397(3). Selected bond angles ($^{\circ}$): N5-O1-C4 113.15(18), O1-C4-C3 105.3(2), N1-C3-C4 111.6(2), O2-N5-O3 129.5(2).

The diffraction data of methyl nitrate **14** were solved in the monoclinic space group $P2_1/c$ with eight formula units per unit cell and a density of 1.608 g cm^{-3} at 173 K (Figure 4). Each molecule is disordered in the same way as **9** and the refinement gives an unsatisfactory $wR2$ value of 30%. The nitrate is twisted out of the planar part of the molecule by 62.8° or 66.0° (N1-C1-C3-O1) and is therefore inversely comparable with structural isomer **9**. The expanded supercell, viewed along the b -axis, shows the same rod-like pattern as **9** with hydrogen bonding between and inside the rods.

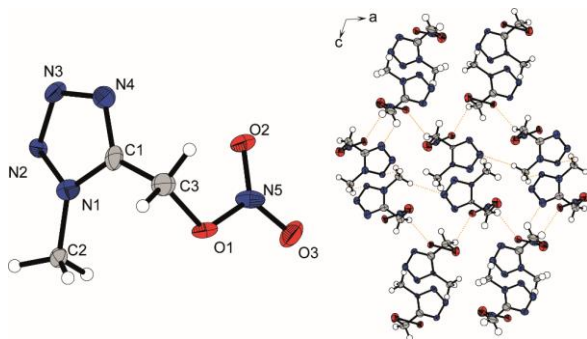


Figure 4 Low temperature crystal structure of **14** with thermal ellipsoids drawn at the 50% probability level and orange dashed lines indicating hydrogen bonding.

The nitrate **15** crystallizes in the monoclinic space group $P2_1/c$ with four formula units per unit cell and a density of 1.576 g cm^{-3} at 173 K (Figure 5). The nitrate group is perpendicular to the tetrazole plane with $-90.3(2)^{\circ}$ (N1-C1-C3-O1). The supercell reveals alternating pairs of molecules along the b -axis, building rods. In the direction of a , these rods are separated by an alkyl layer. In the direction of c non-classic hydrogen bonding is attracting the rods. This results in layers of rods along the c -axis that can slide against each other.

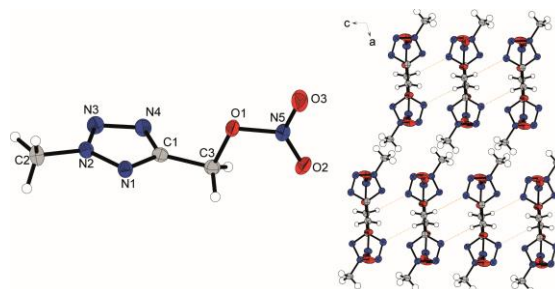


Figure 5 Low temperature crystal structure of **15** with thermal ellipsoids drawn at the 50% probability level and orange dashed lines indicating hydrogen bonding. Selected bond lengths (\AA): N2-C2 1.462(2), C1-C3 1.483(2), O1-C3 1.4577(18), O1-N5 1.3966(18). Selected bond angles ($^{\circ}$): N5-O1-C3 112.31(11), O1-C3-C1 105.14(11), O2-N5-O3 128.65(15).

The nitrate **17** crystallizes in the orthorhombic space group $Pna2_1$ with four formula units per unit cell and a density of 1.650 g cm^{-3} at 101 K (Figure 6). The nitrate groups are twisted out of the triazole plane by $64.0(3)^{\circ}$ (N1-C1-C3-O1) and $98.6(3)^{\circ}$ (N1-C2-C4-O4). A generated supercell shows that the molecules are rigidly fixed in all directions of space by hydrogen bonds. Layers are formed in c -direction where the molecules are attracted by C-H \cdots O bonds. Those layers are bound in b -direction by C-H \cdots N bonds.

Physicochemical Properties and Explosive Performance

The chemical, physical and calculated energetic properties of the investigated substances compared to TNT and PETN are shown in Table 3. The thermal properties of the obtained nitratealkylazoles were analyzed by differential thermal analysis (DTA) (Figure 7).

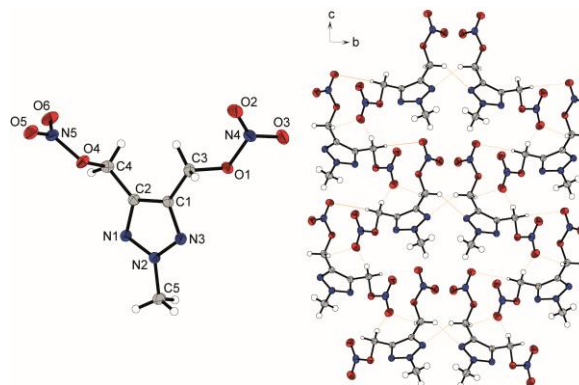


Figure 6 Low temperature crystal structure of **17** with thermal ellipsoids drawn at the 50% probability level and orange dashed lines indicating hydrogen bonding. Selected bond lengths (\AA): N2-

C5 1.451(4), C2-C4 1.485(4), O4-C4 1.461(3), O4-N5 1.397(3)
 Selected bond angles (°): O4-C4-C2 105.8(2), N5-O4-C4 113.11(18),
 O5-N5-O6 128.8(2).

All synthesized solid compounds are melting between 27 and 110 °C. The 1-substituted tetrazoles show higher melting points than their corresponding 2-isomers. The greatest difference is observed for the isomers **10** and **11** with a melting point difference of about 130 °C. The five regioisomers with the formula C₃H₅N₅O₃ (**1-NET**, **2-NET**, **9**, **14**, **15**) are melting between 24 and 70 °C. The more linear molecules 1-NET, 2-NET and 2-M-5-NMT (**15**) are melting close together at 24 to 27 °C, whereas the bulkier ones **9** and **14** are melting at 60 to 70 °C. Concluding for nitroalkylazoles, isomers with similar compositions reveal lower melting points when the molecules show a linear character. For the triazoles, the more symmetric 2-isomer **17** is melting at a higher temperature of 37 °C whereas the 1-isomer **16** is not solidifying below -30 °C. An unexpected result is the thermal behavior of **10**. When adding a methyl group at the 5-position of 1-NET the melting point, other than one might expect, increased by 85 °C. It is shown that some energetics show unexpectedly high melting points due to symmetry and order. [43, 44] Compound **9** contains a shorter alkyl chain that shows a lower degree of freedom, but still, the melting point is 40 °C lower. We conclude that this unexpected low melting point is caused by the disorder of the crystalline compounds **9** and **14**. We observed similar low melting points for disordered crystals in previous studies for mononitramino PETN [45] and monoazido PETN [46]. Both compounds are disordered and show low melting

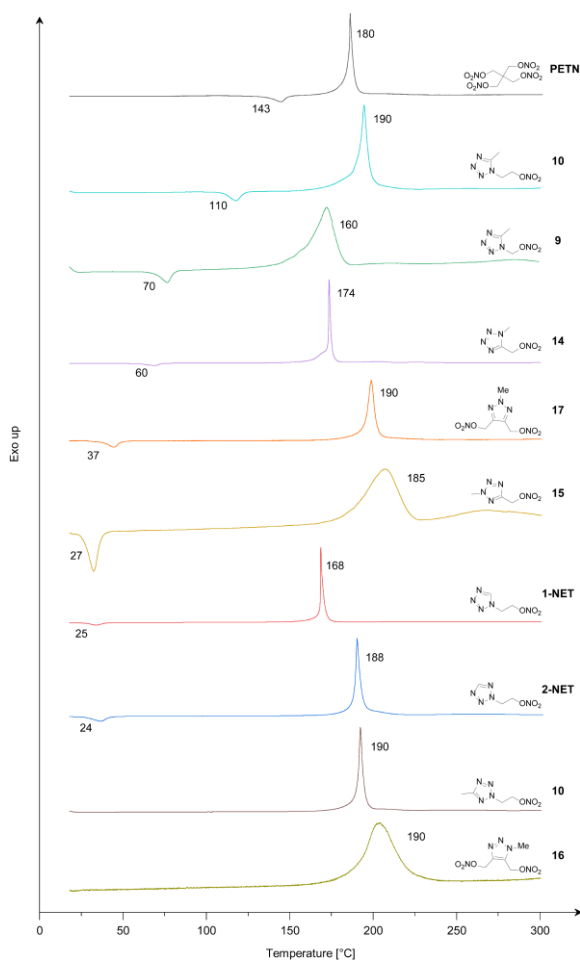


Figure 7 DTA plot of nitroalkylazoles and PETN ordered by melting points (low-bottom to high-top). Indicated melting or decomposition points are onset temperatures.

character. After successful nitration, all energetic materials were investigated for their impact and friction sensitivities. Mostly insensitive compounds were obtained. Of the C₃H₅N₅O₃ isomers (**1-NET**, **2-NET**, **9**, **14**, **15**) the 1-NET, 2-NET and 5-M-1-NMT (**9**) show sensitivity towards impact (2-10 J) whereas both 5-nitratomethyl isomers are far less sensitive (30-40 J). Both nitroethyl compounds and 1-M-5-NMT (**14**) are insensitive towards friction. Compound **9** shows a sensitivity of 96 N and compound **15** shows the highest sensitivity with 60 N which is surprising in comparison to the insensitivity towards impact. The remaining C₄H₇N₅O₃ (**10** and **11**) and C₅H₇N₅O₆ (**16** and **17**) compounds are insensitive towards impact and friction. The sensitivities cannot be correlated with the N+O content, oxygen balance or performance. It is often observed, that low melting compounds exhibit an insensitive character to friction force. This is suspected for 1-NET and 2-NET where we believe that the compound is liquified through friction force and therefore analysis of the liquid compound takes place. Liquid nitrates are generally less sensitive to friction (e.g. NG: >360 N). But this concept is not working for 2-M-5-NMT (**15**).

The densities were calculated from the crystal structures. The density of 2-M-4,5-BNMTri (**17**) with 1.60 g cm⁻³ is the highest of all nitrates investigated. The bulkier molecules of the five C₃H₅N₅O₃ show higher densities than the linear ones. The nitrate **10** crystallizes with the same density than 1-NET, even though **10** contains one methyl group more and has a lower N+O content. Compared to TNT (1.65 g cm⁻³) the observed densities are generally slightly lower. PETN shows a much higher density with 1.78 g cm⁻³. The energetic performance of the solid compounds was calculated with the EXPLOS code. The detonation velocity ranges from 7218 (**10**) to 7551 m s⁻¹ (**14**) which is 6 to 11% higher than TNT with 6798 m s⁻¹. The detonation pressures range from 18.6 to 21.6 kbar and correspond to the calculated velocities. The TNT equivalents were calculated and are between 1.41 and 1.21. The high TNT equivalents can be explained by the higher gas volume produced by the organic nitrates.

Conclusion

Seven nitroalkylazoles with higher oxygen balances than TNT were synthesized. A summary of the physicochemical properties is shown in Figure 8. The synthesis of the starting materials 5-MT and 5-HMT from literature procedures showed unsatisfying results. The original procedures were optimized, so that efficient and reproducible synthesis was possible. Methylation and hydroxyalkylation were evaluated and optimized. Nitration with neat nitric acid showed success for all nitration's except 5-M-1-NMT. Here acetyl nitrate proved to be the better medium.

The observed nitrates outperform the detonation velocity of TNT by 6-11% and have 7-13% higher O+N-contents. Through the alkyl chains, the densities are 3-6% lower than the density of TNT.

Generally, for tetrazoles the N-2 isomers, which are more linear, are melting earlier than the corresponding N-1 isomers, which are bulkier. The N-2 isomers show similar or increased sensitivities compared to the N-1 isomers. 5-M-1-NMT (**9**) (sensitive) and its structural isomer 1-M-5-NMT (**14**) (insensitive) show comparable crystal structures and physical properties but differ strongly in the sensitivity. Both are disordered and show decreased melting points. For the two 1,2,3-triazoles, the more symmetric N-2 isomer shows a higher melting point. Adding a methyl group to 1-NET, yielding 5-M-1-NET (**10**), causes the melting point to increase by 85 °C to

110 °C. 5-M-1-NMT (**9**) and 2-M-5-NMT (**15**) are sensitive towards friction force, whereas the other nitrates are less sensitive than

TNT. Future research on nitroalkylazoles should focus more on

Table 3 Physicochemical properties and calculated explosive performance of nitroalkylazoles (ordered by formula) compared to PETN and TNT.

	Formula	IS [J] ^[a]	FS [N] ^[b]	ρ [g cm ⁻³] ^[c]	N+O [%] ^[d]	Ω_{CO} [%] ^[e]	$T_{\text{melt}}/T_{\text{dec}}$ [°C] ^[f]	$\Delta_f H^0$ [kJ mol ⁻¹] ^[g]	P_{CJ} [kbar] ^[h]	V_{det} [m s ⁻¹] ^[i]	TNT equiv. ^[j]
1-NET	C ₃ H ₅ N ₅ O ₃	10	>360	1.55	74.2	-25.1	25/168	173.7	21.5	7583	1.41
2-NET	C ₃ H ₅ N ₅ O ₃	2	>360	1.57	74.2	-25.1	24/188	147.1	20.0	7420	1.37
5-M-1-NMT (9)	C ₃ H ₅ N ₅ O ₃	3	96	1.58	74.2	-25.1	70/160	143.2	21.2	7524	1.36
1-M-5-NMT (14)	C ₃ H ₅ N ₅ O ₃	>40	>360	1.58	74.2	-25.1	60/174	150.1	21.2	7551	1.37
2-M-5-NMT (15)	C ₃ H ₅ N ₅ O ₃	30	60	1.55	74.2	-25.1	27/185	130.9	20.3	7392	1.34
5-M-1-NET (10)	C ₄ H ₇ N ₅ O ₃	>40	>360	1.55	68.2	-41.6	110/190	99.0	18.6	7218	1.21
5-M-2-NET (11)	C ₄ H ₇ N ₅ O ₃	>40	>360	liq.	68.2	-41.6	ca.-20/190	-	-	-	-
1-M-4,5-BNMTri (16)	C ₅ H ₇ N ₅ O ₆	>40	>360	liq.	71.2	-17.2	<-30/190	-	-	-	-
2-M-4,5-BNMTri (17)	C ₅ H ₇ N ₅ O ₆	>40	>360	1.60	71.2	-17.2	37/190	-37.2	21.6	7416	1.32
PETN [5]	C ₅ H ₈ N ₄ O ₁₂	3.5	54	1.78	78.4	15.2	143/180	-534	30.8	8429	1.64
TNT [5]	C ₇ H ₅ N ₃ O ₆	15	>360	1.65	60.8	-24.7	81/289	-59	18.3	6798	1.01

a Impact sensitivity (BAM Fallhammer). b Friction sensitivity (BAM Friction Tester). c Density from X-ray diffraction analysis recalculated to 298 K. d Combined nitrogen and oxygen content. e Oxygen balance with respect to CO. f Melting and decomposition onset temperature (DTA, 5 °C min⁻¹). g Calculated enthalpy of formation. h Calculated detonation pressure at chapman-jouguet point. i Calculated detonation velocity (EXPLO V6.05.04). j TNT equiv. based on the Power Index.

bulky, N1-substituted and at best symmetric molecules to increase the melting point of the often-low melting alkyl compounds. Thermal behavior and sensitivity are sometimes counter intuitive and must be proven by synthesis and characterization. To accelerate the search for TNT replacements, computational studies providing realistic target molecules are helpful.

There are no conflicts to declare.

Acknowledgements

Financial support of this work by Ludwig-Maximilian University (LMU), the Office of Naval Research (ONR) under Grant ONRN00014-19-1-2078, and the Strategic Environmental Research and Development Program (SERDP) under contract no. W912HQ19C0033 is gratefully acknowledged. The authors would like to thank Prof. Dr. Konstantin Karaghiosoff and Dr. Burkhard Krumm for NMR spectroscopy.

Supplementary materials

Supplementary material associated with this article can be found, in the online version, at [to be added].

References

- [1] J.P. Agrawal, High Energy Materials, Wiley-VCH, Weinheim, 2010.
- [2] R.M. J. Köhler, A. Homburg, Explosivstoffe, Wiley-VCH, Weinheim, 2008.
- [3] T.M. Klapötke, Chemistry of High-Energy Materials 6th edn., De Gruyter, Berlin/Boston, 2022.
- [4] R. Matyáš, J. Pachman, Primary Explosives, 2013.
- [5] T.M. Klapötke, Energetic Materials Encyclopedia 2nd edn., De Gruyter, Berlin/Boston, 2018.
- [6] B.S. Levine, E.M. Furedi, D.E. Gordon, J.J. Barkley, P.M. Lish, Toxic Interactions of the Munitions Compounds TNT and RDX in F344 Rats12, Toxicol. Sci. 15 (1990) 373-380.
- [7] Y. Jehuda, Toxicity and Metabolism of Explosives 1st ed., CRC Press, Boca Raton, 1990.

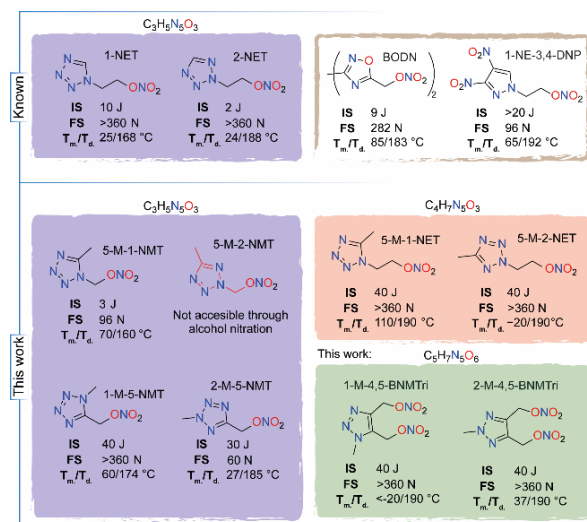


Figure 8 Known nitroalkylazoles with good properties (top right) [15, 17], C₃H₅N₅O₃ nitroalkyltetrazoles (left) [18] and further functionalized azoles (middle and bottom right)

Declaration of Competing Interest

- [8] M. Benz, A. Delage, T.M. Klapötke, M. Kofen, J. Stierstorfer, A rocky road toward a suitable TNT replacement – A closer look at three promising azoles, *Prop., Explos., Pyrotech.* 48 (2023) e202300042.
- [9] P. Ravi, D.M. Badgajar, G.M. Gore, S.P. Tewari, A.K. Sikder, Review on Melt Cast Explosives, *Prop., Explos., Pyrotech.* 36 (2011) 393-403.
- [10] Q. Ma, Z. Zhang, W. Yang, W. Li, J. Ju, G. Fan, Strategies for constructing melt-castable energetic materials: A critical review, *Energetic Materials Frontiers.* 2 (2021) 69-85.
- [11] J.J. Sabatini, E.C. Johnson, A Short Review of Nitric Esters and Their Role in Energetic Materials, *ACS Omega.* 6 (2021) 11813-11821.
- [12] D.E. Chavez, M.A. Hiskey, D.L. Naud, D. Parrish, Synthesis of an Energetic Nitrate Ester, *Angew. Chem. Int. Ed.* 47 (2008) 8307-8309.
- [13] A.A. Larin, D.M. Bystrov, L.L. Fershtat, A.A. Konnov, N.N. Makhova, K.A. Monogarov, D.B. Meerov, I.N. Melnikov, A.N. Pivkina, V.G. Kiselev, N.V. Muravyev, Nitro-, Cyano-, and Methylfuroxans, and Their Bis-Derivatives: From Green Primary to Melt-Cast Explosives, *Molecules.* 25 (2020) 5836.
- [14] C. He, J.n.M. Shreeve, Energetic Materials with Promising Properties: Synthesis and Characterization of 4,4'-Bis(5-nitro-1,2,3-2H-triazole) Derivatives, *Angew. Chem. Int. Ed.* 54 (2015) 6260-6264.
- [15] E.C. Johnson, J.J. Sabatini, D.E. Chavez, R.C. Sausa, E.F.C. Byrd, L.A. Wingard, P.E. Guzmàn, Bis(1,2,4-oxadiazole)bis(methylene) Dinitrate: A High-Energy Melt-Castable Explosive and Energetic Propellant Plasticizing Ingredient, *Org. Process Res. Dev.* 22 (2018) 736-740.
- [16] L. Bauer, M. Benz, T.M. Klapötke, T. Lenz, J. Stierstorfer, Polyazido-methyl Derivatives of Prominent Oxadiazole and Isoxazole Scaffolds: Synthesis, Explosive Properties, and Evaluation, *J. Org. Chem.* 86 (2021) 6371-6380.
- [17] S. Song, F. Chen, Y. Wang, K. Wang, M. Yan, Q. Zhang, Accelerating the discovery of energetic melt-castable materials by a high-throughput virtual screening and experimental approach, *J. Mater. Chem. A.* 9 (2021) 21723-21731.
- [18] M.S. Gruhne, T. Lenz, M. Rösch, M. Lommel, M.H.H. Wurzenberger, T.M. Klapötke, J. Stierstorfer, Nitrateoethyl-5H-tetrazoles: improving the oxygen balance through application of organic nitrates in energetic coordination compounds, *Dalton Trans.* 50 (2021) 10811-10825.
- [19] L.M. Barton, J.T. Edwards, E.C. Johnson, E.J. Bukowski, R.C. Sausa, E.F.C. Byrd, J.A. Orlicki, J.J. Sabatini, P.S. Baran, Impact of Stereo- and Regiochemistry on Energetic Materials, *J. Am. Chem. Soc.* 141 (2019) 12531-12535.
- [20] Y. Ohno, Y. Akutsu, M. Arai, M. Tamura, T. Matsunaga, 5-Methyl-1H-tetrazole, *Acta Cryst. C* 55 (1999) 1014-1016.
- [21] Z.P. Demko, K.B. Sharpless, Preparation of 5-Substituted 1H-Tetrazoles from Nitriles in Water, *J. Org. Chem.* 66 (2001) 7945-7950.
- [22] T.M. Klapötke, A. Penger, C. Pflüger, J. Stierstorfer, M. Sućeska, Advanced Open-Chain Nitramines as Energetic Materials: Heterocyclic-Substituted 1,3-Dichloro-2-nitrazapropane, *Eur. J. Inorg. Chem.* 2013 (2013) 4667-4678.
- [23] J. Zhang, C. He, D.A. Parrish, J.n.M. Shreeve, Nitramines with Varying Sensitivities: Functionalized Dipyrzoly- N-nitromethanamines as Energetic Materials, *Chem. Eur. J.* 19 (2013) 8929-8936.
- [24] P.F. Pagoria, G.S. Lee, A.R. Mitchell, R.D. Schmidt, A review of energetic materials synthesis, *Thermochim. Acta.* 384 (2002) 187-204.
- [25] G. Hervé, C. Roussel, H. Graindorge, Selective Preparation of 3,4,5-Trinitro-1H-Pyrazole: A Stable All-Carbon-Nitrated Arene, *Angew. Chem. Int. Ed.* 49 (2010) 3177-3181.
- [26] N. Fischer, K. Karaghiosoff, Thomas M. Klapötke, J. Stierstorfer, New Energetic Materials featuring Tetrazoles and Nitramines – Synthesis, Characterization and Properties, *Z. anorg. allg. Chem.* 636 (2010) 735-749.
- [27] W.G. Finnegan, R.A. Henry, R. Lofquist, An Improved Synthesis of 5-Substituted Tetrazoles, *J. Am. Chem. Soc.* 80 (1958) 3908-3911.
- [28] J. Nieman, M. Hena, B. Bai, A. S. Kandadai, A. Belovodskiy, Inhibitors of Human Herpesviruses, US20230136702A1, 2021.
- [29] M. Benz, S. Dörrich, T.M. Klapötke, T. Lenz, M. Mouzayek, J. Stierstorfer, 4,5-Bisnitratomethyl and Similar Representatives of the Rare Class of 2-Nitro-1,2,3-triazoles, *Org. Lett.* 25 (2023) 5974-5977.
- [30] A.d. Meijere, *Methods of Organic Chemistry* 4th ed., 4th Edition ed., Georg Thieme Verlag KG, Stuttgart, 1997.
- [31] A.R. Katritzky, J.M. Lagowski, Prototropic Tautomerism of Heteroaromatic Compounds: IV. Five-Membered Rings with Two or More Hetero Atoms, *Advances in Heterocyclic Chemistry*, Academic Press, 1963.
- [32] J.L. Ellingboe, J.H. Runnels, Solubilities of Sodium Carbonate and Sodium Bicarbonate in Acetone-Water and Methanol-Water Mixtures, *J. Chem. Eng.* 11 (1966) 323-324.
- [33] M. Selva, A. Perosa, Green chemistry metrics: a comparative evaluation of dimethyl carbonate, methyl iodide, dimethyl sulfate and methanol as methylating agents, *Green Chem.* 10 (2008) 457-464.
- [34] R.A. Ogg, Jr., The Hydrolysis of Methyl Iodide, *J. Am. Chem. Soc.* 60 (1938) 2000-2001.
- [35] J.P. Guzowski, Jr., E.J. Delaney, M.J. Humora, E. Irdam, W.F. Kiesman, A. Kwok, A.D. Moran, Understanding and Control of Dimethyl Sulfate in a Manufacturing Process: Kinetic Modeling of a Fischer Esterification Catalyzed by H₂SO₄, *Org. Process Res. Dev.* 16 (2012) 232-239.
- [36] R.J. Meyer, *Gmelin Handbook of Inorganic Chemistry* 8th ed., Springer-Verlag Berlin, Heidelberg, 1938.
- [37] G. Dijkstra, W.H. Kruizinga, R.M. Kellogg, An assessment of the causes of the "cesium effect", *J. Org. Chem.* 52 (1987) 4230-4234.
- [38] J.E.H. E. S. Amis, *Solvent Effects on Chemical Phenomena* Vol. 1, Academic Press, New York, 1973.
- [39] R.N. Roberts, R.H. Dinagar, Solubility of Pentaerythritol Tetranitrate, *J. Phys. Chem.* 62 (1958) 1009-1011.
- [40] H. Gao, J.n.M. Shreeve, Azole-Based Energetic Salts, *Chem. Rev.* 111 (2011) 7377-7436.
- [41] J.W.A.M. Janssen, H.J. Koeners, C.G. Kruse, C.L. Habrakern, Pyrazoles. XII. Preparation of 3(5)-nitropyrzoles by thermal rearrangement of N-nitropyrzoles, *J. Org. Chem.* 38 (1973) 1777-1782.
- [42] A.T. Baryshnikov, V.I. Erashko, N.I. Zubanova, B.I. Ugrak, S.A. Shevelev, A.A. Fainzil'berg, A.L. Laikhter, L.G. Mel'nikova, V.V. Semenov, Gem-dinitro compounds in organic synthesis. 3. Syntheses of 4-nitro-1,2,3-triazoles from gem-dinitro compounds, *Bulletin of the Russian Academy of Sciences, Division of chemical science.* 41 (1992) 751-757.
- [43] T. Carnelley, XIII. Chemical symmetry, or the influence of atomic arrangement on the physical properties of compounds, *The London, Edinburgh, and Dublin Philosophical Magazine and Journal of Science.* 13 (1882) 112-130.
- [44] R.J.C. Brown, R.F.C. Brown, Melting Point and Molecular Symmetry, *J. Chem. Educ.* 77 (2000) 724.
- [45] M. Benz, T.M. Klapötke, N. Kölbl, J. Kuch, T. Lenz, E. Parigi, J. Stierstorfer, Melt Castable Derivatives of Pentaerythritol Tetranitrate, *Chem. Eur. J.* 29 (2023) e202204013.
- [46] T. Lenz, T.M. Klapötke, M. Mühlemann, J. Stierstorfer, About the Azido Derivatives of Pentaerythritol Tetranitrate, *Prop., Explos., Pyrotech.* 46 (2021) 723-731.

To be published

Supporting Information

Isomerism of Nitroalkylazoles

Maximilian Benz, Thomas M. Klapötke, Tobias Lenz, Mohamed Mouzayek, Elena Reinhardt and Jörg Stierstorfer

Department of Chemistry, Ludwig-Maximilian University of Munich, Butenandtstr. 5-13(D), D-81377 Munich, Germany;
tmk@cup.uni-muenchen.de

Supplementary Information

Table of Contents

1.	General Considerations	S3
2.	Experimental Part	S4
3.	X-ray Diffraction	S11
4.	Thermal Analysis	S20
5.	Computation	S21
6.	References	S23

1. General Considerations

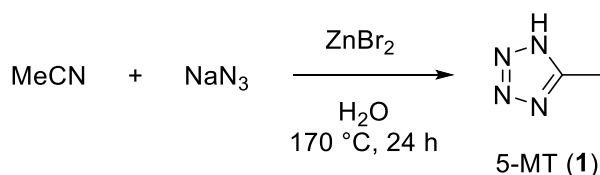
Starting materials were purchased from commercial suppliers (ABCR, Acros Organics, AppliChem, Sigma-Aldrich, VWR) and used without further purification. The nitric acid is 99% pure, white fuming and contains less than 0.4% NO₂. Stirring was performed by a magnetic stir bar if not stated differently. Heating was performed by a heating plate equipped with an oil bath and thermometer. Cooling was performed with an ice water mixture for 5-10 °C.

¹H, ¹³C, ¹⁴N and ¹⁵N NMR spectra were recorded on BRUKER AMX 400 instruments. Samples are placed in regular glass NMR tubes (Ø 5 mm) and measured at 25 °C. Chemical shifts are referenced with respect to tetramethylsilane (1H/13C) and nitromethane (14N/15N). Infrared spectra (IR) were recorded in the region 4000-400 cm⁻¹ on a PERKIN ELMER Spectrum BX-59343 instrument with a SMITHS DETECTION DuraSampl IR II Diamond ATR sensor. The absorption bands are reported in wavenumbers (cm⁻¹). Electrospray ionization (ESI) measurements were performed on a Thermo Finnigan LTQ FT Ultra Fourier Transform ion cyclotron resonance mass spectrometer. The resolution was set to 100,000 at m/z 400. Depending on the sample, mass ranges from 50 to 2000 u were measured. The spray capillary voltage at the IonMax ESI head was 4 kV, the heater capillary temperature was 250 °C, the nitrogen sheath gas flow was 20 and the sweep gas flow was 5 units. Thermal properties were measured via differential thermal analysis (DTA) with an OZM Research DTA 552-Ex instrument at a heating rate of 5 °C/min and in a range of room temperature to 400 °C. All sensitivities toward impact (IS) and friction (FS) were determined according to BAM (Bundesanstalt für Materialforschung und Prüfung) standards using a BAM drop hammer and a BAM friction apparatus by applying the 1 of 6 method.[S1]

CAUTION! Compounds all nitrates are potentially explosive materials. Safety precautions and equipment (such as wearing a leather coat, face shield, Kevlar sleeves, Kevlar gloves, earthed equipment and ear protection) must be used during manipulation.

2. Experimental Part

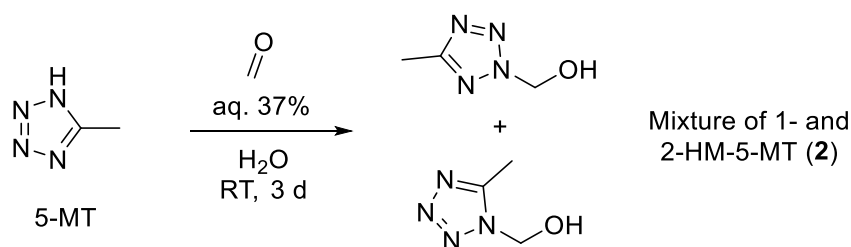
5-Methyltetrazole (1)



5-Methyltetrazole (1) was synthesized according to a modified procedure by Sharpless et.al. [S2] Acetonitrile (1.64 g, 40.0 mmol, 1.0 eq), sodium azide (5.72 g, 80.0 mmol, 2.0 eq) and zinc bromide (9.00 g, 40.0 mmol, 1.0 eq) were dissolved in water (80 mL) and converted to a pressure tube. The reaction flask was heated to 170 °C and stirred vigorously for 24 h using an oil bath. After few hours, a white precipitate is formed. After 24 h, the heating source was removed, and the mixture was cooled to room temperature. Aqueous sodium hydroxide (2 M, 50 mL, 0.1 mol, 2.5 eq) was added to precipitate $Zn(OH)_2$, which was filtered off and washed with a little water (10 mL). (To increase the yield, the amount of water should be as minimal as possible during all washing and workup steps). The filtrate was acidified to pH = 1 using hydrochloric acid (2 M, approx. 40 mL) and saturated with magnesium sulfate. The saturated aqueous solution was extracted with 6-7 equal portions of ethyl acetate (200 mL), dried over anhydrous sodium sulfate. The organic solvent was removed under reduced pressure to obtain a colorless solid. After recrystallization from hot acetone (20 mL) **1** (2.30 g, 27.4 mmol, 68%) was obtained as off-white powder.

1H NMR (DMSO- d_6 , 400 MHz, ppm) δ = 15.94 (br s, 1H), 2.49 (s, 3H); $^{13}C\{^1H\}$ NMR (DMSO- d_6 , 101 MHz, ppm) δ = 152.7, 8.9.

Mixture of 1-hydroxymethyl-5-methyltetrazol and 2-hydroxymethyl-5-methyltetrazol (2)

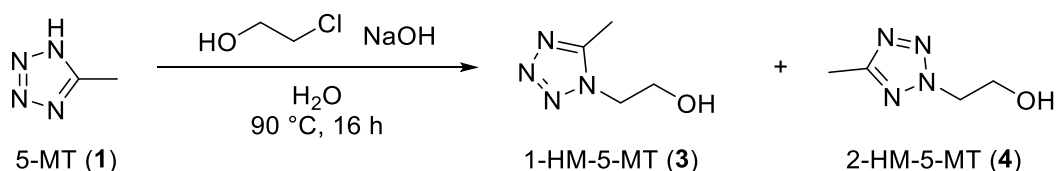


5-Methyltetrazole (1) (0.50 g, 5.95 mmol, 1.0 eq.) was dissolved in water (7 mL) and reacted with formaldehyde (40% aq., 1.0 mL, 0.82 g, 10.9 mmol, 1.8 eq.) and HCl (conc., 1–2 drops) at room temperature for 3 days. The resulting mixture was extracted with EtOAc (3 × 15 mL), dried with $MgSO_4$,

and the solvent was evaporated under reduced pressure to obtain a colorless solid as an isomeric mixture **2** (0.60 g, 5.21 mmol, 88%) in a ratio of 8:1.

IR (ATR, rel. int.): $\tilde{\nu}$ (cm⁻¹) = 3200 (m), 2968 (w), 2910 (w), 1529 (m), 1470 (m), 1413 (m), 1381 (m), 1319 (m), 1270 (m), 1224 (w), 1149 (w), 1093 (vs), 1042 (w), 1012 (m), 972 (w), 758 (vs), 726 (m), 716 (s), 695 (s), 653 (s), 474 (m), 419 (w); **EA** (C₃H₆N₄O, 114.11 g/mol) calc. (found): C 31.58 (31.68), H 5.30 (5.16), N 49.10 (48.19) %; **¹H NMR** (400 MHz, DMSO-*d*₆, 25 °C): δ (ppm) = 7.60 (t, ³J_{H,H} = 8.1 Hz, OH 2-Iso), 7.29 (t, ³J_{H,H} = 7.8 Hz, OH 1-Iso), 5.81 (d, ³J_{H,H} = 8.0 Hz, CH₂ 2-Iso), 5.68 (d, ³J_{H,H} = 7.8 Hz, CH₂ 1-Iso), 2.56 (s, CH₃ 1-Iso), 2.47 (s, CH₃ 2-Iso); **¹³C{¹H} NMR** (101 MHz, DMSO-*d*₆, 25 °C): δ (ppm) = 162.5 (2-Iso), 152.1 (1-Iso), 74.5 (2-Iso), 69.4 (1-Iso), 10.4 (2-Iso), 8.2 (1-Iso); **HR-MS** (EI) m/z: [C₃H₇N₄] **calc.**: 115.0620 [M+H]⁺; **found**: 115.0614.

1-Hydroxyethyl-5-methyltetrazole (**3**) and 2-Hydroxyethyl-5-methyltetrazole (**4**)

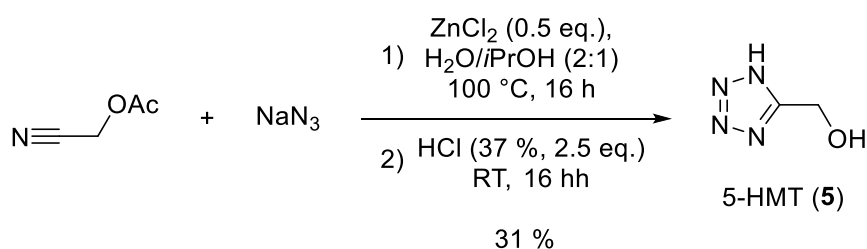


5-Methyltetrazole (**1**) (1.50 g, 17.9 mmol, 1.0 eq) was dissolved in water (50 mL) and sodium hydroxide (0.72 g, 17.9 mmol, 1.0 eq) was added. The mixture was heated to 90 °C with means of an oil bath and 2-chloroethanol (1.58 g, 19.7 mmol, 1.30 mL, 1.1 eq) was added dropwise and further stirred at this temperature for 16 h. After cooling to room temperature, the solvent was evaporated under reduced pressure. The remaining solid was suspended in acetone (70 mL) and refluxed for 1 h. The solid was filtered off and the solvent was evaporated under reduced pressure to obtain a pure mixture of both isomers. Separation was performed using column chromatography with ethyl acetate as eluent. **3** (R_f (EtOAc) = 0.12; 0.89 g, 6.98 mmol, 39%) and **4** (R_f (EtOAc) = 0.50; 0.86 g, 6.74 mmol, 38%) were obtained as colorless liquids.

1-Hydroxyethyl-5-methyltetrazole (3): IR (ATR) $\tilde{\nu}$ (cm⁻¹) = 3422(m), 3378(m), 3350(m), 2930(w), 2883(w), 1531(s), 1411(s), 1308(w), 1249(m), 1129(m), 1067(vs), 954(m), 866(s), 773(m), 715(s), 692(m), 672(m), 641(vs), 536(s), 503(s), 461(s), 450(m), 433(m), 422(s), 403(m); **Elem. Anal.** Calc. for C₄H₈N₄O: C, 37.49; N, 43.73; H, 6.29. Found: C 37.45, N 42.70, H 6.02; **¹H NMR** (Acetone-*d*₆, 400 MHz, ppm): δ = 4.47 (dd, ³J = 5.6, 4.7 Hz, 2H), 3.97 (dd, ³J = 5.6, 4.8 Hz, 2H), 2.56 (s, 3H); **¹³C{¹H} NMR** (Acetone-*d*₆, 101 MHz, ppm): δ = 153.6, 61.4, 50.3, 9.0; **HR-MS** (EI) m/z: [C₄H₉N₄O] **calc.**: 129.0771 (M⁺); **found**: 129.0771.

2-Hydroxyethyl-5-methyltetrazole (4): IR (ATR) $\tilde{\nu}$ (cm⁻¹) = 3371(m), 2926(w), 1508(s), 1434(m), 1367(m), 1253(w), 1193(m), 1157(m), 1069(vs), 1034(s), 957(m), 868(m), 802(w), 740(s), 716(m), 621(s), 559(m), 504(s), 458(m), 449(m), 443(m), 427(m), 402(m); **Elem. Anal.** Calc. for C₄H₈N₄O: C, 37.49; N, 43.73; H, 6.29. Found: C 36.94, N 42.75, H 6.12; **¹H NMR** (Acetone-*d*₆, 400 MHz, ppm): δ = 4.68 (dd, ³*J* = 5.8, 4.8 Hz, 2H), 4.14 (br s, 1H), 4.07 (t, ³*J* = 5.4 Hz, 2H), 2.43 (s, 3H); **¹³C{¹H} NMR** (Acetone-*d*₆, 100 MHz, ppm): δ = 163.2, 60.7, 56.1, 10.7; **HR-MS** (EI) *m/z*: [C₄H₉N₄O] **calc.**:129.0771 (M⁺); **found**: 129.0771.

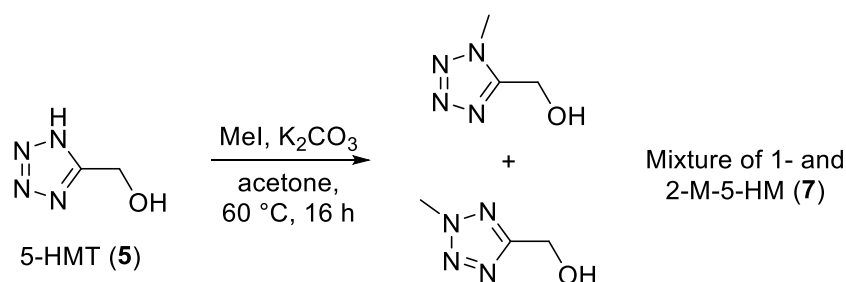
5-Hydroxymethyl-1H-tetrazol (5)



According to modified patents,^[89,90] a solution of cyanomethyl acetate (33.0 g, 333 mmol, 1.0 eq.), ZnCl₂ (22.7 g, 166.5 mmol, 0.5 eq.) and sodium azide (43.3 g, 666 mmol, 2.0 eq.) in a mixture of water (300 mL) and 2-propanol (150 mL) was stirred overnight at 100 °C. After cooling down to RT, conc. HCl (37 %, 69.4 mL, 832 mmol, 2.5 eq.) was slowly added to the mixture upon which the colour changed from orange to clear yellow. The solution was stirred overnight at RT, divided into two portions, and then extracted with EtOAc (5 x 250 mL). The combined organic layers were dried over anhydrous Na₂SO₄, filtrated and the solvent was removed under reduced pressure. The residue was washed with acetonitrile to provide **5** as a colourless solid (10.2 g, 102 mmol, 31%).

¹H-NMR (DMSO-*d*₆, 400 MHz, ppm): δ = 16.27 (br s, 1H), 5.90 (br s, 1H), 4.80 (s, 2H); **¹³C{¹H} NMR** (DMSO-*d*₆, 101 MHz, ppm): δ = 156.6, 53.3; **EA** calcd. for C₂H₄N₄O (100.08 g mol⁻¹): C 24.00, N 55.98, H 4.03 %; found: C 23.93, N 56.11, H 4.19 %.

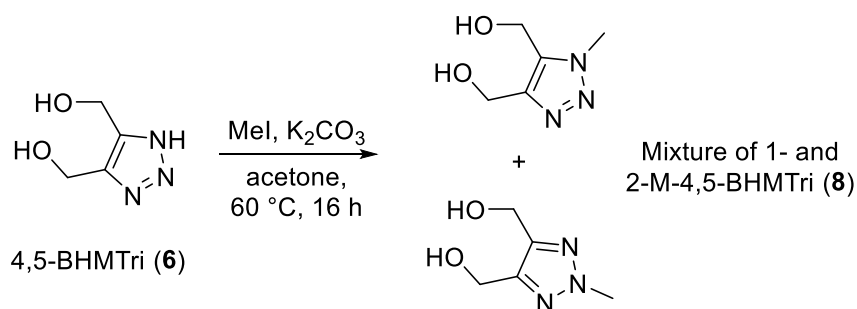
Mixture of 1-methyl-5-hydroxymethyltetrazol and 2-methyl-5-hydroxymethyltetrazol (7)



Methyl iodide (2.84 g, 1.25 mL, 20.0 mmol, 1 eq.) was added to a suspension of 5-hydroxymethyl-1*H*-tetrazol (**5**) (2.00 g, 20.0 mmol, 1 eq.) and K₂CO₃ (2.76 g, 20.0 mmol, 1 eq.) in acetone (350 mL). The mixture was stirred for 16 hours at 60 °C and diluted with EtOAc (150 mL) after cooling down. The suspension was filtrated, and the acetone was evaporated under reduced pressure. The resulting suspension was filtrated again, and the residue was washed with a large amount of ethyl acetate. The solvent along with side products were removed under reduced pressure (20 mbar, 30 min, 80 °C) to provide the regioisomeric mixture **7** as a yellow liquid (2.14 g, 18.7 mmol, 94%) that was used in the next step without separation of the isomers.

IR (ATR): $\tilde{\nu}$ (cm⁻¹) = 3328 (m), 2958 (w), 1473 (m), 1452 (m), 1288 (w), 1190 (w), 1097 (m), 1044 (vs), 1029 (vs), 989 (w), 784 (m), 740 (m), 706 (m), 658 (m), 652 (m); **¹H-NMR** (DMSO-*d*₆, 400 MHz, ppm): δ = 5.82 (t, *J* = 6.0 Hz, 1H), 5.57 (t, ³*J* = 6.0 Hz, 1H), 4.78 (d, ³*J* = 6.0 Hz, 2H), 4.65 (d, ³*J* = 6.0 Hz, 2H), 4.33 (s, 3H), 4.06 (s, 3H); **¹³C{¹H} NMR** (DMSO-*d*₆, 101 MHz, ppm): δ = 166.0, 154.7, 54.0, 52.0, 33.7, 29.6; **HR-MS** (EI, 70 eV): [C₃H₆N₄O] **calc.**: 114.0542 (M⁺); **found**: 114.0536.

Mixture of 1-methyl-4,5-Bishydroxymethyl-1,2,3-triazol and 2-methyl-4,5-bishydroxymethyl-1,2,3-triazol (**8**)

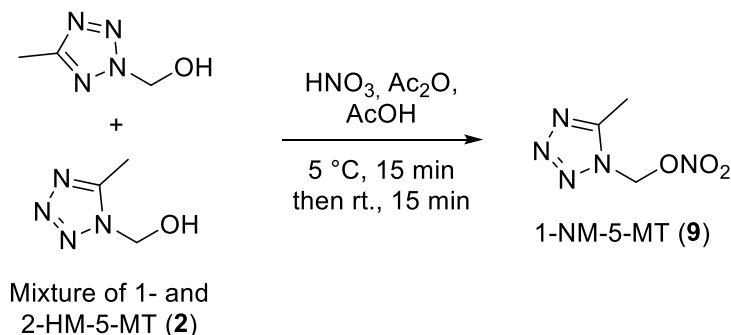


Methyl iodide (0.55 g, 0.24 mL, 3.87 mmol, 1 eq.) was added to a suspension of 4,5-bishydroxymethyl-1,2,3-triazole (**6**)^[LIT] (0.50 g, 3.87 mmol, 1 eq.) and K₂CO₃ (0.54 g, 3.87 mmol, 1 eq.) in acetone (100 mL). The mixture was stirred for 16 hours at 60 °C and after cooling down, filtrated. The solvent was evaporated under reduced pressure and the residue was taken up in a mixture of ethyl acetate (25 mL) and acetone (15 mL) and filtrated again. The residue was washed with a small amount of acetone and the solvent along with side products were removed under reduced pressure (20 mbar, 30 min, 80 °C) to provide mixture **8** as a yellow liquid (0.50 g, 3.5 mmol, 90%) that was used in the next step without separation of the isomers. Separation was investigated but could not be achieved with standard procedures.

IR (ATR): $\tilde{\nu}$ (cm⁻¹) = 3339 (s), 2955 (w), 2881 (w), 1642 (w), 1453 (w), 1320 (w), 1217 (w), 1009 (vs), 797 (m), 650 (m), 646 (m); **¹H-NMR** (DMSO-*d*₆, 400 MHz, ppm): δ = 5.28 (t, ³*J* = 5.5 Hz, 1H), 5.06 (t, ³*J* =

5.6 Hz, 2H), 5.01 (t, $^3J = 5.6$ Hz, 1H), 4.59 (d, $^3J = 5.5$ Hz, 2H), 4.52 – 4.48 (m, 6H), 4.04 (s, 3H), 3.98 (s, 3H); $^{13}\text{C}\{^1\text{H}\}$ NMR (DMSO- d_6 , 101 MHz, ppm): $\delta = 145.6, 144.8, 134.3, 54.2, 53.8, 50.7, 41.0, 34.6$; **HR-MS** (EI, 70 eV): $[\text{C}_5\text{H}_9\text{N}_2\text{O}_2]$ **calc.**: 125.0589 (M – H $_2\text{O}$) $^+$; **found**: 125.0583.

1-Nitratomethyl-5-methyltetrazol (9)



To a solution of acetic acid (1.5 mL) and acetic acid anhydride (7.5 mL), nitric acid (99%, 3 mL) was added dropwise at 5-10 °C. The mixture **2** (768 mg, 8.76 mmol) was then added to the acetyl nitrate solution maintaining the temperature at 0-5 °C (The gas evolution is believed to be associated with the decomposition of the 2-isomer). After the gas evolution has slowed down and the alcohol has gone into solution, the mixture was poured on ice (50 g). The diluted acid was neutralized with sodium bicarbonate and extracted with ethyl acetate (3 x 30 mL) The combined organic layers were washed with brine, dried over sodium sulfate and evaporated at ambient conditions to yield **9** (320 mg, 2.01 mmol, 23%)

BAM drop hammer: 3 J (<500 μm); **Friction tester:** 96 N (<500 μm); **DTA** (5 ° min^{-1}) = 69 °C (endo.), 159 °C (exo.); IR (ATR) $\tilde{\nu}$ (cm^{-1}) = 3045(w), 2943(w), 1664 (vs), 1536 (s), 1375 (s), 1296 (vs), 1278 (s), 1172 (m), 1087 (m), 962 (vs), 835 (vs), 780 (vs), 745 (s), 708 (s), 636 (vs), 592 (s), 426 (m); **Elem. Anal.** ($\text{C}_3\text{H}_5\text{N}_5\text{O}_3$, 159.11 g mol^{-1}): **calc.**: C 22.65, N 44.02, H 3.17; **found**: C 23.20, N 43.49, H 2.98; ^1H NMR (DMSO- d_6 , 400 MHz, ppm) $\delta = 6.81$ (s, 2H), 2.61 (s, 3H); $^{13}\text{C}\{^1\text{H}\}$ NMR (DMSO- d_6 , 101 MHz, ppm) $\delta = 153.8, 73.2, 8.3$; ^{14}N NMR (DMSO- d_6 , 29 MHz, ppm) $\delta = -50$; **HR-MS** (EI) m/z : $[\text{C}_3\text{H}_5\text{N}_5\text{O}_3]$ **calc.**: 160.04651 (M $^+$); **found**: not found.

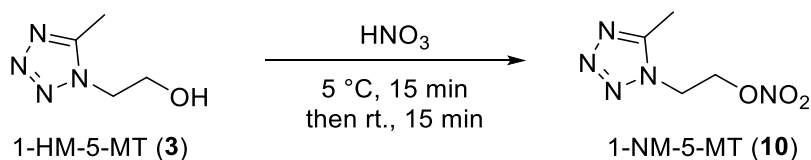
1-Nitrateoethyl-5-methyltetrazole (10) and 2-Nitrateoethyl-5-methyltetrazole (11)

General procedure for nitration:

To 5 °C cold nitric acid (99%, 1 mL/mmol of alcohol) was added alcohol **3** or **4**. The solution was stirred for 15 min and then allowed to warm to room temperature. After 15 min the reaction mixture was poured on ice (20 g/mmol of alcohol). The diluted acid was neutralized with sodium carbonate and the

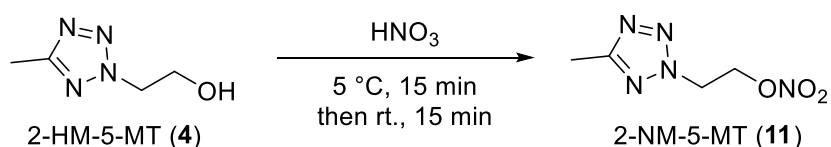
product was extracted with ethyl acetate (3 x 10 mL/mmol of alcohol). The combined organic layers were washed with brine, dried over sodium sulfate and evaporated at ambient conditions to yield **10** as colorless solid and **11** as colorless oil.

1-Nitratoethyl-5-methyltetrazole (10) (0.59 g, 3.41 mmol, 87%) from alcohol **3** (0.50 g, 3.93 mmol) and HNO₃ (4 mL):



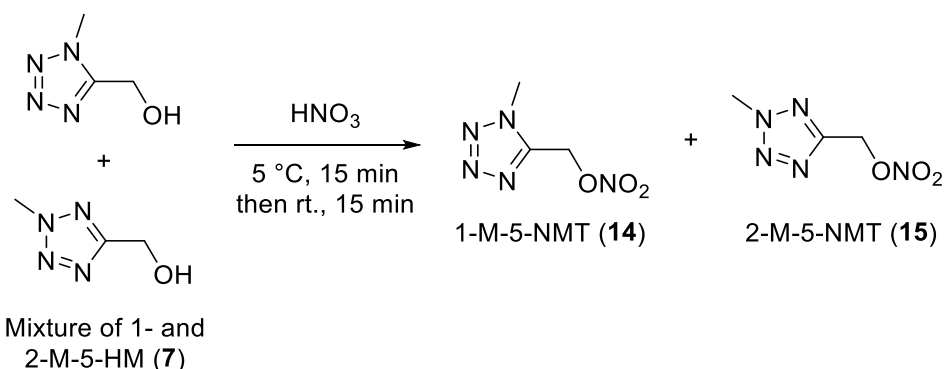
BAM drop hammer: >40 J (<500 μm); **Friction tester:** >360 N (<500 μm); **DTA** (5 ° min⁻¹) = 110 °C (endo.), 190 °C (exo.); **IR** (ATR) $\tilde{\nu}$ (cm⁻¹) = 3025(w), 2986(w), 2915(w), 1635 (vs), 1529 (m), 1440 (m), 1409 (w), 1393 (m), 1386 (m), 1367 (m), 1284 (vs), 1261 (vs), 1099 (m), 1030(vs), 986 (m), 887 (s), 857 (s), 755 (vs), 714 (s), 707 (s), 695 (m), 654 (s), 572 (m), 486 (m); **Elem. Anal.** (C₄H₇N₅O₃, 173.13 g mol⁻¹) calcd.: C 27.75, N 40.45, H 4.08; found: C 27.81, N 40.30, H 3.97; ¹H NMR (DMSO-*d*₆, 400 MHz, ppm) δ = 4.94 (dd, ³J = 5.7, 4.3 Hz, 2H), 4.78 (dd, ³J = 5.7, 4.3 Hz, 2H), 2.54 (s, 3H); ¹³C{¹H} NMR (DMSO-*d*₆, 101 MHz, ppm) δ = 152.6, 70.7, 43.9, 8.2; ¹⁴N NMR (DMSO-*d*₆, 29 MHz, ppm) δ = -43; **HR-MS** (EI) m/z: [C₄H₇N₅O₃] **calc.**:174.06217 (M⁺); **found:** not found.

2-Nitratoethyl-5-methyltetrazole (11) (0.64 g, 3.70 mmol, 95%) from alcohol (4) (0.50 g, 3.93 mmol) and HNO₃ (4 mL):



BAM drop hammer: >40 J (<500 μm); **Friction tester:** >360 N (<500 μm); **DTA** (5 ° min⁻¹) = 190 °C (exo.); **IR** (ATR) $\tilde{\nu}$ (cm⁻¹) = 2967(w), 2960(w), 1634 (s), 1509 (m), 1432 (w), 1382 (w), 1277 (vs), 1199 (w), 1169 (w), 1070 (w), 1031(m), 888 (s), 841 (s), 755 (m), 743 (m), 715 (m), 706 (m), 694 (m), 671 (w), 654 (m), 610 (w), 567 (w), 489 (m), 485 (m), 469 (w), 460 (w), 425 (w), 412 (w), 407 (w); **Elem. Anal.** (C₄H₇N₅O₃, 173.13 g mol⁻¹) calcd.: 27.75, N 40.45, H 4.08; found: C 27.89, N 39.98, H 3.95; ¹H NMR (DMSO-*d*₆, 400 MHz, ppm) δ = 5.08 – 4.98 (m, 4H), 2.47(s, 3H); ¹³C{¹H} NMR (DMSO-*d*₆, 101 MHz, ppm) δ = 162.6, 70.3, 49.8, 10.4; ¹⁴N NMR (DMSO-*d*₆, 29 MHz, ppm) δ = -42; **HR-MS** (EI) m/z: [C₄H₇N₅O₃] **calc.**:174.06217 (M⁺); **found:** not found.

5-Nitratomethyl-2-methyl-tetrazol (**14**) and 5-Nitratomethyl-1-methyl-tetrazol (**15**)



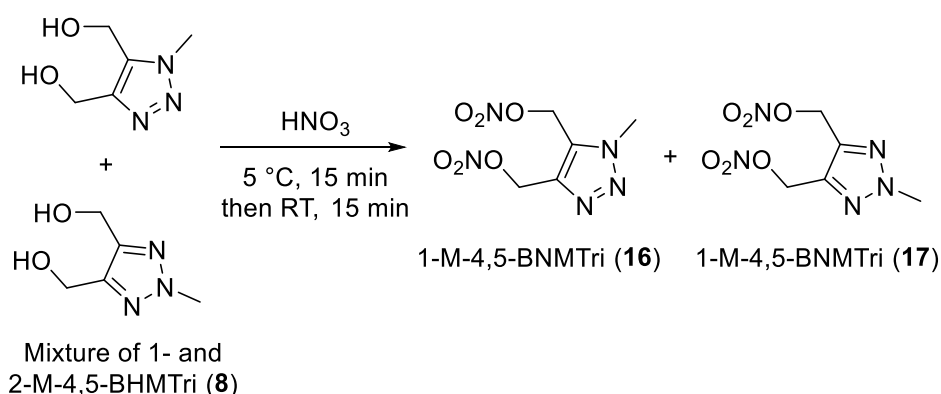
The regioisomeric mixture from the previous step (**7**) (1 g, 8.8 mmol, 1.0 eq.) was added dropwise to HNO₃ (99%, 10 mL) at 0–5 °C. The resulting mixture was stirred at this temperature for 15 min. Cooling was removed, and the mixture was stirred for 15 min before pouring it into ice-water (100 mL). The solution was extracted with ethyl acetate (3 x 50 mL) and the combined extracts were neutralized with sat. aq. NaHCO₃. The organic phase was dried over anhydrous Na₂SO₄, filtrated and the solvent was removed under reduced pressure. The resulting crude was then purified via flash column chromatography (*i*-Hexane/EtOAc, 6:4) to provide both isomers as liquids. The first isomer to elute spontaneously crystallized after three weeks to obtain **15** as a white solid (429 mg, 2.7 mmol, 30%). The second isomer to elute was dissolved in a mixture of acetone and water (1:1) and stored at 3 °C for 3 days to obtain **14** as colourless needle-like crystals (360 mg, 2.3 mmol, 26%).

5-Nitratomethyl-1-methyl-tetrazol (14**): BAM drop hammer: >40 J (<500 μm); Friction tester: >360 N (<500 μm); DTA (5 °C min⁻¹): 60 °C (endo.), 174 °C (exo.); IR (ATR): $\tilde{\nu}$ (cm⁻¹) = 3023 (w), 1652 (vs), 1534 (w), 1478 (m), 1440 (m), 1428 (m), 1356 (m), 1290 (vs), 1264 (s), 1238 (w), 1205 (w), 1100 (m), 1047 (w), 1020 (m), 994 (m), 950 (s), 846 (vs), 792 (s), 748 (s), 724 (m), 712 (s), 672 (s), 646 (vs), 610 (w), 594 (m); Elem. Anal. (C₃H₅N₅O₃, 159.11 g mol⁻¹): calc.: C 22.65, N 44.02, H 3.17%; found: C 22.75, N 43.76, H 3.09%; ¹H-NMR (DMSO-*d*₆, 400 MHz, ppm): δ = 5.99 (s, 2H), 4.12 (s, 3H); ¹³C{¹H} NMR (DMSO-*d*₆, 101 MHz, ppm): δ = 149.5, 62.2, 34.0; ¹⁴N-NMR (DMSO-*d*₆, 29 MHz, ppm): δ = -41.2; HR-MS (ESI, 70 eV): [C₃H₄N₅O₃] calc.: 158.0314 (M-H⁺); found: 158.0307.**

5-Nitratomethyl-2-methyl-tetrazol (15**): BAM drop hammer: 40 J (liquid); Friction tester: 360 N (liquid); BAM drop hammer: 30 J (<500 μm); Friction tester: 60 N (<500 μm); DTA (5 °C min⁻¹): 24 °C (endo.), 185 °C (exo.); IR (ATR): $\tilde{\nu}$ (cm⁻¹) = 3260 (w), 2908 (w), 1642 (s), 1632 (s), 1515 (w), 1453 (m), 1447 (m), 1410 (m), 1374 (w), 1280 (s), 1218 (m), 1199 (m), 1043 (m), 994 (s), 985 (m), 870 (s), 837 (s), 752 (vs), 704 (m), 651 (m), 583 (s); Elem. Anal. (C₃H₅N₅O₃, 159.11 g mol⁻¹): calc.: C 22.65, N 44.02, H 3.17%; found: C 22.86, N 43.82, H 2.88%; ¹H-NMR (DMSO-*d*₆, 400 MHz, ppm): δ = 5.91 (s, 2H), 4.40 (s,**

3H); $^{13}\text{C}\{^1\text{H}\}$ NMR (DMSO- d_6 , 101 MHz, ppm): δ = 159.6, 64.8, 39.8; ^{14}N -NMR (DMSO- d_6 , 29 MHz, ppm): δ = -39.8, -96.5; **HR-MS** (ESI, 70 eV): $[\text{C}_3\text{H}_5\text{N}_5\text{O}_3]$ **calc.**: 160.04652 (M+H $^+$); **found**: 160.04669.

1-methyl-4,5-Bisnitratomethyl-1,2,3-triazol (16) and 2-methyl-4,5-bisnitratomethyl-1,2,3-triazol (17)



The regioisomeric mixture from the previous step (**8**) (500 mg, 3.5 mmol, 1.0 eq.) was added dropwise to HNO_3 (100%, 8 mL) at 0–5 °C. The resulting mixture was stirred at this temperature for 15 min. The cooling-bath was removed, and the mixture was stirred for a further 15 min at RT before pouring it into ice water (50 mL). The solution was extracted with ethyl acetate (3 x 50 mL) and the combined extracts were neutralized with sat. aq. NaHCO_3 . The organic phase was dried over anhydrous Na_2SO_4 , filtrated and the solvent was removed under reduced pressure. The resulting crude was then purified via flash column chromatography (*i*-Hexane/EtOAc, 6:4) to provide first **17** (351 mg, 1.5 mmol, 43%) as a yellowish solid then **16** (347 mg, 1.5 mmol, 43%) as a viscous yellow oil.

4,5-Bisnitratomethyl-1-methyl-1,2,3-triazol (16): BAM drop hammer: >40 J (liquid); **Friction tester:** >360 N (liquid); **DTA** (5 °C min^{-1}): 188 °C (exo.); **IR** (ATR): $\tilde{\nu}$ (cm^{-1}) = 3015 (w), 2971 (w), 1739 (m), 1627 (vs), 1455 (w), 1435 (m), 1365 (m), 1275 (vs), 1230 (m), 1218 (m), 1036 (w), 979 (m), 925 (m), 841 (vs), 751 (s), 696 (w), 680 (w), 650 (m), 621 (m), 595 (m), 578 (w), 527 (w), 469 (w); **Elem. Anal.** ($\text{C}_5\text{H}_7\text{N}_5\text{O}_6$, 233.14 g mol^{-1}): **calc.**: C 25.76, N 30.04, H 3.03%; **found**: C 26.11, N 29.54, H 3.19%; ^1H -NMR (Acetone- d_6 , 400 MHz, ppm): δ = 5.95 (s, 2H), 5.78 (s, 2H), 4.21 (s, 3H); $^{13}\text{C}\{^1\text{H}\}$ NMR (Acetone- d_6 , 101 MHz, ppm): δ = 140.6, 130.4, 66.3, 62.4, 35.8; ^{14}N -NMR (Acetone- d_6 , 29 MHz, ppm): δ = -43.3, -45.5, -72.2, -142.5; **HR-MS** (EI) m/z : [M+H $^+$] Calcd for $\text{C}_5\text{H}_7\text{N}_5\text{O}_6$ 234.0469. Found: not found.

4,5-Bisnitratomethyl-2-methyl-1,2,3-triazol (17)

BAM drop hammer: >40 J (<500 μm); **Friction tester:** >360 N (<500 μm); **DTA** (5 °C min^{-1}): 37 °C (endo.), 194 °C (exo.); **IR** (ATR): $\tilde{\nu}$ (cm^{-1}) = 2971 (w), 1739 (w), 1626 (vs), 1456 (w), 1433 (w), 1365 (w), 1277 (vs), 1217 (w), 1206 (w), 980 (m), 932 (m), 841 (vs), 753 (m), 706 (w), 663 (m), 638 (m), 596 (w)

(w), 580 (w), 482 (w); **EA** ($C_5H_7N_5O_6$, $233.14 \text{ g mol}^{-1}$): **calc.**: C 25.76, N 30.04, H 3.03%; **found**: C 25.98, N 30.39, H 3.03%; **$^1\text{H-NMR}$** (Acetone- d_6 , 400 MHz, ppm): $\delta = 5.76$ (s, 4H), 4.22 (s, 3H); **$^{13}\text{C}\{^1\text{H}\}$ NMR** (Acetone- d_6 , 101 MHz, ppm): $\delta = 140.5, 65.6, 42.5$; **$^{14}\text{N-NMR}$** (Acetone- d_6 , 29 MHz, ppm): $\delta = -43.4, -71.7, -134.5$; **HR-MS** (EI) m/z: $[M+H^+]$ Calcd for $C_5H_7N_5O_6$ 234.0469. Found: 234.0441.

3. X-ray Diffraction

Crystal structure data were obtained from an Oxford Xcalibur3 diffractometer with a Spellman generator (voltage 50 kV, current 40 mA) and a Kappa CCD area for data collection using Mo- $K\alpha$ radiation ($\lambda = 0.71073 \text{ \AA}$) or a Bruker D8 Venture TXS diffractometer equipped with a multilayer monochromator, a Photon 2 detector and a rotation-anode generator (Mo- $K\alpha$ radiation). The data collection was performed using the CRYSTALIS RED software.^[S3] The solution of the structure was performed by direct methods and refined by full-matrix least-squares on F² (SHELXT)^[S4] implemented in the OLEX2^[S5] software suite. The non-hydrogen atoms were refined anisotropically and the hydrogen atoms were located and freely refined. The absorption correction was carried out by a SCALE3 ABSPACK multiscan method.^[S6] The DIAMOND2 plots shown with thermal ellipsoids at the 50% probability level and hydrogen atoms are shown as small spheres of arbitrary radius. The SADABS program embedded in the Bruker APEX3 software was used for multi-scan absorption corrections in all structures.^[S7]

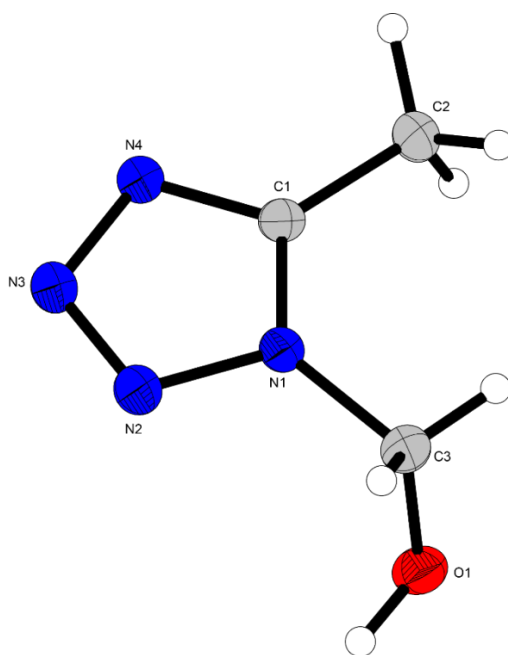


Figure S1. Representation of the molecular unit of N1-isomer of **2**, showing the atom-labeling scheme. Thermal ellipsoids represent the 50% probability level and hydrogen atoms are shown as small spheres of arbitrary radius.

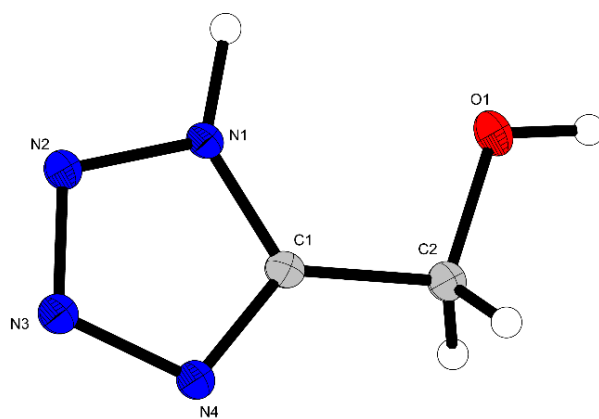


Figure S2. Representation of the molecular unit of **5**, showing the atom-labeling scheme. Thermal ellipsoids represent the 50% probability level and hydrogen atoms are shown as small spheres of arbitrary radius.

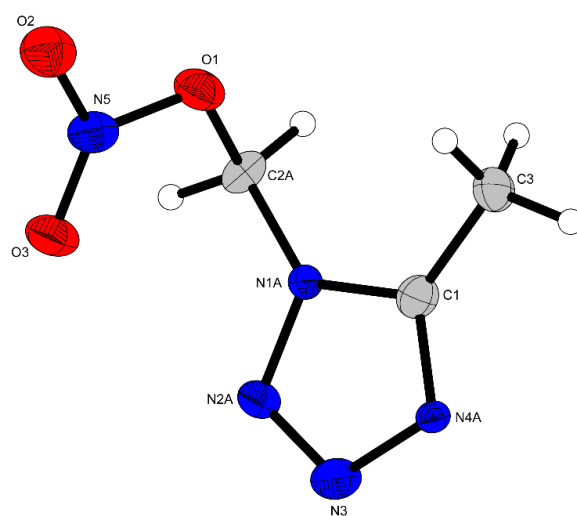


Figure S3. Representation of the molecular unit of **9**, showing the atom-labeling scheme. Thermal ellipsoids represent the 50% probability level and hydrogen atoms are shown as small spheres of arbitrary radius.

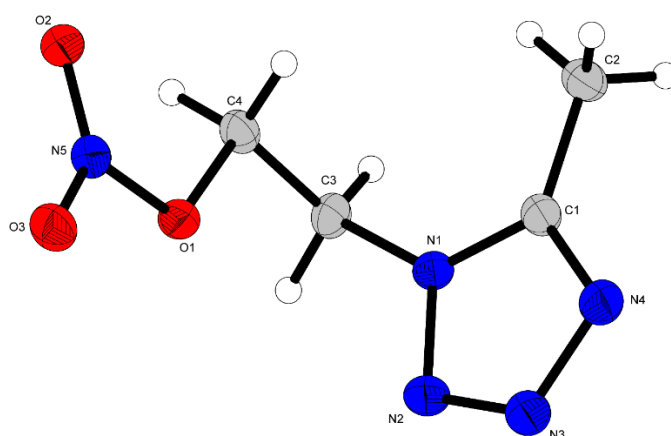


Figure S4. Representation of the molecular unit of **10**, showing the atom-labeling scheme. Thermal ellipsoids represent the 50% probability level and hydrogen atoms are shown as small spheres of arbitrary radius.

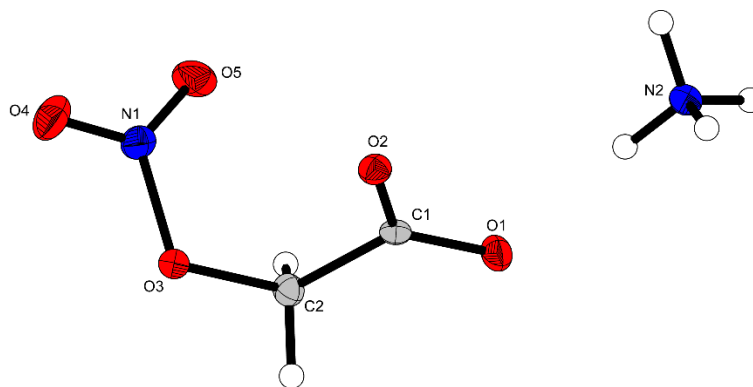


Figure S5. Representation of the molecular unit of **13**, showing the atom-labeling scheme. Thermal ellipsoids represent the 50% probability level and hydrogen atoms are shown as small spheres of arbitrary radius.

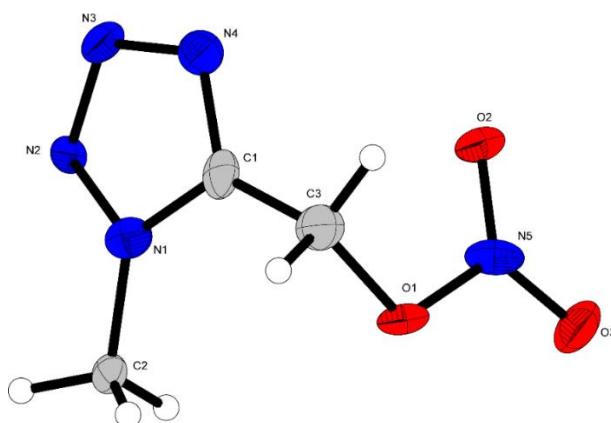


Figure S6. Representation of the molecular unit of **14**, showing the atom-labeling scheme. Thermal ellipsoids represent the 50% probability level and hydrogen atoms are shown as small spheres of arbitrary radius.

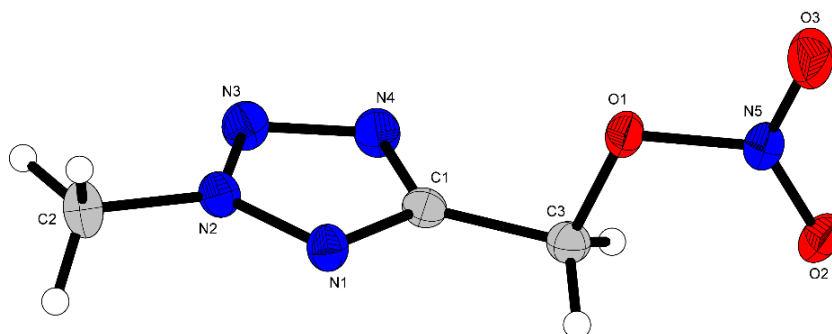


Figure S7. Representation of the molecular unit of **15**, showing the atom-labeling scheme. Thermal ellipsoids represent the 50% probability level and hydrogen atoms are shown as small spheres of arbitrary radius.

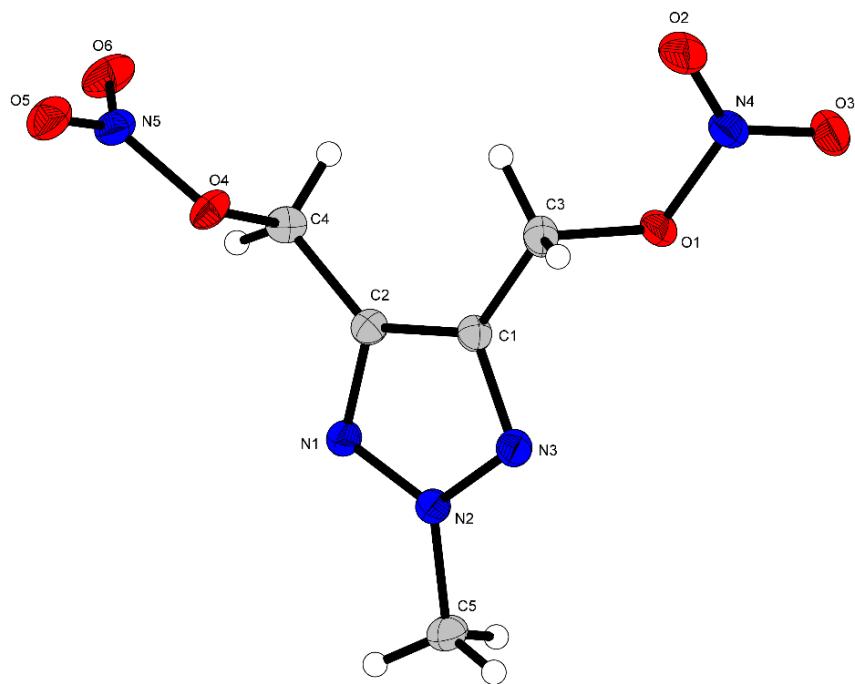


Figure S8. Representation of the molecular unit of **17**, showing the atom-labeling scheme. Thermal ellipsoids represent the 50% probability level and hydrogen atoms are shown as small spheres of arbitrary radius.

Table S1. Crystallographic data of **2**, **5** and **9**.

	N1-isomer of 2	5	9
Formula	C ₃ H ₆ N ₄ O	C ₂ H ₄ N ₄ O	C ₃ H ₅ N ₅ O ₃
FW [g mol ⁻¹]	114.12	100.09	159.12
Crystal system	monoclinic	monoclinic	orthorhombic
Space group	<i>P2₁/c</i> (No. 14)	<i>P2₁/m</i> (No. 11)	<i>P2₁2₁2₁</i> (No. 19)
Color / Habit	colorless block	colorless block	colorless block
Size [mm]	0.20 x 0.50 x 0.50	0.50 x 0.50 x 0.50	0.20 x 0.20 x 0.50
a [Å]	6.4666(9)	4.9015(5)	6.3563(5)
b [Å]	12.6689(11)	6.3166(7)	6.5645(8)
c [Å]	7.1836(11)	6.7767(5)	15.6756(14)
α [°]	90	90	
β [°]	116.420(18)	105.217(7)	
γ [°]	90	90	
V [Å ³]	527.05(14)	202.46(3)	654.08(11)
Z	4	2	4
ρ _{calc.} [g cm ⁻³]	1.438	1.642	1.616
μ [mm ⁻¹]	0.113	0.135	0.143
F(000)	240	104	328
λ _{MoKα} [Å]	0.71073	0.71073	0.71073
T [K]	123	298	123
θ Min-Max [°]	3.2, 26.4	3.1, 26.4	3.4, 26.4
Dataset	-8: 8 ; -15: 15 ; -8: 8	-6: 6 ; -7: 7 ; -8: 8	-7: 7 ; -7: 8 ; -19: 18
Reflections collected	4952	1805	5351
Independent refl.	1069	447	1329
<i>R</i> _{int}	0.030	0.024	0.056
Observed reflections	883	409	1011
Parameters	97	53	139
<i>R</i> ₁ (obs) ^[a]	0.0381	0.0345	0.0498
w <i>R</i> ₂ (all data) ^[b]	0.1042	0.0940	0.1232
<i>S</i> ^[c]	1.05	1.05	1.05
Resd. dens [e Å ⁻³]	-0.15, 0.27	-0.27, 0.22	-0.18, 0.24
Device type	Oxford Xcalibur3	Oxford Xcalibur3	Oxford Xcalibur3
Solution	SHELXT	SHELXT	SHELXT
Refinement	SHELXL-2018	SHELXL-2018	SHELXL-2018
Absorption correction	multi-scan	multi-scan	multi-scan
CCDC	2302431	2302432	2302435

^[a] $R_1 = \sum ||F_o| - |F_c|| / \sum |F_o|$; ^[b] $wR_2 = [\sum [w(F_o^2 - F_c^2)^2] / \sum [w(F_o^2)]]^{1/2}$; $w = [\sigma^2(F_o^2) + (xP)^2 + yP]^{-1}$ and $P = (F_o^2 + 2F_c^2) / 3$;
^[c] $S = (\sum [w(F_o^2 - F_c^2)^2] / (n-p))^{1/2}$ (n = number of reflections; p = total number of parameters).

Table S2. Crystallographic data of **10** and **13**.

	10	13
Formula	C ₄ H ₇ N ₅ O ₃	C ₂ H ₂ NO ₅ , H ₄ N
FW [g mol ⁻¹]	173.15	138.09
Crystal system	monoclinic	monoclinic
Space group	P2 ₁ /n (No. 14)	P21/c (No. 14)
Color / Habit	colorless plate	colorless block
Size [mm]	0.05 x 0.40 x 0.50	0.45 x 0.50 x 0.50
a [Å]	8.9042(11)	6.2146(9)
b [Å]	6.3518(6)	10.6148(11)
c [Å]	12.8406(11)	8.6722(11)
α [°]	90	90
β [°]	94.749(10)	105.274(14)
γ [°]	90	90
V [Å ³]	723.74(13)	551.87(13)
Z	4	4
ρ _{calc.} [g cm ⁻³]	1.589	1.662
μ [mm ⁻¹]	0.136	0.166
F(000)	360	288
λ _{MoKα} [Å]	0.71073	0.71073
T [K]	123	100
θ Min-Max [°]	2.7, 29.1	3.1, 26.4
Dataset	-11: 4 ; -8: 8 ; -16: 17	-5: 7 ; -13: 7 ; -10: 10
Reflections collected	2662	1960
Independent refl.	1637	1115
R _{int}	0.026	0.013
Observed reflections	1117	967
Parameters	137	106
R ₁ (obs) ^[a]	0.0607	0.0323
wR ₂ (all data) ^[b]	0.1915	0.0874
S ^[c]	1.07	1.08
Resd. dens [e Å ⁻³]	-0.52, 0.37	-0.28, 0.18
Device type	Oxford Xcalibur3	Oxford Xcalibur3
Solution	SHELXT	SHELXT
Refinement	SHELXL-2018	SHELXL-2018
Absorption correction	multi-scan	multi-scan
CCDC	2302433	2302430

^[a]R₁ = Σ ||F_o| - |F_c| | / Σ |F_o| ; ^[b]wR₂ = [Σ[w(F_o² - F_c²)²] / Σ[w(F_o)²]^{1/2}; w = [σ²(F_o²) + (xP)² + yP]⁻¹ and P = (F_o² + 2F_c²) / 3; ^[c]S = (Σ[w(F_o² - F_c²)²] / (n - p))^{1/2} (n = number of reflections; p = total number of parameters).

Table S3. Crystallographic data of **15** and **17**.

	15	17
Formula	C ₃ H ₅ N ₅ O ₃	C ₅ H ₇ N ₅ O ₆
FW [g mol ⁻¹]	159.12	233.16
Crystal system	monoclinic	orthorhombic
Space group	<i>P2₁/c</i> (No. 14)	<i>Pna2₁</i> (No. 33)
Color / Habit	colorless plate	colorless block
Size [mm]	0.10 x 0.13 x 0.17	0.25 x 0.40 x 0.50
a [Å]	10.2742(13)	5.7086(4)
b [Å]	8.1612(10)	19.2355(12)
c [Å]	8.2762(10)	8.5454(5)
α [°]	90	
β [°]	104.893(4)	
γ [°]	90	
V [Å ³]	670.65(14)	938.35(10)
Z	4	4
ρ _{calc.} [g cm ⁻³]	1.576	1.650
μ [mm ⁻¹]	0.139	0.151
F(000)	328	480
λ _{MoKα} [Å]	0.71073	0.71073
T [K]	173	101
θ Min-Max [°]	3.2, 27.2	2.1, 32.7
Dataset	-13: 13 ; -10: 10 ; -10: 10	-8: 8 ; -29: 18 ; -12: 12
Reflections collected	11314	10352
Independent refl.	1489	3050
<i>R</i> _{int}	0.052	0.040
Observed reflections	1338	2408
Parameters	120	174
<i>R</i> ₁ (obs) ^[a]	0.0372	0.0467
w <i>R</i> ₂ (all data) ^[b]	0.0977	0.0928
<i>S</i> ^[c]	1.15	1.07
Resd. dens [e Å ⁻³]	-0.23, 0.23	-0.24, 0.24
Device type	Bruker D8 Venture	Oxford Xcalibur3
Solution	TXS	SHELXT
Refinement	SIR-92	SHELXL-2018
Absorption correction	multi-scan	multi-scan
CCDC	2302436	2302434

^[a] $R_1 = \sum ||F_o| - |F_c| | / \sum |F_o|$; ^[b] $wR_2 = [\sum [w(F_o^2 - F_c^2)^2] / \sum [w(F_o^2)^2]]^{1/2}$; $w = [\sigma^2(F_o^2) + (xP)^2 + yP]^{-1}$ and $P = (F_o^2 + 2F_c^2) / 3$;
^[c] $S = (\sum [w(F_o^2 - F_c^2)^2] / (n-p))^{1/2}$ (n = number of reflections; p = total number of parameters).

4. Thermal analysis

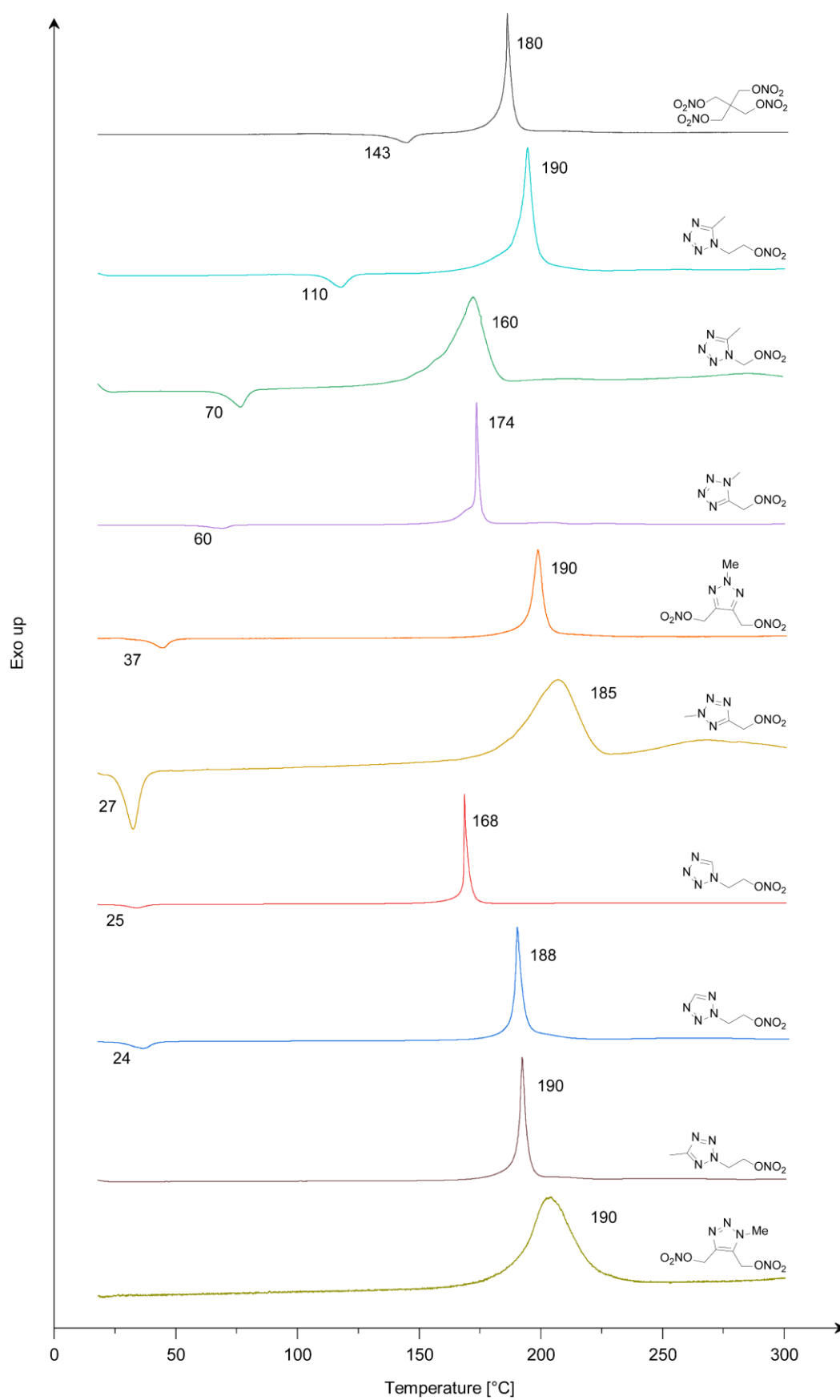


Figure S9. DTA plots of compounds of selected nitrates.

5. Computation

Heat of Formation Computation

All quantum chemical calculations were carried out using the Gaussian G09 program package.^[S8] The enthalpies (H) and free energies (G) were calculated using the complete basis set (CBS) method of Petersson and co-workers to obtain very accurate energies. The CBS models are using the known asymptotic convergence of pair natural orbital expressions to extrapolate from calculations using a finite basis set to the estimated CBS limit. CBS-4 starts with an HF/3-21G(d) geometry optimization; the zero-point energy is computed at the same level. It then uses a large basis set SCF calculation as a base energy, and an MP2/6-31+G calculation with a CBS extrapolation to correct the energy through second order. A MP4(SDQ)/6-31+ (d,p) calculation is used to approximate higher order contributions. In this study, we applied the modified CBS-4M.

Heats of formation of the synthesized ionic compounds were calculated using the atomization method (equation E1) using room temperature CBS-4M enthalpies, which are summarized in Table 4.^[S9, S10]

$$\Delta_f H^\circ_{(g, M, 298)} = H_{(Molecule, 298)} - \sum H^\circ_{(Atoms, 298)} + \sum \Delta_f H^\circ_{(Atoms, 298)} \quad (E1)$$

Table S4. CBS-4M electronic enthalpies for atoms C, H, N and O and their literature values for atomic $\Delta_f H^\circ_{298} / \text{kJ mol}^{-1}$

	$-H^{298}$ [a.u.]	NIST ^[S11]
H	0.500991	218.2
C	37.786156	717.2
N	54.522462	473.1
O	74.991202	249.5

For neutral compounds the sublimation enthalpy, which is needed to convert the gas phase enthalpy of formation to the solid state one, was calculated by the *Trouton* rule.^[S12] For ionic compounds, the lattice energy (U_L) and lattice enthalpy (ΔH_L) were calculated from the corresponding X-ray molecular volumes according to the equations provided by *Jenkins* and *Glasser*.^[S13] With the calculated lattice enthalpy the gas-phase enthalpy of formation was converted into the solid state (standard conditions) enthalpy of formation. These molar standard enthalpies of formation (ΔH_m) were used to calculate the molar solid-state energies of formation (ΔU_m) according to equation E2.

$$\Delta U_m = \Delta H_m - \Delta n RT \quad (E2)$$

(Δn being the change of moles of gaseous components)

The calculation results are summarized in Table S5.

Table S5. Calculation results.

	$-H^{298}$ ^[a] [a.u.]	$\Delta_f H^\circ(g)(M)$ [kJ mol ⁻¹] ^[b]	$\Delta_f H^\circ(s)$ ^[e] [kJ mol ⁻¹]	Δn ^[f]	$\Delta_f U(s)$ ^[g] [kJ kg ⁻¹]
1-NET	-615,780788	229.8	173.7	-6.5	1193.0
2-NET	-615,790916	203,2	147.1	-6,5	1025.9
5-M-1-NMT	-615,789188	207.7	143.2	-6.5	1001.3
1-M-5-NMT	-615,787264	212.8	150.1	-6.5	1044.8
2-M-5-NMT	-615,796959	187.3	130.9	-6.5	923.8
5-M-1-NET	-655,030342	171.0	99.0	-7.5	678.9
2-M-4,5-BNMTri	-918.404869	21.1	-37.2	-9.0	63.7

^[a] CBS-4M electronic enthalpy; ^[b] gas phase enthalpy of formation; ^[c] molecular volumes taken from X-ray structures and corrected to room temperature; ^[d] lattice energy and enthalpy (calculated using Jenkins and Glasser equations); ^[e] standard solid-state enthalpy of formation; ^[f] Δn being the change of moles of gaseous components when formed; ^[g] solid state energy of formation.

The energetic performance was calculated using the explo 5 code with the version 6.04. [S14]

6. References

- [S1] a) Reichel & Partner GmbH, <http://www.reichelt-partner.de>; b) Test methods according to the UN Recommendations on the Transport of Dangerous Goods, *Manual of Test and Criteria*, fourth revised edition, United Nations Publication, New York and Geneva, **2003**, ISBN 92–1-139087–7, Sales No. E.03.VIII.2; 13.4.2 Test 3 a (ii) BAM Fallhammer.
- [S2] Demko, Z. P., Sharpless K. B., *J. Org. Chem.* **2001**, *66*, 24, 7945–7950.
- [S3] *CrysAlisPro*, Oxford Diffraction Ltd. *version 171.33.41*, **2009**.
- [S4] Sheldrick, G.M., *Acta Cryst.* **2015**, *A71*, 3–8.
- [S5] Dolomanov, O. V.; Bourhis, L. J.; Gildea, R. J.; Howard, J. A. K.; Puschmann, H., OLEX2: A complete structure solution, refinement and analysis program, *J. Appl. Cryst.* **2009**, *42*, 339–341.
- [S6] *SCALE3 ABSPACK – An Oxford Diffraction program (1.0.4, gui: 1.0.3)*, Oxford Diffraction Ltd., **2005**.
- [S7] *APEX3*. Bruker AXS Inc., Madison, Wisconsin, USA.
- [S8] Frisch, M. J.; Trucks, G. W.; Schlegel, H. B.; Scuseria, G. E.; Robb, M. A.; Cheeseman, J. R.; Scalmani, G.; Barone, V.; Petersson, G. A.; Nakatsuji, H.; Li, X.; Caricato, M.; Marenich, A. V.; Bloino, J.; Janesko, B. G.; Gomperts, R.; Mennucci, B.; Hratchian, H. P.; Ortiz, J. V.; Izmaylov, A. F.; Sonnenberg, J. L.; Williams-Young, D.; Ding, F.; Lipparini, F.; Egidi, F.; Goings, J.; Peng, B.; Petrone, A.; Henderson, T.; Ranasinghe, D.; Zakrzewski, V. G.; Gao, J.; Rega, N.; Zheng, G.; Liang, W.; Hada, M.; Ehara, M.; Toyota, K.; Fukuda, R.; Hasegawa, J.; Ishida, M.; Nakajima, T.; Honda, Y.; Kitao, O.; Nakai, H.; Vreven, T.; Throssell, K.; Montgomery, J. A., Jr.; Peralta, J. E.; Ogliaro, F.; Bearpark, M. J.; Heyd, J. J.; Brothers, E. N.; Kudin, K. N.; Staroverov, V. N.; Keith, T. A.; Kobayashi, R.; Normand, J.; Raghavachari, K.; Rendell, A. P.; Burant, J. C.; Iyengar, S. S.; Tomasi, J.; Cossi, M.; Millam, J. M.; Klene, M.; Adamo, C.; Cammi, R.; Ochterski, J. W.; Martin, R. L.; Morokuma, K.; Farkas, O.; Foresman, J. B.; Fox, D. J., *Gaussian 09 A.02*, Gaussian, Inc., Wallingford, CT, USA, **2009**.
- [S9] a) Ochterski, J. W.; Petersson, G. A.; Montgomery Jr., J. A., A complete basis set model chemistry. V. Extensions to six or more heavy atoms, *J. Chem. Phys.* **1996**, *104*, 2598–2619; b) Montgomery Jr., J. A.; Frisch, M. J.; Ochterski, J. W.; Petersson, G. A., A complete basis set model chemistry. VII. Use of the minimum population localization method, *J. Chem. Phys.* **2000**, *112*, 6532–6542.
- [S11] a) Curtiss, L. A.; Raghavachari, K.; Redfern, P. C.; Pople, J. A., Assignment of Gaussian-2 and density functional theories for the computation of enthalpies of formation, *J. Chem. Phys.* **1997**, *106*, 1063–1079; b) Byrd, E. F. C.; Rice, B. M., Improved prediction of heats of formation

- of energetic materials using quantum mechanical calculations, *J. Phys. Chem. A* **2006**, *110*, 1005–1013; c) Rice, B. M.; Pai, S. V.; Hare, J., Predicting heats of formation of energetic materials using quantum mechanical calculations, *Comb. Flame* **1999**, *118*, 445–458.
- [S12] Lindstrom, P. J.; Mallard, W. G., (Editors), NIST Standard Reference Database Number 69, <http://webbook.nist.gov/chemistry/> (accessed June **2020**).
- [S12] Westwell, M. S.; Searle, M. S.; Wales, D. J.; Williams, D. H., Empirical correlations between thermodynamic properties and intermolecular forces, *J. Am. Chem. Soc.* **1995**, *117*, 5013–5015; b) Trouton, F., IV. On molecular latent heat, *Philos. Mag.* **1884**, *18*, 54–57.
- [S13] a) Jenkins, H. D. B.; Roobottom, H. K.; Passmore, J.; Glasser, L., Relationships among ionic lattice energies, molecular (formula unit) volumes and thermochemical radii, *Inorg. Chem.* **1999**, *38*, 3609–3620; b) Jenkins, H. D. B.; Tudela, D.; Glasser, L., Lattice potential energy estimation for complex ionic salts from density measurements, *Inorg. Chem.* **2002**, *41*, 2364–2367.
- [S14] Sućeska, M., EXPLO5 V6.02 program, Brodarski Institute, Zagreb, Croatia, **2014**.

4,5-Bisnitratomethyl and Similar Representatives of the Rare Class of 2-Nitro-1,2,3-triazoles

Maximilian Benz, Sabrina Dörrich, Thomas M. Klapötke,* Tobias Lenz, Mohamed Mouzayek, and Jörg Stierstorfer



Cite This: *Org. Lett.* 2023, 25, 5974–5977



Read Online

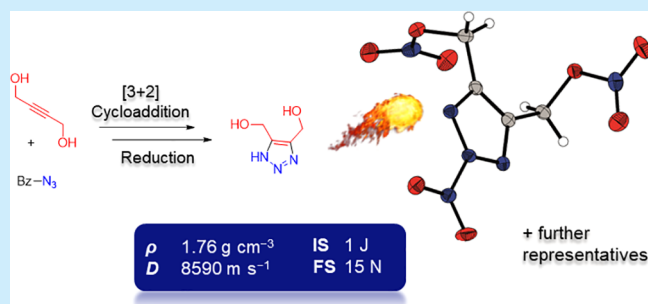
ACCESS |

Metrics & More

Article Recommendations

Supporting Information

ABSTRACT: A [3+2]-cycloaddition toward bishydroxymethyl-1,2,3-triazole makes the title compound available through selective nitration. The obtained sensitive 2-nitrotriazole was shown to have a high density of 1.764 g cm^{-3} and a detonation velocity of 8590 m s^{-1} . It can also be classified as an oxidizer with an oxygen balance toward CO of 12%. Further representatives of this rare class of 2-nitro-1,2,3-triazoles were synthesized. One- and two-dimensional ^{15}N NMR spectroscopy, crystal structure, and elemental analysis were performed.



Traditional energetic materials and their degradation products are often harmful to humans and the environment (e.g., TNT, RDX).¹ Therefore, the need for new materials with low toxicity and additional higher performance is of great interest. Newer advanced materials combine fuel and oxidizer in one molecule through C–NO₂ groups such as TNT. The latest generation now takes less energy from CO formation and more energy from ring tension and N₂ formation (TKX-50, CL-20, ONC).² Nitrogen-rich azoles are often used to achieve a high heat of formation (HOF) and therefore good energy output.³ But those azoles provide fewer opportunities for functionalization and reactions than comparable carbon backbones. The N–H group is increasingly becoming the focus of attention. At this position, alkylation, amination, or oxidation is typically performed.⁴ The less frequent N-nitration is found in pyrazoles and 1,2,4-triazoles.⁵ It can be utilized for C-nitration through rearrangement. Far fewer 1,2,3-triazoles with an N-nitro group are known (Figure 1). Among the energetic compounds are 1,4-dinitrotriazole (A) and polycyclic N-nitro 1,2,3-triazole (B).⁶ Both decompose around 40 °C, and only B is energetically characterized. Less energetic molecules including a 2-nitro-1,2,3-triazole motif are benzotriazole derivatives (C).⁷ The nitro group can also be present at the 1-position as shown for the compound class of D.^{7,8} N-nitro tetrazoles have not been isolated so far. Our group regularly observed the decomposition of acidic N-unsubstituted tetrazoles to the corresponding carboxylic acid. Although the nitro group lowers the HOF, a higher density and better oxygen balance result in an overall increase in the energetic performance.⁹ This work describes the synthesis of three high-energy 2-nitro-1,2,3-triazoles (E–G). The universal-

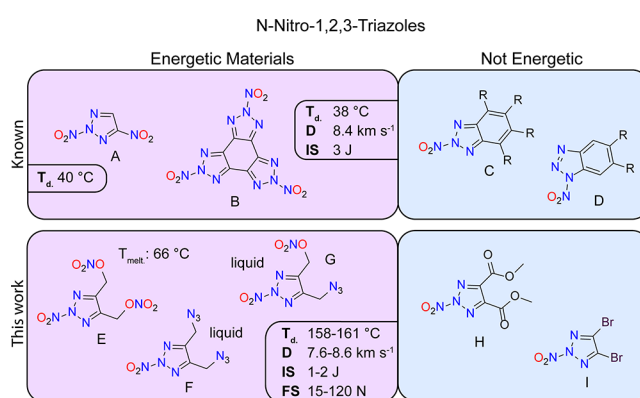


Figure 1. Overview of all known (top A^{6a}, B^{6b}, C,⁷ D^{7,8}) and newly synthesized N-nitro-1,2,3-triazoles (bottom E–I). T_d: decomposition temperature, D: detonation velocity, IS: impact sensitivity, FS: friction sensitivity.

ity of selective nitration is further supported by the syntheses of H and I (Figure 1).

As reported by Sharpless and Loren, 4,5-substituted 1,2,3-triazoles can be synthesized from propargyl halides and sodium azide through [3,3] sigmatropic shift.¹⁰ Therefore, it is not possible to gain 4,5-bishydroxymethyl-1H-1,2,3-triazole (1)

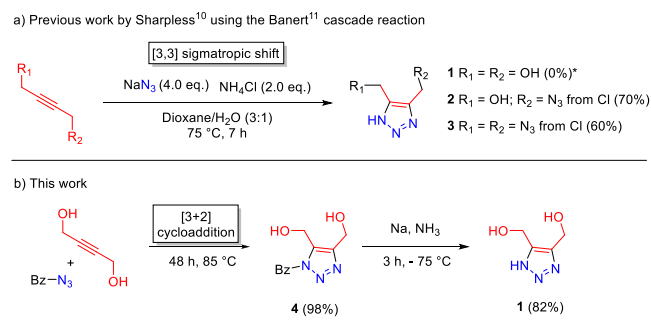
Received: June 26, 2023

Published: August 4, 2023



directly via this route. The work could be reproduced for compounds **2** and **3**. To synthesize **1**, we chose a solvent-free click reaction to synthesize 1-benzyl-protected **4** out of the corresponding alkyne and benzyl azide at 85 °C in excellent yields (Scheme 1). A slight excess of benzyl azide ensures full

Scheme 1. (a) Synthesis of 1,2,3-Triazoles through Azide Exchange As Reported by Sharpless¹⁰ and Developed by Banert;¹¹ (b) Synthetic Pathway toward **1**



conversion. Slow addition of the alkyne and exact temperature control is necessary to avoid thermal runaway. Reductive cleavage of the benzyl group of **4** was performed with sodium in liquid ammonia to give 4,5-bis(hydroxymethyl)-1*H*-1,2,3-triazole (**1**) in 82% yield. During the reaction a solid precipitated and therefore, larger amounts of solvent and adequate stirring should be provided. Palladium-catalyzed deprotection using hydrogen showed no success. The position of the azole-proton was located by crystal structure measurement (Supporting Information).

CAUTION! Compounds **5**–**9** are potentially explosive materials. Safety precautions and equipment (such as wearing a leather coat, face shield, Kevlar sleeves, Kevlar gloves, earthed equipment, and ear protection) must be used during manipulation.

Nitration of **1** using in situ generated acetyl nitrate yields 4,5-bis(nitratomethyl)-2-nitro-1,2,3-triazole (**5**) after recrystallization in very good yields. To investigate if this regioselective nitration is a general trend, energetic compounds **6** and **7** were synthesized through the nitration of **2** and **3**. Selective nitration was observed in good to very good yields. The scope was further extended to the less energetic compounds **8** and **9**, synthesized out of the corresponding 1,2,3-triazoles.¹² The regioselectivity is mainly explained by the steric hindrance of the N1 position, although electronic effects or a NO₂ shift cannot be excluded. Since the instability of N1–NO₂ compared to the N2 position is known,^{6a} decomposition in the nitrating solution might occur. Nitration of neat 1,2,3-1*H*-triazole (**10**) resulted in the decomposition to oxalic acid (Scheme 2). Compounds **5**–**9** are not long-term stable and decompose within months producing NO_x.

Single crystals of compounds **1**, **4**, **5**, **8**, and **9** were obtained by recrystallization. Measurement by low-temperature X-ray diffraction revealed the atomic and molecular structure of the compounds. The data can be found in the CSD database under the numbers 2270383–2270387.

Suitable crystals of compound **5** were obtained by recrystallization from methanol. **5** crystallizes in the monoclinic space group *P*2₁/*c* with four formula units per unit cell and a density of 1.816 g cm⁻³ at 102 K (Figure 2).

Looking at the X–NO₂ bond length, the bond for X=N with 1.429 Å is longer than that for X=O with 1.413 Å. Those bonds

Scheme 2. Selective N2 Nitration toward Triazoles **5**–**10**

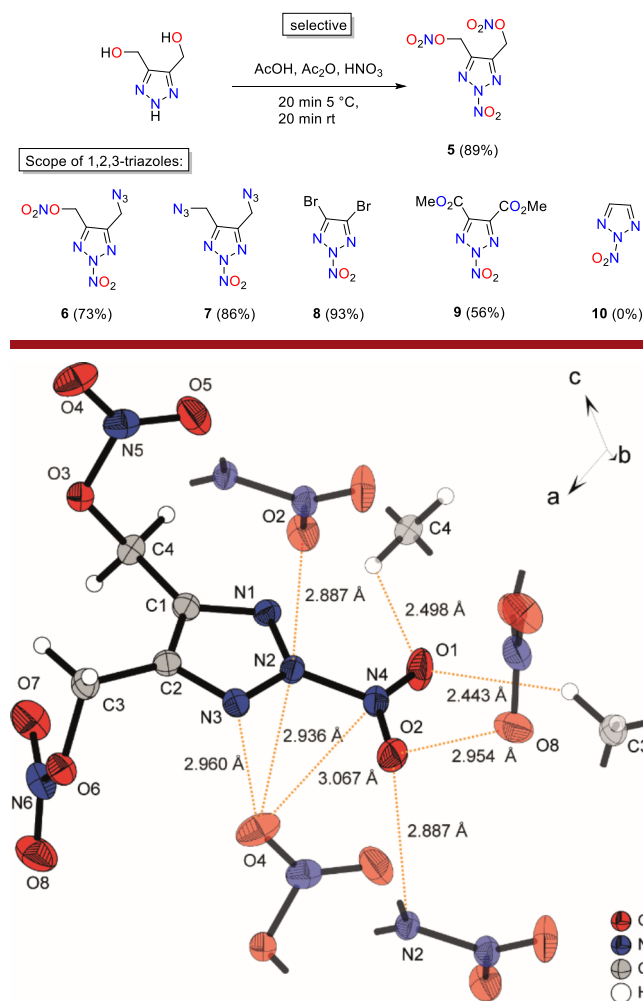


Figure 2. Molecular moiety of **5** is derived from the low-temperature crystal structure measurement. Thermal ellipsoids are drawn at the 50% probability level. Red dashed lines represent electrostatic nitro interactions.

are also longer than the X–NO₂ bonds in RDX (1.361–1.409 Å)¹³ or PETN (1.408 Å).¹⁴ The nitrate groups are twisted out of the triazole plane with torsion of 131° along N1–C1–C4–O3 and –64° along N3–C2–C3–O6. The N2 nitro group is bent out of the ring plane, showing a torsion angle along C2–N3–N2–N4 of –173° and slightly twisted along O2–N4–N2–N3 with –5°. To reveal the molecular interactions, Hirshfeld surface calculation was performed (Supporting Information). The calculation depicts atom distances between molecules that can be assigned to van der Waals interactions by their length. Overall, the molecules are rigidly fixed in all directions of space by attractive and repulsive contacts. Attractive interactions are with O–H (35%) and N–H (6%). Some are in the range of nonclassical hydrogen bonds and therefore strong. The repulsive interactions dominate the structure and are built by O–O (30%) and O–N (23%) contacts. Some of those are within the added van der Waals radii of the participating atoms (O–O: 3.04 Å; N–O: 3.07 Å) and therefore relatively strong.¹⁵

The crystalline compounds **5** and **8** are proven by X-ray crystallography. The liquid compounds **6**, **7** and solid **5** were analyzed through ¹⁵N NMR spectroscopy in advance (Figure

3). The typical shift for the N–NO₂ group is at –70 ppm, whereas the nitrate group O–NO₂ can be found at –50

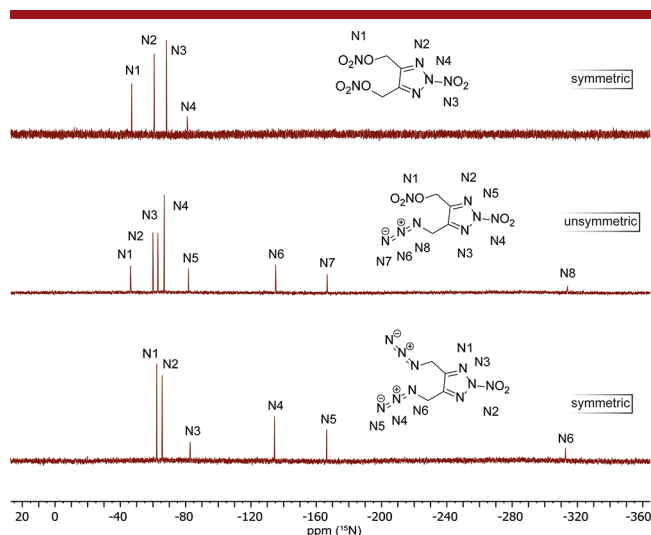


Figure 3. ¹⁵N NMR spectra of **5**, **6**, and **7** measured in acetone-*d*₆.

ppm.^{6,16} The resonances for the nitrogen atoms of the triazole can be found around –60 to –85 ppm. The atom assignment was supported by two-dimensional ¹H–¹⁵N HMBC NMR (Supporting Information). The resonances of the azido groups **6** and **7** can be found at –312–314 ppm (N_α), –134 ppm (N_β), and –166 ppm (N_γ). The symmetries in compounds **5** and **7** can be seen by the smaller number of signals.

To better understand the N–NO₂ bond, the energies of a homolytic cleavage were calculated and compared to those of the O–NO₂ bond. The dissociations were calculated on the CBS-4 M level of theory for the gas phase (Supporting Information). The homolytic dissociation energies are comparable for the two bonds, with 200.9 kJ mol^{–1} for the N–NO₂ bond and 190.7 kJ mol^{–1} for the O–NO₂ bond. This shows that the bonds are comparable stable for dissociation in the gas phase. As the N–NO₂ bond releases NO_x in **7**–**9**, it must be less stable than the O–NO₂ bond in **5** or **6**. Therefore, the authors believe that the decomposition is caused by a different mechanism like hydrolysis.

As shown in Table 1 compounds **5**, **6**, and **7** can be qualified as energetic materials due to their properties. Sensitivities were determined using BAM-standardized machines,¹⁷ and the explosive parameters were calculated with the EXPLO V6.05.04 code.¹⁸ The title compound **5** shows a high detonation velocity of 8590 m s^{–1} and pressure of 323 kbar, exceeding that of already powerful PETN. This is a consequence of the high density and positive heat of formation. Furthermore, the compound still possesses a high oxidation potential with an Ω_{CO} (oxygen balance to CO) of 12%. However, the positive properties come at the cost of a very high sensitivity. With 1 J and 15 N, the compound is in the area of primary explosives. An initiation test toward PETN showed no initiation. The compound melts at 66 °C and decomposes upon heating at about 159 °C. Storage at ambient conditions leads to color change over months.

The azido derivatives **6** and **7** show a higher heat of formation but lower densities. This is typical for organic azides and leads to an overall reduced energy output. The monoazide is moderate and the diazide is very sensitive.

Table 1. Physico-chemical Properties of **5**–**7** Compared to PETN

Formula	5	6	7	PETN ¹⁹
N [%] ^a	31.8	45.9	62.5	17.7
Ω _{CO} [%] ^b	12.1	–6.6	–28.6	15.18
T _{melt.} /T _{dec.} [°C] ^c	66/159	–/158	–/161	143/180
Density [g cm ^{–3}] ^d	1.764	1.524	1.436	1.778
Δ _f H ^o _m [kJ mol ^{–1}] ^e	90.9	536.0	964.5	–484
IS [J] ^f	1	2	1	3.5
FS [N] ^g	15	120	20	54
p _{C-J} [kbar] ^h	323	242	238	313
D [m s ^{–1}] ⁱ	8590	7850	7564	8471

^aNitrogen content. ^bOxygen balance with respect to CO. ^cMelting and decomposition onset temperature (DTA, 5 °C min^{–1}). ^dDensity from X-ray diffraction analysis recalculated to 298 K. ^eCalculated enthalpy of formation. ^fImpact sensitivity (BAM Fallhammer). ^gFriction sensitivity (BAM Friction Tester); EXPLO V6.05.04. ^hCalculated detonation pressure. ⁱCalculated detonation velocity.

In summary, the small building block, bishydroxymethyl-1,2,3-triazole (**1**), was synthesized through a click reaction of the respective diol and benzyl azide followed by subsequent reductive deprotection using sodium. Nitration yields the highly energetic bisnitratomethyl-2-nitro-triazole (**5**), one of the rarely known N-nitro triazoles. X-ray diffraction, ¹⁵N NMR, and elemental analysis prove the existence of the N–NO₂ group at the N2-position. Four other N2-nitrated triazoles were synthesized for general proof, of which two represent highly energetic materials. Compound **5** shows a high density (1.764 g cm^{–3}) and detonation velocity (8590 m s^{–1}) and is very sensitive to external stimuli (IS: 1 J, FS: 15 N).

■ ASSOCIATED CONTENT

Data Availability Statement

The data underlying this study are available in the published article and its Supporting Information.

SI Supporting Information

The Supporting Information is available free of charge at <https://pubs.acs.org/doi/10.1021/acs.orglett.3c02079>.

Experimental part, X-ray diffraction, Computation for heat of formation and bond dissociation, Hirshfeld analysis, NMR spectra and thermal analysis (PDF)

Accession Codes

CCDC 2270383–2270387 contain the supplementary crystallographic data for this paper. These data can be obtained free of charge via www.ccdc.cam.ac.uk/data_request/cif, or by emailing data_request@ccdc.cam.ac.uk, or by contacting The Cambridge Crystallographic Data Centre, 12 Union Road, Cambridge CB2 1EZ, UK; fax: +44 1223 336033.

■ AUTHOR INFORMATION

Corresponding Author

Thomas M. Klapötke – Department of Chemistry, Ludwig-Maximilian University of Munich, D-81377 Munich, Germany; orcid.org/0000-0003-3276-1157; Email: tmk@cup.uni-muenchen.de

Authors

Maximilian Benz – Department of Chemistry, Ludwig-Maximilian University of Munich, D-81377 Munich, Germany

Sabrina Dörrich – Department of Chemistry, Ludwig-Maximilian University of Munich, D-81377 Munich, Germany

Tobias Lenz – Department of Chemistry, Ludwig-Maximilian University of Munich, D-81377 Munich, Germany

Mohamed Mouzayek – Department of Chemistry, Ludwig-Maximilian University of Munich, D-81377 Munich, Germany

Jörg Stierstorfer – Department of Chemistry, Ludwig-Maximilian University of Munich, D-81377 Munich, Germany; orcid.org/0000-0002-2105-1275

Complete contact information is available at:

<https://pubs.acs.org/10.1021/acs.orglett.3c02079>

Author Contributions

Thomas M. Klapötke, Jörg Stierstorfer - Supervision, Conceptualization, Writing—review and editing. Tobias Lenz - Project administration, Conceptualization, Investigation, Writing—original draft. Maximilian Benz - Writing—review and editing. Sabrina Dörrich, Mohamed Mouzayek - Investigation.

Notes

The authors declare no competing financial interest.

ACKNOWLEDGMENTS

Financial support of this work by Ludwig-Maximilian University (LMU), the Office of Naval Research (ONR) under Grant ONR N00014-19-1-2078, and the Strategic Environmental Research and Development Program (SERDP) under contract no. W912HQ19C0033 is gratefully acknowledged. We thank Prof. Konstantin Karaghiosoff for the measurements of the nitrogen NMR spectra.

REFERENCES

- (1) (a) Blessinger, T.; D'Amico, L.; Subramaniam, R.; Brinkerhoff, C. *Toxicological Review of RDX*; U.S. Environmental Protection Agency, 2018. (b) *Technical Fact Sheet –2,4,6-Trinitrotoluene (TNT) in EPA 505-F-21–001*; U.S. Environmental Protection Agency, 2021.
- (2) (a) Brinck, T. *Green Energetic Materials*; Wiley: New York, 2014. (b) Klapötke, T. M. *Chemistry of High Energy Materials*, 6th ed.; De Gruyter: Berlin, 2022. (c) Agrawal, J. P. *High Energy Materials*; Wiley: Weinheim, 2010.
- (3) Gao, G.; Shreeve, J. M. Azole-Based Energetic Salts. *Chem. Rev.* **2011**, *111* (11), 7377–7436.
- (4) (a) Yocca, S. R.; Zeller, M.; Byrd, E. F. C.; Piercey, D. G. 1,5-Diaminotetrazole-4N-oxide (SYX-9). *J. Mater. Chem. A* **2022**, *10* (4), 1876–1884. (b) Chavez, D. E.; Parrish, D. A.; Mitchell, L.; Imler, G. H. Azido and Tetrazolo 1,2,4,5-Tetrazine N-Oxides. *Angew. Chem., Int. Ed.* **2017**, *56* (13), 3575. (c) Larin, A. A.; Fershtat, L. L. Energetic heterocyclic N-oxides. *Mendeleev Commun.* **2022**, *32* (6), 703–713. (d) Benz, M.; Klapötke, T. M.; Lenz, T.; Stierstorfer, J. Tuning the Properties of 5-Azido and 5-Nitramino-tetrazoles. *Chem. Eur. J.* **2022**, *28* (36), No. e202200772.
- (5) (a) Janssen, J. W. A. M.; Koeners, H. J.; Kruse, C. G.; Habrakern, C. L. Pyrazoles XII. *J. Org. Chem.* **1973**, *38* (10), 1777–1782. (b) Yin, P.; Shreeve, J. M. From N-Nitro to N-Nitroamino. *Angew. Chem., Int. Ed.* **2015**, *54* (48), 14513–14517. (c) Tang, Y.; Shreeve, J. M. Nitroxy/Azido-Functionalized Triazoles as Potential Energetic Plasticizers. *Chem. Eur. J.* **2015**, *21* (19), 7285–7291.
- (6) (a) Baryshnikov, A. T.; Erashko, V. I.; Zubanova, N. I.; Ugrak, B. I.; Shevelev, S. A.; Fainzil'berg, A. A.; Laikhter, A. L.; Mel'nikova, L. G.; Semenov, V. V. Gem-Dinitro Compounds in Organic Synthesis. 3. Synthesis of 4-Nitro-1,2,3-Triazoles from Gem-Dinitro Compounds. *Russ. Chem. Bull.* **1992**, *41*, 751–757. (b) Thottempudi, V.; Forohor, F.; Parrish, D. A.; Shreeve, J. M. Tris(triazolo)benzene and Its Derivatives: High-Density Energetic Materials. *Angew. Chem., Int. Ed.* **2012**, *51*, 9881–9885.
- (7) Cohen-Fernandes, P.; Habracken, C. L. On the Nitro Group Transfer from 2-Nitro-4,5,6,7-tetrachloro-2H-benzotriazole and 2-Nitro-2H-phenantro[9,10-d] triazole to Secondary Amines. *J. Heterocyclic Chem.* **1987**, *24*, 1653.
- (8) Zhao, J.-P.; Ding, L. J.; Wang, P.-C.; Liu, Y.; Huang, M.-J.; Zhou, X.-L.; Lu, M. Electrochemical Nonacidic N-Nitrosation/N-Nitration of Secondary Amines through a Biradical Coupling Reaction. *Adv. Synth. Catal.* **2020**, *362*, 5036.
- (9) Chapman, R. D.; Wilson, W. S.; Fronaberger, J. W.; Merwin, L. H.; Ostrom, G. S. Prospects of fused polycyclic nitroazines as thermally insensitive energetic materials. *Thermochem. Acta* **2002**, *384*, 229–243.
- (10) Loren, J. C.; Sharpless, K. B. The Banert Cascade: A Synthetic Sequence to Polyfunctional NH-1,2,3-Triazoles. *Synthesis* **2005**, *9*, 1514–1520.
- (11) (a) Banert, K. Azidobutarien and Azidobutenine. *Chem. Ber.* **1989**, *122*, 1175–1178. (b) Banert, K. Synthesis of 1,2,3-Triazoles from Propargyl Azides by Rearrangement of the Azido Group. – Indication of Short-Lived Allenyl Azides and Triazafulvenes. *Chem. Ber.* **1989**, *122*, 911–918.
- (12) (a) Albrecht, B. K.; Gehling, V. S.; Hewitt, M. C.; Taylor, A. M.; Harmange, J. C. *Bromodomain inhibitors and uses thereof*. Patent WO2012151512 A2, 2012. (b) McDonald, A.; Quian, S. *Therapeutic inhibitory compounds*. Patent WO2018011628 A1, 2018.
- (13) Hakey, P.; Oullette, W.; Zubieta, J.; Korter, T. Redetermination of cyclo-trimethylenetrinitramine. *Acta Crystallogr.* **2008**, *64*, o1428.
- (14) Nieger, M.; Lehmann, J. *CCDC Experimental Crystal Structure Determination* **2003**, 199339.
- (15) (a) Rowland, R. S.; Taylor, R. Intermolecular Nonbonded Contact Distances in Organic Crystal Structures: Comparison with Distances Expected from van der Waals Radii. *J. Phys. Chem.* **1996**, *100* (18), 7384–7391. (b) Mantina, M.; Chamberlin, A. C.; Valero, R.; Cramer, C. J.; Truhlar, D. G. Consistent van der Waals Radii for the Whole Main Group. *J. Phys. Chem. A* **2009**, *113* (19), 5806–5812.
- (16) Benz, M.; Klapötke, T. M.; Kölbl, N.; Kuch, J.; Lenz, T.; Parigi, E.; Stierstorfer, J. Melt Castable Derivatives of Pentaerythritol Tetranitrate. *Chem. Eur. J.* **2023**, *29*, No. e202204013.
- (17) *United Nations Recommendations on the Transport of Dangerous Goods; Manual of Tests and Criteria*; UN: Geneva, 2015.
- (18) Sućeska, M. *EXPLOS V6.04 program*; Brodarski Institute: Zagreb, Croatia, 2020.
- (19) Klapötke, T. M. *Energetic Materials Encyclopedia*, 2nd ed.; De Gruyter, 2021.

Supporting Information

4,5-Bisnitratomethyl and Similar Representatives of the Rare Class of 2-Nitro-1,2,3-triazoles

Maximilian Benz, Sabrina Dörrich, Thomas M. Klapötke*, Tobias Lenz, Mohamed Mouzayek,
Jörg Stierstorfer

*Corresponding Author: Prof. Dr. Thomas M. Klapötke; Department of Chemistry,
Ludwig-Maximilian University of Munich; Butenandtstr. 5-13(D), D-81377
Munich, Germany; tmk@cup.uni-muenchen.de*

Supplementary Information

Table of Contents

1.	General Considerations	S3
2.	Experimental Part	S4
2.	X-ray Diffraction	S6
3.	Differential Thermal Analysis	S12
4.	Computation	S13
5.	Hirshfeld	S16
6.	NMR Spectroscopy	S17
7.	References	S25

1. General Considerations

Starting materials were purchased from commercial suppliers (ABCR, Acros Organics, AppliChem, Sigma-Aldrich, VWR) and used without further purification. The nitric acid is 99% pure and white fuming. Stirring was performed by a magnetic stir bar if not stated differently. Heating was performed by a heating plate equipped with an oil bath and thermometer. Cooling was performed with an ice water mixture for 5-10 °C and an acetone dry ice combination for -70 °C.

¹H, ¹³C, ¹⁴N, and ¹⁵N NMR spectra were recorded on BRUKER AMX 400 instruments. Samples are placed in regular glass NMR tubes (Ø 5 mm) and measured at 25 °C. Chemical shifts are referenced with respect to tetramethylsilane (1H/13C) and nitromethane (14N/15N). Infrared spectra (IR) were recorded in the region 4000-400 cm⁻¹ on a PERKIN ELMER Spectrum BX-59343 instrument with a SMITHS DETECTION DuraSampl IR II Diamond ATR sensor. The absorption bands are reported in wavenumbers (cm⁻¹). Electrospray ionization (ESI) measurements were performed on a Thermo Finnigan LTQ FT Ultra Fourier Transform ion cyclotron resonance mass spectrometer. The resolution was set to 100,000 at m/z 400. Depending on the sample, mass ranges from 50 to 2000 u were measured. The spray capillary voltage at the IonMax ESI head was 4 kV, the heater capillary temperature was 250 °C, the nitrogen sheath gas flow was 20 and the sweep gas flow was 5 units. Thermal properties were measured via differential thermal analysis (DTA) with an OZM Research DTA 552-Ex instrument at a heating rate of 5 °C/min and in a range of room temperature to 400 °C. All sensitivities toward impact (IS) and friction (FS) were determined according to BAM (Bundesanstalt für Materialforschung und Prüfung) standards using a BAM drop hammer and a BAM friction apparatus by applying the 1 of 6 method.[S1]

CAUTION! Compounds **5-9** are potentially explosive materials. Safety precautions and equipment (such as wearing a leather coat, face shield, Kevlar sleeves, Kevlar gloves, earthed equipment and ear protection) must be used during manipulation.

4,5-Bis(bromo)-1*H*-1,2,3-triazole and 4,5-bis(methylcarboxylate)-1*H*-1,2,3-triazole was prepared according to literature known methods.[S2] Synthesis of **1** was performed in a similar way than already described by Izsak *et al.*[S3]

1. Experimental Part

4,5-Bis(hydroxymethyl)-1-benzyl-1,2,3-triazole (4): But-2-yne-1,4-diol (8.6 g, 100 mmol, 1.0 eq.) was added in portions over 30 min to benzyl azide (16.0 g, 120 mmol, 1.2 eq.) under stirring at 70 °C. The resulting solution was stirred for 48 hours at 85 °C and then poured into a crystallizing dish to cool down overnight at RT. The formed precipitate was filtered under reduced pressure and washed with EtOAc to provide **4** as a brown solid (21.5 g, 98.0 mmol, 98%).

¹H-NMR (DMSO-*d*₆, 400 MHz, ppm): δ = 7.37 – 7.22 (m, 5H), 5.59 (s, 2H), 5.41 (t, ³*J* = 5.4 Hz, 1H), 5.04 (t, ³*J* = 5.6 Hz, 1H), 4.55 (d, ³*J* = 5.4 Hz, 2H), 4.52 (d, ³*J* = 5.6 Hz, 2H); ¹³C-NMR (DMSO-*d*₆, 101 MHz, ppm): δ = 144.9, 136.0, 134.1, 128.6, 127.9, 127.6, 54.2, 21.0, 50.9.

4,5-Bis(hydroxymethyl)-1H-1,2,3-triazole (1): 1-Benzyl-(4,5-bis(hydroxymethyl)-1,2,3-triazole (**4**) (32.3 g, 147 mmol, 1 eq.) was added in portions to liquid ammonia (350 mL) under vigorous mechanical stirring at –70 °C. Sodium (13.0 g, 565 mmol, 3.8 eq.) was added in small portions over 2 h until the reaction mixture turned blue. The mixture was stirred for 2 h and then quenched by slowly adding NH₄Cl in portions until the blue color of the mixture disappeared (approx. 1 h) while the temperature was maintained at –70 °C. The mixture was allowed to warm up to RT and quenched with ice water (500 mL). By evaporation at reduced pressure, the volume of the reaction mixture was concentrated to around 100 mL and conc. HCl was added until pH 1 was obtained. The suspension was filtrated, and the solvent of the clear filtrate was removed under reduced pressure. The residue was extracted with hot acetonitrile (5 x 400 mL) and the extracts were stored at 3 °C for 3 days. The formed precipitate was filtered under reduced pressure and washed with cold acetonitrile to provide **1** as a yellowish powder (15.7 g, 121 mmol, 82%).

¹H-NMR (DMSO-*d*₆, 400 MHz, ppm): δ = 4.55 (s, 4H); ¹³C-NMR (DMSO-*d*₆, 101 MHz, ppm): δ = 142.1, 53.6; IR (ATR): $\tilde{\nu}$ (cm⁻¹) = 3024 (s), 2921 (m), 2800 (s), 2711 (s), 2628 (s), 2505 (m), 1838 (w), 1739 (m), 1601 (w), 1515 (w), 1456 (m), 1434 (m), 1385 (m), 1338 (m), 1310 (m), 1257 (w), 1233 (m), 1210 (m), 1175 (w), 1123 (m), 1029 (s), 1009 (vs), 967 (s), 939 (s), 804 (s), 728 (m), 674 (m), 661 (s), 519 (m); EA (C₄H₇N₃O₂, 129.12 g mol⁻¹): calc.: C 37.21, N 32.54, H 5.46%; found: C 36.93, N 32.42, H 5.39%; HR-MS (ESI, 70 eV): [C₄H₇N₃O₂] calc.: 130.0617 (M + H)⁺; found: 130.0613.

General procedure for N-nitration:

Nitric acid (1.5 mL, 1 part) was added dropwise to a mixture of acetic acid (1.5 mL, 1 part) and acetic acid anhydride (7.5 mL, 5 parts) at 5-10 °C. To the cold solution, *H*-triazole was added portion-wise at below 5 °C. The solution was stirred for 20 min at 5 °C, then 20 min at RT and then poured on ice water (50 mL). After extraction with ethyl acetate (3 x) the combined extracts were neutralized with sat. aq. NaHCO₃. The organic phase was dried over anhydrous sodium sulphate and the solvent was removed

under reduced pressure (remove at ambient conditions for sensitive compounds) to yield the crude nitro-triazoles.

4,5-Bis(nitratomethyl)-2-nitro-1,2,3-triazole (5): 4,5-Bis(hydroxymethyl)-1H-1,2,3-triazole (**1**) (250 mg, 1.93 mmol) was used to yield **5** (456 mg, 1.72 mmol, 89%) as a white solid after recrystallization from a small amount of methanol at 4 °C.

^1H NMR (Acetone- d_6 , 400 MHz, ppm) δ = 5.94 (s, 4H); ^{13}C NMR (Acetone- d_6 , 101 MHz, ppm) δ = 143.0, 65.1; ^{15}N NMR (Acetone- d_6 , 41 MHz, ppm) δ = -49.5 (t, 3J = 3.9 Hz), -60.2 (t, 3J = 2.7 Hz), -67.8, -80.3; IR (ATR): $\tilde{\nu}$ (cm^{-1}) = 2853 (vw), 1630 (vs), 1480 (w), 1345 (w), 1269 (vs), 1135 (s), 922 (m), 825 (s), 793 (vs), 728 (s), 586 (w), 578 (w); EA ($\text{C}_4\text{H}_4\text{N}_6\text{O}_6$ = 232.11 g mol $^{-1}$) calcd.: C 18.19, N 31.82, H 1.53%. Found: C 18.35, N 31.76, H 1.53%; Sensitivities: BAM drop hammer: <1 J; BAM friction tester: 15 N; DTA (5 °C min $^{-1}$): 66 °C (endo.), 159 °C (dec.).

4-(Azidomethyl)-5-(nitratomethyl)-2-nitro-1,2,3-triazole (6): 4-(azidomethyl)-5-hydroxymethyl)-1H-1,2,3-triazole (**2**) (250 mg, 1.62 mmol) was used to yield **6** (290 mg, 1.12 mmol, 73%) as a colorless oil after flash column chromatography (iHex/EtOAc, 6/2).

^1H -NMR (DMSO- d_6 , 400 MHz, ppm): δ = 5.85 (s, 2H), 4.83 (s, 2H); ^{13}C -NMR (DMSO- d_6 , 101 MHz, ppm): δ = 144.8, 141.1, 64.3, 43.4; ^{15}N -NMR (Acetone- d_6 , 41 MHz, ppm): δ = -46.0 (t, 3J = 4.0 Hz), -59.6 (t, 3J = 2.7 Hz), -62.7 (t, 3J = 2.8 Hz), -66.5 (s), -81.3 (s), -134.4 (t, 3J = 4.0 Hz), -165.7 (s), -311.9 (s); IR (ATR): $\tilde{\nu}$ (cm^{-1}) = 2919 (vw), 2105 (s), 1639 (vs), 1434 (w), 1365 (w), 1274 (vs), 1218 (m), 1144 (s), 965 (m), 948 (m), 837 (s), 804 (vs), 751 (m), 728 (s), 648 (m), 588 (w); EA ($\text{C}_4\text{H}_4\text{N}_8\text{O}_5$, 244.13 g mol $^{-1}$): calc.: C 19.68, N 45.90, H 1.65%; found: C 20.00, N 45.89, H 1.64%; Sensitivities: BAM drop hammer: 2 J (liquid); friction tester: 120 N (liquid); DTA (5 °C min $^{-1}$): 158 °C (dec.).

4,5-bis(azidomethyl)-2-nitro-1,2,3-triazole (7): 4,5-Bis(azidomethyl)-1H-1,2,3-triazole (**3**) (250 mg, 1.40 mmol) was used to yield **7** (271 mg, 1.21 mmol, 86%) as a colorless oil after flash column chromatography (iHex/EtOAc, 8/12).

^1H NMR (Acetone- d_6 , 400 MHz, ppm) δ = 4.80 (s, 4H); ^{13}C NMR (Acetone- d_6 , 101 MHz, ppm) δ = 145.3, 45.0; ^{15}N NMR (Acetone- d_6 , 41 MHz, ppm) δ = -65.0, -133.9, -166.1, -314.5; IR (ATR) $\tilde{\nu}$ (cm^{-1}) = 2922 (w), 2098 (vs), 1642 (vs), 1481 (vw), 1440 (w), 1328 (w), 1276 (vs), 1143 (vs), 960 (m), 889 (w), 809 (vs), 728 (s), 653 (w), 554 (w); EA ($\text{C}_4\text{H}_4\text{N}_{10}\text{O}_2$ = 224.14 g mol $^{-1}$) calcd.: C 21.43, N 62.49, H 1.80%. Found: C 21.64, N 62.86, H 1.95%; Sensitivities: BAM drop hammer: 1 J; friction tester: 20 N; DTA (5 °C min $^{-1}$): 161 °C (dec.).

4,5-bis(bromo)-2-nitro-1,2,3-triazole (8): 4,5-bis(bromo)-1*H*-1,2,3-triazole (1.00 g, 4.41 mmol) was used to yield **8** (1.11 g, 4.08 mmol, 93%) as colorless solid.

^{13}C NMR (Acetone- d_6 , 101 MHz, ppm) δ = 130.0; ^{14}N NMR (Acetone- d_6 , 29 MHz, ppm) δ = -70; IR (ATR) $\tilde{\nu}$ (cm^{-1}) = 3133 (w), 2962 (w), 2859 (m), 1674 (m), 1644 (vs), 1446 (w), 1379 (m), 1361 (m), 1349 (m), 1315 (m), 1285 (s), 1275 (s), 1165 (s), 1152 (s), 1145 (m), 1100 (m), 1041 (vs), 984 (m), 948 (m), 813 (s), 755 (m), 724 (s), 536 (m), 417 (m); EA ($\text{C}_2\text{Br}_2\text{N}_4\text{O}_2$ = 271.86 g mol^{-1}) calcd.: C 8.84, N 20.61, H 0.00%. Found: C 8.98, N 20.37, H 0.00%; Sensitivities: BAM drop hammer: 3 J; friction tester: 240 N; DTA (5 $^\circ\text{C min}^{-1}$): 89 $^\circ\text{C}$ (endo. Followed by exo.).

4,5-bis(methylcarboxylate)-2-nitro-1,2,3-triazole (9): 4,5-bis(methylcarboxylate)-1*H*-1,2,3-triazole (502 mg, 2.70 mmol) was used to yield **9** (350 mg, 1.52 mmol, 56%) as off-white solid.

^1H NMR (Acetone- d_6 , 400 MHz, ppm) δ = 4.01 (s, 6H); ^{13}C NMR (Acetone- d_6 , 101 MHz, ppm) δ = 159.6, 139.9, 53.9; ^{14}N NMR (Acetone- d_6 , 29 MHz, ppm) δ = -70.5; IR (ATR) $\tilde{\nu}$ (cm^{-1}) = 2964 (vw), 2949 (vw), 1748 (s), 1733 (s), 1672 (s), 1482 (m), 1450 (w), 1430 (m), 1306 (s), 1284 (vs), 1233 (m), 1196 (w), 1145 (s), 1129 (s), 1093 (vs), 988 (m), 945 (w), 834 (s), 804 (vs), 800 (vs), 771 (s), 727 (s), 599 (m); EA ($\text{C}_6\text{H}_8\text{N}_4\text{O}_4$ = 200.15 g mol^{-1}) calcd.: C 31.31, N 24.35, H 2.63%. Found: C 31.37, N 24.07, H 2.43; DTA (5 $^\circ\text{C min}^{-1}$): 60 $^\circ\text{C}$ (endo), 165 $^\circ\text{C}$ (dec.).

2. X-Ray Diffraction

Crystal structure data were obtained from an Oxford Xcalibur3 diffractometer with a Spellman generator (voltage 50 kV, current 40 mA) and a Kappa CCD area for data collection using Mo- $K\alpha$ radiation (λ = 0.71073 Å) or a Bruker D8 Venture TXS diffractometer equipped with a multilayer monochromator, a Photon 2 detector and a rotation-anode generator (Mo- $K\alpha$ radiation). The data collection was performed using the CRYSTALIS RED software.^[S4] The solution of the structure was performed by direct methods and refined by full-matrix least-squares on F2 (SHELXT)^[S5] implemented in the OLEX2 1.3^[S6] software suite. The non-hydrogen atoms were refined anisotropically and the hydrogen atoms were located and freely refined if possible. The absorption correction was carried out by a SCALE3 ABSPACK multiscan method.^[S7] DIAMOND4 plots are shown with thermal ellipsoids at the 50% probability level and hydrogen atoms are shown as small spheres of arbitrary radius. The SADABS program embedded in the Bruker APEX3 software was used for multi-scan absorption corrections in all structures.^[S8] CCDC contain the supplementary crystallographic data for this paper. Their data can be

obtained free of charge from the Cambridge Crystallographic Data Centre. The molecular moieties are represented in **Figure S1** to **Figure S2** and the crystallographic data and structure refinement details are shown in **Table S1** to **S2**. Crystals suitable for measurement were grown by evaporating the solvents at ambient conditions: acetonitrile (**1**), reaction mixture (**4**), methanol (**5**, **8** and **9**).

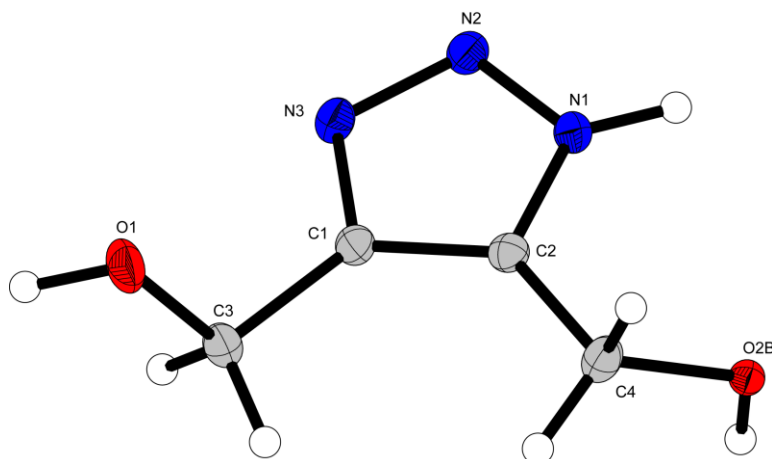


Figure S1. The molecular moiety of **1** is derived from low-temperature crystal structure measurement. Thermal ellipsoids are drawn at the 50 % probability level.

Compound **1** crystallizes in the monoclinic space group $P2_1/c$ with a cell volume of $563.12(14) \text{ \AA}^3$ and four formula units per cell. The cell constants are $a = 7.3284(9) \text{ \AA}$, $b = 6.5102(9) \text{ \AA}$ and $c = 12.2865(18) \text{ \AA}$, with a density of 1.523 g cm^{-3} at 102 K.

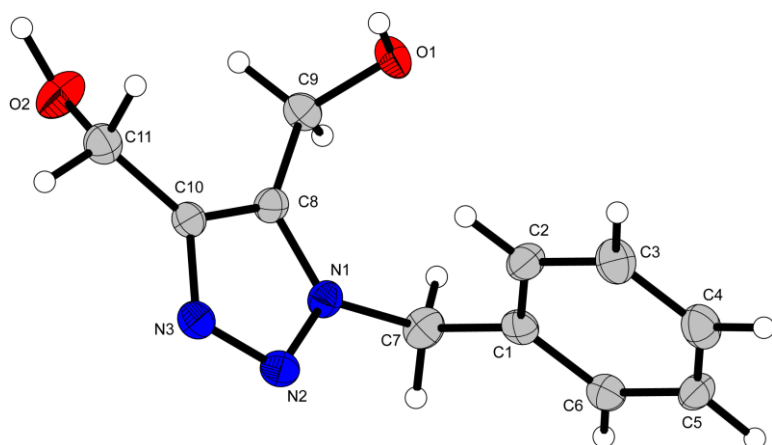


Figure S2. The molecular moiety of **4** derived from low-temperature crystal structure measurement. Thermal ellipsoids are drawn at the 50 % probability level.

Compound **4** crystallizes in the orthorhombic space group $P2_12_12_1$ with a cell volume of $1065.8(3) \text{ \AA}^3$ and four formula units per cell. The cell constants are $a = 9.1325(11) \text{ \AA}$, $b = 9.9724(14) \text{ \AA}$ and $c = 11.7022(17) \text{ \AA}$, with a density of 1.366 g cm^{-3} at 101 K.

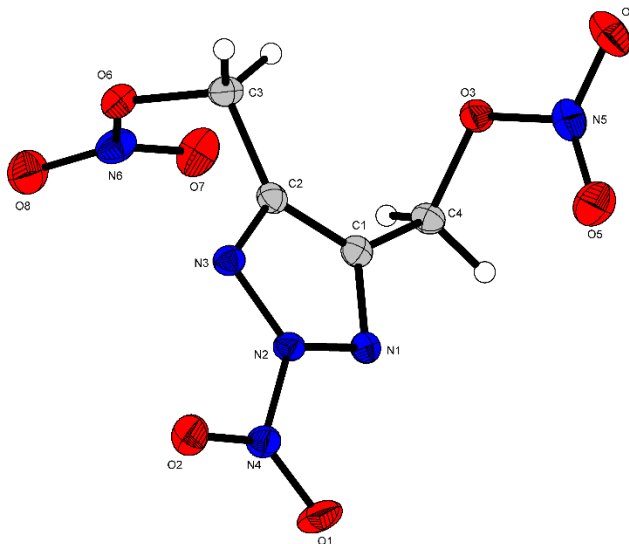


Figure S3. The molecular moiety of **5** derived from low-temperature crystal structure measurement. Thermal ellipsoids are drawn at the 50 % probability level.

Compound **5** crystallizes in the orthorhombic space group $P21/c$ with a cell volume of $966.1(4) \text{ \AA}^3$ and four formula units per cell. The cell constants are $a = 8.5382(18) \text{ \AA}$, $b = 15.893(3) \text{ \AA}$ and $c = 8.0151(15) \text{ \AA}$, with a density of 1.816 g cm^{-3} at 102 K.

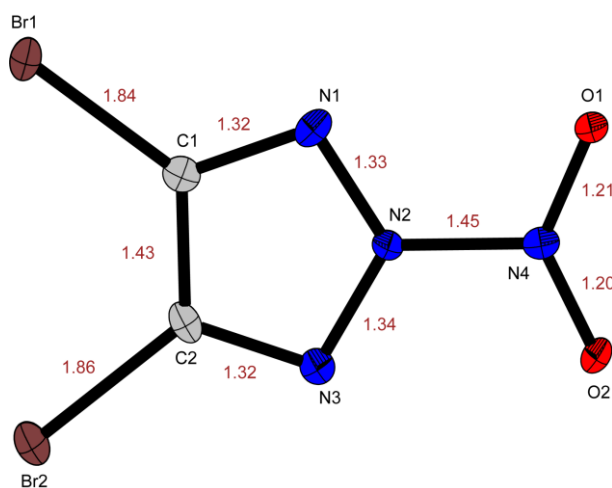


Figure S4. The molecular moiety of **8** derived from low-temperature crystal structure measurement. Thermal ellipsoids are drawn at the 50 % probability level.

Compound **8** crystallizes in the orthorhombic space group $Pbcm$ with a cell volume of $1338.1(2) \text{ \AA}^3$ and eight formula units per cell. The cell constants are $a = 10.499(1) \text{ \AA}$, $b = 15.7769(15) \text{ \AA}$ and $c = 8.0781(6) \text{ \AA}$, with a density of 2.699 g cm^{-3} at 101 K.

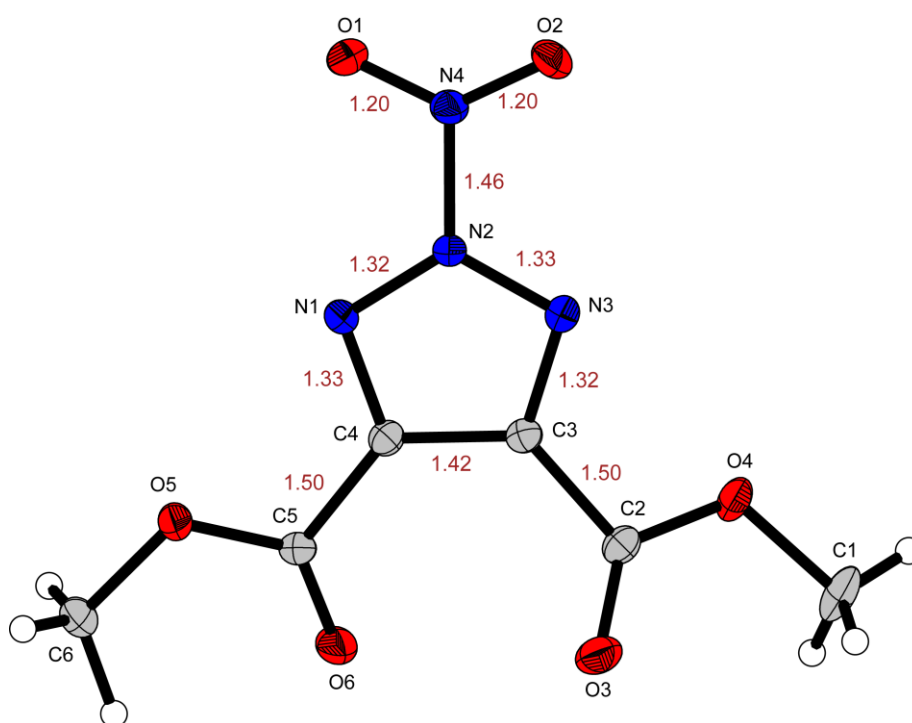


Figure S5. The molecular moiety of **9** derived from low-temperature crystal structure measurement. Thermal ellipsoids are drawn at the 50 % probability level.

Compound **9** crystallizes in the monoclinic space group $P2_1$ with a cell volume of $468.27(3) \text{ \AA}^3$ and two formula units per cell. The cell constants are $a = 6.3706(2) \text{ \AA}$, $b = 9.7460(4) \text{ \AA}$ and $c = 8.1500(3) \text{ \AA}$, with a density of 1.632 g cm^{-3} at 173 K.

Table S1. Crystallographic data and structure refinement details for the prepared compounds **1**, **4** and **5**.

Compound	1	4	5
Formula	C ₄ H ₇ N ₃ O ₂	C ₁₁ H ₁₃ N ₃ O ₂	C ₄ H ₄ N ₆ O ₈
FW [g mol ⁻¹]	129.13	219.24	264.13
Crystal system	monoclinic	orthorhombic	monoclinic
Space group	<i>P</i> 2 ₁ / <i>c</i> (No. 14)	<i>P</i> 2 ₁ 2 ₁ 2 ₁ (No. 19)	<i>P</i> 2 ₁ / <i>c</i> (No. 14)
Color / Habit	colorless block	colorless block	colorless block
Size [mm]	0.10 x 0.10 x 0.50	0.30 x 0.37 x 0.56	0.30 x 0.30 x 0.50
a [Å]	7.3284(9)	9.1325(11)	8.5382(18)
b [Å]	6.5102(9)	9.9724(14)	15.893(3)
c [Å]	12.2865(18)	11.7022(17)	8.0151(15)
α [°]	90		90
β [°]	106.124(13)		117.35(3)
γ [°]	90		90
V [Å ³]	563.12(14)	1065.8(3)	966.1(4)
Z	4	4	4
ρ _{calc.} [g cm ⁻³]	1.523	1.366	1.816
μ [mm ⁻¹]	0.124	0.097	0.176
F(000)	272	464	536
λ _{MoKα} [Å]	0.71073	0.71073	0.71073
T [K]	102	101	102
θ Min-Max [°]	2.9, 26.4	2.7, 26.4	2.6, 26.4
Dataset	-8: 9 ; -8: 8 ; -15: 14	-11: 7 ; -12: 12 ; -14: 11	-10: 10 ; -19: 14 ; -10: 10
Reflections collected	4966	4040	8647
Independent refl.	1152	2176	1972
<i>R</i> _{int}	0.029	0.040	0.047
Observed reflections	894	1485	1555
Parameters	113	198	163
<i>R</i> ₁ (obs) ^[a]	0.0427	0.0606	0.0441
w <i>R</i> ₂ (all data) ^[b]	0.1189	0.0860	0.1430
<i>S</i> ^[c]	1.08	1.12	0.98
Resd. dens [e Å ⁻³]	-0.19, 0.30	-0.20, 0.27	-0.26, 0.32
Device type	Xcalibur Sapphire3	Xcalibur Sapphire3	Xcalibur Sapphire3
Solution	SIR-92	SIR-92	SIR-92
Refinement	SHELXL-2013	SHELXL-2013	SHELXL-2013
Absorption correction	multi-scan	multi-scan	multi-scan
CCDC	2270387	2270383	2270386

^[a] $R_1 = \sum ||F_o| - |F_c|| / \sum |F_o|$; ^[b] $wR_2 = [\sum [w(F_o^2 - F_c^2)^2] / \sum [w(F_o^2)^2]]^{1/2}$; $w = [\sigma^2(F_o^2) + (xP)^2 + yP]^{-1}$ and $P = (F_o^2 + 2F_c^2) / 3$; ^[c] $S = (\sum [w(F_o^2 - F_c^2)^2] / (n - p))^{1/2}$ (n = number of reflections; p = total number of parameters).

Table S2. Crystallographic data and structure refinement details for the prepared compounds **8** and **9**.

Compound	8	9
Formula	2(BrCN ₂ O)	C ₆ H ₆ N ₄ O ₆
FW [g mol ⁻¹]	271.88	230.15
Crystal system	orthorhombic	monoclinic
Space group	<i>Pbcm</i> (No. 57)	<i>P2</i> ₁ (No. 4)
Color / Habit	colorless block	colorless block
Size [mm]	0.05 x 0.10 x 0.50	0.02 x 0.04 x 0.16
a [Å]	10.499(1)	6.3706(2)
b [Å]	15.7769(15)	9.7460(4)
c [Å]	8.0781(6)	8.1500(3)
α [°]		90
β [°]		112.271(1)
γ [°]		90
V [Å ³]	1338.1(2)	468.27(3)
Z	8	2
ρ _{calc.} [g cm ⁻³]	2.699	1.632
μ [mm ⁻¹]	12.057	0.148
F(000)	1008	236
λ _{MoKα} [Å]	0.71073	0.71073
T [K]	101	173
θ Min-Max [°]	1.9, 26.4	3.4, 28.3
Dataset	-13: 11 ; -19: 19 ; -10:	-8: 8 ; -13: 13 ; -10:
	9	10
Reflections collected	10240	9449
Independent refl.	1462	2309
<i>R</i> _{int}	0.052	0.034
Observed reflections	1053	2098
Parameters	109	170
<i>R</i> ₁ (obs) ^[a]	0.0335	0.0308
w <i>R</i> ₂ (all data) ^[b]	0.0820	0.0735
<i>S</i> ^[c]	1.04	1.07
Resd. dens [e Å ⁻³]	-0.52, 0.76	-0.16, 0.22
Device type	Xcalibur Sapphire3	Bruker D8 Venture
Solution	SIR-92	SIR-92
Refinement	SHELXL-2013	SHELXL-2013
Absorption correction	multi-scan	multi-scan
CCDC	2270384	2270385

^[a] $R_1 = \sum ||F_o| - |F_c|| / \sum |F_o|$; ^[b] $wR_2 = [\sum [w(F_o^2 - F_c^2)^2] / \sum [w(F_o^2)]]^{1/2}$; $w = [\sigma^2(F_o^2) + (xP)^2 + yP]^{-1}$ and $P = (F_o^2 + 2F_c^2) / 3$; ^[c] $S = (\sum [w(F_o^2 - F_c^2)^2] / (n-p))^{1/2}$ (n = number of reflections; p = total number of parameters).

3. Differential Thermal Analysis

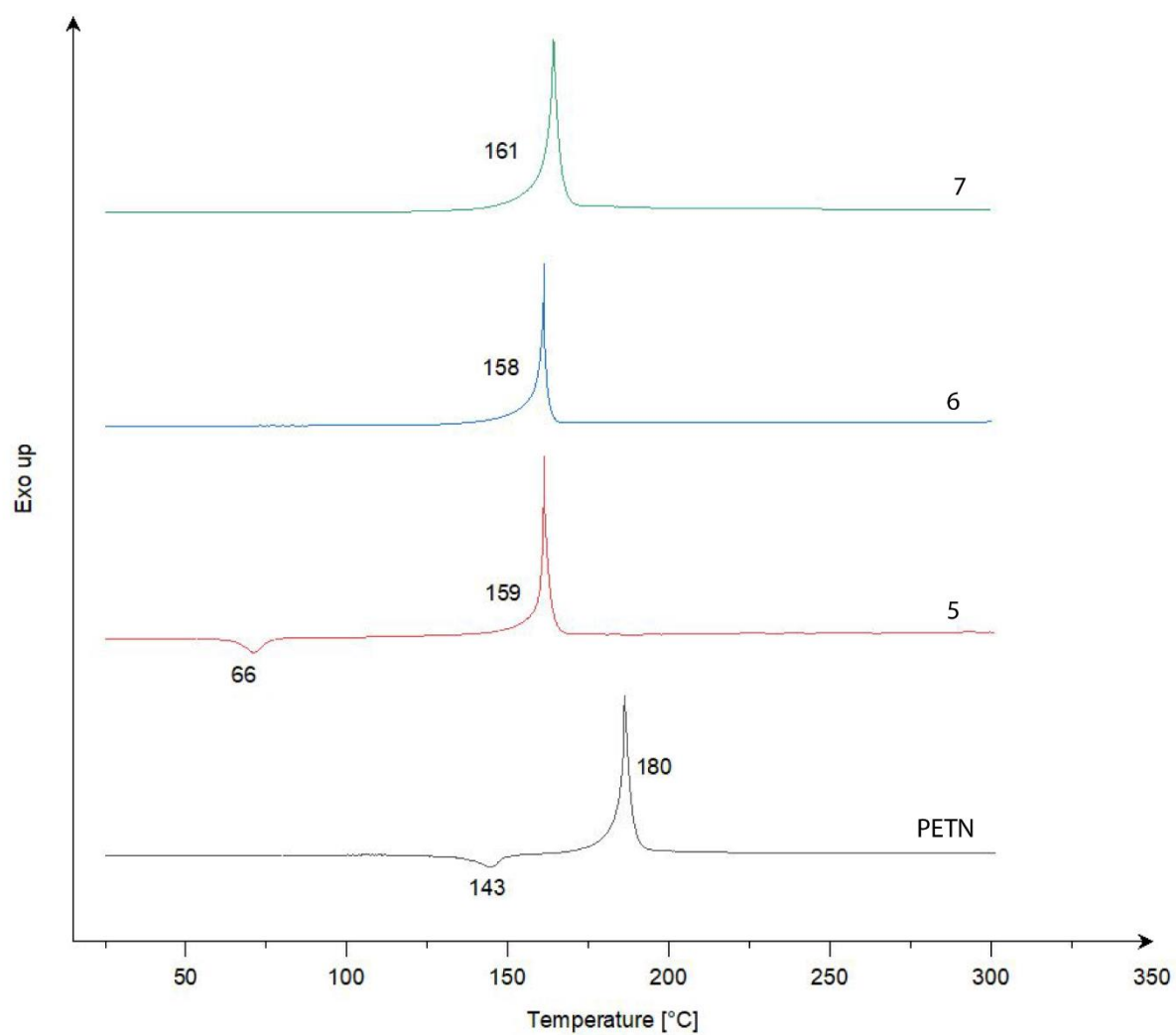


Figure S6. Plots of the differential thermal analysis of PETN, 5, 6, and 7 with a heating rate of 5 K min⁻¹.

4. Computation

Heat of Formation (HOF) Computation

All quantum chemical calculations were carried out using the Gaussian G09 program package.^[S9] The enthalpies (H) and free energies (G) were calculated using the complete basis set (CBS) method of Petersson and co-workers in order to obtain very accurate energies. The CBS models are using the known asymptotic convergence of pair natural orbital expressions to extrapolate from calculations using a finite basis set to the estimated CBS limit. CBS-4 starts with an HF/3-21G(d) geometry optimization; the zero-point energy is computed at the same level. It then uses a large basis set SCF calculation as a base energy, and an MP2/6-31+G calculation with a CBS extrapolation to correct the energy through second order. A MP4(SDQ)/6-31+ (d,p) calculation is used to approximate higher-order contributions. In this study, we applied the modified CBS-4M.

HOF's of ionic compounds were calculated using the atomization method (equation E1) using room temperature CBS-4M enthalpies, which are summarized in **Table S3**.^[S10, S11]

$$\Delta_f H^\circ_{(g, M, 298)} = H_{(Molecule, 298)} - \sum H^\circ_{(Atoms, 298)} + \sum \Delta_f H^\circ_{(Atoms, 298)} \quad (E1)$$

Table S3. CBS-4M electronic enthalpies for atoms C, H, N and O and their literature values for atomic $\Delta_f H^\circ_{298}$ / kJ mol⁻¹

	$-H^{298}$ [a.u.]	NIST ^[S12]
H	0.500991	218.2
C	37.786156	717.2
N	54.522462	473.1
O	74.991202	249.5

For neutral compounds the sublimation enthalpy, which is needed to convert the gas phase enthalpy of formation to the solid state one, was calculated by the *Trouton* rule.^[S13] For ionic compounds, the lattice energy (U_L) and lattice enthalpy (ΔH_L) were calculated from the corresponding X-ray molecular volumes according to the equations provided by *Jenkins and Glasser*.^[S14] With the calculated lattice enthalpy the gas-phase enthalpy of formation was converted into the solid state (standard conditions) enthalpy of formation. These molar standard enthalpies of formation (ΔH_m) were used to calculate the molar solid-state energies of formation (ΔU_m) according to equation E2.

$$\Delta U_m = \Delta H_m - \Delta n RT \quad (E2)$$

(Δn being the change of moles of gaseous components)

The calculation results are summarized in **Table S4**.

Table S4. Calculation results for neutral compounds.

	$-H^{298}$ [a.u.]	$\Delta_f H^\circ(\text{g,M})$ [kJ mol ⁻¹]	$\Delta_f H^\circ(\text{s})$ [kJ mol ⁻¹]	Δn	$\Delta_f U(\text{s})$ [kJ kg ⁻¹]
5	1083.41796	153.6	90.9	-9.0	428.7
6	967.404102	1123.4	536.0	-8.5	2282.0
7	851.387555	1003.5	964.5	-8.0	4391.7

Bond dissociation energy (BDE)

To better understand the rare heteroaromatic N-NO₂ bond, homolytic and heterolytic bond dissociation energies were calculated. Therefore, four reactions were postulated in **Figure S7**, and the HOF of all molecules were calculated for the gas phase (**Table S5**). The HOF of the reactant is subtracted from the sum of the HOF's of the cleavage products. The energy obtained represents the bond dissociation (**Table S6**).

Table S5. Calculation results of radical and ionic fractions of I1 for bond dissociation.

	$-H^{298}$ [a.u.]	$\Delta_f H^\circ(\text{g,M})$ [kJ mol ⁻¹]
I1	1083.41796	153.6
I2	204.863105	30.5
I3	878.47832	324.0
I4	878.482214	313.8
I5	204.500147	983.4
I6	878.654738	-139.2
I7	878.595186	17.2

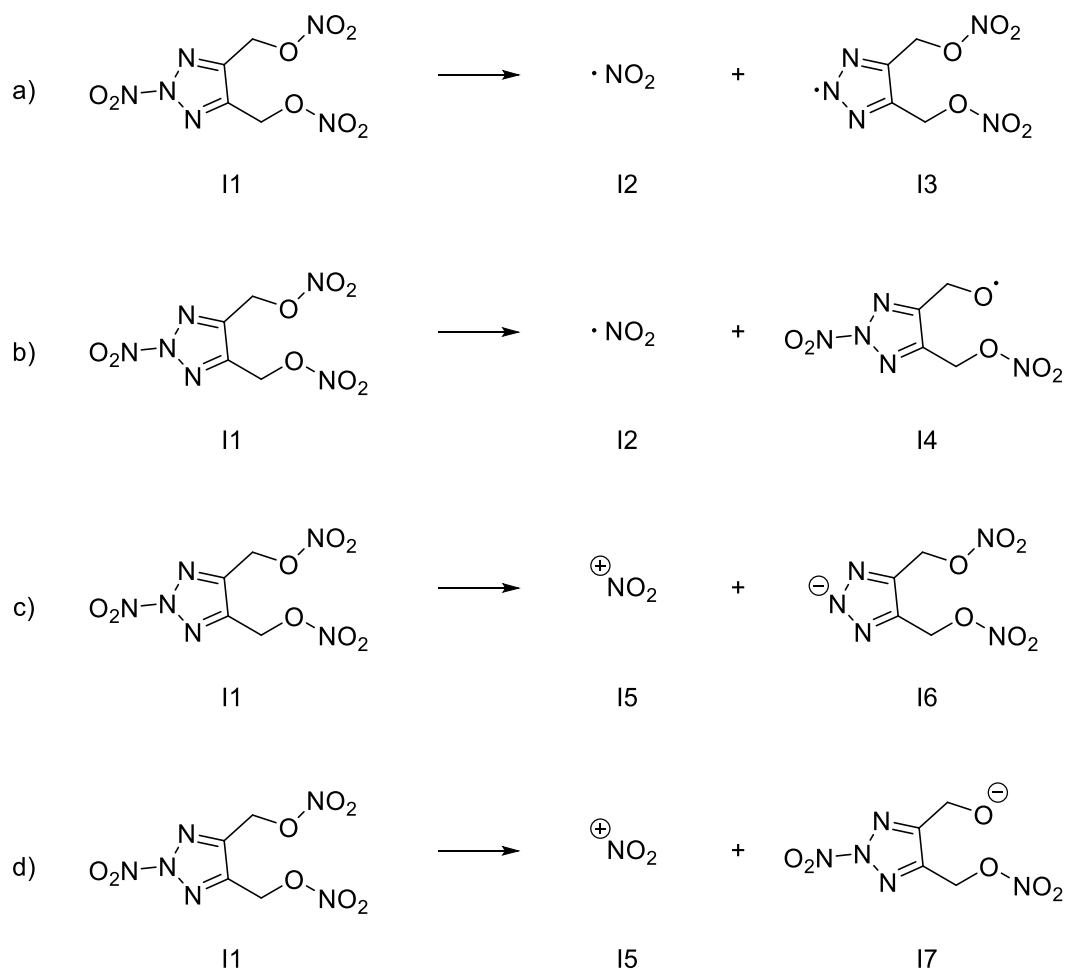


Figure S7. From top to bottom: a) Homolytic cleavage of N-NO₂ (**I1**) to radicals **I2** and **I3**. b) Homolytic cleavage of O-NO₂ (**I1**) to radicals **I2** and **I4**. c) Heterolytic cleavage of N-NO₂ (**I1**) to cation **I5** and anion **I6**. d) Heterolytic cleavage of O-NO₂ (**I1**) to cation **I5** and anion **I7**.

Table S6. Bond dissociation energies for reactions of **Figure S7**.

	$\Delta_f H^\circ(\text{g,M})$ [kJ mol ⁻¹] (I1)	$\Delta_f H^\circ(\text{g,M})$ [kJ mol ⁻¹] (Product)	BDE [kJ mol ⁻¹]
a)	153.6	354.5	200.9
b)	153.6	344.3	190.7
c)	153.6	844.2	690.6
d)	153.6	1000.6	847.0

5. Hirshfeld

A Hirshfeld surface of the molecular moiety of the crystal structure of **5** was generated, analyzed and visualized with the CrystalExplorer21 program. [S15] The contacts and fingerprint plots are represented in **Figure S8** and discussed in the main document. The plot represents atom interactions between molecules. d_e represents the external distance from the atom to the surface whereas d_i shows the inner distance. Close contacts can be found in the lower left corner of each Fingerprint plot. Furthermore, the red dots on the surface illustrate the closest contacts between the molecules. There are discussions about relations between the Hirshfeld surface and impact or friction sensitivity. [S16] The amount of O-O, N-O and N-N close contacts seems to correlate with the sensitivity. It is shown that high amounts of those interactions are indicating a high impact sensitivity. [S17] This agrees for compound **5**.

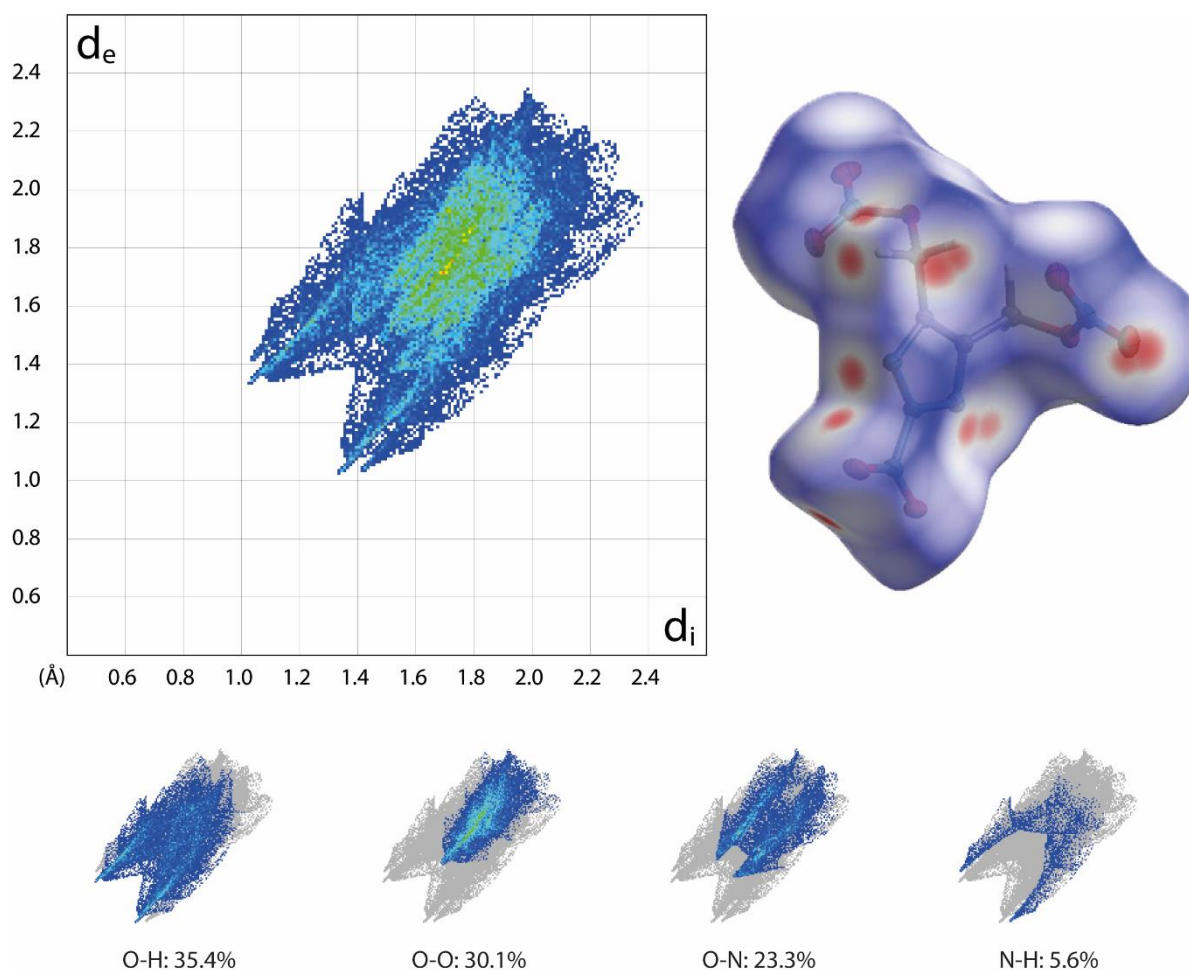
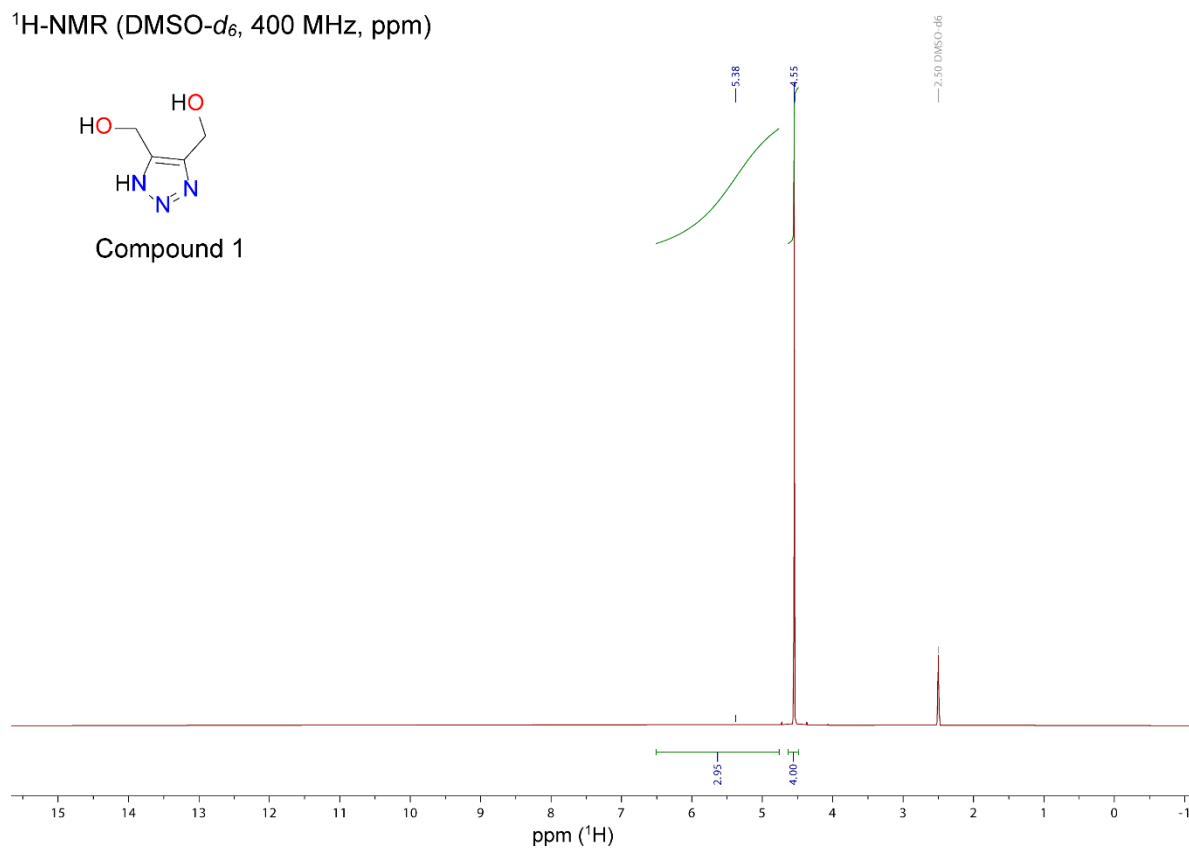
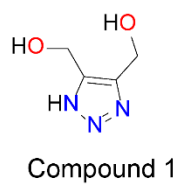


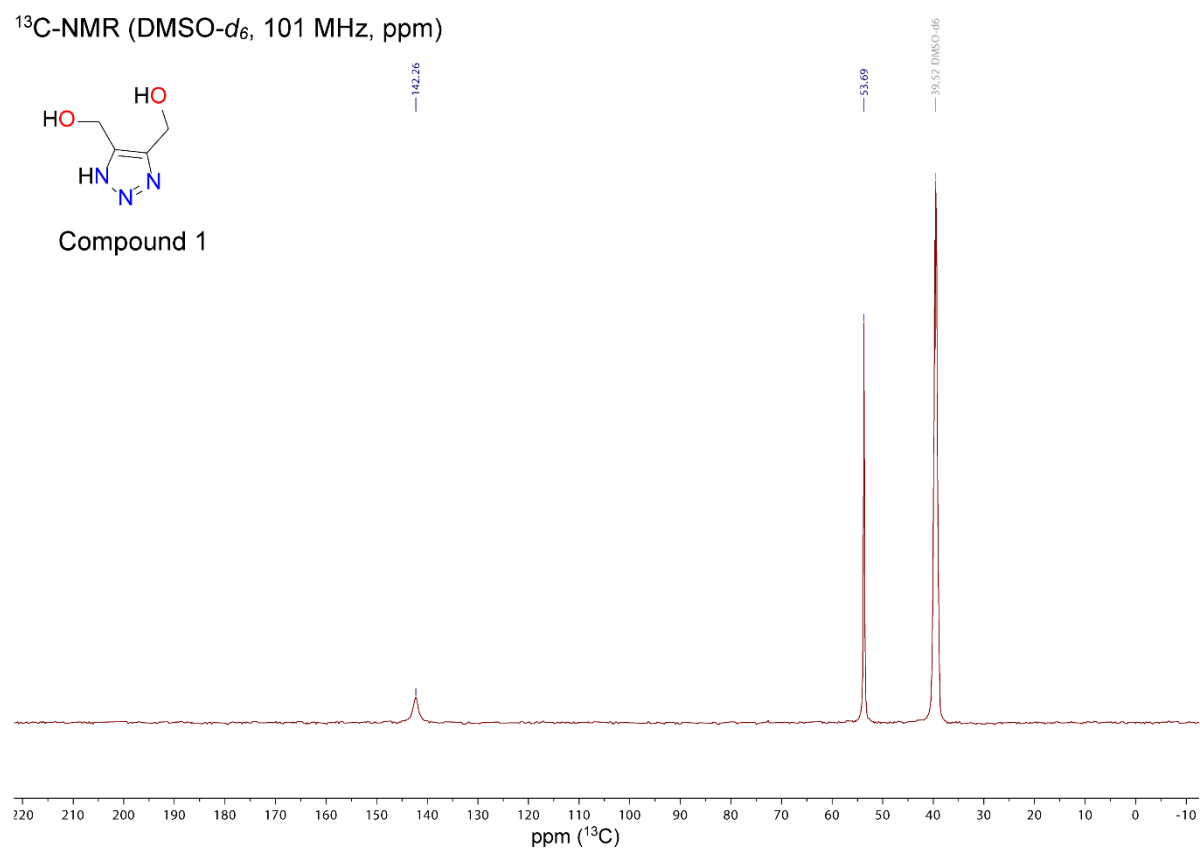
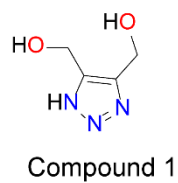
Figure S8 Fingerprint plot, Hirshfeld surface and location of the interactions within the Fingerprint of compound **5**.

6. NMR Spectroscopy

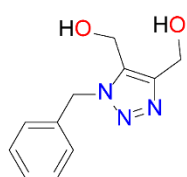
$^1\text{H-NMR}$ (DMSO- d_6 , 400 MHz, ppm)



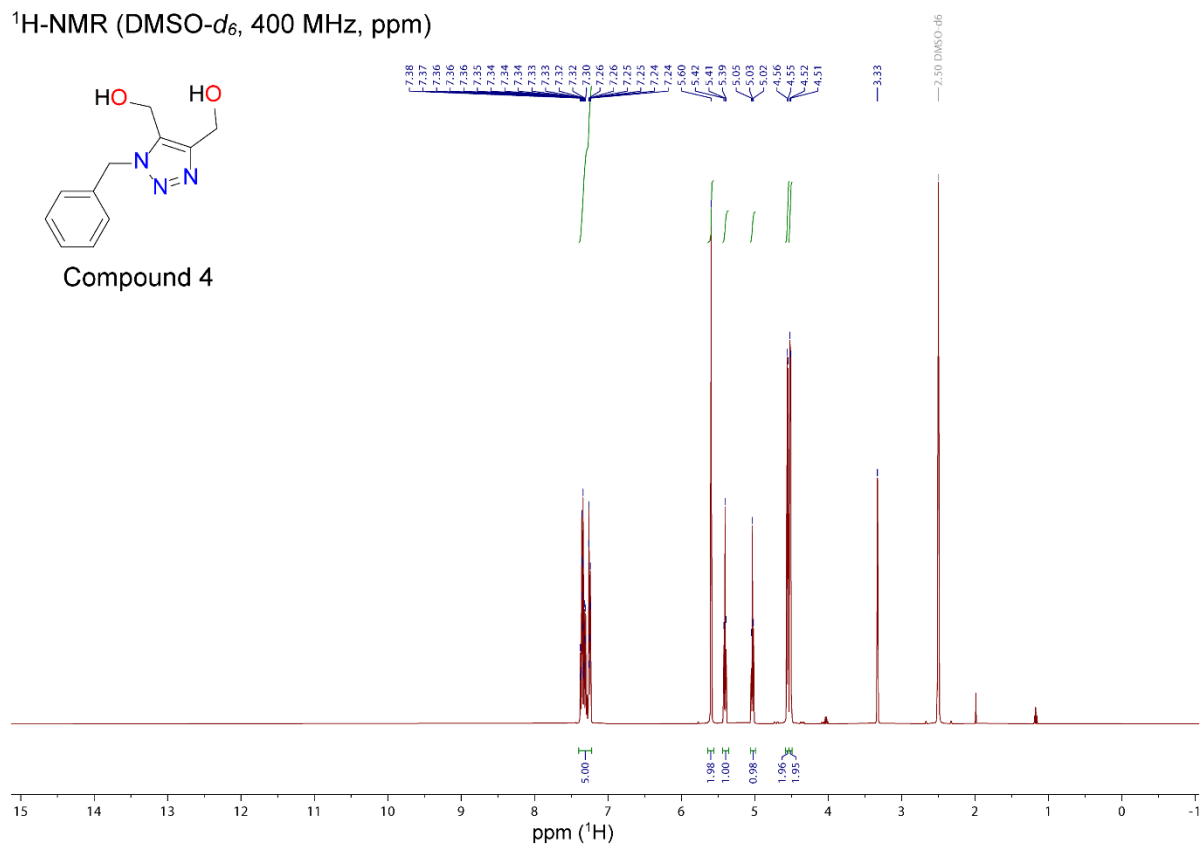
$^{13}\text{C-NMR}$ (DMSO- d_6 , 101 MHz, ppm)



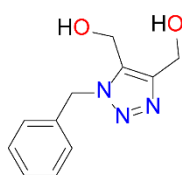
$^1\text{H-NMR}$ ($\text{DMSO-}d_6$, 400 MHz, ppm)



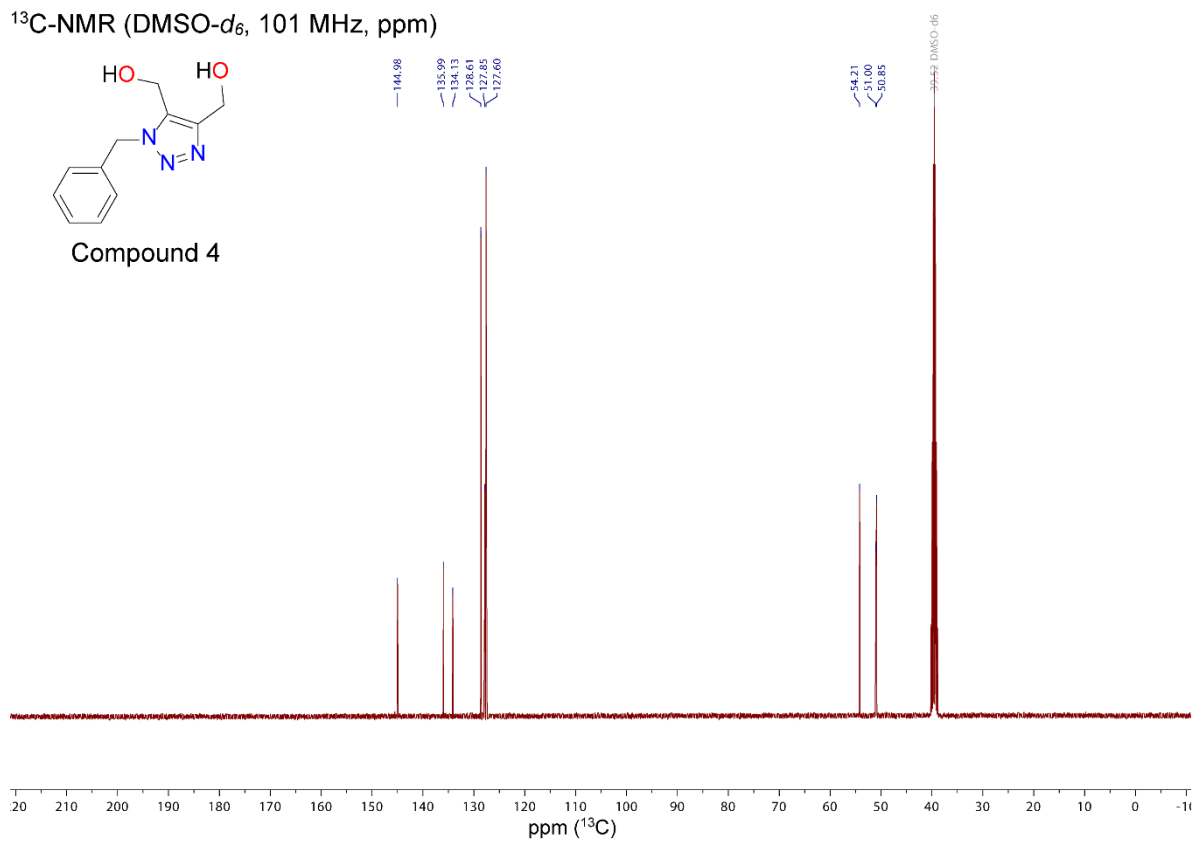
Compound 4



$^{13}\text{C-NMR}$ ($\text{DMSO-}d_6$, 101 MHz, ppm)



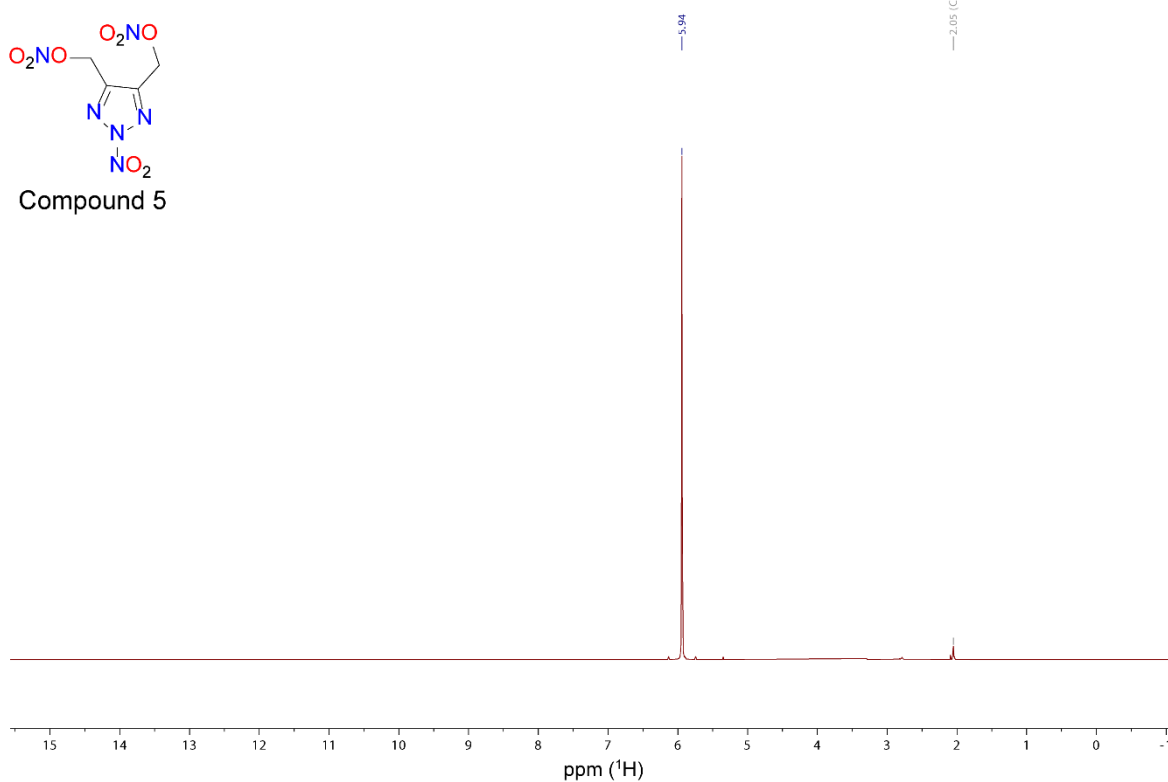
Compound 4



¹H-NMR (Acetone-*d*₆, 400 MHz, ppm)



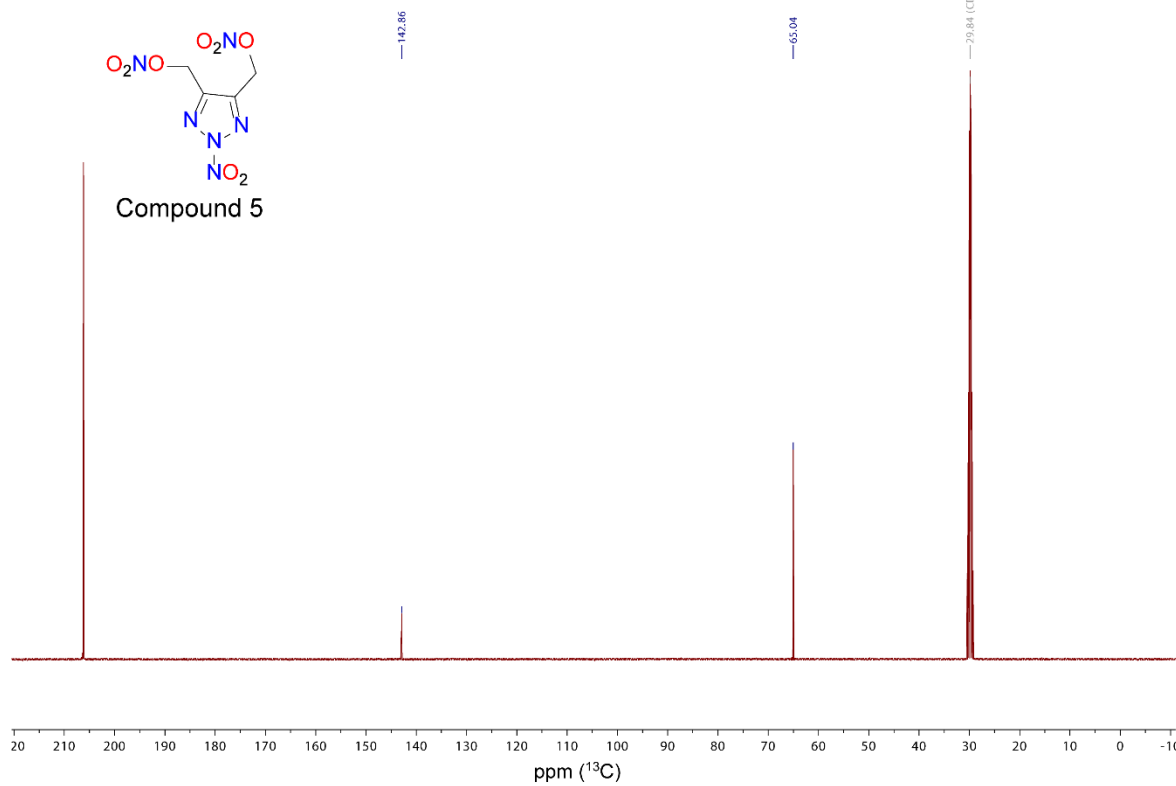
Compound 5



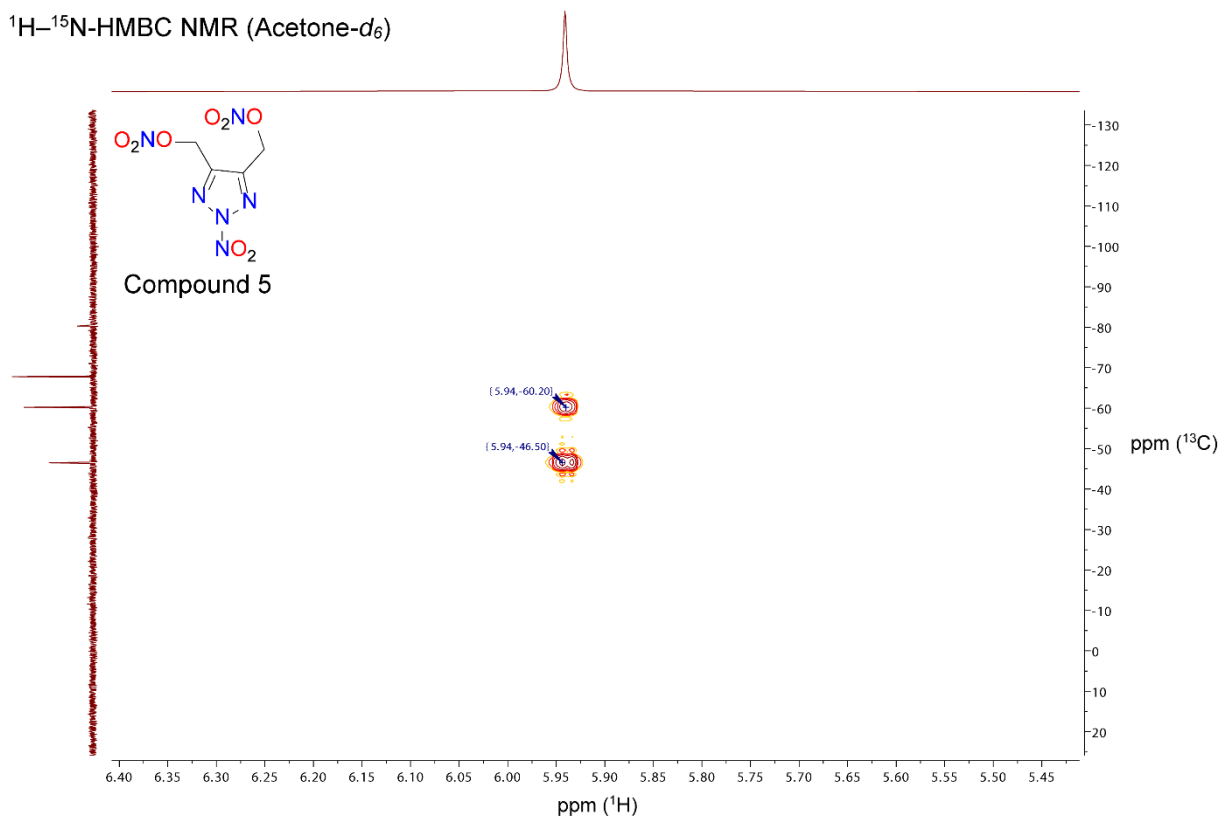
¹³C-NMR (Acetone-*d*₆, 101 MHz, ppm)



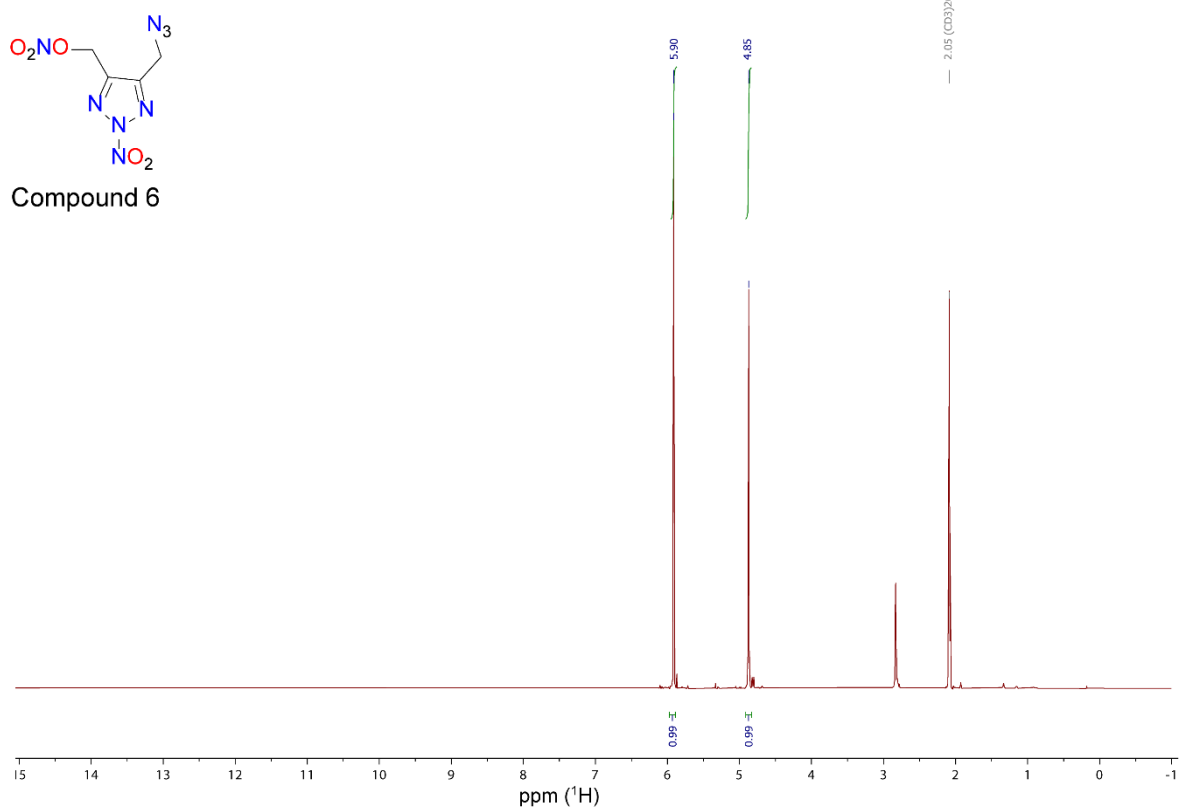
Compound 5



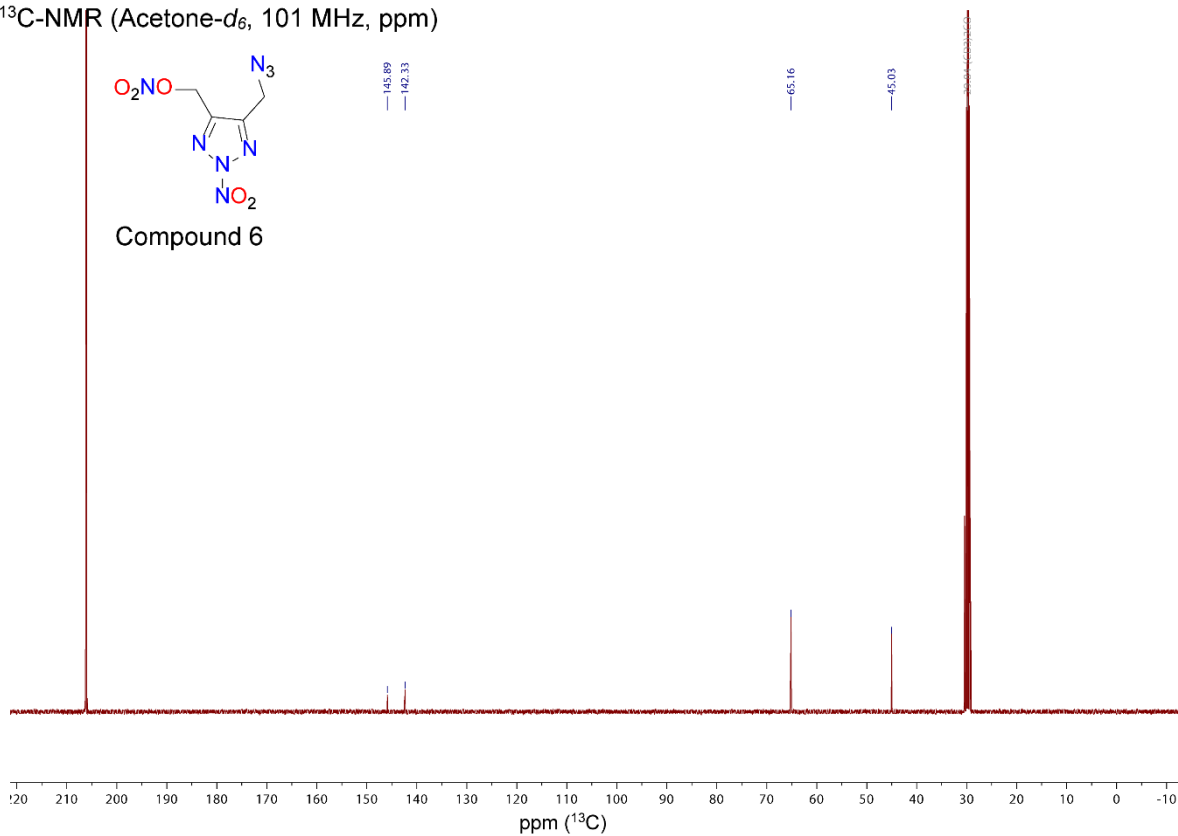
^1H - ^{15}N -HMBC NMR (Acetone- d_6)



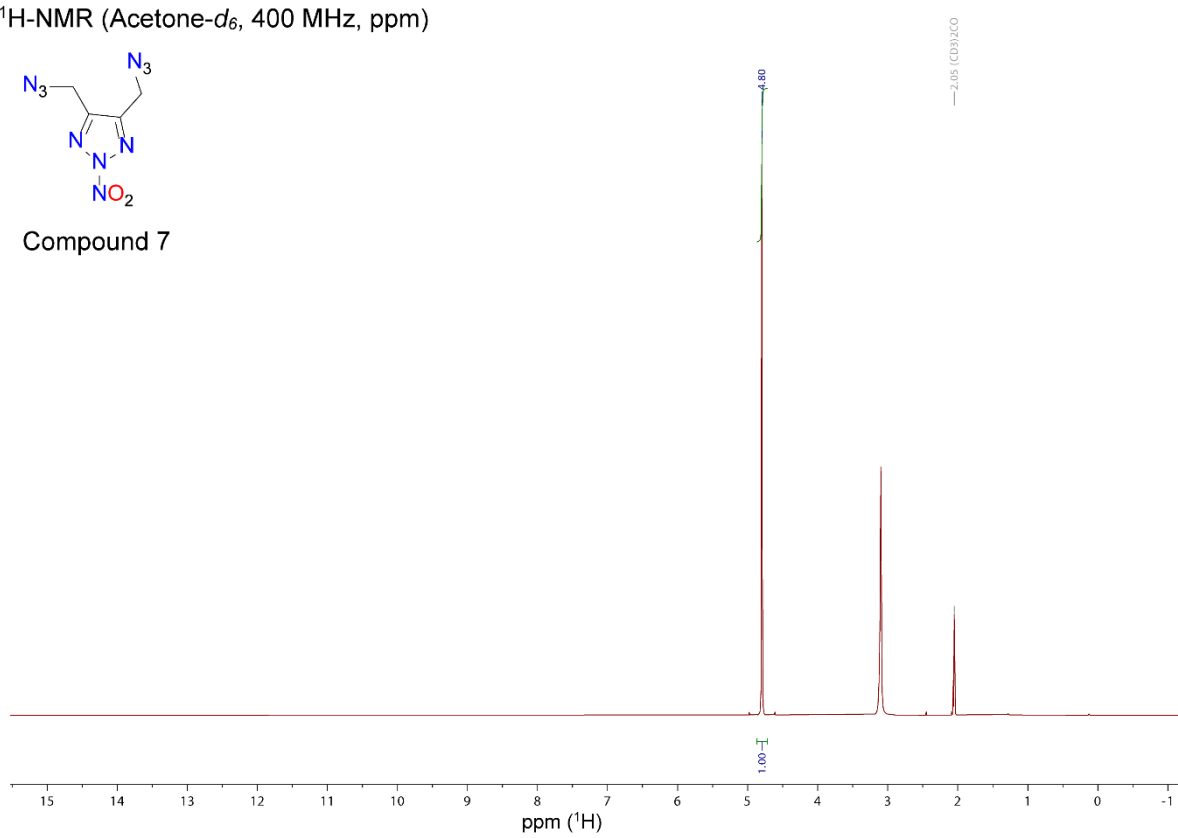
^1H -NMR (Acetone- d_6 , 400 MHz, ppm)



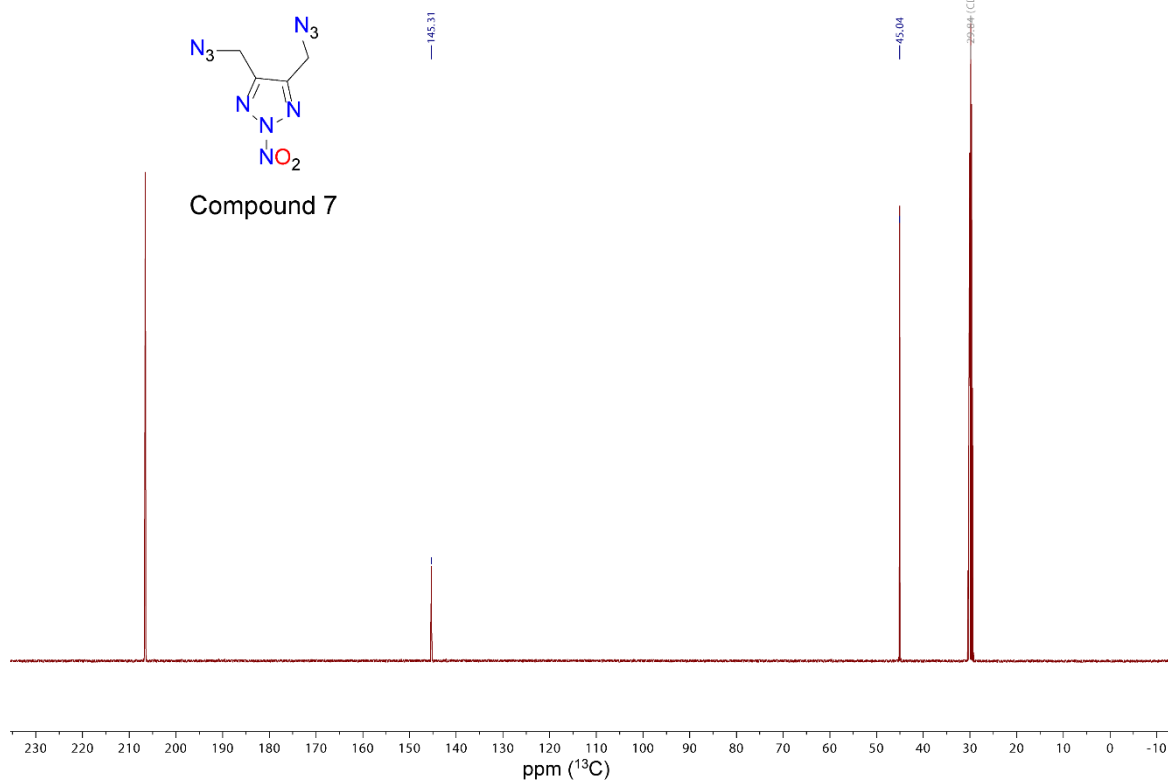
¹³C-NMR (Acetone-*d*₆, 101 MHz, ppm)



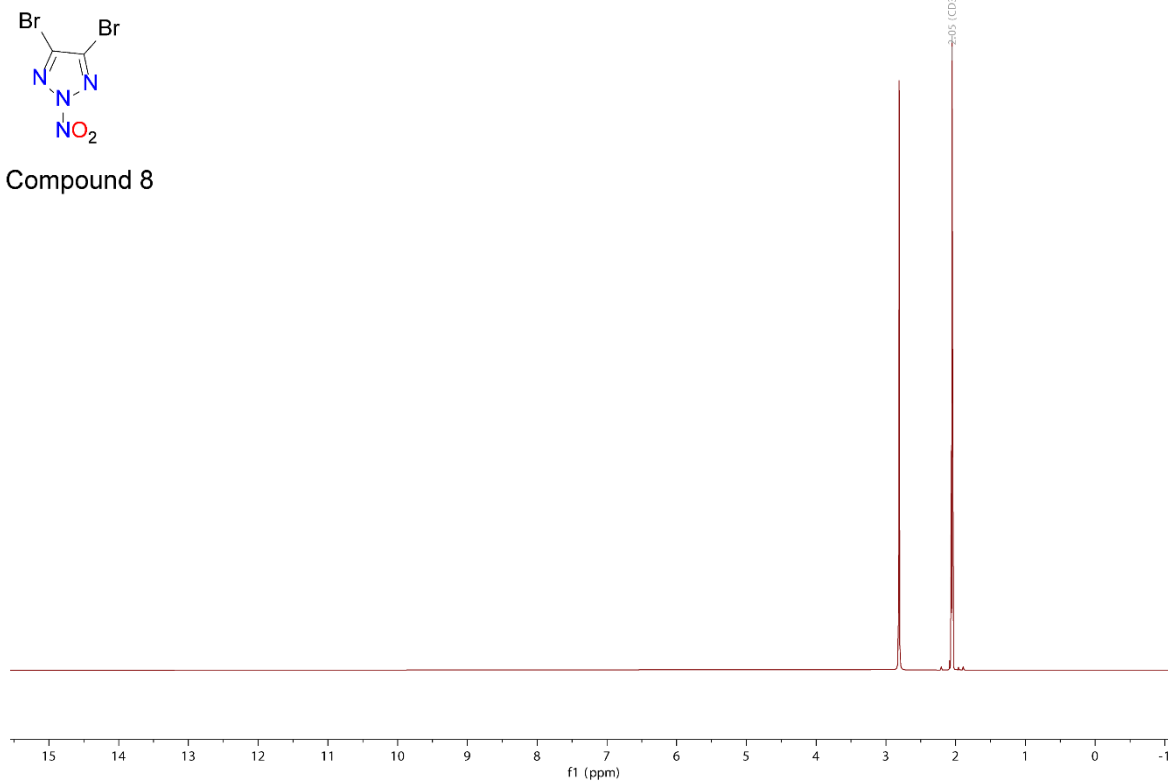
¹H-NMR (Acetone-*d*₆, 400 MHz, ppm)



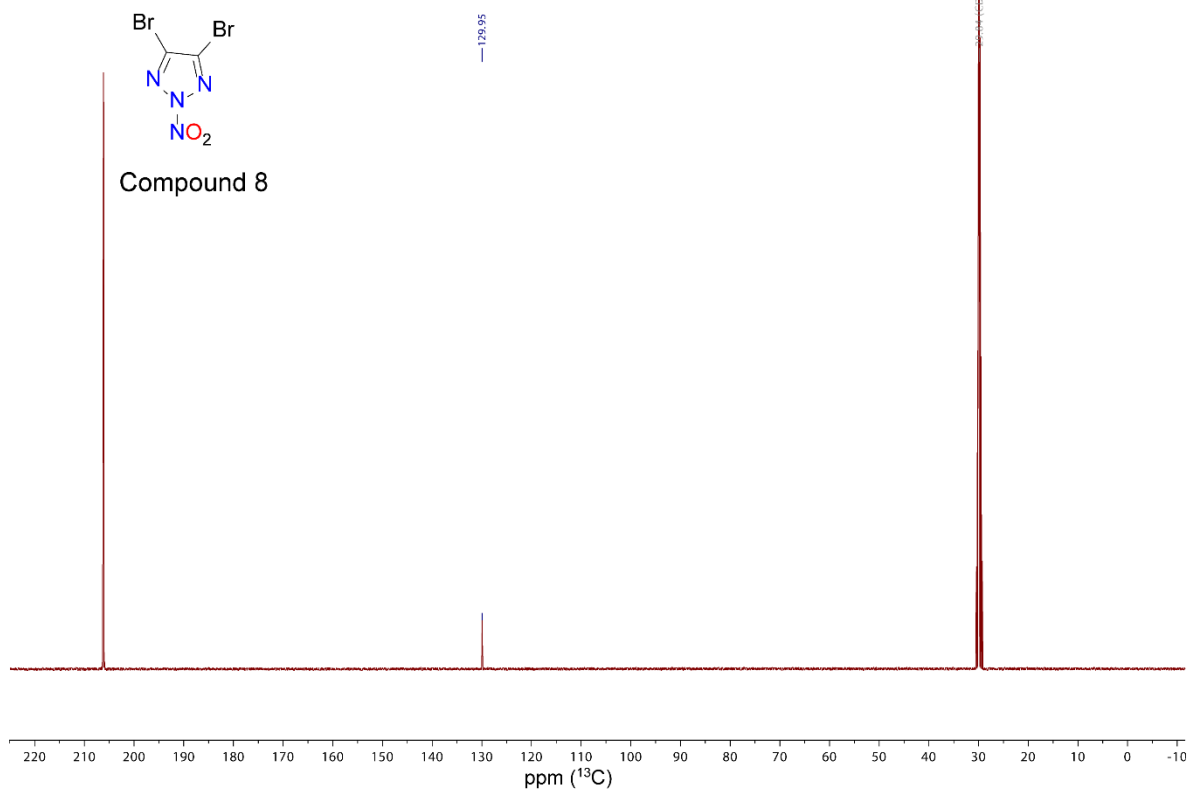
^{13}C -NMR (Acetone- d_6 , 101 MHz, ppm)



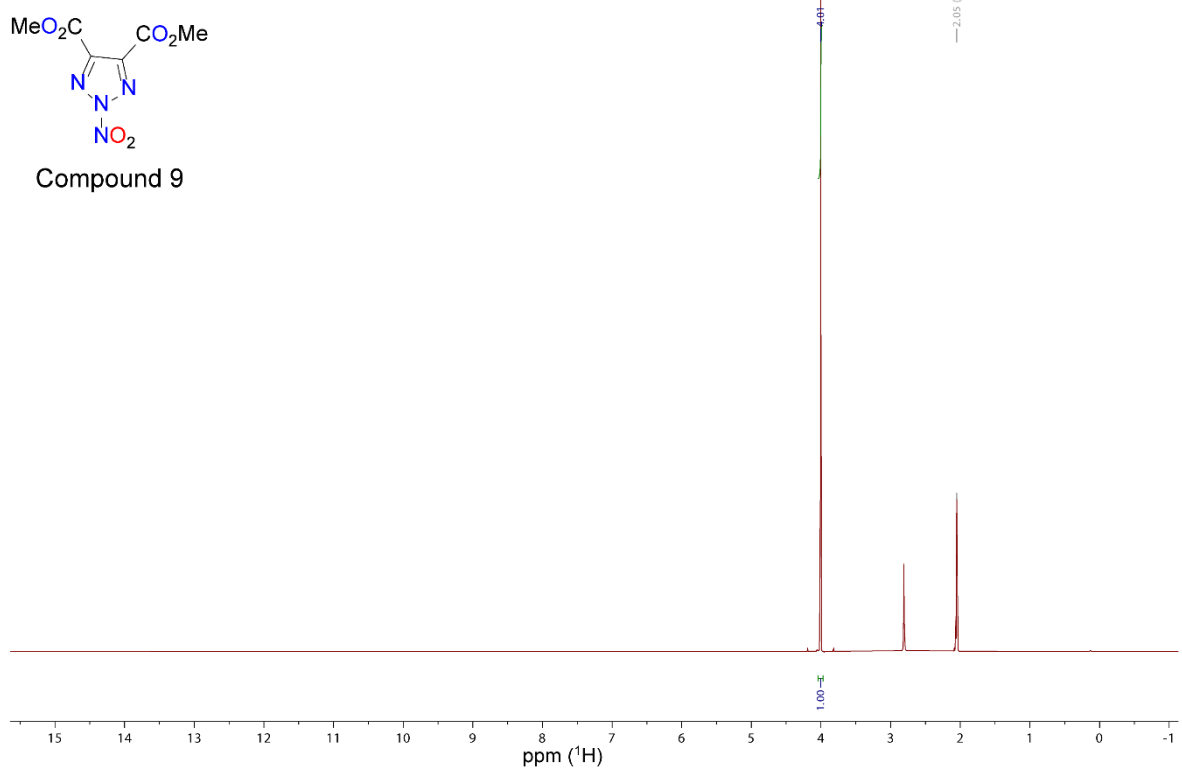
^1H -NMR (Acetone- d_6 , 400 MHz, ppm)



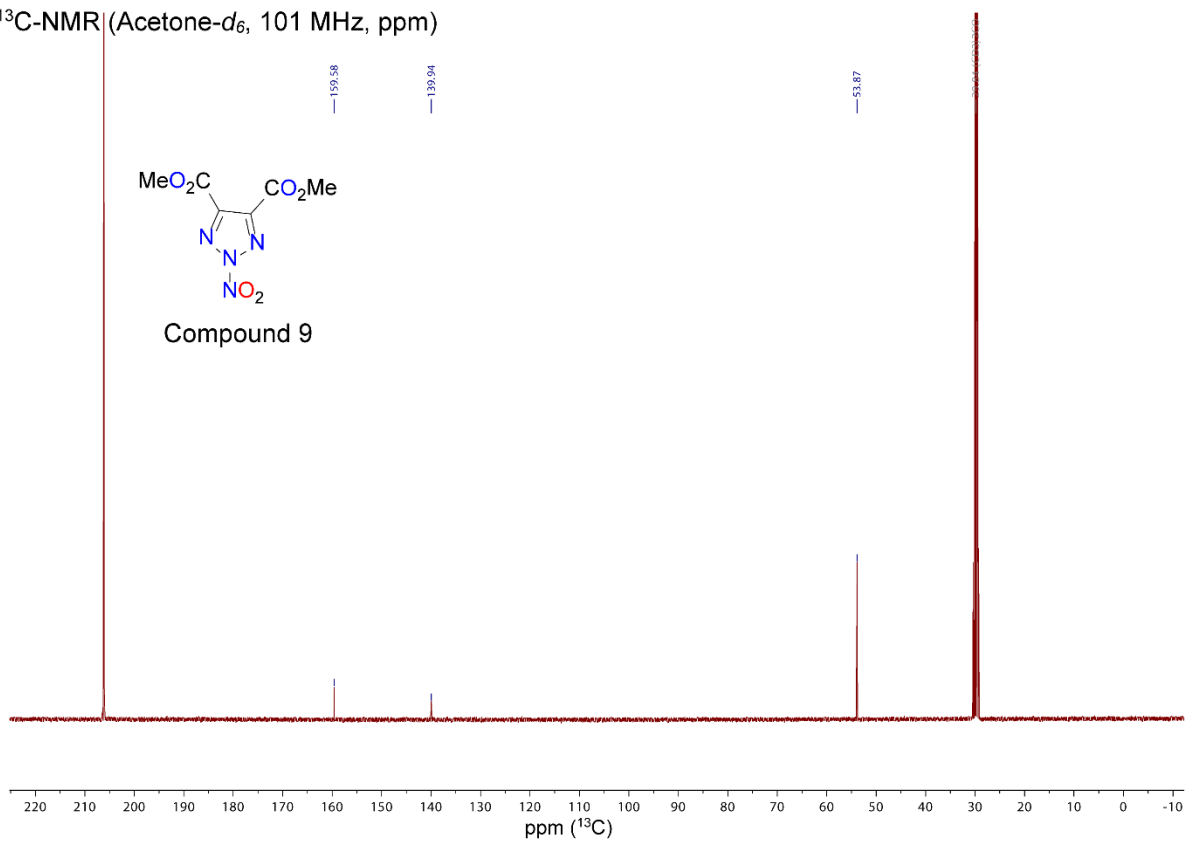
^{13}C -NMR (Acetone- d_6 , 101 MHz, ppm)



^1H -NMR (Acetone- d_6 , 400 MHz, ppm)



^{13}C -NMR (Acetone- d_6 , 101 MHz, ppm)



7. References

- [S1] United Nations, Recommendations on the Transport of Dangerous Goods: Manual of Tests and Criteria; New York and Geneva, **2015**.
- [S2] a) Albrecht, B. K.; Gehling, V. S.; Hewitt, M. C.; Taylor, A. M.; Harmange, J-C. Bromodomain inhibitors and uses thereof, WO2012151512 A2 2012-11-08; b) McDonald, A.; Qui-an, S. Therapeutic inhibitory compounds, WO2018011628 A1 2018-01-18.
- [S3] Izsak, D.; Klapötke, T. M.; Pflüger, C. Energetic derivatives of 5-(5-amino-2H-1,2,3-triazol-4-yl)-1H-tetrazole, *Dalton Trans.* **2015**, *44*, 17054-17063.
- [S4] *CrysAlisPro*, Oxford Diffraction Ltd. *version 171.33.41*, **2009**.
- [S5] Sheldrick, G.M., *Acta Cryst.* **2015**, *A71*, 3–8.
- [S6] Dolomanov, O. V.; Bourhis, L. J.; Gildea, R. J.; Howard, J. A. K.; Puschmann, H., OLEX2: A complete structure solution, refinement and analysis program. *J. Appl. Cryst.* 2009, *42*, 339–341.
- [S7] *SCALE3 ABSPACK – An Oxford Diffraction program* (1.0.4, gui: 1.0.3), Oxford Diffraction Ltd., **2005**.
- [S8] *APEX3*. Bruker AXS Inc., Madison, Wisconsin, USA.
- [S9] Frisch, M. J.; Trucks, G. W.; Schlegel, H. B.; Scuseria, G. E.; Robb, M. A.; Cheeseman, J. R.; Scalmani, G.; Barone, V.; Petersson, G. A.; Nakatsuji, H.; Li, X.; Caricato, M.; Marenich, A. V.; Bloino, J.; Janesko, B. G.; Gomperts, R.; Mennucci, B.; Hratchian, H. P.; Ortiz, J. V.; Izmaylov, A. F.; Sonnenberg, J. L.; Williams-Young, D.; Ding, F.; Lipparini, F.; Egidi, F.; Goings, J.; Peng, B.; Petrone, A.; Henderson, T.; Ranasinghe, D.; Zakrzewski, V. G.; Gao, J.; Rega, N.; Zheng, G.; Liang, W.; Hada, M.; Ehara, M.; Toyota, K.; Fukuda, R.; Hasegawa, J.; Ishida, M.; Nakajima, T.; Honda, Y.; Kitao, O.; Nakai, H.; Vreven, T.; Throssell, K.; Montgomery, J. A., Jr.; Peralta, J. E.; Ogliaro, F.; Bearpark, M. J.; Heyd, J. J.; Brothers, E. N.; Kudin, K. N.; Staroverov, V. N.; Keith, T. A.; Kobayashi, R.; Normand, J.; Raghavachari, K.; Rendell, A. P.; Burant, J. C.; Iyengar, S. S.; Tomasi, J.; Cossi, M.; Millam, J. M.; Klene, M.; Adamo, C.; Cammi, R.; Ochterski, J. W.; Martin, R. L.; Morokuma, K.; Farkas, O.; Foresman, J. B.; Fox, D. J., *Gaussian 09 A.02*, Gaussian, Inc., Wallingford, CT, USA, **2009**.

- [S10] a) Ochterski, J. W.; Petersson, G. A.; Montgomery Jr., J. A., A complete basis set model chemistry. V. Extensions to six or more heavy atoms, *J. Chem. Phys.* **1996**, *104*, 2598–2619; b) Montgomery Jr., J. A.; Frisch, M. J.; Ochterski, J. W.; Petersson, G. A., A complete basis set model chemistry. VII. Use of the minimum population localization method, *J. Chem. Phys.* **2000**, *112*, 6532–6542.
- [S11] a) Curtiss, L. A.; Raghavachari, K.; Redfern, P. C.; Pople, J. A., Assignment of Gaussian-2 and density functional theories for the computation of enthalpies of formation, *J. Chem. Phys.* **1997**, *106*, 1063–1079; b) Byrd, E. F. C.; Rice, B. M., Improved prediction of heats of formation of energetic materials using quantum mechanical calculations, *J. Phys. Chem. A* **2006**, *110*, 1005–1013; c) Rice, B. M.; Pai, S. V.; Hare, J., Predicting heats of formation of energetic materials using quantum mechanical calculations, *Comb. Flame* **1999**, *118*, 445–458.
- [S12] Lindstrom, P. J.; Mallard, W. G., (Editors), NIST Standard Reference Database Number 69, <http://webbook.nist.gov/chemistry/> (accessed June **2020**).
- [S13] Westwell, M. S.; Searle, M. S.; Wales, D. J.; Williams, D. H., Empirical correlations between thermodynamic properties and intermolecular forces, *J. Am. Chem. Soc.* **1995**, *117*, 5013–5015; b) Trouton, F., IV. On molecular latent heat, *Philos. Mag.* **1884**, *18*, 54–57.
- [S14] a) Jenkins, H. D. B.; Roobottom, H. K.; Passmore, J.; Glasser, L., Relationships among ionic lattice energies, molecular (formula unit) volumes and thermochemical radii, *Inorg. Chem.* **1999**, *38*, 3609–3620; b) Jenkins, H. D. B.; Tudela, D.; Glasser, L., Lattice potential energy estimation for complex ionic salts from density measurements, *Inorg. Chem.* **2002**, *41*, 2364–2367.
- [15] a) Spackman, P. R., Turner, M. J., McKinnon, J. J., Wolff, S. K., Grimwood, D. J., Jayatilaka, D., Spackman, M. A., *J. Appl. Cryst.* **2021**, *54*, 1006–1011, <https://doi.org/10.1107/S1600576721002910>; b) Spackman, M. A., Jayatilaka, D., *CrystEngComm* **2009**, *11*, 19–32, <https://doi.org/10.1039/B818330A>.
- [S16] Ma, Y., Zhang, A., Xue, X., Jiang, D., Zhu, Y., Zhang, C., *Cryst. Growth Des.* **2014**, *14*, 6101–6114.
- [S17] Rein, J., Meinhardt, J. M., Hofstra Wahlman, J. L., Sigman, M. S., Lin, S., *Angew. Chem. Int. Ed.* **2023**, e202218213.

Article

Synthesis and Characterization of Azido- and Nitroalkyl Nitropyrzoles as Potential Melt-Cast Explosives

Elena Reinhardt, Tobias Lenz, Lukas Bauer, Jörg Stierstorfer * and Thomas M. Klapötke *

Department of Chemistry, Ludwig-Maximilians-University of Munich, Butenandtstr. 5–13, 81377 Munich, Germany; elrech@cup.uni-muenchen.de (E.R.); tolech@cup.uni-muenchen.de (T.L.); luauch@cup.uni-muenchen.de (L.B.)

* Correspondence: jstch@cup.uni-muenchen.de (J.S.); tmk@cup.uni-muenchen.de (T.M.K.)

Abstract: Desirable advancements in the field of explosive materials include the development of novel melt-castable compounds with melting points ranging from 80 to 110 °C. This is particularly important due to the limited performance and high toxicity associated with TNT (trinitrotoluene). In this study, a series of innovative melt-castable explosives featuring nitroalkyl and azidoalkyl functionalities attached to the 3-nitro-, 4-nitro-, 3,4-dinitropyrazole, or 3-azido-4-nitropyrazole scaffold are introduced. These compounds were synthesized using straightforward methods and thoroughly characterized using various analytical techniques, including single-crystal X-ray diffraction, IR spectroscopy, multinuclear nuclear magnetic resonance (NMR) spectroscopy, mass spectrometry, elemental analysis, and DTA. Furthermore, the energetic properties such as (theoretical) performance data, sensitivities, and compatibilities of the compounds were evaluated and compared among the different structures.

Keywords: melt-cast explosives; nitropyrzoles; nitrate ester; azides; structure elucidation



Citation: Reinhardt, E.; Lenz, T.; Bauer, L.; Stierstorfer, J.; Klapötke, T.M. Synthesis and Characterization of Azido- and Nitroalkyl Nitropyrzoles as Potential Melt-Cast Explosives. *Molecules* **2023**, *28*, 6489. <https://doi.org/10.3390/molecules28186489>

Academic Editors: Vladimir A. Tartakovskiy, Michael S. Klenov and Alexey A. Voronin

Received: 10 August 2023
Revised: 31 August 2023
Accepted: 2 September 2023
Published: 7 September 2023



Copyright: © 2023 by the authors. Licensee MDPI, Basel, Switzerland. This article is an open access article distributed under the terms and conditions of the Creative Commons Attribution (CC BY) license (<https://creativecommons.org/licenses/by/4.0/>).

1. Introduction

Materials that store and release energy are essential for many applications. Energetic materials can store large amounts of energy and release it quickly when stimulated, whether as fuel for rockets and ammunitions or as explosives in the military or civilian sector [1–3]. In the mining industry, the invention of dynamite (nitroglycerin absorbed in kieselguhr) made explosive mining convenient. Today, cheap ammonium nitrate mixed with fuel oil, called ammonium nitrate fuel oil (ANFO), is used for safer handling. The initiation of relatively insensitive ANFO is typically performed by Pentolite, a mixture of pentaerythritol tetranitrate (PETN) that is embedded in a trinitrotoluene (TNT) melt. In the military sector, more robust, high-performance materials are needed. Mixtures of castable compounds such as TNT (Comp-B, Comp-C, Pentolite) or dinitroanisole (DNAN) (IMX-101) with high-performance materials such as hexogen (RDX), octogen (HMX), or PETN are commonly employed and comprise a significant category of military explosives [4,5]. In this procedure, the solid components of the compositions are agitated until they form a homogeneous dispersion within molten TNT. This mixture is then poured into molds or cavities and allowed to solidify as it cools. The inclusion of a melt-castable component, such as TNT, serves as a carrier material, facilitating the shaping of explosive compositions into desired forms and enhancing their loading capacity [5–7]. These traditional materials have several disadvantages that science is trying to solve with new technology and materials. TNT is toxic, and prolonged exposure causes anemia and harms the liver [8]. The production produces red wastewater which is harmful to the environment and disposal is, therefore, problematic [9]. The commonly used explosive RDX is found in air, water, and soil, especially around military facilities. RDX is proven to be toxic and harms the nervous system, urinary system, and prostate of animals. In addition, there is evidence of carcino-

genic potential in animals [10,11]. Therefore, science is looking for more environmentally friendly alternatives with at best better detonation performance and lower sensitivity.

Recent work focusing on the replacement of RDX resulted in high-energy compounds such as CL-20 [12] or TKX-50 [13]. For TNT replacements, a combination of azoles with alkyl functionalities gained attention. Azido or nitrate groups combined with methyl or ethyl groups that are attached to the aromatic ring have proven to be a construction kit for acceptable powerful, low-sensitive, insoluble, and melting compounds [14]. The combinations were also evaluated by computational machine learning methods with good accuracy [15]. Examples of low-melting-point azoles are given in Figure 1.

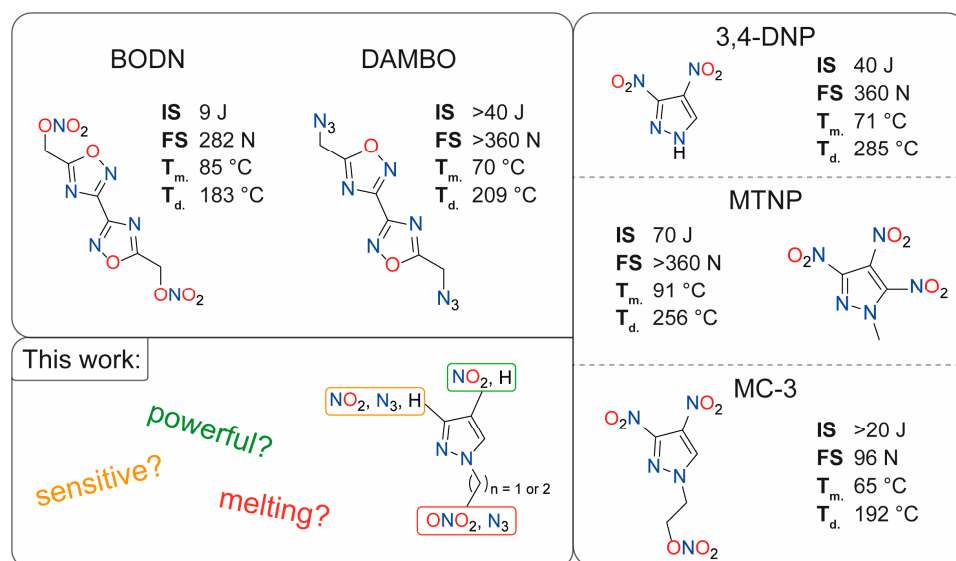


Figure 1. Current examples of energetic materials with suitable melting points based on azoles with bis(1,2,4-oxadiazole)bis(methylene) dinitrate (BODN) [16], diazidomethyl-bisoxadiazole (DAMBO) [17], 3,4-dinitro-1H-pyrazole (3,4-DNP) [18,19], 1-methyl-trinitropyrazole (MTNP) [20], and (MC-3) [15] and sensitivity toward impact and friction as well as their endo- (T_m) or exothermic (T_d) behavior under heating.

The organic nitrate BODN [16] has gained attention due to its desirable properties and higher performance than TNT. The diazido-derivative DAMBO is melts 10 °C lower but has advanced stability and is insensitive. As a general trend, alkyl organic nitrates show acceptable densities and moderate sensitivities but lack thermal stability (typically < 190 °C). Whereas the corresponding azido derivatives show lower densities with better thermal stabilities [21–24]. Recently, nitropyrazoles gained attention as low-melting-point energetic materials (Figure 1). 3,4-DNP shows melting and late decomposition while being sensitive and powerful, but it is acidic and would react with metal shells as is known for picric acid. To overcome the acidity, N–H functionalization, for example, with methyl or nitrateethyl groups, can be performed. MTNP is the most powerful compound in Figure 1 with 8960 m s^{−1} detonation velocity, but is the least efficient to synthesize. Further research has focused on powerful pyrazoles through their combination with ortho azido/nitro groups [25], trinitromethyl moieties [26–28], or alkyl bridges [29–31], and also energetic coordination compounds [32] have been described. To study the effects of different exoporphoric groups (nitro and azido), various chain lengths, and substitution patterns on pyrazoles concerning the properties of potential melt-cast explosives—including attributes such as melting temperature, decomposition temperature, density, and detonation parameters—we utilized the well-known 3-nitro-, 4-nitro-, and 3,4-dinitropyrazoles as building blocks in this work, since compounds based on nitropyrazoles are reported as powerful energetic materials [33–35]. These nitropyrazoles were modified by replacing their acidic N–H position with alkyl azide and nitrate groups, thus customizing their properties to

align with those of a melt-cast explosive. Additionally, we synthesized ortho azido/nitro compounds, resulting in substances with modified properties.

2. Results and Discussion

2.1. Synthesis

The synthesis is divided into two sections: 1. synthesis of nitrate esters, and 2. synthesis of azides (Figure 2). The compounds with these functional groups were synthesized using 3-nitro- [19], 4-nitro- [36] and 3,4-dinitropyrazole [19] backbones, each equipped with either a methyl or an ethyl chain. In both cases, hydroxy moieties acted as the starting compounds. In accordance with literature procedures, 1-hydroxymethyl-3-nitropyrazole compounds (1) and 1-hydroxymethyl-4-nitropyrazole (7) were synthesized by reacting 3-nitropyrazole or 4-nitropyrazole with 40% formaldehyde solution [37]. For the hydroxyethyl groups, compounds (4) and (8), the nitropyrazole rings were deprotonated with potassium carbonate and further reacted with 2-bromoethanol [38].

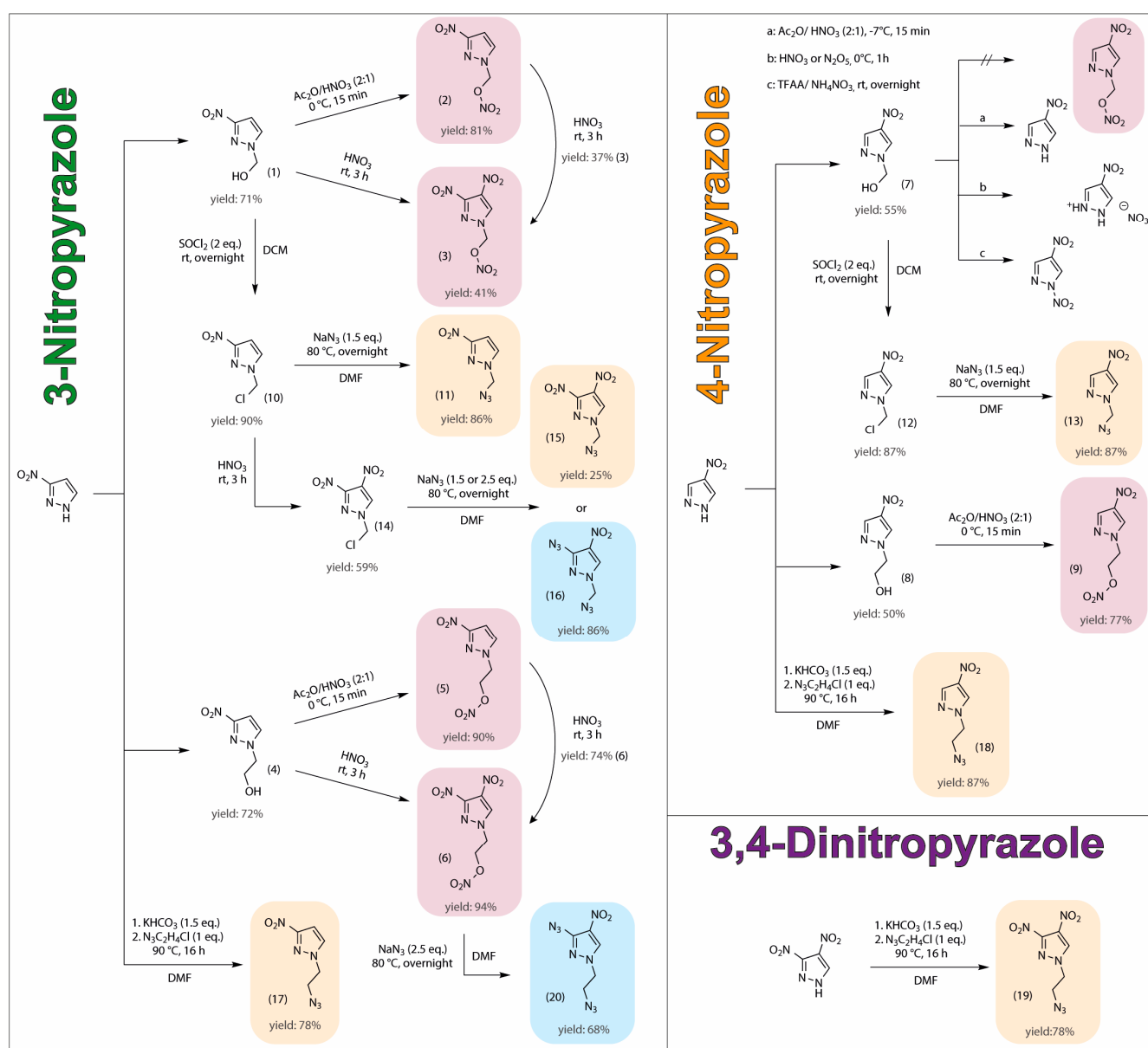


Figure 2. Synthesis overview of azido- and nitratealkyl-nitropyrazoles.

Starting from 1-hydroxymethyl-3-nitropyrazole [37] (**1**) and 1-hydroxyethyl-3-nitropyrazole (**4**) [38], four different compounds were synthesized using different nitrating agents. Acetyl nitrate converted the hydroxy group to a nitrate ester with good yields within a few minutes (**2**: 81%, **5**: 90%). Nitration with fuming nitric acid for three hours led to the additional nitration of the 3-nitropyrazole ring at the C4 position. In this case, the yield of the hydroxyethyl compound (**4**) was significantly better (**6**: 94%) than for the hydroxymethyl compound (**1**) (**3**: 41%). An HPLC study showed that a large percentage of the nitratomethyl moiety was cleaved off during the nitration of OH group. Introducing the nitro group at the C4 position of the pyrazole ring enhances electron withdrawal from the pyrazole ring, leading to the cleavage of the nitratomethyl group. This phenomenon is evident in LC-MS measurements (see SI LC-MS measurements) and results in the lower yield of compound **3**. The cleavage of the nitratomethyl group was also observed at lower temperatures ($-30\text{ }^{\circ}\text{C}$), resulting in approximately the same amount of reaction products. Additionally, compounds (**3**) and (**6**) were synthesized by reacting (**2**) and (**5**) with fuming nitric acid.

Replacing 3-nitropyrazole [19] with 4-nitropyrazole [36] enables successful reaction of the hydroxyethyl compound (**8**) with acetyl nitrate, yielding the desired nitrate ethyl compound (**9**) with a satisfactory yield of 77%. However, attempts to nitrate the hydroxy group of the hydroxymethyl compound (**7**) were unsuccessful. As observed with compound (**3**), the nitratomethyl group formed in this reaction was cleaved off completely, precluding the formation of the desired product. During the reaction of compound (**7**) with acetyl nitrate, only 4-nitropyrazole could be isolated. Upon nitration with fuming nitric acid or N_2O_5 , the major product obtained was the nitrate salt of 4-nitropyrazole. Using TFAA and NH_4NO_3 as the nitration system resulted not only in the cleavage of the nitratomethyl group but also in the nitration of the pyrazole ring at the N1 position.

To synthesize the azidomethyl compounds, the hydroxymethyl compounds (**1**) and (**7**) were initially converted to 1-chloromethylnitropyrazoles [39] (**10**) and (**12**) using thionyl chloride with high yields of 90% and 87%, respectively. Both compounds were further subjected to a substitution reaction, resulting in the successful formation of the desired azidomethyl compounds (**11**) and (**13**) in a good yield (**11**: 86%, **13**: 87%). The attempted nitration of compound (**11**) at the C4 position of the pyrazole ring, using fuming nitric acid, resulted in the substitution of the azido group with a nitrate group, thereby regenerating compound (**3**) among other by-products. To circumvent this issue, the nitro group was first introduced by the previously described method prior to azide exchange, yielding compound **14**. Efforts to prepare 1-azidomethyl-3,4-dinitropyrazole through sodium azide substitution proved challenging. The typical use of 1.5 equivalents resulted in the substitution of the chlorine atom and also in an undesired substitution of the nitro group at the C3 position [30,40], leading to a mixture of compound **15** and the ortho azido/nitro compound **16**, which could be separated by column chromatography. In order to prevent substitution at the nitro group, the reaction was conducted with a precise amount of 1.0 equivalent of sodium azide. While this approach reduced the formation of compound **16**, the reaction remained incomplete and additional by-products were observed. Attempts to address this, by adjusting the reaction temperature or time, proved ineffective. However, increasing the equivalents to 2.5 resulted in the complete substitution of both the chlorine atom and nitro group at the C3 position, leading to full conversion to compound **16**. Upon attempting the conversion of (**6**) to 1-nitrateethyl-3-azido-4-nitropyrazole by replacing the nitro group at the C3 position with an azide moiety, an additional substitution of the nitrate ester with azide occurred, resulting in the formation of compound **20** in a good yield of 68%.

In the synthesis of azidoethyl compounds, the implementation of an azidoethyl transfer method [41] proved advantageous as this method allowed for the elimination of two reaction steps. The procedure involved the in situ deprotonation of nitropyrazoles, followed by their reaction with 1-azido-2-chloroethane (**17**, **18**) or 2-azidoethyl mesylate (**20**) at elevated temperatures using standardized conditions. These reactions were conducted in DMF as the solvent, and the resulting products could be efficiently isolated through

extraction, giving satisfactory yields. If required, the products can be easily purified using column chromatography.

Three of the described compounds (**2**, **3**, **6**) were previously reported in the literature [15]. The synthesis of compound **2** closely followed established literature procedures. Compounds **3** and **6** were synthesized more efficiently, involving fewer steps, by nitration of the OH group and the subsequent introduction of the second nitro group to the pyrazole ring.

2.2. Crystal Structures

Crystals of compounds **1–13**, **16**, **19**, and **20** were obtained either by recrystallization (**1**, **7**: chloroform; **2**, **3**, **5**: methanol; **4**: ether/dichloromethane; **6**, **20**: ethanol; **8**, **16**: ethylacetate, **20**: ether) or directly from the reaction mixture (**9–13**). The crystal structures of the energetic compounds are illustrated in Figure 3. The Supporting Information contains further information on the X-ray measurements and refinements, as well as crystal structure figures for compounds **1**, **4**, **7**, **8**, **10**, and **12**. Additional information on the X-ray structure determinations were deposited in the CCDC database [42], and the corresponding numbers are: **1**: 2255656, **2**: 2255417, **3**: 2255418, **4**: 2255410, **5**: 2255415, **6**: 2255419, **7**: 2255411, **8**: 2255658, **9**: 2255412, **10**: 2255416, **11**: 2255657, **12**: 2255409, **13**: 2255413, **16**: 2261896, **19**: 2255414, **20**: 2269934.

The non-hydrogen atoms' ellipsoids in all structures are depicted at a 50% probability level.

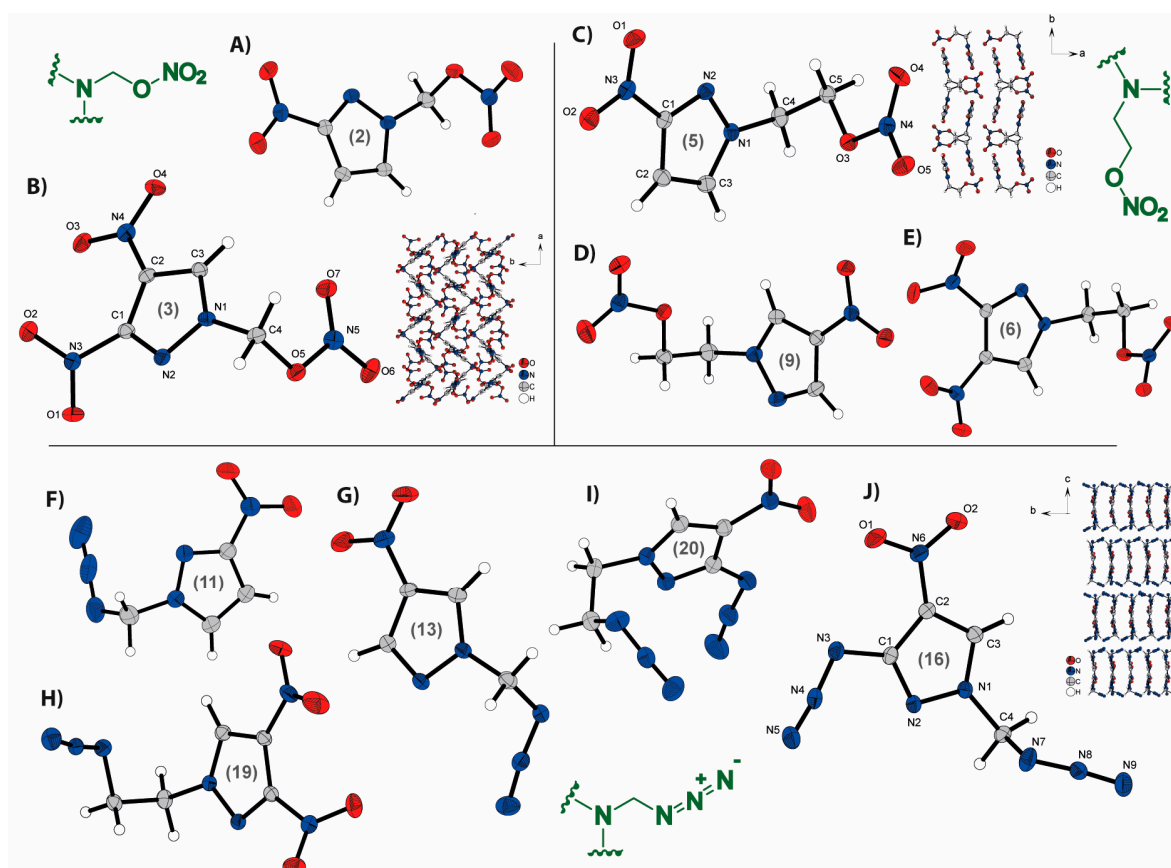


Figure 3. Molecular units of synthesized azido- and nitroalkyl-nitropyrazoles: (A) 1-nitratomethyl-3-nitropyrazole (**2**); (B) 1-nitratomethyl-3,4-dinitropyrazole (**3**) and its extended structure; (C) 1-nitratethyl-3-nitropyrazole (**5**) and its extended structure; (D) 1-nitrateoethyl-4-nitropyrazole (**9**); (E) 1-nitrateoethyl-3,4-dinitropyrazole (**6**); (F) 1-azidomethyl-3-nitropyrazole (**11**); (G) 1-azidomethyl-4-nitropyrazole (**13**); (H) 1-azidoethyl-3,4-dinitropyrazole (**19**); (I) 1-azidoethyl-3-azido-4-nitropyrazole (**20**); (J) 1-azidomethyl-3-azido-4-nitropyrazole (**16**) and its extended structure.

The bond lengths of the pyrazole ring observed in all crystal structures (e.g., **3**: N6–C7 1.344(7), C7–C6 1.364(8); **9**: N1–C3 1.333(2), C2–C1 1.392(2); **11**: N1–N2 1.347(4), C2–C3 1.363(6)) are consistent with the typical range found in substituted pyrazoles [43]. In the mononitrated structures obtained, hydrogen bonds formed with neighboring CH elements cause the nitro group to adopt a nearly planar conformation within the pyrazole ring, regardless of its position at the 3- or 4-position (e.g., **2**: C2–C1–N3–O2 3.0°; **13**: C3–C2–N3–O2 –4.7°). However, when an additional nitro group is introduced at the 4-position of the 3-nitropyrazole, the nitro group at the 3-position undergoes a rotational displacement from the pyrazole plane, while the nitro group at the 4-position retains its planarity with the pyrazole ring (e.g., **3**: C3–C2–N4–O4 –6.5°, C2–C1–N3–O2 –30.6°). The analysis of the nitratomethyl compounds reveals that in both cases, the nitro group of the nitrate ester is positioned away from the pyrazole ring, forming a nearly planar arrangement with the side chain (**2**: C4–O3–N4–O5 –0.4°; **3**: C4–O5–N5–O7 –6.0°). In the nitrateethyl compounds, a gauche conformation is observed between the pyrazole ring and the nitrate ester (e.g., **6**: O5–C5–C4–N1 61.2°). A similar conformation is also observed in the azidoethyl compound. The azide group is nearly perpendicular to the pyrazole ring, resulting in a lower density. In contrast to the corresponding nitrate esters, the azidomethyl compounds have the azido group directed toward the pyrazole ring. However, in the azido-nitro compound **16**, the azido group is oriented in the opposite direction. Both, the nitro group and the azido group in these compounds lie in the same plane as the pyrazole ring (e.g., **16**: N4–N3–C1–N2 6.4° (azido); **20**: O1–N6–C2–C3 177.2° (nitro)), with the azido group pointing away from the nitro group due to electrostatic repulsion.

The mononitrated nitrate ester compounds (**2**, **5**, **9**) exhibit similar extended structures, as illustrated by the example of compound **5** in Figure 3C. These compounds form layered structures, where pyrazole rings are arranged in mirror symmetry, forming a unit within each layer. The side chains are positioned centrally within the layers. The extension of the side chains induces curvature in the layers, leading to a decrease in density (cf. **2**: 1.696 g/cm³, **5**: 1.629 g/cm³). Additionally, the nitro group at the C4 position instead of the C3 position results in an increased spacing between the layers (cf. **5**: 4.5433(14) Å, **9**: 7.6928 (18) Å), further contributing to the reduced density (cf. **5**: 1.629 g/cm³, **9**: 1.613 g/cm³). The dinitrated compounds **3** and **6** display zig-zag structures with acute angles, as exemplified by compound **3** in Figure 3B. This structural arrangement is more pronounced in the methyl derivative **3** than in the ethyl derivative **5**, which likely accounts for the increased sensitivity observed in compound **3** (IS: 4 J). The structural arrangements of the azide compounds (**11**, **13**, **19**) vary and do not exhibit comparable patterns. The dinitro compound (**19**), similar to nitric esters, exhibits a zig-zag structure. The extended structures of the azido-nitro (**16**, **20**) compounds demonstrate a rectangle formation, characterized by distinct orientations within each structure. (All the extended structures of energetic compounds are found in the Supplementary Information).

2.3. Physicochemical Properties

The physicochemical properties of the nitrate esters (**2**, **3**, **5**, **6**, **9**) and azides (**11**, **13**, **15–20**) have been systematically summarized in Table 1. The assessment of their response to external stimuli unveiled that the majority of the investigated compounds exhibit low sensitivity or insensitivity towards impact and friction. Exceptions were observed with the nitrate ester (**3**), which displayed an impact sensitivity value of 4 J, positioning it at the borderline of highly sensitive materials. The manifestation of the unexpectedly increased impact sensitivity for (**3**) becomes apparent upon checking the crystallographic arrangement, wherein distinct zig-zag motifs are prominently observed throughout the extended structure. Moreover, the electrostatic discharge (ESD) sensitivity of the compound was assessed, revealing a value of 51 mJ. This falls below the threshold of the electrostatic charge typically associated with a human being, underscoring the need for cautious handling measures. Moreover, the azido-nitro compounds (**19**) (IS: <1 J, FS: 10 N) and (**20**) (IS: 2 J, FS: 80 N) demonstrated sensitivities in the range of highly sensitive

materials. This can be attributed to the presence of adjacent azido and nitro groups, which result in electrostatic repulsion.

Table 1. Physicochemical properties and detonation parameters of all synthesized energetic compounds compared to TNT [44].

	IS ^a (J)	FS ^b (N)	T _{melt} ^c (°C)	T _{exo.} ^d (°C)	ρ ^e (g/cm ³)	Δ _f H ^o ^f (kJ/mol)	D _{C-J} ^g (m/s)	p _{C-J} ^h (GPa)
(2)	>40	>360	70	161	1.696	−20.2	7675	24.3
(3)	4	288	93	159	1.848	8.7	8668	33.6
(5)	>40	>360	78	198	1.629	−67.1	7163	19.8
(6)	30	>360	61	198	1.734	−43.1	7932	26.7
(9)	>40	>360	52	191	1.613	−65.0	7110	19.5
(11)	>40	>360	40	179	1.513	401.8	6972	19.9
(13)	>40	>360	42	174	1.547	398.7	7100	19.8
(15) ⁱ	>40	>360	/	154	1.58 ^j	433.9	7679	23.1
(17) ⁱ	>40	>360	/	214	1.28 ^j	369.6	6235	11.9
(18) ⁱ	>40	>360	/	214	1.34 ^j	372.1	6483	13.3
(19)	25	>360	50	216	1.664	382.5	7639	22.9
(16)	<1	10	57	157	1.670	755.8	7945	24.4
(20)	2	80	41	172	1.554	707.4	7274	20.1
TNT	15	>360	81	289	1.65	−185	6950	20.5

^a Impact sensitivity (BAM drophammer, method 1 of 6); ^b friction sensitivity (BAM friction tester, method 1 of 6); ^c endothermic event (DTA, β = 5 °C·min^{−1}); ^d temperature of decomposition (DTA, β = 5 °C·min^{−1}); ^e density at 298 K recalculated from X-ray data; ^f heat of formation (calculated using the atomization method and CBS-4M enthalpies); ^g detonation velocity; ^h detonation pressure; ⁱ liquid-oily compounds; ^j volumetric determination.

The vast majority of the compounds are solids, with the exception of the azidomethyl (15) and azidoethyl (17, 18) compounds. Substances with low melting points (11, 13, 20) undergo solidification under cooling conditions. In order to assess their melting and decomposition temperatures, differential thermal analysis (DTA) was performed, employing a controlled heating rate of 5 °C min^{−1}. All solid-state compounds show melting points. It can be generally observed that the azides demonstrate lower melting points (between 40 and 50 °C) compared to their corresponding nitrate esters, while exhibiting around 15–20 °C higher decomposition temperatures (with the exception of 15). The elongation of alkyl chains in both azides and nitrate esters results in higher decomposition temperatures. Consequently, the azidoethyl pyrazoles exhibit the highest decomposition temperatures (e.g., 19: 216 °C). Among the five nitrate esters, three possess melting points within a suitable range (2: 70 °C, 3: 93 °C, 5: 78 °C), whereas the remaining two display slightly lower melting points of 61 (6) and 52 °C (9), respectively. It should be noted, only compound 5 shows a decomposition temperature exceeding 100 °C beyond its melting point (T_{melt}: 78 °C, T_{dec}: 198 °C). The substitution of a nitro group with an azido group on the pyrazole ring does not exhibit a consistent trend regarding thermal behavior.

The examination of the heat of formation and density reveals a general trend wherein the replacement of nitrate esters with azides and the shortening of alkyl chains lead to an increase in the heat of formation but a decrease in density. Accordingly, compounds containing two azido groups exhibit the highest heat of formation values (16: 755.8 kJ/mol, 20: 707.4 kJ/mol). However, there are exceptions observed for the densities of certain pairs of compounds. Specifically, the presence of an additional azido group at the ring (see 15 and 16) leads to increased density (15: 1.58 g/cm³, 16: 1.670 g/cm³). The density significantly outweighs the heat of formation in influencing the detonation parameters. Consequently, despite their lower heat of formation, nitrate esters exhibit superior detonation velocities compared to azides. Among the compounds investigated, three of them exhibit detonation velocities around and above 8000 m/s (3, 6, 16). Compound 3 stands out, with a notable detonation velocity of 8668 m/s accompanied by a density of 1.848 g/cm³.

Compounds 3 and 5 were investigated for their compatibility with HMX and RDX based on their promising detonation velocity and/or the thermal behavior. Differential

thermal analysis (DTA) was employed to evaluate their compatibility. The results revealed that compound **3** is compatible with HMX, showing minimal deviations in melting ($-1\text{ }^{\circ}\text{C}$) and decomposition ($+3\text{ }^{\circ}\text{C}$) temperatures. It exhibited moderate compatibility with RDX, with slight alterations in the thermal behavior ($T_{\text{melt}}: -5\text{ }^{\circ}\text{C}$; $T_{\text{dec}}: +5\text{ }^{\circ}\text{C}$). Compound **5** demonstrated moderate compatibility with RDX and HMX, as indicated by the observed temperature deviations. When combined with RDX, both the melting point and decomposition temperature exhibited a $6\text{ }^{\circ}\text{C}$ shift. Similarly, slight temperature shifts were observed for **5** when mixed with HMX ($T_{\text{melt}}: -4\text{ }^{\circ}\text{C}$; $T_{\text{decom}}: +5\text{ }^{\circ}\text{C}$) (for additional information, see Supplementary Information).

2.4. NMR Spectroscopy

The synthesized compounds were characterized using ^1H , ^{13}C , and, in selected cases, ^{14}N NMR spectroscopy. Specifically, compounds **2**, **3**, and **16** were further characterized by ^{15}N NMR spectroscopy. DMSO- d_6 , CDCl_3 (for ^1H , ^{13}C and ^{14}N NMR), and acetone- d_6 (for ^{15}N NMR, due to slow decomposition in DMSO- d_6) were employed as solvents for the measurements. A summary of the observed chemical shifts of ^1H , ^{13}C , and $^{14,15}\text{N}$ chemical shifts is presented in Figure 4.

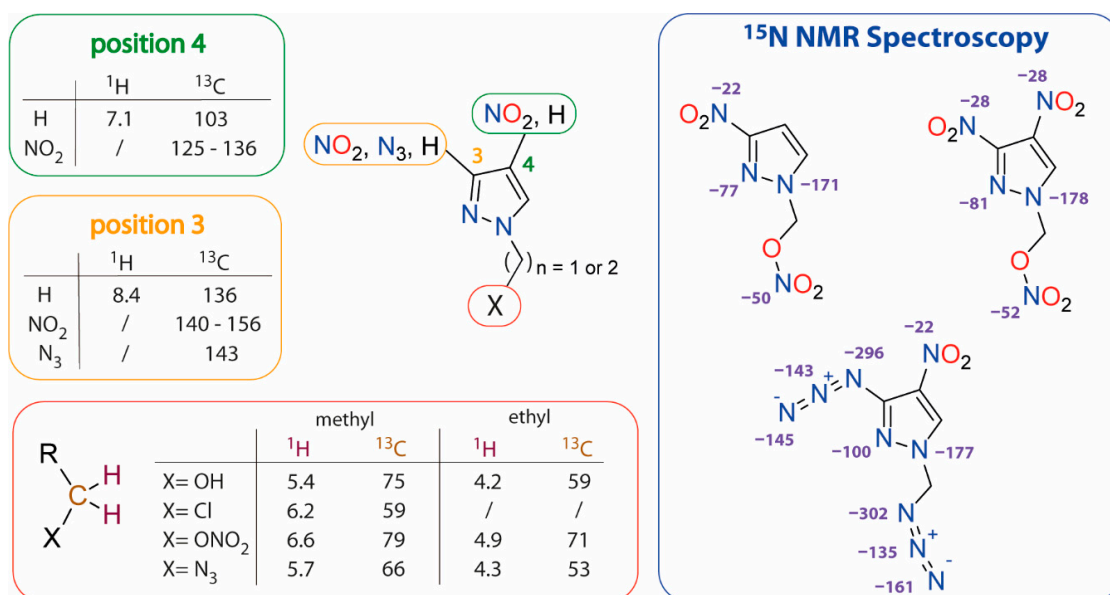


Figure 4. ^1H , ^{13}C , and $^{14,15}\text{N}$ NMR shifts (in ppm) for the synthesized compounds based on nitropyrazole.

The assignment of ^1H and ^{13}C NMR signals is based on comparison with literature data [45,46]. The ^1H and ^{13}C chemical shifts provide valuable insights into the substitution pattern ($-\text{OH}$, $-\text{Cl}$, $-\text{ONO}_2$, $-\text{N}_3$) of the alkyl chain in the pyrazole moiety. The nitrate ester (**2**, **3**) shows the weakest shielding effect to the protons of the alkyl chain, resulting in a downfield shift (6.6 ppm), while the OH group (**1**, **7**) displays the strongest shielding effect, leading to an upfield shift (5.4 ppm). Substituting the nitrate ester with an azide (see **6** and **20**) causes a shift towards higher field (5.7 ppm). The same upfield shift is observed in the case of chlorine-azide exchange ($-\text{Cl}$: 6.2 ppm; $-\text{N}_3$: 5.7 ppm). The influence of different substituents is more pronounced in compounds with a methyl group (**1–3**, **7**, **10–16**) compared to those with an ethyl moiety (**5**, **6**, **9**, **17–20**), although the overall trends remain consistent. Evidence of the substitution at the pyrazole ring can be derived from the observed ^1H and ^{13}C chemical shifts. The proton located at position 3 experiences a larger deshielding effect (**9**, **13**, **18**; 8.4 ppm) compared to that at position 4 (**2**, **5**, **11**, **17**; 7.1 ppm), attributable to its proximity to the pyrazole nitrogen atom. This trend is also reflected in the positions of the ^{13}C NMR signals. Notably, nitration of one of the carbon atoms causes

a downfield shift due to the electron-withdrawing effect of the nitro group. However, the presence of electron-withdrawing groups on the neighboring carbon atom mitigates this effect [47].

The assignment of the ^{14}N and $^{14,15}\text{N}$ NMR signals resulted from the evaluated coupling pattern of ^{15}N NMR spectra and ^1H ^{15}N HMBC spectra (for additional information see Figures S6–S11 in the Supplementary Information). The ^{15}N signal of the N1 atom in compounds **2**, **3**, and **16**, appears at about -175 ppm. In the disubstituted compounds (**3**, **16**), coupling of N1 with the ring proton at position 5 results in a doublet ($^2J_{\text{N,H}} = 2.8\text{--}3.0$ Hz). In the case of the monosubstituted pyrazole (**2**), the N1 signal is split into a doublet of doublets ($^2/3J_{\text{N,H}} = 6.8, 4.4$ Hz) due to coupling also with the second aromatic proton in position 4. The N2 nitrogen of the pyrazole ring exhibits a downfield shift compared to N1 (N1: about $-171\text{--}177$ ppm; N2: $-77\text{--}100$ ppm). Its ^{15}N NMR signal is split into a triplet ($^3J_{\text{N,H}} = 2.6\text{--}2.8$ Hz) due to the 3J coupling with the CH_2 protons. The N2 NMR signal is shifted to higher field when the C3 position is occupied by an azide instead of a nitro group (e.g., **3**: -81 ppm, **16**: -100 ppm), as azides exert a weaker electron-withdrawing effect [46]. The assignment of the nitrogen atoms of the two azido groups was possible by analyzing the splitting pattern of ^{15}N NMR signals and the ^1H ^{15}N HMBC spectrum (see Figures S10 and S11 in the Supplementary Information). The signals of the α and β nitrogen atoms of the azide group bonded to the alkyl chain display triplets ($^2J_{\text{N,H}} = 2.5$ Hz; $^3J_{\text{N,H}} = 5.0$ Hz) resulting from coupling with the CH_2 group. The other azido group (directly bonded to the pyrazole ring) shows singlet signals in the ^{15}N NMR spectrum.

2.5. SSRT (Small-Scale Shock Reactivity Test)

The SSRT test was established by Bohl et al. to measure the explosiveness of a compound on a smaller scale than similar tests such as the Trauzl lead block test [48]. The test setup consists of a steel block with a 7.5 mm wide borehole, which is placed on top of an aluminum witness block. The compound that is tested is filled into the borehole and pressed. To give comparable results with different compounds, the volume is constant and is set to 283 mm^3 in order to account for the filling volume rather than comparing the same mass of energetic material with different filling heights. To ensure optimal energy transfer, the steel and aluminum blocks are placed into a fixating apparatus and a commercial detonator is then placed directly on the pressed compound. The detonation results in a dent in the aluminum witness block that has a characteristic volume for each energetic material that can be compared to each other [49,50]. The volume can be measured either by filling it with standardized sand, or by more technologically advanced optical topographic measurements with a profilometer (Figure 5).

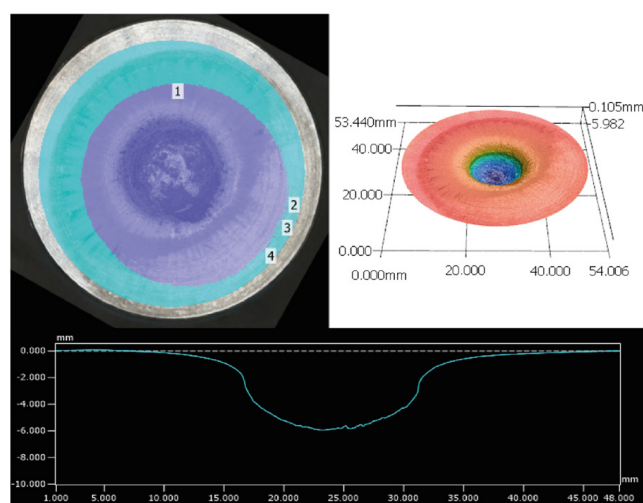


Figure 5. Measured area in cyan and indentations indicated in violet and numbered. Top right: 3D profile with color coded heights. Bottom: 2D profile measurement.

The benefits of the profilometric measurements include, among others, more accurate and operator-independent values, time savings, and better comparability of values between working groups [49]. The compounds tested, 1-nitratomethyl-3,4-dinitropyrazole (**3**) and 1-nitratoethyl-3,4-dinitropyrazole (**6**), both showed good performance in the test setup (Table 2). Compared to established energetic materials, such as HMX or PETN, the methyl derivative (**3**) outperformed both, while the ethyl (**6**) derivative outperformed PETN. Although no single physicochemical value is measured with the SSRT test, valuable conclusions about the explosiveness and general strength of the compound can be drawn. The methyl derivative (**3**) showed a bigger dent volume than the ethyl derivative (**6**), which can be attributed to the increased density, detonation velocity, and detonation pressure.

Table 2. Results of SSRT for **3** and **6** compared to PETN and HMX.

	(3)	(6)	PETN	HMX
Dent volume	1216.36	1135.83	1107.81	1212.39
m (g) ^a	496	447	478	511
ρ (g/cm ³) ^b	1.848	1.664	1.778	1.904
P_{CJ} (kbar) ^c	34.2	27.3	30.8	37.8
V_{det} (m/s) ^d	8734	8004	8429	9193

^a Filling mass; ^b theoretical max. density; ^c detonation pressure; ^d detonation velocity.

3. Materials and Methods

All used materials, methods, and the detailed experimental part can be found in the Supplementary Information.

4. Conclusions

The objective of this research was to synthesize potential melt-castable explosives based on nitropyrazole and incorporating nitratealkyl or azidoalkyl side chains, followed by a thorough comparison of their energetic characteristics. A total of 13 energetic materials were synthesized, consisting of five compounds containing nitratealkyl moiety and eight with azidoalkyl moiety, where the alkyl moiety consisted of methyl or ethyl chains. The nitrate esters were obtained via nitration of the hydroxyl group, while the azides were synthesized through a chlorine-azide exchange reaction. Azidoethyl compounds were directly prepared using an azido ethyl transfer reagent and nitropyrazole. Among these compounds, ten display a solid-state nature with melting points, while the remaining compounds exist in a liquid state. In summary, the investigation reveals that the azido compounds possess superior thermal stability and exhibit higher heats of formation compared to their nitrate ester counterparts. However, this advantage comes at the expense of reduced melting points, leading some compounds to remain in the liquid state. Conversely, the nitrate ester compounds display higher densities, positively influencing their detonation parameters. Notably, compounds **3** and **6**, among others, stand out for their properties. Compound **3** exhibits a high detonation velocity (8668 m/s), while compound **6** demonstrates favorable thermal characteristics (T_{melt} : 78 °C, T_{dec} : 198 °C). Moreover, both compounds show good compatibility with HMX and RDX. Intriguingly, compound **3** outperforms the widely used PETN and HMX in the SSRT, indicating its potential as a highly energetic material.

Supplementary Materials: The following supporting information can be downloaded at: <https://www.mdpi.com/article/10.3390/molecules28186489/s1>. Schemes S1–S5: Synthesis of the presented compounds; Tables S1–S6: Crystallographic data and structure refinement details of the prepared compounds; Table S7: CBS-4M electronic enthalpies for atoms C, H, N and O and their literature values; Table S8: CBS-4M results and calculated gas-phase enthalpies; Tables S9–S11: Physicochemical properties and detonation parameter; Tables S12 and S13: Criteria and results for compatibility measurements; Table S14: Retention time and observed mass for different nitropyrazoles using LC-MS; Tables S15–S20: SSRT results; Table S21: NMR pulse sequences and parameters used for the characterization of the new compounds; Figure S1–S5: Crystal structures; Figure S6–S11: NMR spectra;

Figure S12–S14: DTA spectra; Figures S15 and S16: Combined DTA-TGA spectra; Figures S17 and S18: DTA spectra of compatibility measurements; Figures S19 and S20: LC-MS monitoring of the nitration; Figure S21: Setup of the SSRT experiment. References [19,36–39,50–72] are cited in the Supplementary.

Author Contributions: Methodology, L.B. and J.S.; Investigation, E.R. and T.L.; Writing—original draft, E.R.; Supervision, T.M.K. All authors have read and agreed to the published version of the manuscript.

Funding: The financial support of this work by the Ludwig-Maximilian University (LMU), the Office of Naval Research (ONR) under grant no. ONR N00014-19-1-2078.

Institutional Review Board Statement: Not applicable.

Informed Consent Statement: Not applicable.

Data Availability Statement: The data presented in this study are available in the article and Supplementary Materials.

Acknowledgments: The authors thank Stefan Huber for his help with the sensitivity measurements, Karaghiosoff for ¹⁵N NMR measurements, and Marcus Lommel for single crystal measurements and general support.

Conflicts of Interest: The authors declare no conflict of interest.

Sample Availability: Not applicable.

References

1. Brinck, T. *Green Energetic Materials*; Wiley: New York, NY, USA, 2014.
2. Klapoetke, T.M. *Chemistry of High-Energy Materials*, 6th ed.; De Gruyter: Berlin, Germany; Boston, MA, USA, 2022.
3. Agrawal, J.P. *High Energy Materials*; Wiley: Hoboken, NJ, USA, 2010.
4. Koehler, J.; Meyer, R.; Homburg, A. *Explosivstoffe*, 10th ed.; Wiley: Hoboken, NJ, USA, 2008.
5. Spencer, A.F. Melt-Castable Explosive Composition. U.S. Patent US4747892A, 31 May 1988.
6. Wang, S.-W.; Zhang, Y.-L.; Wu, C.; Xiao, L.; Lin, G.-M.; Hu, Y.-B.; Hao, G.-Z.; Guo, H.; Zhang, G.-P.; Jiang, W. Equal-Material Manufacturing of a Thermoplastic Melt-Cast Explosive Using Thermal-Pressure Coupling Solidification Treatment Technology. *ACS Omega* **2023**, *8*, 16251–16262. [[CrossRef](#)] [[PubMed](#)]
7. Chavez, D.E.; Hiskey, M.A.; Naud, D.L.; Parrish, D. Synthesis of an Energetic Nitrate Ester. *Angew. Chem. Int. Ed.* **2008**, *47*, 8307–8309. [[CrossRef](#)]
8. *Technical Fact Sheet 2–4,6-Trinitrotoluene (TNT)*; U.S. Environmental Protection Agency: Washington, DC, USA, 2021.
9. Maloney, S.W.; Boddu, V.M.; Phull, K.K.; Hao, O.J. *TNT Redwater Treatment by Wet Air Oxidation*; US Army Corps of Engineering: Champaign, IL, USA, 1994.
10. Crouse, L.C.B.; Michie, M.W.; Major, M.; Johnson, M.S.; Lee, R.B.; Paulus, H.I. *Subchronic Oral Toxicity of RDX in Rats*; U.S. Army Center for Health Promotion and Preventive Medicine, Aberdeen Proving Ground: Aberdeen, MD, USA, 2006.
11. Blessinger, T.; D’Amico, L.; Subramaniam, R.; Brinkerhoff, C. *Toxicological Review of RDX*; U.S. Environmental Protection Agency: Washington, DC, USA, 2018.
12. Nair, U.R.; Sivabalan, R.; Gore, G.M.; Geetha, M.; Asthana, S.N.; Singh, H. Hexanitrohexaazaisowurtzitane (CL-20) and CL-20-Based Formulations (Review). *Combust. Explos. Shock. Waves* **2005**, *41*, 121–132. [[CrossRef](#)]
13. Fischer, N.; Fischer, D.; Klapötke, T.M.; Piercey, D.G.; Stierstorfer, J. Pushing the Limits of Energetic Materials—the Synthesis and Characterization of Dihydroxylammonium 5,5′-Bistetrazole-1,1′-Diolate. *J. Mater. Chem.* **2012**, *22*, 20418. [[CrossRef](#)]
14. Sabatini, J.J.; Johnson, E.C. A Short Review of Nitric Esters and Their Role in Energetic Materials. *ACS Omega* **2021**, *6*, 11813–11821. [[CrossRef](#)] [[PubMed](#)]
15. Song, S.; Chen, F.; Wang, Y.; Wang, K.; Yan, M.; Zhang, Q. Accelerating the Discovery of Energetic Melt-Castable Materials by a High-Throughput Virtual Screening and Experimental Approach. *J. Mater. Chem. A* **2021**, *9*, 21723–21731. [[CrossRef](#)]
16. Johnson, E.C.; Sabatini, J.J.; Chavez, D.E.; Sausa, R.C.; Byrd, E.F.C.; Wingard, L.A.; Guzmán, P.E. Bis(1,2,4-Oxadiazole)Bis(Methylene) Dinitrate: A High-Energy Melt-Castable Explosive and Energetic Propellant Plasticizing Ingredient. *Org. Process Res. Dev.* **2018**, *22*, 736–740. [[CrossRef](#)]
17. Bauer, L.; Benz, M.; Klapötke, T.M.; Lenz, T.; Stierstorfer, J. Polyazido-Methyl Derivatives of Prominent Oxadiazole and Isoxazole Scaffolds: Synthesis, Explosive Properties, and Evaluation. *J. Org. Chem.* **2021**, *86*, 6371–6380. [[CrossRef](#)]
18. Ek, S.; Wahlström, L.Y.; Latypov, N. Derivatives of 3(5),4-Dinitropyrazole as Potential Energetic Plasticizers. *J. Chem. Chem. Eng.* **2011**, *5*, 929–935.
19. Bölter, M.F.; Harter, A.; Klapötke, T.M.; Stierstorfer, J. Isomers of Dinitropyrazoles: Synthesis, Comparison and Tuning of Their Physicochemical Properties. *ChemPlusChem* **2018**, *83*, 804–811. [[CrossRef](#)]
20. Ma, Q.; Zhang, Z.; Yang, W.; Li, W.; Ju, J.; Fan, G. Strategies for Constructing Melt-Castable Energetic Materials: A Critical Review. *Energetic Mater. Front.* **2021**, *2*, 69–85. [[CrossRef](#)]

21. Benz, M.; Gruhne, M.S.; Klapötke, T.M.; Krüger, N.; Lenz, T.; Lommel, M.; Stierstorfer, J. Evolving the Scope of 5,5'-Azobistetrazoles in the Search for High Performing Green Energetic Materials. *Eur. J. Org. Chem.* **2021**, *2021*, 4388–4392. [[CrossRef](#)]
22. Lenz, T.; Klapötke, T.M.; Mühlemann, M.; Stierstorfer, J. About the Azido Derivatives of Pentaerythritol Tetranitrate. *Prop. Explos. Pyrotech.* **2021**, *46*, 723–731. [[CrossRef](#)]
23. Lease, N.; Kay, L.M.; Brown, G.W.; Chavez, D.E.; Robbins, D.; Byrd, E.F.C.; Imler, G.H.; Parrish, D.A.; Manner, V.W. Synthesis of Erythritol Tetranitrate Derivatives: Functional Group Tuning of Explosive Sensitivity. *J. Org. Chem.* **2020**, *85*, 4619–4626. [[CrossRef](#)] [[PubMed](#)]
24. Tselinskii, I.V.; Tolstyakov, V.V.; Putis, S.M.; Mel'nikova, S.F. Synthesis and Study of Thermal Stability of 3-Nitro-1,2,4-Triazole N-Nitroso- and N-Azidomethyl Derivatives. *Russ. Chem. Bull.* **2009**, *58*, 2356–2361. [[CrossRef](#)]
25. Yuan, L.; Yuji, L.; Wei, H.; Zhiwei, Z.; Hongwei, Y.; Yongxing, T. Synthesis and Characterization of Pyrazole- and Imidazole-Derived Energetic Compounds Featuring Ortho Azido/Nitro Groups. *FirePhysChem* **2022**, *2*, 140–146. [[CrossRef](#)]
26. Dalinger, I.L.; Vatsadze, I.A.; Shkineva, T.K.; Kormanov, A.V.; Struchkova, M.I.; Suponitsky, K.Y.; Bragin, A.A.; Monogarov, K.A.; Sinditskii, V.P.; Sheremetev, A.B. Novel Highly Energetic Pyrazoles: N-Trinitromethyl-Substituted Nitropyrazoles. *Chem. Asian J.* **2015**, *10*, 1987–1996. [[CrossRef](#)]
27. Zhang, S.; Gao, Z.; Lan, D.; Jia, Q.; Liu, N.; Zhang, J.; Kou, K. Recent Advances in Synthesis and Properties of Nitrated-Pyrazoles Based Energetic Compounds. *Molecules* **2020**, *25*, 3475. [[CrossRef](#)]
28. Ding, L.; Ge, R.; Wang, P.; Li, D.; Lin, Q.; Lu, M.; Xu, Y. A Series of N-Trinitromethyl-Substituted Polynitro-Pyrazoles: High-Energy-Density Materials with Positive Oxygen Balances. *RSC Adv.* **2022**, *12*, 33304–33312. [[CrossRef](#)]
29. Yin, P.; Zhang, J.; Parrish, D.A.; Shreeve, J.M. Energetic N,N'-Ethylene-Bridged Bis(Nitropyrazoles): Diversified Functionalities and Properties. *Chem. Eur. J.* **2014**, *20*, 16529–16536. [[CrossRef](#)]
30. Reinhardt, E.; Thamm, S.; Stierstorfer, J.; Klapötke, T.M. Alkyl-Bridged Nitropyrazoles—Adjustment of Performance and Sensitivity Parameters. *Eur. J. Org. Chem.* **2023**, *26*, e202300304. [[CrossRef](#)]
31. Chinnam, A.K.; Yu, Q.; Imler, G.H.; Parrish, D.A.; Shreeve, J.M. Azo- and Methylene-Bridged Mixed Azoles for Stable and Insensitive Energetic Applications. *Dalton. Trans.* **2020**, *49*, 11498–11503. [[CrossRef](#)] [[PubMed](#)]
32. Myers, T.W.; Chavez, D.E.; Hanson, S.K.; Scharff, R.J.; Scott, B.L.; Veauthier, J.M.; Wu, R. Independent Control of Optical and Explosive Properties: Pyrazole–Tetrazine Complexes of First Row Transition Metals. *Inorg. Chem.* **2015**, *54*, 8077–8086. [[CrossRef](#)] [[PubMed](#)]
33. Chen, D.; Xiong, H.; Yang, H.; Tang, J.; Cheng, G. Nitropyrazole Based Tricyclic Nitrogen-Rich Cation Salts: A New Class of Promising Insensitive Energetic Materials. *FirePhysChem* **2021**, *1*, 71–75. [[CrossRef](#)]
34. He, C.; Zhang, J.; Parrish, D.A.; Shreeve, J.M. 4-Chloro-3,5-Dinitropyrazole: A Precursor for Promising Insensitive Energetic Compounds. *J. Mater. Chem. A* **2013**, *1*, 2863. [[CrossRef](#)]
35. Lei, C.; Yang, H.; Cheng, G. New Pyrazole Energetic Materials and Their Energetic Salts: Combining the Dinitromethyl Group with Nitropyrazole. *Dalton Trans.* **2020**, *49*, 1660–1667. [[CrossRef](#)]
36. Gross, R.S.; Guo, Z.; Dyck, B.; Coon, T.; Huang, C.Q.; Lowe, R.F.; Marinkovic, D.; Moorjani, M.; Nelson, J.; Zamani-Kord, S.; et al. Design and Synthesis of Tricyclic Corticotropin-Releasing Factor-1 Antagonists. *J. Med. Chem.* **2005**, *48*, 5780–5793. [[CrossRef](#)]
37. Meng, W.; Cheng, P.T.W. Noval Glucokinase Activators and Methods of Using Same. WO2011/130459A1, 20 October 2011.
38. Treu, M.; Zahn, S. Karl New 5,8-Dimethyl-9-Phenyl-5,8-Dihydro-6H-Pyrazolo[3,4-H]Quinazolin-2-Yl)-(1H-Pyrazol-3-Yl)-Amines and Derivatives as IGF-1 R/IR Inhibitors. WO2016/180843A1, 17 November 2016.
39. Machin, P.J. Substituierte Phenoxy-Aminopropanol Derivate. EP0034831A2, 2 September 1981.
40. Dalinger, I.; Vatsadze, I.; Shkineva, T.; Popova, G.; Shevelev, S. Efficient Procedure for High-Yield Synthesis of 4-Substituted 3,5-Dinitropyrazoles Using 4-Chloro-3,5-Dinitropyrazole. *Synthesis* **2012**, *44*, 2058–2064. [[CrossRef](#)]
41. Bauer, L.; Kirchhoff, L.; Stierstorfer, J.; Klapötke, T.M. Development of an Azidoethyl-Transfer Reaction Protocol for Azoles. In Proceedings of the 25th NTREM Seminar, Pardubice, Czech Republic, 19–21 April 2023.
42. CCDC Database. Available online: <https://www.ccdc.cam.ac.uk/structures> (accessed on 27 July 2023).
43. Cottrell, T.L. *The Strengths of Chemical Bonds*, 2nd ed.; Butterworths: London, UK, 1958.
44. Klapötke, T.M. *Energetic Materials Encyclopedia*; 2. Auflage-; De Gruyter: Berlin, Germany; Boston, MA, USA, 2021; ISBN 978-3-11-067465-1.
45. Pretsch, E.; Bühlmann, P.; Badertscher, M. *Structure Determination of Organic Compounds: Tables of Spectral Data*; 4. rev.enl. ed.; Springer: Berlin/Heidelberg, Germany, 2009; ISBN 978-3-540-93809-5.
46. Cabildo, P.; Claramunt, R.M.; Elguero, J. ¹³C NMR Chemical Shifts Of N-Unsubstituted- And N-Methyl-Pyrazole Derivatives. *Org. Magn. Reson.* **1984**, *22*, 603–607. [[CrossRef](#)]
47. Viesser, R.V.; Ducati, L.C.; Tormena, C.F.; Autschbach, J. The Unexpected Roles of σ and π Orbitals in Electron Donor and Acceptor Group Effects on the ¹³C NMR Chemical Shifts in Substituted Benzenes. *Chem. Sci.* **2017**, *8*, 6570–6576. [[CrossRef](#)]
48. Sandusky, H.W.; Granholm, R.H.; Bohl, D.G. *Small-Scale Shock Reactivity Test (SSRT)*; Naval Surface Warfare Center, Indian Head Division: Charles County, MD, USA, 2005.
49. Bauer, L.; Benz, M.; Klapötke, T.M.; Selmeier, A. Evaluation of SSRT-Test by Classical Gravimetric Analysis and Optical Topographic Measurement: A Comparative Study. *Propellants Explos. Pyrotech.* **2022**, *47*, e202200113. [[CrossRef](#)]

50. Bauer, L.; Benz, M.; Klapötke, T.M. Linear Correlation Between Confined Explosive Quantity and Dent Volume of an Underlying Aluminium Block Using the SSRT Setup. *Propellants Explos. Pyrotech.* **2022**, *47*, e202100332. [CrossRef]
51. *CrysAlisPro Software*; Version 171.33.41; Rigaku Corporation: Wroclaw, Poland, 2009. Available online: <http://www.rigaku.com> (accessed on 4 July 2023).
52. Sheldrick, G.M. SHELXT Integrated space-group and structure determination. *Acta Cryst.* **2015**, *A71*, 3–8. [CrossRef] [PubMed]
53. Dolomanov, O.V.; Bourhis, L.J.; Gildea, R.J.; Howard, J.A.K.; Puschmann, H.J. OLEX2: A Complete Structure Solution, Refinement and Analysis Program. *Appl. Cryst.* **2009**, *42*, 339–341. [CrossRef]
54. *SCALE3 ABSPACK—An Oxford Diffraction Program*; Version 1.0.4; Rigaku Corporation: Wroclaw, Poland, 2009. Available online: <http://www.rigaku.com> (accessed on 4 July 2023).
55. *APEX3*; Version 2018.7-2; Bruker AXS Inc.: Madison, WI, USA, 2018. Available online: <http://www.bruker.com> (accessed on 4 July 2023).
56. Frisch, M.J.; Trucks, G.W.; Schlegel, H.B.; Scuseria, G.E.; Robb, M.A.; Cheeseman, J.R.; Scalmani, G.; Barone, V.; Petersson, G.A.; Nakatsuji, H.; et al. *Gaussian 16*; Revision A.04; Gaussian, Inc: Wallingford, CT, USA, 2016.
57. Ochterski, J.W.; Petersson, G.A.; Montgomery, J.A. A complete basis set model chemistry. V. Extensions to six or more heavy atoms. *J. Chem. Phys.* **1996**, *104*, 2598–2619. [CrossRef]
58. Montgomery, J.A.; Frisch, M.J.; Ochterski, J.W.; Petersson, G.A. A complete basis set model chemistry. VII. Use of the minimum population localization method. *J. Chem. Phys.* **2000**, *112*, 6532–6542. [CrossRef]
59. Curtiss, L.A.; Raghavachari, K.; Redfern, P.C.; Pople, J.A. Assessment of Gaussian-2 and density functional theories for the computation of enthalpies of formation. *J. Chem. Phys.* **1997**, *106*, 1063–1079. [CrossRef]
60. Rice, B.M.; Pai, S.V.; Hare, J. Predicting heats of formation of energetic materials using quantum mechanical calculations. *Combust. Flame* **1999**, *118*, 445–458. [CrossRef]
61. Byrd, E.F.C.; Rice, B.M. Improved Prediction of Heats of Formation of Energetic Materials Using Quantum Mechanical Calculations. *J. Phys. Chem. A* **2006**, *110*, 1005–1013. [CrossRef]
62. Linstrom, J.; Mallard, W.G. National Institute of Standards and Technology Standard Reference Database Number 69. Available online: <http://www.webbook.nist.gov/chemistry> (accessed on 4 July 2022).
63. Wahler, S.; Chung, P.; Klapoetke, T.M. Training machine learning models based on the structural formula for the enthalpy of vaporization and sublimation and a thorough analysis of Trouton's rules. *J. Energ. Mater.* **2023**. [CrossRef]
64. *STANAG 4147*; Chemical Compatibility of Ammunition Components with Explosives (Non-Nuclear Application). NATO: Brussels, Belgium, 2001.
65. Koehler, J.; Meyer, R.; Homburg, A. *Explosivstoffe*, 6th ed.; Wiley: Weinheim, Germany, 2007.
66. Bundesanstalt für Materialforschung und -Prüfung. Available online: <http://www.bam.de> (accessed on 4 July 2023).
67. *STANAG 4489*; Explosives, Impact Sensitivity Tests. NATO: Brussels, Belgium, 1999.
68. *Standardarbeitsanweisung 4-5.1.02*; Ermittlung der Explosionsgefährlichkeit, hier der Schlagempfindlichkeit mit dem Fallhammer. WIWEB: Erding, Germany, 2002.
69. *STANAG 4489*; Explosives, Friction Sensitivity Tests. NATO: Brussels, Belgium, 2002.
70. *Standardarbeitsanweisung 4-5.1.03*; Ermittlung der Explosionsgefährlichkeit oder der Reibeempfindlichkeit mit dem Reibeapparat. WIWEB: Erding, Germany, 2002.
71. OZM Research. Available online: <http://www.ozm.cz> (accessed on 4 July 2023).
72. Impact: Insensitive > 40 J, Less Sensitive ≤ 35 J, Sensitive ≤ 4 J, Very Sensitive ≤ 3 J; Friction: Insensitive > 360 N, Less Sensitive = 360 N, Sensitive 80 N, Very Sensitive ≤ 80 N, Extreme Sensitive ≤ 10 N; According to the UN Recommendations on the Transport of Dangerous Goods (+) Indicates: Not Safe for Transport. Available online: <https://www.un-ilibrary.org/content/books/9789210019057> (accessed on 4 July 2023).

Disclaimer/Publisher's Note: The statements, opinions and data contained in all publications are solely those of the individual author(s) and contributor(s) and not of MDPI and/or the editor(s). MDPI and/or the editor(s) disclaim responsibility for any injury to people or property resulting from any ideas, methods, instructions or products referred to in the content.

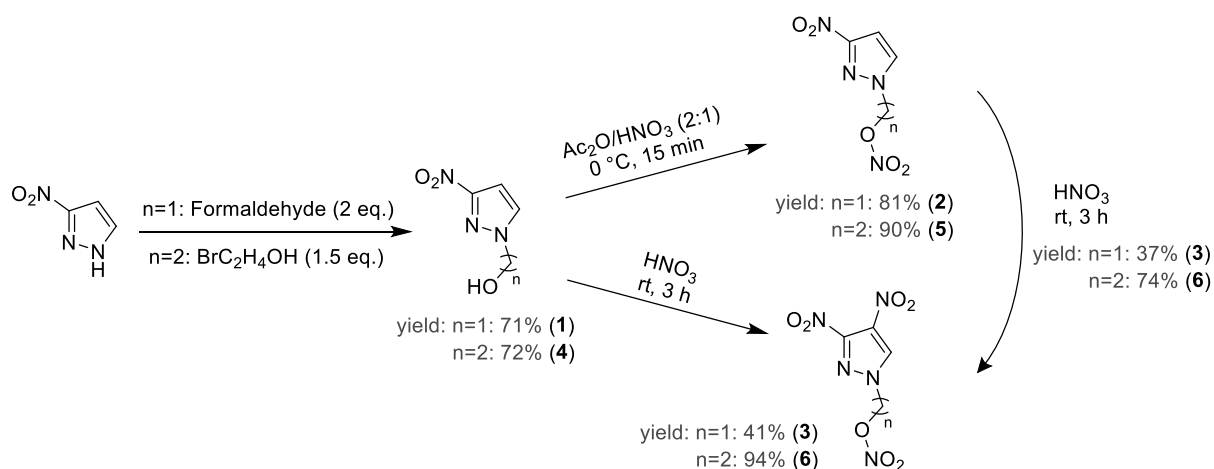
Supporting Information

Table of Content

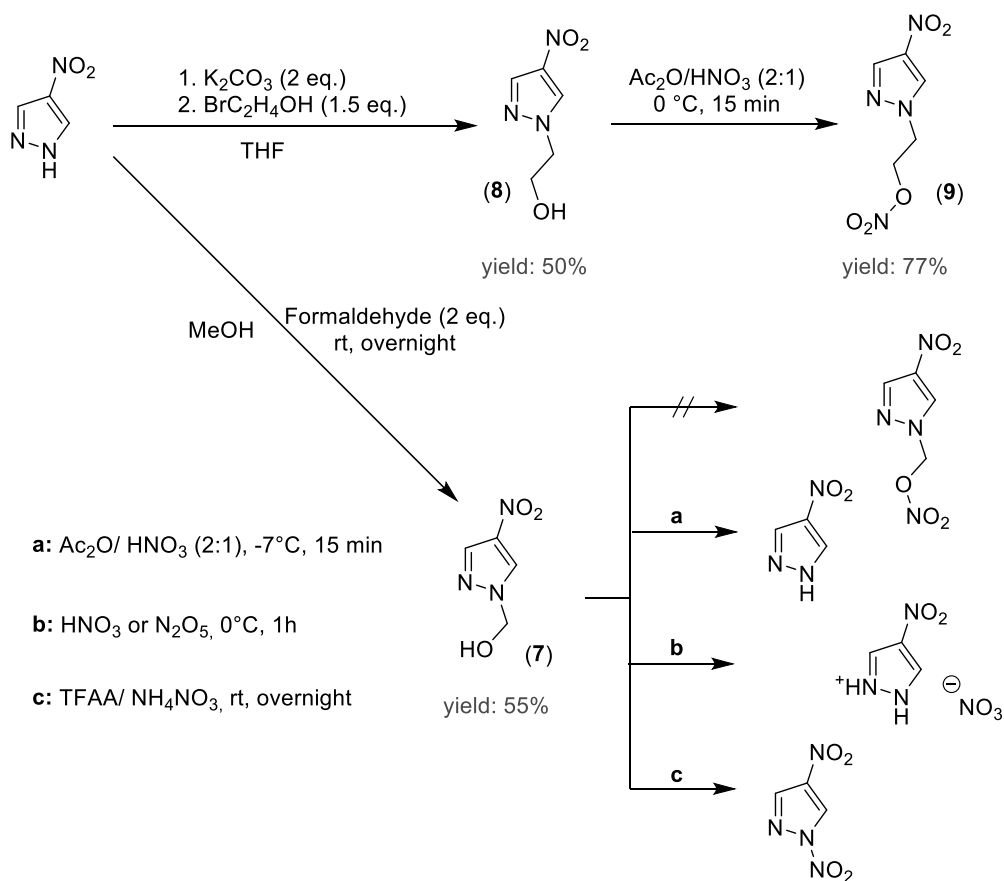
1. Compound overview	1
2. X-ray diffraction.....	3
3. Heat of formation calculation.....	15
4. Physico-chemical properties	16
5. ¹⁵ NMR spectroscopy	18
6. Thermal stability	21
7. Compatibilities	25
8. LC-MS measurements.....	27
9. SSRT (small-scale shock reactivity test).....	30
10. Experimental part and general methods	34
11. References	44

1. Compound overview

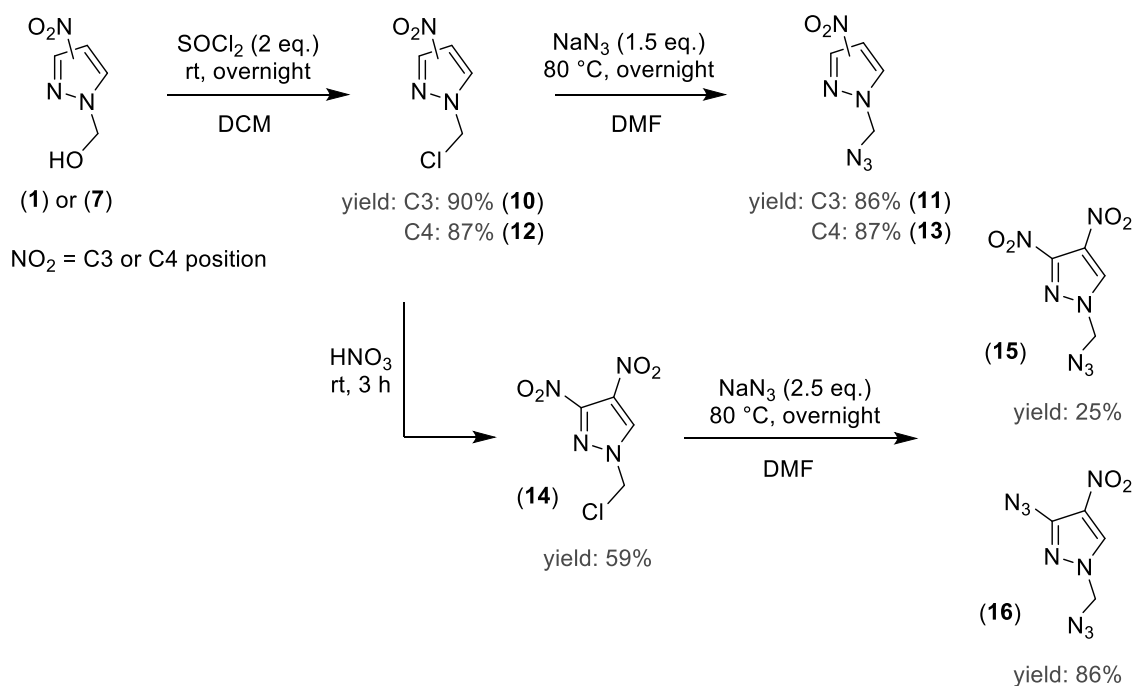
The syntheses and individual compound numbers are shown in the schemes (**S1–S5**) below.



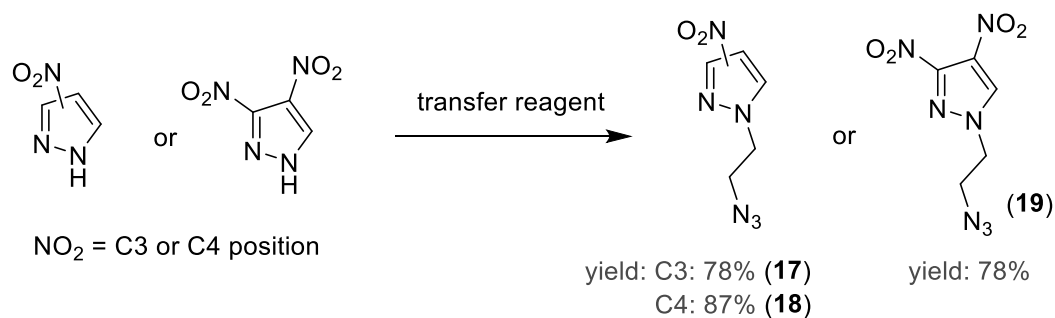
Scheme S1: Synthesis of 1-hydroxyalkyl and 1-nitratoalkyl-nitropyrazoles (**1–6**).



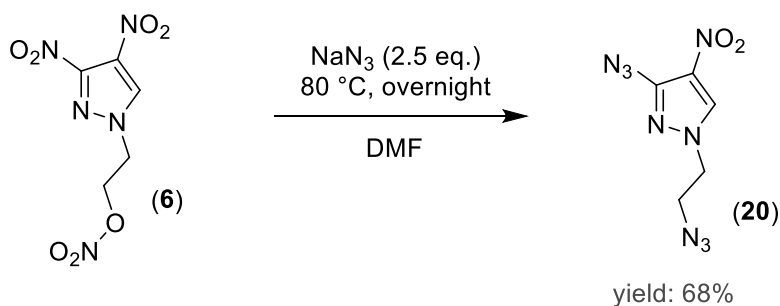
Scheme S2: Synthesis of 1-hydroxyalkyl and 1-nitratoalkyl-4-nitropyrazoles (**7–9**).



Scheme S3: Synthesis of 1-chloromethyl and 1-azidomethyl-nitropyrazoles (**10–15**) and 1-azidomethyl-3-azido-4-nitropyrazole (**16**).



Scheme S4: Synthesis of 1-azidoethyl-nitropyrazoles (**17–19**) using an azido-ethyl-transfer reagent.



Scheme S5: Synthesis of 1-azidoethyl-3-azido-4-nitropyrazole (**20**).

2. X-ray diffraction

Crystalline compounds were measured either on an *Oxford Xcalibur3* diffractometer with a Spellman generator (voltage 50 kV, current 40 mA) and a Kappa CCD area for data collection using Mo-K α radiation ($\lambda = 0.71073 \text{ \AA}$) or a *Bruker D8 Venture TXS* diffractometer equipped with a multilayer monochromator, a Photon 2 detector and a rotation-anode generator (Mo-K α radiation). The data collection was performed using the CrysAlisPro software.^[S1] The solution of the structure was performed by direct methods and refined by full-matrix least-squares on F2 (SHELXT)^[S2] implemented in the OLEX2^[S3] software suite. The non-hydrogen atoms were refined anisotropically and the hydrogen atoms were located and freely refined. The absorption correction was carried out by a SCALE3ABSPACK or SADABS Bruker Apex3 multiscan method.^[S4,5] All DIAMOND2 plots are shown with thermal ellipsoids at the 50% probability level and hydrogen atoms are shown as small spheres of arbitrary radius.

Table S1: Crystallographic data and structure refinement details for the prepared compounds.

	1HM3NPz (1)	1NM3NPz (2)	1NM34DNPz (3)
Formula	C ₄ H ₅ N ₃ O ₃	C ₄ H ₄ N ₄ O ₅	C ₄ H ₃ N ₅ O ₇
FW [g mol ⁻¹]	143.11	188.11	233.11
Crystal system	triclinic	monoclinic	orthorhombic
Space group	<i>P</i> -1 (No. 2)	<i>P</i> 2 ₁ / <i>c</i> (No. 14)	<i>Pna</i> 2 ₁ (No. 33)
Color / Habit	colourless/ plate	colourless/ plates	colourless/ plates
Size [mm]	0.10 x 0.25 x 0.60	0.03 x 0.09 x 0.13	0.10 x 0.25 x 0.70
<i>a</i> [Å]	4.1175(5)	6.5096(3)	9.3876(11)
<i>b</i> [Å]	11.4525(17)	14.8639(7)	10.1407(10)
<i>c</i> [Å]	12.6534(14)	7.7489(4)	17.1149(18)
α [°]	94.378(10)	90	90
β [°]	93.410(9)	105.359(2)	90
γ [°]	96.875(11)	90	90
<i>V</i> [Å ³]	589.24(13)	722.99(6)	1629.3(3)
<i>Z</i>	4	4	8
ρ _{calc.} [g cm ⁻³]	1.613	1.728	1.901
μ [mm ⁻¹]	0.139	0.160	0.183
<i>F</i> (000)	296	384	944
λ _{MoKα} [Å]	0.71073	0.71073	0.71073
<i>T</i> [K]	105	173	105
θ Min-Max [°]	1.6, 26.4	3.5, 26.4	2.3, 26.4
Dataset	-5:5; -14:14; -15:15	-8: 8; -18:18; -8: 9	-11:7; -12:12; -21:21
Reflections collected	9297	12386	5923
Independent refl.	2414	1472	2995
<i>R</i> _{int}	0.056	0.034	0.047
Observed reflections	1872	1291	2236
Parameters	221	134	306
<i>R</i> ₁ (obs) ^[a]	0.0499	0.0365	0.0500
<i>wR</i> ₂ (all data) ^[b]	0.1327	0.1023	0.1047
<i>S</i> ^[c]	1.06	1.21	1.02
Resd. dens [e Å ⁻³]	-0.28, 0.29	-0.24, 0.21	-0.23, 0.34
Device type	Oxford Xcalibur3	D8 Venture	Oxford Xcalibur3
Solution	SHELXT	SHELXT	SIR-92
Refinement	SHELXL-2018	SHELXL-2018	SHELXL-2018
Absorption correction	multi-scan	multi-scan	multi-scan
CCDC	2255656	2255417	2255418

^[a] $R_1 = \sum ||F_o| - |F_c| | / \sum |F_o|$; ^[b] $wR_2 = [\sum [w(F_o^2 - F_c^2)^2] / \sum [w(F_o^2)]]^{1/2}$; $w = [\sigma^2(F_o^2) + (xP)^2 + yP]^{-1}$ and $P = (F_o^2 + 2F_c^2) / 3$; ^[c] $S = \{\sum [w(F_o^2 - F_c^2)^2] / (n-p)\}^{1/2}$ (*n* = number of reflections; *p* = total number of parameters).

Table S2: Crystallographic data and structure refinement details for the prepared compounds.

	1HE3NPz (4)	1NE3NPz (5)	1NE34DNPz (6)
Formula	C ₅ H ₇ N ₃ O ₃	C ₅ H ₆ N ₄ O ₅	C ₅ H ₅ N ₅ O ₇
FW [g mol ⁻¹]	157.14	202.14	247.14
Crystal system	monoclinic	monoclinic	orthorhombic
Space group	<i>P</i> 2 ₁ / <i>c</i> (No. 14)	<i>P</i> 2 ₁ / <i>c</i> (No. 14)	<i>P</i> 2 ₁ 2 ₁ 2 ₁ (No. 19)
Color / Habit	colourless/ block	colourless/ block	colourless/ block
Size [mm]	0.04 x 0.08 x 0.16	0.25 x 0.50 x 0.50	0.03 x 0.06 x 0.12
a [Å]	4.4397(2)	7.1230(11)	8.2650(2)
b [Å]	11.8945(5)	14.488(3)	8.9959(2)
c [Å]	13.0629(6)	7.9349(10)	12.4975(3)
α [°]	90	90	90
β [°]	91.211(2)	102.586(13)	90
γ [°]	90	90	90
V [Å ³]	689.67(5)	799.2(2)	929.20(4)
Z	4	4	4
ρ _{calc.} [g cm ⁻³]	1.513	1.680	1.767
μ [mm ⁻¹]	0.127	0.151	0.166
F(000)	328	416	504
λ _{MoKα} [Å]	0.71073	0.71073	0.71073
T [K]	173	91	173
θ Min-Max [°]	3.1, 26.4	2.8, 26.4	3.0, 26.4
Dataset	-5: 5; -14: 14; -16: 16	-8: 8; -16: 18; -9: 7	-10:10;-11:11;-15:15
Reflections collected	14822	3676	21075
Independent refl.	1410	1627	1897
R _{int}	0.042	0.027	0.033
Observed reflections	1225	1271	1845
Parameters	128	151	174
R ₁ (obs) ^[a]	0.0339	0.0371	0.0239
wR ₂ (all data) ^[b]	0.0874	0.0881	0.0663
S ^[c]	1.13	1.05	1.16
Resd. dens [e Å ⁻³]	-0.24, 0.18	-0.23, 0.19	-0.17, 0.17
Device type	D8 Venture	Oxford Xcalibur3	D8 Venture
Solution	SHELXT	SHELXT	SHELXT
Refinement	SHELXL-2018	SHELXL-2018	SHELXL-2018
Absorption correction	multi-scan	multi-scan	multi-scan
CCDC	2255410	2255415	2255419

^[a]R₁ = Σ ||F_o| - |F_c| | / Σ |F_o|; ^[b]wR₂ = [Σ[w(F_o² - F_c²)] / Σ[w(F_o²)]^{1/2}; w = [σ²(F_o²) + (xP)² + yP]⁻¹ and P = (F_o² + 2F_c²) / 3; ^[c]S = {Σ[w(F_o² - F_c²)] / (n - p)}^{1/2} (n = number of reflections; p = total number of parameters).

Table S3: Crystallographic data and structure refinement details for the prepared compounds.

	1HM4NPz (7)	1HE4NPz (8)	1NE4NPz (9)
Formula	C ₄ H ₅ N ₃ O ₃	C ₅ H ₇ N ₃ O ₃	C ₅ H ₆ N ₄ O ₅
FW [g mol ⁻¹]	143.11	157.14	202.14
Crystal system	monoclinic	monoclinic	monoclinic
Space group	C2/c (No. 15)	P2 ₁ /c (No. 14)	P2 ₁ /c (No. 14)
Color / Habit	colourless/ needle	colourless/ block	colourless/ plates
Size [mm]	0.02 x 0.06 x 0.40	0.06 x 0.08 x 0.16	0.01 x 0.04 x 0.04
a [Å]	21.5247(15)	7.6570(2)	9.8174(5)
b [Å]	4.1038(4)	8.6786(3)	8.3784(4)
c [Å]	12.9782(10)	10.3956(3)	10.9893(6)
α [°]	90	90	90
β [°]	92.166(7)	92.928(1)	115.320(2)
γ [°]	90	90	90
V [Å ³]	1145.59(16)	689.91(4)	817.08(7)
Z	8	4	4
ρ _{calc.} [g cm ⁻³]	1.660	1.513	1.643
μ [mm ⁻¹]	0.143	0.126	0.148
F(000)	592	328	416
λ _{MoKα} [Å]	0.71073	0.71073	0.71073
T [K]	103	173	173
θ Min-Max [°]	3.1, 26.4	3.1, 26.4	3.2, 26.4
Dataset	-26: 26; -5: 5; -16: 16	-9: 9; -10: 10; -12: 12	-12:12;-10:10;-13:13
Reflections collected	7584	14652	14361
Independent refl.	1169	1405	1671
R _{int}	0.038	0.035	0.050
Observed reflections	990	1294	1379
Parameters	111	128	151
R ₁ (obs) ^[a]	0.0298	0.0338	0.0355
wR ₂ (all data) ^[b]	0.0781	0.0897	0.0897
S ^[c]	1.05	1.11	1.13
Resd. dens [e Å ⁻³]	-0.17, 0.24	-0.21, 0.22	-0.23, 0.16
Device type	Oxford Xcalibur3	D8 Venture	D8 Venture
Solution	SHELXT	SHELXT	SHELXT
Refinement	SHELXL-2018	SHELXL-2018	SHELXL-2018
Absorption correction	multi-scan	multi-scan	multi-scan
CCDC	2255411	2255658	2255412

^[a]R₁ = Σ ||F_o| - |F_c| | / Σ |F_o|; ^[b]wR₂ = [Σ[w(F_o² - F_c²)²] / Σ[w(F_o²)]^{1/2}; w = [σ²(F_o²) + (xP)² + yP]⁻¹ and P = (F_o² + 2F_c²) / 3; ^[c]S = {Σ[w(F_o² - F_c²)²] / (n - p)}^{1/2} (n = number of reflections; p = total number of parameters).

Table S4: Crystallographic data and structure refinement details for the prepared compounds.

	1CIM3NPz (10)	1AM3NPz (11)	1CIM4NPz (12)
Formula	C ₄ H ₄ ClN ₃ O ₂	C ₄ H ₄ N ₆ O ₂	C ₄ H ₄ ClN ₃ O ₂
FW [g mol ⁻¹]	161.55	168.13	161.55
Crystal system	orthorhombic	orthorhombic	monoclinic
Space group	<i>Pbca</i> (No. 61)	<i>Pna2</i> ₁ (No. 33)	<i>P2</i> ₁ / <i>c</i> (No. 14)
Color / Habit	colourless/ block	colourless/ plate	colourless/ needle
Size [mm]	0.03 x 0.05 x 0.10	0.01 x 0.04 x 0.08	0.10 x 0.10 x 0.45
a [Å]	6.7667(2)	8.2802(9)	4.2774(4)
b [Å]	12.9917(4)	14.2417(16)	21.208(3)
c [Å]	15.0807(4)	6.1449(8)	7.2323(7)
α [°]	90	90	90
β [°]	90	90	97.183(9)
γ [°]	90	90	90
V [Å ³]	1325.76(7)	724.63(15)	650.93(13)
Z	8	4	4
ρ _{calc.} [g cm ⁻³]	1.619	1.541	1.648
μ [mm ⁻¹]	0.513	0.128	0.523
F(000)	656	344	328
λ _{MoKα} [Å]	0.71073	0.71073	0.71073
T [K]	173	173	93
θ Min-Max [°]	3.1, 26.4	3.6, 26.3	1.9, 26.4
Dataset	-8: 8; -16: 16; -18: 18	-10: 10; -17: 17; -7: 7	-4: 5; -26: 25; -8: 9
Reflections collected	21917	12637	2886
Independent refl.	1357	1480	1329
R _{int}	0.041	0.102	0.032
Observed reflections	1236	1085	935
Parameters	107	125	107
R ₁ (obs) ^[a]	0.0366	0.0447	0.0458
wR ₂ (all data) ^[b]	0.0924	0.0894	0.0996
S ^[c]	1.07	1.07	1.06
Resd. dens [e Å ⁻³]	-0.42, 0.37	-0.16, 0.15	-0.22, 0.28
Device type	D8 Venture	D8 Venture	Oxford Xcalibur3
Solution	SHELXT	SHELXT	SHELXT
Refinement	SHELXL-2018	SHELXL-2018	SHELXL-2018
Absorption correction	multi-scan	multi-scan	multi-scan
CCDC	2255416	2255657	2255409

^[a]R₁ = Σ ||F_o| - |F_c| | / Σ |F_o|; ^[b]wR₂ = [Σ[w(F_o² - F_c²)²] / Σ[w(F_o²)]^{1/2}; w = [σ²(F_o²) + (xP)² + yP]⁻¹ and P = (F_o² + 2F_c²) / 3; ^[c]S = {Σ[w(F_o² - F_c²)²] / (n - p)}^{1/2} (n = number of reflections; p = total number of parameters).

Table S5: Crystallographic data and structure refinement details for the prepared compounds.

	1AM4NPz (13)	1AM3A4NPz(16)	1AE34DNPz(19)
Formula	C ₄ H ₄ N ₆ O ₂	C ₄ H ₃ N ₉ O ₂	C ₅ H ₅ N ₇ O ₄
FW [g mol ⁻¹]	168.13	209.15	227.16
Crystal system	monoclinic	orthorhombic	monoclinic
Space group	<i>C2/c</i> (No. 15)	<i>Pbca</i> (No. 61)	<i>P2₁</i> (No. 4)
Color / Habit	colourless/ block	yellow/ plate	colourless/ plate
Size [mm]	0.30 x 0.40 x 0.50	0.03 x 0.10 x 0.16	0.18 x 0.16 x 0.04
a [Å]	6.4339(9)	12.3345(10)	8.120(2)
b [Å]	11.4490(14)	6.5734(6)	13.319(3)
c [Å]	19.124(2)	20.1402(17)	8.235(2)
α [°]	90	90	90
β [°]	93.367(10)	90	91.83(3)
γ [°]	90	90	90
V [Å ³]	1406.3(3)	1633.0(2)	890.1(1)
Z	8	8	4
ρ _{calc.} [g cm ⁻³]	1.588	1.702	1.695
μ [mm ⁻¹]	0.131	0.142	0.147
F(000)	688	848	464
λ _{MoKα} [Å]	0.71073	0.71073	0.71073
T [K]	123	173	173
θ Min-Max [°]	2.1, 26.4	3.7, 26.4	2.9, 28.2
Dataset	-8: 6; -14: 13; -21: 23	-15:15; -8:8; -25:25	-10:10;-17:17;-10:10
Reflections collected	2960	27146	18061
Independent refl.	1432	1662	4396
R _{int}	0.025	0.067	0.0432
Observed reflections	1067	1526	4122
Parameters	125	148	330
R ₁ (obs) ^[a]	0.0392	0.0400	0.0327
wR ₂ (all data) ^[b]	0.0909	0.1037	0.0819
S ^[c]	1.02	1.20	1.076
Resd. dens [e Å ⁻³]	-0.21, 0.20	-0.30, 0.28	-0.238, 0.144
Device type	Oxford Xcalibur3	D8 Venture	D8 Venture
Solution	SHELXT	SHELXT	SHELXT
Refinement	SHELXL-2018	SHELXL-2018	SHELXL-2018
Absorption correction	multi-scan	multi-scan	multi-scan
CCDC	2255413	2261896	2255414

^[a]R₁ = Σ ||F_o| - |F_c| | / Σ |F_o|; ^[b]wR₂ = [Σ[w(F_o² - F_c²)²] / Σ[w(F_o²)]^{1/2}; w = [σ²(F_o²) + (xP)² + yP]⁻¹ and P = (F_o² + 2F_c²) / 3; ^[c]S = {Σ[w(F_o² - F_c²)²] / (n - p)}^{1/2} (n = number of reflections; p = total number of parameters).

Table S6: Crystallographic data and structure refinement details for the prepared compounds.

1AE3A4NPz (20)	
Formula	C ₅ H ₅ N ₉ O ₂
FW [g mol ⁻¹]	223.18
Crystal system	monoclinic
Space group	<i>P</i> 2 ₁ / <i>c</i> (No. 14)
Color / Habit	colourless/ block
Size [mm]	0.08 x 0.12 x 0.18
a [Å]	10.8862(5)
b [Å]	12.1490(6)
c [Å]	7.0825(4)
α [°]	90
β [°]	91.354(2)
γ [°]	90
V [Å ³]	936.45(8)
Z	4
ρ _{calc.} [g cm ⁻³]	1.583
μ [mm ⁻¹]	0.129
F(000)	456
λ _{MoKα} [Å]	0.71073
T [K]	173
θ Min-Max [°]	3.3, 26.4
Dataset	-13:13; -15:15; -8:8
Reflections collected	16166
Independent refl.	1921
R _{int}	0.041
Observed reflections	1657
Parameters	165
R ₁ (obs) ^[a]	0.0378
wR ₂ (all data) ^[b]	0.0970
S ^[c]	1.12
Resd. dens [e Å ⁻³]	-0.22, 0.22
Device type	D8 Venture
Solution	SIR-92
Refinement	SHELXL-2018
Absorption correction	multi-scan
CCDC	2269934

^[a]R₁ = Σ ||F_o| - |F_c|| / Σ |F_o|; ^[b]wR₂ = [Σ[w(F_o² - F_c²)²] / Σ[w(F_o²)]^{1/2}; w = [σc²(F_o²) + (xP)² + yP]⁻¹ and P = (F_o² + 2F_c²) / 3; ^[c]S = {Σ[w(F_o² - F_c²)²] / (n - p)}^{1/2} (n = number of reflections; p = total number of parameters).

Compound **2** and **3** can be crystallized from methanol, forming colourless platelets. They crystallized in common space groups (**2**: $P2_1/c$; **3**: $Pna2_1$) and have four and eight molecules per unit cell, with a cell volume of $722.99(6) \text{ \AA}^3$ and $1629.3(3) \text{ \AA}^3$, respectively. At 173 K and 105 K, the calculated densities are 1.728 g cm^{-3} and 1.901 g cm^{-3} , respectively. Molecular units and extended structures are illustrated in **Figure S1**.

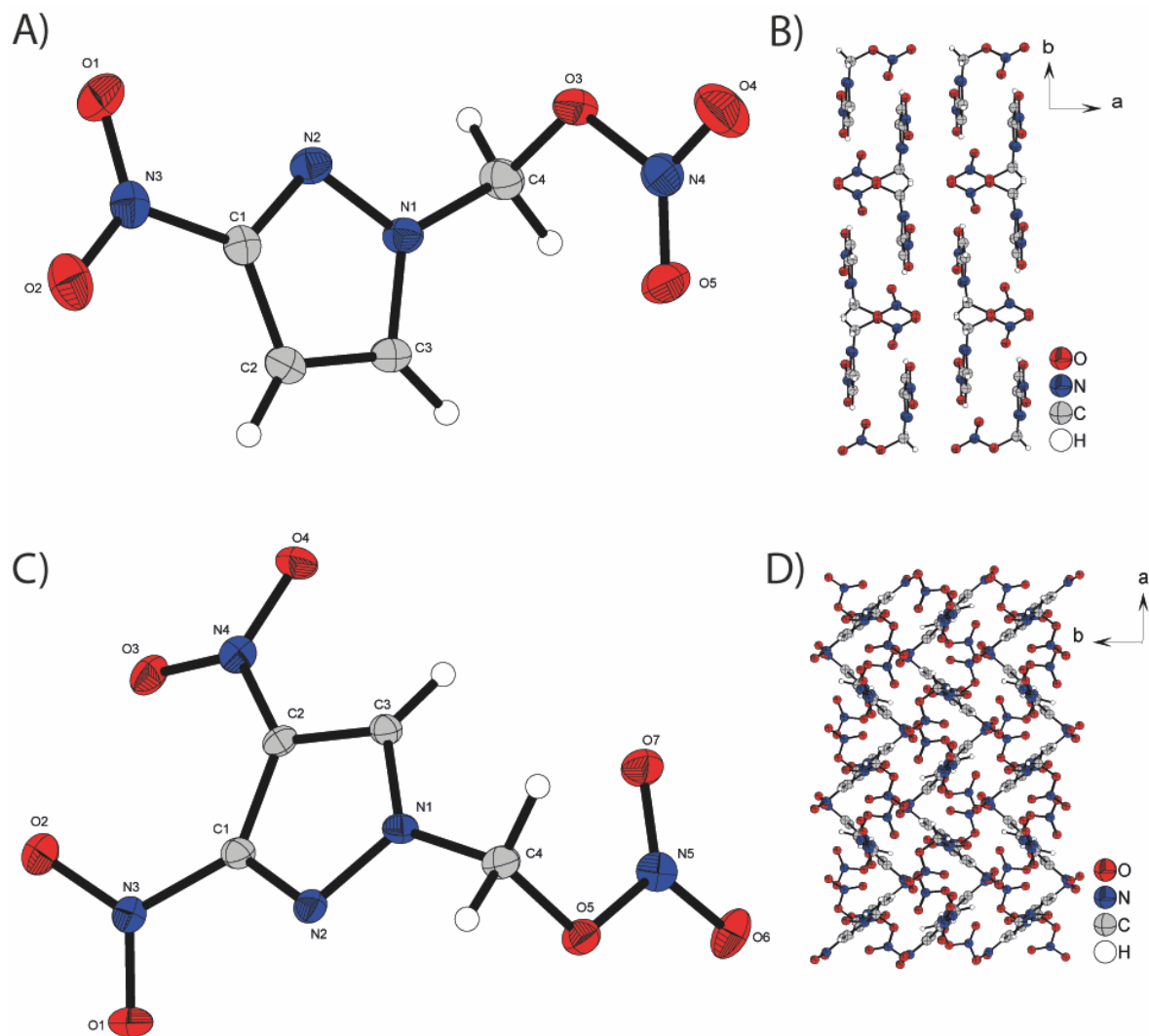


Figure S1: Crystal structures of 1-nitratomethyl-nitropyrazole compounds: **A, B**) 1-nitratomethyl-3-nitropyrazole (**2**); **C, D**) 1-nitratomethyl-3,4-dinitropyrazole (**3**).

Compound **5**, **9** and **6** can be crystallized from methanol or ethanol forming colourless platelets (**9**) or blocks (**5**, **6**). Compounds **5** and **9** have four molecules per unit cell and share common space groups $P2_1/c$. Their cell volumes are $799.2(2) \text{ \AA}^3$ and $817.08(7) \text{ \AA}^3$, while the calculated densities at 91 K and 173 K are 1.680 g cm^{-3} and 1.643 g cm^{-3} , in that order. Compound **6** crystallized in the space group $P2_12_12_1$ with four molecules per unit cell and a cell volume of $929.20(4) \text{ \AA}^3$. At 173 K, the calculated density is 1.767 g cm^{-3} . Molecular units and extended structures are illustrated in **Figure S2**.

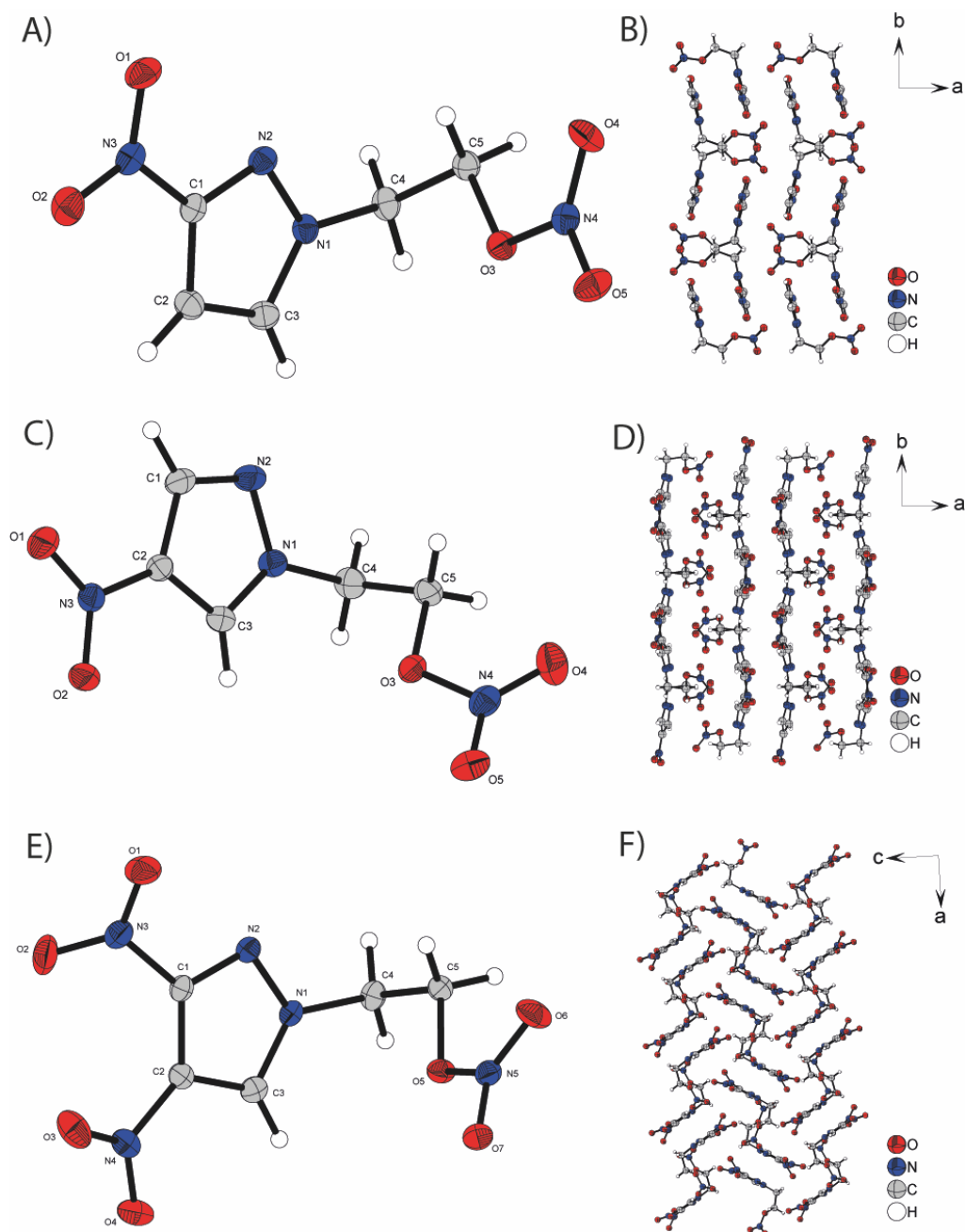


Figure S2: Crystal structures of 1-nitratoethyl-nitropyrazole compounds: **A, B**) 1-nitratoethyl-3-nitropyrazole (**5**); **C, D**) 1-nitratoethyl-4-nitropyrazole (**9**); **E, F**) 1-nitratoethyl-3,4-dinitropyrazole (**6**).

Compound **11**, **13** and **19** crystallized directly from the reaction mixture or ethanol, forming colourless platelets (**11**, **19**) or blocks (**13**). Compounds **11** and **19** precipitated in a common space groups (**11**: $Pna2_1$; **19**: $P2_1$) and have four molecules per unit cell, with a cell volume of $724.63(15) \text{ \AA}^3$ and $890.1(1) \text{ \AA}^3$, respectively. At 173 K, the calculated densities are 1.728 g cm^{-3} and 1.901 g cm^{-3} . At a temperature of 123 K, compound **13** formed a crystal lattice in the $C2/c$ space group, consisting of eight molecules in the unit cell and having a volume of $1406.3(3) \text{ \AA}^3$. The calculated density at this temperature is 1.588 g cm^{-3} . Molecular units and extended structures are illustrated in **Figure S3**.

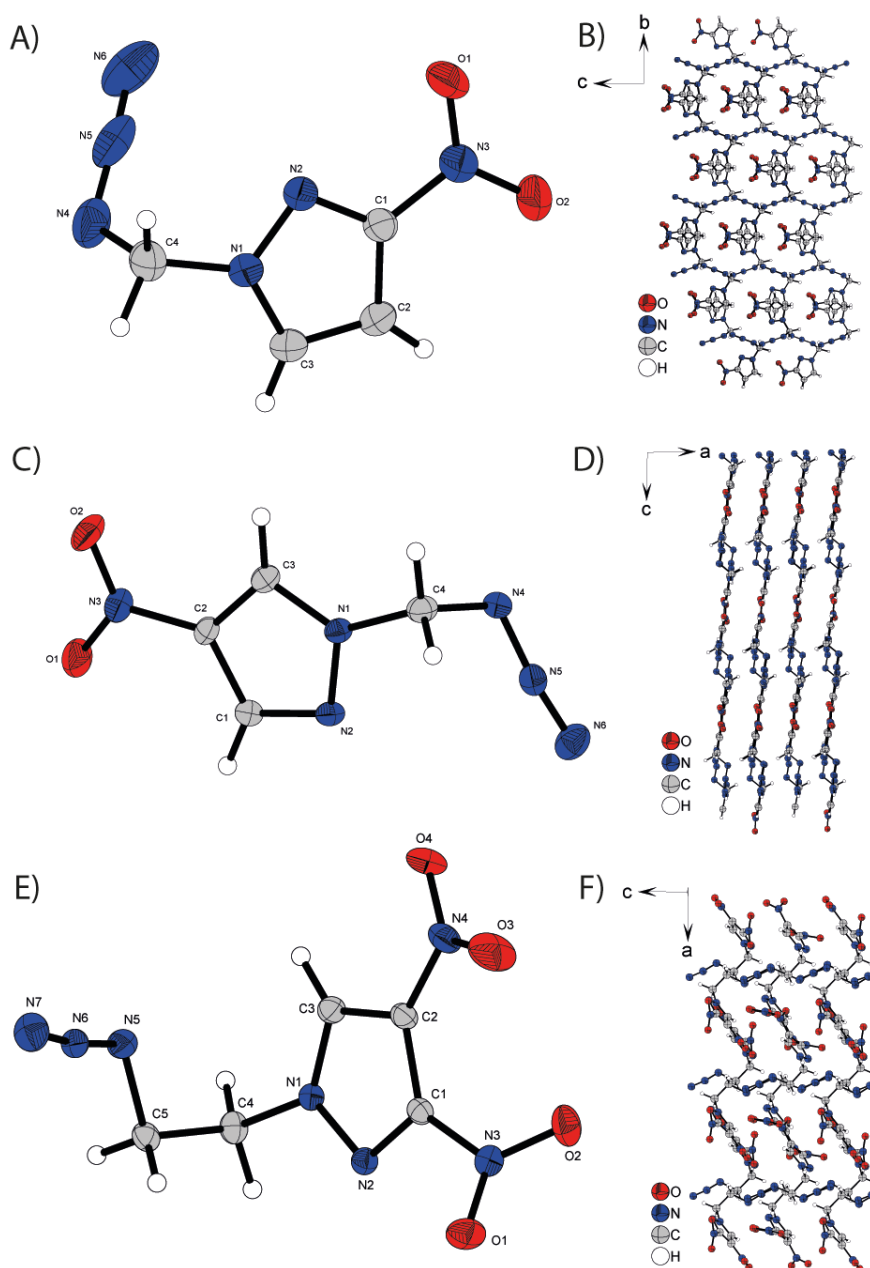


Figure S3: Crystal structures of 1-azidoalkyl-nitropyrazole compounds: **A, B** 1-azidomethyl-3-nitropyrazole (**11**); **C, D** 1-azidomethyl-4-nitropyrazole (**13**); **E, F** 1-azidoethyl-3,4-dinitropyrazole (**19**).

Compound **16** and **20** can be obtained as yellow plates or colorless blocks by crystallization from EtOAc or Et₂O. They crystallize in common space groups (**16**: *Pbca*; **20**: *P2₁/c*) and have eight and four molecules per unit cell, with respective cell volumes of 1633.0(2) Å³ and 936.45(8) Å³. The densities calculated at 173 K are 1.702 g cm⁻³ and 1.583 g cm⁻³. Molecular units and extended structures are illustrated in **Figure S4**.

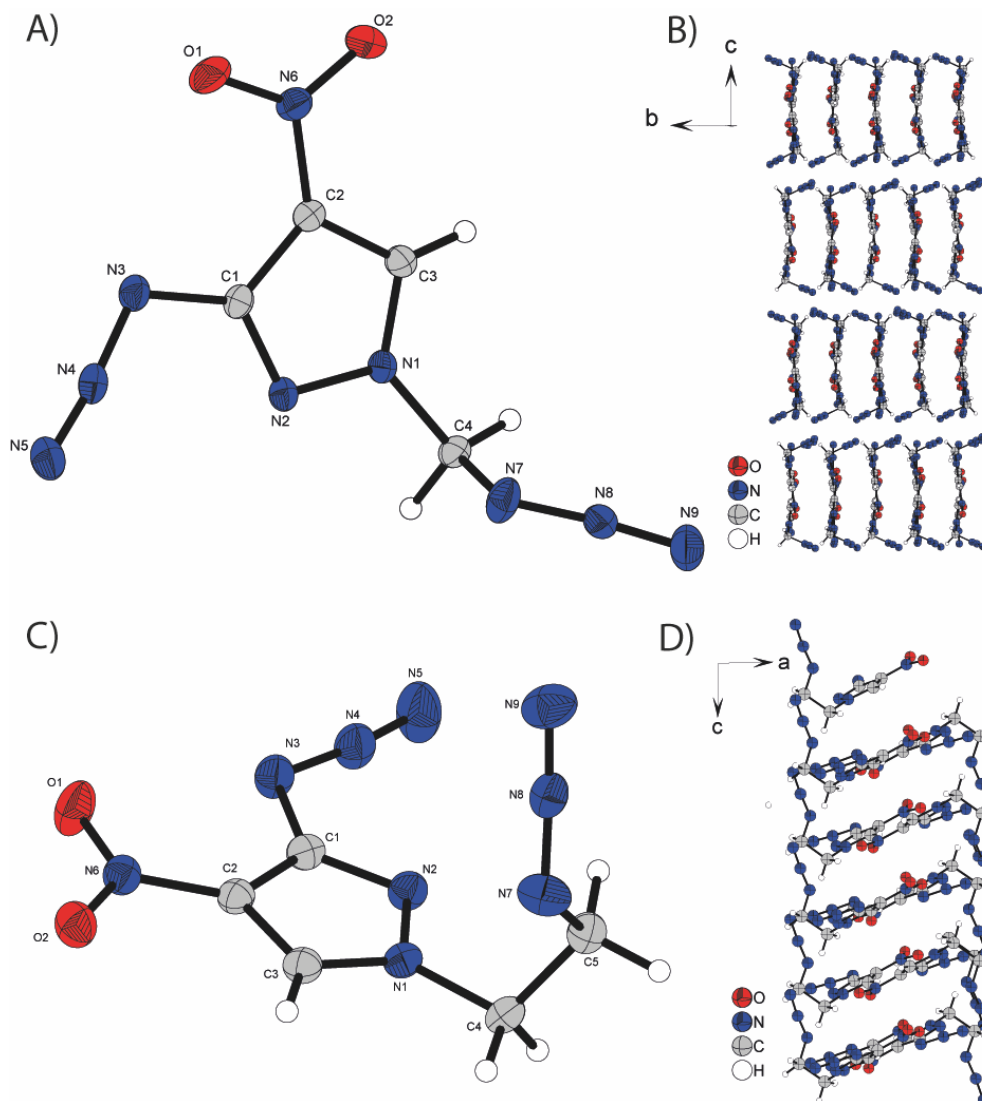
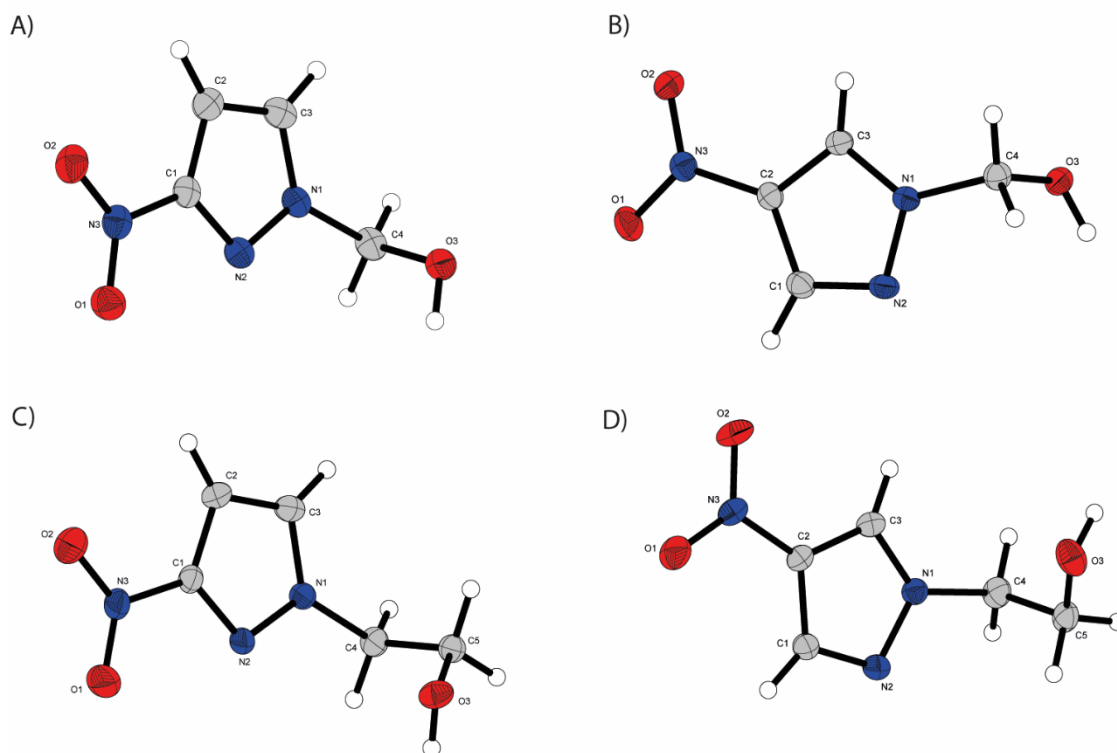


Figure S4: Crystal structures of 1-azidoalkyl-3-azido-4-nitropyrazole compounds: **A, B** 1-azidomethyl-3-azido-4-nitropyrazole (**16**); **C, D** 1-azidoethyl-3-azido-4-nitropyrazole (**20**).

Hydroxy Compounds



Chloro Compounds

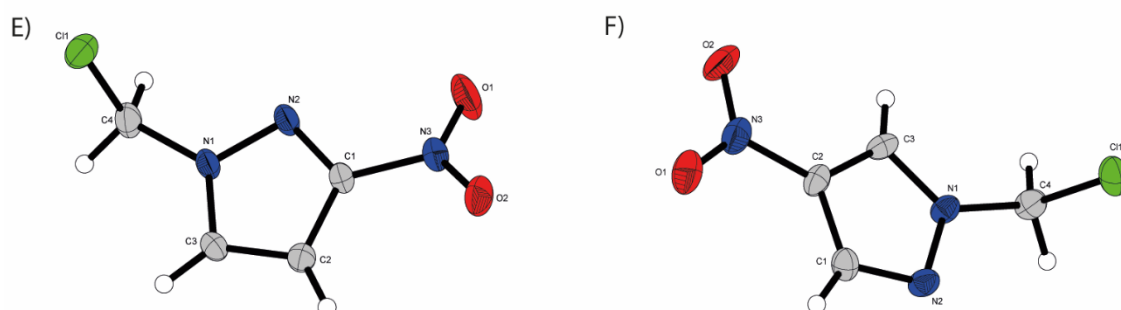


Figure S5: Crystal structures of precursor compounds: **A)** 1-hydroxymethyl-3-nitropyrazole (**1**); **B)** 1-hydroxymethyl-4-nitropyrazole (**7**); **C)** 1-hydroxyethyl-3-nitropyrazole (**4**); **D)** 1-hydroxyethyl-4-nitropyrazole (**8**); **E)** 1-chloromethyl-3-nitropyrazole (**10**); **F)** 1-chloromethyl-4-nitropyrazole (**12**).

3. Heat of formation calculation

All quantum chemical calculations were performed using the Gaussian G09 program package.^[S6] The complete basis set (CBS) method of Petersson and coworkers was used for calculation of enthalpies (H) and free energies (G), listed in Table S6 in order to obtain very accurate energies. The CBS models use the known asymptotic convergence of pair natural orbital expressions to extrapolate from calculations using a finite basis set to the estimated complete basis set limit. CBS-4 starts with a HF/3-21G(d) geometry optimization; the zero-point energy is computed at the same level. It then uses a large basis set SCF calculation as a base energy, and a MP2/6-31+G calculation with a CBS extrapolation to correct the energy through second order. A MP4(SDQ)/6-31+(d,p) calculation is used to approximate higher order contributions. In this study, we applied the modified CBS-4M method (M referring to the use of minimal population localization), which is a re-parametrized version of the original CBS-4 method and also includes some additional empirical corrections.^[S7] The gas-phase enthalpies ($\Delta_f H^\circ(\text{g}, \text{M}, 298)$) of the species were computed according to the atomization energy method (**Equation S1**) using room temperatures CBS-4M enthalpies (**Table S7**).^[S8]

$$\Delta_f H^\circ(\text{g}, \text{M}, 298) = H_{(\text{molecule}, 298)} - \sum H^\circ_{(\text{atoms}, 298)} + \sum \Delta_f H^\circ_{(\text{atoms}, 298)} \quad (\text{Eq. S1})$$

Table S7: CBS-4M electronic enthalpies for atoms C, H, N and O and their literature values.

	$-H^{298} / \text{a.u.}$	$\Delta_f H^\circ_{\text{gas}} [S9]$
H	0.500991	217.998
C	37.786156	716.68
N	54.522462	472.68
O	74.991202	249.18

In order to obtain the energy of formation for the solid phase of all compounds, heat of formations of the condensed phase were calculated by subtracting the heats of sublimation or vaporization, respectively, obtained from RoseBoom 2.3.^[S10]

Table S8: CBS-4M results and calculated gas-phase enthalpies.

	$-H^{298} [a] [\text{a.u.}]$	$\Delta_f H^\circ(\text{g}, \text{M}) [b] [\text{kJ mol}^{-1}]$	$\Delta_{\text{sub}}H / \Delta_{\text{vap}}H [c] [\text{kJ mol}^{-1}]$	$\Delta_f H^\circ(\text{s}) [d] [\text{kJ mol}^{-1}]$
2	-748.781256	83.7	103.9	-20.2
3	-953.057307	122.1	113.4	8.7
5	-788.025077	39.9	107.0	-67.1
6	-992.302632	74.4	117.5	-43.1
9	-788.024279	42.0	107.0	-65.0
11	-632.770512	496.9	95.1	401.8
13	-632.77169	493.8	95.1	398.7
15	-837.045917	537.1	103.2	433.9
17	-672.01395	454.2	84.6	369.6
18	-672.013012	456.7	84.6	372.1
19	-876.291745	488.1	105.6	382.5
16	-796.155912	859.4	103.6	755.8
20	-835.400843	812.8	105.4	707.4

[a] CBS-4M electronic enthalpy; [b] gas phase enthalpy of formation. [c] Calculated with RoseBoom 2.3 [d] Calculated heat of formation for the condensed phase

4. Physico-chemical properties

Table S9: Physicochemical properties and detonation parameter of nitric ester (2, 3, 5, 6, 9) compared to TNT.

	(2)	(3)	(5)	(6)	(9)	TNT
Formula	C ₄ H ₄ N ₄ O ₅	C ₅ H ₃ N ₅ O ₇	C ₅ H ₆ N ₄ O ₅	C ₅ H ₅ N ₅ O ₇	C ₅ H ₆ N ₄ O ₅	C ₇ H ₅ N ₃ O ₆
FW [g·mol ⁻¹]	188.10	233.10	202.14	247.12	202.14	227.13
IS ^[a] [J]	>40	4	>40	30	>40	15
FS ^[b] [N]	>360	288	>360	>360	>360	>360
Ω _{CO₂} ^[d] [%]	-43	-17	-63	-36	-63	-74.0
T _{endo} ^[e] [°C]	70	93	78	61	52	81
T _{exo} ^[f] [°C]	161	159	198	198	191	289
ρ ^[g] [g·cm ⁻³]	1.696	1.848	1.629	1.734	1.613	1.65
Δ _f H ^[h] [kJ·mol ⁻¹]	-20.2	8.7	-67.1	-43.1	-65.0	-185
EXPLOS V6.05 values						
-Δ _ε U ^[i] [kJ·kg ⁻¹]	4869	5693	4398	5152	4399	5022
T _{C-j} ^[j] [K]	3491	4059	3082	3645	3096	3452
ρ _{C-j} ^[k] [GPa]	24.3	33.6	19.8	26.7	19.5	20.5
D _{C-j} ^[l] [m·s ⁻¹]	7675	8668	7163	7932	7110	6950
V ^[m] [dm ³ ·kg ⁻¹]	716	707	730	711	732	633

[a] Impact sensitivity (BAM drophammer, method 1 of 6); [b] friction sensitivity (BAM friction tester, method 1 of 6); [c] electrostatic discharge sensitivity (OZM XSpark10); [d] oxygen balance toward carbon dioxide ($\Omega_{CO_2} = (nO - 2xC - yH/2)/(1600/FW)$); [e] endothermic event (DTA, $\beta = 5$ °C·min⁻¹); [f] temperature of decomposition (DTA, $\beta = 5$ °C·min⁻¹); [g] density at 298 K recalculated from X-ray data; [h] heat of formation (calculated using the atomization method and CBS-4M enthalpies; [i] detonation energy; [j] detonation temperature; [k] detonation velocity; [l] detonation pressure; [m] volume of detonation gases at standard temperature and pressure conditions; [n] determined at LMU.

Table S10: Physicochemical properties and detonation parameter of azides (11, 13, 15, 17, 18, 19) compared to TNT.

	(11)	(13)	(15)	(17)	(18)	(19)	TNT
Formula	C ₄ H ₄ N ₆ O ₂	C ₄ H ₄ N ₆ O ₂	C ₄ H ₃ N ₇ O ₄	C ₅ H ₆ N ₆ O ₂	C ₅ H ₆ N ₆ O ₂	C ₅ H ₅ N ₇ O ₄	C ₇ H ₅ N ₃ O ₆
FW [g·mol ⁻¹]	168.12	168.12	213.11	182.14	182.14	227.14	227.13
IS ^[a] [J]	>40	>40	>40	>40	>40	25	15
FS ^[b] [N]	>360	>360	>360	>360	>360	>360	>360
Ω _{CO₂} ^[d] [%]	-76	-76	-41	-97	-97	-60	-74.0
T _{endo} ^[e] [°C]	40	42	/	/	/	50	81
T _{exo} ^[f] [°C]	179	174	154	214	214	216	289
ρ ^[g] [g·cm ⁻³]	1.513	1.547	1.58 ^[o]	1.28 ^[o]	1.34 ^[o]	1.664	1.65
Δ _f H ^[h] [kJ·mol ⁻¹]	401.8	398.7	433.9	369.6	372.1	382.5	-185
EXPLOS V6.05 values							
-Δ _ε U ^[i] [kJ·kg ⁻¹]	4483	4497	5241	4167	4222	4900	5022
T _{C-j} ^[j] [K]	3380	3314	3998	2910	2914	3483	3452
ρ _{C-j} ^[k] [GPa]	19.9	19.8	23.1	11.9	13.3	22.9	20.5
D _{C-j} ^[l] [m·s ⁻¹]	6972	7100	7679	6235	6483	7639	6950
V ^[m] [dm ³ ·kg ⁻¹]	742	740	768	771	761	738	633

[a] Impact sensitivity (BAM drophammer, method 1 of 6); [b] friction sensitivity (BAM friction tester, method 1 of 6); [c] electrostatic discharge sensitivity (OZM XSpark10); [d] oxygen balance toward carbon dioxide ($\Omega_{CO_2} = (nO - 2xC - yH/2)/(1600/FW)$); [e] endothermic event (DTA, $\beta = 5$ °C·min⁻¹); [f] temperature of decomposition (DTA, $\beta = 5$ °C·min⁻¹); [g] density at 298 K recalculated from X-ray data; [h] heat of formation (calculated using the atomization method and CBS-4M enthalpies; [i] detonation energy; [j] detonation temperature; [k] detonation velocity; [l] detonation pressure; [m] volume of detonation gases at standard temperature and pressure conditions; [n] determined at LMU; [o] volumetric determination.

Table S11: Physicochemical properties and detonation parameter of azides (**16**, **20**) compared to TNT.

	(16)	(20)	TNT
Formula	C ₄ H ₃ N ₉ O ₂	C ₅ H ₅ N ₉ O ₂	C ₇ H ₅ N ₃ O ₆
FW [g·mol ⁻¹]	209.13	223.16	227.13
IS ^[a] [J]	<1	2	15
FS ^[b] [N]	10	80	>360
Ω _{CO₂} ^[d] [%]	-57	-75	-74.0
T _{endo} ^[e] [°C]	57	41	81
T _{exo} ^[f] [°C]	157	172	289
ρ ^[g] [g·cm ⁻³]	1.670	1.554	1.65
Δ _f H ^[h] [kJ·mol ⁻¹]	755.8	707.4	-185
EXPLOS V6.05 values			
-Δ _ε U ^[i] [kJ·kg ⁻¹]	5177	4709	5022
T _{C-J} ^[j] [K]	3812	3416	3452
ρ _{C-J} ^[k] [GPa]	24.4	20.1	20.5
D _{C-J} ^[l] [m·s ⁻¹]	7945	7274	6950
V ^[m] [dm ³ ·kg ⁻¹]	748	751	633

[a] Impact sensitivity (BAM drophammer, method 1 of 6); [b] friction sensitivity (BAM friction tester, method 1 of 6); [c] electrostatic discharge sensitivity (OZM XSpark10); [d] oxygen balance toward carbon dioxide ($\Omega_{CO_2} = (nO - 2xC - yH/2)(1600/FW)$); [e] endothermic event (DTA, $\beta = 5 \text{ }^\circ\text{C}\cdot\text{min}^{-1}$); [f] temperature of decomposition (DTA, $\beta = 5 \text{ }^\circ\text{C}\cdot\text{min}^{-1}$); [g] density at 298 K recalculated from X-ray data; [h] heat of formation (calculated using the atomization method and CBS-4M enthalpies; [i] detonation energy; [j] detonation temperature; [k] detonation velocity; [l] detonation pressure; [m] volume of detonation gases at standard temperature and pressure conditions; [n] determined at LMU.

5. ^{15}N NMR spectroscopy

^{15}N NMR (41 MHz, Aceton- d_6)

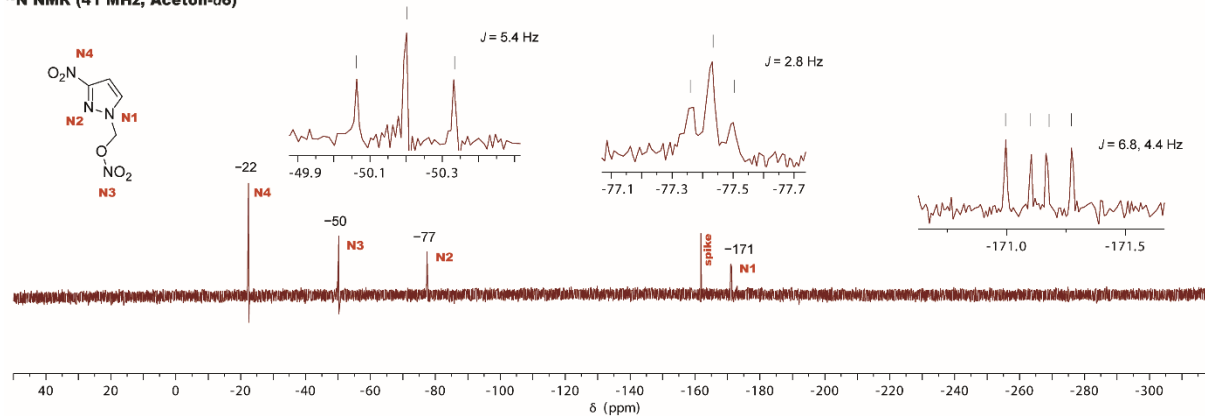


Figure S6: Proton coupled ^{15}N NMR spectrum of compound 2.

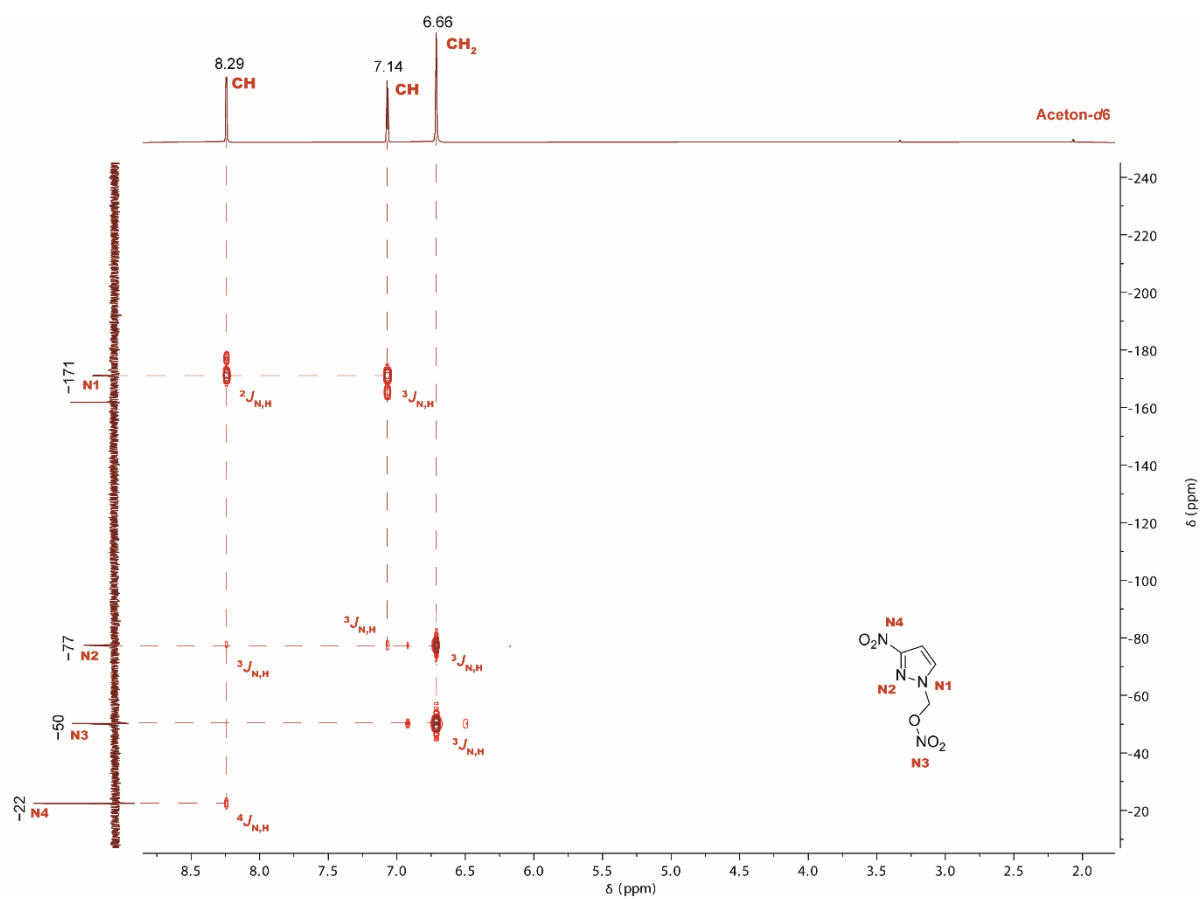


Figure S7: ^1H - ^{15}N HMBC NMR spectrum of compound 2.

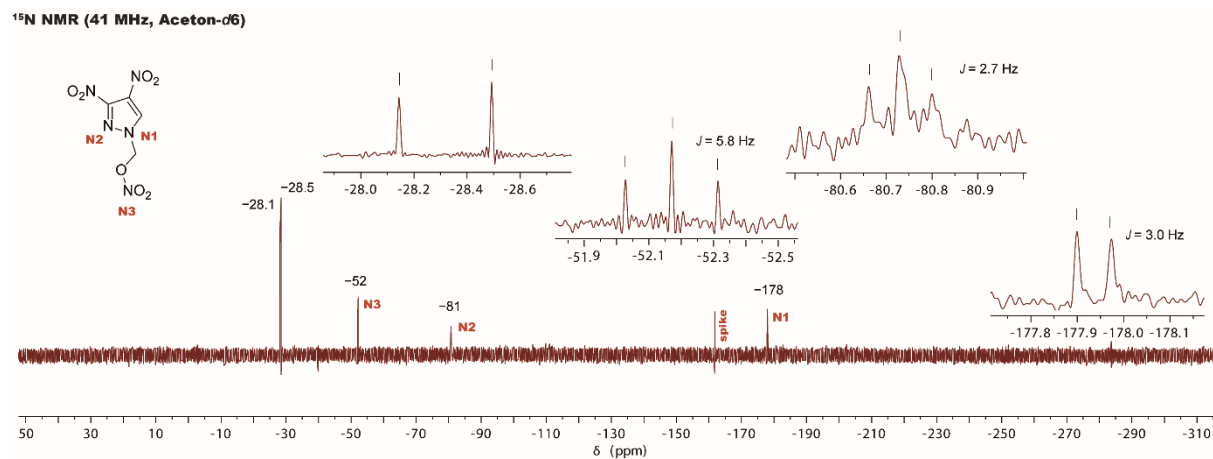


Figure S8: Proton coupled ¹⁵N NMR spectrum of compound 3.

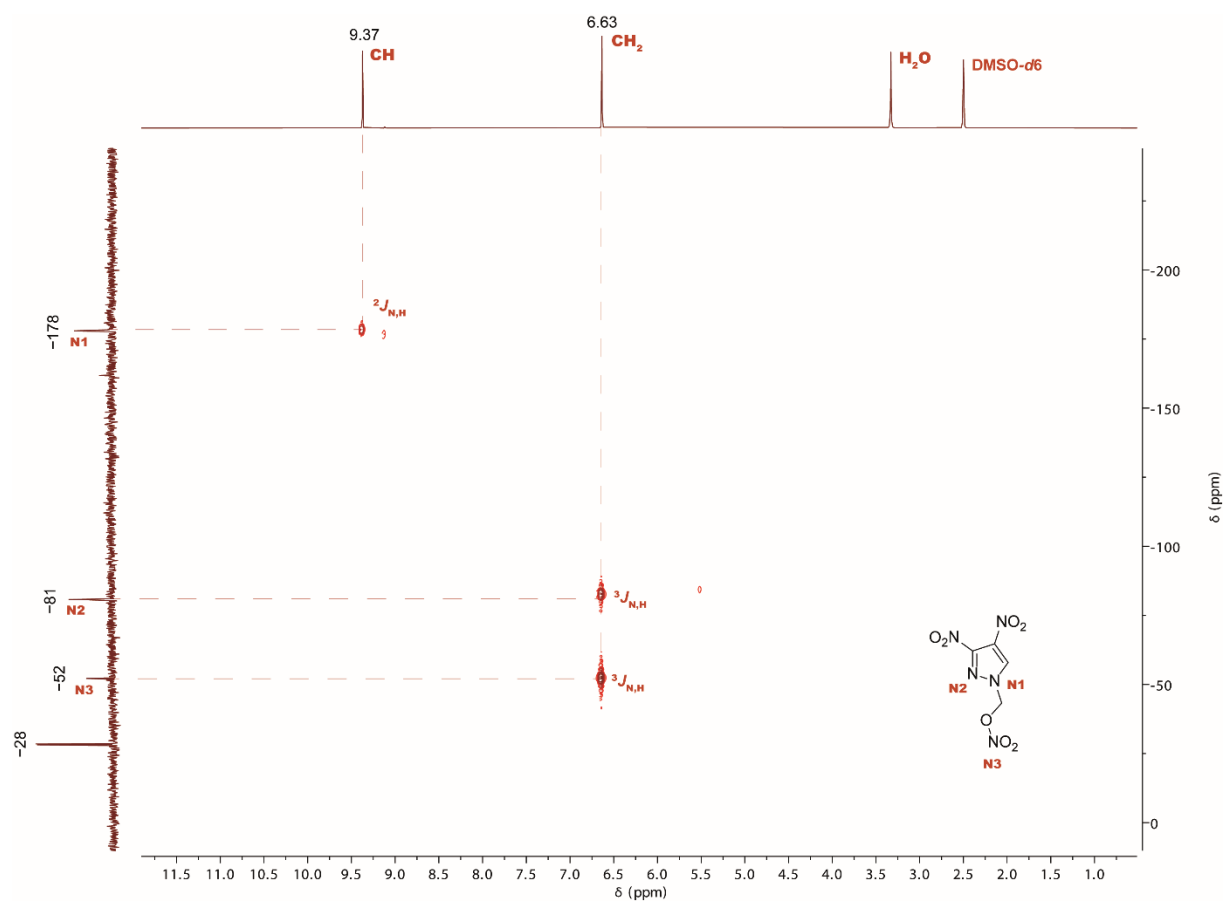


Figure S9: ¹H-¹⁵N HMBC NMR spectrum of compound 3.

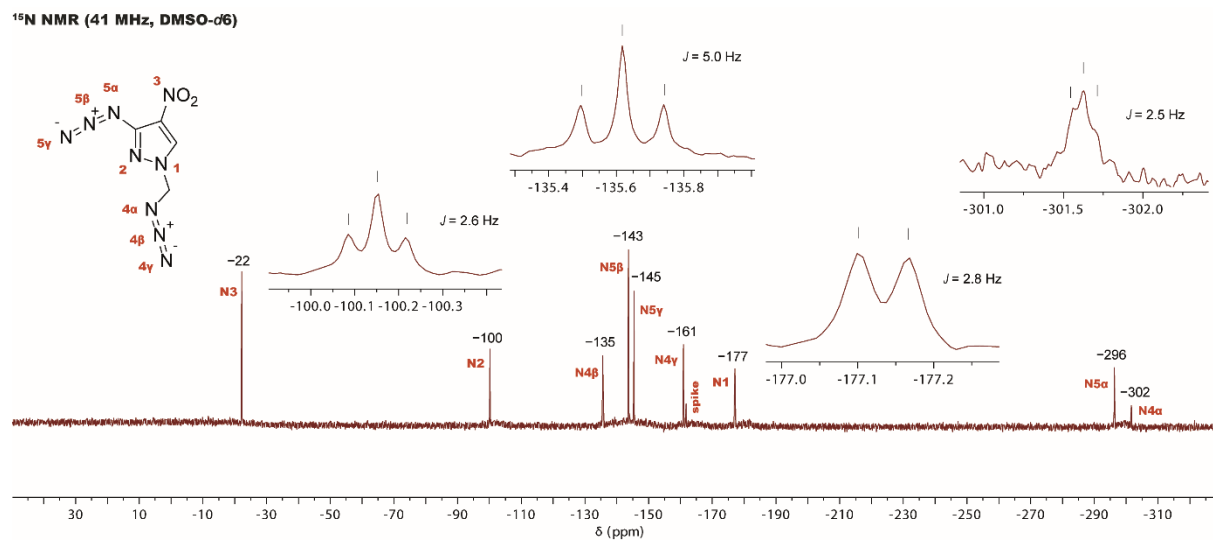


Figure S10: Proton coupled ¹⁵N NMR spectrum of compound 16.

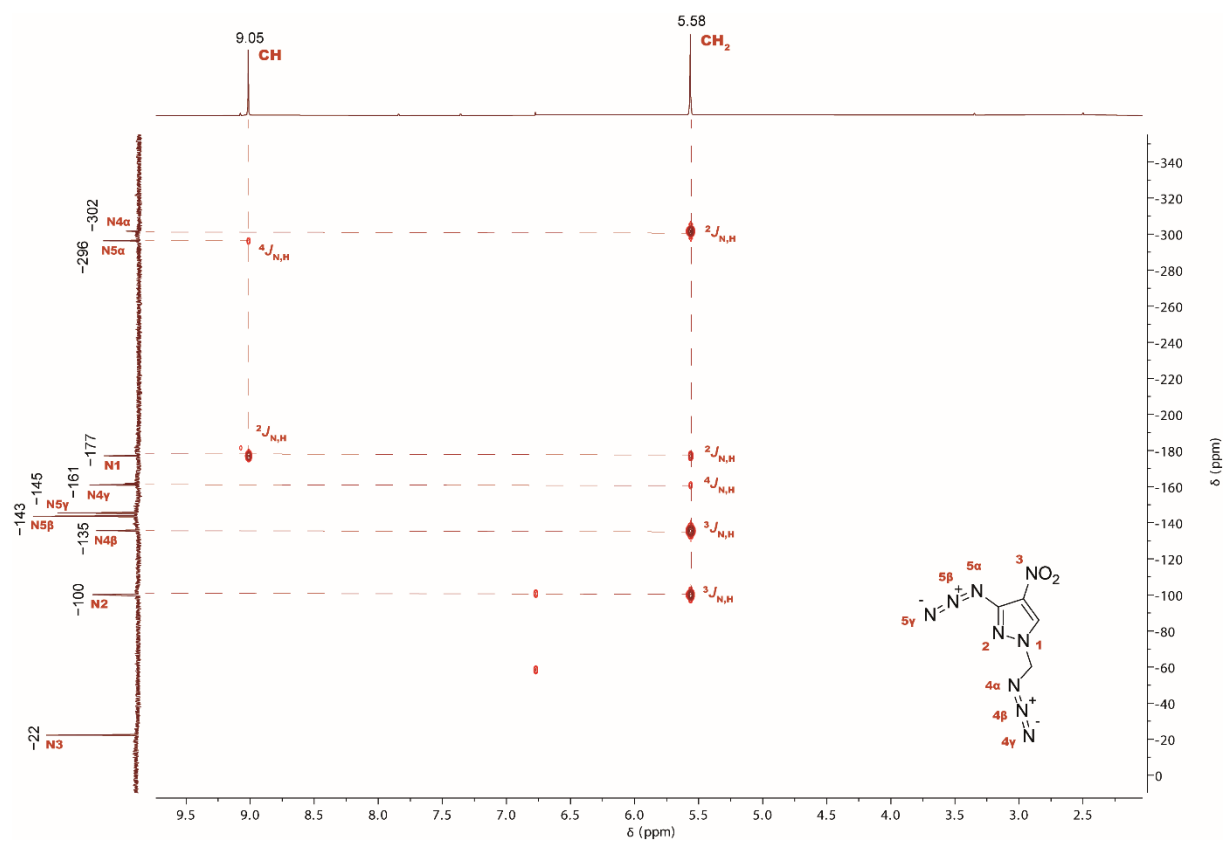


Figure S11: ¹H-¹⁵N HMBC NMR spectrum of compound 16.

6. Thermal stability

Differential thermal analysis (DTA) was measured on an OZM Research DTA 552-Ex device in a range of 25–400 °C at a heating rate of 5 °C min⁻¹. Thermogravimetric measurements (TGA) were performed with a Perkin-Elmer TGA 4000 apparatus using a heating rate of 5 °C min⁻¹ in a slow stream of nitrogen gas (1mL/min).

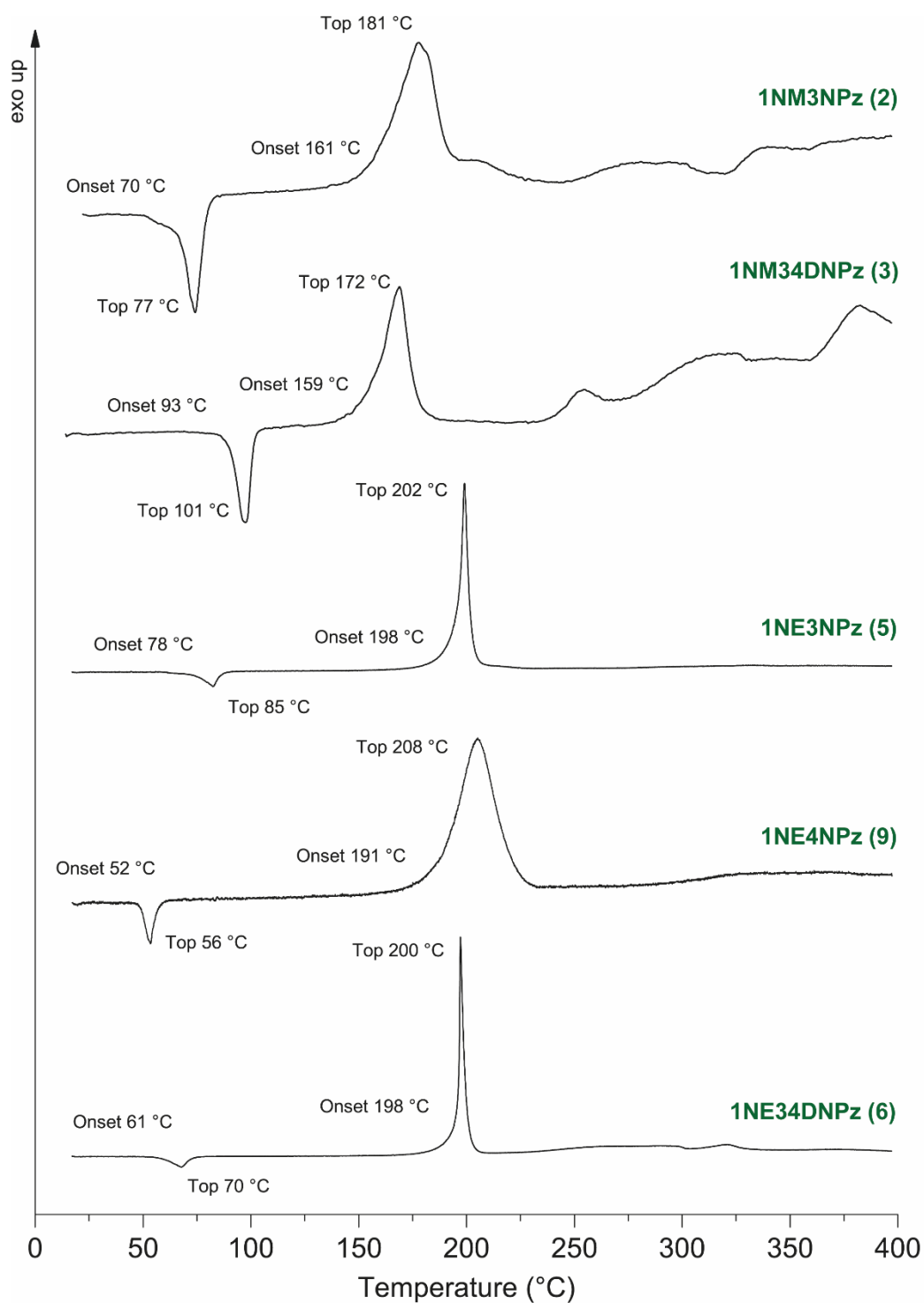


Figure S12: DTA spectra of nitroalkyl-compounds 2, 3, 5, 6 and 9.

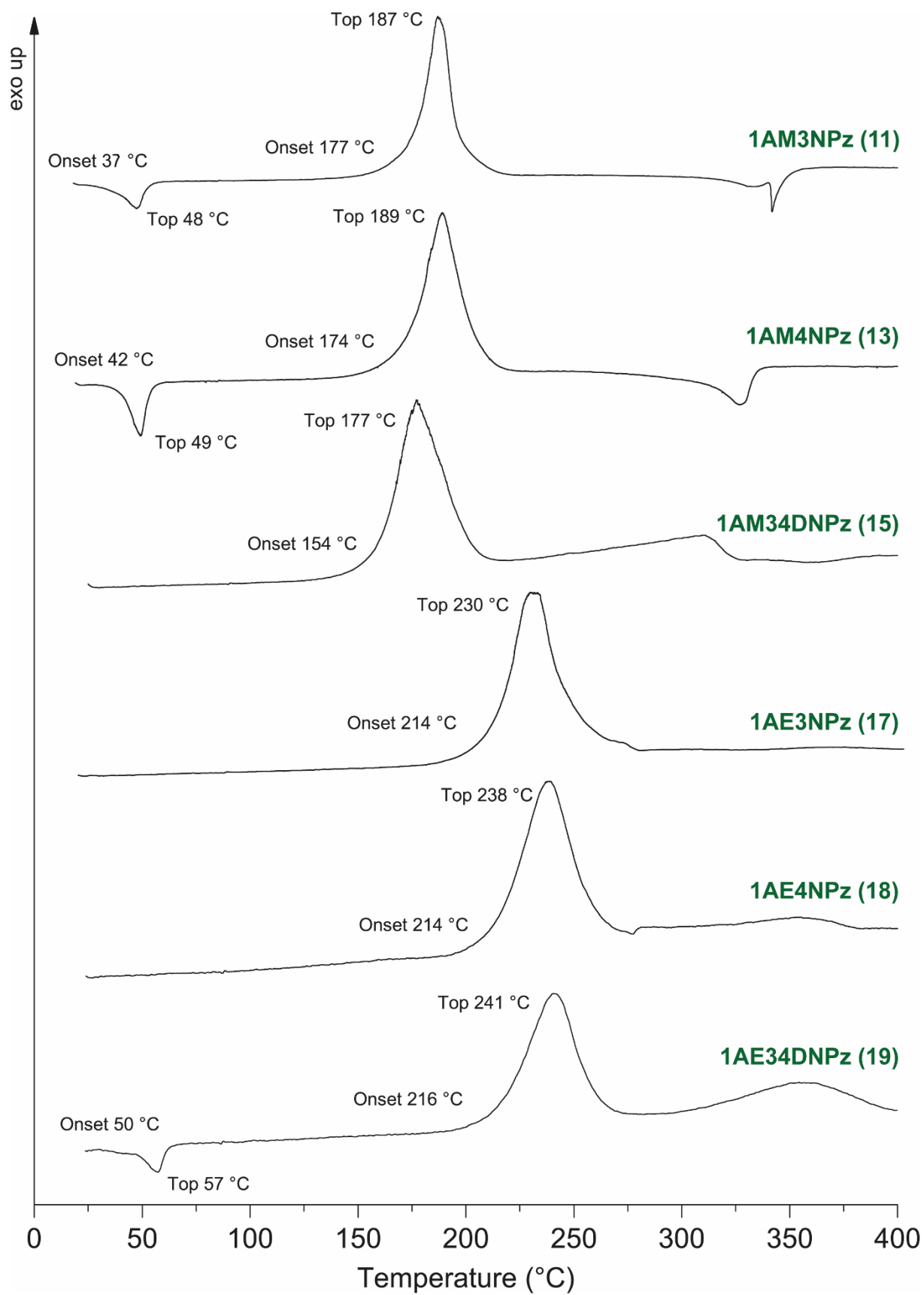


Figure S13: DTA spectra of azidoalkyl-compounds 11, 13, 15, 17, 18 and 19.

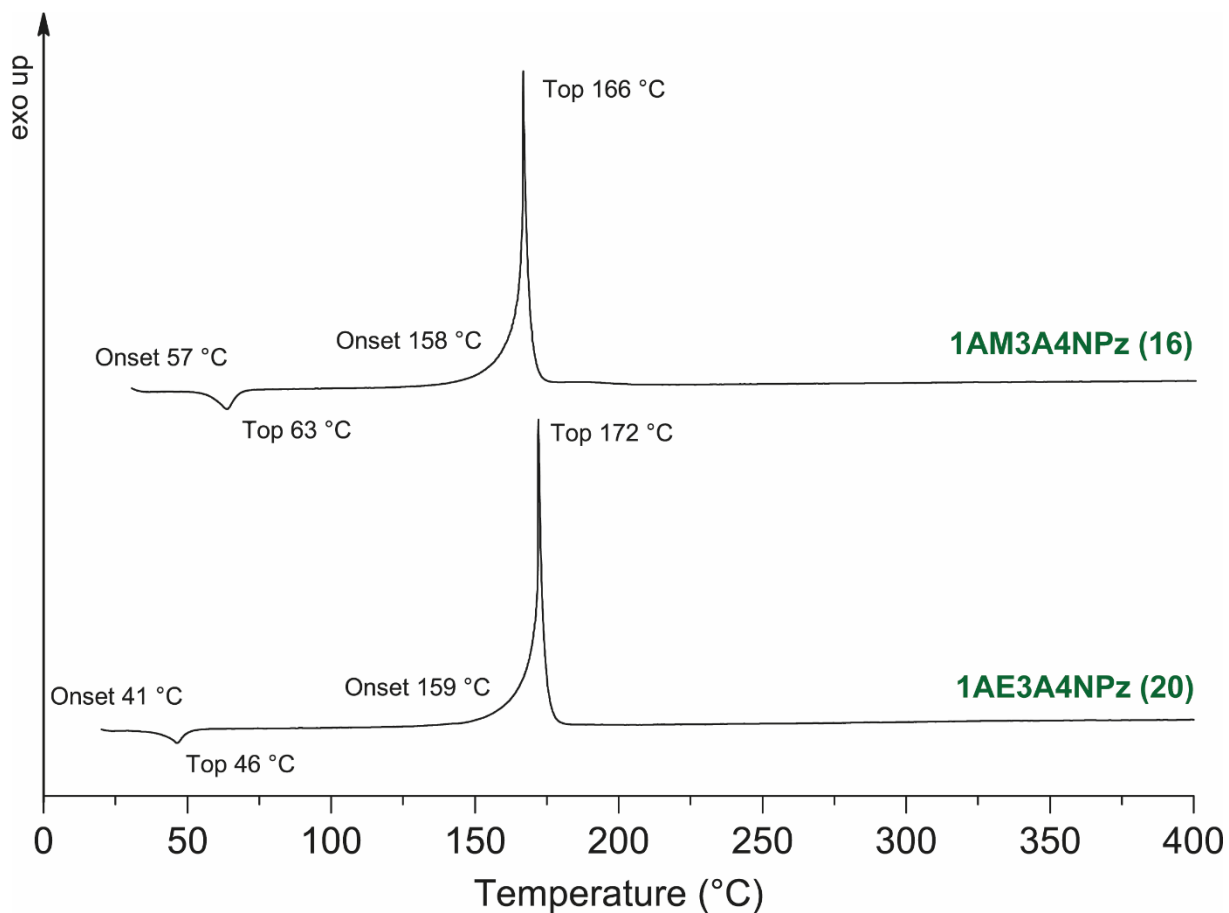


Figure S14: DTA spectra of azidoalkyl-azido-nitro-compounds **16** and **20**.

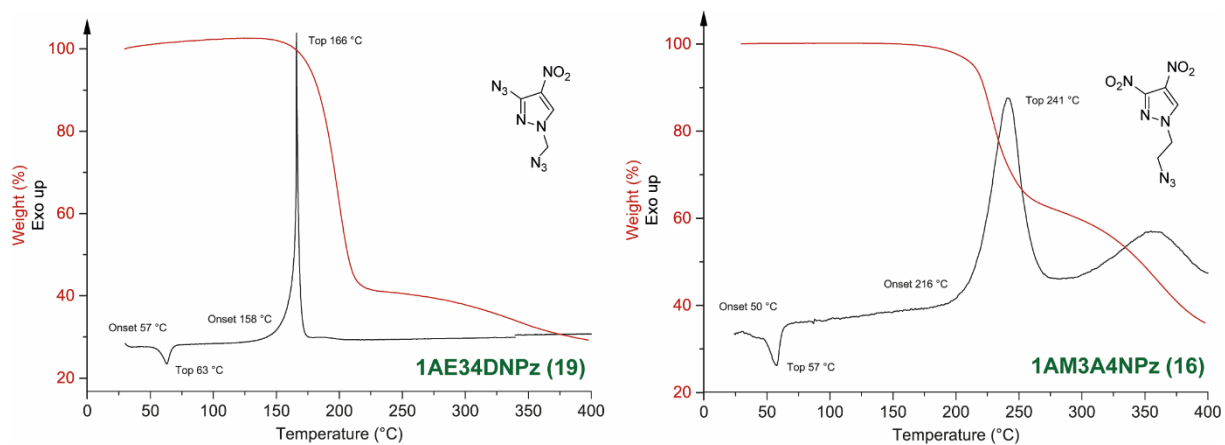


Figure S15: Combined DTA-TGA spectrum of azidoalkyl-compounds **16** and **19**.

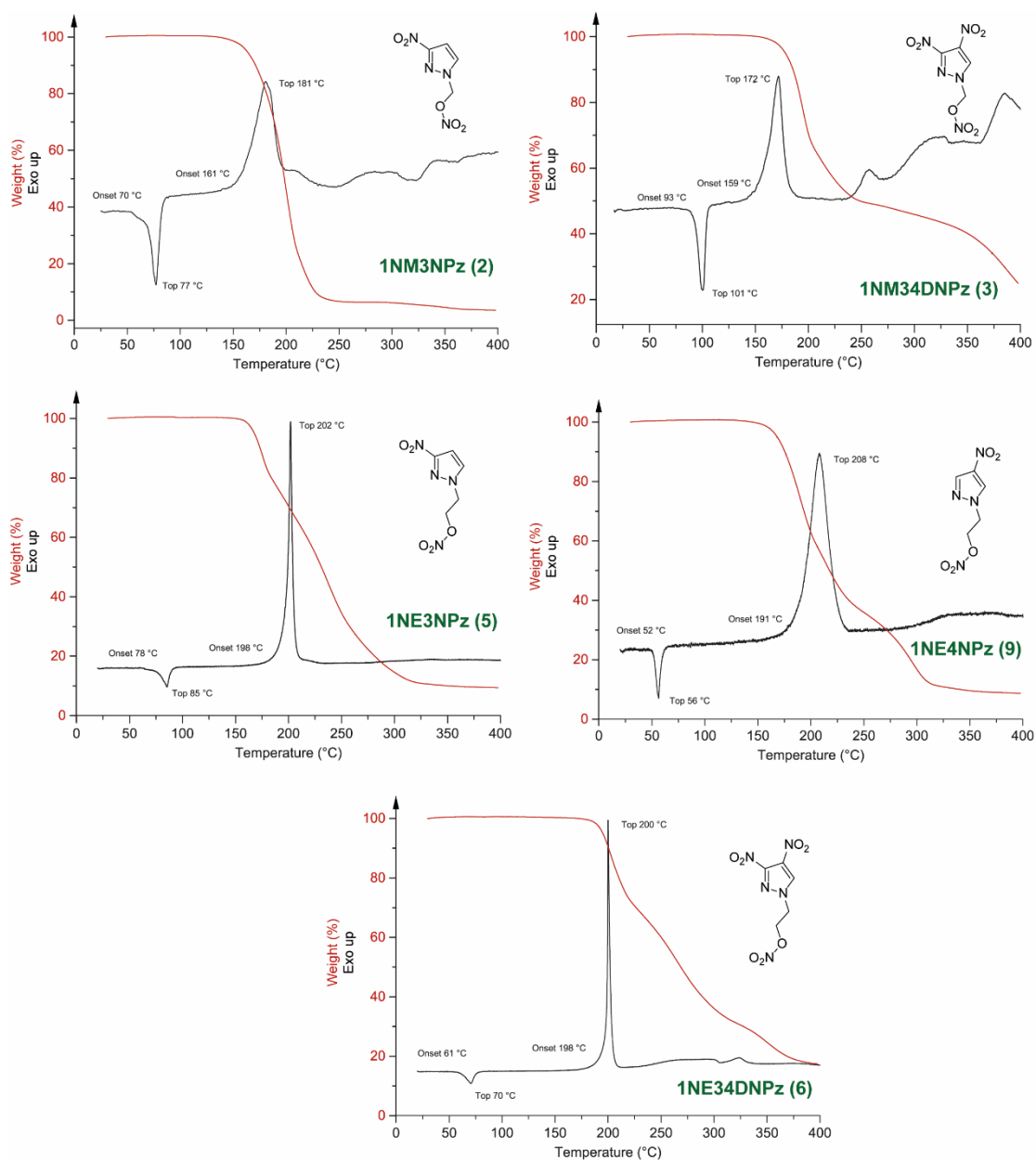


Figure S16: Combined DTA-TGA spectrum of nitroalkyl-compounds 2, 3, 5, 6 and 9.

7. Compatibilities

To ensure the safe handling of energetic substances, it is necessary to consider their thermal stability when they come into contact with other materials. This is particularly important for applications such as explosives and pyrotechnics. In order to assess the compatibility of these substances with various additives, different thermal methods such as differential thermal analysis (DTA), thermogravimetric analysis (TGA), pressure increase in closed systems (PIST), and vacuum stability test (VST) can be utilized. In this study, the DTA method was specifically employed to investigate the compatibility of the energetic substances with different additives (RDX and HMX). Differential thermal analysis (DTA) was measured on an OZM Research DTA 552-Ex device in a range of 25–400 °C at a heating rate of 5 °C min⁻¹. The substances were mixed in the ratio of 1:1.

Compatibilities were evaluated according to the standardized procedure outlined in STANAG 4147.^[S11] The analysis involved determining the difference between the endothermic and exothermic maxima of the pure substance and its mixture with the test component. The criteria for determining compatibilities are presented in **Table S12**.

Table S12: Criteria for compatibilities.

temperature difference	description
$\Delta T \leq 4 \text{ }^{\circ}\text{C}$	compatible
$4 \text{ }^{\circ}\text{C} < \Delta T \leq 20 \text{ }^{\circ}\text{C}$	moderately
$\Delta T > 20 \text{ }^{\circ}\text{C}$	incompatible

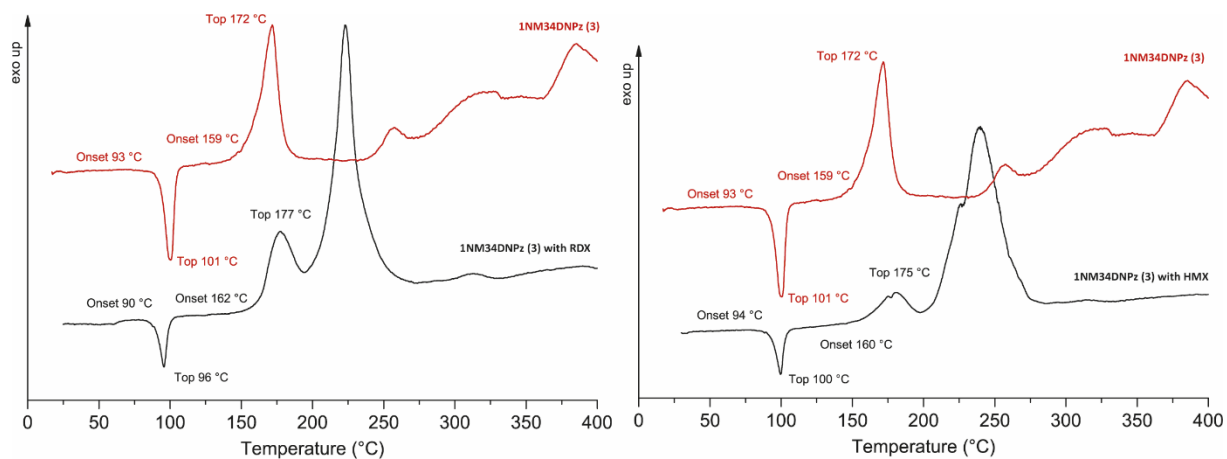


Figure S17: DTA spectra of compatibility measurements of compound **3** with **RDX** (left) and **HMX** (right).

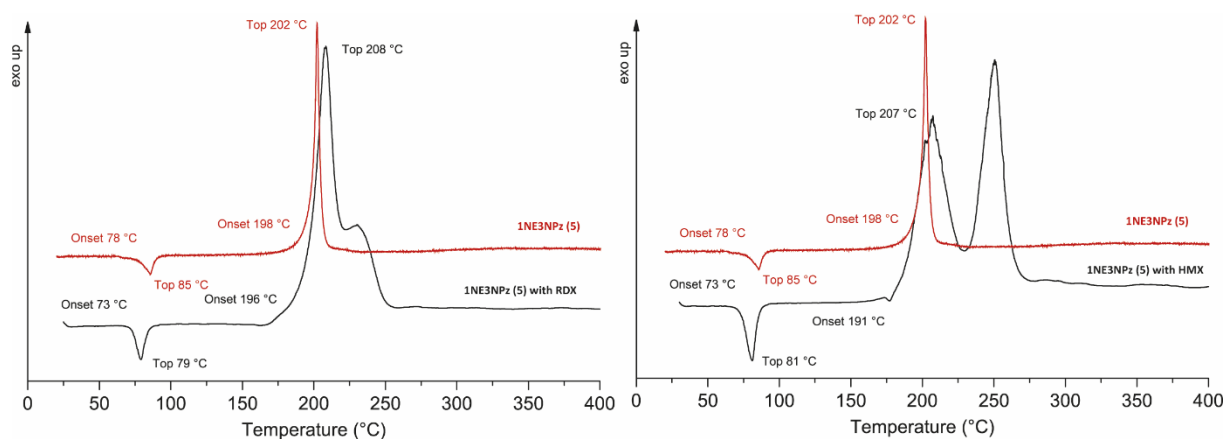


Figure S18: DTA spectra of compatibility measurements of compound **5** with **RDX** (left) and **HMX** (right).

Table S13: Compatibilities of compounds **3** and **5** with **RDX** and **HMX**.

compound	melting [°C]		decompositon [°C]	
	on	top	on	top
1-nitratomethyl-3,4-dinitropyrazole	93	101	159	172
1-nitratomethyl-3,4-dinitropyrazole (RDX)	90	96	162	177
difference (RDX)	3	5	3	5
1-nitratomethyl-3,4-dinitropyrazole (HMX)	94	100	160	175
difference (HMX)	4	1	1	3
1-nittratoethyl-3-nitropyrazole	78	85	198	202
1-nittratoethyl-3-nitropyrazole (RDX)	73	79	196	208
difference (RDX)	5	6	2	6
1-nittratoethyl-3-nitropyrazole (HMX)	73	81	191	207
difference (HMX)	5	4	7	5

8. LC-MS measurements

LC-MS (liquid chromatography – mass spectrometry) analysis was performed on a Shimadzu Prominence HPLC system using a Restek Ultra PFPP column (3 μ m, 150 x 4.6 mm) and a MSQ Plus mass spectrometer from Thermo Scientific in ESI mode. Eluting buffers were buffer A (0.01% formic acid in H₂O) and buffer B (0.01% formic acid in MeCN) with the flow rate set to 0.65 mL/min. The gradient was 0 \rightarrow 7 min, 5% \rightarrow 80% buffer B. The elution was monitored at 220 nm.

For the experimental procedure, 0.5 g of 1-hydroxymethyl-3-nitropyrazole was introduced into a reaction vial containing 4 mL of fuming HNO₃ maintained at the desired temperature. Samples (100 μ L) were taken at specific time intervals: 0 min, 10 min, 30 min, 1h, 2h, 3h, 4h, 5h, and 6h. Each sample was immediately quenched with water (500 μ L) and subjected to extraction with EtOAc (300 μ L). A 100 μ L aliquot of the organic phase was further diluted with an additional 150 μ L of EtOAc and injected into the LC-MS system for analysis.

To enhance compound identification during the experiment, separate measurements of the reactant, product, and potential by-products were performed using LC-MS. This allowed for the determination of specific retention times (**Table S14**) associated with each compound, enabling accurate assignment and analysis.

Table S14: Retention time and observed mass for different nitropyrazoles using LC-MS.

compound	retention time [min]	m/z
3-nitropyrazole	4.58	112
3,4-dinitropyrazole	6.32	157
1-hydroxymethyl-3-nitropyrazole	4.45	112
1-nitratomethyl-3-nitropyrazole	6.79	112
1-nitratomethyl-3,4-dinitropyrazole	7.73	157

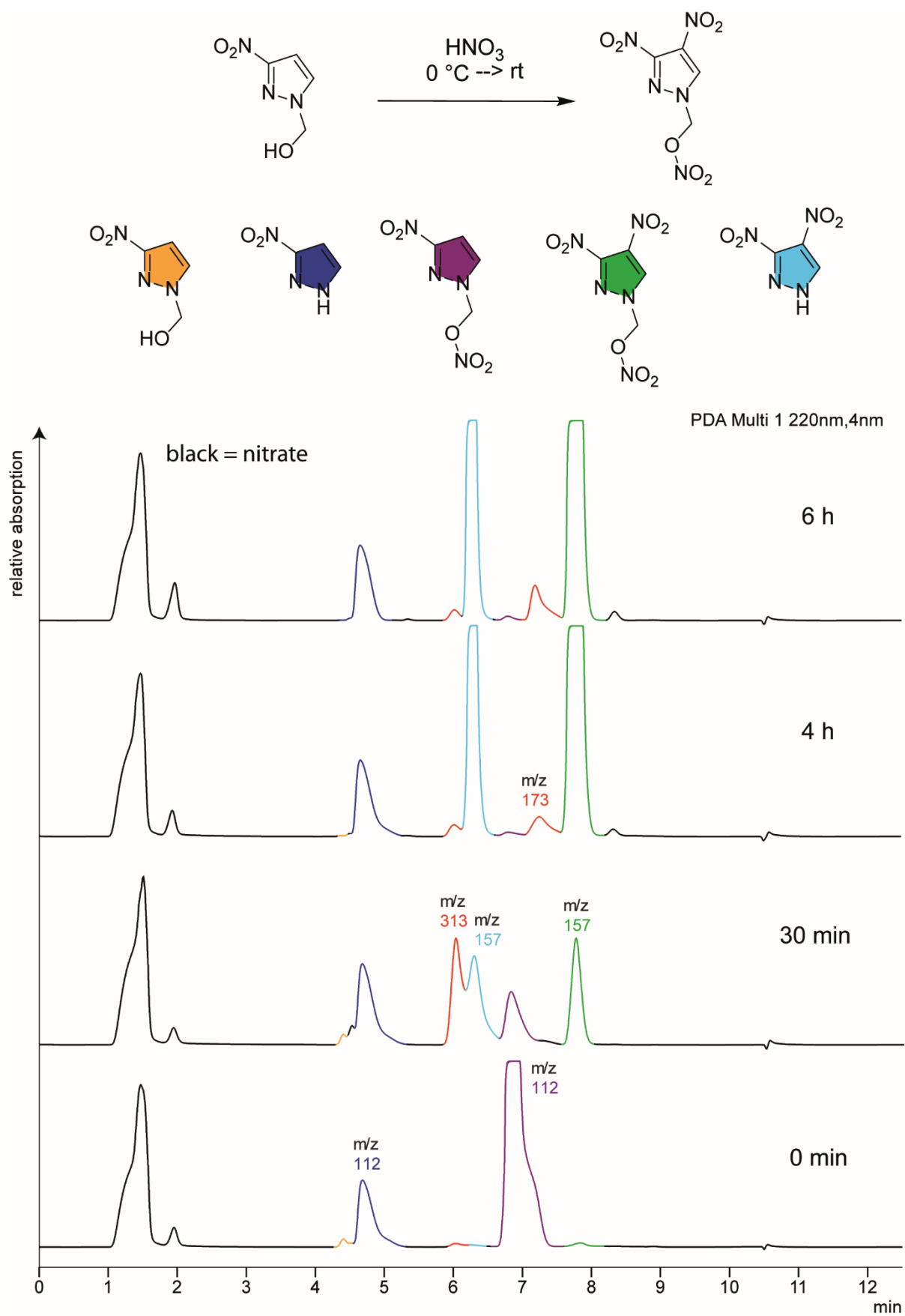


Figure S19: LC-MS monitoring of the nitration of 1-hydroxymethyl-3-nitropyrazole with fuming HNO₃ at 0 °C.

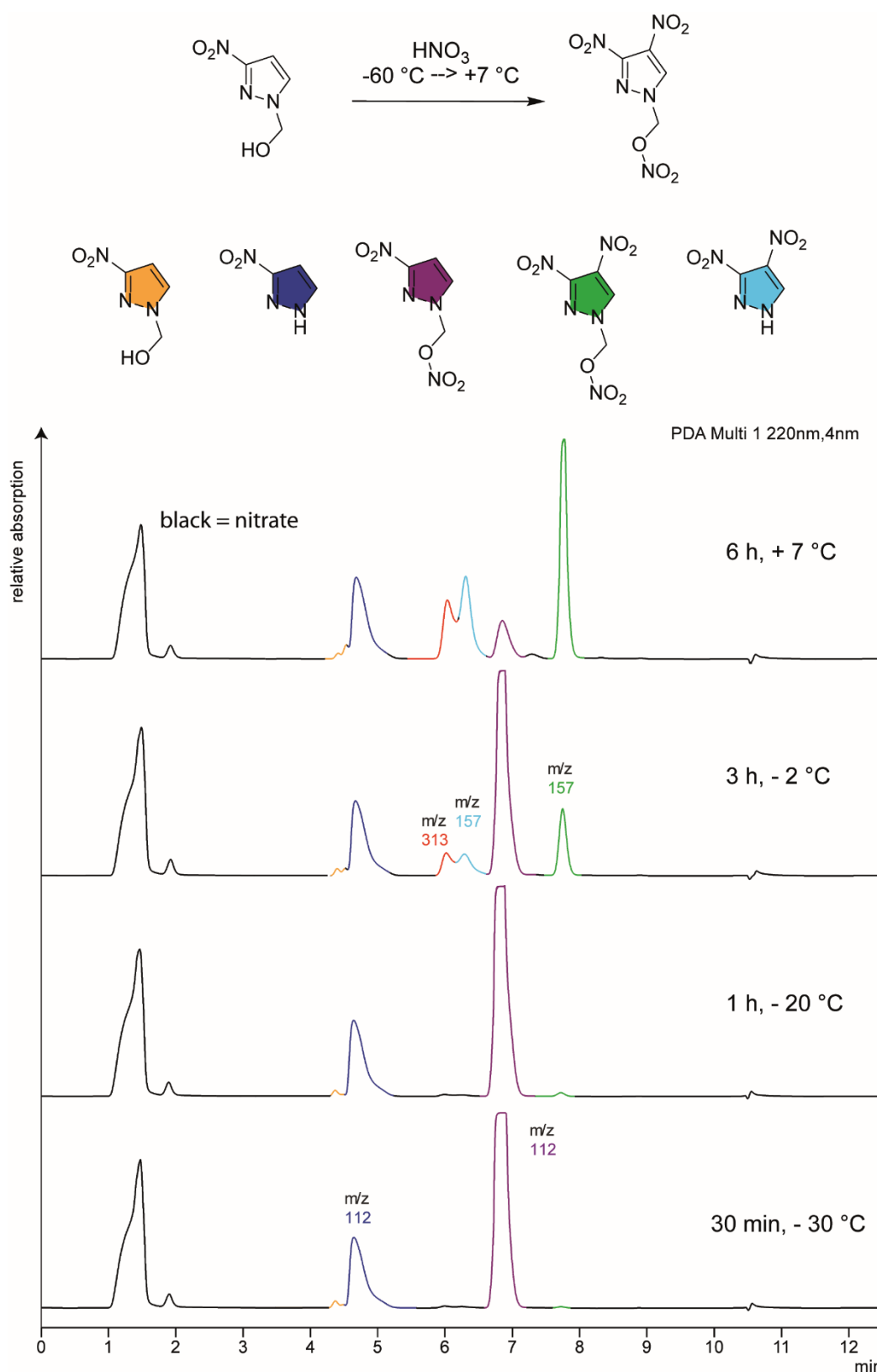


Figure S20: LC-MS monitoring of the nitration of 1-hydroxymethyl-3-nitropyrazole with fuming HNO₃ at -60 °C.

9. SSRT (small-scale shock reactivity test)

To assess the shock reactivity (explosiveness) of the investigated explosives, a small-scale shock reactivity test (SSRT) was conducted. The SSRT is designed to measure the shock reactivity of potentially energetic materials, even below critical diameter, without transitioning to detonation. The test setup combines the advantages of a lead block test^[S12] and a gap test.^[S13] Each compound was compacted into a perforated steel block. No attenuator (between detonator and sample) or air gap (between sample and aluminum block) was used. Initiation of the tested explosive was achieved using a commercially available detonator (Orica-DYNADET-C2-0ms). Dent sizes resulting from the shock were measured non-contactly using the XYZ-axis motorized 3D profilometer VR-5200, manufactured by Keyence (Osaka, Japan).

More information on the test and its implementation is described by Bauer et al.^[S14]

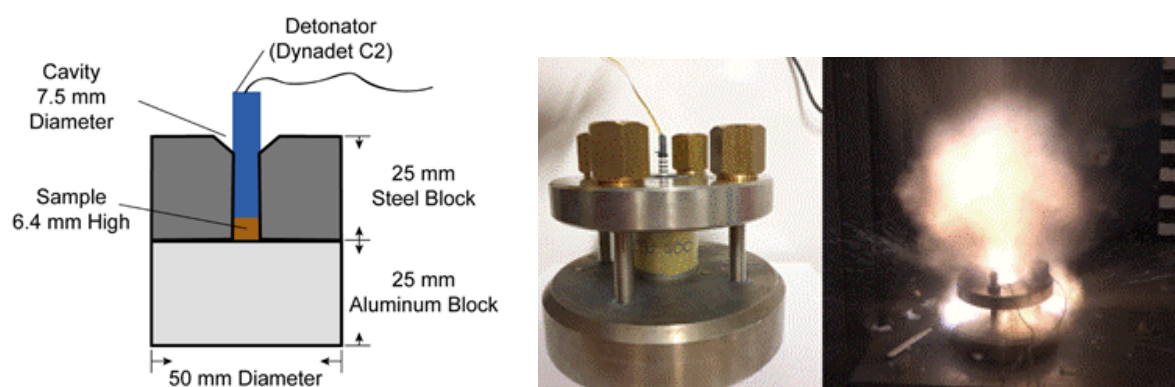


Figure S21: Setup of the SSRT experiment.^[S14]

Evaluation of 1-nitratomethyl-3,4-dinitropyrazole (3)

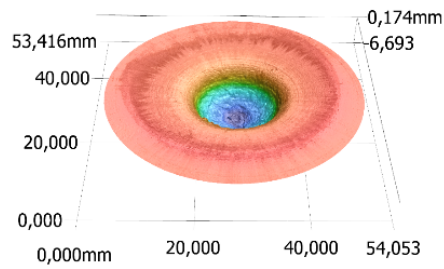
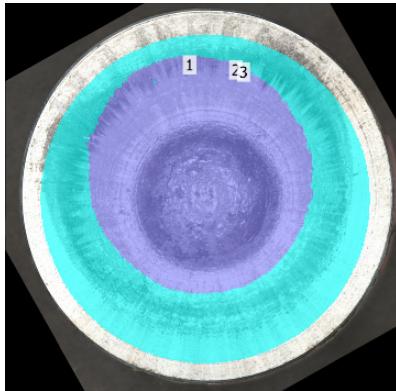


Table S15: SSRT results of 3 (Blast 1).

1-Nitratomethyl-3,4-dinitropyrazole Blast 1	
Measurement 1 [mm ³]	1256,76
Measurement 2 [mm ³]	1257,21
Average Volume [mm³]	1256,98

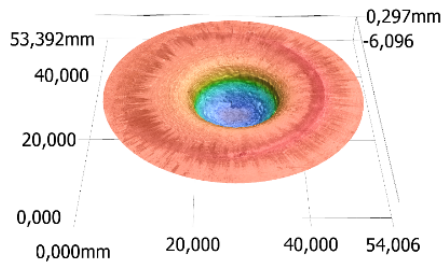
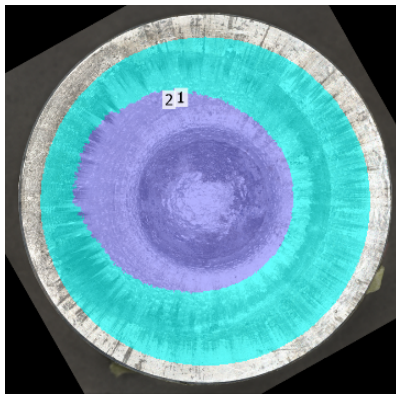
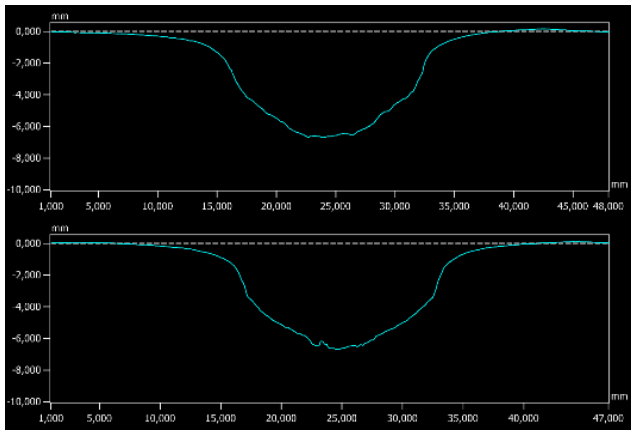
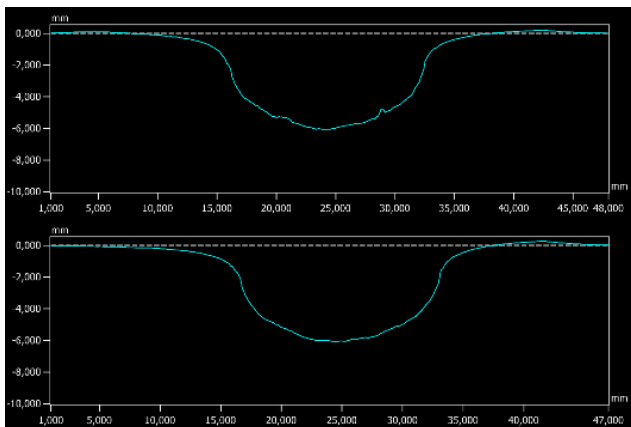


Table S16: SSRT results of 3 (Blast 2).

1-Nitratomethyl-3,4-dinitropyrazole Blast 2	
Measurement 1 [mm ³]	1171,79
Measurement 2 [mm ³]	1170,75
Average Volume [mm³]	1171,27



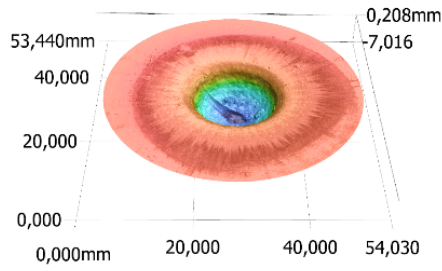
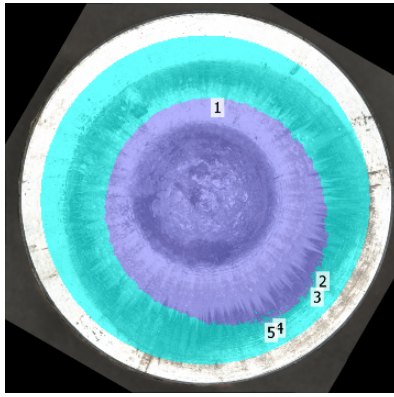
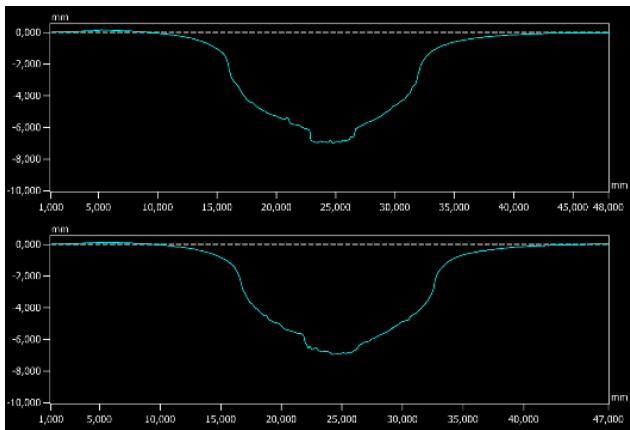


Table S17: SSRT results of 3 (Blast 3).

1-Nitratomethyl-3,4-dinitropyrazole Blast 3	
Measurement 1 [mm ³]	1218,68
Measurement 2 [mm ³]	1223,13
Average Volume [mm³]	1220,90



Evaluation of 1-nitratoethyl-3,4-dinitropyrazole (6)

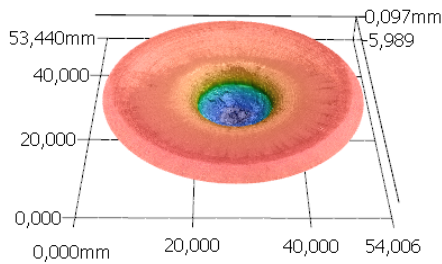
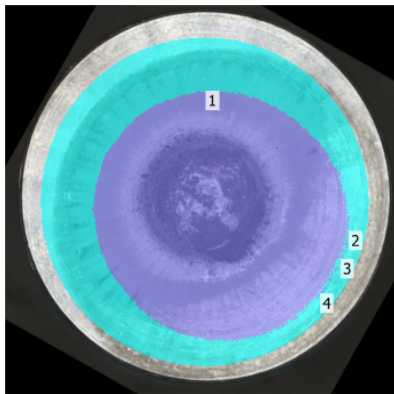
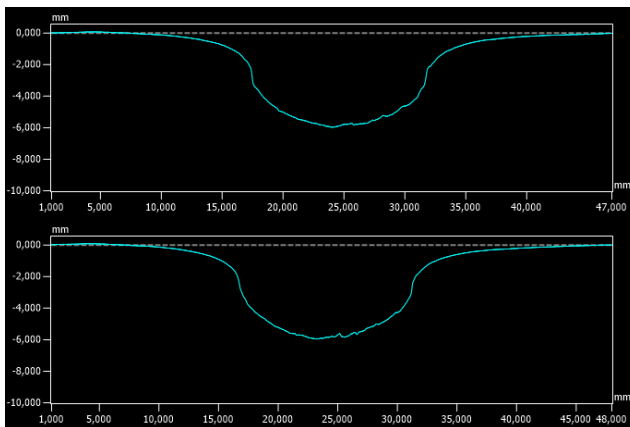


Table S18: SSRT results of 6 (Blast 1).

1-Nitratoethyl-3,4-dinitropyrazole Blast 1	
Measurement 1 [mm ³]	1129,23
Measurement 2 [mm ³]	1130,99
Average Volume [mm³]	1130,11



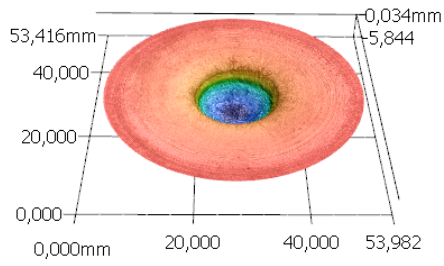
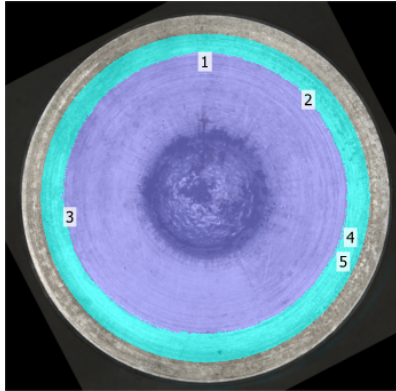


Table S19: SSRT results of 6 (Blast 2).

1-Nitratoethyl-3,4-dinitropyrazole Blast 2	
Measurement 1 [mm ³]	1191,11
Measurement 2 [mm ³]	1179,33
Average Volume [mm³]	1185,22

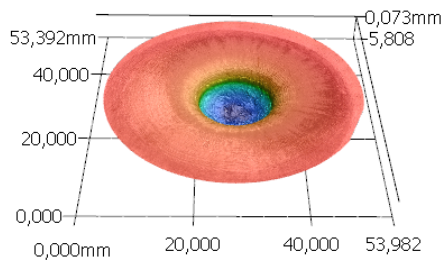
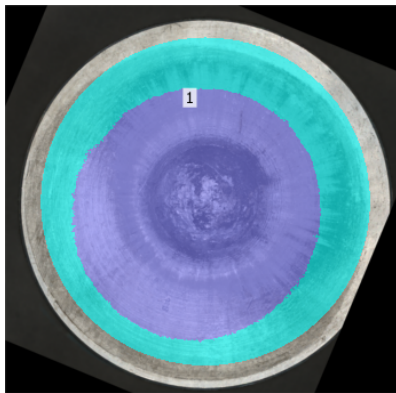
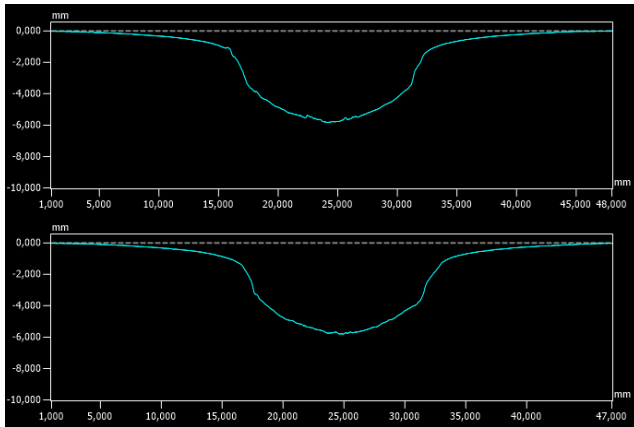
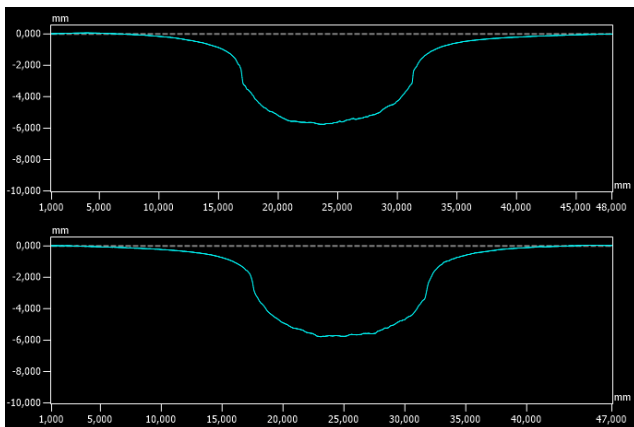


Table S20: SSRT results of 6 (Blast 3).

1-Nitratoethyl-3,4-dinitropyrazole Blast 3	
Measurement 1 [mm ³]	1088,87
Measurement 2 [mm ³]	1095,47
Average Volume [mm³]	1092,17



10. Experimental part and general methods

Caution! Nitropyrazoles are potentially energetic materials with sensitivities toward various stimuli. Therefore, meticulous security precautions (safety glass, face shield, earthed equipment and shoes, Kevlar gloves, and ear plugs) have to be applied while synthesizing and handling the described compounds.

All chemical reagents and solvents were employed as received (Sigma-Aldrich, Acros Organics, ABCR, TCI). NMR spectra were recorded on a 400 MHz instrument (*Bruker AV400* or *Bruker AV400TR*) at room temperature. Chemical shifts (δ) are reported in parts per million (ppm) and refer to tetramethylsilane (^1H , ^{13}C) and nitromethane (^{14}N , ^{15}N) (for more information see **Table S21**). All spectra were analyzed with the software MestReNOVA 10.0 from Mestrelab Research, S. L. Infrared (IR) spectra were recorded with a Perkin-Elmer Spektrum One FT-IR spectrometer in a range of 4000–400 cm^{-1} . Transmittance values are qualitatively described as “very strong” (vs), “strong” (s), “medium” (m), “weak” (w) and “very weak” (vw). Elemental analysis was carried out using an Elementar Vario el or Vario micro by pyrolysis of the sample and subsequent analysis of formed gases (allowed deviation for liquids: +/- 0.5%; for solids: +/- 0.3%). High-resolution mass spectra were recorded with a *Thermo Finnigan LTQ FT-ICR* (ESI) and a *Thermo Finnigan MAT 95* (EI) mass spectrometer. Melting and decomposition points were determined in a range of 25–400 $^{\circ}\text{C}$ at a heating rate of 5 $^{\circ}\text{C min}^{-1}$ through differential thermal analysis (DTA) with an OZM Research DTA 552-Ex instrument. Thermogravimetric measurements were performed with a Perkin-Elmer TGA 4000 apparatus using a heating rate of 5 $^{\circ}\text{C min}^{-1}$ in a slow stream of nitrogen gas (1mL/min). The sensitivity data were determined using a BAM (Bundesanstalt für Materialforschung) drophammer^[S15] according to STANAG 4489^[S16] using a modified instruction^[S17] and a BAM friction tester^[S18] according to STANAG 4487^[S19] using a modified instruction. The electrostatic sensitivity test was carried out using the OZM Electric Spark XSpark10 device^[S20]. The classification is based on the 'UN Recommendations on the Transport of Dangerous Goods'.^[S21]

Table S21: NMR pulse sequences and parameters used for the characterization of the new compounds.

	^1H	^{13}C	^{14}N	^{15}N	$^1\text{H}/^{15}\text{N}$ HMBC
Pulse Sequence	zg30	zgpg30	zgpg	zg30	hmbcqpndqf
Number of Scans	16	2048	5000	15000-39014	32
Receiver Gain	210	210	210	10-14	210
Relaxation Delay (sec)	4.0	0.5	0.2	3.0	2.0
Pulse Width (μs)	10.6	9.3	22.0	16.8	10.6
Acquisition Time (sec)	6.5	1.3	0.6	1.6	0.3
NMR. Freq.(MHz)	400.18	100.64	28.91	40.56	400.18;40.54
Spectral Width (Hz)	10000.0	25252.5	14423.1	20380.4	2994.0;16233.8
Acquired Size (DP)	65536	32768	8192	32768	1024;256

1-Hydroxymethyl-3-nitropyrazole (1)^[S22]

3-Nitropyrazole^[S23] (6.00 g, 53.1 mmol, 1.0 eq.) was dissolved in MeOH (40 mL) and formaldehyde (40% aq., 10 mL, 133 mmol, 2.5 eq.) was added. The reaction mixture was stirred at room temperature overnight and put onto a mixture of water (50 mL) and sat. NaHCO₃ (30 mL). The solution was extracted with CHCl₃ (3 × 50 mL), dried over MgSO₄ and evaporated under reduced pressure. The crude product was recrystallized from CHCl₃ (~100 mL) to obtain 1-hydroxymethyl-3-nitropyrazole (1) (5.41 g, 37.8 mmol, 71%) as colourless crystalline solid.

DTA (5 °C min⁻¹) $T_{melt} = 83$ °C; **¹H NMR** (400 MHz, DMSO-*d*₆, 25 °C): δ (ppm) = 8.08 (d, ³J_{H,H} = 2.6 Hz, 1H), 7.30 (t, ³J_{H,H} = 7.9 Hz, 1H), 7.05 (d, ³J_{H,H} = 2.6 Hz, 1H), 5.48 (d, ³J_{H,H} = 7.9 Hz, 2H); **¹³C{¹H} NMR** (101 MHz, DMSO-*d*₆, 25 °C): δ (ppm) = 155.4, 133.2, 102.9, 75.3; **¹⁴N{¹H} NMR** (29 MHz, DMSO-*d*₆, 25 °C): δ (ppm) = -20; **EA** (C₄H₅N₃O₃, 143.10 g/mol) calc. (found): C 33.57 (33.49), H 3.52 (3.28), N 29.36 (29.46) %; **HRMS** (EI+): *m/z* calculated for C₄H₅N₃O₃ [M]: 143.0331, found: 143.0324; **IR** (ATR, rel. int.): $\tilde{\nu}$ (cm⁻¹) = 3401 (m), 3211 (m), 3158 (m), 3147 (m), 3128 (m), 1537 (s), 1503 (s), 1456 (m), 1409 (m), 1379 (s), 1353 (s), 1284 (s), 1224 (m), 1176 (m), 1167 (s), 1084 (s), 1070 (s), 1050 (vs), 1034 (s), 1017 (m), 1006 (m), 998 (s), 983 (s), 888 (w), 823 (s), 788 (s), 756 (s), 742 (vs), 651 (m), 613 (s), 466 (s), 418 (m).

1-Nitratomethyl-3-nitropyrazole (2)

To cooled acetic acid anhydride (3.0 mL, 31.7 mmol, 4.5 eq.), fuming nitric acid (1.5 mL, 35.9 mmol, 5.1 eq.) was added dropwise while keeping the temperature at 0 °C. To this mixture, 1-hydroxymethyl-3-nitropyrazole (1) (1.00 g, 6.99 mmol, 1.0 eq.) was added portion wise and stirred 15 min at this temperature. The reaction was stirred further at room temperature for 10 min and poured onto ice-water (~30 mL). The precipitate was filtered off, washed with a little amount of water and air dried at room temperature to give 1-nitratomethyl-3-nitropyrazole (2) (1.06 g, 5.64 mmol, 81%) as colourless powder.

DTA (5 °C min⁻¹) $T_{melt} = 70$ °C, $T_{dec} = 161$ °C; **¹H NMR** (400 MHz, DMSO-*d*₆, 25 °C): δ (ppm) = 8.29 (d, ³J_{H,H} = 2.7 Hz, 1H), 7.14 (d, ³J_{H,H} = 2.7 Hz, 1H), 6.66 (s, 2H); **¹³C{¹H} NMR** (101 MHz, DMSO-*d*₆, 25 °C): δ (ppm) = 159.8, 136.6, 103.5, 79.1; **¹⁴N{¹H} NMR** (29 MHz, DMSO-*d*₆, 25 °C): δ (ppm) = -21, -48; **¹⁵N NMR** (41 MHz, Aceton-*d*₆, 25 °C): δ (ppm) = -22.4, -50.2 (t, ³J_{N,H} = 5.4 Hz), -77.4 (t, ³J_{N,H} = 2.8 Hz), -171.1 (dd, ²J_{N,H} = 6.8, 4.4 Hz); **EA** (C₄H₄N₄O₅, 188.10 g/mol) calc. (found): C 25.54 (25.84), H 2.14 (2.18), N 29.79 (29.64) %; **HRMS** (EI+): *m/z* calculated for C₄H₄N₄O₅ [M]: 188.0182, found: 188.0181; **IR** (ATR, rel. int.): $\tilde{\nu}$ (cm⁻¹) = 3156 (w), 3137 (w), 3059 (w), 2938 (w), 1660 (vs), 1552 (s), 1539 (m), 1510 (s), 1451 (m), 1426 (m), 1396 (m), 1377 (m), 1347 (m), 1304 (s), 1283 (s), 1235 (s), 1180 (s), 1069 (m), 1041 (m), 1004 (m), 993 (m), 952 (s), 888 (vw), 831 (s), 821 (vs), 791 (s), 765 (vs), 755 (vs), 655 (s), 632 (s), 615 (s), 589 (m), 545 (m), 446 (s), 413 (m).

1-Nitratomethyl-3,4-dinitropyrazole (3)

Method A: 1-Hydroxymethyl-3-nitropyrazole (1) (3.00 g, 20.9 mmol, 1.0 eq.) was added at 0 °C to fuming nitric acid (15 mL, 359 mmol, 17 eq.) and stirred under ice cooling for 10 min. The reaction mixture was stirred for another 3.5 h at room temperature and poured onto ice-water (~100 mL). The precipitate was filtered off, washed with a little amount of water and air

dried at room temperature to give 1-nitratomethyl-3,4-dinitropyrazole (**3**) (2.00 g, 8.58 mmol, 41%) as colourless powder.

Method B: 1-Nitratomethyl-3-nitropyrazole (**2**) (0.50 g, 2.66 mmol, 1.0 eq.) was added at 0 °C to fuming nitric acid (4 mL, 95.9 mmol, 36 eq.) and stirred at under ice cooling for 10 min. The reaction mixture was stirred further 4 h at room temperature and poured onto ice-water (~20 mL). The precipitate was filtered off, washed with a little amount of water and air dried at room temperature to give 1-nitratomethyl-3,4-dinitropyrazole (**3**) (0.23 g, 0.98 mmol, 37%) as colourless powder.

DTA (5 °C min⁻¹) $T_{melt} = 93$ °C, $T_{dec} = 159$ °C; **¹H NMR** (400 MHz, DMSO-*d*₆, 25 °C): δ (ppm) = 9.37 (s, 1H), 6.63 (s, 2H); **¹³C{¹H} NMR** (101 MHz, DMSO-*d*₆, 25 °C): δ (ppm) = 148.0, 136.2, 127.0, 78.9; **¹⁴N{¹H} NMR** (29 MHz, DMSO-*d*₆, 25 °C): δ (ppm) = -27, -51; **¹⁵N NMR** (41 MHz, Aceton-*d*₆, 25 °C): δ (ppm) = -28.1, -28.5, -52.2 (t, $^3J_{N,H} = 5.8$ Hz), -80.7 (t, $^3J_{N,H} = 2.7$ Hz), -177.9 (d, $^2J_{N,H} = 3.0$ Hz); **EA** (C₄H₃N₅O₇, 233.10 g/mol) calc. (found): C 20.61 (20.74), H 1.30 (1.51), N 30.05 (29.36) %; **HRMS** (EI+): m/z calculated for C₄H₃N₅O₇ [M]: 233.0032, found: 233.0027; **IR** (ATR, rel. int.): $\tilde{\nu}$ (cm⁻¹) = 3169 (w), 3156 (m), 3067 (w), 1648 (s), 1556 (s), 1522 (s), 1460 (m), 1428 (m), 1384 (m), 1364 (s), 1346 (s), 1312 (s), 1282 (vs), 1236 (m), 1145 (vs), 1121 (m), 1056 (w), 1008 (w), 959 (s), 863 (s), 833 (vs), 807 (vs), 766 (s), 754 (s), 741 (s), 683 (m), 663 (s), 622 (s), 600 (m), 583 (s), 496 (s), 430 (m).

1-Hydroxyethyl-3-nitropyrazole (**4**)^[S24]

3-Nitropyrazole^[S23] (4.00 g, 35.4 mmol, 1.0 eq.) was dissolved in THF (40 mL). Potassium carbonate (9.78 g, 70.8 mmol, 2.0 eq.) and 2-bromoethanol (3.8 mL, 6.70 g, 53.6 mmol, 1.5 eq.) were added and the mixture was refluxed at 70 °C for 24 h. The solvent of the resulting suspension was evaporated under reduced pressure and water (40 mL) and ethyl acetate (40 mL) was added to the solid residue. The aqueous phase was extracted with ethyl acetate (2 × 40 mL) and the combined organic phases were dried over MgSO₄, discolored with activated carbon and evaporated. The crude compound solidified over the course of up to 3 d. For purification the residue was triturated with diethyl ether, filtrated, washed with diethyl ether and air dried at room temperature to give 1-hydroxyethyl-3-nitropyrazole (**4**) (4.00 g, 24.5 mmol, 72%) as colourless solid.

DTA (5 °C min⁻¹) $T_{melt} = 72$ °C; **¹H NMR** (400 MHz, DMSO-*d*₆, 25 °C): δ (ppm) = 7.99 (d, $^3J_{H,H} = 2.5$ Hz, 1H), 7.02 (d, $^3J_{H,H} = 2.5$ Hz, 1H), 4.99 (t, $^3J_{H,H} = 5.3$ Hz, 1H), 4.27 (t, $^3J_{H,H} = 5.2$ Hz, 2H), 3.78 (q, $^3J_{H,H} = 5.3$ Hz, 2H); **¹³C{¹H} NMR** (101 MHz, DMSO-*d*₆, 25 °C): δ (ppm) = 155.0, 134.5, 102.5, 59.5, 55.7; **¹⁴N{¹H} NMR** (29 MHz, DMSO-*d*₆, 25 °C): δ (ppm) = -20; **EA** (C₅H₇N₃O₃, 157.13 g/mol) calc. (found): C 38.22 (38.26), H 4.49 (4.24), N 26.74 (26.44) %; **HRMS** (EI+): m/z calculated for C₅H₈N₃O₃ [M]⁺: 158.0560, found: 158.0560; **IR** (ATR, rel. int.): $\tilde{\nu}$ (cm⁻¹) = 3413 (s), 3162 (m), 3114 (m), 1533 (s), 1499 (s), 1460 (m), 1452 (m), 1433 (m), 1407 (m), 1386 (s), 1371 (s), 1359 (s), 1293 (vs), 1253 (m), 1193 (s), 1160 (m), 1080 (m), 1061 (s), 1039 (s), 1012 (m), 1005 (s), 947 (m), 865 (m), 823 (s), 788 (vs), 754 (vs), 676 (w), 657 (w), 622 (m), 576 (m), 538 (m), 500 (m), 426 (m).

1-Nitratoethyl-3-nitropyrazole (**5**)

To cooled acetic acid anhydride (4.0 mL, 42.3 mmol, 6.7 eq.) fuming nitric acid (2.0 mL, 47.9 mmol, 7.5 eq.) was added dropwise while keeping the temperature at 0 °C. To this mixture 1-hydroxyethyl-3-nitropyrazole (**4**) (1.00 g, 6.36 mmol, 1.0 eq.) was added portion

wise and stirred for 10 min at this temperature. The reaction was stirred further at room temperature until everything was dissolved (approx. 15 min) and poured onto ice-water (~40 mL). The precipitate was filtered off, washed with a little amount of water and air dried at room temperature to give 1-nitratoethyl-3-nitropyrazole (**5**) (1.16 g, 5.74 mmol, 90%) as colourless powder.

DTA (5 °C min⁻¹) $T_{melt} = 78$ °C, $T_{dec} = 198$ °C; **¹H NMR** (400 MHz, DMSO-*d*₆, 25 °C): δ (ppm) = 8.11 (d, $^3J_{H,H} = 2.6$ Hz, 1H), 7.07 (d, $^3J_{H,H} = 2.5$ Hz, 1H), 4.95 (t, $^3J_{H,H} = 5.0$ Hz, 2H), 4.67 (t, $^3J_{H,H} = 4.9$ Hz, 2H); **¹³C{¹H} NMR** (101 MHz, DMSO-*d*₆, 25 °C): δ (ppm) = 155.4, 134.8, 103.0, 71.1, 50.2; **¹⁴N{¹H} NMR** (29 MHz, DMSO-*d*₆, 25 °C): δ (ppm) = -21, -44; **EA** (C₅H₆N₄O₅, 202.13 g/mol) calc. (found): C 29.71 (29.51), H 2.99 (3.04), N 27.72 (27.18) %; **HRMS** (EI+): *m/z* calculated for C₅H₆N₄O₅ [M]: 202.0338, found: 202.0333; **IR** (ATR, rel. int.): $\tilde{\nu}$ (cm⁻¹) = 3179 (w), 3130 (m), 1645 (s), 1628 (s), 1550 (m), 1536 (s), 1507 (m), 1470 (w), 1457 (m), 1429 (m), 1382 (s), 1358 (s), 1301 (s), 1279 (vs), 1258 (s), 1206 (w), 1181 (m), 1089 (w), 1059 (m), 1028 (s), 1000 (m), 961 (w), 892 (s), 878 (s), 856 (s), 823 (s), 788 (s), 755 (vs), 709 (s), 690 (m), 648 (w), 611 (m), 566 (m), 542 (w), 498 (m), 431 (w).

1-Nitratoethyl-3,4-dinitropyrazole (**6**)

Method A: 1-Hydroxyethyl-3-nitropyrazole (**4**) (1.00 g, 6.36 mmol, 1.0 eq.) was added at 0 °C to fuming nitric acid (4 mL, 95.9 mmol, 15 eq.) and stirred under ice cooling for 10 min. The reaction mixture was stirred further 3.5 h at room temperature, poured onto ice water (~40 mL), and stored at 4 °C for 2 h for complete precipitation. The precipitate was filtered off, washed with a little amount of water, and air dried at room temperature to give 1-nitratoethyl-3,4-dinitropyrazole (**6**) (1.47 g, 5.95 mmol, 94%) as colourless powder.

Method B: 1-Nitratoethyl-3-nitropyrazole (**5**) (0.96 g, 4.75 mmol, 1.0 eq.) was added at 0 °C to fuming nitric acid (8 mL, 192 mmol, 40 eq.) and stirred at under ice-cooling for 15 min. The reaction mixture was stirred further 4 h at room temperature and poured onto ice-water (~40 mL). The precipitate was filtered off, washed with a little amount of water and air dried at room temperature to give 1-nitratomethyl-3,4-dinitropyrazole (**3**) (0.86 g, 3.48 mmol, 73%) as colourless powder.

DTA (5 °C min⁻¹) $T_{melt} = 61$ °C, $T_{dec} = 198$ °C; **¹H NMR** (400 MHz, DMSO-*d*₆, 25 °C): δ (ppm) = 9.23 (s, 1H), 4.96 (t, $^3J_{H,H} = 4.6$ Hz, 2H), 4.70 (t, $^3J_{H,H} = 4.6$ Hz, 2H); **¹³C{¹H} NMR** (101 MHz, DMSO-*d*₆, 25 °C): δ (ppm) = 147.2, 134.7, 126.3, 70.4 51.1; **¹⁴N{¹H} NMR** (29 MHz, DMSO-*d*₆, 25 °C): δ (ppm) = -26, -43; **EA** (C₅H₅N₅O₇, 247.12 g/mol) calc. (found): C 24.30 (24.24), H 2.04 (1.92), N 28.34 (28.04) %; **HRMS** (EI+): *m/z* calculated for C₅H₅N₅O₇ [M]: 247.0189, found: 247.0185; **IR** (ATR, rel. int.): $\tilde{\nu}$ (cm⁻¹) = 3157 (w), 1639 (s), 1545 (s), 1515 (s), 1476 (w), 1460 (m), 1434 (m), 1412 (w), 1358 (s), 1337 (s), 1308 (m), 1281 (vs), 1248 (m), 1195 (w), 1150 (m), 1122 (w), 1081 (w), 1030 (m), 1020 (m), 966 (w), 902 (s), 862 (s), 808 (s), 759 (s), 750 (s), 715 (m), 706 (w), 667 (w), 641 (w), 596 (m), 574 (m), 504 (w), 455 (w).

1-Hydroxymethyl-4-nitropyrazole (**7**)

4-Nitropyrazole^[S25] (3.00 g, 26.5 mmol, 1.0 eq.) was dissolved in MeOH (20 mL) and formaldehyde (40% aq., 5 mL, 66.6 mmol, 2.5 eq.) was added. The reaction mixture was stirred at room temperature overnight and poured onto a mixture of water (25 mL) and sat. NaHCO₃ (15 mL). The solution was extracted with CHCl₃ (3 × 30 mL), dried over MgSO₄, and evaporated under reduced pressure. The crude product was recrystallized from CHCl₃

(~70 mL) to obtain 1-hydroxymethyl-4-nitropyrazole (**7**) (2.10 g, 14.7 mmol, 55%) as colourless crystalline solid.

DTA (5 °C min⁻¹) $T_{melt} = 98$ °C; **¹H NMR** (400 MHz, DMSO-*d*₆, 25 °C): δ (ppm) = 8.89 (d, ⁴*J*_{H,H} = 0.7 Hz, 1H), 8.28 (d, ⁴*J*_{H,H} = 0.8 Hz, 1H), 7.21 (t, ³*J*_{H,H} = 7.8 Hz, 1H), 5.43 (d, ³*J*_{H,H} = 7.8 Hz, 2H); **¹³C{¹H} NMR** (101 MHz, DMSO-*d*₆, 25 °C): δ (ppm) = 135.7, 135.3, 129.8, 74.9; **¹⁴N{¹H} NMR** (29 MHz, DMSO-*d*₆, 25 °C): δ (ppm) = -18; **EA** (C₄H₅N₃O₃, 143.10 g/mol) calc. (found): C 33.57 (33.59), H 3.52 (3.58), N 29.36 (28.71) %; **HRMS** (EI+): *m/z* calculated for C₄H₅N₃O₃ [M]: 143.0331, found: 143.0309; **IR** (ATR, rel. int.): $\tilde{\nu}$ (cm⁻¹) = 3261 (m), 3139 (m), 3109 (m), 1557 (w), 1536 (m), 1514 (s), 1481 (m), 1457 (m), 1411 (s), 1400 (m), 1356 (w), 1326 (s), 1311 (m), 1293 (s), 1213 (w), 1183 (w), 1114 (m), 1071 (vs), 1028 (m), 1000 (m), 978 (s), 897 (m), 863 (m), 816 (s), 749 (vs), 689 (m), 650 (m), 596 (s), 552 (m), 482 (m).

1-Hydroxyethyl-4-nitropyrazole (**8**)

4-Nitropyrazole^[S25] (4.00 g, 35.4 mmol, 1.00 eq.) was dissolved in THF (40 mL). Potassium carbonate (9.78 g, 70.8 mmol, 2.0 eq.) and 2-bromoethanol (3.8 mL, 6.70 g, 53.6 mmol, 1.5 eq.) were added and the mixture was refluxed at 70 °C for 24 h. The solvent of the resulting suspension was evaporated under reduced pressure and water (40 mL) and ethyl acetate (40 mL) was added to the solid residue. The aqueous phase was extracted with ethyl acetate (2 × 40 mL) and combined organic phases were dried over MgSO₄, discolored with activated carbon and evaporated. For purification, the residue was triturated with diethyl ether, filtrated, washed with diethyl ether and air dried at room temperature to give 1-hydroxyethyl-4-nitropyrazole (**8**) (2.80 g, 17.8 mmol, 50%) as colourless solid.

DTA (5 °C min⁻¹) $T_{melt} = 92$ °C; **¹H NMR** (400 MHz, DMSO-*d*₆, 25 °C): δ (ppm) = 8.80 (d, ⁴*J*_{H,H} = 0.8 Hz, 1H), 8.25 (d, ⁴*J*_{H,H} = 0.7 Hz, 1H), 4.99 (t, ³*J*_{H,H} = 5.4 Hz, 1H), 4.22 (t, ³*J*_{H,H} = 5.4 Hz, 2H), 3.77 (q, ³*J*_{H,H} = 5.4 Hz, 2H); **¹³C{¹H} NMR** (101 MHz, DMSO-*d*₆, 25 °C): δ (ppm) = 135.5, 134.8, 130.9, 59.2, 55.2; **¹⁴N{¹H} NMR** (29 MHz, DMSO-*d*₆, 25 °C): δ (ppm) = -19; **EA** (C₅H₇N₃O₃, 157.13 g/mol) calc. (found): C 38.22 (38.33), H 4.49 (4.34), N 26.74 (26.35) %; **HRMS** (EI+): *m/z* calculated for C₅H₈N₃O₃ [M]⁺: 158.0560, found: 158.0558; **IR** (ATR, rel. int.): $\tilde{\nu}$ (cm⁻¹) = 3379 (m), 3140 (m), 3123 (m), 1559 (w), 1531 (s), 1504 (vs), 1485 (s), 1438 (m), 1429 (s), 1408 (vs), 1376 (m), 1364 (m), 1312 (vs), 1296 (vs), 1208 (m), 1162 (w), 1152 (m), 1127 (s), 1069 (s), 1045 (s), 1002 (s), 991 (m), 943 (m), 890 (s), 871 (m), 849 (m), 818 (vs), 756 (vs), 662 (w), 610 (s), 594 (vs), 556 (s), 511 (m), 423 (m).

1-Nitratoethyl-4-nitropyrazole (**9**)

To cooled acetic acid anhydride (4.0 mL, 42.3 mmol, 6.7 eq.) fuming nitric (2.0 mL, 47.9 mmol, 7.5 eq.) was added dropwise while keeping the temperature at 0 °C. To this mixture, 1-hydroxyethyl-4-nitropyrazole (**8**) (1.00 g, 6.36 mmol, 1.0 eq.) was added portion wise and stirred 20 min at this temperature. The reaction was stirred further 10 min at room temperature and poured onto ice-water (~40 mL). The precipitate was filtered off, washed with a little amount of water and air dried at room temperature to give 1-nitratoethyl-4-nitropyrazole (**9**) (1.01 g, 5.00 mmol, 77%) as colourless powder.

DTA (5 °C min⁻¹) $T_{melt} = 52$ °C, $T_{dec} = 191$ °C; **¹H NMR** (400 MHz, DMSO-*d*₆, 25 °C): δ (ppm) = 8.98 (d, ⁴*J*_{H,H} = 0.7 Hz, 1H), 8.31 (d, ⁴*J*_{H,H} = 0.7 Hz, 1H), 4.94 (t, ³*J*_{H,H} = 4.9 Hz, 2H), 4.60 (t, ³*J*_{H,H} = 5.0 Hz, 2H); **¹³C{¹H} NMR** (101 MHz, DMSO-*d*₆, 25 °C): δ (ppm) = 136.0, 135.1, 131.2, 70.9, 49.8; **¹⁴N{¹H} NMR** (29 MHz, DMSO-*d*₆, 25 °C): δ (ppm) = -19, -43; **EA** (C₅H₆N₄O₅,

202.13 g/mol) calc. (found): C 29.71 (29.79), H 2.99 (2.71), N 27.72 (27.46) %; **HRMS** (EI+): *m/z* calculated for C₅H₆N₄O₅ [M]: 202.0338, found: 202.0333; **IR** (ATR, rel. int.): $\tilde{\nu}$ (cm⁻¹) = 3134 (w), 3122 (m), 1629 (s), 1554 (w), 1529 (m), 1505 (s), 1481 (m), 1439 (m), 1422 (m), 1407 (s), 1361 (m), 1313 (s), 1297 (s), 1276 (vs), 1200 (w), 1183 (w), 1132 (m), 1079 (m), 1029 (w), 1008 (m), 1001 (s), 978 (w), 946 (w), 879 (s), 838 (s), 818 (s), 753 (s), 712 (w), 693 (m), 659 (w), 640 (m), 597 (m), 550 (m), 497 (m), 420 (m).

1-Chloromethyl-3-nitropyrazole (10)^[S26]

Thionyl chloride (3 mL, 41.3 mmol, 2.1 eq.) dissolved in DCM (10 mL) was added dropwise to a cooled solution of 1-hydroxymethyl-3-nitropyrazole (**1**) (2.85 g, 19.9 mmol, 1.0 eq.) in DCM (20 mL). The reaction mixture was stirred 1 h at 5 °C, then overnight at room temperature and evaporated under reduced pressure. The crude product was purified via column chromatography (*i*Hex/EtOAc 3 : 2, *R_f* = 0.5) to give 1-chloromethyl-3-nitropyrazole (**10**) (2.91 g, 18.0 mmol, 90%) as an colourless to yellowish solid. (*Note: Crude product can be used for the conversion to compound 14 which can be purified via column chromatography in the next step.*)

DTA (5 °C min⁻¹) *T_{melt}* = 25 °C; **¹H NMR** (400 MHz, DMSO-*d*₆, 25 °C): δ (ppm) = 8.29 (d, ³*J_{H,H}* = 2.7 Hz, 1H), 7.10 (d, ³*J_{H,H}* = 2.7 Hz, 1H), 6.26 (s, 2H); **¹³C{¹H} NMR** (101 MHz, DMSO-*d*₆, 25 °C): δ (ppm) = 156.5, 135.6, 104.0, 58.7; **¹⁴N{¹H} NMR** (29 MHz, DMSO-*d*₆, 25 °C): δ (ppm) = -22; **EA** (C₄H₄ClN₃O₂, 161.55 g/mol) calc. (found): C 29.74 (30.59), H 2.50 (2.71), N 26.01 (25.14) %; **HRMS** (EI+): *m/z* calculated for C₄H₄ClN₃O₂ [M]: 160.9992, found: 161.0052; **IR** (ATR, rel. int.): $\tilde{\nu}$ (cm⁻¹) = 3157 (w), 3133 (w), 3055 (vw), 1729 (w), 1549 (s), 1510 (s), 1454 (m), 1387 (s), 1352 (m), 1292 (vs), 1247 (m), 1189 (s), 1158 (w), 1100 (w), 1054 (m), 996 (m), 939 (vw), 822 (s), 781 (m), 752 (s), 729 (vs), 718 (s), 642 (m), 610 (w), 538 (w), 441 (w).

1-Azidomethyl-3-nitropyrazole (11)

To a solution of 1-chloromethyl-3-nitropyrazole (**10**) (1.5 g, 9.29 mmol, 1.0 eq.) in DMF (75 mL), sodium azide (0.72 g, 11.1 mmol, 1.2 eq.) was added and the reaction mixture was heated at 80 °C for at least 18 h. The solvent was evaporated under reduced pressure and the residue was taken up in water (~70 mL). The resulting solution was extracted with EtOAc (3 × 50 mL), dried over MgSO₄ and evaporated under reduced pressure to give 1-azidomethyl-3-nitropyrazole (**11**) (1.34 g, 7.97 mmol, 86%) as a yellowish solid.

DTA (5 °C min⁻¹) *T_{melt}* = 40 °C, *T_{dec}* = 179 °C; **¹H NMR** (400 MHz, DMSO-*d*₆, 25 °C): δ (ppm) = 8.22 (d, ³*J_{H,H}* = 2.6 Hz, 1H), 7.13 (d, ³*J_{H,H}* = 2.7 Hz, 1H), 5.74 (s, 2H); **¹³C{¹H} NMR** (101 MHz, DMSO-*d*₆, 25 °C): δ (ppm) = 156.2, 134.9, 103.4, 65.6; **¹⁴N{¹H} NMR** (29 MHz, DMSO-*d*₆, 25 °C): δ (ppm) = -20, -135, -161; **EA** (C₄H₄N₆O₂, 168.12 g/mol) calc. (found): C 28.58 (28.88), H 2.40 (2.69), N 49.99 (49.69) %; **HRMS** (EI+): *m/z* calculated for C₄H₄N₆O₂ [M]: 168.0396, found: 168.0391; **IR** (ATR, rel. int.): $\tilde{\nu}$ (cm⁻¹) = 3160 (w), 3129 (m), 2150 (m), 2116 (s), 2086 (s), 1545 (m), 1502 (m), 1454 (m), 1386 (s), 1370 (s), 1346 (m), 1288 (vs), 1236 (s), 1202 (s), 1174 (s), 1119 (w), 1086 (w), 1058 (s), 1030 (m), 997 (m), 989 (m), 906 (m), 823 (s), 790 (s), 751 (vs), 665 (m), 645 (m), 615 (w), 565 (m), 540 (w), 445 (m).

1-Chloromethyl-4-nitropyrazole (12)^[S26]

Thionyl chloride (3 mL, 41.3 mmol, 2.1 eq.) dissolved in DCM (10 mL) was added dropwise to a cooled solution of 1-hydroxymethyl-4-nitropyrazole (**7**) (2.85 g, 19.9 mmol, 1.0 eq.) in DCM

(20 mL). The reaction mixture was stirred 1 h at 5 °C, then overnight at room temperature and evaporated under reduced pressure. The crude product was purified via column chromatography (*i*Hex/EtOAc 3 : 2, $R_f = 0.7$) to give 1-chloromethyl-4-nitropyrazole (**12**) (2.80 g, 17.3 mmol, 87%) as an colourless to yellowish solid.

DTA (5 °C min⁻¹) $T_{melt} = 38$ °C; **¹H NMR** (400 MHz, DMSO-*d*₆, 25 °C): δ (ppm) = 9.15 (d, $^4J_{H,H} = 0.7$ Hz, 1H), 8.40 (d, $^4J_{H,H} = 0.7$ Hz, 1H), 6.18 (s, 2H); **¹³C{¹H} NMR** (101 MHz, DMSO-*d*₆, 25 °C): δ (ppm) = 137.3, 136.0, 131.9, 58.5; **¹⁴N{¹H} NMR** (29 MHz, DMSO-*d*₆, 25 °C): δ (ppm) = -20; **EA** (C₄H₄ClN₃O₂, 161.55 g/mol) calc. (found): C 29.74 (29.45), H 2.50 (2.51), N 26.01 (25.77) %; **HRMS** (EI+): m/z calculated for C₄H₄ClN₃O₂ [M]: 160.9992, found: 161.0003; **IR** (ATR, rel. int.): $\tilde{\nu}$ (cm⁻¹) = 3125 (m), 3046 (m), 2987 (w), 1553 (m), 1533 (s), 1514 (s), 1498 (s), 1468 (m), 1448 (m), 1406 (s), 1353 (m), 1326 (s), 1310 (s), 1295 (s), 1159 (m), 1133 (s), 1001 (s), 984 (m), 935 (m), 887 (s), 863 (w), 817 (s), 752 (s), 729 (s), 712 (vs), 650 (s), 594 (s), 548 (s), 444 (m).

1-Azidomethyl-4-nitropyrazole (**13**)

To a solution of 1-chloromethyl-3-nitropyrazole (**10**) (1.00 g, 6.19 mmol, 1.0 eq.) in DMF (50 mL) sodium azide (0.61 g, 9.38 mmol, 1.5 eq.) was added and the reaction mixture was heated at 80 °C for min. 18 h. The solvent was evaporated under reduced pressure and the residue was absorbed in water (~50 mL). The resulting solution was extracted with EtOAc (3 × 30 mL), dried over MgSO₄ and evaporated under reduced pressure to give 1-azidomethyl-3-nitropyrazole (**13**) (0.91 g, 5.41 mmol, 87%) as a yellowish solid.

DTA (5 °C min⁻¹) $T_{melt} = 42$ °C, $T_{dec} = 174$ °C; **¹H NMR** (400 MHz, DMSO-*d*₆, 25 °C): δ (ppm) = 9.06 (d, $^4J_{H,H} = 0.7$ Hz, 1H), 8.42 (d, $^4J_{H,H} = 0.8$ Hz, 1H), 5.65 (s, 2H); **¹³C{¹H} NMR** (101 MHz, DMSO-*d*₆, 25 °C): δ (ppm) = 136.9, 135.6, 131.2, 65.3; **¹⁴N{¹H} NMR** (29 MHz, DMSO-*d*₆, 25 °C): δ (ppm) = -18, -135, -160; **EA** (C₄H₄N₆O₂, 168.12 g/mol) calc. (found): C 28.58 (28.57), H 2.40 (2.48), N 49.99 (50.00) %; **HRMS** (EI+): m/z calculated for C₄H₄N₆O₂ [M]: 168.0396, found: 168.0390; **IR** (ATR, rel. int.): $\tilde{\nu}$ (cm⁻¹) = 3120 (s), 3028 (w), 2164 (m), 2129 (s), 2100 (m), 1557 (w), 1531 (s), 1505 (vs), 1468 (s), 1454 (m), 1424 (m), 1407 (s), 1376 (s), 1321 (s), 1285 (vs), 1245 (vs), 1204 (s), 1187 (m), 1130 (s), 1045 (m), 998 (s), 970 (s), 910 (s), 886 (s), 857 (m), 817 (vs), 753 (s), 740 (s), 668 (m), 645 (m), 590 (s), 554 (s), 468 (m).

1-Chloromethyl-3,4-dinitropyrazole (**14**)^[S23]

1-Chloromethyl-3-nitropyrazole (**10**) (2.00 g, 18.6 mmol, 1.0 eq.) was added at 0 °C to fuming nitric acid (12 mL, 288 mmol, 15 eq.) and stirred under ice cooling for 10 min. The reaction mixture was stirred further 3 h at room temperature, poured onto ice-water (~80 mL) and extracted with EtOAc (3 × 50 mL). The combined organic phases were dried over MgSO₄ and the solvent was evaporated under reduced pressure. The crude product was purified via column chromatography (*i*Hex/EtOAc 3 : 7, $R_f = 0.7$) to give 1-chloromethyl-3,4-dinitropyrazole (**14**) (2.26 g, 10.9 mmol, 59%) as an yellowish oil.

¹H NMR (400 MHz, DMSO-*d*₆, 25 °C): δ (ppm) = 9.38 (s, 1H), 6.25 (s, 2H); **¹³C{¹H} NMR** (101 MHz, DMSO-*d*₆, 25 °C): δ (ppm) = 147.8, 135.3, 127.0, 58.8; **¹⁴N{¹H} NMR** (29 MHz, DMSO-*d*₆, 25 °C): δ (ppm) = -27; **EA** (C₄H₃ClN₄O₄, 206.54 g/mol) calc. (found): C 23.26 (23.61), H 1.46 (1.52), N 27.13 (27.08) %; **HRMS** (EI+): m/z calculated for C₄H₃ClN₄O₄ [M]: 205.9843, found: 205.9836; **IR** (ATR, rel. int.): $\tilde{\nu}$ (cm⁻¹) = 3139 (w), 3060 (vw), 1545 (s), 1516 (vs), 1463

(m), 1418 (w), 1362 (s), 1339 (s), 1296 (s), 1171 (w), 1141 (s), 1119 (m), 1010 (w), 946 (vw), 861 (s), 807 (vs), 743 (s), 731 (s), 624 (w), 594 (w), 479 (m), 416 (vw).

1-Azidomethyl-3,4-dinitropyrazole (**15**)

To a solution of 1-chloromethyl-3,4-dinitropyrazole (**14**) (1.86 g, 9.01 mmol, 1.0 eq.) in DMF (75 mL) sodium azide (0.88 g, 13.5 mmol, 1.5 eq.) was added. The reaction mixture was then heated at 80 °C for at least 18 h. Upon cooling to room temperature, the reaction was poured onto ice water (~75 mL) and extracted with EtOAc (3 × 50 mL). The combined organic phases were subsequently washed with NaHCO₃ (9% aq. 50 mL) and LiCl (10% aq. 50 mL), followed by drying over MgSO₄ and evaporation of the solvent to give a mixture of 1-azidomethyl-3,4-dinitropyrazole (**15**) and 1-azidomethyl-3-azido-4-nitropyrazole (**16**) as yellow oil. Compound **15** can be isolated via column chromatography (*i*Hex:EtOAc 7 : 3, *R_f* = 0.3) as yellowish oil (0.48 g, 2.27 mmol, 25%).

DTA (5 °C min⁻¹) *T_{dec}* = 149 °C; **¹H NMR** (400 MHz, DMSO-*d*₆, 25 °C): δ (ppm) = 9.30 (s, 1H), 5.75 (s, 2H); **¹³C{¹H} NMR** (101 MHz, DMSO-*d*₆, 25 °C): δ (ppm) = 140.3, 134.5, 126.6, 66.3; **¹⁴N{¹H} NMR** (29 MHz, DMSO-*d*₆, 25 °C): δ (ppm) = -27, -137; **EA** (C₄H₃N₇O₄, 213.02 g/mol) calc. (found): C 22.54 (22.55), H 1.42 (1.73), N 46.01 (45.70) %; **IR** (ATR, rel. int.): $\tilde{\nu}$ (cm⁻¹) = 3139 (w), 2119 (s), 1542 (s), 1516 (vs), 1462 (m), 1361 (s), 1341 (s), 1300 (s), 1237 (s), 1198 (m), 1139 (s), 1119 (m), 1035 (w), 1005 (w), 913 (m), 861 (s), 807 (vs), 745 (s), 666 (w), 626 (w), 598 (w), 561 (w), 491 (m).

1-Azidomethyl-3-azido-4-nitropyrazole (**16**)

To a solution of 1-chloromethyl-3,4-dinitropyrazole (**14**) (0.50 g, 2.42 mmol, 1.0 eq.) in DMF (25 mL) sodium azide (0.39 g, 6.05 mmol, 2.5 eq.) was added. The reaction mixture was then heated at 80 °C for at least 18 h. Upon cooling to room temperature, the reaction was poured onto ice water (~25 mL) and extracted with EtOAc (3 × 30 mL). The combined organic phases were subsequently washed with NaHCO₃ (9% aq. 30 mL) and LiCl (10% aq. 40 mL), followed by drying over MgSO₄ and evaporation of the solvent to give 1-azidomethyl-3-azido-4-nitropyrazole (**16**) (0.44 g, 2.09 mmol, 86%) as yellowish solid. If desired, the obtained compound can be further purified via column chromatography (EtOAc, *R_f* = 0.7).

DTA (5 °C min⁻¹) *T_{melt}* = 50 °C, *T_{dec}* = 157 °C; **¹H NMR** (400 MHz, DMSO-*d*₆, 25 °C): δ (ppm) = 9.06 (s, 1H), 5.58 (s, 2H); **¹³C{¹H} NMR** (101 MHz, DMSO-*d*₆, 25 °C): δ (ppm) = 143.4, 133.9, 125.1, 65.5; **¹⁴N{¹H} NMR** (29 MHz, DMSO-*d*₆, 25 °C): δ (ppm) = -20, -135, -143; **¹⁵N NMR** (41 MHz, DMSO-*d*₆, 25 °C): δ (ppm) = -22.2, -100.2 (t, ³*J_{N,H}* = 2.6 Hz), -135.6 (t, ²*J_{N,H}* = 5.0 Hz), -143.7, -145.4, -160.9, -177.1 (d, ²*J_{N,H}* = 2.8 Hz), -296.3, -301.6 (t, ²*J_{N,H}* = 2.5 Hz); **EA** (C₄H₃N₉O₂, 209.13 g/mol) calc. (found): C 22.97 (23.85), H 1.45 (1.78), N 60.28 (59.55) %; **HRMS** (EI+): *m/z* calculated for C₄H₃N₉O₂ [M]: 209.0410, found: 209.0402; **IR** (ATR, rel. int.): $\tilde{\nu}$ (cm⁻¹) = 3145 (m), 3042 (w), 2976 (w), 2165 (m), 2134 (vs), 2096 (s), 1536 (s), 1504 (vs), 1474 (vs), 1460 (s), 1441 (m), 1361 (vs), 1307 (s), 1250 (s), 1219 (vs), 1133 (s), 1107 (s), 1033 (m), 995 (m), 908 (s), 871 (s), 852 (s), 812 (w), 792 (s), 757 (s), 736 (s), 680 (m), 666 (s), 621 (vs), 608 (vs), 559 (s), 533 (s), 504 (m), 463 (m).

1-Azidoethyl-3-nitropyrazole (17)

To a solution of 3-nitropyrazole^[S23] (2.00 g, 17.7 mmol, 1.0 eq) in DMF (20 mL) 1-azido-2-chloroethane (1.87 g, 17.7 mmol, 1.0 eq) and potassium hydrogen carbonate (3.67 g, 26.5 mmol, 1.5 eq) were added and the suspension was heated to 90 °C for 16 h. Water (100 mL) was added after cooling down to room temperature and the solution was extracted with EtOAc (3 × 100 mL). The combined organic layers were washed with LiCl solution (10%, 2 × 50 mL) and brine (100 mL), dried over MgSO₄ and the solvent was removed under reduced pressure. 1-Azidoethyl-3-nitropyrazole (**17**) (2.52 g, 13.8 mmol, 78%) was obtained as a yellow liquid. If desired the crude product can be purified further by flash column chromatography (*i*Hex:EtOAc 8 : 2, R_f = 0.2).

DTA (5 °C min⁻¹) T_{dec} = 214 °C; **¹H NMR** (400 MHz, CDCl₃, 25 °C): δ (ppm) = 7.55 (d, ³J_{H,H} = 2.5 Hz, 1H), 6.92 (d, ³J_{H,H} = 2.5 Hz, 1H), 4.32 (t, ³J_{H,H} = 5.1 Hz, 2H) (t, ³J_{H,H} = 5.1 Hz, 2H); **¹³C{¹H} NMR** (101 MHz, CDCl₃, 25 °C): δ (ppm) = 133.2, 103.2, 52.8, 50.4; **¹⁴N{¹H} NMR** (29 MHz, CDCl₃, 25 °C): δ (ppm) = -21, -135, -169; **EA** (C₅H₆N₆O₂, 182.14 g/mol) calc. (found): C 32.97 (33.19), H 3.32 (3.28), 46.14 (46.17) %; **IR** (ATR, rel. int.): $\tilde{\nu}$ (cm⁻¹) = 3157 (w), 3131 (w), 2098 (s), 1542 (s), 1536 (s), 1504 (s), 1456 (m), 1444 (m), 1420 (w), 1382 (s), 1348 (m), 1296 (vs), 1191 (m), 1177 (m), 1053 (m), 999 (m), 939 (vw), 822 (vs), 779 (s), 751 (s), 687 (w), 629 (w), 617 (w), 553 (w), 488 (w), 420 (w).

1-Azidoethyl-4-nitropyrazole (18)

4-Nitropyrazole^[S25] (2.00 g, 17.7 mmol, 1.0 eq) was dissolved in DMF (20 mL), 1-azido-2-chloroethane (1.87 g, 17.7 mmol, 1.0 eq) and potassium hydrogen carbonate (3.67 g, 26.5 mmol, 1.5 eq) were added and the suspension was heated to 90 °C for 16 h. Water (100 mL) was added after cooling down to room temperature and the solution was extracted with EtOAc (3 × 100 mL). The combined organic layers were washed with LiCl solution (10%, 2 × 50 mL) and brine (100 mL), dried over MgSO₄ and the solvent was removed under reduced pressure. 1-Azidoethyl-4-nitropyrazole (**18**) (2.83 g, 15.5 mmol, 87%) was obtained as yellow liquid. If desired the crude product can be purified further by flash column chromatography (*i*Hex:EtOAc 6 : 4, R_f = 0.34).

DTA (5 °C min⁻¹) T_{dec} = 214 °C; **¹H NMR** (400 MHz, CDCl₃, 25 °C): δ (ppm) = 8.21 (s, 1H), 8.12 (s, 1H), 4.28 (t, ³J_{H,H} = 5.5 Hz 2H), 3.82 (t, ³J_{H,H} = 5.5 Hz 2H); **¹³C{¹H} NMR** (101 MHz, CDCl₃, 25 °C): δ (ppm) = 136.6, 129.7, 52.6, 50.2; **¹⁴N{¹H} NMR** (29 MHz, CDCl₃, 25 °C): δ (ppm) = -14, -139, -171; **EA** (C₅H₆N₆O₂, 182.14 g/mol) calc. (found): C 32.97 (33.37), H 3.32 (3.25), N 46.14 (45.64) %; **IR** (ATR, rel. int.): $\tilde{\nu}$ (cm⁻¹) = 3135 (w), 2935 (vw), 2098 (s), 1529 (s), 1506 (vs), 1475 (m), 1440 (m), 1405 (s), 1371 (w), 1351 (m), 1312 (s), 1296 (vs), 1190 (w), 1170 (w), 1129 (m), 1065 (w), 1002 (m), 971 (w), 945 (w), 874 (m), 817 (vs), 753 (vs), 680 (w), 630 (w), 596 (m), 550 (m), 498 (w), 418 (w).

1-Azidoethyl-3,4-dinitropyrazole (19)

3,4-Dinitropyrazole^[S23] (2.00 g, 12.7 mmol, 1.0 eq) was dissolved in DMF (20 mL) and 2-azidoethyl mesylate (2.09 g, 12.7 mmol, 1.0 eq) and potassium hydrogencarbonate (2.62 g, 26.5 mmol, 1.5 eq) were added. The suspension was heated to 90 °C for 16 h. Water (100 mL) was added after cooling down to room temperature and the solution was extracted with EtOAc (3 × 100 mL). The combined organic layers were washed with LiCl solution (10%, 2 × 50 mL) and brine (100 mL), dried over MgSO₄ and the solvent was removed under reduced

pressure. 1-Azidoethyl-3,4-dinitropyrazole (**19**) (2.52 g, 13.8 mmol, 78%) was obtained as yellow liquid. If desired the crude product can be purified further by flash column chromatography (*i*Hex:EtOAc 6 : 4, $R_f = 0.28$).

DTA ($5\text{ }^\circ\text{C min}^{-1}$) $T_{melt} = 50\text{ }^\circ\text{C}$, $T_{dec} = 216\text{ }^\circ\text{C}$; **$^1\text{H NMR}$** (400 MHz, CDCl_3 , $25\text{ }^\circ\text{C}$): δ (ppm) = 8.25 (s, 1H), 4.31 (t, $^3J_{\text{H,H}} = 5.3\text{ Hz}$, 2H), 3.89 (t, $^3J_{\text{H,H}} = 5.5\text{ Hz}$, 2H); **$^{13}\text{C}\{^1\text{H}\}$ NMR** (101 MHz, CDCl_3 , $25\text{ }^\circ\text{C}$): δ (ppm) = 154.4, 132.1, 130.1, 53.7, 49.6; **$^{14}\text{N}\{^1\text{H}\}$ NMR** (29 MHz, CDCl_3 , $25\text{ }^\circ\text{C}$): δ (ppm) = -28, -136; **EA** ($\text{C}_5\text{H}_5\text{N}_7\text{O}_4$, 227.14 g/mol) calc. (found): C 26.44 (26.83), H 2.22 (2.25), N 43.17 (42.78) %; **IR** (ATR, rel. int.): $\tilde{\nu}$ (cm^{-1}) = 3136 (m), 2145 (m), 2102 (s), 1552 (s), 1535 (s), 1512 (vs), 1456 (s), 1443 (m), 1432 (m), 1411 (m), 1362 (s), 1336 (s), 1297 (vs), 1228 (m), 1147 (s), 1118 (m), 1064 (w), 1016 (w), 1003 (m), 935 (w), 859 (s), 805 (s), 756 (m), 746 (s), 702 (w), 668 (w), 642 (m), 626 (m), 593 (m), 557 (m), 503 (m), 443 (m).

1-Azidoethyl-3-azido-4-nitropyrazole (**20**)

To a solution of 1-nitroethyl-3,4-dinitropyrazole (**6**) (1.50 g, 6.07 mmol, 1.0 eq.) in DMF (75 mL) sodium azide (0.99 g, 15.2 mmol, 2.5 eq.) was added. The reaction mixture was then heated at $80\text{ }^\circ\text{C}$ for at least 18 h. Upon cooling to room temperature, the reaction was poured into ice water ($\sim 75\text{ mL}$) and extracted with EtOAc ($3 \times 80\text{ mL}$). The combined organic phases were subsequently washed with NaHCO_3 (9% aq. 50 mL) and LiCl (10% aq. 70 mL), followed by drying over MgSO_4 and evaporation of the solvent to give 1-azidoethyl-3-azido-4-nitropyrazole (**20**) (0.93 g, 4.154 mmol, 68%) as yellow solid. If desired, the obtained compound can be further purified via column chromatography (EtOAc, $R_f = 0.8$).

DTA ($5\text{ }^\circ\text{C min}^{-1}$) $T_{melt} = 41\text{ }^\circ\text{C}$, $T_{dec} = 159\text{ }^\circ\text{C}$; **$^1\text{H NMR}$** (400 MHz, $\text{DMSO-}d_6$, $25\text{ }^\circ\text{C}$): δ (ppm) = 8.98 (s, 1H), 4.31 (t, $^3J_{\text{H,H}} = 5.5\text{ Hz}$, 2H), 3.81 (t, $^3J_{\text{H,H}} = 5.5\text{ Hz}$, 2H); **$^{13}\text{C}\{^1\text{H}\}$ NMR** (101 MHz, $\text{DMSO-}d_6$, $25\text{ }^\circ\text{C}$): δ (ppm) = 142.6, 133.8, 124.4, 51.9, 49.2; **$^{14}\text{N}\{^1\text{H}\}$ NMR** (29 MHz, $\text{DMSO-}d_6$, $25\text{ }^\circ\text{C}$): δ (ppm) = -18, -133, -142; **EA** ($\text{C}_5\text{H}_5\text{N}_9\text{O}_2$, 223.16 g/mol) calc. (found): C 26.91 (27.19), H 2.26 (2.67), N 56.49 (56.24) %; **IR** (ATR, rel. int.): $\tilde{\nu}$ (cm^{-1}) = 3116 (m), 3015 (vw), 2941 (w), 2874 (w), 2341 (w), 2232 (w), 2136 (vs), 2094 (vs), 1732 (w), 1532 (s), 1505 (vs), 1480 (s), 1471 (s), 1449 (m), 1435 (s), 1396 (m), 1381 (s), 1356 (s), 1343 (s), 1303 (vs), 1224 (vs), 1186 (s), 1148 (s), 1069 (m), 991 (m), 937 (w), 869 (s), 838 (m), 785 (m), 755 (s), 678 (m), 639 (s), 612 (s), 550 (w), 532 (m), 505 (m), 498 (s), 415 (m).

11. References

- [S1] CrysAlisPro, Oxford Diffraction Ltd. version 171.33.41, **2009**.
- [S2] G. M. Sheldrick, *Acta Cryst.*, **2015**, A71, 3–8.
- [S3] Dolomanov, O. V., Bourhis, L. J., Gildea, R. J., Howard, J. A. K. & Puschmann, H. J., *Appl. Cryst.*, **2009**, 42, 339–341.
- [S4] SCALE3 ABSPACK – An Oxford Diffraction program (1.0.4, gui: 1.0.3), Oxford Diffraction Ltd., **2005**.
- [S5] APEX3. Bruker AXS Inc., Madison, Wisconsin, USA.
- [S6] M. J. Frisch, G. W. Trucks, H. B. Schlegel, G. E. Scuseria, M. A. Robb, J. R. Cheeseman, G. Scalmani, V. Barone, G. A. Petersson, H. Nakatsuji, X. Li, M. Caricato, A. V. Marenich, J. Bloino, B. G. Janesko, R. Gomperts, B. Mennucci, H. P. Hratchian, J. V. Ortiz, A. F. Izmaylov, J. L. Sonnenberg, D. Williams-Young, F. Ding, F. Lipparini, F. Egidi, J. Goings, B. Peng, A. Petrone, T. Henderson, D. Ranasinghe, V. G. Zakrzewski, J. Gao, N. Rega, G. Zheng, W. Liang, M. Hada, M. Ehara, K. Toyota, R. Fukuda, J. Hasegawa, M. Ishida, T. Nakajima, Y. Honda, O. Kitao, H. Nakai, T. Vreven, K. Throssell, J. A. Montgomery, Jr., J. E. Peralta, F. Ogliaro, M. J. Bearpark, J. J. Heyd, E. N. Brothers, K. N. Kudin, V. N. Staroverov, T. A. Keith, R. Kobayashi, J. Normand, K. Raghavachari, A. P. Rendell, J. C. Burant, S. S. Iyengar, J. Tomasi, M. Cossi, J. M. Millam, M. Klene, C. Adamo, R. Cammi, J. W. Ochterski, R. L. Martin, K. Morokuma, O. Farkas, J. B. Foresman, and D. J. Fox, Gaussian16, Gaussian, Inc., Wallingford, CT, USA, **2016**.
- [S7] a) J. W. Ochterski, G. A. Petersson, J. A. Montgomery, *J. Chem. Phys.* **1996**, 104, 2598–2619; b) J. A. Montgomery, M. J. Frisch, J. W. Ochterski, G. A. Petersson, *J. Chem. Phys.* **2000**, 12, 6532–6542.
- [S8] a) L. A. Curtiss, K. Raghavachari, P. C. Redfern, J. A. Pople, *J. Chem. Phys.* **1997**, 106, 1063–1079; b) B. M. Rice, S. V. Pai, J. Hare, *Combust. Flame* **1999**, 118, 445–458; c) E. F. C. Byrd, B. M. Rice, *J. Phys. Chem. A* **2006**, 110, 1005–1013.
- [S9] P. J. Linstrom, W. G. Mallard (Editors), *National Institute of Standards and Technology Standard Reference Database Number 69*, Gaithersburg MD, 20899, <http://webbook.nist.gov/chemistry/> (July **2022**).
- [S10] S. Wahler, P. Chung, T. M. Klapoetke, **2023**, Training machine learning models based on the structural formula for the enthalpy of vaporization and sublimation and a thorough analysis of Trouton’s rules *J. Energ. Mater* doi.org/10.1080/07370652.2023.2219678.
- [S11] NATO standardization agreement (STANGAG), *Chemical compatibility of ammunition components with explosives (non-nuclear application)*, No. 4147 2. ed., **2001**.
- [S12] R. Meyer, J. Koehler, A. Homburg, *Explosives*, 6th edn., Wiley, Weinheim, **2007**, p. 196–198.
- [S13] R. Meyer, J. Koehler, A. Homburg, *Explosives*, 6th edn., Wiley, Weinheim, **2007**, p. 145.
- [S14] L. Bauer, M. Benz, T. M. Klapoetke, *Propellants Explos. Pyrotech.* **2022**, 47, e202100332.
- [S15] <http://www.bam.de> (July **2022**).
- [S16] NATO Standardization Agreement (STANAG) on Explosives, *Impact Sensitivity Tests*, no. 4489, 1st ed., September 17, **1999**.
- [S17] WIWEB-Standardarbeitsanweisung 4-5.1.02, Ermittlung der Explosionsgefährlichkeit, hier der Schlagempfindlichkeit mit dem Fallhammer, November 8, **2002**.
- [S18] NATO Standardization Agreement (STANAG) on Explosives, *Friction Sensitivity Tests*, no. 4487, 1st ed., August 22, **2002**.
- [S19] WIWEB-Standardarbeitsanweisung 4-5.1.03, Ermittlung der Explosionsgefährlichkeit oder der Reibeempfindlichkeit mit dem Reibeapparat, November 8, **2002**.
- [S20] OZM, <http://www.ozm.cz>. (July **2022**).

[S21] Impact: Insensitive >40 J, less sensitive ≤35 J, sensitive ≤4 J, very sensitive ≤3 J; friction: Insensitive >360 N, less sensitive=360 N, sensitive 80 N, very sensitive ≤80 N, extreme sensitive ≤10 N; According to the UN Recommendations on the Transport of Dangerous Goods (+) indicates: not safe for transport.

[S22] W. Meng, P. T. W. Cheng, Patent WO 2011/130459 A1, **2011**.

[S23] M. F. Boelter, A. Harter, T. M. Klapoetke, J. Stierstorfer *ChemPlusChem* **2018**, *83*, 804–811.

[S24] M. Treu, S. K. Zahn, Patent WO 2016/180843 A1, **2016**.

[S25] R. S. Gross, Z. Guo, B. Dyck, T. Coon, C. Q. Huang, R. F. Lowe, D. Marinkovic, A. Moorjani, J. Nelson, S. Zamani-Kord, D. E. Grigoriadis, S. R. J. Hoare, P. D. Crowe, J. H. Bu, M. Haddach, J. McCarthy, J. Saunders, R. Sullivan, T. Cheng, J. P. Williams, *J. Med. Chem.* **2005**, *48*, 5780–5793.

[S26] P. J. Machin, Patent EP0034831A2, **1981**.

Polyazido-methyl Derivatives of Prominent Oxadiazole and Isoxazole Scaffolds: Synthesis, Explosive Properties, and Evaluation

Lukas Bauer, Maximilian Benz, Thomas M. Klapötke,* Tobias Lenz, and Jörg Stierstorfer

Cite This: *J. Org. Chem.* 2021, 86, 6371–6380

Read Online

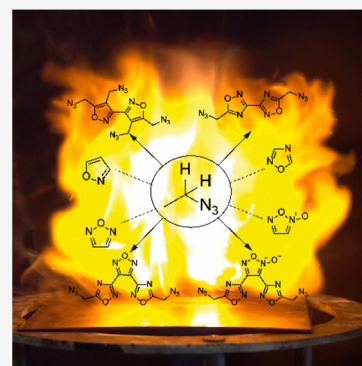
ACCESS |

Metrics & More

Article Recommendations

Supporting Information

ABSTRACT: Recently, different nitrate-methyl-substituted oxadiazoles have been described as potential melt-cast explosives. In this work, corresponding N–O heterocyclic-based compounds with azido-methyl functionalities were synthesized. In each case, the explosophoric azide group is inserted by chlorine–azide exchange during the last synthetic step. All synthesized compounds show interesting characteristics for various applications in the field of energetic materials as energetic plasticizers or as melt-cast explosives. The compounds were extensively analyzed by IR, EA DTA, and multinuclear NMR spectroscopy. Furthermore, the solid compounds 4,4',5,5'-tetrakis(azidomethyl)-3,3'-bisisoxazole (2) and 3,3'-bis(azidomethyl)-5,5'-bis(1,2,4-oxadiazole) (4) were characterized using X-ray diffraction. In addition, the sensitivities toward friction and impact were determined with BAM standard techniques, and the energetic performances of all synthesized azido-methyl compounds were calculated using the EXPLOS code. The properties were compared to recently published, structurally related compounds.



INTRODUCTION

Azide-containing compounds have been indispensable in many areas of chemistry¹ since the discovery of the azide anion by Curtius in 1890.² Despite the toxicity of the azide anion,³ it remains an essential molecular building block and has a great synthetic approach in organic chemistry.⁴ Moreover, as an anion or functionality, azides offer unrivaled and unique properties. Traditionally, azides are widely used in addition⁵ or substitution^{6,7} reactions, as well as in cycloaddition reactions for the production of nitrogen-rich heterocycles, such as 1,2,3-triazoles^{8–10} and tetrazoles.^{11,12} The azide source for these reactions is mostly NaN_3 or trimethylsilylazide (TMSN_3), which are cheap well-manageable chemicals. In addition, there are numerous reactions that benefit from the conversion of azides to isocyanates,¹³ nitrenes,¹⁴ or amines.¹⁵ Therefore, azides are included in numerous substances or at least used as intermediates or reagents toward the synthesis. Nevertheless, many chemists are frightened by the compounds themselves or the use thereof in general since organic azides can have explosive properties.¹

There are various empirical rules, for example, the “Smith rule” or the “rule of six”, which states that “six carbons (or other atoms of approximately equal size) per energetic functional group (azide, diazo, nitro, etc.) should provide sufficient dilution to make the compound relatively safe under appropriate controls and safety procedures”.⁴ However, such rules are guidelines, and one must consider the potential hazards associated with newly prepared azides de novo. Properly characterized and handled organic azides in the form of azido-alkyl functions see widespread use and provide a useful platform for their utilization as energetic materials.^{16–18}

For energetic materials, the high heat of formation inserted by azides (about 360 kJ/mol)¹⁹ and the high nitrogen content, that is inherent in the compound, are exploited in particular. In the research for new green explosives, the azide functionality is advantageous since the resulting polyazides often have low solubility in water, and mainly dinitrogen is formed during combustion.²⁰ Figure 1 shows some azido-methyl-containing compounds that are widely used in almost all fields of high-energy materials such as energetic polymers (A),²¹ energetic plasticizers (B),²² initial explosives (C),²³ or hypergolic liquids (D).²⁴

Yet, there are few examples of heterocyclic-based molecules that contain azido-alkyl units.²² However, recently intensively

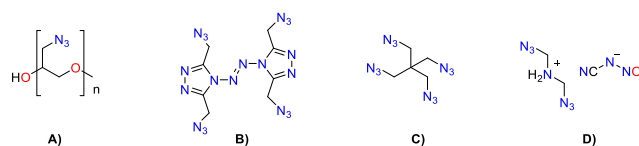


Figure 1. Representative examples for energetic organic compounds containing an alkylazido function: GAP (A), 3,3',5,5'-tetrakis(azidomethyl)-4,4'-azo-1,2,4-triazole (B), tetraazido pentaerythritol (C), and bis(2-azidoethyl)dimethylammonium nitrocyanoamide (D).

Received: January 28, 2021

Published: April 16, 2021



investigated heterocyclic compounds that utilize nitrate-methyl groups, among others as an energy-delivering source, were denoted as promising energetic substances in the field of melt-cast explosives.^{25–29} The chemical structures of the mentioned compounds are depicted in Figure 2. These possible TNT

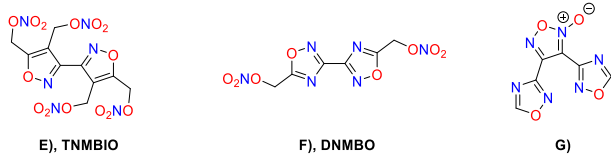


Figure 2. Molecular structures of recently published melt-cast explosives based on isoxazole and oxadiazole scaffolds including tetrakisnitratomethylbisoxazole (TNMBIO) (E), dinitratomethylbisoxadiazole (DNMBO) (F), and bisoxadiazolylfuroxan (G).

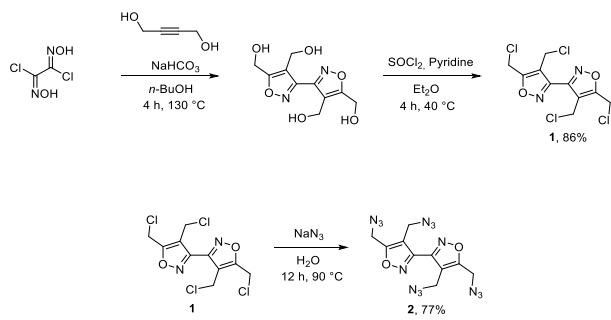
replacements are based on isoxazoles and oxadiazoles, which are characterized above all by high thermal stability and easy chemical availability and synthesis. Even so, they contribute to energy performance through their NO content.^{30–32}

In this study, we present the combination of an azide functionality with established scaffolds to create a new class of low-melting azido-methyl-based explosives.³³ By the structural similarity toward compounds (E)–(G), it was assumed that some properties might be identical or even better.

RESULTS AND DISCUSSION

Starting with known literature precursors reported by Wingard et al.,²⁵ the respective chloromethyl compound **1** was synthesized through classical chlorination reaction with thionyl chloride in pyridine at reflux conditions (Scheme 1). A

Scheme 1. Synthesis of **2** via Chloromethyl Derivative **1**

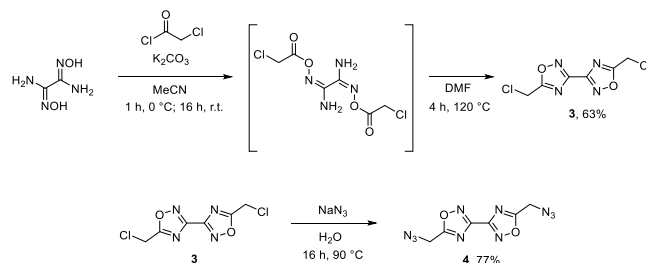


subsequent chlorine–azide exchange yielded **2** in 77% yield. In order to achieve complete conversion of the product, the reaction was stirred at 90 °C for 12 h in water and was then purified by flash column chromatography. Due to the low melting point of 28 °C, it was obtained as oil and solidified by adding a seed crystal at low temperatures.

Compound **4** was previously discovered through a different synthetic pathway by Zhan et al.³⁴ but was investigated intensively for the first time in this study. Starting from diaminoglyoxime, a chloroacetyl unit was added under basic conditions to the oxime functionality by the reaction with the corresponding acid chloride (Scheme 2).

For the subsequent condensation reaction for the formation of the 1,2,4-oxadiazole units, the solvent were required therefore to be switched from MeCN to DMF since reaction temperatures above 100 °C are required. After chlorine–azide

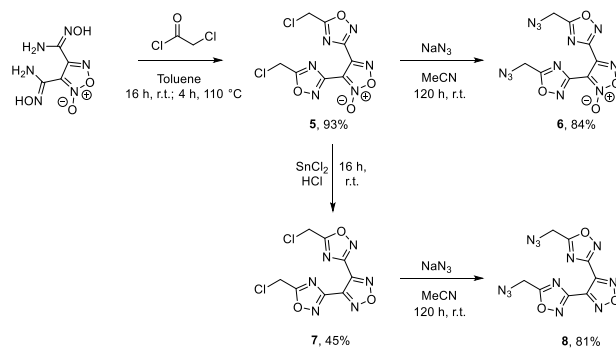
Scheme 2. Synthesis of **4** via Chloromethyl Derivative **3**



exchange in water, the crude product was recrystallized from hot water to yield pure **4** in 77% yield.

The heterocyclic motif of **6** and **8** is a known scaffold for energetic materials. By combining two oxadiazoles through a furoxane or furazane moiety, a high energy content is stored in a molecule that is nevertheless relatively thermally stable and dense.^{30,35} BNFF and its reduced form BNFFa, which are considered as new-generation melt-cast explosives, have therefore been investigated in detail by many research groups.^{36–38} Compounds are synthesized mainly starting from malononitrile.³⁹ Here, the 1,2,4-oxadiazole ring closure was performed similarly for **5** by a reaction of chloroacetyl chloride with bisaminohydroximoylfuroxane in toluene.⁴⁰ To obtain both the furoxan and furazan-containing derivatives as linkers, a reduction of the furoxan ring was performed in hydrochloric acid and tin(II) chloride as a reducing agent to yield compound **7**. The chlorine–azide exchanges for **6** and **8** were performed in acetonitrile with a reaction time of 120 h for both compounds. Trying to shorten the reaction time by heating led to the decomposition of the compounds. After flash column chromatography, **6** and **8** were obtained as yellowish oils. The synthetic pathway is depicted in Scheme 3.

Scheme 3. Synthesis of **6** and **8**



All azido-methyl compounds were characterized with multinuclear NMR, mass spectrometry, and vibrational spectroscopy (IR). Additionally, the thermal behavior was determined by differential thermal analysis (DTA) measurements, and the purity grade was checked by CHN elemental analysis.

The IR spectra of the azido-methyl compounds show strong characteristic azide stretching frequencies in the range between 2200 and 2050 cm⁻¹. For **2**, a broadened band is visible, which indicates an overlap of the two different azide moieties.

Due to the poor solubility or decomposition reactions, different solvents were used for the NMR measurements of the azido-methyl compounds, so no clear continuous trend in the

shift of the NMR resonances compared to the chloromethyl precursors can be established.

In the ^1H and $^{13}\text{C}\{^1\text{H}\}$ spectra of all chloromethyl precursors, proton signals of the methylene groups are found between 5.27 and 4.82 ppm as sharp singlets, and carbon signals appear in a range of 33.7–32.1 ppm. For the azido-methyl moieties, the CH_2 resonances are found between 5.03 and 4.70 ppm in the proton spectra and between 45.2 and 41.8 ppm for the carbon spectra. The remaining heterocyclic carbon signals appear in a range typical for the respective heterocycles.^{25–27}

Proton-coupled ^{15}N measurements were carried out for all azido-methyl compounds and are shown in Figure 3. 2 shows

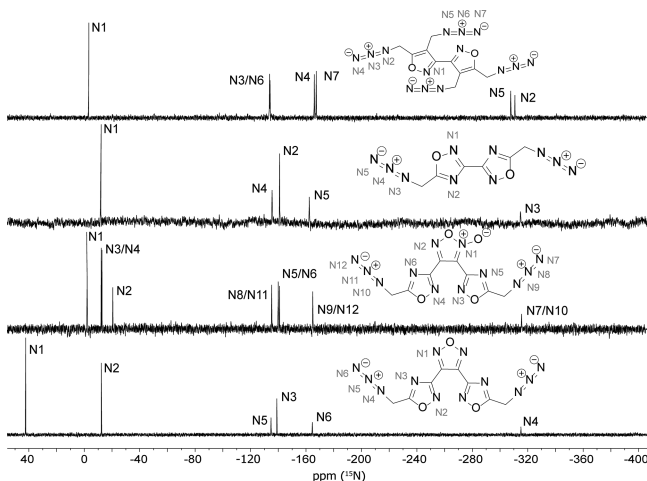


Figure 3. Proton-coupled ^{15}N NMR spectra and assignment of the signals of 2 measured in $\text{DMSO}-d_6$, 4 measured in CDCl_3 , and 6 and 8 measured in $\text{acetone}-d_6$, respectively.

seven sharp signals. The one at -3.2 ppm is assigned to the isoxazole moiety. For the azide resonances, the three typical signals occur in pairs due to their similar surroundings at -310.8 and -307.7 ppm for N_α , -167.5 and -166.0 ppm for N_γ , and -134.1 and -133.7 ppm for N_β and are therefore in the same range as other azido-methyl compounds.⁴¹ The assignment of N_α and N_γ of the different azido groups was possible by information gained from 2D NMR spectroscopy measurements. These spectra can be found in the Supporting Information.

The spectra, especially those with azido-methyl-1,2,4-oxadiazole units (4, 6, and 8), show great similarities. The azide signals are located in close ranges from -314.7 to -315.5 ppm for N_α , -162.3 to -164.9 ppm for N_γ , and -134.7 to -135.5 ppm for N_β . Due to the ^3J coupling with the methylene protons, the latter are split into triplets with coupling constants between 4.3 and 4.5 Hz.

Compound 6 is expected to show six azide signals due to the lack of symmetry in the molecule, which, however, are overlapping because of the small difference in their chemical environment. In the oxadiazole units, in contrast to the azide resonances, two different signals for CNC (-139.9 and -140.9 ppm) and ONC (-12.2 and -12.8 ppm) are still detectable. The remaining heterocyclic signals for 1,2,4-oxadiazole, furoxan, as well as furazan nitrogen atoms show typical shifts.^{30,42}

Single crystals suitable for X-ray diffraction experiments for all chloromethyl precursors 1, 3, 5, and 7 (for more

information check the Supporting Information) and for azido-methyl derivatives 2 and 4 were obtained by slow evaporation or recrystallization from different common solvents.

Compound 2, recrystallized from hot methanol, crystallizes in the monoclinic space group $P2_1/n$ with a cell volume of $753.41(5) \text{ \AA}^3$ and two formula units per cell. The cell constants are $a = 6.9324(3) \text{ \AA}$, $b = 8.6045(3) \text{ \AA}$, and $c = 12.6400(5) \text{ \AA}$, while the density is 1.571 g cm^{-3} at 298 K. The structure is shown in Figure 4. As expected from structurally similar

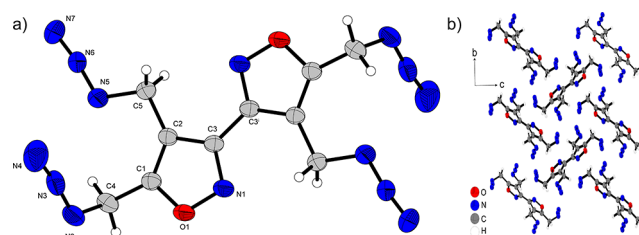


Figure 4. (a) Molecular unit of compound 2, showing the atom labeling scheme. Symmetry code: (i) $-x, 1 - y, 1 - z$. (b) Packing of 2. Thermal ellipsoids represent the 50% probability level, and hydrogen atoms are shown as small spheres of arbitrary radius. Selected bond lengths [Å] and angles [$^\circ$]: $\text{N1}-\text{O1}$ 1.3921(17), $\text{N1}-\text{C3}$ 1.3135(18), $\text{O1}-\text{C1}$ 1.3594(17), $\text{C1}-\text{C2}$ 1.3571(19), $\text{C1}-\text{C4}$ 1.489(2), $\text{N3}-\text{N2}-\text{C4}$ 115.34(13), $\text{N2}-\text{C4}-\text{C1}$ 113.28(13), $\text{N5}-\text{N6}-\text{N7}$ 172.93(16), $\text{N2}-\text{N3}-\text{N4}$ 172.00(19), and $\text{O1}-\text{C1}-\text{C2}-\text{C5}$ 179.67(14).

literature-known compounds, the molecule shows planar assembly of the isoxazole rings. Similarly the angle of $\text{O1}-\text{C1}-\text{C2}-\text{C5}$ $179.67(14)^\circ$ illustrates that the methylene groups are planar with respect to the ring system. Apart from hydrogen atoms, only the azide groups are twisted out of the plane by $115.34(13)^\circ$ for $\text{N3}-\text{N2}-\text{C4}$ and $113.28(13)^\circ$ for $\text{N2}-\text{C4}-\text{C1}$. The bond angles of the azides $\text{N5}-\text{N6}-\text{N7}$ ($172.93(16)^\circ$) and $\text{N2}-\text{N3}-\text{N4}$ ($172.00(19)^\circ$) are also in the range of literature-known azide groups due to negative hyperconjugation. The bond distances in the isoxazole rings are in ranges between single and double bonds with $\text{N}-\text{O}$ (1.3921(17) Å), $\text{N}-\text{C}$ (1.3135(18) Å), $\text{O}-\text{C}$ (1.3594(17) Å), and $\text{C}-\text{C}$ (1.3571(19) Å) for heterocyclic aromatic compounds.²⁵

Compound 4, recrystallized from acetone, crystallizes in the triclinic space group $P-1$ with one formula unit per cell and a density of 1.649 g cm^{-3} at 299 K. The cell constants are $a = 3.9473(3) \text{ \AA}$, $b = 6.7158(4) \text{ \AA}$, and $c = 10.1067(6) \text{ \AA}$, while the volume is 249.92 \AA^3 . The structure is depicted in Figure 5. The heterocyclic rings show clear signs of aromaticity, as the respective bond lengths correspond to the range between single and double bonds ($\text{N2}-\text{C2}$ 1.3713(18) Å , $\text{O1}-\text{C1}$ 1.3385(16) Å , $\text{O1}-\text{N1}$ 1.403(2) Å). The two aromatic 1,2,4-oxadiazole rings form a plane from which the azide moieties twist out with a torsion angle of $81.5(2)^\circ$ ($\text{N4}-\text{N3}-\text{C3}-\text{C1}$). Due to negative hyperconjugation, the azide function shows an angle of $173.5(2)^\circ$ ($\text{N3}-\text{N4}-\text{N5}$). 4 forms a layer-like structure in which the azides and the ring systems are superimposed, respectively. The structure results from the medium-strong hydrogen bridges $\text{C3}-\text{H3A}\cdots\text{N1}$ (2.699(18) Å), $\text{C3}-\text{H3A}\cdots\text{N2}$ (2.779(18) Å), and $\text{C3}-\text{H3B}\cdots\text{N3}$ (2.580(19) Å).

The results of the computed detonation properties of azides 2, 4, 6, and 8, together with the calculated energies of

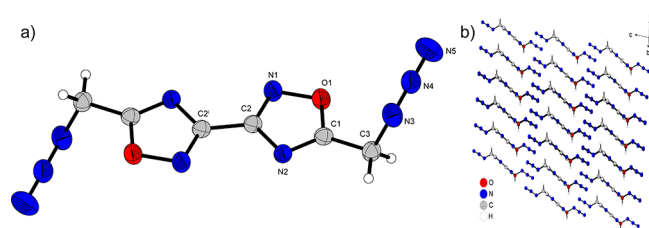


Figure 5. (a) Molecular unit of compound **4**, showing the atom-labeling scheme. Symmetry code: (i) $1 - x 1 - y, -z$. (b) Packing of **4**. Thermal ellipsoids represent the 50% probability level, and hydrogen atoms are shown as small spheres of arbitrary radius. Selected bond distances [Å] and angles [°]: N3–N4 1.237(2), N4–N5 1.138(3), C1–N2 1.292(2), N3–N4–N5 173.5(2), C1–C3–N3 110.70(16), C1–N2–C2 101.84(12), N2–C1–C3–N3 110.88(19), and O1–C1–C3–N3 66.8(2).

formation (details in the Supporting Information) and the corresponding sensitivities, can be found in Table 1. All synthesized compounds are characterized by very high positive enthalpies of formation ($1377.8 \text{ kJ mol}^{-1}$ for **2**, $781.5 \text{ kJ mol}^{-1}$ for **4**, $1079.9 \text{ kJ mol}^{-1}$ for **6**, and $1072.9 \text{ kJ mol}^{-1}$ for **8**), which is a typical feature of organic azides. The limit of “the rule of six” mentioned in the introduction is not even remotely reached by any of the synthesized compounds, yet most of them are classified as nonhazardous.

The tetra-functionalized bisisoxazole derivatives show approximately equal values for impact and friction sensitivity, which are comparable to those PETN ($IS = 3.5 \text{ J}$, $FS = 60 \text{ N}$). For the friction sensitivity of the tetraazido-methyl derivative **2**, a higher sensitivity was expected. However, due to the low melting point, it can be assumed that liquefaction occurs during the performance of the friction test, and thus the sensitivity decreases. The decomposition point of both compounds is slightly above $190 \text{ }^\circ\text{C}$, whereas the melting

point is lowered by almost $100 \text{ }^\circ\text{C}$ by the four azide groups compared to the four nitrate groups (Figure 4). **2** shows a calculated detonation velocity that outperforms TNT ($V_{\text{det}} = 7147 \text{ m s}^{-1}$) but is clearly below the one of TNMBIO ($V_{\text{det}} = 7847 \text{ m s}^{-1}$).²⁵ The huge difference compared to the nitro-methyl derivative mainly results from the distinction of the density of about 0.2 g cm^{-3} .

In contrast to DNMBO, which has moderate sensitivities toward impact and friction ($IS = 8 \text{ J}$, $FS = 282 \text{ N}$), diazidomethyl-bisoxadiazole (**4**) is absolutely insensitive ($IS = >40 \text{ J}$, $FS = >360 \text{ N}$). Only the sensitivity to electrostatic discharge of **4** is higher ($ESD = 60 \text{ mJ}$) compared to the nitro-methyl derivative ($ESD = 125 \text{ mJ}$). Thermal analysis was carried out using DTA experiments. The related plots for azidomethyl compounds **2**, **4**, **6**, and **8** are shown in Figure 6. The thermochemical properties of the two bisoxadiazole compounds are very similar. Thus, **4** has a melting point in a range similar to the corresponding nitrate ester but with a decomposition point of $209 \text{ }^\circ\text{C}$, a significantly higher stability than DNMBO ($T_{\text{dec}} = 183 \text{ }^\circ\text{C}$).²⁶

By substitution of the nitrate group through azide, the same effect is observed as with the compound pair **2**/TNMBIO but to a much weaker extent. The same trend can be seen for the density and the strongly associated detonation parameters. Compound **4** has a density of 1.649 g cm^{-3} coupled with a detonation velocity of 7221 m s^{-1} , which exhibits the same trend compared to the corresponding nitro-methyl derivative (DNMBO), decreasing the density by about 0.2 g cm^{-3} and the detonation velocity by about 900 m s^{-1} . Nevertheless, **4**, like DNMBO, outperforms TNT and shows suitable properties for use as a melt-cast explosive.

Since **6** and **8** are liquids at room temperature, both compounds were only tested toward their impact sensitivity. The impact sensitivity of **6** is 20 J , whereas **8** only shows slight signs of decomposition at a value of 40 J . The decomposition

Table 1. Physicochemical Properties and EXPLO5 Calculation Results of **2**, **4**, **6**, and **8** in Comparison with Nitro-methyl Compounds TNMBIO and DNMBO as Well as TNT

	2	TNMBIO ²⁵	4	DNMBO ²⁶	6	8	TNT
formula	$\text{C}_{10}\text{H}_8\text{N}_{14}\text{O}_2$	$\text{C}_{10}\text{H}_8\text{N}_6\text{O}_{14}$	$\text{C}_6\text{H}_4\text{N}_{10}\text{O}_2$	$\text{C}_6\text{H}_4\text{N}_6\text{O}_8$	$\text{C}_8\text{H}_4\text{N}_{12}\text{O}_4$	$\text{C}_8\text{H}_4\text{N}_{12}\text{O}_3$	$\text{C}_7\text{H}_5\text{N}_3\text{O}_6$
M [g mol ⁻¹]	356.27	436.20	248.17	288.01	332.20	316.20	227.13
IS [J] ^a	2	3	>40	8	20	40	15
FS [N] ^b	64	60	>360	282	-	-	>360
ESD [J] ^c	0.040	0.063	0.060	0.125	-	-	>0.25
ρ (298 K) [g cm ⁻³]	1.571 ^d	1.786	1.649 ^d	1.831	1.80 ^p	1.75 ^p	1.65
N [%] ^e	55.0	19.3	56.4	29.2	50.6	53.2	18.5
Ω [%] ^f	-98.8	0	-77.4	0	-67.4	-75.9	-24.7
T_{melt} [°C] ^g	28	122	70	85	n.d.	n.d.	80
T_{dec} [°C] ^g	192	194	209	183	210	193	295
$\Delta_f H^\circ$ [kJ mol ⁻¹] ^h	1377.8	-395.0	781.5	-79.4	1079.9	1072.9	-59.3
Explos V6.05.02							
$-\Delta_{\text{Ex}} U^0$ [kJ kg ⁻¹] ⁱ	4655	5086	4256	4884	5127	4759	4426
T_{det} [K] ^k	3305	3604	3202	3565	3714	3506	3222
V_0 [L kg ⁻¹] ^l	688	661	702	675	676	672	633
P_{CJ} [kbar] ^m	198	268	192	281	261	227	194
V_{det} [m s ⁻¹] ⁿ	7147	7847	7221	8119	8071	7672	6823
I_s [s] ^o	222	236	219	236	224	226	-

^aImpact sensitivity (BAM drophammer (1 of 6)). ^bFriction sensitivity (BAM friction tester (1 of 6)). ^cElectrostatic discharge device (OZM research). ^dFrom X-ray diffraction analysis recalculated to 298 K. ^eNitrogen content. ^fOxygen balance with respect to CO_2 or carbon dioxide. ^gDecomposition temperature. Melting point (DTA; $\beta = 5 \text{ }^\circ\text{C min}^{-1}$). ^hCalculated enthalpy of formation. ⁱEnergy of explosion. ^kDetonation temperature. ^lVolume of detonation products (assuming only gaseous products). ^mDetonation pressure at the Chapman–Jouguet point. ⁿDetonation velocity. ^oSpecific impulse under isobaric (60 bar) conditions. ^pRecalculated from chloromethyl precursors.

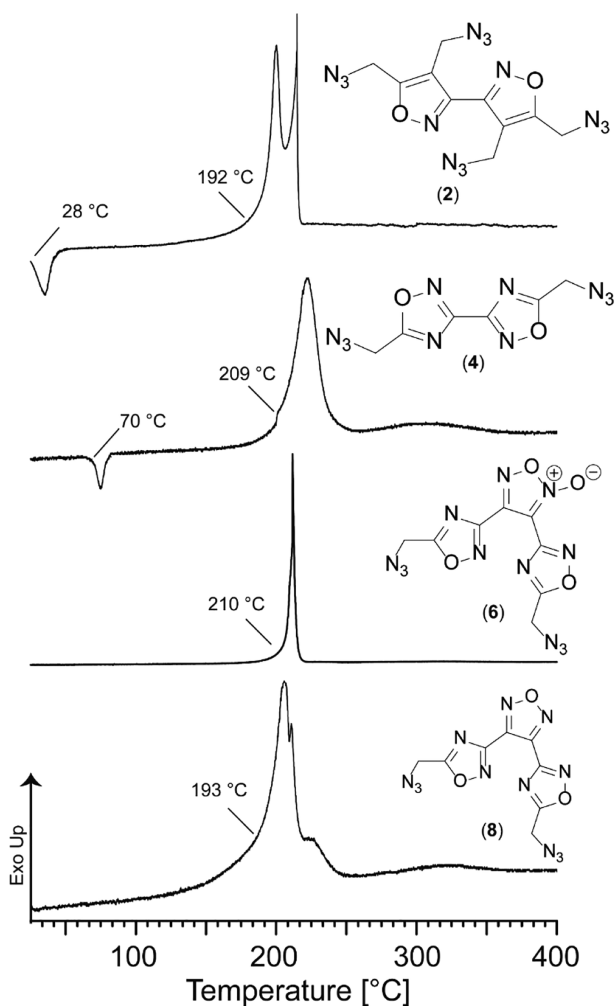


Figure 6. DTA plots of compounds **2**, **4**, **6**, and **8** measured with a heating rate of $5\text{ }^{\circ}\text{C min}^{-1}$. Melting (endo) and decomposition (exo) points are given as onset temperatures.

temperature for both compounds is in the range of $200\text{ }^{\circ}\text{C}$, whereby **6** is marginally more stable and decomposes distinctly more sharply. Despite the flat slope of the curve of **8**, no significant mass loss is observed, which was confirmed by TGA measurements (TGA graphs of **6** and **8** are shown in the [Supporting Information](#)). The densities of **6** and **8** were predicted from the crystal structures of the chloromethyl precursors **5** and **7**, respectively. A comparison of the densities obtained by comparing the densities of various chloromethyl to azido-methyl compounds was considered. The detonation velocities calculated from these densities are in the range of 8071 m s^{-1} for **6** and 7672 m s^{-1} for **8**. As expected, the values of furoxan derivative **6** are generally higher than those of the corresponding furazan derivative **8**, which is related to the higher density caused by the *N*-oxide, which additionally delivers more energy to the system. Both substances would be suitable as energetic plasticizers due to their physicochemical properties.

With the crystal structures of **2** and **4** as well as the respective nitrate-methyl compounds TNMBIO and DNMBIO in hand, a more in-depth analysis of the different sensitivities, which includes the influence of the functional groups, could be carried out. Hence, Hirshfeld surfaces, based on the respective crystal structures of the compounds, were created. ([Figure 7](#)).

The thereof generated 2D fingerprint plots indicate the distance and type of interaction toward the surrounding atoms in the crystal neighborhood with respect to $d_i + d_e$ (d_i : distance from the Hirshfeld surface to the nearest atom interior; d_e : distance from the Hirshfeld surface to the nearest atom exterior).⁴³ Depending on the type, amount, and strength of the respective interactions, relative conclusions about the different sensitivities of similar compounds can be drawn.⁴⁴

In most cases, a large number of equitatomic interactions indicate an increased sensitivity. Since the homoatomic interactions can be assumed to be caused by the same polarization of the atoms, the size of the atoms also plays a decisive role. Therefore, $\text{O}\cdots\text{O}$ interactions have a higher destabilizing effect in the crystal lattice than $\text{N}\cdots\text{N}$ or $\text{H}\cdots\text{H}$ interactions.^{45,46} The same applies to the $\text{O}\cdots\text{N}$, $\text{C}\cdots\text{O}$, and $\text{C}\cdots\text{N}$ interactions, whereby these often do not have such a strong influence on the reduced stability toward external mechanical stimuli. The induced destabilization is a result of close contacts within the crystal layering. By shifting the crystal layers against each other, local hotspots are formed by interlayer repulsion. The vulnerable regions for close interactions are marked as red dots in the Hirshfeld plots. Therefore, it can be concluded that connections with an increased number of red dots or a high frequency of close contacts for repulsive interactions show an increased sensitivity.^{47,48}

Intermolecular hydrogen bridges, which result in $\text{O}\cdots\text{H}$ and $\text{N}\cdots\text{H}$ interactions, form the majority of the stabilizing interactions and are predominantly found in insensitive compounds. In the case of affecting external stimuli, they hinder the slippage of the crystal layers and thus act preventively against the formation of hotspots. Nevertheless, $\text{O}\cdots\text{H}$ and $\text{N}\cdots\text{H}$ contacts create a 3D network and therefore strongly alter the interlayering slide and can sensitize the compounds. However, replacing hard $\text{O}\cdots\text{O}$ and $\text{N}\cdots\text{N}$ contacts by hydrogen bridges often leads to better cushioning of external mechanical stimuli.⁴⁹

However, not only the quantity but also the type of interactions within the crystal layers play an important role for estimating the sensitivities. Even more important for evaluation is the relative strength of the individual interactions, which can be estimated from the position in the 2D plot.⁴⁵

As expected, the main source of positive interactions of the nitrate compounds is $\text{O}\cdots\text{H}$, whereas the majority of negative ones is due to $\text{O}\cdots\text{O}$ contacts. For azides **2** and **4**, $\text{N}\cdots\text{H}$ and $\text{N}\cdots\text{N}$ contacts form the predominant interactions. For the bisisoxazole derivatives TNMBIO and **2**, the measured sensitivities are in the same range. TNMBIO has the highest number of positive interactions of all compounds analyzed, splitting into 44.5% $\text{O}\cdots\text{H}$ and 3.5% $\text{N}\cdots\text{H}$. The $\text{O}\cdots\text{H}$ interactions are presented as some strong interactions ($d_i + d_e = 2.6\text{ \AA}$); however, the majority occurs at larger distances. The $\text{N}\cdots\text{H}$ interactions are completely negligible due to the high distance. TNMBIO has a relatively large number of destabilizing contacts with 29.3% $\text{O}\cdots\text{O}$ and 10.4% $\text{O}\cdots\text{N}$, which occur in the region around $d_i + d_e = 3.2\text{ \AA}$. The intermolecular interactions of **2** are mainly dominated by $\text{N}\cdots\text{N}$ (23.9%), $\text{O}\cdots\text{N}$ (11.9%), and $\text{N}\cdots\text{H}$ (39.0%). Despite the low hydrogen content of the compound, large amounts of destabilizing $\text{H}\cdots\text{H}$ (8.9%) interactions are observed. TNMBIO shows more, albeit weaker, interactions for both attractive and repulsive interactions compared to **2**, so they can be considered as similarly sensitive.

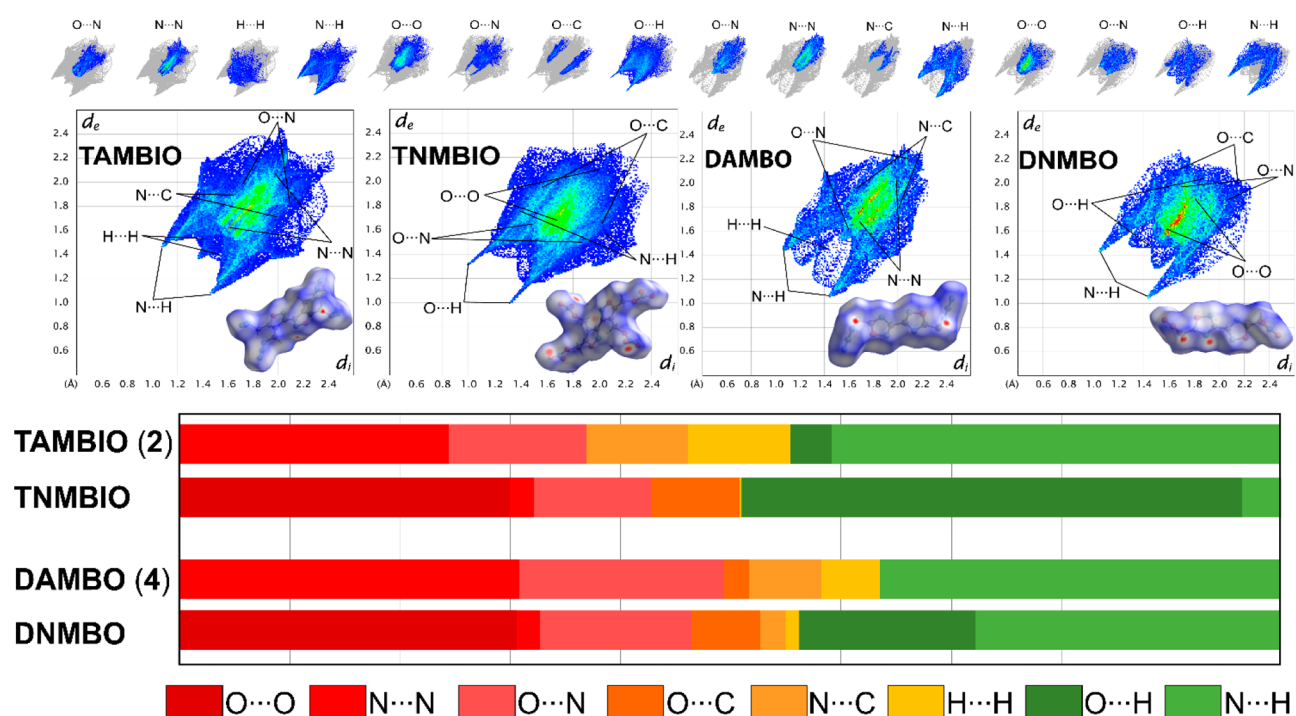


Figure 7. Two-dimensional fingerprint plot in crystal stacking as well as the corresponding Hishfeld surface of TAMBIO (2), TNMBIO, DAMBO (4), and DNMBO. Population of close contacts below.

The repulsive interactions (O...O: 30.5%, O...N: 13.7%, N...N: 2.1%) presented in DNMBO are more abundant than the corresponding attractive ones (O...H: 16.0%, N...H: 27.6%). In general, the high content of O...O in association with low O...H, which forms the strongest interactions due to the highest difference in electronegativity, should be noted. Almost half of all interactions occurring in 4 are due to the negative repulsions of N...N (30.0%) and O...N (18.1%). However, they occur in a range of weak intensity, which makes them rather insignificant. In contrast, 35.3% of N...H interactions occur in a distance range in which medium-strong hydrogen bridges are formed. Therefore, O...O in DNMBO has the predominant importance, destabilizing the compound, which must be weighted more heavily than the N...N and O...N interactions occurring mainly in 4. Unlike in 4, there are no strong stabilizing interactions to counteract this trend. For this reason, the sensitivity of DNMBO should be higher than that of 4, which could also be confirmed by the experimental measurement.

SUMMARY

In summary, four new heterocyclic-based polyazido-methyl compounds were synthesized and characterized intensively. 4 shows promising properties for a melt-cast explosive and therefore as a possible replacement for TNT with $T_{\text{melt}} = 70$ °C and $T_{\text{dec}} = 209$ °C, being thermally more stable than its nitratomethyl derivative DNMBO. Furthermore, it outperforms TNT in terms of detonation velocity. Comparing 4 with its nitratomethyl derivative DNMBO, the sensitivities toward impact and friction are significantly lower, but DNMBO has a detonation velocity of 8119 m s^{-1} , nearly 900 m s^{-1} higher than that of DAMBO (4). Moreover, 2, 6, and 8 show promising values for use as energetic plasticizers. 6 and 8 are presented as liquids, whereas 2 is available as a solid at room temperature, melting at 28 °C. The most promising of these three compounds is 6, which

was obtained as a moderately impact-sensitive liquid, stable up to 210 °C. Further investigations and mixtures therewith should be carried out to study its compatibility with other energetic materials in formulations.

EXPERIMENTAL PART

General Procedures. ^1H , $^{13}\text{C}\{^1\text{H}\}$, and ^{15}N NMR spectra were recorded on BRUKER AMX 400 instruments. Chemical shifts are referenced with respect to tetramethylsilane ($^1\text{H}/^{13}\text{C}\{^1\text{H}\}$) and nitromethane ($^{14}\text{N}/^{15}\text{N}$). Infrared spectra (IR) were recorded in the region $4000\text{--}400 \text{ cm}^{-1}$ on a PERKIN ELMER Spectrum BX-59343 instrument with a SMITHS DETECTION DuraSAMPLIR II Diamond ATR sensor. Mass spectra and high-resolution mass spectra (HR-MS) were recorded using electroionization (EI). HR-MS was recorded on a Finnigan MAT 95Q with an Ion-Trap MS/MS system or a ThermoFisher Q EXACTIVE GC Orbitrap GC-MS/MS. Decomposition temperatures were measured via differential thermal analysis (DTA) with an OZM Research DTA 552-Ex instrument and partly by thermal gravimetric analysis (TGA) with a PerkinElmer TGA4000 at a heating rate of 5 °C/min and in a range of room temperature to 400 °C. All sensitivities toward impact (IS) and friction (FS) were determined according to BAM (Bundesanstalt für Materialforschung und Prüfung) standards using a BAM drop hammer and a BAM friction apparatus by applying the 1 of 6 method.⁵⁰ All energetic compounds were tested for sensitivity toward electrical discharge using an Electric Spark Tester ESD 2010 EN from OZM. Energetic properties have been calculated with the EXPLO5 6.02 computer⁵¹ code using the RT converted and estimated X-ray density and calculated solid-state heats of formation.

CAUTION! All investigated compounds are potentially explosive materials. Safety precautions and equipment (such as wearing a leather coat, face shield, Kevlar sleeves, Kevlar gloves, earthed equipment, and ear plugs) must be used during all manipulations of energetic materials.

4,4',5,5'-Tetrakis(chloromethyl)-3,3'-bisoxazole (1). Tetrakis-hydroxymethyl-bisoxazole (2.00 g, 7.80 mmol, 1.0 equiv) was suspended in Et_2O (40 mL), and SOCl_2 (2.10 mL, 34.0 mmol, 4.4 equiv) and pyridine (2.70 mL, 34.0 mmol, 4.4 equiv) were added

dropwise. The solution was heated to 40 °C with an oil bath for 4 h, adding more SOCl₂ (3.5 g, 2.1 mL, 34 mmol, 4.4 equiv) and pyridine (2.7 g, 2.7 mL, 34 mmol, 4.4 equiv) after 2 h. The brown reaction mixture was filtered and washed with water multiple times. Tetrakis-chloromethyl-bisoxazole (1) was obtained as a brown solid (2.21 g, 6.70 mmol, 86%).

IR (ATR) $\tilde{\nu}$ (cm⁻¹) = 2168(w), 2086(vs), 1620(w), 1438(w), 1418(w), 1337(m), 1265(s), 1221(s), 1179(m), 1139(m), 1067(w), 967(w), 912(m), 879(m), 774(m), 719(m), 654(m), 552(m), 464(m), 438(m), 427(m), 415(m). Elem. Anal. Calcd for C₁₀H₈N₂O₂Cl₄: C, 36.40; N, 8.49; H, 2.44. Found: C, 36.60; N, 8.48; H, 2.51. ¹H NMR (DMSO-*d*₆, 400 MHz, ppm): δ = 5.21 (s, 4H), 4.99 (s, 4H). ¹³C{¹H} NMR (DMSO-*d*₆, 100 MHz, ppm): δ = 167.9, 152.9, 114.9, 33.8, 32.6. HR-MS (EI) *m/z*: [M] Calcd for C₁₀H₈N₂O₂Cl₄ 327.9340. Found: 327.9334.

4,4',5,5'-Tetrakis(azidomethyl)-3,3'-bisoxazole (TAMBIO) (2). Tetrakis-chloromethyl-bisoxazole (1) (1.00 g, 3.00 mmol, 1.0 equiv) and sodium azide (1.00 g, 15.0 mmol, 5.0 equiv) were solved in water (50 mL) and heated to 90 °C with an oil bath and stirred for 12 h at this temperature. The solution was extracted with EtOAc (3 × 50 mL). The organic phase was dried over anhydrous sodium sulfate, and the product was dried in the air. The crude product was purified by flash column chromatography (CHCl₃/NEt₃ 99.9%/0.1%). Tetrakis-azidomethyl-bisoxazole (2) was obtained as a slightly brown liquid that crystallized at 4 °C (0.81 g, 2.30 mmol, 77% yield).

DTA (5 °C min⁻¹): 28 °C (melt), 192 °C (dec). Sensitivities: BAM drop hammer: 2 J (<500 μ m). Friction tester: 64 N (<500 μ m). ESD: 40 mJ (<500 μ m). IR (ATR) $\tilde{\nu}$ (cm⁻¹) = 3016(w), 1623(m), 1448(m), 1411(m), 1393(w), 1270(m), 1252(m), 1138(m), 1105(m), 933(s), 898(m), 883(m), 745(s), 706(vs), 683(vs), 638(m), 615(m), 414(w). Elem. Anal. Calcd for C₁₀H₈N₁₄O₂: C, 33.71; N, 55.04; H, 2.26. Found: C, 33.66; N, 54.63; H, 2.55. ¹H NMR (DMSO-*d*₆, 400 MHz, ppm): δ = 4.95 (s, 4H), 4.70 (s, 4H). ¹³C{¹H} NMR (DMSO-*d*₆, 100 MHz, ppm): δ = 167.4, 153.0, 111.9, 42.8, 41.6. ¹⁵N NMR (DMSO-*d*₆, 41 MHz, ppm) δ = -3.2, -133.7, -134.1, -166.0, -167.5, -307.7, -310.8. HR-MS (EI) *m/z*: [M] Calcd for C₁₀H₈N₁₄O₂ 356.0955. Found: 356.0943.

3,3'-Bis(chloromethyl)-5,5'-bis(1,2,4-oxadiazole) (3). Diaminoglyoxime (2.40 g, 20.3 mmol, 1.0 equiv) was dissolved in acetonitrile (100 mL), and potassium carbonate (5.60 g, 40.6 mmol, 2.0 equiv) was added in one portion. The mixture was cooled to 0 °C with an ice bath, and chloroacetyl chloride (6.50 mL, 81.6 mmol, 4.0 equiv) in acetonitrile (20 mL) was added dropwise over 20 min. The mixture was stirred for 1 h at 0 °C and further overnight at room temperature. The solution was quenched on ice water (100 mL), and the white solid was filtered and washed with small amounts of ice water. Afterward, it was solved in DMF (40 mL) and heated with an oil bath for 4 h to 120 °C. After cooling to room temperature, the mixture was quenched on ice water (100 mL) to yield the white powdered crude product. After recrystallization from hot water (60 mL), 3 was yielded as colorless crystalline needles (3.00 g, 12.7 mmol, 63% yield).

IR (ATR) $\tilde{\nu}$ (cm⁻¹) = 3042(w), 2984(w), 1741(w), 1579(s), 1439(m), 1429(m), 1421(m), 1312(m), 1263(m), 1220(vs), 1144(m), 1022(m), 956(m), 933(w), 920(s), 896(m), 778(w), 749(vs), 681(vs), 653(w), 636(m). Elem. Anal. Calcd for C₆H₄N₄O₂Cl₂: C, 30.66; N, 23.84; H, 1.72. Found: C, 30.42; N, 23.34; H, 2.02. ¹H NMR (DMSO-*d*₆, 400 MHz, ppm) δ = 5.25 (s, 4H). ¹³C{¹H} NMR (DMSO-*d*₆, 100 MHz, ppm) δ = 177.3, 159.7, 33.7. HRMS (EI) *m/z*: [M] Calcd for C₆H₄N₄O₂Cl₂ 233.9711. Found: 233.9707.

3,3'-Bis(azidomethyl)-5,5'-bis(1,2,4-oxadiazole) (DAMBO) (4). 3,3'-Bis(chloromethyl)-5,5'-bis(1,2,4-oxadiazole) (3) (500 mg, 2.13 mmol, 1.0 equiv) was dissolved in water (75 mL), and sodium azide (0.43 g, 6.62 mmol, 3.1 equiv) was added. The mixture was heated to 90 °C with an oil bath and stirred overnight. After cooling to room temperature, the solution was extracted with DCM (3 × 50 mL). The organic phase was dried over anhydrous sodium sulfate and evaporated under reduced pressure to yield the crude product, which was recrystallized from hot water (40 mL). 3,3'-Bis-

(azidomethyl)-5,5'-bi(1,2,4-oxadiazole) (4) was obtained as colorless microcrystals (410 mg, 1.65 mmol, 77% yield).

DTA (5 °C min⁻¹): 70 °C (melt), 209 °C (dec). Sensitivities: BAM drop hammer: >40 J (<500 μ m). Friction tester: >360 N (<500 μ m). ESD: 60 mJ (<500 μ m). IR (ATR) $\tilde{\nu}$ (cm⁻¹) = 3026(w), 2951(w), 2473(vw), 2213(w), 2143(s), 2104(s), 2007(w), 1998(w), 1983(w), 1567(s), 1441(m), 1430(m), 1330(w), 1304(s), 1281(m), 1247(s), 1214(vs), 1196(s), 1196(s), 1054(w), 1038(w), 1024(w), 971(s), 956(m), 915(s), 894(s), 783(s), 688(s), 664(s), 637(s), 555(s), 488(w), 446(w), 430(w), 423(w), 409(m). Elem. Anal. Calcd for C₆H₄N₁₀O₂: C, 29.04; N, 56.44; H, 1.62. Found: C, 29.17; N, 55.19; H, 1.86. ¹H NMR (CDCl₃, 400 MHz, ppm): δ = 4.73 (s, 4H). ¹³C{¹H} NMR (CDCl₃, 100 MHz, ppm): δ = 176.3, 160.0, 45.2. ¹⁵N NMR (CDCl₃, 41 MHz, ppm): δ = -11.8, -135.5, -140.9, -162.3, -314.7. *m/z* (EI+, M = 248.05 g mol⁻¹): 248 (100), 138 (45), 123 (57), 111 (16), 108 (41), 96 (28), 94 (20), 91 (14), 84 (96), 44 (42), 43 (61), 42 (64), 41 (16). HRMS (EI) *m/z*: [M] Calcd for C₆H₄N₁₀O₂ 248.0519. Found: 248.0516.

3,4-Bis(5-(chloromethyl)-1,2,4-oxadiazol-3-yl)-furoxan (5). Bisaminohydroxymoylfuroxan (2.00 g, 9.90 mmol, 1.0 equiv) was dissolved in toluene (50 mL), and chloroacetyl chloride (3.2 mL, 40.2 mmol, 4.1 equiv) in toluene (20 mL) was added dropwise over 20 min. The mixture was stirred at ambient temperature overnight and was subsequently heated to 110 °C with an oil bath and stirred for 4 h at this temperature. After cooling to room temperature, the solvent was evaporated under reduced pressure, and the residue was stirred for 30 min in a mixture of saturated sodium hydrogen carbonate solution (50 mL) and DCM (50 mL). The phases were separated, and the aqueous phase was extracted DCM (2 × 50 mL). The organic phase was dried using sodium sulfate, and the solvent was evaporated under reduced pressure to yield a slightly gray oil, which started to crystallize after several hours on air, which could be identified as 3,4-bis(5-(chloromethyl)-1,2,4-oxadiazol-3-yl)-furoxan (5) (2.94 g, 9.22 mmol, 93%).

IR (ATR) $\tilde{\nu}$ (cm⁻¹) = 3468(w), 3349(w), 3205(w), 3033(w), 2959(w), 2791(w), 1682(w), 1658(m), 1622(vs), 1579(s), 1551(s), 1489(m), 1424(m), 1409(m), 1389(m), 1306(m), 1268(s), 1211(m), 1163(w), 1145(m), 1073(m), 1044(m), 1044(m), 1015(m), 988(m), 972(m), 948(s), 926(s), 902(m), 851(w), 815(s), 788(s), 754(s), 739(s), 690(m), 640(s), 616(m), 571(m), 523(m), 517(m), 496(m), 453(s), 420(s), 412(s), 404(m). Elem. Anal. Calcd for C₈H₄N₆O₄Cl₂: C, 30.12; N, 26.34; H, 1.26. Found: C, 29.89; N, 26.01; H, 1.57. ¹H NMR (DMSO-*d*₆, 400 MHz, ppm): δ = 5.27 (s, 2H), 5.23 (s, 2H). ¹³C{¹H} NMR (DMSO-*d*₆, 100 MHz, ppm): δ = 177.0, 176.7, 158.7, 156.7, 145.1, 106.0, 33.5, 33.4. *m/z* (EI+, M = 317.97 g mol⁻¹): 290 (22), 288 (24), 193 (14), 183 (12), 183 (11), 108 (35), 77 (17), 61 (14), 58 (26), 58 (22), 51 (14), 51 (10), 49 (48), 43 (100), 43 (79), 42 (20). HRMS (EI) *m/z*: [M] Calcd for C₈H₄N₆O₄Cl₂ 317.9671. Found: 317.9667.

3,4-Bis(5-(azidomethyl)-1,2,4-oxadiazol-3-yl)-furoxan (DAMBFF) (6). 3,4-Bis(5-(chloromethyl)-1,2,4-oxadiazol-3-yl)-furoxan (5) (500 mg, 1.57 mmol, 1.0 equiv) was solved in acetonitrile (30 mL), and sodium azide (0.26 g, 4.00 mmol, 2.5 equiv) was added. The mixture was stirred at room temperature for 120 h. Then, the solid was filtered and washed with (2 × 20 mL) of acetonitrile. The filtrate was dried over anhydrous sodium sulfate and reduced at ambient temperature. 3,4-Bis(5-(azidomethyl)-1,2,4-oxadiazol-3-yl)-furoxan (6) was yielded as a slightly yellowish oil (440 mg, 1.32 mmol, 84%) after purification by column chromatography using chloroform/ethyl acetate (24:1) and 0.1% NEt₃ as eluent.

DTA (5 °C min⁻¹): 210 °C (dec). Sensitivities: BAM drop hammer: 20 J (liquid). IR (ATR) $\tilde{\nu}$ (cm⁻¹) = 2101(vs), 1624(s), 1577(s), 1557(m), 1430(m), 1391(m), 1330(m), 1271(s), 1208(m), 1073(m), 1045(m), 1011(m), 971(m), 947(m), 910(m), 814(s), 747(m), 665(m), 555(m), 516(m), 469(m), 462(m), 462(m), 433(m), 426(m), 418(m), 402(m). Elem. Anal. Calcd for C₈H₄N₁₂O₈: C, 28.92; N, 50.60; H, 1.21. Found: C, 28.38; N, 50.26; H, 1.29. ¹H NMR (acetone-*d*₆, 400 MHz, ppm): δ = 5.02 (s, 2H), 4.97 (s, 2H). ¹³C{¹H} NMR (acetone-*d*₆, 100 MHz, ppm): δ = 177.1, 176.9, 159.0, 156.9, 145.1, 105.8, 44.8, 44.7. ¹⁵N NMR

(acetone- d_6 , 41 MHz, ppm): $\delta = -2.1, -12.2, -12.8, -20.6, -135.2, -140.0, -140.9, -164.9, -315.5$. m/z (EI+, $M = 332.02$ g mol $^{-1}$): 332 (10), 325 (12), 303 (13), 302 (88), 297 (28), 295 (77), 290 (13), 288 (18), 230 (13), 230 (100), 225 (29), 223 (91), 200 (25), 193 (23), 108 (46), 92 (15), 90 (10), 78 (14), 77 (10), 77 (13), 54 (12), 51 (10), 49 (28), 42 (17). HRMS (EI) m/z : [M] Calcd for $C_8H_4N_{12}O_4$: 332.0478. Found: 332.0464.

3,4-Bis(5-(chloromethyl)-1,2,4-oxadiazol-3-yl)-furoxan (7). 3,4-Bis(5-(chloromethyl)-1,2,4-oxadiazol-3-yl)-furoxan (5) (1.00 g, 3.13 mmol, 1.0 equiv) was solved in hydrochloric acid (37%, 20 mL), and tin(II) chloride dihydrate (2.70 g, 12.0 mmol, 3.8 equiv) was added. The mixture was stirred overnight at room temperature, poured on ice water (50 mL), and extracted with DCM (5 \times 30 mL). The combined organic phases were dried over anhydrous sodium sulfate and evaporated under reduced pressure to yield 3,4-bis(5-(chloromethyl)-1,2,4-oxadiazol-3-yl)-furoxan (7) as a white solid (0.43 g, 1.42 mmol, 45%).

IR (ATR) $\tilde{\nu}$ (cm $^{-1}$) = 3461(m), 3316(m), 3034(m), 2973(m), 1621(s), 1591(s), 1580(s), 1572(s), 1486(m), 1431(m), 1416(m), 1387(s), 1269(m), 1217(m), 1153(m), 1146(m), 1103(vs), 1074(m), 1021(s), 976(s), 953(s), 936(m), 936(m), 924(m), 912(s), 893(m), 873(s), 776(m), 748(s), 726(s), 717(m), 682(m), 652(s), 643(m), 583(m), 569(s), 452(s), 430(s), 407(s). Elem. Anal. Calcd for $C_8H_4N_6O_3Cl_2$: C, 31.71; N, 33.82; H, 1.33. Found: C, 31.43; N, 33.35; H, 1.51. 1H NMR (CDCl $_3$, 400 MHz, ppm): $\delta = 4.82$ (s, 4H). $^{13}C\{^1H\}$ NMR (CDCl $_3$, 100 MHz, ppm): $\delta = 176.3, 158.8, 143.7, 33.1$. HRMS (EI) m/z : [M - H] $^-$ Calcd for $C_8H_3N_6O_3Cl_2$: 300.9649. Found: 300.9652.

3,4-Bis(5-(azidomethyl)-1,2,4-oxadiazol-3-yl)-furoxan (DAM-BFFa) (8). 3,4-Bis(5-(chloromethyl)-1,2,4-oxadiazol-3-yl)-furoxan (7) (0.50 g, 1.65 mmol, 1.0 equiv) was solved in acetonitrile (30 mL), and sodium azide (0.27 g, 4.13 mmol, 2.5 equiv) was added. The mixture was stirred at room temperature for 120 h. The solid was filtered and washed with (2 \times 20 mL) of acetonitrile. The filtrate was dried over anhydrous sodium sulfate and reduced at ambient temperature. 3,4-Bis(5-(azidomethyl)-1,2,4-oxadiazol-3-yl)-furoxan (8) was yielded as a yellowish oil (0.42 g, 1.33 mmol, 81%) after purification by flash column chromatography using ethyl acetate as eluent.

DTA (5 $^{\circ}C$ min $^{-1}$): 193 $^{\circ}C$ (dec). Sensitivities: BAM drop hammer: 40 J (liquid). IR (ATR) $\tilde{\nu}$ (cm $^{-1}$) = 2933(vw), 2192(w), 2179(w), 2101(vs), 2021(vw), 1723(vw), 1575(m), 1490(w), 1431(m), 1331(m), 1263(s), 1201(m), 1104(s), 1040(w), 1016(m), 979(m), 955(s), 900(s), 767(m), 737(m), 671(m), 622(m), 606(w), 606(w), 554(m), 515(w), 495(w), 482(m), 451(m), 430(m), 423(m), 418(m), 411(m), 405(m). Elem. Anal. Calcd for $C_8H_4N_{12}O_3$: C, 30.39; N, 53.16; H, 1.28. Found: C, 30.55; N, 52.87; H, 1.58. 1H NMR (acetone- d_6 , 400 MHz, ppm): $\delta = 5.03$ (s, 4H). $^{13}C\{^1H\}$ NMR (acetone- d_6 , 100 MHz, ppm): $\delta = 178.1, 159.3, 145.2, 45.7$. ^{15}N NMR (acetone- d_6 , 41 MHz, ppm): $\delta = 42.1, -12.3, -134.7, -138.9, -164.6, -315.4$. HRMS (EI) m/z : [M + H] $^+$ Calcd for $C_8H_5N_{12}O_3$: 317.0602. Found: 317.0602.

ASSOCIATED CONTENT

Supporting Information

The Supporting Information is available free of charge at <https://pubs.acs.org/doi/10.1021/acs.joc.1c00216>.

Author contributions, X-ray diffraction, computation, TGA measurements, NMR spectroscopy, and references (PDF)

Accession Codes

CCDC 2058086–2058091 contain the supplementary crystallographic data for this paper. These data can be obtained free of charge via www.ccdc.cam.ac.uk/data_request/cif, or by emailing data_request@ccdc.cam.ac.uk, or by contacting The Cambridge Crystallographic Data Centre, 12 Union Road, Cambridge CB2 1EZ, UK; fax: +44 1223 336033.

AUTHOR INFORMATION

Corresponding Author

Thomas M. Klapötke – Department of Chemistry, Ludwig-Maximilian University of Munich, D-81377 Munich, Germany; orcid.org/0000-0003-3276-1157; Email: tmk@cup.uni-muenchen.de

Authors

Lukas Bauer – Department of Chemistry, Ludwig-Maximilian University of Munich, D-81377 Munich, Germany

Maximilian Benz – Department of Chemistry, Ludwig-Maximilian University of Munich, D-81377 Munich, Germany

Tobias Lenz – Department of Chemistry, Ludwig-Maximilian University of Munich, D-81377 Munich, Germany

Jörg Stierstorfer – Department of Chemistry, Ludwig-Maximilian University of Munich, D-81377 Munich, Germany; orcid.org/0000-0002-2105-1275

Complete contact information is available at:

<https://pubs.acs.org/doi/10.1021/acs.joc.1c00216>

Notes

The authors declare no competing financial interest.

ACKNOWLEDGMENTS

The financial support of this work by the Ludwig-Maximilian University (LMU), the Office of Naval Research (ONR), under grant no. ONR N00014-19-1-2078, and the Strategic Environmental Research and Development Program (SERDP) under contract no. W912HQ19C0033 is gratefully acknowledged. The authors thank Stefan Huber for his help with the sensitivity measurement. We further thank Dr. Burkhard Krumm and Prof. Konstantin Karaghiosoff for ^{15}N NMR measurements, Dr. Marco Reichel for proofreading of the manuscript, and Jasmin Lechner for providing TGA measurements.

REFERENCES

- Bräse, S.; Gil, C.; Knepper, K.; Zimmermann, V. Organic Azides: An Exploding Diversity of a Unique Class of Compounds. *Angew. Chem., Int. Ed.* **2005**, *44* (33), 5188–5240.
- Curtius, T. Chemische Notizen. *Ber. Dtsch. Chem. Ges.* **1890**, *23* (2), 3033–3041.
- Shan, H.; Chu, Y.; Chang, P.; Yang, L.; Wang, Y.; Zhu, S.; Zhang, M.; Tao, L. Neuroprotective effects of hydrogen sulfide on sodium azide-induced autophagic cell death in PC12 cells. *Mol. Med. Rep.* **2017**, *16* (5), 5938–5946.
- Kolb, H. C.; Finn, M. G.; Sharpless, K. B. Click Chemistry: Diverse Chemical Function from a Few Good Reactions. *Angew. Chem., Int. Ed.* **2001**, *40* (11), 2004–2021.
- Goswami, P. P.; Suding, V. P.; Carlson, A. S.; Topczewski, J. J. Direct Conversion of Aldehydes and Ketones into Azides by Sequential Nucleophilic Addition and Substitution. *Eur. J. Org. Chem.* **2016**, *2016* (28), 4805–4809.
- Doebelin, C.; Schmitt, M.; Antheaume, C.; Bourguignon, J.-J.; Bihel, F. Nucleophilic Substitution of Azide Acting as a Pseudo Leaving Group: One-Step Synthesis of Various Aza Heterocycles. *J. Org. Chem.* **2013**, *78* (22), 11335–11341.
- Miyashita, M.; Mizutani, T.; Tadano, G.; Iwata, Y.; Miyazawa, M.; Tanino, K. Pd-Catalyzed Stereospecific Azide Substitution of α,β -Unsaturated γ,δ -Epoxy Esters with Double Inversion of Configuration. *Angew. Chem., Int. Ed.* **2005**, *44* (32), 5094–5097.
- Miguel-Ávila, J.; Tomás-Gamasa, M.; Olmos, A.; Pérez, P. J.; Mascareñas, J. L. Discrete Cu(i) complexes for azide–alkyne

annulations of small molecules inside mammalian cells. *Chem. Sci.* **2018**, *9* (7), 1947–1952.

(9) Bai, Y.; Feng, X.; Xing, H.; Xu, Y.; Kim, B. K.; Baig, N.; Zhou, T.; Gewirth, A. A.; Lu, Y.; Oldfield, E.; Zimmerman, S. C. A Highly Efficient Single-Chain Metal–Organic Nanoparticle Catalyst for Alkyne–Azide “Click” Reactions in Water and in Cells. *J. Am. Chem. Soc.* **2016**, *138* (35), 11077–11080.

(10) Cui, F.-H.; Chen, J.; Mo, Z.-Y.; Su, S.-X.; Chen, Y.-Y.; Ma, X.-L.; Tang, H.-T.; Wang, H.-S.; Pan, Y.-M.; Xu, Y.-L. Copper-Catalyzed Decarboxylative/Click Cascade Reaction: Regioselective Assembly of 5-Selenotriazole Anticancer Agents. *Org. Lett.* **2018**, *20* (4), 925–929.

(11) Huisgen, R. 1,3-Dipolare Cycloadditionen Rückschau und Ausblick. *Angew. Chem.* **1963**, *75* (13), 604–637.

(12) Boland, Y.; Safin, D. A.; Tinant, B.; Babashkina, M. G.; Marchand-Brynaert, J.; Garcia, Y. Routes to novel mono- and bis-tetrazole compounds: synthesis, spectroscopic and structural characterization. *New J. Chem.* **2013**, *37* (4), 1174–1179.

(13) Gody, G.; Rossner, C.; Moraes, J.; Vana, P.; Maschmeyer, T.; Perrier, S. One-Pot RAFT/“Click” Chemistry via Isocyanates: Efficient Synthesis of α -End-Functionalized Polymers. *J. Am. Chem. Soc.* **2012**, *134* (30), 12596–12603.

(14) Liu, R.; Gutierrez, O.; Tantilillo, D. J.; Aubé, J. Stereocontrol in a Combined Allylic Azide Rearrangement and Intramolecular Schmidt Reaction. *J. Am. Chem. Soc.* **2012**, *134* (15), 6528–6531.

(15) Markiewicz, J. T.; Wiest, O.; Helquist, P. Synthesis of Primary Aryl Amines Through a Copper-Assisted Aromatic Substitution Reaction with Sodium Azide. *J. Org. Chem.* **2010**, *75* (14), 4887–4890.

(16) Wurzenberger, M. H. H.; Gruhne, M. S.; Lommel, M.; Szmhardt, N.; Klapötke, T. M.; Stierstorfer, J. Comparison of 1-Ethyl-5H-tetrazole and 1-Azidoethyl-5H-tetrazole as Ligands in Energetic Transition Metal Complexes. *Chem. - Asian J.* **2019**, *14* (11), 2018–2028.

(17) Shoaf, A. L.; Bayse, C. A. The effect of nitro groups on N2 extrusion from aromatic azide-based energetic materials. *New J. Chem.* **2019**, *43* (38), 15326–15334.

(18) McDonald, K. A.; Seth, S.; Matzger, A. J. Coordination Polymers with High Energy Density: An Emerging Class of Explosives. *Cryst. Growth Des.* **2015**, *15* (12), 5963–5972.

(19) Petrie, M. A.; Sheehy, J. A.; Boatz, J. A.; Rasul, G.; Surya Prakash, G. K.; Olah, G. A.; Christe, K. O. Novel High-Energy Density Materials. Synthesis and Characterization of Triazidocarbenium Dinitramide, -Perchlorate, and -Tetrafluoroborate. *J. Am. Chem. Soc.* **1997**, *119* (38), 8802–8808.

(20) Klapötke, T. M. *Chemistry of High-Energy Materials*; De Gruyter: Boston, Berlin, 2017.

(21) GAP Vandenburg, E. J. Polyethers containing azidomethyl side chains. U.S. Pat. 3,645,917, 1972.

(22) Tang, Y.; Shreeve, J. M. Nitroxy/Azido-Functionalized Triazoles as Potential Energetic Plasticizers. *Chem. - Eur. J.* **2015**, *21* (19), 7285–7291.

(23) Lyssenko, K. A.; Nelubina, Y. V.; Safronov, D. V.; Haustova, O. I.; Kostyanovsky, R. G.; Lenev, D. A.; Antipin, M. Y. Intermolecular N3...N3 interactions in the crystal of pentaerythrityl tetraazide. *Mendeleev Commun.* **2005**, *15* (6), 232–234.

(24) Joo, Y.-H.; Gao, H.; Zhang, Y.; Shreeve, J. M. Inorganic or Organic Azide-Containing Hypergolic Ionic Liquids. As poster published in 1st Korean International Symposium on High Energy Materials, Incheon, Korea, October 6–9, 2009. *Inorg. Chem.* **2010**, *49* (7), 3282–3288.

(25) Wingard, L. A.; Johnson, E. C.; Guzmán, P. E.; Sabatini, J. J.; Drake, G. W.; Byrd, E. F. C.; Sausa, R. C. Synthesis of Bisoxazoletetrakis(methyl nitrate): A Potential Nitrate Plasticizer and Highly Explosive Material. *Eur. J. Org. Chem.* **2017**, *13* (13), 1765–1768.

(26) Johnson, E. C.; Sabatini, J. J.; Chavez, D. E.; Sausa, R. C.; Byrd, E. F. C.; Wingard, L. A.; Guzmán, P. E. Bis(1,2,4-oxadiazole)bis-(methylene) Dinitrate: A High-Energy Melt-Castable Explosive and

Energetic Propellant Plasticizing Ingredient. *Org. Process Res. Dev.* **2018**, *22* (6), 736–740.

(27) Johnson, E. C.; Bukowski, E. J.; Sabatini, J. J.; Sausa, R. C.; Byrd, E. F. C.; Garner, M. A.; Chavez, D. E. Bis(1,2,4-oxadiazolyl) Furoxan: A Promising Melt-Castable Eutectic Material of Low Sensitivity. *ChemPlusChem* **2019**, *84* (4), 319–322.

(28) Johnson, E. C.; Sabatini, J. J.; Chavez, D. E.; Wells, L. A.; Banning, J. E.; Sausa, R. C.; Byrd, E. F. C.; Orlicki, J. A. Bis(Nitroxymethylisoxazolyl) Furoxan: A Promising Standalone Melt-Castable Explosive. *ChemPlusChem* **2020**, *85* (1), 237–239.

(29) Yan, C.; Wang, K.; Liu, T.; Yang, H.; Cheng, G.; Zhang, Q. Exploiting the energetic potential of 1,2,4-oxadiazole derivatives: combining the benefits of a 1,2,4-oxadiazole framework with various energetic functionalities. *Dalton Trans* **2017**, *46* (41), 14210–14218.

(30) Wei, H.; He, C.; Zhang, J.; Shreeve, J. M. Combination of 1,2,4-Oxadiazole and 1,2,5-Oxadiazole Moieties for the Generation of High-Performance Energetic Materials. *Angew. Chem., Int. Ed.* **2015**, *54* (32), 9367–9371.

(31) Cao, Y.; Huang, H.; Lin, X.; Yang, J.; Gong, X. Synthesis and properties of 5,5'-dinitramino-3,3'-bi(1,2,4-oxadiazole) and its energetic salts. *New J. Chem.* **2018**, *42* (14), 11390–11395.

(32) Guzmán, P. E.; Sausa, R. C.; Wingard, L. A.; Pesce-Rodriguez, R. A.; Sabatini, J. J. Synthesis and Characterization of Isoxazole-Based Energetic Plasticizer Candidates EEIN and IDN. *Eur. J. Org. Chem.* **2018**, *2018* (47), 6724–6728.

(33) Schneider, S.; Hawkins, T.; Rosander, M.; Mills, J.; Brand, A.; Hudgens, L.; Warmoth, G.; Vij, A. Liquid Azide Salts. *Inorg. Chem.* **2008**, *47* (9), 3617–3624.

(34) Zhan-Xiong, L.; Yu-Xiang, O.; Bo-Ren, C. Synthesis of two furazano azides. *J. Beijing Inst. Tech.* **2001**, *10* (10), 322–325.

(35) Fischer, D.; Klapötke, T. M.; Reymann, M.; Stierstorfer, J. Dense Energetic Nitraminofurazanes. *Chem. - Eur. J.* **2014**, *20* (21), 6401–6411.

(36) Tsyshkevsky, R.; Pagoria, P.; Zhang, M.; Racoveanu, A.; DeHope, A.; Parrish, D.; Kuklja, M. M. Searching for Low-Sensitivity Cast-Melt High-Energy-Density Materials: Synthesis, Characterization, and Decomposition Kinetics of 3,4-Bis(4-nitro-1,2,5-oxadiazol-3-yl)-1,2,5-oxadiazole-2-oxide. *J. Phys. Chem. C* **2015**, *119* (7), 3509–3521.

(37) Zhang, Y.; Zhou, C.; Wang, B.; Zhou, Y.; Xu, K.; Jia, S.; Zhao, F. Synthesis and Characteristics of Bis(nitrofurazano)furan (BNFF), an Insensitive Material with High Energy-Density. *Propellants, Explos., Pyrotech.* **2014**, *39* (6), 809–814.

(38) Tsyshkevsky, R.; Pagoria, P.; Zhang, M.; Racoveanu, A.; Parrish, D. A.; Smirnov, A. S.; Kuklja, M. M. Comprehensive End-to-End Design of Novel High Energy Density Materials: I. Synthesis and Characterization of Oxadiazole Based Heterocycles. *J. Phys. Chem. C* **2017**, *121* (43), 23853–23864.

(39) Pagoria, P. F.; Zhang, M.-X.; Zuckerman, N. B.; DeHope, A. J.; Parrish, D. A. Synthesis and characterization of multicyclic oxadiazoles and 1-hydroxytetrazoles as energetic materials. *Chem. Heterocycl. Compd.* **2017**, *53* (6), 760–778.

(40) Fershtat, L. L.; Ananyev, I. V.; Makhova, N. N. Efficient assembly of mono- and bis(1,2,4-oxadiazol-3-yl)furoxan scaffolds via tandem reactions of furoxanilamidoximes. *RSC Adv.* **2015**, *5* (58), 47248–47260.

(41) Joo, Y.-H.; Shreeve, J. M. 1,3-Diazido-2-(azidomethyl)-2-propylammonium Salts. *Inorg. Chem.* **2009**, *48* (17), 8431–8438.

(42) He, C.; Tang, Y.; Mitchell, L. A.; Parrish, D. A.; Shreeve, J. M. N-Oxides light up energetic performances: synthesis and characterization of dinitraminobisfuroxans and their salts. *J. Mater. Chem. A* **2016**, *4* (23), 8969–8973.

(43) McKinnon, J. J.; Spackman, M. A.; Mitchell, A. S. Novel tools for visualizing and exploring intermolecular interactions in molecular crystals. *Acta Crystallogr., Sect. B: Struct. Sci.* **2004**, *60* (6), 627–668.

(44) Ma, Y.; Zhang, A.; Zhang, C.; Jiang, D.; Zhu, Y.; Zhang, C. Crystal Packing of Low-Sensitivity and High-Energy Explosives. *Cryst. Growth Des.* **2014**, *14* (9), 4703–4713.

(45) Zhang, C.; Xue, X.; Cao, Y.; Zhou, Y.; Li, H.; Zhou, J.; Gao, T. Intermolecular friction symbol derived from crystal information. *CrystEngComm* **2013**, *15* (34), 6837–6844.

(46) Reichel, M.; Dosch, D.; Klapötke, T.; Karaghiosoff, K. Correlation between Structure and Energetic Properties of Three Nitroaromatic Compounds: Bis(2,4-dinitrophenyl) Ether, Bis(2,4,6-trinitrophenyl) Ether, and Bis(2,4,6-trinitrophenyl) Thioether. *J. Am. Chem. Soc.* **2019**, *141* (50), 19911–19916.

(47) Zhang, J.; Zhang, Q.; Vo, T. T.; Parrish, D. A.; Shreeve, J. n. M. Energetic Salts with π -Stacking and Hydrogen-Bonding Interactions Lead the Way to Future Energetic Materials. *J. Am. Chem. Soc.* **2015**, *137* (4), 1697–1704.

(48) Dosch, D. E.; Reichel, M.; Born, M.; Klapötke, T. M.; Karaghiosoff, K. Investigation of Structure–Property Relationships of Three Nitroaromatic Compounds: 1-Fluoro-2,4,6-trinitrobenzene, 2,4,6-Trinitrophenyl Methanesulfonate, and 2,4,6-Trinitrobenzaldehyde. *Cryst. Growth Des.* **2021**, *21* (1), 243–248.

(49) Spackman, M. A.; McKinnon, J. J. Fingerprinting intermolecular interactions in molecular crystals. *CrystEngComm* **2002**, *4* (66), 378–392.

(50) (a) Reichel & Partner GmbH. <http://www.reichelt-partner.de> (accessed on 28.1.2021). (b) Test methods according to the UN Recommendations on the Transport of Dangerous Goods. *Manual of Test and Criteria*, 4th revised ed.; United Nations Publication: New York and Geneva, 2003. ISBN 92-1-139087-7, Sales No. E.03.VIII.2; 13.4.2 Test 3 a (ii) BAM Fallhammer.

(51) Sućeska, M. *EXPLOS V6.02 program*; Brodarski Institute: Zagreb, Croatia, 2014.

Polyazido-Methyl Derivatives of Prominent Oxadiazole and Isoxazole Scaffolds – Synthesis, Explosive Properties and Evaluation

Lukas Bauer, Maximilian Benz, Thomas M. Klapötke*, Tobias Lenz and Jörg Stierstorfer

Prof. Dr. Thomas M. Klapötke; Department of Chemistry, Ludwig-Maximilian University of Munich; Butenandtstr. 5-13(D), D-81377 Munich, Germany; tmk@cup.uni-muenchen.de

Supplementary Information

Table of Contents

1.	Author Contributions	S3
2.	X-ray Diffraction	S4
3.	Computation	S9
4.	TGA Measurements	S15
5.	NMR Spectroscopy	S16
6.	References	S25

Author Contributions

L.B. Synthesis: Equal

M.B. Writing – Original Draft: Lead ; Writing – Review & Editing: Lead, Synthesis: Lead

T.M.K. Supervision: Lead, Validation: Equal, Resources: Lead

T.L. Writing – Review & Editing: Equal

J.S. Conceptualization: Lead, Project administration: Lead, Validation: Equal

X-ray Diffraction

Crystal structure data were obtained from an Oxford Xcalibur3 diffractometer with a Spellman generator (voltage 50 kV, current 40 mA) and a Kappa CCD area for data collection using Mo- $K\alpha$ radiation ($\lambda = 0.71073 \text{ \AA}$) or a Bruker D8 Venture TXS diffractometer equipped with a multilayer monochromator, a Photon 2 detector and a rotation-anode generator (Mo- $K\alpha$ radiation). The data collection was performed using the CRYSTALIS RED software.^[S1] The solution of the structure was performed by direct methods and refined by full-matrix least-squares on F² (SHELXT)^[S2] implemented in the OLEX2^[S3] software suite. The non-hydrogen atoms were refined anisotropically and the hydrogen atoms were located and freely refined. The absorption correction was carried out by a SCALE3 ABSPACK multiscan method.^[S4] The DIAMOND2 plots shown with thermal ellipsoids at the 50% probability level and hydrogen atoms are shown as small spheres of arbitrary radius. The SADABS program embedded in the Bruker APEX3 software was used for multi-scan absorption corrections in all structures.^[S5] CCDC 2058088 (**1**), 2058090 (**2**), 2058086 (**3**), 2058089 (**4**), 2058087 (**5** · 0.5 H₂O) and 2058091 (**7**) contain the supplementary crystallographic data for this paper. These data can be obtained free of charge from The Cambridge Crystallographic Data Centre.

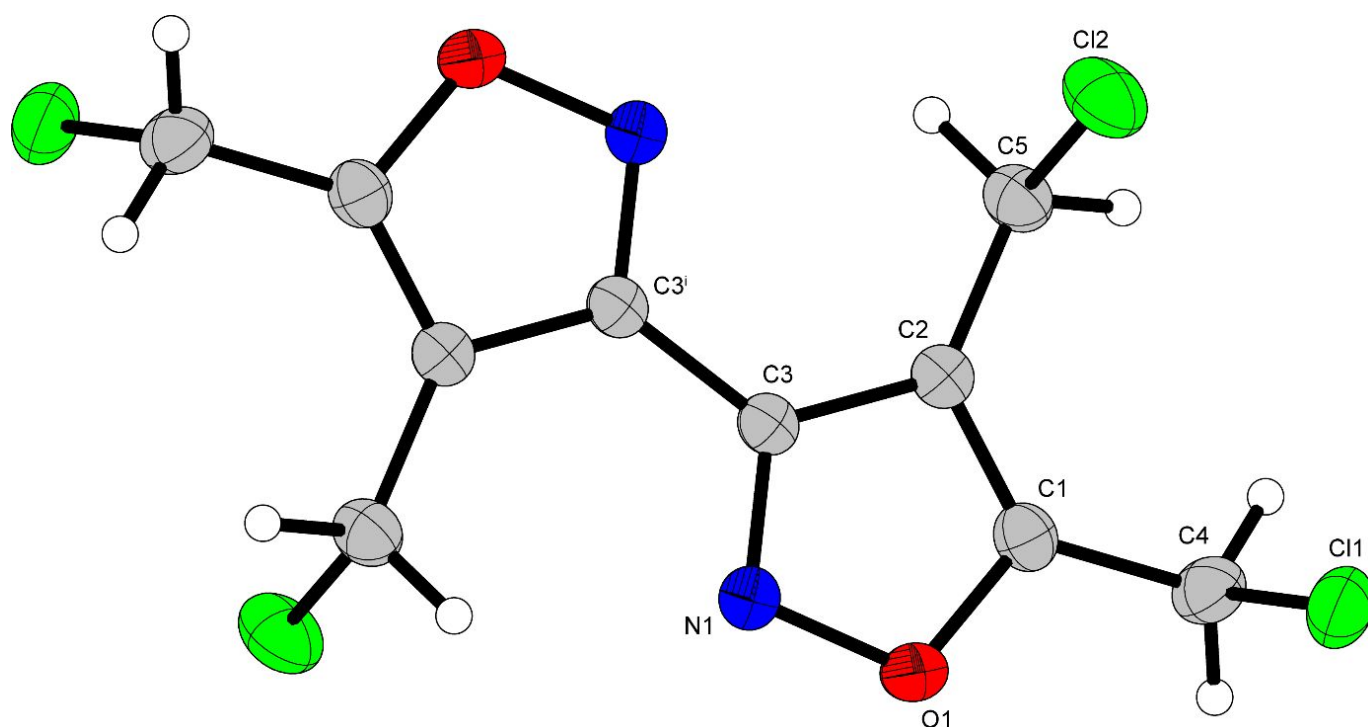


Figure S1. Representation of the molecular unit of **1**, showing the atom-labeling scheme. Thermal ellipsoids represent the 50% probability level and hydrogen atoms are shown as small spheres of arbitrary radius.

1 crystallizes in the monoclinic space group $P2_1/n$ with a cell volume of $651.00(9) \text{ \AA}^3$ and two formula units per cell. The cell constants are $a = 6.8734(5) \text{ \AA}$, $b = 9.3940(7) \text{ \AA}$ and $c = 10.3481(8) \text{ \AA}$, while the density is 1.683 g cm^{-3} at 123 K .

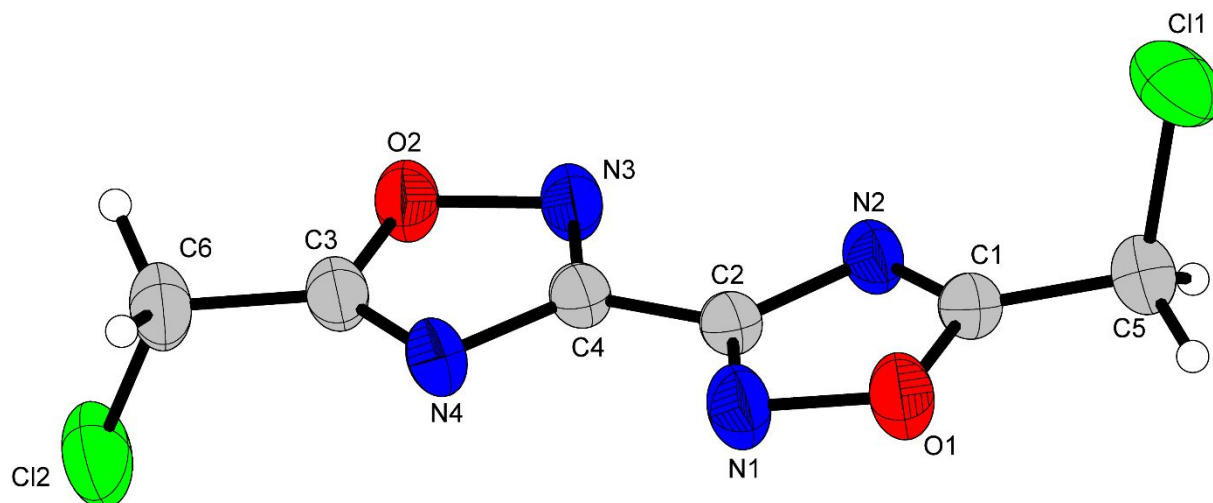


Figure S2. Representation of the molecular unit of **3**, showing the atom-labeling scheme. Thermal ellipsoids represent the 50% probability level and hydrogen atoms are shown as small spheres of arbitrary radius.

3 crystallizes in the monoclinic space group $P2_1/c$ with a cell volume of $1399.84(10) \text{ \AA}^3$ and six formula units per cell. The cell constants are $a = 8.9213(4) \text{ \AA}$, $b = 234125(9) \text{ \AA}$ and $c = 6.9616(3) \text{ \AA}$, while the density is 1.673 g cm^{-3} at $297(2) \text{ K}$. The molecule does not have an intramolecular symmetry like for **1**, **2** and **4**.

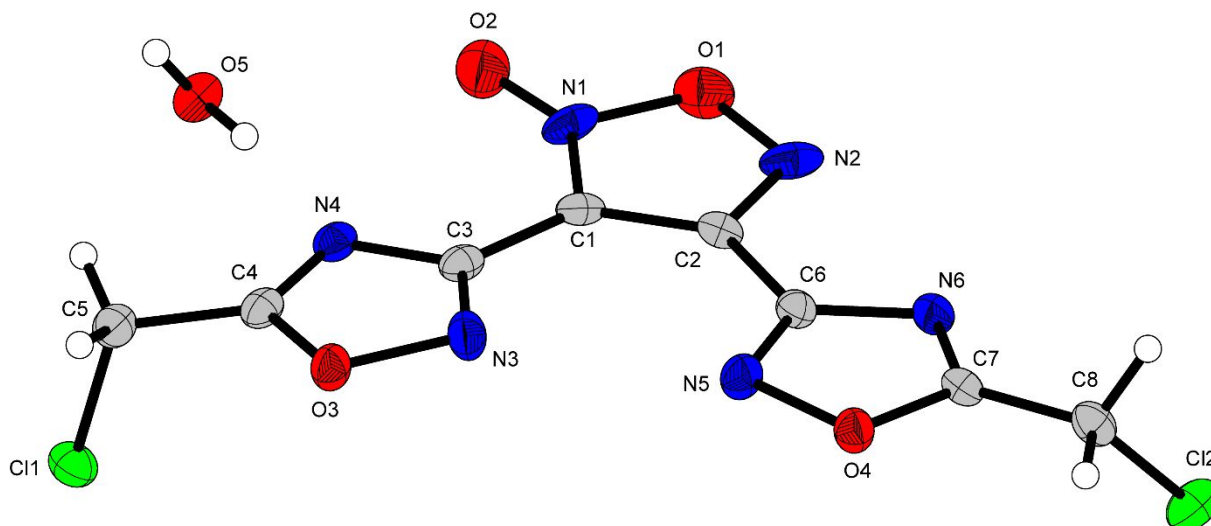


Figure S3. Representation of the molecular unit of **5** · 0.5 H₂O, showing the atom-labeling scheme. Thermal ellipsoids represent the 50% probability level and hydrogen atoms are shown as small spheres of arbitrary radius.

5 crystallizes in the monoclinic space group *C2/c* with a cell volume of 2369.5(4) Å³ and four formula units per cell and with the inclusion of 0.5 molecules of water. The cell constants are $a = 30.944(3)$ Å, $b = 4.7670(4)$ Å and $c = 16.2215(16)$ Å, while the density is 1.839 g cm⁻³ at 103 K.

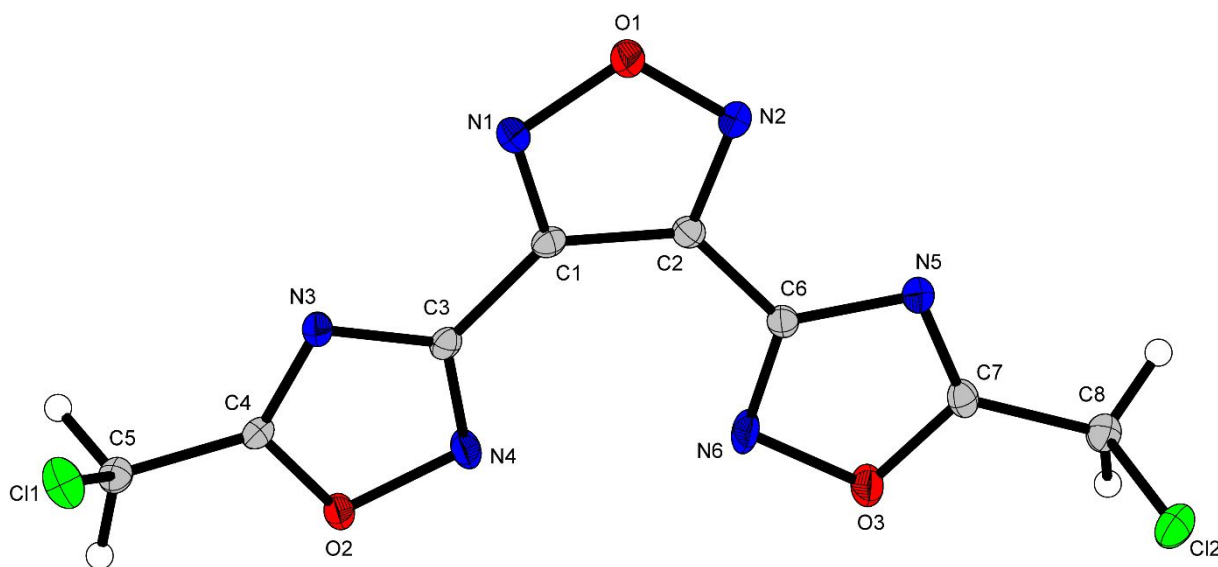


Figure S4. Representation of the molecular unit of **7**, showing the atom-labeling scheme. Thermal ellipsoids represent the 50% probability level and hydrogen atoms are shown as small spheres of arbitrary radius.

Compound **7** crystallizes in the monoclinic space group *P2₁/c* with a cell volume of 1099.82(9) Å³ and four formula units per cell. The cell constants are $a = 15.6285(8)$ Å, $b = 4.6718(2)$ Å and $c = 16.1306(8)$ Å, while the density is 1.830 g cm⁻³ at 102 K.

Table S1. Crystallographic data and structure refinement details for the prepared compounds **1-3**.

Compound	1	2	3
Formula	C ₁₀ H ₈ Cl ₄ N ₂ O ₂	C ₁₀ H ₈ N ₁₄ O ₂	C ₆ H ₄ Cl ₂ N ₄ O ₂
FW [g mol ⁻¹]	329.98	356.30	235.03
Crystal system	monoclinic	monoclinic	monoclinic
Space group	<i>P2₁/n</i> (No. 14)	<i>P2₁/n</i> (No. 14)	<i>P2₁/c</i> (No. 14)
Color / Habit	colorless block	colorless block	colorless platelet
Size [mm]	0.05 x 0.20 x 0.40	0.08 x 0.09 x 0.10	0.02 x 0.04 x 0.10
a [Å]	6.8734(5)	6.9324(3)	8.9213(4)
b [Å]	9.3940(7)	8.6045(3)	23.4125(9)
c [Å]	10.3481(8)	12.6400(5)	6.9616(3)
α [°]	90	90	90
β [°]	103.014(8)	92.218(1)	105.697(1)
γ [°]	90	90	90
V [Å ³]	651.00(9)	753.41(5)	1399.84(10)
Z	2	2	6
ρ _{calc.} [g cm ⁻³]	1.683	1.571	1.673
μ [mm ⁻¹]	0.902	0.122	0.673
F(000)	332	364	708
λ _{MoKα} [Å]	0.71073	0.71073	0.71073
T [K]	123	298	297
θ Min-Max [°]	3.0, 26.4	3.2, 26.4	2.5, 26.4
Dataset	-8: 8 ; -10: 11 ; -10:	-8: 8 ; -10: 10 ; -15:	-11: 11 ; -29: 29 ; -8:
	12	15	8
Reflections collected	4730	12801	23236
Independent refl.	1328	1529	2856
<i>R</i> _{int}	0.031	0.027	0.036
Observed reflections	1089	1365	2307
Parameters	98	134	190
<i>R</i> ₁ (obs) ^[a]	0.0396	0.0378	0.0702
w <i>R</i> ₂ (all data) ^[b]	0.1167	0.1013	0.1736
<i>S</i> ^[c]	1.04	1.09	1.03
Resd. dens [e Å ⁻³]	-0.24, 0.49	-0.19, 0.19	-0.89, 1.09
Device type	Xcalibur Sapphire3	Bruker D8 Venture	Bruker D8 Venture
Solution	SIR-92	SIR-92	SIR-92
Refinement	SHELXL-2013	SHELXL-2013	SHELXL-2013
Absorption correction	multi-scan	multi-scan	multi-scan
CCDC	2058088	2058090	2058086

^[a] $R_1 = \sum ||F_o| - |F_c|| / \sum |F_o|$; ^[b] $wR_2 = [\sum [w(F_o^2 - F_c^2)^2] / \sum [w(F_o^2)^2]]^{1/2}$; $w = [\sigma^2(F_o^2) + (xP)^2 + yP]^{-1}$ and $P = (F_o^2 + 2F_c^2) / 3$; ^[c] $S = (\sum [w(F_o^2 - F_c^2)^2] / (n-p))^{1/2}$ (n = number of reflections; p = total number of parameters).

Table S2. Crystallographic data and structure refinement details for the prepared compounds **4**, **5** and **7**.

Compound	4	5	7
Formula	C ₆ H ₄ N ₁₀ O ₂	C ₈ H ₄ Cl ₂ N ₆ O ₄ · 0.5 H ₂ O	C ₈ H ₄ Cl ₂ N ₆ O ₃
FW [g mol ⁻¹]	248.19	328.08	303.07
Crystal system	triclinic	monoclinic	monoclinic
Space group	<i>P</i> -1 (No. 2)	<i>C</i> 2/ <i>c</i> (No. 15)	<i>P</i> 2 ₁ / <i>c</i> (No. 14)
Color / Habit	colorless rod	colorless needle	colorless rod
Size [mm]	0.02 x 0.03 x 0.10	0.06 x 0.07 x 0.62	0.01 x 0.02 x 0.10
a [Å]	3.9473(3)	30.944(3)	15.6285(8)
b [Å]	6.7158(4)	4.7670(4)	4.6718(2)
c [Å]	10.1067(6)	16.2215(16)	16.1306(8)
α [°]	104.873(2)	90	90
β [°]	90.723(2)	98.007(8)	110.960(2)
γ [°]	104.440(2)	90	90
V [Å ³]	249.92(3)	2369.5(4)	1099.82(9)
Z	1	4	4
ρ _{calc.} [g cm ⁻³]	1.649	1.839	1.830
μ [mm ⁻¹]	0.133	0.579	0.606
F(000)	126	1320	608
λ _{MoKα} [Å]	0.71073	0.71073	0.71073
T [K]	299	103	102
θ Min-Max [°]	3.3, 26.4	2.5, 26.4	3.1, 26.4
Dataset	-4: 4 ; -8: 8 ; -12: 12	-38: 38 ; -5: 5 ; -20: 20	-19: 19 ; -5: 5 ; -20: 20
Reflections collected	4103	13818	17623
Independent refl.	1016	2412	2259
<i>R</i> _{int}	0.022	0.093	0.063
Observed reflections	891	1690	1868
Parameters	90	206	188
<i>R</i> ₁ (obs) ^[a]	0.0396	0.0678	0.0405
w <i>R</i> ₂ (all data) ^[b]	0.1123	0.1770	0.0782
<i>S</i> ^[c]	1.11	1.03	1.11
Resd. dens [e Å ⁻³]	-0.19, 0.23	-0.41, 1.42	-0.31, 0.28
Device type	Bruker D8 Venture	Xcalibur Sapphire3	Bruker D8 Venture
Solution	SIR-92	SIR-92	SIR-92
Refinement	SHELXL-2013	SHELXL-2013	SHELXL-2013
Absorption correction	multi-scan	multi-scan	multi-scan
CCDC	2058089	2058087	20591

^[a] $R_1 = \sum ||F_o| - |F_c|| / \sum |F_o|$; ^[b] $wR_2 = [\sum [w(F_o^2 - F_c^2)^2] / \sum [w(F_o^2)^2]]^{1/2}$; $w = [\sigma^2(F_o^2) + (xP)^2 + yP]^{-1}$ and $P = (F_o^2 + 2F_c^2) / 3$; ^[c] $S = (\sum [w(F_o^2 - F_c^2)^2] / (n-p))^{1/2}$ (n = number of reflections; p = total number of parameters).

Computation

Heat of Formation Computation

All quantum chemical calculations were carried out using the Gaussian G09 program package.^[S6] The enthalpies (H) and free energies (G) were calculated using the complete basis set (CBS) method of Petersson and co-workers in order to obtain very accurate energies. The CBS models are using the known asymptotic convergence of pair natural orbital expressions to extrapolate from calculations using a finite basis set to the estimated CBS limit. CBS-4 starts with an HF/3-21G(d) geometry optimization; the zero-point energy is computed at the same level. It then uses a large basis set SCF calculation as a base energy, and an MP2/6-31+G calculation with a CBS extrapolation to correct the energy through second order. A MP4(SDQ)/6-31+ (d,p) calculation is used to approximate higher order contributions. In this study, we applied the modified CBS-4M.

Heats of formation of the synthesized ionic compounds were calculated using the atomization method (equation E1) using room temperature CBS-4M enthalpies, which are summarized in Table S3.^[S7, S8]

$$\Delta_f H^\circ_{(g, M, 298)} = H_{(Molecule, 298)} - \sum H^\circ_{(Atoms, 298)} + \sum \Delta_f H^\circ_{(Atoms, 298)} \quad (E1)$$

Table S3. CBS-4M electronic enthalpies for atoms C, H, N and O and their literature values for atomic $\Delta_f H^\circ_{298}$ / kJ mol⁻¹

	$-H^{298}$ [a.u.]	NIST ^[S9]
H	0.500991	218.2
C	37.786156	717.2
N	54.522462	473.1
O	74.991202	249.5

For neutral compounds the sublimation enthalpy, which is needed to convert the gas phase enthalpy of formation to the solid state one, was calculated by the *Trouton* rule.^[S10] For ionic compounds, the lattice energy (U_L) and lattice enthalpy (ΔH_L) were calculated from the corresponding X-ray molecular volumes according to the equations provided by *Jenkins* and *Glasser*.^[S11] With the calculated lattice enthalpy the gas-phase enthalpy of formation was converted into the solid state (standard conditions) enthalpy of formation. These molar

standard enthalpies of formation (ΔH_m) were used to calculate the molar solid state energies of formation (ΔU_m) according to equation E2.

$$\Delta U_m = \Delta H_m - \Delta n RT \quad (\text{E2})$$

(Δn being the change of moles of gaseous components)

The calculation results are summarized in Table S4.

Table S4. Calculation results.

	$-H^{298}$ [a.u.]	$\Delta_f H^\circ(\text{g,M})$ [kJ mol ⁻¹]	$\Delta_f H^\circ(\text{s})$ [kJ mol ⁻¹]	Δn	$\Delta_f U(\text{s})$ [kJ kg ⁻¹]
2	1300.713532	1462.6	1377.8	-12.0	1407.5
4	927.565799	846.0	781.5	-8.0	801.3
6	1263.155609	1123.4	1079.9	-10.0	3325.4
8	1188.072180	1116.4	1072.9	-9.5	3467.5

Z-Matrix coordinates for 2, 4, 6 and 8

For all calculated compounds, no imaginary frequencies were obtained. Tables S5-S8 show the atomic positions of compounds **2**, **4**, **6** and **8**, respectively.

Table S5. Z-Matrix positions of **2**.

Atom	Symbolic Z-Matrix		
O	-1.40489	5.33866	8.69814
N	-1.4719	4.48329	7.60194
C	-0.23731	6.0333	8.65103
C	-0.35807	4.68068	6.93441
C	0.47986	5.65608	7.5624
C	-0.06576	7.02041	9.75229
C	-0.13112	3.92382	5.69612
C	1.81046	6.11608	7.05958
N	0.46191	6.41896	11.00233
H	0.5413	7.73545	9.47163
H	-0.93402	7.39127	9.97559
N	0.98271	4.12121	5.02859
C	-0.96905	2.94842	5.06813
N	2.38157	7.08581	8.01129
H	1.68701	6.55663	6.20159
H	2.42111	5.352	6.93669
N	1.596	6.04208	10.95004
O	0.9157	3.26584	3.93239
C	-0.25188	2.5712	3.9795
C	-2.29965	2.48842	5.57095
N	3.46352	7.5452	7.6781
N	2.65198	5.64713	11.05285
C	-0.42343	1.58409	2.87825
N	-2.87076	1.51869	4.61924
H	-2.17621	2.04787	6.42894
H	-2.9103	3.2525	5.69384
N	4.45049	8.04753	7.48473
N	-0.9511	2.18554	1.6282
H	-1.03049	0.86905	3.1589
H	0.44483	1.21323	2.65494
N	-3.95271	1.0593	4.95243
N	-2.08519	2.56242	1.68049
N	-4.93968	0.55697	5.1458
N	-3.14117	2.95737	1.57768

Table S6. Z-Matrix positions of **4**.

Atom	Symbolic Z-Matrix		
O	2.15272	1.90983	2.2545
N	2.07289	3.10042	1.51725
C	1.41608	1.00617	1.59688
C	1.31491	2.76978	0.52113
N	0.8815	1.46881	0.515
C	1.28123	-0.34778	2.20592
C	0.9577	3.73386	-0.52113
N	0.51564	-0.27988	3.45886
H	0.78156	-0.8913	1.63553
H	2.18826	-0.72612	2.32674
N	1.39111	5.03483	-0.515
N	0.19972	3.40323	-1.51725
N	1.18632	0.0707	4.43706
C	0.85652	5.49747	-1.59688
O	0.11988	4.59381	-2.2545
N	1.6969	0.37742	5.40699
C	0.99137	6.85142	-2.20592
N	1.75697	6.78352	-3.45886
H	1.49105	7.39494	-1.63553
H	0.08434	7.22976	-2.32674
N	1.08628	6.43294	-4.43706
N	0.5757	6.12622	-5.40699

Table S7. Z-Matrix positions of **6**.

Atom	Symbolic Z-Matrix		
C	-2.14381	-0.53601	-0.10592
C	-2.14389	-0.536	1.36586
C	-3.55357	-1.24133	4.42691
C	-3.55313	-1.24199	-3.16692
N	-1.39634	0.50894	-0.54997
N	-3.88034	-0.9354	3.1434
N	-1.96073	-2.3079	3.14379
N	-3.88008	-0.93563	-1.88354
N	-1.96069	-2.30846	-1.88338
O	-0.84928	1.27458	0.62995
O	-2.35632	-2.09732	4.42714
O	-2.35606	-2.09822	-3.16684
C	-4.26869	-0.80299	-4.45798
H	-4.64531	-1.66504	-4.96781
H	-5.08071	-0.15116	-4.21173
C	-4.26952	-0.802	5.71765
H	-4.64896	-1.66367	6.22602
H	-5.07958	-0.1478	5.4712
C	-2.89563	-1.58707	2.20355
C	-2.89556	-1.58724	-0.94342
N	-1.39642	0.50896	1.80984
O	-0.63448	1.4985	2.34821
N	-3.31877	-0.09759	6.58988
N	-3.63076	0.17125	7.75101
N	-3.31872	-0.09513	-5.32827
N	-3.60203	0.11247	-6.50914
N	-2.67855	0.70918	8.62504
N	-2.63461	0.62573	-7.38131

Table S8. Z-Matrix position of **8**.

Atom	Symbolic Z-Matrix		
C	-1.39049	-0.35911	-0.07064
C	-1.46993	-0.30066	1.41649
C	-3.74408	-0.71724	4.08702
C	-3.39786	-1.00852	-2.9036
N	-0.27186	0.2978	-0.37554
N	-3.72266	-0.23669	2.82763
N	-2.54619	-2.18084	2.96947
N	-3.49617	-0.42347	-1.69303
N	-2.31946	-2.36784	-1.55629
O	0.27063	0.70512	0.71385
O	-2.81734	-1.85225	4.28063
O	-2.4614	-2.15202	-2.9105
C	-4.19768	-0.55341	-4.13842
H	-5.13122	-1.07527	-4.1709
H	-4.37945	0.49928	-4.07751
C	-4.65751	-0.16297	5.19608
H	-5.59195	-0.68404	5.18214
H	-4.82825	0.88009	5.02942
C	-2.55256	-0.89146	2.33871
C	-2.38143	-1.02993	-1.03999
N	-0.39077	0.37832	1.75316
N	-4.01107	-0.351	6.50286
N	-4.69831	-0.51282	7.51248
N	-3.42886	-0.84825	-5.35616
N	-4.01607	-1.09738	-6.41018
N	-4.08265	-0.69191	8.75703
N	-3.28387	-1.37818	-7.56993

TGA Measurements

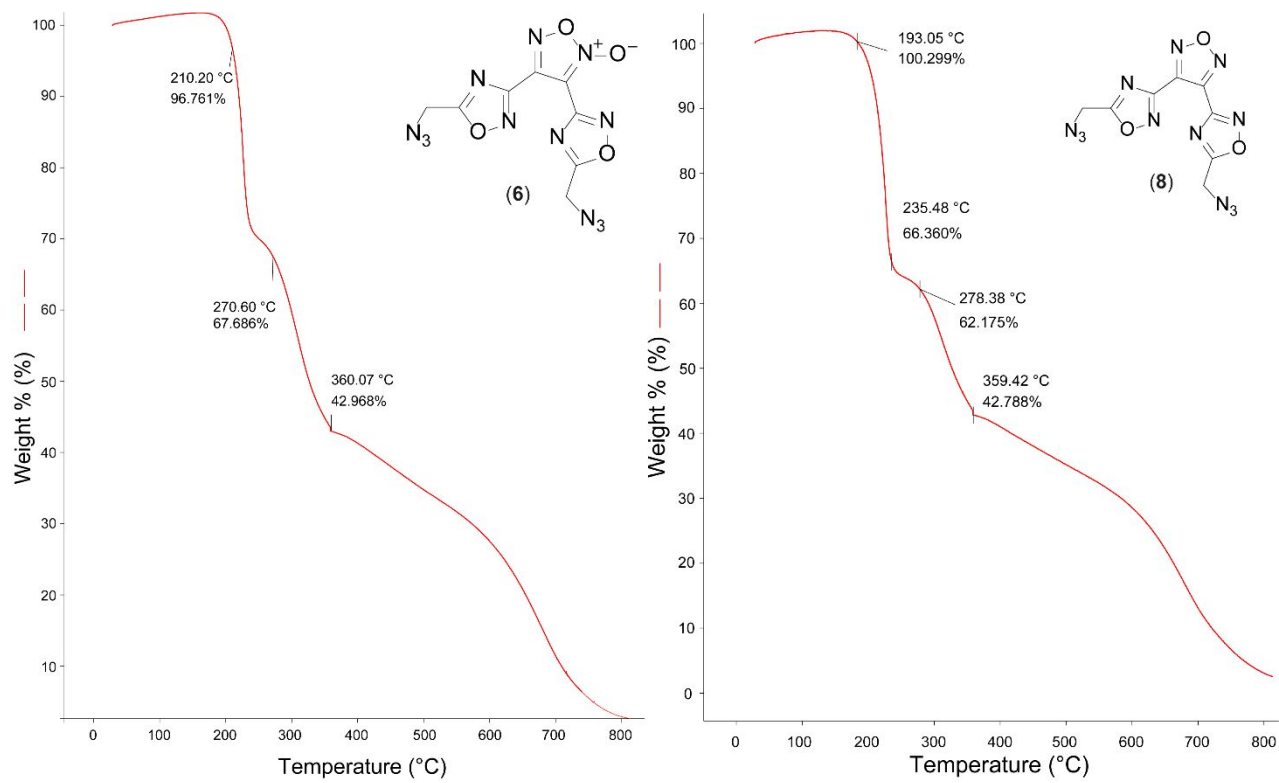
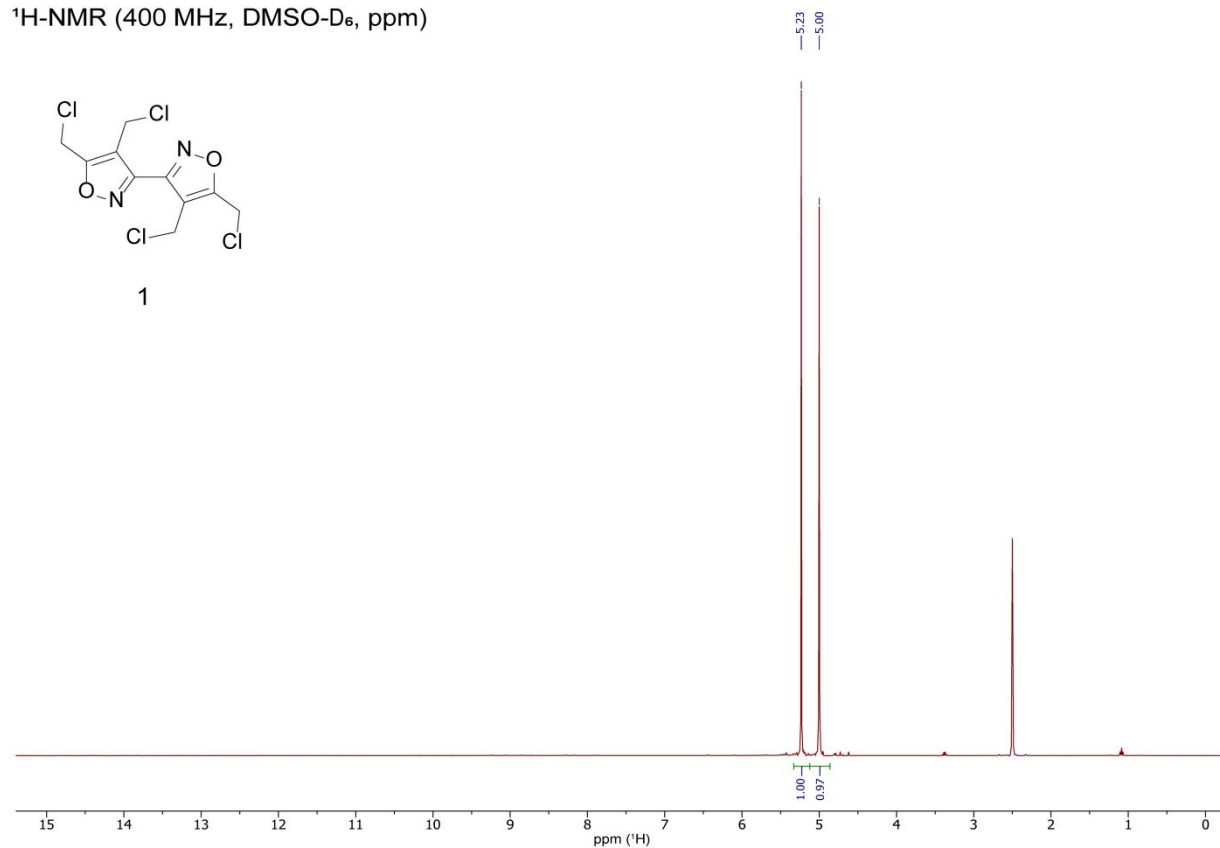


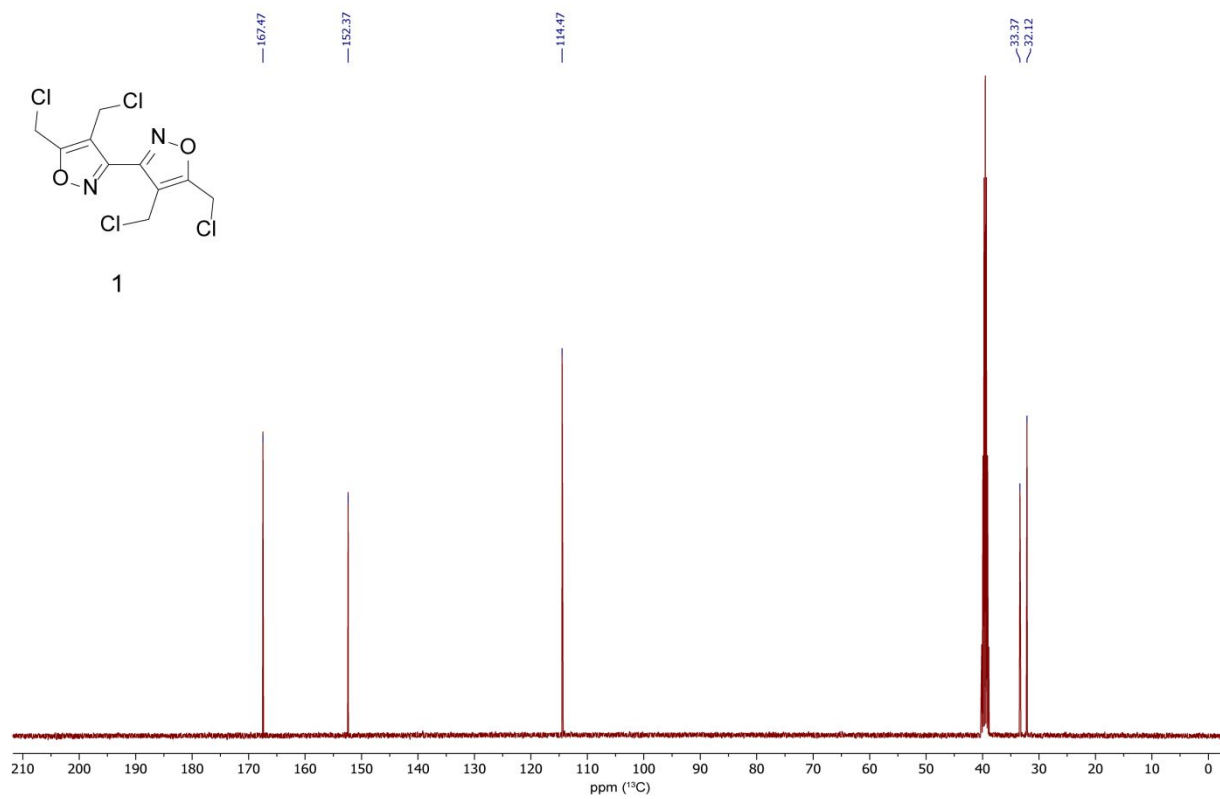
Figure S5. TGA measurements of **6** (left) and **8** (right).

NMR Spectroscopy

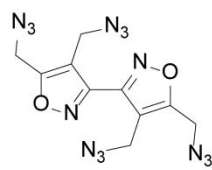
^1H -NMR (400 MHz, DMSO- D_6 , ppm)



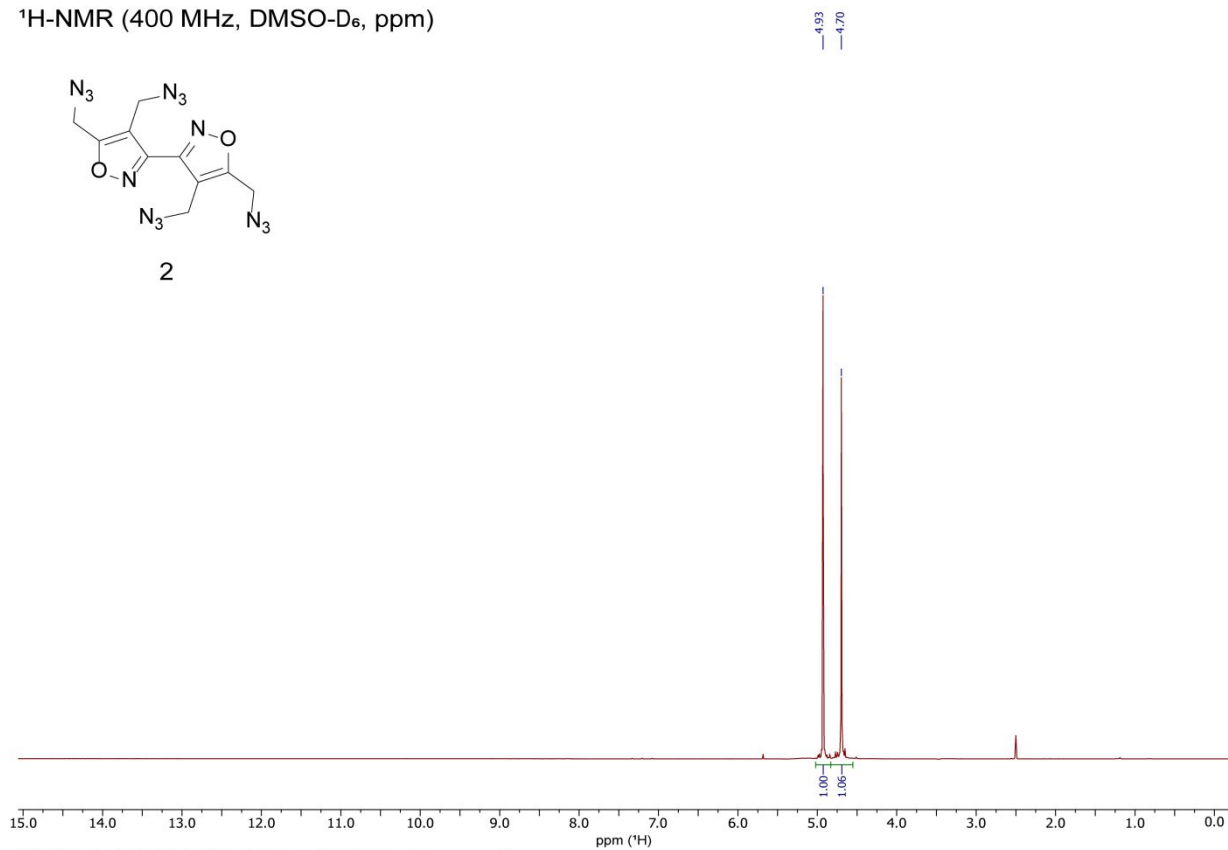
$^{13}\text{C}\{^1\text{H}\}$ -NMR (100 MHz, DMSO- D_6 , ppm)



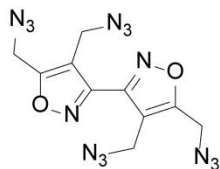
$^1\text{H-NMR}$ (400 MHz, DMSO-D_6 , ppm)



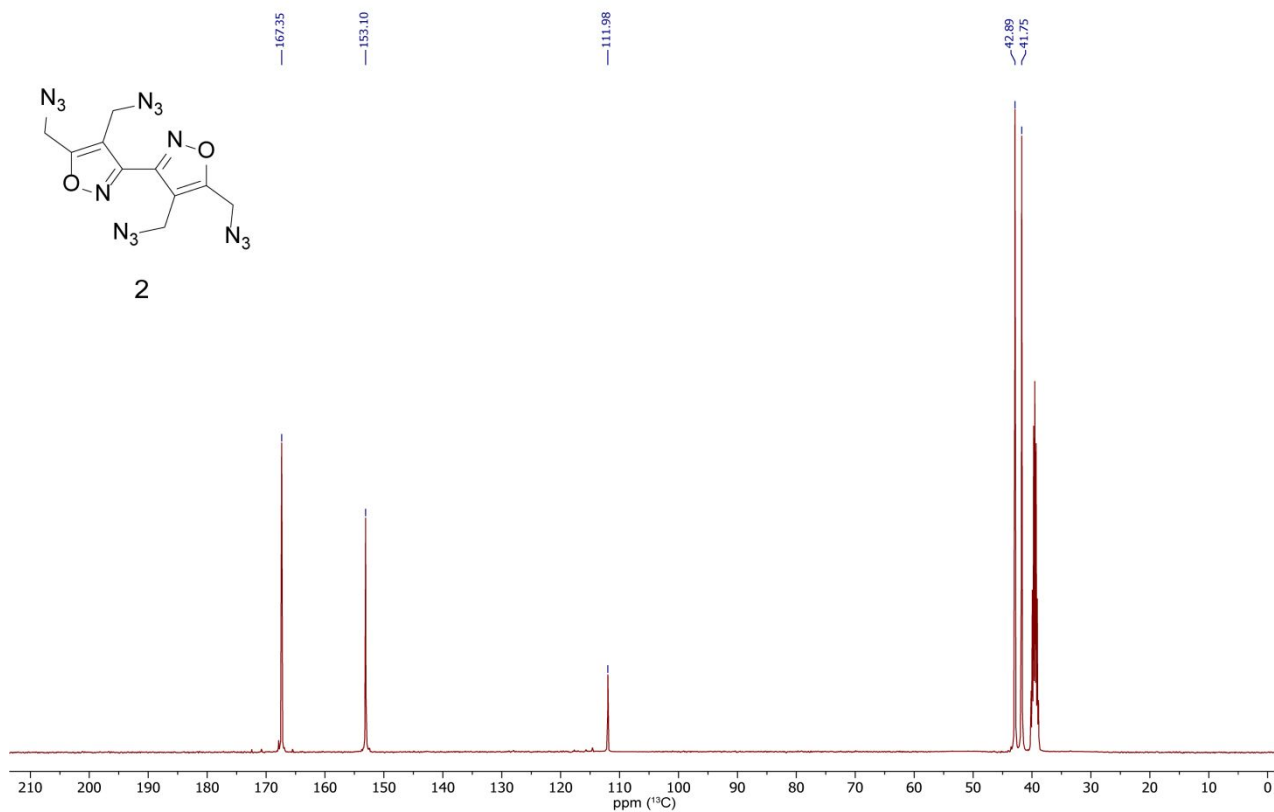
2

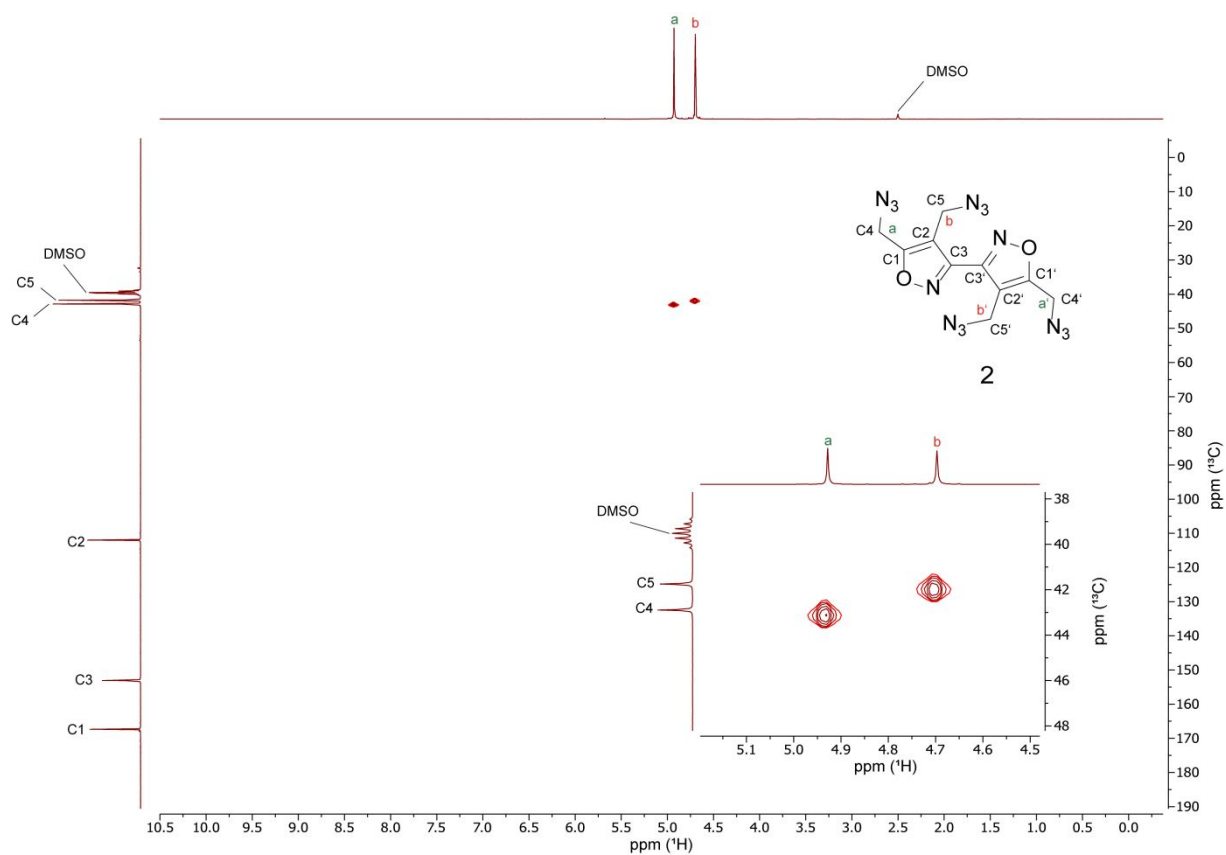
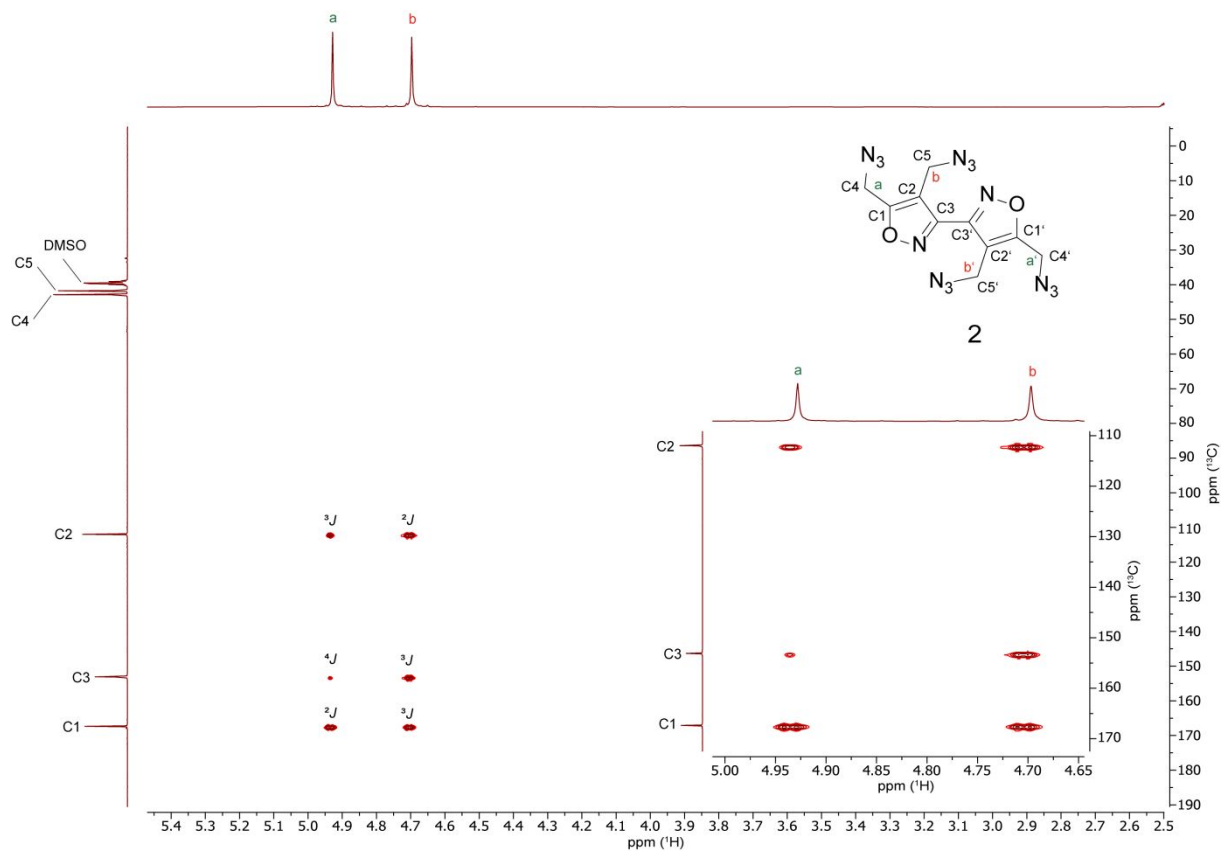


$^{13}\text{C}\{^1\text{H}\}$ -NMR (100 MHz, DMSO-D_6 , ppm)

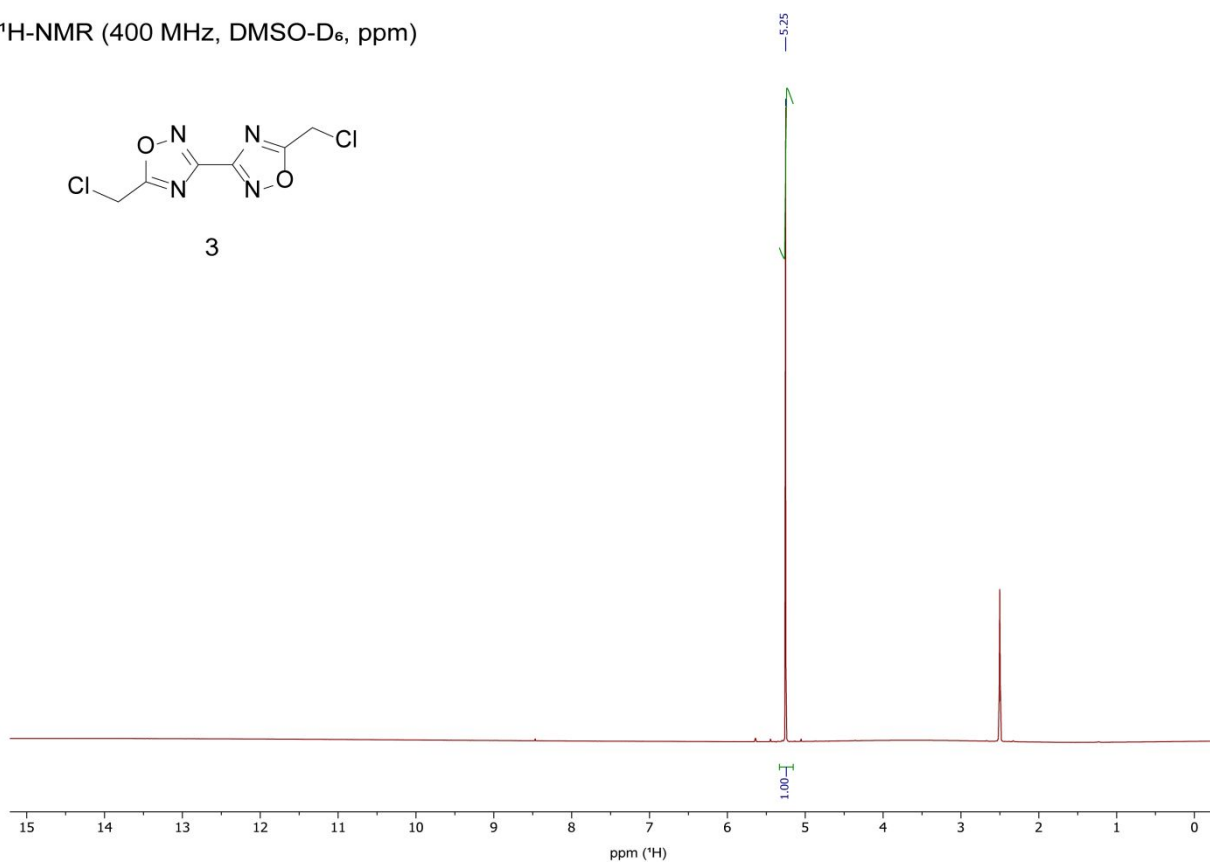
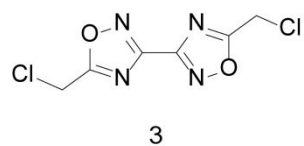


2

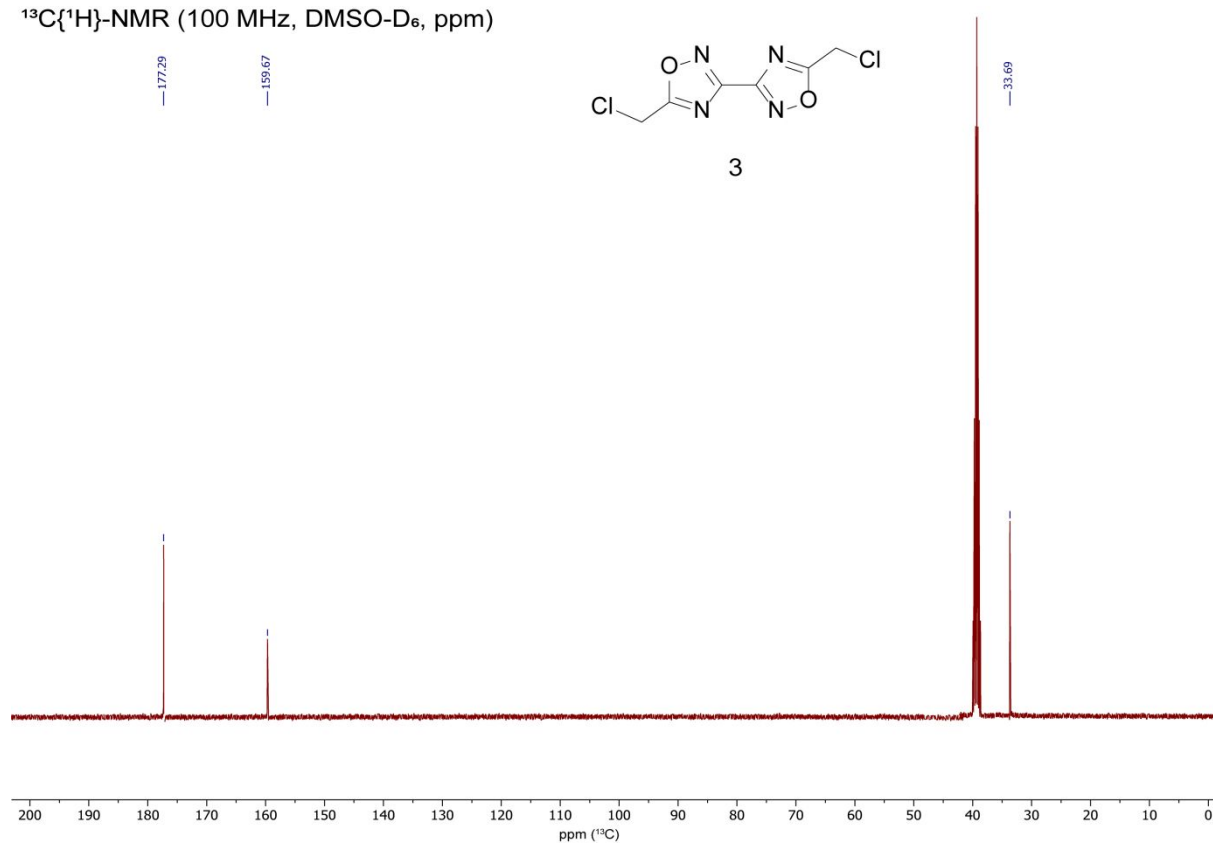
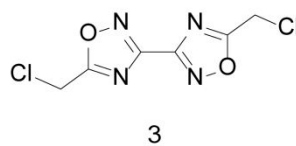




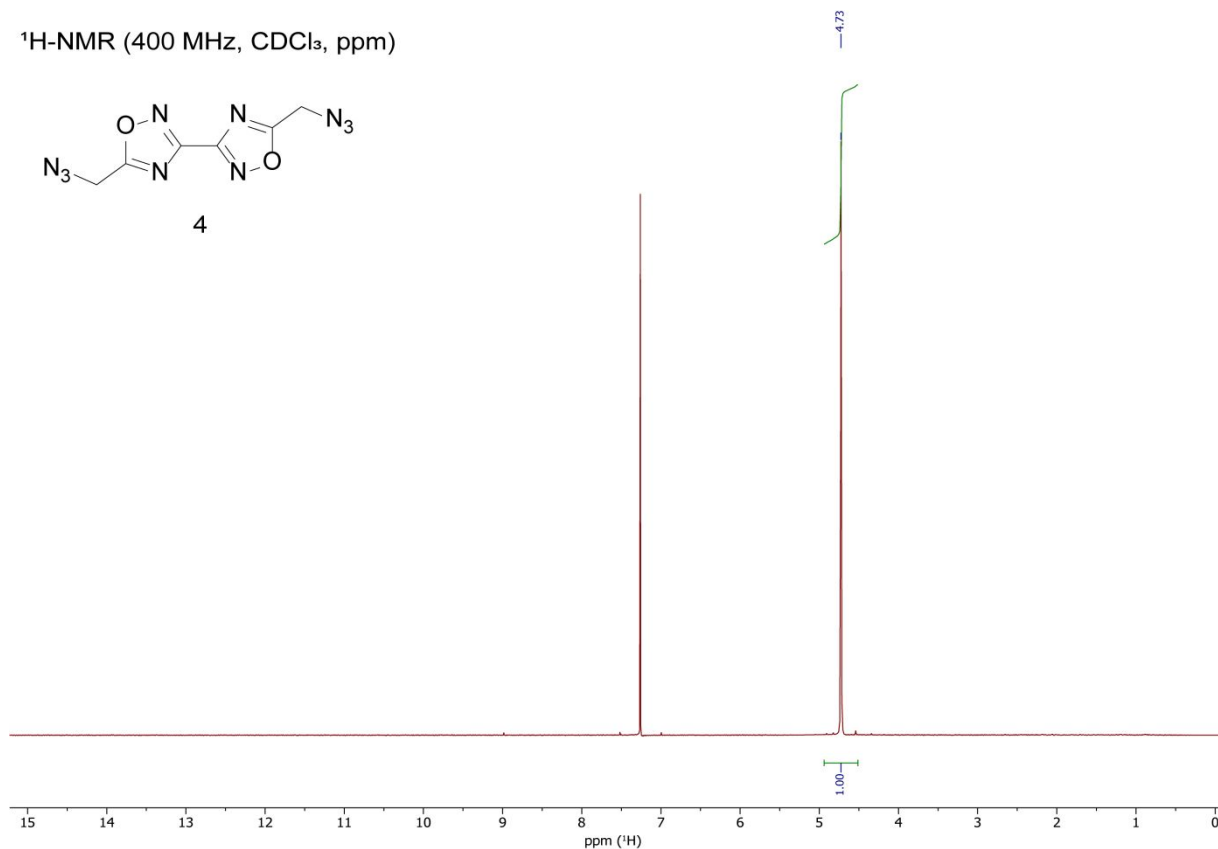
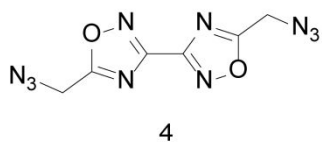
$^1\text{H-NMR}$ (400 MHz, DMSO-D_6 , ppm)



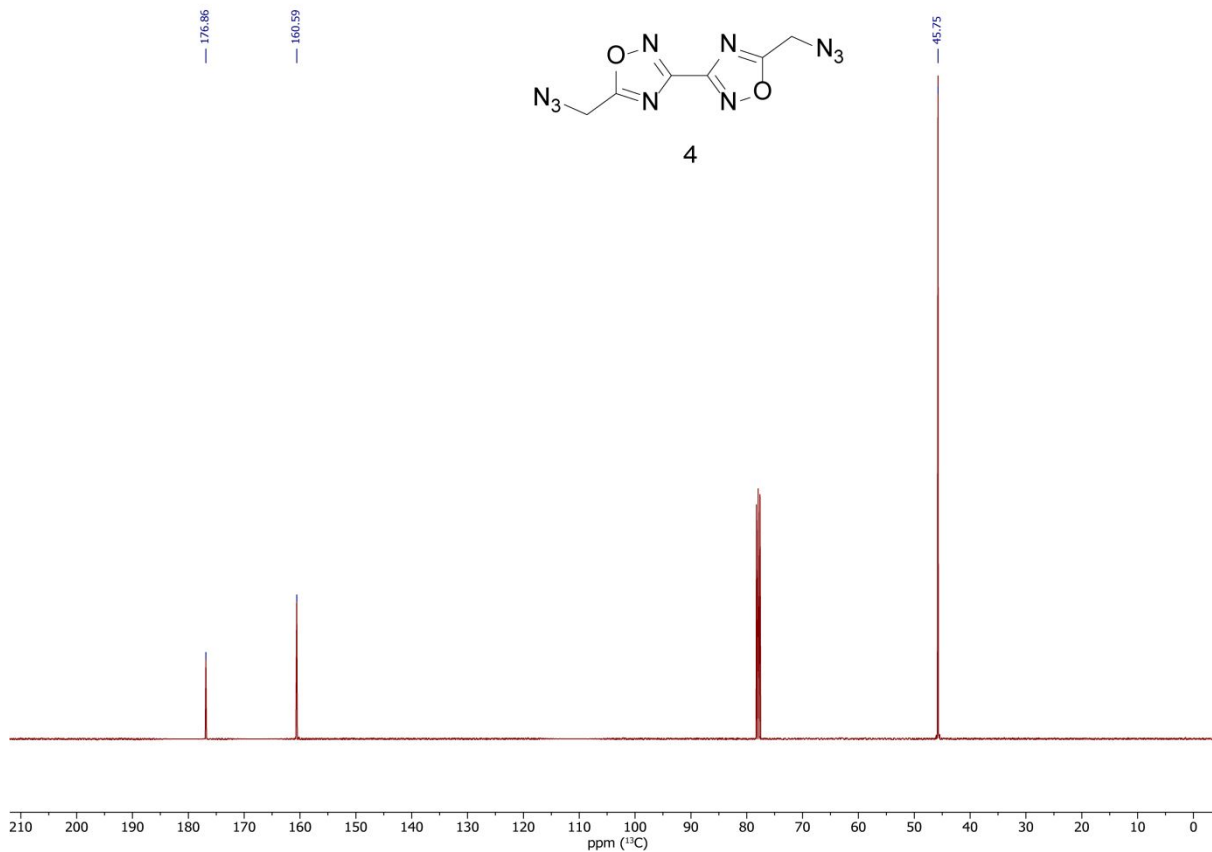
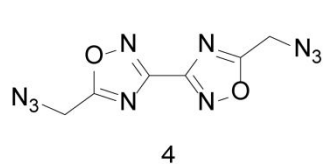
$^{13}\text{C}\{^1\text{H}\}$ -NMR (100 MHz, DMSO-D_6 , ppm)



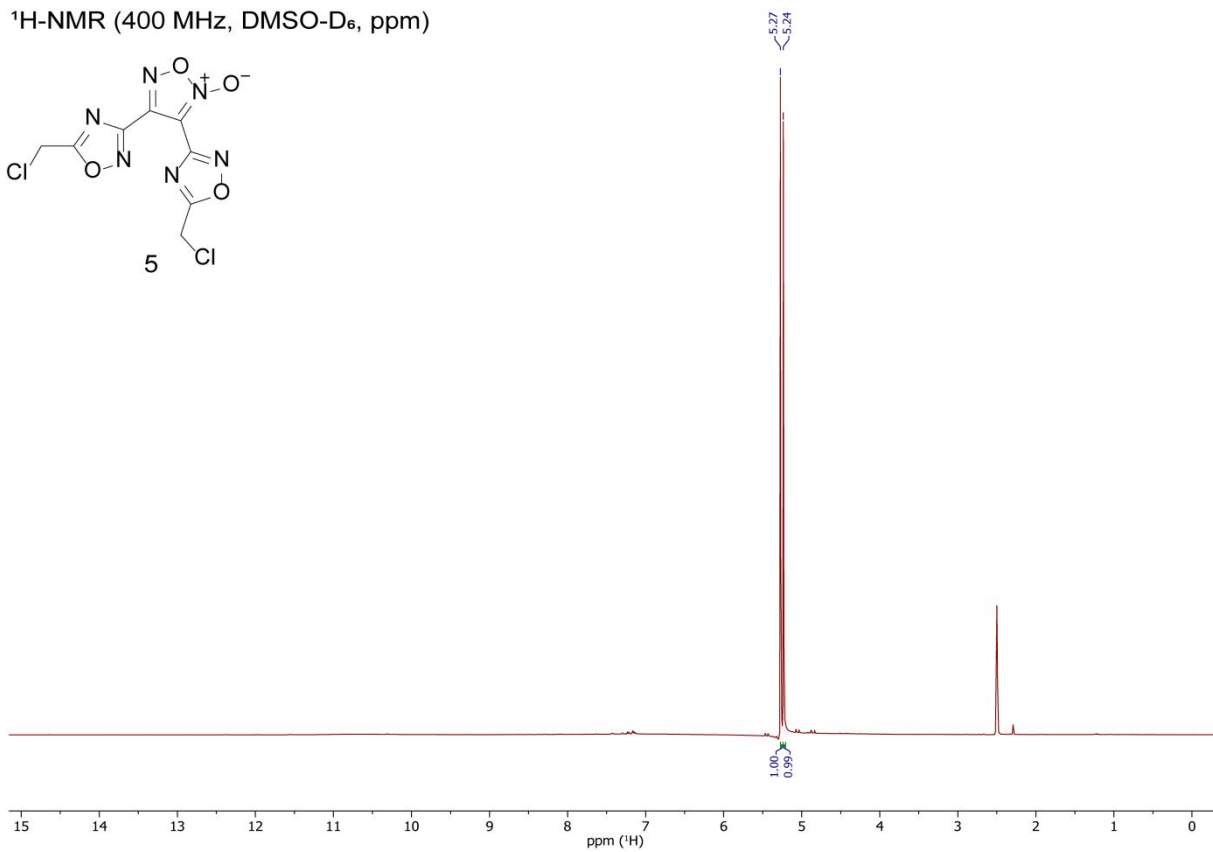
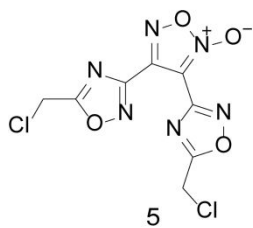
$^1\text{H-NMR}$ (400 MHz, CDCl_3 , ppm)



$^{13}\text{C}\{^1\text{H}\}$ -NMR (100 MHz, CDCl_3 , ppm)



$^1\text{H-NMR}$ (400 MHz, DMSO-D_6 , ppm)



$^{13}\text{C}\{^1\text{H}\}$ -NMR (100 MHz, DMSO-D_6 , ppm)

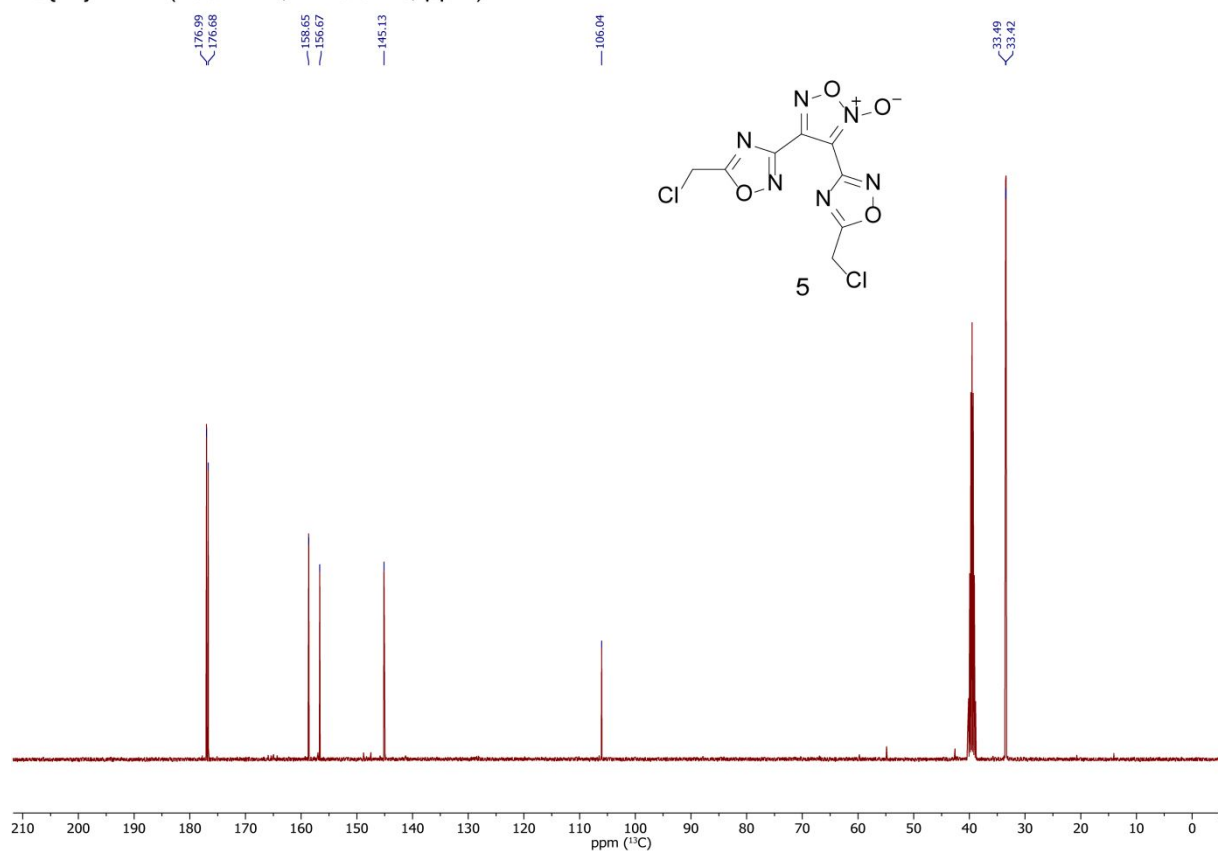
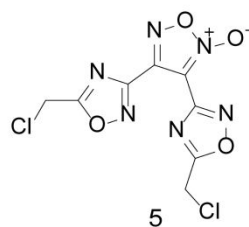
176.99
176.68

158.65
156.67

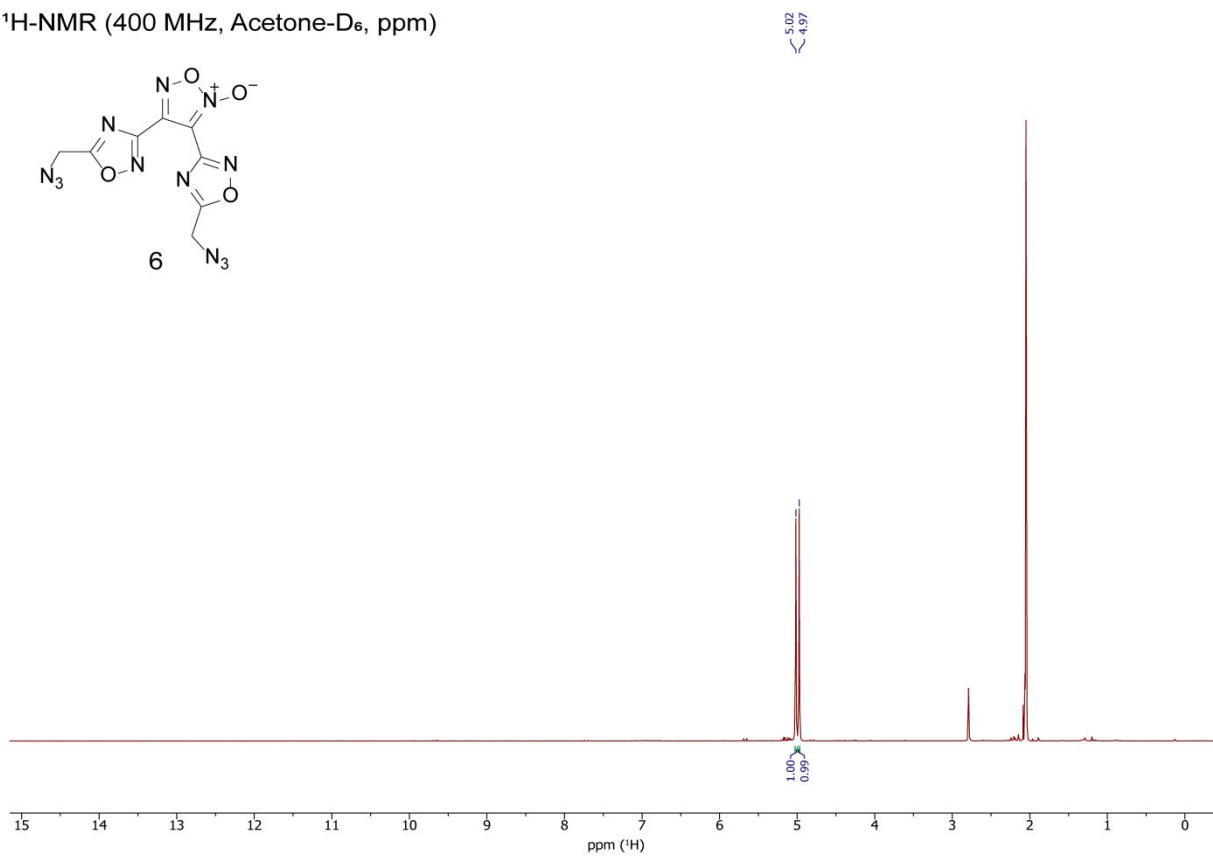
145.13

106.04

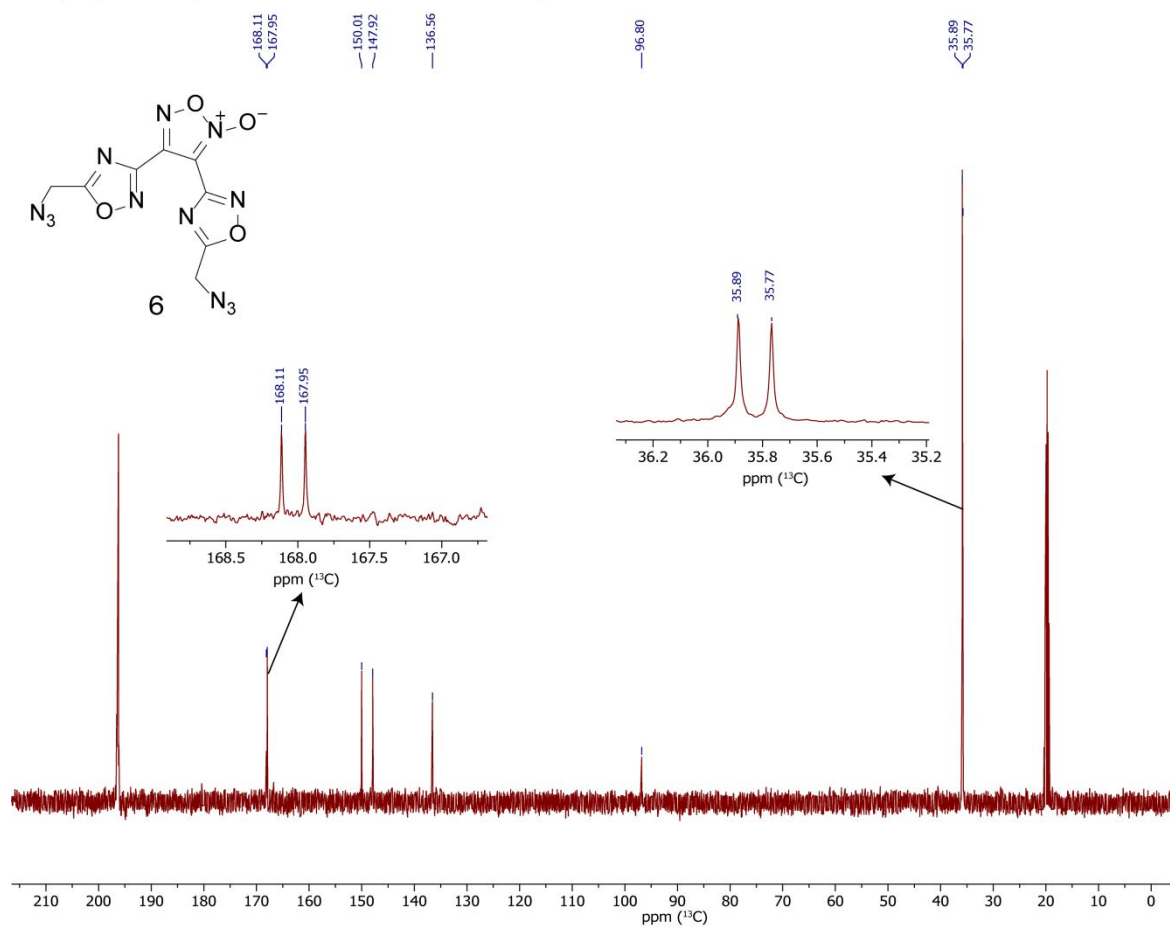
33.49
33.42



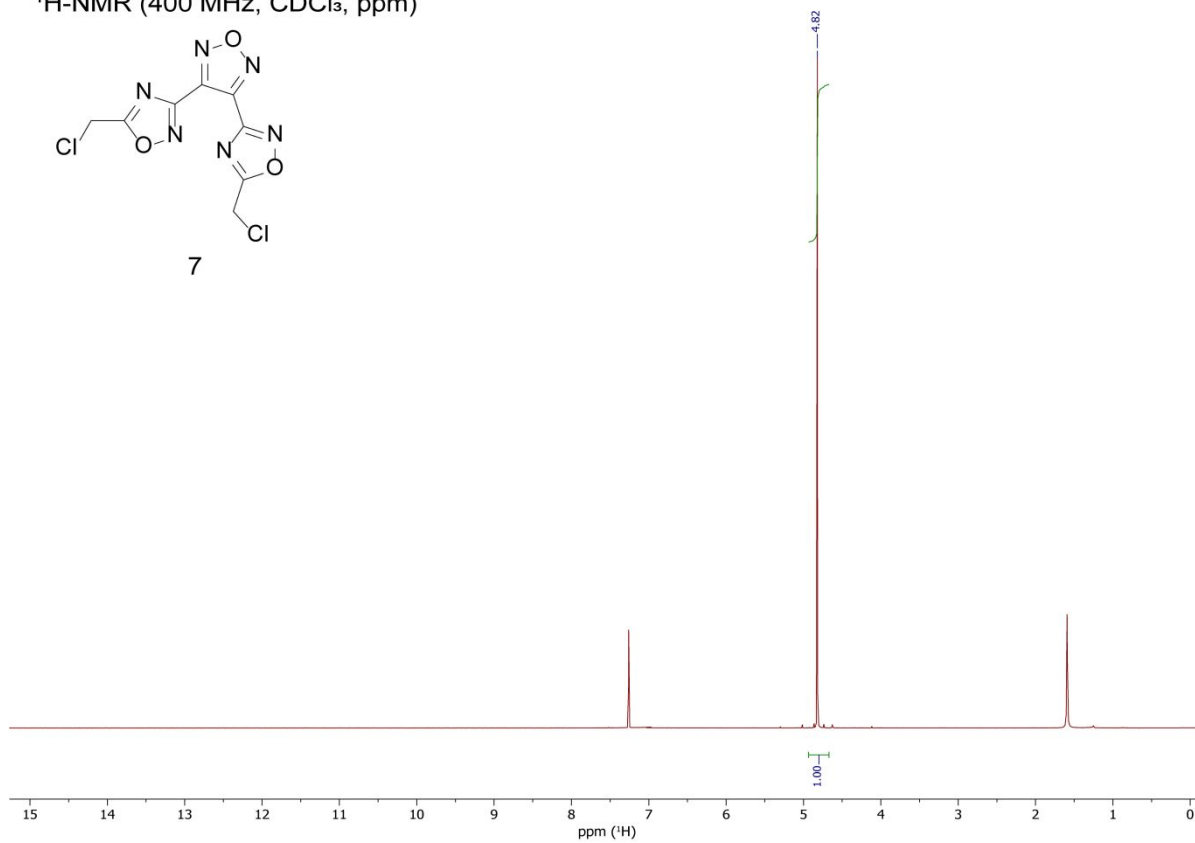
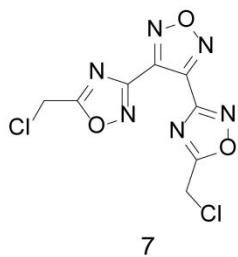
$^1\text{H-NMR}$ (400 MHz, Acetone- D_6 , ppm)



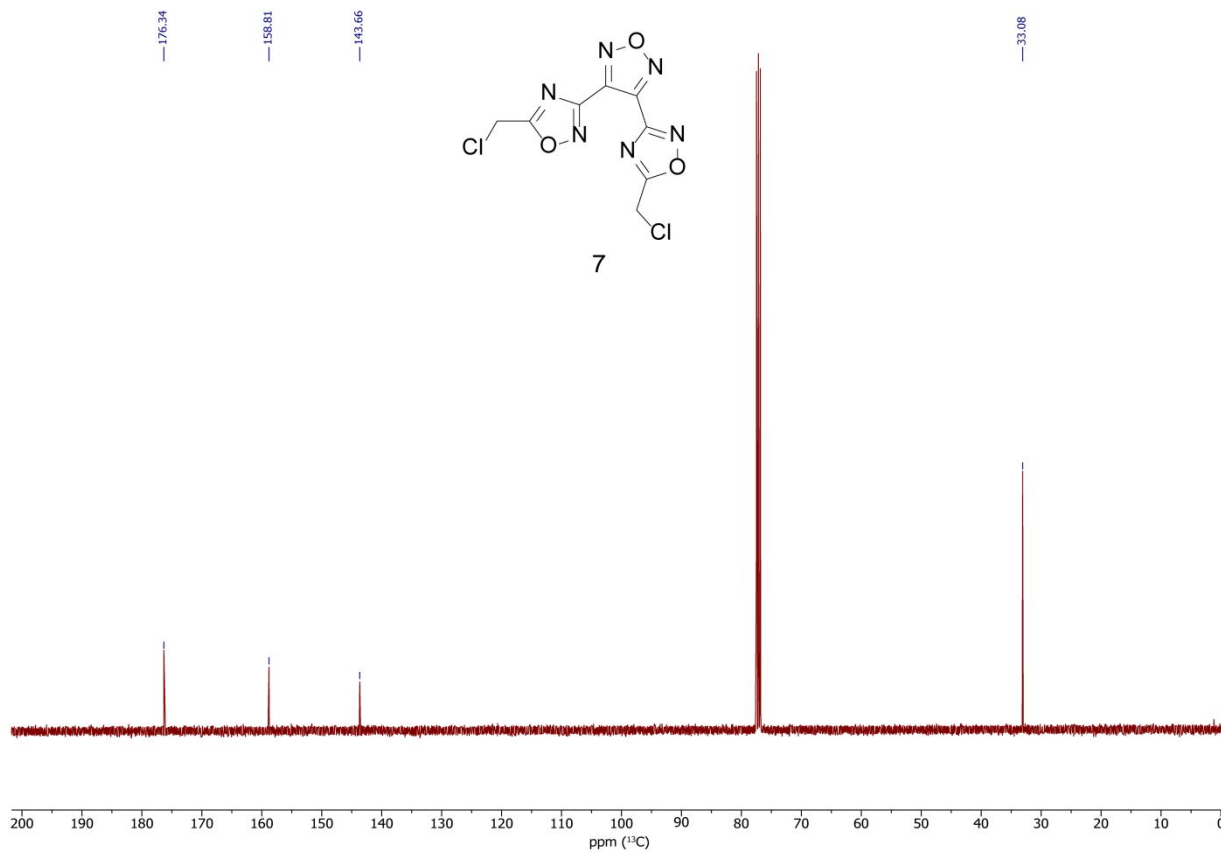
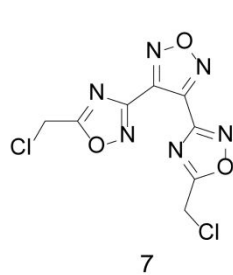
$^{13}\text{C}\{^1\text{H}\}$ -NMR (100 MHz, Acetone- D_6 , ppm)



¹H-NMR (400 MHz, CDCl₃, ppm)



¹³C{¹H}-NMR (100 MHz, CDCl₃, ppm)



References

- [S1] *CrysAlisPro*, Oxford Diffraction Ltd. *version 171.33.41*, **2009**.
- [S2] Sheldrick, G.M., *Acta Cryst.* **2015**, *A71*, 3–8.
- [S3] Dolomanov, O. V.; Bourhis, L. J.; Gildea, R. J.; Howard, J. A. K.; Puschmann, H., OLEX2: A complete structure solution, refinement and analysis program. *J. Appl. Cryst.* 2009, *42*, 339–341.
- [S4] *SCALE3 ABSPACK – An Oxford Diffraction program* (1.0.4, gui: 1.0.3), Oxford Diffraction Ltd., **2005**.
- [S5] *APEX3*. Bruker AXS Inc., Madison, Wisconsin, USA.
- [S6] Frisch, M. J.; Trucks, G. W.; Schlegel, H. B.; Scuseria, G. E.; Robb, M. A.; Cheeseman, J. R.; Scalmani, G.; Barone, V.; Petersson, G. A.; Nakatsuji, H.; Li, X.; Caricato, M.; Marenich, A. V.; Bloino, J.; Janesko, B. G.; Gomperts, R.; Mennucci, B.; Hratchian, H. P.; Ortiz, J. V.; Izmaylov, A. F.; Sonnenberg, J. L.; Williams-Young, D.; Ding, F.; Lipparini, F.; Egidi, F.; Goings, J.; Peng, B.; Petrone, A.; Henderson, T.; Ranasinghe, D.; Zakrzewski, V. G.; Gao, J.; Rega, N.; Zheng, G.; Liang, W.; Hada, M.; Ehara, M.; Toyota, K.; Fukuda, R.; Hasegawa, J.; Ishida, M.; Nakajima, T.; Honda, Y.; Kitao, O.; Nakai, H.; Vreven, T.; Throssell, K.; Montgomery, J. A., Jr.; Peralta, J. E.; Ogliaro, F.; Bearpark, M. J.; Heyd, J. J.; Brothers, E. N.; Kudin, K. N.; Staroverov, V. N.; Keith, T. A.; Kobayashi, R.; Normand, J.; Raghavachari, K.; Rendell, A. P.; Burant, J. C.; Iyengar, S. S.; Tomasi, J.; Cossi, M.; Millam, J. M.; Klene, M.; Adamo, C.; Cammi, R.; Ochterski, J. W.; Martin, R. L.; Morokuma, K.; Farkas, O.; Foresman, J. B.; Fox, D. J., *Gaussian 09 A.02*, Gaussian, Inc., Wallingford, CT, USA, **2009**.
- [S7] a) Ochterski, J. W.; Petersson, G. A.; Montgomery Jr., J. A., A complete basis set model chemistry. V. Extensions to six or more heavy atoms, *J. Chem. Phys.* **1996**, *104*, 2598–2619; b) Montgomery Jr., J. A.; Frisch, M. J.; Ochterski, J. W.; Petersson, G. A., A complete basis set model chemistry. VII. Use of the minimum population localization method, *J. Chem. Phys.* **2000**, *112*, 6532–6542.
- [S8] a) Curtiss, L. A.; Raghavachari, K.; Redfern, P. C.; Pople, J. A., Assignment of Gaussian-2 and density functional theories for the computation of enthalpies of formation, *J. Chem. Phys.* **1997**, *106*, 1063–1079; b) Byrd, E. F. C.; Rice, B. M., Improved prediction of heats of formation of energetic materials using quantum mechanical calculations, *J. Phys. Chem. A* **2006**, *110*, 1005–1013; c) Rice, B. M.; Pai, S. V.; Hare, J., Predicting heats

- of formation of energetic materials using quantum mechanical calculations, *Comb. Flame* **1999**, *118*, 445–458.
- [S9] Lindstrom, P. J.; Mallard, W. G., (Editors), NIST Standard Reference Database Number 69, <http://webbook.nist.gov/chemistry/> (accessed June **2020**).
- [S10] Westwell, M. S.; Searle, M. S.; Wales, D. J.; Williams, D. H., Empirical correlations between thermodynamic properties and intermolecular forces, *J. Am. Chem. Soc.* **1995**, *117*, 5013–5015; b) Trouton, F., IV. On molecular latent heat, *Philos. Mag.* **1884**, *18*, 54–57.
- [S11] a) Jenkins, H. D. B.; Roobottom, H. K.; Passmore, J.; Glasser, L., Relationships among ionic lattice energies, molecular (formula unit) volumes and thermochemical radii, *Inorg. Chem.* **1999**, *38*, 3609–3620; b) Jenkins, H. D. B.; Tudela, D.; Glasser, L., Lattice potential energy estimation for complex ionic salts from density measurements, *Inorg. Chem.* **2002**, *41*, 2364–2367.